

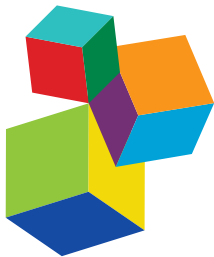
# EPITOPE DISCOVERY AND SYNTHETIC VACCINE DESIGN

EDITED BY: Clarisa Beatriz Palatnik-de-Sousa, Irene da Silva Soares and  
Daniela Santoro Rosa

PUBLISHED IN: *Frontiers in Immunology*



**frontiers** Research Topics



#### Frontiers Copyright Statement

© Copyright 2007-2018 Frontiers Media SA. All rights reserved.

All content included on this site, such as text, graphics, logos, button icons, images, video/audio clips, downloads, data compilations and software, is the property of or is licensed to Frontiers Media SA ("Frontiers") or its licensees and/or subcontractors. The copyright in the text of individual articles is the property of their respective authors, subject to a license granted to Frontiers.

The compilation of articles constituting this e-book, wherever published, as well as the compilation of all other content on this site, is the exclusive property of Frontiers. For the conditions for downloading and copying of e-books from Frontiers' website, please see the Terms for Website Use. If purchasing Frontiers e-books from other websites or sources, the conditions of the website concerned apply.

Images and graphics not forming part of user-contributed materials may not be downloaded or copied without permission.

Individual articles may be downloaded and reproduced in accordance with the principles of the CC-BY licence subject to any copyright or other notices. They may not be re-sold as an e-book.

As author or other contributor you grant a CC-BY licence to others to reproduce your articles, including any graphics and third-party materials supplied by you, in accordance with the Conditions for Website Use and subject to any copyright notices which you include in connection with your articles and materials.

All copyright, and all rights therein, are protected by national and international copyright laws.

The above represents a summary only. For the full conditions see the Conditions for Authors and the Conditions for Website Use.

ISSN 1664-8714  
ISBN 978-2-88945-522-5  
DOI 10.3389/978-2-88945-522-5

#### About Frontiers

Frontiers is more than just an open-access publisher of scholarly articles: it is a pioneering approach to the world of academia, radically improving the way scholarly research is managed. The grand vision of Frontiers is a world where all people have an equal opportunity to seek, share and generate knowledge. Frontiers provides immediate and permanent online open access to all its publications, but this alone is not enough to realize our grand goals.

#### Frontiers Journal Series

The Frontiers Journal Series is a multi-tier and interdisciplinary set of open-access, online journals, promising a paradigm shift from the current review, selection and dissemination processes in academic publishing. All Frontiers journals are driven by researchers for researchers; therefore, they constitute a service to the scholarly community. At the same time, the Frontiers Journal Series operates on a revolutionary invention, the tiered publishing system, initially addressing specific communities of scholars, and gradually climbing up to broader public understanding, thus serving the interests of the lay society, too.

#### Dedication to quality

Each Frontiers article is a landmark of the highest quality, thanks to genuinely collaborative interactions between authors and review editors, who include some of the world's best academicians. Research must be certified by peers before entering a stream of knowledge that may eventually reach the public - and shape society; therefore, Frontiers only applies the most rigorous and unbiased reviews.

Frontiers revolutionizes research publishing by freely delivering the most outstanding research, evaluated with no bias from both the academic and social point of view. By applying the most advanced information technologies, Frontiers is catapulting scholarly publishing into a new generation.

#### What are Frontiers Research Topics?

Frontiers Research Topics are very popular trademarks of the Frontiers Journals Series: they are collections of at least ten articles, all centered on a particular subject. With their unique mix of varied contributions from Original Research to Review Articles, Frontiers Research Topics unify the most influential researchers, the latest key findings and historical advances in a hot research area! Find out more on how to host your own Frontiers Research Topic or contribute to one as an author by contacting the Frontiers Editorial Office: [researchtopics@frontiersin.org](mailto:researchtopics@frontiersin.org)

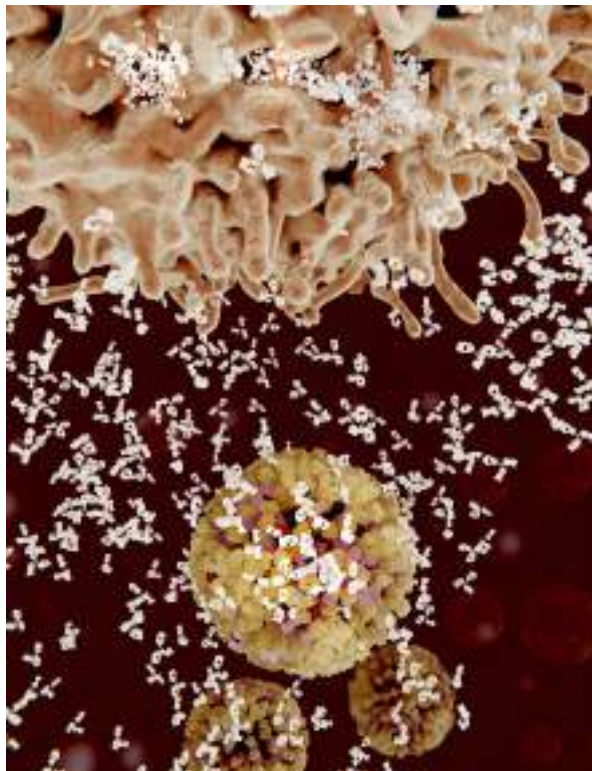
# EPITOPE DISCOVERY AND SYNTHETIC VACCINE DESIGN

Topic Editors:

**Clarisa Beatriz Palatnik-de-Sousa**, Universidade Federal de Rio de Janeiro and Instituto Nacional de Ciência e Tecnologia de Investigação em Imunologia, Brazil

**Irene da Silva Soares**, Universidade de São Paulo, Brazil

**Daniela Santoro Rosa**, Universidade Federal de São Paulo and Instituto Nacional de Ciência e Tecnologia de Investigação em Imunologia, Brazil



Plasma cells (B-cells) segregate specific antibodies to mark and subsequently destroy influenza viruses. 3D rendering.

Image: Juan Gaertner/Shutterstock.com

**Citation:** Palatnik-de-Sousa, C. B., Soares, I. S., Rosa, D. S., eds. (2018). Epitope Discovery and Synthetic Vaccine Design. Lausanne: Frontiers Media. doi: 10.3389/978-2-88945-522-5

# Table of Contents

## 06 Editorial: Epitope Discovery and Synthetic Vaccine Design

Clarisa Beatriz Palatnik-de-Sousa, Irene da Silva Soares and Daniela Santoro Rosa

## SECTION I

### THE IN SILICO APPROACH TO EPITOPE DISCOVERY AND SYNTHETIC VACCINE DESIGN

## 09 The Immune Epitope Database and Analysis Resource in Epitope Discovery and Synthetic Vaccine Design

Ward Flerl, Sinu Paul, Sandeep Kumar Dhanda, Swapnil Mahajan, Xiaojun Xu, Bjoern Peters and Alessandro Sette

## SECTION II

### EPITOPE VACCINES AGAINST VIRUS INFECTIONS

## 25 Enforced OX40 Stimulation Empowers Booster Vaccines to Induce Effective CD4<sup>+</sup> and CD8<sup>+</sup> T Cell Responses against Mouse Cytomegalovirus Infection

Eleni Panagioti, Louis Boon, Ramon Arens and Sjoerd H. van der Burg

## 39 Dendritic Cell Targeting Effectively Boosts T Cell Responses Elicited by an HIV Multiepitope DNA Vaccine

Juliana de Souza Apostólico, Victória Alves Santos Lunardelli, Marcio Massao Yamamoto, Hugo Fernando Santos Souza, Edecio Cunha-Neto, Silvia Beatriz Boscardin and Daniela Santoro Rosa

## 55 A Perspective on the Development of Plant-Made Vaccines in the Fight against Ebola Virus

Sergio Rosales-Mendoza, Ricardo Nieto-Gómez and Carlos Angulo

## 68 Adjusted Particle Size Eliminates the Need of Linkage of Antigen and Adjuvants for Appropriated T Cell Responses in Virus-Like Particle-Based Vaccines

Ariane C. Gomes, Anna Flace, Philippe Saudan, Franziska Zabel, Gustavo Cabral-Miranda, Aadil El Turabi, Vania Manolova and Martin F. Bachmann

## 78 An Approach for a Synthetic CTL Vaccine Design against Zika Flavivirus Using Class I and Class II Epitopes Identified by Computer Modeling

Edecio Cunha-Neto, Daniela S. Rosa, Paul E. Harris, Tim Olson, Alex Morrow, Serban Ciotlos, Charles V. Herst and Reid Martin Rubsamen

## SECTION III

### EPITOPE VACCINES AGAINST BACTERIAL INFECTIONS

## 90 Immunogenicity of a Multi-Epitope DNA Vaccine Encoding Epitopes from Cu–Zn Superoxide Dismutase and Open Reading Frames of *Brucella abortus* in Mice

Emilia Escalona, Darwin Sáez and Angel Oñate

- 100 *Immunogenic Domains and Secondary Structure of Escherichia coli Recombinant Secreted Protein Escherichia coli-Secreted Protein B***  
Bruna Alves Caetano, Letícia Barboza Rocha, Eneas Carvalho, Roxane Maria Fontes Piazza and Daniela Luz

## SECTION IV

### EPITOPE VACCINES AGAINST PROTOZOAN AND FUNGI INFECTIONS

- 108 *A Chimera Containing CD4+ and CD8+ T-Cell Epitopes of the Leishmania donovani Nucleoside Hydrolase (NH36) Optimizes Cross-Protection against Leishmania amazonensis Infection***  
Marcus Vinícius Alves-Silva, Dirlei Nico, Alexandre Morrot, Marcos Palatnik and Clarisa B. Palatnik-de-Sousa
- 126 *Leishmania donovani Nucleoside Hydrolase (NH36) Domains Induce T-Cell Cytokine Responses in Human Visceral Leishmaniasis***  
Micheli Luize Barbosa Santos, Dirlei Nico, Fabrícia Alvisi de Oliveira, Aline Silva Barreto, Iam Palatnik-de-Sousa, Eugenia Carrillo, Javier Moreno, Paula Mello de Luca, Alexandre Morrot, Daniela Santoro Rosa, Marcos Palatnik, Cristiane Bani-Corrêa, Roque Pacheco de Almeida and Clarisa Beatriz Palatnik-de-Sousa
- 145 *F1 Domain of the Leishmania (Leishmania) donovani Nucleoside Hydrolase Promotes a Th1 Response in Leishmania (Leishmania) infantum Cured Patients and in Asymptomatic Individuals Living in an Endemic Area of Leishmaniasis***  
Eugenia Carrillo, Laura Fernandez, Ana Victoria Ibarra-Meneses, Micheli L. B. Santos, Dirlei Nico, Paula M. de Luca, Cristiane Bani Correa, Roque Pacheco de Almeida, Javier Moreno and Clarisa B. Palatnik-de-Sousa
- 158 *A Poly(Lactic-co-Glycolic) Acid Nanovaccine Based on Chimeric Peptides from Different Leishmania infantum Proteins Induces Dendritic Cells Maturation and Promotes Peptide-Specific IFN $\gamma$ -Producing CD8 $^{+}$  T Cells Essential for the Protection against Experimental Visceral Leishmaniasis***  
Evita Athanasiou, Maria Agallou, Spyros Tatsoglou, Olga Kammona, Artemis Hatzigeorgiou, Costas Kiparissides and Evdokia Karagouni
- 183 *LFA-1 Mediates Cytotoxicity and Tissue Migration of Specific CD8 $^{+}$  T Cells after Heterologous Prime-Boost Vaccination against Trypanosoma cruzi Infection***  
Camila Pontes Ferreira, Leonardo Moro Cariste, Fernando Dos Santos Virgílio, Barbara Ferri Moraschi, Caroline Brandão Monteiro, Alexandre M. Vieira Machado, Ricardo Tostes Gazzinelli, Oscar Bruna-Romero, Pedro Luiz Menin Ruiz, Daniel Araki Ribeiro, Joseli Lannes-Vieira, Marcela de Freitas Lopes, Mauricio Martins Rodrigues and José Ronnie Carvalho de Vasconcelos
- 199 *Vaccine Containing the Three Allelic Variants of the Plasmodium vivax Circumsporozoite Antigen Induces Protection in Mice after Challenge with a Transgenic Rodent Malaria Parasite***  
Alba Marina Gimenez, Luciana Chagas Lima, Katia Sanches Françoso, Priscila M. A. Denapoli, Raquel Panatieri, Daniel Y. Bargieri, Jean-Michel Thibierge, Chiara Andolina, Francois Nosten, Laurent Renia, Ruth S. Nussenzweig, Victor Nussenzweig, Rogerio Amino, Mauricio M. Rodrigues and Irene S. Soares

**213 What Is Known about the Immune Response Induced by *Plasmodium vivax* Malaria Vaccine Candidates?**

Carolina López, Yoelis Yépes-Pérez, Natalia Hincapié-Escobar,  
Diana Díaz-Arévalo and Manuel A. Patarroyo

**236 *Plasmodium vivax* Cell-Traversing Protein for Ookinete and Sporozoite: Naturally Acquired Humoral Immune Response and B-Cell Epitope Mapping in Brazilian Amazon Inhabitants**

Rodrigo Nunes Rodrigues-da-Silva, Isabela Ferreira Soares,  
Cesar Lopez-Camacho, João Hermínio Martins da Silva, Daiana de Souza  
Perce-da-Silva, Antônio Têva, Antônia Maria Ramos Franco, Francimere  
Gomes Pinheiro, Lana Bitencourt Chaves, Lilian Rose Pratt-Riccio,  
Arturo Reyes-Sandoval, Dalma Maria Banic and Josué da Costa Lima-Junior

**249 Linear Epitopes of *Paracoccidioides brasiliensis* and Other Fungal Agents of Human Systemic Mycoses As Vaccine Candidates**

Luiz R. Travassos and Carlos P. Taborda

## SECTION V

### IMMUNOGENICITY DETERMINED BY GLYCAN VACCINES

**260 Neoglycoconjugate of Tetrasaccharide Representing One Repeating Unit of the *Streptococcus pneumoniae* Type 14 Capsular Polysaccharide Induces the Production of Opsonizing IgG1 Antibodies and Possesses the Highest Protective Activity As Compared to Hexa- and Octasaccharide Conjugates**

Ekaterina A. Kurbatova, Nelli K. Akhmatova, Elina A. Akhmatova,  
Nadezhda B. Egorova, Natalya E. Yastrebova, Elena V. Sukhova,  
Dmitriy V. Yashunsky, Yury E. Tsvetkov, Marina L. Gening and  
Nikolay E. Nifantiev

**273 The Length of N-Glycans of Recombinant H5N1 Hemagglutinin Influences the Oligomerization and Immunogenicity of Vaccine Antigen**

Agnieszka Katarzyna Maciąga, Maria Anna Pietrzak, Piotr Kosson,  
Mariusz Czarnocki-Cieciura, Krzysztof Śmietanka, Zenon Minta and  
Edyta Kopera



# Editorial: Epitope Discovery and Synthetic Vaccine Design

Clarisa Beatriz Palatnik-de-Sousa<sup>1,2\*</sup>, Irene da Silva Soares<sup>3</sup> and Daniela Santoro Rosa<sup>2,4</sup>

<sup>1</sup>Laboratório de Biologia e Bioquímica de Leishmaniose, Microbiologia Geral, Universidade Federal do Rio de Janeiro, Rio de Janeiro, Brazil, <sup>2</sup>Instituto de Investigação em Imunologia, Faculdade de Medicina, Universidade de São Paulo (USP), São Paulo, Brazil, <sup>3</sup>Department of Clinical and Toxicological Analyses, Universidade de São Paulo, São Paulo, Brazil,

<sup>4</sup>Departamento de Microbiologia, Imunologia e Parasitologia, Universidade Federal de São Paulo (UNIFESP), São Paulo, Brazil

**Keywords:** vaccines, synthetic vaccines, epitopes, T-epitope vaccines, B-cell epitope vaccines, epitope database, immunoinformatics

## Editorial on the Research Topic

### Epitope Discovery and Synthetic Vaccine Design

Traditional and first generation vaccines are composed of live or fixed whole pathogens, while second generation vaccines include, among others, the native protein antigens purified from the pathogen. And furthermore, third-generation vaccines are comprised of DNA plasmids capable of expressing the sequence of the most important pathogen protein antigens in the host. During this evolution of vaccines, there has been a gain in safety, however, with a loss of efficacy that has been compensated for with the use of adjuvants.

The latest step in the evolution of vaccine formulations is the development of epitope vaccines. Epitopes are short amino acid sequences of a protein that can induce a more direct and potent immune response, than the response induced by the whole cognate protein (1).

Moreover, the strategy for developing epitope vaccines requires an accurate knowledge of the amino acid sequence of the immunogenic protein of interest. Therefore, since vaccines against parasite, bacteria, or virus infections and tumors require a cellular immune response for prevention, control, and cure, a strategy called Reverse Vaccinology (RV) was developed. The RV approach uses the information of the codon sequence contained in the DNA of the pathogen to obtain a complementary cDNA, and further translates it to obtain the sequence of the protein of interest. Once these proteins are inside the antigen-presenting cells (APC) of the host, they are processed. The T cell epitopes are then proteolytically cleaved from the protein, and further exposed by the MHC molecules of the APC surface, to interact with the receptors of T cells. Therefore, with the knowledge of the primary sequence of the protein antigen, the epitopes can be identified by cloning the domains or smaller peptides of the protein separately and experimentally determining which one is more immunogenic, or alternatively, by screening the whole protein sequence using *in silico* predictions programs [Flerl et al.; (2, 3)].

The structure of the MHC molecules on APC, MHC class I molecules have a single alpha chain that influences binding, and the binding groove lies between the alpha 1 and alpha 2 domains (Flerl et al.). Since the binding groove is closed, it can only accommodate shorter peptides (8–14 amino acids). The groove binding core has only nine amino acids. MHC class II molecules in contrast, have two chains, alpha and beta that influence binding. The binding groove is open and can accommodate longer peptides (13–25 amino acids) but the binding core has 9 amino acid residues with 0–5 residues flanking on each side. Only the alpha chain is variable in class I molecules, so the nomenclature is “HLA” followed by the locus A, B, or C, an asterisk, and the number of the allele it represents. For class II molecules, both the alpha and beta chains impact binding and both of their chains are variable for the DP and DQ loci. However, for the DR locus, only the beta chain is variable (Flerl et al.). For all the mentioned characteristics, MHC class II binding prediction is more challenging than

## OPEN ACCESS

**Edited and Reviewed by:**  
Marc H. V. Van Regenmortel,  
Centre National de la Recherche  
Scientifique (CNRS), France

**\*Correspondence:**  
Clarisa Beatriz Palatnik-de-Sousa  
immgcpa@micro.ufrj.br

### Specialty section:

This article was submitted to  
Vaccines and Molecular  
Therapeutics,  
a section of the journal  
*Frontiers in Immunology*

**Received:** 03 January 2018  
**Accepted:** 04 April 2018  
**Published:** 18 April 2018

**Citation:**  
Palatnik-de-Sousa CB,  
Soares IS and Rosa DS (2018)  
Editorial: Epitope Discovery  
and Synthetic Vaccine Design.  
*Front. Immunol.* 9:826.  
doi: 10.3389/fimmu.2018.00826

that for class I molecules. Based on different machine learning algorithms, several predictions were developed as tools to identify the T cell epitopes of the protein antigens [Fleri et al.; (2, 3)].

In contrast, for parasite, viral, bacterial infections and tumors, whose prevention control and cure requires the development of a potent antibody response, the problem is more complex. In fact, the majority of B cell epitopes are discontinuous epitopes composed of amino acid residues located on separate regions of the protein, and which are joined together by the folding of the chain (4). These groups of residues cannot be isolated as such from the antigen. Therefore, the strategy used for these cases is called structural based reverse vaccinology (SBRV), and it focuses on the use of monoclonal antibodies against the protein antigen. There are six complementary determining regions (4) or antigen-binding regions (ABRs) (5), in the antibody molecule that can interact with the antigen. An antigen-binding site, also called a paratope, which is a small region (of 10–15 amino acids) is the part of the antibody that recognizes and binds to an antigen. However, each ABR differs significantly in its amino acid composition and tends to bind different types of amino acids on the surface of proteins. In spite of these differences, the combined preference of the six ABRs does not allow the epitopes to be distinguished from the rest of the protein surface. These findings explain the poor success of past and newly proposed methods for predicting protein epitopes (4, 5). SBRV strategy is used to study the interaction of the complex composed of the monoclonal antibody with the protein in order to identify to which amino acids of the antigen protein, the ABR or paratope of the monoclonal antibody binds. The objective of this approach is to elucidate the potential amino acid sequence of the discontinuous epitope indirectly. However, the search for the epitopes that interact with antibodies is a much more difficult task to which successful prediction algorithms are about non-existing. Consequently, this strategy has not achieved much success (4, 5).

The inability of synthetic linear peptides to effectively mimic the discontinuous epitopes is one of the reasons for the failure of many B cell synthetic vaccines to induce the synthesis of neutralizing antibodies. These facts partially explain why even though more than a thousand synthetic B cell peptides have been identified, only 125 of them have progressed to phase I, 30 of them to Phase II, and none of them have succeeded in phase III trials or have been licensed for human use (4).

Hence, while RV generally refers to the *in silico* analysis of the entire pathogen genome to identify all the antigens that the pathogen is able to express, the SBRV refers to the approach which tries to generate a vaccine from the known crystallographic structure of the neutralizing antibodies bound to the epitopes (6).

In the case of infections that are preventable by an antibody response, the term antigenicity has frequently been confused with immunogenicity (7). In fact, the epitopes of some viral antigens are often wrongly considered as immunogens, when they are only antigens, since they can interact with a variety of antibodies raised against a virus, but they are not capable of inducing the synthesis of the neutralizing antibodies engaged in protection (7). Previously, it was thought, that if an antigenic epitope bound strongly to a neutralizing monoclonal antibody *in vitro*, it would

be also able to induce the synthesis of neutralizing antibodies when used as a vaccine. However, this is not true (7).

Additionally, other concepts have been developed in association to the RV strategy (6). The concept of RV 1.0 is an approach based on bioinformatics and animal immunization and challenge used to determine which antigens are more appropriate for vaccination (8). In contrast, the concept of RV 2.0 refers to a strategy that obtains monoclonal antibodies from the few individuals that make a strong antibody response against natural infection. These monoclonal antibodies guide the vaccine design in the reversal direction of the normal flow of vaccines to anti-bodies (8).

Furthermore, the concept of “rational vaccine design” was used very often creating the expectation of having the same success as the strategy of “rational drug design” obtained before. However, the “rational drug design” is related to the development of chemical analogs that are perfect inhibitors of the active site of important vital enzymes of the pathogen. In contrast, investigators involved in the development of the HIV vaccine claimed that they use the “rational vaccine design” whereas in fact they only improved the antigenic binding capacity of one epitope with respect to only one paratope, and not the immunogenic capacity of an epitope to elicit neutralizing antibodies. These conclusions generated strong criticism [Van Regenmortel; (9)].

In contrast, the present Research Topic uses the concept of “Epitope Discovery and Synthetic Vaccine Design” as illustrated by Kao and Hodges (1). These authors demonstrated that synthetic vaccines based on short peptides, which represent immunogenic epitopes are able to impair and even exceeded the protective potential of the native cognate whole protein. They found higher antibody titers directed to the receptor-binding domain of the Pilus A of *Pseudomonas aeruginosa*, which has 14 amino acids than to the whole pilin native protein. The titers against the native pilin of the animals immunized with the synthetic peptide-conjugate were higher, than the titers of animals immunized with the whole pilin protein. In addition, the affinities of the anti-peptide sera for the intact pilin receptor-binding domain were significantly higher than affinities of anti-pilin protein sera (1).

We support the development of epitope vaccines that combine immunoinformatics and experimental biological approaches (Alves-Silva et al.; Barbosa Santos et al.). We used an immuno-informatic approach to improve the efficacy of existing vaccines composed of protein antigens that were selected according to their relevance in previous experimental biological results. Our results also showed that vaccines composed of the immunogenic domains, optimize and even exceed the protective potential induced by the whole protein (1). For instance, we achieved 33% optimization of vaccine efficacy by using a recombinant chimera, which contains the two domains that hold the most immunogenic epitopes of the Nucleoside hydrolase NH36 of *Leishmania*, instead of the whole NH36 protein (Alves-Silva et al.). These two domains (F1 and F3) hold the most potent epitopes for the generation of prophylactic protection against *Leishmania (L.) amazonensis* infection (Alves-Silva et al.). Vaccination with the NH36 protein reduces the lesion sizes by 55% (10). However, vaccination with the F1 and the F3 domains independently determined respective reductions of 70 and 77%, and the F1F3 chimera induced a reduction of 82% in the footpad lesion sizes (Alves-Silva et al.).

This enthusiasm coming after the advent of immunoinformatic tools and the finding of epitopes *via in silico* predictions should not devalue the empirical foundations of all experimental science involved in the development of the vaccines that control diseases until present (6). On the contrary, both the empirical and *in silico* tools should be used together in the development of new synthetic epitope vaccines that offer advantages over traditional vaccines. They are chemically defined antigens free from deleterious effects. Additionally, in contrast to live-attenuated vaccines, they do not revert to virulence in immunocompromised subjects, and different from genetic vaccines, they do not involve ethical questions.

With this Research Topic, we believed we have made significant contributions to the development of synthetic epitope vaccines that may help in the prevention, treatment, and control of infectious diseases and cancer.

## REFERENCES

1. Kao DJ, Hodges RS. Advantages of a synthetic peptide immunogen over a protein immunogen in the development of an anti-pilus vaccine for *Pseudomonas aeruginosa*. *Chem Biol Drug Des* (2009) 74:33–42. doi:10.1111/j.1747-0285.2009.00825.x
2. Jensen KK, Andreatta M, Marcatili P, Buus S, Greenbaum JA, Yan Z, et al. Improved methods for predicting peptide binding affinity to MHC class II molecules. *Immunology* (2018). doi:10.1111/imm.12889
3. Jurtz V, Paul S, Andreatta M, Marcatili P, Peters B, Nielsen M. NetMHCpan-4.0: improved peptide-MHC class I interaction predictions integrating eluted ligand and peptide binding affinity data. *J Immunol* (2017) 199:3360–8. doi:10.4049/jimmunol.1700893
4. Van Regenmortel MHV. Synthetic peptide vaccines and the search for neutralization B cell epitopes. *Open Vaccine J* (2009) 2:33–44. doi:10.2174/1875035401002010033
5. Kunik V, Ofran Y. The indistinguishability of epitopes from protein surface is explained by the distinct binding preferences of each of the six antigen-binding loops. *Protein Eng Des Sel* (2013) 26:599–609. doi:10.1093/protein/gzt027
6. Van Regenmortel MHV. Two meanings of reverse vaccinology and the empirical nature of vaccine science. *Vaccine* (2011) 29:7875. doi:10.1016/j.vaccine.2011.08.063
7. Van Regenmortel MHV. Immune systems rather than antigenic epitopes elicit and produce protective antibodies against HIV. *Vaccine* (2017) 35:1985–6. doi:10.1016/j.vaccine.2017.03.017
8. Burton DR. What are the most powerful immunogen design vaccine strategies? Reverse vaccinology 2.0 shows great promise. *Cold Spring Harb Perspect Biol* (2017) 9(11):a030262. doi:10.1101/cshperspect.a030262
9. Van Regenmortel MHV. Structure-based reverse vaccinology failed in the case of HIV because it disregarded accepted immunological theory. *Int J Mol Sci* (2016) 17:1591. doi:10.3390/ijms17091591
10. Nico D, Claser C, Borja-Cabrera GP, Travassos LR, Palatnik M, Soares IS, et al. Adaptive immunity against *Leishmania* nucleoside hydrolase maps its c-terminal domain as the target of the CD4+ T cell-driven protective response. *PLoS Negl Trop Dis* (2010) 4(11):e866. doi:10.1371/journal.pntd.0000866

## AUTHOR CONTRIBUTIONS

CP-d-S, DSR, and ISS wrote and approved the final text of this Editorial.

## ACKNOWLEDGMENTS

The authors thank David Straker for language review.

## FUNDING

This work was supported by Conselho Nacional de Desenvolvimento Científico e Tecnológico (CNPQ) [Fellowships, 310977/2014-2 to CP-d-S and grant 404400/2012-4 to CP-d-S] and Fundação Carlos Chagas de Amparo à Pesquisa do Estado de Rio de Janeiro (FAPERJ) [grant E-26-201.583/2014, E-26-102957/2011 and E-26/111.682/2013 to CP-d-S].

8. Burton DR. What are the most powerful immunogen design vaccine strategies? Reverse vaccinology 2.0 shows great promise. *Cold Spring Harb Perspect Biol* (2017) 9(11):a030262. doi:10.1101/cshperspect.a030262
9. Van Regenmortel MHV. Structure-based reverse vaccinology failed in the case of HIV because it disregarded accepted immunological theory. *Int J Mol Sci* (2016) 17:1591. doi:10.3390/ijms17091591
10. Nico D, Claser C, Borja-Cabrera GP, Travassos LR, Palatnik M, Soares IS, et al. Adaptive immunity against *Leishmania* nucleoside hydrolase maps its c-terminal domain as the target of the CD4+ T cell-driven protective response. *PLoS Negl Trop Dis* (2010) 4(11):e866. doi:10.1371/journal.pntd.0000866

**Conflict of Interest Statement:** The authors declare that the research was conducted in the absence of any commercial or financial relationships that could be construed as a potential conflict of interest.

Copyright © 2018 Palatnik-de-Sousa, Soares and Rosa. This is an open-access article distributed under the terms of the Creative Commons Attribution License (CC BY). The use, distribution or reproduction in other forums is permitted, provided the original author(s) and the copyright owner are credited and that the original publication in this journal is cited, in accordance with accepted academic practice. No use, distribution or reproduction is permitted which does not comply with these terms.



# Enforced OX40 Stimulation Empowers Booster Vaccines to Induce Effective CD4<sup>+</sup> and CD8<sup>+</sup> T Cell Responses against Mouse Cytomegalovirus Infection

Eleni Panagioti<sup>1</sup>, Louis Boon<sup>2</sup>, Ramon Arens<sup>3</sup> and Sjoerd H. van der Burg<sup>1\*</sup>

<sup>1</sup> Department of Medical Oncology, Leiden University Medical Center, Leiden, Netherlands, <sup>2</sup> Bioceros, Utrecht, Netherlands,

<sup>3</sup> Department of Immunohematology and Blood Transfusion, Leiden University Medical Center, Leiden, Netherlands

## OPEN ACCESS

### Edited by:

Irene S. Soares,  
University of São Paulo, Brazil

### Reviewed by:

Yasmin Thanavala,  
Roswell Park Cancer Institute, USA  
Daniel Olive,  
Institut national de la santé et de la  
recherche médicale, France

### \*Correspondence:

Sjoerd H. van der Burg  
shvdburg@lumc.nl

### Specialty section:

This article was submitted to  
Vaccines and Molecular  
Therapeutics,  
a section of the journal  
*Frontiers in Immunology*

Received: 24 November 2016

Accepted: 30 January 2017

Published: 20 February 2017

### Citation:

Panagioti E, Boon L, Arens R and van der Burg SH (2017) Enforced OX40 Stimulation Empowers Booster Vaccines to Induce Effective CD4<sup>+</sup> and CD8<sup>+</sup> T Cell Responses against Mouse Cytomegalovirus Infection. *Front. Immunol.* 8:144.  
doi: 10.3389/fimmu.2017.00144

There is an imperative need for effective preventive vaccines against human cytomegalovirus as it poses a significant threat to the immunologically immature, causing congenital disease, and to the immune compromised including transplant recipients. In this study, we examined the efficacy of synthetic long peptides (SLPs) as a CD4<sup>+</sup> and CD8<sup>+</sup> T cell-eliciting preventive vaccine approach against mouse CMV (MCMV) infection. In addition, the use of agonistic OX40 antibodies to enhance vaccine efficacy was explored. Immunocompetent C57BL/6 mice were vaccinated in a prime-boost vaccination regimen with SLPs comprising various MHC class I- and II-restricted peptide epitopes of MCMV-encoded antigens. Enforced OX40 stimulation resulted in superior MCMV-specific CD4<sup>+</sup> and CD8<sup>+</sup> T cell responses when applied during booster SLP vaccination. Vaccination with a mixture of SLPs containing MHC class II epitopes and OX40 agonistic antibodies resulted in a moderate reduction of the viral titers after challenge with lytic MCMV infection. Markedly, the combination of SLP vaccines containing both MHC class I and II epitopes plus OX40 activation during booster vaccination resulted in polyfunctional (i.e., IFN- $\gamma$ <sup>+</sup>, TNF<sup>+</sup>, IL-2<sup>+</sup>) CD4<sup>+</sup> and CD8<sup>+</sup> T cell responses that were even higher in magnitude when compared to those induced by the virus, and this resulted in the best containment of virus dissemination. Our results show that the induction of strong T cell responses can be a fundamental component in the design of vaccines against persistent viral infections.

**Keywords:** cytomegalovirus, synthetic long peptides, prophylactic vaccination, T cells, OX40 costimulation

## INTRODUCTION

It is estimated that 60–80% of people worldwide are infected by the prototypic  $\beta$ -herpesvirus human cytomegalovirus (HCMV). CMV establishes low-level viral persistence within immunocompetent hosts without clinical symptoms. However, it can cause life-threatening disease in the immunological immature (unborn babies and newborns) and immunocompromised individuals (e.g., bone marrow and organ transplant recipients) (1, 2). Although new antiviral drugs against CMV are in clinical development, the most commonly used agents display toxicity. Importantly, no licensed prophylactic or therapeutic vaccines exist for CMV at present. Consequently, there is an imperative

need to identify potent vaccine modalities to prevent HCMV infection (3–5).

CD4<sup>+</sup> and CD8<sup>+</sup> T cell responses play a critical role in controlling CMV infection in both mouse and human. While CD4<sup>+</sup> T cells seem to be more crucial in the early phase after infection, CD8<sup>+</sup> T cells are imperative during latency and harbor superior protective properties upon rechallenge (6–9). Moreover, adoptive transfer approaches established the pivotal role of CMV-specific CD4<sup>+</sup> and CD8<sup>+</sup> T cells in orchestrating virus replication control (10–12). During CMV infection, CD4<sup>+</sup> and CD8<sup>+</sup> T cell responses either follow the traditional course comprised by massive expansion followed by rapid contraction and maintenance at low levels or instead do not undergo contraction but remain at high frequency or even expand gradually. The latter has been described as memory T cell inflation and has been observed for a restricted set of immunodominant CMV antigens (13–16). Memory inflation is thought to occur due to low-level persistent antigenic priming and requires certain costimulatory receptor-ligand pairs of which CD27–CD70 and OX40–OX40L interactions are important (17, 18). Phenotypically inflationary T cells exhibit effector-like properties without signs of exhaustion (14, 16, 19). The comparable nature of the T cell response to mouse CMV (MCMV) and HCMV is also found for B cell and NK cell responses and is likely related to the similarities of both viruses in tropism, pathology, and the establishment of latent infection that reactivates upon immunosuppression (20, 21).

Recently, we demonstrated that synthetic long peptide (SLP) vaccines, designed to exclusively induce MHC class I-restricted CD8<sup>+</sup> T cells, were able to elicit robust and polyfunctional T cell responses that led to reduced MCMV replication in C57BL/6 and BALB/c mouse strains after challenge (22). However, live MCMV vaccines were more efficient which prompted us to further improve the SLP vaccine efficacy. Since CD4<sup>+</sup> helper T cells promote long-term maintenance of memory CD8<sup>+</sup> T cells, also during MCMV infection (23, 24), and display direct antiviral capabilities (12, 25), the induction of CD4<sup>+</sup> T cells may improve the efficacy of the SLP vaccine. Here, we analyzed the potency of SLP vaccines inducing MCMV-specific CD4<sup>+</sup> T cells, either alone or in conjunction with SLPs eliciting MCMV-specific CD8<sup>+</sup> T cells. Enforced OX40 signaling was used to enhance the expansion of both CD4<sup>+</sup> and CD8<sup>+</sup> T cell subsets. We show that combined administration of SLPs eliciting CD4<sup>+</sup> and CD8<sup>+</sup> T cells and OX40 stimulation during booster vaccination leads to a startling increase of both the T cell magnitude and polyfunctionality, ultimately leading to efficient control of lytic MCMV infection.

## ANIMALS AND METHODS

### Mice

Wild-type female C57BL/6 mice (8–10 weeks) were purchased from Charles River Laboratories (L'Arbresle, France) and Ly5.1 (SJL; CD45.1) congenic mice on a C57BL/6 genetic background were obtained from The Jackson Laboratory. Mice were bred and housed under specific-pathogen-free conditions at the Central Animal Facility of Leiden University Medical Center (LUMC).

Experimental procedures were approved by the LUMC Animal Experiments Ethical Committee and conducted according to the Dutch Experiments on Animals Act and the Council of Europe (#13156 and #14187).

### Viral Infections

Virus stocks were prepared from salivary glands of BALB/c mice infected with MCMV-Smith [American Type Culture Collection (ATCC)]. The viral titers of the produced virus stocks were determined by viral plaque assays with mouse NIH-3T3 Embryonic Fibroblasts (ATCC). C57BL/6 mice were infected intraperitoneally (i.p.) with  $5 \times 10^4$  PFU MCMV in 400 µl of PBS. 60 days post-booster vaccination or infection, mice were rechallenged with  $5 \times 10^4$  PFU MCMV. Viral loads in spleen, liver, and lungs were determined by real-time PCR at day 5 post challenge as described previously (26). Due to differences in peak viral replication, the viral load in the salivary glands was not measured.

### Peptides and Vaccination

Short (9–10 aa) and long (20–21 aa) peptides containing MHC class I-restricted T cell epitopes (22) and 15 aa long peptides containing MHC class II epitopes (15) were produced at the GMP-peptide facility of the LUMC. The purity (75–90%) of the synthesized peptides was determined by HPLC and the molecular weight by mass spectrometry. All peptide sequences used in this study are listed and described in Table S1 in Supplementary Material. Both single and mixed SLP vaccines were administered subcutaneously (s.c.) at the tail base by delivery of 50 µg of each SLP and 20 µg CpG (ODN 1826, InvivoGen) in a total volume of 50 µl in PBS. Booster SLP vaccinations were provided after 2 weeks. At the indicated times (during prime and/or booster vaccination), mice were injected i.p. with 150 µg agonistic OX40 mAb (clone OX86) dissolved in 150 µl of PBS. All SLP vaccine administrations were well tolerated without adverse events and signs of hypersensitivity.

### Flow Cytometry

To evaluate CD4<sup>+</sup> and CD8<sup>+</sup> T cell responses, cell surface and intracellular cytokine staining in splenocytes and blood lymphocytes were performed as previously described (27). In brief, to determine the cytokine production capacity, single-cell suspensions from spleens were stimulated with short MHC class I peptides (2 µg/ml) for 5 h in the presence of brefeldin A (GolgiPlug; BD Pharmingen) or with long MHC class II peptides (5 µg/ml) for 8 h of which the last 6 h in presence of brefeldin A. MHC class I tetramers specific for the M45<sub>985–993</sub>, M57<sub>816–824</sub>, m139<sub>419–426</sub>, M38<sub>316–323</sub>, and IE3<sub>416–423</sub> MCMV epitopes were used. Fluorochrome-conjugated mAbs were obtained from BD Biosciences, Biolegend, or eBioscience. Flow cytometry gating strategies are shown in Figure S6 in Supplementary Material. All data were acquired on a LSRFortessa cytometer (BD Biosciences) and analyzed with FlowJo-V10 software (Tree Star).

### Antibody Detection by ELISA

Total IgG, IgG<sub>2b</sub>, IgG<sub>2c</sub>, IgG<sub>3</sub>, IgE, and IgA concentrations were determined by ELISA in serum samples as previously

described (26). Briefly, Nunc-Immuno Maxisorp plates (Fisher Scientific) were coated overnight with 2 µg/ml MHC class II SLPs in bicarbonate buffer, and after blocking (skim milk powder, Fluka BioChemika) sera from mice (i) chronically infected, (ii) long term vaccinated with MHC class II SLP vaccines and anti-OX40 mAb treated (i.p. during booster vaccination only), or (iii) uninfected were added. Next, plates were incubated with various HRP-conjugated antibodies (SouthernBiotech) to detect different immunoglobulin isotypes. Plates were developed with TMB substrate (Sigma Aldrich), and the color reaction was stopped by the addition of 1 M H<sub>2</sub>SO<sub>4</sub>. To serve as a positive control, a peptide from the M2 protein (eM2) of influenza A virus with known ability to induce antibodies and corresponding serum was used. Optical density was read at 450 nm (OD<sub>450</sub>) using a Microplate reader (Model 680, Bio-Rad).

## Adoptive T Cell Transfers

The secondary expansion potential of the SLP vaccine-induced antigen-specific CD8<sup>+</sup> T cells receiving agonistic OX40 mAb only during booster vaccination was determined by adoptive transfers. Splenic memory (day 65) CD8<sup>+</sup> T cells from SLP vaccinated CD45.1<sup>+</sup> congenic mice were negatively enriched with magnetic sorting using the CD8<sup>+</sup> T cell isolation kit (Miltenyi Biotec). 2 × 10<sup>6</sup> total CD8<sup>+</sup> T cells were retro-orbitally injected (in a total volume of 200 µl in PBS) into naive CD45.2<sup>+</sup> recipients. Recipient mice were rested for 2 h and concomitantly infected with 5 × 10<sup>4</sup> PFU MCMV. Subsequently, in order to quantify the number of the vaccine antigen-specific CD8<sup>+</sup> T cells that was transferred, a representative amount of cells was stained with MHC class I tetramers and with fluorochrome labeled antibodies against CD44, CD3, CD4, and CD8. The number of the donor's vaccine-specific T cells transferred was ranging between 8 × 10<sup>3</sup> and 2.5 × 10<sup>4</sup> cells for the group that did not receive OX40 mAb and between 1.8 × 10<sup>4</sup> and 4.5 × 10<sup>4</sup> cells for the OX40 mAb boosted group. 6 days later, the number of vaccine-specific CD8<sup>+</sup> T cells of the donor was measured (based on the expression of the CD45.1 marker) by flow cytometry, and the fold expansion was calculated.

## Statistical Analyses

Statistics were calculated using the unpaired Student's *t*-test or ANOVA in GraphPad Prism software (GraphPad Software Inc., USA). \**P* < 0.05, \*\**P* < 0.01, \*\*\**P* < 0.001, and \*\*\*\**P* < 0.00001.

## RESULTS

### Prime/Boost Vaccination with SLPs Inducing MCMV-Specific CD4<sup>+</sup> T Cell Responses

MHC class II epitopes from MCMV-encoded proteins have previously been identified by us in the C57BL/6 mouse strain (MHC haplotype H-2<sup>b</sup>) (15), and five immunogenic epitopes (i.e., m18<sub>872–886</sub>, M25<sub>409–423</sub>, m139<sub>560–574</sub>, m142<sub>24–38</sub>, and m09<sub>133–147</sub>) were selected for the SLP vaccine platform (Table S1 in Supplementary Material). Initially, the potential of single SLP-based vaccines in eliciting CD4<sup>+</sup> T cell responses was assessed in a prime/boost

vaccination setting (2 weeks apart) with the TLR9 ligand CpG as adjuvant. At day 8 after the first SLP vaccination, CD4<sup>+</sup> T cell responses were not detected by polychromatic intracellular cytokine staining (data not shown) but they became detectable in the spleen at day 8 after the booster SLP vaccination (Figure 1A). However, these responses were relatively low when compared to SLP-induced CD8<sup>+</sup> T cell responses (22). Analysis of the cytokine profile revealed the presence of single IFN-γ, double IFN-γ/TNF, and triple IFN-γ/TNF/IL-2 cytokine-producing CD4<sup>+</sup> T cell populations (Figure 1B).

For clinical applications multiple SLPs need to be combined in order to deal with MHC heterogeneity. Moreover, the breadth of SLP vaccines is important for the efficacy (22). Hence, mice were vaccinated with a mixture of the five SLPs, and the CD4<sup>+</sup> T cell response for each individual peptide epitope was measured. CD4<sup>+</sup> T cell reactivity to all MHC class II epitopes was detected (Figure 1C), albeit that the response to each individual peptide was lower when compared to single SLP vaccination, suggesting that competition among CD4<sup>+</sup> T cell peptide epitopes occurs in multivalent vaccines. Moreover, in comparison to the CD4<sup>+</sup> T cell response observed after MCMV infection, vaccination with a mixture of MHC class II SLPs resulted in lower numbers of MCMV-specific T cells (Figure 1C). Nevertheless, the cytokine polyfunctionality of the SLP-elicited CD4<sup>+</sup> T cells was augmented compared to MCMV-induced CD4<sup>+</sup> T cells (Figure 1D). Taken together, these results show that prime/boost vaccination with a mixture of MHC class II epitope-containing SLPs elicits polyfunctional MCMV-specific CD4<sup>+</sup> T cell responses, but in magnitude these are lower as compared to those induced by the virus itself.

### Enforced OX40 Triggering during Booster Vaccination Shows Superior Induction of SLP-Elicited CD4<sup>+</sup> T Cell Responses

Next, we attempted to augment the magnitude of the SLP-induced CD4<sup>+</sup> T cell responses. As OX40-mediated signals are important for enhancing CD4<sup>+</sup> T cell expansion and survival (28), we decided to use an agonistic OX40 antibody that provides *in vivo* OX40 stimulation. First, we investigated the scheduling of the agonistic OX40 antibody administration (i.e., during priming only, during booster only or during priming and booster) in order to obtain the most optimal CD4<sup>+</sup> T cell stimulation (Figure 2A). The magnitude of the T cell response elicited by the SLP containing the M25<sub>409–423</sub> epitope was measured 8 days post-booster vaccination in the spleen. OX40 stimulation clearly increased the magnitude of the M25<sub>409–423</sub>-specific CD4<sup>+</sup> T cell responses, and remarkably, this was most prominent when the mice received agonistic OX40 antibody during the booster vaccination only (Figures 2B,C). Markedly, a >100-fold increase in IFN-γ<sup>+</sup> CD4<sup>+</sup> T cells was observed when compared to SLP vaccination without enforced OX40 stimulation, whereas the response was 17-fold and 5-fold higher than in mice receiving OX40 antibody during priming only or during both priming and booster vaccination, respectively (Figure 2C). In addition, there was a striking gain in cytokine polyfunctionality when agonistic OX40 antibody

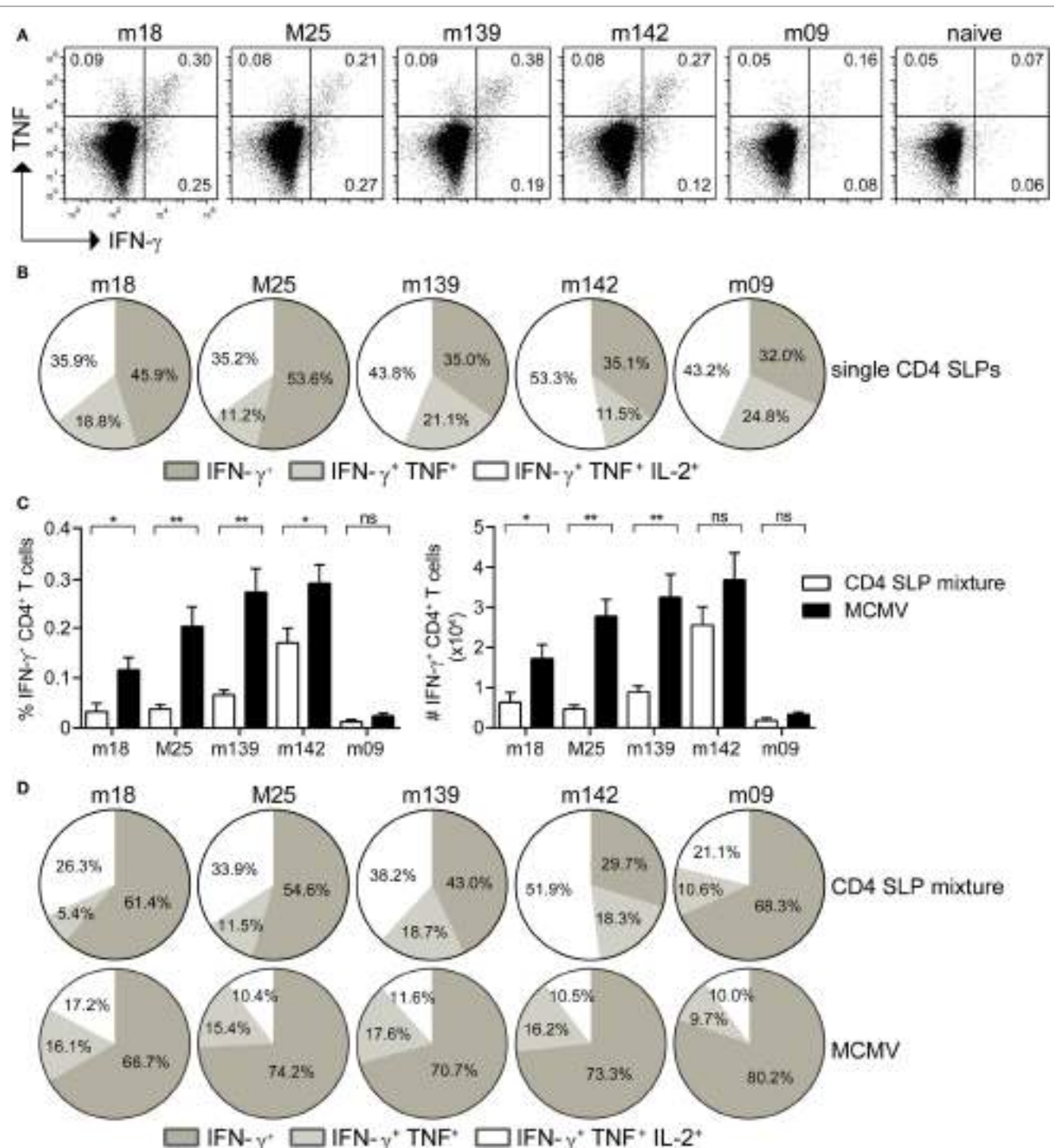


**FIGURE 1 | Prime-boost synthetic long peptide (SLP) vaccination with combined MHC class II SLPs provokes the induction of strong and polyfunctional CD4 $^{+}$  T cell responses. (A)** At day 8 post-booster vaccination with single SLPs containing MHC class II epitopes, the magnitude of the CD4 $^{+}$  T cell responses specific to the indicated epitopes was determined by intracellular cytokine staining after restimulation with peptide. Representative plots show percentages of IFN- $\gamma$  versus TNF cytokine production of the vaccine-elicited CD4 $^{+}$  T cells. **(B)** Pie charts depict the percentages of the single (IFN- $\gamma$ ), double (IFN- $\gamma$ /TNF), and triple (IFN- $\gamma$ /TNF/IL-2) cytokine producers of each antigen-specific CD4 $^{+}$  T cell population at day 8 post-booster vaccination with single MHC class II SLPs. **(C)** Percentages (left) and total numbers (right) of splenic SLP and MCMV-specific IFN- $\gamma$  $^{+}$  CD4 $^{+}$  T cells at day 8 post-booster vaccination with a mixture of all five MHC class II SLPs are shown. **(D)** Pie charts depict the percentages of the single (IFN- $\gamma$ ), double (IFN- $\gamma$ /TNF), and triple (IFN- $\gamma$ /TNF/IL-2) cytokine producers of each antigen-specific CD4 $^{+}$  T cell population at day 8 after booster vaccination with a mixture of all five MHC class II SLPs. Data represent mean values and are representative of three independent experiments ( $n = 4$ –5 per group). \* $P < 0.05$ ; \*\* $P < 0.01$ ; ns, not significant.

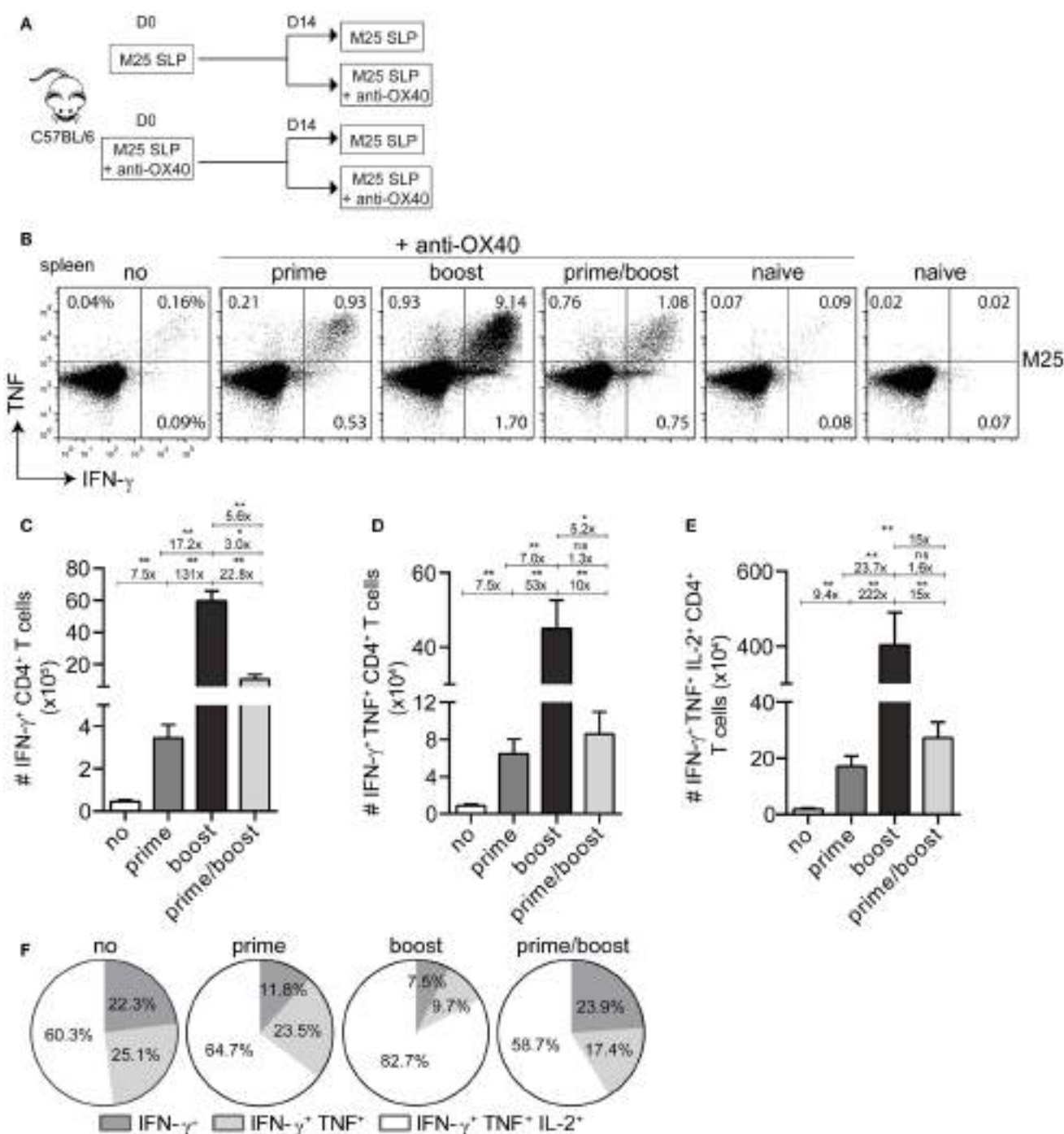


**FIGURE 2 | Activation of the OX40 axis during booster vaccination with a single MHC class II synthetic long peptide (SLP) vaccine propels increment of the vaccine-induced CD4<sup>+</sup> T cell response. (A)** Scheme of the experimental procedure and the vaccination timeline. Wild-type C57BL/6 mice were vaccinated (i) s.c. with M25<sub>409-423</sub> MHC class II SLP alone or (ii) with M25<sub>409-423</sub> MHC class II SLP (s.c.) along with anti-OX40 mAb (i.p.). Two weeks after prime vaccination mice from group (i) and (ii) were divided into two groups, respectively, and a booster immunization was administered. Half mice received only the M25<sub>409-423</sub> SLP and the other half were injected anti-OX40 mAb in addition to the M25<sub>409-423</sub> SLP. **(B)** The total size of the splenic M25<sub>409-423</sub> SLP vaccine-induced CD4<sup>+</sup> T cells from each group was measured by intracellular cytokine staining. Representative plots depict percentages of IFN- $\gamma$  versus TNF cytokine producing CD4<sup>+</sup> T cell populations at day 8 post-booster vaccination. **(C)** Total numbers of splenic IFN- $\gamma$ <sup>+</sup> producing M25<sub>409-423</sub> antigen-specific CD4<sup>+</sup> T cells at day 8 post booster SLP vaccination and differential anti-OX40 mAb treatment are shown. **(D)** Total double (IFN- $\gamma$ /TNF) and **(E)** triple (IFN- $\gamma$ /TNF/IL-2) cytokine producers of M25<sub>409-423</sub> vaccine-specific CD4<sup>+</sup> T cells measured in spleen at day 8 post-booster vaccination. Fold differences among each population are also depicted **(F)**. Pie charts show the percentages of the single (IFN- $\gamma$ ), double (IFN- $\gamma$ /TNF), and triple (IFN- $\gamma$ /TNF/IL-2) cytokine producers of each M25<sub>409-423</sub>-specific CD4<sup>+</sup> T cell population upon vaccination with M25<sub>409-423</sub> SLP and anti-OX40 mAb. Data represent mean values and are representative of three independent experiments ( $n = 5-6$  per group). \* $P < 0.05$ ; \*\* $P < 0.01$ ; ns, not significant.

was provided during booster vaccination only (**Figures 2D–F**). Compared to SLP vaccination, the increase in absolute numbers of triple IFN- $\gamma$ /TNF/IL-2 producers was even >200-fold (**Figure 2E**).

Next, we examined whether the strong increase in MCMV-specific CD4 $^{+}$  T cells by administration of agonistic OX40 antibody during booster vaccination was also evident in case of a mixture of SLPs. Clearly, at day 8 post-booster vaccination, a strong increase in both percentages and absolute numbers of the peptide-specific IFN- $\gamma$  $^{+}$  CD4 $^{+}$  T cells was observed for all epitopes in the mixture (**Figure 3A**). In addition, administration of OX40 antibody dramatically improved the cytokine polyfunctional traits (**Figure 3B**). Most profoundly, OX40 stimulation augmented the IL-2 production capacity of the vaccine-induced CD4 $^{+}$  T cells (**Figures 3B,C**). Together, these results demonstrate that activation of the OX40 axis during booster SLP vaccination leads to superior CD4 $^{+}$  T cell expansion and induction of cytokine polyfunctionality.

Having established a powerful means to augment SLP vaccines containing MHC class II epitopes, we tested if the used SLPs may comprise unidentified class I epitopes and/or linear B cell epitopes leading to CD8 $^{+}$  T cells and antibody responses, respectively. However, intracellular cytokine staining did not reveal any induction of MCMV-specific CD8 $^{+}$  T cells and SLP-specific antibody ELISAs were negative (Figures S1A,B in Supplementary Material). Furthermore, increased percentages of activated NK cells were also not detected after SLP vaccination (Figure S1C in Supplementary Material), indicating that the intended MHC class II epitope-containing SLPs with enforced OX40 stimulation exclusively activate antigen-specific CD4 $^{+}$  T cell responses.

## Provision of OX40 Stimulation during Booster Vaccination Also Advances SLP-Induced CD8 $^{+}$ T Cell Responses

To improve our previously reported CD8 $^{+}$  T cell eliciting SLP vaccine modality (22), we here envisaged to combine both MHC class I and II epitope-containing SLPs. We, therefore, also analyzed the impact of OX40 engagement on vaccine-induced CD8 $^{+}$  T cells in a similar scheduling experiment using a SLP exclusively containing the CD8 $^{+}$  T cell peptide epitope M57<sub>816–824</sub> (Figure S2A in Supplementary Material). Consistent with the results described for CD4 $^{+}$  T cells, mice that were vaccinated and treated with agonistic OX40 antibody during booster vaccination displayed the strongest SLP-induced CD8 $^{+}$  T cell response in both blood and spleen (Figures S2B–F in Supplementary Material). The number of SLP-induced CD8 $^{+}$  T cells, determined either by IFN- $\gamma$  reactivity or by MHC class I tetramer binding, at the peak after the boost were similar, indicating that OX40 stimulation during SLP vaccination (provided either during priming, during booster or during prime/boost) induces functional (non-exhausted) CD8 $^{+}$  T cells (Figures S2C,D in Supplementary Material). The cell-surface phenotype based on KLRG1 and CD127 of the vaccine-induced CD8 $^{+}$  T cells at the peak of the response after the booster was comparable (Figure S2G in Supplementary Material).

Next, the impact of OX40 stimulation during booster vaccination was evaluated for a mixture of MHC class I epitope-containing SLPs. Longitudinal analysis of the SLP-specific CD8 $^{+}$  T cell response revealed that OX40 stimulation during booster vaccination clearly amplifies the expansion of all SLP vaccine-induced CD8 $^{+}$  T cells measured in blood and spleen (**Figures 4A,B**), although this effect was relatively lower when compared to that seen for CD4 $^{+}$  T cells. At the peak of the response, 8 days after booster SLP vaccination, the magnitude of the IFN- $\gamma$  $^{+}$ CD8 $^{+}$  T cell response specific for each MHC class I-restricted epitope was again proportional to the MHC class I tetramer response (data not shown). However, the polyfunctional cytokine profile was improved upon OX40 stimulation (**Figures 4C,D**). In particular, OX40 stimulation augmented the percentages and absolute number of the triple cytokine producers (**Figures 4C,D**).

To gain insight into the mechanisms underlying the apparent impact of OX40 stimulation during booster vaccination, we examined the expression of the pro-apoptotic protein BCL-2, a known target of OX40 triggering and implicated in T cell survival (29). BCL-2 expression was upregulated by the vaccine-specific CD8 $^{+}$  T cells when OX40 stimulation was provided during booster vaccination compared to no OX40 stimulation (**Figure 4E**). Moreover, when agonistic OX40 antibody was administered during both primary and booster vaccination, BCL-2 expression was downregulated. These results indicate that stimulation of OX40 can bolster vaccine-induced CD8 $^{+}$  T cell expansion through a BCL-2-dependent mechanism, if this stimulation is correctly scheduled.

Over time, the SLP-induced CD8 $^{+}$  T cell responses contracted, yet the OX40 boosted epitope-specific CD8 $^{+}$  T cell responses to M38, M45, and M57 were maintained at higher levels (**Figure 5A**). At the memory phase (60 days after booster vaccination), there were higher percentages and numbers of triple (IFN- $\gamma$ /TNF/IL-2) cytokine-producing vaccine-induced CD8 $^{+}$  T cells in mice that received agonistic OX40 antibody during booster vaccination (except for m139<sub>419–426</sub>) (**Figures 5B,C**).

We also tested the impact of the *in vivo* OX40 stimulation on the secondary expansion potential, a hallmark of memory T cells. We performed adoptive transfer experiments in which congenically marked (CD45.1 $^{+}$ ) memory CD8 $^{+}$  T cells from SLP vaccinated mice were isolated and transferred into naïve recipient mice, which were subsequently challenged with MCMV (Figure S3A in Supplementary Material). Overall, the SLP-induced memory CD8 $^{+}$  T cells isolated from mice that also received OX40 stimulation during booster vaccination expanded better compared to the vaccine only group (Figures S3B,C in Supplementary Material).

Subsequently, we examined whether OX40 stimulation is able to further improve the prophylactic efficacy of the combined MHC class I SLP vaccine. At day 60, post-booster vaccination, mice were virally challenged and the titers were quantified in spleen, liver, and lungs. Similar to our previous study (22), vaccination with a mixture of MHC class I SLPs resulted in reduction of the virus titers (**Figure 5D**). Mice that received OX40 stimulation during the booster showed increased potency to control the virus compared to mice that received no extra stimulation of

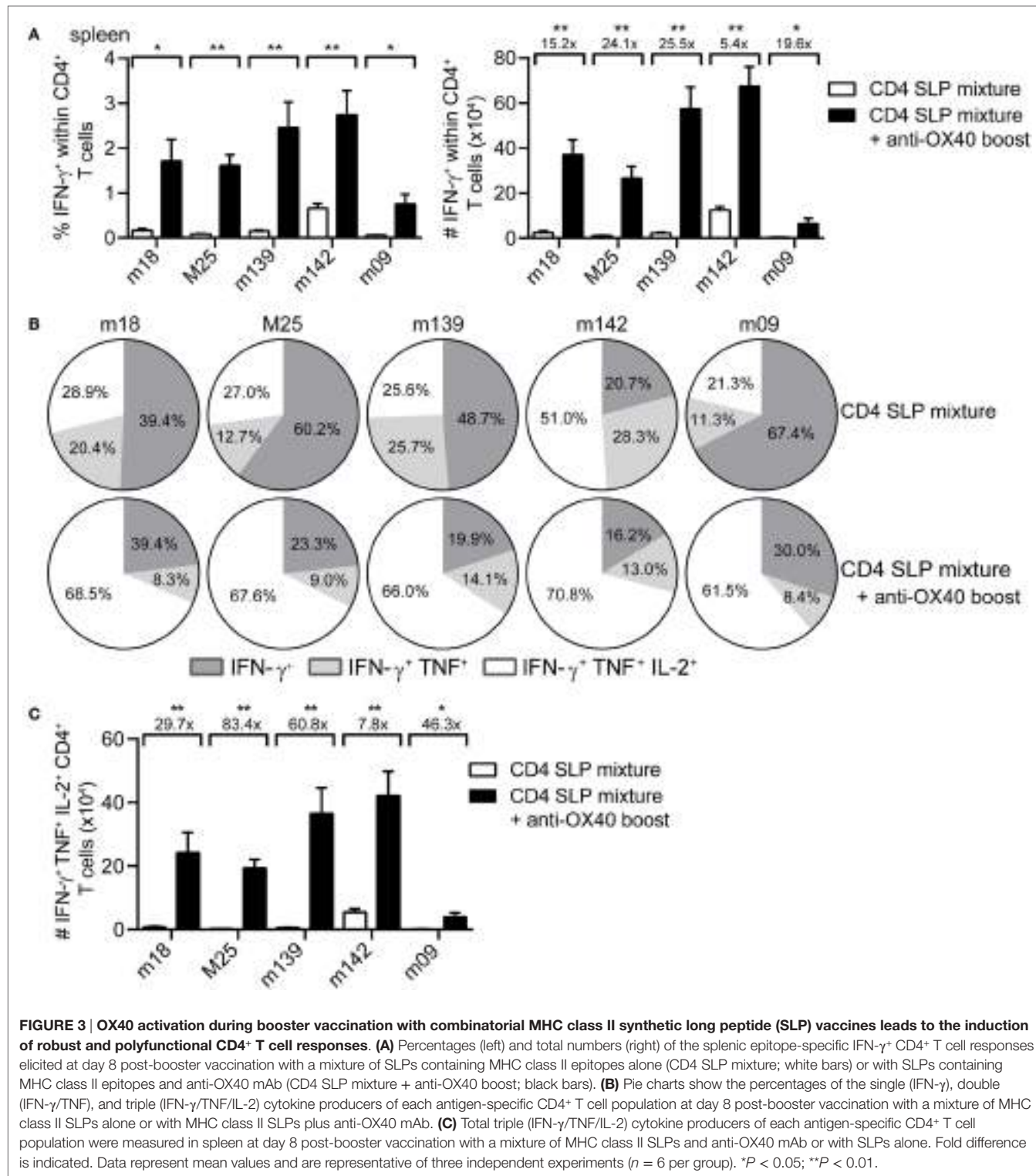


**FIGURE 3 |** OX40 activation during booster vaccination with combinatorial MHC class II synthetic long peptide (SLP) vaccines leads to the induction of robust and polyfunctional CD4<sup>+</sup> T cell responses. **(A)** Percentages (left) and total numbers (right) of the splenic epitope-specific IFN- $\gamma$ <sup>+</sup> CD4<sup>+</sup> T cell responses elicited at day 8 post-booster vaccination with a mixture of SLPs containing MHC class II epitopes alone (CD4 SLP mixture; white bars) or with SLPs containing MHC class II epitopes and anti-OX40 mAb (CD4 SLP mixture + anti-OX40 boost; black bars). **(B)** Pie charts show the percentages of the single (IFN- $\gamma$ ), double (IFN- $\gamma$ /TNF), and triple (IFN- $\gamma$ /TNF/IL-2) cytokine producers of each antigen-specific CD4<sup>+</sup> T cell population at day 8 post-booster vaccination with a mixture of MHC class II SLPs alone or with MHC class II SLPs plus anti-OX40 mAb. **(C)** Total triple (IFN- $\gamma$ /TNF/IL-2) cytokine producers of each antigen-specific CD4<sup>+</sup> T cell population were measured in spleen at day 8 post-booster vaccination with a mixture of MHC class II SLPs and anti-OX40 mAb or with SLPs alone. Fold difference is indicated. Data represent mean values and are representative of three independent experiments ( $n = 6$  per group). \* $P < 0.05$ ; \*\* $P < 0.01$ .

OX40 (Figure 5D). All together, these data suggest that enforced OX40 stimulation during booster SLP vaccination does not only impact the expansion of activated CD8<sup>+</sup> T cells but also has a long-lasting constructive influence on the magnitude and the functional profile of the vaccine-elicited CD8<sup>+</sup> T cells leading to more effective viral control.

## SLP Vaccines Inducing Both CD4<sup>+</sup> and CD8<sup>+</sup> T Cells Confer Superior Protection against MCMV Infection

To evaluate if the provision of CD4<sup>+</sup> T cells would benefit the CD8<sup>+</sup> T cell response, C57BL/6 mice were vaccinated with a

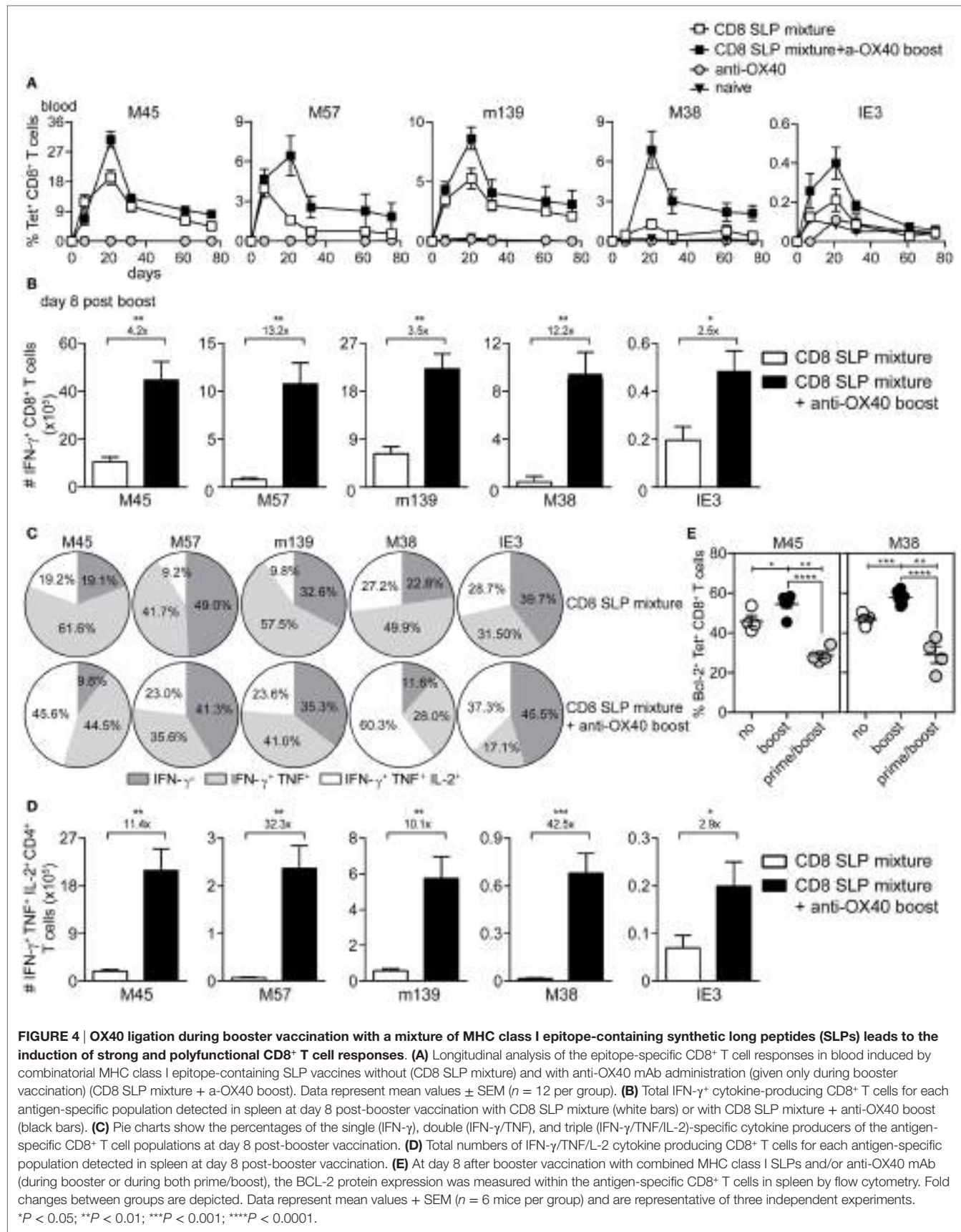


**FIGURE 4 | OX40 ligation during booster vaccination with a mixture of MHC class I epitope-containing synthetic long peptides (SLPs) leads to the induction of strong and polyfunctional CD8<sup>+</sup> T cell responses. (A)** Longitudinal analysis of the epitope-specific CD8<sup>+</sup> T cell responses in blood induced by combinatorial MHC class I epitope-containing SLP vaccines without (CD8 SLP mixture) and with anti-OX40 mAb administration (given only during booster vaccination) (CD8 SLP mixture + α-OX40 boost). Data represent mean values ± SEM ( $n = 12$  per group). **(B)** Total IFN-γ<sup>+</sup> cytokine-producing CD8<sup>+</sup> T cells for each antigen-specific population detected in spleen at day 8 post-booster vaccination with CD8 SLP mixture (white bars) or with CD8 SLP mixture + anti-OX40 boost (black bars). **(C)** Pie charts show the percentages of the single (IFN-γ<sup>+</sup>), double (IFN-γ<sup>+</sup>TNF<sup>+</sup>), and triple (IFN-γ<sup>+</sup>TNF<sup>+</sup>IL-2<sup>+</sup>)-specific cytokine producers of the antigen-specific CD8<sup>+</sup> T cell populations at day 8 post-booster vaccination. **(D)** Total numbers of IFN-γ<sup>+</sup>TNF<sup>+</sup>L-2<sup>+</sup> cytokine producing CD8<sup>+</sup> T cells for each antigen-specific population detected in spleen at day 8 post-booster vaccination. **(E)** At day 8 after booster vaccination with combined MHC class I SLPs and/or anti-OX40 mAb (during booster or during both prime/boost), the BCL-2 protein expression was measured within the antigen-specific CD8<sup>+</sup> T cells in spleen by flow cytometry. Fold changes between groups are depicted. Data represent mean values + SEM ( $n = 6$  mice per group) and are representative of three independent experiments.

\* $P < 0.05$ ; \*\* $P < 0.01$ ; \*\*\* $P < 0.001$ ; \*\*\*\* $P < 0.0001$ .

mixture of either all 5 MHC class I epitope-containing SLPs or with a mixture of all 5 MHC class I and all 5 class II epitope-containing SLPs (Table 1 in Supplementary Material). Agonistic

OX40 mAb was provided during the boost only. The CD8<sup>+</sup> T cell response after the prime vaccination was higher when the SLP vaccine contained a mixture of MHC class I and II peptide

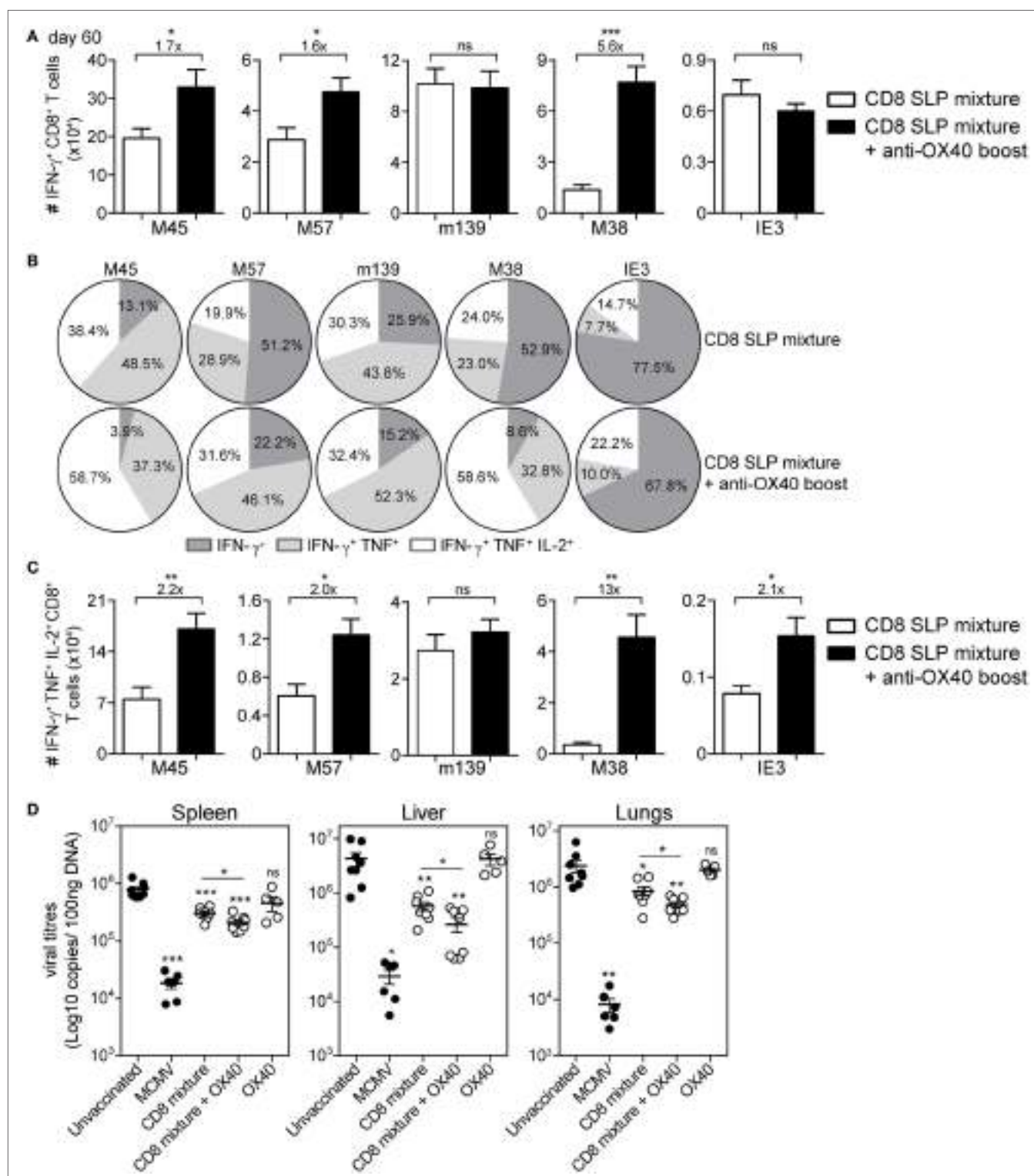


FIGURE 5 | Continued

**FIGURE 5 | Continued**

**Agonistic OX40 mAb administration during booster vaccination leads to improved memory synthetic long peptide (SLP)-elicited CD8<sup>+</sup> T cell responses.** **(A)** Total single IFN- $\gamma$ <sup>+</sup> cytokine-producing CD8<sup>+</sup> T cells for each antigen-specific population detected in spleen at day 60 post-booster vaccination with combinatorial MHC class I SLPs and anti-OX40 mAb (provided during booster vaccination) (CD8 SLP mixture + anti-OX40 boost) or with MHC class I SLPs alone (CD8 SLP mixture). Fold changes between groups are depicted. Data represent mean values + SEM ( $n = 6$  per group). **(B)** Pie charts show the percentages of the single (IFN- $\gamma$ ), double (IFN- $\gamma$ /TNF), and triple (IFN- $\gamma$ /TNF/IL-2) cytokine producers of each antigen-specific CD8<sup>+</sup> T cell population in spleen at day 60 post-booster vaccination with a mixture of MHC class I SLPs and anti-OX40 mAb (administered only during booster vaccination) or with MHC class I SLPs alone. **(C)** Total triple IFN- $\gamma$ <sup>+</sup>/TNF<sup>+</sup>/IL-2<sup>+</sup>-producing CD8<sup>+</sup> T cells for each antigen-specific population detected in spleen at day 60 post-booster vaccination. Fold changes between groups are depicted. Data represent mean values + SEM ( $n = 6$  per group). **(D)** Different groups of mice [unvaccinated (naive), mouse CMV (MCMV) infected (live-virus vaccine), vaccinated with a mixture of all 5 MHC class I SLPs, vaccinated with a mixture of all five MHC class I SLPs and anti-OX40 mAb (given only during booster vaccination), or treated with a-OX40 mAb only] were challenged at day 60 postvaccination/infection with  $5 \times 10^4$  PFU salivary gland-derived MCMV Smith. At day 5, post challenge spleen, liver, and lungs were harvested and the viral genome copies were determined by qPCR. The viral titers of individual mice are depicted ( $n = 5$ –8 mice per group). Mean ± SEM is indicated. The detection limit was below 1,000 genome copies as measured in naive mice. Experiments were performed twice with similar outcome. \* $P < 0.05$ ; \*\* $P < 0.01$ ; \*\*\* $P < 0.001$ ; ns, not significant as compared to the unvaccinated group unless otherwise indicated.

epitopes (Figure 6A; Figure S4A in Supplementary Material), stressing the importance of CD4<sup>+</sup> T cell help during the priming. Also, the phenotype of the vaccine-induced CD8<sup>+</sup> T cells after prime vaccination revealed slightly more effector-type (KLRG-1<sup>+</sup>CD127<sup>-</sup>) CD8<sup>+</sup> T cells when CD4<sup>+</sup> T cell help was provided (Figure S4B Supplementary Material), whereas the polyfunctionality of the vaccine-induced CD8<sup>+</sup> T cells remained unchanged (data not shown). However, at day 7/8 after booster SLP vaccination, the effect of CD4<sup>+</sup> T cell help on the magnitude of the vaccine-induced CD8<sup>+</sup> T cell response was no longer detectable in blood (Figure 6A) and spleen (Figure 6B). At this time-point, also no difference in the CD8<sup>+</sup> T cell cytokine polyfunctionality and phenotype was found (Figures 6C,D). Furthermore, the size and polyfunctionality of the CD4<sup>+</sup> T cells responses induced at the peak response after combined MHC class I and II SLP vaccination was similar to vaccination with MHC class II SLPs only (Figures S5A,B in Supplementary Material). Taken together, vaccination with a mixture of MHC class I and II epitope-containing SLPs resulted in enhanced primary CD8<sup>+</sup> T cell expansion compared to vaccination with class I epitope-containing SLPs only, but no additional effects of the helper T cells were observed after the enforced OX40 stimulation provided during booster vaccination.

Ultimately, we analyzed the prophylactic efficacy of the SLP-induced MCMV-specific CD4<sup>+</sup> and CD8<sup>+</sup> T cells to control viral replication. At day 60 post-booster SLP vaccination, mice were infected with MCMV and 5 days later the viral titers were quantified. The viral load of unvaccinated (naive) mice challenged with MCMV was found significantly higher in spleen, liver, and lungs compared to the viral load of mice that received earlier a virulent virus as a vaccine. This result suggests that pre-existing immunity to MCMV can inhibit virus replication during subsequent infection (Figure 7). Furthermore, the viral titers of mice that had received the virulent virus-based vaccine were similar to those measured during chronic MCMV infection, indicating that this is the maximum of immune control that can be achieved. Mice vaccinated with the mixture of SLPs containing MHC class II epitopes plus OX40 triggering during booster vaccination displayed significant reduction in viral load in all tested organs (Figure 7), indicating that the SLP-induced MCMV-specific CD4<sup>+</sup> T cells display direct antiviral

properties. Vaccination with the mixture of MHC class I SLPs plus anti-OX40 during booster resulted in a more efficient reduction of viral load in all organs. Strikingly, mice that received a mixture of MHC class I and II epitope-containing SLPs and OX40 stimulation during booster vaccination displayed the strongest reduction in viral load (Figure 7). Notably, the SLP vaccine-induced reduction in viral load in the spleen and liver was almost as effective as to what is observed after vaccination with virulent virus. Thus, SLP vaccines comprising a mixture of MHC class I and II SLPs has the highest protection potency compared to similar vaccines that elicit merely MCMV-specific CD4<sup>+</sup> or CD8<sup>+</sup> T cell responses. All together, we conclude that OX40 activation during booster vaccination empowers SLP-induced memory CD4<sup>+</sup> and CD8<sup>+</sup> T cells to efficiently counteract lytic MCMV infection.

## DISCUSSION

In this study, we show that SLP-based vaccine strategies eliciting vigorous polyfunctional CD4<sup>+</sup> and CD8<sup>+</sup> T cell responses are highly effective against MCMV infection. While SLP-based vaccines that evoke solely CD8<sup>+</sup> T cell responses display already efficacy against lytic MCMV infection (22), vaccination with a mixture of various immunodominant MHC class II and MHC class I MCMV epitopes and the combination with enforced OX40 stimulation results in superior vaccine efficacy. Former explored CMV vaccines focused mainly on the induction of neutralizing antibodies and thus far did not show substantial efficacy (3–5). Our finding that SLP-based vaccines that merely provoke CD4<sup>+</sup> and CD8<sup>+</sup> T cell responses are almost as efficient as a virulent vaccine suggests that the inclusion of T cell-stimulating antigens should facilitate the design of more efficient vaccines against CMV.

Signals through the OX40 costimulatory receptor are known to regulate expansion and survival of both CD4<sup>+</sup> and CD8<sup>+</sup> T cells after antigen encounter (28, 30). Consistent with this, OX40 had a robust effect on the magnitude of the effector SLP vaccine-induced CD4<sup>+</sup> and CD8<sup>+</sup> T cells and on their capacity to induce “Th1” cytokine responses (especially IL-2). This effect of OX40 costimulatory signals was stronger when agonistic antibody to OX40 was provided during booster SLP vaccination.

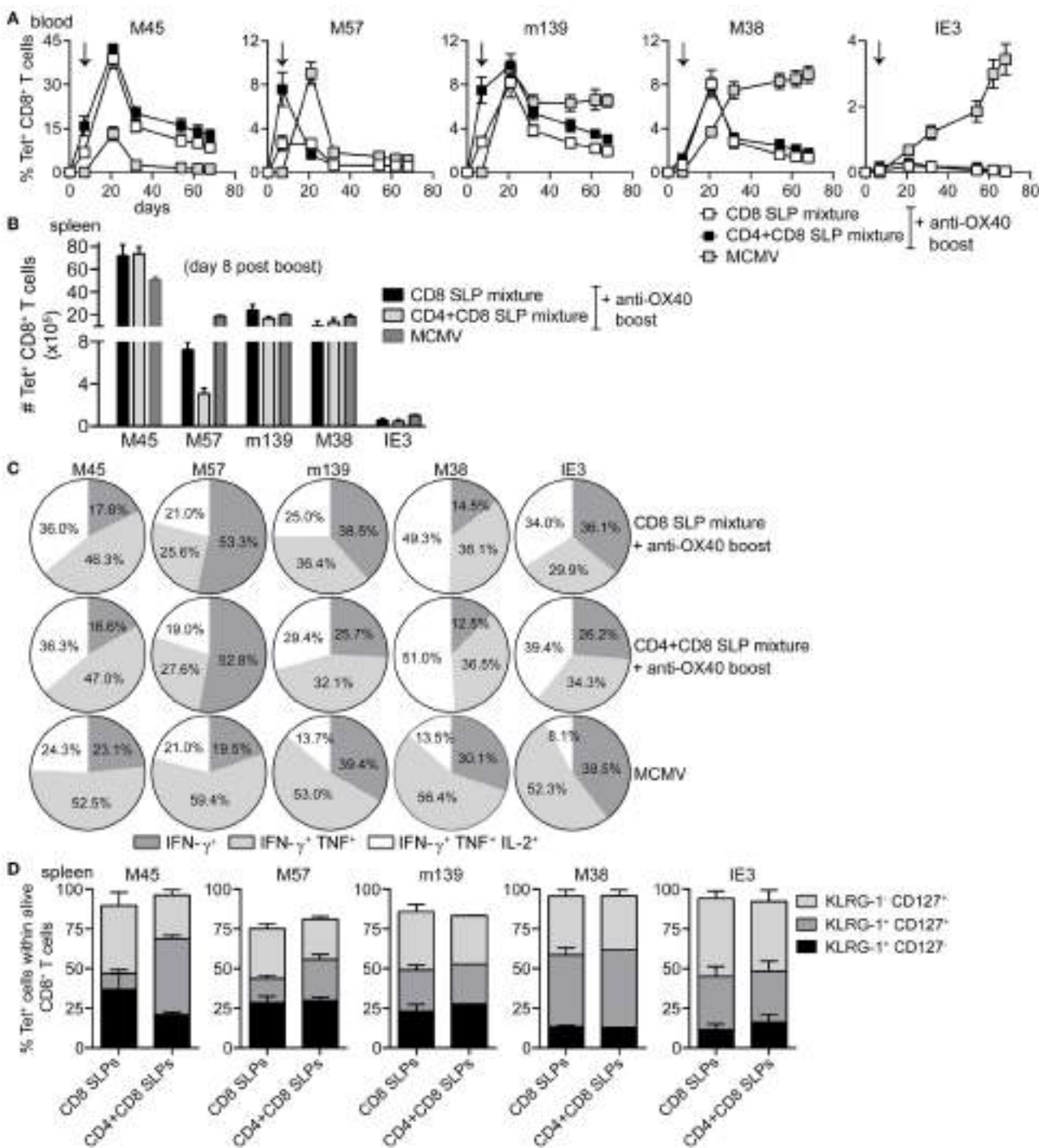


**FIGURE 6 | Combination of MHC class I and II epitope-containing synthetic long peptide (SLP) vaccines and OX40 agonistic mAb during booster vaccination leads to robust induction of both CD4<sup>+</sup> and CD8<sup>+</sup> T cell responses.** C57BL/6 mice were vaccinated s.c. with a combination of all MHC class I epitope-containing SLPs (CD8 SLP) or with a combination of all MHC class I and II epitope-containing SLPs (CD4 + CD8 SLP). In both groups agonistic OX40 mAb was administered i.p. during booster vaccination. **(A)** Kinetics of the antigen-specific CD8<sup>+</sup> T cells measured by MHC class I tetramer staining in blood. Data shown are mean values  $\pm$  SEM ( $n = 18$  mice/group). **(B)** Total MHC class I tetramer-specific CD8<sup>+</sup> T cells induced by combinatorial MHC class I or MHC class I plus MHC class II SLP vaccination compared to MCMV infection at day 8 post-booster vaccination in spleen. Data represent mean values ( $n = 5$  mice/group). **(C)** The cytokine production capacity of the splenic SLP vaccine-induced CD8<sup>+</sup> T cells was examined by intracellular cytokine staining at day 8 after booster vaccination. Pie charts depict the percentages of the single (IFN- $\gamma$ ), double (IFN- $\gamma$ /TNF), and triple (IFN- $\gamma$ /TNF/IL-2) cytokine producers of each antigen-specific CD8<sup>+</sup> T cell populations at day 8 post-booster vaccination. **(D)** Phenotypic analysis of the combinatorial SLP vaccine-induced CD8<sup>+</sup> T cells in spleen at day 8 post-booster vaccination. Data represent mean values ( $n = 5$  mice/group) and are representative of three independent experiments.

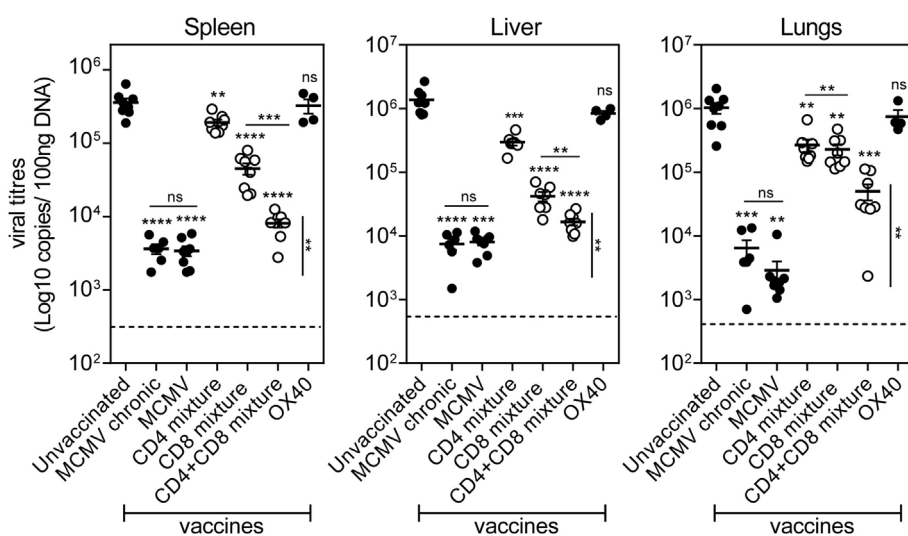


**FIGURE 7 | Prime-boost vaccination with a combination of MHC class I and II epitope-containing synthetic long peptides (SLPs) exhibits increased potency to protect against lytic mouse CMV (MCMV) infection.** Unvaccinated (naive), MCMV (live-virus vaccine), combined MHC class II SLPs (CD4 mixture), combined MHC class I SLPs (CD8 mixture), combined MHC class I and II SLPs (CD4 + CD8 mixture), and anti-OX40 mAb only treated C57BL/6 mice were challenged 60 days post-booster vaccination/infection with  $5 \times 10^4$  PFU salivary gland-derived MCMV Smith. At day 5 post challenge, liver, lungs, and spleen were harvested and the viral genome copies were quantified by qPCR. To further evaluate the efficacy of the vaccines, the viral titers of chronically infected (MCMV chronic/day 60) mice were also measured. The viral titers of individual mice are depicted ( $n = 4-8$  per group). Statistical significance between the unvaccinated group and the rest of the groups is indicated with asterisks above each group. A statistical comparison between the CD4 + CD8 mixture group and the MCMV (live-virus vaccine) and MCMV chronic group was also performed (vertical statistical bar). For both comparisons the statistical difference was found the same ( $^{**}P < 0.01$ ). The detection limit was below 1,000 genome copies as measured in naive mice. Experiment was performed twice with similar outcome. Statistical difference is indicated  $^{**}P < 0.01$ ;  $^{***}P < 0.001$ ;  $^{****}P < 0.0001$ ; ns, not significant as compared to the unvaccinated group unless otherwise indicated.

We hypothesize that primed T cells more rapidly and stronger upregulated OX40 leading to greater benefit during enforced OX40 stimulation. OX40 ligation seems to work better on CD4<sup>+</sup> T cells as compared to CD8<sup>+</sup> T cells, which may be related to the higher expression of OX40 on CD4<sup>+</sup> T cells (31, 32). Due to its capacity to regulate both CD4<sup>+</sup> and CD8<sup>+</sup> T cells, OX40 is a promising candidate in immunotherapy of chronic viral infections and cancer (30). In this study, we did not detect toxicity of OX40 agonistic antibodies but a better understanding of potential side-effects is required.

CD4<sup>+</sup> T cell responses in CMV infection have been long known as important contributors to control primary infection (8, 33). In MCMV infection, CD4<sup>+</sup> T cells direct the quality and persistence of inflammatory CD8<sup>+</sup> T cells and B cell responses (23, 24, 34). Here, we show that vaccine-induced CD4<sup>+</sup> T cells solely can confer moderate protection against acute MCMV infection. These results are consistent with other reports showing CD4<sup>+</sup> T cell effectiveness against MCMV and HCMV (8, 12, 25, 35–37). Furthermore, we observed that addition of CD4<sup>+</sup> T cell help during vaccination with MHC class I SLP vaccines promoted priming of naïve CD8<sup>+</sup> T cells. After booster vaccination in settings wherein OX40 costimulation was enhanced, no additional effects of CD4 help on the magnitude and phenotype of the CD8<sup>+</sup> T cells were observed, suggesting that enforced OX40 stimulation during booster vaccination may replace the need for CD4 help signals. On this basis, the improved prophylactic vaccine efficacy

of the combined MHC class I and II SLP vaccines appears to be more additive rather than synergistic.

Another interesting observation was that the vaccine efficacy was somewhat better in liver and spleen than in lungs. A possible explanation for this discrepancy is that the SLP-induced CD8<sup>+</sup> T cells are better capable to control the virus (lowering the viral titers) in the spleen and liver than the SLP-induced CD4<sup>+</sup> T cells. A marked difference in the efficacy of SLP-induced CD4<sup>+</sup> and CD8<sup>+</sup> T cells as observed in liver and spleen is not found in the lungs and can thus be dictated by the tissue environment. Differences in site-specific control of MCMV-specific CD4<sup>+</sup> and CD8<sup>+</sup> T cells is known to be especially important in the salivary glands but for other tissues this may be important as well (33). Nevertheless, the combined SLP vaccines inducing both CD4<sup>+</sup> and CD8<sup>+</sup> T cell responses clearly improved the efficacy of the vaccine in all organ tissues. In this respect, it is of interest to note that SLP-based vaccines can be further refined by different prime-booster regimens, inclusion of B cell epitopes and by combinations with adjuvants, immunomodulatory antibodies, or other vaccine platforms (38).

This study provided evidence that SLP-based vaccines eliciting broad CD4<sup>+</sup> and CD8<sup>+</sup> T cell responses can effectively control lytic MCMV infection without contribution by humoral responses. The use of OX40 as an adjuvant for MCMV peptide immunization strongly bolstered the development of effective CD4<sup>+</sup> and CD8<sup>+</sup> T cells. Future studies to examine the ability

of the SLP vaccine-induced T cells and OX40 costimulation to boost immune responses in immunocompromised settings of CMV infection or other chronic viral infections are strongly encouraged by these promising findings. Taken together, our data highlight the importance of designing CMV vaccines that elicit effective CD4<sup>+</sup> and CD8<sup>+</sup> T cell responses.

## AUTHOR CONTRIBUTIONS

EP, RA, and SB designed research. EP and RA performed the experiments and analyzed the data. LB contributed essential reagents. EP, RA, and SB wrote the manuscript.

## REFERENCES

- Gandhi MK, Khanna R. Human cytomegalovirus: clinical aspects, immune regulation, and emerging treatments. *Lancet Infect Dis* (2004) 4(12):725–38. doi:10.1016/S1473-3099(04)01202-2
- Boppana SB, Ross SA, Fowler KB. Congenital cytomegalovirus infection: clinical outcome. *Clin Infect Dis* (2013) 57(Suppl 4):S178–81. doi:10.1093/cid/cit629
- Krause PR, Bialek SR, Boppana SB, Griffiths PD, Laughlin CA, Ljungman P, et al. Priorities for CMV vaccine development. *Vaccine* (2013) 32(1):4–10. doi:10.1016/j.vaccine.2013.09.042
- Wang D, Fu TM. Progress on human cytomegalovirus vaccines for prevention of congenital infection and disease. *Curr Opin Virol* (2014) 6:13–23. doi:10.1016/j.coviro.2014.02.004
- McCormick AL, Mocarski ES. The immunological underpinnings of vaccinations to prevent cytomegalovirus disease. *Cell Mol Immunol* (2015) 12(2):170–9. doi:10.1038/cmi.2014.120
- Reddehase MJ, Mutter W, Munch K, Buhring HJ, Koszinowski UH. CD8-positive T lymphocytes specific for murine cytomegalovirus immediate-early antigens mediate protective immunity. *J Virol* (1987) 61(10):3102–8.
- Polic B, Hengel H, Krmpotic A, Trgovcich J, Pavic I, Luccaroni P, et al. Hierarchical and redundant lymphocyte subset control precludes cytomegalovirus replication during latent infection. *J Exp Med* (1998) 188(6):1047–54. doi:10.1084/jem.188.6.1047
- Gamadia LE, Remmerswaal EB, Weel JF, Bemelman F, van Lier RA, ten Berge IJ. Primary immune responses to human CMV: a critical role for IFN-gamma-producing CD4<sup>+</sup> T cells in protection against CMV disease. *Blood* (2003) 101(7):2686–92. doi:10.1182/blood-2002-08-2502
- Arens R, Loewendorf A, Her MJ, Schneider-Ohrum K, Shellam GR, Janssen E, et al. B7-mediated costimulation of CD4 T cells constrains cytomegalovirus persistence. *J Virol* (2011) 85(1):390–6. doi:10.1128/JVI.01839-10
- Riddell SR, Watanabe KS, Goodrich JM, Li CR, Agha ME, Greenberg PD. Restoration of viral immunity in immunodeficient humans by the adoptive transfer of T cell clones. *Science* (1992) 257(5067):238–41. doi:10.1126/science.1352912
- Rausch G, Einsele H, Sinzger C, Wernet D, Kuntz G, Assenmacher M, et al. Rapid generation of combined CMV-specific CD4<sup>+</sup> and CD8<sup>+</sup> T-cell lines for adoptive transfer into recipients of allogeneic stem cell transplants. *Blood* (2004) 103(9):3565–72. doi:10.1182/blood-2003-09-3056
- Jeitziner SM, Walton SM, Torti N, Oxenius A. Adoptive transfer of cytomegalovirus-specific effector CD4<sup>+</sup> T cells provides antiviral protection from murine CMV infection. *Eur J Immunol* (2013) 43(11):2886–95. doi:10.1002/eji.201343690
- Karrer U, Siervo S, Wagner M, Oxenius A, Hengel H, Koszinowski UH, et al. Memory inflation: continuous accumulation of antiviral CD8<sup>+</sup> T cells over time. *J Immunol* (2003) 170(4):2022–9. doi:10.4049/jimmunol.170.4.2022
- Munks MW, Cho KS, Pinto AK, Siervo S, Klennerman P, Hill AB. Four distinct patterns of memory CD8 T cell responses to chronic murine cytomegalovirus infection. *J Immunol* (2006) 177(1):450–8. doi:10.4049/jimmunol.177.1.450
- Arens R, Wang P, Sidney J, Loewendorf A, Sette A, Schoenberger SP, et al. Cutting edge: murine cytomegalovirus induces a polyfunctional CD4 T cell response. *J Immunol* (2008) 180(10):6472–6. doi:10.4049/jimmunol.180.10.6472
- O'Hara GA, Welten SP, Klennerman P, Arens R. Memory T cell inflation: understanding cause and effect. *Trends Immunol* (2012) 33(2):84–90. doi:10.1016/j.it.2011.11.005
- Humphreys IR, Loewendorf A, De TC, Schneider K, Benedict CA, Munks MW, et al. OX40 costimulation promotes persistence of cytomegalovirus-specific CD8 T cells: a CD4-dependent mechanism. *J Immunol* (2007) 179(4):2195–202. doi:10.4049/jimmunol.179.4.2195
- Welten SP, Redeker A, Franken KL, Benedict CA, Yagita H, Wensveen FM, et al. CD27-CD70 costimulation controls T cell immunity during acute and persistent cytomegalovirus infection. *J Virol* (2013) 87(12):6851–65. doi:10.1128/JVI.03305-12
- Klennerman P, Oxenius A. T cell responses to cytomegalovirus. *Nat Rev Immunol* (2016) 16(6):367–77. doi:10.1038/nri.2016.38
- Krmpotic A, Cubic I, Polic B, Lucin P, Jonjic S. Pathogenesis of murine cytomegalovirus infection. *Microbes Infect* (2003) 5(13):1263–77. doi:10.1016/j.micinf.2003.09.007
- Holtappels R, Bohm V, Podlech J, Reddehase MJ. CD8 T-cell-based immunotherapy of cytomegalovirus infection: “proof of concept” provided by the murine model. *Med Microbiol Immunol* (2008) 197(2):125–34. doi:10.1007/s00430-008-0093-2
- Panagioti E, Redeker A, van Duiken S, Franken KL, Drijfhout JW, van der Burg SH, et al. The breadth of synthetic long peptide vaccine-induced CD8<sup>+</sup> T cell responses determines the efficacy against mouse cytomegalovirus infection. *PLoS Pathog* (2016) 12(9):e1005895. doi:10.1371/journal.ppat.1005895
- Snyder CM, Loewendorf A, Bonnett EL, Croft M, Benedict CA, Hill AB. CD4<sup>+</sup> T cell help has an epitope-dependent impact on CD8<sup>+</sup> T cell memory inflation during murine cytomegalovirus infection. *J Immunol* (2009) 183(6):3932–41. doi:10.4049/jimmunol.0900227
- Walton SM, Torti N, Mandaric S, Oxenius A. T-cell help permits memory CD8<sup>(+)</sup> T-cell inflation during cytomegalovirus latency. *Eur J Immunol* (2011) 41(8):2248–59. doi:10.1002/eji.201141575
- Verma S, Weiskopf D, Gupta A, McDonald B, Peters B, Sette A, et al. Cytomegalovirus-specific CD4 T cells are cytolytic and mediate vaccine protection. *J Virol* (2015) 90(2):650–8. doi:10.1128/jvi.02123-15
- Redeker A, Welten SP, Arens R. Viral inoculum dose impacts memory T-cell inflation. *Eur J Immunol* (2014) 44(4):1046–57. doi:10.1002/eji.201343946
- Arens R, Loewendorf A, Redeker A, Siervo S, Boon L, Klennerman P, et al. Differential B7-CD28 costimulatory requirements for stable and inflationary mouse cytomegalovirus-specific memory CD8 T cell populations. *J Immunol* (2011) 186(7):3874–81. doi:10.4049/jimmunol.1003231
- Croft M. Control of immunity by the TNFR-related molecule OX40 (CD134). *Annu Rev Immunol* (2010) 28:57–78. doi:10.1146/annurev-immunol-030409-101243
- Rogers PR, Song J, Gramaglia I, Killeen N, Croft M. OX40 promotes Bcl-xL and Bcl-2 expression and is essential for long-term survival of CD4 T cells. *Immunity* (2001) 15(3):445–55. doi:10.1016/S1074-7613(01)00191-1

## FUNDING

This work was funded by grants from the European Commission [FP7 Marie Curie Action, Grant number: 316655, VacTrain (SB, RA, and EP)], the Macropa Foundation (RA), and the Gisela Thier Foundation (RA).

## SUPPLEMENTARY MATERIAL

The Supplementary Material for this article can be found online at <http://journal.frontiersin.org/article/10.3389/fimmu.2017.00144/full#supplementary-material>.

30. Linch SN, McNamara MJ, Redmond WL. OX40 agonists and combination immunotherapy: putting the pedal to the metal. *Front Oncol* (2015) 5:34. doi:10.3389/fonc.2015.00034
31. Baum PR, Gayle RB III, Ramsdell F, Srinivasan S, Sorensen RA, Watson ML, et al. Molecular characterization of murine and human OX40/OX40 ligand systems: identification of a human OX40 ligand as the HTLV-1-regulated protein gp34. *EMBO J* (1994) 13(17):3992–4001.
32. al-Shamkhani A, Birkeland ML, Puklavec M, Brown MH, James W, Barclay AN. OX40 is differentially expressed on activated rat and mouse T cells and is the sole receptor for the OX40 ligand. *Eur J Immunol* (1996) 26(8):1695–9. doi:10.1002/eji.1830260805
33. Jonjic S, Mutter W, Weiland F, Reddehase MJ, Koszinowski UH. Site-restricted persistent cytomegalovirus infection after selective long-term depletion of CD4+ T lymphocytes. *J Exp Med* (1989) 169(4):1199–212. doi:10.1084/jem.169.4.1199
34. Welten SP, Redeker A, Toes RE, Arens R. Viral persistence induces antibody inflation without altering antibody avidity. *J Virol* (2016) 90(9):4402–11. doi:10.1128/JVI.03177-15
35. Casazza JP, Betts MR, Price DA, Precopio ML, Ruff LE, Brenchley JM, et al. Acquisition of direct antiviral effector functions by CMV-specific CD4+ T lymphocytes with cellular maturation. *J Exp Med* (2006) 203(13):2865–77. doi:10.1084/jem.20052246
36. van Leeuwen EM, Remmerswaal EB, Heemskerk MH, ten Berge IJ, van Lier RA. Strong selection of virus-specific cytotoxic CD4+ T-cell clones during primary human cytomegalovirus infection. *Blood* (2006) 108(9):3121–7. doi:10.1182/blood-2006-03-006809
37. Pachnio A, Ciauriz M, Begum J, Lal N, Zuo J, Beggs A, et al. Cytomegalovirus infection leads to development of high frequencies of cytotoxic virus-specific CD4+ T cells targeted to vascular endothelium. *PLoS Pathog* (2016) 12(9):e1005832. doi:10.1371/journal.ppat.1005832
38. Arens R, van Hall T, van der Burg SH, Ossendorp F, Mелиef CJ. Prospects of combinatorial synthetic peptide vaccine-based immunotherapy against cancer. *Semin Immunol* (2013) 25(2):182–90. doi:10.1016/j.smim.2013.04.008

**Conflict of Interest Statement:** This study has been conducted by the Leiden University Medical Center (LUMC) that holds a patent on the synthetic long peptides as vaccine (US 7.202.034). SB is named as inventor on this patent. LB is a shareholder of Bioceros that holds a patent on anti-human OX40 mAbs. The other authors declare no conflict of interest.

Copyright © 2017 Panagioti, Boon, Arens and van der Burg. This is an open-access article distributed under the terms of the Creative Commons Attribution License (CC BY). The use, distribution or reproduction in other forums is permitted, provided the original author(s) or licensor are credited and that the original publication in this journal is cited, in accordance with accepted academic practice. No use, distribution or reproduction is permitted which does not comply with these terms.



# Dendritic Cell Targeting Effectively Boosts T Cell Responses Elicited by an HIV Multiepitope DNA Vaccine

**Juliana de Souza Apostólico<sup>1,2†</sup>, Victória Alves Santos Lunardelli<sup>1†</sup>,**  
**Marcio Massao Yamamoto<sup>3</sup>, Higo Fernando Santos Souza<sup>3</sup>,**  
**Edecio Cunha-Neto<sup>2,4,5</sup>, Silvia Beatriz Boscardin<sup>2,3</sup> and Daniela Santoro Rosa<sup>1,2\*</sup>**

<sup>1</sup>Department of Microbiology, Immunology and Parasitology, Federal University of São Paulo (UNIFESP/EPM), São Paulo, Brazil, <sup>2</sup>Institute for Investigation in Immunology (III), INCT, São Paulo, Brazil, <sup>3</sup>Department of Parasitology, Institute of Biomedical Sciences, University of São Paulo, São Paulo, Brazil, <sup>4</sup>Laboratory of Clinical Immunology and Allergy-LIM60, University of São Paulo School of Medicine, São Paulo, Brazil, <sup>5</sup>Laboratory of Immunology, Heart Institute (InCor), University of São Paulo School of Medicine, São Paulo, Brazil

## OPEN ACCESS

### Edited by:

Lee Mark Wetzer,  
Boston University School of  
Medicine, USA

### Reviewed by:

Diana Dudziak,  
University Hospital of Erlangen,  
Germany  
Laura Bonifaz,  
Instituto Mexicano del Seguro Social  
(IMSS), Mexico

### \*Correspondence:

Daniela Santoro Rosa  
dsantororosa@gmail.com

<sup>†</sup>These authors have contributed  
equally to this work.

### Specialty section:

This article was submitted to  
Vaccines and Molecular  
Therapeutics,  
a section of the journal  
*Frontiers in Immunology*

**Received:** 17 November 2016

**Accepted:** 20 January 2017

**Published:** 07 February 2017

### Citation:

Apostólico JdS, Lunardelli VAS,  
Yamamoto MM, Souza HFS,  
Cunha-Neto E, Boscardin SB and  
Rosa DS (2017) Dendritic Cell  
Targeting Effectively Boosts T Cell  
Responses Elicited by an HIV  
Multiepitope DNA Vaccine.  
*Front. Immunol.* 8:101.  
doi: 10.3389/fimmu.2017.00101

Despite several efforts in the last decades, an efficacious HIV-1 vaccine is still not available. Different approaches have been evaluated, such as recombinant proteins, viral vectors, DNA vaccines, and, most recently, dendritic cell (DC) targeting. This strategy is based on DC features that place them as central for induction of immunity. Targeting is accomplished by the use of chimeric monoclonal antibodies directed to DC surface receptors fused to the antigen of interest. In this work, we targeted eight promiscuous HIV-derived CD4<sup>+</sup> T cell epitopes (HIVBr8) to the DEC205<sup>+</sup> DCs by fusing the multiepitope immunogen to the heavy chain of αDEC205 (αDECHIVBr8), in the presence of the TLR3 agonist poly (I:C). In addition, we tested a DNA vaccine encoding the same epitopes using homologous or heterologous prime-boost regimens. Our results showed that mice immunized with αDECHIVBr8 presented higher CD4<sup>+</sup> and CD8<sup>+</sup> T cell responses when compared to mice that received the DNA vaccine (pVAXHIVBr8). In addition, pVAXHIVBr8 priming followed by αDECHIVBr8 boosting induced higher polyfunctional proliferative and cytokine-producing T cell responses to HIV-1 peptides than homologous DNA immunization or heterologous αDEC prime/DNA boost. Based on these results, we conclude that homologous prime-boost and heterologous boosting immunization strategies targeting CD4<sup>+</sup> epitopes to DCs are effective to improve HIV-specific cellular immune responses when compared to standalone DNA immunization. Moreover, our results indicate that antigen targeting to DC is an efficient strategy to boost immunity against a multiepitope immunogen, especially in the context of DNA vaccination.

**Keywords:** HIV, dendritic cells, multiepitope vaccine, CD4<sup>+</sup> T cell, monoclonal antibody

## INTRODUCTION

Since HIV was discovered in the 1980s, there has been a remarkable progress in the treatment for AIDS. Despite impressive advances in the scientific knowledge and numerous trials, a safe and effective preventive HIV vaccine is still not available. The majority of licensed vaccines provide protection against other pathogens by the induction of neutralizing antibodies (nAbs), but strategies that

focused on the development of an effective humoral immunity for HIV have failed so far. The RV144 trial was the only to demonstrate some level of efficacy (~31.2%) against HIV infection by inducing env-specific CD4<sup>+</sup> T cells as well as antibodies that were able to bind to HIV, but not to neutralize it (1, 2). Moreover, the tested vaccine regimen induced proliferating CD4<sup>+</sup> T cells with a cytotoxic profile (3). A T cell vaccine able to elicit potent cellular immune responses showed marked protection against simian immunodeficiency (SIV) challenge in non-human primates (4). Janes et al. (5) showed that Gag-specific T cells induced by the Merck Ad5Gag-nef-pol vaccine were associated with reduced viremia after HIV-1 infection.

The role of CD4<sup>+</sup> T cells to support immunity places them as key for viral clearance, ensuring homeostasis. The important role of CD4 T cell responses during HIV (6) and non-human primate SIV infection is now clear (7). They can provide help for CD8<sup>+</sup> cytotoxic T cells to control virus replication (8), especially in the mucosal region (9). In addition, HIV-specific CD4<sup>+</sup> T cell responses promote B cell differentiation leading to generation or maintenance of nAbs in natural infection (10). Furthermore, HIV-specific CD4<sup>+</sup> T cells can control viral replication by direct cytotoxicity (11) or indirectly through the secretion of soluble antiviral mediators (CCL3, CCL4, and CCL5) (12). A polyfunctional Gag-specific CD4<sup>+</sup> T cell response was inversely correlated with virus load and directly with the HIV-specific CD8<sup>+</sup> T cell response in HIV-infected long-term non-progressor individuals (13). Furthermore, expression of specific HLA class II alleles has a considerable impact on the control of HIV replication. HLA-DRB1\*15:02 is significantly associated with HIV control (14) and elite controllers that express HLA-DRB1\*13 and HLA-DQB1\*06 class II HLA molecule showed superior mucosal Gag-specific CD4<sup>+</sup> T cell responses that produced simultaneously IFN $\gamma$ , TNF $\alpha$ , and IL-2 when compared to non-controllers or individuals in highly active antiretroviral therapy (HAART) (9). Thus, it is now accepted that an effective vaccine should also promote broad and polyfunctional CD4<sup>+</sup> T responses against HIV infection (15).

The inclusion of appropriate HIV-1 epitopes recognized by CD4<sup>+</sup> T cells may thus play an essential role in the induction of immune responses to a HIV vaccine candidate. Our group has previously described a set of conserved HIV-1 CD4<sup>+</sup> T cell epitopes from the whole proteome of the HIV-1 B subtype consensus that promiscuously bound to multiple HLA-DR, -DQ, and -DP molecules. Peripheral blood mononuclear cells from 90% of HIV-seropositive individuals recognized these epitopes, and the strongest responses were found among long-term non-progressors (16). Epitope-based vaccines focus responses on epitopes with desirable properties and prevent responses to neutral or deleterious epitopes (17). A DNA vaccine encoding the mentioned conserved epitopes (HIVBr18) induced broad specific CD4<sup>+</sup> and CD8<sup>+</sup> T responses in transgenic mice expressing human HLA class II alleles (HLA-DR2, -DR4, -DQ6, and -DQ8) (18). Furthermore, HIVBr18 promoted high magnitude, broad, and polyfunctional CD4<sup>+</sup> and CD8<sup>+</sup> T cell responses to 8 out of 18 vaccine-encoded peptides in BALB/c mice (19). This epitope-based vaccine concept may cope with HIV genetic variability, since it induces a broad T cell response focused on

conserved HIV epitopes, and may also provide increased population coverage, given the promiscuity of HLA class II binding to multiple epitopes.

DNA vaccines are relatively easy and cheap to produce, being promising agents to control epidemics in remote, resource-poor locations (20). However, DNA vaccines have shown limited immunogenicity in non-human primates and in humans, possibly due to the low amount of the expressed antigen (21). For this reason, different approaches have been pursued in order to overcome this hurdle (22). Dendritic cells (DCs) have the ability to link innate and adaptive immunity because they are able to effectively acquire, process, and present a myriad of pathogen-derived epitopes mainly to T cells (23). In mouse spleen and lymph nodes, two major subtypes of resident DCs have been described: the CD11c<sup>+</sup>CD8 $\alpha$ <sup>+</sup> DCs that additionally express high levels of DEC205 endocytic receptor and the CD11c<sup>+</sup>CD8 $\alpha$ <sup>-</sup> that express the DCIR2 receptor (24, 25). *In vivo* antigen targeting to the CD11c<sup>+</sup>CD8 $\alpha$ <sup>+</sup> DCs was first demonstrated when two model antigens were fused to a monoclonal antibody (mAb) directed to the DEC205<sup>+</sup> receptor. Ovalbumin and hen egg lysozyme were successfully coupled to the  $\alpha$ DEC205 mAb, and effective presentation to either CD4<sup>+</sup> or CD8<sup>+</sup> T cells was observed, eliciting both robust humoral and cellular responses (26, 27). Different pathogen-derived antigens were shown to be efficiently processed and presented to T cells when targeted to the CD11c<sup>+</sup>CD8 $\alpha$ <sup>+</sup> DCs through  $\alpha$ DEC205 mAb, such as *Plasmodium yoelii* (28), *Plasmodium falciparum* (29), *Trypanosoma cruzi* (30), *Mycobacterium tuberculosis* (31), HIV (32–34), and dengue virus (35). Furthermore, it was shown that targeting of HIV antigens using  $\alpha$ DEC205 mAb could be an efficient vaccine platform. A single dose of  $\alpha$ DEC205-Gag mAb in the presence of poly (I:C) induced protective CD4<sup>+</sup> T responses when mice were challenged with recombinant vaccinia virus expressing Gag (33). In addition,  $\alpha$ DEC205-p24 in the presence of poly (I:C) led to strong polyfunctional CD4<sup>+</sup> profile that was able to induce proliferating and cytokine-producing T cells (32). HIV p24 targeted to CD11c<sup>+</sup>CD8 $\alpha$ <sup>+</sup> DCs also induced Th1 CD4<sup>+</sup> T cells as well as cross-presentation to CD8<sup>+</sup> T cells (36). Immunization with an anti-human DEC205-p24 mAb induced IFN $\gamma$ - and IL-2-producing cells and was able to elicit high titers of anti-human IgG in transgenic mice (37).  $\alpha$ DEC205-Gag targeting was also shown to assist a protective response to a DNA vaccine by mobilizing CD8<sup>+</sup> T cells after challenge (38). More recently,  $\alpha$ DEC205-p24 mAb was evaluated for intranasal immunization, and it was able to induce HIV-specific immunity in the gastrointestinal tract (34).

In recent years, evidence has shown that heterologous prime-boost vaccination was an effective strategy to generate powerful antibody responses (39, 40), to improve the magnitude and quality of T cell responses (41), and to induce protection against different pathogens (42), including HIV. We thus hypothesized that targeting HIV CD4<sup>+</sup> T cell epitopes to DCs using the  $\alpha$ DEC205 mAb would be able to induce higher specific cellular responses against HIV-1 when compared to a DNA vaccine encoding the same epitopes. In the current study, we assessed the polyfunctionality of HIV-specific T cell responses induced by  $\alpha$ DEC205 mAb and the DNA vaccine HIVBr8 in homologous and

heterologous prime-boost immunization regimens. Our results showed that immunization with  $\alpha$ DECHIVBr8 solely or heterologous prime-boost with HIVBr8 followed by  $\alpha$ DECHIVBr8 was able to induce broader and polyfunctional CD4 $^{+}$  and CD8 $^{+}$  T cells when compared to the DNA vaccine alone.

## MATERIALS AND METHODS

### Epitopes

The sequences of HIV-1 epitopes selected for this study were previously described by Fonseca et al. (16) and are the following: p6 (32–46), p17 (73–89), pol (785–799), gp160 (188–201), rev (11–27), vpr (65–82), vif (144–158), and nef (180–194) (Table 1). These epitopes were derived from the previously described DNA vaccine HIVBr18 (18, 19) and comprise the eight mentioned epitopes (HIVBr8) that can bind to I-Ad and are recognized by T cells from immunized BALB/c mice. The epitopes were assembled in tandem and are separated by GPGPG at C and N termini to avoid the creation of junctional epitopes that may interfere with processing and presentation (43).

### Cloning the DNA Sequence Encoding HIV-1 Epitopes: pVAXHIVBr8 Generation

The HIVBr8 nucleotide sequence was codon optimized, and a Kozak sequence was included at the 5' end to improve mammalian expression. The artificial gene (Genscript) was cloned between the *Hind*III and *Xhol* restriction sites of the pVAX1 vector (Invitrogen) to generate the pVAXHIVBr8 plasmid that was amplified using DH5 $\alpha$  cells. The pVAXHIVBr8 was purified using the Endofree Plasmid Giga Kit (Qiagen) according to the manufacturer's instructions. The yield and quality of purified DNA was determined by spectrophotometry at 260 nm and confirmed by agarose gel electrophoresis.

### Fusion of HIV-Derived CD4 $^{+}$ T Cell Epitopes to the $\alpha$ DEC205 Antibody: $\alpha$ DECHIVBr8 mAb Generation

Plasmids encoding the light and heavy chains of the mouse  $\alpha$ DEC205 antibody were kindly provided by Dr. Michel C.

**TABLE 1 | Amino acid sequence of HIV epitopes.**

Epitope	Sequence
p6 (32–46)	DKELYPLASLRLSLFG
p17 (73–89)	EELRSLYNTVATLYCVH
pol (785–799)	GKIIILVAHVVASGYI
gp160 (188–201)	NTSYRLISCNTSVI
rev (11–27)	ELLKTVRLIKFLYQSNP
vpr3 (65–82)	QQLLFIHFRIGCRHSRIG
vif (144–158)	SLQYLALVALVALVAPKK
nef (180–194)	VLEWRFDSRLAFHHV

The sequences of HIV-1 epitopes selected for this study were previously described by Fonseca et al. (16). These epitopes were derived from the previously described DNA vaccine HIVBr18 (18, 19) and comprise the eight mentioned epitopes (HIVBr8) that can bind to I-Ad and are recognized by T cells from immunized BALB/c mice.

Nussenzweig (The Rockefeller University). The artificial HIVBr8 gene was produced (Genscript), digested from pUC57 vector, and cloned in frame with the carboxyl terminus of the heavy chain of the mouse DEC205 (clone NLDC145) between the 5' *Xho*I and 3' *Not*I sites. Large-scale preparation of plasmids pDECHIVBr8, empty pDEC (a negative non-fused control), and pDEC kappa (encoding the  $\alpha$ DEC205 kappa light chain) were prepared using Maxi Plasmid Purification Kit (Qiagen), according to the manufacturer's instructions. The yield and quality of purified DNA were determined by spectrophotometry at 260 nm and confirmed by agarose gel electrophoresis.

### Expression and Purification of $\alpha$ DECHIVBr8 mAb

The chimeric  $\alpha$ DEC and  $\alpha$ DECHIVBr8 mAbs were produced and purified after transfection of human embryonic kidney 293T cells (ATCC, CRL-11268) exactly as described (35).

### Immunoblot

Approximately 1  $\mu$ g of the  $\alpha$ DEC and  $\alpha$ DECHIVBr8 mAbs were run on 12% SDS-PAGE gels under reducing conditions, and subsequently transferred to nitrocellulose membranes (GE Healthcare) at 100 V for 90 min in transfer buffer (glycine 39 mM, Tris 48 mM, SDS 10% and methanol 20%, pH 8.3). After transfer, nitrocellulose membranes were blocked in PBS 0.02% Tween-20 (PBST), 5% non-fat milk, and 2.5% BSA, overnight at 4°C. Membranes containing the reduced mAbs were then incubated with peroxidase-labeled goat anti-mouse IgG Fc specific (1:5,000, Jackson Laboratories) plus peroxidase-labeled goat anti-mouse IgG kappa (1:3,000, SouthernBiotech) for 60 min at room temperature. After three washes with PBST, the reaction was developed using chemiluminescence (ECL kit, GE Healthcare) and captured on Kodak film.

### Binding Assay

Binding assays were performed using CHO cells expressing either the mouse DEC205 (CHOmDEC) or DCIR2 (CHOmDCIR2) receptors, kindly provided by Dr. Michel Nussenzweig (The Rockefeller University). Purified mAbs were diluted to 4, 2, or 1  $\mu$ g/mL and incubated with the CHOmDEC or CHOmDCIR2 cells at 4°C for 30 min, exactly as described by Henriques et al. (35). Next, the cells were washed and incubated with anti-mouse IgG1-PE (clone A85-1, BD Biosciences) for 30 min at 4°C. Additionally, 4, 2, or 1  $\mu$ g/mL of  $\alpha$ DEC or  $\alpha$ DECHIVBr8 mAbs were incubated with 5 million splenocytes at 4°C for 40 min and then incubated with anti-CD49b-biotin (clone DX5), anti-CD19-biotin (clone 1D3), anti-CD3-biotin (clone 145-2C11), Streptavidin-APCCy7, anti-CD11c-APC (HL3), anti-IAIE-FITC (clone 2G9), anti-CD8-Pacific Blue (clone 53-6.7), and anti-IgG1-PE (clone A85-1). All monoclonal antibodies were purchased from BD Biosciences. Fifty thousand events were acquired for the analysis of binding to CHO cells and 3 million for the analysis of binding to splenocytes. Samples were acquired using FACS Canto II flow cytometer (BD Biosciences) and analyzed using the FlowJo software (version 9.9, Tree Star, San Carlos, CA, USA).

## Animals and Immunization

The 6- to 8-week-old female BALB/c (H-2<sup>d</sup>) mice were purchased from Centro de Desenvolvimento de Modelos Experimentais para Medicina e Biologia (CEDEME), Brazil. Groups of six animals were immunized with two doses—2 weeks apart—of 4 µg of αDEC1HIVBr8 mAb in the presence of 50 µg of adjuvant poly (I:C) (Invivogen) delivered intraperitoneally (IP) or subcutaneously (SC), or with two doses of 100 µg of the DNA vaccine pVAXHIVBr8 by intramuscular route (IM). The control groups were immunized with 4 µg of αDEC in the presence of 50 µg of poly (I:C) or with pVAX (empty vector). Furthermore, for heterologous prime-boost regimen, other groups received one dose of the mAb followed by one dose of DNA vaccine or *vice versa*. The control groups were immunized with one dose of αDEC mAb together with poly (I:C) followed by one dose with pVAX or *vice versa*.

## Spleen Cell Isolation for Immune Assays

Two weeks after the last immunization, mice were euthanized and spleens were removed aseptically. After obtaining single cell suspensions, cells were washed in 10 mL of RPMI 1640 (Gibco). Cells were then resuspended in R-10 [RPMI supplemented with 10% of fetal bovine serum (Gibco)], 2 mM L glutamine (Gibco), 10 mM Hepes (Gibco), 1 mM sodium pyruvate (Gibco), 1% v/v non-essential amino acids solution (Gibco), 40 µg/mL of gentamicin, 20 µg/mL of peflacin, and 5 × 10<sup>-5</sup> M 2-mercaptoethanol (Gibco). The viability of cells was evaluated using 0.2% Trypan Blue exclusion dye to discriminate between live and dead cells. Cell concentration was estimated with the aid of a cell counter (Countess, Invitrogen) and adjusted in cell culture medium.

## T Cell ELISpot Assay

Splenocytes from immunized mice were obtained as previously described and assayed for their ability to secrete IFNγ after *in vitro* stimulation with 5 µM of individual or pooled HIV-1 peptides using the ELISpot assay. The ELISpot assay was performed using mouse IFNγ ELISpot Ready-SET-Go! (eBiosciences) according to the manufacturer's instructions. Spots were counted using an AID ELISpot Reader System (Autoimmun Diagnostika GmbH, Germany). The cutoff was 15 SFU per million splenocytes.

## Analysis of Polyfunctional HIV-Specific T Cell Responses by Multiparametric Flow Cytometry

To analyze HIV-specific T cell expansion, proliferation, and cytokine production, splenocytes from immunized mice were labeled with carboxyfluorescein succinimidyl ester (CFSE) (19). In summary, freshly isolated splenocytes were resuspended (50 × 10<sup>6</sup>/mL) in PBS and labeled with 1.25 µM of CFSE (Molecular Probes) at 37°C for 10 min. The reaction was quenched with RPMI 1640 supplemented with 10% FBS (R10), and cells were washed with R10 before resuspension in RPMI 1640. Cells were cultured in 96-well round-bottomed plates (5 × 10<sup>5</sup>/well in triplicates) for 5 days at 37°C and 5% CO<sub>2</sub> with medium only or pooled HIV-1 peptides (5 µM). After 4 days of incubation,

cells were restimulated in the presence of 2 µg/mL anti-CD28 (BD Pharmingen), 5 µM of individual or pooled HIV-1 peptides and brefeldin A GolgiPlug™ (BD Pharmingen) for further 12 h. After the incubation period, cells were washed with FACS buffer (PBS with 0.5% BSA and 2 mM EDTA) and surface stained with anti-CD3 APCCy7 (clone 145-2C11), anti-CD4 PerCP (clone RM4-5), and anti-CD8 Pacific Blue (clone 53-6.7) monoclonal antibodies for 30 min at 4°C. Cells were fixed and permeabilized using Cytofix/Cytoperm™ kit (BD Pharmingen), according to the manufacturer's instructions. After permeabilization, cells were washed with Perm/Wash buffer (BD Biosciences) and stained intracellularly with anti-IL2 PE (clone JES6-5H4), anti-TNFα PECy7 (clone MP6-XT22), and anti-IFNγ APC (clone XMG1.2) monoclonal antibodies for 30 min at 4°C. Following staining, cells were washed twice and resuspended in FACS buffer. All antibodies were from BD Pharmingen. Samples were acquired on a FACSCanto II flow cytometer (BD Biosciences) and then analyzed using FlowJo software (version 9.9, Tree Star, San Carlos, CA, USA). To analyze cellular polyfunctionality, we used the Boolean gating platform (FlowJo software) to create several combinations of the three cytokines (IL-2, TNFα, and IFNγ) within the CFSE<sup>low</sup> population resulting in seven distinct patterns. The percentages of cytokine-producing cells were calculated by subtracting background values. For each experiment performed, unstained and all single-color controls were processed to allow proper compensation.

## Data Analysis

Statistical significance (*p*-values) was calculated by using a two-way ANOVA and Bonferroni's or one-way ANOVA and Tukey honest significant difference. Statistical analysis and graphical representation of data was performed using GraphPad Prism version 5.0 software.

## Ethics Statement

Mice were housed and manipulated under SPF conditions in the animal care facilities of the Division of Immunology, Federal University of São Paulo (UNIFESP). This study was carried out in accordance with the recommendations of the National Institutes of Health Guide for the Care and Use of Laboratory Animals and the Brazilian National Law (11.794/2008). The protocol (number 3226180814) was approved by the Institutional Animal Care and Use Committee (CEUA) of Federal University of São Paulo.

## RESULTS

### αDEC1HIVBr8 mAb Binds Specifically the DEC205 Receptor

In an attempt to induce a T cell response against HIV, we cloned eight CD4<sup>+</sup> T cell epitopes in fusion with the heavy chain of the DEC205 receptor. αDEC1HIVBr8 and control αDEC205 mAbs were purified and analyzed in 12% SDS polyacrylamide gel under reducing conditions. **Figure 1A** shows an immunoblot in which both mAbs were transferred to a nitrocellulose membrane and incubated with anti-mouse total IgG and anti-mouse IgG kappa

chain. Two bands that correspond to the heavy chain (~50 kDa) and to the light chain were detected. In the  $\alpha$ DECHIVBr8 mAb preparation, we detected the light chain (~25 kDa) and also a band of ~70 kDa that corresponds to the heavy chain of  $\alpha$ DEC205 fused with the HIVBr8 sequence. Next, we tested whether the  $\alpha$ DECHIVBr8 mAb retained its binding capacity to either CHO cells expressing the mouse DEC205 receptor or to the CD11c $^+$ CD8 $\alpha^+$  spleen DCs. **Figure 1B** shows that  $\alpha$ DECHIVBr8 mAb was able to specifically bind to CHO cells expressing the mouse DEC205 receptor in a dose-dependent manner but not to CHO cells expressing the mouse DCIR2 receptor. The control  $\alpha$ DEC205 mAb showed the same binding pattern. More interestingly, the  $\alpha$ DECHIVBr8 mAb was able bind specifically to the murine CD11c $^+$ CD8 $\alpha^+$  DCs but not to the CD11c $^+$ CD8 $\alpha^-$  DCs, showing its specificity for DCs that express DEC205 *in vivo*. As expected, the control  $\alpha$ DEC205 mAb also bound to the CD11c $^+$ CD8 $\alpha^+$  DCs (**Figure 1C**). Taken together, these results showed that the  $\alpha$ DECHIVBr8 mAb was successfully produced and retained its capacity to bind to murine DCs expressing DEC205.

### Immunization with the $\alpha$ DECHIVBr8 mAb Induces Higher Immune Responses than the pVAXHIVBr8 DNA Vaccine

We initially evaluated the cellular immune responses against the pooled HIV peptides in BALB/c mice immunized with one or two doses of  $\alpha$ DECHIVBr8 mAb (4  $\mu$ g) in the presence of poly (I:C) and compared to two doses of the pVAXHIVBr8 DNA vaccine (100  $\mu$ g) (**Figure 2A**). Splenocytes from mice immunized with two doses of the  $\alpha$ DECHIVBr8 mAb presented a higher number of specific IFN $\gamma$ -producing cells when compared to mice immunized with two doses of the DNA vaccine (about 280 and 180 SFU/10 $^6$ , respectively). In addition, no significant difference was observed when the groups that received one or two doses of the  $\alpha$ DECHIVBr8 mAb were compared (**Figure 2B**). Notably, when specific cellular proliferation was evaluated, mice

that received two doses of  $\alpha$ DECHIVBr8 mAb displayed higher frequency of specific CD4 $^+$  (12%, **Figure 2C**) and CD8 $^+$  (8.5%, **Figure 2D**) T cells that proliferated when compared to all the other groups. Significantly, these were almost twofold higher than the numbers found in the group receiving two doses of pVAX-HIVBr8 (6.6% CD4 $^+$  and 4.8% specific CD8 $^+$  T cells). Control groups that were immunized with  $\alpha$ DEC mAb or pVAX plasmid did not show specific IFN $\gamma$  production or T cell proliferation. Of note, the number of CD4 $^+$  and CD8 $^+$  T cells that proliferated in mice immunized with two doses of the  $\alpha$ DECHIVBr8 mAb was higher than the number detected in mice immunized with just one dose. These results led us to conclude that two doses are more effective to induce higher immune responses.

Next, we decided to address if the route of immunization would alter the efficacy of the  $\alpha$ DECHIVBr8 mAb immunization. For that purpose, mice were immunized with two doses of the  $\alpha$ DEC or  $\alpha$ DECHIVBr8 in the presence of poly (I:C) by intraperitoneal (IP) or subcutaneous (SC) route (**Figure 3A**). As shown in **Figure 3B**, IP immunization with the  $\alpha$ DECHIVBr8 mAb was able to induce higher IFN $\gamma$ -producing cells than the SC immunization. Similar results were obtained when we measured the percentage of specific proliferating CD4 $^+$  and CD8 $^+$  T cells (**Figures 3C,D**, respectively). Control mice immunized with  $\alpha$ DEC205 mAb did not show significant production of IFN $\gamma$  or proliferation independently of the route used. We subsequently characterized the profile of polyfunctional T cells. Using multiparameter flow cytometry, we detected antigen-specific T cells (CD4 $^+$  and CD8 $^+$ ) based on their ability to proliferate (CFSE dilution assay) and produce the effector cytokines IFN $\gamma$ , TNF $\alpha$ , and IL2 simultaneously. Boolean combinations of proliferating and cytokine-positive populations indicated that immunization by IP route was most effective to induce higher percentage CD4 $^+$  T cells that proliferated and produced simultaneously IFN $\gamma$ /IL2/TNF $\alpha$  or IFN $\gamma$ /TNF $\alpha$  or TNF $\alpha$  only (**Figure 3E**). Also, IP immunization induced a higher percentage of CD8 $^+$  T cells that proliferated and produced IFN $\gamma$ /IL2/TNF $\alpha$  simultaneously when compared to the group immunized by SC route (**Figure 3F**). We can conclude

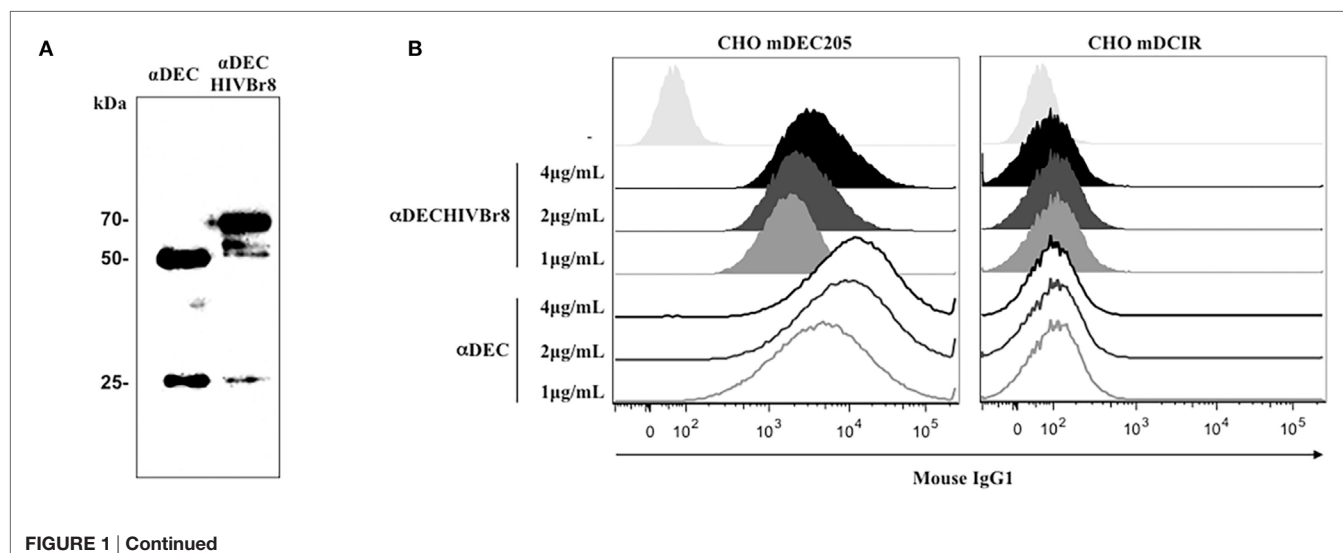
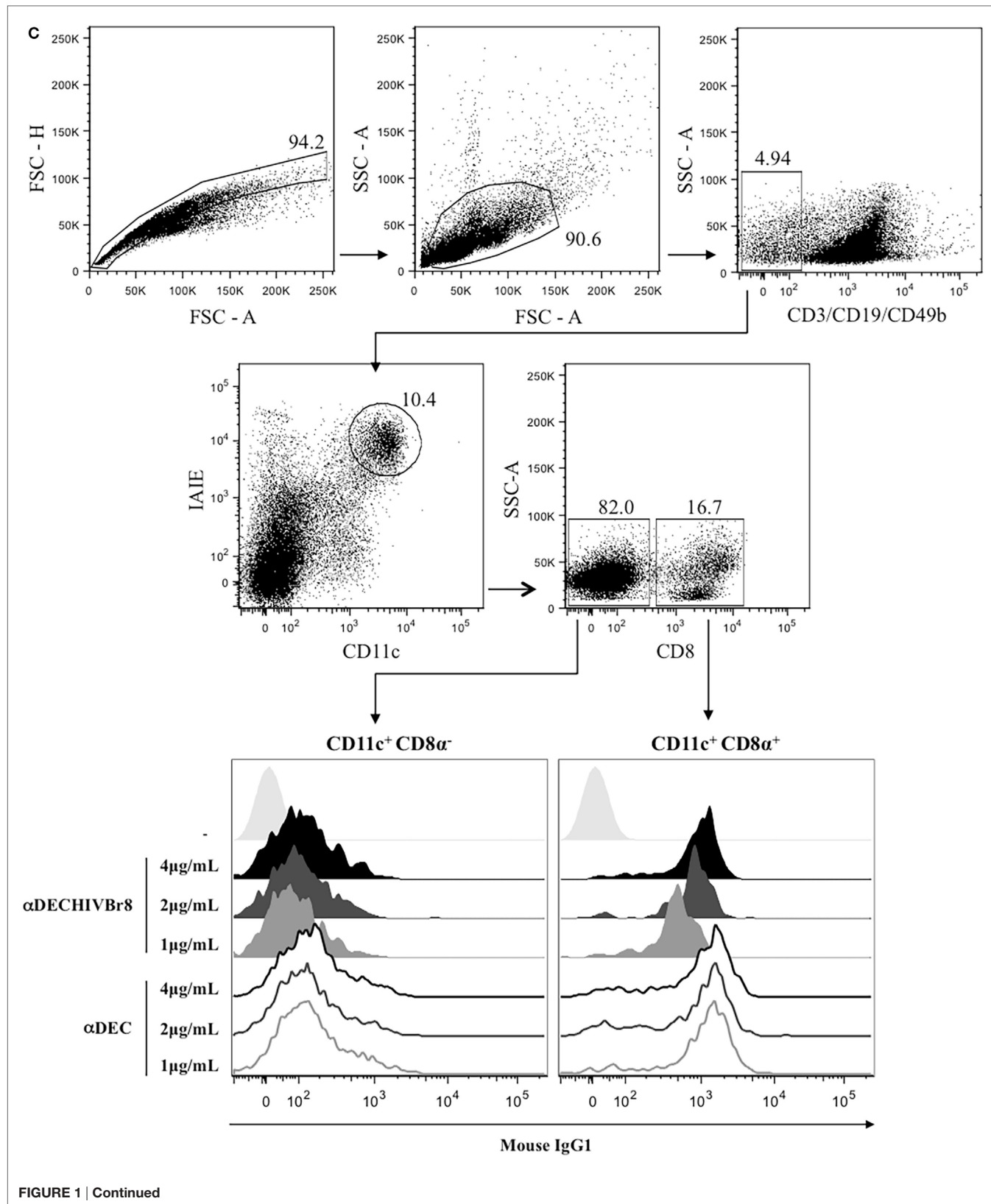
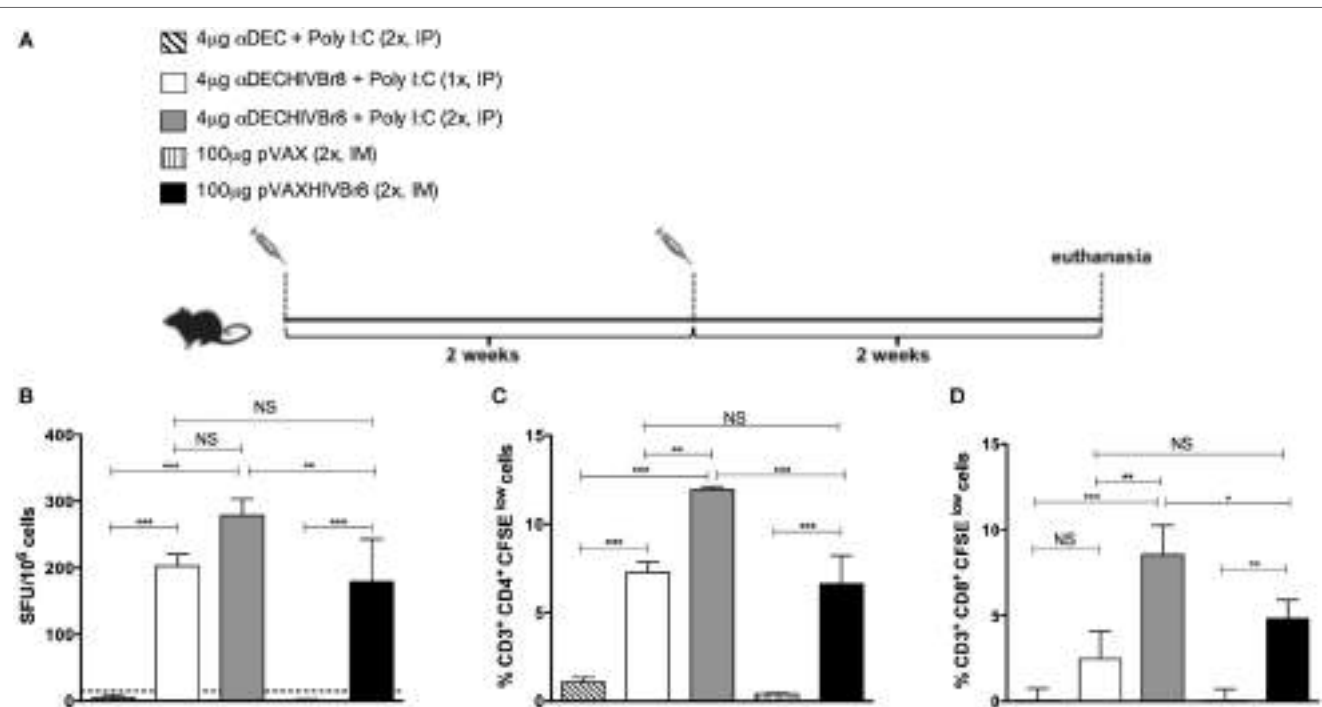


FIGURE 1 | Continued



**FIGURE 1 | Continued**

**The chimeric  $\alpha$ DECHIVBr8 was successfully produced and retained its ability to bind to cells expressing the DEC205 receptors.** (A) One microgram of each monoclonal antibody (mAb) was run on 12% SDS-PAGE under reducing conditions. An immunoblot was performed using peroxidase-labeled goat anti-mouse IgG Fc specific and peroxidase-labeled goat anti-mouse IgG kappa. Molecular weight (kilodaltons),  $\alpha$ DEC (control), and  $\alpha$ DECHIVBr8; (B) CHO cells expressing either DEC205 (left) or DCIR2 (right) receptors were incubated with 4, 2, or 1  $\mu$ g/mL of  $\alpha$ DEC (control) or  $\alpha$ DECHIVBr8, following staining with anti-mouse IgG1 PE antibody. Fifty thousand events were acquired in FACS Canto II and analysis was performed using FlowJo software; (C) 5 million splenocytes from BALB/c mice were incubated with 4, 2, or 1  $\mu$ g/mL of the chimeric  $\alpha$ DECHIVBr8 or  $\alpha$ DEC mAbs. Splenocytes were then incubated with a pool of fluorescent antibodies and gated as singlets and CD3-CD19-CD49b<sup>-</sup>. Dendritic cells were selected as CD11c<sup>+</sup> IAI<sup>+</sup> and subsequently divided into CD8 $\alpha^+$  and CD8 $\alpha^-$ . Binding was detected on  $3 \times 10^6$  cells using an anti-mouse IgG1-PE antibody. Analysis was performed using FlowJo software.



**FIGURE 2 | Immunization with the chimeric  $\alpha$ DECHIVBr8 monoclonal antibody induces higher immune responses when compared to immunization with the pVAXHIVBr8 DNA vaccine.** BALB/c mice ( $n = 6$ ) were immunized with one or two doses of 4  $\mu$ g of  $\alpha$ DEC or  $\alpha$ DECHIVBr8 in the presence of poly I:C adjuvant (IP) or two doses of 100  $\mu$ g of pVAX or pVAXHIVBr8 DNA vaccine (IM). (A) Immunization scheme. Fifteen days after the second dose, the spleen of each animal was removed and the splenocytes (B) were cultured in the presence of pooled HIV-1 peptides (5  $\mu$ M) for 18 h to evaluate the number of IFN- $\gamma$ -producing cells by ELISpot assay. SFU, spot forming units. Cutoff = 15 SFU/ $10^6$  cells and is represented by the dotted line. (C,D) Splenocytes were labeled with carboxyfluorescein succinimidyl ester (CFSE) (1.25  $\mu$ M) and cultured in the presence of pooled HIV-1 peptides (5  $\mu$ M) for 5 days to evaluate specific proliferation. After staining with fluorochrome-labeled anti-CD3, anti-CD4, and anti-CD8 monoclonal antibodies, cells were analyzed by flow cytometry. CFSE dilution on gated CD3<sup>+</sup>CD4<sup>+</sup> (C) or CD3<sup>+</sup>CD8<sup>+</sup> (D) cells was used as readout for antigen-specific proliferation. One million events were acquired in a live lymphocyte gate. The percent of proliferating CD4<sup>+</sup> and CD8<sup>+</sup> CFSE<sup>low</sup> cells was determined in the CD3<sup>+</sup> cell population. The percentage of proliferating T cells was calculated subtracting by the values of stimulated from non-stimulated cultures. NS, not significant; \* $p < 0.05$ ; \*\* $p < 0.01$ ; \*\*\* $p < 0.001$ . Data represent mean  $\pm$  SD.

that immunization using two doses of the  $\alpha$ DECHIVBr8 mAb by the IP route was better to induce T cell responses with greater magnitude and more polyfunctional than those induced by the pVAXHIVBr8 DNA vaccine encoding the same epitopes.

### Homologous or Heterologous $\alpha$ DECHIVBr8 Prime-Boost Enhances IFN- $\gamma$ Production, T Cell Proliferation, and Polyfunctional T Cells

To test whether a heterologous prime-boost strategy would work with chimeric mAb, groups of mice were then immunized with

one dose of  $\alpha$ DECHIVBr8 mAb (prime) followed by one dose of the pVAXHIVBr8 DNA vaccine (boost), or *vice versa*, and compared to the homologous prime-boost immunization strategy (two doses of chimeric mAb or DNA vaccine) (Figure 4A). Two weeks after the boost, splenocytes from immunized mice were incubated with pooled peptides and specific IFN $\gamma$  production was measured by ELISpot assay. We detected the highest numbers of IFN $\gamma$ -producing cells against the pooled peptides in mice that received two doses of  $\alpha$ DECHIVBr8 and in the group receiving pVAXHIVBr8 priming followed by  $\alpha$ DECHIVBr8 mAb boosting (Figure 4B). Interestingly, mice primed with  $\alpha$ DECHIVBr8 mAb and boosted with pVAXHIVBr8 showed a lower response when

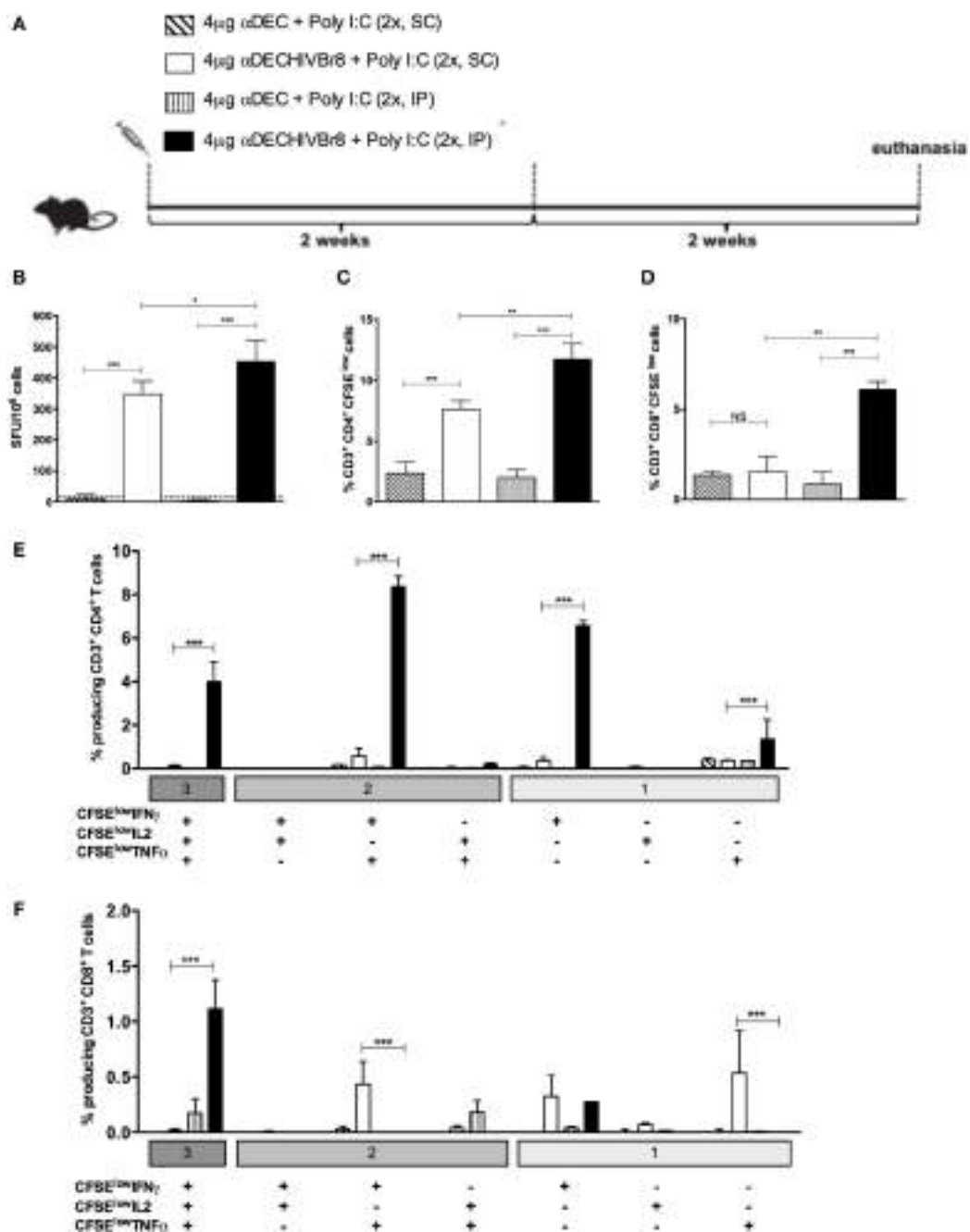


**FIGURE 3 |** The intraperitoneal route elicits higher T cell responses in the spleen than subcutaneous administration of the chimeric αDECHIVBr8 monoclonal antibody. BALB/c mice ( $n = 6$ ) were immunized with two doses of 4 µg of αDEC or αDECHIVBr8 in the presence of poly (I:C) adjuvant by intraperitoneal (IP) or subcutaneous (SC) routes. **(A)** Immunization scheme. Fifteen days after the second dose, the spleen of each animal was removed and the splenocytes **(B)** were cultured in the presence pooled HIV-1 peptides (5 µM) for 18 h to evaluate the number of IFN- $\gamma$ -producing cells by ELISpot assay. SFU, spot forming units. Cutoff = 15 SFU/ $10^6$  cells and is represented by the dotted line. **(C,D)** Splenocytes were labeled with carboxyfluorescein succinimidyl ester (CFSE) (1.25 µM) and cultured in the presence of pooled HIV-1 peptides (5 µM) for 5 days to evaluate specific proliferation. After staining with fluorochrome-labeled anti-CD3, anti-CD4, and anti-CD8 monoclonal antibodies, cells were analyzed by flow cytometry. CFSE dilution on gated CD3<sup>+</sup>CD4<sup>+</sup> **(C)** or CD3<sup>+</sup>CD8<sup>+</sup> **(D)** cells was used as readout for antigen-specific proliferation. For detection of cytokine-producing T cells, cells were pulsed on day 4 for 12 h with pooled peptides in the presence of anti-CD28 and brefeldin A. Cells were then surface stained with anti-CD3, CD4, and CD8, permeabilized, and stained for intracellular cytokines. Multiparameter flow cytometry was used to determine the frequency of IFN $\gamma$ , IL2-, or TNF $\alpha$ -producing CD4<sup>+</sup> and CD8<sup>+</sup> T cells **(E,F)**. After gating on proliferating (CFSE<sup>low</sup>) and cytokine-producing cells, Boolean combinations were then created using FlowJo software to determine the frequency of each response based on all possible combinations of cytokine-producing CD4<sup>+</sup> **(E)** and CD8<sup>+</sup> **(F)** T cells. One million events were acquired in a live lymphocyte gate. The percentage of proliferating and cytokine-producing T cells was calculated subtracting the values of stimulated from non-stimulated cultures. NS, not significant; \* $p < 0.05$ ; \*\* $p < 0.01$ ; \*\*\* $p < 0.001$ . Data represent mean  $\pm$  SD.

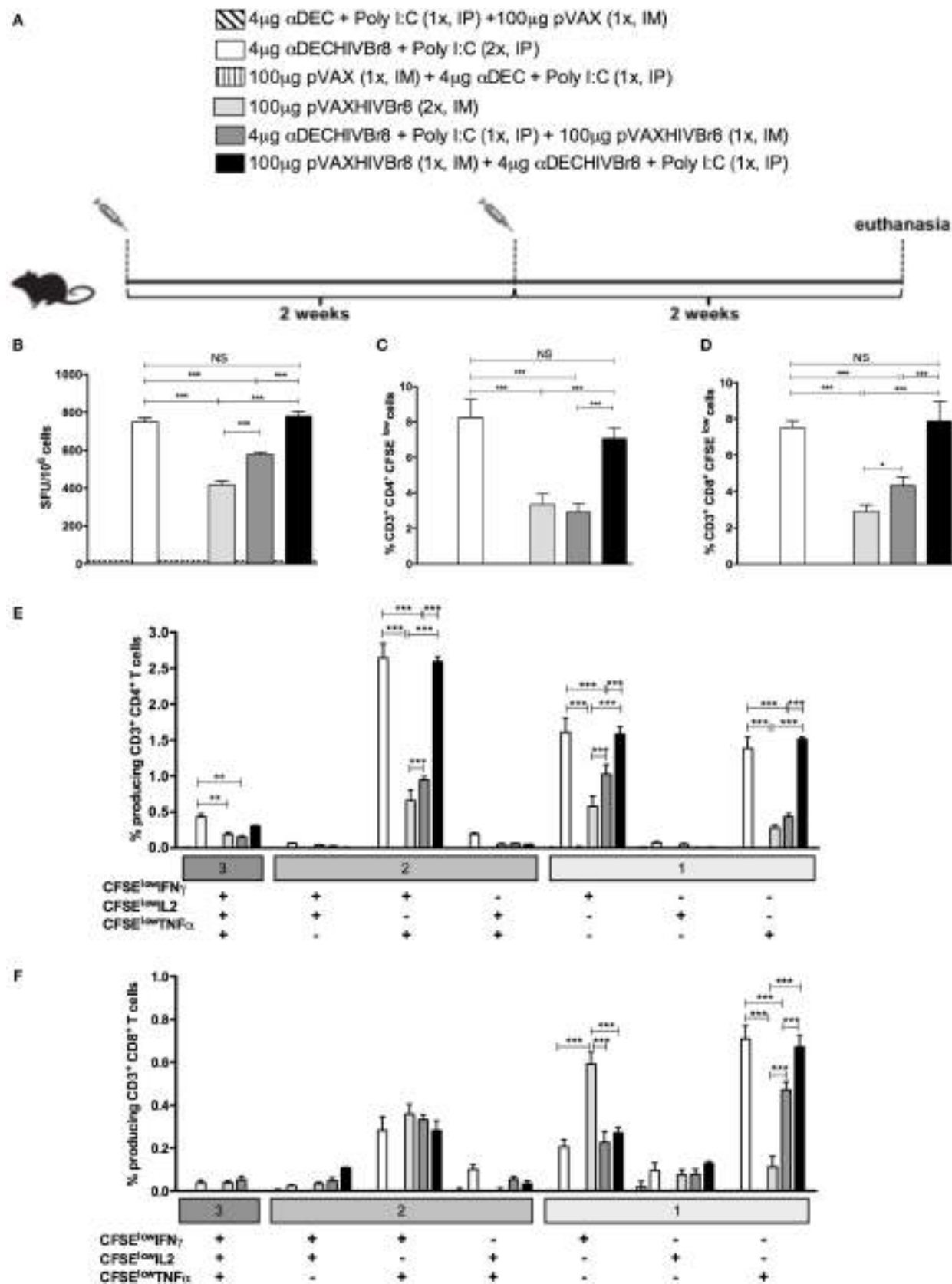


FIGURE 4 | Continued

**FIGURE 4 | Continued**

**Homologous  $\alpha$ DECHIVBr8 monoclonal antibody (mAb) immunization or heterologous prime-boost induces polyfunctional T cell responses.** BALB/c mice ( $n = 6$ ) were immunized with two doses of 4  $\mu$ g of  $\alpha$ DECHIVBr8 in the presence of poly (I:C) adjuvant (IP) or two doses of 100  $\mu$ g of pVAXHIVBr8 DNA vaccine (IM). For heterologous regimens, mice were immunized with one dose of  $\alpha$ DECHIVBr8 followed by one dose of DNA vaccine or vice versa. The control groups were immunized with one dose of  $\alpha$ DEC mAb together with poly (I:C) followed by one dose with pVAX or vice versa. **(A)** Immunization scheme. Fifteen days after the second dose, the spleen of each animal was removed and the splenocytes **(B)** were cultured in the presence of pooled HIV-1 peptides (5  $\mu$ M) for 18 h to evaluate the number of IFN- $\gamma$ -producing cells by ELISpot assay. SFU, spot forming units. Cutoff = 15 SFU/ $10^6$  cells and is represented by the dotted line. **(C,D)** Splenocytes were labeled with carboxyfluorescein succinimidyl ester (CFSE) (1.25  $\mu$ M) and cultured in the presence of pooled HIV-1 peptides (5  $\mu$ M) for 5 days to evaluated specific proliferation. After staining with fluorochrome-labeled anti-CD3, anti-CD4, and anti-CD8 monoclonal antibodies, cells were analyzed by flow cytometry. CFSE dilution on gated CD3+CD4+ **(C)** or CD3+CD8+ **(D)** cells was used as readout for antigen-specific proliferation; For detection of cytokine-producing T cells, cells were pulsed on day 4 for 12 h with pooled peptides in the presence of anti-CD28 and brefeldin A. Cells were then surface stained with anti-CD3, CD4, and CD8, permeabilized, and stained for intracellular cytokines. Multiparameter flow cytometry was used to determine the frequency of IFN $\gamma$ -, IL2-, or TNF $\alpha$ -producing CD4+ and CD8+ T cells **(E,F)**. After gating on proliferating (CFSE $^{low}$ ) and cytokine-producing cells, Boolean combinations were then created using FlowJo software to determine the frequency of each response based on all possible combinations of cytokine-producing CD4+ **(E)** and CD8+ **(F)** T cells. One million events were acquired in a live lymphocyte gate. The percentage of proliferating and cytokine-producing T cells was calculated subtracting the values of stimulated from non-stimulated cultures. NS, not significant; \* $p < 0.05$ ; \*\* $p < 0.01$ ; \*\*\* $p < 0.001$ . Data represent mean  $\pm$  SD.

compared to the two previously described groups. Finally, mice immunized with two doses of pVAXHIVBr8 presented the lowest number of IFN $\gamma$ -producing cells (416 SFU/ $10^6$  cells, **Figure 4B**). A similar pattern was observed when we analyzed the percent of CD4+ and CD8+ specific proliferation (**Figures 4C,D**, respectively): mice immunized with two doses of  $\alpha$ DECHIVBr8 mAb displayed 8.23% of CD4+ and 7.49% of CD8+ T cell specific proliferation, while pVAXHIVBr8 (prime)/ $\alpha$ DECHIVBr8 (boost) displayed 7.04 and 7.86%, respectively. Lower percentages were observed in mice immunized with two doses of pVAXHIVBr8 or  $\alpha$ DECHIVBr8 mAb (prime)/pVAXHIVBr8 (boost). In addition, we characterized the phenotype and functionality of antigen-specific CD4+ and CD8+ T cells based on their ability to proliferate (CFSE $^{low}$ ) and produce IFN $\gamma$ , TNF $\alpha$ , and IL2 individually or in combinations (Figure S1 in Supplementary Material). **Figure 4E** shows once more that immunization with two doses of  $\alpha$ DECHIVBr8 and pVAXHIVBr8 (prime)/ $\alpha$ DEC205-HIVBr8 (boost) were most effective to induce higher percentage of CD4+ T cells that proliferated and produced simultaneously IFN $\gamma$ /TNF $\alpha$  or IFN $\gamma$  only or TNF $\alpha$  only. When we analyzed the CD8+ T cells, two doses of pVAXHIVBr8 DNA vaccine showed a higher percentage of CD8+ T cell proliferating and producing only IFN $\gamma$  when compared to the other groups (**Figure 4F**). By contrast, CD8+ T cells from mice immunized with two doses of  $\alpha$ DECHIVBr8 and pVAXHIVBr8 (prime)/ $\alpha$ DECHIVBr8 (boost) were able to proliferate and mainly produce TNF $\alpha$ .  $\alpha$ DEC and pVAX immunized mice displayed negligible percentages of specific proliferating/cytokine-producing T cells. Extended comparative analysis revealed that  $\alpha$ DECHIVBr8 and  $\alpha$ DECHIVBr8 (prime)/pVAXHIVBr8 (boost) immunized mice displayed higher frequency of non-proliferating (CFSE $^{high}$ ) IFN $\gamma$ +/IL2+/TNF $\alpha$ + and CFSE $^{high}$  IFN $\gamma$ +/TNF $\alpha$ +-producing CD4+ T cells when compared to other groups (Figure S2A in Supplementary Material). Analysis of CD8+ T cell compartment demonstrated that  $\alpha$ DECHIVBr8 (prime)/pVAXHIVBr8 (boost) was the most efficient strategy to induce CFSE $^{high}$  IFN $\gamma$ +/IL2+/TNF $\alpha$ + and CFSE $^{high}$  IFN $\gamma$ + cells, while  $\alpha$ DECHIVBr8 immunization induced higher frequency of CFSE $^{high}$  TNF $\alpha$ + cells (Figure S2B in Supplementary Material). Taken together, these results showed that homologous immunization with  $\alpha$ DECHIVBr8 mAb or heterologous pVAXHIVBr8

(prime)/ $\alpha$ DECHIVBr8 (boost) were able to induce broad specific cellular responses, and polyfunctional CD4+ and CD8+ T cells that proliferated and produced effector Th1 cytokines to epitopes encoded by the chimeric mAb and the DNA vaccine.

In an attempt to improve the cellular immune response induced by the DNA vaccination alone and compare it to the homologous immunization with  $\alpha$ DECHIVBr8 or with the heterologous pVAXHIVBr8 (prime)/ $\alpha$ DECHIVBr8 (boost), we decided to administer one additional dose of either  $\alpha$ DECHIVBr8 or pVAXHIVBr8. In this way, the homologous immunization groups received three doses of either  $\alpha$ DECHIVBr8 or pVAXHIVBr8, while the heterologous immunization group received one dose of pVAXHIVBr8 followed by two boosters of  $\alpha$ DECHIVBr8. Control groups received three doses of either  $\alpha$ DEC or pVAX (**Figure 5A**). To assess the magnitude of the immune response, we evaluated specific IFN $\gamma$ -producing cells in splenocytes from immunized mice stimulated with pooled peptides (**Figure 5B**). Once again, we observed no difference between animals immunized with three doses of  $\alpha$ DECHIVBr8 and animals immunized with pVAXHIVBr8 once/ $\alpha$ DECHIVBr8 twice. By contrast, the group immunized with pVAXHIVBr8 thrice presented a lower number of specific IFN $\gamma$ -producing cells. In addition, as observed with the administration of two doses, CD4+ and CD8+ T cells (**Figures 5C,D**, respectively) from mice immunized with three doses of  $\alpha$ DECHIVBr8, and one dose pVAXHIVBr8 followed by two doses of  $\alpha$ DECHIVBr8 displayed higher T cell proliferation against the pooled HIV-1 peptides than three doses of pVAXHIVBr8. By contrast, mice immunized with three doses of pVAXHIVBr8 continued to present a lower percentage of proliferation when compared to the two previous groups.  $\alpha$ DEC and pVAX immunized mice presented negligible numbers of IFN $\gamma$ -producing cells and T cell proliferation. Boolean combinations of proliferating and cytokine-positive populations indicated that homologous immunization with  $\alpha$ DECHIVBr8 (3 $\times$ ) or with pVAXHIVBr8 (1 $\times$ )/ $\alpha$ DECHIVBr8 (2 $\times$ ) induced polyfunctional CD4+ T cells that proliferated and produced simultaneously IFN $\gamma$ /TNF $\alpha$ , or IFN $\gamma$ , or TNF $\alpha$  only (**Figure 5E**). Similar results were observed when CD8+ T cells were analyzed (**Figure 5F**). CD4+ and CD8+ T cells from mice immunized with the controls  $\alpha$ DEC and pVAX displayed negligible percentages of specific

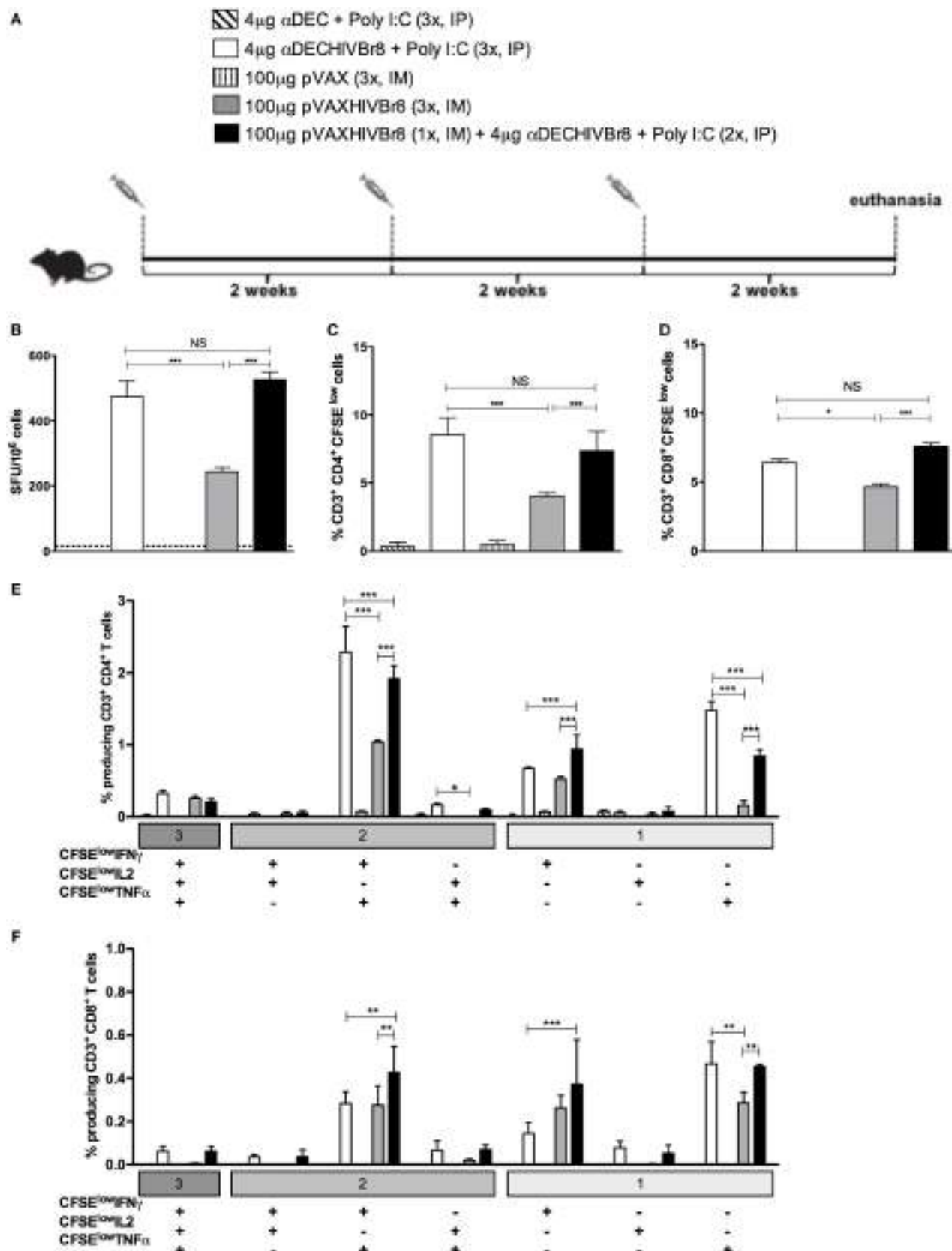
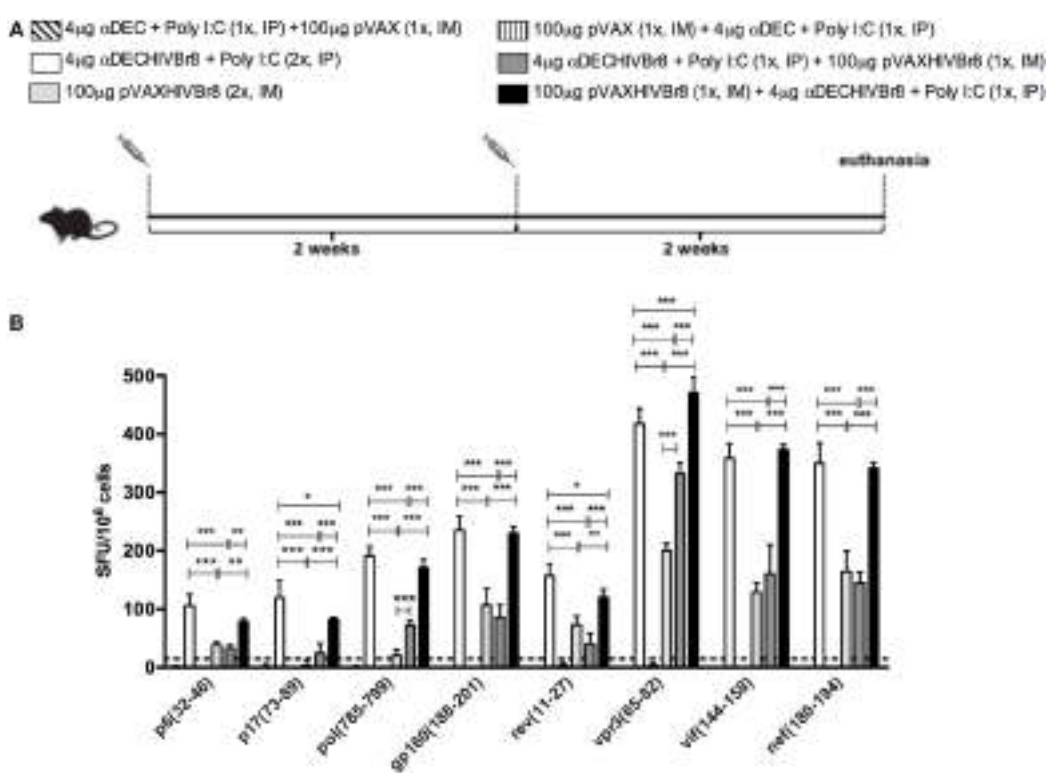


FIGURE 5 | Continued

**FIGURE 5 | Continued**

**The chimeric  $\alpha$ DECHIVBr8 monoclonal antibody (mAb) is more immunogenic even with increased doses of the DNA vaccine.** BALB/c mice ( $n = 6$ ) were immunized with three doses of 4  $\mu$ g of  $\alpha$ DECHIVBr8 in the presence of poly (I:C) adjuvant (IP) or three doses of 100  $\mu$ g of pVAXHIVBr8 DNA vaccine (IM). For heterologous regimens, mice were immunized with one dose of DNA vaccine followed by two doses of the chimeric mAb. **(A)** Immunization scheme. Fifteen days after the second dose, the spleen of each animal was removed and the splenocytes **(B)** were cultured in the presence of pooled HIV-1 peptides (5  $\mu$ M) for 18 h to evaluate the number of IFN- $\gamma$ -producing cells by ELISpot assay. SFU, spot forming units. Cutoff = 15 SFU/10<sup>6</sup> cells and is represented by the dotted line. **(C,D)** Splenocytes were labeled with carboxyfluorescein succinimidyl ester (CFSE) (1.25  $\mu$ M) and cultured in the presence of pooled HIV-1 peptides (5  $\mu$ M) for 5 days to evaluate specific proliferation. After staining with fluorochrome-labeled anti-CD3, anti-CD4, and anti-CD8 monoclonal antibodies, cells were analyzed by flow cytometry. CFSE dilution on gated CD3 $^+$ CD4 $^+$  **(C)** or CD3 $^+$ CD8 $^+$  **(D)** cells was used as readout for antigen-specific proliferation. For detection of cytokine-producing T cells, cells were pulsed on day 4 for 12 h with pooled peptides in the presence of anti-CD28 and brefeldin A. Cells were then surface stained with anti-CD3, CD4, and CD8, permeabilized, and stained for intracellular cytokines. Multiparameter flow cytometry was used to determine the frequency of IFN $\gamma$ -, IL2-, or TNF $\alpha$ -producing CD4 $^+$  and CD8 $^+$  T cells **(E,F)**. After gating on proliferating (CFSE $^{low}$ ) and cytokine-producing cells, Boolean combinations were then created using FlowJo software to determine the frequency of each response based on all possible combinations of cytokine-producing CD4 $^+$  **(E)** and CD8 $^+$  **(F)** T cells. One million events were acquired in a live lymphocyte gate. The percent of proliferating CD4 $^+$  and CD8 $^+$  CFSE $^{low}$  cells was determined in the CD3 $^+$  cell population. The percentage of proliferating and cytokine-producing T cells was calculated subtracting the values of stimulated from non-stimulated cultures. NS, not significant; \* $p < 0.05$ ; \*\* $p < 0.01$ ; \*\*\* $p < 0.001$ . Data represent mean  $\pm$  SD.



**FIGURE 6 | Immunization with homologous or heterologous prime-boost induces broad T cell responses.** BALB/c mice ( $n = 6$ ) were immunized with two doses of 4  $\mu$ g of  $\alpha$ DECHIVBr8 in the presence of poly (I:C) adjuvant (IP) or two doses of 100  $\mu$ g of pVAXHIVBr8 DNA vaccine (IM). For heterologous regimens, mice were immunized with one dose of the DNA vaccine followed by one dose of monoclonal antibody. **(A)** Immunization scheme. Fifteen days after the last immunization, splenocytes were cultured **(B)** with individual HIV-1 peptides (5  $\mu$ M) for 18 h to evaluate the number of IFN- $\gamma$ -producing cells by ELISpot assay, SFU, spot forming units. Cutoff = 15 SFU/10<sup>6</sup> cells and is represented by the dotted line.

proliferating/cytokine-producing T cells. Taken together, these results indicate that an additional dose of pVAXHIVBr8 does not improve the magnitude of the T cell responses over immunization with  $\alpha$ DECHIVBr8 mAb.

### Immunization with Chimeric $\alpha$ DECHIVBr8 mAb Induces Broad T Cell Responses

To evaluate whether immunization induces broad T cell responses, splenocytes from mice immunized with two doses of

$\alpha$ DECHIVBr8 and pVAXHIVBr8 or heterologous prime-boost regimens (Figure 6A) were incubated with each of the eight individual HIV-1 peptides present in the chimeric mAb or DNA vaccine. We detected IFN $\gamma$ -producing cells against all tested peptides. Immunization with two doses of  $\alpha$ DECHIVBr8 mAb or with pVAXHIVBr8 (prime)/ $\alpha$ DECHIVBr8 (boost) elicited significantly higher numbers of IFN $\gamma$ -producing cells when compared to mice immunized with two doses of pVAXHIVBr8 or that received  $\alpha$ DECHIVBr8 (prime)/pVAXHIVBr8 (boost) (Figure 6B).

In summary, our results demonstrate that immunization of BALB/c mice with two or three doses of  $\alpha$ DECHIVBr8 mAb or heterologous prime-boost with pVAXHIVBr8 followed by  $\alpha$ DECHIVBr8 were able to induce specific immune responses with a higher number of IFN $\gamma$ -producing cells, and polyfunctional CD4 $^{+}$  and CD8 $^{+}$  T cells that proliferated and produced effector Th1 cytokines.

## DISCUSSION

In this paper, we provide the first evidence that a multiepitopic vaccine can be targeted to DCs *via* DEC205 mAb. Furthermore, homologous prime-boosting with the  $\alpha$ DECHIVBr8, or heterologous DNA prime followed by  $\alpha$ DECHIVBr8 boosting encoding the same epitopes, can induce T cell responses of higher magnitude, polyfunctionality, and breadth than homologous prime-boost with the DNA vaccine.

In a previous study, our group demonstrated that a DNA vaccine encoding 18 HIV-derived promiscuous and preserved CD4 $^{+}$  T cell epitopes (16) was able to induce broad CD4 $^{+}$  and CD8 $^{+}$  T cell responses in different strains of HLA class II transgenic mice (DR2, DR4, DQ6, and DQ8) (18). Furthermore, the HIVBr18 DNA vaccine induced polyfunctional and long-lived CD4 $^{+}$  and CD8 $^{+}$  T cells responses to 8/18 HIV peptides encoded by the DNA vaccine (19). Despite promising, DNA vaccines show reduced immunogenicity in humans (21), and in the last decades, several strategies have been developed in order to increase the immunogenicity of these vaccines (17).

Initial attempts at developing a vaccine against HIV have focused mainly on the induction of humoral immune response against the viral gp120 protein and were not able to confer protection (44). In order to improve the induced immune response, the RV144 trial performed an immunization scheme that included a prime with a viral vector followed by a boost with Env protein and reported ~30% of protection in vaccinated individuals (1). A more detailed analysis of the immunized and protected individuals did not show CD8 $^{+}$  responses but CD4 $^{+}$  T cell responses to HIV correlated with reduced acquisition (2). Although the importance of CD8 $^{+}$  cytotoxic T cells as a first response against HIV (45, 46) is well established, a strong CD4 $^{+}$  T cell response is of utmost importance for the slow progression to AIDS (8). A recent study showed that untreated HIV-infected controllers presented higher Gag-specific CD4 $^{+}$  T cell responses and higher titers of nAbs against Env (10). Moreover, in non-human primates, depletion of CD4 $^{+}$  T cells markedly reduced protection mediated by vaccination after SIV challenge (47). Hence, an effective vaccine against HIV should induce specific cytotoxic responses as well as CD4 $^{+}$  T cell responses.

In an attempt to improve the HIV-specific cellular response, we targeted eight previously recognized epitopes derived from the HIVBr18 DNA vaccine directly to DCs. This is accomplished by the use of DC receptor-specific mAbs fused to the antigen of interest. We produced an  $\alpha$ DEC205 chimeric mAb containing the sequence of eight HIV-derived CD4 $^{+}$  T cell epitopes ( $\alpha$ DECHIVBr8) (18, 19) and compared DC targeting through  $\alpha$ DECHIVBr8 mAb with the DNA vaccine pVAXHIVBr8. We initially showed that the  $\alpha$ DECHIVBr8 mAb was successfully

produced and retained its ability to bind to the DEC205 receptor, especially to the CD11c $^{+}$ CD8 $\alpha^{+}$  DCs that naturally express the DEC205 receptor. The use of chimeric  $\alpha$ DEC205 to deliver HIV antigens, especially Gag, to DCs has been previously reported (32, 33). Targeting Gag to CD8 $\alpha^{+}$  DCs leads to a strong polyfunctional CD4 $^{+}$  (32, 37) and also CD8 $^{+}$  T cell responses (36) including in the gastrointestinal tract (34).

To address the minimum number of doses to induce specific immune responses, BALB/c mice were immunized with one or two doses of  $\alpha$ DECHIVBr8 in the presence of poly (I:C) or with pVAXHIVBr8 DNA vaccine. We found that mice immunized with two doses of chimeric  $\alpha$ DECHIVBr8 mAb developed a stronger CD4 $^{+}$  and CD8 $^{+}$  T cell response when compared to mice that received one dose of  $\alpha$ DECHIVBr8 mAb or two doses of the DNA vaccine after stimulation with pooled HIV-1 peptides, demonstrating the effectiveness of the approach in the context of a chimeric multiepitope vaccine antigen. Next, we determined which immunization route was more effective. BALB/c received two doses of  $\alpha$ DECHIVBr8 plus poly (I:C) by intraperitoneal (IP) or subcutaneous (SC) route. Although some studies have demonstrated the efficacy of the subcutaneous immunization with  $\alpha$ DEC mAbs (27, 48), we detected a stronger CD4 $^{+}$  and CD8 $^{+}$  T cell response when  $\alpha$ DECHIVBr8 was delivered IP. These results confirm what has already been demonstrated by other studies that used the IP route and showed high magnitude of specific cellular immune responses against different pathogens such as *Yersinia pestis* (49), *Plasmodium* sp. (28), papilloma virus (50), *Leishmania major* (51), Epstein–Barr virus (52), dengue virus (35), *T. cruzi* (30), and HIV (32, 33).

Some studies on the clinical course of HIV-1 have associated CD4 $^{+}$  T cells exhibiting polyfunctional profile with better control of disease. In elite controllers, superior polyfunctional CD4 $^{+}$  T cell response is observed when compared to non-controller individuals in HAART (53–55), including in the mucosal region (56). In RV144 trial analysis, vaccinees with polyfunctional CD4 $^{+}$  T cell responses against HIV peptides were found to have a lower rate of infection (57). Besides, the presence of specific HLA class II (DRB1\*13, DQB1\*06, and DRB1\*15:02)-restricted CD4 $^{+}$  T cell responses (9, 14) play an important role in HIV immune control. In the present study, we show the induction of both polyfunctional CD4 $^{+}$  and CD8 $^{+}$  T cell responses after immunization with  $\alpha$ DECHIVBr8 in the presence of poly (I:C).

When antigens are targeted to the DEC205 $^{+}$  DC population, they can be presented to CD4 $^{+}$  (58) as well as to CD8 $^{+}$  T cells (48). Other studies showed that antigens encapsulated in nanoparticles and targeted to the DEC205 $^{+}$  DCs are presented by MHC class I and induce specific CD8 $^{+}$  T cell responses (59, 60). This phenomenon can be explained by the ability of the CD11c $^{+}$ CD8 $\alpha^{+}$  DCs to perform cross-presentation (61). Our study demonstrates that targeting promiscuous HIV epitopes to CD8 $\alpha^{+}$  DC induce both CD4 $^{+}$  and CD8 $^{+}$  T cell-mediated immunity.

In recent years, several studies have shown that heterologous prime-boost immunization is able to increase the magnitude and quality of the immune response to many pathogens, including HIV (39). This approach started to be used in attempt to develop vaccines against pathogens that require more robust

humoral and cellular immune responses such as HIV (62), *M. tuberculosis*, and *Plasmodium* sp. (42). In this work, we found that pVAXHIVBr8 DNA vaccine priming followed by boost with the  $\alpha$ DECHIVBr8 mAb boosting increased the overall magnitude of the responses against HIV peptides when the opposite was tested (priming with  $\alpha$ DECHIVBr8 followed by pVAXHIVBr8 boost). Our results have shown that receiving two doses of  $\alpha$ DECHIVBr8 mAb or a pVAXHIVBr8/ $\alpha$ DECHIVBr8 heterologous prime-boost induced a stronger CD4<sup>+</sup> and CD8<sup>+</sup> polyfunctional T cell response than any other immunization schemes tested. DNA vaccines have been shown to be most effective when administrated as a prime in vaccine formulations (63, 64). In our model, chimeric  $\alpha$ DEC205 mAb was more effective as a boost exceptionally when the analysis was performed in non-proliferating (CFSE<sup>high</sup>) cytokine-producing cells. Of note, targeted  $\alpha$ DEC205-Gag has been successfully used as a priming platform followed by recombinant vaccinia as boost to induce robust cellular immunity (34, 65).

In an attempt to improve the pVAXHIVBr8 magnitude, we immunized mice with three doses in the homologous or heterologous prime-boost regimens. We analyzed the ability of the cells from immunized mice to produce cytokines and proliferate at the same time. Overall, we observed the same phenomenon that occurred in animals that received only two doses showing that an additional dose of pVAXHIVBr8 did not increase the magnitude to the same level as immunization with  $\alpha$ DECHIVBr8 (3x) or with pVAXHIVBr8 prime (1x)/ $\alpha$ DECHIVBr8 (2x).

Our results have shown that immunization with two doses of  $\alpha$ DECHIVBr8 mAb or with pVAXHIVBr8 followed by  $\alpha$ DECHIVBr8 boost elicited higher magnitude T cell responses against all the peptides indicating a broad T cell response. Indeed, recent efficacy trials of T cell-based HIV vaccines showed that for protection, it is necessary to induce broad T cell responses toward conserved epitopes (2, 46, 66). An adenovirus-based SIV vaccine encoding eight virus proteins elicited broad T cell responses that reduced viremia after heterologous challenge (67) and the vaccine-induced response correlated with higher CD4<sup>+</sup> T cell responses (68). Hence, vaccine candidates that expand the breadth of CD4<sup>+</sup> and CD8<sup>+</sup> T cell responses must be developed in order to provide optimal T-cell responses that may cope with the diverse circulating strains of HIV (69).

Our results provide evidence that multiepitope targeting to DCs can provide superior CD4<sup>+</sup> and CD8<sup>+</sup> T cell responses as compared to DNA vaccines alone. Given the known protective potential of CD4<sup>+</sup> T responses elicited by  $\alpha$ DEC205 mAb DC-targeted immunization (33), direct DC targeting, or the combination of DNA priming followed by DC targeting, is a promising platform for increasing HIV immunity after vaccination.

## AUTHOR CONTRIBUTIONS

JA, SB, and DR conceived and designed the experiments. JA, VL, MY, HS, and DR performed the experiments. JA and DR analyzed

the data and prepared the figures. DR, SB, and EC-N contributed with reagents and materials. JA, SB, and DR wrote the manuscript. SB, EC-N, and DR performed the final review of the article. All the authors read and approved the final article.

## ACKNOWLEDGMENTS

The authors thank Mr. Geová Santos for assistance at the animal facility.

## FUNDING

This research was supported by the Fundação de Amparo à Pesquisa do Estado de São Paulo (FAPESP, 2014/15061-8 and 2013/11442-4) and the Brazilian National Research Council (CNPq)/Institute for Investigation in Immunology. JA, VL, EC-N, and SB received fellowships from CNPq/FAPESP. HS received a fellowship from CAPES.

## SUPPLEMENTARY MATERIAL

The Supplementary Material for this article can be found online at <http://journal.frontiersin.org/article/10.3389/fimmu.2017.00101/full#supplementary-material>.

**FIGURE S1 | Flow cytometer analysis of cellular proliferation and intracellular cytokine production.** Representative dot plots of a seven-color flow cytometry panel used for the detection of carboxyfluorescein succinimidyl ester (CFSE), IFN $\gamma$ -, IL2-, and TNF $\alpha$ -producing T cells after *in vitro* stimulation with pooled HIV peptides. After gating on proliferating (CFSE<sup>low</sup>) or non-proliferating (CFSE<sup>high</sup>) and cytokine-producing cells, Boolean combinations were then created using FlowJo software to determine the frequency of each response based on all possible combinations of cytokine-producing T cells. The frequency of IFN $\gamma$ -, IL2-, or TNF $\alpha$  cytokine-producing CFSE<sup>low</sup> or CFSE<sup>high</sup> CD4<sup>+</sup> T cells is displayed.

**FIGURE S2 | Homologous  $\alpha$ DECHIVBr8 monoclonal antibody (mAb) immunization or heterologous prime-boost induces polyfunctional T cell responses.** BALB/c mice ( $n = 6$ ) were immunized with two doses of 4  $\mu$ g of  $\alpha$ DECHIVBr8 in the presence of poly (I:C) adjuvant (IP) or two doses of 100  $\mu$ g of pVAXHIVBr8 DNA vaccine (intramuscular). For heterologous regimens, mice were immunized with one dose of  $\alpha$ DECHIVBr8 followed by one dose of DNA vaccine or vice versa. The control groups were immunized with one dose of  $\alpha$ DEC mAb together with poly (I:C) followed by one dose with pVAX or vice versa. Fifteen days after the second dose, the spleen of each animal was removed and the splenocytes were labeled with carboxyfluorescein succinimidyl ester (CFSE) (1.25  $\mu$ M) and cultured in the presence of pooled HIV-1 peptides (5  $\mu$ M) for 5 days to evaluated specific proliferation. For detection of cytokine-producing T cells, cells were pulsed on day 4 for 12 h with pooled peptides in the presence of anti-CD28 and brefeldin A. Cells were then surface stained with anti-CD3, CD4, and CD8, permeabilized, and stained for intracellular cytokines. Multiparameter flow cytometry was used to determine the frequency of IFN $\gamma$ -, IL2-, or TNF $\alpha$ -producing CD4<sup>+</sup> and CD8<sup>+</sup> T cells. After gating on non-proliferating (CFSE<sup>high</sup>) and cytokine-producing cells, Boolean combinations were then created using FlowJo software to determine the frequency of each response based on all possible combinations of cytokine-producing CD4<sup>+</sup> (A) and CD8<sup>+</sup> (B) T cells. One million events were acquired in a live lymphocyte gate. The percentage of proliferating and cytokine-producing T cells was calculated subtracting the values of stimulated from non-stimulated cultures. NS, not significant; \* $p < 0.05$ ; \*\* $p < 0.01$ ; \*\*\* $p < 0.001$ . Data represent mean  $\pm$  SD.

## REFERENCES

1. Berks-Ngarm S, Pitisuttithum P, Nitayaphan S, Kaewkungwal J, Chiu J, Paris R, et al. Vaccination with ALVAC and AIDSVAX to prevent HIV-1 infection in Thailand. *N Engl J Med* (2009) 361(23):2209–20. doi:10.1056/NEJMoa0908492
2. McElrath MJ, Haynes BF. Induction of immunity to human immunodeficiency virus type-1 by vaccination. *Immunity* (2010) 33(4):542–54. doi:10.1016/j.immuni.2010.09.011
3. de Souza MS, Ratto-Kim S, Chuenarom W, Schuetz A, Chantakulkij S, Nuntapinit B, et al. The Thai phase III trial (RV144) vaccine regimen induces T cell responses that preferentially target epitopes within the V2 region of HIV-1 envelope. *J Immunol* (2012) 188(10):5166–76. doi:10.4049/jimmunol.1102756
4. Hansen SG, Piatak M Jr, Ventura AB, Hughes CM, Gilbride RM, Ford JC, et al. Immune clearance of highly pathogenic SIV infection. *Nature* (2013) 502(7469):100–4. doi:10.1038/nature12519
5. Janes H, Friedrich DP, Krambrink A, Smith RJ, Kallas EG, Horton H, et al. Vaccine-induced gag-specific T cells are associated with reduced viremia after HIV-1 infection. *J Infect Dis* (2013) 208(8):1231–9. doi:10.1093/infdis/jit322
6. Rosenberg ES, Billingsley JM, Caliendo AM, Boswell SL, Sax PE, Kalams SA, et al. Vigorous HIV-1-specific CD4+ T cell responses associated with control of viremia. *Science* (1997) 278(5342):1447–50. doi:10.1126/science.278.5342.1447
7. Sacha JB, Giraldo-Vela JP, Buechler MB, Martins MA, Maness NJ, Chung C, et al. Gag- and Nef-specific CD4+ T cells recognize and inhibit SIV replication in infected macrophages early after infection. *Proc Natl Acad Sci U S A* (2009) 106(24):9791–6. doi:10.1073/pnas.0813106106
8. Pancre V, Delhem N, Yazdanpanah Y, Delanoye A, Delacre M, Depil S, et al. Presence of HIV-1 Nef specific CD4 T cell response is associated with non-progression in HIV-1 infection. *Vaccine* (2007) 25(31):5927–37. doi:10.1016/j.vaccine.2007.05.038
9. Ferre AL, Hunt PW, McConnell DH, Morris MM, Garcia JC, Pollard RB, et al. HIV controllers with HLA-DRB1\*13 and HLA-DQB1\*06 alleles have strong, polyfunctional mucosal CD4+ T-cell responses. *J Virol* (2010) 84(21):11020–9. doi:10.1128/JVI.00980-10
10. Ranasinghe S, Soghoian DZ, Lindqvist M, Ghebremichael M, Donaghey F, Carrington M, et al. HIV-1 antibody neutralization breadth is associated with enhanced HIV-specific CD4+ T cell responses. *J Virol* (2016) 90(5):2208–20. doi:10.1128/JVI.02278-15
11. Soghoian DZ, Jessen H, Flanders M, Sierra-Davidson K, Cutler S, Pertel T, et al. HIV-specific cytolytic CD4 T cell responses during acute HIV infection predict disease outcome. *Sci Transl Med* (2012) 4(123):123ra25. doi:10.1126/scitranslmed.3003165
12. Lusso P. HIV and the chemokine system: 10 years later. *EMBO J* (2006) 25(3):447–56. doi:10.1038/sj.emboj.7600947
13. Boaz MJ, Waters A, Murad S, Easterbrook PJ, Vyakarnam A. Presence of HIV-1 Gag-specific IFN-gamma+IL-2+ and CD28+IL-2+ CD4 T cell responses is associated with nonprogression in HIV-1 infection. *J Immunol* (2002) 169(11):6376–85. doi:10.4049/jimmunol.169.11.6376
14. Ranasinghe S, Cutler S, Davis I, Lu R, Soghoian DZ, Qi Y, et al. Association of HLA-DRB1-restricted CD4(+) T cell responses with HIV immune control. *Nat Med* (2013) 19(7):930–3. doi:10.1038/nm.3229
15. Virgin HW, Walker BD. Immunology and the elusive AIDS vaccine. *Nature* (2010) 464(7286):224–31. doi:10.1038/nature08898
16. Fonseca SG, Coutinho-Silva A, Fonseca LA, Segurado AC, Moraes SL, Rodrigues H, et al. Identification of novel consensus CD4 T-cell epitopes from clade B HIV-1 whole genome that are frequently recognized by HIV-1 infected patients. *AIDS* (2006) 20(18):2263–73. doi:10.1097/01.aids.0000253353.48331.5f
17. Rosa DS, Ribeiro SP, Fonseca SG, Almeida RR, Santana VC, Apostolico JdeS, et al. Multiple approaches for increasing the immunogenicity of an epitope-based anti-HIV vaccine. *AIDS Res Hum Retroviruses* (2015) 31(11):1077–88. doi:10.1089/AID.2015.0101
18. Ribeiro SP, Rosa DS, Fonseca SG, Mairena EC, Postol E, Oliveira SC, et al. A vaccine encoding conserved promiscuous HIV CD4 epitopes induces broad T cell responses in mice transgenic to multiple common HLA class II molecules. *PLoS One* (2010) 5(6):e11072. doi:10.1371/journal.pone.0011072
19. Rosa DS, Ribeiro SP, Almeida RR, Mairena EC, Postol E, Kalil J, et al. A DNA vaccine encoding multiple HIV CD4 epitopes elicits vigorous polyfunctional, long-lived CD4+ and CD8+ T cell responses. *PLoS One* (2011) 6(2):e16921. doi:10.1371/journal.pone.0016921
20. Wedrychowicz H. Antiparasitic DNA vaccines in 21st century. *Acta Parasitol* (2015) 60(2):179–89. doi:10.1515/ap-2015-0026
21. Kutzler MA, Weiner DB. DNA vaccines: ready for prime time? *Nat Rev Genet* (2008) 9(10):776–88. doi:10.1038/nrg2432
22. Rosa DS, Apostolico JdeS, Boscardin SB. DNA vaccines: how much have we accomplished in the last 25 years? *J Vaccines Vaccin* (2015) 6:283. doi:10.4172/2157-7560.10000283
23. Merad M, Sathe P, Helft J, Miller J, Mortha A. The dendritic cell lineage: ontogeny and function of dendritic cells and their subsets in the steady state and the inflamed setting. *Annu Rev Immunol* (2013) 31:563–604. doi:10.1146/annurev-immunol-020711-074950
24. Shortman K, Liu YJ. Mouse and human dendritic cell subtypes. *Nat Rev Immunol* (2002) 2(3):151–61. doi:10.1038/nri746
25. Dudziak D, Kamphorst AO, Heidkamp GF, Buchholz VR, Trumppheller C, Yamazaki S, et al. Differential antigen processing by dendritic cell subsets in vivo. *Science* (2007) 315(5808):107–11. doi:10.1126/science.1136080
26. Hawiger D, Inaba K, Dorsett Y, Guo M, Mahnke K, Rivera M, et al. Dendritic cells induce peripheral T cell unresponsiveness under steady state conditions in vivo. *J Exp Med* (2001) 194(6):769–79. doi:10.1084/jem.194.6.769
27. Bonifaz LC, Bonnyay DP, Charalambous A, Darguste DI, Fujii S, Soares H, et al. In vivo targeting of antigens to maturing dendritic cells via the DEC-205 receptor improves T cell vaccination. *J Exp Med* (2004) 199(6):815–24. doi:10.1084/jem.20032220
28. Boscardin SB, Hafalla JC, Masilamani RF, Kamphorst AO, Zebroski HA, Rai U, et al. Antigen targeting to dendritic cells elicits long-lived T cell help for antibody responses. *J Exp Med* (2006) 203(3):599–606. doi:10.1084/jem.20051639
29. Tewari K, Flynn BJ, Boscardin SB, Kastenmueller K, Salazar AM, Anderson CA, et al. Poly(I:C) is an effective adjuvant for antibody and multi-functional CD4+ T cell responses to *Plasmodium falciparum* circumsporozoite protein (CSP) and alphaDEC-CSP in non human primates. *Vaccine* (2010) 28(45):7256–66. doi:10.1016/j.vaccine.2010.08.098
30. Rampazo EV, Amorim KN, Yamamoto MM, Panatieri RH, Rodrigues MM, Boscardin SB. Antigen targeting to dendritic cells allows the identification of a CD4 T-cell epitope within an immunodominant *Trypanosoma cruzi* antigen. *PLoS One* (2015) 10(2):e0117778. doi:10.1371/journal.pone.0117778
31. Silva-Sánchez A, Meza-Perez S, Flores-Langarica A, Donis-Maturano L, Estrada-Garcia I, Calderon-Amador J, et al. ESAT-6 targeting to DEC205+ antigen presenting cells induces specific-T cell responses against ESAT-6 and reduces pulmonary infection with virulent *Mycobacterium tuberculosis*. *PLoS One* (2015) 10(4):e0124828. doi:10.1371/journal.pone.0124828
32. Trumppheller C, Caskey M, Nchinda G, Longhi MP, Mizenina O, Huang Y, et al. The microbial mimic poly IC induces durable and protective CD4+ T cell immunity together with a dendritic cell targeted vaccine. *Proc Natl Acad Sci U S A* (2008) 105(7):2574–9. doi:10.1073/pnas.0711976105
33. Trumppheller C, Finke JS, Lopez CB, Moran TM, Moltedo B, Soares H, et al. Intensified and protective CD4+ T cell immunity in mice with anti-dendritic cell HIV gag fusion antibody vaccine. *J Exp Med* (2006) 203(3):607–17. doi:10.1084/jem.20052005
34. Ruane D, Do Y, Brane L, Garg A, Bozzacco L, Kraus T, et al. A dendritic cell targeted vaccine induces long-term HIV-specific immunity within the gastrointestinal tract. *Mucosal Immunol* (2016) 9(5):1340–52. doi:10.1038/mi.2015.133
35. Henriques HR, Rampazo EV, Goncalves AJ, Vicentini EC, Amorim JH, Panatieri RH, et al. Targeting the non-structural protein 1 from dengue virus to a dendritic cell population confers protective immunity to lethal virus challenge. *PLoS Negl Trop Dis* (2013) 7(7):e2330. doi:10.1371/journal.pntd.0002330
36. Idoyaga J, Lubkin A, Fiorese C, Lahoud MH, Caminschi I, Huang Y, et al. Comparable T helper 1 (Th1) and CD8 T-cell immunity by targeting HIV gag p24 to CD8 dendritic cells within antibodies to Langerin, DEC205, and Clec9A. *Proc Natl Acad Sci U S A* (2011) 108(6):2384–9. doi:10.1073/pnas.1019547108
37. Cheong C, Choi JH, Vitale L, He LZ, Trumppheller C, Bozzacco L, et al. Improved cellular and humoral immune responses in vivo following targeting of HIV Gag to dendritic cells within human anti-human DEC205 monoclonal antibody. *Blood* (2010) 116(19):3828–38. doi:10.1182/blood-2010-06-288068

38. Nchinda G, Amadu D, Trumpheller C, Mizenina O, Uberla K, Steinman RM. Dendritic cell targeted HIV gag protein vaccine provides help to a DNA vaccine including mobilization of protective CD8+ T cells. *Proc Natl Acad Sci U S A* (2010) 107(9):4281–6. doi:10.1073/pnas.1000621107
39. Ratto-Kim SCJ, Cox JH, Excler JL, Valencia-Micolta A, Thelian D, Lo V, et al. Heterologous prime-boost regimens using rAd35 and rMVA vectors elicit stronger cellular immune responses to HIV proteins than homologous regimens. *PLoS One* (2012) 7(9):e45840. doi:10.1371/journal.pone.0045840
40. Iyer SS, Gangadhara S, Victor B, Shen X, Chen X, Nabi R, et al. Virus-like particles displaying trimeric simian immunodeficiency virus (SIV) envelope gp160 enhance the breadth of DNA/modified vaccinia virus ankara SIV vaccine-induced antibody responses in rhesus macaques. *J Virol* (2016) 90(19):8842–54. doi:10.1128/JVI.01163-16
41. Wille-Reece U, Flynn BJ, Lore K, Koup RA, Miles AP, Saul A, et al. Toll-like receptor agonists influence the magnitude and quality of memory T cell responses after prime-boost immunization in nonhuman primates. *J Exp Med* (2006) 203(5):1249–58. doi:10.1084/jem.20052433
42. Cabrera-Mora M, Fonseca JA, Singh B, Zhao C, Makarova N, Dmitriev I, et al. A recombinant chimeric Ad5/3 vector expressing a multistage plasmodium antigen induces protective immunity in mice using heterologous prime-boost immunization regimens. *J Immunol* (2016) 197(7):2748–61. doi:10.4049/jimmunol.1501926
43. Livingston B, Crimi C, Newman M, Higashimoto Y, Appella E, Sidney J, et al. A rational strategy to design multiepitope immunogens based on multiple Th lymphocyte epitopes. *J Immunol* (2002) 168(11):5499–506. doi:10.4049/jimmunol.168.11.5499
44. Flynn NM, Forthal DN, Harro CD, Judson FN, Mayer KH, Para MF, et al. Placebo-controlled phase 3 trial of a recombinant glycoprotein 120 vaccine to prevent HIV-1 infection. *J Infect Dis* (2005) 191(5):654–65. doi:10.1086/428404
45. Watkins DI. The hope for an HIV vaccine based on induction of CD8+ T lymphocytes – a review. *Mem Inst Oswaldo Cruz* (2008) 103(2):119–29. doi:10.1590/S0074-02762008000200001
46. Watkins DI, Burton DR, Kallas EG, Moore JP, Koff WC. Nonhuman primate models and the failure of the Merck HIV-1 vaccine in humans. *Nat Med* (2008) 14(6):617–21. doi:10.1038/nm.f.1759
47. Vaccari M, Boasso A, Ma ZM, Cecchinato V, Venzon D, Doster MN, et al. CD4+ T-cell loss and delayed expression of modulators of immune responses at mucosal sites of vaccinated macaques following SIV(mac251) infection. *Mucosal Immunol* (2008) 1(6):497–507. doi:10.1038/mi.2008.60
48. Bonifaz L, Bonnyay D, Mahnke K, Rivera M, Nussenzweig MC, Steinman RM. Efficient targeting of protein antigen to the dendritic cell receptor DEC-205 in the steady state leads to antigen presentation on major histocompatibility complex class I products and peripheral CD8+ T cell tolerance. *J Exp Med* (2002) 196(12):1627–38. doi:10.1084/jem.20021598
49. Do Y, Koh H, Park CG, Dudziak D, Seo P, Mehandru S, et al. Targeting of LcrV virulence protein from *Yersinia pestis* to dendritic cells protects mice against pneumonic plague. *Eur J Immunol* (2010) 40(10):2791–6. doi:10.1002/eji.201040511
50. Stahl-Hennig C, Eisenblatter M, Jasny E, Rzehak T, Tenner-Racz K, Trumpheller C, et al. Synthetic double-stranded RNAs are adjuvants for the induction of T helper 1 and humoral immune responses to human papillomavirus in rhesus macaques. *PLoS Pathog* (2009) 5(4):e1000373. doi:10.1371/journal.ppat.1000373
51. Soares H, Waechter H, Glaichenhaus N, Mougneau E, Yagita H, Mizenina O, et al. A subset of dendritic cells induces CD4+ T cells to produce IFN-gamma by an IL-12-independent but CD70-dependent mechanism *in vivo*. *J Exp Med* (2007) 204(5):1095–106. doi:10.1084/jem.20070176
52. Gurur C, Strowig T, Brilot F, Pack M, Trumpheller C, Arrey F, et al. Targeting the nuclear antigen 1 of Epstein-Barr virus to the human endocytic receptor DEC-205 stimulates protective T-cell responses. *Blood* (2008) 112(4):1231–9. doi:10.1182/blood-2008-03-14802
53. Owen RE, Heitman JW, Hirschhorn DF, Lanteri MC, Biswas HH, Martin JN, et al. HIV+ elite controllers have low HIV-specific T-cell activation yet maintain strong, polyfunctional T-cell responses. *AIDS* (2010) 24(8):1095–105. doi:10.1097/QAD.0b013e3283377a1e
54. Emu B, Sinclair E, Favre D, Moretto WJ, Hsue P, Hoh R, et al. Phenotypic, functional, and kinetic parameters associated with apparent T-cell control of human immunodeficiency virus replication in individuals with and without antiretroviral treatment. *J Virol* (2005) 79(22):14169–78. doi:10.1128/JVI.79.22.14169-14178.2005
55. Potter SJ, Lacabaratz C, Lambotte O, Perez-Patrigon S, Vingert B, Sinet M, et al. Preserved central memory and activated effector memory CD4+ T-cell subsets in human immunodeficiency virus controllers: an ANRS EP36 study. *J Virol* (2007) 81(24):13904–15. doi:10.1128/JVI.01401-07
56. Ferre AL, Hunt PW, Critchfield JW, Young DH, Morris MM, Garcia JC, et al. Mucosal immune responses to HIV-1 in elite controllers: a potential correlate of immune control. *Blood* (2009) 113(17):3978–89. doi:10.1182/blood-2008-10-182709
57. Corey L, Gilbert PB, Tomaras GD, Haynes BF, Pantaleo G, Fauci AS. Immune correlates of vaccine protection against HIV-1 acquisition. *Sci Transl Med* (2015) 7(310):310rv7. doi:10.1126/scitranslmed.aac7732
58. Jiang W, Swiggard WJ, Heufler C, Peng M, Mirza A, Steinman RM, et al. The receptor DEC-205 expressed by dendritic cells and thymic epithelial cells is involved in antigen processing. *Nature* (1995) 375(6527):151–5. doi:10.1038/375151a0
59. Saluja SS, Hanlon DJ, Sharp FA, Hong E, Khalil D, Robinson E, et al. Targeting human dendritic cells via DEC-205 using PLGA nanoparticles leads to enhanced cross-presentation of melanoma-associated antigen. *Int J Nanomedicine* (2014) 9:5231–46. doi:10.2147/IJN.S66639
60. Cruz LJ, Rosalia RA, Kleinovink JW, Rueda F, Lowik CW, Ossendorp F. Targeting nanoparticles to CD40, DEC-205 or CD11c molecules on dendritic cells for efficient CD8(+) T cell response: a comparative study. *J Control Release* (2014) 192:209–18. doi:10.1016/j.jconrel.2014.07.040
61. Kastenmuller W, Kastenmuller K, Kurts C, Seder RA. Dendritic cell-targeted vaccines – hope or hype? *Nat Rev Immunol* (2014) 14(10):705–11. doi:10.1038/nri3727
62. Costa M, Pollara J, Edwards RW, Seaman M, Gorny MK, Montefiori D, et al. Fc receptor mediated activities by Env-specific human mAbs generated from volunteers receiving the DNA prime-protein boost HIV vaccine DP6-001. *J Virol* (2016) 90(22):10362–78. doi:10.1128/JVI.01458-16
63. Woodland DL. Jump-starting the immune system: prime-boosting comes of age. *Trends Immunol* (2004) 25(2):98–104. doi:10.1016/j.it.2003.11.009
64. Lu S. Combination DNA plus protein HIV vaccines. *Springer Semin Immunopathol* (2006) 28(3):255–65. doi:10.1007/s00281-006-0028-1
65. Flynn BJ, Kastenmuller K, Wille-Reece U, Tomaras GD, Alam M, Lindsay RW, et al. Immunization with HIV Gag targeted to dendritic cells followed by recombinant New York vaccinia virus induces robust T-cell immunity in nonhuman primates. *Proc Natl Acad Sci U S A* (2011) 108(17):7131–6. doi:10.1073/pnas.1103869108
66. Sekaly RP. The failed HIV Merck vaccine study: a step back or a launching point for future vaccine development? *J Exp Med* (2008) 205(1):7–12. doi:10.1084/jem.20072681
67. Wilson NA, Keel BF, Reed JS, Piaskowski SM, MacNair CE, Bett AJ, et al. Vaccine-induced cellular responses control simian immunodeficiency virus replication after heterologous challenge. *J Virol* (2009) 83(13):6508–21. doi:10.1128/JVI.00272-09
68. Martins MA, Wilson NA, Reed JS, Ahn CD, Klimentidis YC, Allison DB, et al. T-cell correlates of vaccine efficacy after a heterologous simian immunodeficiency virus challenge. *J Virol* (2010) 84(9):4352–65. doi:10.1128/JVI.02365-09
69. Corey L, McElrath MJ, Kublin JG. Post-step modifications for research on HIV vaccines. *AIDS* (2009) 23(1):3–8. doi:10.1097/QAD.0b013e32830e6d6d

**Conflict of Interest Statement:** The authors declare that the research was conducted in the absence of any commercial or financial relationships that could be construed as a potential conflict of interest.

Copyright © 2017 Apostólico, Lunardelli, Yamamoto, Souza, Cunha-Neto, Boscardin and Rosa. This is an open-access article distributed under the terms of the Creative Commons Attribution License (CC BY). The use, distribution or reproduction in other forums is permitted, provided the original author(s) or licensor are credited and that the original publication in this journal is cited, in accordance with accepted academic practice. No use, distribution or reproduction is permitted which does not comply with these terms.



# A Perspective on the Development of Plant-Made Vaccines in the Fight against Ebola Virus

Sergio Rosales-Mendoza<sup>1\*</sup>, Ricardo Nieto-Gómez<sup>1</sup> and Carlos Angulo<sup>2\*</sup>

<sup>1</sup>Laboratorio de Biofarmacéuticos Recombinantes, Facultad de Ciencias Químicas, Universidad Autónoma de San Luis Potosí, San Luis Potosí, San Luis Potosí, Mexico, <sup>2</sup>Grupo de Inmunología & Vacunología, Centro de Investigaciones Biológicas del Noroeste, SC., La Paz, Baja California Sur, Mexico

## OPEN ACCESS

### Edited by:

Daniela Santoro Rosa,  
Federal University of São Paulo,  
Brazil

### Reviewed by:

Tomasz Pniewski,  
Institute of Plant Genetics (PAN),  
Poland

Chad Edward Mire,  
University of Texas Medical Branch,  
USA

### \*Correspondence:

Sergio Rosales-Mendoza  
rosales.s@fcq.uaslp.mx;  
Carlos Angulo  
eangulo@cibnor.mx

### Specialty section:

This article was submitted to  
Vaccines and Molecular  
Therapeutics,  
a section of the journal  
*Frontiers in Immunology*

Received: 27 October 2016

Accepted: 20 February 2017

Published: 10 March 2017

### Citation:

Rosales-Mendoza S, Nieto-Gómez R and Angulo C (2017) A Perspective on the Development of Plant-Made Vaccines in the Fight against Ebola Virus.

Front. Immunol. 8:252.

doi: 10.3389/fimmu.2017.00252

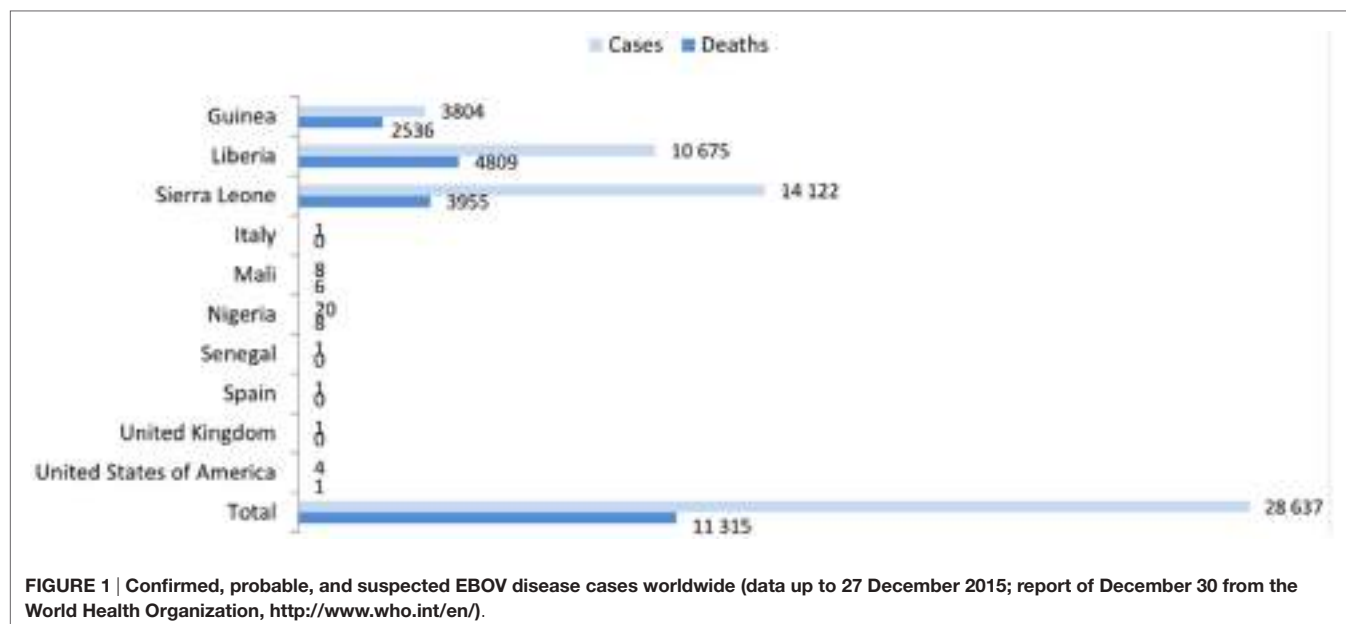
The Ebola virus (EBOV) epidemic indicated a great need for prophylactic and therapeutic strategies. The use of plants for the production of biopharmaceuticals is a concept being adopted by the pharmaceutical industry, with an enzyme for human use currently commercialized since 2012 and some plant-based vaccines close to being commercialized. Although plant-based antibodies against EBOV are under clinical evaluation, the development of plant-based vaccines against EBOV essentially remains an unexplored area. The current technologies for the production of plant-based vaccines include stable nuclear expression, transient expression mediated by viral vectors, and chloroplast expression. Specific perspectives on how these technologies can be applied for developing anti-EBOV vaccines are provided, including possibilities for the design of immunogens as well as the potential of the distinct expression modalities to produce the most relevant EBOV antigens in plants considering yields, posttranslational modifications, production time, and downstream processing.

**Keywords:** Ebola virus, mucosal immunization, low-cost vaccine, global vaccination, molecular pharming, glycoprotein antigen, VP antigen

## INTRODUCTION

The last *Zaire Ebola virus* (EBOV) epidemic outbreak in Guinea, which began in December 2013, quickly spread and six West-African countries were greatly affected (Guinea, Liberia, Sierra Leone, Mali, Nigeria, and Senegal). There have also been reports of cases within health-care workers from the USA, Spain, and the United Kingdom. Fortunately, the overall case incidence has dropped, and no reports on confirmed cases during the last week of December 2015 were generated. Nonetheless, according to a report on December 27, 2015, there have been 25,637 confirmed, probable, or suspected cases of EBOV disease (EVD) in Guinea, Liberia, and Sierra Leone (Figure 1), with over 11,000 reported deaths, which surpasses all previous EBOV outbreaks combined (World Health Organization<sup>1</sup>). Therefore, the EBOV constitutes an imminent and serious threat to public health, as well as a potential bioterrorism agent (1). EBOV represents one of the three genera composed of the family Filoviridae (2). The EBOV genus comprises five species: (1) *Sudan ebolavirus* (SUDV), (2) *Zaire ebolavirus* (ZEBOV), (3) *Côte d'Ivoire ebolavirus* (also known as Ivory Coast ebolavirus or Tai Forest ebolavirus, TAFV), (4) *Reston ebolavirus* (RESTV), and (5) *Bundibugyo ebolavirus*. All of these

<sup>1</sup><http://www.who.int/en/>.



species, with the exception of the RESTV, have shown to cause disease in human beings (3, 4). After an incubation period of 3–21 days, the EVD generally progresses quickly, with symptoms of fever, diarrhea, vomiting, systemic inflammatory response syndrome, organ dysfunction, and hemorrhagic manifestations that end in death (5).

Despite the substantial efforts made to develop rational prophylactic and chemotherapeutic interventions, no licensed countermeasures are available for the treatment of EVD as of now. EBOV is introduced into the human population through close contact with bodily fluids of infected animals such as primates and fruit bats. EBOV then spreads through human-to-human transmission *via* direct contact (through broken skin or mucous membranes) with bodily fluids of infected people. Therefore, most efficient measures to control the EVD spread consist of the isolation of patients establishing strict barrier nursing procedures to protect health-care workers (5). Looking at this situation, the development of effective therapeutics for the prevention and treatment of EBOV infections is urgently needed. In the case of immunotherapies, achieving broad and long-lasting humoral immunity at the mucosa and systemic levels against many EBOV species as possible is a key goal (6). The most advanced immunotherapy against EVD is ZMapp (Mapp Biopharmaceutical, San Diego, CA, USA), a drug consisting of humanized monoclonal antibodies (mAbs) capable of neutralizing the EBOV. This treatment, based on passive immunity, has been successful in non-human primates (NHPs) and efforts for its licensing and introduction into the market are ongoing (7). ZMapp has already been used on a compassionate basis to treat a few patients of EVD; however, the clinical efficacy of this specific cocktail as a treatment of EVD in humans remains uncertain (8). Vaccination is the ideal approach to fight this disease since prophylaxis could be achieved through the administration of a minimum number of doses. Vaccinology offers a myriad of possibilities for the development of vaccines

against EBOV, and according to the ClinicalTrials.gov database,<sup>2</sup> 47 studies of Ebola vaccine trials have been registered. One of the biggest challenges in achieving global vaccination is developing production platforms accessible to developing countries. For instance, protein subunit vaccines are obtained, distributed, and administered through processes requiring complex downstream steps, cold chain, and delivery systems that involve specialized personnel and equipment. All of these aspects hamper vaccination availability and usage in developing countries. Therefore, the next-generation platforms for vaccine production, distribution, and delivery have been proposed to develop low-cost and broad coverage vaccination strategies. In this context, plant-based platforms constitute an attractive technology with the following attributes: (i) since the use of sophisticated bioreactors and complex downstream processing are avoided, the cost of a plant-derived product is 10–50 times lower than products derived from the fermentation with *Escherichia coli* (9) and 140 times lower when compared to baculovirus-infected insect cells (10); (ii) high biosynthetic capacity derived from a machinery that performs folding, assembly, and glycosylation; (iii) the plant systems offer high safety in the sense that they are not hosts of human or animal pathogens, in contrast to mammalian-based production systems where the risk of contamination with viruses and prions exists. Moreover, many plant tissues and fruits are safe for human consumption and thus can be used as oral delivery vehicles for vaccines, thereby avoiding the purification and processing required for conventional injectable vaccines. Therefore, plant-made oral vaccines can be easily formulated with freeze-dried plant material, which not only increases antigen concentration but also produces a material stable at room temperature avoiding the cold chain maintenance required for other delivery systems (11). This

<sup>2</sup><https://clinicaltrials.gov>

perspective constitutes the ideal case for vaccine development, and it has been consolidated in recent years with the successful delivery of many vaccines and other biopharmaceuticals by the oral route in test animals (12–14). The technology of plant-based vaccines and the current advances have been recently reviewed by distinct groups (15–17). During the last years, clinical trials have been conducted to evaluate the immunogenicity and safety of influenza virus vaccines with positive outcomes (18–21), which has stimulated the interest of the pharmaceutical industry in these platforms (**Table 1**).

In this review, the use of the technology of plant-based vaccines to develop attractive EBOV vaccines is placed in perspective. After describing the molecular approaches to express antigens in the plant cell, the relevant aspects of EBOV as well as conventional vaccines under development were summarized; finally, the perspectives on how plant systems may lead to EBOV vaccines are identified and discussed.

## CURRENT EXPERIMENTAL VACCINES TO FIGHT EBOV

While the precise mechanisms for immune protection against the EBOV infection are likely complex, it is noteworthy that vaccination against the EBOV surface glycoprotein (GP) is both necessary and sufficient for protection against virus infection as has been evidenced by several successful vaccination approaches (23, 24). This evidence suggests an important role of the GP in virus survival within the host. Several studies have pointed out that the humoral responses induced by these vaccines are strongly associated with protection (25–27), although some reports have clearly demonstrated that the cellular response aided in infection clearance as well (28).

The most advanced vaccines against EBOV are based on the viral GP that has demonstrated protection against EBOV in NHPs. It is important to point out that in 2002, the US Food and Drug Administration introduced the “animal rule” concept that aims to facilitate the licensing of vaccine or drug treatments against infection by the EBOV as well as other highly lethal human pathogens for which the efficacy evaluation in human beings would be unethical and field trials unreasonable (29). The application of the “animal rule” allows for the approval of any EBOV vaccine candidate based on efficacy testing in animal models, with defined immune correlates of protection, as well as

Phase I and II clinical trials for safety and immunogenicity testing in human beings. Therefore, the development of animal models is critical for the evaluation and eventual approval of EBOV vaccine candidates. Promising animal models for investigating EBOV vaccines include Guinea pig (30), mouse (31), Syrian Golden hamster (32), marmoset (33), and ferret (34, 35). However, NHP models of EBOV infection, especially the model of cynomolgus macaques, have a stronger predictive value for human diseases and immune protection, and thus, it is the preferred model for EBOV vaccine development (24). Therefore, this review will focus on the most advanced vaccines that have been tested in NHPs and clinical trials. New promising vaccine candidates evaluated using other animal models will be mentioned briefly.

Overall, the candidate vaccines against the EBOV developed thus far can be divided into three categories: non-replicative expressing vector-based vaccines, replication-competent viral vector-based vaccines, and viral antigen-based vaccines (36). Most of the successful vaccines against the EVD rely on viral vectors in whose genome the EBOV GP gene was introduced (37). The vector-based vaccines have been evaluated in NHP and in clinical trials, whose outcomes are summarized in the following sections. Viruses used as vaccine vectors include vesicular stomatitis virus (VSV) (38), recombinant adenovirus replicons (39), recombinant parainfluenza virus (40), recombinant rabies virus (RABV) (41), and recombinant Venezuelan equine encephalitis virus (VEEV) (42). Protein-based vaccines such as virus-like particles (VLPs) have also demonstrated EVD protection in NHPs, but the characterization of most of the candidates has been performed in small animal models (43, 44). A general overview on the progress achieved for each type of vaccine is described in the following sections.

### Non-Replicative Vector-Based Vaccines

Sullivan et al. (45) reported the first proof of concept on protection against EBOV infection by vaccination. The study revealed that priming with an EBOV GP DNA vaccine followed by boosting with a recombinant adenovirus-5 replicon expressing GP conferred complete protection against a lethal EBOV challenge in NHPs. Although promising and safe for human beings, the use of the most advanced adenovirus 5 replicon-based vaccine faces the problem of pre-existing immunity against the viral vector as well as a relatively low immunogenicity in human beings, since the antibody titers against GP were less than 300, while titers of

**TABLE 1 | Evaluations of plant-made vaccines in clinical trials reported over the last years.**

Target disease	Antigen	Expression platform	Outcomes	Reference
Influenza virus, 2009 pandemic A/California/04/2009 (H1N1) strain	Hemagglutinin	Plant virus-based transient expression technology in <i>Nicotiana benthamiana</i> plants	Safety and immunogenicity of the plant-produced subunit H1N1 influenza vaccine was proven. No serious adverse effects were observed	Cummings et al. (20)
Influenza virus, A/Indonesia/05/2005 (H5N1) strain	Hemagglutinin	Plant virus-based transient expression technology in <i>N. benthamiana</i> plants	Safety and immunogenicity of the plant-produced subunit H5N1 influenza vaccine was proven. No serious adverse effects were observed	Chichester et al. (19)
H1N1 A/California/7/09 (H1) or H5N1 A/Indonesia/5/05 (H5)	Hemagglutinin	Plant virus-based transient expression technology in <i>N. benthamiana</i> plants	Besides strong antibody responses, both vaccines elicited significantly greater poly-functional CD4(+) T cell responses H1 vaccine induced poly-functional CD8(+) T cell responses	Landry et al. (22)

2,000 are associated with the protection of NHPs (46). An interesting alternative that may solve the problem derived from the pre-existing immunity against the vaccination vector consists in the use of Chimpanzee adenovirus-based vaccines (47).

Another encouraging example is a VEEV replicon that has been employed for EBOV vaccine development. VEEV replicons expressing EBOV GP and *Sudan ebolavirus* (SUDV) GP protected NHPs against a lethal EBOV as well as SUDV challenge when administered a single [ $1 \times 10^{10}$  focus-forming units (FFU)] simultaneous intramuscular vaccination (42). However, similar to adenovirus replicons, the requirement of high vaccine doses and a pre-existing immunity to VEEV will likely be the major obstacles for human application of this kind of vaccine. A mutant form of the EBOV, without the VP30 gene that is required for virus replication, was evaluated in mice and guinea pigs, and it was shown to confer complete protection against a lethal EBOV challenge after two immunizations (48). Moreover, the efficacy of this new replication-defective viral vector-based vaccine was also confirmed to confer immunoprotection in NHPs when administered by the intraperitoneal route twice at 3-week intervals with  $1 \times 10^6$  FFU of Ebola ΔVP30 virus. However, this approach raised concerns with respect to virulence reversion, and thus, a new version of the vaccine consisted of the virus inactivated with hydrogen peroxide was generated, which remained antigenic and protective in NHPs when administered intramuscularly ( $1 \times 10^7$  FFU) one or two times with a 4-week interval (49).

Two replication-incompetent vectored vaccines have reached Phase III clinical trials: human adenovirus serotype 26 (Ad26) expressing the Ebola virus Mayinga variant GP (Ad26.ZEBOV) and Modified Vaccinia Virus Ankara-Bavarian Nordic Filo-vector (MVA-BN-Filo). Remarkably, Ad26.ZEBOV and MVA-BN-Filo vaccines resulted in sustained elevation of specific immunity, and no vaccine-related serious adverse events were observed in Phase I clinical trial. In this evaluation, the vaccinated (i.m.) groups were (1) with MVA-BN-Filo as prime vaccine on day 1 boosted by Ad26.ZEBOV on day 29 or day 57; and (2) with a priming dose of Ad26.ZEBOV boosted by MVA-BN-Filo on day 29 or day 57 (50). Therefore, Phases II and III were pursued. Moreover, the Phase IV, named “Long-term Safety Follow-up of Participants Exposed to the Candidate Ebola Vaccines Ad26.ZEBOV and/or MVA-BN-Filo” is active but not open for participant recruitment yet.

## Replication-Competent Viral Vector-Based Vaccines

This category includes rhabdovirus-based viral vectors, including the VSV and RABV, and paramyxovirus-based vectors such as recombinant human parainfluenza virus 3 (HPIV3) expressing EBOV GP separately or in combination with nucleoprotein (NP). The potential of this kind of vaccine platform was shown when the recombinant VSV expressing the GPs of ZEBOV (strain Mayinga) was generated using the infectious clone for the VSV Indiana serotype. A single intramuscular immunization, measured in plaque-forming units (PFU) of the virus particles, of cynomolgus macaques ( $1 \times 10^7$  PFU) demonstrated to protect NHPs against a lethal challenge ( $1 \times 10^3$  PFU) of ZEBOV (strain Kikwit) isolated from a patient from the 1995 EBOV outbreak in

Kikwit (38). Similarly, Marzi et al. (51) found complete protection of NHPs against ZEBOV (strain Makona) following the administration of a single dose given as late as 7 days before challenge in VSV-EBOV GP vaccinated animals. Looking to explore practical delivery routes, effective protection of NHPs was observed when the vaccine was administered either orally or intranasally with the subsequent EBOV challenge (52, 53). These findings opened the path to explore mucosal vaccination as a feasible strategy in combating the EVD. Furthermore, this vaccine platform showed potential as an early treatment since it induced beneficial effects in NHPs infected with the EBOV (54) and in individuals who have experienced incidental exposure or high-risk occupational exposure to the EBOV such as a needle stick handling (55, 56). Interestingly, a single intramuscular immunization ( $1 \times 10^7$  PFU in the caudal thigh) of the full-length parent RABV vaccine expressing the EBOV GP also conferred complete protection in rhesus macaques after a challenge with 1,000 PFU of the EBOV (strain Mayinga). However, its potency was lower when compared to recombinant VSV-based vaccines (41), such as the attenuated vesiculovax recombinant VSV-based vaccines expressing the EBOV GP, which protects macaques from a lethal challenge after a single dose (57). Another vaccine platform uses a paramyxovirus-based vector, such as the recombinant HPIV3 expressing EBOV GP alone or in combination with NP. These vaccines were constructed by inserting a transcription cassette encoding the EBOV (Mayinga strain) GP gene between the HPIV3 P and M genes alone or in combination with a cassette encoding the NP inserted between the HPIV3 HN and L genes. Rhesus monkeys were protected against the EBOV infection after receiving two doses of  $2 \times 10^7$  tissue culture infectious dose (TCID50) (days 0 and 28) of combined intranasal and intratracheal inoculation and an intraperitoneal challenge on day 67 (39 days following the second vaccine dose) with 1,000 PFU of the EBOV (Zaire species, Mayinga strain) (40). This study reinforces the practical feasibility of immunization against the EVD via the respiratory tract (58). However, since these vaccine platforms are replication competent, their side effects for human vaccination is a major concern and merits further research. Recently, Phase I and II clinical trials have been conducted, and the results showed that rVSV-ZEBOV is immunogenic but also mild to moderate reactogenic. rVSV-ZEBOV used at  $1-5 \times 10^7$  PFU (Phase I) provoke fever (25%) and oligoarthritis (22%) in vaccinated volunteers (6). A reduced dose of  $3 \times 10^5$  (Phase II) PFU decreases viremia and reactogenicity but also antibody response levels without reducing the risk of vaccine-induced side effects (59). Remarkably, a Phase III trial in Guinea highlighted that the rVSV-ZEBOV is highly efficacious when administered in a single  $2 \times 10^7$  PFU dose (estimated vaccine efficacy of 100%) and safe in preventing the EVD, while the assessment of vaccine-derived adverse events revealed promising outcomes (2 serious adverse events in 5,837 vaccinees) (60, 61).

## Viral Protein/DNA-Based Vaccines

Konduru et al. (62) provided the first proof of concept that a subunit vaccine based on purified GP could elicit protective immune responses against the EBOV. In their study, a ZEBOV GP-Fc fusion protein was constructed coding for the C-terminal

end (1–637 aa) of the extracellular domain from the ZEBOV GP (Mayinga strain) and the crystallizable fragment (Fc) from human IgG1. The ZEBOV GP-Fc protein fusion was produced in transfected Chinese hamster ovary cells. C57BL/6 mice were intraperitoneally vaccinated (i.p.) with 100 µg of purified ZEBOVGP-Fc in complete Freund's adjuvant and boosts (25 µg in incomplete Freund's adjuvant) were administered at 21, 45, and 60 days post-priming. A 90% of protection in the vaccinated mice was achieved after a lethal challenge by i.p. injection with 1,000 PFU of mouse-adapted ZEBOV. Similar results were obtained by Phoolcharoen et al. (63) in which the GP was fused to a mAb that recognizes an epitope in the GP, resulting in the production of EBOV immune complexes (EICs). Remarkably, the EICs were produced in *Nicotiana benthamiana* plants by transient expression. The purified EICs were tested in mice, administered by the subcutaneous route four times on days 0, 21, 42, and 63, and the immunogenic properties determined. Although antigen–antibody immune complexes were efficiently processed and presented to immune effector cells, they found that co-delivery of the EIC with toll-like receptor (TLR) agonists elicited a more robust antibody response in mice than the EICs alone. Among the compounds tested, polyinosinic:polycytidylic acid (poly I:C, a TLR-3 agonist) was highly effective as an adjuvant. After vaccinating mice with EIC plus poly I:C, 80% of the animals were protected against a lethal challenge with live EBOV. These results are encouraging but further research is needed to optimize the immunogenicity of this vaccine and test its efficacy in NHP models with the subsequent determination of its safety in clinical trials. Another viral antigen-based vaccine strategy is the use of VLP that can direct the target antigen to antigen presenting cells, such as dendritic cells, stimulating antibody, and cellular immune responses. Interestingly, three i.m. immunizations at 42-day intervals with enveloped EBOV VLPs containing the EBOV GP, NP, and VP40 matrix protein, along with RIBI adjuvant, conferred protection to NHPs against a lethal challenge with EBOV, thus providing the first evidence that protective immunity can be elicited by non-viral vector-based vaccines in NHPs (43). Moreover, the versatility of VLPs should be noted that they can either be used as carriers of immune-stimulating molecules or enriched with chimeric EBOV GP carrying additional epitopes as an approach to enhance immune responses.

It is also important to note that the results on three DNA vaccines (INO-4201, -4202, and -4212) and one recombinant protein subunit vaccine (EBOV GP1,2 with Matrix-M) have not been published yet and probably will bring new perspectives in the race of developing new Ebola vaccines (64). DNA vaccines expressing the EBOV GP have also been tested in human beings during Phase I clinical trials with safe and immunogenic properties when applied under a scheme comprising three i.m. doses (2, 4, and 8 mg) on days 0, 28, and 56 (65) and an homologous boost (2 mg) at week 32 or after (66).

## PERSPECTIVES FOR EBOV VACCINE DEVELOPMENT

Despite the milestone of establishing durable protection against the EBOV, future developments are required to increase qualitative

or quantitative resolution of the protective and non-protective humoral immune responses (67). Two encouraging vaccines based on GP have been evaluated under Phase I and Phase II clinical trials (**Table 2**) showing durable protection in the cynomolgus macaque model (47, 68, 69). Based on promising data from the initial clinical trials, gathered in the late 2014, the WHO in combination with the Health Ministry of Guinea, Médecins Sans Frontières from Epicentre, and The Norwegian Institute of Public Health launched a Phase III trial in Guinea on March 7, 2015. This trial tested the VSV-EBOV (VSVΔG-ZEBOV-GP) vaccine for efficacy and effectiveness in preventing the EVD (60). The results indicated that the vaccine is highly efficacious and safe, and likely effective in the population when delivered during an EVD outbreak via a ring vaccination strategy (60). In addition, the plan includes testing another advanced vaccine called ChAd3 (ChAd3-ZEBOV-GP; GSK). The follow-up study to compare the safety and efficacy of the ChAd3 Ebola Zaire and VSVΔG-ZEBOV-GP virus vaccines through Phase II/III clinical trials in volunteers from Liberia led to promising results upon the first 4 months, and serious adverse effects were not reported (24, 64, 70). ChAd3 is an example that the current EBOV vaccines require cell-based production and storage at low temperature, thereby creating obstacles in scalable manufacturing and shelf-life in developing countries (67).

Overall, non-replicative vector-based vaccines face the problem of pre-existing immunity and/or the induction of anti-vector immune responses that may decrease their efficacy, while viral replication-competent vaccines face important human safety or adverse side effects concerns. By contrast, the vaccine strategies based on viral protein antigens are not affected by those issues. In this context, plant-made vaccines can be a reasonable alternative in the fight against the EVD.

## HOW COULD EBOV PLANT-BASED VACCINES BE DEVELOPED?

The key steps involved in the development of plant-made vaccine prototypes include the following: design putative functional immunogens and develop genetically engineered plants expressing the antigen or establishing viral vector-based platforms for transient expression, estimate yields and antigenic properties of the target antigen, assess the immunogenic potential of the candidate vaccine in test animals in terms of protective immunity and safety, and perform clinical trials once preclinical studies have provided acceptable outcomes (**Figure 2**).

## POSSIBILITIES FOR THE DESIGN OF IMMUNOGENS

A successful proof of concept on EBOV plant-based vaccines will include the design and production of full-length viral proteins such as GP, matrix viral protein (VP40), and NP antigens, as well as chimeric proteins carrying conserved protective epitopes capable of inducing anti-EBOV neutralizing antibodies. Examples of the latter approach include the following linear epitopes: EQHHRRRTDN, VIKLDISEA, and LITNTIAGV (25). Hopefully, the current knowledge on the protective EBOV sequences as well

**TABLE 2 | Current EBOV Food and Drug Administration-approved vaccine trials.<sup>a</sup>**

Vaccine platform	Trial type	Start date <sup>b</sup>	Location	Enrollment <sup>c</sup>	Sponsor
Chimpanzee adenovirus vector (ChAd3-ZEBOV-GP)	Phase I a/b dose escalating	2014 August	USA (Georgia and Maryland)	26	National Institute of Allergy and Infectious Diseases, USA
	Phase Ia dose escalating	2014 September	United Kingdom	60	University of Oxford, UK
	Phase I/II	2014 October	Lausanne, Switzerland	120	University of Lausanne Hospitals, Switzerland
	Phase Ib dose escalating	2014 November	Mali, Africa	40	University of Maryland, USA
Vesicular stomatitis virus vector (VSV-DG-ZEBOV-GP) (37, 53)	Phase Ia dose escalating	2014 August	USA (National Institutes of Health, Maryland)	120	NewLink Genetics, USA
	Phase Ia dose escalating	2014 October	USA (Walter Reed Army Institute of Research, Maryland)	117	NewLink Genetics, USA
	Phase I/II	2014 November	Geneva, Switzerland	115	University Hospital, Geneva, Switzerland
	Phase I	2014 November	Germany	30	Hamburg-Eppendorf, Germany
Human adenovirus serotype 26 (Ad26) expressing the Ebola virus Mayinga variant glycoprotein (GP) (Ad26.ZEBOV) and Modified Vaccinia Virus Ankara-Bavarian Nordic Filo-vector (MVA-BN Filo), in a heterologous prime-boost regimen	Phase III	2015 September	Kambia, Sierra Leone	This study is currently recruiting participants	Crucell Holland BV

<sup>a</sup>Information was collected from public records provided by the U.S. National Institutes of Health and is current as of March 2016 (<https://clinicaltrials.gov/ct2/home>).

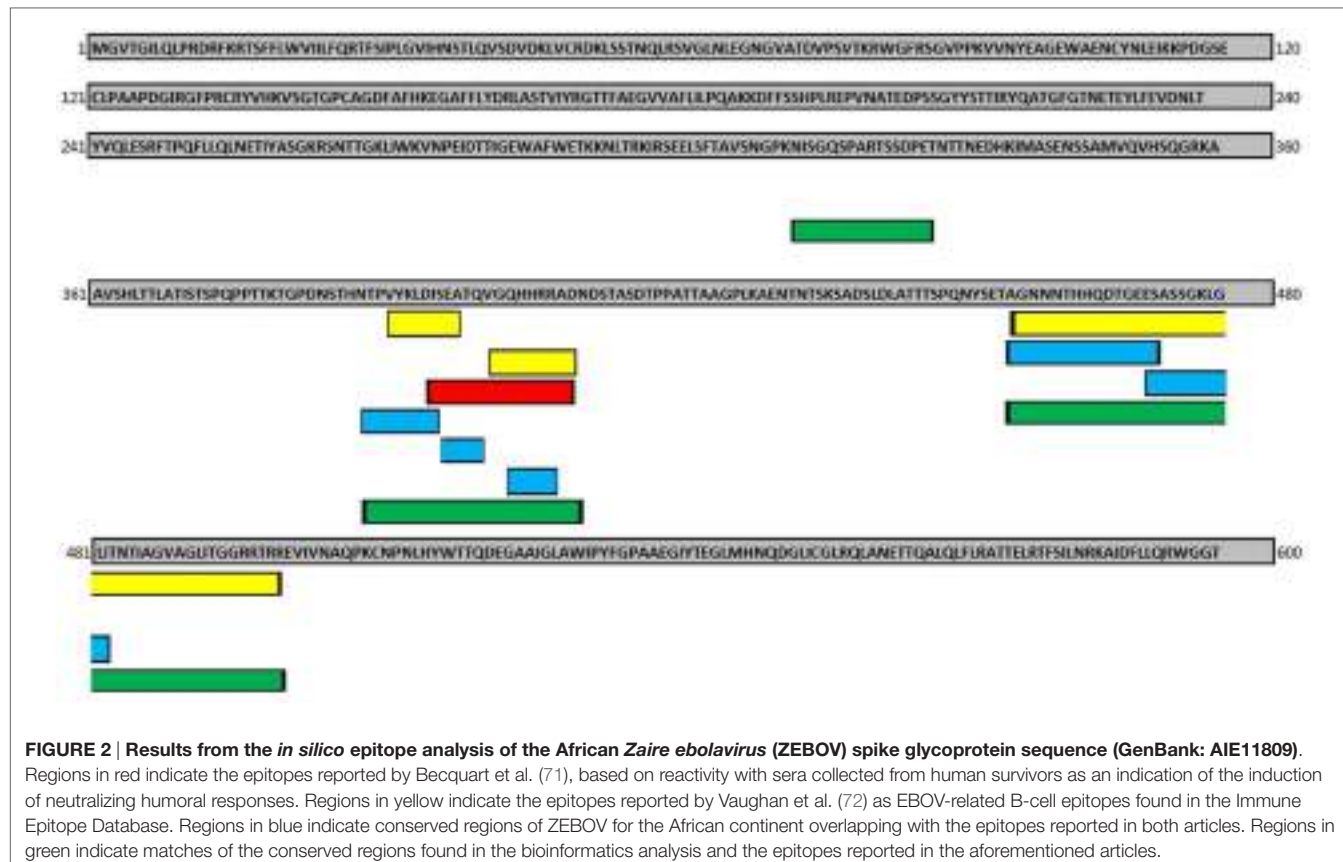
<sup>b,c</sup>May represent proposed dates and enrollments, respectively.

as the technologies to produce heterologous proteins in plant cells will accelerate the development of plant-made vaccine candidates against EBOV.

Regarding epitope vaccines, Wilson et al. (25) reported a GP epitope that is conserved among all Ebola viruses demonstrating that a specific mAb was able to protect mice from a lethal EBOV infection. Subsequently, it was found that although some EBOV GP epitopes induce an antibody-dependent enhancement of EBOV infection, antibodies against other specific EBOV GP epitopes were required to control an EBOV infection (73). Another recent study demonstrated that a linkage region (aa 393–556) of the GP (called MFL) contains a furin cleavage site and an internal fusion loop responsible for important viral functions (74). This region was the major contributor to immunogenicity in terms of the induction of humoral immune responses and neutralizing antibodies against the EBOV (75). Interestingly, the study by Becquart et al. (71), using sera from infected patients, identified specific B-cell epitopes in four EBOV proteins [GP, NP, and matrix viral protein (VP40 and VP35)]. Among them, the specific immunodominant VP40 and GP epitopes were detected by IgG antibodies from asymptomatic individuals and symptomatic Gabonese EBOV infected survivors, respectively. These findings strongly suggest that an effective epitopic subunit vaccine should induce humoral IgG responses targeting specific GP and VP40 epitopes. One interesting approach in the design of an epitope-based vaccine capable of triggering protective immune responses is the use of immunoinformatic tools. In this regard, the potential of inducing both humoral and cell-mediated immunity by T and B cells against the EBOV epitopes was recently assessed by Khan et al. (76). From the complete proteomes of EBOVs, the amino acid sequences were retrieved using UniProt Knowledge Base and bioinformatic analyses were conducted to study antigenicity,

solvent-accessible regions, surface accessibility, flexibility, MHC class-I-binding epitopes (cellular immune response), and B-cell-binding epitopes (antibody immune response) from those proteins. The *in silico* capability of each protein sequence to initiate an immune response allowed for the identification of the most promissory L protein comprise of 128 amino acids, which is also known as RNA-dependent RNA polymerase. This protein reached the highest antigenicity score in VaxiJen analysis among all the query proteins. The downstream bioinformatic analysis showed that the 9-mer epitope TLASIGTAF was the selected potential epitope-based vaccine candidate for inducing cytotoxic T cell immune responses by considering its overall epitope conservancy (76.60%), human population coverage (53–81%), and the affinity for highest number of MHC-I (HLA) molecules ( $n = 12$ ). Similarly, the L protein was evaluated to identify B cell epitopes and the 9-mer epitope PEEQEQA (spanning region from 42 to 50 amino acids) of the L protein was the most potential B cell epitope to induce antibody-mediated immune responses. However, it should be considered that L protein is the last one expressed during viral replication, and thus, a vaccine targeting only this antigen may result in low efficacy. Therefore, vaccine design should contemplate a combination of L protein epitopes with those of early proteins, such as GP. Thus, the combination of experimental data with immunoinformatic prediction approaches opens up a new horizon to design effective multiepitopic vaccines able to induce protective antibody immune responses against the EBOV. In fact, the Immune Epitope Database and Analysis Resource<sup>3</sup> has reported an integrative immunopredictive and experimental analysis for “functional epitopes.” These epitopes

<sup>3</sup>[www.iedb.com](http://www.iedb.com).

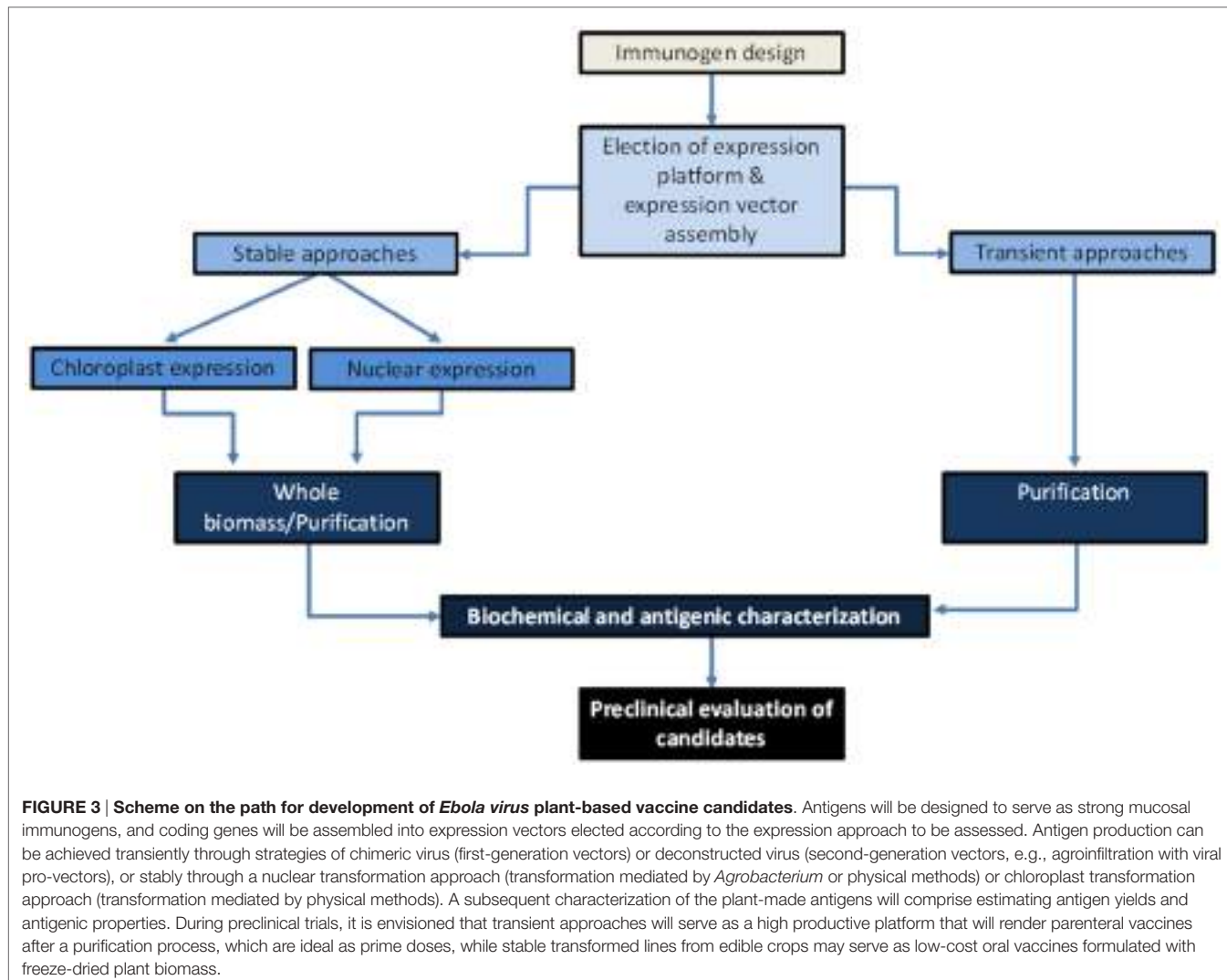


are identified using assays that demonstrate their potential to induce positive outcomes when virus neutralization assays or challenge experiments are performed. A high percentage of the selected epitopes were from the GP (55%) and NP (33%) proteins. The functional EBOV-related B cell epitopes were only found in these two proteins (72). On the other hand, an *in silico* analysis to identify EBOV conserved sequences among the EBOV variants, matching with the abovementioned functional analysis, has allowed the identification of a set of promising GP Zaire EBOV B-cell epitopes comprising the following sequence: NISGQSPARTSSDPE, NTPVYKLDISEATQVGQHHRRAD, and TAGNNNTHHQDTGEE SASSGKLGLITNTI AGVAGLI TGGRRTTR. These sequences are considered promising candidates for multiepitopic vaccine design (**Figure 3**).

Since vaccines administered through mucosal membranes, mainly by oral route, are the most convenient approach for mass vaccination, the developments in this direction are a priority. However, epitopes are not good immunogens *per se* and thus must be coupled to carrier proteins or adjuvant sequences that favor uptake and efficient antigen presentation. Antigen uptake at the mucosa can be aided by the use of transmucosal carriers, such as the B subunits from either the cholera toxin (CTB) or the enterotoxigenic *E. coli* heat-labile toxin (LTB). These proteins produce oligomeric structures that bind the GM1 ganglioside on the surface of gut epithelial cells, mediating the translocation into the submucosal compartment where the antigen can be processed by dendritic cells with the subsequent induction of

adaptive immune responses (77). These properties enable both CTB and LTB to be highly immunogenic and serve as effective carrier proteins and adjuvants for unrelated coupled antigens (78, 79). Therefore, the designed chimeric proteins, through genetic fusion, are proposed as candidates that could result in immunogens capable of inducing strong anti-EBOV antibody responses using oral immunization under the plant-based vaccine concept. This idea is also supported by the proven oral immunogenic activity of CTB- and LTB-based chimeric antigens produced in plants (79, 80). Therefore, specific EBOV epitopes in the form of CTB- or LTB-based chimeras could serve as candidates to induce immunoprotective humoral responses against the EBOV. Other strategies might include the design of chimeras comprising target epitopes and cell penetrating peptides, such as those derived from the HIV-1 Tat protein or the *Drosophila melanogaster* Antennapedia homeodomain (penetratin), which increase the cellular uptake of large molecules (81, 82).

Another attractive possibility in developing plant-based EBOV vaccines could be based on VLPs. It is well established that plants can synthesize structural viral proteins that self assemble into VLPs. These structures are macromolecular complexes that typically are highly immunogenic due to their complexity. Two types of VLPs can be produced: those based only on structural viral proteins and those based on envelope viral proteins associated to a membrane layer from the plant cell. VLPs derived from bluetongue virus, Norwalk virus, influenza virus, Hepatitis B virus (HBV) (nucleocapsid antigen), human papilloma virus, and



*rotavirus* have been successfully assembled in plants (83). These viral proteins have also been engineered to display unrelated epitopes and thus serve, as in the case of CTB and LTB, as immunogenic carriers. This strategy has been successfully applied in a number of cases (80, 84).

Another alternative for immunogen design consists of recombinant immune complexes (RICs). RICs rely on the production of self-polymerized chimeras, whose monomeric form is comprised of the antigen of interest fused to the heavy chain of a mAb against the same antigen of interest. This has been found to be an effective strategy to increase antigen accumulation in transgenic plants enhancing immunogenicity (85).

## EXPRESSION AND DELIVERY POSSIBILITIES

High antigen yields will constitute a key factor in the flowchart to define the viability of the vaccination approach. In particular when oral vaccine development is pursued, high doses of antigen are typically required. If this aspect is addressed, the ambitious

goal of developing oral vaccines will be greatly favored. Oral vaccines constitute the most attractive immunization approach since they offer easier and safer administration as well as the possibility of inducing mucosal and systemic immune responses. Although low expression levels were a limitation in the initial attempts at exploring the viability of plant-based vaccines, it is envisioned that the current optimized expression platforms will allow the production of the targeted antigens at acceptable yields to reach the required level in the plant biomass that could reasonably constitute an oral dose (86).

Each expression modality possesses particular advantages but at the same time imposes some limitations. Therefore, the selection of the expression platform should follow a case-by-case analysis contemplating the nature of the elected antigen, the delivery approach, and the required time response (Table 3). For instance, viral vector-based systems offer high yields, efficient production of complex glycosylated proteins, and the shortest production time among the plant-based platforms. However, since these processes are based in *Nicotiana* species and agroinfiltration, parenteral vaccines can only be produced

after an extensive purification process to obtain an antigen free of bacterial compounds and toxic plant metabolites (87). Therefore, VLP-based EBOV vaccines using the GP or VP40 antigens can be ideally produced in viral vector-based platforms as a quick response to epidemics, parenterally immunizing the population at risk. However, it should be considered that these vaccines will not result in low-cost formulations and will require sterile devices and trained personnel for administration. In fact, there is one approved patent covering the production of EBOV VLPs in plants (88). A report by Phoolcharoen et al. (89), where a geminiviral vector was used for expression of the EIC in leaves of *N. benthamiana*, illustrates the potential for producing functional EBOV antigens at convenient yields.

In the case of transplastomic approaches, the average yields are lower than those of the viral expression vector but still considered convenient. However, it should be considered that the time for generating transplastomic lines is very long and no complex post-translational modifications, such as glycosylation, occur in this organelle (90). Therefore, this platform is ideal for the production of epitope-based vaccines where no complex antigens requiring glycosylation are targeted. One attractive avenue consists in the use of edible plant species for which chloroplast transformation has been established. This is the case of lettuce, which was used for the production of some vaccines (91–93).

By contrast, stable nuclear expression also offers high biosynthetic capacity and propagation of cells in bioreactors. The time for generating transformed lines depends on the species but is generally shorter than that required for transplastomic approaches. Yields are in general modest but can be optimized using several approaches such as organelle targeting and formation of protein

bodies (94). Interestingly, several edible plant species can be efficiently transformed. For instance, lettuce can be transformed efficiently using *Agrobacterium tumefaciens* (95). Another interesting species is the carrot (*Daucus carota*), for which there are efficient protocols for *Agrobacterium*-mediated transformation (96, 97). This host, *D. carota*, is relevant considering that the first plant-made biopharmaceutical for human use introduced into the market (Taliglucerase), which is a glucocerebrosidase for Gaucher's disease treatment, was expressed in carrot cell cultures. This fact implies that the production processes and the regulatory framework are already in place for this system (98). In fact, the company that developed this process is also working on validating the oral delivery of a recombinant product using carrot cells (99).

## CONSIDERATIONS FOR PLANT-BASED EBOV VACCINES IN PRECLINICAL EVALUATIONS

The antigenic and immunogenic properties of the target immunogens should be evaluated through molecular and immunological analyses. At the same time, these techniques will allow antigen quantification. For strategies based on LTB or CTB as carriers, proper folding and formation of pentameric structures produced in plants can be assessed by evaluating their interaction with the GM1 receptor in GM1-ELISA assays. Positive signals for this analysis imply that the chimeric protein is assembled into the pentameric form, and therefore, a proper uptake can be expected at the mucosa.

On the other hand, VLPs are usually detected *via* electron microscopy, which provides evidence of their successful assembly.

**TABLE 3 | Identified expression options for specific EBOV immunogens using the available plant expression technologies.**

			Available expression platforms
Possible immunogens	Full-length glycoprotein	Highly recommended	Stable nuclear transformation Advantages: well established for edible crops to be used in oral vaccines Limitations: expression is often low and should be optimized
			Transient nuclear vector-mediated expression Advantages: high yields
			Chloroplast expression Advantages: high yields
	Full-length VP40	Highly recommended	Reports related to this approach: a patent registered by D'aoust et al. (88) claims the expression of virus-like particle (VLP) in plants, comprised of the influenza transmembrane domain, and the cytoplasmic tail; fused to ectodomain from a non-influenza virus trimeric surface protein, covering EBOV
	Multi-epitope proteins	Highly recommended	Reports related to this approach: a patent registered by D'aoust et al. (88) claims the expression of VLPs in plants, comprised the influenza transmembrane domain, and the cytoplasmic tail; fused to ectodomain from a non-influenza virus trimeric surface protein, covering EBOV
	Immune complexes	Highly recommended	Reports related to this approach: Phoolcharoen et al. (89) expressed EBOV immune complex in leaves of <i>Nicotiana benthamiana</i> using a geminiviral vector
			Highly recommended
			To be determined
			Highly recommended
			To be determined

VLPs have the ability to stimulate strong immune responses upon oral delivery. In fact, it is considered that the compact and highly ordered structures of VLPs can provide resistance to digestive proteases (100). It is worth mentioning that the antigenic proteins for the HBV are one of the most studied models for production of plant-derived VLPs (101). It has been widely demonstrated that HBV VLP carriers spontaneously assemble in plant cells, resulting in VLPs that preserve their structure (102).

In terms of posttranslational modifications, glycosylation is of particular relevance in the production of vaccines based on GP. It should be considered that distinct glycosylation processes occur in plants with respect to mammalian cells: complex type glycans in plants possess, unlike GPs in mammals, a  $\beta(1,2')$ -xylose residue, and/or an  $\alpha(1,3')$ -fucose residue linked to the core glycan (103), and a second N-acetylglucosamine (GlcNAc) is enzymatically added to the mannose core, and lack of  $\beta(1,4')$ -galactose- and sialic acid-containing complex type glycans as well as the bi-antennary N-glycans production found in mammals. However, these differences on glycosylation do not necessarily result in a non-functional or low quality product. In fact, in the case of vaccines, there is the possibility that differential glycans associated with the plant-derived antigen could enhance immunogenicity (104). Moreover, recent advances in the plant glycoengineering allow human-like glycomodification and optimization of the desired glycan structures for enhancing safety and functionality of recombinant vaccines (105).

Another important consideration is the use of rodent or large animal models mentioned above that will allow assessing the immunogenicity and immunoprotective potential of the plant-made EBOV vaccine candidates.

Two cases can be highlighted as examples of how the above mentioned methodologies have resulted in desirable vaccine prototypes: (i) a plant-based vaccine candidate against malaria has been produced in plants by using a transplastomic expression approach. Fusion proteins consisting of CTB along with the antigens malaria apical membrane antigen-1 (AMA1) or merozoite surface protein-1 were produced in lettuce and tobacco leaves; these candidates induced humoral responses and protective immunity against a cholera toxin challenge. Moreover, both oral and injectable vaccination with CTB-AMA1 resulted in the blocking of the parasite from entering the erythrocytes (13). It should also be considered that LTB has been successfully produced in several crops, including corn and potato (106, 107). The potato-made LTB was used to conduct a pioneering Phase I clinical trial, showing its capacity to achieve seroconversion with no major adverse effects following an oral immunization scheme (106). (ii) A vaccine prototype against *Mycobacterium tuberculosis* has been developed following an approach based on RICs. The early secreted Ag85B and the latency-associated Acr antigen were expressed in tobacco plants as fusion proteins along with an anti-Acr antibody. Remarkably, *Bacillus Calmette–Guérin* (BCG)-immunized mice boosted intranasally with TB-RICs showed a significant reduction in *M. tuberculosis* lung infection in comparison with the group immunized only with BCG (108).

Based on the current evidence on the efficacy of several plant-based vaccines orally administered (16), it is proposed that

plant-based formulations may result in strong immune responses that could provide immunoprotection against EBOV. It should also be considered that plant-based vaccines could be applied as oral boosters in prime-boost immunization approaches. This focus has proven useful in many plant-based vaccine prototypes, including those against *Yersinia pestis*, HBV, and *M. tuberculosis* (11, 108, 109). All of the aspects mentioned in this article are critical in defining the feasibility of performing evaluations of the plant-based vaccine candidates in clinical trials.

## CONCLUDING REMARKS

There is an urgent need to develop efficacious vaccines against the EVD. Although preclinical trials are continuously reported for EBOV vaccine prototypes, efforts to develop low-cost vaccine production platforms should be contemplated. Plant-made vaccines offer the potential to address large-scale vaccine production at low cost, thereby facilitating the success of global vaccination programs, especially in developing and poorer countries where coverage is problematic mainly due to vaccine costs. Only one plant-made vaccine candidate has been developed against the EBOV thus far. Therefore, systematic efforts are required to expand this important research field. The path to address this objective will include (i) the design of protective antigens based on the current knowledge of the EBOV immunogenic determinants and on efficacious immunogenic carriers, preferably those that are highly effective in mucosal membranes; (ii) achieving sufficient antigen yields in edible plant biomass to establish models for oral immunization using minimally processed plant biomass; and (iii) validating the safety as well as the immunogenic and immunoprotective potential of plant-made vaccine candidates in test animals.

Each expression platform offers particular advantages, and the election should be based on the nature of the chosen antigen, the required time response, and desired delivery route. In conclusion, the continuing effort toward the development of plant-made vaccines prototypes could lead to important data to select approaches with the realistic goal of providing efficacious and cost-effective strategies to protect against the EVD. Thus, we encourage research in this direction to accelerate the fight against this deadly disease.

## AUTHOR CONTRIBUTIONS

SR-M designed the content of the review, wrote the plant sciences aspects, and corrected the full manuscript. RN-G performed the epitope analysis, made the figures and participated in the general writing of the manuscript. CA designed in part the content of the review, and wrote the immunology and virology aspects.

## FUNDING

The current investigations from the group are supported by CONACYT/México (grant 271182 to SR-M and grant 151818 to CA). Omar Gonzalez edited the English version of this manuscript.

## REFERENCES

- Kosal ME. A new role for public health in bioterrorism deterrence. *Front Public Health* (2014) 2:278. doi:10.3389/fpubh.2014.00278
- Jun SR, Leuze MR, Nookaew I, Überbacher EC, Land M, Zhang Q, et al. Ebolavirus comparative genomics. *FEMS Microbiol Rev* (2015) 39:764–78. doi:10.1093/femsre/fuv031
- Marsh GA, Haining J, Robinson R, Foord A, Yamada M, Barr JA. Ebola Reston virus infection of pigs: clinical significance and transmission potential. *J Infect Dis* (2011) 204:S804–9. doi:10.1093/infdis/jir300
- Kuhn JH, Becker S, Ebihara H, Geisbert TW, Johnson KM, Kawaoka Y, et al. Proposal for a revised taxonomy of the family Filoviridae: classification, names of taxa and viruses, and virus abbreviations. *Arch Virol* (2010) 155:2083–103. doi:10.1007/s00705-010-0814-x
- Lado M, Walker NF, Baker P, Haroon S, Brown CS, Youkee D, et al. Clinical features of patients isolated for suspected Ebola virus disease at Connaught Hospital, Freetown, Sierra Leone: a retrospective cohort study. *Lancet Infect Dis* (2015) 15:1024–33. doi:10.1016/S1473-3099(15)00137-1
- Agnandji ST, Huttner A, Zinser ME, Njuguna P, Dahlke C, Fernandes JF, et al. Phase 1 trials of rVSV Ebola vaccine in Africa and Europe. *N Engl J Med* (2016) 374:1647–60. doi:10.1056/NEJMoa1502924
- Qiu X, Wong G, Audet J, Bello A, Fernando L, Alimonti JB, et al. Reversion of advanced Ebola virus disease in nonhuman primates with ZMapp. *Nature* (2014) 514:47–53. doi:10.1038/nature13777
- Tully CM, Lambe T, Gilbert SC, Hill AS. Emergency Ebola response: a new approach to the rapid design and development of vaccines against emerging diseases. *Lancet Infect Dis* (2015) 15:356–9. doi:10.1016/S1473-3099(14)71071-0
- Avesani L, Bortesi L, Santi L, Falorni A, Pezzotti M. Plant-made pharmaceuticals for the prevention and treatment of autoimmune diseases: where are we? *Expert Rev Vaccines* (2010) 9:957–69. doi:10.1586/erv.10.82
- Avesani L, Merlin M, Gecchele E, Capaldi S, Brozzetti A, Falorni A, et al. Comparative analysis of different biofactories for the production of a major diabetes autoantigen. *Transgenic Res* (2014) 23:281–91. doi:10.1007/s11248-013-9749-9
- Alvarez ML, Pinyerd HL, Crisantes JD, Rigano MM, Pinkhasov J, Walmsley AM, et al. Plant-made subunit vaccine against pneumonic and bubonic plague is orally immunogenic in mice. *Vaccine* (2006) 24:2477–9. doi:10.1016/j.vaccine.2005.12.057
- Su J, Zhu L, Sherman A, Wang X, Lin S, Kamesh A, et al. Low cost industrial production of coagulation factor IX bioencapsulated in lettuce cells for oral tolerance induction in hemophilia. *Biomaterials* (2015) 70:84–93. doi:10.1016/j.biomaterials.2015.08.004
- Davoodi-Semiroomi A, Schreiber M, Nalapalli S, Verma D, Singh ND, Banks RK, et al. Chloroplast-derived vaccine antigens confer dual immunity against cholera and malaria by oral or injectable delivery. *Plant Biotechnol J* (2010) 8:223–42. doi:10.1111/j.1467-7652.2009.00479.x
- Monreal-Escalante E, Govea-Alonso DO, Hernández M, Cervantes J, Salazar-González JA, Romero-Maldonado A, et al. Towards the development of an oral vaccine against porcine cysticercosis: expression of the protective HP6/TSOL18 antigen in transgenic carrots cells. *Planta* (2016) 243:675–85. doi:10.1007/s00425-015-2431-0
- Hernández M, Rosas G, Cervantes J, Fragoso G, Rosales-Mendoza S, Sciuotto E. Transgenic plants: a 5-year update on oral antipathogen vaccine development. *Expert Rev Vaccines* (2014) 13:1523–36. doi:10.1586/14760584.20.14.953064
- Chan HT, Daniell H. Plant-made oral vaccines against human infectious diseases – are we there yet? *Plant Biotechnol* (2015) 13:1056–70. doi:10.1111/pbi.12471
- Streatfield SJ, Kushnir N, Yusibov V. Plant-produced candidate countermeasures against emerging and reemerging infections and bioterror agents. *Plant Biotechnol J* (2015) 13:1136–59. doi:10.1111/pbi.12475
- Ward BJ, Landry N, Trépanier S, Mercier G, Dargis M, Couture M. Human antibody response to N-glycans present on plant-made influenza virus-like particle (VLP) vaccines. *Vaccine* (2014) 32:6098–106. doi:10.1016/j.vaccine.2014.09.030
- Chichester JA, Jones RM, Green BJ, Stow M, Miao F, Moonsammy G, et al. Safety and immunogenicity of a plant-produced recombinant hemagglutinin-based influenza vaccine (HAI-05) derived from A/Indonesia/05/2005 (H5N1) influenza virus: a phase 1 randomized, double-blind, placebo-controlled, dose-escalation study in healthy adults. *Viruses* (2012) 4:3227–44. doi:10.3390/v4113227
- Cummings JF, Guerrero ML, Moon JE, Waterman P, Nielsen RK, Jefferson S, et al. Safety and immunogenicity of a plant-produced recombinant monomer hemagglutinin-based influenza vaccine derived from influenza A (H1N1) pdm09 virus: a phase 1 dose-escalation study in healthy adults. *Vaccine* (2014) 32:2251–9. doi:10.1016/j.vaccine.2013.10.017
- Bosch D, Schots A. Plant glycans: friend or foe in vaccine development? *Expert Rev Vaccines* (2010) 9:835–42. doi:10.1586/erv.10.83
- Landry N, Pillet S, Favre D, Poulin JF, Trépanier S, Yassine-Diab B, et al. Influenza virus-like particle vaccines made in *Nicotiana benthamiana* elicit durable, poly-functional and cross-reactive T cell responses to influenza HA antigens. *Clin Immunol* (2014) 154(2):164–77. doi:10.1016/j.clim.2014.08.003
- Pavot V. Ebola virus vaccines: where do we stand? *Clin Immunol* (2016) 173:44–9. doi:10.1016/j.clim.2016.10.016
- Mire CE, Geisbert TW, Feldmann H, Marzi A. Ebola virus vaccines – reality or fiction? *Expert Rev Vaccines* (2016) 15:1421–30. doi:10.1080/14760584.2016.1178068
- Wilson JA, Hevey M, Bakken R, Guest S, Bray M, Schmaljohn AL. Epitopes involved in antibody-mediated protection from Ebola virus. *Science* (2000) 287:1664–6. doi:10.1126/science.287.5458.1664
- Wong G, Richardson JS, Pillet S, Patel A, Qiu X, Alimonti J, et al. Immune parameters correlate with protection against Ebola virus infection in rodents and nonhuman primates. *Sci Transl Med* (2012) 4:158ra146. doi:10.1126/scitranslmed
- Marzi A, Engelmann F, Feldmann F, Haberthur K, Shupert WL, Brining D, et al. Antibodies are necessary for rVSV/ZEBOV-GP-mediated protection against lethal Ebola virus challenge in nonhuman primates. *Proc Natl Acad Sci U S A* (2013) 110:1893–8. doi:10.1073/pnas.1209591110
- Sullivan NJ, Hensley L, Asiedu C, Geisbert TW, Stanley D, Johnson J, et al. CD8+ cellular immunity mediates rAd5 vaccine protection against Ebola virus infection of nonhuman primates. *Nat Med* (2011) 17:1128–31. doi:10.1038/nm.2447
- Food and Drug Administration. (2014). Available from: <http://www.fda.gov/BiologicsBloodVaccines/GuidanceComplianceRegulatoryInformation/default.htm>
- Connolly BM, Steele KE, Davis KJ, Geisbert TW, Kell WM, Jaax NK, et al. Pathogenesis of experimental Ebola virus infection in guinea pigs. *J Infect Dis* (1999) 179(Suppl 1):S203–17. doi:10.1086/514305
- Bray M, Davis K, Geisbert T, Schmaljohn C, Huggins J. A mouse model for evaluation of prophylaxis and therapy of Ebola hemorrhagic fever. *J Infect Dis* (1998) 178:651–61. doi:10.1086/515386
- Ebihara H, Zivcec M, Gardner D, Falzarano D, LaCasse R, Rosenke R, et al. A Syrian golden hamster model recapitulating Ebola hemorrhagic fever. *J Infect Dis* (2013) 207:306–18. doi:10.1093/infdis/jis626
- Carrión R Jr, Ro Y, Hoosien K, Ticer A, Brasky K, de la Garza M, et al. A small nonhuman primate model for filovirus-induced disease. *Virology* (2011) 420:117–24. doi:10.1016/j.virol.2011.08.022
- Cross RW, Mire CE, Borisevich V, Geisbert JB, Fenton KA, Geisbert TW. The domestic ferret (*Mustela putorius furo*) as a lethal infection model for 3 species of ebolavirus. *J Infect Dis* (2016) 214:565–9. doi:10.1093/infdis/jiw209
- Kozak R, He S, Kroeker A, de La Vega MA, Audet J, Wong G, et al. Ferrets infected with Bundibugyo virus or Ebola virus recapitulate important aspects of human filovirus disease. *J Virol* (2016) 90:9209–23. doi:10.1128/JVI.01033-16
- Ye L, Yang C. Development of vaccines for prevention of Ebola virus infection. *Microbes Infect* (2015) 17:98–108. doi:10.1016/j.micinf.2014.12.004
- Hoelen T, Groseth A, Feldmann H. Current Ebola vaccines. *Expert Opin Biol Ther* (2012) 12:859–72. doi:10.1517/14712598.2012.685152
- Jones SM, Feldmann H, Stroher U, Geisbert JB, Fernando L, Grolla A, et al. Live attenuated recombinant vaccine protects nonhuman primates against Ebola and Marburg viruses. *Nat Med* (2005) 11:786–90. doi:10.1038/nm1258
- Sullivan N, Geisbert T, Geisbert J, Shedlock D, Xu L, Lamoreaux L, et al. Immune protection of nonhuman primates against Ebola virus with single low-dose adenovirus vectors encoding modified GPs. *PLoS Med* (2006) 3:e177. doi:10.1371/journal.pmed.0030177

40. Bukreyev A, Rollin PE, Tate MK, Yang L, Zaki SR, Shieh WJ, et al. Successful topical respiratory tract immunization of primates against Ebola virus. *J Virol* (2007) 81:6379–88. doi:10.1128/JVI.00105-07
41. Blaney JE, Marzi A, Willet M, Papaneri AB, Wirlbach C, Feldmann F, et al. Antibody quality and protection from lethal Ebola virus challenge in non-human primates immunized with rabies virus based bivalent vaccine. *PLoS Pathog* (2013) 9:e1003389. doi:10.1371/journal.ppat.1003389
42. Herbert AS, Kuehne AI, Barth JF, Ortiz RA, Nichols DK, Zak SE, et al. Venezuelan equine encephalitis virus replicon particle vaccine protects non-human primates from intramuscular and aerosol challenge with Ebolavirus. *J Virol* (2013) 87:4952–64. doi:10.1128/JVI.03361-12
43. Warfield KL, Swenson DL, Olinger GG, Kalina WV, Aman MJ, Bavari S. Ebola virus-like particle-based vaccine protects nonhuman primates against lethal Ebola virus challenge. *J Infect Dis* (2007) 196(Suppl 2):S430–7. doi:10.1086/520583
44. Swenson DL, Wang D, Luo M, Warfield KL, Woraratanadarm J, Holman DH, et al. Vaccine to confer to nonhuman primates complete protection against multistrain Ebola and Marburg virus infections. *Clin Vaccine Immunol* (2008) 15:460–7. doi:10.1128/CVI.00431-07
45. Sullivan NJ, Sanchez A, Rollin PE, Yang ZY, Nabel GJ. Development of a preventive vaccine for Ebola virus infection in primates. *Nature* (2000) 408:605–9. doi:10.1038/35046108
46. Ledgerwood JE, Costner P, Desai N, Holman L, Enama ME, Yamshchikov G, et al. A replication defective recombinant Ad5 vaccine expressing Ebola virus GP is safe and immunogenic in healthy adults. *Vaccine* (2010) 29:304–13. doi:10.1016/j.vaccine.2010.10.037
47. Stanley DA, Honko AN, Asiedu C, Trefry JC, Lau-Kilby AW, Johnson JC, et al. Chimpanzee adenovirus vaccine generates acute and durable protective immunity against Ebola virus challenge. *Nat Med* (2014) 20:1126–9. doi:10.1038/nm.3702
48. Halfmann P, Ebihara H, Marzi A, Hatta Y, Watanabe S, Suresh M, et al. Replication-deficient Ebolavirus as a vaccine candidate. *J Virol* (2009) 83:3810–5. doi:10.1128/JVI.00074-09
49. Marzi A, Halfmann P, Hill-Batorski L, Feldmann F, Shupert WL, Neumann G, et al. Vaccines. An Ebola whole-virus vaccine is protective in nonhuman primates. *Science* (2015) 348:439–42. doi:10.1126/science.aaa4919
50. Milligan ID, Gibani MM, Sewell R, Clutterbuck EA, Campbell D, Plested E, et al. Safety and immunogenicity of novel adenovirus type 26- and modified vaccinia Ankara-vectored Ebola vaccines: a randomized clinical trial. *JAMA* (2016) 315:1610–23. doi:10.1001/jama.2016.4218
51. Marzi A, Robertson SJ, Haddock E, Feldmann F, Hanley PW, Scott DP, et al. Ebola vaccine. VSV-EBOV rapidly protects macaques against infection with the 2014/15 Ebola virus outbreak strain. *Science* (2015) 349:739–42. doi:10.1126/science.aab3920
52. Geisbert TW, Daddario-Dicaprio KM, Geisbert JB, Reed DS, Feldmann F, Grolla A, et al. Vesicular stomatitis virus-based vaccines protect nonhuman primates against aerosol challenge with Ebola and Marburg viruses. *Vaccine* (2008) 26:6894–900. doi:10.1016/j.vaccine.2008.09.082
53. Qiu X, Fernando L, Alimonti JB, Melito PL, Feldmann F, Dick D, et al. Mucosal immunization of cynomolgus macaques with the VSVDeltaG/ZEBOVGP vaccine stimulates strong Ebola GP-specific immune responses. *PLoS One* (2009) 4:e5547. doi:10.1371/journal.pone.0005547
54. Geisbert TW, Daddario-DiCaprio KM, Williams KJ, Geisbert JB, Leung A, Feldmann F, et al. Recombinant vesicular stomatitis virus vector mediates postexposure protection against Sudan Ebola hemorrhagic fever in nonhuman primates. *J Virol* (2008) 82:5664–8. doi:10.1128/JVI.00456-08
55. Lai L, Davey R, Beck A, Xu Y, Suffredini AF, Palmore T, et al. Emergency postexposure vaccination with vesicular stomatitis virus-vectored Ebola vaccine after needlestick. *JAMA* (2015) 313:1249–55. doi:10.1001/jama.2015.10933
56. Günther S, Feldmann H, Geisbert TW, Hensley LE, Rollin PE, Nichol ST, et al. Management of accidental exposure to Ebola virus in the biosafety level 4 laboratory, Hamburg, Germany. *J Infect Dis* (2011) 204(Suppl 3):S785–90. doi:10.1093/infdis/jir298
57. Mire CE, Matassov D, Geisbert JB, Latham TE, Agans KN, Xu R, et al. Single dose attenuated Vesiculovax vaccines protect primates against Ebola Makona virus. *Nature* (2015) 520:688–91. doi:10.1038/nature14428
58. DiNapoli JM, Yang L, Samal SK, Murphy BR, Collins PL, Bukreyev A. Respiratory tract immunization of non-human primates with a Newcastle disease virus-vectored vaccine candidate against Ebola virus elicits a neutralizing antibody response. *Vaccine* (2010) 29:17–25. doi:10.1016/j.vaccine.2010.10.024
59. Huttner A, Dayer JA, Yerly S, Combescure C, Auderset F, Desmeules J, et al. The effect of dose on the safety and immunogenicity of the VSV Ebola candidate vaccine: a randomised double-blind, placebo-controlled phase 1/2 trial. *Lancet Infect Dis* (2015) 15:1156–66. doi:10.1016/S1473-3099(15)00154-1
60. Henao-Restrepo AM, Longini IM, Egger M, Dean NE, Edmunds WJ, Camacho A, et al. Efficacy and effectiveness of an rVSV-vectored vaccine expressing Ebola surface glycoprotein: interim results from the guinea ring vaccination cluster-randomised trial. *Lancet* (2015) 386:857–66. doi:10.1016/S0140-6736(15)61117-5
61. Henao-Restrepo AM, Camacho A, Longini IM, Watson CH, Edmunds WJ, Egger M, et al. Efficacy and effectiveness of an rVSV-vectored vaccine in preventing Ebola virus disease: final results from the Guinea ring vaccination, open-label, cluster-randomised trial (Ebola Ça Suffit!). *Lancet* (2017) 389:505–18. doi:10.1016/S0140-6736(16)32621-6
62. Konduru K, Bradfute SB, Jacques J, Manangeeswaran M, Nakamura S, Morshed S, et al. Ebola virus glycoprotein Fc fusion protein confers protection against lethal challenge in vaccinated mice. *Vaccine* (2011) 29:2968–77. doi:10.1016/j.vaccine.2011.01.113
63. Phoolcharoen W, Dye JM, Kilbourne J, Piensook K, Pratt WD, Arntzen CJ, et al. A nonreplicating subunit vaccine protects mice against lethal Ebola virus challenge. *Proc Natl Acad Sci USA* (2011) 108:20695–700. doi:10.1073/pnas.1117715108
64. Martina KA, Jahrling PB, Bavari S, Kuhn JH. Ebola virus disease candidate vaccines under evaluation in clinical trials. *Expert Rev Vaccines* (2016) 15:1101–12. doi:10.1080/14760584.2016.1187566
65. Martin JE, Sullivan NJ, Enama ME, Gordon IJ, Roederer M, Koup RA, et al. A DNA vaccine for Ebola virus is safe and immunogenic in a phase I clinical trial. *Clin Vaccine Immunol* (2006) 13:1267–77. doi:10.1128/CVI.00162-06
66. Sarwar UN, Costner P, Enama ME, Berkowitz N, Hu Z, Hendel CS, et al. Safety and immunogenicity of DNA vaccines encoding Ebola virus and Marburgvirus wild-type glycoproteins in a phase I clinical trial. *J Infect Dis* (2015) 211:549–57. doi:10.1093/infdis/jiu511
67. Cooper CL, Bavari S. A race for an Ebola vaccine: promises and obstacles. *Trends Microbiol* (2015) 23:65–6. doi:10.1016/j.tim.2014.12.005
68. Mire CE, Geisbert JB, Agans KN, Satterfield BA, Versteeg KM, Fritz EA, et al. Durability of a vesicular stomatitis virus-based marburg virus vaccine in nonhuman primates. *PLoS One* (2014) 9:e94355. doi:10.1371/journal.pone.0094355
69. Wong G, Audet J, Fernando L, Fausther-Bovendo H, Alimonti JB, Kobinger GP, et al. Immunization with vesicular stomatitis virus vaccine expressing the Ebola glycoprotein provides sustained long-term protection in rodents. *Vaccine* (2014) 32:5722–9. doi:10.1016/j.vaccine.2014.08.028
70. Kennedy SB, Neaton JD, Lane HC, Kieh MWS, Massaquoi MBF, Touchette NA, et al. Implementation of an Ebola virus disease vaccine clinical trial during the Ebola epidemic in Liberia: design, procedures, and challenges. *Clin Trials* (2016) 13:49–56. doi:10.1177/1740774515621037
71. Becquart P, Mahlaköiv T, Nkoghe D, Leroy EM. Identification of continuous human B-cell epitopes in the VP35, VP40, nucleoprotein and glycoprotein of Ebola virus. *PLoS One* (2014) 9:e96360. doi:10.1371/journal.pone.0096360
72. Vaughan K, Ponomarenko J, Sette A. (2014). *Ebola Virus Related Immune Epitope Data Curated in the IEDB*. Available from: <http://help.iedb.org/entries/51011785-Ebola-virus-related-immune-epitope-data-curated-in-the-IEDB>
73. Takada A, Ebihara H, Feldmann H, Geisbert TW, Kawaoka Y. Epitopes required for antibody-dependent enhancement of Ebola virus infection. *J Infect Dis* (2007) 196(Suppl 2):S347–56. doi:10.1086/520581
74. Lee JE, Saphire EO. Ebola virus glycoprotein structure and mechanism of entry. *Future Virol* (2009) 4:621–35. doi:10.2217/fvl.09.56
75. Wang Y, Liu Z, Dai Q. A highly immunogenic fragment derived from Zaire Ebola virus glycoprotein elicits effective neutralizing antibody. *Virus Res* (2014) 189:254–61. doi:10.1016/j.virusres.2014.06.001
76. Khan MA, Hossain MU, Rakib-Uz-Zaman SM, Morshed MN. Epitope-based peptide vaccine design and target site depiction against Ebola viruses: an immunoinformatics study. *Scand J Immunol* (2015) 82:25–34. doi:10.1111/sji.12302

77. Spangler BD. Structure of cholera toxin and the related *Escherichia coli* heat-labile enterotoxin. *Microbiol Rev* (1992) 56:622–47.
78. Guan C, Ji J, Jin C, Wang G, Li X, Guan W. Expression of cholera toxin B subunit-lumbrokinase in edible sunflower seeds – the use of transmucosal carrier to enhance its fusion protein's effect on protection of rats and mice against thrombosis. *Biotechnol Prog* (2014) 30:1029–39. doi:10.1002/btpr.1963
79. Rosales-Mendoza S, Soria-Guerra RE, Moreno-Fierros L, Govea-Alonso DO, Herrera-Díaz A, Korban SS, et al. Immunogenicity of nuclear-encoded LTB:ST fusion protein from *Escherichia coli* expressed in tobacco plants. *Plant Cell Rep* (2011) 30:1145–52. doi:10.1007/s00299-011-1023-0
80. Yu J, Langridge WH. A plant-based multicomponent vaccine protects mice from enteric diseases. *Nat Biotechnol* (2001) 19:548–52. doi:10.1038/89297
81. Frankel AD, Pabo CO. Cellular uptake of the tat protein from human immunodeficiency virus. *Cell* (1988) 55:1189–93. doi:10.1016/0092-8674(88)90263-2
82. Derossi D, Joliot AH, Chassaing G, Prochiantz A. The third helix of the Antennapedia homeodomain translocates through biological membranes. *J Biol Chem* (1994) 269:10444–50.
83. Scotti N, Rybicki EP. Virus-like particles produced in plants as potential vaccines. *Expert Rev Vaccines* (2013) 12:211–24. doi:10.1586/erv.12.147
84. Marusic C, Rizza P, Lattanzi L, Mancini C, Spada M, Belardelli F, et al. Chimeric plant virus particles as immunogens for inducing murine and human immune responses against human immunodeficiency virus type 1. *J Virol* (2001) 75:8434–9. doi:10.1128/JVI.75.18.8434-8439.2001
85. Chargelegue D, Drake P, Obregon P, Prada A, Fairweather N, Ma JK. Highly immunogenic and protective recombinant vaccine candidate expressed in transgenic plants. *Infect Immun* (2005) 73:5915–22. doi:10.1128/IAI.73.9.5915-5922.2005
86. Komarova TV, Baschieri S, Donini M, Marusic C, Benvenuto E, Dorokhov YL. Transient expression systems for plant-derived biopharmaceuticals. *Expert Rev Vaccines* (2010) 9:859–76. doi:10.1586/erv.10.85
87. Thuenemann EC, Meyers AE, Verweij J, Rybicki EP, Lomonossoff GP. A method for rapid production of heteromultimeric protein complexes in plants: assembly of protective bluetongue virus-like particles. *Plant Biotechnol J* (2013) 11(7):839–46. doi:10.1111/pbi.12076
88. D'aoust M, Couture M, Lavoie P, Vezina L. *Virus Like Particle Production in Plants*. U.S. Patent No 20,130,344,100 (2013).
89. Phoolcharoen W, Bhoo SH, Lai H, Ma J, Arntzen CJ, Chen Q, et al. Expression of an immunogenic Ebola immune complex in *Nicotiana benthamiana*. *Plant Biotechnol J* (2011) 9:807–16. doi:10.1111/j.1467-7652.2011.00593.x
90. Salazar-González JA, Monreal-Escalante E, Herrera Diaz A, Koop HU, Rosales-Mendoza S. Plastid-based expression strategies. In: Mendoza SR, editor. *Genetically Engineered Plants as a Source of Vaccines Against Wide Spread Diseases – An Integrated View*. New York, NY: Springer (2014). p. 61–78.
91. Lelivelt CL, van Dun KM, de Snoo CB, McCabe MS, Hogg BV, Nugent JM. Plastid transformation in lettuce (*Lactuca sativa* L.) by polyethylene glycol treatment of protoplasts. *Methods Mol Biol* (2014) 1132:317–30. doi:10.1007/978-1-62703-995-620
92. Ruhrlman T, Ahangari R, Devine A, Samsam M, Daniell H. Expression of cholera toxin B-proinsulin fusion protein in lettuce and tobacco chloroplasts – oral administration protects against development of insulinitis in non-obese diabetic mice. *Plant Biotechnol J* (2007) 5:495–510. doi:10.1111/j.1467-7652.2007.00259.x
93. Lakshmi PS, Verma D, Yang X, Lloyd B, Daniell H. Low cost tuberculosis vaccine antigens in capsules: expression in chloroplasts, bio-encapsulation, stability and functional evaluation in vitro. *PLoS One* (2013) 8:e54708. doi:10.1371/journal.pone.0054708
94. Alvarez ML, Topal E, Martin F, Cardineau GA. Higher accumulation of F1-V fusion recombinant protein in plants after induction of protein body formation. *Plant Mol Biol* (2010) 72:75–89. doi:10.1007/s11103-009-9552-4
95. Curtis IS. Lettuce (*Lactuca sativa* L.). *Methods Mol Biol* (2006) 343:449–58. doi:10.1385/1-59745-130-4:449
96. Rosales-Mendoza S, Soria-Guerra RE, de Jesús Olivera-Flores MT, López-Revilla R, Argüello-Astorga GR, Jiménez-Bremont JF, et al. Expression of *Escherichia coli* heat-labile enterotoxin b subunit (LTB) in carrot (*Daucus carota* L.). *Plant Cell Rep* (2007) 26:969–76. doi:10.1007/s00299-007-0310-2
97. Balestrazzi A, Carbonera D, Celli R. Transformation of *Daucus carota* hypocotyls mediated by *Agrobacterium tumefaciens*. *J Genet Breed* (1991) 45:135–40.
98. Pastores GM, Petakov M, Giraldo P, Rosenbaum H, Szer J, Deegan PB, et al. A phase 3, multicenter, open-label, switchover trial to assess the safety and efficacy of taliglucerase alfa, a plant cell-expressed recombinant human glucocerebrosidase, in adult and pediatric patients with Gaucher disease previously treated with imiglucerase. *Blood Cells Mol Dis* (2014) 53:253–60. doi:10.1016/j.bcmd.2014.05.004
99. Shaaltiel Y, Gingis-Velitski S, Tzaban S, Fiks N, Tekoah Y, Aviezer D. Plant-based oral delivery of β-glucocerebrosidase as an enzyme replacement therapy for Gaucher's disease. *Plant Biotechnol J* (2015) 13:1033–40. doi:10.1111/pbi.12366
100. Smith ML, Richter L, Arntzen CJ, Shuler ML, Mason HS. Structural characterization of plant-derived hepatitis B surface antigen employed in oral immunization studies. *Vaccine* (2003) 21:4011–21. doi:10.1016/S0264-410X(03)00268-8
101. Meador LR, Mor TS. Meeting report VLPNPV: session 5: plant based technology. *Hum Vaccin Immunother* (2014) 10:3068–73. doi:10.4161/21645515.2014.979693
102. Huang Z, Elkin G, Maloney BJ, Beuhner N, Arntzen CJ, Thanavala Y, et al. Virus-like particle expression and assembly in plants: hepatitis B and Norwalk viruses. *Vaccine* (2005) 23:1851–8. doi:10.3748/wjg.v9.i5.996
103. Lerouge P, Bardor M, Pagny S, Gomord V, Faye L. N-glycosylation of recombinant pharmaceutical glycoproteins produced in transgenic plants: towards an humanisation of plant N-glycans. *Curr Pharm Biotechnol* (2000) 1:347–54. doi:10.2174/1389201003378843
104. Hamorsky KT, Kouokam JC, Jurkiewicz JM, Nelson B, Moore LJ, Husk AS, et al. N-glycosylation of cholera toxin B subunit in *Nicotiana benthamiana*: impacts on host stress response, production yield and vaccine potential. *Sci Rep* (2015) 5:8003. doi:10.1038/srep08003
105. Kim HS, Jeon JH, Lee KJ, Ko K. N-glycosylation modification of plant-derived virus-like particles: an application in vaccines. *Biomed Res Int* (2014) 2014:249519. doi:10.1155/2014/249519
106. Tacket CO, Mason HS, Losonsky G, Clements JD, Levine MM, Arntzen CJ. Immunogenicity in humans of a recombinant bacterial antigen delivered in a transgenic potato. *Nat Med* (1998) 4(5):607–9. doi:10.1038/nm0598-607
107. Chikwamba RK, Scott MP, Mejía LB, Mason HS, Wang K. Localization of a bacterial protein in starch granules of transgenic maize kernels. *Proc Natl Acad Sci U S A* (2003) 100:11127–32. doi:10.1073/pnas.1836901100
108. Pepponi I, Diogo GR, Stylianou E, van Dolleweerd CJ, Drake PM, Paul MJ, et al. Plant-derived recombinant immune complexes as self-adjuvanting TB immunogens for mucosal boosting of BCG. *Plant Biotechnol J* (2014) 12:840–50. doi:10.1111/pbi.12185
109. Pniewski T, Kapusta J, Bociag P, Wojciechowicz J, Kostrzak A, Gdula M, et al. Low-dose oral immunization with lyophilized tissue of herbicide-resistant lettuce expressing hepatitis B surface antigen for prototype plant-derived vaccine tablet formulation. *J Appl Genet* (2011) 52:125–36. doi:10.1007/s13353-010-0001-5

**Conflict of Interest Statement:** The authors declare that the research was conducted in the absence of any commercial or financial relationships that could be construed as a potential conflict of interest.

Copyright © 2017 Rosales-Mendoza, Nieto-Gómez and Angulo. This is an open-access article distributed under the terms of the Creative Commons Attribution License (CC BY). The use, distribution or reproduction in other forums is permitted, provided the original author(s) or licensor are credited and that the original publication in this journal is cited, in accordance with accepted academic practice. No use, distribution or reproduction is permitted which does not comply with these terms.



# Adjusted Particle Size Eliminates the Need of Linkage of Antigen and Adjuvants for Appropriated T Cell Responses in Virus-Like Particle-Based Vaccines

OPEN ACCESS

**Edited by:**

Clarisa B. Palatnik-de-Sousa,  
Federal University of Rio de Janeiro, Brazil

**Reviewed by:**

Arun Kumar,  
Health Sciences North, Canada

David Peabody,  
University of New Mexico  
School of Medicine, USA

**\*Correspondence:**

Vania Manolova

vania.manolova@viforpharma.com;  
Martin F. Bachmann  
martin.bachmann@ndm.ox.ac.uk

<sup>†</sup>These authors share last authorship.

**#Present address:**

Anna Flace and Vania Manolova,  
Vifor (International) AG, Schlieren,  
Switzerland

**Specialty section:**

This article was submitted to  
Vaccines and Molecular Therapeutics,  
a section of the journal  
*Frontiers in Immunology*

**Received:** 25 October 2016

**Accepted:** 16 February 2017

**Published:** 06 March 2017

**Citation:**

Gomes AC, Flace A, Saudan P, Zabel F, Cabral-Miranda G, Turabi AE, Manolova V and Bachmann MF (2017) Adjusted Particle Size

*Eliminates*

*the Need of Linkage of Antigen and Adjuvants for Appropriated T Cell Responses in Virus-Like Particle-Based Vaccines.*

*Front. Immunol.* 8:226.

doi: 10.3389/fimmu.2017.00226

**Ariane C. Gomes<sup>1</sup>, Anna Flace<sup>2†</sup>, Philippe Saudan<sup>2</sup>, Franziska Zabel<sup>3</sup>,**

**Gustavo Cabral-Miranda<sup>1</sup>, Aadil El Turabi<sup>1</sup>, Vania Manolova<sup>2\*†‡</sup> and Martin F. Bachmann<sup>1,4\*†</sup>**

<sup>1</sup>The Jenner Institute, Oxford University, Oxford, UK, <sup>2</sup>Cytos Biotechnology AG, Schlieren, Switzerland, <sup>3</sup>Dermatology, University Hospital, Zürich, Switzerland, <sup>4</sup>Immunology, Inselspital, Bern, Switzerland

Since the discovery of the first virus-like particle (VLP) derived from hepatitis B virus in 1980 (1), the field has expanded substantially. Besides successful use of VLPs as safe autologous virus-targeting vaccines, the powerful immunogenicity of VLPs has been also harnessed to generate immune response against heterologous and even self-antigens (2–4). Linking adjuvants to VLPs displaying heterologous antigen ensures simultaneous delivery of all vaccine components to the same antigen-presenting cells. As a consequence, antigen-presenting cells, such as dendritic cells, will process and present the antigen displayed on VLPs while receiving costimulatory signals by the VLP-incorporated adjuvant. Similarly, antigen-specific B cells recognizing the antigen linked to the VLP are simultaneously exposed to the adjuvant. Here, we demonstrate in mice that physical association of antigen, carrier (VLPs), and adjuvant is more critical for B than T cell responses. As a model system, we used the E7 protein from human papilloma virus, which spontaneously forms oligomers with molecular weight ranging from 158 kDa to 10 MDa at an average size of 50 nm. E7 oligomers were either chemically linked or simply mixed with VLPs loaded with DNA rich in non-methylated CG motifs (CpGs), a ligand for toll-like receptor 9. E7-specific IgG responses were strongly enhanced if the antigen was linked to the VLPs. In contrast, both CD4<sup>+</sup> and CD8<sup>+</sup> T cell responses as well as T cell-mediated protection against tumor growth were comparable for linked and mixed antigen formulations. Therefore, our data show that B cell but not T cell responses require antigen-linkage to the carrier and adjuvant for optimal vaccination outcome.

**Keywords:** VLPs, vaccines, HPV, CpG, adjuvant

## INTRODUCTION

Most prophylactic vaccines are designed to induce strong antibody responses, while many therapeutic vaccines against chronic viral infections and cancer aim to induce T cell responses (5, 6). However, for many vaccines currently under development, this dictum is challenged, and strong B and T cell responses are likely required to achieve protection. Thus, understanding the rules that

govern induction of B versus T cell responses and identifying commonalities and differences between them represents an important goal in vaccinology and immunology.

Formulation of vaccines in adjuvants usually enhances both B and T helper ( $T_H$ ) responses (7). However, it is often unclear whether the adjuvants enhance B cell responses directly or indirectly, via enhancing follicular  $T_H$  cell responses. We have recently shown that the adjuvant CpGs linked to antigen enhances B cell responses by activating B cells directly through TLR9 recognition (8, 9), which required internalization of the CpG. By contrast, CpGs mixed with antigen may primarily enhance B cell responses by facilitating Th cell activation, thereby increasing antibody responses indirectly (10–12). As a general rule, it is important that the immunological target cells [dendritic cells (DCs) or B cells] are simultaneously activated by the adjuvant and exposed to the antigen (5, 13). One way to ensure co-exposure to antigen and adjuvant is the physical linkage of the two components. Something readily achieved by conjugation with covalent chemical bonds or by packaging adjuvant into liposomes or virus-like particles (VLPs). However, for good manufacturing practice production, covalent linkage might be a complicated and costly endeavor, especially if the antigen is complex or if the goal is patient-specific vaccination. Hence, a simple admixed formulation could be advantageous under these circumstances.

The trafficking of antigen from the periphery to lymph nodes (LN<sub>s</sub>) or the spleen is essential to drive T cell and B cell activation (5), and it is well established that one of the main factors governing influx to the LN<sub>s</sub> is the size of the particles (14–16). Particles in the nanometer range can flow freely within the lymph, rapidly reaching LN<sub>s</sub> where they can encounter relevant B cells and APCs that will activate CD4<sup>+</sup> and CD8<sup>+</sup> T cells (17–19). By simply mixing antigens and adjuvants of similar size, it may be possible to target the same individual cells within the LN<sub>s</sub>. To test this, we generated particulate adjuvants and antigens of similar size, mixed them freely before injecting the formulation into mice, then observed if they indeed were draining to the same cells within LN<sub>s</sub>. As adjuvant, we used VLPs derived from Q $\beta$  bacteriophages packaged with CpGs, having a size of 30 nm. The recombinant oncoprotein E7 derived from the human papilloma virus (HPV) was chosen as the target antigen as it forms oligomers with a size of around 50 nm (20). To test the impact of antigen size and co-drainage, we also used the immunodominant peptide E7<sub>49–57</sub> derived from the E7 protein, representing a H2-D $b$ -restricted CTL epitope (12). We found that covalent linkage was essential for maximal B cell for peptide and particle-based vaccine responses, regardless of the size of the antigen. In contrast, an admixed formulation of E7 oligomers with CpG-loaded VLPs was sufficient to induce optimal CD4<sup>+</sup> and CD8<sup>+</sup> T cell responses that proved to be protective as a therapeutic vaccine when tested in an HPV tumor model. Mixing free E7<sub>49–57</sub> peptide with CpG-loaded VLPs, however, failed to induce strong T cell responses, suggesting that adjusted particle size may be sufficient to co-deliver antigen and adjuvants to the same DCs for optimal T cell induction, eliminating the requirement for the linkage of the two entities.

## MATERIALS AND METHODS

### VLP and E7 Production

HPV-E7 protein containing a short C-terminal GGC linker was recombinantly expressed in *Escherichia coli*, solubilized from the inclusion body fraction by 8M urea and purified using affinity and size-exclusion chromatography. The denatured protein migrated as a 14-kDa single band in reducing SDS-PAGE (data not shown). After refolding by dilution and dialysis against NaCl-MES-containing buffer, E7 protein spontaneously formed oligomers. Q $\beta$  VLP production and purification have been described in detail elsewhere (21).

### CpG ODN and Antigen Sequence

CpGs 1668 with phosphorothioate backbone were purchased from Invivogen (sequence: 5' tccatgacgttcttgatgc 3'). The protein and peptides E7<sub>49–57</sub> were produced in a modified version with additional 3 aa (GGC) added to the C terminus E7 (Proimmune, UK) to allow coupling to VLPs. E7 protein sequence UniProt database: P03129. E7<sub>49–57</sub> peptide sequence: RAHYNIVTFGGC.

### Measurement of Anti-E7 and Anti-VLP Antibodies by ELISA

Anti-VLP and anti-E7 antibody titers were measured in the serum of mice vaccinated 21 days earlier with unmodified VLP. A total of 96-well plates were coated overnight with 5  $\mu$ g/mL of unmodified VLP or 5  $\mu$ g/mL of E7 oligomers. After blocking for 2 h with 2% bovine serum albumin phosphate-buffered saline (PBS), serum obtained from vaccinated or control mice (diluted 1:500 to 1:12,500) was added and plates were incubated for 2 h at room temperature. After washing the plates three times with PBS-0.05% Tween, horseradish peroxidase-labeled goat anti-mouse immunoglobulin G (IgG-HRP) (Jackson ImmunoResearch, UK) was added for 1 h, followed by the addition of 3,3',5,5'-tetramethylbenzidine (TMB) Sigma, as a substrate before reading the optical density (OD) at 450 nm (OD<sub>450</sub>). Titers are expressed as serum dilutions at the half-maximal OD (OD<sub>50</sub>).

### Association ELISA

Plates (Nunc-Immuno MaxiSorp) were coated with anti-E7 antibody, each of the vaccine preparations were added at a concentration corresponding to 60 ng/mL of E7 protein. Following washing and incubations, anti-Q $\beta$  monoclonal antibody was added followed by secondary detection antibody goat anti-mouse IgG-HRP and TMB. Data expressed in OD<sub>450</sub>.

### Vaccine Preparation

Vaccines were prepared by chemical coupling as described elsewhere (2). Purified Q $\beta$  VLPs (2 mg/mL in PBS) were derivatized by a 1-h incubation at room temperature with a 10-fold molar excess of succinimidyl-6-( $\beta$ -maleimidopropionamido)hexanoate (Pierce, Rockford, IL, USA). Free cross-linker was removed by diafiltration with Amicon Ultra Centrifugal Filters, 100 kDa MWCO. Derivatized Q $\beta$  VLPs and E7<sub>49–57</sub>-GGC (peptide at five-fold molar excess) or E7 protein were then incubated for 3 h at room temperature to allow cross-linking. Unbound material was

removed by diafiltration with Amicon Ultra centrifugal filters, 100 kDa MWCO for the peptide and size exclusion for the E7 protein. Efficiency of cross-linking was analyzed by SDS-PAGE.

### Packaging of CpG into Q $\beta$ VLPs

Performed as described elsewhere (22). Briefly, bacterial RNA trapped into VLPs during recombinant expression was digested with RNase A (Merck) for 5 h at 37°C. RNase-treated VLPs were combined with 120 nM/mL of CpG and incubated for further 3 h at 37°C. Excess of CpG was removed by dialysis against PBS.

### Immunization and Trafficking Experiments

C57BL/6 mice (9–12 weeks old; Harlan) were injected s.c. with 80  $\mu$ g of either vaccine formulation. Blood was collected from the tail vein and serum and PBMCs separated for further analysis.

E7 protein or E7<sub>49–57</sub> was labeled with AlexaFluor 488 C5-maleamide as described by the manufacturer and with Q $\beta$

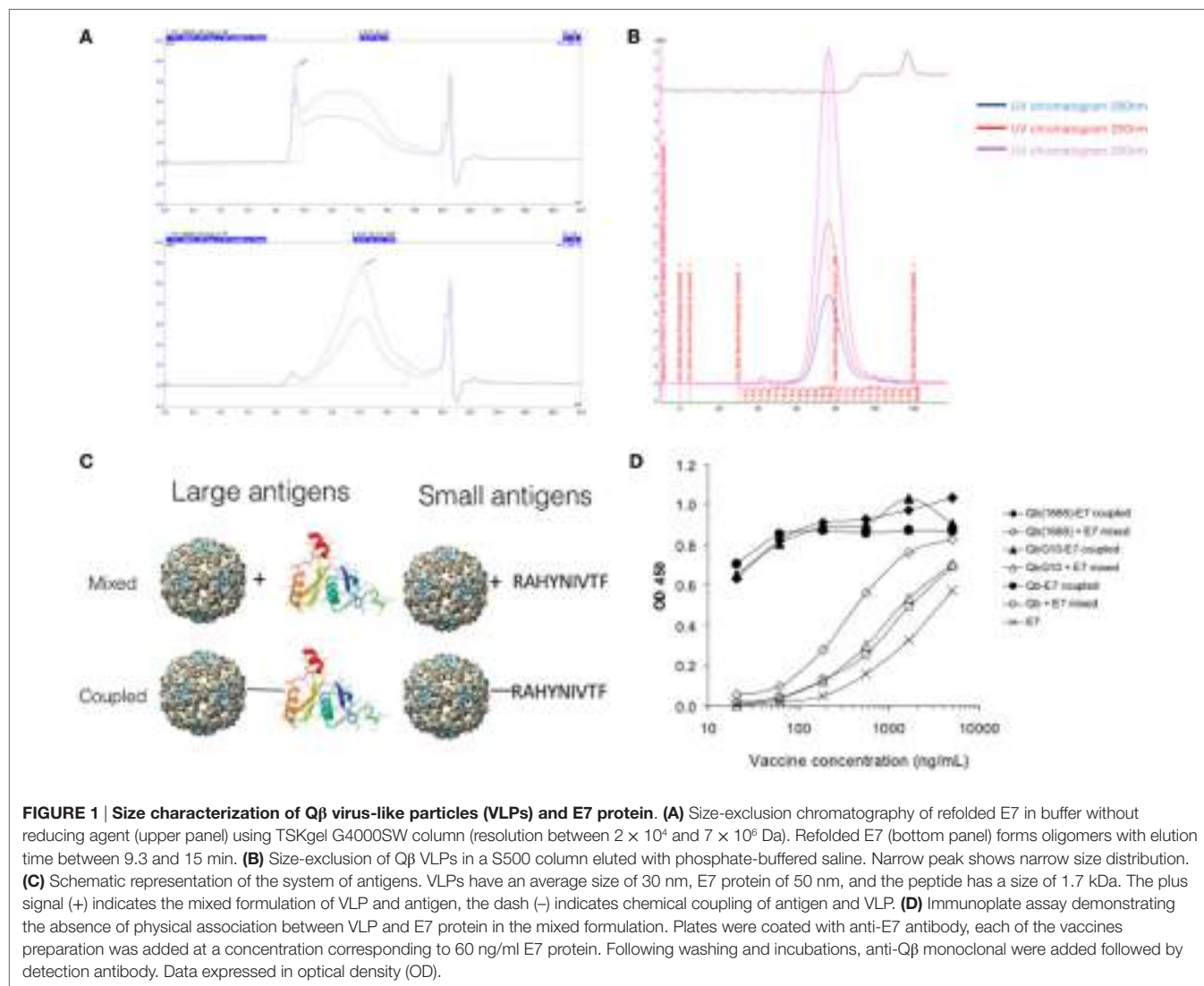
labeled with AlexaFluor 647 or PE as instructed by the manufacturer (all from Thermo Fischer). C57BL/6 mice (9–12 weeks old; Harlan) were injected s.c. with 30  $\mu$ g of VLP and peptide into the hind leg.

All mouse experiments have been performed in accordance with the local welfare legislation and under valid animal experimentation licenses.

### Cells and Flow Cytometry

Popliteal and inguinal LNs were isolated and a single-cell suspension was prepared by incubating LN with 1 mg/mL collagenase D (Roche) and 0.04 mg/mL DNase I (Boehringer) in 5% FSC containing DMEM, for 30 min at 37°C. Organ pieces were passed through a 70- $\mu$ m cell strainer and stained for cell-specific markers. The following fluorochrome-labeled antibodies were used: CD11c, CD8a (all from eBioscience), F4/80, Live/Dead Aqua cell stain (all from Life Technologies).

Spleens were isolated smashed through a 70- $\mu$ m cell strainer using the plunger of a syringe (Falcon), red blood cells were lysed



with ACK solution (Lonza). The following fluorochrome-labeled antibodies were used: CD3, CD8a, Live-Dead dye, IFN $\gamma$ , TNF $\alpha$ , and IL-17 (eBioscience).

Primary culture of DCs from LNs of a naïve mice were harvested and incubated for 24 h with 10 nM of E7<sub>49-51</sub> conjugated with Alexa488 and 1  $\mu$ g/mL of Q $\beta$  conjugated with Alexa647. CD11c $^+$  F4/80 $^-$  DCs were subsequently analyzed by flow cytometry for uptake of peptide and Q $\beta$ .

## Tumor Model

Female C57BL/6 mice at age of 10–11 weeks were injected with  $1.5 \times 10^5$  TC-1 cells expressing HPV16 E7 oncoprotein. Eight days post injection of tumor cells, mice developed palpable tumors and were subjected to a weekly immunization schedule with E7 coupled or mixed to Q $\beta$ (1668) for 49 days. Tumor size was recorded daily and was calculated as follows:  $W^*W^*L/2$ , where  $W$  is tumor width (centimeters) and  $L$  is tumor length (centimeters). Mice showing signs of suffering or reaching tumor size larger than 1,000 cm $^3$  were euthanized.

## RESULTS

### Characterization of Q $\beta$ -VLPs and E7

Size-exclusion chromatography analysis of refolded E7 showed a wide distribution elution profile corresponding to molecular weights between 17 kDa and 10 MDa (void volume of the column, **Figure 1A**, upper panel). The refolded E7 was treated under reducing conditions, which narrowed the molecular weight distribution to a major peak with average size of 670 kDa (**Figure 1A**, bottom panel) and demonstrated the role of disulfide bonds in E7 multimerization, as described elsewhere (20). The 14 kDa capsid protein of the Q $\beta$  bacteriophage is expressed in *E. coli* and self-assembles to form a VLP with molecular weight of approximately 3 MDa. Electron microscopy and dynamic light scattering (not shown) demonstrates that Q $\beta$  VLPs are single particles with average diameter of 30 nm. The size-exclusion profile demonstrated a narrow size distribution of the VLP on a S500 column (GE) (**Figure 1B**). Thus, Q $\beta$  VLPs and non-reduced E7 oligomers exhibit roughly comparable sizes of 30–50 nm.

### Q $\beta$ and E7 Protein Are Physically Associated by Chemical Coupling but Not by Mixing

In order to compare the immunogenicity of mixed and covalently linked antigen and VLP, the E7 protein containing a short cysteine-containing linker (-GGC) was chemically cross-linked via the free cysteine to surface lysine on Q $\beta$  using the hetero-bi-directional cross-linker, SMPH. The efficiency of the cross-linking was assessed by separation on SDS-PAGE under reducing conditions and analyzed by Western blot (**Figure 2**). Alternatively, purified Q $\beta$  and E7 protein were simply mixed. The model of mixed and coupled formulations is represented in **Figure 1C**. To assess whether mixing would result in spontaneous association of Q $\beta$  to E7 oligomers, a sandwich ELISA assay was

performed using anti-Q $\beta$  VLP capture antibodies and anti-E7 detection antibodies. The assay demonstrated that E7 was only associated with Q $\beta$  VLPs upon chemical coupling, while simple mixing did not result in any physical association (**Figure 1D**). To ensure that loading of VLPs with CpGs did not alter the binding properties of VLPs, the ELISA was repeated with Q $\beta$  VLPs loaded with B-type CpG 1668 (Q $\beta$ (1668)). Similarly, no association between E7 and Q $\beta$  VLPs could be observed (**Figure 1D**). VLPs loaded with CpG are represented as Q $\beta$ (1668), while “Q $\beta$ ” will be used to indicate unmodified VLPs (naturally loaded with *E. coli*-derived ssRNA).

### Linkage of Q $\beta$ and E7 Is Not Required for Uptake by the Same DCs

Drainage of Q $\beta$  and E7 was assessed by labeling particles with Phycoerythrine (PE) and Alexa488, respectively. Flow cytometry analysis demonstrated that a subpopulation of resident DCs of draining LNs simultaneously took up both E7 and Q $\beta$  VLPs (**Figure 3A**). A total of 23% of cDCs (CD11c $^{high}$ F4/80 $^-$ ) from the popliteal LN were double positives for Q $\beta$  and the antigen E7-Alexa488. Thus, antigen and adjuvants, i.e., E7 and Q $\beta$  VLPs, were taken up simultaneously *in vivo* by the same DCs.

To confirm the hypothesis that antigen and VLP size was the limiting factor on antigen and VLP distribution, the E7 derived peptide H2-D $b$  E7<sub>49-57</sub> was used as antigen instead of the E7

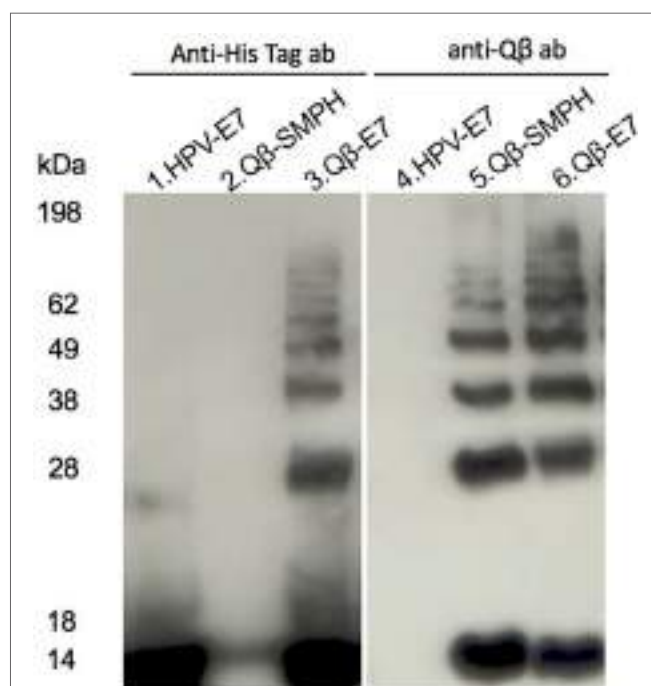


**FIGURE 2 | Biochemical analysis of the coupling of Q $\beta$  and hPV.E7.**

HPV-E7 (lane 1 and 4), SMPH reacted Q $\beta$  (2 and 5), and coupled Q $\beta$ -E7 (3 and 6) were separated by SDS-PAGE under reducing conditions and analyzed by Western blot. HPV-E7 was detected in lanes 1–3 by anti-His tag antibody (His Tag Ab), and lanes 4–6 were assayed with anti-Q $\beta$  specific antibody (Q $\beta$  Ab).

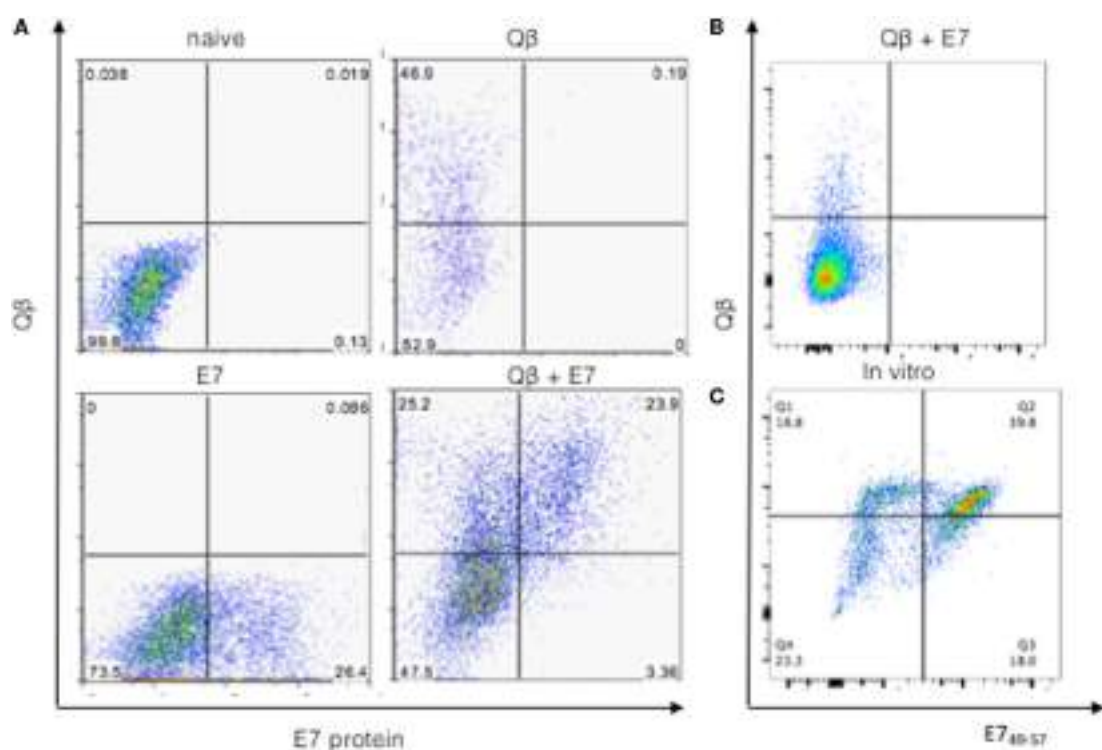


**FIGURE 3 | Draining of Q $\beta$  virus-like particle (VLP) and antigens to LNs.** **(A)** Q $\beta$ -VLP mixed with E7 oligomers are taken up by the same population of DCs in the draining lymph nodes. Mice were injected either with Q $\beta$ -VLP-Alexa488 or E7-phycoerythrin (PE) or a mixture of both particles (100  $\mu$ g of each). The uptake of the fluorescent proteins into DCs of the draining lymph node (popliteal) was analyzed by flow cytometry. Frequency plot is gated on DCs (CD11c $^+$  F4/80 $^-$ ). **(B)** Frequency plot of cells from draining LNs 24 h postinjection with 100  $\mu$ g of Q $\beta$ -Alexa647 and 100  $\mu$ g of E7<sub>49-57</sub> peptide labeled with Alexa Fluor 488. **(C)** *In vitro* uptake of Q $\beta$ -Alexa647 and E7<sub>49-57</sub> Alexa488. Single cell preparation draining LN of naïve C57BL/6 mice was prepared and pulsed for 24 h with 1  $\mu$ g/mL VLP and 10 nM of peptide. Frequency plot is gated on DCs (CD11c $^+$  F4/80 $^-$ ).

protein. Injection of free peptide E7<sub>49-57</sub> labeled likewise with Alexa488 and Q $\beta$  VLPs labeled with Alexa647 did not result in simultaneous uptake by DCs in draining LNs (Figure 3B). As a matter of fact, the peptide could not be found in LNs 24 h after injection, indicating that small peptides do not drain efficiently to LNs and are not efficiently transported by DCs.

To exclude potential methodological limitations in visualizing peptide interaction with DCs by flow cytometry, an *in vitro* pulsing experiment was performed. Primary cultures of DCs from LNs of a naïve mice were incubated for 24 h with the peptide E7<sub>49-51</sub> conjugated to Alexa488 and Q $\beta$  conjugated to Alexa647. CD11c $^+$  F4/80 $^-$  DCs were subsequently analyzed by flow cytometry for uptake of peptide and Q $\beta$ . As shown in Figure 3C, almost 50% of the DCs simultaneously interacted with the peptide and Q $\beta$ , which confirmed the capacity of small peptides to interact with DCs *in vitro* and suggested that subcutaneously injected small peptides do not efficiently traffic to the LN.

## Packaging of CpG into VLPs Is Necessary to Induce T Cell Responses

The contribution of the vaccine components for generation of CD4 $^+$  and CD8 $^+$  T cell responses was investigated by injecting

mice with E7 protein either alone or mixed with CpG and Q $\beta$ (1668) either coupled or mixed with E7. The production of IFN $\gamma$  by CD4 $^+$  and CD8 $^+$  T cells was measured 8 days after vaccination. E7 alone or mixed with free CpG induced low percentage of E7-specific T cells. E7 protein mixed or coupled with Q $\beta$ (1668) efficiently induced T cells producing IFN $\gamma$  demonstrating the superior T cell immunogenicity of a vaccine containing VLPs-packaged CpGs (Figures 4A,B). More importantly, levels of CD4 $^+$  and CD8 $^+$  T cell responses induced by E7 protein either mixed or coupled to Q $\beta$ (1668) were similar, suggesting that chemical association of the antigen and adjuvant is dispensable for priming (Figures 4A,B) T cell responses.

## Mixing of Antigens and CpG-Loaded VLP of Similar Size Is Sufficient for Induction of Strong T Cell Responses

After establishing that Q $\beta$ (1668) was necessary to induce IFN $\gamma$  production by CD8 $^+$  T cells in response to E7 and that DCs simultaneously take up antigen and VLP if simply mixed, it was investigated whether such formulation was sufficient for induction of protective T cell responses or whether covalent

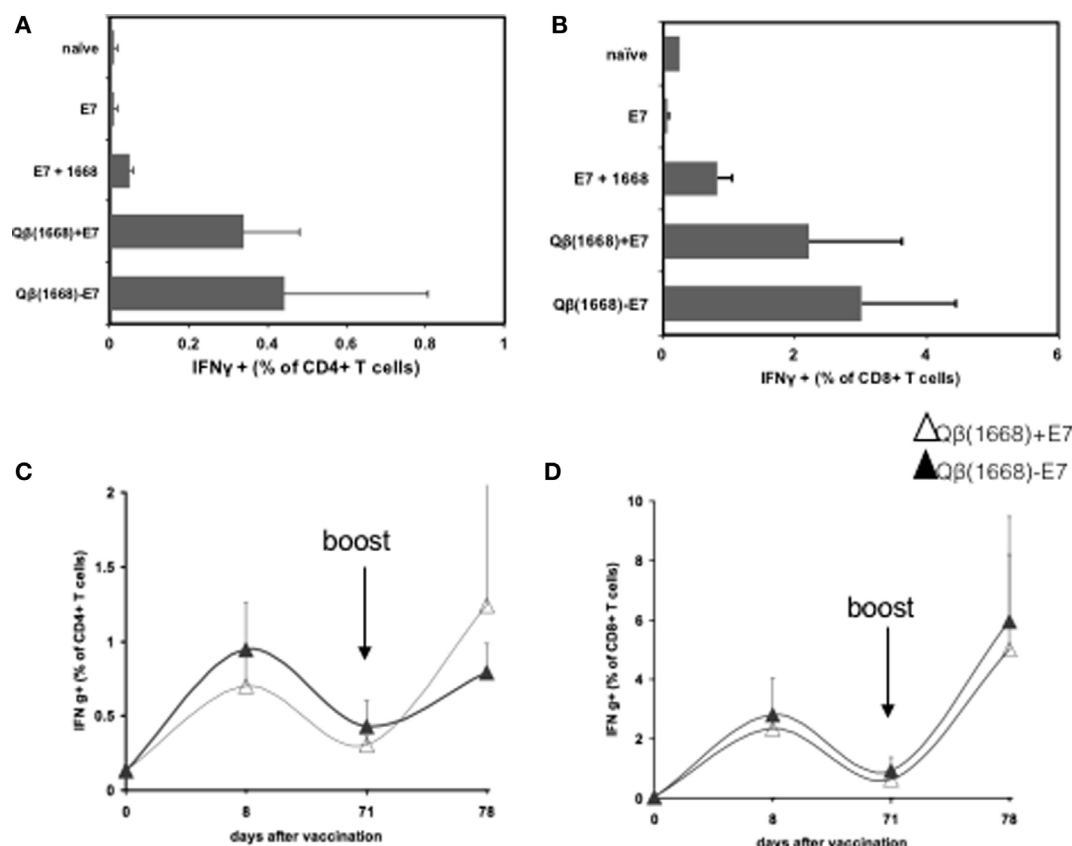


**FIGURE 4 | Coupling of similar size antigens to VLPs is not required for cytokine production by T cells.** C57BL/6 mice were immunized, and T cell responses were assessed 8 days later. **(A)** IFN $\gamma$  production by CD4+ T cells after immunization with E7 protein, E7 mixed with 1668, Q $\beta$ (1668) + E7 mixed and Q $\beta$ (1668) – E7 coupled. **(B)** IFN $\gamma$  production by CD8+ T cells after immunization with E7 protein, E7 mixed with 1668, Q $\beta$ (1668) + E7 mixed, and Q $\beta$ (1668) – E7 coupled. Mice were immunized with mixed or coupled vaccines. Boost was administered 70 days after first dose, blood was collected on days 0, 8, 71, and 78 for IFN $\gamma$  measurements. **(C)** Kinetics of IFN $\gamma$  production by CD4+ T cells from blood. **(D)** Kinetics of IFN $\gamma$  production by CD8+ T cells from blood. Data represented as mean + SD  $n = 5$  mice per group.

linkage of E7 oligomers to Q $\beta$ (1668) VLPs was necessary. First, the kinetics and duration of the response were measured. E7 was either chemically coupled to or mixed with Q $\beta$ (1668) and C57BL/6 mice were immunized s.c. in a prime-boost scheme 70 days apart. T cell responses were followed in the blood by intracellular cytokine staining for IFN $\gamma$ . Both experimental groups mounted strong primary CD4+ and CD8+ T cell responses that had declined by day 70 and were strongly increased after the boost injection (Figures 4C,D, respectively). CD4+ and CD8+ T cells from the blood were analyzed by intracellular cytokine staining upon *in vitro* stimulation on day 78.

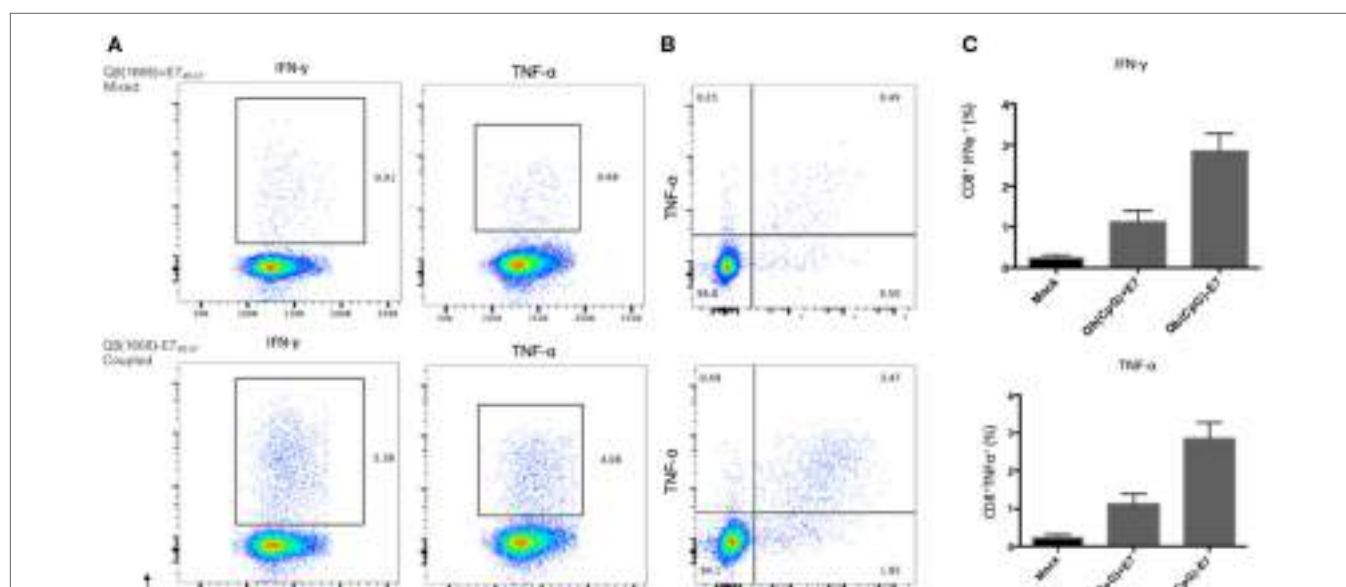
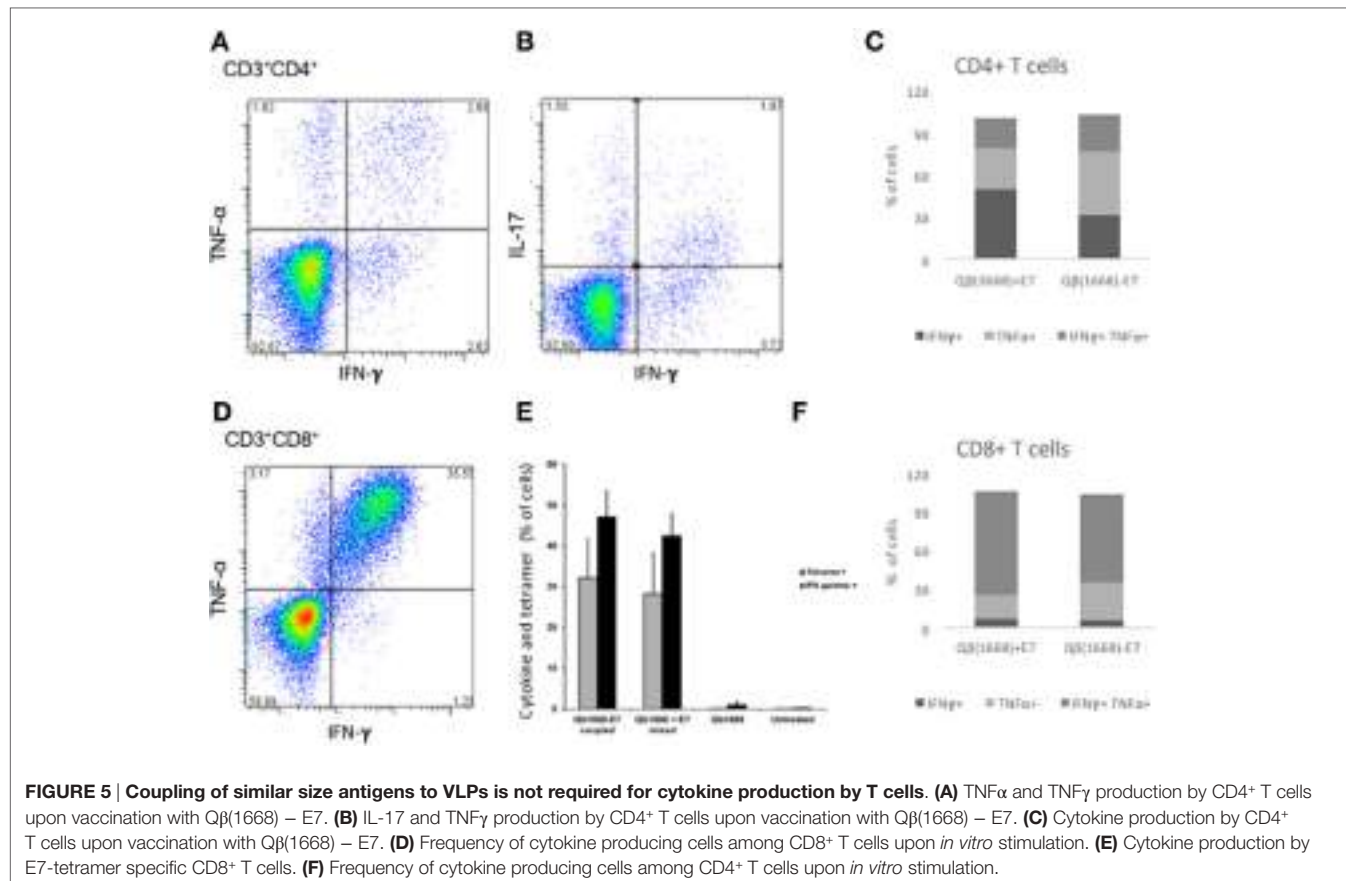
To further investigate the cytokine production of splenic T cells, spleens were collected on day 78. Both vaccination regimens induced strong CD8+ and CD4+ T cell responses expressing multiple cytokines (Figure 5) and induction of multifunctional CD4+ T cells producing IFN $\gamma$ , TNF $\alpha$ , and IL-17 (Figure 5A,B) were observed. For CD8+ T cells, a strong induction of TNF $\alpha$  and IFN $\gamma$ -producing T cells was detected (Figure 5D,E). The number

of tetramer-positive cells was roughly similar to the frequency of IFN $\gamma$ -producing CD8+ T cells (Figure 5E). Thus, as observed in the blood, linked E7 protein induced similar frequencies of cytokine-producing T cells compared to the mixed formulation in splenic T cells (Figure 5).

In marked contrast to the results obtained with particulate E7 proteins, for small peptides, linkage to the VLP was essential. Specifically, mice immunized with the peptide E7<sub>49–57</sub> coupled to Q $\beta$ (1668) generated strong CD8+ T cell responses. In contrast, E7<sub>49–57</sub> mixed to Q $\beta$ (1668) failed to induce good production of IFN $\gamma$  and TNF $\alpha$  by CD8+ T cells significantly above background (Figure 6).

## Mixing of E7 Protein with Q $\beta$ (1668) Is Sufficient for Eradication of Established Tumors

In order to assess the therapeutic capacity of the vaccine-induced T cells, mice were injected with TC-1 cells expressing HPV16



E7 oncoprotein. Eight days post injection of tumor cells, mice developed palpable tumors and were subjected to a weekly immunization schedule with E7 coupled or mixed to Q $\beta$ (1668) for 49 days (**Figure 7A**). In untreated mice, as well as mice injected with Q $\beta$ (1668) only, tumors grew unrestrained and 50% of mice reached severity scores requiring euthanasia by day 32 (**Figure 7B**). In contrast, both coupled and mixed formulation of Q $\beta$ (1668) and E7 protein were able to induce strong protection against tumor growth resulting in survival rate of more than 80% until the end of the study. In an additional study, vaccination with E7 mixed with Q $\beta$ (1668) extended the survival of tumor bearing mice to more than 3 months (data not shown). Therefore, covalent linkage of the E7 to Q $\beta$ (1668) VLPs is not required for induction of protective T cell responses against solid tumor.

### Covalent Linkage of E7 Oligomers to CpG-Loaded VLPs Is Required for Induction of Optimal B Cell Responses

In order to understand whether the same rules would apply to B cells, the importance of covalent linkage of E7 to Q $\beta$  VLPs for

induction of optimal antibody responses was assessed. Serum collected from mice immunized with E7 coupled or mixed with Q $\beta$ (1668) were analyzed for E7-specific antibody response by ELISA. Importantly, only covalent coupling but not simple mixing of E7 and Q $\beta$ (1668) was able to enhance the antibody response against E7 (**Figure 8A**). Conversely, the antibody levels raised against Q $\beta$  were higher in the mixed formulation when compared to the coupled counterpart (**Figure 8B**). Antibody induction against the E7<sub>49-57</sub> peptide also required covalent linkage, as in the absence of linkage, antibody levels induced were comparable to the background (**Figure 8C**). Hence, in contrast to T cell responses, B cell responses appear to require physical linkage of antigen and adjuvants in order to induce appropriate levels of antibody responses irrespective of the size of the antigen.

## DISCUSSION

In the current study, we demonstrated in an HPV model that a particulate VLP-based vaccine containing CpG exerts distinct adjuvant effects in B and T cells. While for T cells, the concomitant

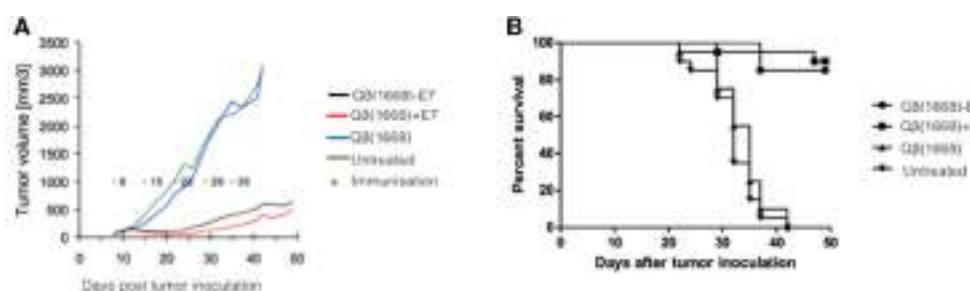


**FIGURE 7 | Simply mixing of similar size antigen and adjuvant is enough for protection against tumor.** **(A)** Tumor growth after tumor challenge in immunized mice with mixed and coupled vaccines or controls was monitored over 50 posttumor inoculation. **(B)** C57BL/6 female mice ( $n = 5$  per group) were injected i.v. with  $1.5 \times 10^5$  TC-1 cells expressing HPV-16 E7 oncoprotein. Crosses indicate the weekly immunization schedule with E7 coupled or mixed to Q $\beta$ (1668) for 49 days. **(B)** Percent of survival and tumor growth in immunized groups was monitored over time and represented in a Kaplan–Meier survival curve and analysed using the Log-rank test;  $^*P < 0.05$ .

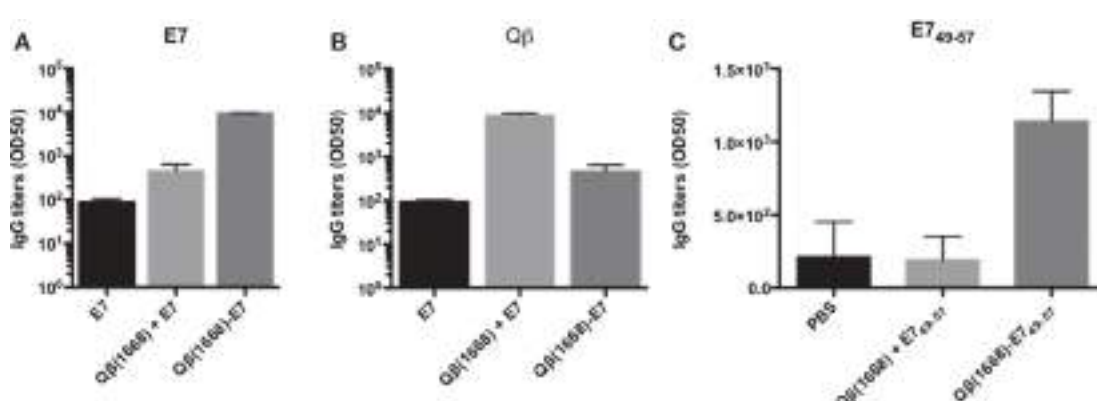


**FIGURE 8 | Covalent linkage is required for optimal responses of B cells.** **(A)** Antibody titers for IgG against E7 expressed in log scale of OD50 on day 71. **(B)** Total IgG titers expressed in log scale of OD50 against Q $\beta$  at day 71 measured by ELISA. Mean with SEM in log transformed titers. **(C)** Antibody titers expressed in OD50 against the peptide E7<sub>49-57</sub>. Values as mean ( $n = 5$ ) plus SEM.

draining of antigen and adjuvant to LNs and subsequent uptake by APCs is enough for T cell-mediated cytokine production and protection against the expansion of tumors, for B cells, appropriate presentation of antigens by linkage to VLPs is required for induction of optimal antibody levels.

This dichotomy may be explained by mechanistic differences in the induction of innate and adaptive immune responses. The innate arm of the immune system represented by DCs is able to recognize certain pathogen and danger-associated patterns (23). However, specific receptor-ligand interaction is not required in order to induce phagocytosis and activation (24). Thus, DCs will non-specifically take up both antigen and VLP. This is strictly different for B cells, which take up particles in an antigen-specific fashion. For B cells to be exposed to CpGs packaged within VLPs, they need to take up the particles via their B cell receptors (BCR), which will be followed by internalization of the VLP plus their CpG cargo (25). Therefore, E7-specific B cells will fail to take up VLPs loaded with CpGs unless E7 is linked to the VLPs. In addition to that, VLPs are potent activators of B cells (26, 27) and the presentation of the coupled antigens in the surface of the VLPs in a geometrically defined and repetitive manner promotes cross-linking of the BCR, which helps surpass the threshold for cellular activation (28). In the case of large antigens such as E7, the coupling is limited by steric hindrance of the proteins, limiting the number of copies of E7 that can be exposed. However, our data suggest that even with relatively low valency of the antigen, coupling exerts a positive impact on the level of antibodies produced.

For priming of T cell responses, activation of the DCs presenting the specific antigen is required (29). The simultaneous uptake of antigen and adjuvants by DCs, but not by T cells is critical (30). However, in contrast to B cells, DCs take up particulate antigens non-specifically without need for antigen-specific receptors (31). Given that DCs on average can accommodate and take up 70 particles (at a size of about 30 nm) (32), most DCs will take up reasonable numbers of both particle species at the same time. Therefore, simple co-exposure of DCs to particulate antigen and adjuvants is sufficient for simultaneous uptake of both entities. This guarantees that DCs will be appropriately activated providing optimal signaling to T cells.

Of particular note, the conclusions from this study are in agreement with a growing body of evidence that proposes that the size of antigens conveys major influence on factors driving immunity (14, 15, 17, 18). Peptides are well known to be unable to induce relevant immune responses; this is likely a result of inefficient drainage, degradation, or uptake by resident DCs *in vivo*.

## REFERENCES

1. Weimer T, Salfeld J, Will H. Expression of the hepatitis B virus core gene in vitro and in vivo. *J Virol* (1987) 61:3109–13.
2. Spohn G, Jennings GT, Martina BE, Keller I, Beck M, Pumpens P, et al. A VLP-based vaccine targeting domain III of the West Nile virus E protein protects from lethal infection in mice. *Virology* (2010) 7:146. doi:10.1186/1743-422X-7-146
3. Roldão A, Mellado MCM, Castilho LR, Carrondo MJ, Alves PM. Virus-like particles in vaccine development. *Expert Rev Vaccines* (2010) 9:1149–76. doi:10.1586/erv.10.115

that do not migrate to the LNs. A position that appears to have been confirmed here, as administered peptides failed to charge LN resident DCs.

Collectively, these observations are important for vaccine development, as they elucidate distinct requirements for induction of optimal B versus T cell responses and indicate that the use of both particulate antigens and adjuvants with similar size avoids the necessity of conjugating the two entities together. This may be especially important for the development of patient-specific vaccines. VLPs are an attractive platform for personalized vaccines considering the convenience of production and low costs.

Based on the findings of this work, a new advantage is attributed to such nanoparticles, as we show that covalent linkage of antigen and adjuvants might not be necessary to obtain protective tumor-specific T cells. This knowledge can be used to design antigens that would not require coupling, which would streamline the manufacturing process and increase cost-savings. Also, this simple system of mixed and coupled vaccines stands as an attractive tool to explore the dynamic of humoral and cellular responses and how they interact.

## ETHICS STATEMENT

This study was carried out in accordance with the recommendations of the Animals (Scientific Procedures) Act 1986 (ASPA) and European Directive 2010/63/EU on the protection of animals used for scientific purposes.

## AUTHOR CONTRIBUTIONS

AG, AF, and FZ performed the experiments. MB, VM, and PS designed the experiments. AG, VM, and MB wrote the manuscript. GC-M and AT provided technical support.

## ACKNOWLEDGMENTS

We thank Joshua Blight for critical reading of the manuscript and Fabiana Leorati for scientific advice and support.

## FUNDING

This project was partially funded by the Science without Borders scheme (CNPq, Brazil), Research support grant from Kellogg College (Oxford, UK) and Swiss Cancer League (KFS-2993-08-2012).

4. Hemann EA, Kang S-M, Legge KL. Protective CD8 T cell-mediated immunity against influenza A virus infection following influenza virus-like particle vaccination. *J Immunol* (2013) 191:2486–94. doi:10.4049/jimmunol.1300954
5. Zinkernagel RM. On natural and artificial vaccinations. *Annu Rev Immunol* (2003) 21:515–46. doi:10.1146/annurev.immunol.21.120601.141045
6. Pennock ND, Kedl JD, Kedl RM. T cell vaccinology: beyond the reflection of infectious responses. *Trends Immunol* (2016) 37:170–80. doi:10.1016/j.it.2016.01.001
7. Grun JL, Maurer PH. Different T helper cell subsets elicited in mice utilizing two different adjuvant vehicles: the role of endogenous interleukin 1 in

- proliferative responses. *Cell Immunol* (1989) 121:134–45. doi:10.1016/0008-8749(89)90011-7
8. Hou B, Saudan P, Ott G, Wheeler ML, Ji M, Kuzmich L, et al. Selective utilization of toll-like receptor and MyD88 signaling in B cell for enhancement of the anti-viral germinal center response. *Immunity* (2012) 34:375–84. doi:10.1016/j.jimmuni.2011.01.011
  9. Jegerlehner A, Maurer P, Bessa J, Hinton HJ, Kopf M, Bachmann MF. TLR9 signaling in B cells determines class switch recombination to IgG2a. *J Immunol* (2007) 178:2415–20. doi:10.4049/jimmunol.178.4.2415
  10. Krieg AM. Therapeutic potential of toll-like receptor 9 activation. *Nat Rev Drug Discov* (2006) 5:471–84. doi:10.1038/nrd2059
  11. Schwarz K, Meijerink E, Speiser DE, Tissot AC, Cielens I, Renhof R, et al. Efficient homologous prime-boost strategies for T cell vaccination based on virus-like particles. *Eur J Immunol* (2005) 35:816–21. doi:10.1002/eji.200425755
  12. Milan R, Ivan S, Jana S, Jana B, Hana P, Marie I, et al. Induction of protective immunity against MHC class I-deficient, HPV16-associated tumors with peptide and dendritic cell-based vaccines. *Int J Oncol* (2010) 36:545–51. doi:10.3892/ijo-00000528
  13. Katsikis PD, Schoenberger SP, Mourao-sa D, Roy S. Crossroads between Innate and Adaptive Immunity. Vol. 785. Switzerland: Springer International Publishing (2013).
  14. Fifis T, Gamvrellis A, Crimeen-Irwin B, Pietersz GA, Li J, Mottram PL, et al. Size-dependent immunogenicity: therapeutic and protective properties of nano-vaccines against tumors. *J Immunol* (2004) 173:3148–54. doi:10.4049/jimmunol.173.5.3148
  15. Jia R, Guo JH, Fan MW. The effect of antigen size on the immunogenicity of antigen presenting cell targeted DNA vaccine. *Int Immunopharmacol* (2012) 12:21–5. doi:10.1016/j.intimp.2011.08.016
  16. Reddy ST, van der Vlies AJ, Simeoni E, Angeli V, Randolph GJ, O’Neil CP, et al. Exploiting lymphatic transport and complement activation in nanoparticle vaccines. *Nat Biotechnol* (2007) 14:103. doi:10.1038/nbt1332
  17. Manolova V, Flace A, Bauer M, Schwarz K, Saudan P, Bachmann MF. Nanoparticles target distinct dendritic cell populations according to their size. *Eur J Immunol* (2008) 38:1404–13. doi:10.1002/eji.200737984
  18. Yue H, Wei W, Yue Z, Lv P, Wang L, Ma G, et al. Particle size affects the cellular response in macrophages. *Eur J Pharm Sci* (2010) 41:650–7. doi:10.1016/j.ejps.2010.09.006
  19. Bachmann MF, Jennings GT. Vaccine delivery: a matter of size, geometry, kinetics and molecular patterns. *Nat Rev Immunol* (2010) 10:787–96. doi:10.1038/nri2868
  20. Alonso LG, García-Alai MM, Smal C, Centeno JM, Iacono R, Castaño E, et al. The HPV16 E7 viral oncoprotein self-assembles into defined spherical oligomers. *Biochemistry* (2004) 43:3310–7. doi:10.1021/bi036037o
  21. Kozlovska TM, Cielens I, Dreilinna D, Dišlers A, Baumanis V, Osea V, et al. Recombinant RNA phage Qβ capsid particles synthesized and self-assembled in *Escherichia coli*. *Gene* (1993) 137:139–43. doi:10.1016/0378-1119(93)90261-Z
  22. Storni T, Ruedl C, Schwarz K, Schwendener RA, Renner WA, Bachmann MF. Nonmethylated CG motifs packaged into virus-like particles induce protective cytotoxic T cell responses in the absence of systemic side effects. *J Immunol* (2004) 172:1777–85. doi:10.4049/jimmunol.172.3.1777
  23. Janeway CA, Medzhitov R. Innate immune recognition. *Annu Rev Immunol* (2002) 20:197–216. doi:10.1146/annurev.immunol.20.083001.084359
  24. Buckwalter MR, Albert ML. Orchestration of the immune response by dendritic cells. *Curr Biol* (2009) 19:355–61. doi:10.1016/j.cub.2009.03.012
  25. Eckl-Dorna J, Batista FD. BCR-mediated uptake of antigen linked to TLR9 ligand stimulates B-cell proliferation and antigen-specific plasma cell formation. *Blood* (2009) 113:3969–77. doi:10.1182/blood-2008-10-185421
  26. Bachmann MF, Hengartner H, Zinkernagel RM. T helper cell-independent neutralizing B cell response against vesicular stomatitis virus: role of antigen patterns in B cell induction? *Eur J Immunol* (1995) 25:3445–51. doi:10.1002/eji.1830251236
  27. Zabel F, Kündig TM, Bachmann MF. Virus-induced humoral immunity: on how B cell responses are initiated. *Curr Opin Virol* (2013) 3:357–62. doi:10.1016/j.coviro.2013.05.004
  28. Dintzis HM, Dintzis RZ, Vogelstein B. Molecular determinants of immunogenicity: the immunon model of immune response. *Proc Natl Acad Sci U S A* (1976) 73:3671–5. doi:10.1073/pnas.73.10.3671
  29. Masson F, Mount AM, Wilson NS, Belz GT. Dendritic cells: driving the differentiation programme of T cells in viral infections. *Immunol Cell Biol* (2008) 86:333–42. doi:10.1038/icb.2008.15
  30. MartIn-Fontecha A, Sebastiani S, Höpken UE, Uggioni M, Lipp M, Lanzavecchia A, et al. Regulation of dendritic cell migration to the draining lymph node: impact on T lymphocyte traffic and priming. *J Exp Med* (2003) 198:615–21. doi:10.1084/jem.20030448
  31. López-Bravo M, Ardagán C. In vivo induction of immune responses to pathogens by conventional dendritic cells. *Immunity* (2008) 29:343–51. doi:10.1016/j.jimmuni.2008.08.008
  32. Keller SA, Schwarz K, Manolova V, von Allmen CE, Kinzler MG, Bauer M, et al. Innate signaling regulates cross-priming at the level of DC licensing and not antigen presentation. *Eur J Immunol* (2010) 40:103–12. doi:10.1002/eji.200939559

**Conflict of Interest Statement:** MB declares to be involved in a number of companies developing VLP-based vaccines. FZ is an employee of Hypopet AG. The other authors declare no further conflicts of interest.

Copyright © 2017 Gomes, Flace, Saudan, Zabel, Cabral-Miranda, Turabi, Manolova and Bachmann. This is an open-access article distributed under the terms of the Creative Commons Attribution License (CC BY). The use, distribution or reproduction in other forums is permitted, provided the original author(s) or licensor are credited and that the original publication in this journal is cited, in accordance with accepted academic practice. No use, distribution or reproduction is permitted which does not comply with these terms.



# An Approach for a Synthetic CTL Vaccine Design against Zika Flavivirus Using Class I and Class II Epitopes Identified by Computer Modeling

Edecio Cunha-Neto<sup>1,2,3</sup>, Daniela S. Rosa<sup>2,4</sup>, Paul E. Harris<sup>5</sup>, Tim Olson<sup>6</sup>, Alex Morrow<sup>6</sup>, Serban Ciotlos<sup>6</sup>, Charles V. Herst<sup>6</sup> and Reid Martin Rubsamen<sup>6,7\*</sup>

## OPEN ACCESS

### Edited by:

Laurent Rénia,  
Agency for Science, Technology and  
Research (A\*STAR), Singapore

### Reviewed by:

Daniel Olive,  
Institut national de la santé  
et de la recherche médicale  
(INSERM), France

Sarah Rowland-Jones,  
Oxford University, United Kingdom

### \*Correspondence:

Reid Martin Rubsamen  
reidrubsamen@alum.mit.edu

### Specialty section:

This article was submitted to  
Vaccines and Molecular  
Therapeutics,  
a section of the journal  
*Frontiers in Immunology*

Received: 22 December 2016

Accepted: 16 May 2017

Published: 09 June 2017

### Citation:

Cunha-Neto E, Rosa DS, Harris PE,  
Olson T, Morrow A, Ciotlos S,  
Herst CV and Rubsamen RM (2017)  
*An Approach for a Synthetic CTL  
Vaccine Design against Zika Flavivirus  
Using Class I and Class II Epitopes  
Identified by Computer Modeling.*  
*Front. Immunol.* 8:640.  
doi: 10.3389/fimmu.2017.00640

<sup>1</sup>Laboratory of Clinical Immunology and Allergy-LIM60, University of São Paulo School of Medicine, São Paulo, Brazil,

<sup>2</sup>Institute for Investigation in Immunology (III) INCT, São Paulo, Brazil, <sup>3</sup>School of Medicine, Heart Institute (Incor), University of São Paulo, São Paulo, Brazil, <sup>4</sup>Department of Microbiology, Immunology and Parasitology, Federal University of São Paulo (UNIFESP/EPM), São Paulo, Brazil, <sup>5</sup>Endocrinology Division, Department of Medicine, School of Medicine, Columbia University, New York, NY, United States, <sup>6</sup>Flow Pharma, Inc., Redwood City, CA, United States, <sup>7</sup>Department of Anesthesia, Critical Care and Pain Medicine, Massachusetts General Hospital, Boston, MA, United States

The threat posed by severe congenital abnormalities related to Zika virus (ZKV) infection during pregnancy has turned development of a ZKV vaccine into an emergency. Recent work suggests that the cytotoxic T lymphocyte (CTL) response to infection is an important defense mechanism in response to ZKV. Here, we develop the rationale and strategy for a new approach to developing cytotoxic T lymphocyte (CTL) vaccines for ZKV flavivirus infection. The proposed approach is based on recent studies using a protein structure computer model for HIV epitope selection designed to select epitopes for CTL attack optimized for viruses that exhibit antigenic drift. Because naturally processed and presented human ZKV T cell epitopes have not yet been described, we identified predicted class I peptide sequences on ZKV matching previously identified DNV (Dengue) class I epitopes and by using a Major Histocompatibility Complex (MHC) binding prediction tool. A subset of those met the criteria for optimal CD8+ attack based on physical chemistry parameters determined by analysis of the ZKV protein structure encoded in open source Protein Data File (PDB) format files. We also identified candidate ZKV epitopes predicted to bind promiscuously to multiple HLA class II molecules that could provide help to the CTL responses. This work suggests that a CTL vaccine for ZKV may be possible even if ZKV exhibits significant antigenic drift. We have previously described a microsphere-based CTL vaccine platform capable of eliciting an immune response for class I epitopes in mice and are currently working toward *in vivo* testing of class I and class II epitope delivery directed against ZKV epitopes using the same microsphere-based vaccine.

**Keywords:** Zika vaccine, epitope, CTL vaccine, protein folding, dengue, flavivirus, computer model

## 1. INTRODUCTION

As of Fall 2016, the Zika Virus (ZKV) pandemic continues its northward spread in the Americas. The CDC estimates at least 4,100 cases in the United States and up to 29,000 cases in Puerto Rico. Those cases in Puerto Rico include 672 pregnant women (1). Using a data-driven global stochastic epidemic model to project past and future spread of the ZKV in the Americas, it has been estimated that the large population centers of Florida, New York, and New Jersey will be seeing significant numbers of imported cases (acquired by travel) of ZKV infection (2) by the end of Fall 2016. In South America, the new case rate of ZKV infection is tapering off, however, researchers in Brazil warn that official statistics may significantly underestimate the size of the ZKV epidemic based on improved serological tools that have become recently available. In any event, when a significant proportion of the population is infected with a viral infection and become immune, the epidemic can migrate to an area with a larger susceptible individual pool. Given the alarming news that significant brain defects were detected in newborns of 42% women infected with ZKV during pregnancy, including the third trimester (29%) (3), the public health threat of ZKV in pregnant women is even higher than expected before. Taken together, recent estimates put 1.65 million childbearing women in the Americas at risk of ZKV infection. As yet no phase II trials of a ZKV vaccine have been initiated. We review critical aspects of the unique pathogenesis of ZKV infection which will need to be considered when evaluating the efficacy of such vaccines and designing next iterations of possible ZKV vaccines to improve vaccine efficacy. In this article, we will also highlight details of the vaccines currently under consideration for Phase I and Phase II clinical trials, develop the argument that vaccines that evoke antibody responses need careful scrutiny, outline the rationale why our group is focusing on developing a “pure” CTL vaccine, and enumerate many of the challenges that will need to be overcome to develop an effective ZKV CTL vaccine.

### 1.1. Genome and Protein Structure of ZKV

ZKV is a small enveloped plus strand RNA virus belonging to the genus Flavivirus, which includes many human pathogenic viruses, such as Dengue virus (DNV), yellow fever virus (YFV), West Nile Virus (WNV), and hepatitis C virus (HCV). ZKV has a 10.8 kb RNA genome, containing a single open reading frame flanked by a 5'-UTR (106 nt long) and a 3'-UTR (428 nt long). The open reading frame encodes a polyprotein precursor, which is processed into three structural proteins [capsid (C), premembrane (prM), and envelope (E)] and seven non-structural proteins (NS1, NS2A, NS2B, NS3, NS4A, NS4B, and NS5). The viral E protein is the major surface glycoprotein of flavivirus, and the non-structural NS3 and NS5 encode essential enzyme activities for viral reproduction. The E protein is divided into three discernible domains (Domain I, Domain II, and Domain III). Domain I is involved in the envelope structure organization, and Domain II and Domain III are related to the monomers interaction and receptor binding, respectively (4).

### 1.2. Protective Immune Responses to Flaviviruses: Role of T Cells

Significant information is available about the protective role of T cell responses against other flaviviruses of clinical importance. Prevention of infection is achieved primarily by neutralizing antibodies but T cell responses (both CD4+ and CD8+) are of utmost importance for virus clearance. Cytotoxic CD8+ T cells are critical to eliminate virus-infected cells while CD4+ T cells provide help to cytotoxic CD8+ T cells and antibody production (5, 6). DNV-specific CD8+ T cells play a protective role in natural DNV infection both in humans and in animal models (7) and polyfunctional CD8+ responses are associated with protection against disease (8). CD8+ T cell immunity has been shown to be protective against WNV infection (9). Vaccination with a tetravalent DNV vaccine elicits CD8+ T cell responses against highly conserved epitopes (10). Similar, the live-attenuated 17D-based YFV vaccine elicits potent and long-lasting CD8+ T cell responses (11–13). Progress toward understanding the role of CD4+ T cell immunity in flavivirus infection is recent. YFV 17D-204 vaccination and adoptive transfer experiments demonstrate that CD4+ T cells contributed to protection against virulent YFV (14). Similar CD4+ responses have been found to be critical for protection against DNV challenge (15) and for the prevention of encephalitis during WNV infection (16). More recently, the CTL response in a murine ZKV model has shown to be crucial for protection against ZKV infection, both in CD8 depletion experiments in mice and passive transfer of memory CD8+ T cells to naive mice exposed to infection. Furthermore, deletion of the CD8a<sup>-/-</sup> gene leads to 100% death after infection. This CD8+ T cell response is cytotoxic, polyfunctional, and targeted to several H-2D-restricted epitopes (17).

## 2. SPECIFIC POTENTIAL ADVANTAGES OF CTL VERSUS ANTIBODY VACCINE FOR ZKV

### 2.1. Caveats of Antibody-Inducing ZKV Vaccines

Following the acute phase infection of ZKV (with or without clinical symptoms), the persistence of biomarkers of ZKV infection (e.g., viral RNA in semen) suggest that some cells may be chronically infected. The wide distribution of types and anatomical locations of cells permissive for ZKV infection, sometimes beyond the easy reach of antibodies (e.g., blood-brain barrier), suggest that a cell mediated immune response will be critical for immune surveillance of chronically infected cells. While there can be little doubt that a ZKV vaccine stimulating a neutralizing antibody response will be a key resource in limiting viremia during the acute phase of ZKV infection, there are some concerns regarding the exact nature of the antibody response provoked. The exact pathological mechanism which drives Guillain-Barré syndrome (GBS) remains unknown although there seems to a general consensus that antiglycolipid antibodies play an important role, although not every GBS patient develop this type of antibody. As discussed earlier, there is an increased incidence

of GBS associated with ZKV infection (18, 19), but it is not known whether antiganglioside antibodies have a role in this specific comorbidity of ZKV infection. Each of the four different DNV serotypes (DNV 1–4) provoke cross-reactive antibody responses that may contribute to the increased disease severity observed following subsequent infection with a different serotype. The first DNV infection is either subclinical or result in a mild disease, and results in long lasting immunity to the serotype. The next DNV infection, if initiated by a different serotype, can induce severe, potentially lethal disease termed Dengue hemorrhagic fever/Dengue shock syndrome (20, 21). The immunopathogenesis of severe disease is not completely understood. One model, termed antibody-dependent enhancement (ADE), works as follows: anti-DNV antibodies evoked by the primary infection, which were once neutralizing but are not with the current serotype, bind the second serotype viral particles and promote antibody mediated phagocytosis by myeloid antigen-presenting cells which in turn become infected serving as a future reservoir for infectious virions with impaired functional activity (22). Of note are recent reports demonstrating that preexisting anti DNV abs can enhance ZKV infection (23, 24). Conversely, preexisting serum anti-ZKV antibodies were able to enhance DNV infection *in vitro* (25). This is due to the high serological crossreactivity between both flaviviruses which may not be cross-neutralizing. This crossreactivity is so relevant that it has delayed the development of highly specific, non-DNV crossreactive serodiagnostic tests for ZKV infection. An additional concern for flavivirus vaccination-induced pathogenic antibodies in humans came from the recent reports of severe DNV breakthrough infections requiring hospitalization, after vaccination of seronegative volunteers with an antibody-inducing DNV attenuated virus tetravalent vaccine (Dengvaxia®), a phenomenon possibly related to ADE (26). This is a special concern since epidemics of both flaviviruses occur simultaneously in the same regions (27). Their research using a mouse model exhibiting much of the same symptoms/pathology of Dengue fever in humans, concluded “a sub-protective humoral response may, under some circumstances, have pathological consequences.” This group has since shifted their focus to inducing CD8+ T cell-mediated immunity to DNV (7, 28–31). Furthermore, the possibility that preexisting non-neutralizing anti-ZKV antibody-dependent enhancement could facilitate infection of fetal–mother interface tissues and contribute to fetal ZKV infection has not been excluded yet. Of note, currently studied ZKV candidate vaccines currently in the pipeline, either in the preclinical or phase I trial (one ongoing trial) phases, aim to elicit antibodies and are all based on whole envelope proteins, or whole inactivated or live attenuated virus (32). Preclinical studies using vaccines encoding whole ZKV preM/E proteins in DNA form, using adenovirus vectors, or whole inactivated ZKV in non-human primate models have been able to elicit neutralizing antibodies and protection after ZKV challenge (33, 34).

Taken together, these findings suggest caution in needed in the development of whole protein ZKV vaccines where evoked antibody responses that are not neutralizing may possibly enhance infection or be pathogenic (i.e., autoimmune) or could facilitate infection of maternal–fetal interface tissue.

## 2.2. Epitope-Based T Cell Vaccines

Given the concerns with antibody-inducing flavivirus vaccines, one possible alternative would be to harness the power of the T cell immune response in protecting against flavivirus infection, as mentioned above. A recent report has shown that CD8+ T cell prevent antigen induced antibody-dependent enhancement of Dengue disease in a murine model and several studies have identified DNV T cell epitopes appropriate for inclusion in a T cell-based vaccine (31, 35–38). Another recent study shows the critical role of CTL response for protection against ZKV infection in a mouse model; this article identifies ZKV H-2D restricted epitopes recognized by CD8+ T cells from infected mice (17). Recent clinical trials have demonstrated the efficacy of T-cell-inducing vaccines against a number of diseases (39), but immunization with whole proteins may favor responses to regions subject to antigenic drift and immune escape. A way to counteract this is to focus the response into specific desirable epitopes. The T cell epitope-based vaccine approach may target the immune response only to desirable and relevant epitopes, instead of the whole protein. Relevant epitopes include those that come from conserved viral protein regions, and/or where mutations could lead to reduced viral fitness, and those that bind to multiple MHC variant molecules—thus potentially recognized by the majority of the target population—while avoiding regions that are poorly immunogenic, variable and subject to antigenic drift, or that could cause a harmful response (40). These targeted immune responses could lead to increased potency, as well as increasing safety (41, 42). There are several ongoing clinical trials of T cell epitope-based Influenza vaccines aiming to be universal vaccines (43). Mapping and selection of potential immunogenic T cell epitopes is a crucial step that may be performed either with the aid of bioinformatics tools and experimental confirmation or by empirical approach using peptide library spanning the antigen full sequence.

## 2.3. Antigenic Drift: Parallels to Chronic HIV Infection and Implications for Vaccine Design

In chronic HIV infection there exists a reservoir of latent, transcriptionally silent viral infection within the resting memory CD4+ T cell compartment and specific myeloid lineage cells (e.g., CD14+/CD16+ monocytes) [reviewed in Ref. (44, 45)]. The resting CD4+ memory cells have long life spans, can remain quiescent, and similar to some of the ZKV tissue targets such placental, neuronal, and gonadal tissues as recently described in mice (46), may reside in immune-privileged sites such as the B cell follicle of lymph nodes, allowing escape from existing immune surveillance mechanisms (47). While the mechanism that triggers active replication in HIV+ CD4+ memory cells is poorly understood, interruption of antiretroviral therapy is associated with the resumption of viral replication. Unfortunately, preexisting HIV-1-specific CD8+ T cell responses have shown to be ineffective [reviewed in Ref. (48)] due to viral evolution of CTL epitopes, resulting in a limited repertoire of effective of cytotoxic T cell-mediated immune responses (49) and progression to AIDS. In HIV infection there are selection pressures exerted by

the cellular immune system which result in antigenic drift in new virions (50).

A recent murine model study has demonstrated the potential importance of the CTL response to ZKV infection where H-2D restricted CTL epitopes were identified (17). Studies of HIV specific CTL responses in a subset of HIV+ individuals may also prove informative. HIV controllers (i.e., individuals who are HIV+ yet maintain low viral loads and do not progress to AIDS) have been carefully studied (51). HIV controller status is associated with the ability to develop CTL responses to regions of HIV proteins critical for maintenance of their structure–function (and viral fitness). Pereyra et al. (51) demonstrated that it may be possible to predict CTL class I epitopes favored by HIV controllers and suggested that CTL vaccines designed to evoke cellular immune responses to MHC class I restricted epitopes found within viral protein regions resistant to antigenic drift could lead to improved efficacy of HIV vaccines perhaps mimicking what happens naturally in HIV controllers. Our group has been inspired by these studies and has selected this general approach in the development of a CTL vaccine for ZKV.

Flaviviruses mutate in response to immune system pressure, both by antibodies and T cells. It has been reported that HLA class I-binding residues of a CD8+ T cell epitope encompassing the conserved catalytic site of DNV NS3 protease suffer variation that can abrogate HLA class I binding, suggesting evasion of DNV from a specific CD8+ T cell response by antigenic drift (52). Antigenic drift in ZKV has not been thoroughly studied, but a phylogenetic analysis of contemporary human isolates show a common ancestor and as many as 34 amino acid substitutions relative to the common ancestors with most of the variation contained within the prM protein (53, 54), suggesting that ZKV does not undergo viral evolution as fast as HIV does. However, a recent phylogenetic study on 17 whole ZKV genomes from human isolates in the present epidemic has shown the mutation rate varies between 12 and 25 bases (0.12–0.25% of the polyprotein) per year since the 2013 Polynesia outbreak. The latest sequence shows 64 mutations; and overall, 62 non-synonymous amino acid changes were observed among all sequences analyzed, demonstrating that the ZKV continues to mutate at a rapid rate during the current epidemic (55). The rationale of focusing CTL attack to ZKV protein regions that are “intolerant” to amino acid substitutions thus remains sound.

## 2.4. ZKV HLA Class I Epitope Identification: HLA Binding and Structural Entropy

Human class I epitopes have not yet been formally identified for ZKV. Some authors have published ZKV MHC class II epitope prediction based on MHC binding search engines alone (35, 56, 57). In order to generate a realistic list of MHC-I binding peptides on ZKV E and M proteins, not only did we use a binding prediction tool, but we also performed matching known DNV class I epitopes to peptides on ZKV. This is warranted due to the antigenic similarity of DNV and ZKV, which display 44–68% sequence identity, as well as the reported crossreactivity to ZKV of DNV envelope-specific antibodies (58). An additional layer of

identification was the structural entropy analysis described in the next section.

We generated the predicted ZKV epitope list using the sequence of ZKV Strain H/PF/2013 (GenBank Accession number: KJ776791.2) (59). This strain was isolated from an infected patient during the French Polynesia epidemic in 2013–2014. The E and M protein amino acid sequences were run through the MHC-I Binding Predictions tool available on IEDB (60). This tool combines data from multiple prediction methods, which include artificial neural networks stabilized matrices. Choosing only those alleles that occur in at least 1% of the human population, we generated a list of predicted epitopes for MHC-A and B alleles. Percentile rank is calculated by comparing a given predicted peptide's IC<sub>50</sub> (concentration of the query peptide which inhibits 50% of a reference peptide binding) against those of a random set drawn from (61) where smaller rank indicates higher affinity. The highest ranking MHC-A and -B alleles are presented in **Tables 1** and **2**.

In order to maximize matching known DNV class I epitopes against the ZKV sequences, we were indiscriminate with respect to the DNV strain sequences. We used epitope sequence data from all of DNV strains 1–4, as downloaded from IEDB. Alignments between predicted ZKV epitopes and DNV were calculated using MAFFT (62) and webPRANK (63).

A recent study by Stettler (58) indicated ZKV/DNV cross-recognition observed for antibodies may not also be present for T-cell epitopes. Because more work is needed on this topic, and in order to analyze a larger set of potential ZKV epitopes, the class I epitopes listed in **Tables 1** and **2** are initially predicted, and only afterward aligned to DNV. Allowing for sequence divergence between DNV and ZKV, as well as keeping in mind the antigenic divergence between strains of ZKV, we did not require strict conservation between the predicted ZKV epitopes and the DNV epitopes they were compared to. As such, non-homologous but predicted epitopes were included in these tables. There are no table entries for epitopes matched to DNV but not predicted. Reported HLA specificities refer specifically to ZKV epitope predictions.

### 2.4.1. Computing Structural Entropy to Select Class I Epitopes for a CTL Vaccine

X-ray crystallography can be used to generate a PDB file containing a complete mathematical representation of the three-dimensional properties of a protein (64). Software is available which can take a PDB file as input and predict changes in the protein's three-dimensional structure after specified amino acid substitutions. One example of such a program is FoldX, which compute whole-protein free energy changes resulting from these specified amino acid changes (65).

Pereyra-Heckerman described an index they call structural entropy (*SE*) which codifies the extent to which a free energy change will occur after CTL escape at that epitope (51). A low *SE* indicates that at least one amino acid position in an epitope, a relatively high change in the protein's free energy is expected to occur after mutations to one or more amino acids in that epitope. They analyzed class I epitope targets preferred by HIV controllers and reported that these individuals have a statistically significant preference to attack class I epitopes associated with a low *SE*.

**TABLE 1** | Structural entropy (SE) calculated by the authors for DNV homologous and/or MHC binding predicted class I epitopes on ZKV E.

Epitope	SE	Source	Start	Stop	1° Allele	2° Allele	%RankΔ 1° ↔ 2°
ALGGVLIFL	1.57	Dengue/Predicted	490	498	HLA-A*02	HLA-B*58	6.9
LTMNNKHWLV	1.73	Dengue/Predicted	204	213	HLA-A*02	HLA-B*08	1.45
GLFGKGSLV	1.78	Dengue/Predicted	106	114	HLA-A*02	HLA-B*08	16.7
TMNNKHWLV	1.84	Dengue/Predicted	205	213	HLA-A*02	HLA-B*08	1.55
YYLTMNNKHW	1.86	Dengue/Predicted	202	211	HLA-A*23	HLA-B*53	0.4
QEGAVHTAL	1.89	Dengue/Predicted	261	269	HLA-B*40	HLA-A*32	23.8
AVHTALAGA	1.96	Dengue/Predicted	264	272	HLA-A*30	HLA-B*07	1.6
YSLCTAAFTF	1.98	Dengue/Predicted	305	314	HLA-A*23	HLA-B*53	0.3
KEWFHDPL	2.08	Dengue/Predicted	215	223	HLA-B*40	HLA-A*02	8.3
SQILIGTLLM	2.09	Dengue/Predicted	464	473	HLA-B*15	HLA-A*26	2.25
SYSLCTAAF	2.10	Dengue/Predicted	304	312	HLA-A*23	HLA-B*15	2.4
TPHWNNKEAL	2.13	Dengue/Predicted	233	242	HLA-B*07	HLA-A*23	46.25
ILIGTLLMW	2.13	Dengue/Predicted	466	474	HLA-B*57	HLA-A*33	42.65
DTAWDFGSV	2.13	Dengue/Predicted	426	434	HLA-A*68	HLA-B*51	12.8
LALGGVLIF	2.14	Dengue/Predicted	489	497	HLA-B*53	HLA-A*23	1.5
HKEWFHDPL	2.15	Dengue/Predicted	214	223	HLA-B*40	HLA-A*32	0.45
MAVLGDTAW	2.16	Dengue/Predicted	421	429	HLA-B*53	HLA-A*32	5.2
RMAVLGDTAW	2.17	Dengue/Predicted	420	429	HLA-B*58	HLA-A*24	3.9
ILIGTLLMWL	2.17	Dengue/Predicted	466	475	HLA-A*02	HLA-B*15	5.5
VSYSLCTAAF	2.18	Dengue/Predicted	303	312	HLA-A*24	HLA-B*15	1.25
RLKGVSYSL	2.20	Dengue/Predicted	299	307	HLA-A*32	HLA-B*08	0.3
FKSLFGGMSW	2.28	Dengue/Predicted	453	462	HLA-B*58	HLA-A*23	3.5
KSLFGGMSW	2.28	Dengue/Predicted	454	462	HLA-B*57	HLA-A*32	0.15
KMMLELDPPF	2.33	Predicted	373	382	HLA-A*02	HLA-B*44	0.4
EFKDAHAKR	2.61	Dengue/Predicted	244	252	HLA-A*33	HLA-B*08	57.8

Start-Stop positions are relative to the ZKV E protein. %RankΔ reflects the absolute value of the difference between the best fit, primary (1°) and secondary (2°) allele percentile rank. Larger numbers for %RankΔ indicate a larger preference for the 1° allele.

**TABLE 2** | Structural entropy (SE) calculated by the authors for DNV homologous and/or MHC binding predicted class I epitopes on ZKV M.

Epitope	SE	Source	Start	Stop	1° Allele	2° Allele	%RankΔ 1° ↔ 2°
VMILLIAPA	1.83	Predicted	65	74	HLA-A*30	HLA-B*15	0.45
LVMILLIAPA	1.87	Dengue/Predicted	64	73	HLA-A*02	HLA-B*08	2.75
YLVMILLIA	1.89	Dengue/Predicted	63	71	HLA-A*02	HLA-B*35	1.75
VMILLIAPAY	1.93	Predicted	65	74	HLA-A*30	HLA-B*15	0.45
IYLVIMILLI	2.02	Dengue/Predicted	62	70	HLA-A*23	HLA-B*51	0.2
ALAAAAIAWL	2.24	Predicted	43	52	HLA-A*02	HLA-B*15	4.2
SQKVYIYLM	2.26	Dengue/Predicted	58	66	HLA-B*15	HLA-A*30	3.8
LLGSSTSQKV	2.25	Dengue/Predicted	52	61	HLA-A*02	HLA-B*51	17.35
TSQKVYIYLV	2.33	Dengue/Predicted	56	65	HLA-A*68	HLA-B*57	0.55
LIRVENWIFR	2.37	Dengue/Predicted	29	38	HLA-A*31	HLA-B*57	31.25
VTLPSHSTR	2.58	Predicted	2	11	HLA-A*11	HLA-B*57	6.55
LPSHSTRKL	2.65	Predicted	3	12	HLA-B*07	HLA-A*02	4.65
SQTWLESREY	2.79	Predicted	16	25	HLA-B*15	HLA-A*30	1.45
RSQTWLESR	2.81	Predicted	15	23	HLA-A*31	HLA-B*57	6.25
KLQTRSQTW	2.84	Predicted	11	19	HLA-A*32	HLA-B*57	0.2

Start-Stop positions are relative to the ZKV M protein. %RankΔ reflects the absolute value of the difference between the best fit, primary (1°), and secondary (2°) allele percentile rank. Larger numbers for %RankΔ indicate a larger preference for the 1° allele.

Identifying SE may be a key criterion for picking class I epitope CTL attack points especially for vaccines targeting pathogens that exhibit viral escape due to antigenic drift. Designing vaccines that focus cellular immunity toward these structurally critical regions of proteins may prove advantageous. Pereyra-Heckerman's observation that HIV controllers preferentially target epitopes with a low SE suggests that it may be possible to design vaccines based entirely on an *in silico* analysis of the protein structure.

SE is calculated using a four-step process. First, a 20-element free energy change vector is created for each amino acid position

within each class I epitope codifying the free energy change computed after each of all possible 20 amino acid substitutions at that amino acid position. Note that one of those substitutions will be the amino acid for itself resulting in a free energy change of "zero" for one of the entries in the 20-element free energy change vector. Second, each 20-element free energy change vector associated with each amino acid in the epitope is converted into a 20 element Boltzmann probability distribution. A particularly high Boltzmann distribution entry indicates that there is a relatively high probability of that particular amino acid occurring at that

position. The first and second steps are implemented in equation (1) taken from Pereyra-Heckerman. Third, each Boltzmann distribution is converted into a single Shannon entropy value shown in Pereyra-Heckerman equation (2). A Low Shannon entropy indicates a Boltzmann distribution with at least one entry significantly higher than the others, indicating a relatively high preference for the wild type. Fourth, the *SE* is calculated by taking the mean of the Shannon entropies for the individual amino acids in the epitope.

$$p_{ij} = E | f_{ij} | = \frac{e^{-|ddG_{ij}|}}{\sum_{k=1}^{20} e^{-|ddG_{ik}|}} \quad (1)$$

$$E | H_i | = -\sum_{j=1}^{20} p_{ij} \ln(p_{ij}) \quad (2)$$

In systems with many possible energy states, the Boltzmann distribution is typically used to compute the relative probability of each energy state occurring. The Boltzmann distribution is used here, in the context of amino acid substitutions, to estimate the probability of each substitution occurring by considering how

much each substitution changes the protein's energy relative to the wild type. We assume that the wild type is the most likely state, and compute the Boltzmann distribution from the free energy changes relative to the wild type, generating a distribution of probabilities for each substitution. Amino acids that do not cause large energy changes will have a high probability, large-valued entry in the Boltzmann distribution, and mutations which cause large energy changes will have low Boltzmann values. We can think of the values in the Boltzmann Distribution as measuring the "naturalness" of each mutation at the given site.

The ZKV structural entropy data was generated using the PDB file (64) uploaded to RCSB by Sirohi et al. in March of 2016 (66). Protein structure data was available for ZKV E and M proteins only. The original DNA sequence used to generate this protein structure was based on the ZKV Strain H/PF/2013 (GenBank Accession number: KJ776791.2) (59). The ZKV E protein has been identified as the main source of H-2D-restricted MHC class I epitopes recognized by CD8+ T cells from ZKV-infected mice (17).

*SE* data for class I epitopes identified on ZKV E are shown in **Table 1** and for ZKV M in **Table 2**. Qualitative heat maps showing



Heat map coding *SE* for epitopes on ZKV E Protein. Rotation A.



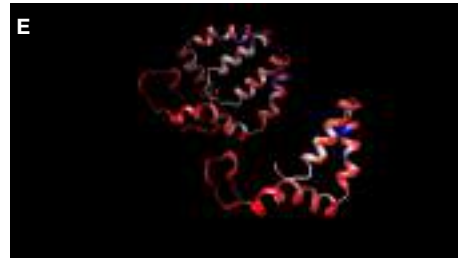
Heat map coding *SE* for epitopes on ZKV E Protein. Rotation B.



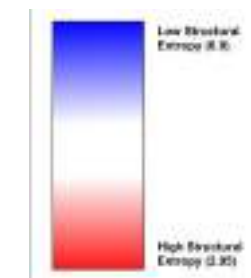
Heat map coding *SE* for epitopes on ZKV E Protein. Rotation C.



Heat map coding *SE* for epitopes on ZKV M Protein. Rotation A.



Heat map coding *SE* for epitopes on ZKV M Protein. Rotation B.



*SE* heat map color key

**FIGURE 1** | Three-dimensional ribbon view of ZKV E and M with moving-window-calculated *SE* values shown in heat map format. Note that the color coded *SE* regions do not represent *SE* values for specific epitope sequences.

*SE* values computed using moving windows across all amino acids in ZKV E and ZKV M are shown in **Figure 1**. These heat maps are not based on the specific epitope sequences identified in the tables. They are qualitative and are intended to show the distribution of *SE* values throughout the proteins. Note that low *SE* regions, shown in blue, are in the minority. By ranking the epitopes in order of *SE* in **Tables 1** and **2**, we list the epitopes predicted to be the best CTL targets based on Pereyra-Heckerman first.

## 2.5. Mapping of Potential Epitopes in ZKV Capable of Binding to Multiple HLA Class II Molecules

The rational selection of CD4+ T cell epitopes in vaccine formulation is crucial for successful application of vaccination strategies that focus on induction of CD8+ T cell immunity, given the role of CD4+ T cell response in long-term maintenance of CD8+ T cell-dependent protective immunity. Recently, CD4+ T cells with cytotoxic features have been identified in PBMC from patients with chronic viral infections (67–70). Bioinformatics tools for identification of HLA class II epitopes have been reviewed by Ref. (71). The TEPIPOPE HLA-DR binding prediction algorithm (72) and the derived ProPred algorithm (73) use the concept that each HLA-DR pocket in the antigen-binding groove can be characterized by “pocket profiles,” a quantitative representation of the interaction of all natural amino-acid residues with a given pocket, creating a matrix incorporated in the TEPIPOPE and ProPred softwares. For each HLA-DR specificity, the algorithms generated a binding score corresponding to the algebraic sum of the strength of interaction between each residue and pocket, which correlated with binding affinity. Peptide scores along a scanned protein sequence are normalized for each HLA-DR as the proportion of the best binder peptides (74). Since the software predicts binding to a significant number of HLA-DR specificities (25 in the case of TEPIPOPE, 51 for PROPPRED), it is also capable of predicting promiscuous peptide ligands each capable of binding to multiple HLA class II variant molecules (58). The TEPIPOPE prediction algorithm has been successfully applied to the identification of dozens of promiscuous T cell epitopes frequently recognized in 59 antigenic proteins from several human pathogens including viruses, bacteria, protozoa, fungi, and helminths (HIV, SIV, CMV, *M. tuberculosis*, *P. vivax*, *P. brasiliensis*, *S. mansoni*), and *in silico* prediction correlated with promiscuity in HLA-binding assays and frequency of T cell recognition by exposed individuals (75). This has led to several epitope-based vaccines which were shown to be immunogenic using conventional or and HLA class II-transgenic mice (71, 76) and protective (77) in mice. The incorporation of a promiscuous CD4+ T cell epitope in a recombinant protein-based *P. vivax* vaccine led to significant increase in its immunogenicity (41). A recent study from our group in non-human primates showed that a HIV CD4+ T cell epitope-based DNA vaccine was highly immunogenic and induced significant responses to most encoded epitopes in all animals tested (unpublished observations). Vaccines encoding promiscuous peptides able to bind to multiple HLA-DR molecules may thus allow wide population

coverage. Here, we used the TEPIPOPE and ProPred algorithms to identify potential “promiscuous” CD4+ T cell epitopes—predicted to bind to multiple HLA-DR molecules—derived from conserved regions of ZKV majority/consensus E and M protein sequences from circulating strains in the recent epidemic in Brazil and Polynesia.

## 2.6. Selection of ZKV Sequences and Promiscuous HLA Class II Epitope Prediction

The amino acid sequences derived from the ZKV strains BeH-818995 (Genbank accession number KU365777.1), BeH819015 (Genbank accession number KU365778.1), BeH815744 (Genbank accession number KU365780.1), BeH819966 (Genbank accession number KU365779.1), SPH2015 (Genbank accession number KU321639.1), and SSABR1 (Genbank accession number KU707826.1), isolated in Brazil; and the H/PF/2013 strain (Genbank accession number KJ776791.2) isolated in French Polynesia were assembled and aligned with Clustal W (MegAlign, DNASTAR, Madison, WI, USA, **Figure 2**). We scanned the generated consensus sequence with the TEPIPOPE and ProPred algorithms. We selected ZKV M and E peptides (**Table 3**) whose sequences were predicted to bind to at least 2/3 out of the 25 or 51 HLA-DR molecules in the TEPIPOPE or ProPred matrixes, respectively, corresponding to an inner nonamer core selected as the HLA binding motif with flanking amino acids added when possible at either or both N- and C-terminal ends, to increase the efficiency of *in vitro* peptide presentation to CD4+ T cells.

## 2.7. Potential Synthetic CTL Vaccine Platforms for Class I and Class II Epitope Delivery

H-2D-restricted class I epitopes, when injected intradermally without adjuvants, produce a weak immune response in C57BL/6 mice. Methods have been described for eliciting immune responses to class I. For example, the target epitopes are linked together as a “string of beads” (78). In another example, the DNA corresponding to the desired string of epitopes is inserted in a modified vaccinia Ankara (MVA) vector. Immune responses have been elicited in mice using this technique (79). A DNA string has also been administered with electroporation (80). Immune responses in Macaques have been elicited in this manner (81). In order to add and subtract epitopes from the formulation used in these types of vaccines, new linker elements must be identified and proper presentation of the desired epitopes after “string-of-beads” processing by antigen-presenting cells confirmed (82).

The use of a biodegradable, PLGA microsphere-based vaccine delivery platform allows one or more unmodified peptides to easily be incorporated into the vaccine formulation (83). The limitations of PLGA microsphere-based vaccines have been described in the literature. For example, double-emulsion sphere fabricating technologies may degrade the tertiary structure of the

A Majority	AVTLPSHSTRKLQTRSQTWLESREYTKHLIRVENWIFRNPGFALAAAAIAWLLGSSTSQKVIVLYVMILLIAPAYS							
	10	20	30	40	50	60	70	
M ZIKA BeH815744	AVTLPSHSTRKLQTRSQTWLESREYTKHLIRVENWIFRNPGFALAAAAIAWLLGSSTSQKVIVLYVMILLIAPAYS							75
M ZIKA BeH818995	AVTLPSHSTRKLQTRSQTWLESREYTKHLIRVENWIFRNPGFALAAAAIAWLLGSSTSQKVIVLYVMILLIAPAYS							75
M ZIKA BeH819966	AVTLPSHSTRKLQTRSQTWLESREYTKHLIRVENWIFRNPGFALAAAAIAWLLGSSTSQKVIVLYVMILLIAPAYS							75
M ZIKA BeH819815	AVTLPSHSTRKLQTRSQTWLESREYTKHLIRVENWIFRNPGFALAAAAIAWLLGSSTSQKVIVLYVMILLIAPAYS							75
M ZIKA SPH2015	AVTLPSHSTRKLQTRSQTWLESREYTKHLIRVENWIFRNPGFALAAAAIAWLLGSSTSQKVIVLYVMILLIAPAYS							75
M ZIKA SSABR1	AVTLPSHSTRKLQTRSQTWLESREYTKHLIRVENWIFRNPGFALAAAAIAWLLGSSTSQKVIVLYVMILLIAPAYS							75
M ZIKA HPF2013	AVTLPSHSTRKLQTRSQTWLESREYTKHLIRVENWIFRNPGFALAAAAIAWLLGSSTSQKVIVLYVMILLIAPAYS							75
B Majority	IRCIGVSNRDFVEGMSGGTWVDVLEHGGCVTVMAQDKPTVDIELVTTTYSNMAEVRSYCYEASISOMASDRCPQGEA							
	10	20	30	40	50	60	70	80
E ZIKA BeH815744	IRCIGVSNRDFVEGMSGGTWVDVLEHGGCVTVMAQDKPTVDIELVTTTYSNMAEVRSYCYEASISOMASDRCPQGEA							80
E ZIKA BeH818995	IRCIGVSNRDFVEGMSGGTWVDVLEHGGCVTVMAQDKPTVDIELVTTTYSNMAEVRSYCYEASISOMASDRCPQGEA							80
E ZIKA BeH819966	IRCIGVSNRDFVEGMSGGTWVDVLEHGGCVTVMAQDKPTVDIELVTTTYSNMAEVRSYCYEASISOMASDRCPQGEA							80
E ZIKA BeH819815	IRCIGVSNRDFVEGMSGGTWVDVLEHGGCVTVMAQDKPTVDIELVTTTYSNMAEVRSYCYEASISOMASDRCPQGEA							80
E ZIKA SPH2015	IRCIGVSNRDFVEGMSGGTWVDVLEHGGCVTVMAQDKPTVDIELVTTTYSNMAEVRSYCYEASISOMASDRCPQGEA							80
E ZIKA SSABR1	IRCIGVSNRDFVEGMSGGTWVDVLEHGGCVTVMAQDKPTVDIELVTTTYSNMAEVRSYCYEASISOMASDRCPQGEA							80
E ZIKA HPF2013	IRCIGVSNRDFVEGMSGGTWVDVLEHGGCVTVMAQDKPTVDIELVTTTYSNMAEVRSYCYEASISOMASDRCPQGEA							80
Majority	YLDKQSDTQYVCKRTLVDRGWNGCGLFGKGSVLTCAKFACSKIKMTGKSIOPENLEYRIMLSVHGSQLHSQMIVNDTGHE							
	90	100	110	120	130	140	150	160
E ZIKA BeH815744	YLDKQSDTQYVCKRTLVDRGWNGCGLFGKGSVLTCAKFACSKIKMTGKSIOPENLEYRIMLSVHGSQLHSQMIVNDTGHE							160
E ZIKA BeH818995	YLDKQSDTQYVCKRTLVDRGWNGCGLFGKGSVLTCAKFACSKIKMTGKSIOPENLEYRIMLSVHGSQLHSQMIVNDTGHE							160
E ZIKA BeH819966	YLDKQSDTQYVCKRTLVDRGWNGCGLFGKGSVLTCAKFACSKIKMTGKSIOPENLEYRIMLSVHGSQLHSQMIVNDTGHE							160
E ZIKA BeH819815	YLDKQSDTQYVCKRTLVDRGWNGCGLFGKGSVLTCAKFACSKIKMTGKSIOPENLEYRIMLSVHGSQLHSQMIVNDTGHE							160
E ZIKA SPH2015	YLDKQSDTQYVCKRTLVDRGWNGCGLFGKGSVLTCAKFACSKIKMTGKSIOPENLEYRIMLSVHGSQLHSQMIVNDTGHE							160
E ZIKA SSABR1	YLDKQSDTQYVCKRTLVDRGWNGCGLFGKGSVLTCAKFACSKIKMTGKSIOPENLEYRIMLSVHGSQLHSQMIVNDTGHE							160
E ZIKA HPF2013	YLDKQSDTQYVCKRTLVDRGWNGCGLFGKGSVLTCAKFACSKIKMTGKSIOPENLEYRIMLSVHGSQLHSQMIVNDTGHE							160
Majority	DENRAKVEITPNSPRAEATLGGFGSLGLDCEPRTGLDFSDOLYYLTWNKHLVHKEWFHDIPLPWHAAGDTGTPHMNNKE							
	170	180	190	200	210	220	230	240
E ZIKA BeH815744	DENRAKVEITPNSPRAEATLGGFGSLGLDCEPRTGLDFSDOLYYLTWNKHLVHKEWFHDIPLPWHAAGDTGTPHMNNKE							240
E ZIKA BeH818995	DENRAKVEITPNSPRAEATLGGFGSLGLDCEPRTGLDFSDOLYYLTWNKHLVHKEWFHDIPLPWHAAGDTGTPHMNNKE							240
E ZIKA BeH819966	DENRAKVEITPNSPRAEATLGGFGSLGLDCEPRTGLDFSDOLYYLTWNKHLVHKEWFHDIPLPWHAAGDTGTPHMNNKE							240
E ZIKA BeH819815	DENRAKVEITPNSPRAEATLGGFGSLGLDCEPRTGLDFSDOLYYLTWNKHLVHKEWFHDIPLPWHAAGDTGTPHMNNKE							240
E ZIKA SPH2015	DENRAKVEITPNSPRAEATLGGFGSLGLDCEPRTGLDFSDOLYYLTWNKHLVHKEWFHDIPLPWHAAGDTGTPHMNNKE							240
E ZIKA SSABR1	DENRAKVEITPNSPRAEATLGGFGSLGLDCEPRTGLDFSDOLYYLTWNKHLVHKEWFHDIPLPWHAAGDTGTPHMNNKE							240
E ZIKA HPF2013	DENRAKVEITPNSPRAEATLGGFGSLGLDCEPRTGLDFSDOLYYLTWNKHLVHKEWFHDIPLPWHAAGDTGTPHMNNKE							240
Majority	ALVEFKDAHAKRQTVVVLGSQEAVHTALAGALEAEADGAKGRILSSGHLKCRLKMDKLRKGVSYSLCTAAFTFTKIPAE							
	250	260	270	280	290	300	310	320
E ZIKA BeH815744	ALVEFKDAHAKRQTVVVLGSQEAVHTALAGALEAEADGAKGRILSSGHLKCRLKMDKLRKGVSYSLCTAAFTFTKIPAE							320
E ZIKA BeH818995	ALVEFKDAHAKRQTVVVLGSQEAVHTALAGALEAEADGAKGRILSSGHLKCRLKMDKLRKGVSYSLCTAAFTFTKIPAE							320
E ZIKA BeH819966	ALVEFKDAHAKRQTVVVLGSQEAVHTALAGALEAEADGAKGRILSSGHLKCRLKMDKLRKGVSYSLCTAAFTFTKIPAE							320
E ZIKA BeH819815	ALVEFKDAHAKRQTVVVLGSQEAVHTALAGALEAEADGAKGRILSSGHLKCRLKMDKLRKGVSYSLCTAAFTFTKIPAE							320
E ZIKA SPH2015	ALVEFKDAHAKRQTVVVLGSQEAVHTALAGALEAEADGAKGRILSSGHLKCRLKMDKLRKGVSYSLCTAAFTFTKIPAE							320
E ZIKA SSABR1	ALVEFKDAHAKRQTVVVLGSQEAVHTALAGALEAEADGAKGRILSSGHLKCRLKMDKLRKGVSYSLCTAAFTFTKIPAE							320
E ZIKA HPF2013	ALVEFKDAHAKRQTVVVLGSQEAVHTALAGALEAEADGAKGRILSSGHLKCRLKMDKLRKGVSYSLCTAAFTFTKIPAE							320
Majority	TLHGTVTVEVQYAGTDGPCKVPAQMAVDMQTLTPVGRLLITANPVITESTENSMMLELDPPFGDSYIVIGVGEKKITHM							
	330	340	350	360	370	380	390	400
E ZIKA BeH815744	TLHGTVTVEVQYAGTDGPCKVPAQMAVDMQTLTPVGRLLITANPVITESTENSMMLELDPPFGDSYIVIGVGEKKITHM							400
E ZIKA BeH818995	TLHGTVTVEVQYAGTDGPCKVPAQMAVDMQTLTPVGRLLITANPVITESTENSMMLELDPPFGDSYIVIGVGEKKITHM							400
E ZIKA BeH819966	TLHGTVTVEVQYAGTDGPCKVPAQMAVDMQTLTPVGRLLITANPVITESTENSMMLELDPPFGDSYIVIGVGEKKITHM							400
E ZIKA BeH819815	TLHGTVTVEVQYAGTDGPCKVPAQMAVDMQTLTPVGRLLITANPVITESTENSMMLELDPPFGDSYIVIGVGEKKITHM							400
E ZIKA SPH2015	TLHGTVTVEVQYAGTDGPCKVPAQMAVDMQTLTPVGRLLITANPVITESTENSMMLELDPPFGDSYIVIGVGEKKITHM							400
E ZIKA SSABR1	TLHGTVTVEVQYAGTDGPCKVPAQMAVDMQTLTPVGRLLITANPVITESTENSMMLELDPPFGDSYIVIGVGEKKITHM							400
E ZIKA HPF2013	TLHGTVTVEVQYAGTDGPCKVPAQMAVDMQTLTPVGRLLITANPVITESTENSMMLELDPPFGDSYIVIGVGEKKITHM							400

**FIGURE 2 |** Alignment of ZKV M (A) and E (B) proteins with epitope identification.

**TABLE 3** | Model-predicted class II epitopes on ZKV E and ZKV M proteins.

Epitope ID	Epitope sequence	Interacting HLA-DR alleles	% predicted/51
M (58–77)	SQKVIYLVMLIAPAYSIR	DRB1*0101, DRB1*0102, DRB1*0301, DRB1*0305, DRB1*0306, DRB1*0307, DRB1*0308, DRB1*0309, DRB1*0311, DRB1*0401, DRB1*0402, DRB1*0404, DRB1*0405, DRB1*0408, DRB1*0410, DRB1*0421, DRB1*0423, DRB1*0426, DRB1*0701, DRB1*0703, DRB1*0801, DRB1*0802, DRB1*0804, DRB1*0806, DRB1*0813, DRB1*0817, DRB1*1101, DRB1*1102, DRB1*1104, DRB1*1106, DRB1*1107, DRB1*1114, DRB1*1120, DRB1*1121, DRB1*1128, DRB1*1301, DRB1*1302, DRB1*1304, DRB1*1305, DRB1*1307 DRB1*1311, DRB1*1321, DRB1*1322, DRB1*1323, DRB1*1327, DRB1*1328, DRB1*1501, DRB1*1502, DRB1*1506, DRB5*0101, DRB5*0105	100
E (130–149)	QPENLEYRIMLHSVGSQHSG	DRB1*0101, DRB1*0102, DRB1*0301, DRB1*0305, DRB1*0309, DRB1*0401, DRB1*0402, DRB1*0404, DRB1*0405, DRB1*0408, DRB1*0410, DRB1*0421, DRB1*0423, DRB1*0426, DRB1*0701, DRB1*0703, DRB1*0801, DRB1*0802, DRB1*0804, DRB1*0806, DRB1*0813, DRB1*0817, DRB1*1101, DRB1*1102, DRB1*1104, DRB1*1106, DRB1*1107, DRB1*1114, DRB1*1120, DRB1*1121, DRB1*1128, DRB1*1301, DRB1*1302, DRB1*1304, DRB1*1305, DRB1*1307, DRB1*1311, DRB1*1321, DRB1*1322, DRB1*1323, DRB1*1327, DRB1*1328, DRB1*1501, DRB1*1502, DRB5*0101, DRB5*0105	92
E (289–308)	KCRLKMDKLRLKGVSYSLCT	DRB1*0301, DRB1*0305, DRB1*0306, DRB1*0307, DRB1*0308, DRB1*0309, DRB1*0311, DRB1*0401, DRB1*0402, DRB1*0404, DRB1*0405, DRB1*0408, DRB1*0410, DRB1*0421, DRB1*0423, DRB1*0426, DRB1*0801, DRB1*0802, DRB1*0804, DRB1*0806, DRB1*0813, DRB1*0817, DRB1*1101, DRB1*1102, DRB1*1104, DRB1*1106, DRB1*1107, DRB1*1114, DRB1*1120, DRB1*1121, DRB1*1128, DRB1*1301, DRB1*1302, DRB1*1304, DRB1*1305, DRB1*1307, DRB1*1311, DRB1*1321, DRB1*1322, DRB1*1323, DRB1*1327, DRB1*1328, DRB5*0101, DRB5*0105	86

delivered antigen due to exposure to solvents or high temperatures used during spray drying processes (84). In a previous report, we manufactured our microspheres avoiding double emulsion sphere manufacturing technology using a precision spray drying process that operates at room temperature (85).

In contrast to previous studies which incorporated only a single peptide epitope in spheres (86), we showed that it was possible to elicit an immune response from each of two epitopes delivered simultaneously, when the two epitopes were loaded into the same spheres or different spheres.

This is an important consideration, especially because the HLA restricted nature of the class I epitopes being delivered will require the development of a “master vaccine” containing enough different peptide epitopes to cover a target population.

The fact that the majority of the epitopes listed in the first four rows of **Tables 1** and **2** have the best predicted HLA match as HLA\*02 suggests that a vaccine directed against these class I epitopes could readily tested in Brazil where the frequency of HLA A\*02 frequency varies from 21.7 to 47.5% between states (87).

### 3. CONCLUDING REMARKS

The search for rapid development of safe and effective vaccines against ZKV is a global public health emergency. Testing multiple vaccine platforms in parallel may speed up and increase the likelihood of finding a good vaccine. We have proposed a rationale for ZKV epitope selection and design of T cell epitope-based vaccine against ZKV virus. Selection of candidate ZKV structure-constrained HLA class I epitopes able to bind an array of HLA class I supertypic molecules, and promiscuous class II T cell

epitopes capable of binding to multiple HLA class II molecules could provide wide HLA and population coverage for such a vaccine which could be delivered using the synthetic, adjuvanted microsphere vaccine as outlined above or other techniques for epitope immunization that we discussed.

### ETHICS STATEMENT

This study was carried out in accordance with the policies and procedures established by the WIRB Institutional Review Board with written informed consent from all subjects. All subjects gave written informed consent in accordance with the Declaration of Helsinki. The protocol was approved by the WIRB.

### AUTHOR CONTRIBUTIONS

RR, EC-N, DR, and PH wrote the manuscript. All authors reviewed the manuscript. All authors directly participated in the research described with EC-N and DR performing modeling predictions of class II epitopes and AM, TO, SC, and RR performing class I epitope identification and SE calculations for class I epitopes.

### FUNDING

The work described was funded in part by Flow Pharma, Inc. and through an in-kind grant of Azure platform cloud computer time by Microsoft Corporation which was used for class I epitope SE calculations. EC-N is supported by grants from CNPq (Brazilian National Scientific Council) and FAPESP (São Paulo State Research Foundation) 13/50302-3.

## REFERENCES

- CDC. *Zika Virus Case Counts in the US*. (2016). Available from: <http://www.cdc.gov/zika/geo/unitedstates.html>
- Zhang Q, Sun K, Chinazzi M, Pastore-Pinotti A, Dean NE, Rojas DP, et al. Projected spread of Zika virus in the Americas. *bioRxiv* (2016). doi:10.1101/066456
- Brasil P, Pereira JP, Gabaglia J, Damasceno CR, Wakimoto LM, Nogueira R, et al. Zika virus infection in pregnant women in Rio de Janeiro – preliminary report. *N Engl J Med* (2016). doi:10.1056/NEJMoa1602412
- Ye Q, Liu Z, Han J, Jiang T, Li X, Qin C. Genomic characterization and phylogenetic analysis of Zika virus circulating in the Americas. *Infect Genet Evol* (2016) 43:43–9. doi:10.1016/j.meegid.2016.05.004
- Sant A, McMichael A. Revealing the role of CD4(+) T cells in viral immunity. *J Exp Med* (2012) 209(8):1391–5. doi:10.1084/jem.20121517
- Swain S, McKinstry K, Strutt. Expanding roles for CD4+ T cells in immunity to viruses. *Nat Rev Immunol* (2012) 12(2):136–48. doi:10.1038/nri3152
- Yauch L, Zellweger M, Kotturi M, Qutubuddin A, Sidney J, Peters B, et al. A protective role for dengue virus-specific CD8+ T cells. *J Immunol* (2009) 182(8):4865–73. doi:10.4049/jimmunol.0801974
- Weiskopf D, Bangs D, Sidney J, Kolla R, Silva AD, de Silva A, et al. Dengue virus infection elicits highly polarized CX3CR1+ cytotoxic CD4+ T cells associated with protective immunity. *Proc Natl Acad Sci U S A* (2015) 112(31):E4256–63. doi:10.1073/pnas.1505956112
- Netland J, Bevan M. CD8 and CD4 T cells in West Nile virus immunity and pathogenesis. *Viruses* (2013) 5(10):2573–84. doi:10.3390/v5102573
- Weiskopf D, Angelo M, Bangs D, Sidney J, Paul S, Peters B, et al. The human CD8+ T cell responses induced by a live attenuated tetravalent dengue vaccine are directed against highly conserved epitopes. *J Virol* (2015) 89(1):120–8. doi:10.1128/JVI.02129-14
- Akondy R, Johnson L, Nakaya H, Edupuganti S, Mulligan M, Lawson B, et al. Initial viral load determines the magnitude of the human CD8 T cell response to yellow fever vaccination. *Proc Natl Acad Sci U S A* (2015) 112(10):3050–5. doi:10.1073/pnas.1500475112
- Bassi M, Kongsgaard M, Steffensen M, Fenger C, Rasmussen M, Skødt K, et al. CD8+ T cells complement antibodies in protecting against yellow fever virus. *J Immunol* (2015) 194(3):1141–53. doi:10.4049/jimmunol.1402605
- Marraco SF, Soneson C, Po G, Allard M, Maillard SA, Montandon N, et al. Long-lasting stem cell-like memory CD8+ T cells with a naïve-like profile upon yellow fever vaccination. *Sci Transl Med* (2015) 7(282):4111–6. doi:10.1126/scitranslmed.aaa3700
- Watson A, Lam L, Klimstra W, Ryman K. The 17D-204 vaccine strain-induced protection against virulent yellow fever virus is mediated by humoral immunity and CD4+ but not CD8+ T cells. *PLoS Pathog* (2016) 12(7):e1005786. doi:10.1371/journal.ppat.1005786
- Chen H-W, Hu H-M, Wu S-H, Chiang C-Y, Hsiao Y-J, Wu C-K, et al. The immunodominance change and protection of CD4+ T-cell responses elicited by an envelope protein domain III-based tetravalent dengue vaccine in mice. *PLoS One* (2015) 10(12):e0145717. doi:10.1371/journal.pone.0145717
- Brien J, Uhrlaub J, Nikolich-Zugich J. West Nile virus-specific Cd4 T cells exhibit direct antiviral cytokine secretion and cytotoxicity and are sufficient for antiviral protection. *J Immunol* (2008) 181(12):8568–75. doi:10.4049/jimmunol.181.12.8568
- Ngono E, Vizcarra E, Tang W, Sheets N, Kim K, Gorman M, et al. Mapping and role of the CD8+ T cell response during primary Zika virus infection in mice. *Cell Host Microbe* (2017) 21(1):35–46. doi:10.1016/j.chom.2016.12.010
- Cao-Lormeau V, Blake A, Mons S, Lastere S, Roche C, Vanhomwegen J, et al. Guillain-Barre syndrome outbreak associated with Zika virus infection in French polynesia: a case-control study. *Lancet* (2016) 387(10027):1531–9. doi:10.1016/S0140-6736(16)00562-6
- Parra B, Lizarazo J, Jimenez-Arango JA, Zea-Vera AF, Gonzalez-Manrique G, Vargas J, et al. Guillain-Barre syndrome associated with Zika virus infection in colombia. *N Engl J Med* (2016) 375(16):1513–23. doi:10.1056/NEJMoa1605564
- Guzman MG, Alvarez M, Halstead SB. Secondary infection as a risk factor for dengue hemorrhagic fever/dengue shock syndrome: an historical perspective and role of antibody-dependent enhancement of infection. *Arch Virol* (2013) 158(7):1445–59. doi:10.1007/s00705-013-1645-3
- Guzman MG, Alvarez M, Rodriguez-Roche R, Bernardo L, Montes T, Vazquez S, et al. Neutralizing antibodies after infection with dengue 1 virus. *Emerg Infect Dis* (2007) 13(2):282–6. doi:10.3201/eid1302.060539
- Schmid M, Diamond MS, Harris E. Dendritic cells in dengue virus infection: targets of virus replication and mediators of immunity. *Front Immunol* (2014) 5:647. doi:10.3389/fimmu.2014.00647
- Dejnirattisai W, Supasa P, Wongwiwat W, Rouvinski A, Barba-Spaeth G, Duangchinda T, et al. Dengue virus serocross-reactivity drives antibody-dependent enhancement of infection with Zika virus. *Nat Immunol* (2016) 17: 1102–8. doi:10.1038/ni.3515
- Paul LM, Carlin ER, Jenkins MM, Tan AL, Barcellona CM, Nicholson CO, et al. Dengue virus antibodies enhance Zika virus infection. *bioRxiv* (2016). doi:10.1101/050112
- Kawiecki A, Christofferson R. Zika virus-induced antibody response enhances dengue virus serotype 2 replication in vitro. *J Infect Dis* (2016) 214(9):1357–60. doi:10.1093/infdis/jiw377
- Russell P, Halstead S. Challenges to the design of clinical trials for live-attenuated tetravalent dengue vaccines. *PLoS Negl Trop Dis* (2016) 10:8. doi:10.1371/journal.pntd.0004854
- Zellweger RM, Prestwood TR, Shresta S. Enhanced infection of liver sinusoidal endothelial cells in a mouse model of antibody-induced severe dengue disease. *Cell Host Microbe* (2010) 7(2):128–39. doi:10.1016/j.chom.2010.01.004
- Dudley DW, Aliotta MT, Mohr EL, Weiler AM, Lehrer-Brey G, Weisgrau KL, et al. A rhesus macaque model of Asian-lineage Zika virus infection. *Nat Commun* (2016) 7:12204. doi:10.1038/ncomms12204
- Yauch LE, Prestwood TR, May MM, Morar MM, Zellweger RM, Peters B, et al. CD4+ T cells are not required for the induction of dengue virus-specific CD8+ T cell or antibody responses but contribute to protection after vaccination. *J Immunol* (2010) 185(9):5405–16. doi:10.4049/jimmunol.1001709
- Zellweger RM, Tang WW, Eddy WE, King K, Sanchez MC, Shresta S. CD8+ T cells can mediate short-term protection against heterotypic dengue virus re-infection in mice. *J Virol* (2015) 89(12):6494–505. doi:10.1128/JVI.00036-15
- Zellweger R, Eddy WE, Tang WW, Miller R, Shresta S. CD8+ T cells prevent antigen-induced antibody-dependent enhancement of dengue disease in mice. *J Immunol* (2014) 193(8):4117–24. doi:10.4049/jimmunol.1401597
- Vaccine Pipeline Tracker. (2016). Available from: [http://www.who.int/immunization/research/vaccine\\_pipeline\\_tracker\\_spreadsheet/en/](http://www.who.int/immunization/research/vaccine_pipeline_tracker_spreadsheet/en/)
- Abbink P, Larocca R, de La Barrera R, Bricault C, Moseley E, Boyd M, et al. Protective efficacy of multiple vaccine platforms against Zika virus challenge in rhesus monkeys. *Science* (2016) 353(6304):1129–32. doi:10.1126/science.aaah6157
- Dowd K, Ko S, Morabito K, Yang E, Pelc R, DeMaso C, et al. Rapid development of a DNA vaccine for Zika virus. *Science* (2016) 354(6309):237–40. doi:10.1126/science.aai3197
- Alam A, Ali S, Ahamed S, Malik M, Ishrat R. From ZikV genome to vaccine: in silico approach for the epitope-based peptide vaccine against Zika virus envelope glycoprotein. *Immunology* (2016) 149(4):386–99. doi:10.1111/imm.12656
- Khan A, Miotto O, Heiny A, Salmon J, Srinivasan K, Nascimento E, et al. A systematic bioinformatics approach for selection of epitope-based vaccine targets. *Cell Immunol* (2006) 244(2):141–7. doi:10.1016/j.cellimm.2007.02.005
- Sánchez-Burgos G, Ramos-Castañeda J, Cedillo-Rivera R, Dumonteil E. Immunogenicity of novel dengue virus epitopes identified by bioinformatic analysis. *Virus Res* (2006) 153(1):113–20. doi:10.1016/j.virusres.2010.07.014
- Shi J, Sun J, Wu M, Hu N, Li J, Li Y, et al. Inferring protective CD8+ T-cell epitopes for NS5 protein of four serotypes of dengue virus Chinese isolates based on HLA-a, -b and -c allelic distribution: implications for epitope-based universal vaccine design. *PLoS One* (2015) 10(9):e0138729. doi:10.1371/journal.pone.0138729
- Gilbert S. T-cell-inducing vaccines – what's the future? *Immunology* (2012) 135(1):19–26. doi:10.1111/j.1365-2567.2011.03517.x
- Borthwick N, Ahmed T, Ondondo B, Hayes P, Rose A, Ebrahimsa U, et al. Vaccine-elicited human T cells recognizing conserved protein regions inhibit HIV-1. *Mol Ther* (2014) 22(2):464–75. doi:10.1038/mt.2013.248
- Rosa D, Iwai L, Tzelepis F, Bargieri D, Medeiros M, Soares I, et al. Immunogenicity of a recombinant protein containing the *Plasmodium vivax* vaccine candidate msp1(19) and two human CD4+ T-cell epitopes

- administered to non-human primates (*Callithrix jacchus jacchus*). *Microbes Infect* (2006) 8(8):2130–7. doi:10.1016/j.micinf.2006.03.012
42. Soria-Guerra R, Nieto-Gomez R, Govea-Alonso D, Rosales-Mendoza S. An overview of bioinformatics tools for epitope prediction: implications on vaccine development. *J Biomed Inform* (2014) 53:405–14. doi:10.1016/j.jbi.2014.11.003
  43. Sridhar S. Heterosubtypic T-cell immunity to influenza in humans: challenges for universal T-cell influenza vaccines. *Front Immunol* (2016) 7:195. doi:10.3389/fimmu.2016.00195
  44. Kimata JT, Rice AP, Wang J. Challenges and strategies for the eradication of the HIV reservoir. *Curr Opin Immunol* (2016) 42:65–70. doi:10.1016/j.co.2016.05.015
  45. Abbas W, Tariq M, Iqbal M, Kumar A, Herbein G. Eradication of HIV-1 from the macrophage reservoir: an uncertain goal? *Viruses* (2015) 7:1578–98. doi:10.3390/v7041578
  46. Govero J, Esakkyp P, Scheaffer S, Fernandez E, Drury A, Platt D, et al. Zika virus infection damages the testes in mice. *Nature* (2016) 540:438–42. doi:10.1038/nature20556
  47. Connick E, Folkvord JM, Lind KT, Rakasz EG, Miles B, Wilson NA, et al. Compartmentalization of simian immunodeficiency virus replication within secondary lymphoid tissues of rhesus macaques is linked to disease stage and inversely related to localization of virus-specific CTL. *J Immunol* (2014) 193(11):5613–25. doi:10.4049/jimmunol.1401161
  48. Douek DC. Disrupting T-cell homeostasis: how HIV-1 infection causes disease. *AIDS Rev* (2003) 5(3):172–7.
  49. Streck H, Jolin JS, Qi Y, Yassine-Diab B, Johnson RC, Kwon DS, et al. Human immunodeficiency virus type 1-specific CD8+ T-cell responses during primary infection are major determinants of the viral set point and loss of CD4+ T cells. *J Virol* (2009) 83(15):7641–8. doi:10.1128/JVI.00182-09
  50. Rademeyer C, Korber B, Seaman MS, Giorgi EE, Thebus R, Robles A, et al. Features of recently transmitted HIV-1 clade c viruses that impact antibody recognition: implications for active and passive immunization. *PLoS Pathog* (2016) 12(7):e1005742. doi:10.1371/journal.ppat.1005742
  51. Pereyra F, Heckerman D, Carlson JM, Soghoian CK, Karel D, Goldenthal A, et al. HIV control is mediated in part by CD8+ T-cell targeting of specific epitopes. *J Virol* (2014) 88(22):12937–48. doi:10.1128/JVI.01004-14
  52. Schein C, Zhou B, Braun W. Stereophysical variability plots highlight conserved antigenic areas in flaviviruses. *Virol J* (2005) 2:40. doi:10.1186/1743-422X-2-40
  53. Faria NR, Rdo SA, Kraemer MU, Souza R, Cunha MS, Hill SC, et al. Zika virus in the Americas: early epidemiological and genetic findings. *Science* (2016) 352(6283):345–9. doi:10.1126/science.aaf5036
  54. Wang L, Valderramas SG, Wu A, Ouyang S, Li C, Brasil P, et al. From mosquitos to humans: genetic evolution of Zika virus. *Cell Host Microbe* (2016) 19(5):561–5. doi:10.1016/j.chom.2016.04.006
  55. Logan I. Zika – how fast does this virus mutate? *Dongwuxue Yanjiu* (2016) 37(2):110–5. doi:10.13918/j.issn.2095-8137.2016.2.110
  56. Ashfaq U, Ahmed B. De novo structural modeling and conserved epitopes prediction of Zika virus envelop protein for vaccine development. *Viral Immunol* (2016) 29(7):1–8. doi:10.1089/vim.2016.0033
  57. Shawan M, Mahmud H, Hasan M, Parvin M, Rahman N, Rahman SMB. In silico modeling and immunoinformatics probing disclose the epitope based peptide vaccine against Zika virus envelope glycoprotein. *Indian J Pharm Biol Res* (2014) 2(4):44–57.
  58. Stettler K, Beltramello M, Espinosa DA, Graham V, Cassotta A, Bianchi S, et al. Specificity, cross-reactivity and function of antibodies elicited by Zika virus infection. *Science* (2016) 353(6301):823–6. doi:10.1126/science.aaf8505
  59. Zika-Strain. *Complete Coding Sequence of Zika Virus from a French Polynesia Outbreak in 2013*. (2014). Available from: <https://www.ncbi.nlm.nih.gov/pmc/articles/PMC4047448/>
  60. IEDB. *IEDB MHC-I Binding Predictions Tool*. (2013). Available from: <http://tools.iedb.org/mhci/reference/>
  61. UniProtKB/Swiss-Prot. (2016). Available from: <https://www.ebi.ac.uk/uniprot>
  62. Katoh K, Misawa K, Kuma K, Miyata T. Mafft: a novel method for rapid multiple sequence alignment based on fast Fourier transform. *Nucleic Acids Res* (2002) 30(14):3059–66. doi:10.1093/nar/gkf436
  63. Löytynoja A, Goldman N. webPRANK: a phylogeny-aware multiple sequence aligner with interactive alignment browser. *BMC Bioinformatics* (2010) 11:579. doi:10.1186/1471-2105-11-579
  64. RCSB PDB Policies and References. (2013). Available from: [http://www.rcsb.org/pdb/static.do?p=general\\_information/about\\_pdb/policies\\_references.html](http://www.rcsb.org/pdb/static.do?p=general_information/about_pdb/policies_references.html)
  65. Schymkowitz J, Borg J, Stricher F, Nys R, Rousseau F, Serrano L. The foldx web server: an online force field. *Nucleic Acids Res* (2005) 33:W382–8. doi:10.1093/nar/gki387
  66. Sirohi D, Chen Z, Sun L, Klose T, Pierson TC, Rossman MG, et al. The 3.8 Å resolution cryo-EM structure of Zika virus. *Science* (2016) 22:467–70. doi:10.1126/science.aaf5316
  67. Aslan N, Yurdaydin C, Wiegand J, Greten T, Ciner A, Meyer M, et al. Cytotoxic CD4 T cells in viral hepatitis. *J Viral Hepat* (2006) 13(8):505–14. doi:10.1111/j.1365-2893.2006.00723.x
  68. Marshall N, Swain S. Cytotoxic CD4 T cells in antiviral immunity. *J Biomed Biotechnol* (2011) 2011:954602. doi:10.1155/2011/954602
  69. Sáez-Borderías A, Gumá M, Angulo A, Bellosillo B, Pende D, López-Botet M. Expression and function of nkg2d in CD4+ T cells specific for human cytomegalovirus. *Eur J Immunol* (2006) 36(12):3198–206. doi:10.1002/eji.200636682
  70. Soghoian D, Jessen H, Flanders M, Sierra-Davidson K, Cutler S, Pertel T, et al. HIV-specific cytolytic CD4 T cell responses during acute HIV infection predict disease outcome. *Sci Transl Med* (2012) 29(4):123–5. doi:10.1126/scitranslmed.3003165
  71. Rosa D, Ribeiro S, Cunha-Neto E. CD4+ T cell epitope discovery and rational vaccine design. *Arch Immunol Ther Exp (Warsz)* (2010) 32(2):121–30. doi:10.1007/s00005-010-0067-0
  72. Sturniolo T, Bono E, Ding J, Raddrizzani L, Tuereci O, Sahin U, et al. Generation of tissue-specific and promiscuous HLA ligand databases using DNA microarrays and virtual HLA class II matrices. *Nat Biotechnol* (1999) 17(6):555–61. doi:10.1038/9858
  73. Singh H, Raghava G. Propred: prediction of HLA-DR binding sites. *Bioinformatics* (2001) 17(12):1236–7. doi:10.1093/bioinformatics/17.12.1236
  74. Hammer J, Belunis C, Bolin D, Papadopoulos J, Walsky R, Higelin J. High-affinity binding of short peptides to major histocompatibility complex class II molecules by anchor combinations. *Proc Natl Acad Sci U S A* (1994) 91:4456–60. doi:10.1073/pnas.91.10.4456
  75. LK LI, Yoshida M, Sidney J, Shikanai-Yasuda M, Goldberg A, Juliano M, et al. In silico prediction of peptides binding to multiple HLA-DR molecules accurately identifies immunodominant epitopes from gp43 of *Paracoccidioides brasiliensis* frequently recognized in primary peripheral blood mononuclear cell responses from sensitized individuals. *Mol Med* (2003) 9:209–19.
  76. Ribeiro S, Rosa D, Fonseca S, Mairena E, Postol E, Oliveira S, et al. A vaccine encoding conserved promiscuous HIV CD4 epitopes induces broad T cell responses in mice transgenic to multiple common HLA class II molecules. *PLoS One* (2010) 5(6):e11072. doi:10.1371/journal.pone.0011072
  77. Garcia T, Fonseca C, Pacifico L, Fdo VD, Marinho F, Penido M, et al. Peptides containing T cell epitopes, derived from Sm14, but not from paramyosin, induce a Th1 type of immune response, reduction in liver pathology and partial protection against *Schistosoma mansoni* infection in mice. *Acta Trop* (2008) 106(3):162–7. doi:10.1016/j.actatropica.2008.03.003
  78. Whilton JL, Sheng N, Oldstone MBA, McKee TA. A “string-of-beads” vaccine, comprising linked mini genes, confers protection from lethal-dose virus challenge. *J Virol* (1993) 67(1):348–52.
  79. Mothe B. *DNA-MVA Prime-Boost Vaccine Eliciting T-Cell Specificities Associated with HIV-1 Control is Highly Immunogenic in Mice and Breaks CTL Immuno-Dominance*. Barcelona, Spain (2013).
  80. Kopycinski J, Cheeseman H, Ashraf A, Gill D, Hayes P, Hannaman D. A DNA-based candidate HIV vaccine delivered via in vivo electroporation induces CD4 responses toward the 4-7-binding v2 loop of HIV gp120 in healthy volunteers. *Clin Vaccine Immunol* (2012) 19(9):1557–9. doi:10.1128/CVI.00327-12
  81. Mullins J. *Refocusing CTL and Antibody Responses with p24 gag Conserved Elements Vaccines*. Barcelona, Spain (2013).
  82. Groot AD, Marcon L, Bishop E, Rivera D, Kutzler M, Weiner D, et al. HIV vaccine development by computer assisted design: the GAIA vaccine. *Vaccine* (2005) 23(17–18):2136–48. doi:10.1016/j.vaccine.2005.01.097
  83. Rubsamen RM, Herst CV, Lloyd PM, Heckerman DE. Eliciting cytotoxic t-lymphocyte responses from synthetic vectors containing one or two epitopes in a c57bl/6 mouse model using peptide-containing biodegradable

- microspheres and adjuvants. *Vaccine* (2014) 32:4111–6. doi:10.1016/j.vaccine.2014.05.071
84. Jain S, O'Hagan D, Singh M. The long-term potential of biodegradable poly(lactide co-glycolide) micro particles as the next-generation vaccine adjuvant. *Expert Rev Vaccines* (2007) 28:13. doi:10.1586/erv.11.126
85. Martin-Banderas LF, Flores-Mosquera M, Riesco-Chueca P, Rodriguez-Gil A, Cebolla A, Chávez S. Flow focusing: a versatile technology to produce size-controlled and specific-morphology microparticles. *Small* (2005) 1(7):688–92. doi:10.1002/smll.200500087
86. Waechterle-Men Y, Allmen E, Gander B, Scandella E, Schlosser E, Schmidtke G. Encapsulation of proteins and peptides into biodegradable poly(D,L-lactide-co-glycolide) microspheres prolongs and enhances antigen presentation by human dendritic cells. *Vaccine* (2006) 24(11):1847–57. doi:10.1016/j.vaccine.2005.10.032
87. Salvadori L, Santana F, Marcos E. Frequency of alleles and haplotypes of the human leukocyte antigen system in Bauru, São Paulo, Brazil. *Rev Bras Hematol Hemoter* (2014) 36(2):108–14. doi:10.5581/1516-8484.20140026

**Conflict of Interest Statement:** RR is CEO of Flow Pharma, Inc. RR, AM, TO, SC, and CH have received compensation in the form of cash and/or stock from Flow Pharma, Inc. All other authors declare that the research was conducted in the absence of any commercial or financial relationships that could be construed as a potential conflict of interest.

Copyright © 2017 Cunha-Neto, Rosa, Harris, Olson, Morrow, Ciotlos, Herst and Rubsamen. This is an open-access article distributed under the terms of the Creative Commons Attribution License (CC BY). The use, distribution or reproduction in other forums is permitted, provided the original author(s) or licensor are credited and that the original publication in this journal is cited, in accordance with accepted academic practice. No use, distribution or reproduction is permitted which does not comply with these terms.



# Immunogenicity of a Multi-Epitope DNA Vaccine Encoding Epitopes from Cu–Zn Superoxide Dismutase and Open Reading Frames of *Brucella abortus* in Mice

Emilia Escalona, Darwin Sáez and Angel Oñate\*

Laboratory of Molecular Immunology, Department of Microbiology, Faculty of Biological Sciences, Universidad de Concepción, Concepción, Chile

## OPEN ACCESS

### Edited by:

Clarisa B. Palatnik-de-Sousa,  
Federal University of Rio de Janeiro,  
Brazil

### Reviewed by:

Daniel Olive,  
Institut national de la santé et de la  
recherche médicale, France  
Pablo Penalosa,  
Northwestern University, USA

### \*Correspondence:

Angel Oñate  
aonate@udec.cl

### Specialty section:

This article was submitted to  
Vaccines and Molecular  
Therapeutics, a section of the  
journal Frontiers in Immunology

Received: 14 November 2016

Accepted: 25 January 2017

Published: 09 February 2017

### Citation:

Escalona E, Sáez D and Oñate A  
(2017) Immunogenicity of a  
Multi-Epitope DNA Vaccine Encoding  
Epitopes from Cu–Zn Superoxide  
Dismutase and Open Reading  
Frames of *Brucella abortus* in Mice.  
*Front. Immunol.* 8:125.  
doi: 10.3389/fimmu.2017.00125

Brucellosis is a bacterial zoonotic disease affecting several mammalian species that is transmitted to humans by direct or indirect contact with infected animals or their products. In cattle, brucellosis is almost invariably caused by *Brucella abortus*. Live, attenuated *Brucella* vaccines are commonly used to prevent illness in cattle, but can cause abortions in pregnant animals. It is, therefore, desirable to design an effective and safer vaccine against *Brucella*. We have used specific *Brucella* antigens that induce immunity and protection against *B. abortus*. A novel recombinant multi-epitope DNA vaccine specific for brucellosis was developed. To design the vaccine construct, we employed bioinformatics tools to predict epitopes present in Cu–Zn superoxide dismutase and in the open reading frames of the genomic island-3 (BAB1\_0260, BAB1\_0270, BAB1\_0273, and BAB1\_0278) of *Brucella*. We successfully designed a multi-epitope DNA plasmid vaccine chimera that encodes and expresses 21 epitopes. This DNA vaccine induced a specific humoral and cellular immune response in BALB/c mice. It induced a typical T-helper 1 response, eliciting production of immunoglobulin G2a and IFN- $\gamma$  particularly associated with the Th1 cell subset of CD4 $^{+}$  T cells. The production of IL-4, an indicator of Th2 activation, was not detected in splenocytes. Therefore, it is reasonable to suggest that the vaccine induced a predominantly Th1 response. The vaccine induced a statistically significant level of protection in BALB/c mice when challenged with *B. abortus* 2308. This is the first use of an *in silico* strategy to design a multi-epitope DNA vaccine against *B. abortus*.

**Keywords:** brucellosis, *Brucella abortus*, multi-epitope DNA vaccine, genomic island 3, Cu–Zn SOD

## INTRODUCTION

Brucellosis, caused by facultative Gram-negative intracellular coccobacilli grouped in the genus *Brucella* (1), is a zoonotic disease with a high incidence and prevalence worldwide. Brucellosis affects mammals, and it can considerably undermine the health and productivity of domestic livestock. The most frequent clinical symptom in livestock after *Brucella* infection is abortion (2). In humans, the disease has a wide spectrum of clinical manifestations. They range from

simple fever to major complications in which function in the nervous, digestive, genital-urinary, cardiovascular, and muscular systems is compromised, sometimes leading to death (3). Brucellosis can impose a significant economic burden on animal production (reduction in milk production, abortions, delayed in conception). In cattle, it has been estimated that more than 300,000 animals, out of the 1.4 billion in the world, are infected (4). Brucellosis is one of the most common zoonotic diseases in humans, with more than 500,000 cases reported annually. However, depending upon the system of controls and the socioeconomic conditions, official reports only account for a fraction of the true incidence of this disease, and different countries have reported from 0.09 to 1603 cases per million inhabitants (5).

Infection by *Brucella* spp. is usually associated to an acute inflammatory reaction, the principal mechanism against local proliferation of *Brucella* organisms. Infection initially prompts an innate immune response that reduces the number of bacteria (6). The innate response activates immunity mediated by cells, in which CD4+ and CD8+ T lymphocytes, macrophages (MΦ), dendritic cells (DCs), and pro-inflammatory cytokines, such as interferon-gamma (IFN- $\gamma$ ) and tumor necrosis factor-alpha (TNF- $\alpha$ ), participate to confer protection (7). Although the host raises strong immune response, *Brucella abortus* has the capacity to survive inside MΦ and DCs, expressing a number of virulence factors that allow it to reach its replicative niche and to avoid immune-mediated destruction (8). It has been shown that antigen O protects *Brucella* from intracellular death mechanisms, while lipid A is involved in evasion of the innate immune system during the first stages of infection (9). Some additional virulence factors have been reported to be involved in intracellular replication and immune evasion. These include VirB type IV secretion (10), BTP1, a seven-helix transmembrane protein that prevents maturation of DCs (11), a BvrR/BvrS regulatory system of two components (12), and the RNA chaperone protein Hfq (13). *B. abortus* contains a Cu-Zn superoxide dismutase (SOD1), an homodimeric metalloenzyme (14). SOD1 catalyzes the dismutation of the superoxide anion  $O_2^-$  to  $O_2$  and  $H_2O_2$ , detoxifying superoxide radicals generated during the host antimicrobial immune response (15). It has been observed that a DNA vaccine with the gene sequence for this protein (*sodC*) is highly immunogenic (16, 17).

One characteristic of *Brucella* is a limited genetic diversity. This is manifested by the small number of differences responsible for host preferences and by virulence restrictions (18). The *Brucella* genome incorporates transfer-acquired mobile elements referred to as genomic islands (GIs). Nine GIs have been identified in *Brucella* (19). GI-3 is present in *B. abortus*, *Brucella melitensis*, and *Brucella ovis*. This GI contains 25 genes, many of which have unknown function, and several pseudogenes (20). GI-3 in *B. abortus* 2308 includes open reading frame (ORF) BAB1\_0260, BAB1\_0270, BAB1\_0273, BAB1\_0278, and BAB1\_0278a. Our group has reported that BAB1\_0270, described as a zinc-dependent metallopeptidase protein, and BAB1\_0278, which has homology with the GcrA superfamily, are involved in *Brucella* virulence. Their deletion affects the capacity of *Brucella* to invade phagocytic cells and to survive within them (21, 22). Furthermore,

DNA vaccine encoding BAB1\_0270 (23), BAB1\_0278 (24), and BAB1\_0278a, a hypothetical ABC-type transporter (25), were able to induce an immune response and protection against *B. abortus* 2308 infection. Immunization with the recombinant flagellar protein (BAB1\_0260) also induced protection (26). Based on bioinformatics analysis BAB1\_0273, a possible DNA-binding protein, is a putative antigen.

Despite the existence of effective commercial vaccines against brucellosis and a diagnostic test, it has not been possible to eradicate the disease. The main vaccines currently used for cattle are based on live bacteria attenuated to decrease their pathogenicity. Cattle are often vaccinated with *B. abortus* S19 or RB51, which, although providing good protection, may induce abortion if administered to gravid females (27), and are potentially infectious to humans (28). Recent advances in genomics, proteomics, recombinant DNA techniques, and vaccinology have made possible the development of safer vaccines, which overcome the drawbacks associated with live-attenuated vaccines. For example, DNA vaccines offer the possibility of inducing both humoral and cellular immune responses, and potentially can prolong the expression of an antigen (29). The use of epitopes in the design of this type of vaccine is a new alternative in the development of multi-epitope DNA vaccines (30–32). In this strategy, an informed selection of antigenic determinants that correlate with immunogenicity was used.

In this study, we have predicted antigenic determinants using bioinformatics tools from any ORF codified in GI-3 from *B. abortus* and designed a multi-epitope chimeric DNA vaccine. Humoral, cell-mediated, and protective immunity induced by this multi-epitope DNA vaccine was examined in BALB/c mice.

## MATERIALS AND METHODS

### Animals

Seven- to eight-week-old female isogenic BALB/c mice (obtained from the Instituto de Salud Pública, Santiago, Chile) were randomly allocated to three groups. Mice were kept in conventional animal facilities and received water and food *ad libitum*. All animals were handled in accordance with the regulations of the Bioethics Committee of the Faculty of Biological Sciences, Universidad de Concepción regulations. The Bioethics and Safety committee of the Faculty of Biological Sciences of the Universidad de Concepción approved this study. All efforts were made to minimize animal suffering.

### Bacterial Strains

*Escherichia coli* strain BL21 (DE3) pLys (Novagen, Madison, WI, USA) was used as the host strain for expression of recombinant multi-epitope protein and *E. coli* DH5 $\alpha$  (Invitrogen, San Diego, CA, USA) was used for obtaining plasmids. Both strains were grown at 37°C in LB broth. The virulent *B. abortus* 2308 and the attenuated strain RB51 were obtained from our culture collection. Bacterial cells were grown under aerobic conditions in Trypticase soy broth (Difco Laboratories, Detroit, MI, USA) for 72 h at 37°C.

## Epitope Prediction

The selected protein sequences (**Table 1**) were obtained from the NCBI Database. To find promising epitopes, we used the Immune Epitope Database (33). This database contains epitope information from 99% of all papers published about immune epitopes (33). We used the T Cell Epitope Prediction Tools to find peptides binding to MHC class I and class II molecules. Epitope prediction was performed for H2-D<sup>d</sup>, H2-K<sup>d</sup>, H2-L<sup>d</sup> alleles and H2-IE<sup>d</sup>, H2-IA<sup>d</sup> alleles, and MHC-I and MHC-II haplotypes in BALB/c mice. We used a consensus method consisting of a combination of the Stabilized Matrix Method (34), Artificial Neural Network (35), and Scoring Matrices derived from Combinatorial Peptide Libraries (36). We set a threshold <20 of percentile rank and selected all peptides lower than this.

## Construction of Recombinant Plasmids

pVAX1 vector (Thermo Fisher Scientific Inc., MA, USA), designed for use in the development of DNA vaccines, and pQE80L bacterial lacI<sub>Q</sub> vector (Qiagen), for expressing N-terminally 6xHis-tagged proteins, were used to induce the expression of recombinant protein. The multi-epitope genes were chemically synthesized by GenScript, Inc. (Piscataway, NJ, USA), with codon optimization for mouse and *E. coli*. The Kozak or Shine-Dalgarno sequence was included in the respective genes. The genes were inserted into pUC57 to generate two expression vectors: pUC57-MEBe (expressing to the recombinant protein) and pUC57-MEBm (used to construct the DNA vaccine). Both constructs were digested with *Bam*H-I and subcloned into

*Bam*H-I-*Pst*I-digested pVAX1 or *Bam*H-I-*Pst*I-digested pQE80L. We obtained pV-MEB (multi-epitope DNA vaccine for *Brucella*) and pQE80L-MEB plasmids and confirmed them by restriction digestion analysis (**Figure 1**). We observed 1140 base pairs (bp) corresponding to MEBm fragment (A) and 1098 bp corresponding to MEBe fragment (B), respectively.

## Immunization

BALB/c mice were randomly divided into three groups consisting of 10 mice per group. Group 1 was injected with 100 µg of the pV-MEB vaccine in 100 µl of phosphate buffer saline (PBS), divided into two injections of 50 µl, in each posterior tibialis muscle. As negative controls, groups of mice received either 100 µg pVAX1 in 100 µl of PBS or 100 µl of PBS, injected as described above for the experimental group (23). All groups were immunized three times at 15-day intervals.

## Purification of Recombinant Multi-Epitope Protein

To obtain the multi-epitope recombinant protein, *E. coli* BL-21 were chemically transformed with pQE80L-MEBe, and we standardized the protocols to carry out the purification of the rMEB protein. Transformed bacteria were grown in LB broth at 37°C to mid-log phase [optical density at 600 nm (OD<sub>600</sub>), 0.6–0.8]. To induce the expression of recombinant protein, bacteria were cultured with 0.5 mM Isopropyl β-D-1-thiogalactopyranoside (IPTG) for 4 h at 27°C to induce the

**TABLE 1 |** *Brucella abortus* proteins used to design the multi-epitope DNA vaccine.

Protein name	Locus tag	Position	Genebank ID	Length (aa)
Copper/Zinc superoxide dismutase	BAB2_0535	AM040265.1:534069–534590	CAJ12701.1	173
Flagellar protein FlgJ	BAB1_0260	AM040264.1:263739–265859	CAJ10216.1	706
Zinc-dependent metallopeptidase	BAB1_0270	AM040264.1:270965–271513	CAJ10226.1	182
Hypothetical DNA-binding protein	BAB1_0273	AM040264.1:272920–273165	CAJ10229.1	81
Hypothetical GcrA protein	BAB1_0278	AM040264.1:275602–275838	CAJ10234.1	78
Hypothetical ABC-type transporter	BAB1_0278a	AM040264.1:275322–275654	EEP63779.1	110

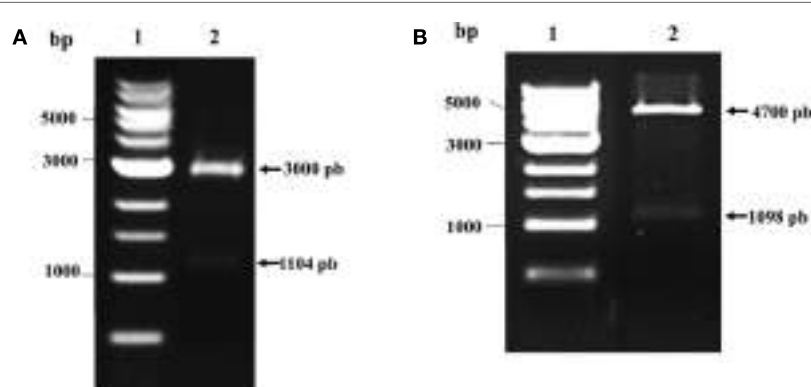


**FIGURE 1 |** Verification of pV-MEB DNA vaccine and pQE80L-MEB plasmids. **(A)** Restriction analysis of pV-MEB plasmid digested with *Bam*H-I and *Pst*I (line 1). **(B)** Restriction analysis of pQE80L-MEB plasmid digested with *Bam*H-I and *Pst*I (line 1). LM, DNA size marker (1 kb DNA ladder).

expression of recombinant protein. Thereafter, the transformed bacterial cells were collected by centrifugation and then disrupted by sonication in Tris-HCl buffer plus 0.2 mM of phenylmethylsulfonyl fluoride (PMSF). This preparation was centrifuged at 12,000 g for 20 min, the soluble fraction was saved and the insoluble fraction was denatured with Denaturing Binding Buffer (0.2 mM PMSF; 20 mM Tris-HCl pH 8; 0.5 M NaCl; 6 M Urea; 10 mM Imidazole). The his-tagged rMEB protein was purified by Ni<sup>2+</sup>-chelated affinity chromatography with HisTrap FF crude columns (GE Healthcare Life Sciences), according to the manufacturer's instructions. The elution was performed with 100 mM of Imidazole. The eluate was concentrated and desalinated using a filter with a molecular weight exclusion of 10 kDa (Amicon ultra 100 K, Millipore, MA, USA). Protein concentration was determined by the Pierce™ BCA Protein Assay kit (Thermo Fisher Scientific Inc.). Recombinant multi-epitope proteins were stored at -20°C for later use as antigens in a indirect enzyme-linked immunosorbent assay (ELISA) and lymphocyte proliferation assays.

## Humoral Immune Response

The antibody isotype IgG, IgG1, and immunoglobulin G2a (IgG2a) titers were measured from peripheral blood using an ELISA. Serum was collected 2 days before each immunization and 15 days after the last immunization. Ninety-six-well polystyrene microtiter plates (Thermo Fisher Scientific Inc., MA, USA) were coated with 1 µg/ml of rMEB or 10 µg/ml of crude *Brucella* protein (CBP) (37), diluted in 0.05 M carbonate-bicarbonate buffer (pH 9.6). After overnight incubation at 4°C, the plates were blocked with 0.8% gelatin in Tris-buffered saline for 1 h at 37°C. Serial twofold dilutions of sera containing primary antibodies from test and control animals were added and incubated for 3 h at room temperature. Isotype-specific horseradish peroxidase-conjugated anti-mouse IgG (US Biological, Life Sciences) was added at 1:1000 dilution. After 30 min of incubation at room temperature, 200 µl of substrate solution (Sigma-Aldrich, Inc.) was added to each well. Results were read using a VictorX3 Multilabel Plate Reader (PerkinElmer, USA) at 450 nm. All assays were done in triplicate.

## Culture of Splenocytes and Lymphocyte Proliferation

Four weeks after the last immunization, mice were euthanized and their spleens removed under aseptic conditions. The splenocytes were cultured, at a concentration of  $4 \times 10^6$  viable cells/ml (100 µl per well), at 37°C under 5% CO<sub>2</sub> in a 96-well flat-bottom plate (Nunc, Denmark), previously sensitized with 2 µg/ml or 10 µg/ml of recombinant proteins (rMEB), or 2 µg/ml or 10 µg/ml CBP. Splenocytes were cultured in RPMI 1640 medium (Thermo Fisher Scientific, MA, USA) supplemented with 10% heat-inactivated fetal calf serum (GIBCO BRL), penicillin-streptomycin (50 UI of penicillin; 50 µg/ml streptomycin), and amphotericin B (0.25 µg/ml). After 72 h, cells were pulsed for 8 h with 0.4 µCi thymidine (50 µCi/mmol; Amersham, UK) per well and the radioactivity incorporated in the DNA measured using a scintillation counter. Concanavalin A (ConA) (Sigma

Aldrich, MO, USA), at a concentration of 10 µg/ml was used as proliferative positive control and 10 µg/ml albumin protein or 10 µg/ml total *E. coli* protein (CEP) were used as proliferative negative control. Cell proliferation data were expressed as the stimulation index of triplicate cultures from a cell pool from each group. These were obtained by dividing the amount of <sup>3</sup>H-Thymidine incorporated (c.p.m.) in antigen-stimulated cell cultured by the c.p.m. obtained from cells cultured without antigen (38).

## Cytokine ELISAs

The levels of IFN-γ and IL-4 secreted were measured by antigen-capture ELISA. Briefly, spleens were aseptically removed from experimental and control mice, disaggregated to single cells, re-suspended in Red Blood Cell buffer (Promega, Madison, WI, USA) to eliminate erythrocytes, and washed three times using incomplete RPMI 1640 (Thermo Fisher Scientific, MA). Cells were adjusted to a concentration of  $4 \times 10^6$  viable cells per ml in RPMI 1640 supplemented with 10% fetal calf serum (Thermo Fisher Scientific, MA, USA) and antibiotic/antimycotic solution (100 UI penicillin, 100 µg/ml streptomycin, and 0.25 µg/ml amphotericin B). Spleen cell suspensions were cultured in 24-well plates (Nunc, Denmark) and stimulated with the recombinant multi-epitope *B. abortus* protein (rMEB) at 2 or 10 µg/ml CBPs or medium alone. They were incubated for 48 h at 37°C under 5% CO<sub>2</sub> to induce, *in vitro*, the expression of cytokines. After centrifugation at 400 × g for 10 min, supernatants were collected and cytokines quantified by ELISA sandwich using the Mouse IFN-γ and IL-4 ELISA kits (eBiosciences, San Diego, CA, USA), following the manufacturer's instructions. All assays were performed in triplicate.

## Protection Experiment

The protection experiments were performed as previously described (16). Briefly, 4 weeks after last vaccination, four mice from each group were challenged by intraperitoneal injection of  $10^4$  CFU *B. abortus* 2308 per animal. Two weeks later, infected mice were euthanized and their spleens were homogenized in PBS, with the homogenate serially diluted and cultured in Petri dishes containing agar Columbia supplemented with 5% sheep blood (bioMériex, Santiago, Chile) for 72 h at 37°C. Bacterial counts were recorded and the number of CFU per spleen calculated. This experiment was repeated twice. When the immunizations were initiated, one reference-vaccinated control group was immunized with  $1 \times 10^8$  CFU *B. abortus* RB51 per mouse. Results are reported as units of protection represented by the difference between mean ± SD of log<sub>10</sub> CFU/spleen of the PBS control groups with respect to mean ± SD of log<sub>10</sub> CFU/spleen values of experimental groups.

## Statistical Analysis

The immune response in mice was analyzed using a two-way analysis of variance (ANOVA) and the protective response was analyzed using a one-way ANOVA. Data were analyzed using Prism 5.0 (GraphPad software). Differences were considered significant if  $P < 0.05$ .

## RESULTS

### Epitope Prediction

Using the Immune Epitope Database (IEDB, [www.iedb.org](http://www.iedb.org)), we identified epitopes suitable for constructing a multi-epitope DNA chimeric vaccine against *B. abortus*. The epitopes identified (**Table 1**) are specific for MHC class I and MHC class II molecules. However, while all sequences had putative epitopes for MHC class I and class II molecules, the BAB1\_0278 ORF only showed epitopes for MHC class I (**Table 2**). Peptides were selected based on having a lower percentile rank score. Non-redundant peptides were selected to construct the DNA vaccine. An immunodominant peptide of the Cu, Zn superoxide dismutase protein from *B. abortus*, described previously in the literature (39), was also included in the vaccine sequence. Finally, 21 epitopes were used to construct the DNA vaccine. To connect the epitopes, we used a GDGDG linker sequence, a rationally designed sequences used to link multi-epitope vaccines (40). The final design of the multi-epitope vaccine is shown in **Figure 2A**.

### Production of Recombinant Multi-Epitope Protein of *Brucella*

To construct the recombinant protein, *E. coli* BL21 (DE3) cells were transformed with the pQE80L-MEB plasmid and expression of the 6xHis-Tagged protein was induced. The recombinant protein was mainly expressed in the soluble fraction of the transformed bacteria after their sonication (**Figure 2B**, lane 4). The recombinant protein of *B. abortus* (rMEB) was induced and detected by Western blot. Its weight was ~37 kDa, the expected mass (**Figure 2C**).

### Humoral Immune Response of Immunized Mice

Specific antibodies for rMEB and CBPs were measured in order to evaluate the humoral immune response. We performed ELISAs to detect specific IgG, IgG1, and IgG2a antibodies induced in mice against rMEB and CBP. Serum from mice immunized with multi-epitope DNA vaccine for *Brucella* (pV-MEB) contained

**TABLE 2 |** Epitope prediction by computer modeling.

		Allele	Pi	Pf	Peptide	Peptide selected
Cu-Zn SOD	MHC-I	H-2-Ld	60	68	TPGYHGFHV	TPGYHGFHV
		H-2-Kd	92	102	HYDPGNTHHHHL	HYDPGNTHHHHL
	MHC-II	H2-IAd	6	20	IASTMVLMAFPFAAE	IASTMVLMAFPFAAE
		H2-IAd	5	19	FIASTMVLMAFPFAFA	FIASTMVLMAFPFAFA
		H2-IAd	7	21	ASTMVLMAFPFAFAES	ASTMVLMAFPFAFAES
	BAB1_0260	H-2-Kd	199	207	NYARSGVAI	NYARSGVAI
		H-2-Kd	311	322	SYAAPRQGGVNI	SYAAPRQGGVNI
		H-2-Ld	114	122	APGNNNFFGI	APGNNNFFGI
		H-2-Ld	155	166	SPQDSVAGYADF	SPQDSVAGYADF
	MHC-II	H2-IAd	353	367	NDPMRALQAQKLQLE	NDPMRALQAQKLQLEM
BAB1_0270	MHC-I	H-2-Ld	35	43	FPVMDFLEL	FPVMDFLEL
		H-2-Ld	128	138	EPQANQFAGEL	EPQANQFAGEL
	MHC-II	H2-IAd	46	60	CQRGMVDLRIKTQQ	CQRGMVDLRIKTQQ
		H2-IAd	45	59	LCQRGMVDLRIKTQ	LCQRGMVDLRIKTQ
		H2-IAd	155	169	MQRHSVSRGAAIDL	MQRHSVSRGAAIDL
		H2-IAd	154	168	VMQRHSVSRGAADIR	VMQRHSVSRGAADIR
		H2-IAd	153	167	DVMQRHSVSRGAADI	DVMQRHSVSRGAADI
BAB1_0273	MHC-I	H-2-Kd	35	43	RYEGGSGVL	RYEGGSGVL
		H-2-Kd	48	60	QYIEALIAVLTAA	QYIEALIAVLTAA
		H-2-Kd	48	56	QYIEALIAV	QYIEALIAV
	MHC-II	H2-IAd	3	17	ITAEQLRAARALLKM	ITAEQLRAARALLKM
		H2-IAd	9	23	RAARALLKMEQRALA	RAARALLKMEQRALA
BAB1_0278	MHC-I	H-2-Ld	7	16	SPLSEALPMF	SPLSEALPMF
		H-2-Ld	7	15	SPLSEALPM	SPLSEALPM
		H-2-Ld	21	28	SPHEGFLRL	SPHEGFLRL
		H-2-Ld	21	31	SPHEGFLRLADL	SPHEGFLRLADL
BAB1_0278a	MHC-I	H-2-Ld	22	32	FPANKKNGYAL	FPANKKNGYAL
	MHC-II	H2-IAd	44	58	SAPASIQEADDFLLA	SAPASIQEADDFLLA
		Pi	Pf	Peptide	Reference	
Cu-Zn SOD	-	-	75	86	GGAPGEKDGVIPAG	Tabatabai and Pugh (39)

Pi, initial position of peptides in each protein; Pf, final position of peptides in each protein.

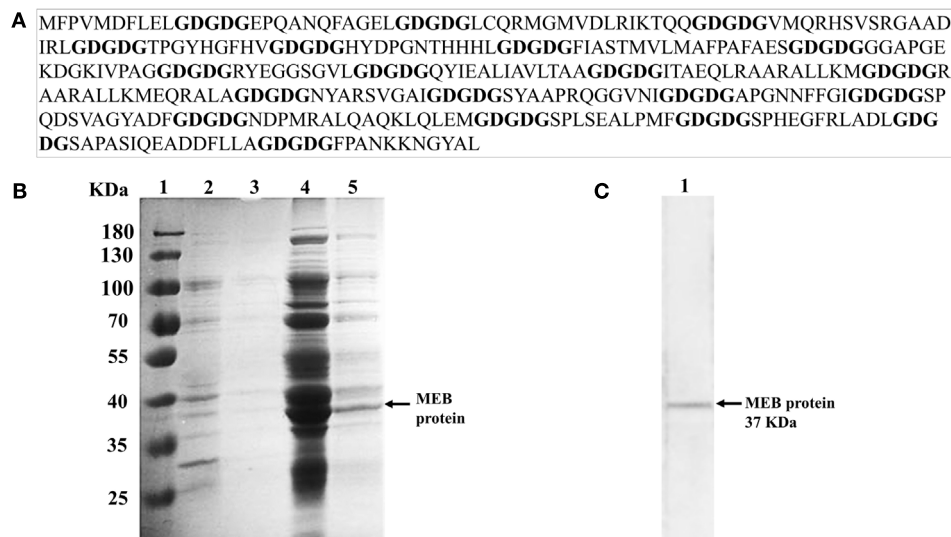


**FIGURE 2 | MEB DNA vaccine design and identification of rMEB protein. (A)** Multi-epitope vaccine sequence spaced by GDGDG linker sequence. **(B)** SDS-PAGE analysis of rMEB. Lane 1, marker; lane 2, total proteins obtained from insoluble extract from *Escherichia coli* transformed with pQE80L-MEB plasmid; lane 3, eluent from Ni<sup>2+</sup>-chelated affinity chromatography of the insoluble extract from *E. coli*; lane 4, total proteins obtained from the soluble extract from *E. coli* transformed with pQE80L-MEB plasmid; lane 5, eluent from Ni<sup>2+</sup>-chelated affinity chromatography of the soluble extract from *E. coli*. **(C)** Western blot analysis of rMEB with anti-His-tag monoclonal antibody.

significant titers of IgG specific for rMEB at 30 days after the first immunization. IgG titers were higher at 45 days, compared to the negative-control groups pVAX and PBS (Figure 3A). The same pattern was observed for IgG against CBPs (Figure 3B). No rMEB- or CBP-specific IgG1 was detected in serum from mice immunized with pV-MEB (Figures 3C,D). Titers of IgG2a antibodies specific for rMEB proteins significantly differed between the pV-MEB groups immunized ( $P < 0.05$ ) only after the second immunization between pV-MEB groups immunized, compared to PBS and pVAX controls (Figure 3E). On the other hand, a significant titer of IgG2a specific for CBP was observed after the third immunization with pV-MEB, compared to PBS and pVAX negative controls (Figure 3F).

## Cellular Immune Response

To evaluate the cellular immune response, splenocytes were obtained from mice immunized with pV-MEB, p-VAX, or PBS at 30 days after the last immunization. *In vitro* stimulation using splenocytes from pV-MEB mice immunized with 10 or 2 µg/ml rMEB protein resulted in a significant increase in cell proliferation in relation to the control group ( $P < 0.001$  and  $P < 0.05$ , respectively; Figure 4A). *In vitro* stimulation using splenocytes from pV-MEB mice immunized with 10 and 2 µg/ml of CBP also induced a significant increase in splenocytes proliferation ( $P < 0.001$  and  $P < 0.01$ , respectively; Figure 4B). In this assay, 10 µg/ml of ConA was used as lymphoproliferation control. It induced a strong lymphoproliferative response in all experimental groups (data not shown). *In vitro* stimulation of splenocytes with 10 µg/ml crude *E. coli* protein and 10 µg/ml albumin did not induce proliferation across the different experimental groups (Figure 4C).

IFN- $\gamma$  levels in supernatants from cultures of splenocytes obtained from the pV-MEB immunization group re-stimulated with rMEB or CBP were significantly higher than those in the negative-control groups ( $P < 0.001$ , respectively) (Figure 5A). There were no significant difference in levels of IL-4 secretion between the experimental and control groups (Figure 5B).

## Protection against Virulent *B. abortus* Challenged

The protective capacity provided by the pV-MEB DNA vaccine was evaluated 6 weeks after the last immunization. Immunized mice were challenged with 10<sup>4</sup> CFU *B. abortus* 2308, and after 2 weeks their spleens were removed, homogenized, and cultured. The results showed that pV-MEB DNA vaccine confers protection against *B. abortus* 2308. The DNA vaccine induced 1.14 log<sub>10</sub> units of protection ( $P > 0.005$ ; Figure 6) compared to the PBS control group. By comparison, vaccination with live *B. abortus* strain RB51 induced 2.85-log units of protection.

## DISCUSSION

Brucellosis is a worldwide zoonotic disease of increasing incidence. Vaccination of livestock is considered the best prevention method, but it is necessary to generate safer and more effective vaccine formulations (41). The availability of bioinformatics tools and databases allow the design of vaccines without the need for *in vitro* manipulation of a pathogenic microorganism. Using “reverse vaccinology” approach, *in silico* genomic databases are screened to identify antigenic sequences for new vaccines (42). This allows the identification of antigens that would be difficult

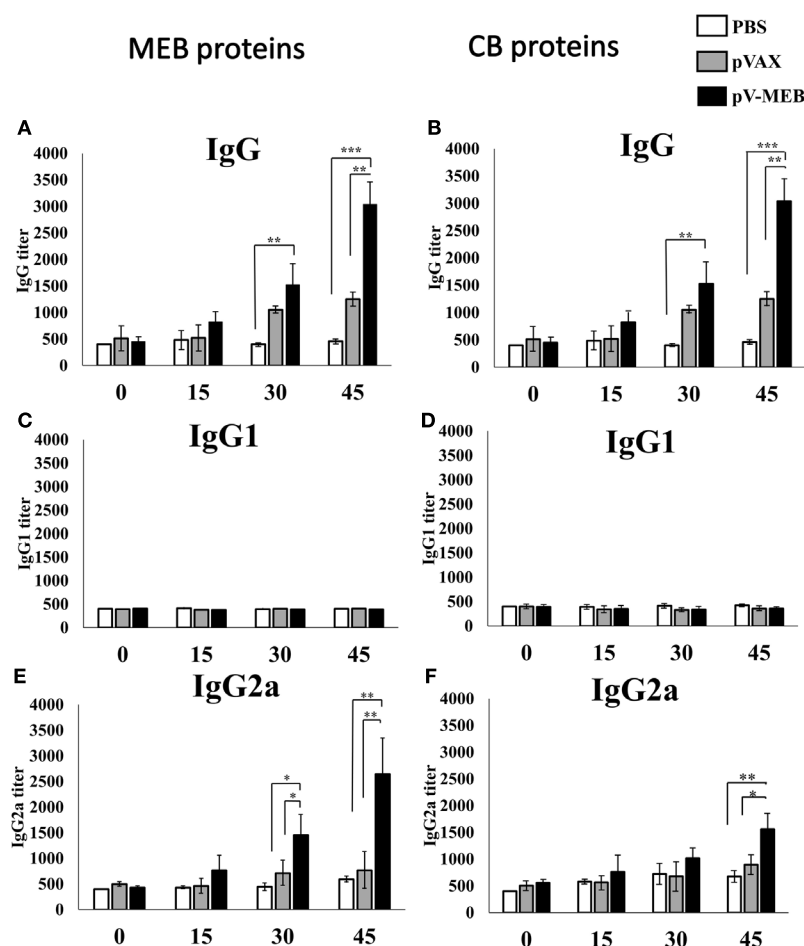


**FIGURE 3 | Titers of specific IgG (A,B), IgG1 (C,D), and immunoglobulin G2a (E,F) production after immunization with recombinant pV-MEB vaccine.** Sera obtained from each group of mice were used for detection of antibodies against purified rMEB proteins (A,C,D) and crude *Brucella* proteins (B,D,F) by indirect enzyme-linked immunosorbent assay. Sera obtained at days 0, 15, 30, and 45 post-immunization were serially diluted in phosphate buffer saline and used in the assay (\* $P < 0.05$ , \*\* $P < 0.01$ , and \*\*\* $P < 0.001$ ).

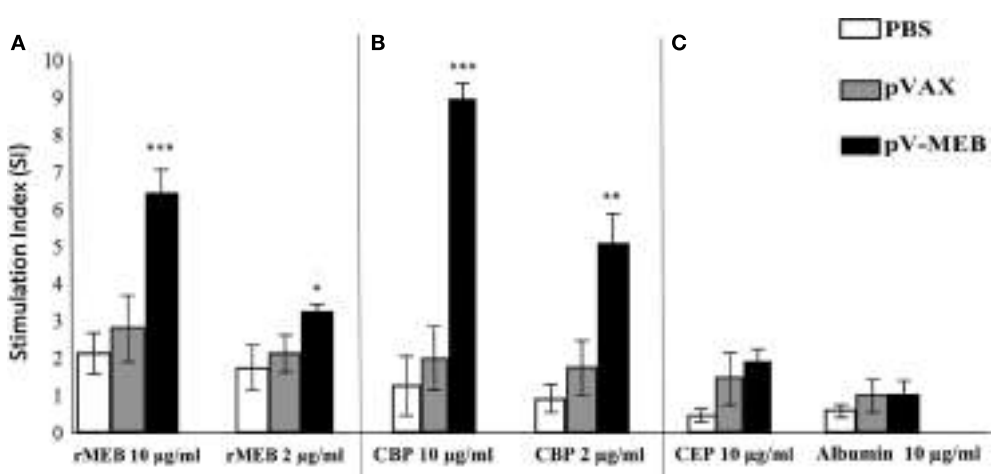


**FIGURE 4 | Lymphocyte proliferation assay after *in vitro* stimulation with (A) 10 or 2 µg/ml recombinant protein, (B) 10 or 2 µg/ml *Brucella abortus* total proteins (CBP), and (C) 10 µg/ml of crude *Escherichia coli* proteins and 10 µg/ml of albumin as control.** Results are shown as mean  $\pm$  SD of the stimulation index of  $^3\text{H}$ -thymidine, incorporated from mouse splenocytes ( $n = 5$ ) (\* $P < 0.05$ , \*\* $P < 0.01$ , and \*\*\* $P < 0.001$ ).

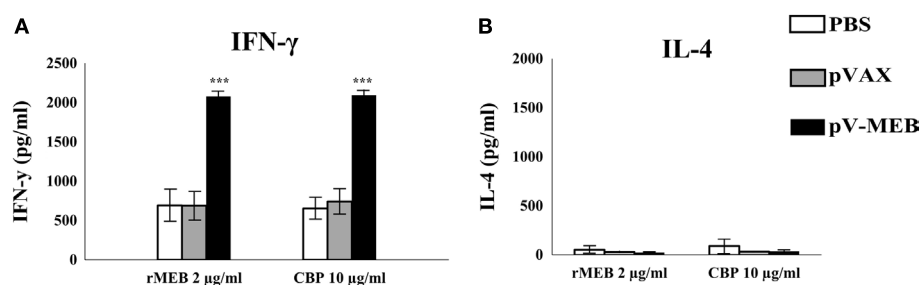
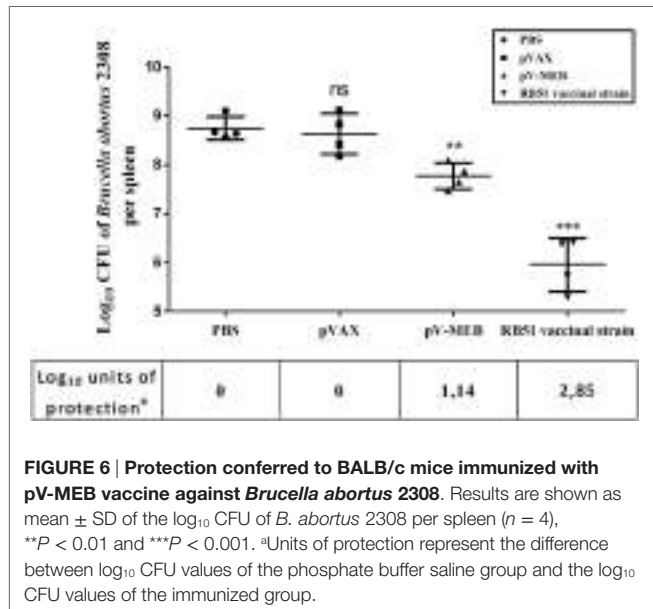


**FIGURE 5 | Determination of IFN- $\gamma$  (A) or IL-4 (B) production.** Splenocytes from pV-MEB pVAX or phosphate buffer saline (PBS) groups were obtained 30 days after the last immunization, and were re-stimulated *in vitro* with 2  $\mu$ g/ml of recombinant MEB proteins or 10  $\mu$ g/ml of crude *Brucella* proteins. Each bar represents the geometric mean  $\pm$  SD (error bars) of the response in spleen cells from individual mice. \*\*\* $P$  < 0.001, statistically significant difference compared to the PBS group.



using traditional methods (42). It has been observed that recombinant protein vaccines induce a humoral/Th2 immune response and it is suggested that a boost with a protein improve the protective efficacy of the antibodies (43). The effect of DNA vaccines, however, is based toward a Th1 response (44–46).

DNA vaccine have a number of advantages, including ease storage, flexibility of antigen codification, and the presence of CpG motifs, which improve the immune response (45). Mono-antigenic DNA vaccines induce a good immune response, but tend to induce less protection against pathogens compared to poly-antigenic vaccine (47, 48). In the case of *B. abortus*, the three antigens: BCSP31, Cu-Zn SOD, and L7/L12 ribosomal proteins, when giving together as part of a formulation, improve the immune response against pathogenic *B. abortus* (49).

Within the last few years, the use of epitopes in vaccines has become a valid alternative for improving the efficacy of traditional vaccine, based on a “natural” form of the pathogen (50). Multi-epitope peptide DNA vaccines are effective against some viruses (30, 51, 52) and they are potentially effective against some bacteria such as *Helicobacter pylori* (53) and in cancer prevention (54, 55).

Multi-epitope DNA vaccines more faithfully mimic antigen processing and presentation during natural infection (30). In addition, multi-epitope DNA vaccines induce more potent immunoreaction than whole protein vaccine (30). Since the epitopes are derived from multiple antigens and packaged into a relatively small delivery vehicle, the vaccine can induce powerful cross-reactive responses toward multiple antigens and elicit a strong humoral and cellular immune response (56). In this study, we used bioinformatics methods to identify epitopes on antigenic proteins of *B. abortus* and to design a multi-epitope chimeric DNA vaccine. We performed the epitope prediction using bioinformatics resources available online, including NetChop, SYFPEITHI, or BIMAS. However, these database had a 50% prediction assertiveness about the prediction (57). The predictive power of the IEDB has been expanded with the provision of a large number of published epitopes and full-scale MHC-binding peptides (58), so we opted to use the IEDB server. In order to design a rational vaccine against *Brucella*, we focused on finding MHC class I or MHC class II binding peptides known to orchestrate primarily a T-cell immune response, since *B. abortus* is known as a facultative intracellular pathogen (59). We selected 21 dominant epitopes from ORFs present within GI-3 and proteins described as antigens of immunological interest (Table 1). Peptides were selected based on their low percentile score using observed redundant sequences as a further selection criterion, choosing peptides with non-redundant sequences (Table 2). For the theoretical binding of peptides we used the “GDGDG” sequence as spacer (Figure 2A) (40). The introduction of GDGDG spacers does not preclude the possibility that such linear arrangements of epitopes might contain other cryptic epitopes. The presence of this spacer at 15–20 residue intervals might help create some secondary and possibly tertiary structure, thereby facilitating antigen expression (40). Then, we constructed the *B. abortus* multi-epitope chimeric DNA vaccine using of chemical gene synthesis (pV-MEB).

We, next, proceeded to evaluate the immunogenicity and protective efficacy conferred by immunization with the multi-epitope vaccine, peptides present in Cu-Zn superoxide dismutase and the ORFs present within GI-3 (BAB1\_0260, BAB1\_0270, BAB1\_0273, and BAB1\_0278) of *B. abortus* (16, 21–26). The results showed that immunization with pV-MEB triggers a MEB-specific humoral and cellular immune response in BALB/c mice.

At systemic level pV-MEB promotes the stimulation of MEB-specific IgG2, indicating an adequate induction of a Th1 response. *In vitro* stimulation of splenocytes from pV-MEB immunized mice induced the highest proliferation in response to antigen, confirming the *in vivo* translation of the *MEB* synthetic gene and subsequent induction of a cell-mediated immune response. We used albumin and *E. coli* proteins as control of proliferation and in both cases splenocytes did not proliferate. Therefore, the immune response inducing by pV-MEB DNA vaccine was specific to MEB protein and *Brucella* antigens. Antigen-stimulated splenocytes from vaccinated mice produced IFN- $\gamma$ . The level of IFN- $\gamma$  and the *in vitro* proliferation of splenocytes stimulated by MEB recombinant protein demonstrated that pV-MEB DNA vaccine induces a strong immunoreaction and a polarized Th1 response against *Brucella* infection, which is associated to effective clearance of intracellular pathogens, so essential feature for a *Brucella* vaccine (7, 59). The immunogenicity induced by pV-MEB DNA recombinant plasmid was evaluated by challenging immunized mice with *B. abortus* 2308 strain. Our results confirmed that immunization with pV-MEB induced immunogenicity associated with significant protection, but protection induced by attenuated *B. abortus* RB51 was more robust.

In conclusion, we have shown that a *B. abortus* multi-epitope chimeric DNA vaccine (pV-MEB) elicits strong humoral and

## REFERENCES

- Percin D. Microbiology of *Brucella*. *Recent Pat Antiinfect Drug Discov* (2012) 8:13–7. doi:10.2174/1574891X11308010004
- Seleem M, Boyle S, Sriranganathan N. Brucellosis: a re-emerging zoonosis. *Vet Microbiol* (2010) 140:392–8. doi:10.1016/j.vetmic.2009.06.021
- Atluri V, Xavier M, de Jong M, den Hartigh A, Tsolis RM. Interactions of the human pathogenic *Brucella* species with their hosts. *Annu Rev Microbiol* (2011) 65:523–41. doi:10.1146/annurev-micro-090110-102905
- de Figueiredo P, Ficht T, Rice-Ficht A, Rossetti C, Adams L. Pathogenesis and immunobiology of brucellosis: review of *Brucella*-host interactions. *Am J Pathol* (2015) 185:1505–17. doi:10.1016/j.ajpath.2015.03.003
- Pappas G, Papadimitriou P, Akritidis N, Christou L, Tsianos E. The new global map of human brucellosis. *Lancet Infect Dis* (2006) 6:91–9. doi:10.1016/S1473-3099(06)70382-6
- Carvalho N, Mol J, Xavier M, Paixao T, Lagew A, Santos R. Pathogenesis of Bovine brucellosis. *Vet J* (2010) 184:146–55. doi:10.1016/j.tvjl.2009.04.010
- Brandão A, Oliveira F, Carvalho N, Vieira L, Azevedo V, Macedo G, et al. Host susceptibility to *Brucella abortus* infection is more pronounced in IFN- $\gamma$  knockout than IL-12/β 2-microglobulin double-deficient mice. *Clin Dev Immunol* (2012) 2012:589494. doi:10.1155/2012/589494
- Pappas G, Akritidis N, Bositkovski M, Tsianos E. Brucellosis. *N Engl J Med* (2005) 352:2325–36. doi:10.1056/NEJMra050570
- Haag A, Myka K, Arnold MF, Caro-Hernández P, Ferguson G. Importance of lipopolysaccharide and cyclic β-1,2-glucans in *Brucella*-mammalian infections. *Int J Microbiol* (2010) 2010:124509. doi:10.1155/2010/124509
- Celli J, de Chastellier C, Franchini D, Pizarro-Cerda J, Moreno E, Gorvel J. *Brucella* evades macrophage killing via VirB-dependent sustained interactions with the endoplasmic reticulum. *J Exp Med* (2003) 198:545–56. doi:10.1084/jem.20030088
- Salcedo S, Marchesini M, Lalouard H, Fuguier E, Jolly G, Balor S, et al. *Brucella* control of dendritic cell maturation is dependent on the TIR-containing protein Btp1. *PLoS Pathog* (2008) 4(2):e21. doi:10.1371/journal.ppat.0040021
- Viadas C, Rodríguez M, Sangari F, Gorvel J, García-Lobo J, López-Góñi I. Transcriptome analysis of the *Brucella abortus* BvrR/BvrS two-component regulatory system. *PLoS One* (2010) 5:e10216. doi:10.1371/journal.pone.0010216
- Lei S, Zhong Z, Ke Y, Yang M, Xu X, Ren H, et al. Deletion of the small RNA chaperone protein Hfq down regulates genes related to virulence and confers cellular protective immunity. Future studies must include an array of epitopes or combination of peptides and adjuvants as alternatives to conventional vaccine design. This study provides a starting point for the development of multi-epitope DNA vaccines against *B. abortus*.
- EE: construction of recombinant plasmid, analysis *in silico* of determination of epitopes, evaluation of immune response, evaluation of antibodies specificity by ELISA, and writing and discussion of the results. DS: immunization trial, lymphocyte proliferation assays, and protection experiment. AO: programming and monitoring the experiments, performing the analysis, and discussion and writing the manuscript. AO is principal investigator at the FONDECYT grant that funded this work.
- AUTHOR CONTRIBUTIONS**
- ACKNOWLEDGMENTS**
- This work was supported by Grant 1130093 from the Fondo Nacional de Desarrollo Científico y Tecnológico (FONDECYT), Santiago, Chile. The authors wish to thank Professor Nelson Fernández (University of Essex, UK) for critical reading and editing of the manuscript.
- protection against wild-type *Brucella* challenge in mice. *Front Microbiol* (2016) 20(6):1570. doi:10.3389/fmicb.2015.01570
- Beck B, Tabatabai L, Mayfield J. A protein isolated from *Brucella abortus* is a Cu-Zn superoxide dismutase. *Biochemistry* (1990) 29:372–6. doi:10.1021/bi00454a010
- Pratt A, DiDonate M, Shim D, Cabelli D, Bruns C, Belzer C, et al. Structural, functional, and immunogenic insights on Cu, Zn superoxide dismutase pathogenic virulence factors from *Neisseria meningitidis* and *Brucella abortus*. *J Bacteriol* (2015) 197:3834–47. doi:10.1128/JB.00343-15
- Oñate A, Céspedes S, Cabrera A, Rivers R, Gonzalez A, Munoz C, et al. A DNA vaccine encoding Cu, Zn superoxide dismutase of *Brucella abortus* induces protective immunity in BALB/c mice. *Infect Immun* (2003) 71:4857–61. doi:10.1128/IAI.71.9.4857-4861.2003
- Muñoz-Montesino C, Andrews A, Rivers R, González-Smith A, Folch H, Céspedes S, et al. Intraspleen delivery of a DNA vaccine coding for superoxide dismutase (SOD) of *Brucella abortus* induces SOD-specific CD4+ and CD8+ T cells. *Infect Immun* (2004) 72:2081–7. doi:10.1128/IAI.72.4.2081-2087.2004
- Gándara B, Merino A, Rogel M, Martínez-Romero E. Limited genetic diversity of *Brucella* spp. *J Clin Microbiol* (2001) 39:235–40. doi:10.1128/JCM.39.1.235-240.2001
- Rajashekara G, Glasner J, Glover D, Splitter G. Comparative whole-genome hybridization reveals genomic islands in *Brucella* species. *J Bacteriol* (2004) 186(15):5040–51. doi:10.1128/JB.186.15.5040-5051.2004
- Ratnshana V, Sturgill D, Ramamoorthy S, Reichow S, He Y, Lathigra R, et al. Molecular targets for rapid identification of *Brucella* spp. *BMC Microbiol* (2006) 22(6):13. doi:10.1186/1471-2180-6-13
- Ortiz-Román L, Riquelme-Neira R, Vidal R, Oñate A. Roles of genomic island 3 (GI-3) BAB1\_0267 and BAB1\_0270 open reading frames (ORFs) in the virulence of *Brucella abortus* 2308. *Vet Microbiol* (2014) 172:279–84. doi:10.1016/j.vetmic.2014.05.005
- Céspedes S, Salgado P, Retamal-Díaz A, Vidal R, Oñate A. Roles of genomic island 3 (IG3) BAB1\_0278 and BAB1\_0263 open reading frames (ORFs) in the virulence of *Brucella abortus* in BALB/c mice. *Vet Microbiol* (2012) 156:1–7. doi:10.1016/j.vetmic.2011.09.025
- Gómez L, Alvarez F, Fernández P, Flores M, Molina R, Coloma R, et al. Immunogenicity and protective response induced by recombinant plasmids based on the BAB1\_0267 and BAB1\_0270 open reading frames of *Brucella*

- abortus* 2308 in BALB/c mice. *Front Cell Infect Microbiol* (2016) 6:117. doi:10.3389/fcimb.2016.00117
24. Sisilema-Egas F, Céspedes S, Fernández P, Retamal-Díaz A, Sáez D, Oñate A. Evaluation of protective effect of DNA vaccines encoding the BAB1\_0263 and BAB1\_0278 open reading frames of *Brucella abortus* in BALB/c mice. *Vaccine* (2012) 30:7286–91. doi:10.1016/j.vaccine.2012.09.039
  25. Riquelme-Neira R, Retamal-Díaz A, Acuña F, Riquelme P, Rivera A, Sáez D, et al. Protective effect of a DNA vaccine containing an open reading frame with homology to an ABC-type transporter present in the genomic island 3 of *Brucella abortus* in BALB/c mice. *Vaccine* (2013) 31:3663–7. doi:10.1016/j.vaccine.2013.06.013
  26. Li X, Xu J, Xie Y, Qiu Y, Fu S, Yuan X, et al. Vaccination with recombinant flagellar proteins FlgJ and FliN induce protection against *Brucella abortus* 544 infection in BALB/c mice. *Vet Microbiol* (2012) 161:137–44. doi:10.1016/j.vetmic.2012.07.016
  27. Dorneles E, Lima G, Teixeira-Carvalho A, Araújo M, Martins-Filho O, Sriranganathan N, et al. Immune response of calves vaccinated with *Brucella abortus* S19 or RB51 and revaccinated with RB51. *PLoS One* (2015) 10(9):e0136696. doi:10.1371/journal.pone.0136696
  28. Schurig G, Sriranganathan N, Corbel M. Brucellosis vaccines: past, present and future. *Vet Microbiol* (2002) 90:479–96. doi:10.1016/S0378-1135(02)00255-9
  29. Ingolotti M, Kawelekar O, Shedlock D, Muthumani K, Weiner D. DNA vaccines for targeting bacterial infections. *Expert Rev Vaccines* (2010) 9:747–63. doi:10.1586/erv.10.57
  30. Zhao C, Sun Y, Zhao Y, Wang S, Yu T, Du F, et al. Immunogenicity of a multi-epitope DNA vaccine against hantavirus. *Hum Vaccin Immunother* (2012) 8:208–15. doi:10.4161/hv.18389
  31. Wu M, Li M, Yue Y, Xu W. DNA vaccine with discontinuous T-cell epitope insertions into HSP65 scaffold as a potential means to improve immunogenicity of multi-epitope *Mycobacterium tuberculosis* vaccine. *Microbiol Immunol* (2016) 60:634–45. doi:10.1111/1348-0421.12410
  32. Xu Q, Cui N, Ma X, Wang F, Li H, Shen F, et al. Evaluation of a chimeric multi-epitope-based DNA vaccine against subgroup J avian leukosis virus in chickens. *Vaccine* (2016) 34:3751–6. doi:10.1016/j.vaccine.2016.06.004
  33. Salimi N, Flerl W, Peters B, Sette A. The immune epitope database: a historical retrospective of the first decade. *Immunology* (2012) 137:117–23. doi:10.1111/j.1365-2567.2012.03611.x
  34. Peters B, Sette A. Generating quantitative models describing the sequence specificity of biological processes with the stabilized matrix method. *BMC Bioinformatics* (2005) 6:132. doi:10.1186/1471-2105-6-132
  35. Nielsen M, Lundsgaard C, Worning P, Lauemøller S, Lamberth K, Buus S, et al. Reliable prediction of T-cell epitopes using neural networks with novel sequence representations. *Protein Sci* (2003) 12:1007–17. doi:10.1110/ps.0239403
  36. Sidney J, Assarsson E, Moore C, Ngo S, Pinilla C, Sette A, et al. Quantitative peptide binding motifs for 19 human and mouse MHC class I molecules derived using positional scanning combinatorial peptide libraries. *Immunome Res* (2008) 4:2. doi:10.1186/1745-7580-4-2
  37. Oñate A, Andrew A, Beltran A, Eller G, Schurig G, Folch H. Frequent exposure of mice to crude *Brucella abortus* proteins down-regulates immune response. *J Vet Med B Infect Dis Vet Public Health* (2000) 47:677–82. doi:10.1046/j.1439-0450.2000.00402.x
  38. González M, Andrews E, Folch H, Sáez D, Cabrera A, Salgado P, et al. Cloning, expression and immunogenicity of the translation initiation factor 3 homologue of *Brucella abortus*. *Immunobiol* (2009) 214:113–20. doi:10.1016/j.imbio.2008.07.004
  39. Tabatabai L, Pugh G. Modulation of immune responses in Balb/c mice vaccinated with *Brucella abortus* Cu-Zn superoxide dismutase synthetic peptide vaccine. *Vaccine* (1994) 12:919–24. doi:10.1016/0264-410X(94)90035-3
  40. Livingston B, Crimi C, Newman M, Higashimoto Y, Appella E, Sidney J, et al. A rational strategy to design multiepitope immunogens based on multiple Th lymphocyte epitopes. *J Immunol* (2002) 168:5499–506. doi:10.4049/jimmunol.168.11.5499
  41. Deqiu S, Donglou X, Jiming Y. Epidemiology and control of brucellosis in China. *Vet Microbiol* (2002) 90:165–82. doi:10.1016/S0378-1135(02)00252-3
  42. Rappuoli R. Reverse vaccinology. *Curr Opin Microbiol* (2000) 3:445–50. doi:10.1016/S1369-5274(00)00119-3
  43. Barouch D, Alter G, Broge T, Linde C, Ackerman M, Brown E, et al. Protective efficacy of adenovirus/protein vaccines against SIV challenges in rhesus monkeys. *Science* (2015) 349:320–4. doi:10.1126/science.aab3886
  44. Da'Dara A, Skelly P, Walker C, Harn D. A DNA-prime/protein-boost vaccination regimen enhances Th2 immune responses but not protection following *Schistosoma mansoni* infection. *Parasite Immunol* (2003) 25:429–37. doi:10.1111/j.1365-3024.2003.00651.x
  45. Gurunathan S, Klinman D, Seder R. DNA vaccines: immunology, application, and optimization. *Ann Rev Immunol* (2000) 18:927–74. doi:10.1146/annurev.immunol.18.1.927
  46. Gurunathan S, Stobie L, Prussin C, Sacks D, Glaichenhaus N, Iwasaki A, et al. Requirements for the maintenance of Th1 immunity *in vivo* following DNA vaccination: a potential immunoregulatory role for CD8+ T cells. *J Immunol* (2000) 165:915–24. doi:10.4049/jimmunol.165.2.915
  47. Cui Y, He S, Xue M, Zhang J, Wang H, Yao Y. Protective effect of a multiantigenic DNA vaccine against *Toxoplasma gondii* with co-delivery of IL-12 in mice. *Parasite Immunol* (2008) 30:309–13. doi:10.1111/j.1365-3024.2008.01025.x
  48. Qu D, Yu H, Wang S, Cai W, Du A. Induction of protective immunity by multiantigenic DNA vaccine delivered in attenuated *Salmonella typhimurium* against *Toxoplasma gondii* infection in mice. *Vet Parasitol* (2009) 166:220–7. doi:10.1016/j.vetpar.2009.08.016
  49. Yu D, Hu X, Cai H. A combined DNA vaccine encoding BCSP31, SOD, and L7/L12 confers high protection against *Brucella abortus* 2308 by inducing specific CTL responses. *DNA Cell Biol* (2007) 26:435–43. doi:10.1089/dna.2006.0552
  50. Sette A, Fikes J. Epitope-based vaccines: an update on epitope identification, vaccine design and delivery. *Curr Opin Immunol* (2003) 15:461–70. doi:10.1016/S0952-7915(03)00083-9
  51. Depla E, Van der Aa A, Livingston B, Crimi C, Allosery K, De Brabandere V, et al. Rational design of a multiepitope vaccine encoding T-lymphocyte epitopes for treatment of chronic hepatitis B virus infections. *J Virol* (2008) 82:435–50. doi:10.1128/JVI.01505-07
  52. Tian L, Wang H, Lu D, Zhang Y, Wang T, Kang R. The immunoreactivity of a chimeric multi-epitope DNA vaccine against IBV in chickens. *Biochem Biophys Res Commun* (2008) 377:221–5. doi:10.1016/j.bbrc.2008.09.125
  53. Moss S, Moise L, Lee D, Kim W, Zhang S, Lee J, et al. HelicoVax: epitope-based therapeutic *Helicobacter pylori* vaccination in a mouse model. *Vaccine* (2011) 29:2085–91. doi:10.1016/j.vaccine.2010.12.130
  54. Nezafat N, Ghasemi Y, Javadi G, Khoshnoud M, Omidinia E. A novel multi-epitope peptide vaccine against cancer: an *in silico* approach. *J Theor Biol* (2014) 349:121–34. doi:10.1016/j.jtbi.2014.01.018
  55. Mahmoodi S, Nezafat N, Barzegar A, Negahdaripour M, Nikanfar A, Zarghami N, et al. Harnessing bioinformatics for designing a novel multi-epitope peptide vaccine against breast cancer. *Curr Pharm Biotechnol* (2016) 17:1110–4. doi:10.2174/138920101766160914191106
  56. Xiong A, Peng R, Zhuang J, Gao F, Li Y, Cheng Z, et al. Chemical gene synthesis: strategies, softwares, error corrections, and applications. *FEMS Microbiol Rev* (2008) 32:522–40. doi:10.1111/j.1574-6976.2008.00109.x
  57. Schuler MM, Nastkic M-D, Stevanović S. SYFPEITHI, database for searching and T-cell epitope prediction. In: Flower DR, editor. *Immunoinformatics. Predicting Immunogenicity in silico*. Totowa, NJ: Humana Press (2007). p. 75–94.
  58. Vita R, Overton J, Greenbaum J, Ponomarenko J, Clark J, Cantrell J, et al. The immune epitope database (IEDB) 3.0. *Nucleic Acids Res* (2015) 43:D405–12. doi:10.1093/nar/gku938
  59. Golding B, Scott D, Scharf O, Huang L, Zaitseva M, Lapham C, et al. Immunity and protection against *Brucella abortus*. *Microbes Infect* (2001) 3:43–8. doi:10.1016/S1286-4579(00)01350-2

**Conflict of Interest Statement:** The authors declare that the research was conducted in the absence of any commercial or financial relationships that could be construed as a potential conflict of interest.

Copyright © 2017 Escalona, Sáez and Oñate. This is an open-access article distributed under the terms of the Creative Commons Attribution License (CC BY). The use, distribution or reproduction in other forums is permitted, provided the original author(s) or licensor are credited and that the original publication in this journal is cited, in accordance with accepted academic practice. No use, distribution or reproduction is permitted which does not comply with these terms.



# Immunogenic Domains and Secondary Structure of *Escherichia coli* Recombinant Secreted Protein *Escherichia coli*-Secreted Protein B

Bruna Alves Caetano<sup>1</sup>, Letícia Barboza Rocha<sup>1</sup>, Eneas Carvalho<sup>2†</sup>, Roxane Maria Fontes Piazza<sup>1\*</sup> and Daniela Luz<sup>1</sup>

## OPEN ACCESS

### Edited by:

Daniela Santoro Rosa,  
Federal University of  
São Paulo, Brazil

### Reviewed by:

Eric Cox,  
Ghent University, Belgium  
Jorge Blanco,  
Universidade de Santiago de  
Compostela, Spain  
Nora Lía Padola,  
National University of Central Buenos  
Aires, Argentina

### \*Correspondence:

Roxane Maria Fontes Piazza  
roxane@butantan.gov.br

### †Present address:

Eneas Carvalho,  
Laboratório de Bacteriologia,  
Instituto Butantan, São Paulo,  
São Paulo, Brazil

### Specialty section:

This article was submitted to  
Vaccines and Molecular  
Therapeutics,  
a section of the journal  
*Frontiers in Immunology*

Received: 11 October 2016

Accepted: 05 April 2017

Published: 24 April 2017

### Citation:

Caetano BA, Rocha LB, Carvalho E,  
Piazza RMF and Luz D (2017)  
Immunogenic Domains and  
Secondary Structure of *Escherichia coli*  
Recombinant Secreted Protein  
*Escherichia coli*-Secreted Protein B.  
*Front. Immunol.* 8:477.  
doi: 10.3389/fimmu.2017.00477

<sup>1</sup>Laboratório de Bacteriologia, Instituto Butantan, São Paulo, São Paulo, Brazil, <sup>2</sup>Centro de Biotecnologia, Instituto Butantan, São Paulo, São Paulo, Brazil

Several pathogenic bacteria are able to induce the attaching and effacing (A/E) lesion. The A/E lesion is caused by effector proteins, such as *Escherichia coli*-secreted protein B (EspB), responsible together with *Escherichia coli*-secreted protein D for forming a pore structure on the host cell, which allows the translocation of effector proteins. Different variants of this protein can be found in *E. coli* strains, and during natural infection or when this protein is injected, this leads to variant-specific production of antibodies, which may not be able to recognize other variants of this bacterial protein. Herein, we describe the production of a hybrid recombinant EspB toxin that comprises all known variants of this protein. This recombinant protein could be useful as an antigen for the production of antibodies with broad-range detection of EspB-bearing bacteria, or as an antigen that could be used in vaccine formulation to generate antibodies against different EspB variants, thereby increasing immunization potential. In addition, the recombinant protein allowed us to analyze its secondary structure, to propose the immunogenic regions of EspB variants, and also to characterize anti-EspB antibodies. Our results suggest that this hybrid protein or a protein composed of the conserved immunogenic regions could be used for a variety of clinical applications.

**Keywords:** *Escherichia coli*-secreted protein B, *Escherichia coli*, protein structure, peptide sequence, immunogenic domain

## INTRODUCTION

Gram-negative pathogenic bacteria, such as enteropathogenic *Escherichia coli* (EPEC), enterohemorrhagic *Escherichia coli* (EHEC), and *Citrobacter rodentium* are able to induce attaching and effacing (A/E) lesion (1–3). The A/E lesion is characterized by intimate intestinal epithelium adhesion, microvillus effacing, pedestal formation for effector protein translocation and the aggregation of actin and other cytoskeletal elements at the bacterial binding sites, caused by effector proteins, which are secreted into the enterocyte by a type III secretion system (T3SS) (4). The genes encoding the T3SS are located in pathogenicity islands and have many conserved structural components. The system structure consists of a syringe-like conformation, with a protein complex anchored on the bacterial membrane and a needle-shaped protein crossing the extracellular space to the host membrane, where a pore for the translocation of effector proteins is assembled (5, 6).

Enteropathogenic *Escherichia coli* and EHEC are the main bacterial agents associated with diarrhea among children under 5 years old, and both pathogens are able to induce the A/E lesion (7). Among the virulence factors comprising the T3SS of these bacteria are the secreted proteins (Esps). The Esp responsible for the syringe-like structure of T3SS is secreted protein A (EspA), which is the needle-shaped protein of approximately 25 kDa, while secreted proteins B [*Escherichia coli*-secreted protein B (EspB)] and D [*Escherichia coli*-secreted protein D (EspD)] are responsible for the pore structure assembled in the eukaryotic membrane (8).

*Escherichia coli*-secreted protein B is approximately 37 kDa in size and forms the pore assembled “needle tip” in the host cell membrane together with EspD. Also, EspB participates in phagocytosis evasion and binding to eukaryotic cell myosin, inhibition of actin interaction, and damage to the microvilli (9). There are three variants of EspB, i.e.,  $\alpha$ ,  $\beta$ , and  $\gamma$ , where the  $\alpha$  variant is subdivided into 1, 2, and 3. Allele frequency studies have shown  $\alpha$  EspB to be the most prevalent, followed by  $\beta$  EspB (5, 10–13). The EspB genetic sequence varies between all variants, as demonstrated by the necessity of different primer sets for DNA amplification in gene detection studies. However, there is no clear correlation between an EspB protein subtype and a specific serogroup of EPEC and EHEC (11–13).

Several studies have used EspB protein as an antigen for the recognition of EPEC and EHEC strains (14–17), but they employed an EspB obtained by *espB* gene amplification from specific EPEC strains—mainly the prototype (E2348/69; O127:H6). Thus, the antibodies generated are against the specific EspB variant present in these strains. Therefore, the detection coverage in these methods is limited by the variant strain, which may result in other variants not being effectively recognized, thereby reducing bacterial recognition.

Nevertheless, eliciting antibodies against bacterial colonization factors have been proposed as a vaccination strategy to prevent pathogenic *E. coli* infection (18). Antibodies against the T3SS proteins, such as EspA, EspB, and EspD, have been detected in the serum from patients with diarrheagenic *E. coli* infections, demonstrating their immunogenic potential (19–22). Previous studies have shown EspB as a target for vaccine formulations in the veterinary field, ranging from transferred maternal colostral antibodies and intramuscular immunization in cattle (18, 23), to oral and intranasal immunization in mice (24, 25). Vaccine development against enteric pathogens that are able to induce strong mucosal immune responses capable of preventing intestinal colonization are of great importance to protect humans and animals from pathologies (21, 23).

Herein, we synthetically constructed a hybrid recombinant EspB (rEspB), representative of all known variants to date, and characterized its secondary structure, which allowed us to propose an immunogenic domain.

## MATERIALS AND METHODS

### Bacterial Strains, Plasmid, and Supplies

The *E. coli* strains used were DH5 $\alpha$  [F $^{-}$   $\Phi$ 80lacZ $\Delta$ M15  $\Delta$ (*lacZYA-argF*) U169 *recA1 endA1 hsdR17* ( $r_k^-, m_k^+$ ) *phoA supE44 thi-1 gyrA96 relA1*  $\lambda^-$ ] and BL21 (DE3) [F $^{-}$  *ompT hsdS<sub>B</sub>* ( $r_B^-, m_B^-$ ) *gal*

*dcm* (DE3)] from Invitrogen (CA, USA). The plasmid used was pET28a(+) containing a 6-histidine tag (His-tag) at both the N- and C-terminal from Novagen (Darmstadt, Germany). T4 ligase and T4 buffer DNA ligase (2 $\times$ ) were purchased from Promega Corporation (WI, USA). The enzymes used (*Bam*H I and *Hind*III) and the induction agent isopropyl  $\beta$ -D-1-thiogalactopyranoside (IPTG) were obtained from Thermo Scientific (MA, USA). The monoclonal anti-polyHistidine antibody produced in mouse, anti-mouse IgG (whole molecule) peroxidase antibody and 3'3'-diaminobenzidine (DAB) were purchased from Sigma-Aldrich (MO, USA). Luria-Bertani (LB) medium was from BD (NJ, USA), and kanamycin from Gibco (MA, USA).

### Synthetic Gene Design

The EspB synthetic gene was developed considering common regions of all known EspB variants to date, by alignment of  $\alpha$ 1,  $\alpha$ 2,  $\alpha$ 3,  $\beta$ , and  $\gamma$  EspB sequences (GenBank number: AAC38396.1, AEW69664.1, AEW69663.1, CAA74174.1, and CAA65654.1) using the Basic Local Alignment Search Tool (BLAST). The synthetic gene for the hybrid rEspB protein was assembled on the basis of the most prevalent amino acids among the variants for each position of the protein sequence (Figure 1). The restriction enzymes were selected with the support program BioEdit version 7.2.0, and the restriction sites for the enzymes *Bam*H I and *Hind*III were inserted into the conserved sequence upstream and downstream, respectively (Figure S1 in Supplementary Material), while no stop codon was added in the sequence. The predicted recombinant protein had a molecular weight of 24.6 kDa. The EspB gene was manufactured by GenScript (NJ, USA) and cloned into pUC57 vector.

### Cloning

Chemically competent *E. coli* BL21 (DE3) were obtained using the Chung and Miller protocol, with modifications (26). The gene of interest was excised from pUC57 by restriction enzyme digestion and then cloned into the pET28a expression vector. The reaction mixture consisting of 2  $\mu$ L of deionized water, 5  $\mu$ L of the gene, 1  $\mu$ L of the pET28a vector, 1  $\mu$ L of T4 DNA ligase (3 IU), and 2  $\mu$ L of T4 buffer DNA ligase (2 $\times$ ) was incubated at 24°C for 1 h, followed by a 4°C incubation for 18 h.

For *E. coli* BL21 (DE3) transformation, 1  $\mu$ L of plasmid was incubated with 2  $\mu$ L of 5 $\times$  KCM buffer (0.5 M KCl, 0.15 M CaCl<sub>2</sub>, and 0.25 M MgCl<sub>2</sub>) and 7  $\mu$ L of deionized water on ice for 5 min, followed by the addition of 10  $\mu$ L of chemically competent cells; after 20 min, the solution was transferred to 24°C for 10 min. Subsequently, 200  $\mu$ L of LB culture medium were added and the sample was incubated at 37°C for 1 h. The cells were then streaked on a LB agar plate containing 50  $\mu$ g/mL of kanamycin and incubated at 37°C for 18 h.

### Expression and Purification

BL21 His-EspB transformant was cultivated in 10 mL of LB medium containing 50  $\mu$ g/mL kanamycin at 37°C for 18 h with stirring at 250 rpm. The culture was then added to 500 mL of LB medium supplemented with 0.2% glucose and 50  $\mu$ g/mL of kanamycin, and further grown at 37°C for 2 h at 250 rpm. After reaching an optical density of 0.6–0.8 (OD<sub>600</sub>), IPTG was added to

alpha 1	AVFESQNKAIDEKKAGATAALIGGAISSVLGILGSFAAINSATKGASDVAQQRAASTSAKSI
alpha 2	AVFESQNKAIDEKKAGATAALIGGAISSVLGILGSFAAINSATKGASDAVQQRAASTSAKSI
alpha 3	AVFESQNKAISEKKAGATAALIGGAISSVLGILGSFAAINSATKGASDAVQQRAASTSARSI
beta	AVFESQNKAIDEKKAATAALVGGAISSVLGILGSFAAINSATKGASDIAQKTASTSSKAI
gamma	AVFESQNKAIEEKKAATAALVGIISSALGILGSFAAMNNAAKGAGEIAEKASSASSKAA
rEspB	AVFESQNKAIDEKKAGATAALIGGAISSVLGILGSFAAINSATKGASDIAQQRRAASTSAKSI
alpha 1	GTVSEASTKALAKASEGIADAADDAAGAMQQTIAATAAKAASRTSGITDDVATSAQKASQVA
alpha 2	GTASEASTKVLAKASESIADAADDAAS-MQQTIAAAAAsRTSGVTDDVAASAQKASQVA
alpha 3	STASEASTKALAKASESIADAADDAAS-VQQTIAAAAAsRTSGVTDDVAASAQKASQVA
beta	DAASDTATKTLTAKATESVADAVE DASSVMQQMTTATRAGSRTSDVADDIADSAQRASQLA
gamma	GAASEVANKALVKATESVADVAEEASSAMQKAMATTKAASRASGVADEVA---KATDFA
rEspB	GTASEASTKVLAKASESIADAADDAASAMQQTIAATAAKAASRTSGVTDDVAASAQKASQVA
alpha 1	EEAADAAQELAQKAGLLSRPTAAAGRISGSTPFIVVTSLAEGTKTLPTTISESVKSNHDIN
alpha 2	EEAADAAQELAEKAGLLSRPTAAAGRISGSTSFIVVTSLAEGTKTLPTTISESVKSNHDIN
alpha 3	EEAAGAAQELAEKAGLLSRPTAAAGRISGSTSFIVVTSLAEGTKTLPTTISESVKSNHDIS
beta	ENAAADA---AQKASRASRFMADVDRITGSPFIAVTSLAEGTKTLPTVSESVKSNHEIS
gamma	EDLADA---AEKTSRINKLLNSVDKLTNTTAFVAVTSLAEGTKTLPTTISESVRSTHEVN
rEspB	EEAADAAQELAEKAGLLSRPTAAAGRISGSTPFIVVTSLAEGTKTLPTTISESVKSNHDIN
alpha 1	EQRAKSVENLQASNLDTYKQDVVRRAQDDISSRLRDMLTTARDLTDLINRMGQAARLAG
alpha 2	EQRAKSLENLQTSNLENYKQDVVRRAQDDISSRLRDMLTTARDLTDLINRMGQAARLAG
alpha 3	EQRAKSVENLQASNLENYKQDVVRTQDDISSRLRDMLTTARDLTDLINRLQGSARLAG
beta	EQRYSKVENPQQGNLDLYKQEVRRAQDDIASRLRDMLTAARDLTDLQNRMGQSVRLAG
gamma	EQRAKSLENPQQGNLELYKQDVVRTQDDITTRLRDITSAVRDLLEVQNRMGQSRLAG
rEspB	EQRAKSVENLQQSNLENYKQDVVRRAQDDISSRLRDMLTTARDLTDLINRMGQASRLAG

**FIGURE 1 | Recombinant *Escherichia coli*-secreted protein B (rEspB) conserved domain.** Alignment of all EspB variants known to date. Shown in black are the conserved regions and in colors the divergent amino acids along the whole protein sequence, in which we used the most prevalent amino acids among the variants.

a final concentration of 1 mM, and the culture was then incubated at 37°C for 4 h at 250 rpm. The cells were separated in a 5804 R centrifuge (Eppendorf, Hamburg, Germany) at 10,000 × g for 10 min, and the supernatant discarded. The pellet was resuspended in 60 mL of ligation buffer (20 mM Tris-HCl, pH 7.9, containing 0.5 M NaCl) with 1% 100× protease inhibitor cocktail and 50 µg/mL lysozyme, and allowed to stand in an ice bath for 30 min. The cells were lysed by three cycles of sonication for 10 min, with the amplitude set at 30% (Sonopuls Bandelin, Berlin, Germany). The lysate was centrifuged at 10,000 × g for 10 min and the resulting pellet was solubilized with 30 mL of buffer with 8 M urea, with stirring at 4°C for 18 h.

Purification was performed by metal affinity chromatography by gravity flow. Following urea treatment, 2 mL of Ni-NTA Agarose (Qiagen, NW, Germany) were added to the solubilized pellet and the suspension incubated at 4°C for 18 h with gentle shaking. The suspension was centrifuged at 30 × g for 1 min and pellet-containing agarose was gently transferred to a polypropylene column (Qiagen, NW, Germany). rEspB protein was eluted with buffer containing different concentrations of imidazole: 10, 20, 50, 100, 150, 200, 300, 400, and 500 mM. The eluted protein was refolded by long-term dialysis and subsequently

concentrated by osmosis with PEG 4000. SDS-PAGE (12%) and immunoblotting were used to confirm the purification. The recombinant protein was quantified with a NanoDrop Lite Spectrophotometer (Thermo Scientific, MA, USA) and stored at 4°C. Identification of rEspB protein was performed by liquid chromatography coupled to mass spectrometry (LC-MS/MS). After SDS-PAGE analysis, protein bands were subjected to *in gel* trypsin digestion (27) and the resulting peptide mixture was analyzed by LC-MS/MS as described elsewhere (28). LTQ-Orbitrap Velos raw data were searched against a target database (UniProt restricted to *E. coli*; 22,940 sequences) using Mascot search engine (Matrix Science, UK).

## Structure Analysis

Protein secondary structure was confirmed after refolding by circular dichroism (CD). The CD spectra were recorded between 190 and 260 nm using a quartz cuvette (0.1-mm path length) in a JASCO J-810 Spectropolarimeter (Jasco Corporation, Japan). After buffer-background subtraction (10 mM sodium phosphate buffer, pH 8.0), the CD data were converted to mean residue ellipticity [θ] units (degree × cm<sup>2</sup> dmol<sup>-1</sup>). CD spectra were obtained at three different pH (7.0, 8.0, and 9.0) and at temperatures ranging

from 5 to 95°C. The results were analyzed on the online server DICHROWEB (29–31), using the analysis program CDSSTR (32–34).

## Epitope Mapping

Antibody-binding epitopes were determined by designing a CelluSpots® peptide array (INTAVIS Bioanalytical Instruments AG, NW, Germany), with 384 dots containing the full protein sequence divided in peptides with 11 amino acids/dots, having 8 overlapping amino acids. The sequences in the array were derived from the rEspB protein, which represents the  $\alpha$  variants, as well as the full  $\beta$  and  $\gamma$  sequences (Table S1 in Supplementary Material) (5, 10, 11, 13). The assay was performed following the manufacturer's recommendations: briefly, the slides were blocked by immersion in 1% BSA at 4°C for 18 h with shaking. Anti-EspB monoclonal antibody (mAb) (10  $\mu$ g/mL) and polyclonal antibody (pAb) (30  $\mu$ g/mL) were incubated at 24°C for 4 h with stirring. The slides were washed three times with 0.05% Tween in PBS (0.01 M, pH 7.2) for 5 min. The slides were then incubated with peroxidase-conjugated anti-mouse IgG antibody (1:5,000) at 24°C for 2 h with stirring. Detection was performed with DAB and hydrogen peroxide and the reaction stopped with distilled water.

## Antibodies

Polyclonal serum was obtained from a New Zealand White female rabbit (60 days old) after immunizing intramuscularly, three times with 2-week intervals, using a dose of 100  $\mu$ g of rEspB protein adsorbed to 2.5 mg alum ( $\text{Al}^{3+}$ ) as adjuvant. Serum was obtained 45 days after the first immunization. Immune serum reactivity was tested by indirect ELISA (35). Serum samples were obtained just before immunization from the auricular vein, which were used as the negative control in specific antibody evaluation. The anti-EspB mAb A5 was raised in the present study as in previous work by our group where mAb 4D9 was obtained (17).

## RESULTS

### rEspB Protein

The hybrid rEspB protein was obtained from the *E. coli* BL21 transformed with a plasmid harboring the hybrid *espB* gene. Restriction analysis confirmed that all clones had the same plasmid profile, and synthetic gene cloning was confirmed by sequencing. The protein was expressed in inclusion bodies; thus,

urea treatment was necessary before the purification process. Since there was no stop codon in the cloned gene and since pET28a was the expression vector, the recombinant protein was expressed with two His-tag tails, one at each end of it. The protein was eluted using different imidazole concentrations, with effective elution occurring between 100 and 200 mM imidazole (Figure 2).

### EspB Protein Characterization

To confirm the identity of rEspB, protein bands indicated in Figure 2A were subjected to mass spectrometric analysis, which resulted in the identification of nine tryptic peptides (<sup>95</sup>AGATAALIGGAISVVLGILGSFAAINSATK<sup>124</sup>, <sup>216</sup>AGLLSR<sup>221</sup>, <sup>222</sup>FTAAAGR<sup>228</sup>, <sup>229</sup>ISGSTPFIVVTSLAEGTK<sup>246</sup>, <sup>247</sup>TLPTTISE-SVK<sup>257</sup>, <sup>258</sup>SNHDINEQR<sup>266</sup>, <sup>288</sup>AQDDISSR<sup>295</sup>, <sup>298</sup>DMTTTAR<sup>304</sup>, and <sup>305</sup>DLTDLINR<sup>312</sup>), confirming the expression and isolation of protein EaeB (UniProt entry EAEB\_ECO27).

### Secondary Structure Prediction under Different Conditions

The EspB CD spectra showed a negative ellipticity band at 222 nm, which corresponds to  $\alpha$ -helix structure (36). This secondary structure was observed at all pH tested; however, ellipticity was closer to 0 at pH 7.0, indicating less  $\alpha$ -helix content under this condition when compared to pH 8.0 and 9.0. Indeed, deconvolution analysis showed a higher level of unordered content at pH 7.0 and, on the other hand, an increase in  $\alpha$ -helix content at pH 8.0 and 9.0 (Figure 3; Table S2 in Supplementary Material). Effects on protein secondary structures were observed at a higher temperature, indicating protein denaturation by heat (Figure 4; Table S3 in Supplementary Material).

Treatment with temperatures over 60°C resulted in altered secondary structure stability, showing this to be the necessary temperature to denature the rEspB protein. There was a slight reversible loss of secondary structure after heating to 95°C and gradual cooling to 5°C. Close to the storage temperature, at 5°C, EspB protein secondary structure exhibited approximately 18%  $\alpha$ -helix, 20%  $\beta$ -sheet and 20% turns, and 42% irregular structures. As the temperature increased, the proportion of turns and irregular structures tended to be the same, while the  $\alpha$ -helix content decreased and  $\beta$ -sheet content increased. Above 60°C, there were no more alterations in secondary structure, with  $\alpha$ -helix around 5% and  $\beta$ -sheet 31%.

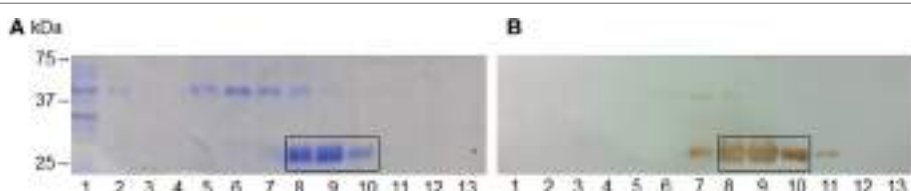


**FIGURE 2 |** *Escherichia coli*-secreted protein B (EspB) protein SDS-PAGE and immunoblotting purification profile. **(A)** 12% SDS-PAGE; **(B)** immunoblotting; (1) flow through; (2–4) wash with 20 mM Tris-HCl, pH 7.9, containing 0.5 M NaCl; (5–13) elution fractions with increasing imidazole concentration, respectively, 10, 20, 50, 100, 150, 200, 250, 300, and 400 mM. The steps where EspB was effectively eluted are highlighted.

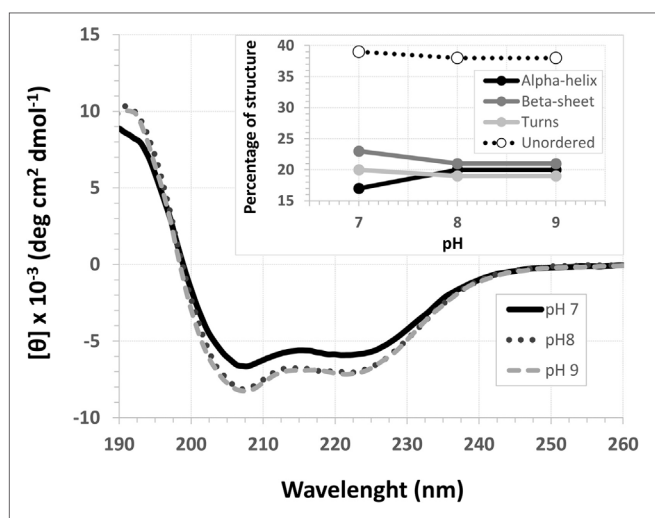


**FIGURE 3 |** pH circular dichroism spectra profile of *Escherichia coli*-secreted protein B (EspB) protein. EspB profile at pH 7.0, 8.0 and 9.0, showing maintenance of structure at pH 8.0 and 9.0. Inset shows the percentage of secondary structure for each pH tested.

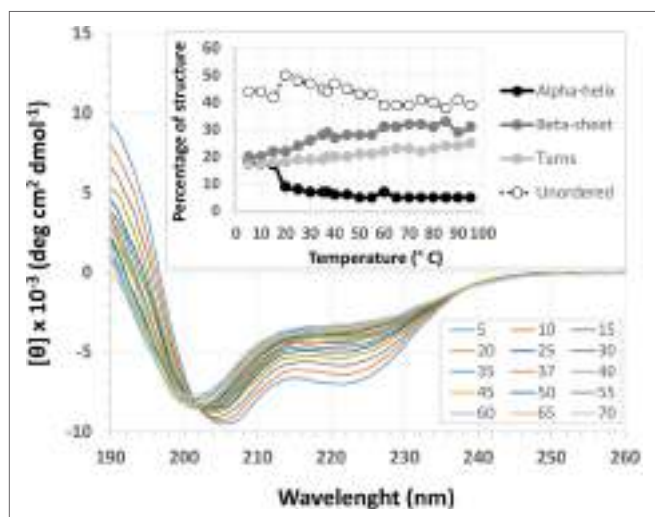


**FIGURE 4 |** Temperature circular dichroism spectra of *Escherichia coli*-secreted protein B (EspB) protein. Secondary structure of EspB at different temperatures ranging from 5 to 95°C, showing the loss of structure when approaching 0 mean residue ellipticity  $[\theta]$ . Inset shows the variation in the percentage of secondary structure for each temperature tested.

## Antibody-Binding Epitopes and Probable Immunogenic Domain of EspB

The anti-EspB pAb generated against the hybrid rEspB was able to recognize several dots on the peptide array, suggesting that those epitopes are involved in antibody binding. The pAb reacted with 11 points on  $\alpha$  EspB, 4 on  $\beta$  EspB, and 5 on  $\gamma$  EspB (Table 1). Several spots were adjacent to each other, which resulted in three sequences for the  $\alpha$  variant (<sup>198</sup>ASQVAEEAAD<sup>208</sup>, <sup>231</sup>GSTPFIVVTSLAEG<sup>244</sup>, and <sup>264</sup>EQRAKSVENLQASNLDTYKQDVRRQAQDDISSR<sup>295</sup>)

**TABLE 1 |** Binding epitopes of individual antibodies recognized by peptide array.

<i>Escherichia coli</i> -secreted protein B (EspB) variant	Polyclonal antibody (pAb)	Monoclonal antibody (mAb) 4D9	mAb A5
$\alpha$ EspB	ASQVAEEAAD VAEEAADAQAE GSTPFIVVTS PFIVVTSLAEG DINEQRAKSVE EQRAKSVENLQ VENLQQSNLEN LQQSNLENYKQ SNLENYKQDVR KQDVRRQAQDDI VRRAQDDISSR	DAAQELAEKAG ARDLTDLINRM	AVFESQNKAID EAADAAQELAE DAAQELAECAG ARDLTDLINRM LTDLINRMGQA
$\beta$ EspB	TPFIAVTSLAE NFQQGNLDLYK QGNLDLYKQEV EVRAQDDIAS	KGASDIAQKTA MTTAARDLTL AARDLTDLQNR	AITASAINTSSL GKMRVILQDYQ VRILQDYQQQQ LQDYQQQQQLSQ QLAVFESQNKA AARDLTDLQNR
$\gamma$ EspB	TTAVFAVTSLA FVAVTSLAEGT ENFQQGNLELY LYKQDVRRTQD QDVRRTQDDIT	AAGAASEVANK AASEVANKALV	AAGAASEVANK

and the same two sequences for the  $\beta$  and  $\gamma$  variants (<sup>232</sup>STPFIVVTSLAEGT<sup>245</sup> and <sup>271</sup>ENLQASNLDTYKQDVRRQAQDDISS<sup>294</sup>). The common domain between all sequences could be defined as <sup>232</sup>STPFIVVTSLAEG<sup>244</sup> and <sup>271</sup>ENLQASNLDTYKQDVRRQAQDDISS<sup>294</sup>.

The mAbs 4D9 and A5 were used for comparison with the pAb, since they were obtained against the  $\alpha$  EspB variant. Individually, mAb 4D9 reacted with 2 points on  $\alpha$  EspB, 3 on  $\beta$  EspB, and 2 on  $\gamma$  EspB, and mAb A5 reacted with 5 points on  $\alpha$  EspB, 6 on  $\beta$  EspB, and 1 on  $\gamma$  EspB (Table 1). The common region between the mAbs was two dots on  $\alpha$  EspB (<sup>127</sup>DAAQELAEKAG<sup>137</sup> and <sup>223</sup>ARDLTDLINRM<sup>233</sup>), one dot on  $\beta$  EspB (<sup>295</sup>AARDLTDLQNR<sup>305</sup>), and one dot on  $\gamma$  EspB (<sup>139</sup>AAGAASEVANK<sup>149</sup>) (Figure S2 in Supplementary Material).

Another BLAST alignment of the two major sequences recognized by the pAb was performed against non-redundant protein sequences (nr) within bacteria (taxid:2) to evaluate if the sequences actually correlated with EspB and had 100% identity to the enterobacterial EspB protein from *E. coli* (data not shown).

## DISCUSSION

*Escherichia coli*-secreted protein B protein is translocated into the host cell through a T3SS and together with EspD is responsible for assembling a multimeric pore in the eukaryotic membrane, contributing to the hallmarks of the A/E lesion. Due to this characteristic, EspB has a major importance in bacterial virulence and its detection can be used as a diagnostic tool for diarrheagenic *E.*

*coli* infections. However, the allele diversity of EspB in immune response leads to specific antibodies that may not be able to recognize different variant bacterial strains.

Considering that EspB can be found in EPEC and EHEC, both related to severe diarrhea cases in human, its diagnosis and prevention are of great value for public health. Besides, since cattle are a natural reservoir of EHEC and a source for human infection, veterinary diagnosis and prevention are of major importance as well (37, 38). Vaccine strategies to prevent EPEC and EHEC infections employing EspB as an antigen have been proposed in mice and cattle, contemplating the veterinary field (18, 23–25). We obtained a hyperimmune serum from rabbits recognizing EspB, demonstrating the protein antigenic ability. Furthermore, it is known that in cases of infection, antibodies against EspB can be found in human serum (19–21), thus making EspB a target protein for the development of diagnostic tests and vaccine formulations.

In addition, EPEC and EHEC EspB protein showed less than 50% identity when compared to the homologs from *Salmonella enterica*, *Yersinia enterocolitica*, and *Pseudomonas aeruginosa*, suggesting that a diagnostic test for EspB can be specific for EPEC and EHEC. Based on EspB detection, previous studies proposed diagnostic methods for human infection by EPEC and EHEC, such as an immunochromatographic test (16) and latex agglutination test (15, 17), while ELISA was proposed for herd diagnosis (37). All of those methods rely on antibody recognition ability, and they used heterologous EspB protein obtained from the *espB* gene amplified from specific strains, which can result in ineffective antigen recognition, since other EspB variants may not be effectively recognized by the antibody. It is worth mentioning that mAb 4D9, described by our group, reacted with 2 points on  $\alpha$  EspB, 3 on  $\beta$  EspB, and 2 on  $\gamma$  EspB, thus supporting our previous results, which were 97% sensitivity, 98% specificity, and 97% efficiency for a rapid agglutination latex test. All EspB variants were detected by the mAb in the peptide array assay; however, when used for strain recognition, the mAb did not recognize the different variants (17). One hypothesis is that in the peptide array the epitopes are linearized; thus, the antibody identifies small parts of an epitope that is recognized when the protein presents quaternary structure.

Therefore, the use of an EspB protein that comprises and represents all known variants as an antigen and for antibody development continues to be necessary. Thus, herein, a hybrid recombinant protein EspB was developed and characterized in terms of secondary structure, thermostability, and immunogenic region.

For that purpose, a rEspB protein comprising all known variants was designed and expressed. The His-tag tails did not affect secondary structure. The percentage of unordered structures decreased as pH increased from 7.0 to 8.0 and then remained stable when pH increased from 8.0 to 9.0. This finding suggests that the secondary structure of EspB has greater proportions of  $\alpha$ -helix and  $\beta$ -sheet and turns at pH 8.0 and 9.0 when compared to pH 7.0 (Figure 3; Table S2 in Supplementary Material). Moreover, our data suggest that this increase in the percentage of ordered secondary structures was due to an increase in  $\alpha$ -helix content; on the other hand, the percentage of  $\beta$ -sheets and turns was slightly

reduced when pH increased. This increase in the proportion of ordered secondary structures at pH 8.0 and 9.0 may produce a change in the biological activity (in efficacy or even specificity) of this protein at this basic pH. EspB is mostly composed of irregular structures, followed by almost equal proportions of  $\alpha$ -helix and  $\beta$ -sheet and turns. In regard to temperature stability, the  $\alpha$ -helix content tended to decrease with temperature increase, while the  $\beta$ -sheet proportion increased with temperature (Figure 4; Table S3 in Supplementary Material). Either way, at temperatures above 60°C, the change in secondary structure halts, leading us to believe that, in this range, EspB is heat denatured, showing a heat-sensitivity characteristic.

Furthermore, the epitope mapping assay analyses allowed not only the characterization of antibody/epitope binding described here but also the proposal of an EspB immunogenic consensus domain. pAb is generated by humoral immune response, and their recognizing domain shows the EspB protein sites capable of activating the immune system. We identified two common epitopes between all known EspB subtypes (<sup>232</sup>STPFIVVTS LAEG<sup>244</sup> and <sup>271</sup>ENLQASNLD TYKQDV RRAQDDISS<sup>294</sup>). The peptides were aligned with the EspB protein of the prototype EPEC strain E2348/69 and showed 100% identity with two regions at the C-terminus, indicating the antibody molecule binding site to EspB. These regions were also present among the binding sites of all antibodies tested, even the mAb obtained against only  $\alpha$  EspB, indicating that they are, indeed, conserved immunogenic domains for this protein.

This recombinant protein can be used in clinical applications, such as antigen for antibody production, enabling not only the diagnosis of A/E-producing pathogens by EspB protein recognition but also as an alternative therapy for the disease by eliciting neutralizing antibodies against different EspB variants. Moreover, rEspB itself can serve as an antigen in a vaccine formulation to generate host antibodies able to prevent disease occurrence. In conclusion, we developed and obtained a hybrid rEspB protein capable of inducing antibody response against all known EspB subtypes, which can be a promising tool to be used as antigen for antibody development for the diagnosis and prevention of A/E lesion-producing pathogens.

## ETHICS STATEMENT

The experiments were conducted in agreement with the Ethical Principles in Animal Research, adopted by the Brazilian College of Animal Experimentation, and they were approved by the Ethical Committee for Animal Research of Butantan Institute (5492021015).

## AUTHOR CONTRIBUTIONS

RP conceived and designed the experiments, analyzed the data, contributed reagents/materials/analysis tools, and wrote the paper. BC conceived and designed the experiments, performed the experiments, analyzed the data, and wrote the paper. LR and DL conceived and designed the experiments, analyzed the data, and wrote the paper. EC performed the experiments, analyzed the data, and wrote the paper.

## ACKNOWLEDGMENTS

The authors thank Dr. Solange M. T. Serrano (Laboratório Especial de Toxinologia Aplicada, Instituto Butantan, São Paulo, Brazil) for support in the identification of rEspB by mass spectrometry and Dr. Waldir P. Elias (Laboratório de Bacteriologia, Instituto Butantan, São Paulo, Brazil) for helpful discussions and suggestions. This work was supported by grants from São Paulo Research Foundation (FAPESP 2011/12928-2; 2013/06589-6) and from Conselho Nacional de Desenvolvimento Científico e Tecnológico (CNPq) awarded to RP. BC was a recipient of Coordenação de Aperfeiçoamento de Pessoal de Nível Superior (CAPES) fellowship (AUXPE/PROAP - 1364/2013). DL is a PNPD/CAPES postdoctoral fellow (PNPD20132071). LR was a FAPESP postdoctoral fellow (2012/090906-2). Dr. A. Leyva helped with English editing of the manuscript.

## REFERENCES

- Moon HW, Whipp SC, Argenzio RA, Levine MM, Giannella RA. Attaching and effacing activities of rabbit and human enteropathogenic *Escherichia coli* in pig and rabbit intestines. *Infect Immun* (1983) 41:1340–51.
- Knutton S, Baldwin T, Williams PH, McNeish AS. Actin accumulation at sites of bacterial adhesion to tissue culture cells: basis of a new diagnostic test for enteropathogenic and enterohemorrhagic *Escherichia coli*. *Infect Immun* (1989) 57:1290–8.
- Gaytán MO, Martínez-Santos VI, Soto E, González-Pedrajo B. Type three secretion system in attaching and effacing pathogens. *Front Cell Infect Microbiol* (2016) 21(6):129. doi:10.3389/fcimb.2016.00129
- Knutton S, Lloyd DR, Mcneish AS. Adhesion of enteropathogenic *Escherichia coli* to human intestinal enterocytes and cultured human intestinal mucosa. *Infect Immun* (1987) 55(1):69–77.
- Elliott SJ, Wainwright LA, Mcdaniel TK, Jarvis KG, Deng YK, Lai LC, et al. The complete sequence of the locus of enterocyte effacement (LEE) from enteropathogenic *Escherichia coli* E2348/69. *Mol Microbiol* (1998) 28(1):1–4. doi:10.1046/j.1365-2958.1998.00783.x
- Costa TR, Felisberto-Rodrigues C, Meir A, Prevost MS, Redzej A, Trokter M, et al. Secretion systems in Gram-negative bacteria: structural and mechanistic insights. *Nat Rev Microbiol* (2015) 13(6):343–59. doi:10.1038/nrmicro3456
- Lanata CF, Fischer-Walker CL, Olascoaga AC, Torres CX, Aryee MJ, Black RE. Global causes of diarrheal disease mortality in children <5 years of age: a systematic review. *PLoS One* (2013) 8(9):e72788. doi:10.1371/journal.pone.0072788
- Garmendia J, Frankel G, Crepin VF. Enteropathogenic and enterohemorrhagic *Escherichia coli* infections: translocation, translocation, translocation. *Infect Immun* (2005) 73(5):2573–85. doi:10.1128/IAI.73.5.2573-2585.2005
- Loadt PB, Kaper JB. Post-transcriptional processing of the LEE4 operon in enterohaemorrhagic *Escherichia coli*. *Mol Microbiol* (2009) 71(2):273–90. doi:10.1111/j.1365-2958.2008.06530.x
- Ebel F, Deibel C, Kresse AU, Guzmán CA, Chakraborty T. Temperature- and medium-dependent secretion of proteins by Shiga toxin-producing *Escherichia coli*. *Infect Immun* (1996) 64(11):4472–9.
- Mairena EC, Neves BC, Trabulsi LR, Elias WP. Detection of LEE 4 region-encoded genes from different enteropathogenic and enterohemorrhagic *Escherichia coli* serotypes. *Curr Microbiol* (2004) 48(6):412–8. doi:10.1007/s00284-003-4164-8
- Garrido P, Blanco M, Moreno-Paz M, Briones C, Dahbi G, Blanco J, et al. STEC-EPEC oligonucleotide microarray: a new tool for typing genetic variants of the LEE pathogenicity island of human and animal Shiga toxin-producing *Escherichia coli* (STEC) and enteropathogenic E-coli (EPEC) strains. *Clin Chem* (2006) 52(2):192–201. doi:10.1373/clinchem.2005.059766
- Contreras CA, Ochoa TJ, Ruiz J, Lacher DW, Durand D, Debroy C, et al. Genetic diversity of locus of enterocyte effacement genes of enteropathogenic *Escherichia coli* isolated from Peruvian children. *J Med Microbiol* (2012) 61 (Pt 8):1114–20. doi:10.1099/jmm.0.045443-0

## SUPPLEMENTARY MATERIAL

The Supplementary Material for this article can be found online at <http://journal.frontiersin.org/article/10.3389/fimmu.2017.00477/full#supplementary-material>.

### FIGURE S1 | Sequence coding for *Escherichia coli*-secreted protein B (EspB) protein.

The sequence has 245 amino acids, and 241 encoding for EspB protein. The underlined sequences represent the cleavage sites of the restriction enzymes *Bam*H I, upstream, and *Hind* III, downstream.

### FIGURE S2 | Antibodies binding epitope by peptide array.

The dots indicate the linear sequence of 11 peptides that the monoclonal antibody (mAb) 4D9, mAb A5, and polyclonal antibody (pAb) bind, respectively. From top to bottom, the array was designed containing the recombinant *Escherichia coli*-secreted protein B (rEspB) sequence, which represents the  $\alpha$  variants and  $\beta$  and  $\gamma$  sequences, highlighted in bars. The two sides of the slide are duplicate of the sequence.

- Frankel G, Phillips AD, Novakova M, Field H, Candy DC, Schauer DB, et al. Intimin from enteropathogenic *Escherichia coli* restores murine virulence to a *Citrobacter rodentium* eaeA mutant: induction of an immunoglobulin A response to intimin and EspB. *Infect Immun* (1996) 64(12):5315–25.
- Lu Y, Toma C, Honma Y, Iwanaga M. Detection of EspB using reversed passive latex agglutination: application to determination of enteropathogenic *Escherichia coli*. *Diagn Microbiol Infect Dis* (2002) 43(1):7–12. doi:10.1016/S0732-8893(02)00363-2
- Nakasone N, Toma C, Lu Y, Iwanaga M. Development of a rapid immuno-chromatographic test to identify enteropathogenic and enterohemorrhagic *Escherichia coli* by detecting EspB. *PLoS Negl Trop Dis* (2014) 8(9):e3150. doi:10.1371/journal.pntd.0003150
- Rocha LB, Santos AR, Munhoz DD, Cardoso LT, Luz DE, Andrade FB, et al. Development of a rapid agglutination latex test for diagnosis of enteropathogenic and enterohemorrhagic *Escherichia coli* infection in developing world: defining the biomarker, antibody and method. *PLoS Negl Trop Dis* (2014) 8(9):e3150. doi:10.1371/journal.pntd.0003150
- Rabinovitz BC, Vilte DA, Larzábal M, Abdala A, Galarza R, Zotta E, et al. Physiopathological effects of *Escherichia coli* O157:H7 inoculation in weaned calves fed with colostrum containing antibodies to EspB and intimin. *Vaccine* (2014) 32:3823–9. doi:10.1016/j.vaccine.2014.04.073
- Martinez MB, Taddei CR, Ruiz-Tagle A, Trabulsi LR, Girón JA. Antibody response of children with enteropathogenic *Escherichia coli* infection to the bundle-forming pilus and locus of enterocyte effacement-encoded virulence determinants. *J Infect Dis* (1999) 179(1):269–74. doi:10.1086/314549
- Loureiro I, Frankel G, Adu-Bobie J, Dougan G, Trabulsi LR, Carneiro-Sampaio MM. Human colostrum contains IgA antibodies reactive to enteropathogenic *Escherichia coli* virulence-associated proteins: intimin, BfpA, EspA, and EspB. *J Pediatr Gastroenterol Nutr* (1998) 27(2):166–71. doi:10.1097/00005176-199808000-00007
- Guirro M, de Souza RL, Piazza RM, Guth BE. Antibodies to intimin and *Escherichia coli*-secreted proteins EspA and EspB in sera of Brazilian children with hemolytic uremic syndrome and healthy controls. *Vet Immunol Immunopathol* (2013) 152(1–2):121–5. doi:10.1016/j.vetimm.2012.09.016
- Asper DJ, Karmali MA, Townsend H, Rogan D, Potter AA. Serological response of Shiga toxin-producing *Escherichia coli* type III secreted proteins in sera from vaccinated rabbits, naturally infected cattle, and humans. *Clin Vaccine Immunol* (2011) 18:1052–7. doi:10.1128/CVI.00068-11
- Vilte DA, Larzábal M, Garbaccio S, Gammella M, Rabinovitz BC, Elizondo AM, et al. Reduced faecal shedding of *Escherichia coli* O157:H7 in cattle following systemic vaccination with gamma-intimin C280 and EspB proteins. *Vaccine* (2011) 29:3962–8. doi:10.1016/j.vaccine.2011.03.079
- Ahmed B, Loos M, Vanrompay D, Cox E. Oral immunization with *Lactococcus lactis*-expressing EspB induces protective immune responses against *Escherichia coli* O157:H7 in a murine model of colonization. *Vaccine* (2014) 32(31):3909–16. doi:10.1016/j.vaccine.2014.05.054
- Rabinovitz BC, Larzábal M, Vilte DA, Cataldi A, Mercado EC. The intranasal vaccination of pregnant dams with intimin and EspB confers protection in

- neonatal mice from *Escherichia coli* (EHEC) O157:H7 infection. *Vaccine* (2016) 34(25):2793–7. doi:10.1016/j.vaccine.2016.04.056
26. Chung CT, Miller RH. A rapid and convenient method for the preparation and storage of competent bacterial cells. *Nucleic Acids Res* (1988) 16(8):3580. doi:10.1093/nar/16.8.3580
27. Hanna SL, Sherman NE, Kinter MT, Goldberg JB. Comparison of proteins expressed by *Pseudomonas aeruginosa* strains representing initial and chronic isolates from a cystic fibrosis patient: an analysis by 2-D gel electrophoresis and capillary column liquid chromatography-tandem mass spectrometry. *Microbiology* (2000) 146(Pt 10):2495–508. doi:10.1099/00221287-146-10-2495
28. Zelanis A, Tashima AK, Rocha MM, Furtado MF, Camargo AC, Ho PL, et al. Analysis of the ontogenetic variation in the venom proteome/peptidome of *Bothrops jararaca* reveals different strategies to deal with prey. *J Proteome Res* (2010) 9(5):2278–91. doi:10.1021/pr901027r
29. Whitmore L, Wallace BA. Protein secondary structure analyses from circular dichroism spectroscopy: methods and reference databases. *Biopolymers* (2008) 89(5):392–400. doi:10.1002/bip.20853
30. Whitmore L, Wallace BA. DICHROWEB: an online server for protein secondary structure analyses from circular dichroism spectroscopic data. *Nucleic Acids Res* (2004) 32:W668–73. doi:10.1093/nar/gkh371
31. Lobley A, Whitmore L, Wallace BA. DICHROWEB: an interactive website for the analysis of protein secondary structure from circular dichroism spectra. *Bioinformatics* (2002) 18:211–2. doi:10.1093/bioinformatics/18.1.211
32. Compton LA, Johnson WC Jr. Analysis of protein circular dichroism spectra for secondary structure using a simple matrix multiplication. *Anal Biochem* (1986) 155(1):155–67. doi:10.1016/0003-2697(86)90241-1
33. Manavalan P, Johnson WC Jr. Variable selection method improves the prediction of protein secondary structure from circular dichroism spectra. *Anal Biochem* (1987) 167(1):76–85. doi:10.1016/0003-2697(87)90135-7
34. Sreerama N, Woody RW. Estimation of protein secondary structure from CD spectra: comparison of CONTIN, SELCON and CDSSTR methods with an expanded reference set. *Anal Biochem* (2000) 287(2):252–60. doi:10.1006/abio.2000.4880
35. Engvall E, Perlmann P. Enzyme-linked immunosorbent assay (ELISA): quantitative assay of immunoglobulin. *Immunochemistry* (1971) 8(9):871–4. doi:10.1016/0019-2791(71)90454-X
36. Kelly SM, Jess TJ, Price NC. How to study proteins by circular dichroism. *Biochim Biophys Acta* (2005) 1751(2):119–39. doi:10.1016/j.bbapap.2005.06.005
37. Joris MA, Vanrompay D, Verstraete K, De Reu K, De Zutter L, Cox E. Use of antibody responses against locus of enterocyte effacement (LEE)-encoded antigens to monitor enterohemorrhagic *Escherichia coli* infections on cattle farms. *Appl Environ Microbiol* (2013) 79(12):3677–83. doi:10.1128/AEM.01029-13
38. Bolton DJ, Ennis C, McDowell D. Occurrence, virulence genes and antibiotic resistance of enteropathogenic *Escherichia coli* (EPEC) from twelve bovine farms in the north-east of Ireland. *Zoonoses Public Health* (2014) 61(2):149–56. doi:10.1111/zph.12058

**Conflict of Interest Statement:** The authors declare that the research was conducted in the absence of any commercial or financial relationships that could be construed as a potential conflict of interest.

Copyright © 2017 Caetano, Rocha, Carvalho, Piazza and Luz. This is an open-access article distributed under the terms of the Creative Commons Attribution License (CC BY). The use, distribution or reproduction in other forums is permitted, provided the original author(s) or licensor are credited and that the original publication in this journal is cited, in accordance with accepted academic practice. No use, distribution or reproduction is permitted which does not comply with these terms.



# A Chimera Containing CD4+ and CD8+ T-Cell Epitopes of the *Leishmania donovani* Nucleoside Hydrolase (NH36) Optimizes Cross-Protection against *Leishmania amazonensis* Infection

Marcus Vinícius Alves-Silva<sup>1,2</sup>, Dirlei Nico<sup>1</sup>, Alexandre Morrot<sup>3</sup>, Marcos Palatnik<sup>4</sup> and Clarisa B. Palatnik-de-Sousa<sup>1,5\*</sup>

## OPEN ACCESS

### Edited by:

Nahid Ali,  
Indian Institute of Chemical Biology,  
India

### Reviewed by:

Owen Kavanagh,  
York St John University, UK  
Leonardo Freire-de-Lima,  
Federal University of Rio de Janeiro,  
Brazil

### \*Correspondence:

Clarisa B. Palatnik-de-Sousa  
immcpa@micro.ufrj.br

### Specialty section:

This article was submitted to  
Vaccines and Molecular  
Therapeutics,  
a section of the journal  
*Frontiers in Immunology*

Received: 18 November 2016

Accepted: 20 January 2017

Published: 23 February 2017

### Citation:

Alves-Silva MV, Nico D, Morrot A, Palatnik M and Palatnik-de-Sousa CB (2017) A Chimera Containing CD4+ and CD8+ T-Cell Epitopes of the *Leishmania donovani* Nucleoside Hydrolase (NH36) Optimizes Cross-Protection against *Leishmania amazonensis* Infection. *Front. Immunol.* 8:100.  
doi: 10.3389/fimmu.2017.00100

<sup>1</sup>Laboratório de Biologia e Bioquímica de Leishmaniose, Departamento de Microbiologia Geral, Instituto de Microbiologia Paulo de Góes, Universidade Federal do Rio de Janeiro, Rio de Janeiro, Rio de Janeiro, Brazil, <sup>2</sup>Programa de Pós-Graduação em Biotecnologia Vegetal e Bioprocessos, Centro de Ciências da Saúde, Universidade Federal do Rio de Janeiro, Rio de Janeiro, Rio de Janeiro, Brazil, <sup>3</sup>Laboratório de Imunologia Integrada, Departamento de Imunologia, Instituto de Microbiologia Paulo de Góes, Universidade Federal do Rio de Janeiro, Rio de Janeiro, Rio de Janeiro, Brazil, <sup>4</sup>Programa de Pós-Graduação em Clínica Médica, Faculdade de Medicina-Hospital Universitário Clementino Fraga Filho, Universidade Federal do Rio de Janeiro, Rio de Janeiro, Rio de Janeiro, Brazil, <sup>5</sup>Faculdade de Medicina, Instituto de Investigação em Imunologia, Universidade de São Paulo (USP), São Paulo, São Paulo, Brazil

The *Leishmania donovani* nucleoside hydrolase (NH36) and NH A34480 of *Leishmania amazonensis* share 93% of sequence identity. In mice, the NH36 induced protection against visceral leishmaniasis is mediated by a CD4+ T cell response against its C-terminal domain (F3). Besides this CD4+ Th1 response, prevention and cure of *L. amazonensis* infection require also additional CD8+ and regulatory T-cell responses to the NH36 N-terminal (F1 domain). We investigated if mice vaccination with F1 and F3 domains cloned in tandem, in a recombinant chimera, with saponin, optimizes the vaccine efficacy against *L. amazonensis* infection above the levels promoted by the two admixed domains or by each domain independently. The chimera induced the highest IgA, IgG, and IgG2a anti-NH36 antibody, IDR, IFN-γ, and IL-10 responses, while TNF-α was more secreted by mice vaccinated with F3 or all F3-containing vaccines. Additionally, the chimera and the F1 vaccine also induced the highest proportions of CD4+ and CD8+ T cells secreting IL-2, TNF-α, or IFN-γ alone, TNF-α in combination with IL-2 or IFN-γ, and of CD4+ multifunctional cells secreting IL-2, TNF-α, and IFN-γ. Correlating with the immunological results, the strongest reductions of skin lesions sizes were determined by the admixed domains (80%) and by the chimera (84%), which also promoted the most pronounced and significant reduction of the parasite load (99.8%). Thus, the epitope presentation in a recombinant chimera optimizes immunogenicity and efficacy above the levels induced by the independent or admixed F1 and F3 domains. The multiparameter analysis disclosed that the Th1-CD4+ T helper response induced by the chimera is mainly directed against its FRYPRPKHCHTQVA epitope. Additionally, the YPPEFKTKL epitope of F1 induced the second most important CD4+ T cell response, and, followed by the

DVAGIVGVPVAAGCT, FMLQILDFYTKVYE, and ELLAITTVGNQ sequences, also the most potent CD8+ T cell responses and IL-10 secretion. Remarkably, the YPPEFKTKL epitope shows high amino acid identity with a multipotent PADRE sequence and stimulates simultaneously the CD4+, CD8+ T cell, and a probable T regulatory response. With this approach, we advanced in the design of a NH36 polytope vaccine capable of inducing cross-protection to cutaneous leishmaniasis.

**Keywords:** nucleoside hydrolases, T-cell epitope vaccines, visceral and cutaneous leishmaniasis, *Leishmania amazonensis*, PADRE epitopes

## INTRODUCTION

Leishmaniasis is a complex of protozoan vector-borne diseases of recent increased worldwide incidence (1). Clinical manifestations of the disease range from visceral leishmaniasis (VL), the most severe and fatal syndrome with 400,000 new cases/year, characterized by a strong suppression of the CD4+ T-cell response, to tegumentary leishmaniasis, with 7 to 1.2 million new annual cases and variable degrees of T-cell immunity (2). Clinical cases of cutaneous leishmaniasis (CL), the most benign form of tegumentary leishmaniasis, show skin ulcers and a T cell-mediated active immune response, which is often responsible of self-healing or worsening of the disease (2). Mucocutaneous leishmaniasis (MCL), on the other hand, involves an exacerbated immune inflammatory response and lesions of cutaneous and mucosal tissues, while diffuse cutaneous leishmaniasis (DCL), the anergic form of disease, is associated to high *Leishmania*-specific inhibition of the T-cell responses (3). A few patients also develop the borderline disseminated leishmaniasis (4).

Afghanistan, Algeria, Colombia, Brazil, Iran, Syria, Ethiopia, North Sudan, Costa Rica, and Peru are the 10 countries with higher incidence of CL, and together they account for 70–75% of the estimated global occurrence (2). Regarding the ethyological agents of tegumentary leishmaniasis, *Leishmania amazonensis* is a causative agent of CL, MCL, and DCL in Northern, South America, and Brazil (3–7).

Chemotherapy of leishmaniasis is highly toxic, and many cases of resistance or recurrent disease were reported (8–10). Alternatively, vaccine-mediated prevention or cure of CL was assayed with first generation formulations since the 80s, achieving, however, no more than 50% efficacy (8, 11). Only one vaccine based on *L. amazonensis* lysate is licensed at present for immuno-chemotherapy in Brazil (8).

Since three licensed vaccines against canine VL are available at present (12–14), one feasible approach to induce cross-protection against CL would be to use the vaccine antigens that are conserved in the *Leishmania* genus (15, 16) and already demonstrated to confer protection against VL (12, 17–19), the most immunosuppressive and severe form of the disease.

The *Leishmania donovani* nucleoside hydrolase (NH36) (17) is the main antigen of the Leishmune® vaccine, the first licensed veterinary vaccine against canine VL (12, 18). Leishmune® shows 76–80% vaccine efficacy (18, 19), and its use in endemic areas already promoted the decrease of the canine and the human incidence of VL (12).

Nucleoside hydrolases are enzymes of the DNA metabolism of bacteria, fungi, and protozoa which release exogenous purines or pyrimidines from nucleosides, in microorganisms that are not able to synthesize them, enabling in this way an efficient pathogen replication. They are absent in mammals (20, 21).

Vaccination with the NH of *L. donovani*, NH36, in its native form, protected mice against *L. donovani* infection (22), and in its DNA or recombinant protein forms induced efficacy against mice (17, 23, 24) and dog infections by *Leishmania chagasi* (25), and against mice challenged with *Leishmania mexicana* (23), *Leishmania major* (26), and *L. amazonensis* (27–29), the respective agents of cutaneous and diffuse leishmaniasis. NHs are considered strong phylogenetic markers of the genus *Leishmania* (15, 16), and their amino acid sequences are strongly conserved (29, 30). In fact, the sequence of *L. donovani* NH36 is homologous to the NH sequences of all the studied species of *Leishmania*: *L. major* (95%) (31), *L. chagasi* (99%), *Leishmania infantum* (99%), *L. amazonensis* (93%) (28), *L. mexicana* (93%), *Leishmania braziliensis* (84%), and *Leishmania tropica* (97%) (32).

Therefore, NH36 becomes a good candidate for the development of a cross-protective and universal vaccine against leishmaniasis. Using recombinant generated proteins covering the whole sequence of NH36, and saponin, in previous work, we demonstrated that protection against mice VL is mediated by a CD4+ T cell response against epitopes of the NH36 C-terminal domain (F3) (17). On the other hand, prevention (28) and cure of mice CL (29) caused by *L. amazonensis* are determined by a CD4+-Th1 cell-mediated response toward the F3 protein and a CD8+ and regulatory T-cell responses directed to the N-terminal (F1) domain of NH36, which promoted simultaneous increased secretions of IFN- $\gamma$ , TNF- $\alpha$ , and IL-10 (29).

Additionally, the F3 vaccine promoted in mice a 36 and 40% respective higher average protection than those generated by the NH36-vaccine against VL, induced by *L. chagasi* (17), and CL, caused by *L. amazonensis* (28). These results confirmed that the use of the domain containing the relevant epitopes enhances the efficacy over that induced by the cognate whole protein (33).

Multisubunit vaccines against leishmanial infection have been shown to be more promising (34). Additionally, the most efficient protection is considered to be determined by diverse T cells that respond to a group of the pathogen-derived epitopes (35). Recent research in immunity to leishmaniasis disclosed the importance of multifunctional CD4+ and CD8+ T cells in the generation of a Th1 response to control infection (34, 36, 37). According to that, it has been suggested that the *in silico* tools should be used to

search in the *Leishmania* genome for potential candidates with both CD4+ and CD8+ T cell-stimulating competences. Epitope mapping could then be used to design a polyepitope vaccine that could carry conserved epitopes, which bind to many HLA or MHC allotypes, or which are present in many species of a *Leishmania* genus (34).

Although the whole NH36 protein would be easier to work with, it would be also much less potent. In fact, according to the philosophy of the development of T-epitope vaccines, the whole cognate protein is less potent than the domains that contain the important epitopes. The domains are also more immunogenic than the isolated epitopes. Our aim, in this investigation, was to increase potency and optimize the vaccine. In agreement to that, we were able to show that a combination of these domains in a chimera even enhances the protective efficacy demonstrated for each domain independently. Our results support that the use of the domain containing the relevant epitopes enhances the vaccine efficacy over that induced by the cognate whole protein (33).

In fact, we evaluated if the administration of F1 and F3 domains of NH36 expressed in tandem, as a recombinant chimera, optimizes the immunogenicity and vaccine efficacy against mice infection by *L. amazonensis*, above the levels promoted by the two admixed domains and by each protein administered alone. We additionally identified the most important epitopes of F1 and F3 responsible for the generation of the cellular immune response. In this investigation, we aimed to progress in the development of a universal NH36 T-cell epitope vaccine capable of protecting against the infection by *L. amazonensis*.

## MATERIALS AND METHODS

### Ethical Statement

This study was carried out in accordance with the recommendations of National Institutes of Health, USA. The protocol was approved by the Comissão de Avaliação da Utilização de Animais em Pesquisa do Centro de Ciência da Saúde (CEUA), Universidad Federal do Rio de Janeiro (CONCEA, Brazil, 01200.001568/2013-87, IMPPG-016).

### Recombinant Antigens Expression and Purification and Epitopes

NH36 is composed of 314 amino acids (Genbank access number AY007193, SwissProt-UniProt access number Q8WQX2-LEIDO). The N-terminal (F1, amino acid sequences 1–103), the central (F2, amino acids 104–198), and the C-terminal (F3, amino acids 199–314) domains were cloned in the pET28 plasmid system, between the restriction sites of *Nco*I and *Xho*I (17). Furthermore, the F1F3 recombinant chimera containing the sequence of the F1 followed by the F3 protein, cloned between the restriction sites of *Nco*I and *Xho*I was obtained with optimized codons in the PET28b expression vector by GenScript (NJ, USA). All the recombinant proteins used in this investigation were expressed with a six His-Tag at their C-terminals.

For protein expression, pET28bNH36, pET28bF1, pET28bF3, or pET28bF1F3-transformed *E. coli* BI21DE3 bacteria were amplified into 2 l of LB culture medium with kanamycin.

Expression was induced with 1 mM IPTG (isopropyl-beta-D-thiogalactopyranoside—Fermentas) for 4 h at 37°C, and cultures were centrifuged. The pellets were sonicated and further centrifuged for 20 min under 14,000 rpm at 4°C. The recombinant proteins were more concentrated in the pellets, which were purified by affinity column chromatography with Ni-NTA resin according to the manufacturer's instructions (Qiagen). Briefly, each pellet was incubated with 10–15 ml urea buffer (8 M urea, 1 M Na<sub>2</sub>HPO<sub>4</sub>, 1 M NaH<sub>2</sub>PO<sub>4</sub>, and 1 M Tris-HCl) pH 8.0, for 2 h, on ice. Then, the suspension was homogenized by successive passages through 20 ml syringes with 1.2 mm × 40 mm needles, until complete dissolution and centrifuged for 15 min at 14,000 rpm at 4°C. The supernatants containing the solubilized proteins were loaded on the Ni-NTA column previously equilibrated with urea buffer. Then, the column was washed with 5 volumes of urea buffer, pH 8.0, for removal of non-specifically bound proteins and with additional 5 volumes of urea buffer, pH 6.4–6.5, for removal of bacterial proteins containing His residues. The recombinant antigens were recovered in 10 volumes of urea buffer pH 4.5, dialyzed overnight against PBS at 4°C, and preserved with 1 mM PMSF and 5% glycerol at –80°C (17). The absence of LPS was confirmed using the LAL QCL-1000 kit (Lonza).

Furthermore, CD4+ T cell epitopes predicted by the Protean Pad program based on the A. Sette algorithm for the H2<sup>d</sup> haplotype of Balb/c mice (IA<sup>d</sup> and IE<sup>d</sup> alleles) (17) and the CD8+ T cell epitopes (H2 L<sup>d</sup> haplotype), identified by the HLA peptide motif search<sup>1</sup> and the SYFPEITHI<sup>2</sup> programs (17) were synthetized by GenScript (NJ, USA). A model of the structure of the NH36 monomer and of the spatial distribution of the predicted epitopes in F1 and F3 is represented in Figure S1 in Supplementary Material.

### Vaccine Efficacy Assay

Groups of BALB/c females (2-month old) were randomized by corporal weight and immunized with three subcutaneous doses of each respective vaccine: F1 (100 µg), F3 (100 µg), F1 (50 µg), and F3 (50 µg) administered as a simple mixture (F1 + F3), and F1F3 chimera (100 or 200 µg). All antigens were formulated with 100 µg of Riedel de Haen saponin (Sigma, St. Louis, MO, USA) in 0.2 ml of 0.9% NaCl saline solution and injected subcutaneously in the back, at weekly intervals (17, 28, 29). Control animals received only saline. Mice were infected subcutaneously in the right hind footpads with 10<sup>6</sup> stationary phase infective promastigotes of *L. amazonensis* IFLA/BR/67/PH8, 10 days after the last vaccine dose. Briefly, infective parasites were obtained from hamsters footpads in 10% fetal calf serum, 50 U penicillin, and 50 µg streptomycin/ml (Cultilab, Brazil) supplemented Schneider's Drosophila medium (Sigma). Parasites were then cultured using a 1/5 serial dilution, in 24-well plates, at 26°C, during 3 days. On day 4, 400 µl of promastigote suspensions was amplified through three successive passages in Schneider's supplemented medium and finally, the stationary-phase parasites

<sup>1</sup>[http://bimas.dcrt.nih.gov/molbio/hla\\_bind/](http://bimas.dcrt.nih.gov/molbio/hla_bind/)

<sup>2</sup><http://www.syfpeithi.de/>

were centrifuged, washed twice, suspended in saline solution, counted in a hemocytometer, and used for infection.

The evolution of lesion sizes in footpads was monitored weekly, with a Mitutoyo® pachymeter. Measures of the infected footpads were subtracted from the contra-lateral controls injected only with saline.

At week 12, mice were euthanized with CO<sub>2</sub> and their parasite load determined by a limiting dilution assay. Briefly, the infected paws were removed under aseptic conditions and washed with Schneider's medium. Fragments of bones, nails, and skin were chirurgically removed. The remaining tissue was chopped into small pieces and suspended into 1 ml supplemented Schneider's medium. A 1/5 serial dilution of this suspension was obtained in a 24-well plate that was further incubated at 26°C for 4 days, with daily observation in an inverted microscope. The number of promastigotes present at the last well containing visible parasites was quantified in a hemocytometer.

The anti-NH36 antibody response was assessed in sera, and the intradermal response to leishmanial antigen, and the secretion and intracellular expression of cytokines by antigen-stimulated CD4 and CD8 lymphocytes were studied 1 week after complete vaccination and on week 12 after infection.

### Antibody Assay in Sera

Anti-NH36 antibodies were assayed in the sera of mice, using a standard ELISA assay. Plates were treated with 2 µg NH36 per well in carbonate–bicarbonate buffer pH 9.6, washed with 0.018 M PBS, pH 7.2, 1% non-fat milk, and 0.05% Tween-20 buffer (PBS\*), and further incubated with diluted sera samples in PBS\* for 1 h at 37°C. Then, plates were washed and treated with peroxidase-conjugated goat anti-mouse-IgA, IgM, IgG1, or IgG2a antibodies (1:4,000) (Southern Biotechnology Associates, Birmingham, AL, USA) or with protein-A-peroxidase (Kirkegaard & Perry Laboratories, Gaithersburg, MD, USA, EEUU) at 1:1,000 dilution in PBS\*. Reaction was developed with ortho-phenylenediamine buffer (Sigma), interrupted with 1 N sulfuric acid, and monitored at 492 nm. Results were expressed as the mean of absorbance values of 1/100 diluted sera of each animal, in triplicates, in double-blind tests.

### Intradermal Skin Test (IDR)

Mice were injected in their right front footpad with 0.1 ml 0.9% NaCl saline solution containing the lysate of 10<sup>7</sup> freeze-thawed stationary-phase *L. amazonensis* infective promastigotes obtained as described in Section “Vaccine Efficacy Assay.” The footpad swelling was monitored with a Mitutoyo apparatus, both before and at 0, 24, and 48 h after lysate injection. Each measure was subtracted from the values of the left front footpads injected with only saline (28).

### Secreted Cytokines Assay

Spleens were excised, and single-cell suspensions were prepared in 1 ml RPMI medium (Sigma, Co) supplemented with 10% fetal calf serum (Nutricell, Campinas, São Paulo, Brazil), 1% L-glutamine, and 5 mM 2-β-mercaptoethanol. Then, cells were counted in a hemocytometer, distributed into a 96-well

plate (10<sup>6</sup>/well), and incubated with 5 µg/well NH36, or with no addition, for 72 h *in vitro*, at 37°C with 5% of CO<sub>2</sub>. Culture supernatants were collected and assayed for IFN-γ, TNF-α, and IL-10 using the OptEIA mouse ELISA Set II kits (Becton and Dickinson, BD-Biosciences, USA) according to the manufacturer's instructions. The sensitivity of the assay was established with a range of 0–1,000 pg/ml for TNF-α and IL-10 and of 0–200 pg/ml for IFN-γ. Reactions were developed using biotinylated anti-cytokine antibodies, streptavidin (SAv-HRP) enzymatic reagent, and TMB (Zymed, USA). Absorbances were monitored at 655 nm.

### Intracellular Cytokine Staining (ICS) and Flow Cytometry

Splenocytes suspended in RPMI medium were distributed into 96-well Costar plates (10<sup>6</sup>/well) and stimulated with 25 µg/ml recombinant NH36 or with no addition, for 24 h at 37°C with 5% CO<sub>2</sub> according to the results of previous experiments. The intracellular expression of IL-2, TNF-α, and IFN-γ by CD4+ and CD8+ T cells was determined by multiparameter analysis (36, 37) after incubation with 10 µg/ml brefeldin (Sigma) for 4 h at 37°C, 5% CO<sub>2</sub>. After washing with FACS buffer (PBS containing 2% bovine fetal calf, 0.1% sodium azide), splenocytes were labeled for 20 min at 4°C, in the dark with rat anti-mouse-CD4FITC (clone GK1.5) and -CD8FITC (clone 53-6.7) monoclonal antibodies (R&D systems, Inc.). Cells were then fixed with 4% para-formaldehyde, washed and treated with FACS buffer containing 0.5% saponin (Sigma), and further stained with IFN-γAPC, IL-2-PerCP-Cy5.5, and TNF-αPE monoclonal antibodies (BD-Pharmingen). For ICS, gating for CD4+ ad CD8+ T cells was performed, and 100,000 events were acquired in a Becton Dickinson FACScalibur. Data were analyzed using the FlowJo program (Tree Star, USA).

### Epitope Assays

Splenocytes of mice vaccinated with the chimera (100 µg/dose) or saline solution and further challenged with 10<sup>6</sup> promastigotes of *L. amazonensis* were incubated *in vitro* with 25 µg/ml of NH36, F1F3 chimera, each one of the CD4 predicted epitopes of F1 (ELLAITTGVGNQ and DVAGIVGPVAAGCT) and F3 domains (FMLQILDYTKVYE, FRYPRPKHCCHTQVA, and KFWCLVIDALKRIG), with the highest scored CD8 predicted epitope of the F1 protein (YPPEKTKL), or with the mixture of all the epitopes, at week 11 after infection. The epitope-specific cellular immune response was studied through the analysis of the cytokine secretion to supernatants and by multiparameter cytometry, as described above.

### Statistical Methods

Means were compared by the Kruskal–Wallis and Mann–Whitney methods. Spearman's two-tailed correlation test was used for correlation analysis. Furthermore, the slope of the curves of variation of lesion sizes along the time was calculated as the best-fit values (GraphPad Prism6 software). All experiments were performed at least twice, and the indicated error bars are based on the SE.

## RESULTS

### The F1F3 Chimera Optimizes the Antibody Response

We investigated, for all variables, if the vaccine containing the mixture of the F1 and F3 domains (F1 + F3) was more potent than the F1 and F3 vaccines independently. Our strategy also involved the use of the chimera at the dosage of 100 µg, in order to make a fair comparison with the simple addition of the two domains (F1 + F3), since both vaccines are composed of approximately 50 µg of each F1 and F3 proteins. Additionally, we also used the chimera at the dosage of 200 µg, to disclose any potential dose-response effect of increased efficacy determined by a higher dose of the antigen.

Initially, we compared the antibody response generated by the vaccines, both after complete immunization and after challenge by *L. amazonensis* (Figures 1 and 2). In contrast to what observed for the IgM antibodies (Figures 1C,D), the F1 protein alone did not induce any anti-NH36 antibodies of the IgG class or subclasses. The F3 vaccine on the other hand enhanced the IgM and all IgG antibodies against NH36 above the saline controls ( $p < 0.0001$  for all comparisons) (Figures 1C,D and 2A–F). The IgM antibodies were equally enhanced by the F3 and the chimera vaccines before challenge and by the F3 vaccine after challenge (Figure 1).

Furthermore, the admixed domains induced more IgG, IgG1, and IgG2a antibodies than the F3 or the F1 vaccines did independently ( $p < 0.007$  for both) indicating that the administration of both proteins simultaneously potentiates the effect (Figures 1A,B and 2).

Remarkably, the chimera vaccine optimized the antibody response by inducing the highest IgA, IgG, and IgG2a anti-NH36 responses (Figures 1A,B and 2A–C,E,F). In fact, the dose of 200 µg determined additional increases of 19%, in the absorbency values, above those of the F1 + F3 and chimera (100 µg) vaccines ( $p < 0.0001$  for both) revealing maximal optimization of the IgG response (Figure 2A). The 200 µg F1F3 chimera was also the strongest formulation for the IgG class after challenge ( $p < 0.0148$  for all comparisons) (Figure 2B) while the admixed proteins (F1 + F3) were no longer superior to the F3 vaccine.

Noteworthy and in agreement with what described for the IgG response, after immunization, the chimeras induced the most potent and optimized IgG2a response (Figure 2E). The dosage of 100 µg exhibited an increase of 20% ( $p < 0.0001$ ) in the IgG2a antibody titers, above the F1 + F3 vaccine, indicating that the presentation of the epitopes in tandem increases the efficacy. Additionally, and similar to what described for IgG (Figure 1A), the maximal IgG2a antibody response was induced by the 200 µg chimera vaccine, which promoted a 19% higher IgG2a response than the same vaccine at 100 µg dosage ( $p < 0.0001$ ), indicating

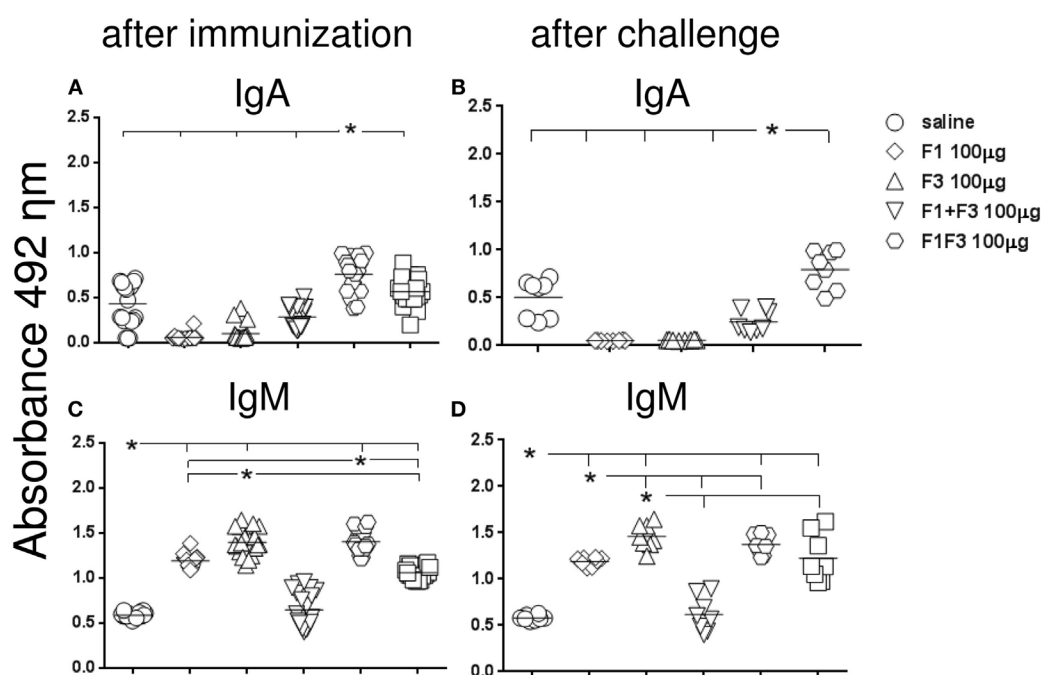


**FIGURE 1 | Chimera enhances the IgA and, together with F3, the IgM anti-NH36 antibody response.** BALB/c mice were immunized with three subcutaneous doses of each respective vaccine: F1 (100 µg), F3 (100 µg), F1 (50 µg), and F3 (50 µg) administered as a simple mixture (F1 + F3), and F1F3 chimera (100 or 200 µg), all formulated in 100 µg of saponin. Anti-NH36 antibodies were measured by an ELISA assay in the sera of mice after vaccination (A,C) and on week 12 after infection with *Leishmania amazonensis* (B,D). Data are means and individual results of two independent experiments, each one with 8–10 animals per treatment. The chimera vaccine induced the highest IgA response (A,B). The IgM antibodies were equally enhanced by the F3 and the chimera vaccines before challenge and by the F3 vaccine after challenge (C,D).

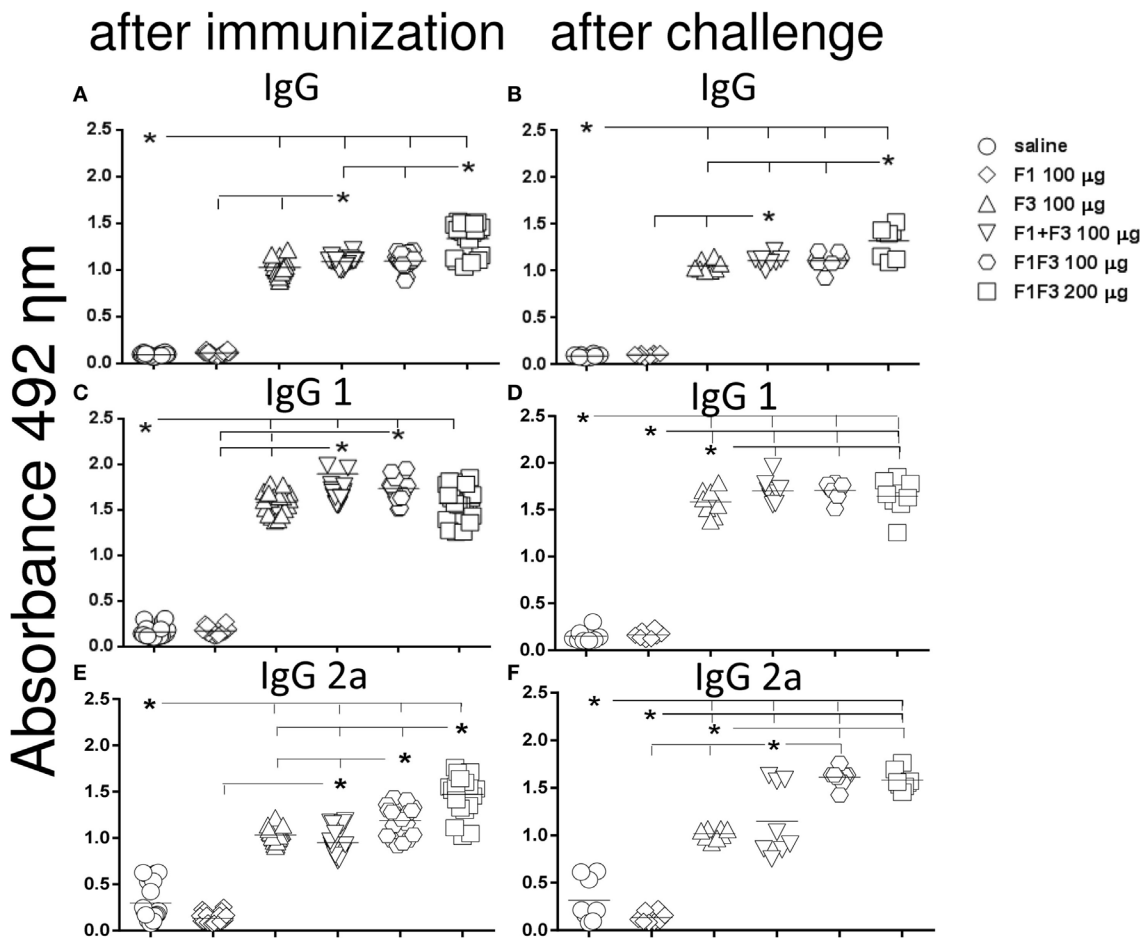


**FIGURE 2 | Chimera increased the IgG, IgG1, and IgG2a antibody levels.** Anti-NH36 antibodies were measured by an ELISA assay in the sera of mice vaccinated with F1, F3, the addition of F1 and F3, or the F1F3 chimera in formulation with saponin and after infection with *Leishmania amazonensis*. Data are means and individual results of two independent experiments, each one with 8–10 animals per treatment. The F1 protein alone did not induce any increase in IgG, IgG1, or IgG2a antibodies while the F3 did (**A–F**). The mixture of domains enhanced the IgG, IgG1, and IgG2a antibody responses above the F3 and F1 proteins (**A–D,F**). The chimera, however, induced the strongest IgG and IgG2a anti-NH36 responses (**A–C,E,F**) being, at the dosage of 100 µg, more potent than the domain mixture (**E,F**), and at the dosage of 200 µg, stronger than at the dosage of 100 µg (**A,B,E**).

a dose-response effect (**Figure 2E**). Optimization of the IgG2a antibody response was also detected as a result of the impact of *L. amazonensis* infection when the two chimera-vaccine dosages showed a 28% increased potency above the F1 + F3 vaccine ( $p < 0.007$  for the two comparisons) (**Figure 2F**).

For the IgG1 subtype, the admixed domains were as potent as the chimera (100 µg) (**Figures 2C,D**).

We concluded that the presentation of the F1 and F3 proteins in a recombinant chimera determined a stronger effect than the simultaneous delivery of both independent domains, for the induction of IgA, IgG, and IgG2a anti-NH36 antibodies. An increasing dose-response was additionally detected for the chimera in the IgG (before and after challenge) and IgG2a (before challenge) antibodies. In contrast, the chimera at the dosage of 100 µg was even more potent than at 200 µg, for the IgA and IgM (before and after challenge) and IgG1 (after immunization) antibodies, and was as strong as at 200 µg dosage, for the IgG1

and IgG2a (after challenge) response. These results suggest that the optimization effect is more related to the concomitant presentation of the F1 and F3 epitopes in tandem, rather than to an increased antigen concentration.

### The F1F3 Chimera Optimizes the Intradermal Response to *L. amazonensis* Antigen

The induction a cellular immune response was initially assessed by IDR. At all times, all formulations developed more potent IDR reactions than the saline controls and the F1 vaccine ( $p < 0.0001$  for all comparisons) (**Figures 3A–D**). Maximal skin tests were achieved in mice vaccinated with the chimera (**Figure 3**).

Although the chimera at 100 µg dosage was more potent than the admixed proteins (**Figures 3A,B,D**), and the F3 vaccine (**Figure 3D**), the dosage of 200 µg was the strongest formulation, which induced the largest skin tests (**Figures 3A–D**). In fact, at

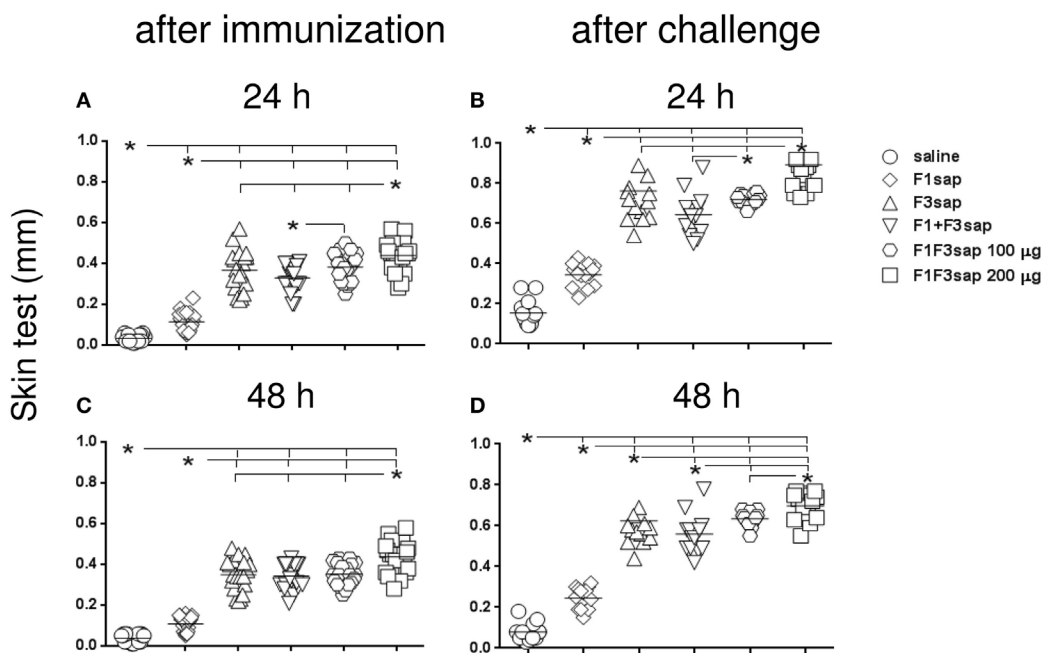


**FIGURE 3 | Chimera optimizes the intradermal response against *Leishmania amazonensis* antigen.** The IDR to the lysate of *L. amazonensis* infective promastigotes was measured in mice vaccinated with F1, F3, the addition of F1 and F3 proteins, or the F1F3 chimera, in formulation with saponin, after vaccination (**A,C**) and on week 12 after challenge with *L. amazonensis* (**B,D**), at 24 and 48 h after antigen injection. Data are means and individual results of two independent experiments, each one with 8–10 animals per treatment. All formulations were more potent than the saline controls and the F1 vaccine (**A–D**). The chimera, at 100 µg dosage, was more potent than the addition of domains (**A,B,D**), and the F3 vaccine (**D**), but the dosage of 200 µg was the strongest formulation (**A–D**). After challenge (**B,D**) and 48 h after antigen injection (**C,D**), all vaccines enhanced the skin tests.

the dosage of 100 µg, the chimera was already 13% more potent than the addition of F1 + F3 proteins ( $p < 0.0232$ ) disclosing the optimization effect that was due to the presentation of the epitopes in tandem. The additional 13% ( $p < 0.0263$ ) enhancement generated by the 200 µg dosage disclosed a dose-response effect (Figure 3A).

After challenge, and in contrast to what described for antibodies, all the vaccines induced significant increases of skin tests ( $p < 0.0001$ ). Actually, after infection, the skin tests of mice vaccinated with the F3, F1 + F3, 100, and 200 µg chimera vaccines were 47, 52, 53, and 51% larger than before challenge, respectively ( $p < 0.0001$ , for all comparisons) (Figures 3A,B). At 48 h after antigen injection also, respective IDR increases of 44, 38, 44, and 38% were also observed for the F3, F1 + F3, 100, and 200 µg chimera vaccines ( $p < 0.0001$  for all comparisons) (Figures 3C,D).

Our results disclosed the chimera at the 200 µg dosage as the strongest formulation. However, at the dosage of 100 µg, the chimera was already capable of inducing the most pronounced enhancement of skin tests after infection, being even more efficacious than the admixed domains. These results confirm the chimera capability for optimization of vaccine efficacy and suggest that efficacy could be even enhanced by using increased chimera dosages (Figures 3A–D).

The IDR response after immunization is highly correlated to the IgG ( $p < 0.0001$ ,  $R = 0.7552$ ,  $R^2 = 0.5703$ ) and the IgG2a ( $p < 0.0001$ ,  $R = 0.8839$ ,  $R^2 = 0.7813$ ) antibody responses. Also,

after infection, the IgG ( $p < 0.0001$ ,  $R = 0.7009$ ,  $R^2 = 0.4912$ ) and IgG2a antibody levels ( $p < 0.0001$ ,  $R = 0.8364$ ,  $R^2 = 0.6995$ ) were correlated to the IDR results.

### Secretion of IFN- $\gamma$ , TNF- $\alpha$ , and IL-10 Increased in Response to the F1F3 Chimera

After immunization, all vaccines increased the IFN- $\gamma$  secretion to PBMC supernatants above the levels induced by the saline controls ( $p < 0.0022$ ), indicating the triggering of a Th1-immune response. Mice vaccinated with F3-containing vaccines secreted more IFN- $\gamma$  than those treated only with the F1 protein ( $p < 0.0022$ ). The main performance was, however, determined by the chimera at 100 µg dosage, which was 19% stronger than the admixed domains and 20% more potent than the 200 µg dosage ( $p < 0.0022$  for both comparisons) (Figure 4A). After infection, and as observed for skin tests and IgG2a antibodies, the two dosages of the chimera showed codominance of the IFN- $\gamma$  secretion (Figure 4B) above the F1 and F3 vaccines independently or formulated together ( $p < 0.0002$  for all comparisons). IFN- $\gamma$  levels induced by the chimeras after challenge were 56–44% lower (Figure 4B).

As observed for IFN- $\gamma$  and also indicating the rise of a Th1 response, TNF- $\alpha$  was initially more secreted by mice vaccinated with F3 than with F1 ( $p < 0.0022$ ) (Figure 4C) and by all vaccines

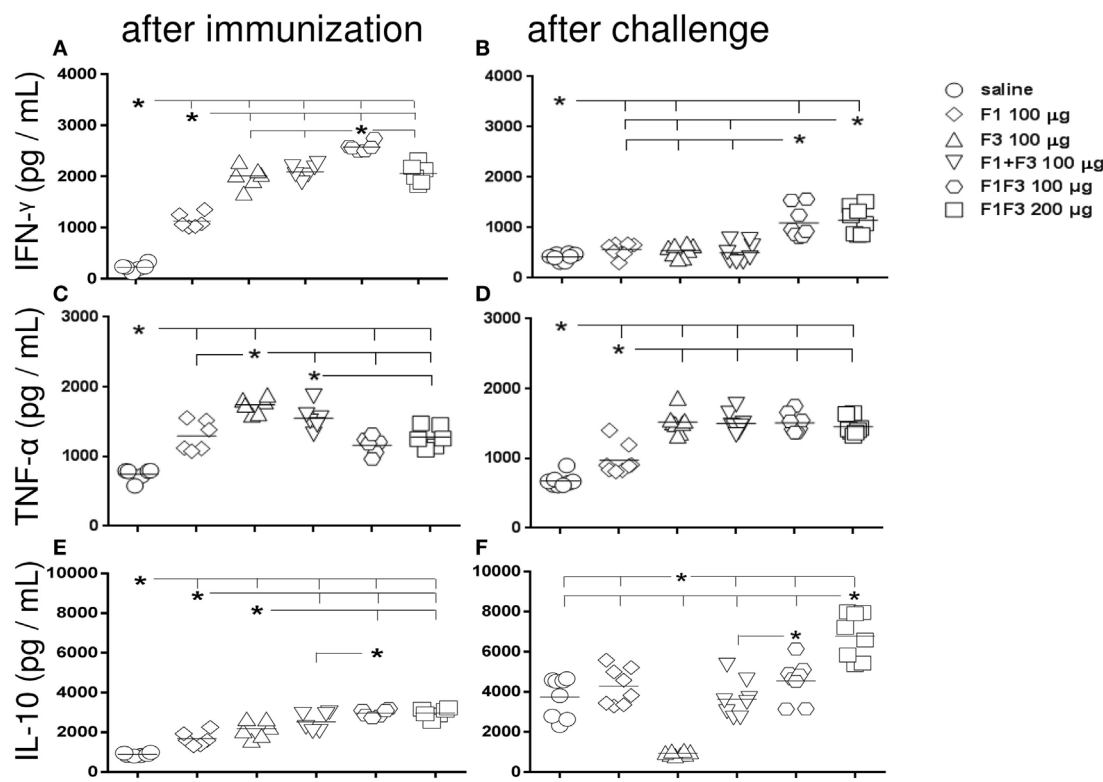


**FIGURE 4 |** Chimera potentiates the secretion of IFN- $\gamma$  and IL-10 while TNF- $\alpha$  is generated in response to all F3-containing vaccines. Secretions of IFN- $\gamma$  (**A,B**), TNF- $\alpha$  (**C,D**), and IL-10 (**E,F**), as measured by an ELISA assay in the supernatant of splenocytes, both after immunization with F1, F3, the addition of F1 and F3 proteins, or the F1F3 chimera in formulation with saponin, and after challenge with *Leishmania amazonensis*, are expressed in picograms per milliliter. Data are means and individual results of two independent experiments, each one with 8–10 animals per treatment. After immunization, the F3-containing vaccines secreted more IFN- $\gamma$  than the F1 vaccine. The chimera at 100 µg dosage was stronger than the admixed proteins and the 200 µg dosage (**A**). After infection, the two dosages of the chimera were equally potent (**B**) above the F1 and F3 vaccines independently or formulated together. However, the IFN- $\gamma$  levels after challenge were lower (**B**). TNF- $\alpha$  was initially more secreted by mice vaccinated with F3 than with F1 (**C**) and by all vaccines containing the F3 domain, after challenge (**D**). The chimeras or the admixed proteins enhanced IL-10 secretion after immunization, above the F1 or F3 vaccines (**E**). After challenge, IL-10 secretion was null in F3-vaccinated mice, but it was increased by the other vaccines with maximal performance achieved by the chimera (200 µg) (**F**). A dose-response increase in IFN- $\gamma$  (**B**) and IL-10 (**F**) secretion was observed with the increment of the chimera dosage.

containing the F3 domain, including the chimeras, after challenge (**Figure 4D**).

Additionally and suggesting a potential regulatory immune response, mice vaccinated with the chimeras or with the admixed proteins secreted more IL-10 after immunization than mice vaccinated with F1 or F3 proteins alone ( $p < 0.015$  for all comparisons) (**Figure 4E**). Noteworthy, IL-10 secretion was higher in mice vaccinated with 100 µg of the chimera than with the F1 + F3 addition, both before and after challenge (**Figures 4E,F**).

Remarkably, after challenge, however, IL-10 secretion was null only in F3-vaccinated mice while it was increased by all vaccines containing F1 and achieved the maximal values in the 200 µg chimera vaccine (**Figure 4F**). In fact, after infection, the IL-10 levels were 2.3 times reduced ( $p < 0.0007$ ) in F3-vaccinated mice, while increases of 2.6 ( $p < 0.0007$ ), 1.4 ( $p < 0.0200$ ), 1.5 ( $p < 0.0023$ ), and 2.3 times ( $p < 0.0007$ ) were detected in mice vaccinated with the F1, F1 + F3, and the chimera vaccine at 100 and 200 µg dosage, respectively (**Figures 4E,F**).

Lastly, a dose-response increase in IFN- $\gamma$  and IL-10 secretion was observed with the increment of the chimera dosage to 200 µg.

### The F1F3 Chimera Induces the Highest Proportions of CD4+ and CD8+ T Cells Secreting One, Any Combination of Two and Three Cytokines

The effector function and quality of the T cell immune response were assessed after infection, by multiparameter-flow cytometry analysis.

The chimera vaccine at 100 µg/dose induced the highest proportions of all types of CD4+-cytokine secreting T cells (**Figure 5**). In fact, the 100 µg/dose chimera was more potent than the F3 ( $p < 0.0469$ ) and F1 + F3 vaccines ( $p < 0.0391$ ) inducing elevated proportions of CD4+ T cells secreting IL-2, TNF- $\alpha$ , or IFN- $\gamma$  alone (**Figures 5A–C**), TNF- $\alpha$  in combination

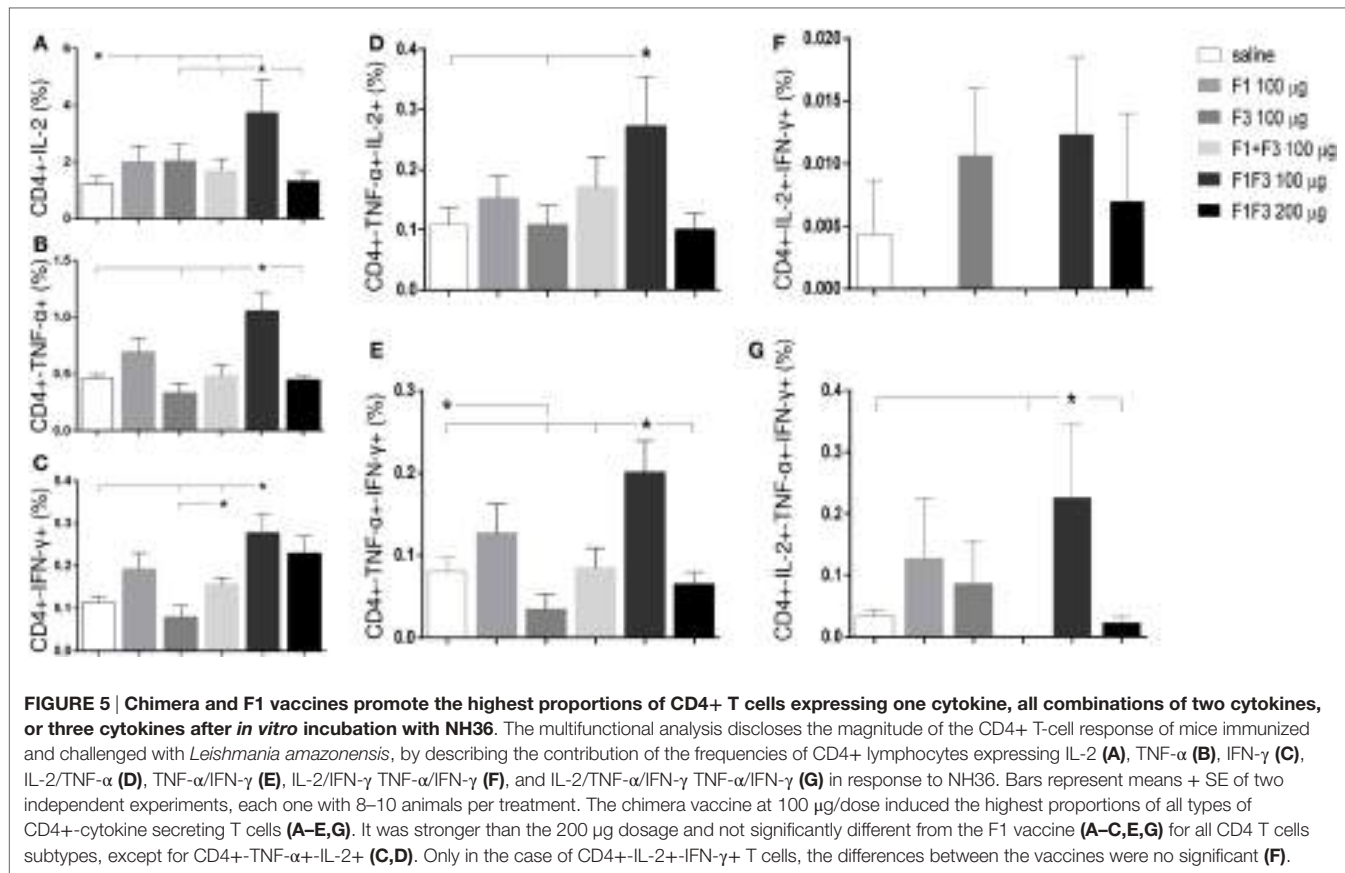


**FIGURE 5 |** Chimera and F1 vaccines promote the highest proportions of CD4+ T cells expressing one cytokine, all combinations of two cytokines, or three cytokines after *in vitro* incubation with NH36. The multifunctional analysis discloses the magnitude of the CD4+ T-cell response of mice immunized and challenged with *Leishmania amazonensis*, by describing the contribution of the frequencies of CD4+ lymphocytes expressing IL-2 (A), TNF-α (B), IFN-γ (C), IL-2/TNF-α (D), TNF-α/IFN-γ (E), IL-2/IFN-γ TNF-α/IFN-γ (F), and IL-2/TNF-α/IFN-γ TNF-α/IFN-γ (G) in response to NH36. Bars represent means + SE of two independent experiments, each one with 8–10 animals per treatment. The chimera vaccine at 100 µg/dose induced the highest proportions of all types of CD4+-cytokine secreting T cells (A–E,G). It was stronger than the 200 µg dosage and not significantly different from the F1 vaccine (A–C,E,G) for all CD4 T cells subtypes, except for CD4+-TNF-α+IL-2+ (Figures 5C,D). Our results indicate that it was stronger than the 200 µg dosage and not significantly different from the F1 vaccine (A–C,E,G) for all CD4 T cells subtypes, except for CD4+-TNF-α+IL-2+ (Figures 5C,D). Only in the case of CD4+-IL-2+IFN-γ+ T cells, the differences between the vaccines were no significant (F).

with IL-2 or IFN-γ (Figures 5D,E) and multifunctional cells secreting IL-2, TNF-α, and IFN-γ simultaneously (Figure 5G). Additionally, the 100 µg dose was stronger than the 200 µg dosage ( $p < 0.0391$ ) and not significantly different than the F1 vaccine (Figures 5A–C,E,G) for all CD4 T cells subtypes, except for CD4+-TNF-α+IL-2+ (Figures 5C,D). Our results indicate the presence of important CD4+ epitopes in F1 (Figures 5A–E,G) and suggest that the presentation of the epitopes in tandem by the chimera represents the best approach for optimization of the Th1 response. Only in the case of CD4+-IL-2+IFN-γ+ T cells, the differences between the vaccines were no significant (Figure 5F).

Regarding the cytotoxic response (Figure 6), the admixed proteins were not capable of inducing higher CD8+ T cell proportions than the F1 or F3 domains independently (Figure 6). Furthermore, as described for CD4+ T cells (Figure 5), the chimera vaccine, at the dosage of 100 µg, also promoted the highest proportions of CD8+ T cell expressing IL-2, TNF-α, or IFN-γ (Figures 6A–C) and TNF-α, in combination with IL-2 or IFN-γ (Figures 6D,E). This did not occur for the CD8+ multifunctional T cells which, in contrast to what observed for CD4+ T cells, showed no significant differences between treatments (Figures 6F,G).

At 100 µg dosage, the chimera was more potent than at 200 µg for the increase of the proportions of CD8+-TNF-α+ ( $p < 0.0078$ ) and CD8+-IFN-γ+ secreting T cells ( $p < 0.0078$ ).

Additionally, and similar to what described for CD4+ T cells (Figure 5), the 100 µg chimera vaccine was stronger than the F1 vaccine in CD8+-TNF-α+IFN-γ T cells and as potent as the F1 vaccine in induction of most types of CD8+-cytokine secreting T cells (Figures 6A,B,D,E), except for cells secreting only IFN-γ (Figure 6C). Our results also indicate that important epitopes for CD8+ T cells are located in the F1 domain.

The multifunctional flow cytometry confirmed that in order to optimize the antigen presentation to T cells, the exposure of the F1 and F3 domains cloned in tandem is needed. The simple addition of the two domains was not effective in triggering the cellular immune response. We conclude that the chimera at the dosage of 100 µg generated the strongest protection against the parasite challenge but was not significantly different from the F1 vaccine.

## Vaccine Efficacy Is Optimized by the F1F3 Chimera Formulation

The evolution of the infection was monitored by the increase of the skin lesion sizes up to week 12 after infection. The linear regression analysis revealed significantly different degrees of vaccine-induced protection disclosed by the decreased slopes of their respective curves:  $0.3033 \pm 0.016$  for the F1,  $0.2257 \pm 0.012$  for the F3,  $0.1973 \pm 0.009$  for the F1 + F3,  $0.1793 \pm 0.008$  for the F1F3 100 µg, and  $0.1640 \pm 0.007$  for

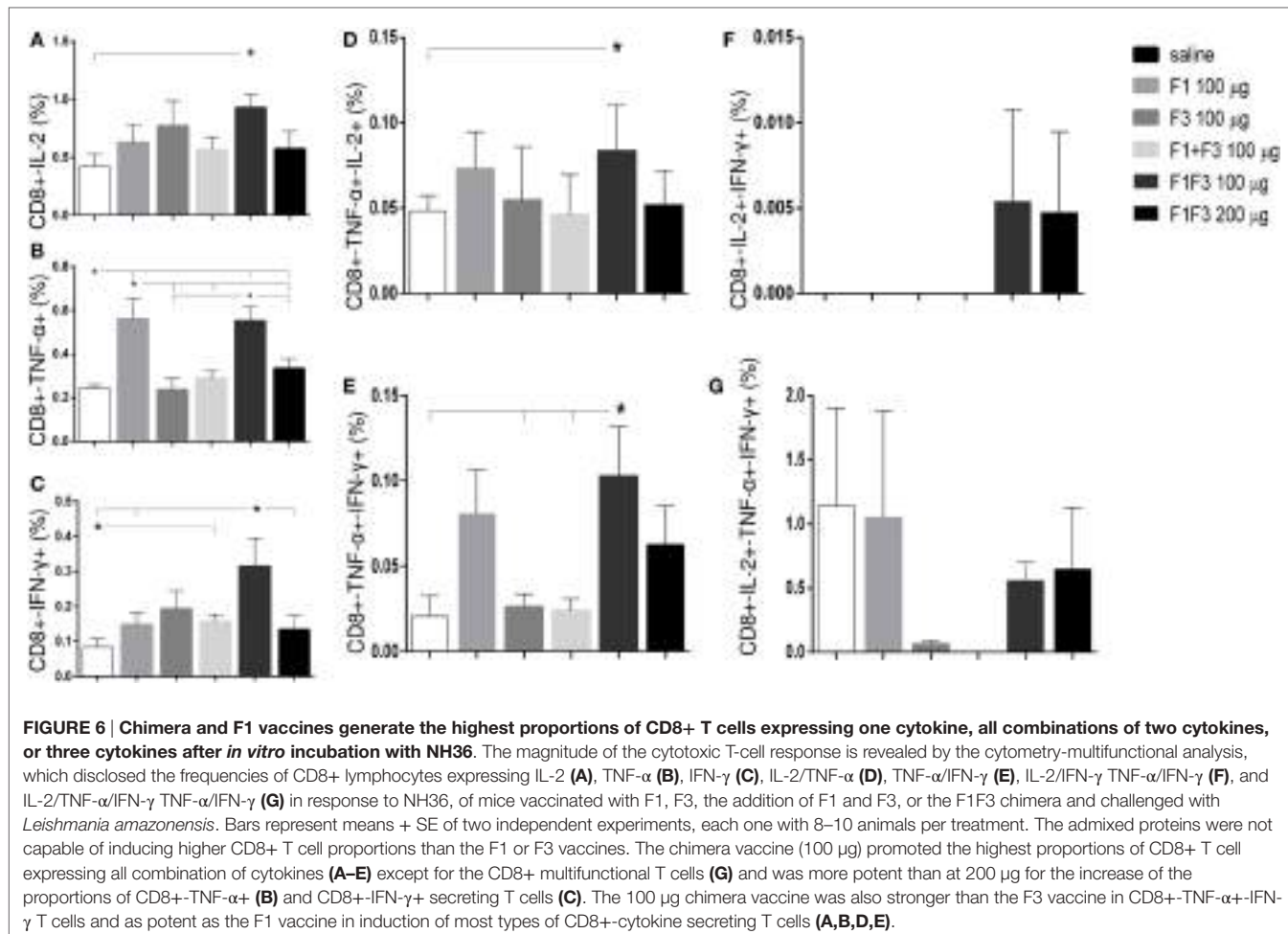


**FIGURE 6 |** Chimera and F1 vaccines generate the highest proportions of CD8+ T cells expressing one cytokine, all combinations of two cytokines, or three cytokines after *in vitro* incubation with NH36. The magnitude of the cytotoxic T-cell response is revealed by the cytometry-multifunctional analysis, which disclosed the frequencies of CD8+ lymphocytes expressing IL-2 (A), TNF- $\alpha$  (B), IFN- $\gamma$  (C), IL-2/TNF- $\alpha$  (D), TNF- $\alpha$ /IFN- $\gamma$  (E), IL-2/IFN- $\gamma$  TNF- $\alpha$ /IFN- $\gamma$  (F), and IL-2/TNF- $\alpha$ /IFN- $\gamma$  TNF- $\alpha$ /IFN- $\gamma$  (G) in response to NH36, of mice vaccinated with F1, F3, the addition of F1 and F3, or the F1F3 chimera and challenged with *Leishmania amazonensis*. Bars represent means + SE of two independent experiments, each one with 8–10 animals per treatment. The admixed proteins were not capable of inducing higher CD8+ T cell proportions than the F1 or F3 vaccines. The chimera vaccine (100 µg) promoted the highest proportions of CD8+ T cell expressing all combination of cytokines (A–E) except for the CD8+ multifunctional T cells (G) and was more potent than at 200 µg for the increase of the proportions of CD8+TNF- $\alpha$  (B) and CD8+IFN- $\gamma$ - secreting T cells (C). The 100 µg chimera vaccine was also stronger than the F3 vaccine in CD8+TNF- $\alpha$ +IFN- $\gamma$  T cells and as potent as the F1 vaccine in induction of most types of CD8+cytokine secreting T cells (A,B,D,E).

the F1F3 200 µg vaccines. Except for the F1 vaccine, all formulations induced protection and decreased the lesion sizes in comparison to saline controls ( $p < 0.0351$  for all comparisons) (Figure 7A). Furthermore, the F1 + F3 vaccine and the chimeras were more efficacious than the F1 vaccine ( $p < 0.0500$ ) (Figure 7A) and equally potent until week 8 after infection. By the end of the experiment, on week 12, however, the strongest reduction in lesion sizes was determined by the combination of F1 + F3 domains and by the chimera, at the 100 and 200 µg dosages, which induced 80, 82, and 84% of protection, respectively (Figure 7A).

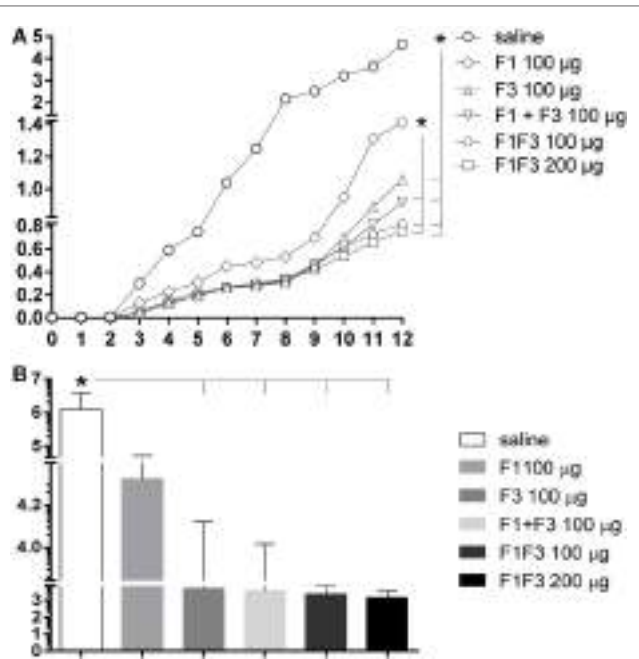
Additionally, the parasite load was evaluated after euthanasia by a limiting dilution assay on week 12 after infection (Figure 7B). While the saline controls exhibited 1,259,770 promastigotes, the chimera vaccines at 100 µg/dose decreased the parasite load to 2,423 ( $p < 0.0040$ ) and at 200 µg/dose, to 1,424 ( $p < 0.0062$ ). Our results indicate that the presentation of epitopes in tandem in a recombinant chimera exceeds the protection generated by the mixture of the recombinant domains F1 and F3. In fact, efficacies of 99.8 and 99.9% were achieved using the chimera at 100 and 200 µg/dose, respectively. The measures of footpad lesions at week 12 after infection and

the  $\log_{10}$  number of parasites in lesions were highly correlated ( $p < 0.001$ ,  $R = 0.5640$ ,  $R^2 = 0.3181$ ).

The increases in the antibody response were good surrogates for protection. In fact, we detected significant negative correlations between the increase of all antibody subtypes and the decrease of footpad lesion sizes and of the number of parasites. The IgG2a increase for instance was negatively correlated to the size of footpad lesions ( $p < 0.0001$ ,  $R = -0.6026$  before and  $p = 0.0029$ ,  $R = -0.4246$  after infection) and to the number of parasites in lesions ( $p = 0.0293$ ,  $R = -0.3147$  before and  $p = 0.0031$ ,  $R = -0.4177$  after infection).

Additionally, the IDR ( $p < 0.0001$ ,  $R = -0.7815$ ) and the frequencies of multifunctional CD4+ ( $p < 0.0500$ ,  $R = -0.2803$ ) and CD8+ T cells ( $p < 0.0001$ ,  $R = -0.7837$ ) expressing IL-2, TNF- $\alpha$ , and IFN- $\gamma$ , after infection, were strong correlates of prophylactic efficacy. In agreement to that, the number of parasites in lesions was also negatively correlated with the IDR ( $p = 0.0012$ ,  $R = -0.4531$ ) and the CD8 T cells expressing IL-2, TNF- $\alpha$ , and IFN- $\gamma$  ( $p = 0.0012$ ,  $R = -0.4531$ ).

We conclude that vaccination with the F1F3 chimera optimizes the cross-species vaccine efficacy against *L. amazonensis* infection above the levels reached by the admixed domains.



## CD4+ and CD8+ T-Cell Epitopes of the F1 and F3 Domains Exceed the Cellular Immune Response Generated by the Chimera

Toward the design of a potential synthetic vaccine, we further investigated which of the predicted F1 and F3 domains' T-cell epitopes target the optimized cellular immune response and induce *in vitro* T cell responses even stronger than the chimera.

The *in silico* prediction for CD4+ T cell epitopes performed before (17) mapped two sequences of CD4+ T cell epitopes of BALB/c mice in F1 (ELLAITTGVGNQ and DVAGIVGVPVAAGCT) and three more sequences in the F3 domain (FMLQILDFTKVE, FRYPRPKHCHTQVA, and KFWCLVIDALKRIG) (Table 1). Additionally, the highest scored CD8+ epitope (YPPEFKTKL) of the NH36 protein was identified in the F1 domain (17) (Table 1). We here compared the secretion

**TABLE 1 | IFN- $\gamma$ /IL-10 and TNF- $\alpha$ /IL-10 ratios secreted in response to the predicted synthetic epitopes of NH36.**

Amino acid location <sup>a</sup>	Predicted for	Domain	Sequences	IFN- $\gamma$ /IL-10	TNF- $\alpha$ /IL-10
0219-40	CD4	F1	ELLAITTGVGNQ	0.18	0.81
54-68	CD4	F1	DVAGIVGVPVAAGCT	0.14	0.59
92-100	CD8	F1	YPPEFKTKL	0.96	0.49
217-230	CD4	F3	FMLQILDFTKVE	0.64	0.60
278-291	CD4	F3	FRYPRPKHCHTQ	0.92	1.72
298-311	CD4	F3	KFWCLVIDALKRIG	0.29	1.00

<sup>a</sup>The *in silico* predicted epitopes for CD4+ and CD8+ lymphocytes of Balb/c mice were previously described by Nico et al. (17).

of cytokines induced by each one of these epitopes alone or mixed together, using the NH36 and F1F3 chimera antigens as controls, in mice vaccinated with the chimera, on week 11 after *L. amazonensis* challenge.

Actually, several epitopes induced higher cytokine secretion than the NH36 and their chimera cognate proteins in vaccinated mice and that their controls in saline treated mice. Among them, remarkably, the YPPEFKTKL epitope of F1 and the FMLQILDFTKVE epitope of the F3 domain promoted the highest levels of IFN- $\gamma$  (Figure 8A), and together with ELLAITTGVGNQ and DVAGIVGVPVAAGCT epitopes, also the strongest secretion of TNF- $\alpha$  (Figure 8B) and IL-10 (Figure 8C).

In contrast, the two other CD4+ predicted epitopes of F3, FRYPRPKHCHTQVA and KFWCLVIDALKRIG, induced a moderate but significant secretion of TNF- $\alpha$  (Figure 8B) and no secretion or poor levels of IL-10 (Figure 8C), respectively, when compared to the untreated saline controls.

These results suggested the induction of a mixed Th1/Th2 immunity in response to the FMLQILDFTKVE of F3, and the YPPEFKTKL, ELLAITTGVGNQ, and DVAGIVGVPVAAGCT predicted epitopes of the F1 domain. In contrast, the two final CD4 predicted epitopes of F3, FRYPRPKHCHTQVA and KFWCLVIDALKRIG generated a main Th1 response, with a predominant TNF- $\alpha$  production and low IL-10 secretion (Figure 8).

Calculation of the IFN- $\gamma$ /IL-10 and TNF- $\alpha$ /IL-10 secreted ratios confirmed the generation of the Th1 response (Table 1). In fact, the FRYPRPKHCHTQVA sequence of F3 induced an elevated IFN- $\gamma$ /IL-10 and the highest TNF- $\alpha$ /IL-10 ratio. The KFWCLVIDALKRIG epitope also generated a high TNF- $\alpha$ /IL-10 ratio, which was followed by the ELLAITTGVGNQ sequence. Interestingly, the YPPEFKTKL epitope also promoted a high IFN- $\gamma$ /IL-10 ratio (Table 1).

The multiparameter cytometry analysis disclosed that the FRYPRPKHCHTQVA epitope as the most potent enhancer of the CD4+-TNF- $\alpha$ , -IFN- $\gamma$ , -TNF- $\alpha$ -IL-2, -TNF- $\alpha$ -IFN- $\gamma$  and -IFN- $\gamma$ -IL-2 T cell proportions (Figure 9), confirming its capability of raising a specific Th1 response (Figures 8B,C). The YPPEFKTKL epitope was the second most important sequence which, although predicted as a CD8 epitope, also stimulated the increase of the proportions of CD4+ T cells producing TNF- $\alpha$ , IFN- $\gamma$ , IL-2-IFN- $\gamma$  and TNF- $\alpha$ -IFN- $\gamma$ , as much as the chimera did (Figure 9). Additionally, the multifunctional IL-2-TNF- $\alpha$ -IFN- $\gamma$ -secreting CD4+ T-cells were only raised in response to the

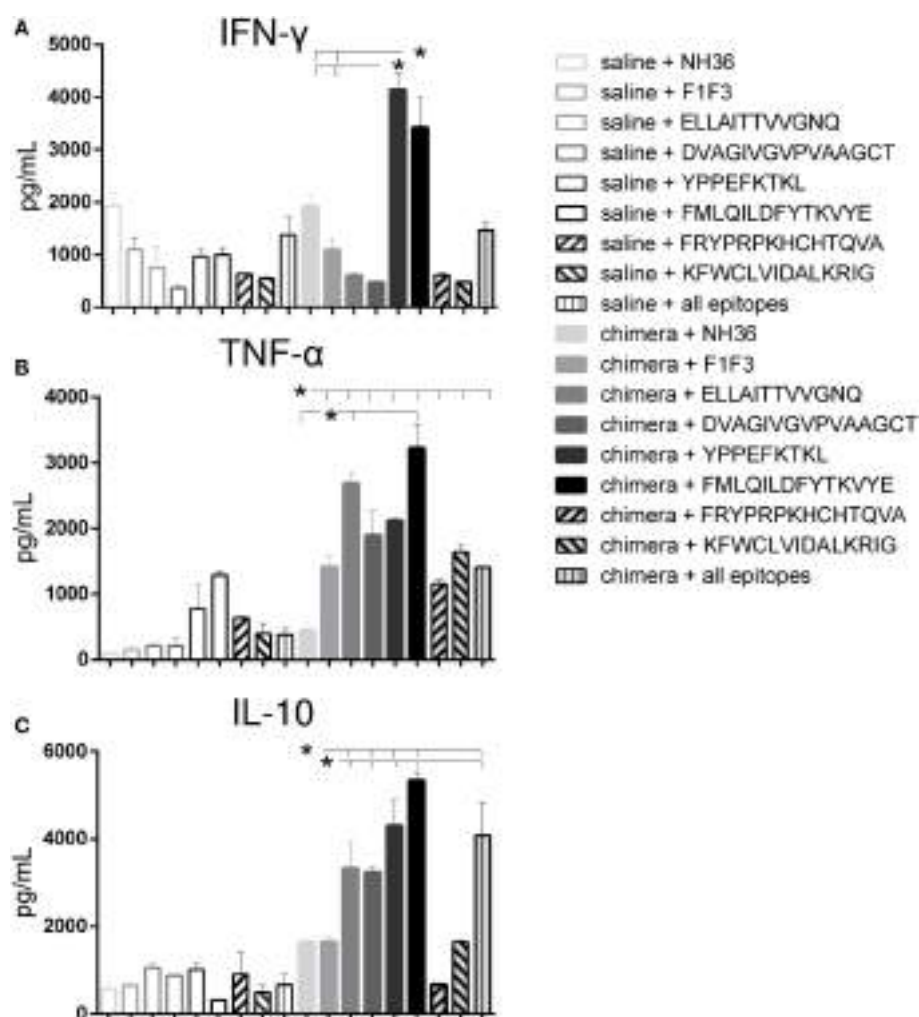


**FIGURE 8 |** The YPPEFKTKL and FMLQILDFTKVE epitopes promote the highest IFN- $\gamma$  and IL-10 levels, and together with DVAGIVGVPAAGCT and ELLAITTGVGNQ, the strongest TNF- $\alpha$  secretion of splenocytes of chimera-vaccinated mice. Splenocytes of mice vaccinated with 100  $\mu$ g of the chimera were incubated *in vitro* with 10  $\mu$ g/ml of NH36, F1F3 chimera, each one of the CD4 predicted epitopes of F1 (ELLAITTGVGNQ and DVAGIVGVPAAGCT) and F3 domains (FMLQILDFTKVE, FRYPRPKHCHTQVA, and KFWCLVIDALKRIG) and with the highest scored CD8 predicted epitope of the F1 protein (YPPEFKTKL), or with the mixture of all the epitopes, at week 11 after infection. Secretions of IFN- $\gamma$  (A), TNF- $\alpha$  (B), and IL-10 (C) were measured by an ELISA assay in the supernatants of splenocytes and expressed in picograms per milliliter. Data are means + SE of two independent experiments, each one with 8–10 animals per treatment. The YPPEFKTKL epitope of F1 and the FMLQILDFTKVE epitope of the F3 domain promoted the highest levels of IFN- $\gamma$  (A), and together with ELLAITTGVGNQ and DVAGIVGVPAAGCT epitopes, also the strongest secretion of TNF- $\alpha$  (B) and IL-10 (C). In contrast, the FRYPRPKHCHTQVA and KFWCLVIDALKRIG of F3 induced a moderate but significant secretion of TNF- $\alpha$  (B) and no secretion or poor levels of IL-10 (C).

FRYPRPKHCHTQVA, FMLQILDFTKVE, and the admixed epitopes. In contrast, no epitope increased the percent of CD4+ T cells secreting only IL-2 above the levels promoted by the chimera (**Figure 9**).

Regarding the cytotoxic response, YPPEFKTKL was the most potent epitope. Alone, it induced higher proportions of CD8+ T cells secreting IFN- $\gamma$  and IFN- $\gamma$  in combination with IL-2 than the chimera; together with DVAGIVGVPAAGCT and KFWCLVIDALKRIG, the highest frequencies of CD8+IL-2+ T cells and combined only with DVAGIVGVPAAGCT, the highest proportions of CD8+-TNF- $\alpha$ +-IFN- $\gamma$ + T cells. Furthermore, DVAGIVGVPAAGCT was the only epitope

to increase the frequencies of CD8+-TNF- $\alpha$ +-IL-2+ T cells (**Figure 10**). In contrast, the cytotoxic T cells secreting only TNF- $\alpha$  were increased in response to the ELLAITTGVGNQ and the FMLQILDFTKVE epitopes (**Figure 10**).

## DISCUSSION

NH36 is an important phylogenetic marker, highly conserved among the species of the *Leishmania* genus. Thus, it became a strong candidate antigen for the development of a bivalent cross-protective vaccine against both visceral and CL (17, 28, 29, 38). We previously demonstrated that the F3 protein of NH36 hosts

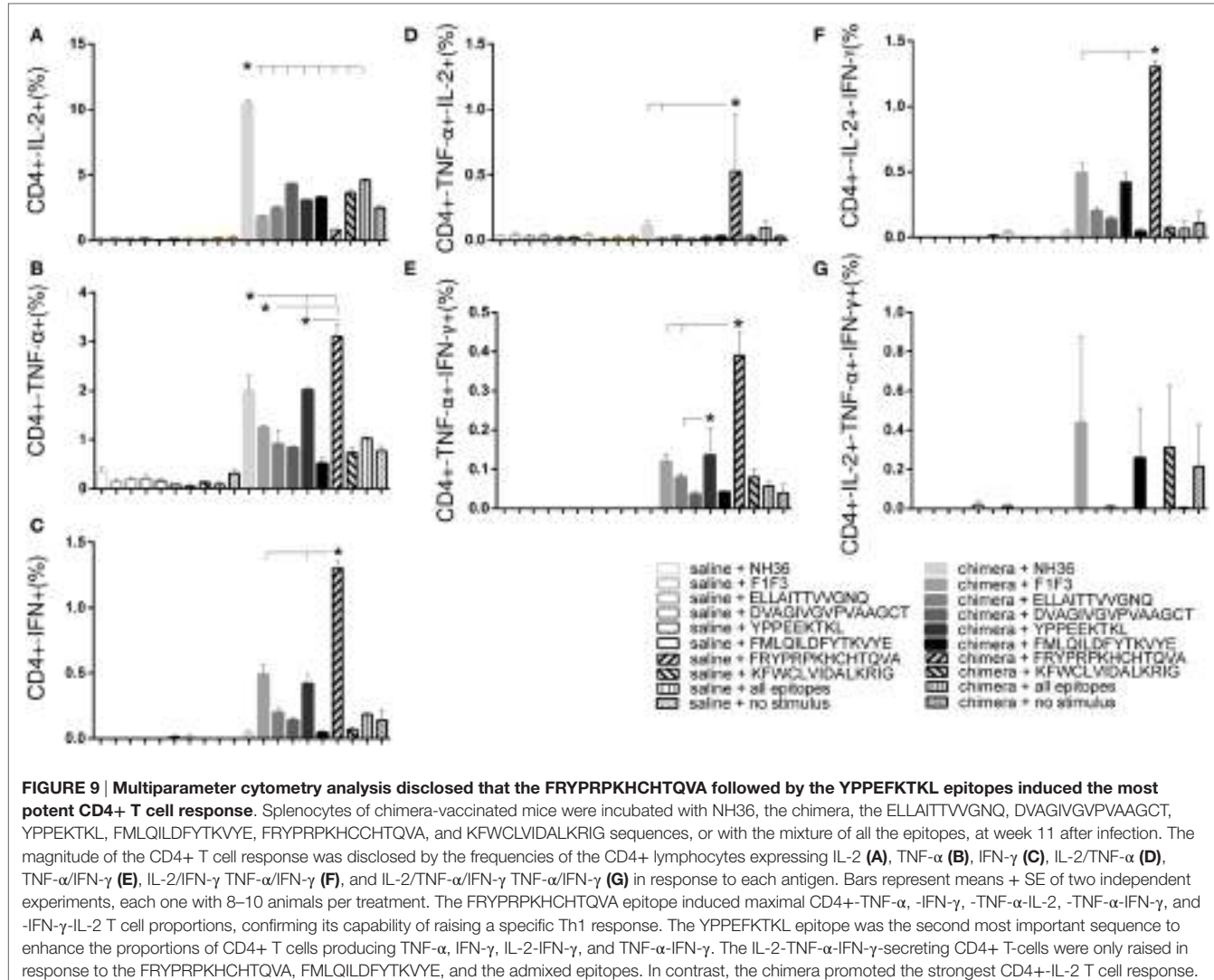


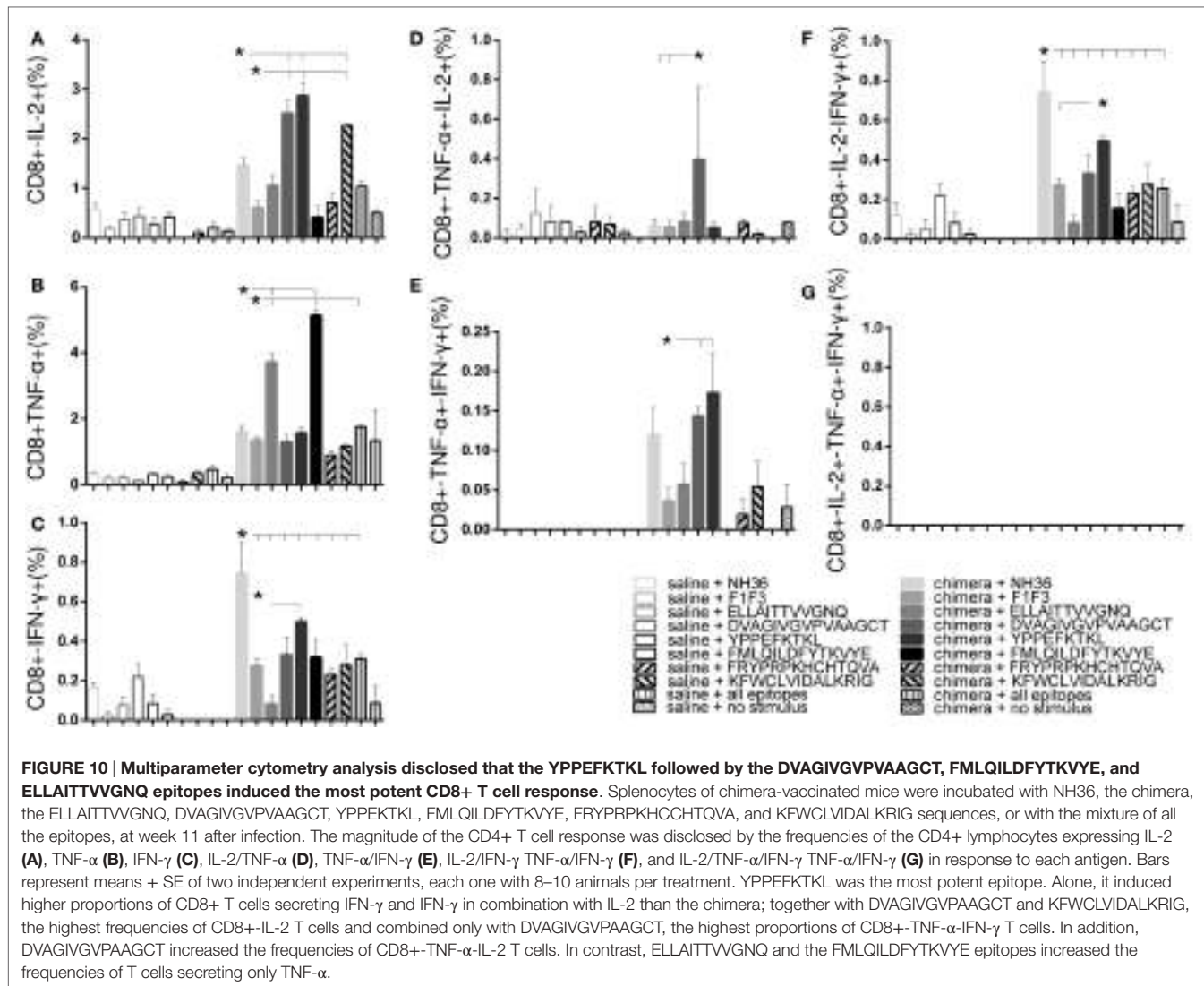
**FIGURE 9 | Multiparameter cytometry analysis disclosed that the FRYPRPKHCHTQVA followed by the YPPEFKTKL epitopes induced the most potent CD4+ T cell response.** Splenocytes of chimera-vaccinated mice were incubated with NH36, the chimera, the ELLAITTVGNQ, DVAGIVGVPAAGCT, YPPEEKTKL, FMLQILDFTKVYE, FRYPRPKHCHTQVA, and KFWCLVIDALKRIG sequences, or with the mixture of all the epitopes, at week 11 after infection. The magnitude of the CD4+ T cell response was disclosed by the frequencies of the CD4+ lymphocytes expressing IL-2 (A), TNF- $\alpha$  (B), IFN- $\gamma$  (C), IL-2/TNF- $\alpha$  (D), TNF- $\alpha$ /IFN- $\gamma$  (E), IL-2/IFN- $\gamma$  TNF- $\alpha$ /IFN- $\gamma$  (F), and IL-2-TNF- $\alpha$ -IFN- $\gamma$  TNF- $\alpha$ /IFN- $\gamma$  (G) in response to each antigen. Bars represent means + SE of two independent experiments, each one with 8–10 animals per treatment. The FRYPRPKHCHTQVA epitope induced maximal CD4+TNF- $\alpha$ , -IFN- $\gamma$ , -TNF- $\alpha$ -IL-2, -TNF- $\alpha$ -IFN- $\gamma$ , and -IFN- $\gamma$ -IL-2 T cell proportions, confirming its capability of raising a specific Th1 response. The YPPEFKTKL epitope was the second most important sequence to enhance the proportions of CD4+ T cells producing TNF- $\alpha$ , IFN- $\gamma$ , IL-2-IFN- $\gamma$ , and TNF- $\alpha$ -IFN- $\gamma$ . The IL-2-TNF- $\alpha$ -IFN- $\gamma$ -secreting CD4+ T-cells were only raised in response to the FRYPRPKHCHTQVA, FMLQILDFTKVYE, and the admixed epitopes. In contrast, the chimera promoted the strongest CD4+IL-2 T cell response.

the immunodominant CD4+ epitopes necessary for protection against *L. chagasi* (17) and *L. amazonensis* (17, 28) infections. Instead, the F1 protein codominance with F3, in protection against *L. amazonensis* infection, is mediated mostly by CD8+ epitopes (28). Accordingly, the highest scored epitope for CD8+ T cells, YPPEFKTKL, was identified in the sequence of the F1 protein (17). The finding of 93% sequence homology between the NH36 of *L. donovani* and the A34480 NH of *L. amazonensis* encouraged even more the idea of a NH-based bivalent vaccine against both leishmaniasis (28).

According to the philosophy of the T cell polytope vaccine development, efficacy increases using antigens that contain enriched proportions of the relevant epitopes (34, 35). Searching for the optimization of the vaccine efficacy against *L. amazonensis* infection, in this investigation, we used the F1 and F3 domains of NH36 through several approaches. First, we investigated if the simple mixture of F1 and F3 vaccines increased the efficacy above the levels induced by the F1 and F3 vaccines independently. Second, we asked if the presentation of F1 and F3 domains cloned

in tandem, as a chimera, was more efficacious than the presentation of the admixed proteins. Third, we assayed if the chimera-induced protection could be enhanced in a dose-response manner by doubling the vaccine concentration. Finally, we identified the most important epitopes for CD4+ and CD8+ T cells included in the chimera that could be combined in a future synthetic polytope vaccine capable to induce cross-protection to CL.

Confirming that the F3 and F1 domains contain the epitopes responsible for the NH36-induced immune protection, higher efficacy was obtained by vaccination with each one of these proteins rather than with the whole NH36 cognate protein (17, 28, 29, 33). Additionally, the cross-protective capabilities of the NH36 vaccines can be explained by the high identity of the sequences of predicted epitopes of the two *Leishmania* NHs (28). In fact, the CD4+ epitope ELLAITTVGNQ and the CD8+ epitope YPPEEKTKL of the F1 domain of NH36 (17) are completely conserved in the sequence of NH A34480 of *L. amazonensis* (28). Likewise, the DVAGIVGVPAAGCT epitope for CD4+ T cells of F1, and the three epitopes for CD4+



T cells of F3, FMLQILDFYTKVYE, FRYPRPKHCHTQVA, and KFWCLVIDALKRIG differ in only one amino acid (28).

Strong IgG1, IgG2a, and/or IgG2b anti-NH36 antibody responses were described after mice vaccination with the gene of NH36 (23, 24, 27), with the NH36 recombinant protein in combination with saponin (17, 28, 29), CPG and polyacrylate glycolide particles (39), and the GLA-SE adjuvant (40), or with the NH36 cloned with a sterol 24-C-methyl transferase (NS), and used with GLA-SE adjuvant (30). Furthermore, higher IgG2/IgG1 antibody ratios were also found after immunotherapy of *Leishmania infantum chagasi*-infected dogs with NH36-DNA (25). Additionally, human vaccination with NS determined a preferential increase in IgG1 and IgG3 subclasses, which are dependent of Th1-like cytokines (30).

Vaccination with F3, but not with F1, induced higher IgG2a antibody levels than NH36, in mice challenged with *L. chagasi* (17). In contrast, IgG2a, IgG1 antibody levels were similar in mice challenged with *L. amazonensis* (28, 29). Although protection against leishmaniasis depends more, on the cellular than on the humoral immune response, it is worth to note that these increased

antibody subtypes are strong surrogates predictive of protection (41), which indicate the decrease of parasite load (17, 28, 29) and that could also be the basis of the development of a transmission blocking vaccine (38, 42).

We previously identified in the F3 domain, the epitopes AVQKRVKEVGTAAFFML (202–219), VYEKERNTYATV (228–239), and FRYPRPKHCHTQVA (278–291), as the most relevant targets of the anti-NH36 antibody response in mice (17). Supporting our results, two B cell epitopes for dog and human antibodies were confirmed in the sequence of NH36 by other group (43). These epitopes, called peptide 17 and 18 (43), overlap with the sequences AVQKRVKEVGTAAFFML and NQTLEKVRNARLVADVAG that we previously described in the F3 and F1 domains, respectively (17). Interestingly, the peptide 17 diagnosed with 100% sensitivity canine and human VL (43). These results disclose the universal nature of the B cell epitopes of NH36.

We further demonstrated that the admixed F1 + F3 vaccine induced more IgG, IgG1, and IgG2a antibodies than the F3 or the F1 vaccines did independently, suggesting a potentiated

immunogenicity. However, the presentation of the domains cloned in tandem as the chimera was superior and exceeded the IgG and IgG2a response above the admixed domains showing an additional dose-response effect.

Our results demonstrate that the delivery of the F1 and F3 domains cloned in tandem, rather than as a simple mixture, increases the probabilities of a single antigen presenting cell to exhibit simultaneously both the CD8+ and CD4+ epitopes to lymphocytes, optimizing the immunogenicity. This might occur through cross-priming when MHC class II molecules can present both, exogenous molecules acquired by antigen presenting cells and endogenous degraded antigens (44, 45). Therefore, our results suggest that not only the composition of the epitopes and subunits is critical but also how the epitopes are exposed in the tridimensional structure of the vaccine antigen (46). In fact, only the tandem arrangement, but not the independent subunits containing an HIV epitope represented the most efficient immunogenic conformation (46). Another advantage of the presentation of the epitopes in a recombinant chimera is that it facilitates the scaling-up of the antigen, reducing the production yield time and cost, when large amounts of antigen for clinical phase III and IV assays are needed.

Regarding the generation of the cellular immune response, the F3 domain induced stronger IDR than the F1 protein in mice vaccinated against *L. chagasi* (17) and *L. amazonensis* (28, 29). In this investigation, we showed that the admixed antigens were even better than F3, but also, that the chimera induced the strongest IDR after infection and an increased a dose-response effect. Supporting our previous descriptions (17, 28, 29), the IDR was an important correlate of protection that increased along with the decrease of parasite load, indicating the generation of a robust cellular immune response against *L. amazonensis* optimized by vaccination with the chimera.

We confirmed here our previous results showing that mice vaccinated with F3 and challenged with *L. amazonensis* increase the IFN- $\gamma$  and TNF- $\alpha$  secretion but have a null IL-10 response (28, 29). Mice vaccinated with the F1 domain, on the other hand, secreted IFN- $\gamma$ , TNF- $\alpha$ , and IL-10, suggesting the simultaneous stimulation of T reg subsets and the presence of epitopes for Tregs along its sequence (28, 29). In this investigation, vaccination with the chimera induced a concomitant higher expression of IFN- $\gamma$  and IL-10 than the admixed domains, and a dose-response effect. This is remarkable considering that IL-10 has been shown to be related both to the pathology and the control of CL (47) and that IFN- $\gamma$  has also a dual role, as inducer of effector mechanisms and, conversely, as a mediator of inflammation and pathogenesis (48). Increased CD4+ T cell proportions secreting IFN- $\gamma$  with low proportions of CD4+-IL-4 T cells were also described in mice vaccinated with NH36 and challenged with *L. mexicana* (40).

We additionally demonstrated that the chimera vaccine at 100  $\mu$ g/dose induced the highest proportions of all types of CD4+ and CD8+ T cells secreting IL-2, TNF- $\alpha$ , or IFN- $\gamma$  alone, TNF- $\alpha$  in combination with IL-2 or IFN- $\gamma$ , and the highest percentage of CD4+ multifunctional cells secreting IL-2, TNF- $\alpha$ , and IFN- $\gamma$  simultaneously. In fact, the chimera optimized the induction of a CD4+ Th1 immune response by promoting the highest

proportions of CD4+ effector and long-term memory potential T cells, being the strongest vaccine at all the steps of the CD4 T cell differentiation (36). Thus, and confirming the *in silico* prediction (17) important epitopes for CD4+ T cells are present both in the F1 and F3 domains and their presentation in tandem, in the chimera, improve significantly their immunogenicity. This very desirable performance was observed also for the cytotoxic immune response. The highest proportions of all subtypes of CD8+-cytokine secreting T cells were observed in response to the chimera, except for the multifunctional cells. As detected for the CD4+ T cells, F1 was the second most important vaccine for the induction of the cytotoxic response while no enhancement was induced by the admixed antigens.

The immunotherapeutic effect induced by the F1 or F3 domains against *L. amazonensis* infection was predicted by the frequencies of the CD4+ and CD8+ T cells producing IL-2 or TNF- $\alpha$  or both (29). Total frequencies and frequencies of double-cytokine CD4 T cell producers were enhanced by F1 and F3 vaccines. In contrast to what described for prophylactic vaccination with the chimera, no increases in CD4+ multifunctional T cells were observed after immunotherapy with the independent domains (29). On the other, the F1 vaccine was codominant in prophylaxis with the chimera, for both CD4+ and CD8+ T cells (this investigation) and promoted the highest proportions of CD8+ multifunctional T cells when used for immunotherapy (29).

The reduction of parasite load and sizes of lesions confirmed the predictions of the immunological assays. Cross-protection to *L. amazonensis* infection was maximal (99.8–99.9%) in mice vaccinated with the chimera. As described before, and in spite of raising a strong CD4+ and CD8+ T cell immunogenic response, the F1 vaccine was less protective (17, 28).

We concluded that the chimera optimized the immune cross-protection against *L. amazonensis*, above the levels induced by the F1 and F3 domains either admixed or independently. Our results indicated the development of a Th1-immune response mediated by CD4+ T cell epitopes of the F3 and F1 domains, a cytotoxic response induced by F1 and the potential presence of T reg epitopes in the F1 domain determining also a potential regulatory response. The three arms of immunity increased by the presentation of the F1 and F3 epitopes in tandem in the F1F3 chimera.

Progressing toward the definition of a polytope vaccine, we were further able to identify the epitopes of NH36 responsible for the cross-protection against *L. amazonensis* infection. Confirming that they are the target of the immune response, some epitopes exceeded the levels of cytokine secretion induced by the chimera (33). The FMLQILDFYTKVYE and YPPEFKTKL sequences promoted, respectively, a 3.2- and 3.8-fold enhance in IFN- $\gamma$ , a 3.2- and 2.9-fold increase in IL-10, and a 2.3- and 1.5-fold augment of TNF- $\alpha$  secretion above the levels generated by the chimera.

Additionally, we further elucidated that the main Th1 response induced by the NH36 and the chimera was due to the FRYPRPKHCHTQVA epitope of F3, which generated elevated IFN- $\gamma$ /IL-10 and TNF- $\alpha$ /IL-10 ratios and the highest proportions of CD4+-TNF- $\alpha$ , -TNF- $\alpha$ -IL-2, -TNF- $\alpha$ -IFN- $\gamma$ , -IFN- $\gamma$ -IL-2, and multifunctional IL-2-TNF- $\alpha$ -IFN- $\gamma$  T cells.

The FRYPRPKHCHTQVA epitope might be the reason for the CD4+ Th1 TNF- $\alpha$ -mediated protection induced by F3 and previously detected against both visceral (17) and CL in mice [(this investigation) (28, 29)]. In fact, only the FRYPRPKHCHTQVA sequence determined a high CD4+ response with strong IFN- $\gamma$ , TNF- $\alpha$  secretion, and null IL-10 response, as already described for the F3 vaccine (17, 29).

Although first predicted as a CD8 epitope (17, 28), the YPPEFKTKL sequence of F1 also contributed to the CD4+ T cell response. In fact, it was the second most important CD4+ epitope, which stimulated a high IFN- $\gamma$ /IL-10 ratio and increased proportions of CD4+ T cells producing TNF- $\alpha$ , IFN- $\gamma$ , IL-2-IFN- $\gamma$ , and TNF- $\alpha$ -IFN- $\gamma$ . Additionally, the YPPEFKTKL and DVAGIVGVPAAGCT epitopes were the most important sequences inducing the CD8+ T cell response. Likewise, the ELLAITTVVGNQ and the FMLQILDFYTKVYE epitopes also induced elevated frequencies of CD8-TNF- $\alpha$  T cells, although they were predicted as CD4+ T cell epitopes of mice (17, 28). In agreement with that, the AFMLQILDF sequence was also predicted as a human epitope of CD8+ T cells binding the HLA-A\*2402 and HLA-B\*4402, HLA-A\*01 molecules (49).

We demonstrated that the YPPEFKTKL epitope capabilities of stimulating both the CD4+ and CD8+ T cell response, with intense production of pro-inflammatory cytokines, indicating its potential PAN epitope nature (50). YPPEFKTKL was the only predicted epitope for CD8+ T cells identified in the F1 domain (17) and because of that, it is probably the responsible for the CD8- T cell mediated vaccine protection against *L. amazonensis* infection, attributed to the F1 vaccine (28). The enhancement of the IL-10 secretion induced by the F1 vaccine [(this investigation) (28, 29)] and YPPEFKTKL indicate that this sequence might also be a T regulatory epitope, which deserves better characterization. Supporting its universality and biological relevance, the YPPEFKTKL sequence was also predicted with high scores for the binding of the human Class I HLA-A\*2402 and HLA-B\*0702 molecules, induced the IFN- $\gamma$  secretion by PBMC of asymptomatic, IDR positive human individuals infected with *L. infantum* and was found to be highly conserved in the NH sequence of all the studied *Leishmania* species (49).

For its multiple capabilities, the YPPEFKTKL epitope might be considered as a Pan epitope candidate (51–53). In fact, the sequence MDEPTLLYV was described as a PANDR epitope of the A15 hexon protein of adenovirus (52) while the synthetic more preferably PADRE peptide composition is aKXVAAWTLKAAA (54). In order to constitute a PADRE epitope, the peptide should contain defined amino acids in R1, R2, R3, R4, and R5 (54). Remarkably, and as expected for a PADRE sequence (54), the YPPEFKTKL contains Y as the R2 residue, four residues in R3, where three to five amino acids are needed, and the sequences KT followed by TKL in R4, while the expected combinations for R4 are KT, TLK, or WTLK (54). The adenovirus epitope contains TLL instead of TLK in the place of R4 (52).

YPPEFKTKL of *L. donovani* maintains identical sequence in the NHs of *L. infantum chagasi*, *L. infantum*, *L. amazonensis*, *L. major*, and *L. mexicana* (49). TKL is substituted with TNL in *L.*

*tropica* while the second residue of R2, P, is substituted by S in the NHs of *L. braziliensis* and *Leishmania panamensis*, both of the subgenus *Vianna* (49).

Another common feature of the NH36 epitopes to PADRE sequences is found in the KFWCLVIDALKRIG CD4+ predicted epitope of F3, which shares with the aKFVAAWTLKAAA of the PADRE sequence the first KF residues (54). This epitope induced a mild secretion of IFN- $\gamma$ , TNF- $\alpha$ , and IL-10 and increased frequencies of CD4+ multifunctional T cells.

In spite the intense research on development of anti-*Leishmania* vaccines in animals models (11, 55) only a few of them are the basis of potential synthetic or epitope vaccines. The kmp-11 (56), the amastigote A2 (57), and the polytope vaccine containing LPG-3, LmSTI-1, CPB, and CPC (58) present epitopes for the CD8+ T cells. On the other hand, the LACK158–173 peptide (59), the amastigote A2 antigen (57), and the MML-triple fusion *L. major* vaccine expressed in adenovirus (37) determined a Th1-biased CD4 T cell response.

In this investigation, we demonstrated that arrangement of the epitopes of the NH of *L. donovani* NH36 in tandem, in a chimera, improved the cross-protection to CL caused by *L. amazonensis*. We found that the chimera optimized the vaccine efficacy, probably by increasing the probabilities of cross-presentation as a strategy to enhance immunity (44, 45). We further advanced in the identification of the most relevant epitopes responsible for the immune responses generated by the subunit vaccines (17, 28, 29). We found potent epitopes for the generation of the CD4+-Th1, cytotoxic and potential T regulatory response and recognized among them at least one with PADRE capabilities (54). The data gathered in our work will help in the development of a polytope vaccine against visceral and CL, which will allow to fight the disease with enhanced efficacy.

## AUTHOR CONTRIBUTIONS

MA-S and DN conducted the experiments, MA-S, DN and AM acquired data, MA-S, DN, MP, and CP-d-S analyzed data. CP-d-S designed research studies. MA-S and CP-d-S prepared the figures. CP-d-S wrote the manuscript, and all authors have read and approved the final manuscript.

## ACKNOWLEDGMENTS

MA-S was a recipient of an MSc fellowship from Coordenação de Aperfeiçoamento de Pessoal de Nível Superior (CAPES), Brazil.

## FUNDING

This work was supported by Conselho Nacional de Desenvolvimento Científico e Tecnológico (CNPQ) fellowship 310977/2014-2 and grant 404400/2012-4 (to CP-d-S) and by Fundação Carlos Chagas Filho de Amparo à Pesquisa do Estado do Rio de Janeiro (FAPERJ) grants E-26-201.583/2014 and E-26/111.682/2013 (to CP-d-S) and fellowships E-26/102415/2010 and E-26/201747/2015 (to DN).

## SUPPLEMENTARY MATERIAL

The Supplementary Material for this article can be found online at <http://journal.frontiersin.org/article/10.3389/fimmu.2017.00100/full#supplementary-material>.

**FIGURE S1 | Monomer of *Leishmania donovani* nucleoside hydrolase (NH36).** (A) Illustration of the tridimensional structure of the NH36 monomer

was obtained by homology modeling to the sequence of the NH of *Leishmania major* template (RCSB PDB code: 1EZR; crystal structure of NH of *L. major*) with the sequences of the N-terminal (F1, amino acids 1–103 in lime green), central (F2, amino acids 104–198 in gray), and C-terminal (F3, amino acids 199–314 in cyan) moieties, using the Modeller 9.10 software. (B) MHC class II-IAd and IEd, haplotype H2d CD4+ T cell epitopes (dark blue) and of MHC class I Ld-CD8+ T cell predicted epitopes (red) of the C-terminal and N-terminal moieties. This illustration was modified from Nico et al. (29) and reproduced with authorization of the authors.

## REFERENCES

1. World Health Organization. *WHO Report on Global Surveillance of Epidemic-Prone Infectious Diseases – Leishmaniasis*. (2016). Available from: [http://www.who.int/csr/resources/publications/CSR\\_ISR\\_2000\\_1leish/en/](http://www.who.int/csr/resources/publications/CSR_ISR_2000_1leish/en/)
2. Alvar J, Vélez ID, Bern C, Herrero M, Desjeux P, Cano J, et al. Leishmaniasis worldwide and global estimates of its incidence. *PLoS One* (2012) 7(5):e35671. doi:10.1371/journal.pone.0035671
3. Da-Cruz AM, Bittar R, Mattos M, Oliveira-Neto MP, Nogueira R, Pinho-Ribeiro V, et al. T-cell-mediated immune responses in patients with cutaneous or mucosal leishmaniasis: long-term evaluation after therapy. *Clin Diagn Lab Immunol* (2002) 9(2):251–6.
4. Silveira FT, Lainson R, Corbett CE. Clinical and immunopathological spectrum of American cutaneous leishmaniasis with special reference to the disease in Amazonian Brazil: a review. *Mem Inst Oswaldo Cruz* (2004) 99(3):239–51. doi:10.1590/S0074-02762004000300001
5. Silveira FT, Lainson R, De Castro Gomes CM, Laurenti MD, Corbett CE. Immunopathogenic competences of *Leishmania* (*V.*) *braziliensis* and *L.* (*L.*) *amazonensis* in American cutaneous leishmaniasis. *Parasite Immunol* (2009) 31(8):423–31. doi:10.1111/j.1365-3024.2009.01116.x
6. Mendes Wanderley JL, Costa JF, Borges VM, Barcinski M. Subversion of immunity by *Leishmania amazonensis* parasites: possible role of phosphatidylserine as a main regulator. *J Parasitol Res* (2012) 2012:981686. doi:10.1155/2012/981686
7. França-Costa J, Van Weyenbergh J, Boaventura VS, Luz NF, Malta-Santos H, Oliveira MC, et al. Arginase I, polyamine, and prostaglandin E2 pathways suppress the inflammatory response and contribute to diffuse cutaneous leishmaniasis. *J Infect Dis* (2015) 211(3):426–35. doi:10.1093/infdis/jiu455
8. Mayrink W, Botelho AC, Magalhães PA, Batista SM, de Lima AO, Genaro O, et al. Immunotherapy, immunochemotherapy and chemotherapy for American cutaneous leishmaniasis treatment. *Rev Soc Bras Med Trop* (2006) 39(1):14–21. doi:10.1590/S0037-86822006000100003
9. Croft SL, Sundar S, Fairlamb AH. Drug resistance in leishmaniasis. *Clin Microbiol Rev* (2006) 19(1):111–26. doi:10.1128/CMR.19.1.111-126.2006
10. Perez-Franco JE, Cruz-Barrera ML, Robayo ML, Lopez MC, Daza CD, Bedoya A, et al. Clinical and parasitological features of patients with American cutaneous leishmaniasis that did not respond to treatment with meglumine antimoniate. *PLoS Negl Trop Dis* (2016) 10(5):e0004739. doi:10.1371/journal.pntd.0004739
11. Palatnik-de-Sousa CB. Vaccines for leishmaniasis in the fore coming 25 years. Review. *Vaccine* (2008) 26(14):1709–24. doi:10.1016/j.vaccine.2008.01.023
12. Palatnik-de-Sousa CB, Silva-Antunes I, de Morgado AA, Menz I, Palatnik M, Lavor C. Decrease of the incidence of human and canine visceral leishmaniasis after dog vaccination with Leishmune in Brazilian endemic areas. *Vaccine* (2009) 27(27):3505–12. doi:10.1016/j.vaccine.2009.03.045
13. Regina-Silva S, Feres AM, França-Silva JC, Dias ES, Michalsky ÉM, de Andrade HM, et al. Field randomized trial to evaluate the efficacy of the Leish-Tec® vaccine against canine visceral leishmaniasis in an endemic area of Brazil. *Vaccine* (2016) 34(19):2233–9. doi:10.1016/j.vaccine.2016.03.019
14. Starita C, Gavazza A, Lubas G. Hematological, biochemical, and serological findings in healthy canine blood donors after the administration of CaniLeish® vaccine. *Vet Med Int* (2016) 2016:4601893. doi:10.1155/2016/4601893
15. Lukes J, Mauricio IL, Schönian G, Dujardin JC, Soteriadou K, Dedet JP, et al. Evolutionary and geographical history of the *Leishmania donovani*
16. Mauricio IL, Yeo M, Baghaei M, Doto D, Pratlong F, Zemanova E, et al. Towards multilocus sequence typing of the *Leishmania donovani* complex: resolving genotypes and haplotypes for five polymorphic metabolic enzymes (ASAT, GPI, NH1, NH2, PGD). *Int J Parasitol* (2006) 36(7):757–69. doi:10.1016/j.ijpara.2006.03.006
17. Nico D, Claser C, Borja-Cabrera GP, Travassos LR, Palatnik M, Soares IS, et al. Adaptive immunity against *Leishmania* nucleoside hydrolase maps its c-terminal domain as the target of the CD4+ T cell-driven protective response. *PLoS Negl Trop Dis* (2010) 4(11):e866. doi:10.1371/journal.pntd.0000866
18. da Silva VO, Borja-Cabrera GP, Correia Pontes NN, de Souza EP, Luz KG, Palatnik M, et al. A phase III trial of efficacy of the FML-vaccine against canine kala-azar in an endemic area of Brazil (São Gonçalo do Amarante, RN). *Vaccine* (2000) 19(9–10):1082–92. doi:10.1016/S0264-410X(00)00339-X
19. Borja-Cabrera GP, Correia Pontes NN, da Silva VO, Paraguai de Souza E, Santos WR, Gomes EM, et al. Long lasting protection against canine kala-azar using the FML-QuilA saponin vaccine in an endemic area of Brazil (São Gonçalo do Amarante, RN). *Vaccine* (2002) 20(27–28):3277–84. doi:10.1016/S0264-410X(02)00294-3
20. Iovane E, Giabbai B, Muzzolini L, Matafora V, Fornili A, Minici C, et al. Structural basis for substrate specificity in group I nucleoside hydrolases. *Biochemistry* (2008) 47(15):4418–26. doi:10.1021/bi702448s
21. Versées W, Goeminne A, Berg M, Vandemeulebroucke A, Haemers A, Augustyn K, et al. Crystal structures of *T. vivax* nucleoside hydrolase in complex with new potent and specific inhibitors. *Biochim Biophys Acta* (2009) 1794(6):953–60. doi:10.1016/j.bbapap.2009.02.011
22. Paraguai de Souza E, Bernardo RR, Palatnik M, Palatnik de Sousa CB. Vaccination of Balb/c mice against experimental visceral leishmaniasis with the GP36 glycoprotein antigen of *Leishmania donovani*. *Vaccine* (2001) 19(23–24):3104–15. doi:10.1016/S0264-410X(01)00031-7
23. Aguilera-Be I, Zardo RS, Paraguai de Souza E, Borja-Cabrera GP, Rosado-Vallado M, Mut-Martin M, et al. Cross-protective efficacy of a prophylactic *Leishmania donovani* DNA vaccine against visceral and cutaneous murine leishmaniasis. *Infect Immun* (2005) 73(2):812–9. doi:10.1128/IAI.73.2.812-819.2005
24. Gamboa-León R, Paraguai de Souza E, Borja Cabrera GP, Santos FN, Miyashiro LM, Pinheiro RO, et al. Immunotherapy against visceral leishmaniasis with the nucleoside hydrolase-DNA vaccine of *L. donovani*. *Vaccine* (2007) 24(22):4863–73. doi:10.1016/j.vaccine.2006.03.005
25. Borja-Cabrera GP, Santos FB, Picillo E, Gravino E, Manna L, Palatnik de Sousa CB. Nucleoside hydrolase DNA vaccine against canine visceral leishmaniasis. *Proc Vaccinol* (2009) 1(1):104–9. doi:10.1016/j.provac.2009.07.019
26. Al-Wabel MA, Tonui WK, Cui L, Martin SK, Titus RG. Protection of susceptible BALB/c mice from challenge with *Leishmania major* by nucleoside hydrolase, a soluble exo-antigen of *Leishmania*. *Am J Trop Med Hyg* (2007) 77(6):1060–5.
27. Souza LOP, Palatnik de Sousa CB. The nucleoside hydrolase DNA vaccine VR1012NH36 in prophylactic vaccination against mice tegumental leishmaniasis. *Proc Vaccinol* (2009) 1(1):120–3. doi:10.1016/j.provac.2009.07.022
28. Nico D, Gomes DC, Alves-Silva MV, Freitas EO, Morrot A, Bahia D, et al. Cross-protective immunity to *Leishmania amazonensis* is mediated by CD4+ and CD8+ epitopes of *Leishmania donovani* nucleoside hydrolase terminal domains. *Front Immunol* (2014) 5:189. doi:10.3389/fimmu.2014.00189
29. Nico D, Gomes DC, Palatnik-de-Sousa I, Morrot A, Palatnik M, Palatnik-de-Sousa CB. *Leishmania donovani* nucleoside hydrolase terminal domains

- in cross-protective immunotherapy against *Leishmania amazonensis* murine infection. *Front Immunol* (2014) 5:273. doi:10.3389/fimmu.2014.00273
30. Coler RN, Duthie MS, Hofmeyer KA, Guderian J, Jayashankar L, Vergara J, et al. From mouse to man: safety, immunogenicity and efficacy of a candidate leishmaniasis vaccine LEISH-F3+GLA-SE. *Clin Transl Immunol* (2015) 4:e35. doi:10.1038/cti.2015.6
  31. Cui L, Rajasekariah GR, Martin SK. A nonspecific nucleoside hydrolase from *Leishmania donovani*: implications for purine salvage by the parasite. *Gene* (2001) 280(1–2):153–62. doi:10.1016/S0378-1119(01)00768-5
  32. NIH. *Blast-Basic Local Alignment Search Tool*. National Institute of Health (NIH) (2016). Available from: <http://blast.ncbi.nlm.nih.gov/Blast.cgi>
  33. Kao DJ, Hedges RS. Advantages of a synthetic peptide immunogen over a protein immunogen in the development of an anti-pilus vaccine for *Pseudomonas aeruginosa*. *Chem Biol Drug Res* (2009) 74:33–42. doi:10.1111/j.1747-0285.2009.00825
  34. Seyed N, Taheri T, Rafati S. Post-genomics and vaccine improvement for *Leishmania*. *Front Microbiol* (2016) 7:467. doi:10.3389/fmicb.2016.00467
  35. De Groot AS, Sbai H, Aubin CS, McMurry J, Martin W. Immuno-informatics: mining genomes for vaccine components. *Immunol Cell Biol* (2002) 80(3):255–69. doi:10.1046/j.1440-1711.2002.01092.x
  36. Seder RA, Darrah PA, Roederer M. T cell quality in memory and protection: implications for vaccine design. *Nat Rev* (2008) 8(4):247–58. doi:10.1038/nri2274
  37. Darrah PA, Patel DT, De Luca PM, Lindsay RWB, Davey DF, Flynn BG, et al. Multifunctional T<sub>H</sub>1 cells define a correlate of vaccine-mediated protection against *Leishmania major*. *Nat Med* (2007) 13(7):843–50. doi:10.1038/nm1592
  38. Palatnik de Sousa CB, de Barbosa AF, Oliveira SM, Nico D, Bernardo RR, Santos WR, et al. FML vaccine against canine visceral leishmaniasis: from second-generation to synthetic vaccine. *Expert Rev Vaccines* (2008) 7(6):833–51. doi:10.1586/14760584.7.6.833
  39. Hudspeth EM, Wang Q, Seid CA, Hammond M, Wei J, Liu Z, et al. Expression and purification of an engineered, yeast-expressed *Leishmania donovani* nucleoside hydrolase with immunogenic properties. *Hum Vaccin Immunother* (2016) 12(7):1707–20. doi:10.1080/21645515.2016.1139254
  40. McAtee CP, Seid CA, Hammond M, Hudspeth E, Keegan BP, Liu Z, et al. Expression, purification, immunogenicity and protective efficacy of a recombinant nucleoside hydrolase from *Leishmania donovani*, a vaccine candidate for preventing cutaneous leishmaniasis. *Protein Expr Purif* (2016) 130:129–36. doi:10.1016/j.pep.2016.10.008
  41. Plotkin SA. Vaccines: correlates of vaccine-induced immunity. *Clin Infect Dis* (2008) 47(3):401–9. doi:10.1086/589862
  42. Saraiva EM, de Figueiredo Barbosa A, Santos FN, Borja-Cabrera GP, Nico D, Souza LO, et al. The FML-vaccine (Leishmune) against canine visceral leishmaniasis: a transmission blocking vaccine. *Vaccine* (2006) 24(13):2423–31. doi:10.1016/j.vaccine.2005.11.061
  43. Costa MM, Penido M, dos Santos MS, Doro D, de Freitas E, Michalik MS, et al. Improved canine and human visceral leishmaniasis immuno-diagnosis using combinations of synthetic peptides in enzyme-linked immunosorbent assay. *PLoS Negl Trop Dis* (2012) 6(5):e1622. doi:10.1371/journal.pntd.0001622
  44. Leung CS. Endogenous antigen presentation of MHC class II epitopes through non-autophagic pathways. *Front Immunol* (2015) 6:464. doi:10.3389/fimmu.2015.00464
  45. Chow KV, Sutherland RM, Zhan Y, Lew AM. Heterogeneity, functional specialization and differentiation of monocyte-derived dendritic cells. *Immunol Cell Biol* (2016). doi:10.1038/icb.2016.104
  46. Sun Z, Zhu Y, Wang Q, Ye L, Dai Y, Su S, et al. An immunogen containing four tandem 10E8 epitope repeats with exposed key residues induces antibodies that neutralize HIV-1 and activates an ADCC reporter gene. *Emerg Microbes Infect* (2016) 5:e65. doi:10.1038/emi.2016.86
  47. Ji J, Masterson J, Sun J, Soong L. CD4 CD25 regulatory T cells restrain pathogenic responses during *Leishmania amazonensis* infection. *J Immunol* (2005) 174(11):7147–53. doi:10.4049/jimmunol.174.11.7147
  48. Carneiro MB, Lopes ME, Vaz LG, Sousa LM, dos Santos LM, de Souza CC, et al. IFN- $\gamma$ -dependent recruitment of CD4(+) T cells and macrophages contributes to pathogenesis during *Leishmania amazonensis* infection. *J Interferon Cytokine Res* (2015) 35(12):935–47. doi:10.1089/jir.2015.0043
  49. Santos ML, Nico D, Oliveira FA, Barreto AS, De Sousa IP, Carrillo E, et al. *Leishmania donovani*-nucleoside hydrolase (NH36) domains induce T-cell cytokine responses in human visceral leishmaniasis. *Front Immunol* (2017) 8:227. doi:10.3389/fimmu.2017.00227
  50. Haveman LM, Bierings M, Legger E, Klein MR, de Jager W, Otten HG, et al. Novel pan-DR-binding T cell epitopes of adenovirus induce pro-inflammatory cytokines and chemokines in healthy donors. *Int Immunopharmacol* (2006) 18(11):1521–9. doi:10.1016/j.intimm/dx1085
  51. Alexander J, Sidney J, Southwood S, Ruppert J, Oseroff C, Maewal A, et al. Development of high potency universal DR-restricted helper epitopes by modification of high affinity DR-blocking peptides. *Immunity* (1994) 1(9):751–61. doi:10.1016/S1074-7613(94)80017-0
  52. Ghaffari-Nazari H, Tavakkol-Afshari J, Jaafari MR, Tahaghoghi-Hajghorbani S, Masoumi E, Jalali SA. Improving multi-epitope long peptide vaccine potency by using a strategy that enhances CD4+ T help in BALB/c mice. *PLoS One* (2015) 10(11):e0142563. doi:10.1371/journal.pone.0142563
  53. El Bissati K, Chentoufi AA, Krishack PA, Zhou Y, Woods S, Dubey JP, et al. Adjuvanted multi-epitope vaccines protect HLA-A\*11:01 transgenic mice against *Toxoplasma gondii*. *JCI Insight* (2016) 1(15):e85955. doi:10.1172/jci.insight.85955
  54. Alexander JL, Defrees S, Sette A. *Induction of Immune Response against Desired Determinants*. US patent No WO 1997026784 A1 (1997).
  55. Kaye PM, Aebsicher T. Visceral leishmaniasis: immunology and prospects for a vaccine. *Clin Microbiol Infect* (2011) 17(10):1462–70. doi:10.1111/j.1469-0691.2011.03610.x
  56. Basu R, Roy S, Walden P. HLA class I-restricted T cell epitopes of the kinetoplastid membrane protein-11 presented by *Leishmania donovani*-infected human macrophages. *J Infect Dis* (2007) 195(9):1373–80. doi:10.1086/513439
  57. Fernandes AP, Coelho EA, Machado-Coelho GL, Grimaldi G Jr, Gazzinelli RT. Making an anti-amastigote vaccine for visceral leishmaniasis: rational, update and perspectives. *Curr Opin Microbiol* (2012) 15(4):476–85. doi:10.1016/j.mib.2012.05.002
  58. Seyed N, Taheri T, Vauchy C, Dosset M, Godet Y, Eslamifar A, et al. Immunogenicity evaluation of a rationally designed polytope construct encoding HLA-A\*0201 restricted epitopes derived from *Leishmania major* related proteins in HLA-A2/DR1 transgenic mice: steps toward polytope vaccine. *PLoS One* (2014) 9(10):e108848. doi:10.1371/journal.pone.0108848
  59. Kedzierska K, Curtis JM, Valkenburg SA, Hatton LA, Kiu H, Doherty PC, et al. Induction of protective CD4+ T cell-mediated immunity by a *Leishmania* peptide delivered in recombinant influenza viruses. *PLoS One* (2012) 7(3):e33161. doi:10.1371/journal.pone.0033161

**Conflict of Interest Statement:** DN, MP, and CP-d-S are inventors of the patent file PI1015788-3 (INPI Brazil). MA-S and AM declares no conflict of interest.

The reviewer LFL declared a shared affiliation, though no other collaboration, with the authors to the handling Editor, who ensured that the process nevertheless met the standards of a fair and objective review.

Copyright © 2017 Alves-Silva, Nico, Morrot, Palatnik and Palatnik-de-Sousa. This is an open-access article distributed under the terms of the Creative Commons Attribution License (CC BY). The use, distribution or reproduction in other forums is permitted, provided the original author(s) or licensor are credited and that the original publication in this journal is cited, in accordance with accepted academic practice. No use, distribution or reproduction is permitted which does not comply with these terms.



# ***Leishmania donovani* Nucleoside Hydrolase (NH36) Domains Induce T-Cell Cytokine Responses in Human Visceral Leishmaniasis**

**Micheli Luize Barbosa Santos<sup>1</sup>, Dirlei Nico<sup>2</sup>, Fabrícia Alvisi de Oliveira<sup>1</sup>, Aline Silva Barreto<sup>1</sup>, Iam Palatnik-de-Sousa<sup>3</sup>, Eugenia Carrillo<sup>4</sup>, Javier Moreno<sup>4</sup>, Paula Mello de Luca<sup>5</sup>, Alexandre Morrot<sup>6</sup>, Daniela Santoro Rosa<sup>7,8</sup>, Marcos Palatnik<sup>9</sup>, Cristiane Bani-Corrêa<sup>10</sup>, Roque Pacheco de Almeida<sup>1,7</sup> and Clarisa Beatriz Palatnik-de-Sousa<sup>2,7\*</sup>**

## OPEN ACCESS

### **Edited by:**

Jude Ezech Uzonna,  
University of Manitoba, Canada

### **Reviewed by:**

Ricardo Fujiwara,  
Universidade Federal de Minas  
Gerais, Brazil  
Nahid Ali,  
Indian Institute of Chemical Biology,  
India

### **\*Correspondence:**

Clarisa Beatriz Palatnik-de-Sousa  
immgcpa@micro.ufrj.br

### **Specialty section:**

This article was submitted to  
Vaccines and Molecular  
Therapeutics,  
a section of the journal  
*Frontiers in Immunology*

**Received:** 27 September 2016

**Accepted:** 16 February 2017

**Published:** 07 March 2017

### **Citation:**

Barbosa Santos ML, Nico D, de Oliveira FA, Barreto AS, Palatnik-de-Sousa I, Carrillo E, Moreno J, de Luca PM, Morrot A, Rosa DS, Palatnik M, Bani-Corrêa C, de Almeida RP and Palatnik-de-Sousa CB (2017) *Leishmania donovani* Nucleoside Hydrolase (NH36) Domains Induce T-Cell Cytokine Responses in Human Visceral Leishmaniasis. *Front. Immunol.* 8:227.  
doi: 10.3389/fimmu.2017.00227

<sup>1</sup>Laboratório de Biologia Molecular, Hospital Universitário, Departamento de Medicina, Universidade Federal de Sergipe (HU-UFS), Aracaju, Sergipe, Brazil, <sup>2</sup>Laboratório de Biologia e Bioquímica de Leishmania, Departamento de Microbiologia Geral, Instituto de Microbiologia Paulo de Góes, Universidade Federal do Rio de Janeiro (UFRJ), Rio de Janeiro, Rio de Janeiro, Brazil, <sup>3</sup>Laboratório de Biometrologia, Programa de Pós-Graduação em Metrologia, Pontifícia Universidade Católica do Rio de Janeiro, Rio de Janeiro, Rio de Janeiro, Brazil, <sup>4</sup>WHO Collaborating Centre for Leishmaniasis, Instituto de Salud Carlos III, Centro Nacional de Microbiología, Madrid, Comunidad de Madrid, Spain, <sup>5</sup>Laboratório de Imunoparasitologia, Instituto Oswaldo Cruz (IOC), Rio de Janeiro, Rio de Janeiro, Brazil, <sup>6</sup>Laboratório de Imunologia Integrada, Departamento de Imunologia, Instituto de Microbiologia Paulo de Góes, Universidade Federal do Rio de Janeiro (UFRJ), Rio de Janeiro, Rio de Janeiro, Brazil, <sup>7</sup>Faculdade de Medicina, Instituto de Investigação em Imunologia, Universidade de São Paulo (USP), São Paulo, Brazil, <sup>8</sup>Laboratório de Vacinas experimentais, Departamento de Microbiologia, Imunologia e Parasitologia, Universidade Federal de São Paulo (UNIFESP), São Paulo, São Paulo, Brazil, <sup>9</sup>Laboratório de Imunohematologia, Faculdade de Medicina, Hospital Universitário Clementino Fraga Filho, Universidade Federal do Rio de Janeiro (UFRJ), Rio de Janeiro, Rio de Janeiro, Brazil, <sup>10</sup>Departamento de Morfologia, Universidade Federal de Sergipe (HU-UFS), Aracaju, Sergipe, Brazil

Development of immunoprotection against visceral leishmaniasis (VL) focused on the identification of antigens capable of inducing a Th1 immune response. Alternatively, antigens targeting the CD8 and T-regulatory responses are also relevant in VL pathogenesis and worthy of being included in a preventive human vaccine. We assessed in active and cured patients and VL asymptomatic subjects the clinical signs and cytokine responses to the *Leishmania donovani* nucleoside hydrolase NH36 antigen and its N-(F1), central (F2) and C-terminal (F3) domains. As markers of VL resistance, the F2 induced the highest levels of IFN- $\gamma$ , IL-1 $\beta$ , and TNF- $\alpha$  and, together with F1, the strongest secretion of IL-17, IL-6, and IL-10 in DTH $^{+}$  and cured subjects. F2 also promoted the highest frequencies of CD3 $^{+}$ CD4 $^{+}$ IL-2 $^{+}$ TNF- $\alpha$  $^{-}$ IFN- $\gamma$  $^{-}$ , CD3 $^{+}$ CD4 $^{+}$ IL-2 $^{+}$ TNF- $\alpha$  $^{+}$ IFN- $\gamma$  $^{-}$ , CD3 $^{+}$ CD4 $^{+}$ IL-2 $^{+}$ TNF- $\alpha$  $^{-}$ IFN- $\gamma$  $^{+}$ , and CD3 $^{+}$ CD4 $^{+}$ IL-2 $^{+}$ TNF- $\alpha$  $^{+}$ IFN- $\gamma$  $^{+}$  T cells in cured and asymptomatic subjects. Consistent with this, the IFN- $\gamma$  increase was correlated with decreased spleen ( $R = -0.428$ ,  $P = 0.05$ ) and liver sizes ( $R = -0.428$ ,  $P = 0.05$ ) and with increased hematocrit counts ( $R = 0.532$ ,  $P = 0.015$ ) in response to F1 domain, and with increased hematocrit ( $R = 0.512$ ,  $P = 0.02$ ) and hemoglobin counts ( $R = 0.434$ ,  $P = 0.05$ ) in response to F2. Additionally, IL-17 increases were associated with decreased spleen and liver sizes in response to F1 ( $R = -0.595$ ,  $P = 0.005$ ) and F2 ( $R = -0.462$ ,  $P = 0.04$ ). Conversely, F1 and F3 increased the CD3 $^{+}$ CD8 $^{+}$ IL-2 $^{+}$ TNF- $\alpha$  $^{-}$ IFN- $\gamma$  $^{-}$ , CD3 $^{+}$ CD8 $^{+}$ IL-2 $^{+}$ TNF- $\alpha$  $^{+}$ IFN- $\gamma$  $^{-}$ , and CD3 $^{+}$ CD8 $^{+}$ IL-2 $^{+}$ TNF- $\alpha$  $^{+}$ IFN- $\gamma$  $^{+}$  T cell frequencies of VL patients correlated with increased spleen and liver sizes and decreased hemoglobin and hematocrit values.

Therefore, cure and acquired resistance to VL correlate with the CD4<sup>+</sup>-Th1 and Th-17 T-cell responses to F2 and F1 domains. Clinical VL outcomes, by contrast, correlate with CD8<sup>+</sup> T-cell responses against F3 and F1, potentially involved in control of the early infection. The *in silico*-predicted NH36 epitopes are conserved and bind to many HL-DR and HLA and B allotypes. No human vaccine against *Leishmania* is available thus far. In this investigation, we identified the NH36 domains and epitopes that induce CD4<sup>+</sup> and CD8<sup>+</sup> T cell responses, which could be used to potentiate a human universal T-epitope vaccine against leishmaniasis.

**Keywords:** human visceral leishmaniasis, nucleoside hydrolase, recombinant domains, T cell epitopes, epitope vaccine design, *Leishmania donovani*, *Leishmania infantum chagasi*

## INTRODUCTION

Visceral leishmaniasis (VL) is a severe chronic vector-borne protozoan disease. Approximately 400,000 new cases of VL and 30,000 deaths are reported annually (1), and the worldwide incidence is increasing due to co-infection with HIV and the expanded geographical range of the insect vector subsequent to global warming (2). The disease is caused by *Leishmania donovani* in India, Asia, and East Africa; by *Leishmania infantum chagasi* in America; and by *Leishmania infantum* in the Middle East, Central Asia, China, and the Mediterranean (2). Bangladesh, India, Nepal, Sudan, Ethiopia, and Brazil concentrate 90% of the VL worldwide incidence (2). Clinical findings of VL range from asymptomatic cases with self-resolving infection and an anti-*Leishmania* integral immune response to severe cases characterized by intermittent fever, malaise, weight loss, cachexia, hepatomegaly, splenomegaly, hypergammaglobulinemia, anemia, leukopenia, thrombocytopenia, strong suppression of the CD4<sup>+</sup> T-cell immune response, and death, if untreated (3). Chemotherapy is highly toxic, and the long-term use of this treatment can select for resistant parasites (4).

Asymptomatic subjects and cured individuals from endemic areas have an effective CD4<sup>+</sup>-Th1 immune response against *Leishmania* and are resistant to the disease on the basis of a positive *Leishmania*-specific delayed-type hypersensitivity (DTH<sup>+</sup>) skin test response (4–6). Delayed-type of hypersensitivity response (DTH) is mediated by the Th1 subset of CD4<sup>+</sup> cells (7) and lost during severe VL (4–6). Identification of the antigens and HLA-restricted epitopes correlating with the natural resistance and cure of VL, and of the epitopes recognized during the severe disease is necessary to guide the development of a rational vaccine and to understand the precise immune mechanisms required for controlling parasite growth (4, 5).

Visceral leishmaniasis is associated with polarization to a Th2 immune response with increased production of IL-10 and TGF- $\beta$  (8) and depletion of the Th1 cytokines IFN- $\gamma$ , TNF- $\alpha$ , IL-2, and IL-12 produced by PBMCs in response to leishmanial lysates (4, 8, 9). The development of successful protection or resistance to VL requires, the generation of potent and durable Th1 parasite-specific memory responses, characterized by the production of IFN- $\gamma$ , IL-2, and TNF- $\alpha$  by multifunctional CD4<sup>+</sup> T cells (4, 10–13). Additionally, the assessment of the balance between immunoregulatory mechanisms, including pro-inflammatory

IFN- $\gamma$  and TNF- $\alpha$ , and the secretion of IL-17 and the regulatory cytokine IL-10 (4, 8) is required. Furthermore, CD8 T cells were also recently described, as contributing to the cure or pathology of VL (8, 14).

Many *Leishmania* antigens have been tried as potential vaccine candidates with varied immune responses and diverse species-specific protection (14–16). Leishmune® is the first licensed second-generation vaccine against VL. It is composed of the FML glycoproteic antigen of *L. donovani* and saponin (17–19). Its recent use has already resulted in the reduction of the incidence of dog and human VL in Brazil (20). The nucleoside hydrolase of *L. donovani* (NH36) is the Leishmune® main antigen and one of the promising candidates for vaccination against VL (17). Notably, NH36 is a vital enzyme of *Leishmania* that releases purines or pyrimidines from foreign DNA to be used in the synthesis of parasite DNA. Because it is absent from mammalian cells, it is a good target for differential chemotherapy (21, 22).

Vaccination with recombinant NH36 protein or DNA, protected mice from *L. donovani* (23), *Leishmania major* (24), *L. infantum chagasi* (25, 26), *L. mexicana* (25), and *Leishmania amazonensis* (12, 13) infections and also protected dogs infected with *L. infantum chagasi* through a Th1 immune response mediated by IFN- $\gamma$ -producing CD4<sup>+</sup> T cells (27). After vaccination with the recombinant NH36 in the mouse model, we described the achievement of 88% prophylactic protection (26) and 91% cure of VL (28), and 65–81% cure of cutaneous leishmaniasis (CL) (13).

NH36 is a strong phylogenetic marker of the *Leishmania* genus (11, 13, 29) that mediates high levels of vaccine cross-protection. In fact, the amino acid sequence of *L. donovani* NH36 shows high identity with the NH sequences of *L. major* (95–96%) (11, 30), *L. mexicana* (93%), *L. infantum chagasi* (99%), *L. infantum* (99%), *Leishmania tropica* (97%), *Leishmania braziliensis* (84%) (31), and *L. amazonensis* (93%) (12).

Our objective was to determine the major epitopes that contribute to protective responses, and this was done directly from the whole NH36 molecule. In fact, the *in silico* prediction disclosed the epitopes of NH36 for mice (12, 26) and human histocompatibility complex molecules (this investigation). However, although this information would allow the direct design of a synthetic epitope vaccine, the results of the immunological assays *in vivo* not always confirm the *in silico* predictions (32), and the synthetic epitopes alone are not enough immunogenic to be used as vaccine candidate antigens (14). Our strategy then

was to identify through immunological assays the presence of the important epitopes in shorter sequences of the NH36 antigen that would be, therefore, more potent than the whole cognate protein and more immunogenic than the isolated epitopes.

Knowing that NH36 was a vital parasite enzyme (33, 34), a conserved molecule of the *Leishmania* genus (29), and an important antigen (35), we designed three subunit vaccines that would cover the whole sequence of NH36. Since NH36 has 314 amino acids, we subcloned and obtained its N-terminal (F1) domain (amino acids 1–103), the central (F2) domain (amino acids 104–198), and the C-terminal (F3) domain (amino acids 199–314) (26). We first vaccinated mice with NH36 and used these domains to stimulate the splenocyte secretion of IFN- $\gamma$  and TNF- $\alpha$  (36). Furthermore, we vaccinated mice with each one of the three domains and studied the cytokine secretion and intracellular staining in response to NH36, the DTH, and the reduction of parasite load after infection with *L. infantum chagasi* (26). In both studies, F1 and F3 domains induced the strongest immune response (26, 36). However, mouse protection against *L. infantum chagasi* challenge was mediated by a CD4 $^{+}$  Th1 response directed only against F3 and was higher (88%) than that generated by the NH36 protein (68%) (26). The increases in DTH and in ratios of TNF- $\alpha$ /IL-10 CD4 $^{+}$ -producing cells were the strong correlates of this protection, which was confirmed by *in vivo* depletion with monoclonal antibodies (26). In agreement, the *in silico* prediction identified three MHC class II-restricted epitopes in the F3 domain (26). On the other hand, prevention (12) and cure (13) of *L. amazonensis* infection in mice were determined also by a CD4 $^{+}$  T-cell-driven response to F3 but with an additional CD8 $^{+}$  T-cell response directed to the F1 domain. Coincidentally, one highly scored epitope for MHC class I-restricted molecules was detected in the sequence of F1 (12, 26). In the meantime, the predictions of one MHC class II- and two MHC class I-restricted epitopes in the F2 domain were not confirmed by any immunologic or parasitological assay developed in the mice models of VL or CL (12, 13, 26). Our results then confirmed that both, the *in silico* predictions and the *in vivo* immunological assays, are needed to improve the definition of a T-cell epitope vaccine (32).

To this point, however, the NH36 epitopes recognized by the human major histocompatibility class I and II complexes (HLAs) were not yet described. In this investigation, we aimed to identify the main domains and epitopes of NH36 to be included in a future vaccine against human VL. For that purpose, we evaluated the clinical outcomes of VL patients, cured subjects, and asymptomatic individuals of a Brazilian endemic area and assessed their correlations with cytokine expression, and with the induction of CD3 $^{+}$ CD4 $^{+}$  and CD3 $^{+}$ CD8 $^{+}$  multifunctional T cells, in response to the defined domains of NH36. We used these correlations as tools for identification of the domains of NH36 responsible for the cellular immune responses generated during resistance and progression of the disease. We were able to demonstrate the generation of Th1 and Th17 cells and regulatory cytokines, as well as a CD3 $^{+}$ CD4 $^{+}$  Th1 multifunctional T-cell response, in cured and asymptomatic subjects. We additionally disclosed the generation of a CD3 $^{+}$ CD8 $^{+}$  multifunctional T-cell response in VL patients. Finally, we identified the most immunodominant epitopes of *L. donovani* NH36 for the generation of CD4 and CD8 T cell immune

responses in individuals infected with *L. infantum chagasi*. A rationale combination of the domains or epitopes that enhance both arms of T-cell immunity will contribute to the development of a universal protective or therapeutic vaccine against human VL and to the understanding of VL pathology.

## MATERIALS AND METHODS

### Ethics

The protocols were performed according to the guidelines and regulations of the Brazilian National Council of Health resolution 196/96 (CAAE 0162.0.107.000-09). The protocols were performed according to the guidelines and regulations of the Brazilian National Council of Health resolution 196/96 (CAAE 0162.0.107.000-09) and were approved by the Research Ethics Committee of the Universidade Federal de Sergipe. The objectives of the study were explained to all invited participants who gave written informed consent in accordance to the Declaration of Helsinki. Participants were explained about the low risks of the procedures. Only small samples of venous blood were collected from them, and no invasive procedure was performed.

### Patients

This study was performed with patients who were admitted to the UFS University Hospital, SE, Brazil, between March 2013 and March 2015. They were clinically diagnosed with VL based on fever, weight loss, anemia, spleen and liver enlargement, pancytopenia, hypergammaglobulinemia, positive culture in NNN media (Sigma-Aldrich), and positive serum reactivity to the rK39 antigen (KalazarDetect® Rapid Test, INBIOS International Inc., Seattle, WA, USA). Pregnant women, patients receiving immunosuppressive treatments, and those with diabetes or HIV or HTLV-1 co-infections were excluded. Cure was monitored 180 days after therapy with Glucantime®. Household contacts or patient relatives with no signs of disease were recruited and skin-tested for DTH with *Leishmania* promastigote lysate kindly provided by Centro de Produção e Pesquisa de Imunobiológicos (CPPI, Paraná, Brazil). Indurations of diameters  $\geq 5$  mm, detectable at 48 h after antigen injection, were considered positive. Hematological, hematocrit, and hemoglobin evaluation of patients and DTH $^{+}$  subjects was performed. Increases in the spleen and liver sizes were measured in centimeters, below the ribs' lower edge. Healthy subjects from the endemic area were included as negative controls. A total of 67 individuals were included in this study: 16 healthy controls, 14 patients with active VL, 17 cured patients, and 20 asymptomatic DTH $^{+}$  subjects. The group of untreated patients was increased to 41 individuals in order to establish the correlations between the increases of spleen and liver sizes.

### Recombinant Antigens and Epitopes

NH36 [EMBL, Genbank, and DDJB databases, access number AY007193 GENBANK (AY007193 and AAG02281.1 access codes) and in SWISS-PROT (Q8WQX2 UNi-Prot access code)] and its N-terminal (F1, amino acids 1–103), central (F2, amino acids 104–198), and C-terminal (F3, amino acids 199–314) domains were cloned in *E. coli* (26), expressed, and purified as modified

from the methods of Rodrigues et al. (37) and Saini et al. (38). Briefly, protein expression was induced in bacterial suspensions with 1 mM IPTG, for 4 h at 37°C. The cells were sonicated, and the insoluble pellets were washed twice with 10 mM Tris-HCl pH 8.0 and 0.5% CHAPS and further treated for 2 h at 37°C, under agitation, with a solubilization buffer composed of 20 mM Tris-HCl pH 8.0, 500 mM NaCl, 10% glycerol, and 8 M urea. Then, the suspension was homogenized by successive passages through 20-ml syringes with 1.2 mm × 40 mm needles followed by centrifugation, for 30 min at 14,000 rpm. The supernatant was loaded on a Ni-NTA chromatography column previously equilibrated with solubilization buffer. After sample application, the column was washed with three volumes of solubilization buffer containing 20 mM imidazole. Next, the column was washed with three volumes of the same buffer containing 5 mM reduced glutathione, 0.1% Triton X-100, and each one of the decreasing concentrations of a urea gradient (6–1 M), and buffer with no urea added for refolding. Elution of the proteins was achieved using 250 mM imidazole in refolding buffer without urea and confirmed by protein assay and 15% SDS-PAGE. The proteins were finally dialyzed against 50 mM Tris-HCl, pH 8, 50 mM NaCl, 50% glycerol, and 0.1 mM DTT and the absence of LPS was confirmed using the LAL QCL-1000 kit (Lonza). The purification process yielded 1 mg protein antigen per liter of bacterial culture. The homology between the sequence of *L. donovani* NH36 (GenBank: AAG02281.1) and *Leishmania infantum chagasi* NH (Lch-NH) (GenBank: AAS48353.1) was determined using NIH-NCBI Standard Protein BLAST software. A molecular model was obtained by homology modeling using the Modeller 9.10 software and data for the nucleoside hydrolase from a *L. major* template (RCSB PDB code: 1EZR; crystal structure of nucleoside hydrolase of *L. major*) (39).

For control purposes, in order to further demonstrate that NH36 is a component of SLA, we also assayed if sera of mice vaccinated with three doses of 100 µg of either NH36, F1, F2, or F3 recombinant antigens formulated with 100 µg saponin, with a weekly interval, recognized the SLA of *L. infantum chagasi* (2 µg/well) in a standard ELISA assay using peroxidase-conjugated protein A (26).

HLA-DR-binding CD4 epitopes were mapped with the TEPIPOPE program. CD8 epitopes were identified using SYFPEITHI software. The predicted epitopes were synthetized by GenScript (NJ, USA). The analysis of the identity of the epitopes in the different leishmanial species was performed using the sequences of nucleoside hydrolase of *Leishmania* species of PubMed Protein Databank and the sequence of *L. amazonensis* NH A34480 (12).

## Cytokine Secretion

PBMCs were obtained from heparinized vein blood using a standard Ficoll-Hypaque procedure, washed twice with RPMI 1640 and counted microscopically with Trypan Blue. The cells were plated ( $2 \times 10^5$ /well) and stimulated with 10 µg/ml of NH36, F1, F2, and F3, stationary phase *L. donovani* promastigote lysate or with no addition for 72 h at 30°C and 5% CO<sub>2</sub>. The secretion of IFN-γ, TNF-α, IL-1β, IL-4, IL-6, IL-12p70, IL-10, and IL-17 into the supernatants was evaluated with a Multiplex® MAP-Luminex

MAP® kit and analyzed using Milliplex Analyst 5.1 software (Merck Millipore, Billerica, MA, USA), according to the manufacturer's instructions. The sensitivity of the assay was established with a range of 8–15,000 pg/ml recombinant cytokines. We further assessed the IFN-γ secretion by PBMC of asymptomatic subjects in response to the synthetic predicted epitopes using the Invitrogen™ NOVEX™ IFN-γ Human Ultrasensitive Magnetic Bead kit (USA).

## Intracellular Cytokine Staining

PBMCs ( $2 \times 10^6$ /well) were *in vitro* cultured in 96-well/plates with 10 µg/ml of NH36, F1, F2, and F3, stationary phase *L. donovani* promastigote lysate or with no addition, for 6 h, followed by the addition of Brefeldin A (GolgiPlus, BD Biosciences, Franklin Lakes, NJ, USA), and further incubation for 12 h. The plates were centrifuged at 1,430 rpm for 5 min at 4°C, washed with PBS, and blocked with 2% fetal goat and 2% fetal bovine calf sera. The cells were further stained for surface markers with V500 mouse anti-human CD3 clone UCHT1 (RUO), FITC mouse anti-human CD4 clone RPA-T4 (RUO), and PE-Cy5 mouse anti-human CD8 clone RPA-T8 (RUO) monoclonal antibodies (BD Biosciences Pharmingen, San Diego, CA, USA), washed with PBS, and fixed and permeabilized with the Cytofix/Cytoperm mixture (BD Biosciences, Pharmingen, San Diego, CA, USA) for 20 min. The cells were then stained for the intracellular expression of cytokines with anti-IL-2-BV421 (clone 5344.111), anti-TNF-α-PE (clone Mab 11), and anti-IFN-γ-PE-Cy7 (clone B27) antibodies (BD Biosciences Pharmingen), washed with Perm Wash buffer (BD Biosciences Pharmingen), and resuspended in PBS. A minimum of 30,000 events were acquired on a BD FACSCanto II™ flow cytometer and analyzed using FlowJo software (Tree Star Inc., Ashland, OR, USA). All T cell frequencies were recorded after background subtraction of cells incubated without antigen.

For multiparameter cytometry analysis, the gated single-cell lymphocyte population was additionally gated for CD3 expression and subsequently for CD4 or CD8 expression. Production of each cytokine (IL-2, TNF-α, and IFN-γ) were analyzed individually inside CD3<sup>+</sup>CD4<sup>+</sup> or CD3<sup>+</sup>CD8<sup>+</sup> T cells gate. Boolean gating was used to generate combinations of cytokine expression and types of lymphocytes in order to identify lymphocytes expressing one cytokine or any combination of two cytokines or three cytokines (Figure S5 in Supplementary Material).

## Statistical Analysis

Kruskal-Wallis and Mann-Whitney tests were used for means comparison, and Spearman's two-tailed correlation test was used for correlation analysis using GraphPad Prism 6.03 software. All experiments were performed at least twice, and the indicated error bars are based on the SEM.

## RESULTS

### Clinical Outcomes of VL Patients

Clinical examination and laboratory exams of patients before treatment revealed the typical sign of VL: hepatomegaly, splenomegaly, leukopenia, neutropenia, eosinopenia, lymphopenia,

monocytopenia, thrombocytopenia, and decreased hematocrit and hemoglobin levels (**Table 1**). Conversely and as expected for their natural resistance status to infection, all outcomes remained at normal levels in DTH<sup>+</sup> asymptomatic subjects and in cured subjects, except for eosinophils, monocytes, and platelets.

## Expression and Purification of NH36 and Its Domains

Each bacterial clone codifying for the sequences of the recombinant NH36 and its F1, F2, and F3 domains was cultured into 2 l of bacterial culture media and induced for expression with IPTG. Conditions of expression and purification of the antigens are summarized in Figure S1A in Supplementary Material. The yield of each expression batch was 4.62 mg for NH36, 5.00 mg for F1, 3.5 mg for F2, and 3.75 mg for F3. The antigens were maintained at -80°C until use. A standardization study proved that the protein concentration was preserved at -80°C until at least 24 months after purification. SDS-PAGE analysis disclosed that the expressed proteins showed their expected molecular weights: 34,238.6 Da for NH36, 10,845.5 Da for F1, 10,327.9 Da for F2, and 13,101.1 Da for F3 (Figure S1B in Supplementary Material).

## Cytokine Secretion in Response to NH36 Domains

We investigated which NH36 domains target the cellular immune response. The secretion of most cytokines was enhanced in cured and DTH<sup>+</sup> subjects above the levels detected in patients before treatment, except for IL12p70 (**Figure 1**). Additionally, the secretion of IFN-γ, IL-17, and IL-10 was lower in patients before treatment than in healthy controls of endemic areas.

We observed discrete, but significant, differences between the immunogenicity of NH36 domains. The F2 peptide alone induced the highest levels of IFN-γ, IL-1β, and TNF-α. Furthermore, F1

and F2 domains together promoted the strongest secretion of IL-17, IL-6, and IL-10 in DTH<sup>+</sup> and cured subjects (**Figure 1**). Noteworthy, SLA induced lower levels of IL-1β and IL-10 than F1 and F2 domains (**Figure 1**). F2 was also the predominant domain that secreted higher levels of IL12p70 than SLA, but in patients before treatment. Conversely, IL-4 secretion was promoted only by SLA in cured and DTH<sup>+</sup> individuals (**Figure 1**). We also show that serum antibodies of mice vaccinated with NH36, F1, F2, or F3 domains and saponin recognize the SLA antigen of *L. infantum chagasi* in an ELISA assay, indicating that NH36 is an antigenic component of SLA (Figure S2 in Supplementary Material).

We further investigated if this Th1 response correlates with the natural resistance to VL. In fact, the IFN-γ increase in response to F1, and the secretion of IL-17 in response to F1 and F2, strongly correlates with the decreases of spleen and liver sizes, which are signals of resistance to *Leishmania* infection (**Table 2**; Figure S3 in Supplementary Material). The increases in liver and spleen sizes are highly correlated ( $R = 0.796, P < 0.0001$ ) (Figure S4 in Supplementary Material).

Furthermore, the increase of IFN-γ secretion in response to F1 and F2 domains correlates with the increase of hematocrit and, in response to the F2 peptide, also correlates with the increment in Hg concentration (**Table 2**; Figure S4 in Supplementary Material). Likewise, IL-17 secretion in response to F1 correlated with the increase in monocyte counts and Hg concentration (**Table 2**; Figure S4 in Supplementary Material). Increases in hematocrit, hemoglobin concentration and monocyte counts are markers of resistance and cure of VL.

We found also significant correlations between the IL-17 and IL-6 secretions promoted by NH36 and the decreases in spleen and liver weights (**Table 2**). Also, the increases in monocyte counts and IL-6 secretion in response to NH36 were correlated.

## Intracellular Expression of Cytokines in Response to NH36 Domains

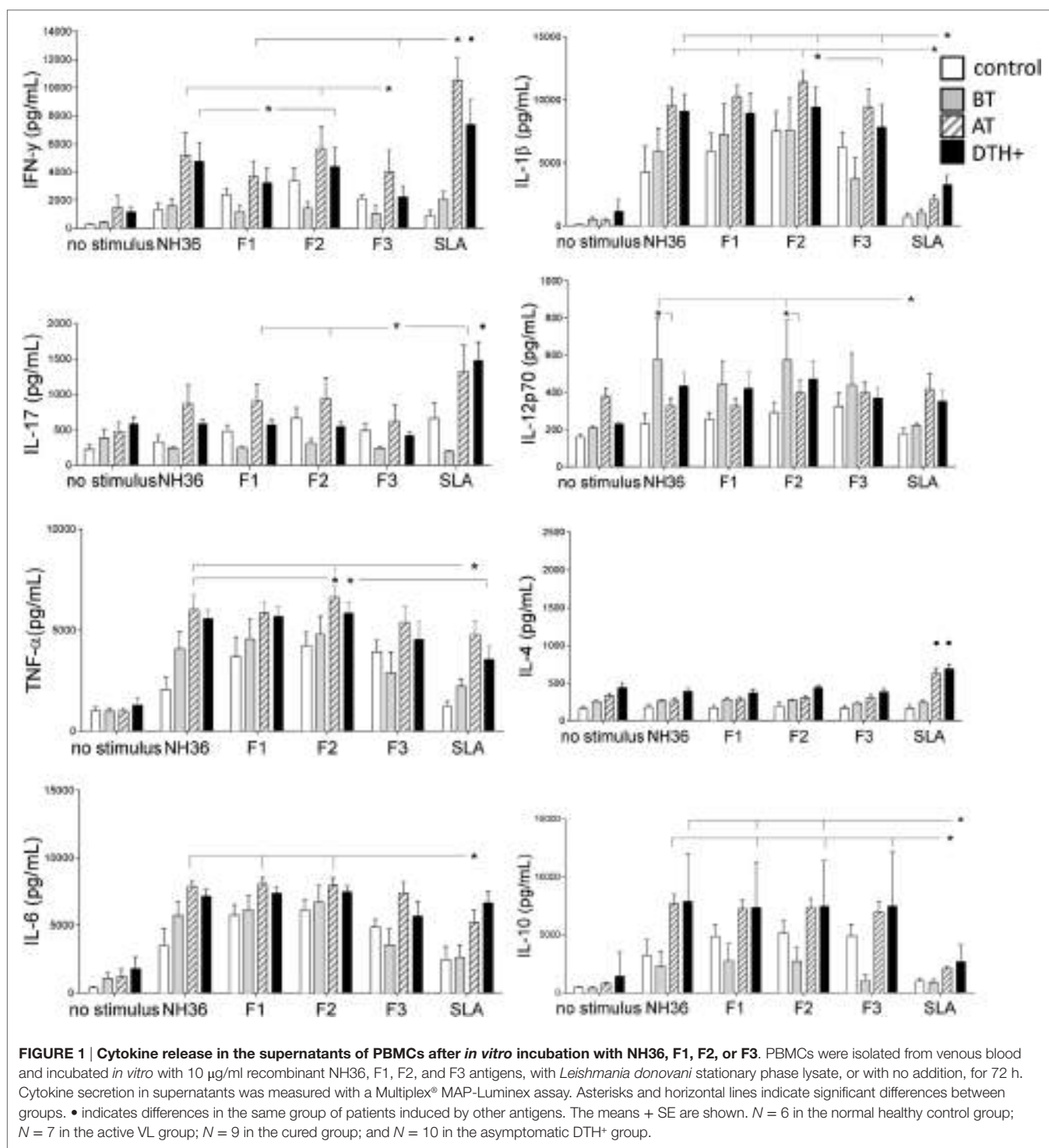
We further investigated the cellular immune response to NH36 domains by multiparameter cytometry analysis. The strategy that we used for the analysis of multifunctional T cell response using multiparameter flow cytometry is summarized in Figure S5 in Supplementary Material. The total frequencies of CD3<sup>+</sup>CD4<sup>+</sup> T cells were reduced in patients with active VL ( $P < 0.031$ ), compared to DTH<sup>+</sup> subjects (**Figure 2A**). This is in agreement to the lower IFN-γ secretion found in VL patients (**Figure 1**).

In DTH<sup>+</sup> subjects, the NH36 domains induced higher frequencies of CD4 T cells secreting one, two (except for CD3<sup>+</sup>CD4<sup>+</sup>IL-2<sup>-</sup>TNF-α<sup>+</sup>IFN-γ<sup>-</sup>), and three cytokines compared to those in cured individuals ( $P < 0.031$ ) or controls ( $P < 0.031$ ), suggesting the involvement of CD4 epitopes in natural resistance to VL (**Figure 2A**). Confirming the results of cytokine expression, F2 was the predominant inducer of the CD4<sup>+</sup> Th1 response and alone induced the highest frequencies of CD3<sup>+</sup>CD4<sup>+</sup>IL-2<sup>+</sup>TNF-α<sup>+</sup>IFN-γ<sup>-</sup> and CD3<sup>+</sup>CD4<sup>+</sup>IL-2<sup>+</sup>TNF-α<sup>-</sup>IFN-γ<sup>+</sup> T cells. Furthermore, together with NH36, F2 induced the highest single (CD3<sup>+</sup>CD4<sup>+</sup>IL-2<sup>+</sup>TNF-α<sup>-</sup>IFN-γ<sup>-</sup>) and total (CD3<sup>+</sup>CD4<sup>+</sup>IL-2<sup>+</sup>) frequencies of IL-2<sup>+</sup> and of multifunctional CD4 T cells (CD3<sup>+</sup>CD4<sup>+</sup>IL-2<sup>+</sup>TNF-α<sup>+</sup>IFN-γ<sup>+</sup>) (**Figure 2A**), and the lowest

**TABLE 1 | Comparison of clinical outcomes.**

Clinical outcomes	VL patients	Cured patients	Asymptomatic DTH <sup>+</sup> subjects				
			Mean (SE)	Mean (SE)	P value	Mean (SE)	P value
Spleen increase in cm	1.7 (0.6)	0 (0)	0.002	0 (0)	0.001		
Liver increase in cm	0.8 (0.3)	0 (0)	0.045	0 (0)	0.027		
Leukocytes per mm <sup>3</sup>	2,384 (477)	6,047 (1,234)	0.018	7,556 (674)	0.001		
Neutrophils per mm <sup>3</sup>	712 (285)	3,407 (780)	0.010	4,941 (701)	0.001		
Eosinophils per mm <sup>3</sup>	18.5 (7.7)	93.9 (52)	0.183	337.3 (66)	0.001		
Lymphocytes per mm <sup>3</sup>	1,094 (244)	2,068 (368)	0.045	2,724 (454)	0.008		
Monocytes per mm <sup>3</sup>	297 (72.3)	433 (32.4)	0.097	543 (59)	0.019		
Hematocrit (%)	28.4 (2.6)	40.9 (2.3)	0.006	41.4 (1.5)	0.004		
Hemoglobin (gr/dl)	8.9 (0.8)	13.7 (0.8)	0.002	13 (0.5)	0.002		
Platelets per 10 <sup>3</sup> /μl	123.4 (25.9)	169.8 (14.4)	0.184	262.1 (14.2)	0.001		

P values express the significance of the differences to the clinical outcomes of visceral leishmaniasis (VL) patients before treatment. Means + SE. N = 9 VL patients before treatment, N = 8 cured VL patients, and N = 10 asymptomatic DTH<sup>+</sup> subjects.



proportions of CD3<sup>+</sup>CD4<sup>+</sup>IL-2<sup>-</sup>TNF-α<sup>-</sup>IFN-γ<sup>+</sup> T cells, in DTH<sup>+</sup> and cured subjects.

Additionally, single producers of IL-2 (CD3<sup>+</sup>CD4<sup>+</sup>IL-2<sup>+</sup>TNF-α<sup>-</sup>IFN-γ<sup>-</sup>) represented the predominant fraction of the CD4 response in cured patients, while single producers of TNF-α (CD3<sup>+</sup>CD4<sup>+</sup>IL-2<sup>-</sup>TNF-α<sup>+</sup>IFN-γ<sup>-</sup>) were the major fraction in DTH<sup>+</sup> subjects (Figure 2B). The F2 domain generated the most

potent response, and this was confirmed by the finding that it stimulated the highest percentages of CD3<sup>+</sup>CD4<sup>+</sup>IL-2<sup>+</sup>TNF-α<sup>-</sup>IFN-γ<sup>-</sup> single producers (55 and 50%), CD3<sup>+</sup>CD4<sup>+</sup>IL-2<sup>+</sup>TNF-α<sup>+</sup>IFN-γ<sup>-</sup> (23 and 5%), CD3<sup>+</sup>CD4<sup>+</sup>IL-2<sup>+</sup>TNF-α<sup>-</sup>IFN-γ<sup>+</sup> (3 and 3%), and CD3<sup>+</sup>CD4<sup>+</sup>IL-2<sup>+</sup>TNF-α<sup>+</sup>IFN-γ<sup>+</sup> multifunctional T cells (0.89 and 47%) in cured and DTH<sup>+</sup> individuals, respectively. These results confirm that this domain generates the most advanced

**TABLE 2 | Correlation between clinical status, cytokine secretion and frequencies of CD4<sup>+</sup> and CD8<sup>+</sup> lymphocytes secreting one, two, or three cytokines, in response to NH36 domains.**

Cytokines	NH36		F1		F2		F3	
	R value	P value	R value	P value	R value	P value	R value	P value
IFN- $\gamma$	Spleen size		-0.428	0.050				
	Liver size		-0.428	0.050				
	Hematocrit		0.532	0.015	0.512	0.020		
	Hemoglobin				0.434	0.050		
IL-17	Spleen size	-0.546	0.012	-0.595	0.005	-0.462	0.040	
	Liver size	-0.546	0.012	-0.595	0.005	-0.462	0.040	
	Monocytes	0.539	0.014	0.580	0.007			
	Hemoglobin			0.466	0.038			
IL-6	Spleen size	-0.464	0.039					
	Liver size	-0.464	0.039					
CD3 <sup>+</sup> CD4 <sup>+</sup> IL-2 <sup>-</sup> TNF- $\alpha$ <sup>+</sup> IFN- $\gamma$ <sup>-</sup>	Neutrophils	0.452	0.027	0.437	0.003			
CD3 <sup>+</sup> CD4 <sup>+</sup> IL-2 <sup>-</sup> TNF- $\alpha$ <sup>+</sup> IFN- $\gamma$ <sup>+</sup>	Monocytes			0.458	0.024			
	Hematocrit					0.432	0.035	
	Neutrophils						-0.432	0.035
CD3 <sup>+</sup> CD4 <sup>+</sup> IL-2 <sup>-</sup> TNF- $\alpha$ <sup>+</sup> IFN- $\gamma$ <sup>+</sup>	Platelets	0.476	0.019			0.454	0.026	
CD3 <sup>+</sup> CD4 <sup>+</sup> IL-2 <sup>-</sup> TNF- $\alpha$ <sup>+</sup> IFN- $\gamma$ <sup>+</sup>	Leukocytes			0.405	0.050			
CD3 <sup>+</sup> CD8 <sup>+</sup> IL-2 <sup>-</sup> TNF- $\alpha$ <sup>+</sup> IFN- $\gamma$ <sup>-</sup>	Spleen size			0.424	0.034			
	Hemoglobin			-0.534	0.006			
	Hematocrit			-0.526	0.007			
CD3 <sup>+</sup> CD8 <sup>+</sup> IL-2 <sup>-</sup> TNF- $\alpha$ <sup>+</sup> IFN- $\gamma$ <sup>+</sup>	Eosinophils			0.412	0.045			
	Monocytes	0.672	0.001	0.766	0.001	0.406	0.049	0.480
CD3 <sup>+</sup> CD8 <sup>+</sup> IL-2 <sup>-</sup> TNF- $\alpha$ <sup>+</sup> IFN- $\gamma$ <sup>+</sup>	Liver size						0.557	0.005
CD3 <sup>+</sup> CD8 <sup>+</sup> IL-2 <sup>-</sup> TNF- $\alpha$ <sup>+</sup> IFN- $\gamma$ <sup>+</sup>	Monocytes	0.566	0.004			0.599	0.002	
CD3 <sup>+</sup> CD8 <sup>+</sup> IL-2 <sup>-</sup> TNF- $\alpha$ <sup>+</sup> IFN- $\gamma$ <sup>+</sup>	Spleen size			0.445	0.029			
	Liver size			0.603	0.002			
	Leukocytes					0.421	0.040	
	Neutrophils					0.412	0.046	

Non-parametric Spearman two-tailed correlation analysis between the outcomes of clinical variables and cytokines secreted in vitro, or frequencies of CD3<sup>+</sup>CD4<sup>+</sup> and CD3<sup>+</sup>CD8<sup>+</sup> T cells secreting 1+, 2+, and 3+ cytokines in vitro, in response to incubation with NH36, F1, F2, or F3 antigens.

stage of differentiation of the CD4 response (**Figures 2A,B**). F1 and F3, on the other hand, induced the highest frequencies of CD3<sup>+</sup>CD4<sup>+</sup>IL-2<sup>-</sup>TNF- $\alpha$ <sup>+</sup>IFN- $\gamma$ <sup>-</sup> and CD3<sup>+</sup>CD4<sup>+</sup>IL-2<sup>-</sup>TNF- $\alpha$ <sup>+</sup>IFN- $\gamma$ <sup>+</sup> single producers (**Figure 2B**).

We found interesting correlations between the clinical outcomes of VL and T cell immunity to NH36 antigens. As correlates of VL resistance or cure, the increases of frequencies of CD3<sup>+</sup>CD4<sup>+</sup>IL-2<sup>-</sup>TNF- $\alpha$ <sup>+</sup>IFN- $\gamma$ <sup>-</sup>, CD3<sup>+</sup>CD4<sup>+</sup>IL-2<sup>-</sup>TNF- $\alpha$ <sup>+</sup>IFN- $\gamma$ <sup>+</sup>, and multifunctional CD3<sup>+</sup>CD4<sup>+</sup>IL-2<sup>-</sup>TNF- $\alpha$ <sup>+</sup>IFN- $\gamma$ <sup>+</sup> T cells induced by F1 were significantly associated with the increases in neutrophil, monocyte, and leukocyte counts, respectively (**Table 2**). Additionally, the increases in CD3<sup>+</sup>CD4<sup>+</sup>IL-2<sup>-</sup>TNF- $\alpha$ <sup>+</sup>IFN- $\gamma$ <sup>+</sup> frequencies generated by F2 correlated with the neutrophil counts, and the increase in CD3<sup>+</sup>CD4<sup>+</sup>IL-2<sup>-</sup>TNF- $\alpha$ <sup>+</sup>IFN- $\gamma$ <sup>+</sup> correlated with the platelets counts. In contrast and as a marker of susceptibility to VL, the F3 induced CD3<sup>+</sup>CD4<sup>+</sup>IL-2<sup>-</sup>TNF- $\alpha$ <sup>+</sup>IFN- $\gamma$ <sup>+</sup> T cell frequency was inversely correlated with the hematocrit values (**Table 2**).

Additionally, the analysis of the cytotoxic response disclosed that the total frequency of CD3<sup>+</sup>CD8<sup>+</sup> T cells (**Figure 3A**) was lower in patients and higher in DTH<sup>+</sup> and cured subjects. However, unlike the predominant enhancement of CD3<sup>+</sup>CD4<sup>+</sup>

T-cell frequencies, observed in DTH<sup>+</sup> individuals (**Figure 2A**), the frequencies of CD3<sup>+</sup>CD8<sup>+</sup> T cells producing cytokines, except for the single producers of TNF- $\alpha$  (CD3<sup>+</sup>CD8<sup>+</sup>IL-2<sup>-</sup>TNF- $\alpha$ <sup>+</sup>IFN- $\gamma$ <sup>-</sup>) and IFN- $\gamma$  (CD3<sup>+</sup>CD8<sup>+</sup>IL-2<sup>-</sup>TNF- $\alpha$ <sup>+</sup>IFN- $\gamma$ <sup>+</sup>), were higher in patients with active VL ( $P < 0.028–0.050$ ) (**Figure 3A**), suggesting the importance of CD8 epitopes in the development of the disease.

F1 and F3 induced the highest single and total frequencies of CD8 T cells secreting IL-2 (CD3<sup>+</sup>CD8<sup>+</sup>IL-2<sup>-</sup>TNF- $\alpha$ <sup>+</sup>IFN- $\gamma$ <sup>-</sup> and CD3<sup>+</sup>CD8<sup>+</sup>IL-2<sup>+</sup>) and of multifunctional CD8 T cells (CD3<sup>+</sup>CD8<sup>+</sup>IL-2<sup>-</sup>TNF- $\alpha$ <sup>+</sup>IFN- $\gamma$ <sup>+</sup>), and F3 alone induced the highest proportions of CD3<sup>+</sup>CD8<sup>+</sup>IL-2<sup>-</sup>TNF- $\alpha$ <sup>+</sup>IFN- $\gamma$ <sup>-</sup> and CD3<sup>+</sup>CD8<sup>+</sup>IL-2<sup>-</sup>TNF- $\alpha$ <sup>+</sup>IFN- $\gamma$ <sup>+</sup> T cells (**Figure 3A**). F2 promoted low frequencies of CD3<sup>+</sup>CD8<sup>+</sup>IL-2<sup>-</sup>TNF- $\alpha$ <sup>+</sup>IFN- $\gamma$ <sup>-</sup> cells in DTH<sup>+</sup> subjects. NH36 induced higher frequencies of CD3<sup>+</sup>CD8<sup>+</sup>IL-2<sup>-</sup>TNF- $\alpha$ <sup>+</sup>IFN- $\gamma$ <sup>-</sup> T cells in cured patients, while the CD3<sup>+</sup>CD8<sup>+</sup>IL-2<sup>-</sup>TNF- $\alpha$ <sup>+</sup>IFN- $\gamma$ <sup>+</sup> T-cell frequencies were enhanced in DTH<sup>+</sup> individuals ( $P < 0.0286$ ), regardless of the antigen used (**Figure 3A**).

Furthermore, in patients before treatment, F1 and F3 induced the highest percentages of CD3<sup>+</sup>CD8<sup>+</sup>IL-2<sup>-</sup>TNF- $\alpha$ <sup>+</sup>IFN- $\gamma$ <sup>+</sup> multifunctional cells (3.17 and 0.84%, respectively), while F1 promoted

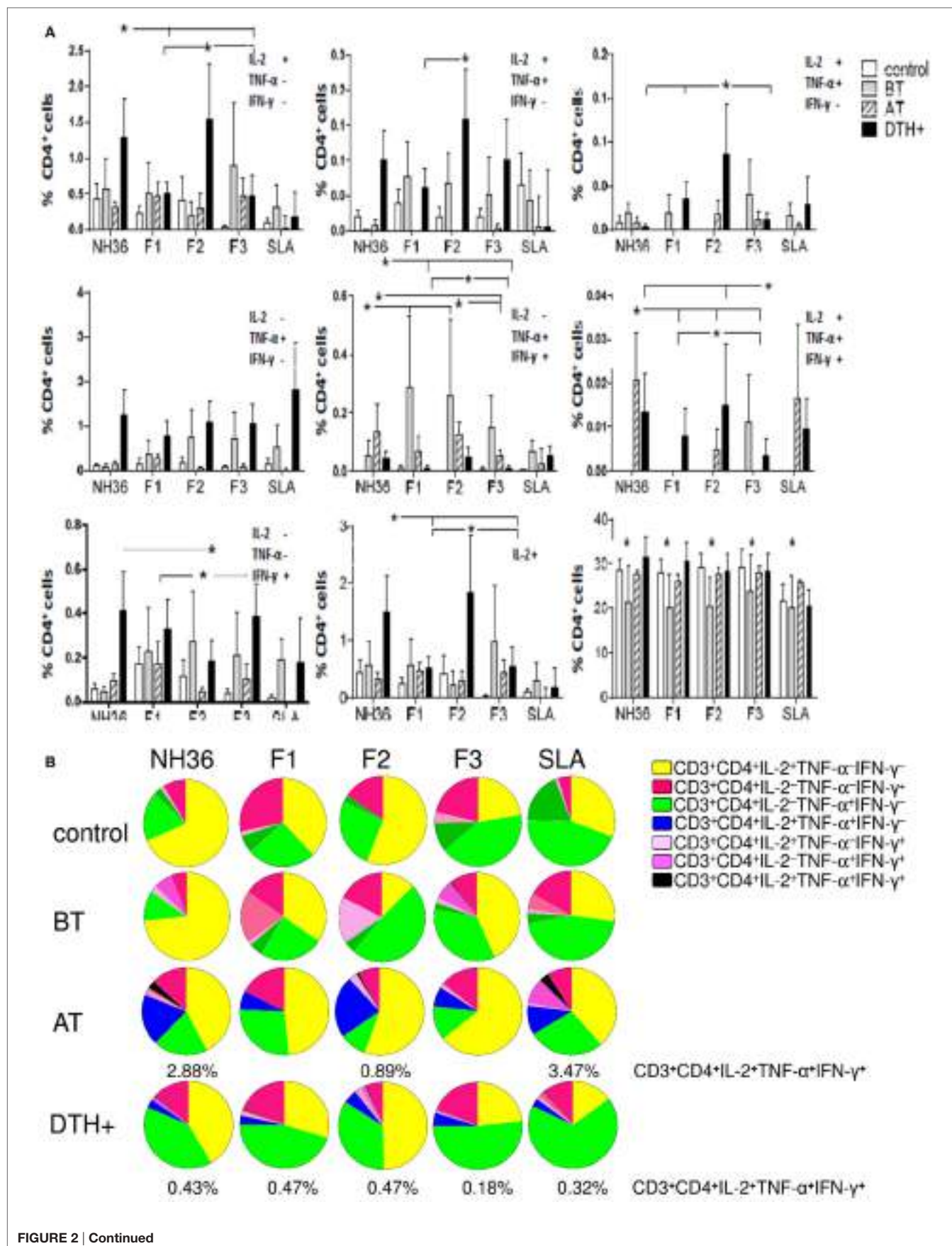


FIGURE 2 | Continued

**FIGURE 2 | Continued**

**Distinct quality of CD4 T cell response induced by NH36 or its domains.** PBMCs were incubated *in vitro* with 10 µg/ml recombinant NH36, F1, F2, and F3 antigens or with no antigenic stimulation for 6 h and further treated with brefeldin A for additional 12 h. Then, the cells were stained for surface CD3 and CD4 markers, fixed, permeabilized, and stained for the intracellular expression of IL-2, TNF- $\alpha$ , and IFN- $\gamma$ . Multiparametric flow cytometry was used to determine (A) the frequencies of CD3 $^+$ CD4 $^+$  lymphocytes and of CD3 $^+$ CD4 $^+$  lymphocytes single producers of each one of the three cytokines (CD3 $^+$ CD4 $^+$ IL-2 $^+$ TNF- $\alpha$  $^+$ IFN- $\gamma$  $^-$ , CD3 $^+$ CD4 $^+$ IL-2 $^+$ TNF- $\alpha$  $^+$ IFN- $\gamma$  $^+$ , and CD3 $^+$ CD4 $^+$ IL-2 $^+$ TNF- $\alpha$  $^+$ IFN- $\gamma$  $^+$ ), double producers (CD3 $^+$ CD4 $^+$ IL-2 $^+$ TNF- $\alpha$  $^+$ IFN- $\gamma$  $^-$ , CD3 $^+$ CD4 $^+$ IL-2 $^+$ TNF- $\alpha$  $^+$ IFN- $\gamma$  $^+$ , and CD3 $^+$ CD4 $^+$ IL-2 $^+$ TNF- $\alpha$  $^+$ IFN- $\gamma$  $^+$ ), and multifunctional CD3 $^+$ CD4 $^+$  T cells (CD3 $^+$ CD4 $^+$ IL-2 $^+$ TNF- $\alpha$  $^+$ IFN- $\gamma$  $^+$ ); as well as the total frequencies of CD3 $^+$ CD4 $^+$  cells producing IL-2 (CD3 $^+$ CD4 $^+$ IL-2 $^+$ ) and (B) the fraction of the total CD3 $^+$ CD4 $^+$  T cell response comprising cells expressing all three cytokines, any two cytokines, or any one cytokine in healthy individuals (control  $N = 10$ ), active visceral leishmaniasis (VL) patients before therapy (BT  $N = 7$ ), cured VL patients after therapy (AT  $N = 9$ ), and in asymptomatic DTH $^+$  individuals (DTH $^+$   $N = 10$ ). The frequencies of each cytokine expressing phenotype were recorded after background subtraction of cells incubated without antigen. Results in panel (A) are expressed as means  $\pm$  SE. Asterisks and horizontal lines indicate significant differences from all other groups.

the highest fraction of the CD3 $^+$ CD8 $^+$ IL-2 $^+$ TNF- $\alpha$  $^+$ IFN- $\gamma$  $^+$  T cells (68%) and F3, the highest contribution of CD3 $^+$ CD8 $^+$ IL-2 $^+$ TNF- $\alpha$  $^+$ IFN- $\gamma$  $^+$  T cells (74%) (**Figure 3B**). Cured and DTH $^+$  subjects showed an enhanced fraction of CD3 $^+$ CD8 $^+$ IL-2 $^+$ TNF- $\alpha$  $^+$ IFN- $\gamma$  $^+$  secreting lymphocytes. A multifunctional CD3 $^+$ CD8 $^+$  T cell contribution was also found in cured patients, in response to F2 and in DTH $^+$  subjects in response to F2 and F3. Interestingly, F1 and F3 promoted the highest frequencies of CD8 T cells secreting only IFN- $\gamma$  (CD3 $^+$ CD8 $^+$ IL-2 $^+$ TNF- $\alpha$  $^+$ IFN- $\gamma$  $^+$ ), in DTH $^+$  subjects (**Figure 3B**).

In addition, we analyzed if the cytotoxic response was correlated with the clinical outcomes (**Table 2**). As a marker of the advancement of the disease, F1 induced increased frequencies of CD3 $^+$ CD8 $^+$ IL-2 $^+$ TNF- $\alpha$  $^+$ IFN- $\gamma$  $^+$  T cells, which were correlated with increased spleen sizes and decreased hemoglobin and hematocrit values. Additionally, F1, together with F3, increased the frequencies of multifunctional CD3 $^+$ CD8 $^+$  T cells, which were correlated with the increased spleen and liver sizes (**Table 2**). As an additional marker of the progression of the disease, F3 also induced an increase in the frequencies of CD3 $^+$ CD8 $^+$ IL-2 $^+$ TNF- $\alpha$  $^+$ IFN- $\gamma$  $^+$  T cells, which correlated with an increase in liver size. Conversely, as a marker of resistance, F2 increased the frequency of multifunctional cells, which was correlated with increased leukocyte and neutrophil counts. Furthermore, F2, together with NH36, enhanced proportions of CD3 $^+$ CD8 $^+$ IL-2 $^+$ TNF- $\alpha$  $^+$ IFN- $\gamma$  $^+$  T cells which were correlated with the monocyte counts (**Table 2**).

Additionally, the cytokine responses of the CD4 $^+$  (**Figure 2A**) and CD8 $^+$  T cells (**Figure 3A**) induced by the SLA antigen were inferior, or did not differ from those promoted by NH36 and its domains.

## Mapping of the CD4 $^+$ and CD8 $^+$ T Cell Epitopes

Aiming to map the epitopes responsible for the described T cell response against NH36 domains, we first compared the sequence of the gene of *L. donovani* NH36 to the sequence of the NH gene of the close related species *L. infantum chagasi*, which is the etiological agent of VL in Brazil (**Figure 4A**). While NH36 of *L. donovani* is composed of 314 amino acids, the NH of *L. infantum chagasi* was described as containing 297 amino acids. The Blast analysis comparing the two sequences indicated 99% homology (**Figure 4A**). The difference between the two proteins is based on only one amino acid at position 192. The aspartate (D)

residue of *L. donovani* NH36 is substituted with asparagine (N) in the Lch-NH sequence (**Figure 4A**). This result suggests that the recombinant domains of *L. donovani* NH36 could generate a successful cross-protection against infection by *L. infantum chagasi*.

Additionally, confirming our experimental results, the TEPITOPE program, with a 3% threshold, identified one epitope for CD4 T cells in the F1 domain and two epitopes in the F2 domain of NH36 (**Table 3**). These three CD4 epitopes showed high percent of predicted binding to HLA-DR molecules (**Table 3**) and are highly promiscuous. In fact, the epitope “AAGCTKPLVRGVRNASQIHG” of F1 (64–93) binds to 20 among the 25 most frequent human HLA DR molecules (DRB1 $^*$ 0301, DRB1 $^*$ 0401, DRB1 $^*$ 0402, DRB1 $^*$ 0404, DRB1 $^*$ 0405, DRB1 $^*$ 0410, DRB1 $^*$ 0801, DRB1 $^*$ 0802, DRB1 $^*$ 0804, DRB1 $^*$ 0806, DRB1 $^*$ 1101, DRB1 $^*$ 1104, DRB1 $^*$ 1106, DRB1 $^*$ 1107, DRB1 $^*$ 1305, DRB1 $^*$ 1307, DRB1 $^*$ 1311, DRB1 $^*$ 1321, DRB1 $^*$ 1501, and DRB1 $^*$ 1502). The epitope “GRHAVQLIIDLIMSHEPKTI” of F2 (102–121) binds to 21 of the 25 most frequent human HLA DR molecules (DRB1 $^*$ 0102, DRB1 $^*$ 0301, DRB1 $^*$ 0401, DRB1 $^*$ 0402, DRB1 $^*$ 0404, DRB1 $^*$ 0405, DRB1 $^*$ 410, DRB1 $^*$ 0421, DRB1 $^*$ 0801, DRB1 $^*$ 0802, DRB1 $^*$ 0804, DRB1 $^*$ 0806, DRB1 $^*$ 1101, DRB1 $^*$ 1104, DRB1 $^*$ 1106, DRB1 $^*$ 1107, DRB1 $^*$ 1305, DRB1 $^*$ 1311, DRB1 $^*$ 1321, DRB1 $^*$ 1501, and DRB1 $^*$ 1502). Additionally, the epitope “DRVKEVVLMGGGYHTGNASP” of F2 (144–163) binds to 19 of the 25 most frequent human HLA DR molecules (DRB1 $^*$ 0101, DRB1 $^*$ 0102, DRB1 $^*$ 0404, DRB1 $^*$ 0405, DRB1 $^*$ 0410, DRB1 $^*$ 0801, DRB1 $^*$ 0802, DRB1 $^*$ 0804, DRB1 $^*$ 0806, DRB1 $^*$ 1101, DRB1 $^*$ 1104, DRB1 $^*$ 1106, DRB1 $^*$ 1107, DRB1 $^*$ 1307, DRB1 $^*$ 1311, DRB1 $^*$ 1321, DRB1 $^*$ 1501, DRB1 $^*$ 1502, and DRB5 $^*$ 0101) (**Figures 4A,B**).

Also supporting our experimental results, two and three CD8 epitopes for the HLA class I molecules were predicted in the sequences of F1 and F3 domains, respectively (**Table 3**), by the SYFPEITHI software (**Figures 4A,C**), while no epitope for CD8 was predicted in the sequence of F2.

The CD4 and CD8 epitopes (**Figure 4A**) are completely conserved and have identical composition in the sequences of NH of *L. donovani*, *L. infantum chagasi*, and *L. infantum* (**Tables 4** and **5**), which are the three species causing VL. Minor variations in 1–3 or 1 amino acids were detected in the CD4 $^+$  and CD8 $^+$  epitopes, respectively, of all other species, which also belong to the subgenus *Leishmania*. Additionally, variations in 3–5 and 1–4 amino acids were observed in the sequences of CD4 $^+$  and CD8 $^+$  epitopes of *Leishmania panamensis* and *L. braziliensis*, which are species that belong to the genus *Viannia* (**Tables 4** and **5**). The

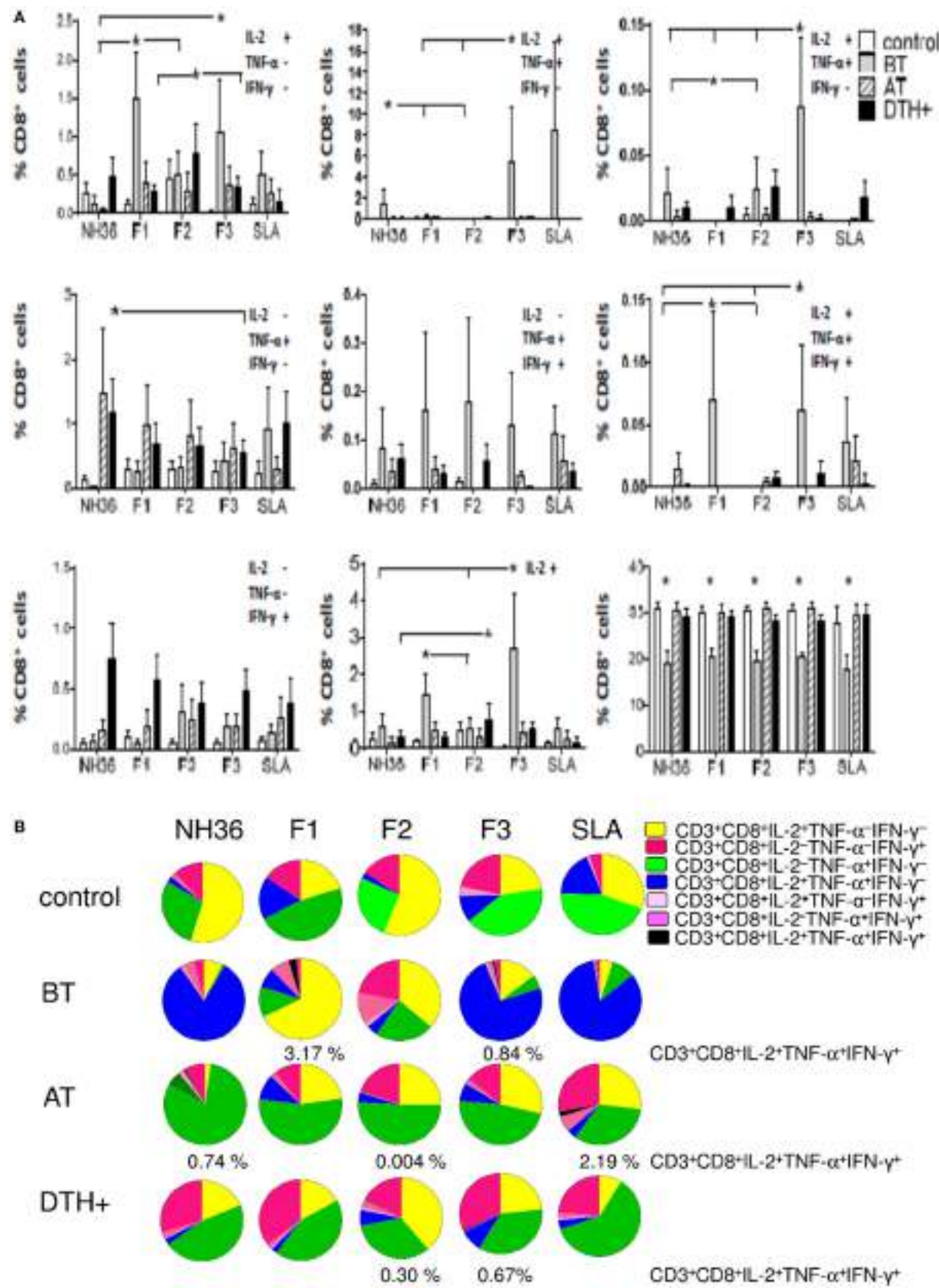


FIGURE 3 | Continued

**FIGURE 3 | Continued**

**Distinct quality of CD8 T cell response induced by NH36 or its domains.** PBMCs were incubated *in vitro* with 10 µg/ml recombinant NH36, F1, F2, and F3 antigens or with no antigenic stimulation for 6 h and further treated with brefeldin A for additional 12 h. Then the cells were stained for surface CD3 and CD8 markers, fixed, permeabilized and stained for the intracellular expression of IL-2, TNF- $\alpha$ , and IFN- $\gamma$ . Multiparametric flow cytometry was used to determine (A) the frequencies of CD3 $^+$ CD8 $^+$  lymphocytes, and of CD3 $^+$ CD8 $^+$  lymphocytes single producers of each one of the three cytokines (CD3 $^+$ CD8 $^+$ IL-2 $^+$ TNF- $\alpha$ IFN- $\gamma$  $^+$ , CD3 $^+$ CD8 $^+$ IL-2 $^+$ TNF- $\alpha$ IFN- $\gamma$  $^-$ , and CD3 $^+$ CD8 $^+$ IL-2 $^+$ TNF- $\alpha$ IFN- $\gamma$  $^+$ ), double producers (CD3 $^+$ CD8 $^+$ IL-2 $^+$ TNF- $\alpha$ IFN- $\gamma$  $^+$ , CD3 $^+$ CD8 $^+$ IL-2 $^+$ TNF- $\alpha$ IFN- $\gamma$  $^-$ , and CD3 $^+$ CD8 $^+$ IL-2 $^+$ TNF- $\alpha$ IFN- $\gamma$  $^+$ ), and multifunctional CD8 T cells (CD3 $^+$ CD8 $^+$ IL-2 $^+$ TNF- $\alpha$ IFN- $\gamma$  $^+$ ); as well as the total frequencies of CD8 T cells producing IL-2 (CD3 $^+$ CD8 $^+$ IL2 $^+$ ) and (B) the fraction of the total CD3 $^+$ CD8 $^+$  T cell response comprising cells expressing all three cytokines, any two cytokines, or any one cytokine in healthy individuals (control  $N = 10$ ), active visceral leishmaniasis (VL) patients before therapy (BT  $N = 7$ ), cured VL patients after therapy (AT  $N = 9$ ), and in asymptomatic DTH $^+$  individuals (DTH $^+$   $N = 10$ ). The frequencies of each cytokine expressing phenotype were recorded after background subtraction of cells incubated without antigen. Results in panel (A) are expressed as means + SE. Asterisks and horizontal lines indicate significant differences from all other groups.

presence of these highly conserved epitopes explain the high degree of cross-species recognition displayed by lymphocytes of patients infected with *L. infantum chagasi* against the *L. donovani* NH36 recombinant domains.

In order to confirm the accuracy of the *in silico* predictions, the CD4 predicted epitopes of F2 and F1 and the CD8 predicted epitopes of F1 and F3 domains were chemically synthetized and incubated *in vitro* with PBMC of asymptomatic DTH $^+$  subjects. The secretion of IFN- $\gamma$  to PBMC supernatants in response to those epitopes was assessed by an ELISA assay (Figure 5). The three predicted epitopes for CD4 $^+$  T cells promoted IFN- $\gamma$  secretion. The IFN- $\gamma$  response generated by the epitope F2 (102–121) was 85% higher (mean = 5.35 pg/ml;  $P = 0.006$ ) than that induced by the F2 epitope (144–163) (mean + 0.79 pg/ml), and 60% stronger ( $P = 0.050$ ) than that induced by the F1 (64–93) epitope (mean = 2.14 pg/ml) (Figure 5). Levels of IFN- $\gamma$  secreted after incubation with the F2 (102–121) epitope were not different from those obtained in response to the SLA complex antigen indicating that this is the major epitope responsible for the immunodominance of the F2 domain detected in all previous immunological assays. IFN- $\gamma$  secretion was also directed against two predicted epitopes for the CD8 T cells of the F1 domain (sequences 20–28 and 92–100), which were no different from SLA antigen, but not for the epitopes of the F3 domain (Figure 5).

## DISCUSSION

Patients of this study showed the typical clinical outcomes of VL (3, 4, 8, 40). On the other hand, no alterations were detected in cured or DTH $^+$  individuals, whose PBMCs secreted the most pro-inflammatory cytokines, mainly in response to F2 and F1, and also secreted higher levels of TNF- $\alpha$  and IL-1 $\beta$  than those induced by the *L. donovani* lysate. The antigenic predominance of F2 is related to the finding of two predicted CD4 T cell epitopes in its sequence, while only one epitope is located in F1, and none is located in F3. Confirming these results, the additional increases in the secretion of IFN- $\gamma$  and IL-17, in response to F2 and F1 were highly correlated with the reduction of VL clinical signs, suggesting that F2 and F1 are indeed the NH36 markers of the Th1-mediated cure or resistance to VL (9). In agreement to those results, the epitopes (102–121 and 144–163) of F2 and the sequence (64–93) of F1 induced the highest IFN- $\gamma$  responses in DTH $^+$  individuals. Therefore, our immunological results supported the *in silico* predictions of epitopes for CD4 $^+$  T cells.

Epidemiological studies performed in Brazil (6, 41, 42) and Kenya (43) have shown that a positive DTH response is a marker for developing acquired resistance to human VL (5, 41, 43). In the north east of Brazil, where the present study was also developed, the DTH $^+$  response was proved to be under genetic control (6, 42, 43) with some genotypes associated to DTH $^+$  subjects and others to DTH $^-$  subjects (42). A DTH positive phenotype is considered not only a measure of acquired resistance to natural infection (41, 43), but also, the only correlate with date of protection in human vaccine trials (44–46). Our results are thus relevant considering that we described the conserved domains and epitopes of *L. donovani*, *L. infantum*, and Lch-NHs that promote Th1 responses in DTH $^+$  subjects and, because of that, which correlate with the resistance to *L. infantum chagasi* infection.

While the hallmark of VL is associated with an impairment of Th1 responses and a depressed cell-mediated immune response characterized by the failure of PBMCs of untreated patients to produce IFN- $\gamma$  in response to leishmanial antigens (47–49), in our study, the F2 peptide alone promoted the highest secretion of IFN- $\gamma$ , IL-1 $\beta$ , and TNF- $\alpha$  in cured and DTH $^+$  subjects. In fact, the IFN- $\gamma$  and TNF- $\alpha$  levels produced by DTH $^+$  subjects in response to F2 are two or three orders of magnitude higher, respectively, than those detected in cured patients from India in response to SLA, and one order of magnitude higher than those obtained in response to the antigens LACK and TRYP (4). Also, similar to our results, cured patients of India produce IFN- $\gamma$  and TNF- $\alpha$  in response to antigens (48, 49) providing correlates of resistance (4). Additionally, Th1 responses including a robust TNF- $\alpha$  response directed against NH36 were also recently described in human healthy subjects vaccinated with an NH36-fusion protein (11). The pro-inflammatory enhanced cytokine secretion in response to F2 and F1 domains indicated that they are the targets of the anti-NH36 immune response related to VL resistance.

We therefore revealed in our study the main domains and epitopes of NH36 which can be considered as potential candidates for a T-epitope vaccine for humans. Indeed, while prediction programs and pre-clinical studies in mice indicated the importance of three CD4 epitopes of F3, and two of F1 (26) in the generation of protection against visceral and CL, our study conversely describes two CD4 epitopes for humans in the F2 and one in F1. Therefore, the F2 domain, which is not relevant for mouse immunity (12, 13, 26), is however responsible for the generation of the strongest Th1 responses in humans.

A Ld-NH36 <sub>1</sub>	MPRKIIILCDPGIDDOAVAFLAHGNPEVLLAIZTTVVGNOTLEKVTRNARLVAADVAGIVG	68
Lch-NH <sub>1</sub>	MPRKIIILCDPGIDDOAVAFLAHGNPEVLLAIZTTVVGNOTLEKVTRNARLVAADVAGIVG	68
Ld-NH36 <sub>61</sub>	VPAAGCTKPLVRGVNRNASQIHGTGMGNVSYPPFEKTKLGRHAVOLIIDLIMSHEPKT	128
Lch-NH <sub>61</sub>	VPAAGCTKPLVRGVNRNASQIHGTGMGNVSYPPFEKTKLGRHAVOLIIDLIMSHEPKT	128
Ld-NH36 <sub>121</sub>	ELVPTGGLTNIAMAVRLEPRIVDRVKEVVLMGGGYHTGNASVAEFDNVFVDPEAAHVFL	188
Lch-NH <sub>121</sub>	ELVPTGGLTNIAMAVRLEPRIVDRVKEVVLMGGGYHTGNASVAEFDNVFVDPEAAHVFL	188
Ld-NH36 <sub>181</sub>	NESWNVTMVGQLDLTHQALATPAVQKRVKEVGTKPAAFMILCLDFYTKVYKERNTYATVH	248
Lch-NH <sub>181</sub>	NESWNVTMVGQLDLTHQALATPAVQKRVKEVGTKPAAFMILCLDFYTKVYKERNTYATVH	248
Ld-NH36 <sub>241</sub>	DPCAVAYVIDPTVMITTEQVVPVDIELNGALTIGMTVADFRYPRPKHCHTOAVKLDFD	297
Lch-NH <sub>241</sub>	DPCAVAYVIDPTVMITTEQVVPVDIELNGALTIGMTVADFRYPRPKHCHTOAVKLDFD	297

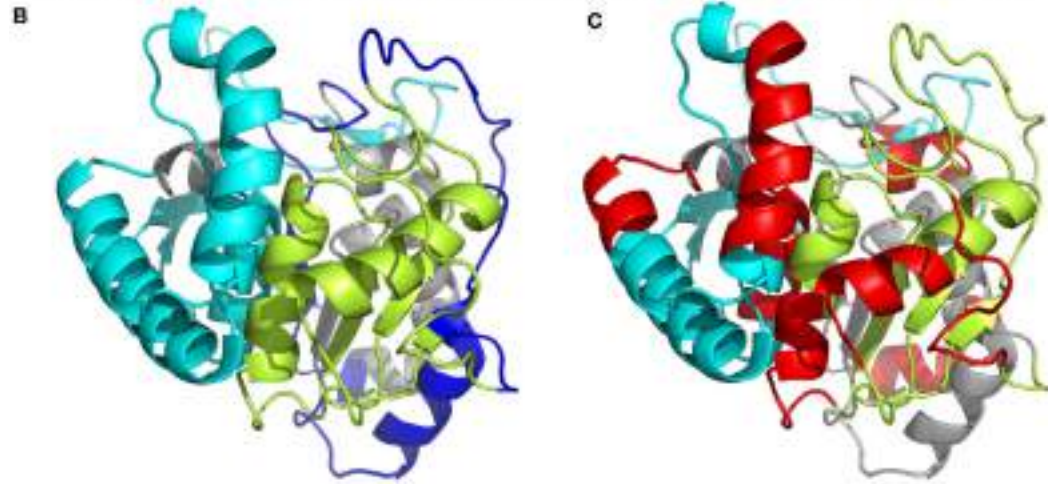


**FIGURE 4 | Spatial distribution of epitopes in the monomer of the *Leishmania donovani* nucleoside hydrolase NH36 (Ld-NH36) and homology to the sequence of *Leishmania infantum chagasi* NH (Lch-NH). (A)** Blast of the sequences of Ld-NH36 and Lch-NH with the sequences of the predicted epitopes for HLA class II molecules identified with a 3% threshold by the TEPIPOPE program shown in blue boxes and the epitopes for HLA class I molecules identified by the SYFPEITHI software shown in red boxes. **(B)** The NH36 monomer model obtained by homology modeling to the sequence of the nucleoside hydrolase of *Leishmania major*. The model shows the N-terminus (F1, amino acids 1–103) in lime green, the central domain (F2, amino acids 104–198) in gray, and the C-terminus (F3, amino acids 199–314) in cyan. The CD4<sup>+</sup> T-cell epitopes are plotted in dark blue, and **(C)** the sequences of the CD8<sup>+</sup> T-cell epitopes are labeled in red.

**TABLE 3 | Peptide sequences of the NH36 antigen selected by the TEPIPOPE and SYFPEITHI algorithms.**

Amino acid location	Lymphocytes	Domain	Sequences	Prediction of molecular binding	
				HLA-DR (%) <sup>a</sup>	HLA-A and B scores <sup>b</sup>
64–93	CD4	F1	AAGCTKPLVRGVNRNASQIH	80	—
102–121	CD4	F2	GRIHAVQLIIDLIMSHEPKT	84	—
144–163	CD4	F2	DRVKEVLMGGGYHTGNASP	76	—
20–28	CD8	F1	FLAHGNPEV	—	28 (A*02:01)
92–100	CD8	F1	YPPEFKTKL	—	21 (B*0702)
197–205	CD8	F3	ALATPAVQK	—	34 (A*03)
211–219	CD8	F3	AFMLQILDF	—	19 (B*4402) 17 (A*2402)
221–229	CD8	F3	ILDFYTKVY	—	27 (A*01)

<sup>a</sup>Predictions were calculated using the TEPIPOPE algorithm using 3% threshold.

<sup>b</sup>Predictions obtained using the SYFPEITHI algorithm.

IL-1 $\beta$ , which is highly induced by F2, is a pro-inflammatory cytokine secreted by monocytes and macrophages, which promotes inflammatory responses that activate protective immunity. In agreement to that, the increase in IL-1 $\beta$  secretion of cured and DTH $^{+}$  subjects of the same endemic area, was associated with

the decrease of the parasite load of infected macrophages (50). Furthermore, host resistance to infections by *L. major* (24), *L. amazonensis*, *L. brasiliensis*, and *L. infantum chagasi*, which share a high degree of identity in their NH sequences (13, 31), has also been described to be mediated by IL-1 $\beta$  (51). Thus, the IL-1 $\beta$

**TABLE 4 | Conserved epitopes for CD4<sup>+</sup> T cells within the genus *Leishmania*.**

<i>Leishmania</i> species	Epitope CD4-F1 (64–93)	Epitope CD4-F2 (102–121)	Epitope CD4-F2 (144–163)
<i>L. donovani</i>	AAGCTKPLVRGVRNASQIHG	GRHAVQLIIDLIMSHEPKTI	DRVKEVLMGGGYHTGNASP
<i>L. infantum chagasi</i>	AAGCTKPLVRGVRNASQIHG	GRHAVQLIIDLIMSHEPKTI	DRVKEVLMGGGYHTGNASP
<i>L. infantum</i>	AAGCTKPLVRGVRNASQIHG	GRHAVQLIIDLIMSHEPKTI	DRVKEVLMGGGYHTGNASP
<i>L. amazonensis</i>	AAGCAKPLVRGVRNASQIHG	SRHAVQLIIDLIMSHEPKTI	ERVKKVVLGGGYHTANASP
<i>L. major</i>	AAGCTKPLVRGVRNASIHIIG	GRHAVQLIIDLIMSHEPKTI	DRVKEVLMGGGYHTGNASP
<i>L. tropica</i>	AAGCTKPLVRGVRNASQIHG	GRHAVQLIIDLIMSHEPKTI	DRVKEVLMGGGYHTGNASP
<i>L. mexicana</i>	AAGCAKPLVRGVRNASQIHG	SRHAVQVIIIDLMSHEPKTI	ERVKEVLMGGGYHTANASP
<i>L. braziliensis</i>	AAGCCKPLVRKVRTAPQIHG	KRHAVHLIELIMSHPKSI	ERVKEVLMGGSCCIGNASP
<i>L. panamensis</i>	AAGCCKPLVRKVRTAPQIHG	KRHAVHLIELIMSHPKSI	ERVKEVLMGGSCCIGNASP

The amino acids that are different from those of the sequence described in the Nucleoside hydrolase NH36 of *L. donovani*.

**TABLE 5 | Conserved epitopes for CD8<sup>+</sup> T cells of the genus *Leishmania*.**

<i>Leishmania</i> species	CD8-F1 (20–28)	CD8-F1 (92–100)	CD8-F3 (197–205)	CD8-F3 (216–224)	CD8-F3 (221–229)
<i>L. donovani</i>	FLAHGNPEV	YPPEFKTKL	ALATPAVQK	AFMLQILDF	ILDFTKVV
<i>L. infantum chagasi</i>	FLAHGNPEV	YPPEFKTKL	ALATPAVQK	AFMLQILDF	ILDFTKVV
<i>L. infantum</i>	FLAHGNPEV	YPPEFKTKL	ALATPAVQK	AFMLQILDF	ILDFTKVV
<i>L. amazonensis</i>	FLAYGNPEI	YPPEFKTKL	ALATPAVRK	AFMLQILDF	ILDFTKVV
<i>L. major</i>	FLAHGNPEI	YPPEFKTKL	ALATPAVQK	AFMLQILDF	ILDFTKVV
<i>L. tropica</i>	FLAHGNPEI	YPPEFKTNL	ALATPEVQK	AFMLQILDF	ILDFTKVV
<i>L. mexicana</i>	F LAYGNPEI	YPPEFKTKL	ALATPAVRK	AFMLQILDF	ILDFTKVV
<i>L. braziliensis</i>	LLAYGNPEI	YPSEFKTKL	ALATPEVLQ	DFILKILEF	I LEFYTKVV
<i>L. panamensis</i>	LLAYGNPEI	YPSEFKTKL	ALATPEVLQ	DFILKILEF	I LEFYTEVY

The amino acids that are different from those of the sequence described in the Nucleoside hydrolase NH36 of *L. donovani*.

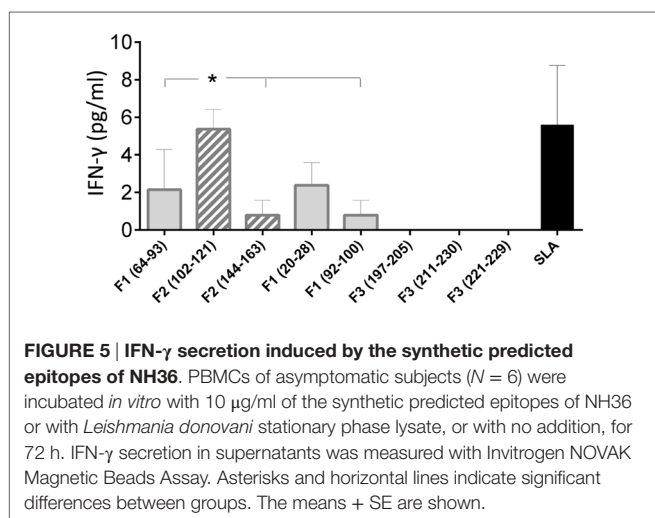


**FIGURE 5 | IFN-γ secretion induced by the synthetic predicted epitopes of NH36.** PBMCs of asymptomatic subjects ( $N = 6$ ) were incubated *in vitro* with 10  $\mu$ g/ml of the synthetic predicted epitopes of NH36 or with *Leishmania donovani* stationary phase lysate, or with no addition, for 72 h. IFN- $\gamma$  secretion in supernatants was measured with Invitrogen NOVAK Magnetic Beads Assay. Asterisks and horizontal lines indicate significant differences between groups. The means + SE are shown.

secretion induced by the F2 domain could contribute to the basis of this cross-species resistance induced by NH36.

IL-12 secretion by VL untreated patients was higher in response to F2 than to SLA. As in our study, similar or higher levels of IL-12 were detected in the sera of infected untreated patients and subclinical DTH<sup>+</sup> subjects from Bangladesh (52) and Brazil (53). IL-12 is associated with macrophage activation, parasite phagocytosis, and a protective host response that upregulates

IFN- $\gamma$  synthesis, cytolytic activity, and Th1 cell differentiation (3). Therefore, the finding of increased levels of IL-12p70 in untreated patients in response to F2 might indicate its involvement in the generation of an early inflammatory response as an attempt to control infection (53, 54).

Enlarged spleen and livers and decreased hemoglobin, albumin, and hematocrit counts correlate with the clinical variables (55–58) and the increased blood parasite load found in VL (55). By contrast, in our study, the increase of both IL-17 and IL-6 secretion in response to F1 and F2 correlated with decreases in spleen and liver sizes, which are parameters of cure and asymptomatic VL (56, 58).

The increased secretion of IL-17 in response to F1 also correlated with an increase in monocytes as well as with an increase hemoglobin counts. IL-17 is a classical effector of innate immunity that induces the expression of many inflammatory mediators, including IL-6 (8). Our results then indicate the efficient induction of a Th17 response by the F2 and F1 domains that contributes in the cure and control of the infection.

Besides inducing Th1 and Th17 responses, the F2 and F1 domains also promoted the secretion of IL-10, a cytokine which was correlated with immunosuppression defects (8, 59) and, together with IL-6, with the severity of human VL (60). This kind of mixed Th1/Th2 response was also previously described for VL (49). In fact, in our study, IFN- $\gamma$ , IL-17, and IL-10 were co-expressed by PBMCs of healthy, cured, and DTH<sup>+</sup> subjects and their secretion was lower in untreated patients. Since

DTH<sup>+</sup> is a marker of acquired resistance to VL (5, 42, 43), the increased IL-10 secretion in response to NH36 domains, in cured and DTH<sup>+</sup> subjects is more associated with resistance and cure of VL than with a Th2 response. As we described here for the NH36 domains, another *Leishmania* vaccine candidate, the LaPSA-38S antigen induced specific Th1 responses and protection in mice and promoted significant levels of IFN-γ, granzyme B, and IL-10 in patients cured from cutaneous *L. major* infection and in high responders asymptomatic subjects infected with *L. major* or *L. infantum* (61). A higher secretion of TNF-α in response to LaPSA-38S was also found in the *L. infantum* high responders (61). As described for LaPSA-38S protein, the NH36 domains were able to induce a mixed Th1 and Th2/Treg cytokine response in individuals with immunity to *L. infantum chagasi* indicating that it may be exploited as a vaccine candidate. The IL-10 elevated secretion in response to NH36 domains might be determined by the increased secretion of TNF-α (60, 62) and might serve as a tool for control of tissue damage caused by the enhanced inflammatory response. The increased secretion of IL-10 in response to NH36 also suggests the presence of Treg epitopes in its domains. Confirming that, it was described that the parasite-induced IFN-γ and IL-1β act on DCs and macrophages to promote the production of IL-27, which blocks the generation of Th17 cells and facilitates the generation of IL-10-producing T cells (8). Remarkably, this ability of modulating the immune response, and promoting similar levels of IFN-γ, TNF-α, and IL-10 associated to resistance was also found after human vaccination with an NH36-fusion protein (11), in DTH<sup>+</sup> asymptomatic CL patients (63), in *L. infantum*-infected asymptomatic dogs (64), and in mice vaccinated with F1 (26). Therefore, our results suggest that a combination of CD4 Th1 and/or potential regulatory epitopes of F2 and F1 modulate the human immune response against the parasite. This seems to be also the case for IL-6, which is produced by APCs and involved in the control of Th1/Th2 differentiation during CD4 T cell activation and is found in the plasma of VL patients and asymptomatic subjects in Brazil (65). The F2 and F1 domains could be therefore the basis of tools for prevention, control, or new methods of immunotherapy of this severe potentially lethal disease.

Optimal vaccine protection is achieved by developing a population of multifunctional IL-2<sup>+</sup>TNF-α<sup>+</sup>IFN-γ<sup>+</sup> producing CD4 T cells that can mediate effector functions quickly, and by having a memory T-cell reservoir that secretes IL-2, TNF-α, or both and shows effector potential (66). Consistent with this, F2 induced the most robust cytokine responses and the highest frequencies of CD3<sup>+</sup>CD4<sup>+</sup>IL-2<sup>+</sup>TNF-α<sup>+</sup>IFN-γ<sup>+</sup> effector T cells, CD3<sup>+</sup>CD4<sup>+</sup>IL-2<sup>+</sup>TNF-α<sup>+</sup>IFN-γ<sup>-</sup>, and CD3<sup>+</sup>CD4<sup>+</sup>IL-2<sup>+</sup>TNF-α<sup>+</sup>IFN-γ<sup>-</sup> T cells in asymptomatic individuals. F2 also most efficiently promoted the expression of IL-2 and TNF-α by CD4<sup>+</sup> T cells and promoted the development of multifunctional T cells in cured patients, followed by F1 in DTH<sup>+</sup> subjects. The correlations observed between the increases in proportions of multifunctional, CD3<sup>+</sup>CD4<sup>+</sup>IL-2<sup>+</sup>TNF-α<sup>+</sup>IFN-γ<sup>+</sup>, and CD3<sup>+</sup>CD4<sup>+</sup>IL-2<sup>+</sup>TNF-α<sup>+</sup>IFN-γ<sup>-</sup> T cells and leukocytes, neutrophils, and monocytes induced by F1 also confirm that, for some variables, F1 is co-dominant with F2. The increased

IFN-γ secretion of PBMC of asymptomatic subjects in response to the predicted CD4<sup>+</sup> epitopes of F2 (102–121 and 144–163) and F1 (69–93) explains those results. Confirming the relevance of NH36 in cross-species protection, enhanced frequencies of anti-NH36 IL-2, TNF-α, or IFN-γ-producing CD4<sup>+</sup> T cells, indicating the generation of a memory-response, have also been reported, in asymptomatic patients of Bangladesh (11) and in mice vaccinated after *L. amazonensis* infection (12, 13, 25, 26).

Unlike CD4 lymphocytes, following antigenic stimulation, naïve CD8 T cells differentiate into activated effector cells that can transform into CD8<sup>+</sup>IL2<sup>+</sup>TNF-α<sup>+</sup>IFN-γ<sup>+</sup> effector cells or into multifunctional CD8<sup>+</sup>IL2<sup>+</sup>TNF-α<sup>+</sup>IFN-γ<sup>+</sup> memory cells (66). We described that the CD8<sup>+</sup> T cells response against F1 and F3 is related to the advancement of the disease as most of the CD8<sup>+</sup> phenotypes are increased in untreated patients. However, positive correlations were found between the increases in CD3<sup>+</sup>CD8<sup>+</sup>IL2<sup>+</sup>TNF-α<sup>+</sup>IFN-γ<sup>-</sup>, CD3<sup>+</sup>CD8<sup>+</sup>IL2<sup>+</sup>TNF-α<sup>+</sup>IFN-γ<sup>+</sup>, and CD3<sup>+</sup>CD8<sup>+</sup>IL2<sup>+</sup>TNF-α<sup>+</sup>IFN-γ<sup>+</sup> T cell frequencies and the increases in spleen and liver sizes. These positive correlations indicate that, in these untreated patients, the CD8<sup>+</sup> T cells could be involved in an early attempt to control the parasite loads of liver and spleens. Supporting the multiparameter analysis two synthetic predicted CD8<sup>+</sup> epitopes of the F1 domain induced the IFN-γ secretion by PBMC of DTH<sup>+</sup> subjects.

In agreement to our results, in CL models, CD8 T cells producing IFN-γ were considered as very important for directing Th2-type responses toward Th1 (67) and for establishing long-term memory that protects against re-infections (68). Memory CD8 T cells have been shown to be responsible for resistance against re-infection (69) and for promoting long-lasting protection, which is lost in their absence (70, 71). This evidence could also explain our finding of high percentages of CD3<sup>+</sup>CD8<sup>+</sup>IL-2<sup>+</sup>TNF-α<sup>+</sup>IFN-γ<sup>+</sup> single positive cells observed in the DTH<sup>+</sup> group, which represent the immune resistance to VL, after stimulation with F1 and F3 domains.

We further described the prediction of two promiscuous epitopes for CD4<sup>+</sup> lymphocytes in the F2, and one in the F1 domain, which are all capable of binding to at least 19 of the 25 most frequent human HLA-DR molecules. These predictions were confirmed by the ability of F2 and F1 domains to induce CD4 Th1 responses, and the competence of the respective synthetic predicted epitopes, mainly the F2 (102–121) followed by the F1 (64–93), to promote the IFN-γ secretion by PBMC of DTH<sup>+</sup> subjects. These results are very impressive considering that HLA class II prediction is more difficult and less reliable (14).

In this investigation, we demonstrated that F2 and F1 domains induce a strong CD4<sup>+</sup>-Th1 response in cured and DTH<sup>+</sup> subjects, whereas the F1 and F3 domains promote a higher CD8<sup>+</sup> T cell pro-inflammatory response in untreated patients and an increase in the CD3<sup>+</sup>CD8<sup>+</sup>IL-2<sup>+</sup>TNF-α<sup>+</sup>IFN-γ<sup>+</sup> T cell proportions in DTH<sup>+</sup> subjects. Both CD4 and CD8 responses can be related to the control and resistance to *L. infantum chagasi* infection.

Our objective in this study was to determine which are the more immunogenic domains of NH36. This would allow us to confirm the relevance of the epitopes disclosed by the *in silico*

prediction programs and to define a rationale combination of the domains and/or epitopes to be used in a future universal vaccine against leishmaniasis, capable of enhancing both arms of T-cell immunity.

The epitopes were indeed identified by the prediction programs directly, on the sequence of the whole NH36 molecule, both for mice (26, 28) and human histocompatibility complex molecules (this manuscript). However, although the identification of the epitopes would allow the direct design of a synthetic epitope vaccine, it has been reported that the results of the immunological assays *in vivo* not always confirm the *in silico* predictions (32), and that the synthetic epitopes alone are not enough immunogenic to be used as vaccine candidate antigens (14). Our strategy then was to identify through immunological assays the presence of the important epitopes in the domains of the NH36 antigen that would therefore be more immunogenic than the whole cognate NH36 protein and more potent than the isolated epitopes, when used in vaccination.

The reason for evaluating the individual domains of the same antigen in order to identify the epitopes is that the domains, which contain potent epitopes, will be more potent than the whole antigen. This will indeed allow the selection of the truly relevant epitopes among all epitopes disclosed by the *in silico* software. The immunogenic domains in fact concentrate the immunogenic power of the whole antigen. Hence, for instance, if we use for incubation with PBMC one molecule of NH36, among its 314 amino acids, 40 of them compose the sequences of the three epitopes for CD4 located in F3. This means that one molecule of NH36 has 12.7% (40/314) of its sequence constituted by epitopes for CD4 T cells. If by contrast, we vaccinate only with a molecule of F3, which is composed by 115 amino acids, the 40 amino acids of the CD4 epitopes would represent now 34.8% (40/115) of the antigen, and this is what induce a threefold increase in the immunogenic effect. We are, in this way, exposing PBMC to a higher molar concentration of the relevant epitopes. That is why more protection is expected to be generated by the domain that contains the epitopes than by the whole NH36. A higher molar concentration of the epitopes is expected to be found in it than in the whole cognate protein.

In agreement with this idea, the F3 vaccine promoted in mice a 36% higher average protection than the NH36 vaccine. This average increased protection induced by the F3 vaccine above the level promoted by the NH36 vaccine included: a 32.06% higher IDR, 24 h after immunization, a 34.1% higher IDR 48 h after immunization, a 21.4% higher IDR 48 h after challenge, a 37.39% enhanced IFN- $\gamma$ /IL-10 CD4 $^{+}$  T cell ratios, a 27. 18% stronger reduction of parasite load by *in vivo* depletion with anti-CD4 monoclonal antibody, a 57.99% increment in reduction of the parasite load of *L. chagasi*, and a 47% reduction in parasite load by *L. amazonensis* (26). That means that while the NH36 vaccine reduces the *L. chagasi* parasite load in 37%, the F3 reduces it in 88% (26).

Additionally, the F3 vaccine was 40% average more protective than the NH36 vaccine against *L. amazonensis* infection (28). This included a 27.58% stronger IDR, 48 h after challenge, a 20.04 and 11.64% enhanced secretion of IFN- $\gamma$  and TNF- $\alpha$  to supernatants, respectively, and a 93.03% reduced *L. amazonensis*

parasite load (28). The calculation was performed according the following equation = (F3 – NH36/F3) values × 100 and allowed us to obtain the protective effect increment (26).

Noteworthy, for mice, the prediction software had disclosed two epitopes for CD4 in F1, one in F2, and three in F3. On the other hand, one epitope for CD8 T cells was disclosed in F1 and two in F2 (26). The immunological *in vivo* assays, on the other hand, only confirmed the relevance of the three epitopes for CD4 of F3 and of the single epitope for CD8 T cells of F1 (26, 28, 29). Therefore, the immunological assays only partially confirmed the *in silico* prediction for the mice model (32). No response against the F2 domain was observed in vaccinated mice. In fact, the F3 domain induced the strongest CD4-mediated protection against VL infection (26) and, besides F3, the F1 domain induced an additional CD8-mediated response against *L. amazonensis* infection (26, 28).

Therefore, if the domains, which contain the important epitopes, are more potent than the whole protein, the need of evaluation the individual domains in order to confirm the epitopes is justified. In order to increase potency and optimize a vaccine, for instance, the domains could be even combined in a chimera that would be expected to be even more potent than the single domains. Our results support those of Kao et al. for the *Pseudomonas aeruginosa* Type IV pilus vaccine (72). The authors compared antisera raised against the PAK strain monomeric pilin protein (29–144) and a synthetic peptide containing the main receptor-binding domains (RBDs) of the pili (128–144). They showed that not only does the synthetic peptide generated higher titers of RBD-specific antibodies but that the anti-peptide antibodies have a higher affinity for the native protein than the anti-pilin (72). The strategy of using the domains that concentrate the most relevant epitopes was the basis of the development of the vaccines against human malaria (central and C-terminal domain) (73), HIV (CD4 and co-receptor binding domains) (74), and influenza [extracellular domain of matrix protein 2 (M2e)] (75).

In this investigation, we are not analyzing vaccinated individuals that have a strong response to the correct epitopes. We are studying instead human VL cured and DTH $^{+}$  subjects, trying to detect to what portion of the NH36 molecule the acquired resistance and immunity of these patients is directed. These individuals, although representing the Th1 pole of the immune response to VL, and being expected to have the strongest naturally acquired immune resistance to VL (41–43), display milder immune responses, in *in vitro* assays, if compared to vaccinated subjects. Therefore, the search for immunogenicity is more difficult, and small signals of increase of the immune reactivity should be considered in order to map the best immunogenic domain.

It is worth to note that the predicted epitopes are different in mice and in human histocompatibility complexes. For humans the *in silico* programs disclosed two epitopes for CD3 $^{+}$ CD4 $^{+}$  T cells in F2 and one in F1, and further three epitopes for CD3 $^{+}$ CD8 $^{+}$  T cells in F1 and additional three in F3. In agreement to that, we were able to show that the most pronounced CD4-Th1 response was directed against F2 and F1 domains, and the strongest CD8 $^{+}$  response target the F1 and F3 proteins.

In fact, the F2 induced 76% higher frequencies of CD3<sup>+</sup>CD4<sup>+</sup>IL-2<sup>+</sup>TNF- $\alpha$ <sup>+</sup>IFN- $\gamma$ <sup>-</sup> than F1, in DTH<sup>+</sup> subjects, and 100% higher proportions of multifunctional IL-2<sup>+</sup>TNF- $\alpha$ <sup>+</sup>IFN- $\gamma$ <sup>+</sup> T cells than F1 and F3, respectively, in cured patients. Additionally, in DTH<sup>+</sup> individuals, F2 increased the CD3<sup>+</sup>CD4<sup>+</sup>IL-2<sup>+</sup>TNF- $\alpha$ <sup>+</sup>IFN- $\gamma$ <sup>-</sup> T cell frequencies 67% more than F1 and 69% more than F3. F2 also enhanced the CD3<sup>+</sup>CD4<sup>+</sup>IL-2<sup>+</sup> T cell proportions 72% more than F1 and 70% more than F3. Furthermore, F2 was 59 and 87% stronger than F1 and F3 domains, respectively, but most important, it was 96% more potent than NH36, in the enhancement of the frequencies of CD3<sup>+</sup>CD4<sup>+</sup>IL-2<sup>+</sup>TNF- $\alpha$ <sup>+</sup>IFN- $\gamma$ <sup>+</sup> T cells of the DTH<sup>+</sup> subjects.

Accordingly, F2 was the only domain that retained the capabilities of NH36 to enhance the IFN- $\gamma$  secretion. Additionally, F2 increased the TNF- $\alpha$  secretion 10% more than NH36, and 28% more than the very potent SLA, in cured subjects.

Similar to our results of multiparameter analysis, the increased IFN- $\gamma$  secretion by PBMC of DTH<sup>+</sup> subjects, in response to the synthetic epitopes predicted for CD4<sup>+</sup> T cells disclosed, the F2 (102–121) epitope which promoted a 86 and 60% higher secretion of IFN- $\gamma$  than the sequences F2 (144–163) and F1 (64–94), respectively.

Regarding the induction of the CD8<sup>+</sup> T cell response, the reactivity was higher in untreated patients. F1 and F3 increased the frequencies of CD3<sup>+</sup>CD8<sup>+</sup>IL-2<sup>+</sup>TNF- $\alpha$ <sup>+</sup>IFN- $\gamma$ <sup>-</sup> T cells above the levels of NH36, by 90 and 89%, respectively. Also, F1 was 59% and F3, 78% more potent than NH36 in the enhancement of the frequencies of CD3<sup>+</sup>CD8<sup>+</sup>IL-2<sup>+</sup> T cells. F3 was additionally 77% stronger than NH36, in the increase of the CD3<sup>+</sup>CD8<sup>+</sup>IL-2<sup>+</sup>TNF- $\alpha$ <sup>+</sup>IFN- $\gamma$ <sup>+</sup> T cell frequencies. Finally, F1 was 99% and F3, 100% stronger than NH36, in the enhancement of the multifunctional CD3<sup>+</sup>CD8<sup>+</sup>IL-2<sup>+</sup>TNF- $\alpha$ <sup>+</sup>IFN- $\gamma$ <sup>+</sup> T cell proportions.

Accordingly, the two synthetic predicted epitopes for CD8 T cells of the F1 domain, F1 (20–28) and F1 (92–100), promoted the secretion of IFN- $\gamma$  of PBMC of DTH<sup>+</sup> subjects. The F3 epitopes however did not. This is possible due to the fact that the PBMC incubated with the synthetic epitopes belonged to DTH<sup>+</sup> subjects and not to untreated patients. The analysis should be extended to untreated patients in order to give more information.

We conclude that, in this investigation, the information disclosed by the immunological assays with the domains was mostly supported by the *in silico* predictions. The use of the single immunogenic domains also induced protective effect increments above those promoted by NH36 and/or the other domains. These results will allow us to guide the initiation of the development of a synthetic vaccine against leishmaniasis.

The importance of our findings is enhanced considering three rare achievements (76): (1) we found CD4 Th1-cell epitopes of a CD4 T cell mediated immunosuppressive disease; (2) they are highly promiscuous and bind to many HL-DR allotypes; and (3) they are extremely conserved and present in *Leishmania* of two subgenera that cause visceral, cutaneous, diffuse, and mucocutaneous leishmaniasis.

Previously, all of the vaccine approaches against leishmaniasis have focused on the stimulation of the CD4 T cell response and have neglected the important contribution of CD8 T cells (14). However defined epitopes for both CD4 (LACK) (77)

and CD8 (KMP11; GP63, CPB, CPA, Lpg2, histone 3 variant, histone H4)-mediated protective responses against *Leishmania* (78, 79) were described. Recently, it has been proposed that vaccine design will improve through the search for potential candidates that share both CD4- and CD8 T-cell-stimulating capabilities (NH36, A2, P4) (8, 12–14, 26, 80) and through their expression as polytope or poly-epitope vaccines (14, 81). Recently published data indicate that CD8 T cells are very important in protection against *L. major* infection induced by a polytope DNA construct expressing individual MHC-I-restricted peptides in BALB/c mice (82). In that study, the vaccine stimulation of CD8 T-cells resulted in partial protection which was abolished by CD8 T-cell depletion resulting in a predominant Th2 response. This directly confirmed the role of CD8 T-cells in early-stage Th1 response polarization (82). We also previously described that the protection of mice against *L. amazonensis* infection induced by F1 was mediated by CD8 T cells and was abolished by CD8 T cell depletion (12). The present investigation represents a step forward in the definition of the epitopes for CD8 T cells involved in IFN- $\gamma$  secretion by human PBMC.

Our results confirm the relevance of NH36 in immune regulation in human VL and identified its immunodominant domains and epitopes that could guide the design of a rational and cross-protective T-cell vaccine against human leishmaniasis.

## AUTHOR CONTRIBUTIONS

MS, FO, DN, and AB conducted the experiments; MS, DN, CB-C, and IP-d-S acquired data; MS, CB-C, MP, CP-d-S, PL, and DR analyzed data; CP-d-S, RA, and PL designed research studies; EC, JM, and AM provided reagents; CP-d-S wrote the manuscript. All the authors have read and approved the final manuscript.

## FUNDING

This work was supported by the following: Conselho Nacional de Desenvolvimento Científico e Tecnológico (CNPQ) (Fellowships 300639/2003-1 to MP, 310977/2014-2 to CP-d-S, 310797/2015-2 to AM, and grant 404400/2012-4 to CP-d-S, MP, PL, RA, JM, EC, and AM); by Fundação Carlos Chagas de Amparo à Pesquisa do Estado de Rio de Janeiro (FAPERJ) (grant E-26-201.583/2014, E-26-102957/2011, and E-26/111.682/2013 to CP-d-S, and fellowships E-26/102415/2010 and E-26/201747/2015 to DN); by Coordenação de Aperfeiçoamento de Pessoal de Nível Superior (grant 23038.005304/2011-0 to MS), by CNPQ-Fundação de Apoio à Pesquisa e a Inovação Tecnológica do Estado de Sergipe-PRONEX (12/2009); and by FAPITEC CNPq (PRONEX) (019.203.02712/2009-8) to RA. EC was supported by a research contract funded via VII PN I+D+I 2013–2016 and FEDER Funds (RICET RD12/0018/0003).

## SUPPLEMENTARY MATERIAL

The Supplementary Material for this article can be found online at <http://journal.frontiersin.org/article/10.3389/fimmu.2017.00227/full#supplementary-material>.

**FIGURE S1 | Schematic of NH36 and domains fermentation and purification process.** Expression and purification protocol (**A**). SDS-PAGE (15 %) with Coomassie Blue staining. The slot of the gel showing the run of the NH36 protein is a part of the same gel that has been lined up to be next to the F3 protein. The original gel contained two other proteins between the F3 and the NH36 antigen that were irrelevant to this investigation (**B**).

**FIGURE S2 | NH36 is a component of SLA.** Serum antibodies of mice vaccinated with NH36, F1, F2, or F3 domains and saponin recognize the SLA antigen of *L. infantum chagasi* in an ELISA assay.

**FIGURE S3 | Correlation between the secretion of IFN- $\gamma$  and IL-17 secretion in response to F1 and F2 and the increases in spleen and liver sizes.** The levels of IFN- $\gamma$  (pg/ml) in response to F1 (**A,B**) and of IL-17 (pg/ml) in response to F1 (**C,D**) and F2 (**E,F**) were assessed in the supernatants of PBMC of patients before treatment ( $n = 4$ ), cured ( $n = 7$ ), and DTH $^+$  subjects ( $n = 9$ ) by the Multiplex® MAP-Luminex assay and were correlated to their increases in spleen and liver sizes. Correlation was calculated using the Spearman two-tailed correlation test.  $R$  and  $p$  values are summarized in **Table 2**. Diagonal lines represent linear regression.

## REFERENCES

- Alvar J, Vélez ID, Bern C, Herrero M, Desjeux P, Cano J, et al. Leishmaniasis worldwide and global estimates of its incidence. *PLoS One* (2012) 7:e35671. doi:10.1371/journal.pone.0035671
- Palatnik-de-Sousa CB, Day MJ. One Health: the global challenge of epidemic and endemic leishmaniasis. *Parasit Vectors* (2011) 4:197. doi:10.1186/1756-3305-4-197
- Khadem F, Uzonna JE. Immunity to visceral leishmaniasis: implications for immunotherapy. *Future Microbiol* (2014) 9:901–15. doi:10.2217/fmb.14.43
- Singh OP, Stober CB, Singh AK, Blackwell JM, Sundar S. Cytokine responses to novel antigens in an Indian population living in an area endemic for visceral leishmaniasis. *PLoS Negl Trop Dis* (2012) 6:e1874. doi:10.1371/journal.pntd.0001874
- Stober CB, Jeronimo SM, Pontes NN, Miller EN, Blackwell JM. Cytokine responses to novel antigens in a peri-urban population in Brazil exposed to *Leishmania infantum chagasi*. *Am J Trop Med Hyg* (2012) 87:663–70. doi:10.4296/ajtmh.2012.12-0180
- Jeronimo SM, Duggal P, Ettinger NA, Nascimento ET, Monteiro GR, Cabral AP, et al. Genetic predisposition to self-curing infection with the protozoan *Leishmania chagasi*: a genomewide scan. *J Infect Dis* (2007) 196:1261–9. doi:10.1086/521682
- Cher DJ, Mosmann TR. Two types of murine helper T cell clone. II. Delayed-type hypersensitivity is mediated by TH1 clones. *J Immunol* (1987) 138:3688–94.
- Kumar R, Nylen S. Immunobiology of visceral leishmaniasis. *Front Immunol* (2012) 3:251. doi:10.3389/fimmu.2012.00251
- Carvalho EM, Barral A, Pedral-Sampaio D, Barral-Netto M, Badaró R, Rocha H, et al. Immunologic markers of clinical evolution in children recently infected with *Leishmania donovani chagasi*. *J Infect Dis* (1992) 165:535–40. doi:10.1093/infdis/165.3.535
- Darrah PA, Patel DT, De Luca PM, Lindsay RW, Davey DF, Flynn BJ, et al. Multifunctional TH1 cells define a correlate of vaccine-mediated protection against *Leishmania major*. *Nat Med* (2007) 13:843–50. doi:10.1038/nm1592
- Coler RN, Duthie MS, Hofmeyer KA, Guderian J, Jayashankar L, Vergara J, et al. From mouse to man: safety, immunogenicity and efficacy of a candidate leishmaniasis vaccine LEISH-F3+GLA-SE. *Clin Transl Immunol* (2015) 4:e35. doi:10.1038/cti.2015.6
- Nico D, Gomes DC, Alves-Silva MV, Freitas EO, Morrot A, Bahia D, et al. Cross-protective immunity to *Leishmania amazonensis* is mediated by CD4+ and CD8+ epitopes of *Leishmania donovani* nucleoside hydrolase terminal domains. *Front Immunol* (2014) 5:189. doi:10.3389/fimmu.2014.00189
- Nico D, Gomes DC, Palatnik-de-Sousa I, Morrot A, Palatnik M, Palatnik-de-Sousa CB. *Leishmania donovani* nucleoside hydrolase terminal domains in cross-protective immunotherapy against *Leishmania amazonensis* murine infection. *Front Immunol* (2014) 5:273. doi:10.3389/fimmu.2014.00273
- Seyed N, Taheri T, Rafati S. Post-genomics and vaccine improvement for *Leishmania*. *Front Microbiol* (2016) 7:467. doi:10.3389/fmicb.2016.00467
- Kaye PM, Aebscher T. Visceral leishmaniasis: immunology and prospects for a vaccine. *Clin Microbiol Infect* (2011) 17:1462–70. doi:10.1111/j.1469-0961.2011.03610.x
- Singh B, Sundar S. Leishmaniasis: vaccine candidates and perspectives. *Vaccine* (2012) 30:3834–42. doi:10.1016/j.vaccine.2012.03.068
- Palatnik-de-Sousa CB, Barbosa Ade F, Oliveira SM, Nico D, Bernardo RR, Santos WR, et al. The FML-vaccine against canine visceral leishmaniasis: from the second generation to the synthetic vaccine. *Exp Rev Vaccines* (2008) 7:833–51. doi:10.1586/14760584.7.6.833
- Saraiva EM, de Figueiredo Barbosa A, Santos FN, Borja-Cabrera GP, Nico D, Souza LO, et al. The FML-vaccine (Leishmune®) against canine visceral leishmaniasis: transmission blocking vaccine. *Vaccine* (2006) 24:2423–31. doi:10.1016/j.vaccine.2005.11.061
- Nogueira FS, Moreira MA, Borja-Cabrera GP, Santos FN, Menz I, Parra LE, et al. Leishmune vaccine blocks the transmission of canine visceral leishmaniasis: absence of *Leishmania* parasites in blood, skin and lymph nodes of vaccinated exposed dogs. *Vaccine* (2005) 23:4805–10. doi:10.1016/j.vaccine.2005.05.011
- Palatnik-de-Sousa CB, Silva-Antunes I, Morgado Ade A, Menz I, Palatnik M, Lavor C. Decrease of the incidence of human and canine visceral leishmaniasis after dog vaccination with Leishmune in Brazilian endemic areas. *Vaccine* (2009) 27:3505–12. doi:10.1016/j.vaccine.2009.03.045
- Freitas EO, Nico D, Guan R, Meyer-Fernandes JR, Clinch K, Evans GB, et al. Immucillins impair *Leishmania (L.) infantum chagasi* and *Leishmania (L.) amazonensis* multiplication in vitro. *PLoS One* (2015) 10:e0124183. doi:10.1371/journal.pone.0124183
- Freitas EO, Nico D, Alves-Silva MV, Morrot A, Clinch K, Evans GB, et al. Immucillins ImmA and ImmH are effective and non-toxic in the treatment of experimental visceral leishmaniasis. *PLoS Negl Trop Dis* (2015) 9:e0004297. doi:10.1371/journal.pntd.0004297
- Paraguai de Souza E, Bernardo RR, Palatnik M, Palatnik de Sousa CB. Vaccination of Balb/c mice against experimental visceral leishmaniasis with the GP36 glycoprotein antigen of *Leishmania donovani*. *Vaccine* (2001) 19:3104–15. doi:10.1016/S0264-410X(01)00031-7
- Al-Wabel MA, Tonui WK, Cui L, Martin SK, Titus RG. Protection of susceptible BALB/c mice from challenge with *Leishmania major* by nucleoside hydrolase, a soluble exo-antigen of *Leishmania*. *Am J Trop Med Hyg* (2007) 77:1060–5.
- Aguilar-Be I, da Silva Zardo R, Paraguai de Souza E, Borja-Cabrera GP, Rosado-Vallado M, Mut-Martin M, et al. Cross-protective efficacy of a prophylactic *Leishmania donovani* DNA vaccine against visceral and

**FIGURE S4 | Correlation between cytokines secretion in culture supernatants and clinical and hematological variables.** The levels of IFN- $\gamma$  and IL-17 (pg/ml) in response to F1 (**A–C**) and F2 (**D,E**) were assessed in the supernatants of PBMC of patients before treatment ( $n = 4$ ), cured ( $n = 7$ ), and DTH $^+$  subjects ( $n = 9$ ) by the Multiplex® MAP-Luminex assay were correlated to the hematological parameters. Additionally, we show the correlation between the increases in spleen and liver increased sizes of 41 untreated VL patients (**F**). Correlation was calculated using the Spearman two-tailed correlation test.  $R$  and  $p$  values are summarized in **Table 2**. Diagonal lines represent linear regression.

**FIGURE S5 | Strategy for the analysis of multifunctional T cell response using a seven-color flow cytometry panel to simultaneously analyze multiple cytokines at the single-cell level in PBMC cultures.** After single cells selection (FSC-A  $\times$  FSC-H), lymphocytes were selected according to a FSC-A versus SSC-A dot plot, followed by CD3 $^+$  gating. Afterwards, CD3 $^+$ CD4 $^+$  and CD3 $^+$ CD8 $^+$  lymphocytes were evaluated inside the CD3 $^+$  gate. CD3 $^+$ CD4 $^+$  and CD3 $^+$ CD8 $^+$  T-cell phenotypes were plotted against each cytokine individually: tumor necrosis factor- $\alpha$  (TNF- $\alpha$ ), interleukin (IL)-2, and interferon- $\gamma$  (IFN- $\gamma$ ). Boolean gating was performed to generate the frequencies of the possible seven combinations of cytokine producing CD4 $^+$  and CD8 $^+$  cells using FlowJo software.

- cutaneous murine leishmaniasis. *Infect Immun* (2005) 73:812–9. doi:10.1128/IAI.73.2.812-819.2005
26. Nico D, Claser C, Borja-Cabrera GP, Travassos LR, Palatnik M, Soares IS, et al. Adaptive immunity against *Leishmania* nucleoside hydrolase maps its c-terminal domain as the target of the CD4+ T cell-driven protective response. *PLoS Negl Trop Dis* (2010) 4:e866. doi:10.1371/journal.pntd.0000866
27. Borja-Cabrera GP, Santos FB, Picillo E, Gravino E, Manna L, Palatnik-de-Sousa CB. Nucleoside hydrolase DNA vaccine against visceral leishmaniasis. *Procedia Vaccinol* (2009) 1:104–9. doi:10.1016/j.provac.2009.07.019
28. Gamboa-León R, Paraguai de Souza E, Borja-Cabrera GP, Santos FN, Myashiro LM, Pinheiro RO, et al. Immunotherapy against visceral leishmaniasis with the nucleoside hydrolase-DNA vaccine of *Leishmania donovani*. *Vaccine* (2006) 24:4863–73. doi:10.1016/j.vaccine.2006.03.005
29. Mauricio IL, Yeo M, Baghaei M, Doto D, Pratlong F, Zemanova E, et al. Towards multilocus sequence typing of the *Leishmania donovani* complex: resolving genotypes and haplotypes for five polymorphic metabolic enzymes (ASAT, GPI, NH1, NH2, PGD). *Int J Parasitol* (2006) 36:757–69. doi:10.1016/j.ijpara.2006.03.006
30. Cui L, Rajasekariah GR, Martin SK. A nonspecific nucleoside hydrolase from *Leishmania donovani*: implications for purine salvage by the parasite. *Gene* (2001) 280:153–62. doi:10.1016/S0378-1119(01)00768-5
31. *Blast-Basic Local Alignment Search Tool*. National Institute of Health (NIH) (2014). Available from: <http://blast.ncbi.nlm.nih.gov/Blast.cgi>
32. De Groot AS, McMurry J, Moise L. Prediction of immunogenicity: in silico paradigms, ex vivo and in vivo correlates. *Curr Opin Pharmacol* (2008) 8:620–6. doi:10.1016/j.coph.2008.08.002
33. Versées W, Goeminne A, Berg M, Vandemeulebroucke A, Haemers A, Augustyns K, et al. Crystal structures of *T. vivax* nucleoside hydrolase in complex with new potent and specific inhibitors. *Biochim Biophys Acta* (2009) 1794:953–60. doi:10.1016/j.bbapap.2009.02.011
34. Iovane E, Giabbai B, Muzzolini L, Matafora V, Fornili A, Minici C, et al. Structural basis for substrate specificity in group I nucleoside hydrolases. *Biochemistry* (2008) 47:4418–26. doi:10.1021/bi702448s
35. Palatnik de Sousa CB, Gomes EM, Paraguai de Souza E, Santos WR, Macedo SR, Medeiros LV, et al. The FML (Fucose Mannose Ligand) of *Leishmania donovani*. A new tool in diagnosis, prognosis, transfusional control and vaccination against human Kala-azar. *Rev Soc Bras Med Trop* (1996) 29:153–63. doi:10.1590/S0037-86821996000200008
36. Nico D, Claser C, Rodrigues MM, Soares IS, Palatnik-de-Sousa CB. Cloning of the Nucleoside hydrolase of *Leishmania donovani* aiming at the development of a synthetic vaccine against visceral leishmaniasis. *Procedia Vaccinol* (2009) 1:115–9. doi:10.1016/j.provac.2009.07.021
37. Rodrigues MHC, Rodrigues KM, Oliveira TR, Cómodo AN, Rodrigues MM, Kocken CH, et al. Antibody response of naturally infected individuals to recombinant *Plasmodium vivax* apical membrane antigen. *Int J Parasitol* (2005) 35:185–92. doi:10.1016/j.ijpara.2004.11.003
38. Saini DK, Pant N, Das TK, Tyagi JS. Cloning, overexpression, purification and matrix-assisted refolding of DevS (Rv 3132c) histidine protein kinase of *Mycobacterium tuberculosis*. *Protein Expr Purif* (2002) 25:203–8. doi:10.1006/prep.2002.1628
39. Shi W, Schramm VL, Almo SC. Nucleoside hydrolase from *Leishmania major*. Cloning, expression, catalytic properties, transition state inhibitors, and the 2.5-å crystal structure. *J Biol Chem* (1999) 274:21114–20. doi:10.1074/jbc.274.30.21114
40. Potestio M, D'Agostino P, Romano GC, Milano S, Ferlazzo V, Aquino A, et al. CD4+ CCR5+ and CD4+ CCR3+ lymphocyte subset and monocyte apoptosis in patients with acute visceral leishmaniasis. *Immunology* (2004) 113:260–8. doi:10.1046/j.1365-2567.2004.01948.x
41. Jeronimo SM, Duggal P, Braz RF, Cheng C, Monteiro GR, Nascimento ET, et al. An emerging peri-urban pattern of infection with *Leishmania chagasi*, the protozoan causing visceral leishmaniasis in northeast Brazil. *Scand J Infect Dis* (2004) 36:443–9. doi:10.1080/00365540410020451
42. Jeronimo SM, Holst AK, Jamieson SE, Francis R, Martins DR, Bezerra FL, et al. Genes at human chromosome 5q31.1 regulate delayed-type hypersensitivity responses associated with *Leishmania chagasi* infection. *Genes Immun* (2007) 8:539–51. doi:10.1038/sj.gene.6364422
43. Ho M, Siongok TK, Lyerly WH, Smith DH. Prevalence and disease spectrum in a new focus of visceral leishmaniasis in Kenya. *Trans R Soc Trop Med Hyg* (1982) 76:741–6. doi:10.1016/0035-9203(82)90095-5
44. Mayrink W, da Costa CA, Magalhaes PA, Melo MN, Dias M, Lima AO, et al. A field trial of a vaccine against American dermal leishmaniasis. *Trans R Soc Trop Med Hyg* (1979) 73:385–7. doi:10.1016/0035-9203(79)90159-7
45. Antunes CM, Mayrink W, Magalhaes PA, Costa CA, Melo MN, Dias M, et al. Controlled field trials of a vaccine against new world cutaneous leishmaniasis. *Int J Epidemiol* (1986) 15:572–80. doi:10.1093/ije/15.4.572
46. Khalil EA, El Hassan AM, Zijlstra EE, Mukhtar MM, Ghalib HW, Musa B, et al. Autoclaved *Leishmania major* vaccine for prevention of visceral leishmaniasis: a randomised, double-blind, BCG-controlled trial in Sudan. *Lancet* (2000) 356:1565–9. doi:10.1016/S0140-6736(00)03128-7
47. Carvalho EM, Badaró R, Reed SG, Jones TC, Johnson WD Jr. Absence of gamma interferon and interleukin 2 production during active visceral leishmaniasis. *J Clin Invest* (1985) 76:2066–9. doi:10.1172/JCI112209
48. Sacks DL, Lal SL, Shrivastava SN, Blackwell J, Neva FA. An analysis of T cell responsiveness in Indian kala-azar. *J Immunol* (1987) 138:908–13.
49. Saha S, Mondal S, Ravindran R, Bhowmick S, Modak D, Mallick S, et al. IL-10 and TGF-beta-mediated susceptibility in kala-azar and post-kala-azar dermal leishmaniasis: the significance of amphotericin B in the control of *Leishmania donovani* infection in India. *J Immunol* (2007) 179:5592–603. doi:10.4049/jimmunol.179.8.5592
50. de Oliveira FA, Barreto AS, Bomfim LG, Leite TR, Dos Santos PL, de Almeida RP, et al. Soluble CD40 ligand in sera of subjects exposed to *Leishmania infantum* infection reduces the parasite load in macrophages. *PLoS One* (2015) 10(10):e0141265. doi:10.1371/journal.pone.0141265
51. Lima-Junior DS, Costa DL, Carregaro V, Cunha LD, Silva AL, Mineo TW, et al. Inflammasome-derived IL-1 $\beta$  production induces nitric oxide-mediated resistance to *Leishmania*. *Nat Med* (2013) 19:909–15. doi:10.1038/nm.3221
52. Kurkjian KM, Mahmudovic AJ, Kellar KL, Haque R, Bern C, Secor WE. Multiplex analysis of circulating cytokines in the sera of patients with different clinical forms of visceral leishmaniasis. *Cytometry A* (2006) 69:353–8. doi:10.1002/cyto.a.20256
53. Costa DL, Rocha RL, Carvalho RM, Lima-Neto AS, Harhay MO, Costa CH, et al. Serum cytokines associated with severity and complications of kala-azar. *Pathog Glob Health* (2013) 107:78–87. doi:10.1179/204773213Y.0000000078
54. Costa AS, Costa GC, Aquino DM, Mendonça VR, Barral A, Barral-Netto M, et al. Cytokines and visceral leishmaniasis: a comparison of plasma cytokine profiles between the clinical forms of visceral leishmaniasis. *Mem Inst Oswaldo Cruz* (2012) 107:735–9. doi:10.1590/S0074-02762012000600005
55. Bhattacharya P, Ghosh S, Ejazi SA, Rahaman M, Pandey K, Ravi Das VN, et al. Induction of IL-10 and TGF $\beta$  from CD4+CD25+FoxP3+ T cells correlates with parasite load in Indian kala-azar patients infected with *Leishmania donovani*. *PLoS Negl Trop Dis* (2016) 10(2):e0004422. doi:10.1371/journal.pntd.0004422
56. Mondal D, Alvar J, Hasnain MG, Hossain MS, Ghosh D, Huda MM, et al. Efficacy and safety of single-dose liposomal amphotericin B for visceral leishmaniasis in a rural public hospital in Bangladesh: a feasibility study. *Lancet Glob Health* (2014) 2:e51–7. doi:10.1016/S2214-109X(13)70118-9
57. Sundar S, Goyal AK, Mandal AK, Makharla MK, Singh VP, Murray HW. Amphotericin B lipid complex in the management of antimony unresponsive Indian visceral leishmaniasis. Spleen size regression in cure. *J Assoc Physicians India* (1999) 47:186–8.
58. Lucero E, Collin SM, Gomes S, Akter F, Asad A, Kumar Das A, et al. Effectiveness and safety of short course liposomal amphotericin B (AmBisome) as first line treatment for visceral leishmaniasis in Bangladesh. *PLoS Negl Trop Dis* (2015) 9(4):e0003699. doi:10.1371/journal.pntd.0003699
59. Nylén S, Sacks D. Interleukin-10 and the pathogenesis of human visceral leishmaniasis. *Trends Immunol* (2007) 28:378–84. doi:10.1016/j.it.2007.07.004
60. Ato M, Stäger S, Engwerda CR, Kaye PM. Defective CCR7 expression on dendritic cells contributes to the development of visceral leishmaniasis. *Nat Immunol* (2002) 3:1185–91. doi:10.1038/ni861
61. Chamakh-Ayari R, Bras-Gonçalves R, Bahi-Jaber N, Petitdidier E, Markikou-Ouni W, Aoun K, et al. In vitro evaluation of a soluble *Leishmania* promastigote surface antigen as a potential vaccine candidate against human leishmaniasis. *PLoS One* (2014) 9:e92708. doi:10.1371/journal.pone.0092708

62. Kaye PM, Svensson M, Ato M, Maroof A, Polley R, Stager S, et al. The immunopathology of experimental visceral leishmaniasis. *Immunol Rev* (2004) 201:239–53. doi:10.1111/j.0105-2896.2004.00188.x
63. Follador I, Araújo C, Bacellar O, Araújo CB, Carvalho LP, Almeida RP, et al. Epidemiologic and immunologic findings for the subclinical form of *Leishmania braziliensis* infection. *Clin Infect Dis* (2002) 34:E54–8. doi:10.1086/340261
64. Chamizo C, Moreno J, Alvar J. Semi-quantitative analysis of cytokine expression in asymptomatic canine leishmaniasis. *Vet Immunol Immunopathol* (2005) 103:67–75. doi:10.1016/j.vetimm.2004.08.010
65. Ramos PK, Carvalho KI, Rosa DS, Rodrigues AP, Lima LV, Campos MB, et al. Serum cytokine responses over the entire clinical-immunological spectrum of human *Leishmania (L.) infantum chagasi* infection. *Biomed Res Int* (2016) 2016:6937980. doi:10.1155/2016/6937980
66. Seder RA, Darrah PA, Roederer M. T-cell quality in memory and protection: implications for vaccine design. *Nat Rev Immunol* (2008) 8:247–58. doi:10.1038/nri2274
67. Uzonna JE, Joyce KL, Scott P. Low dose *Leishmania major* promotes a transient T helper cell type 2 response that is down-regulated by interferon  $\gamma$ -producing CD8+ T cells. *J Exp Med* (2004) 199:1559–66. doi:10.1084/jem.20040172
68. Okwor IB, Jia P, Mou Z, Onyilagha C, Uzonna JE. CD8+ T cells are preferentially activated during primary low dose *Leishmania major* infection but are completely dispensable during secondary anti-*Leishmania* immunity. *PLoS Negl Trop Dis* (2014) 8:e3300. doi:10.1371/journal.pntd.0003300
69. Müller I. Role of T cell subsets during the recall of immunologic memory to *Leishmania major*. *Eur J Immunol* (1992) 22:3063–9. doi:10.1002/eji.1830221206
70. Gurunathan S, Stobie L, Prussin C, Sacks DL, Glaichenhaus N, Iwasaki A, et al. Requirements for the maintenance of Th1 immunity in vivo following DNA vaccination: a potential immunoregulatory role for CD8+ T cells. *J Immunol* (2000) 165:915–24. doi:10.4049/jimmunol.165.2.915
71. Mendez S, Gurunathan S, Kamhawi S, Belkaid Y, Moga MA, Skeiky YA, et al. The potency and durability of DNA- and protein-based vaccines against *Leishmania major* evaluated using low-dose intradermal challenge. *J Immunol* (2001) 166:5122–8. doi:10.4049/jimmunol.166.8.5122
72. Kao DJ, Hodges RS. Advantages of a synthetic peptide immunogen over a protein immunogen in the development of an anti-pilus vaccine for *Pseudomonas aeruginosa*. *Chem Biol Drug Des* (2009) 74:33–42. doi:10.1111/j.1747-0285.2009.00825.x
73. Plassmeyer ML, Reiter K, Shimp RL Jr, Kotova S, Smith PD, Hurt DE, et al. Structure of the *Plasmodium falciparum* circumsporozoite protein, a leading malaria vaccine candidate. *J Biol Chem* (2009) 284:26951–63. doi:10.1074/jbc.M109.013706
74. Liu H, Bi W, Wang Q, Lu L, Jiang S. Receptor binding domain based HIV vaccines. *Biomed Res Int* (2015) 2015:594109. doi:10.1155/2015/594109
75. Kolpe A, Schepens B, Fiers W, Saelens X. M2-based influenza vaccines: recent advances and clinical potential. *Expert Rev Vaccines* (2017) 16:123–36. doi:10.1080/14760584.2017.1240041
76. Parra-López C, Calvo-Calle JM, Cameron TO, Vargas LE, Salazar LM, Patarroyo ME, et al. Major histocompatibility complex and T cell interactions of a universal T-cell epitope from *Plasmodium falciparum* circumsporozoite protein. *J Biol Chem* (2006) 281:14907–17. doi:10.1074/jbc.M511571200
77. Launois P, Pingel S, Himmelrich H, Locksley R, Louis J. Different epitopes of the LACK protein are recognized by V beta 4 V alpha 8 CD4+ T cells in H-2b and H-2d mice susceptible to *Leishmania major*. *Microbes Infect* (2007) 9:1260–6. doi:10.1016/j.micinf.2007.05.017
78. Basu R, Roy S, Walden P. HLA class I-restricted T cell epitopes of the kinetoplastid membrane protein-11 presented by *Leishmania donovani*-infected human macrophages. *J Infect Dis* (2007) 195:1373–80. doi:10.1086/513439
79. Duarte A, Queiroz AT, Tosta R, Carvalho AM, Barbosa CH, Bellio M, et al. Prediction of CD8+ epitopes in *Leishmania braziliensis* proteins using EPIBOT: in silico search and in vivo validation. *PLoS One* (2015) 10:e0124786. doi:10.1371/journal.pone.0124786
80. Fernandes AP, Coelho EA, Machado-Coelho GL, Grimaldi G Jr, Gazzinelli RT. Making an anti-amastigote vaccine for visceral leishmaniasis: rational, update and perspectives. *Curr Opin Microbiol* (2012) 15:476–85. doi:10.1016/j.mib.2012.05.002
81. De Groot AS, Sbai H, Aubin CS, McMurry J, Martin W. Immuno-informatics: mining genomes for vaccine components. *Immunol Cell Biol* (2002) 80:255–69. doi:10.1046/j.1440-1711.2002.01092.x
82. Zandieh M, Kashi T, Taheri T, Zahedifard F, Taslimi Y. Assessment of protection induced by DNA and live vaccine encoding *Leishmania* MHC class I restricted epitopes against *L. major* challenge in Balb/c mice model. *J Microb Biochem Technol* (2015) 7:427–38. doi:10.4172/1948-5948.1000250

**Conflict of Interest Statement:** DN, MP, and CP-d-S are inventors of the patent file PI1015788-3 (INPI, Brazil). MS, IP-d-S, EC, JM, PL, CB-C, AM, DR, and RA declare no conflict of interest.

Copyright © 2017 Barbosa Santos, Nico, de Oliveira, Barreto, Palatnik-de-Sousa, Carrillo, Moreno, de Luca, Morrot, Rosa, Palatnik, Bani-Corrêa, de Almeida and Palatnik-de-Sousa. This is an open-access article distributed under the terms of the Creative Commons Attribution License (CC BY). The use, distribution or reproduction in other forums is permitted, provided the original author(s) or licensor are credited and that the original publication in this journal is cited, in accordance with accepted academic practice. No use, distribution or reproduction is permitted which does not comply with these terms.



# F1 Domain of the *Leishmania (Leishmania) donovani* Nucleoside Hydrolase Promotes a Th1 Response in *Leishmania (Leishmania) infantum* Cured Patients and in Asymptomatic Individuals Living in an Endemic Area of Leishmaniasis

OPEN ACCESS

**Edited by:**

Rashika El Ridi,  
Cairo University, Egypt

**Reviewed by:**

Rajiv Kumar,  
Banaras Hindu University, India  
Clara Lúcia Barbéria,  
Universidade Federal de São Paulo,  
Brazil

**\*Correspondence:**

Clarisa B. Palatnik-de-Sousa  
immgcpa@micro.utfpr.br

<sup>†</sup>These authors have contributed  
equally to this work.

**Specialty section:**

This article was submitted to  
Vaccines and Molecular  
Therapeutics, a section of the journal  
*Frontiers in Immunology*

**Received:** 07 April 2017

**Accepted:** 13 June 2017

**Published:** 12 July 2017

**Citation:**

Carrillo E, Fernandez L, Ibarra-Meneses AV, Santos MLB, Nico D, de Luca PM, Correa CB, de Almeida RP, Moreno J and Palatnik-de-Sousa CB (2017) F1 Domain of the *Leishmania (Leishmania) donovani* Nucleoside Hydrolase Promotes a Th1 Response in *Leishmania (Leishmania) infantum* Cured Patients and in Asymptomatic Individuals Living in an Endemic Area of Leishmaniasis. *Front. Immunol.* 8:750.  
doi: 10.3389/fimmu.2017.00750

Eugenio Carrillo<sup>1†</sup>, Laura Fernandez<sup>1†</sup>, Ana Victoria Ibarra-Meneses<sup>1</sup>,  
Micheli L. B. Santos<sup>2</sup>, Dirlei Nico<sup>3</sup>, Paula M. de Luca<sup>4</sup>, Cristiane Bani Correa<sup>5</sup>,  
Roque Pacheco de Almeida<sup>2,6</sup>, Javier Moreno<sup>1</sup> and Clarisa B. Palatnik-de-Sousa<sup>3,6\*</sup>

<sup>1</sup>WHO Collaborating Centre for Leishmaniasis, Centro Nacional de Microbiología, Instituto de Salud Carlos III, Madrid, Spain

<sup>2</sup>Departamento de Medicina, Hospital Universitário, Universidade Federal de Sergipe, Aracaju, Brazil, <sup>3</sup>Instituto de Microbiologia Paulo de Góes, Universidade Federal do Rio de Janeiro, Rio de Janeiro, Brazil, <sup>4</sup>Laboratório de Imunoparásitologia, Instituto Oswaldo Cruz, Rio de Janeiro, Brazil, <sup>5</sup>Departamento de Morfologia, Universidade Federal de Sergipe, Aracaju, Brazil, <sup>6</sup>Instituto Nacional de Ciência e Tecnologia de Investigações em Imunologia, São Paulo, Brazil

The *Leishmania (Leishmania) donovani* nucleoside hydrolase NH36 is the main antigen of the Leishmune® vaccine and one of the promising candidates for vaccination against visceral leishmaniasis. The antigenicity of the N-terminal (F1), the central (F2), or the C-terminal recombinant domain (F3) of NH36 was evaluated using peripheral blood mononuclear cells (PBMC) from individuals infected with *L. (L.) infantum* from an endemic area of visceral leishmaniasis of Spain. Both NH36 and F1 domains significantly increased the PBMC proliferation stimulation index of cured patients and infected asymptomatic individuals compared to healthy controls. Moreover, F1 induced a 19% higher proliferative response than NH36 in asymptomatic exposed subjects. In addition, in patients cured from visceral leishmaniasis, proliferation in response to NH36 and F1 was accompanied by a significant increase of IFN-γ and TNF-α secretion, which was 42–43% higher, in response to F1 than to NH36. The interleukin 17 (IL-17) secretion was stronger in asymptomatic subjects, in response to F1, as well as in cured cutaneous leishmaniasis after NH36 stimulation. While no IL-10 secretion was determined by F1, a granzyme B increase was detected in supernatants from cured patients after stimulation with either NH36 or F1. These data demonstrate that F1 is the domain of NH36 that induces a recall cellular response in individuals with acquired resistance to the infection by *L. (L.) infantum*. In addition, F1 and NH36 discriminated the IgG3 humoral response in patients with active visceral leishmaniasis due to *L. (L.) donovani* (Ethiopia) and *L. (L.) infantum* (Spain) from that of endemic and non-endemic area controls. NH36 showed higher reactivity with sera from *L. (L.) donovani*-infected individuals, indicating species specificity. We conclude that the F1 domain, previously characterized as an inducer

of the Th1 and Th17 responses in cured/exposed patients infected with *L. (L.) infantum chagasi*, may also be involved in the generation of a protective response against *L. (L.) infantum* and represents a potential vaccine candidate for the control of human leishmaniasis alone, or in combination with other HLA epitopes/antigens.

**Keywords:** human visceral leishmaniasis, cutaneous leishmaniasis, nucleoside hydrolase, B cell epitopes, T cell epitopes, adaptive immunity

## INTRODUCTION

Leishmaniasis is a vector-born infectious disease caused by a group of protozoan parasites of the genus *Leishmania*. *Leishmania (L.) infantum* infection is endemic in parts of the Mediterranean basin, Asia, and Central and South America, where it is widespread and represents a serious public health problem. In Spain, the infection can be either asymptomatic or manifest in both cutaneous (CL) and visceral (VL) forms (1, 2), the last one being fatal if untreated (3).

While vaccination has been considered as a very effective tool for the eradication of canine visceral leishmaniasis (canine VL) (4, 5) and four veterinary vaccines were already licensed (6–9), there is still no vaccine available for use in humans. In Europe, there are two veterinary vaccines, one composed of the 54 kDa native excreted/secreted protein (Canileish) (6) and the other a chimera recombinant multiprotein protein Q, which contains the acidic ribosomal proteins Lip2a, Lip2b, P0, and histone H2A (7) (Latifend). In Brazil, the FML glycoprotein extract of *L. (L.) donovani* (Leishmune®) (8–11) was the first commercial vaccine in the world licensed in 2003. After that, the A2 recombinant protein of *L. (L.) infantum chagasi* (Leish-Tec®) (12) was also licensed in Brazil, in 2007 (13).

While untreated VL patients showed a failure in the T-cell proliferative response to leishmanial antigens, recovery from disease and resolution of infection correlate with the induction of a memory Th1 response in cured/exposed asymptomatic *Leishmania*-infected individuals (14, 15). The ability of vaccine candidates to elicit a Th1 response in infected hosts is indicative of the respective antigen presentation during infection and its potential to generate protection, if used as a component in a vaccine formulation. Many *Leishmania* antigens have been assayed as vaccine candidates in animal models with variable success (16–18). The main antigen of Leishmune® is the *L. (L.) donovani* nucleoside hydrolase (NH36) (8). Vaccination with NH36 DNA has proven to induce protection against murine cutaneous and visceral leishmaniasis (19–25) as well as against canine VL (26, 27) mediated by a CD4+ T-cell-dependent interferon (IFN)- $\gamma$  response (21). Furthermore, the N-terminal domain (F1, amino acids 1–103), the central domain (F2, amino acids 104–198), or the C-terminal recombinant domain (F3, amino acids 199–314) of NH36 have been tested as vaccine candidates against *L. (L.) infantum chagasi* challenge, and F1- and F3-vaccinated mice induced increased levels of IFN- $\gamma$  and tumor necrosis factor (TNF) (22). Protection in mice against *L. (L.) infantum chagasi* infection was mediated by a CD4+ T-cell response to the F3 domain. The intradermal response to leishmanial antigen (IDR) and an increased tumor necrosis

factor alpha (TNF- $\alpha$ ) secretion were the strong correlates of this F3 domain-induced protection (22).

In contrast, prevention and cure of cutaneous leishmaniasis caused by *L. (L.) amazonensis* involved a CD8+ T-cell response to the F1 domain, besides the CD4+ T-cell response to the F3 domain (23, 24). We recently described that the *in silico*-predicted epitopes of *L. (L.) donovani*-NH36 are highly conserved in the nucleoside hydrolase of *L. amazonensis* (24). This justifies the high cross-protection obtained against *L. (L.) amazonensis* infection of mice, after vaccination with F1 and F3 (23–25). Furthermore, a recombinant chimera composed of the F1 and F3 domains cloned in tandem optimized that vaccine efficacy (25).

The *in silico* analysis revealed that the predicted epitopes of NH36 for HLA-DR and HLA-A and B histocompatibility molecules of humans (28) slightly differ from those described for MHC molecules of mice (22, 24). In spite of that difference, the F1 domain, which induced a CD8+ T-cell-mediated protection against cutaneous leishmaniasis of mice (22, 24, 25), shares important epitopes for the generation of a Th1 and CD8+ T-cell responses of human VL patients infected with *L. (L.) infantum chagasi* from Sergipe, Brazil (28). However, while *L. (L.) infantum chagasi* is the etiological agent of VL in America, the disease is caused by *L. (L.) infantum* in Europe. We recently showed that the epitopes of NH36 recognized by the histocompatibility molecules of humans are highly conserved among species of the *Leishmania* genus that cause both the visceral and the cutaneous forms of leishmaniasis in all continents (28). In addition, we identified the NH36 domains, which are the markers of VL resistance, in asymptomatic and cured subjects and of clinical VL outcomes, in a Brazilian endemic area of *L. (L.) infantum chagasi* infection (28).

As a further step in the development of a universal vaccine, able to protect against human VL in Europe and America, the identification of the main immunogenic domains of *L. (L.) donovani*-NH36 recognized by human asymptomatic and cured patients, infected by *L. (L.) infantum*, in Europe is necessary. In addition, it is important to identify if the domains of NH36 are recognized differently by patients infected by *L. (L.) infantum*, which develop the visceral, or the cutaneous form of leishmaniasis (1, 2).

In this investigation, we report the recognition of NH36 and its domains by peripheral blood mononuclear cells (PBMC) of *Leishmania*-exposed and cured individuals from an *L. (L.) infantum* endemic area of Spain. The proliferation to NH36 and F1 domains was accompanied by a statistical increase in IFN- $\gamma$ , TNF- $\alpha$ , interleukin (IL)-17, and granzyme secretion. Our data demonstrate that F1 is a potential candidate for the development of a synthetic human vaccine formulation against VL in Europe and America.

## MATERIALS AND METHODS

### Ethical Statement

This study was approved by the Hospital de Fuenlabrada (Madrid) Ethics and Research Committee (APR 12-65 and APR 14-64). In addition, the protocols for the collection of sera samples of healthy blood donors of the Hospital Universitário Clementino Fraga Filho (HUCFFo)-Blood Transfusion service of the Universidade Federal do Rio de Janeiro (Rio de Janeiro, Brazil) were approved by the Comité de Ética em Pesquisa of the HUCFFo-Faculdade de Medicina according to the GM-MS 158-2016 regulation of the Brazilian Ministry of Health. All participants gave their written informed consent.

### Blood and Sera Samples

Subjects included in this study were residents of Fuenlabrada, an *L. (L.) infantum* postoutbreak area of Madrid, Spain. Blood samples were obtained from the patients of the Hospital de Fuenlabrada, from 2013 to 2015, and forwarded to the Instituto de Salud Carlos III, where the immunological assays were performed. Patients clinically diagnosed with either visceral (VL) or cutaneous leishmaniasis (CL) were treated with liposomal amphotericin B or with intralesional meglumine antimoniate, respectively. Three months after the end of the treatment, cure was confirmed in 16 patients. Their PBMC were used for a preliminary screening of antigenicity in a cell lymphoproliferation assay. Further lymphoproliferation analysis and quantification of cytokines secreted to the supernatants were performed in antigen-stimulated PBMC from additional 10 patients cured from visceral leishmaniasis (CVL) and eight individuals cured from cutaneous leishmaniasis (CCL).

In addition, healthy blood donors of the Hospital de Fuenlabrada-Blood Bank ( $n = 41$ ) were screened according to their response to the soluble *Leishmania* antigen (SLA) in an *in vitro* PBMC proliferation assay. Among them, 11 donors reacted positively and were considered as *Leishmania*-infected asymptomatic subjects. Moreover, 30 subjects with negative reaction in the SLA proliferation assay were considered as endemic area normal healthy controls and were randomly distributed for lymphoproliferative assays ( $n = 17$ ) and cytokine analyses ( $n = 13$ ).

For ELISA, we analyzed sera samples of 33 *L. (L.) infantum*-VL cases from Spain. Their clinical status was confirmed by positive results in the direct agglutination test results (DAT) and rK39 serological assays. Furthermore, 24 cases of *L. (L.) donovani*-VL infection from Amhara, Ethiopia, were confirmed by their positive DAT results and negative delayed type of hypersensitivity (DTH) reactions to leishmanial antigen (29). Asymptomatic subjects, in contrast, showed DAT-negative and DTH-positive responses. All the sera samples of *L. (L.) infantum*- and *L. (L.) donovani*-infected individuals belong to the Instituto de Salud Carlos III-WHO Collaborating Center for Leishmaniasis-Biobank. This biobank is registered in the National Registry of Biobanks with reference C.000898 (in accordance with the regulation established by RD1716/2011 Spain).

We also included, as controls, 25 sera samples of healthy blood donors from the Hospital de Fuenlabrada-Blood Bank and 23 sera of healthy blood donors from Rio de Janeiro, a VL

non-endemic area of Brazil (NEC), collected at the HUCFFo-Blood Transfusion service, who tested negatively for hepatitis B and C, HIV, syphilis, HTV, and Chagas disease.

### Antigens

Soluble *Leishmania* antigen (SLA) was obtained from a stationary phase-promastigote culture of *L. (L.) infantum* (JPC strain, MCAN/ES/98/LLM-722). Briefly, promastigotes were washed in PBS and centrifuged at 1,000 g for 20 min at 4°C. The *Leishmania* pellet was suspended in lysis buffer (50 mM Tris/5 mM EDTA/HCl, pH 7), submitted to a freeze and thaw procedure, and sonicated and centrifuged at 27,000 g for 4 h at 4°C. The supernatant was aliquoted in sterile conditions and stored at -20°C. Protein concentration in the extract was determined using the Pierce BCA Protein Assay Kit (Thermo Scientific, USA) following the manufacturer's instructions.

Nucleotide and amino acid sequence data of NH36 are available in the EMBL, GenBank™, and DDJB databases under the accession codes AY007193 and AAG02281.1, respectively, and in the SWISS-PROT database under the accession code Q8WQX2. The recombinant NH36 antigen, composed of a sequence of 314 amino acids, i.e., N-terminal (F1, amino acids 1–103), central (F2, amino acids 104–198), and C-terminal (F3, amino acids 199–314) domains, was cloned in *E. coli* (22) and expressed and purified as modified from the methods of Rodrigues et al. (30) and Saini et al. (31).

Briefly, the protein expression was induced in bacterial suspensions with 1 mM IPTG for 4 h and disrupted by sonication. Pellets were washed with 0.5% CHAPS in 10 mM Tris HCl, pH 8.0, and solubilized in a 20 mM Tris HCl, pH 8.0, 500 mM NaCl, 10% glycerol, 8 M urea-containing buffer. After centrifugation, the proteins in supernatants were purified in a Ni-NTA column using imidazol, refolded with urea and reduced glutathione, and dialyzed. Absence of LPS was confirmed using the "Limulus Amebocyte Lysate" QCL-1000, Lonza kit. The fractions containing the NH36, F1, F2, and F3 recombinant antigens were recovered, dialyzed, and preserved at -80°C. The yield of each expression batch was 4.62 mg for NH36, 5.00 mg for F1, 3.5 mg for F2, and 3.75 mg for F3.

The NH sequences of *L. (L.) infantum* (PubMed databank code: AMP43260.1 and CA F05930.1) were compared with those of NH36 of *L. (L.) donovani* using the PubMed NIH-Blast protein tool.

### PBMC Culture and Cell Proliferation Assay

Peripheral blood mononuclear cells were isolated from heparinized blood by Ficoll-Hypaque gradient (Lymphocytes Isolation Solution, Rafer, UK). PBMC were washed with PBS and suspended in RPMI 1640 (Lonza, Sweden) supplemented with 10% fetal bovine serum and 100 U/ml penicillin/streptomycin (Lonza, Sweden). Aliquots containing  $2 \times 10^5$  cells/well were distributed in 96-well plates and cultured with supplemented RPMI 1640 medium alone or with the addition of 10 µg/ml of SLA, NH36, F1, F2, or F3 at 37°C in a 5% CO<sub>2</sub> incubator. Bromodeoxyuridine (BrDU) was added 16 h before the end of the 5-day incubation period, and the cell proliferation was measured by BrDU incorporation using the Cell Proliferation Biotrak ELISA System Kit

(GE Healthcare life Science, UK). Absorbance values were read at 450 nm in a microplate photometer (Multiskan FC, Thermo Scientific, USA), and results were expressed as stimulation indexes (SI), which represent the ratio between the absorbance mean of stimulated cells and the absorbance mean of unstimulated cells. Supernatants were collected and stored at -20°C until analyzed for cytokine secretion.

### Multiplex Analysis of Cytokines

The levels of the secreted IFN- $\gamma$ , TNF- $\alpha$ , IL-10, IL-17A, and granzyme B were measured in 50  $\mu$ l of the supernatants from SLA, NH36, and F1 (10  $\mu$ g/ml) stimulated PBMC by flow cytometry analysis using the BD Cytometric Bead Array Human Flex set (Becton & Dickinson Bioscience, USA), as previously described (32). Data were acquired in an FACSCalibur cytometer and analyzed using the FCAP Array software Version 3.0 (Becton & Dickinson Bioscience, USA).

### ELISA

MaxiSorp 96-well plates were coated with 100  $\mu$ l/well of 20  $\mu$ g/ml of NH36 and F1 recombinant proteins diluted in carbonate buffer (15 mM Na<sub>2</sub>CO<sub>3</sub>, 28 mM NaHCO<sub>3</sub>, pH 9.6). After blocking with 1% BSA supplemented with PBS for 1 h at 37°C, plates were incubated with 100  $\mu$ l of 1:200 diluted sera samples in PBS -0.05% Tween 20, for 1 h at 37°C. Plates were subsequently incubated with 1/2,000 diluted mouse antihuman IgG3 HRP conjugate (Invitrogen, USA) for 30 min at 37°C, and immune complexes were revealed with SIGMAFAST OPD peroxidase substrate (Sigma-Aldrich, USA). The absorbance was measured at 492 nm using a microplate photometer (Multiskan FC, Thermo Scientific, USA). The cutoff values were calculated using the receiver operating characteristic (ROC) analysis (33, 34) using the Graphpad Prism6 program and the three categories of accuracy based on AUC-ROC analysis, as described by Solano Gallego et al. (33). We additionally calculated the cutoff values using the Youden index (35–37).

### Statistical Analysis

Data were analyzed using the Mann-Whitney *U* test of the GraphPad Prism version 5.0 software (GraphPad Software, La Jolla, CA, USA). Significance was set at  $p \leq 0.05$ .

## RESULTS

### F1 Is the Main Domain of NH36 Recognized by the Lymphoproliferative Response of VL Cured and Asymptomatic Individuals

In VL, the cellular immune response to leishmanial antigens is lost during the active disease but is maintained in the infected asymptomatic subjects and cured individuals. We, therefore, decided to study the lymphoproliferative response of these three populations to the NH36 and its domains, using samples of *L. (L.) infantum*-infected subjects obtained from the endemic area of Spain.

An initial screening with NH36, F1, F2, and F3 disclosed that only the NH36 ( $p = 0.042$ ) and F1 ( $p = 0.019$ ) domains induced significant differences between cured leishmaniasis patients and negative controls (Figure 1A). Both NH36 and F1 promoted 1.4-fold increases of their respective SI, which were 30–31% higher in cured patients than in negative controls (Figure 1A).

Based on the cellular immune response results, we decided to focus this study in testing the antigenicity of NH36 and F1 in asymptomatic individuals and patients cured of VL and CL, from the same VL endemic area of Spain. Incubation with either NH36 or F1 induced higher lymphoproliferative responses in PBMC of asymptomatic subjects and cured VL and CL patients than in endemic area controls (Figure 1B). The responses of asymptomatic individuals to NH36 or F1 antigens were not different from those of the cured VL or CL patients. However, it is worth to note that, in the asymptomatic subjects, the F1 domain induced a 19% higher stimulation index than NH36, equivalent to 1.2-fold increase. This result confirmed the antigenic predominance of F1 in acquired resistance to the disease (Figure 1B). We, therefore, concluded that the lymphoproliferative response of cured and asymptomatic subjects against the NH36 antigen is mainly directed toward its F1 immunodominant domain.

Similar to what detected for NH36 and F1 (Figure 1B), we also observed SLA-mediated stimulation in asymptomatic and cured patients (Figure 1C), but with higher SI, as expected for being composed of multiple antigens. In contrast to NH36 and F1, which stimulated PBMC of cured CL, VL, and asymptomatic patients to a similar extent, the SLA complex was preferably recognized by the asymptomatic subjects and cured VL patients (Figure 1C).

### F1 Enhances the Th1 and Th17 Cytokine and Cytotoxic Responses

Regarding the Th1-cytokine response, both NH36 and F1 promoted higher IFN- $\gamma$  secretion in asymptomatic subjects and cured CL and VL patients than in their respective endemic area controls ( $p < 0.0001$ ) (Figure 2A). The highest IFN- $\gamma$  secretion was observed in cured VL patients against the F1 domain. In fact, the F1 peptide induced 42% more IFN- $\gamma$  secretion than NH36 (1.7-fold increase) (Figure 2A). Stimulation with SLA, in contrast, also promoted higher IFN- $\gamma$  secretion in all groups of patients than in controls ( $p < 0.0001$ ). The highest response to SLA was observed in asymptomatic individuals and, to a lower extent, in cured VL patients (Figure 2B).

As observed for IFN- $\gamma$  (Figure 2A), a similar performance was observed for TNF- $\alpha$  secretion, which was also more pronounced in cured VL patients, in this case against both the NH36 antigen and the F1 domains (Figure 2C), and was 43% higher in response to F1 than to NH36 (1.8-fold increase). SLA stimulation, in contrast, promoted less TNF- $\alpha$  secretion than the F1 domain (Figure 2C) and a main response observed in asymptomatic subjects ( $p \leq 0.0001$ ) (Figure 2D).

In addition, IL-17A was secreted by all groups of patients, in response to NH36 (Figure 2E), and by asymptomatic and cured CL patients, in response to F1 (Figure 2F). The highest NH36-specific IL-17A was observed in cured CL patients, while

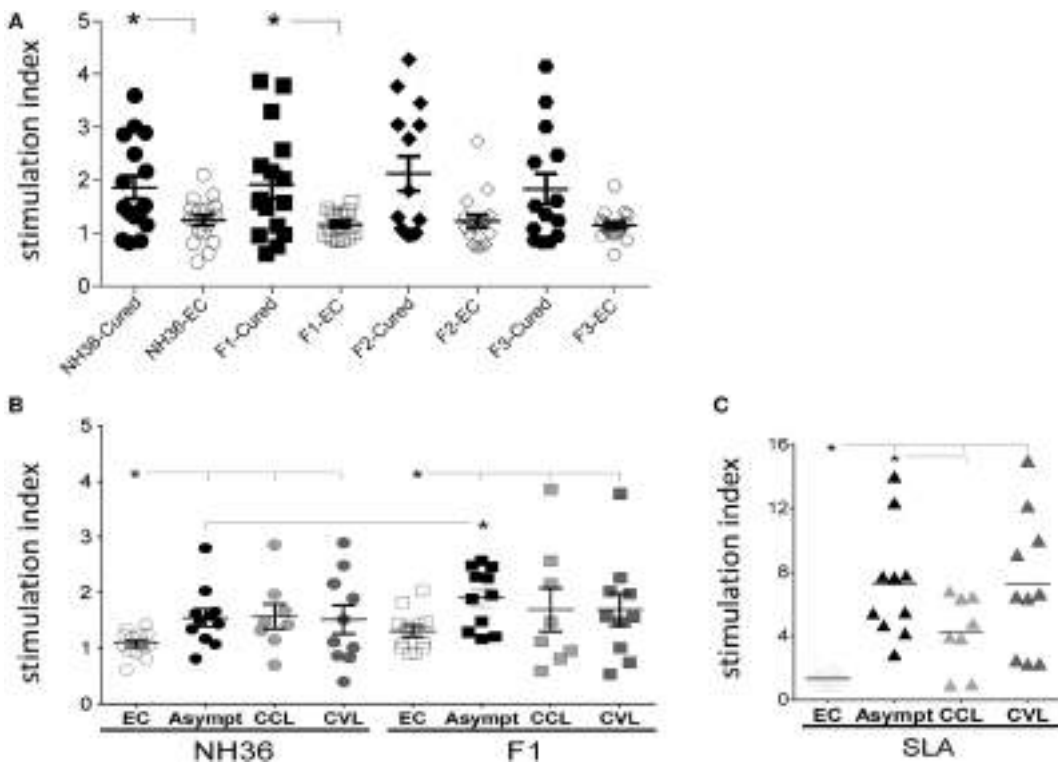


**FIGURE 1 |** F1 significantly enhances the lymphoproliferative response of cured and asymptomatic visceral leishmaniasis (VL) patients. **(A)** A preliminary screening of the specific proliferation to F1, F2, F3, and NH36 antigens was performed using peripheral blood mononuclear cells from cured VL patients and negative endemic controls (EC) ( $n = 14–16$ ). **(B)** Anti-NH36 and anti-F1 proliferative responses were assessed in EC ( $n = 13$ ), asymptomatic subjects (Asympt) ( $n = 11$ ), cured cutaneous leishmaniasis (CCL) ( $n = 8$ ), and cured VL patients (CVL) ( $n = 10$ ). **(C)** Soluble *Leishmania* antigen (SLA) proliferative responses was assessed in EC ( $n = 10$ ), asymptomatic subjects (Asympt) ( $n = 10$ ), CCL ( $n = 8$ ), and cured VL patients (CVL) ( $n = 10$ ). Each symbol represents one individual; bars represent the mean of the experimental groups. Mann–Whitney test was used to compare clinical groups ( $p \leq 0.05$ ).

asymptomatic developed the most pronounced response to F1 (Figure 2E). As observed for IFN- $\gamma$  (Figure 2B) and TNF- $\alpha$  secretion (Figure 2D), SLA stimulation induced a specific increase in IL-17A in asymptomatic individuals. The potency of the NH36 and F1 antigens is remarkable when compared with that of SLA control, which in spite of being composed of many *Leishmania* proteins and PAMPs and being expected to potentiate the cytokine response, promoted a much lower secretion of TNF- $\alpha$  and IL-17A (Figures 2D,F).

Regarding the Th2-cytokine response to the antigens, the global antigen-specific IL-10 response was very low. In fact, while no increase in IL-10 secretion was observed against F1, only PBMC of cured VL patients, incubated with NH36, secreted IL-10 (Figure 3A). SLA, in contrast, stimulated IL-10 secretion in all groups of patients ( $p \leq 0.05$ ) and was predominant in asymptomatic subjects (Figure 3B), as detected for IFN- $\gamma$ , TNF- $\alpha$ , and IL-17A secretions (Figures 2B,D,F).

Suggesting that NH36 and F1 are capable of triggering a potential Th1 response, the IFN- $\gamma$ /IL-10 and TNF- $\alpha$ /IL-10 ratios induced by both antigens were higher in asymptomatic individuals and cured CL and VL patients than in the endemic area controls (Table 1). In addition, in response to both antigens, the TNF- $\alpha$ /IL-10 ratios were higher than the IFN- $\gamma$ /IL-10 ratios (Table 1).

Moreover, F1 was more potent than NH36 in the development of the IFN- $\gamma$ /IL-10 and TNF- $\alpha$ /IL-10 ratios, in all groups of patients (Table 1). This means that the capability of inducing an enhancement of IFN- $\gamma$ /IL-10 and TNF- $\alpha$ /IL-10 ratios is enriched in F1 (Table 1). Calculation of this enrichment increment disclosed that F1 is 38% more potent than NH36 in the induction of IFN- $\gamma$ /IL-10 by cured VL patients. In addition, F1 is 39 and 42% stronger than NH36 in an increase in the TNF- $\alpha$ /IL-10 ratios in asymptomatic subjects and cured VL patients, respectively (Table 1).

Furthermore, as an indicator of the activity of CD8 $^{+}$  T and cytotoxic cells, we measured the secretion of granzyme B. PBMC of cured VL and CL patients stimulated with either NH36 or F1 secreted more granzyme B than negative controls (Figure 3C), indicating the induction of cytotoxic activity by both antigens. SLA stimulation, in contrast, increased the granzyme B secretion from PBMC of the asymptomatic subjects ( $p \leq 0.0001$ ) and the cured VL ( $p = 0.0075$ ) and CL patients ( $p \leq 0.0001$ ) (Figure 3D).

Our results disclosed that the F1 domain was more potent than the cognate NH36 protein in the induction of IFN- $\gamma$  and TNF- $\alpha$  secretions in cured VL patients, did not enhance the secretion of IL-10, and promoted, together with NH36, an increased cytotoxic activity in patients cured from CL and VL. In addition, F1 together with NH36 stimulated the IL-17A secretion by PBMC of asymptomatic individuals.

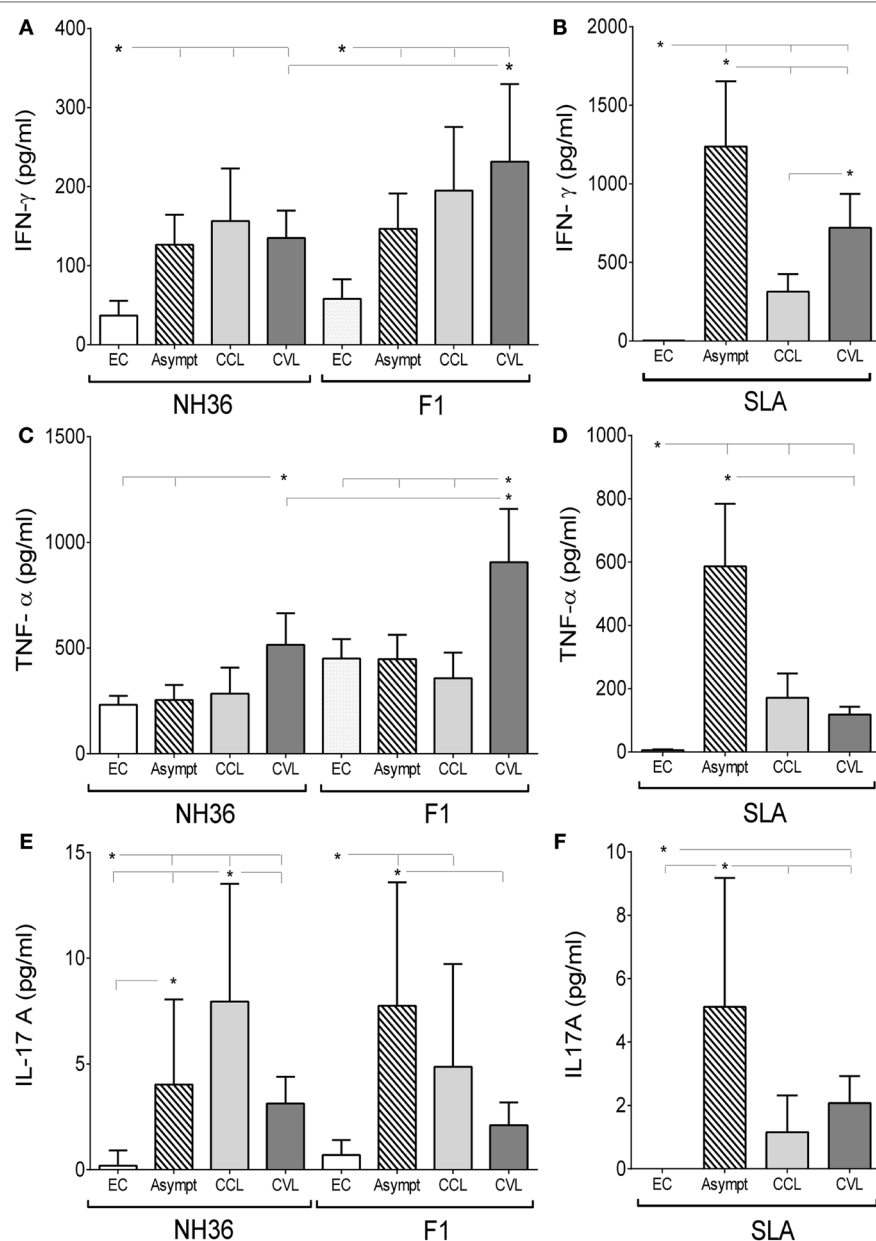


**FIGURE 2 |** F1 and NH36 enhance the peripheral blood mononuclear cells (PBMC) secretion of interferon (IFN)- $\gamma$ , tumor necrosis factor alpha (TNF- $\alpha$ ), and interleukin (IL)-17A. The secretion of IFN- $\gamma$  (A), TNF- $\alpha$  (C), and IL-17A (E) was assessed in supernatants of NH36- and F1-stimulated PBMC of endemic negative controls (EC,  $n = 13$ ), asymptomatic subjects (Asympt,  $n = 11$ ), cured cutaneous leishmaniasis (CCL,  $n = 8$ ) and cured visceral leishmaniasis (CVL,  $n = 10$ ) patients from visceral leishmaniasis endemic area. Supernatants of PBMC stimulated by the soluble *Leishmania* antigen (SLA) control were also assayed for IFN- $\gamma$  (B), TNF- $\alpha$  (D), and IL-17A (F) secretions. Each symbol represents one individual; bars represent the mean of the experimental groups. Mann-Whitney test was used to compare clinical groups ( $^*p \leq 0.05$ ).

## NH36 and F1 Are Recognized by IgG3 Antibodies of Patients Infected by *L. (L.) donovani* and *L. (L.) infantum* with Active VL

We followed our analysis aiming to elucidate the cross-species capabilities of the NH36 antigen and extended the analysis of the humoral response to the antigens, using sera samples of patients

from Ethiopia infected with *L. (L.) donovani* and patients from Spain infected with *L. (L.) infantum* (Figure 4).

The IgG3 antibody subtype has been described as a serological marker of VL, and its decrease after successful treatment suggests that it may be a useful tool for diagnosis. The anti-NH36 IgG3 antibodies were 55% higher in patients with active VL from Ethiopia, caused by *L. (L.) donovani*, than in patients infected with *L. (L.) infantum* ( $p = 0.004$ ) and also higher than

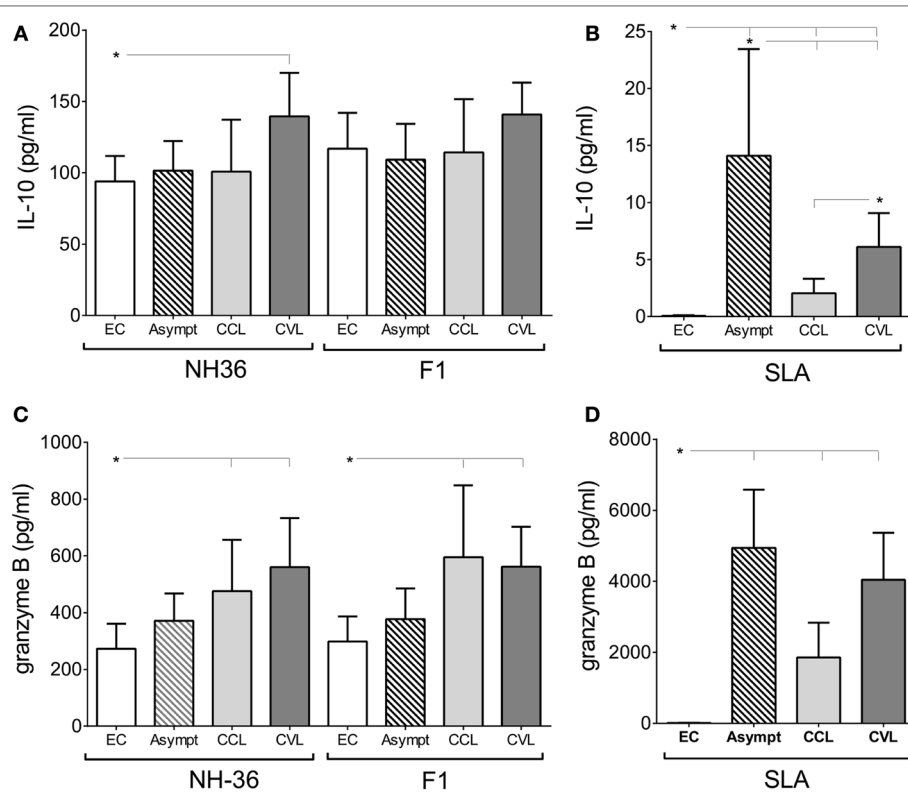


**FIGURE 3** | Granzyme B secretion is increased in response to NH36 and F1, while only NH36 induces the increased secretion of interleukin (IL)-10. IL-10 (**A**) and granzyme B (**C**) secretions in response to NH36, and F1, was assessed in stimulated supernatants from endemic negative controls (EC,  $n = 13$ ), asymptomatic subjects (Asympt,  $n = 11$ ), cured cutaneous leishmaniasis (CCL,  $n = 8$ ) and cured visceral leishmaniasis (CVL,  $n = 10$ ) patients from a visceral leishmaniasis area. The control IL-10 (**B**) and granzyme B (**D**) responses induced by soluble *Leishmania* antigen (SLA) were also assayed. Mann–Whitney test was used to compare clinical groups (\* $p \leq 0.05$ ).

**TABLE 1** | Superiority of the F1 over the NH36 antigen in interferon (IFN)- $\gamma$  and tumor necrosis factor alpha (TNF- $\alpha$ )/interleukin (IL)-10 ratios.

Antigens	F1				NH36				
	Patients	Endemic controls (EC)	Asym. <sup>a</sup>	Cured cutaneous leishmaniasis (CCL)	CVL	EC	Asym.	CCL	CVL
IFN- $\gamma$ (pg/ml)		58	147	195	231	37	126	156	135
TNF- $\alpha$ (pg/ml)		451	448	357	906	232	254	285	516
IL-10 (pg/ml)		117	109	114	141	94	102	101	140
IFN- $\gamma$ /IL-10 ratio		0.5	1.3	1.7	1.6	0.4	1.2	1.6	1
TNF- $\alpha$ /IL-10 ratio		3.9	4.1	3.1	6.4	2.4	2.5	2.8	3.7
IFN- $\gamma$ /IL-10 ratio % enrichment		20	8	6	38	—	—	—	—
TNF- $\alpha$ /IL-10 ratio % enrichment		38	39	10	42	—	—	—	—

Calculation was performed according to the following equation = (F1-NH36/F1) values  $\times 100$  = protective increment. doi: 10.1371/journal.pntd.0000866.t003

<sup>a</sup>Asymptomatic.

in uninfected controls of both non-endemic and endemic areas ( $p \leq 0.0001$  for both) (Figure 4). The IgG3 reactivity to NH36 was also higher in patients infected with *L. (L.) infantum* than in non-endemic and endemic area controls. In contrast, there was no significant difference between the anti-F1 IgG3 reactivity of LV patients infected either by *L. (L.) donovani* ( $p \leq 0.01$ ) or by *L. (L.) infantum* ( $p \leq 0.0001$ ), although both were respectively higher than those observed in the non-endemic and endemic control subjects (Figure 4).

Noteworthy, the response of patients infected with *L. (L.) donovani* from Ethiopia was 35% higher against NH36 than against F1 ( $p \leq 0.01$ ) (Figure 4).

The accuracy of these results was confirmed by calculation of the cutoff values by the Receiver operating characteristic (ROC) analysis and the Youden test (Table 2). In both methods, the maximal accuracy values are equal to 1. In fact, NH36 discriminated the sera of *L. (L.) donovani* infection from controls with the highest accuracy values ( $0.9 < \text{AUC-ROC} \leq 1$ ) (Table 2).

Sera of *L. (L.) infantum* infection, in contrast, were separated from sera of non-endemic area with moderate accuracy values ( $0.7 < \text{AUC-ROC} \leq 0.89$ ) and from sera of endemic area controls with low accuracy values ( $0.5 < \text{AUC-ROC} \leq 0.69$ ) (Table 2). As illustrated in Figure 5, the sensitivities and specificities obtained

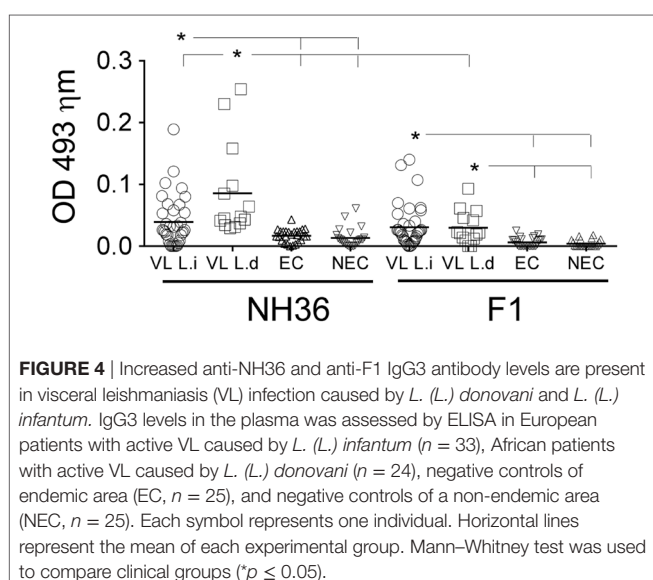


**FIGURE 4 |** Increased anti-NH36 and anti-F1 IgG3 antibody levels are present in visceral leishmaniasis (VL) infection caused by *L. (L.) donovani* and *L. (L.) infantum*. IgG3 levels in the plasma was assessed by ELISA in European patients with active VL caused by *L. (L.) infantum* ( $n = 33$ ), African patients with active VL caused by *L. (L.) donovani* ( $n = 24$ ), negative controls of endemic area (EC,  $n = 25$ ), and negative controls of a non-endemic area (NEC,  $n = 25$ ). Each symbol represents one individual. Horizontal lines represent the mean of each experimental group. Mann-Whitney test was used to compare clinical groups (\* $p \leq 0.05$ ).

**TABLE 2 |** Cross-species IgG3 reactivity of the NH36 antigen.

Comparisons	Cut-off ROC	AUC	Cut-off Youden	Youden index
NH36 VL Ld x NEC	0.0315	0.9479	0.0280	0.8030
NH36 VL Ld x EC	0.0300	0.9849	0.0270	0.8510
NH36 VL Li x NEC	0.0180	0.7100	0.0280	0.3030
NH36 VL Li x EC	0.0205	0.6484	0.0270	0.3510
F1 VL Ld x NEC	0.0185	0.8661	0.0100	0.5770
F1 VL Ld x EC	0.0200	0.8255	0.0130	0.6320
F1 VL Li x NEC	0.0170	0.8624	0.0100	0.4500
F1 VL Li x EC	0.0200	0.8087	0.0130	0.5040

VL Ld, visceral leishmaniasis caused by infection with *Leishmania* (*Leishmania*) *donovani*; VL Li, visceral leishmaniasis caused by infection with *Leishmania* (*L.* *infantum*).

in the NH36 ELISA against samples of *L. (L.) donovani*-infected patients were maximal and gave the best receiver operating characteristic (ROC) curves. Calculation of cutoff values by Youden test also confirmed that NH36 displays the best performance against sera of VL patients infected with *L. (L.) donovani* (0.8030 and 0.8510) (Table 2).

In contrast, and different from what observed for NH36, F1 recognized the sera of individuals infected with either *L. (L.) donovani* or *L. (L.) infantum*, with similar moderate ROC-AUC values (0.8087–0.8661) (Table 2) and with lower and similar Youden indexes than NH36.

We investigated further the possible reason for the higher antigenicity of NH36 against the sera of patients infected with *L. (L.) donovani*. Figure 6 summarizes the sequence homology and alignment found between the NH36 of *L. (L.) donovani*, and two reported sequences of NH of *L. (L.) infantum*. The analysis revealed 99% of homology with differences in only one amino acid: aspartic acid in NH36 of *L. (L.) donovani* was substituted by asparagine in NHs of *L. (L.) infantum*.

## DISCUSSION

F1 is the main domain of NH36 recognized by the lymphoproliferative response of *L. (L.) infantum*-cured and asymptomatic individuals. In the asymptomatic subjects, the F1 domain induced a 19% higher stimulation index than NH36 domain. This result confirmed its antigenic predominance in acquired resistance to the disease. Coincidentally and supporting its cross-protective capabilities, we recently described that the F2 together with F1 was the strongest immunogenic domains of NH36 that were recognized by asymptomatic and cured VL patients infected with *L. (L.) infantum chagasi* in North East Brazil (28). In fact, F1 promoted a higher secretion of IFN- $\gamma$ , IL-1 $\beta$ , IL-17, IL-12p70, and TNF- $\alpha$  in these patients than in endemic area controls (28).

In this investigation, we show that the lymphoproliferative responses to F1 and NH36 of cured/exposed *L. (L.) infantum*-infected subjects were accompanied by a specific IFN- $\gamma$  secretion. Furthermore, the levels of IFN- $\gamma$  and TNF- $\alpha$  and the IFN- $\gamma$ /IL-10 and TNF- $\alpha$ /IL-10 ratios were higher in response to F1 than to NH36 in cured VL patients, suggesting the triggering of a Th1

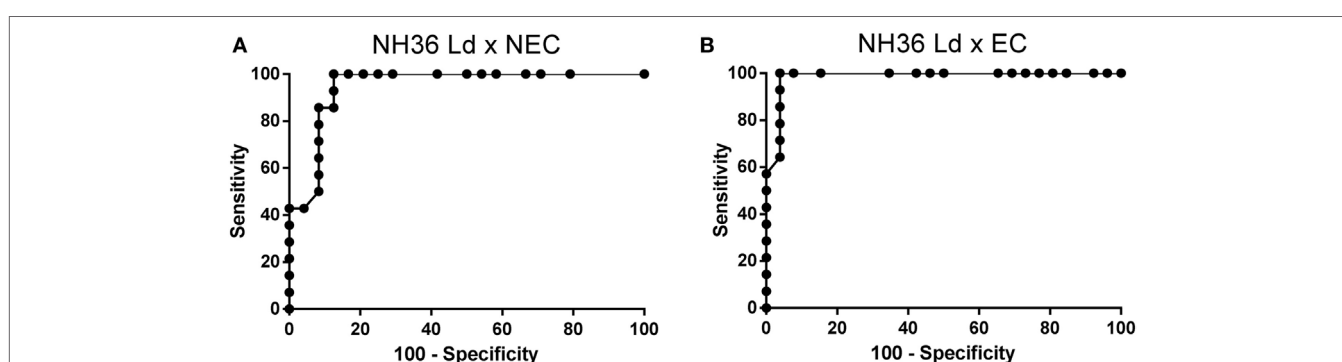


**FIGURE 5 |** Sensitivities and specificities of NH36 ELISA for IgG3 antibodies. Receiver operating characteristics (ROC) curve for NH36-based ELISAs applied on *Leishmania* (*Leishmania*) *donovani* visceral leishmaniasis cases versus (A) NEC and (B) endemic controls (EC).

Ld-NH36 <sup>1</sup>	MPRKIILDCDPGIDDAVAIFLAHGNPEVELLAITTGGNQTLKVRNARLVADVAGIVG	60
Li-NH 1	MPRKIILDCDPGIDDAVAIFLAHGNPEVELLAITTGGNQTLKVRNARLVADVAGIVG	60
Ld-NH36 61	VPVAAGCTKPLVRGVRNASQIHGETGMGNVSYPPEFKTKLDGRHAVQLIIDLIMSHEPKT	120
Li-NH 61	VPVAAGCTKPLVRGVRNASQIHGETGMGNVSYPPEFKTKLDGRHAVQLIIDLIMSHEPKT	120
Ld-NH36 121	ITLVPTGGLTNIAMAVRLEPRIVDRVKEVVLMGGGYHTGNASPVAEFNVFDPEAAHIVF	180
Li-NH 121	ITLVPTGGLTNIAMAVRLEPRIVDRVKEVVLMGGGYHTGNASPVAEFNVFDPEAAHIVF	180
Ld-NH36 181	NESWNVTMVG[ ]LTHQALATP[ ]AVOKRVKEVGTKPAAFML[ ]QILDFTYTKVYEKERNTYATVH	240
Li-NH 181	NESWNVTMVG[ ]LTHQALATP[ ]AVOKRVKEVGTKPAAFML[ ]QILDFTYTKVYEKERNTYATVH	240
Ld-NH36 241	DPCAVAYVIDPTVMTTEQPVVDIELNGALTGMTVADFRYPRPKHCHTQAVKLDFDKFW	300
Li-NH 241	DPCAVAYVIDPTVMTTEQPVVDIELNGALTGMTVADFRYPRPKHCHTQAVKLDFDKFW	300
Ld-NH36 301	CLVIDALKRIGDPO 314	
Li-NH 301	CLVIDALKRIGDPO 314	

**FIGURE 6 |** Sequence analysis of nucleoside hydrolases of *Leishmania* (*Leishmania*) *donovani* and *Leishmania* (*Leishmania*) *infantum*. The sequences of the nucleoside hydrolases NH36 of *L. (L.) donovani* AAG02281.1 (Ld-NH36) and *L. (L.) infantum* AMP43260.1 and CA F05930.1 (Li-NH) were aligned using the BLASTP GenBank program. The line in the middle of the two sequences shows the amino acids shared by the two NHs. The peptide sequence of the strongest B-cell epitope of F3 (position 202–219) (22) and the substitution of aspartic acid in Ld-NH36 for asparagine in Ld-NHs are marked by empty black squares.

response probably due to the F1 domain epitopes. Noteworthy, the SLA complex antigen induced levels of TNF- $\alpha$  not different from NH36 and F1, in asymptomatic subjects, and lower than NH36, in cured patients. In addition, IL-17A was secreted by asymptomatic and cured CL patients, in response to F1. The SLA control promoted a much lower secretion of TNF- $\alpha$  and IL-17A. These findings correlate with our previous observations showing that NH36 and F1 domains are strong inducers of the Th1 response. Both vaccines indeed promote increased frequencies of CD4 $^{+}$  T cells secreting IL-2, TNF- $\alpha$ , and both TNF- $\alpha$  and IL-2 together (22–24), which are, according to the CD4 $^{+}$  T-cell differentiation model proposed by Seder et al. (38), the reservoirs of memory CD4 $^{+}$  T cells that also exhibit effector potential.

Our results support the recent report of Santos et al. (28) who described a predicted epitope for CD4 $^{+}$  T cells in F1, which is highly conserved in the *Leishmania* genus and is highly promiscuous (amino acids 64–93, AAGCTKPLVRGVRNASQIHG). This epitope shows 80% probabilities of molecular binding to 18/25 HLA-DR most common molecules (28). The composition of this epitope is identical in the species that cause visceral leishmaniasis [*L. (L.) donovani*, *L. (L.) infantum*, and *L. (L.) infantum chagasi*] (28). Therefore, our data support the evidence raised by Mauricio et al. (39, 40) that consider *L. (L.) infantum* and *L. (L.) infantum chagasi* as the same species.

In addition, as markers of VL resistance, the F2 together with F1 induced the strongest secretion of IL-17, IL-6, and IL-10 in asymptomatic DTH $^{+}$  and cured human subjects infected with *L. (L.) infantum chagasi* in Brazil (28). Consistent with this, the IFN- $\gamma$  increase was correlated with decreased spleen and liver sizes and with increased hematocrit counts, in response to F1 domain (28). Furthermore, IL-17 increases were associated with decreased spleen and liver sizes in response to F1 (28).

Vaccination with NH36 has proven to protect against murine cutaneous and visceral leishmaniasis (19–24) and canine visceral

leishmaniasis (26, 27), through an IFN- $\gamma$ -CD4 response (21, 24). Preclinical assays with F1sap vaccine have demonstrated the induction of a cellular protective Th1 immune response characterized by the secretion of IFN- $\gamma$  by CD4 $^{+}$  triple-cytokine producers and the secretion of IFN- $\gamma$  and TNF- $\alpha$  into the splenocyte supernatants (24). Some antigens have been previously proposed as potential synthetic vaccines against leishmaniasis, like KMP-11 recognized by human CD8 $^{+}$  lymphocytes and by many different HLA receptors (41), or Leish110f fusion protein (42). Our results suggest that F1 domain of *L. (L.) donovani*-NH36 may be consequently involved in the generation of a protective response against *L. (L.) infantum* human infection and represents a potential vaccine candidate for human leishmaniasis by itself, or in combination with other HLA epitopes/antigens.

Furthermore, an increment in IL-17A secretion was observed in response to NH36 in PBMC from cured/exposed *Leishmania*-infected subjects and to F1 in cured CL and asymptomatic subjects. During the leishmaniasis epidemics in Fuenlabrada, all the infections were caused by *L. (L.) infantum*, as confirmed by PCR analysis, but the main reservoirs were hares and not dogs (1). Two-third of the cases corresponded to cutaneous leishmaniasis, and only one-third of the cases corresponded to visceral leishmaniasis. A total of 15.2% of the patients were foreigners, born in Sub-Saharan Africa. Among them, visceral leishmaniasis was predominant, while in patients from Spain, cutaneous leishmaniasis was the most frequent outcome (1, 43). In addition, near Madrid, in the past, the number of human cases has never been so high and the infection was more prevalent in children and in immunocompromised adults. In this outbreak, in contrast, only 14.1% of the affected were children and 15% were immunocompromised individuals (43). The probable genetic background basis of the different outcomes should be further investigated. An increase in IL-17 secretion has been previously reported in exposed but healthy, resistant subjects who did not

develop VL (44). An increase in IL-17A after PBMC stimulation has been also described in cutaneous leishmaniasis caused by *L. (L.) braziliensis* (45). The mechanisms by which IL-17 mediates protection are not understood, but it has been recently described that IL-17A and IFN- $\gamma$  synergistically promote *L. (L.) infantum* killing (46). An increase in IL-17A and IFN- $\gamma$  after SLA incubation in asymptomatic and cured VL solid organ transplant patients has been previously reported (32). Here, we also described that PBMC from cured/exposed *L. (L.) infantum*-infected subjects after NH36 and F1 stimulations produced both IL-17A and IFN- $\gamma$  and there are no changes in the secretion of IL-10. The IL-17A response against F1 was higher in asymptomatic subjects, disclosing its relationship with the resistance to the disease.

Furthermore, the protection elicited by IL-17 against infection is associated with the downregulation of regulatory T cells and IL-10 production, while benefiting the Th1 response and improving the leishmanicidal activity of macrophages in an NO-dependent manner (46). As widely reported for IFN- $\gamma$ , a protective role of IL-17 has been described to induce in vaccine-induced immunity (44). These results reinforce the potential of F1 as a vaccine to protect against *L. (L.) infantum* human infection.

Our results also showed that supernatants stimulated with F1 or NH36 from *L. (L.) donovani* increased the levels of granzyme B in cured individuals from *L. (L.) infantum* cutaneous and visceral infection. It has been previously described the ability of some peptides from *L. major* to elicit the production of granzyme B (47). Granzyme B is secreted mainly from CD8 $^{+}$  cytotoxic lymphocytes and natural killer cells and is one of the primary molecules in effector cell-mediated killing. Our results support the description of the FLAHGNPEV- (amino acids 20–28 HLA-A and B score 28 A\*02:01) and YPPEFKTKL (score 21 B\*0702)-predicted epitopes for CD8 $^{+}$  T cells in the F1 sequence (28). Both epitopes show identical sequence in *L. (L.) donovani* and *L. (L.) infantum* species (28) and induced the secretion of IFN- $\gamma$  by PBMC of asymptomatic, *L. (L.) infantum chagasi*-infected subjects (28). In agreement with our results, F1 increased the CD8 $^{+}$ IL-2 $^{+}$ , CD8 $^{+}$ IL-2 $^{+}$ TNF- $\alpha$  $^{+}$ , and CD8 $^{+}$ IL-2 $^{+}$ TNF- $\alpha$  $^{+}$ IFN- $\gamma$  $^{+}$  T-cell frequencies of *L. (L.) infantum chagasi* VL patients that correlated with increased spleen and liver sizes and decreased hemoglobin and hematocrit values (28). Therefore, while cure and acquired resistance to VL correlated to the CD4 $^{+}$  Th1 and Th17 T-cell responses to F1, clinical VL outcomes, in *L. (L.) infantum chagasi*-infected individuals in contrast, correlated to CD8 $^{+}$  T-cell responses against F1, potentially involved in control of the early infection (28).

In addition, we recently observed that the predicted epitopes for CD8 $^{+}$  T cells of F1 induced *in vitro* stimulating activity on both the CD4 $^{+}$  and the CD8 $^{+}$  T-cell populations in mice vaccinated against cutaneous leishmaniasis. The F1 epitope (92–100, YPPEFKTKL) promoted simultaneously the highest frequencies of CD4 $^{+}$ IFN- $\gamma$  $^{+}$ TNF- $\alpha$  $^{+}$ , CD8 $^{+}$ TNF- $\alpha$  $^{+}$ , and CD8 $^{+}$ IFN- $\gamma$  $^{+}$  T cells (25). This sequence could also be a PADRE epitope since the synthetic more preferably PADRE peptide composition is aKX-VAATLKAa (48). In fact, YPPEFKTKL contains Y as the R2 residue, four residues in R3, where 3–5 amino acids are needed, and the sequences KT followed by TKL in R4, while the expected combinations for R4 are KT, TLK, or WTLK (40). This evidence

strengthens the relevance of the YPPEFKTKL epitope and partially explains the immunogenic potency of the F1 domain.

Recently, the involvement of CD4 $^{+}$  T cells producing granzyme B was described in the immune response against *Leishmania* antigens (47). F1 has also two epitopes for CD4 $^{+}$ , and this could be related with the high amount of granzyme B produced after stimulation, with similar levels to those induced by SLA. Furthermore, a strong correlation has been observed between IFN- $\gamma$  and granzyme B productions in response to *L. (L.) major*-excreted/secreted proteins and SLA (32, 47). While we found similar figures after SLA stimulation, F1 and NH36 produced an increase in both IFN- $\gamma$  and granzyme B in cured patients and IFN- $\gamma$  in asymptomatic individuals. Granzyme B has recently suggested as a new marker for cured/exposed *Leishmania*-infected subjects (49), and stimulation with F1 and NH36 could also help to potentially discriminate between cured and asymptomatic individuals exposed to *L. (L.) infantum* (49).

Regarding the humoral response, the IgG3 antigen-specific humoral response is decreased after successful VL treatment and has diagnostic value in *L. (L.) donovani*-infected patients from India (50). In our investigation, increased levels of IgG3 human antibodies directed against NH36 and F1 allowed the differentiation of clinical status. Although with relatively low absorbance values, both antigens were able to significantly discriminate sera of active disease from controls. NH36 was 55% more potent in the recognition of sera from patients infected with *L. (L.) donovani* than those infected with *L. (L.) infantum*, indicating a species specificity of this antigen for humoral immune responses. In addition, in patients infected with *L. (L.) donovani*, the absorbance values directed against NH36 were higher than those directed against F1, indicating that the most potent B epitopes are not located in F1 but probably in other NH36 domains. In agreement with that, we described, in 2010, the sequences of the NH36 epitopes for antibodies predicted by the Protean Pad program (22). Two predicted epitopes belong to the F1 domain (amino acids 40–57, NQTLEKVTRNARLVADVAG and 94–108, PEFKTKLDGRHAVQLDGRHAVQL), one was located in F2 domain (114–126, MSHEPKTITLVPT), and three epitopes correspond to the F3 domain (202–219, AVQKRVKEVGTKPAAFML, IEDB 139695; 228–239, VYEKERNTYATV, IEDB 139948; 278–291, FRYPRPKHCHTQVA, IEDB 139752) (22). In the same work, we demonstrated that the three epitopes of F3 developed the strongest reactivity against the sera of healthy dogs vaccinated with Leishmune® (22).

Confirming our previous results, in 2012, two linear B-cell-predicted epitopes for dog and human antibodies were identified along the sequence of NH36 (51). One of them, called peptide 18 (TTVVGNQTLEKVT), is located in the F1 domain, overlaps with the single antibody epitope identified by our group before (NQTLEKVTRNARLVADVAG) (22), and displayed high sensitivities and specificities in the diagnosis of canine and human cases of VL caused by *L. (L.) infantum chagasi* in Brazil (51). F1 was also the domain mostly recognized by sera of *L. (L.) infantum chagasi*-infected dogs, after immunotherapy with the NH36 DNA vaccine (26). The second epitope called peptide 17 (TPAVQKRVKEVGTKP) (51) belongs to the F3 domain and

overlaps with the epitope AVQKRVKEVGTKPAAFML described by our group before, which induced the strongest inhibition of binding of anti-NH36 antibodies (31.4%) of dogs vaccinated with Leishmune® (22). Peptide 17 showed 100% sensitivity and 94% specificity in the diagnosis of human cases of VL due to *L. (L.) infantum chagasi* infection (51).

The finding of the most antigenic B-cell epitopes in the F3 domains of NH36 (22) explain why, in this investigation, NH36 was a more potent antigen than the F1 domain alone, mainly in the detection of antibodies raised by *L. (L.) donovani* infection.

In addition, in our investigation, a species specificity was noted in the reactivity of NH36 with IgG3 of human sera. In fact, we demonstrated that the sera of patients infected with *L. (L.) donovani* reacted more with the NH36 antigen of *L. (L.) donovani* than the sera of patients infected with *L. (L.) infantum*. This species specificity was, however, not detected against the F1 domain, which was equally recognized by the sera of patients from Ethiopia and Spain; therefore, its basis would be related to the epitopes of other NH36 domains. To investigate this possibility, the sequences of NHs of the two parasites were aligned. They share 99% of identity, the only difference being one amino acid located at position 192. Indeed, aspartic acid in NH36 of *L. (L.) donovani* is substituted by asparagine in NH of *L. (L.) infantum*. Aspartic acid is a charged amino acid residue, while asparagine is a non-charged but polar amino acid. Conformational B epitopes are enriched in charged and polar amino acids (51, 52). The importance of the substitution of aspartic acid for asparagine in position 192 might be enhanced by the fact that only nine residues separate it from the most immunogenic epitope of F3, which is responsible for 31% of the inhibition of binding of NH36 to antibodies of Leishmune®-vaccinated dogs (202–219, AVQKRVKEVGTKPAAFML) (22). Therefore, the substitution of one charged amino acid in the vicinity of the most important epitope of F3 might explain the higher antigenicity found in NH36 of *L. (L.) donovani*. Our assumption of the importance of this area is supported by the description of the predicted epitope 17, also in this region, but which starts at amino acid 200 (51), instead of 202 (22).

In contrast, the similar AUC and Youden index values determined by F1 in the assay of sera of patients infected with *L. (L.) donovani* and *L. (L.) infantum* might indicate the importance of the predicted epitopes for antibodies in the sequence of F1 (amino acids 40–57, NQTLEKVTRNARLVADVAG and 94–108, PEFKTKLDGRHAVQLDGRHAVQL) (22), which are completely conserved in the NHs of the two *Leishmania* species.

It is worth to note that the presence of anti-NH36 antibodies in sera of human and dog patients infected with *L. (L.) infantum chagasi* was previously demonstrated (51, 53, 54). In this article, we described for the first time the recognition of NH36 by antibodies generated by human infections with *L. (L.) infantum* and *L. (L.) donovani*.

Our data demonstrates that F1 peptide induces a recall cellular response similar or higher to the one induced by NH36, a recombinant antigen that has protected mice from infection by several *Leishmania* species and dogs from *L. (L.) infantum chagasi* infection. No human vaccine against *Leishmania* is available thus

far. The F1 domain of *L. (L.) donovani*-NH36, which contributes to protection against human infection by *L. (L.) infantum chagasi* (28), may also be involved in the generation of a protective response against *L. (L.) infantum* infection and represents a potential universal vaccine candidate for the control of human visceral leishmaniasis alone, or in combination with other HLA epitopes/antigens.

## ETHICS STATEMENT

This study was approved by the Hospital de Fuenlabrada (Madrid) Ethics and Research Committee (APR 12–65 and APR 14–64). In addition, the protocols for the collection of sera samples of healthy blood donors of the Hospital Universitário Clementino Fraga Filho (HUCFFo)-Blood Transfusion service of the Universidade Federal do Rio de Janeiro (Rio de Janeiro, Brazil) were approved by the Comité de Ética em Pesquisa of the HUCFFo-Faculdade de Medicina-UFRJ, Brazil, according to the GM-MS 158-2016 regulation of the Brazilian Ministry of Health. All participants gave their written informed consent.

## AUTHOR CONTRIBUTIONS

LF, AI-M, and DN conducted the experiments; LF, AI-M, MS, DN, and CC acquired the data; LF, AI-M, and CP-d-S analyzed the data; CP-d-S, RA, PL, and JM designed the research studies; EC and JM provided reagents; EC and CP-d-S wrote the manuscript. All authors have read and approved the final manuscript.

## ACKNOWLEDGMENTS

We are grateful to Dr. Juan Victor San Martín of Hospital de Fuenlabrada, Madrid, Spain, for the collection of blood samples and to Professor Carmen Martins Nogueira, technical responsible of the Blood Transfusion service of the Hospital Universitário Clementino Fraga-Filho-Blood Transfusion service of the Universidade Federal do Rio de Janeiro, Rio de Janeiro, Brazil, for the non-endemic area control sera samples.

## FUNDING

This work was supported by Conselho Nacional de Desenvolvimento Científico e Tecnológico (CNPQ) (fellowships 300639/2003-1 to MP, 310977/2014-2 to CP-d-S, and grant 404400/2012-4 to CP-d-S, MP, PL, RA, JM, EC); Fundação Carlos Chagas de Amparo à Pesquisa do Estado de Rio de Janeiro (FAPERJ) (grant E-26-201.583/2014, E-26-102957/2011, and E-26/111.682/2013 to CP-d-S and fellowships E-26/102415/2010 and E-26/201747/2015 to DN); Coordenação de Aperfeiçoamento de Pessoal de Nível Superior (grant 23038.005304/2011-0 to MS); CNPQ-Fundação de Apoio à Pesquisa e a Inovação Tecnológica do Estado de Sergipe-PRONEX (12/2009); and FAPITEC CNPq-(PRONEX) (019.203.02712/2009-8) to RA. EC was supported by a research contract funded via VII PN I+D+I 2013–2016 and FEDER Funds (RICET RD12/0018/0003).

## REFERENCES

- Arce A, Estrada A, Ordobas M, Sevilla S, Garcia N, Moratilla L, et al. Re-emergence of leishmaniasis in Spain: community outbreak in Madrid, Spain, 2009 to 2012. *Euro Surveill* (2013) 18:20546. doi:10.2807/1560-7917.EU2013.18.30.20546
- Ibarra-Meneses AV, Carrillo E, Sanchez C, Garcia-Martinez J, Lopez Lacomba D, San Martin JV, et al. Interleukin-2 as a marker for detecting asymptomatic individuals in areas where *Leishmania infantum* is endemic. *Clin Microbiol Infect* (2016) 22(739):e1–4. doi:10.1016/j.cmi.2016.05.021
- Chappuis F, Sundar S, Hailu A, Ghalib H, Rijal S, Peeling RW, et al. Visceral leishmaniasis: what are the needs for diagnosis, treatment and control? *Nat Rev Microbiol* (2007) 5:873–82. doi:10.1038/nrmicro1748
- Kumar R, Engwerda C. Vaccines to prevent leishmaniasis. *Clin Transl Immunol* (2014) 3:e13. doi:10.1038/cti.2014.4
- Dye C. The logic of visceral leishmaniasis control. *Am J Trop Med Hyg* (1996) 55:125–30. doi:10.4269/ajtmh.1996.55.125
- Oliva G, Nieto J, Foglia Manzillo V, Cappiello S, Fiorentino E, Di Muccio T, et al. A randomised, double-blind, controlled efficacy trial of the LiESP/QA-21 vaccine in naïve dogs exposed to two *Leishmania infantum* transmission seasons. *PLoS Negl Trop Dis* (2014) 8:e3213. doi:10.1371/journal.pntd.0003213
- Carcelén J, Iniesta V, Fernández-Cotrina J, Serrano F, Parejo JC, Corraliza I, et al. The chimerical multi-component Q protein from *Leishmania* in the absence of adjuvant protects dogs against an experimental *Leishmania infantum* infection. *Vaccine* (2009) 27:5964–73. doi:10.1016/j.vaccine.2009.07.069
- Palatnik-de-Sousa CB, Barbosa Ade F, Oliveira SM, Nico D, Bernardo RR, Santos WR, et al. The FML-vaccine against canine visceral leishmaniasis: from the second generation to the synthetic vaccine. *Expert Rev Vaccines* (2008) 7:833–51. doi:10.1586/14760584.7.6.833
- Saraiva EM, de Figueiredo Barbosa A, Santos FN, Borja-Cabrera GP, Nico D, Souza LO, et al. The FML-vaccine (Leishmune®) against canine visceral leishmaniasis: a transmission blocking vaccine. *Vaccine* (2006) 24:2423–31. doi:10.1016/j.vaccine.2005.11.061
- Parra LE, Borja-Cabrera GP, Santos FN, Souza LO, Palatnik-de-Sousa CB, Menz I. Safety trial using the Leishmune vaccine against canine visceral leishmaniasis in Brazil. *Vaccine* (2007) 25:2180–6. doi:10.1016/j.vaccine.2006.11.057
- Palatnik-de-Sousa CB, Silva-Antunes I, Morgado Ade A, Menz I, Palatnik M, Lavor C. Decrease of the incidence of human and canine visceral leishmaniasis after dog vaccination with Leishmune in Brazilian endemic areas. *Vaccine* (2009) 27:3505–12. doi:10.1016/j.vaccine.2009.03.045
- Fernandes AP, Coelho EA, Machado-Coelho GL, Grimaldi G Jr, Gazzinelli RT. Making an anti-amaстigote vaccine for visceral leishmaniasis: rational, update and perspectives. *Curr Opin Microbiol* (2012) 15:476–85. doi:10.1016/j.mib.2012.05.002
- Foroughi-Parvar F, Hatam G. Vaccines for canine leishmaniasis. *Adv Prev Med* (2014) 2014:569193. doi:10.1155/2014/569193
- Kemp M, Kurtzhals JA, Bendtzen K, Poulsen LK, Hansen MB, Koech DK, et al. *Leishmania donovani*-reactive Th1- and Th2-like T-cell clones from individuals who have recovered from visceral leishmaniasis. *Infect Immun* (1993) 61:1069–73.
- Reed SG, Scott P. T-cell and cytokine responses in leishmaniasis. *Curr Opin Immunol* (1993) 5:524–31. doi:10.1016/0952-7915(93)90033-O
- Seyed N, Taheri T, Rafati S. Post-genomics and vaccine improvement for *Leishmania*. *Front Microbiol* (2016) 7:467. doi:10.3389/fmicb.2016.00467
- Kaye PM, Aebsicher T. Visceral leishmaniasis: immunology and prospects for a vaccine. *Clin Microbiol Infect* (2011) 17:1462–70. doi:10.1111/j.1469-0993.2011.03610.x
- Singh B, Sundar S. Leishmaniasis: vaccine candidates and perspectives. *Vaccine* (2012) 30:3834–42. doi:10.1016/j.vaccine.2012.03.068
- Paraguai de Souza E, Bernardo RR, Palatnik M, Palatnik de Sousa CB. Vaccination of Balb/c mice against experimental visceral leishmaniasis with the GP36 glycoprotein antigen of *Leishmania donovani*. *Vaccine* (2001) 19:3104–15. doi:10.1016/S0264-410X(01)00031-7
- Al-Wabel MA, Tonui WK, Cui L, Martin SK, Titus RG. Protection of susceptible BALB/c mice from challenge with *Leishmania major* by nucleoside hydrolase, a soluble exo-antigen of *Leishmania*. *Am J Trop Med Hyg* (2007) 77:1060–5.
- Aguilar-Be I, da Silva Zardo R, Paraguai de Souza E, Borja-Cabrera GP, Rosado-Vallado M, Mut-Martin R, et al. Cross-protective efficacy of a prophylactic *Leishmania donovani* DNA vaccine against visceral and cutaneous murine leishmaniasis. *Infect Immun* (2005) 73:812–9. doi:10.1128/IAI.73.2.812-819.2005
- Nico D, Claser C, Borja-Cabrera GP, Travassos LR, Palatnik M, Soares IS, et al. Adaptive immunity against *Leishmania* nucleoside hydrolase maps its c-terminal domain as the target of the CD4+ T cell-driven protective response. *PLoS Negl Trop Dis* (2010) 4:e866. doi:10.1371/journal.pntd.0000866
- Nico D, Gomes DC, Palatnik-de-Sousa I, Morrot A, Palatnik M, Palatnik-de-Sousa CB. *Leishmania donovani* nucleoside hydrolase terminal domains in cross-protective immunotherapy against *Leishmania amazonensis* murine infection. *Front Immunol* (2014) 5:273. doi:10.3389/fimmu.2014.00273
- Nico D, Gomes DC, Alves-Silva MV, Freitas EO, Morrot A, Bahia D, et al. Cross-protective immunity to *Leishmania amazonensis* is mediated by CD4+ and CD8+ epitopes of *Leishmania donovani* nucleoside hydrolase terminal domains. *Front Immunol* (2014) 5:189. doi:10.3389/fimmu.2014.00189
- Alves-Silva MV, Nico D, Morrot A, Palatnik M, Palatnik-de-Sousa CB. A chimera containing CD4+ and CD8+ T-cell epitopes of the *Leishmania donovani* nucleoside hydrolase (NH36) optimizes cross-protection against *Leishmania amazonensis* infection. *Front Immunol* (2017) 8:100. doi:10.3389/fimmu.2017.00100
- Borja-Cabrera GP, Santos FB, Nico D, Gravino AE, Manna L, Palatnik M, et al. The Leishmune's nucleoside hydrolase DNA vaccine as an aid in immunotherapy of canine visceral leishmaniasis. *Procedia Vaccinol* (2012) 6:64–73. doi:10.1016/j.provac.2012.04.009
- Borja-Cabrera GP, Picillo E, Gravino E, Manna L, Palatnik de Sousa CB. Nucleoside hydrolase DNA vaccine against canine visceral leishmaniasis. *Procedia Vaccinol* (2009) 1:104–9. doi:10.1016/j.provac.2009.07.019
- Santos MLB, Nico D, de Oliveira FA, Barreto AS, Palatnik-de-Sousa I, Carrillo E, et al. *Leishmania donovani* nucleoside hydrolase (NH36) domains induce T-cell cytokine responses in human visceral leishmaniasis. *Front Immunol* (2017) 8:227. doi:10.3389/fimmu.2017.00227
- Sordo L, Gadisa E, Custodio E, Cruz I, Simón F, Abraham Z, et al. Low prevalence of *Leishmania* infection in post-epidemic areas of Libo Kemkem, Ethiopia. *Am J Trop Med Hyg* (2012) 86:955–8. doi:10.4269/ajtmh.2012.11-0436
- Rodrigues MHC, Rodrigues KM, Oliveira TR, Cômodo AN, Rodrigues MM, Kocken CH, et al. Antibody response of naturally infected individuals to recombinant *Plasmodium vivax* apical membrane antigen. *Int J Parasitol* (2005) 35:185–92. doi:10.1016/j.ijpara.2004.11.003
- Saini DK, Pant N, Das TK, Tyagi JS. Cloning, overexpression, purification and matrix-assisted refolding of DevS (Rv 3132c) histidine protein kinase of *Mycobacterium tuberculosis*. *Protein Expr Purif* (2002) 25:203–8. doi:10.1006/prep.2002.1628
- Carrillo E, Carrasco-Antón N, López-Medrano F, Salto E, Fernández L, San Martín JV, et al. Cytokine release assays as tests for exposure to *Leishmania*, and for confirming cure from leishmaniasis, in solid organ transplant recipients. *PLoS Negl Trop Dis* (2015) 9:e0004179. doi:10.1371/journal.pntd.0004179
- Solano Gallego L, Villanueva-Saz S, Carbonell M, Trotta M, Furlanello T, Natale A. Serological diagnosis of canine leishmaniosis: comparison of three commercial ELISA tests (Leiscan, ID screen and *Leishmania* 96), a rapid test (Speed Leish K) and an in-house IFAT. *Parasit Vectors* (2014) 7:111. doi:10.1186/1756-3305-7-111
- Chauhan IS, Shukla R, Krishna S, Sekhri S, Kaushik U, Baby S, et al. Recombinant *Leishmania* Rab6 (rLdRab6) is recognized by sera from visceral leishmaniasis patients. *Exp Parasitol* (2016) 170:135–47. doi:10.1016/j.exppara.2016.09.010
- Palatnik-de-Sousa CB, Gomes EM, Paraguai-de-Souza E, Palatnik M, Luz K, Borojevic R. *Leishmania donovani*: titration of antibodies to the fucose-mannose ligand as an aid in diagnosis and prognosis of visceral leishmaniasis. *Trans R Soc Trop Med Hyg* (1995) 89:390–3. doi:10.1016/0035-9203(95)90022-5
- Cabrera GP, Da Silva VO, Da Costa RT, Reis AB, Mayrink W, Genaro O, et al. The fucose-mannose ligand-ELISA in the diagnosis and prognosis of canine visceral leishmaniasis in Brazil. *Am J Trop Med Hyg* (1999) 61:296–301. doi:10.4269/ajtmh.1999.61.296
- Hajian-Tilaki K. Receiver operating characteristic (ROC) curve analysis for medical diagnostic test evaluation. *Caspian J Intern Med* (2013) 4:627–35.

38. Seder RA, Darrah PA, Roederer M. T-cell quality in memory and protection: implications for vaccine design. *Nat Rev Immunol* (2008) 8:247–58. doi:10.1038/nri2274
39. Mauricio IL, Howard MK, Stothard JR, Miles MA. Genomic diversity in the *Leishmania donovani* complex. *Parasitology* (1999) 119:237–46. doi:10.1017/S0031182099004710
40. Mauricio IL, Stothard JR, Miles MA. The strange case of *Leishmania chagasi*. *Parasitol Today* (2000) 16:188–9. doi:10.1016/S0169-4758(00)01637-9
41. Basu R, Roy S, Walden P. HLA class I-restricted T cell epitopes of the kinetoplastid membrane protein-11 presented by *Leishmania donovani*-infected human macrophages. *J Infect Dis* (2007) 195:1373–80. doi:10.1086/513439
42. Bertholet S, Goto Y, Carter L, Bhatia A, Howard RF, Carter D, et al. Optimized subunit vaccine protects against experimental leishmaniasis. *Vaccine* (2009) 27:7036–45. doi:10.1016/j.vaccine.2009.09.066
43. Carrillo E, Moreno J, Cruz I. What is responsible for a large and unusual outbreak of leishmaniasis in Madrid? *Trends Parasitol* (2013) 29:579–80. doi:10.1016/j.pt.2013.10.007
44. Pitta MG, Romano A, Cabantous S, Henri S, Hammad A, Kouriba B, et al. IL-17 and IL-22 are associated with protection against human Kala-azar caused by *Leishmania donovani*. *J Clin Invest* (2009) 119:2379–87. doi:10.1172/JCI38813
45. Novoa R, Bacellar O, Nascimento M, Cardoso TM, Ramasawmy R, Oliveira WN, et al. IL-17 and regulatory cytokines (IL-10 and IL-27) in *L. braziliensis* infection. *Parasite Immunol* (2011) 33:132–6. doi:10.1111/j.1365-3024.2010.01256.x
46. Nascimento MS, Carregaro V, Lima-Junior DS, Costa DL, Ryffel B, Duthie MS. Interleukin 17A acts synergistically with interferon gamma to promote protection against *Leishmania infantum* infection. *J Infect Dis* (2015) 211:1015–26. doi:10.1093/infdis/jiu531
47. Naouar I, Boussoffara T, Chenik M, Gritli S, Ben Ahmed M, Belhadj Hmida N, et al. Prediction of T cell epitopes from *Leishmania major* potentially excreted/secreted proteins inducing granzyme B production. *PLoS One* (2016) 11(1):e0147076. doi:10.1371/journal.pone.0147076
48. Alexander JL, Defrees S, Sette A. *Induction of Immune Response against Desired Determinants*. US patent No WO 1997026784 A1 (1997).
49. Chamakh-Ayari R, Bras-Goncalves R, Bahi-Jaber N, Petididier E, Markikou-Ouni W, Aoun K, et al. In vitro evaluation of a soluble *Leishmania* promastigote surface antigen as a potential vaccine candidate against human leishmaniasis. *PLoS One* (2014) 9(5):e92708. doi:10.1371/journal.pone.0092708
50. Anam K, Afrin F, Banerjee D, Pramanik N, Guha SK, Goswami RP, et al. Immunoglobulin subclass distribution and diagnostic value of *Leishmania donovani* antigen-specific immunoglobulin G3 in Indian Kala-azar patients. *Clin Diagn Lab Immunol* (1999) 6:231–5.
51. Costa MM, Penido M, dos Santos MS, Doro D, de Freitas E, Michalick MS, et al. Improved canine and human visceral leishmaniasis immunodiagnosis using combinations of synthetic peptides in enzyme-linked immunosorbent assay. *PLoS Negl Trop Dis* (2012) 6(5):e1622. doi:10.1371/journal.pntd.0001622
52. Zheng W, Ruan J, Hu G, Wang K, Hanlon M, Gao J. Analysis of conformational B-cell epitopes in the antibody-antigen complex using the depth function and the convex hull. *PLoS One* (2015) 10(8):e0134835. doi:10.1371/journal.pone.0134835
53. Palatnik de Sousa CB, Gomes EM, de Souza EP, dos Santos WR, de Macedo SR, de Medeiros LV, et al. The FML (fucose mannose ligand) of *Leishmania donovani*. A new tool in diagnosis, prognosis, transfusional control and vaccination against human Kala-azar. *Rev Soc Bras Med Trop* (1996) 29:153–63. doi:10.1590/S0037-86821996000200008
54. Santana DM, Borja-Cabrera GP, Paraguai de Souza E, Sturm NR, Palatnik de Sousa CB, Campbell DA. Nucleoside hydrolase from *Leishmania donovani* is an antigen diagnostic for visceral leishmaniasis. *Mol Biochem Parasitol* (2002) 120:315–9. doi:10.1016/S0166-6851(02)00010-5

**Conflict of Interest Statement:** DN and CP-d-S are the inventors of the patent file PI1015788-3 (INPI Brazil). EC, LF, AI-M, MS, PL, CC, RA, and JM declare no conflict of interest.

Copyright © 2017 Carrillo, Fernandez, Ibarra-Meneses, Santos, Nico, de Luca, Correa, de Almeida, Moreno and Palatnik-de-Sousa. This is an open-access article distributed under the terms of the Creative Commons Attribution License (CC BY). The use, distribution or reproduction in other forums is permitted, provided the original author(s) or licensor are credited and that the original publication in this journal is cited, in accordance with accepted academic practice. No use, distribution or reproduction is permitted which does not comply with these terms.



# A Poly(Lactic-co-Glycolic) Acid Nanovaccine Based on Chimeric Peptides from Different *Leishmania infantum* Proteins Induces Dendritic Cells Maturation and Promotes Peptide-Specific IFN $\gamma$ -Producing CD8 $^{+}$ T Cells Essential for the Protection against Experimental Visceral Leishmaniasis

OPEN ACCESS

**Edited by:**

Daniela Santoro Rosa,  
Federal University of São  
Paulo, Brazil

**Reviewed by:**

Urszula Krzych,  
Walter Reed Army Institute of  
Research, United States  
Laura Bonifaz,  
Instituto Mexicano del Seguro  
Social (IMSS), Mexico

**\*Correspondence:**

Evdokia Karagouni  
ekaragouni@pasteur.gr

**Specialty section:**

This article was submitted to  
Vaccines and Molecular  
Therapeutics,  
a section of the journal  
*Frontiers in Immunology*

**Received:** 04 January 2017

**Accepted:** 26 May 2017

**Published:** 13 June 2017

**Citation:**

Athanasiou E, Agallou M,  
Tatsoglou S, Kammona O,  
Hatzigeorgiou A, Kiparissides C and  
Karagouni E (2017) A Poly(Lactic-co-  
Glycolic) Acid Nanovaccine Based on  
Chimeric Peptides from Different  
*Leishmania infantum* Proteins  
Induces Dendritic Cells Maturation and  
Promotes Peptide-Specific  
IFN $\gamma$ -Producing CD8 $^{+}$  T Cells  
Essential for the Protection against  
Experimental Visceral Leishmaniasis.  
*Front. Immunol.* 8:684.  
doi: 10.3389/fimmu.2017.00684

Evita Athanasiou<sup>1</sup>, Maria Agallou<sup>1</sup>, Spyros Tatsoglou<sup>2</sup>, Olga Kammona<sup>3</sup>,  
Artemis Hatzigeorgiou<sup>2</sup>, Costas Kiparissides<sup>3,4</sup> and Evdokia Karagouni<sup>1\*</sup>

<sup>1</sup>Laboratory of Cellular Immunology, Department of Microbiology, Hellenic Pasteur Institute, Athens, Greece, <sup>2</sup>DIANA-Lab, Hellenic Pasteur Institute, Athens, Greece, <sup>3</sup>Laboratory of Polymer Reaction Engineering, Chemical Process and Energy Resources Institute, Centre for Research and Technology-Hellas, Thessaloniki, Greece, <sup>4</sup>Laboratory of Chemical Engineering B, Department of Chemical Engineering, Aristotle University of Thessaloniki, Thessaloniki, Greece

Visceral leishmaniasis, caused by *Leishmania* (*L.*) *donovani* and *L. infantum* protozoan parasites, can provoke overwhelming and protracted epidemics, with high case-fatality rates. An effective vaccine against the disease must rely on the generation of a strong and long-lasting T cell immunity, mediated by CD4 $^{+}$  T<sub>H1</sub> and CD8 $^{+}$  T cells. Multi-epitope peptide-based vaccine development is manifesting as the new era of vaccination strategies against *Leishmania* infection. In this study, we designed chimeric peptides containing HLA-restricted epitopes from three immunogenic *L. infantum* proteins (cysteine peptidase A, histone H1, and kinetoplastid membrane protein 11), in order to be encapsulated in poly(lactic-co-glycolic) acid nanoparticles with or without the adjuvant monophosphoryl lipid A (MPLA) or surface modification with an octapeptide targeting the tumor necrosis factor receptor II. We aimed to construct differentially functionalized peptide-based nanovaccine candidates and investigate their capacity to stimulate the immunomodulatory properties of dendritic cells (DCs), which are critical regulators of adaptive immunity generated upon vaccination. According to our results, DCs stimulation with the peptide-based nanovaccine candidates with MPLA incorporation or surface modification induced an enhanced maturation profile with prominent IL-12 production, promoting allogeneic T cell proliferation and intracellular production of IFN $\gamma$  by CD4 $^{+}$  and CD8 $^{+}$  T cell subsets. In addition, DCs stimulated with the peptide-based nanovaccine candidate with MPLA incorporation exhibited a robust transcriptional

activation, characterized by upregulated genes indicative of vaccine-driven DCs differentiation toward type 1 phenotype. Immunization of HLA A2.1 transgenic mice with this peptide-based nanovaccine candidate induced peptide-specific IFN $\gamma$ -producing CD8 $^{+}$  T cells and conferred significant protection against *L. infantum* infection. Concluding, our findings supported that encapsulation of more than one chimeric multi-epitope peptides from different immunogenic *L. infantum* proteins in a proper biocompatible delivery system with the right adjuvant is considered as an improved promising approach for the development of a vaccine against VL.

**Keywords:** *Leishmania*, chimeric peptides, peptide-based vaccine, poly(lactic-co-glycolic) acid nanoparticles, dendritic cell transcriptome

## INTRODUCTION

Leishmaniasis, a group of vector-borne parasitic diseases caused by dimorphic protozoan flagellates of the genus *Leishmania*, is highly diverse and complex with a wide spectrum of clinical forms in humans, ranging from the self-healing cutaneous leishmaniasis (CL) to the potentially fatal visceral leishmaniasis (VL). With an estimated incidence of 0.3 million cases and over than 30,000 deaths per year, VL has emerged as a serious global problem and important public health concern with major clinical and socio-economic impacts (1, 2). In South Europe, Central, and South America, VL is caused by *Leishmania* (*L.*) *infantum* (synonym *L. chagasi*) and is transmitted as a zoonosis with the domestic dog serving as the main reservoir of the parasite, especially in the urban and suburban areas (3).

Current control tactics for VL rely on chemotherapy to alleviate the disease and on vector control to reduce transmission. Since the arsenal of drugs available is limited and chemotherapy gathers many disadvantages with most prominent the toxicity and the emergence of resistance, the development of a prophylactic, safe, and cost affordable vaccine is considered high priority. The success of vaccine development depends on understanding the immunology of host-pathogen interactions, choosing appropriate antigenic candidates, and selecting the right adjuvant and/or delivery vehicle.

It is well established that CD4 $^{+}$  T helper type 1 ( $T_{H1}$ ) cells are critical for the control of *L. infantum* infection owing to their ability to produce IFN $\gamma$ , which activates macrophages to kill parasites *via* nitric oxide (NO) production leading to reduction in parasitic burden (4, 5). However, nowadays, it is clear that CD8 $^{+}$  T cells also play an important role in the mechanisms involved in cure of and resistance to VL, either by production of IFN $\gamma$  and macrophage activation or by direct killing of parasitized macrophages, or *via* a combination of both effects (6, 7). Thus, an effective vaccine against the disease must rely on the generation of a strong and long-lasting T cell immunity (7).

Almost a decade ago, T cell epitope prediction *via* bioinformatics analysis of protein sequences has been proposed as an alternative for rational vaccine development (8). Recent immunoinformatics approaches utilize multiple algorithms for predicting epitopes, HLA-binding, transporter of antigen processing (TAP) affinity, proteasomal cleavage, etc., in order to explore the use of peptide epitopes with the highest probability

of inducing protective immune responses (9). Such bioinformatics tools predict promiscuous epitopes presented by different HLA supertypes, providing a way to surmount the obstacle of HLA heterogeneity in human populations through the design of “polytope vaccines” against several pathogens. Although an ideal “polytope vaccine” for human population seems to be still difficult to achieve, several research groups have studied the protective potential of epitope vaccines against *Leishmania* infectious challenges in experimental models (10, 11). Peptide-based vaccines offer considerable advantages over other vaccine types, such as cost-effective production, safety, stability under different conditions, high specificity due to defined epitopes, and decreased chance of stimulating a response against self-antigens. On the other hand, they have drawbacks including low immunogenicity and rapid degradation by endopeptidase or exopeptidase activity in the injection site or in circulation. Thus, peptides need to be combined with delivery systems and/or adjuvants such as immune modulators in order to properly activate the innate and adaptive arms of the immune system (12).

Several studies have indicated that peptide-based vaccines may benefit from particulate delivery systems that mimic the size and structure of a pathogen, facilitating uptake by dendritic cells (DCs) and increasing the probability of peptide cross-presentation (13–15). DCs are the most proficient antigen-presenting cells in capturing, processing, and presenting antigens, as well as triggering T cell responses. Further, they exclusively own the capacity of primary activating naïve T lymphocytes. Classically, extracellular antigens are taken up by DCs, processed into short peptides, and presented on major histocompatibility complex (MHC) class II molecules to activate CD4 $^{+}$  T cells. However, intracellular phagocytosis of exogenous antigens mediated by nanoparticles (NPs) can dramatically enhance cross-presentation, where the antigen is processed in the cytoplasm for presentation on MHC class I molecules activating CD8 $^{+}$  T cell responses (16, 17). Among particulate delivery systems, poly(lactic-co-glycolic) acid (PLGA) polymers have received considerable interests in recent years for potent use in antigen delivery, due to the numerous advantages they provide. Commercially available at different molecular weights (MW) and co-polymer compositions, PLGA polymers are biodegradable and biocompatible, protect the encapsulated molecules from degradation, allow co-encapsulation of antigens and immune modulators in the same particle, offer the possibility of sustained release, can undergo surface modification, and be

targeted to antigen-presenting cells, while their particulate nature can increase uptake and cross-presentation (18, 19). PLGA NPs have already been tested as antigen-delivery systems in different experimental models toward the development of an effective vaccine against leishmaniasis with encouraging results (20–22).

In the process of vaccine development against infectious diseases, there is often a strong need to monitor a great number of compounds for their immunogenicity. A functional high-throughput screen of candidate vaccines can be carried out to test their ability to activate innate immune cells *in vitro*, since such assays could be predictive of *in vivo* immunogenicity. DCs play pivotal role in the induction of adaptive immunity priming naïve T cells, and, consequently, in orchestration of immune responses upon vaccination. Thus, *in vitro* assays monitoring DCs activation after stimulation represent a robust biological platform to predict the immunological potential of novel vaccine compounds and, therefore, could be considered as a tool for the preclinical assessment of their immunogenicity (23, 24). Moreover, recently, the scientific community has focused its interest on the definition of transcriptional signatures to study immune responses induced by already existing and candidate vaccines (25, 26). Data obtained from the gene-expression profile of DCs stimulated with different antigens, adjuvants, antigen-delivery systems, or candidate vaccines may guide the development of an improved vaccination strategy (24, 27, 28).

In this study, we designed synthetic long peptides (chimeric peptides) using proper amino acid (aa) linkers and multi-epitope peptides containing HLA class I-restricted epitopes of the *L. infantum* proteins cysteine peptidase A (CPA), histone H1, and kinetoplastid membrane protein 11 (KMP-11). Each chimeric peptide was encapsulated in PLGA NPs alone or in combination with the adjuvant monophosphoryl lipid A (MPLA), or in PLGA NPs surface modified with an octapeptide (p8) mimicking the TNF $\alpha$ -docking region with tumor necrosis factor receptor II (TNFRII), with the view of constructing experimental peptide-based nanovaccines. In the context of a cell-based preclinical

system, we aimed to compare the capacity of the differentially functionalized nanovaccine candidates to stimulate the immunomodulatory properties of DCs, which are critical regulators of vaccine-induced immunity, in order to select the most promising for *in vivo* evaluation. To that end, the expression of activation markers, the production of cytokines, the ability to stimulate allogeneic T cells, and the gene-expression profile of bone marrow-derived DCs from HLA A2.1 transgenic mice were examined. From the *in vitro* screening, the mix of PLGA nanoformulations with MPLA incorporation emerged as a promising peptide-based nanovaccine and thus, its ability to promote antigen-specific CD8 $^{+}$  T cell responses and to confer protection against *L. infantum* infection was evaluated in HLA A2.1 transgenic mice, a strain that enables the modeling of human T cell immune responses to HLA A\*0201-restricted epitopes.

## MATERIALS AND METHODS

### Chimeric Peptide Design and Synthesis

Two multi-epitope peptides of CPA (CPA\_p2: 160–189 aa and CPA\_p3: 273–302 aa), two multi-epitope peptides of histone H1 (H1\_p1: 1–20 aa and H1\_p3: 43–61 aa), and one multi-epitope peptide of KMP-11 (KMP-11\_p1: 4–23 aa), derived from a previously described *in silico* analysis of the three *L. infantum* proteins (29) and designed in a way to contain HLA-restricted epitopes (Table 1), formed the basis for the design of chimeric peptides (one for each protein) with the use of proper linkers. HLA A\*0201-restricted epitopes derived from the *L. infantum* proteins and included in the chimeric peptides were predicted using the online available algorithms SYFPEITHI (30) and EpiJen (31) with a cutoff score adjusted to  $\geq 18$  and  $< 50$  nM, respectively (Table 2). SYFPEITHI was also used for the *in silico* prediction of potent H2-Kb- or H2-Db-restricted epitopes (Table 2). The chimeric peptides (chCPAp, chH1p, and chKMP-11p) were synthesized by GeneCust (Labbx, Dudelange, Luxembourg) with  $\geq 95\%$  purity. Synthetic chimeric peptides were dissolved in DMSO or dH<sub>2</sub>O,

**TABLE 1 |** Chimeric peptides containing multi-epitope peptides of the *Leishmania infantum* immunogenic proteins cysteine peptidase A (CPA), histone H1, and kinetoplastid membrane protein 11 (KMP-11).

Name	Sequence (NH <sub>2</sub> – ... -COOH)	Multi-epitope peptide	HLA supertypes	Linker	Length (aa)	Molecular weights (Da)
chCPAp	GNIEQQWALKNHSVLSEQVLVSCDNIDD <b>AA</b> Y LYFGGVVTLCFGLSLNHGVLVGFNQRQAKP	CPA_p2 and CPA_p3	HLA-A2 (A*0201) HLA-A3 (A*03) HLA-A24 (A*2402) HLA-DRB1 HLA-DPA1 HLA-DQA1	AA	65	6,778.77
chH1p	MSSDSAVAALSAAMTSPQKS <b>AA</b> Y AGAKKKAGAKKAVRKVATPKK	H1_p1 and H1_p3	HLA-A2 (A*0201) HLA-A3 (A*03) HLA-DRB1 HLA-DQA1	AA	43	4,236.02
chKMP-11p	AKFVAAWTLKAAA <b>HEYGAEALERAG</b> TYEEFSAKLDRLDEEFNRKM	PADRE and KMP-11_p1	HLA-A2 (A*0201) HLA-A3 (A*03) HLA-A24 (A*2402) HLA-DRB1 HLA-DPA1 HLA-DQA1	HEYGAEALERAG	45	5,135.79

**TABLE 2** | HLA A\*0201, H2-Db, and H2-Kb restricted epitopes included in the chimeric peptides from the *Leishmania infantum* immunogenic proteins cysteine peptidase A (CPA), histone H1, and kinetoplastid membrane protein 11 (KMP-11).

Name	Sequence (NH <sub>2</sub> ... -COOH)	HLA A*0201-restricted epitopes	H2-Db restricted epitopes	H2-Kb restricted epitopes
chCPAp	GNIEQQWALKNHSVLSEQVLVSCDNIDD <b>AY</b> LYFGGVTLCFGSLNHGVLVGFNROAKP	<i>Nonamers</i> 160-GNIEQQWAL-168 168-LKNHSLVSL-176 172-SLVSLSQEV-180 175-SLSEQVLS-183 273-LYFGGVVTL-281 277-GVVTLCFGL-285 279-VTLCFGLSL-287 283-FGLSLNHGV-291 284-GLSLNHGV-292 286-SLNHGVLV-294 <i>Decamers</i> 167-ALKNHSLSL-176 172-SLVSLSQEV-181 173-LVSLSEQVLS-182 175-SLSEQVLS-184 284-GLSLNHGV-293 285-LSLNHGVLV-294 286-SLNHGVLV-295	<i>Nonamers</i> 166-WALKNHSLV-174 284-GLSLNHGV-292 <i>Decamers</i> 276-GGVTLCFGL-285 284-GLSLNHGV-293	No predicted epitopes
chH1p	MSSDSAVAALSAAMTPQKS <b>AY</b> AGAKKAGAKKAVRKVATPKK	<i>Nonamers</i> 2-SSDSAVAAL-10 49- GAKKAVRKV-57 <i>Decamers</i> 1-MSSDSAVAAL-10 48-AGAKKAVRKV-57	<i>Decamers</i> 5-SAVAALSAAM-14	No predicted epitopes
chKMP-11p	AKFVAATWLKAAA <b>HEYGAEALERAG</b> TYEEFSAKLDRLDEEFNRKM	<i>Nonamers</i> 2-ATTYEEFSA-10 11-KLDRLDEEF-19 <i>Decamers</i> 3-TTYEEFSAKL-12 14-RLDEEFNRKM-23	<i>Decamers</i> 10-AKLDRLDEEF-19	No predicted epitopes

The cutoff score was adjusted to  $\geq 18$  for SYFPEITHI and  $< 50$  nM for EpiJen.

according to their hydrophobicity, by vigorous pipetting and stored at  $-80^{\circ}\text{C}$  in aliquots until use.

## Construction and Characterization of Nanoformulations Based on PLGA NPs

Poly(lactic-*co*-glycolic) acid 75:25 (Resomer RG752H, MW: 4–15 kDa), polyvinyl alcohol (PVA; MW: 30–70 kDa, 87–90% hydrolyzed), MPLA from *Salmonella minnesota*, phosphate-buffered saline (PBS; 10 $\times$ , pH 7.4), *N*-(3-Dimethylaminopropyl)-*N'*-ethylcarbodiimide hydrochloride (EDC), and *N*-hydroxysuccinimide 98% (NHS) were purchased from Sigma-Aldrich (Vienna, Austria). All the other reagents were of analytical grade and commercially available. PLGA NPs containing the chimeric peptide (chCPAp, chH1p, or chKMP-11p) and the adjuvant MPLA were prepared by the double emulsion method, as previously described (32). Briefly, 2.9 ml of a PLGA chloroform solution (31 mg/ml) were mixed with 0.1 ml of an MPLA solution (10 mg/ml) in methanol:chloroform (1:4 v/v). Water-in-oil (w/o) emulsion was then formed by adding 0.3 ml of the chimeric peptide solution in PBS at a final concentration of 6.6 mg/ml into the PLGA/MPLA solution. The emulsification was performed in an ice bath with the aid of a microtip sonicator (Vibra Cell VC-505; Sonics, Newtown, CO, USA) at 40% amplitude for 45 s. Subsequently, the primary emulsion (w/o) was added into 12 ml of

1% (w/v) PVA aqueous solution. The mixture was then emulsified *via* sonication at 40% amplitude for 2 min. The resulting double (w/o/w) emulsion was stirred overnight to allow the evaporation of chloroform. The PLGA NPs were then purified by means of four successive centrifugation–redispersion cycles in sterilized water, at 13,860  $\times$  g for 10 min at  $4^{\circ}\text{C}$  and were subsequently lyophilized (ScanVac Freezedryers CoolSafe 55-9; LaboGene ApS, Lyngé, Denmark). For the preparation of the PLGA NPs loaded with each of the chimeric peptides, the same volume of peptide solution as previously was added into 3 ml of a PLGA chloroform solution at a final concentration of 30 mg/ml. Lyophilized PLGA NPs were stored at  $4^{\circ}\text{C}$ .

For specific purposes, PLGA NPs were surface modified with a synthetic octapeptide (p8: CYTYQGKL; JPT, Berlin, Germany) that mimics the TNF $\alpha$ -docking region with the TNFRII. The peptide was conjugated to NPs *via* a two-step carbodiimide method (33, 34). Accordingly, 1.5 ml of a 7 wt% EDC solution and 1.5 ml of a 0.3 wt% NHS solution both prepared in 20 mM HEPES/NaOH buffer containing 1% (v/v) Pluronic F-68 at pH 7 were added into 1 ml of PLGA NPs (empty or loaded with each of the chimeric peptides) dispersion in the same buffer at a final concentration of 20 mg/ml, in order to activate the PLGA carboxyl groups (35). The mixture was then stirred end-over-end for 2 h at room temperature. The residual reagents were removed

by centrifugation at  $13,860 \times g$  for 10 min at  $25^{\circ}\text{C}$ . Subsequently, 0.3 ml of 0.1% (w/v) p8 solution in 20 mM HEPES/NaOH buffer containing 1% (v/v) Pluronic F-68 at pH 7 were added to the PLGA NPs dispersion, and the mixture was incubated for 18 h at room temperature. To saturate free-coupling sites, 500  $\mu\text{L}$  of 20% (w/v) glycine in 20 mM HEPES/NaOH buffer containing 1% (v/v) Pluronic F-68 at pH 7.0 was added and incubated end-over-end for 1 h at  $25^{\circ}\text{C}$ . The PLGA NPs were subsequently purified by means of two successive centrifugation–redispersion cycles at  $13,860 \times g$  for 10 min at  $25^{\circ}\text{C}$  in the same buffer. The finally collected NPs were subsequently lyophilized and stored at  $4^{\circ}\text{C}$ .

The surface morphology of the PLGA NPs was observed by scanning electron microscopy (SEM) (JEOL JSM 6300). Accordingly, the lyophilized NPs were first double coated with a gold layer under vacuum and then examined by SEM. The average particle diameter of the PLGA NPs was determined by photon correlation spectroscopy and their zeta potential by aqueous electrophoresis measurements (Nano ZS90; Malvern Instruments Ltd., Malvern, UK). The measurements were performed with aqueous dispersions of NPs prior to their lyophilization.

## Quantification of Antigen, Adjuvant, and Targeting Ligand and *In Vitro* Release Studies

The MicroBCA Protein assay kit (Thermo Scientific, Rockford, IL, USA) was employed to determine the chimeric peptide load (wt%) in the PLGA NPs according to the manufacturer's instructions. Briefly, 2.5 mg of lyophilized PLGA NPs was dissolved in 0.25 ml DMSO for 1 h following a further dissolution in 1.25 ml of 0.05 N NaOH/0.5% (v/v) SDS for 3 h at  $25^{\circ}\text{C}$ . PLGA NPs without encapsulated chimeric peptide were used as controls. The absorbance of the samples was measured at 562 nm using a microplate reader (EL808IU-PC, BioTek Instruments Inc., Winooski, VT, USA). Peptide encapsulation efficiency (%) was calculated by the ratio of the peptide mass in the PLGA NPs over the total mass of peptide used. Peptide load (wt%) was calculated by the ratio of the encapsulated mass of peptide over the total mass of PLGA NPs.

A Limulus Amebocyte Lysate (LAL) kit (Lonza, Walkersville, MD, USA) was used for the determination of the MPLA load (wt%) in the PLGA NPs according to the manufacturer's instructions. Briefly, a standard curve was established using different concentrations of aqueous MPLA solutions ranging from 0.01 to 10 ng/ml, which was found to be linear for the MPLA concentration range used with a correlation coefficient of  $R^2 = 0.9994$ . The encapsulation efficiency (%) of MPLA was calculated by the ratio of the measured MPLA mass in the PLGA NPs over the total mass of MPLA in the recipe. Similarly, the MPLA load (wt%) was calculated by the ratio of encapsulated MPLA mass over the total mass of the PLGA NPs.

A UV-Vis spectrophotometer (Lambda 35; PerkinElmer, Waltham, MA, USA) was used for the determination of p8 amount (wt%) conjugated on the PLGA NPs surface. Accordingly, 2.5 mg of lyophilized p8-conjugated PLGA NPs was dissolved in 0.25 ml DMSO for 1 h following a further dissolution in 1.25 ml 0.05 N NaOH/0.5% (v/v) SDS for 3 h. The absorbance of the samples

was measured at 492 nm. The calibration curve was found to be linear over the p8 concentration range of 0.3125–70  $\mu\text{g}/\text{ml}$  with a correlation coefficient of  $R^2 = 0.9982$ . Conjugation efficiency (%) of p8 was calculated by the ratio of the measured p8 mass on the PLGA NPs over the total mass of p8 used. Similarly, p8 load (wt%) was calculated by the ratio of conjugated p8 mass over the total mass of the PLGA NPs.

For the assessment of the *in vitro* release of the chimeric peptides and MPLA, PLGA NPs were dispersed in PBS at a final concentration of 1 mg/ml and incubated at  $37^{\circ}\text{C}$  in a thermomixer (Eppendorf) under constant stirring at  $120.7 \times g$ . At predetermined time points (0, 1, 2, 4, 6, 12, 24, 48 h, and 1, 2 weeks), 1 ml of the dispersion was centrifuged at  $13,860 \times g$  for 10 min at  $4^{\circ}\text{C}$ . The supernatants were collected, and the amount of the chimeric peptide or MPLA was determined using the MicroBCA or the LAL kit, respectively.

## Experimental Animals and Ethics Statement

B6.Cg-Tg(HLA-A/H2-D)2Enge/J humanized transgenic mice, provided by the Jackson Laboratory (Bar Harbor, ME, USA), were used in this study. These transgenic mice express an interspecies hybrid class I MHC gene, *aad*, which contains the alpha-1 and alpha-2 domains of the human HLA-A2.1 gene and the alpha-3 transmembrane and cytoplasmic domains of the mouse H-2D<sup>d</sup> gene, under the direction of the human HLA-A2.1 promoter, while they are created on a C57BL/6 background. BALB/c mice, also used in this study, were obtained from the breeding unit of the Hellenic Pasteur Institute (Athens, Greece). Both strains were reared in institutional facilities under specific pathogen-free conditions at ambient temperature of  $25^{\circ}\text{C}$ , receiving a diet of commercial food pellets and water *ad libitum*; female mice 6–8 weeks old were used. Animal protocols had been approved by the institutional Animal Bioethics Committee regulating according to the National Law 2013/56 and the EU Directive 2010/63/EU for animal experiments and complied with the ARRIVE guidelines. All efforts were made to minimize animal suffering.

## Generation and Characterization of DCs

Dendritic cells were generated from pluripotent bone marrow stem cells obtained from HLA A2.1 transgenic mice in the presence of recombinant mouse granulocyte macrophage colony-stimulating factor (rmGM-CSF) as previously described (36). Briefly,  $3.5 \times 10^6$  bone marrow cells obtained from the tibias and femurs of mice were seeded in a 100 mm Petri dish in 10 ml of RPMI-1640 medium (Biochrom AG, Berlin, Germany) supplemented with 2 mM L-glutamine, 10 mM HEPES, 100 U/ml penicillin, 100  $\mu\text{g}/\text{ml}$  streptomycin (complete RPMI-1640 medium), 10% (v/v) heat-inactivated fetal bovine serum (FBS; Gibco, Paisley, UK), and 20 ng/ml rmGM-CSF (Peprotech, London, UK) and cultured for 7 days at  $37^{\circ}\text{C}$  and 5% CO<sub>2</sub>. On days 3 and 6, loosely adherent cells were harvested and resuspended in fresh culture medium supplemented with the same dose of rmGM-CSF. On day 7, non-adherent cells were collected and characterized; cell viability was >95% as determined by trypan blue exclusion, and the percentage of CD11c<sup>+</sup>CD8α<sup>-</sup> cells was >85% as assessed by R-phycocerythrin

(R-PE)-conjugated hamster anti-mouse CD11c (clone HL3; BD Biosciences, Erembodegem, Belgium) and FITC-conjugated rat anti-mouse CD8 $\alpha$  (clone Lyt2; BD Biosciences) monoclonal antibodies (mAbs) and flow cytometry. For each sample, 10,000 cells were analyzed on a FACS Calibur (Becton-Dickinson, San Jose, CA, USA), and the data were processed using FlowJo V10 software (Tree Star Inc., Ashland, OR, USA).

## Stimulation of DCs and Analysis of Their Maturation and Functional Differentiation Profile by Flow Cytometry

To analyze the effect of differentially functionalized PLGA nanoformulations on DCs maturation and functional differentiation, DCs were harvested on day 7, seeded in 24-well plates at a density of  $1 \times 10^6$  cells/ml, and cultured for 24 h at 37°C and 5% CO<sub>2</sub> in the presence of (i) PLGA, (ii) PLGA-MPLA, (iii) p8-PLGA, (iv) PLGA-chCPAp, (v) PLGA-chH1p, (vi) PLGA-chKMP-11p, (vii) a mix of PLGA-chCPAp, PLGA-chH1p, and PLGA-chKMP-11p (mix A), (viii) PLGA-chCPAp-MPLA, (ix) PLGA-chH1p-MPLA, (x) PLGA-chKMP-11p-MPLA, (xi) a mix of PLGA-chCPAp-MPLA, PLGA-chH1p-MPLA, and PLGA-chKMP-11p-MPLA (mix B), (xii) p8-PLGA-chCPAp, (xiii) p8-PLGA-chH1p, (xiv) p8-PLGA-chKMP-11p, and (xv) a mix of p8-PLGA-chCPAp, p8-PLGA-chH1p, and p8-PLGA-chKMP-11p (mix C). In parallel, DCs were cultured under the same conditions in the presence of each soluble chimeric peptide or a mix of soluble chimeric peptides with or without the adjuvant MPLA (mix D or mix E, respectively). Unstimulated DCs or DCs stimulated with 1 µg/ml LPS (Sigma-Aldrich) were used as negative and positive control, respectively. The optimal dose for each chimeric peptide encapsulated in PLGA NPs was determined at 2 µg according to preliminary experiments (data not shown). At the end of incubation, cells were washed with FACS buffer [3% (v/v) FBS in PBS] and then labeled with R-PE-conjugated 1:100 diluted rat anti-mouse CD40 (clone 3/23; BD Biosciences), hamster anti-mouse CD80 (clone 16-10A1; BD Biosciences), rat anti-mouse CD86 (clone GL-1; BD Biosciences), mouse anti-mouse MHC I H-2 Kb/H-2 Db (clone 5041.16.1; Acris, Herford, Germany), or 1:200 diluted rat anti-mouse MHCII I-Ab chain, H2-Eb1 (clone NIMR; Acris), or 1:10 diluted mouse anti-human HLA-ABC (clone G46-2.6; BD Biosciences) mAbs for 30 min at 4°C in the dark. For intracellular staining, cells were subjected to 2.5 µg/ml brefeldin A (Applichem, Darmstadt, Germany) during the last 4 h of culture and then they were fixed with 2% (w/v) paraformaldehyde (PFA; Sigma-Aldrich) in PBS and stained with PE-conjugated 1:100 diluted anti-mouse IL-12p40/p70 (clone C15.6; BD Biosciences) mAb in permeabilization buffer [0.1% (v/v) saponin in FACS buffer] for 30 min at 4°C in the dark. After a washing step with FACS buffer, cells were analyzed by flow cytometry, and data were processed as previously described.

## Mixed Leukocyte Reaction (MLR) Induced by Stimulated DCs

Spleens from BALB/c mice were aseptically excised and teased into single-cell suspension in complete RPMI-1640 medium supplemented with 10% (v/v) FBS. Red blood cells were removed

by treating spleen cells with ammonium chloride lysis solution, pH 7.2 (ACK; 0.15 M NH<sub>4</sub>Cl, 1 mM KHCO<sub>3</sub>, 0.1 mM Na<sub>2</sub>EDTA). Lysis reaction was stopped by adding ice-cold complete RPMI-1640 medium, and spleen cells were washed twice. DCs that have been stimulated as described above for 24 h were washed and co-cultured with  $2 \times 10^5$  naïve spleen cells at different ratios (1:5, 1:10, or 1:20) in 96-well round-bottom plates for 96 h at 37°C and 5% CO<sub>2</sub>. Spleen cells cultured in medium alone or in the presence of 6 µg/ml concanavalin A (Con A; Sigma-Aldrich) served as negative and positive control of T cell proliferation, respectively. Cells were pulsed with 1 µCi/ml of <sup>3</sup>[H]-thymidine (<sup>3</sup>[H]-TdR; PerkinElmer, MA, USA) for the last 18 h of the culture period and then were harvested. The <sup>3</sup>[H]-TdR incorporation was determined on a microplate scintillation counter (Microbeta Trilux, Wallac, Turku, Finland). All samples were run in triplicate.

In parallel, DCs stimulated for 24 h with (i) the mix of PLGA-chCPAp, PLGA-chH1p, and PLGA-chKMP-11p nanoformulations (mix A), (ii) the mix of PLGA-chCPAp-MPLA, PLGA-chH1p-MPLA, and PLGA-chKMP-11p-MPLA nanoformulations (mix B), (iii) the mix of p8-PLGA-chCPAp, p8-PLGA-chH1p, and p8-PLGA-chKMP-11p nanoformulations (mix C), (iv) the mix of soluble chimeric peptides (mix D), and (v) the mix of the soluble chimeric peptides with the adjuvant MPLA (mix E) were co-cultured with  $1 \times 10^6$  naïve spleen cells from BALB/c mice at a ratio of 1:5 in 24-well plates for 48 h at 37°C and 5% CO<sub>2</sub>. Cells were exposed to 2.5 µg/ml brefeldin A during the last 4 h of culture and then washed with FACS buffer and fixed with 2% (w/v) PFA in PBS. Fixed cells were stained with APC-conjugated hamster anti-mouse CD3e (clone 145-2C11), FITC-conjugated rat anti-mouse CD4 (clone RM4-5) or CD8 $\alpha$  (clone 53-6.7) mAbs, and R-PE-conjugated rat anti-mouse IFN $\gamma$  (clone XMG1.2) or IL-4 (clone BVD4-1D11) mAbs in permeabilization buffer for 30 min at 4°C in the dark. All mAbs used in the protocol were purchased from BD Biosciences. After a washing step with FACS buffer, 20,000 cells from each sample were analyzed by flow cytometry, and data were processed as previously described.

## RNA Extraction and Microarray Assay

To analyze the effect of differentially functionalized PLGA nanoformulations on DCs gene expression, DCs were stimulated with (i) the mix of PLGA-chCPAp, PLGA-chH1p, and PLGA-chKMP-11p nanoformulations (mix A), (ii) the mix of PLGA-chCPAp-MPLA, PLGA-chH1p-MPLA, and PLGA-chKMP-11p-MPLA nanoformulations (mix B), (iii) the mix of p8-PLGA-chCPAp, p8-PLGA-chH1p, and p8-PLGA-chKMP-11p nanoformulations (mix C), and (iv) the mix of soluble chimeric peptides (mix D) at 37°C and 5% CO<sub>2</sub>, for 18 h. DCs cultured in medium alone were used as a reference group. Total RNA was isolated with Trizol Reagent (Invitrogen, Karlsruhe, Germany) and purified on a Qiagen RNeasy column (Qiagen, Hilden, Germany) according to the manufacturer's instructions. RNA was quantified with ND-1000 Nanodrop (Thermo Fisher Scientific, Wilmington, DE, USA), and RNA integrity was assessed using the RNA 6000 NanoLabChip kit on Agilent Bioanalyzer 2100 (Agilent Technologies, Inc., Palo

Alto, CA, USA). Only samples with intact total RNA profiles (retention of both ribosomal bands and the broad central peak of mRNA) and RIN > 7.0 were utilized in microarray analysis. Approximately 300 ng of total RNA were used to generate biotinylated complementary RNA (cRNA) for each group using the GeneChip® WT PLUS Reagent Kit protocol for whole transcript (WT) expression array, Rev3. Poly-A RNA control added to the RNA test samples as exogenous positive control, and the RNA was reverse transcribed to double-stranded cDNA, and biotinylated cRNA was synthesized and purified according to the protocol. A second cycle of cDNA synthesis followed along with a second purification step. Then, 6 µg of the single-stranded DNA was fragmented, labeled with the appropriate labeling reagent, and hybridized to GeneChip® Mouse Gene 2.0 ST arrays (Affymetrix, UK). Hybridization took place for 16 h in an Affymetrix GeneChip® Hybridization Oven 640. Affymetrix GeneChip® Fluidics Station 450 was used to wash and stain the arrays with streptavidin–phycoerythrin according to the standard antibody amplification protocol for eukaryotic targets. Arrays were scanned on Affymetrix GeneChip® Scanner 3000 at 570 nm. The Affymetrix eukaryotic hybridization control and Poly-A RNA control were used to ensure efficiency of hybridization and cRNA amplification. Images and data were acquired and analyzed using the Affymetrix® GeneChip® Command Console® Software (AGCC), where initial quality control of the experiment was performed. AGCC was also used to perform robust multi-array average (RMA) normalization and probe set summarization steps on the raw signal intensity files. Principal component analysis (PCA) and heatmap representation of individual values were conducted utilizing appropriate open-source software. Differential expression analysis was performed for stimulated vs. unstimulated DCs utilizing one-way ANOVA ( $p < 0.05$ ) and a  $\pm 0.585\log_2$  (fold change) threshold on mean gene-expression levels. Probe sets that were unannotated or that mapped to the same gene in a many-to-one fashion were removed from the subsequent analysis. Microarray raw files and RMA-summarized data have been deposited in Gene Expression Omnibus under accession number GSE92869.

## Functional Analysis of Gene-Expression Profiling

Mapping of array-specific probe sets to Entrez Gene IDs was conducted using up-to-date annotation package mogene20st-transcriptcluster.db in R. Significantly deregulated genes [ $p < 0.05$ ,  $\pm 0.585\log_2$  (fold change) threshold] from each comparison (mix A–D vs. reference) were subjected to functional enrichment analysis with the R package *clusterProfiler* (37), setting parameters “*pvalueCutoff*” = 0.05 and “*pAdjustMethod*” = “*fdr*” for multiple comparisons. Terms from Gene Ontology (Biological Process) database slice (38) were tested for enrichment. Mappings between GO terms and Entrez Gene IDs relied on regularly updated R package org.Mm.eg.db. R package *Pathview* (39) was utilized to superimpose differentially expressed genes upon KEGG pathways. Red and green colors signify upregulation and downregulation on stimulated DCs, respectively.

## Immunization and Analysis of Antigen-Specific T Cell Responses

HLA A2.1 transgenic mice ( $n = 5$ ) were immunized subcutaneously in the upper and dorsal region with the mix of PLGA-chCPAp-MPLA, PLGA-chH1p-MPLA, and PLGA-chKMP-11p-MPLA nanoformulations (mix B) in a total volume of 100 µl sterile PBS. Taking into account the chimeric peptide and MPLA loads of the above nanoformulations, each mouse received in total 6 µg of chimeric peptides (2 µg of each chimeric peptide) with 3 µg MPLA. Two booster doses—also subcutaneously injected—followed at a 2-week interval. Control groups ( $n = 5$  mice/group) received PLGA-MPLA nanoformulations in PBS or only PBS.

Two weeks after the last immunization, mice were euthanized, and spleens were removed aseptically. To analyze antigen-specific T cell proliferation, single-cell suspensions were prepared in complete RPMI-1640 medium supplemented with 10% (v/v) FBS, as previously described. Spleen cells were cultured in 96-well round bottom plates at a density of  $2 \times 10^5$  cells/200 µl/well in the presence of 5 µg/ml soluble chCPAp or chH1p or chKMP-11p for 96 h at 37°C and 5% CO<sub>2</sub>. Spleen cells cultured in medium alone or in the presence of 6 µg/ml Con A served as negative and positive control of T cell proliferation, respectively. Cells were pulsed with 1 µCi/ml of <sup>3</sup>[H]-TdR for the last 18 h of the culture period and then were harvested. The <sup>3</sup>[H]-TdR incorporation was determined on a microplate scintillation counter. All samples were run in triplicate, and the results were expressed as Δcpm (cpm of stimulated spleen cells – cpm of unstimulated spleen cells).

In parallel, intracellular cytokine staining and flow cytometry were performed in the spleen cell suspensions from immunized mice in order to identify antigen-specific IFNγ-producing CD8<sup>+</sup> T cells. In brief,  $1 \times 10^6$  spleen cells were cultured in 24-well plates in the presence of 5 µg/ml soluble chCPAp or chH1p or chKMP-11p for 48 h, according to previously described protocols (29, 40), at 37°C and 5% CO<sub>2</sub>. Spleen cells cultured in medium alone served as negative control. Spleen cells were exposed to 2.5 µg/ml brefeldin A during the last 4 h of culture and then washed with FACS buffer and fixed with 2% (w/v) PFA in PBS. After fixation, spleen cells were stained with APC-conjugated anti-CD3, PE-conjugated anti-IFNγ, and FITC-conjugated anti-CD8 mAbs in permeabilization buffer and analyzed with flow cytometry, as previously described.

## Parasites, Infection Protocol, and Evaluation of Parasite Burden by a Limiting Dilution Assay

A strain of *L. infantum* (MHOM/GR/2001/GH8) originally isolated from a Greek patient suffering from VL (41) was cultured *in vitro* and maintained infective through serial passage in BALB/c mice, as previously described (36). Immunized with the mix B and non-immunized (received only PBS) HLA A2.1 transgenic mice ( $n = 5$ /group) were infected by injecting intravenously  $2 \times 10^7$  stationary phase *L. infantum* promastigotes in 100 µl PBS, 2 weeks after the final booster dose. Mice immunized with PLGA-MPLA nanoformulations and then infected were used as a control group. The protective effect of immunization with the mix B was assessed in liver and spleen of the infected

mice at 1 and 2 months post-infection. The protective effect was determined in comparison with the non-immunized control group according to the formula: percentage of reduction in parasite burden = (number of parasites from the non-immunized infected control group – number of parasites from the immunized infected group)/(number of parasites from the non-immunized infected control group) × 100.

The parasite burden was assessed by a limiting dilution assay following well-established protocols (42) with minor modifications. Briefly, livers and spleens were removed aseptically from the euthanized mice and weighed. Suspensions of liver or spleen tissue were prepared in Schneider's *Drosophila* medium (Biosera, Boussens, France) supplemented with 100 U/ml penicillin, 100 µg/ml streptomycin, and 20% (v/v) FBS to 1 mg/ml final concentration. Serial twofold dilutions of the tissue suspensions were plated in 96-well culture plates and incubated at 26°C for 7 days. After the incubation period, the presence or absence of viable and motile promastigotes was recorded in each well. The reciprocal of the highest dilution that was positive for parasites was considered to be the number of parasites per milligram of tissue. The total parasite burden was calculated by reference to the whole organ weight.

## Statistical Analysis

Results are derived from at least two independent experiments and are expressed as the mean value ± SD. One-way ANOVA and Tukey's multiple comparisons test or two-way ANOVA and Bonferroni multiple comparisons test were performed, when required, to assess statistical differences using the GraphPad Prism software (version 5.0; San Diego, CA, USA). The probability (*p*) of <0.05 was considered to indicate statistical significance.

## RESULTS

### Design and Construction of Experimental Peptide-Based Nanovaccines

#### Design of Chimeric Peptides from the Immunogenic *L. infantum* Proteins CPA, Histone H1, and KMP-11

In a previous study based on an *in silico* analysis of the *L. infantum* proteins CPA, histone H1, and KMP-11, multi-epitope peptides

were designed in a way that each peptide contained at least one HLA class I-restricted epitope scored very high, as well as adjacent or overlapping HLA class II-restricted epitopes scored also high (29). All the multi-epitope peptides also contained more than one epitopes with high-binding affinity to HLA A\*0201 (**Table 2**), the most prevalent among HLA A2 allelic variants (43) with 72.2% coverage in Caucasians (44). The multi-epitope peptide sequences were also checked for the presence of H2-Db- or H2-Kb-restricted epitopes. No epitopes were predicted with binding affinity to H2-Kb allele, whereas a small number of epitopes were predicted with binding affinity to H2-Db allele with great overlap with the HLA A\*0201 epitopes. Selected multi-epitope peptides were linked together with proper aa linkers in order to design longer chimeric peptides (**Table 1**). More specifically, the tripeptide AAY was used as a linker between the multi-epitope peptides of CPA (CPA\_p2 and CPA\_p3) and histone H1 (H1\_p1 and H1\_p3), while the motif HEYGAELERAG was used as a linker between the multi-epitope peptide of KMP-11 (KMP-11\_p1) and PADRE, a synthetic pan HLA DR-binding epitope of 13 residues (AKFVAAWTLKAAA) that binds to a wide spectrum of human and mouse MHC class II alleles and induce T<sub>H</sub> cell responses.

### Physicochemical Characterization of PLGA-Based Antigen-Delivery Systems

Chimeric peptides were synthesized and each of them was encapsulated in PLGA NPs alone or in combination with the MPLA adjuvant, or in PLGA NPs surface modified with the octapeptide p8. The different nanoformulations and their characteristics are summarized in **Table 3**. Both chimeric peptide-loaded and chimeric peptide/MPLA-loaded PLGA NPs had an average diameter in the range of 291.4–413.5 nm and a negative zeta potential value, varying from -31.6 to -10.6 mV. The negative zeta potential values of the blank PLGA NPs are due to the carboxyl groups residing on the surface of NPs that are negatively charged at physiological pH (45). The observed slight decrease in the absolute zeta potential value of the chimeric peptide loaded PLGA NPs can be attributed to the presence of antigen that partially neutralizes the free anionic surface carboxyl groups. On the other hand, the negative zeta potential values observed for the chimeric peptide/MPLA-loaded PLGA NPs are due to the combined negative

**TABLE 3 |** Properties of synthesized nanoformulations based on poly(lactic-co-glycolic) acid (PLGA) nanoparticles.

Formulation name	Average size (nm)	z potential (mV)	Peptide load (wt%)	Peptide EE (%)	Monophosphoryl lipid A (MPLA) load (wt%)	MPLA EE (%)	p8 load (wt%)	p8 CE (%)
PLGA-chCPAp	291.4 ± 3.1	-31.6 ± 2.0	1.84 ± 0.04	86.44 ± 1.86	-	-	-	-
PLGA-chH1p	341.8 ± 2.8	-15.0 ± 0.2	1.41 ± 0.20	64.59 ± 7.10	-	-	-	-
PLGA-chKMP-11p	341.0 ± 1.2	-20.1 ± 0.2	1.84 ± 0.10	84.57 ± 2.37	-	-	-	-
PLGA-chCPAp-MPLA	374.5 ± 12.5	-16.1 ± 0.2	1.89 ± 0.03	87.35 ± 1.35	0.50 ± 0.06	45.44 ± 5.02	-	-
PLGA-chH1p-MPLA	413.5 ± 4.5	-10.6 ± 0.1	1.44 ± 0.08	65.30 ± 2.04	0.98 ± 0.01	92.85 ± 1.05	-	-
PLGA-chKMP-11p-MPLA	299.9 ± 1.05	-19.8 ± 0.1	1.80 ± 0.06	82.06 ± 0.99	0.81 ± 0.06	75.19 ± 4.80	-	-
p8-PLGA-chCPAp	392.2 ± 0.8	-4.0 ± 0.1	1.84 ± 0.04	86.44 ± 1.86	-	-	0.83 ± 0.14	49.62 ± 5.41
p8-PLGA-chH1p	421.1 ± 2.1	-5.5 ± 0.1	1.41 ± 0.20	64.59 ± 7.10	-	-	0.77 ± 0.09	53.06 ± 3.15
p8-PLGA-chKMP-11p	424.1 ± 3.8	-4.3 ± 0.2	1.84 ± 0.10	84.57 ± 2.37	-	-	0.73 ± 0.08	51.68 ± 2.90

Results are presented as mean ± SD (n = 3).

EE, encapsulation efficiency; CE, conjugation efficiency.

charges of the PLGA carboxyl groups and MPLA molecules that have a zeta potential value of approximately  $-50$  mV in water. Further, PLGA was successfully conjugated with p8 resulting in partial neutralization of the free anionic carboxyl groups residing on the PLGA NPs surface and thus explaining the decrease of the absolute values of zeta potential of the functionalized NPs ( $-4.0$  to  $-5.5$  mV) (46).

The *in vitro* release profiles of each chimeric peptide and MPLA from the PLGA NPs in PBS at  $37^{\circ}\text{C}$  are shown in **Figure 1**. About 45% of the total amount of chCPAp (**Figure 1A**) and chKMP-11p (**Figure 1C**) and 25% of the total amount of chH1p (**Figure 1B**) are released from the PLGA NPs during the first hour, possibly reflecting the release of antigen located near the NPs external surface and/or in the pores connected to the surface. This initial burst release of antigen was followed by a phase of slight sustained release. Thus, approximately 45% of chCPAp, 30% of chH1p, and 60% of chKMP-11p were released after 2 weeks since the polymer matrix was not completely hydrolyzed during this period. Regarding MPLA, it is apparent that it exhibits a similar release profile to that of the chimeric peptides. However, only 10–20% of the total MPLA amount was released after 2 weeks of incubation in PBS at  $37^{\circ}\text{C}$ .

### The MPLA Incorporation in PLGA Nanoformulations or the Surface Modification with p8 Induced a Strong DCs Maturation Profile

The capacity of the synthesized PLGA-based nanoformulations to directly activate and induce maturation of CD11c<sup>+</sup> bone marrow-derived DCs after 24 h stimulation was assessed by flow cytometry, measuring the surface expression of the hallmark DCs maturation and T-cell co-stimulation markers MHC class I, MHC class II, CD40, CD80, and CD86. According to preliminary experiments, the optimum dose of each chimeric peptide encapsulated in PLGA NPs for efficient DCs maturation was determined at 2  $\mu\text{g}$  (data not shown). As depicted in **Figures 2A,B**, the encapsulation of chimeric peptides in PLGA NPs resulted in a significant increase in the number of DCs expressing CD40, CD80, CD86, MHC class I, and MHC class II molecules, in comparison to DCs stimulated with soluble peptides (CD40:  $72.40 \pm 1.27$  vs.  $35.53 \pm 3.41\%$ ,  $p < 0.001$ ; CD80:  $81.20 \pm 1.56$  vs.  $56.20 \pm 2.78\%$ ,  $p < 0.001$ ; CD86:  $74.33 \pm 3.99$  vs.  $43.20 \pm 1.13\%$ ,  $p < 0.001$ ; murine MHC class I:  $82.15 \pm 4.31$  vs.  $71.60 \pm 2.26\%$ ,  $p < 0.05$ ; murine MHC class II:  $82.35 \pm 0.35$  vs.  $62.03 \pm 2.97\%$ ,  $p < 0.001$ ; hybrid HLA class I:  $39.50 \pm 0.30$  vs.  $22.55 \pm 3.82\%$ ,  $p < 0.001$ ). Regarding the mean fluorescence index (MFI) values (**Figure 2C**), significant increase was observed only for CD80, murine MHC class I, and MHC class II molecules in comparison to DCs stimulated with soluble peptides (CD80:  $754 \pm 26.87$  vs.  $503 \pm 70.29$ ,  $p < 0.05$ ; murine MHC class I:  $432 \pm 50.91$  vs.  $237 \pm 27.58$ ,  $p < 0.01$ ; MHC class II:  $3,990 \pm 718.74$  vs.  $2,370 \pm 15.56$ ,  $p < 0.01$ ). It must be noted that DCs stimulated with each of the PLGA-chCPAp, PLGA-chH1p, and PLGA-chKMP-11p nanoformulations exhibited a similar maturation profile to that of the DCs stimulated with the mix of these nanoformulations (mix A), in comparison to DCs

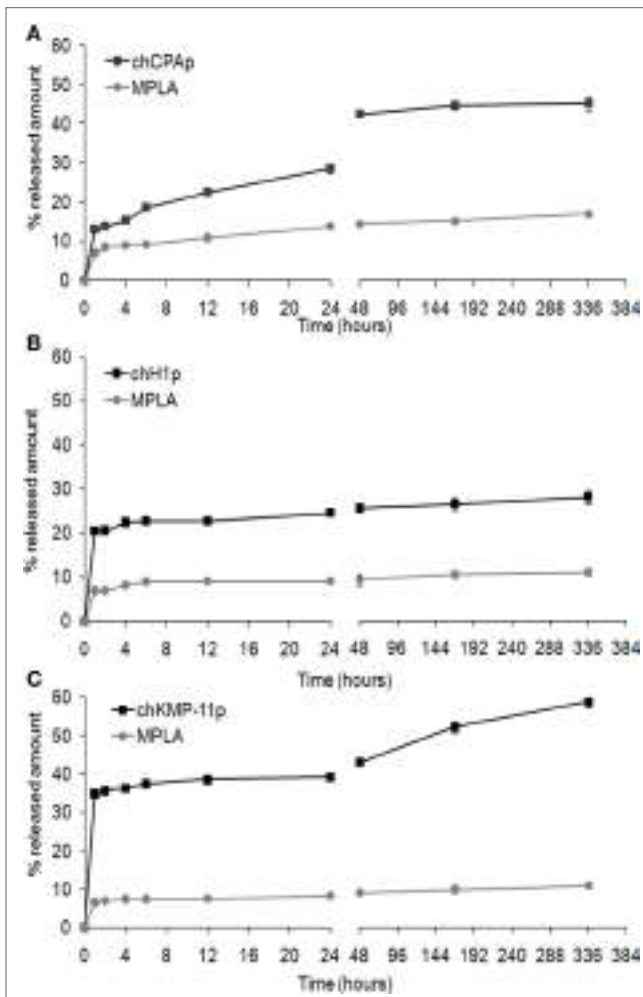


**FIGURE 1 |** *In vitro* release profile of the chimeric peptides from peptide-based poly(lactic-co-glycolic) acid (PLGA) nanoformulations. Time-dependent release of chCPAp and monophosphoryl lipid A (MPLA) adjuvant from PLGA-chCPAp-MPLA nanoformulations **(A)**, chH1p and MPLA adjuvant from PLGA-chH1p-MPLA nanoformulations **(B)**, and chKMP-11p and MPLA adjuvant from PLGA-chKMP-11p-MPLA nanoformulations **(C)** into PBS at  $37^{\circ}\text{C}$ . Data represent the mean  $\pm$  SD of three independent experiments.

stimulated with the relevant soluble chimeric peptide (Figure S1 in Supplementary Material). The above results confirm that PLGA NPs are promising delivery systems of immunogenic peptides in the development of peptide-based vaccines.

The MPLA incorporation as well as the surface modification of PLGA NPs with p8 further increased DCs maturation. More specifically, as shown in **Figures 3A,B**, stimulation of DCs with the mix of PLGA-chCPAp-MPLA, PLGA-chH1p-MPLA, and PLGA-chKMP-11p-MPLA nanoformulations (mix B) led to a significant increase in the number of DCs expressing the co-stimulatory molecules CD40 ( $80.73 \pm 3.46$  vs.  $72.40 \pm 1.27\%$ ,  $p < 0.05$ ) and CD86 ( $86.75 \pm 2.33$  vs.  $74.33 \pm 3.99\%$ ,  $p < 0.01$ ), as well as the MHC class I molecules (murine MHC class I:  $93.05 \pm 0.78$  vs.  $82.15 \pm 4.31\%$ ,  $p < 0.01$ ; hybrid HLA class I:  $71.65 \pm 4.17$  vs.  $39.50 \pm 0.30\%$ ,  $p < 0.001$ ), in comparison to DCs stimulated with the mix A. This was also accompanied by a significant increase

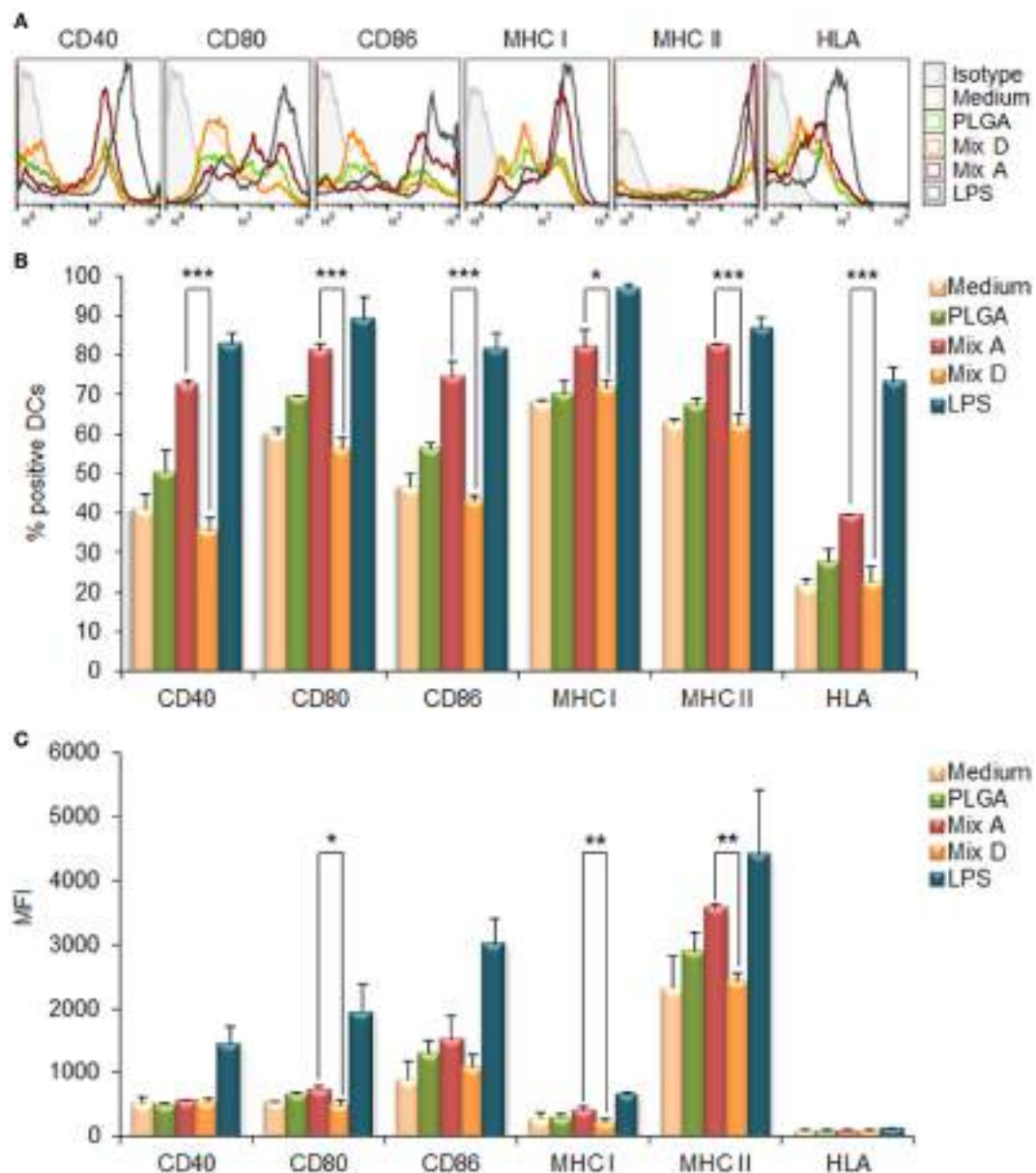
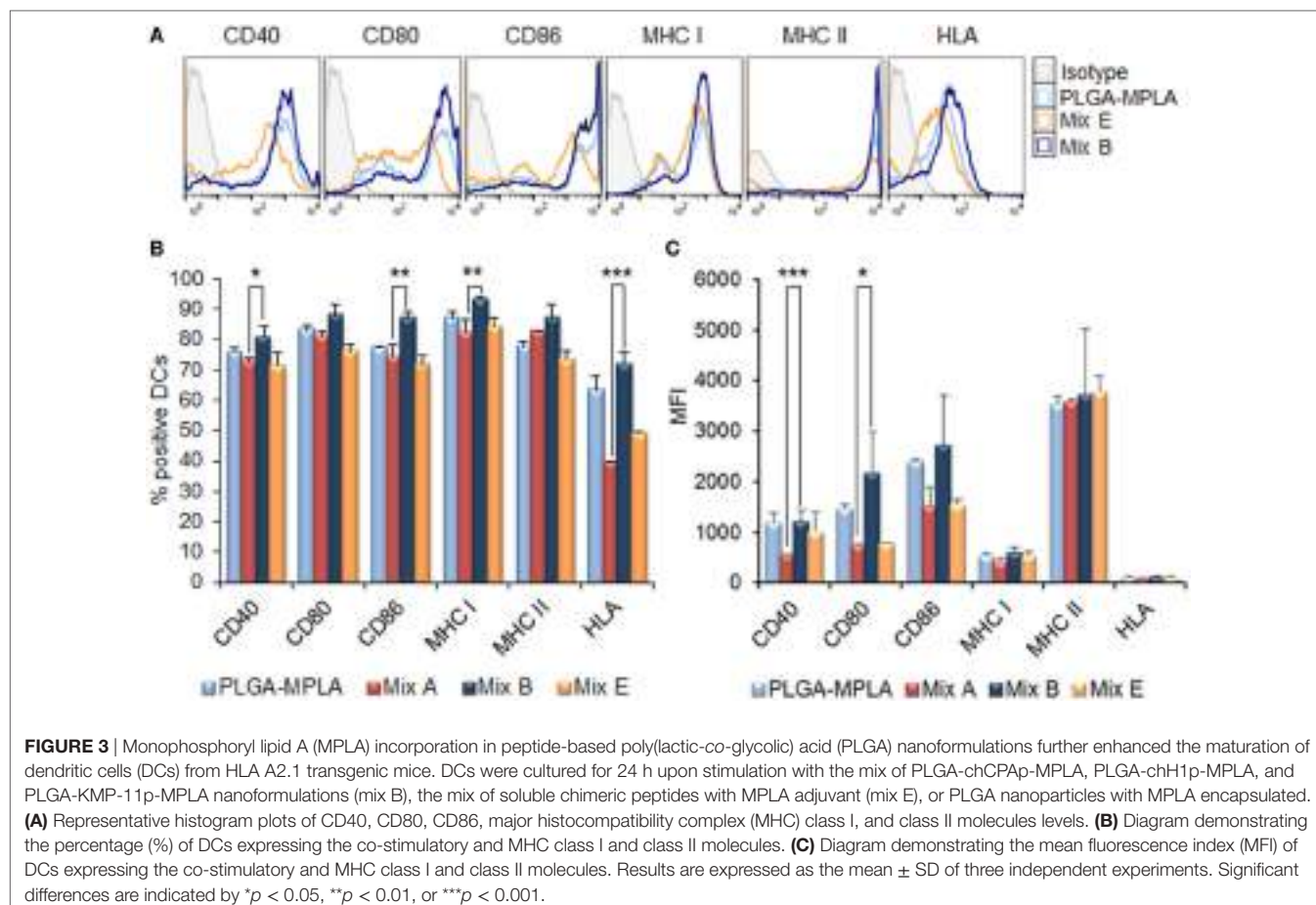


**FIGURE 2 |** Encapsulation of chimeric peptides in poly(lactic-co-glycolic) acid (PLGA) nanoparticles (NPs) induced a strong maturation profile in dendritic cells (DCs) from HLA A2.1 transgenic mice. DCs were cultured for 24 h upon stimulation with the mix of PLGA-chCPAp, PLGA-chH1p, and PLGA-KMP-11p nanoformulations (mix A), the mix of soluble chimeric peptides (mix D), or empty PLGA NPs (control group). DCs cultured in medium alone or in the presence of 1  $\mu$ g/ml LPS were used as negative and positive control, respectively. **(A)** Representative histogram plots of CD40, CD80, CD86, major histocompatibility complex (MHC) class I, and class II molecules levels. **(B)** Diagram demonstrating the percentage (%) of DCs expressing the co-stimulatory and MHC class I and class II molecules. **(C)** Diagram demonstrating the mean fluorescence index (MFI) of DCs expressing the co-stimulatory and MHC class I and class II molecules. Results are expressed as the mean  $\pm$  SD of three independent experiments. Significant differences are indicated by \* $p$  < 0.05, \*\* $p$  < 0.01, or \*\*\* $p$  < 0.001.

in the MFI values for CD40 ( $1,338 \pm 81.32$  vs.  $618 \pm 72.75$ ,  $p < 0.0001$ ) and CD80 ( $1,338 \pm 81.32$  vs.  $618 \pm 72.75$ ,  $p < 0.0001$ ) molecules (Figure 3C). Regarding the surface modification with p8, as depicted in Figures 4A,B, stimulation of DCs with the mix of p8-PLGA-chCPAp, p8-PLGA-chH1p, and p8-PLGA-chKMP-11p nanoformulations (mix C) significantly also enhanced the presence of DCs expressing the co-stimulatory molecules CD40 ( $18.40 \pm 1.57$  vs.  $72.40 \pm 1.27\%$ ,  $p < 0.001$ ) and CD86 ( $83.60 \pm 4.95$

vs.  $74.33 \pm 3.99\%$ ,  $p < 0.01$ ), as well as the MHC class I molecules (murine MHC class I:  $90.25 \pm 5.02$  vs.  $82.15 \pm 4.31\%$ ,  $p < 0.05$ ; hybrid HLA class I:  $73.50 \pm 0.05$  vs.  $39.50 \pm 0.30\%$ ,  $p < 0.001$ ), in comparison to DCs stimulated with the mix A. In addition, a significant increase was observed in the MFI values of DCs stimulated with the mix C in comparison to DCs stimulated with the mix A for all the co-stimulatory and MHC class I molecules except from the MHC class II molecule (CD40:  $1,084 \pm 28.93$  vs.



618  $\pm$  72.75,  $p$  < 0.0001; CD80: 1,715  $\pm$  223.45 vs. 754  $\pm$  26.87,  $p$  < 0.001; CD86: 2,529  $\pm$  201.52 vs. 1,680  $\pm$  347.19,  $p$  < 0.01; murine MHC class I: 537  $\pm$  31.82 vs. 432  $\pm$  50.91,  $p$  < 0.05; HLA class I: 122  $\pm$  4.24 vs. 96  $\pm$  2.26,  $p$  < 0.05). The above results concerning DCs stimulated with the mix B or the mix C were comparable to that observed in the case of DCs cultured in the presence of LPS (positive control of maturation; CD40: 82.80  $\pm$  2.86%; CD80: 89.10  $\pm$  5.61%; CD86: 81.63  $\pm$  3.84%; murine MHC class I: 96.53  $\pm$  1.34%; murine MHC class II: 86.63  $\pm$  2.73%; hybrid HLA class I: 73.30  $\pm$  3.36%) (Figures 2A,B). Moreover, similar results were obtained from DCs stimulated with each of the PLGA-chCPAp-MPLA, PLGA-chH1p-MPLA, and PLGA-chKMP-11p-MPLA nanoformulations (Figure S2 in Supplementary Material) or each of the p8-PLGA-chCPAp, p8-PLGA-chH1p, and p8-PLGA-chKMP-11p nanoformulations (Figure S3 in Supplementary Material), in comparison to DCs stimulated with each of PLGA-chCPAp, PLGA-chH1p, and PLGA-chKMP-11p nanoformulations, respectively. It is noteworthy that the significant ( $p$  < 0.001) increase observed in the number of DCs expressing the hybrid HLA-A2.1 molecule confirmed the successful design of the chimeric peptides to harbor T cell epitopes with high-binding affinity to HLA class I molecules.

Furthermore, as demonstrated in Figure 5, stimulation of DCs with the mix B (Figure 5A) or the mix C (Figure 5B) resulted in a significant increase of DCs that intracellularly produced IL-12

(26.94  $\pm$  2.74 and 37.60  $\pm$  1.43, respectively, vs. 12.16  $\pm$  2.20%,  $p$  < 0.001), compared to DCs stimulated with the mix A. This observation supports the functional differentiation of DCs toward DC1 type. The high percentage of DCs that produced IL-12 (22.11  $\pm$  0.53%) in response to p8-PLGA NPs indicated a role of the synthetic octapeptide in this biological process.

### DCs Stimulated with the Mix of PLGA Nanoformulations with MPLA Incorporation or Surface Modification Promoted Allogeneic T Cell Proliferation and IFN $\gamma$ Production by CD4 $^{+}$ and CD8 $^{+}$ T Cells

Since the peptide-based PLGA nanoformulations and especially those with MPLA incorporation or surface modification proved capable to induce DCs maturation and IL-12 production, mixed leukocyte cultures were performed in order to investigate the capacity of these DCs to promote *in vitro* T cell proliferation. For this purpose, DCs stimulated with the peptide-based PLGA nanoformulations were co-cultured with allogeneic spleen cells at different stimulator/responder ratios and their proliferative potential was determined by  $^3$ H-TdR incorporation. The results obtained indicated that the optimum stimulator/responder ratio was that of 1:5. As shown in Figure 6, DCs stimulated with the

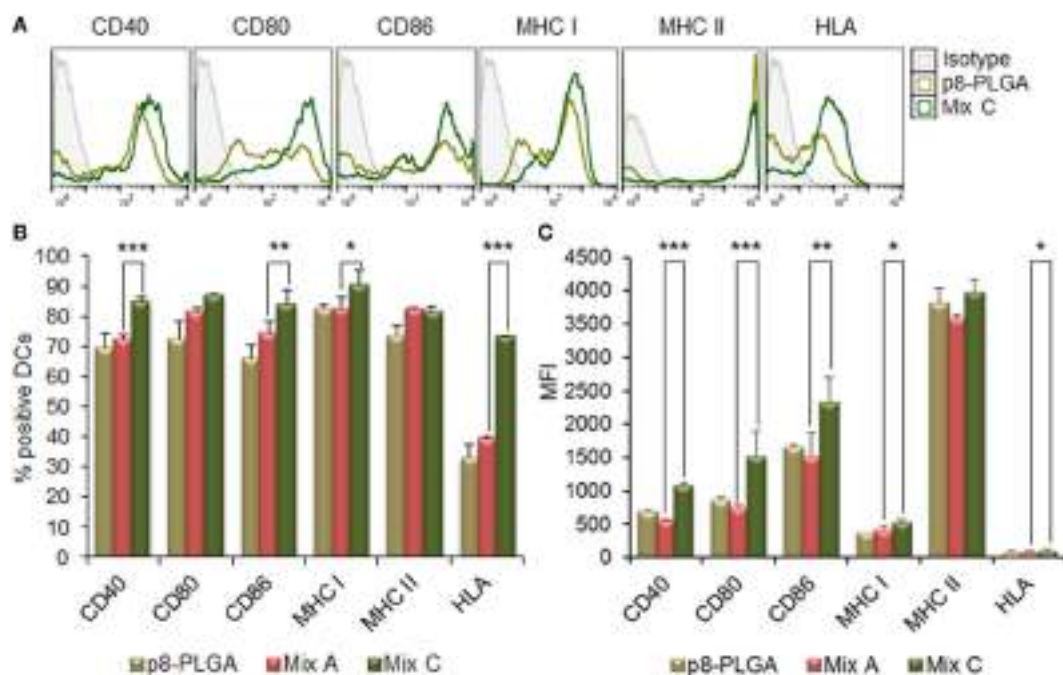


**FIGURE 4 |** Surface modification of peptide-based poly(lactic-co-glycolic) acid (PLGA) nanoformulations with p8 also enhanced the maturation of dendritic cells (DCs) from HLA A2.1 transgenic mice. DCs were cultured for 24 h upon stimulation with the mix of p8-PLGA-chCPAp, p8-PLGA-chH1p, and p8-PLGA-KMP-11p nanoformulations (mix C) or PLGA nanoparticles surface modified with p8. **(A)** Representative histogram plots of CD40, CD80, CD86, major histocompatibility complex (MHC) class I, and class II molecules levels. **(B)** Diagram demonstrating the percentage (%) of DCs expressing the co-stimulatory and MHC class I and class II molecules. **(C)** Diagram demonstrating the mean fluorescence index (MFI) of DCs expressing the co-stimulatory and MHC class I and class II molecules. Results are expressed as the mean  $\pm$  SD of three independent experiments. Significant differences are indicated by \* $p$  < 0.05, \*\* $p$  < 0.01, or \*\*\* $p$  < 0.001.

mix of PLGA-chCPAp, PLGA-chH1p, and PLGA-chKMP-11p nanoformulations (mix A) proved able to promote T cell proliferation (cpm:  $10,895 \pm 953$ ) compared to unstimulated DCs stimulated (cpm:  $8,330 \pm 1,167$ ). However, the incorporation of the MPLA adjuvant, as well as the surface modification with p8, remarkably enhanced the competency of stimulated DCs to efficiently present the processed antigenic peptides to T cells. In more details, DCs stimulated with the mix of PLGA-chCPAp-MPLA, PLGA-chH1p-MPLA, and PLGA-chKMP-11p-MPLA nanoformulations (mix B) or the mix of p8-PLGA-chCPAp, p8-PLGA-chH1p, and p8-PLGA-chKMP-11p nanoformulations (mix C) triggered significantly increased lymphoproliferative responses in comparison to unstimulated DCs (cpm mix B:  $26,014 \pm 1,828$  vs.  $8,330 \pm 1,167$ ,  $p$  < 0.001; cpm mix C:  $23,626 \pm 776$  vs.  $8,330 \pm 1,167$ ,  $p$  < 0.001). It is noteworthy that DCs stimulated with PLGA-MPLA or p8-PLGA also induced T cell proliferation at significant levels compared to unstimulated DCs ( $p$  < 0.001) at the ratio 1:5. This difference was not observed at ratio 1:20 in contrast to DCs stimulated with mix B or mix C. Spleen cells cultured in medium alone and *in vitro* stimulated with the mitogen ConA were used as positive control of proliferation (cpm:  $40,118 \pm 1,936$ , data not shown).

Flow cytometry analysis was conducted to unveil the presence of CD4<sup>+</sup> T cells producing IL-4 (indicative of T<sub>H</sub>2 polarization) or IFN $\gamma$  (indicative of T<sub>H</sub>1 polarization), as well as IFN $\gamma$ -producing CD8<sup>+</sup> T cells. Flow cytometry results revealed no increase in the

population of IL-4-producing CD4<sup>+</sup> T cells in comparison to T cells co-cultured with unstimulated DCs (Figures 7A,D,G). On the contrary, a significant increase was observed in the populations of IFN $\gamma$ -producing CD4<sup>+</sup> T cells (Figures 7B,E,H) and CD8<sup>+</sup> T cells (Figures 7C,F,I) upon activation by DCs stimulated with the mix of PLGA-chCPAp, PLGA-chH1p, and PLGA-chKMP-11p (Mix A; CD4<sup>+</sup> T cells:  $12.0 \pm 0.14\%$ ,  $p$  < 0.01 and CD8<sup>+</sup> T cells:  $5.4 \pm 0.05\%$ ,  $p$  < 0.01) compared to unstimulated DCs. A further increase in IFN $\gamma$ -producing CD4<sup>+</sup> and CD8<sup>+</sup> T cells was observed upon activation with DCs stimulated with PLGA-chCPAp-MPLA, PLGA-chH1p-MPLA, and PLGA-chKMP-11p-MPLA nanoformulations (mix B; CD4<sup>+</sup> T cells:  $13.0 \pm 0.28\%$ ,  $p$  < 0.001 and CD8<sup>+</sup> T cells:  $5.88 \pm 0.14\%$ ,  $p$  < 0.001) or the mix of p8-PLGA-chCPAp, p8-PLGA-chH1p, and p8-PLGA-chKMP-11p nanoformulations (mix C; CD4<sup>+</sup> T cells:  $14.85 \pm 0.49\%$ ,  $p$  < 0.001 and CD8<sup>+</sup> T cells:  $7.16 \pm 0.86\%$ ,  $p$  < 0.01).

## Transcriptome Analysis of DCs Stimulated with the Differentially Functionalized PLGA Nanoformulations Revealed that MPLA Incorporation Induced the Most Robust Transcriptional Activation

In an attempt to unveil changes in the gene-expression profile of DCs stimulated with the differentially functionalized PLGA nanoformulations for 18 h, transcriptome analysis was performed

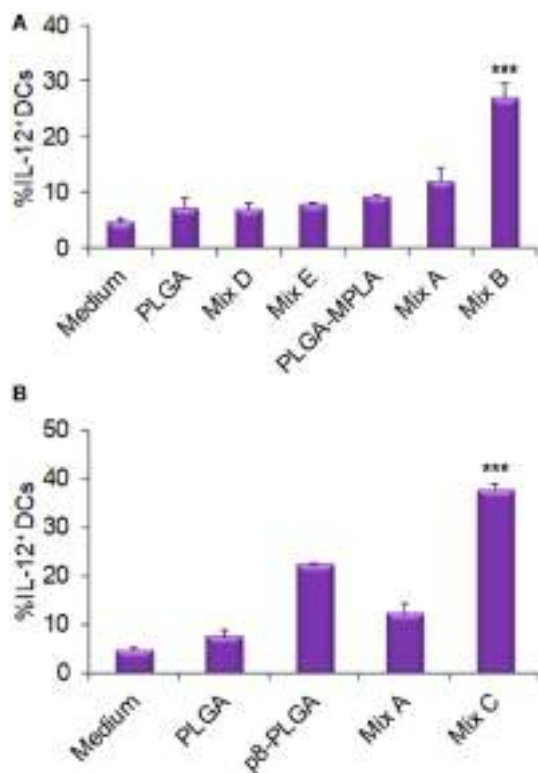


**FIGURE 5 |** Functional differentiation of dendritic cells (DCs) stimulated with the differentially functionalized peptide-based poly(lactic-co-glycolic) acid (PLGA) nanoformulations in terms of IL-12 production. DCs were cultured for 24 h upon stimulation with the mix of PLGA-chCPAp, PLGA-chH1p, and PLGA-chKMP-11p nanoformulations (mix A), the mix of PLGA-chCPAp-MPLA, PLGA-chH1p-MPLA, and PLGA-chKMP-11p-MPLA nanoformulations (mix B), the mix of p8-PLGA-chCPAp, p8-PLGA-chH1p, and p8-PLGA-chKMP-11p nanoformulations (mix C), the mix of soluble chimeric peptides (mix D), and the mix of soluble chimeric peptides plus MPLA (mix E). DCs cultured in medium alone were used as negative control. DCs were also stimulated with empty PLGA nanoparticles (NPs), PLGA NPs with MPLA encapsulated, and PLGA NPs surface modified with p8 as control groups. The diagrams indicate the effect of MPLA incorporation (**A**) or the effect of surface modification with p8 (**B**) in the percentage of DCs producing IL-12. Results are expressed as the mean  $\pm$  SD of three independent experiments. Significant differences between DCs stimulated with the mix B or the mix C and DCs stimulated with the mix A are indicated by \*\*\* $p < 0.001$ .

using microarrays. PCA and Pearson correlation analysis of samples displayed satisfactory replicate resemblance (Figures 8A,B). Microarray data analysis revealed considerable differences in the gene-expression profiles of DCs stimulated with the different mixes of peptide-based PLGA nanoformulations or the mix of soluble chimeric peptides (Figures 8C,D). The highest number of differentially expressed genes was observed in DCs stimulated with the PLGA-chCPAp-MPLA, PLGA-chH1p-MPLA, and PLGA-chKMP-11p-MPLA nanoformulations (mix B, 2,104 differentially expressed genes; 1,027 up- and 1,077 downregulated), followed by DCs stimulated with the p8-PLGA-chCPAp, p8-PLGA-chH1p, and p8-PLGA-chKMP-11p nanoformulations (mix C, 1,273 differentially expressed genes; 527 up- and 746 downregulated), and then DCs stimulated with the PLGA-chCPAp, PLGA-chH1p, and

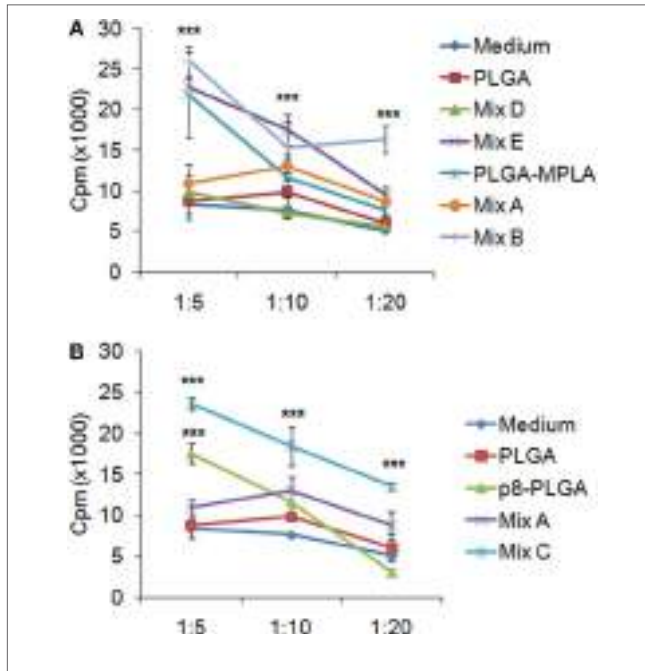


**FIGURE 6 |** T cell priming induced by dendritic cells (DCs) stimulated with the differentially functionalized peptide-based poly(lactic-co-glycolic) acid (PLGA) nanoformulations. Spleen cells from naïve BALB/c mice were primed *in vitro* by DCs stimulated for 24 h with the mix of PLGA-chCPAp, PLGA-chH1p, and PLGA-chKMP-11p nanoformulations (mix A), the mix of PLGA-chCPAp-MPLA, PLGA-chH1p-MPLA, and PLGA-chKMP-11p-MPLA nanoformulations (mix B), the mix of p8-PLGA-chCPAp, p8-PLGA-chH1p, and p8-PLGA-chKMP-11p nanoformulations (mix C), the mix of soluble chimeric peptides (mix D), and the mix of soluble chimeric peptides plus MPLA (mix E). Cultures were pulsed for the last 18 h with 1  $\mu$ Ci of [<sup>3</sup>H]-TdR, and the proliferative potential was measured by [<sup>3</sup>H]-TdR incorporation. The diagrams indicate the effect of MPLA incorporation (**A**) or the effect of surface modification with p8 (**B**) in the capacity of DCs stimulated with the mix B or the mix C to induce T cell priming. Samples were run in triplicates. Results are depicted as cpm  $\pm$  SD from three independent experiments. Significant differences are indicated by \*\*\* $p < 0.001$ .

PLGA-chKMP-11p nanoformulations (mix A, 847 differentially expressed genes; 278 up- and 569 downregulated). Importantly, much milder differences were observed for DCs stimulated with the mix of soluble chimeric peptides (mix D, 191 differentially expressed genes; 69 up- and 122 downregulated) compared to unstimulated DCs. Therefore, the hierarchy of potency in inducing gene-expression changes was mix B > mix C > mix A > mix D, stressing that the overall magnitude of activation was much higher in DCs stimulated with the mix B.

Enrichment analysis of differentially expressed genes for GO terms (Biological Processes) revealed that DCs stimulated with the mix B or the mix C exhibited a higher number of significantly enriched terms compared to DCs stimulated with the mix A, while no significant enrichment was observed in the case of DCs stimulated with the mix D. More specifically, DCs stimulated with the mix B or the mix C shared common genes involved in cytokine production (GO:0001819), inflammatory response (GO:0050727), leukocyte cell-cell adhesion (GO:0007159), and cellular response to cytokine stimulus (GO:0071345), as well as in other biological processes related to antigen processing and presentation or adaptive

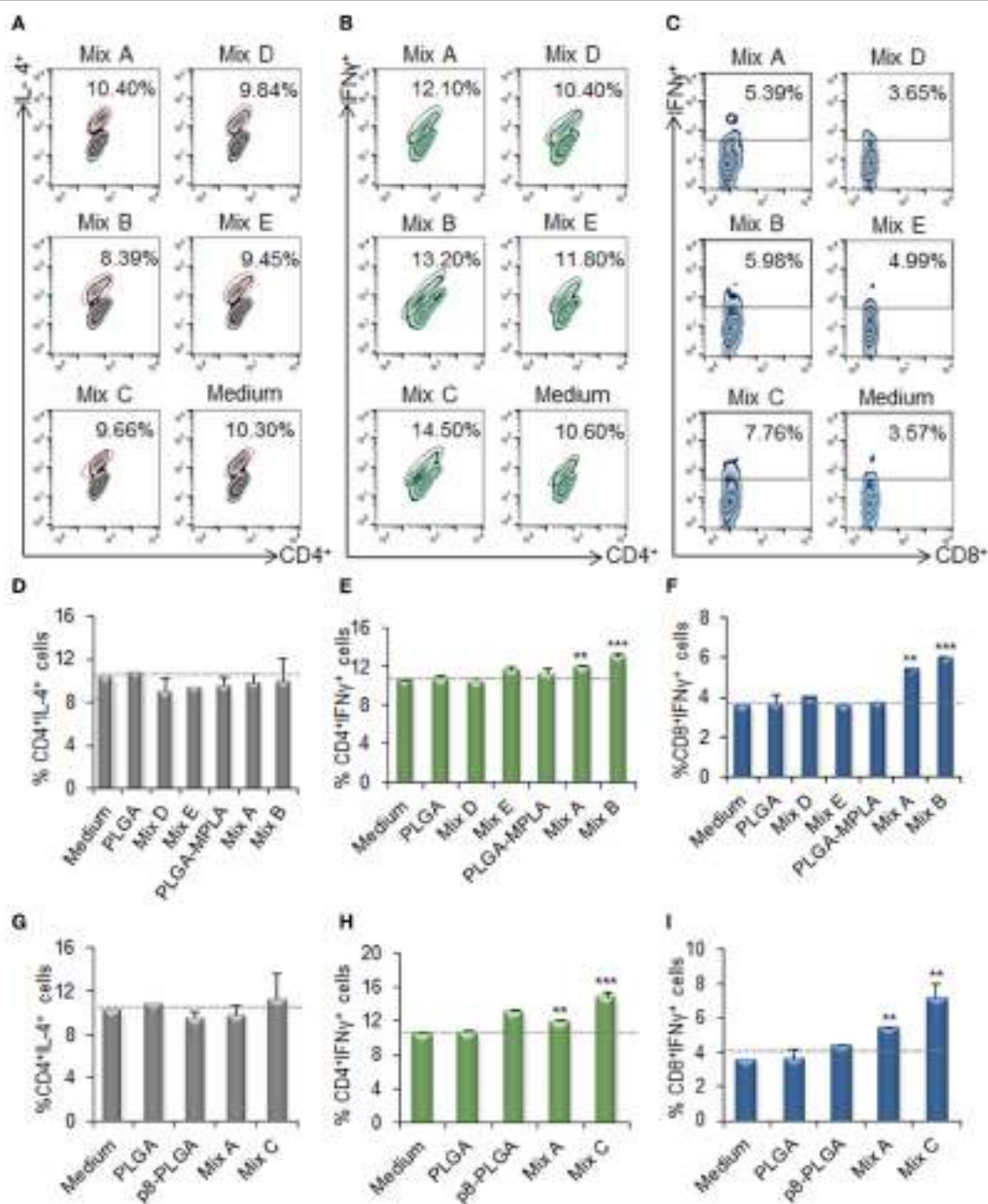


**FIGURE 7 |** IFN $\gamma$ -producing CD4<sup>+</sup> and CD8<sup>+</sup> T cells among the spleen cell populations primed by dendritic cells (DCs) stimulated with the mix B or C. Spleen cells from naïve BALB/c mice were primed *in vitro* by DCs stimulated for 24 h with the different mixes of differentially functionalized nanoformulations (mix A, mix B, and mix C), the mix of soluble chimeric peptides (mix D), and the mix of soluble chimeric peptides plus monophosphoryl lipid A (MPLA) (mix E). Then, spleen cells were stained and analyzed by flow cytometry. The representative contour plots depict IL-4-producing CD4<sup>+</sup> T cells (**A**), and IFN $\gamma$ -producing CD4<sup>+</sup> (**B**) and CD8<sup>+</sup> (**C**) T cells. Diagram showing the percentage of (**D,G**) IL-4-producing CD4<sup>+</sup> T cells, (**E,H**) IFN $\gamma$ -producing CD4<sup>+</sup>, and (**F,I**) IFN $\gamma$ -producing CD8<sup>+</sup> T cells. Results are expressed as the mean  $\pm$  SD and significant differences between T cells activated by DCs stimulated with mix A, mix B or mix C and T cells activated by unstimulated DCs are indicated by  $^{**}p < 0.01$ , or  $^{***}p < 0.001$ .

immunity (Data Sheet S1 in Supplementary Material). Focusing on a number of the most significantly enriched GO terms (Figure 8D; Table 4), genes encoding pro-inflammatory cytokines, such as *Il12b*, *Il6*, type-I, and II IFN-response elements (*Irf7*, *Stat5a*, *Irf8*, *Gbp5*, *Ido1*, *Stat1*, *Ifi205*, etc.) and DCs maturation markers (*Cd40*) were upregulated in both groups. However, a much higher number

of upregulated genes involved in the above biological processes were found to be specifically expressed in DCs stimulated with the mix B. Between these specifically upregulated genes, they were identified IFN-response genes (*Ifih1*, *Ifit1*, *Ifit2*, *Igip1*, *Irg1*, *Gbp2*, and *Gbp4*), inflammation-related genes (*Il10*, *Il23a*, *Il15*, and *Saa3*), and genes encoding chemokines that act to recruit leukocytes

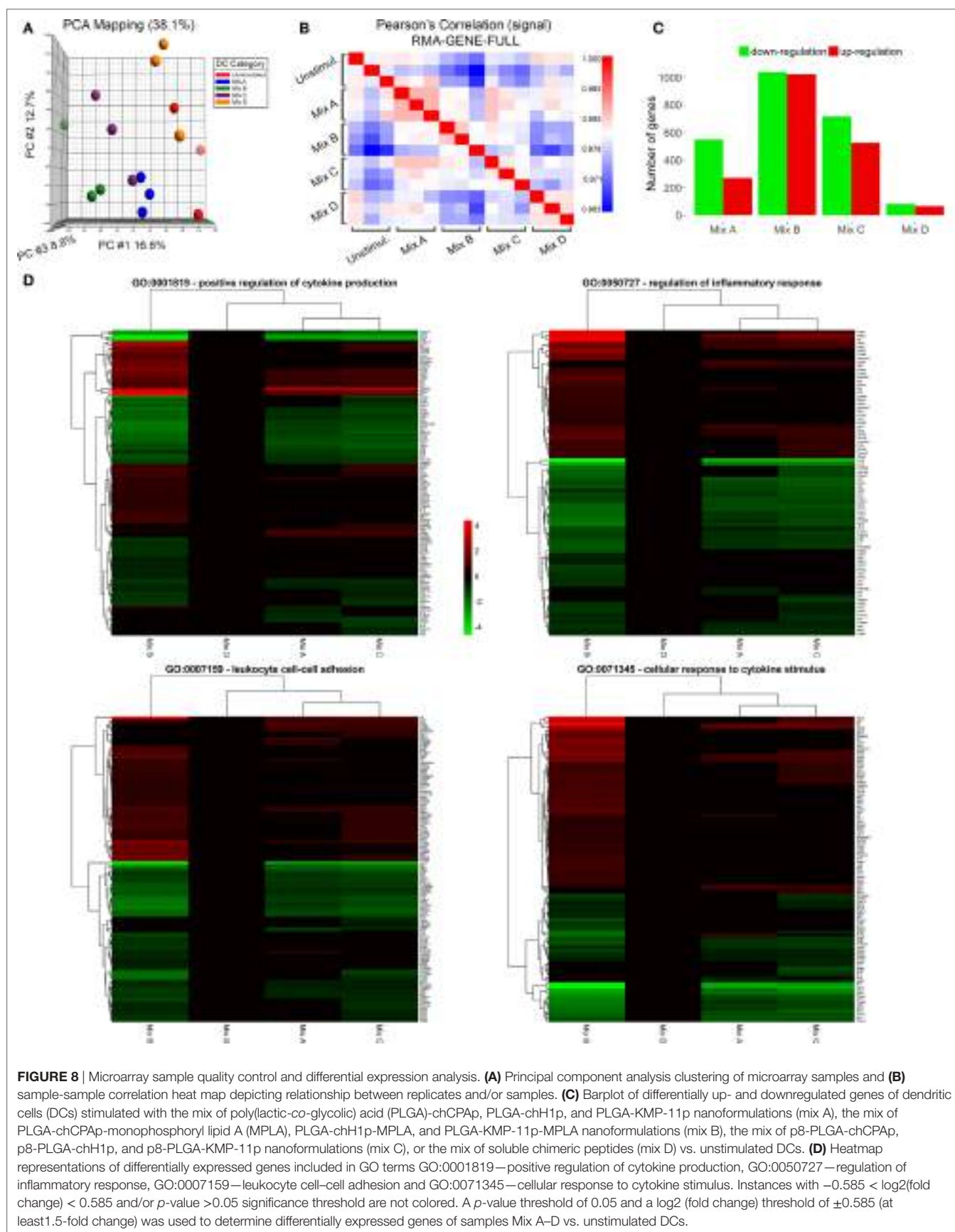


**TABLE 4** | Unique or common upregulated genes in dendritic cells stimulated with mix B or mix C that enriched GO terms related to immune response.

	Mix B			Mix C			Genes in common	
	FDR	Unique genes		FDR	Unique genes			
GO:0001819 Positive regulation of cytokine production	5.28E-27	Ddx60, Lgals9, Dhx58, Il1f6, Clec4e, Tnfsf15, Il10, Eif2ak2, Ifih1, Il23a, Serpine1, Tnfsf4, Ticam1, Ddit3, Flot1, Lum, Sema7a, Tir1, Cd1d1, Il15, Casp4, Cd274, Hilpda, Ripk2, Slamf1, Ccl3, Cx3cl1, Mif		8.77E-22	Adra2a, Afap1l2, F2rl1, Cd244, Cd28		Irf7, Rsd2, Hc, Bcl3, Stat5a, Ccl4, Src, Tnfsf9, Il12b, Il23r, Cd40, Irf8, Ido1, Gbp5, Il6, Flt3, Ptgs2, Cyp1b1	
GO:0050727 Regulation of inflammatory response	2.29E-20	Lgals9, Il1r1, Serping1, Fabp4, Il10, Ednrb, Serpine1, Tnfsf4, Gstp1, Hamp, Sema7a, Socs3, Casp4, Irg1, Ccl3, Cx3cl1, Mvk, Pde5a, Tnfaip6, Mif		4.55E-16	Ier3, Cd28		Slc7a2, Nos2, Stat5a, Adora2a, Ccl4, Ppard, Il12b, Il2ra, Stk39, Dusp10, Ido1, Gbp5, Il6, Ptgs2	
GO:0007159 Leukocyte cell-cell adhesion	7.91E-18	Lgals9, Batf, Cav1, Itgav, Clec4e, Cd80, Itga5, Gadd45g, Tnfsf8, Prex1, Il23a, Tnfsf4, Dll4, Gstp1, Ebi3, Cd1d1, Il15, Fkbp1a, Cd274, Psmb10, Ripk2, Slamf1, Nck2, Cd86, Pde5a, Hsp90aa1, Zc3h12d, Kit		1.19E-15	Olr1, Stx11, F2rl1, Cd244, Pdcld1lg2, Cd28		Rsd2, Hsph1, Cdk6, Btla, Foxp1, Satb1, Fyn, Bcl3, Stat5a, Adora2a, Runx2, Wash1, Tnfsf9, Il12b, Il2ra, Ido1, Tcf7, Il6, Flt3	
GO:0071345 Cellular response to cytokine stimulus	3.25E-17	Gm4951, Ifit1, Ifit2, Saa3, Igtp, Zbp1, Cav1, Il1r1, Pml, Il1f6, Igtp1, Dcn, Cxcl9, Adar, Osm, Acs1, Keap1, Serpine1, Pyrin1, Hsp90ab1, Il1rn, Gbp4, Il3ra, Ebi3, Dapk3, Cxcl5, Socs3, Fkbp1a, Gbp3, Hax1, Pias4, Tjp2, Cish, Cib1, Irg1, Ripk2, Cxcl1, Stat3, Cdip1, Ccl3, Cx3cl1, Gbp2, Ccl17, Gbp2b, Kit		1.91E-09	Ptpf, F2rl1, Csf1		Irf7, Ifi205, Nos2, Nfil3, Stat2, Ikbkb, Socs1, Stat1, Stat5a, Ccl4, Il12b, Txndc17, Il23r, Gbp5, Il6, Flt3, Cxcl3	

(*Ccl3*, *Cx3cl1*, *Mif*, and *Cxcl1*). Moreover, a remarkable number of genes was identified characteristic for the type 1 DCs phenotype that could induce a subsequent CD8<sup>+</sup> T cell activation (*Psmb10*, *Hsp90aa1*, *Hsp90ab1*, *Igtp*, *Ccl3*, *Dhx58*, *Tnfsf8*, *Il15*, *Olr*, etc.) and CD4<sup>+</sup> T<sub>H1</sub> polarization (*Cd86*, *Cish*, *Dll4*, *Cxcl9*, *Cx3cl1*, *Osm*, *Il1f6*, *Tnfsf15*, *Kit*, *Clec4e*, etc.) (Table 4; Figure 9). Overall, the above findings suggested that DCs exposed to mix B could probably be in a more advanced state of maturity and functional differentiation and might be able to induce specific T cell responses.

## Immunization of HLA A2.1 Transgenic Mice with the Mix of Peptide-Based PLGA Nanoformulations with MPLA Incorporation Promoted Peptide-Specific IFN $\gamma$ -Producing CD8<sup>+</sup> T Cell Populations

The *in vitro* screening of the differentially functionalized PLGA nanoformulations in DCs gave precedence to the mix of PLGA-chCPAp-MPLA, PLGA-chH1p-MPLA, and PLGA-chKMP-11p-MPLA nanoformulations (mix B) to be evaluated *in vivo* in terms of immunogenicity, as a promising peptide-based nanovaccine. For this purpose, HLA A2.1 transgenic mice were subcutaneously injected with the mix B and boosted twice in a 2-week interval (Figure 10A). The specific T cell expansion induced by each of the chimeric peptides was initially assessed by  $^3\text{H}$ -TdR incorporation. As shown in Figure 10B, chCPAp, chH1p, and chKMP-11p induced proliferation of spleen cells from mice immunized with mix B compared to spleen cells from non-immunized mice (received only PBS), upon *in vitro* stimulation. More specifically, chKMP-11p induced the strongest proliferation ( $\Delta\text{cpm}$ :  $7,908 \pm 1,886$  vs.  $65 \pm 20$ ,  $p < 0.01$ ), followed by chH1p ( $\Delta\text{cpm}$ :  $3,764 \pm 643$  vs.  $42 \pm 6$ ,  $p < 0.01$ ) and chCPAp ( $\Delta\text{cpm}$ :  $2,232 \pm 112$  vs.  $66 \pm 5$ ,  $p < 0.05$ ). Mice immunized with PLGA-MPLA nanoformulations did not show specific T cell

expansion. Spleen cells cultured in medium alone and *in vitro* stimulated with the mitogen ConA were used as positive control of proliferation ( $\Delta\text{cpm}$ :  $39,726 \pm 3,061$ , data not shown).

Flow cytometry analysis was then performed to detect peptide-specific IFN $\gamma$ -producing CD8<sup>+</sup> T cell populations (Figures 10C,D). The highest number of peptide-specific IFN $\gamma$ -producing CD8<sup>+</sup> T cells was observed upon *in vitro* stimulation with chKMP-11p of spleen cells from mice immunized with mix B compared to spleen cells from non-immunized mice ( $1.34 \pm 0.35$  vs.  $0.22 \pm 0.03\%$ ,  $p < 0.05$ ). Chimeric peptides chH1p and chCPAp were also able to stimulate specific IFN $\gamma$ -producing CD8<sup>+</sup> T cells to a lower level ( $0.53 \pm 0.05$  vs.  $0.21 \pm 0.02\%$ ,  $p < 0.01$  and  $0.41 \pm 0.06$  vs.  $0.20 \pm 0.02\%$ ,  $p < 0.05$ , respectively). It must be also noted that spleen cells from mice immunized with PLGA-MPLA nanoformulations did not exhibit IFN $\gamma$ -producing CD8<sup>+</sup> T cell populations, similar to spleen cells from non-immunized mice.

## Immunization of HLA A2.1 Transgenic Mice with the Mix of Peptide-Based PLGA Nanoformulations with MPLA Incorporation Conferred Protection against *L. infantum* Infection

In order to investigate whether the peptide-specific T cell responses observed in HLA A2.1 transgenic mice immunized with the mix of PLGA-chCPAp-MPLA, PLGA-chH1p-MPLA, and PLGA-chKMP-11p-MPLA nanoformulations (mix B) could confer protection against *L. infantum* infection, immunized and non-immunized mice were infected intravenously with *L. infantum* promastigotes and the parasite burden was assessed in liver and spleen by a limiting dilution assay 1 and 2 months post-infection (Figure 11A). According to the infection kinetics in HLA A2.1 transgenic mice, the parasite burden reached a peak at 1 month post-infection in the liver (Figure 11B) and at 2 months

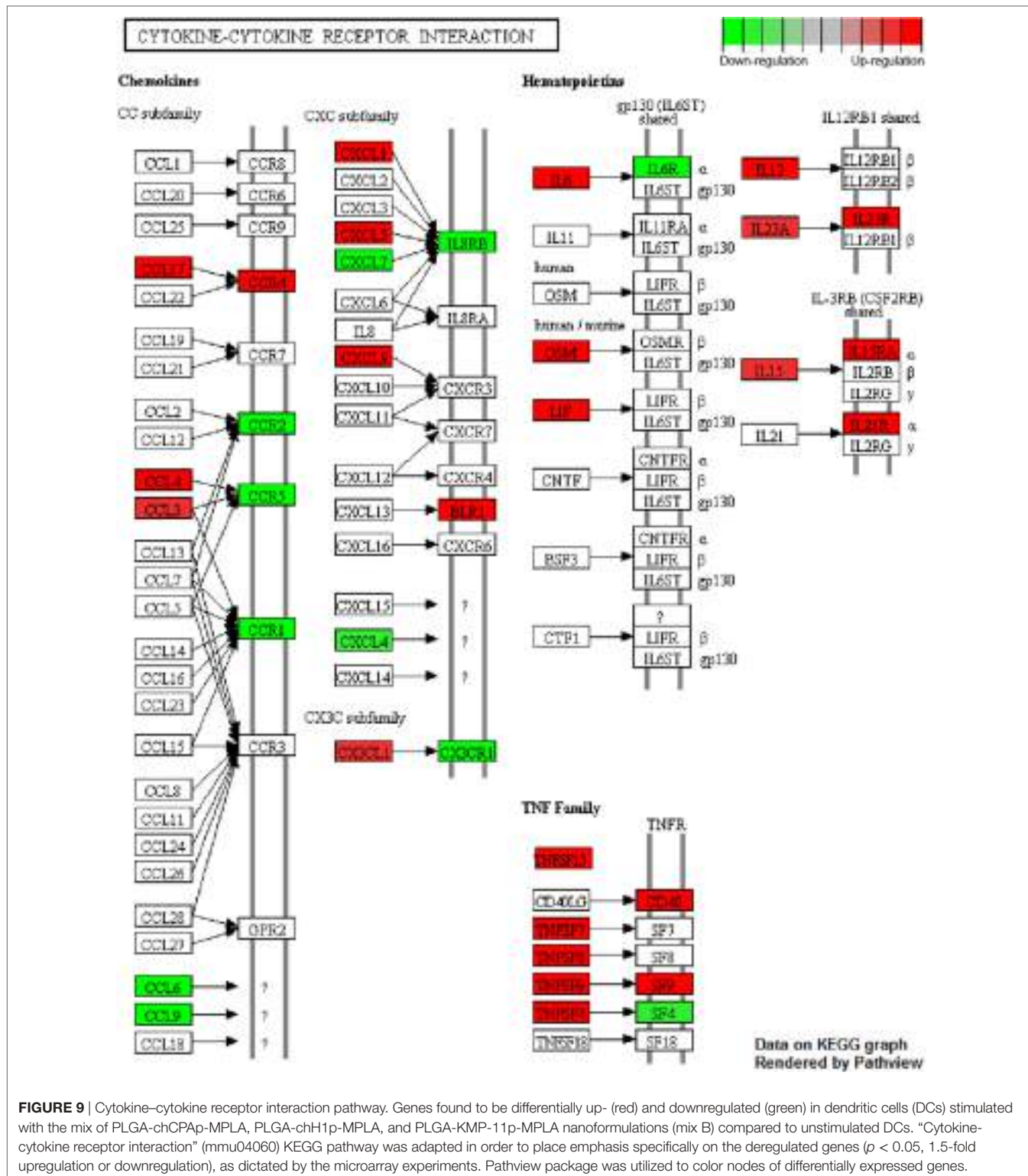


**FIGURE 9 |** Cytokine-cytokine receptor interaction pathway. Genes found to be differentially up- (red) and downregulated (green) in dendritic cells (DCs) stimulated with the mix of PLGA-chCPAp-MPLA, PLGA-chH1p-MPLA, and PLGA-KMP-11p-MPLA nanoformulations (mix B) compared to unstimulated DCs. “Cytokine-cytokine receptor interaction” (mmu04060) KEGG pathway was adapted in order to place emphasis specifically on the deregulated genes ( $p < 0.05$ , 1.5-fold upregulation or downregulation), as dictated by the microarray experiments. Pathview package was utilized to color nodes of differentially expressed genes.

post-infection in the spleen (Figure 11D), followed by a decrease in both organs. The results obtained indicated that immunization with the mix B reduced significantly hepatic and splenic parasite burden 1 month post-infection by 72.81% ( $p < 0.01$ , Figure 11C) and 61.98% ( $p < 0.05$ , Figure 11E), respectively,

compared to the non-immunized control group. Assessment of the parasite burden 2 months post-infection revealed a maintenance of the protective effect with 64.4% reduction of parasite burden in the liver ( $p < 0.01$ , Figure 11C) and 73.64% reduction of parasite burden in the spleen ( $p < 0.05$ , Figure 11E).

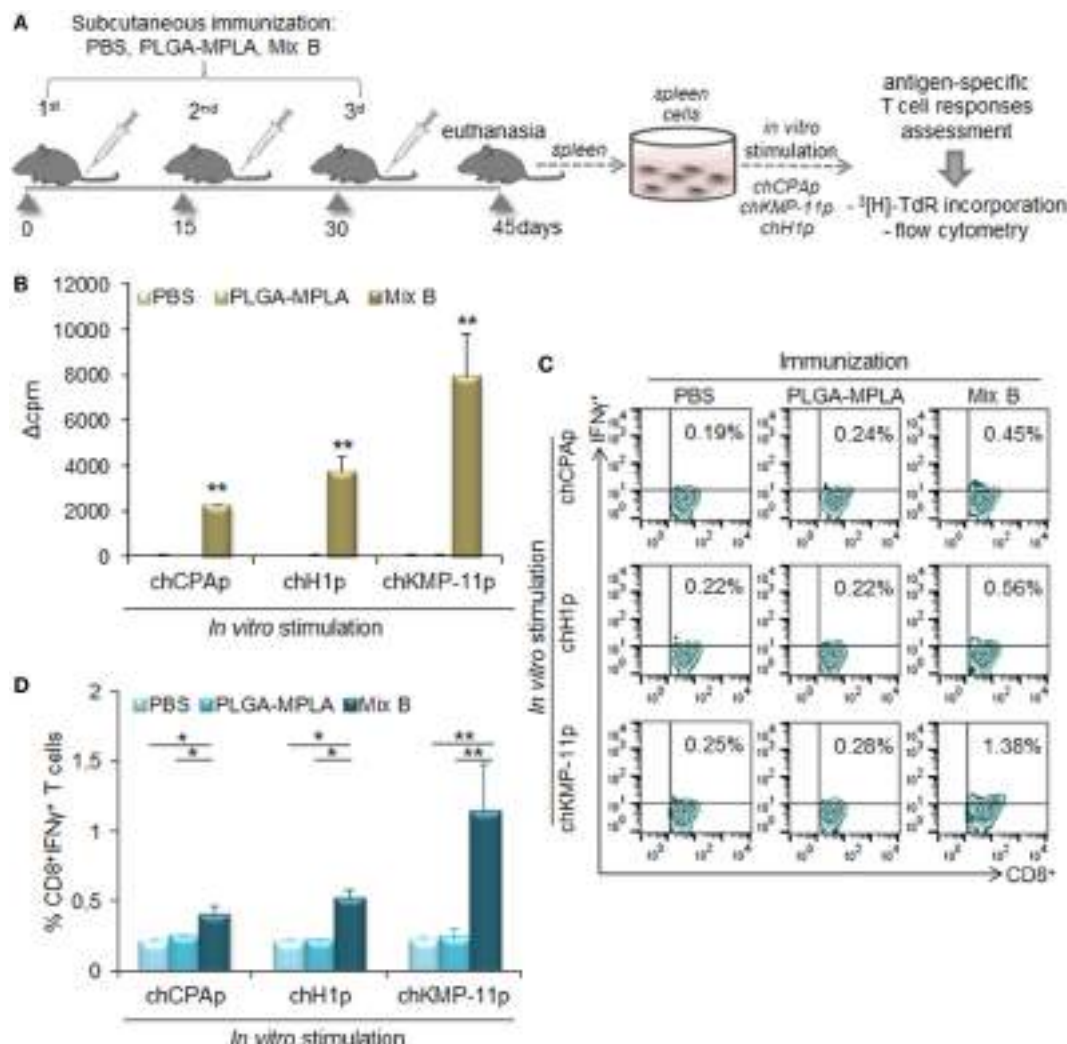


**FIGURE 10 |** Immunization with the mix of peptide-based poly(lactic-co-glycolic) acid (PLGA) nanoformulations with monophosphoryl lipid A (MPLA) incorporation induced peptide-specific T cell responses in HLA A2.1 transgenic mice. **(A)** Immunization scheme. Mice were subcutaneously immunized with the mix of PLGA-chCPAp-MPLA, PLGA-chH1p-MPLA, and PLGA-KMP-11p-MPLA nanoformulations (mix B), PLGA-MPLA nanoformulations or only PBS. Two weeks after the last boosting dose, the spleen of each mouse was aseptically removed and spleen cells were stimulated *in vitro* with each of the chimeric peptides (chCPAp, chH1p, and chKMP-11p) in order to assess induced peptide-specific T cell responses. **(B)** Peptide-specific T cell expansion was measured by  $^3\text{H}$ -TdR incorporation. Samples were run in triplicates. Results are represented as  $\Delta\text{cpm} \pm \text{SD}$  ( $\text{cpm}$  of stimulated spleen cells –  $\text{cpm}$  of unstimulated spleen cells), and significant differences are indicated by  $^{**}p < 0.01$ . **(C,D)** *In vitro*-stimulated spleen cells were stained with fluorochrome-labeled anti-CD3, anti-CD8, and anti-IFN $\gamma$  monoclonal antibodies and analyzed with flow cytometry. **(C)** The representative contour plots depict the peptide-specific IFN $\gamma$ -producing CD8 $+$  T cells. **(D)** The diagrams show the percentage of peptide-specific IFN $\gamma$ -producing CD8 $+$  T cells. Results are expressed as the mean  $\pm$  SD and significant differences between spleen cells from mice immunized with mix B and spleen cells from mice immunized with PLGA-MPLA or PBS are indicated by  $^{*}p < 0.05$  or  $^{**}p < 0.01$ .

It also must be noted that immunization with PLGA-MPLA nanoformulations did not confer protection against *L. infantum* infection, indicating that the protective effect observed in liver and spleen of immunized with the mix B HLA A2.1 transgenic mice was peptide specific.

## DISCUSSION

Immunoinformatics analyses based on algorithms that predict with high accuracy immunodominant epitopes on protein antigens could greatly enhance “polytope vaccine” design and

development against infectious diseases, such as VL, since the most efficient immune response to pathogens is derived from different T cells that respond to an ensemble of pathogen-derived specific epitopes (47). Different research groups have focused on MHC class I- and/or MHC class II-restricted epitope prediction from *Leishmania* spp. vaccine candidates such as A2, GP63, KMP-11, CPs, LmsTI-1, TSA, LeIF, and LPG-3 with the view of a peptide-based vaccine generation against CL or VL (36, 48–51). Following this promising approach, in a previous study, we performed an *in silico* analysis of the *L. infantum* proteins CPA, histone H1, and KMP-11 in order to identify

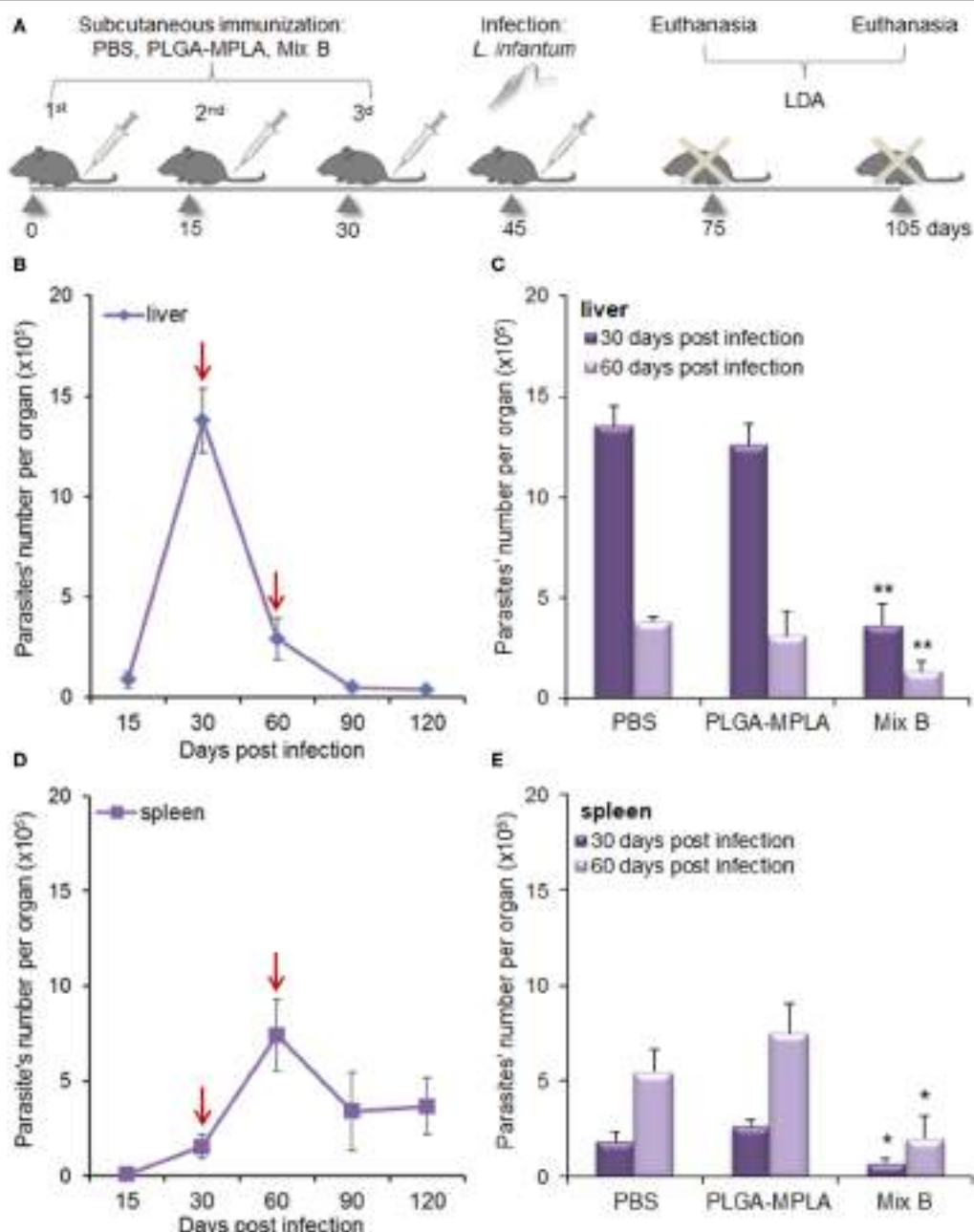


**FIGURE 11** | Immunization with the mix of peptide-based poly(lactic-co-glycolic) acid (PLGA) nanoformulations with monophosphoryl lipid A (MPLA) incorporation conferred significant protection against *Leishmania infantum* infection in HLA A2.1 transgenic mice. **(A)** Immunization and infection scheme. Mice were subcutaneously immunized with the mix of PLGA-chCPAp-MPLA, PLGA-chH1p-MPLA, and PLGA-KMP-11p-MPLA nanoformulations (mix B), PLGA-MPLA nanoformulations or only PBS. Two weeks after the last boosting dose, immunized and non-immunized mice were infected intravenously with  $2 \times 10^7$  *L. infantum* promastigotes and parasite burden was evaluated 1 and 2 months post-infection with a limiting dilution assay. **(B,D)** Time course of infection in liver (**B**) and spleen (**D**) of HLA A2.1 transgenic mice infected with *L. infantum* promastigotes. Red arrows indicate the time points selected for the evaluation of immunization's protective effect. **(C,E)** Parasite burden in the liver (**C**) and the spleen (**E**) of immunized and non-immunized mice 1 and 2 months post-infection with *L. infantum*. Results are presented as the mean  $\pm$  SD of five individual mice per group and significant differences between the parasite burden of immunized with mix B mice and the parasite burden of non-immunized mice are indicated by \**p* < 0.05 or \*\**p* < 0.01.

T cell epitopes presented on mouse and human MHC class I and II molecules and design multi-epitope peptides that were validated in terms of immunogenicity in BALB/c mice (29). Among these multi-epitope peptides, CPA\_p2, CPA\_p3, H1\_p1, and

H1\_p3 proved capable to induce a T cell response characterized by CD8<sup>+</sup> and CD4<sup>+</sup> T cell priming with IFN $\gamma$  production in immunized mice, whereas KMP-11\_p1 abrogated the secretion of IL-10.

The *in silico* analysis of the three *L. infantum* proteins also revealed a remarkable number of binding epitopes to HLA A\*0201 allele. Among HLA A2 allelic variants, HLA A\*0201 is the most prevalent and common in all ethnic groups, hence its peptide-binding motif is commonly used for epitope prediction of proteins from viruses such as hepatitis B and C viruses, human immunodeficiency virus, Epstein–Barr virus, human papillomavirus (43), as well as *Leishmania* parasites (51, 52). All the multi-epitope peptides contained more than one HLA A\*0201-restricted epitopes and were used for the design of longer chimeric peptides, with the use of appropriate linkers. Such an approach can help to overcome the fact that peptides shorter than 30 amino acids long may bind directly to MHC class I or II molecules of non-professional antigen-presenting cells, thereby potentially stimulating tolerance or anergy (53, 54).

Linkers have a pivotal role in functional and structural features of a peptide-based vaccine, since tandem fusion of peptides may result in generation of a new “protein” with novel characteristics and potent loss of the predicted MHC class I- or II-restricted epitopes. Linkers starting with alanine are more frequently used when targeting CD8<sup>+</sup> T cell responses, as the chance of proteasomal cleavage increases once the first amino acid next to the C-terminal peptide is alanine (55). Thus, the multi-epitope peptides of CPA (CPA\_p2 and CPA\_p3) and histone H1 (H1\_p1 and H1\_p3) were linked together by AAY, a short amino acid motif that is documented to support epitope generation and has been used in several studies on epitope vaccine design against cancer or infectious diseases (56–59). The two alanine residues flanking the C-terminal support C-terminal cleavage of the epitope without negatively influencing the N-terminal cleavage of the adjacent epitope (60), and further the generation of the C-terminal provides a suitable site for binding to TAP transporter or other chaperons (61).

KMP-11 derived multi-epitope peptide (KMP-11\_p1) was used in conjunction with the pan DR epitope (PADRE), a universal synthetic 13 aa peptide with high-binding affinity to 15 of the 16 most common HLA-DR molecules that is specifically engineered to be immunogenic in humans (62). CD4<sup>+</sup> T cells are well documented to play a central role in priming and maintenance of CD8<sup>+</sup> T cell effector functions, and thus PADRE could be considered a crucial component of prophylactic or immunotherapeutic vaccines against tumors and intracellular pathogens. Indeed, PADRE has been shown to augment the potency of vaccines designed to stimulate a cellular immune response (62). Multi-epitope peptides targeting CD8<sup>+</sup> T cell responses in conjunction with PADRE and a signaling peptide proved capable to increase memory CD8<sup>+</sup> T cells producing IFN $\gamma$  and elicit protective immunity in transgenic mice challenged with *Toxoplasma gondii* (63). In another study, the use of PADRE in combination with a synthetic multi-epitope peptide derived from the tumor-associated antigen Her2/neu improved vaccine potency in terms of IFN $\gamma$  producing CD4<sup>+</sup> and CD8<sup>+</sup> T cells expansion in mice (64). PADRE and KMP-11\_p1 were fused together via the linker HEYGAELERAG that provides the specific cleavage target for both proteasomal and lysosomal degradation system enhancing epitope presentation (57). This 12 aa peptide consists of five appropriate cleavage sites Y3-G4, A5-E6,

A7-L8, L8-E9, and R10-A11 specified for eukaryotic proteasome complexes in which A5-E6 is superior cleavage site (65) and has been used in a number of studies on multi-epitope peptide-based vaccine strategy combating cancer and intracellular infectious agents (57, 66, 67).

Antigen presentation is a crucial step in the initiation of an effective immune response and DCs own the unique ability to efficiently present processed antigenic peptides to T cells in the context of MHC class I or II molecules, playing a pivotal role in the orchestration of the adaptive immune response. Peptides are weak immune stimulators, and proper particulate delivery systems and/or adjuvants are needed to enhance their immunogenicity providing efficacious targeting of DCs. Thus, each chimeric peptide was synthesized and encapsulated in PLGA NPs (~300 nm) alone or in combination with MPLA adjuvant, or in PLGA NPs surface modified with the octapeptide p8 aiming their effective delivery to DCs. PLGA NPs are well suited for vaccine delivery due to the numerous advantages they offer including safety and endocytosis by DCs. A previous study has demonstrated that PLGA NPs 300 nm in average size exhibited low toxicity and were efficiently internalized by antigen-presenting cells—macrophages, B cells, and DCs—in vitro and in vivo (68). In the same study, PLGA NPs surface modified with p8 were proved to be internalized more efficiently by DCs *in vitro*.

This is the first report, to the best of our knowledge, describing the design and construction of an experimental nanovaccine against *L. infantum* infection based on a mix of PLGA NPs loaded with different synthetic long peptides from CPA, histone H1, and KMP-11 proteins, alone or in combination with the adjuvant MPLA, or a mix of PLGA NPs surface modified with the octapeptide p8 and loaded with the different synthetic long peptides. Since each chimeric peptide contained more than one HLA A2\*0201-restricted epitopes, the effect of these peptide-based PLGA nanoformulations was examined in bone marrow-derived DCs isolated from transgenic mice expressing an interspecies hybrid MHC class I gene with the alpha-1 and alpha-2 domains of the human HLA-A2.1 gene, with the view of selecting the most promising nanovaccine candidate for *in vivo* evaluation. This transgenic strain enables the modeling of human T cell immune responses to HLA-A2.1 presented antigens and may be precious tool in hand to study the immunogenicity of *in silico* selected peptides for vaccination purposes. Many vaccine trials primarily reported as protective in wild-type animals exhibit a moderate efficacy in humans, partially due to the fact that human and animal MHC molecules may have different influence on the outcome of an immune response (69). Humanized transgenic mice expressing human HLA molecules have shown promising results despite subtle differences in the antigen-processing machinery including proteasome cleavage and TAP molecules affinity for peptides (70), since the immunological hierarchy is approximately the same in both models and about 80% of peptides immunogenic in one are also immunogenic in the other (71).

Apart from enhancing antigen uptake, the main rationale behind DCs targeting remains the efficient antigen presentation to CD4<sup>+</sup> and CD8<sup>+</sup> T cells that requires beforehand the development of a strong maturation profile. In this study, the encapsulation of chimeric peptides in PLGA NPs resulted in a significant increase

in the number of DCs expressing the co-stimulatory molecules CD40, CD80, CD86, as well as the murine MHC class I and II molecules and the hybrid HLA-A2.1 molecule compared to DCs stimulated with the mix of soluble chimeric peptides. Previous studies have demonstrated that PLGA NPs loaded with soluble antigen or peptides strengthened DCs maturation in comparison to antigens in a soluble form or empty PLGA NPs (68, 72). Microarray data analysis strongly supported these findings, since DCs stimulated with the mix of soluble chimeric peptides exhibited a gene-expression profile similar to that of unstimulated DCs without enriched GO terms relevant to immune response. Both flow cytometry and microarray results demonstrated that MPLA incorporation in the peptide-based PLGA nanoformulations, as well as surface modification with p8 further enhanced DCs maturation. Particulate delivery of TLR ligands, such as MPLA adjuvant, offers several advantages over their administration in a soluble form. Delivery of TLR ligands in PLGA NPs would permit the use of very small doses and limit the non-specific immune activation and/or toxicity that may result upon systemic administration, as well as it may facilitate a sustained TLR signaling in DCs (73). A list of earlier studies have shown superior DCs and/or T cells activation when antigens were co-delivered in PLGA NPs with MPLA adjuvant (32, 68, 74–76). On the other hand, the attachment of targeting moieties on PLGA NPs surface cannot only facilitate the uptake by DCs, but can also enhance DCs maturation and ultimately lead to improving the effectiveness of vaccine formulation (73).

It is noteworthy that the significant increase in the number of DCs expressing the hybrid HLA-A2.1 confirms the achievement of antigen cross-presentation and the successful design of chimeric peptides to harbor epitopes that target mainly CD8<sup>+</sup> T cell responses (Figures 2–4). PLGA NPs can escape from endosomes and extrude through endosomal membrane into the cytoplasm, where encapsulated antigens can be released, processed by the proteasome, and cross-presented by MHC class I molecules (73). In complement with the above findings, T cell proliferation assay and flow cytometry results demonstrated that both DCs stimulated with the mix of PLGA-chCPAp-MPLA, PLGA-chH1p-MPLA, and PLGA-chKMP-11p-MPLA nanoformulations (mix B) and DCs stimulated with the mix of p8-PLGA-chCPAp, p8-PLGA-chH1p, and p8-PLGA-chKMP-11p nanoformulations (mix C) were proved capable to activate CD8<sup>+</sup> T cell populations with IFN $\gamma$  production (Figure 7). Microarray data analysis provided robust evidence for the accuracy of the results obtained from flow cytometry, since it revealed upregulated genes (*Tap1*, *Tap2*, *Psme2*, *Tapbp*, etc.) related to antigen processing and presentation in the context of MHC class I molecules in both DCs stimulated with mix B or mix C (Data Sheet S1 in Supplementary Material). However, a number of genes exclusively upregulated in DCs stimulated with mix B indicated a greater potency of these peptide-based PLGA nanoformulations to promote CD8<sup>+</sup> T cell responses (Data Sheet S1 in Supplementary Material; Table 4). Among them, *Psmb10* encodes the proteasome subunit beta type-10, a protein with major role in the immune system as part of an immunoproteasome formed by replacing constitutive beta subunits with inducible beta subunits that possess specific cleavage properties aiding in the release of peptides directed to MHC class

I antigen presentation (77). *Hsp90aa1* and *Hsp90ab1* encode the two forms—inducible and constitutive, respectively—of the cytosolic heat shock protein 90 alpha, an endogenous chaperon that associates with the N-terminally extended peptides after proteasomal degradation (78) and is essential for cross-presentation of both soluble and cell-associated antigens by DCs (79). Interferon gamma induced protein 3 (IRGM3), encoded by *Igtp*, is a p47 GTPase that also controls cross-presentation in DCs. IRGM3-deficient DCs were proved to exhibit a major impairment in their ability to cross-present phagocytized antigens to CD8<sup>+</sup> T cells (80). Chemokine (C-C motif) ligand 3 and 4, encoded by *Ccl3* and *Ccl4*, respectively, are produced at the immunological synapse between DCs and T cells and increase the chance for migrating CCR5-expressing CD8<sup>+</sup> T cells to contact DCs by a factor of 2–4 (81). Furthermore, upregulation of *Dhx58* suggested the presence of LPG2, a RIG-I-like receptor that is required for controlling antigen-specific CD8<sup>+</sup> T cell survival and fitness during peripheral T cell number expansion in response to virus infection (82), while upregulation of *Tnfsf8* indicated the expression of CD135 which is the ligand for CD30 whose signaling plays important role in the generation of long-lived memory CD8<sup>+</sup> T cells (83). *Il15* and *Il15ra* were also found exclusively upregulated in DCs stimulated with mix B. Interestingly, previous studies have shown that coordinate expression of IL-15 and IL-15R $\alpha$  by the same accessory cells such as DCs is required for supporting both NK and CD8<sup>+</sup> memory T cell homeostasis (84, 85).

As mentioned earlier, CD8<sup>+</sup> T cell responses are crucial mediators of immunity against intracellular pathogens like *L. infantum* parasites and a protective peptide-based vaccine targeting such immune responses might open a new way toward the battle over VL. Nevertheless, CD4<sup>+</sup> T<sub>H1</sub> cells also play a central role in *Leishmania*-specific response and thus they must be taken into account in vaccination strategies against the disease. Both DCs stimulated with the mix B or mix C were characterized by IL-12 production (Figure 5), a pro-inflammatory cytokine with great importance in the activation of T<sub>H1</sub> cell responses (86), and promoted allogeneic T cell proliferation and IFN $\gamma$  production by CD4<sup>+</sup> T cells (Figures 6 and 7), required for the immunity against VL. It can be argued that the nature of nanoformulations has a contribution to this fact, since in a previous study PLGA-based NPs loaded with CpG were proved to induce greater cytokine production and T cell proliferation than the oligonucleotide alone (87). Further, the presence of IL-4-producing CD4<sup>+</sup> T cells in the same population density as in the case of T cells co-cultured with unstimulated DCs indicated the absence of a T<sub>H2</sub> response (Figure 7) that is unwilling in the fight against VL.

Microarray data analysis further supported these findings unveiling up- (*Il6*, *Il12b*, *Ccl4*, *Cxcl3*, *Tnfsf9*, etc.) and downregulated genes (*Icos-l*, etc.) involved in T<sub>H</sub> cell aggregation and activation (Data Sheet S1 in Supplementary Material; Figures 8 and 9; Table 4). However, the presence of upregulated genes exclusively expressed in DCs stimulated with mix B demonstrated that these specific cells might be in a more advanced state of maturity and functional differentiation in terms of T<sub>H</sub> polarization than DCs stimulated with mix C (Table 4). For example, a number of upregulated genes involved in the regulation of cytokine production or in the response to cytokine stimulus, such as *Cish*, *Il1f6*, *Osm*, *Cxcl9*,

*Tnfsf15*, *Ddit3*, and *Dll4*, are considered markers of T cell activation and polarization toward T<sub>H1</sub> cells. *Cish* is identified as a STAT5 target gene and encodes a cytokine-inducible SH2-containing protein that plays a crucial role in type 1 DCs development (T<sub>H1</sub> polarization), as well as in DC-mediated cytotoxic T cell activation, since *Cish* knockdown was found to reduce the expression of MHC class I, co-stimulatory molecules and pro-inflammatory cytokines in bone marrow-derived DCs (88). Delta-like 4 (DLL4) is a protein encoded by the *Dll4* gene and its expression by DCs is critical for eliciting T cell responses. Activated DLL4<sup>+</sup> DCs were more capable to promote T<sub>H1</sub> and T<sub>H17</sub> differentiation than unstimulated DCs (89). Furthermore, CXCL9 is a well-known T<sub>H1</sub> attractant molecule, whereas oncostatin M—encoded by the *Osm* gene—is a pleiotropic cytokine that was found to induce the allogeneic stimulatory capacity of DCs by promoting the production of IL-12 and increase the production of IFNγ by T cells in MLRs that would be expected to contribute to the T<sub>H1</sub> polarization of the immune response (90). *Il1f6* encodes the cytokine IL36A whose signaling pathway activates DCs and amplifies T<sub>H1</sub> responses by enhancing proliferation and T<sub>H1</sub> polarization of naïve CD4<sup>+</sup> T cells (91).

The *in vitro* screening promoted the peptide-based PLGA nanoformulations with MPLA incorporation as a promising nanovaccine candidate and, therefore, immunization of HLA A2.1 transgenic mice was performed to unveil the induction of peptide-specific CD8<sup>+</sup> T cell responses. Results obtained confirmed the ability of PLGA nanoformulations with MPLA incorporation to target efficiently DCs, promoting peptide presentation through MHC class I molecules and thus inducing peptide-specific IFNγ-producing CD8<sup>+</sup> T cells (Figure 10). This finding provides evidence that the peptide-specific response is attributed to the HLA A\*0201 epitopes predicted by the *in silico* analysis and included in the chimeric peptides. According to the *in silico* analysis chimeric peptides also contain H2-D<sub>b</sub> restricted epitopes that might impact the TCR repertoire and further investigation is required. However, a study, focused on the use of this strain of transgenic mice as a model of human immune responses, revealed an extended epitope overlap in human Dryvax vaccines expressing HLA A\*0201 and HLA A2.1 transgenic mice (92). In a previous study of our group, a single peptide of CPA (CPA\_p2) co-encapsulated with MPLA in PLGA NPs induced CPA\_p2-specific cellular and humoral immune responses and conferred acute protection against *L. infantum* infection in BALB/c mice, mediated by IFNγ-producing CD8<sup>+</sup> T cells (93). Encapsulating more than one and longer synthetic peptides derived from three different immunogenic *Leishmania* proteins, more intense CD8<sup>+</sup> T cell responses were achieved, required in the immunity developed against VL. This tactics is in agreement with other studies underlining that vaccines designed to address a broad range of specificities are capable of inducing polyclonal effector T cells promoting protection (51, 94, 95).

Protection assays conducted in HLA A2.1 transgenic mice confirmed that this tactics could be considered as an improved strategy in terms of prophylactic efficacy against *L. infantum* infection (Figure 11). HLA A2.1 transgenic mice are created on a C57BL/6 background characterized by susceptibility to

*L. infantum* infection with a cure profile on the infection outcome (96). The selection of the specific time points for the estimation of immunization's protective effect was based on the infection kinetics in these mice. According to the time course of infection, the parasite burden reached a peak at 1 month post-infection in the liver and at 2 months post-infection in the spleen, followed by a decrease in both visceral organs. The results obtained from the limiting dilution assay revealed a significant reduction in hepatic and splenic parasite burden at 1 month post-infection by 72.81 and 61.98%, respectively, compared to the non-immunized control group. It is of particular interest that this protective effect was preserved at 2 months post-infection in both visceral organs (64.4 and 73.64% reduction in liver and spleen, respectively) indicating that immunization could accelerate the self-curing profile. The above findings combined with the fact that mice immunized with PLGA-MPLA nanoformulations exhibited comparable levels of parasite burden with the non-immunized mice provide evidence that the peptide-based PLGA nanoformulations with MPLA incorporation conferred a significant peptide-specific protection against *L. infantum* infection that was maintained 2 months post-infection before starting the self-curing phase on the infection outcome.

Conclusively, our findings supported that the encapsulation of more than one chimeric multi-epitope peptides from different immunogenic *L. infantum* proteins in a proper biocompatible delivery system with the right adjuvant is considered as an improved promising approach for the development of a vaccine against VL, since it induced a strong maturation profile in DCs and enabled them to present efficiently the pathogen-derived peptides to T cells inducing peptide-specific CD8<sup>+</sup> T cells with IFNγ production and conferring significant protection against *L. infantum* infection.

## ETHICS STATEMENT

This study was carried out in accordance with the recommendations of National Law 2013/56 and the EU Directive 2010/63/EU for animal experiments and complied with the ARRIVE guidelines. The protocol was approved by the institutional Animal Bioethics Committee.

## AUTHOR CONTRIBUTIONS

Conceived and designed the experiments: EK. Performed the experiments: EA, MA, and OK. Performed the bioinformatics analysis of the microarray data: ST, AH, and EA. Analyzed the data: EA, MA, ST, OK, AH, CK, and EK. Wrote the paper: EA and EK. All the authors critically revised the work, approved the version to be published, and agreed to be accountable for its content.

## ACKNOWLEDGMENTS

The authors thank Dr. Vaggelis Harokopos and Dr. Pantelis Hatzis at the Genomics Facility in the Biomedical Sciences Research Center “Alexander Fleming” for their assistance regarding the RNA integrity screening, probe synthesis, hybridization, and scanning. The authors also thank Dr. Olga Koutsoni, Dr. Dimitra

Toubanaki, and Dr. Maritsa Margaroni at the Laboratory of Cellular Immunology in the Hellenic Pasteur Institute for their partial technical assistance regarding mice handling, RNA extraction, and flow cytometry, respectively.

## FUNDING

This work was mainly supported by the grants “SYNERGASIA” (09SYN-14-643) and “KRIPIΣ” (MIS 450598) co-financed by the European Union and the National Ministry of Education and Religion Affairs under the Operational Strategic Reference Framework (NSFR 2007–2013), awarded to EK. The work was also

partially supported by “NGS-infect” grant financed by SIEMENS AG. EA and MA were awarded post-doctoral fellowships by the Hellenic Pasteur Institute and the State Scholarships Foundation (IKY) under “IKY FELLOWSHIPS OF EXCELLENCE FOR POSTGRADUATE STUDIES IN GREECE—SIEMENS PROGRAM” (Contract No.: SR22954), respectively.

## SUPPLEMENTARY MATERIAL

The Supplementary Material for this article can be found online at <http://journal.frontiersin.org/article/10.3389/fimmu.2017.00684/full#supplementary-material>.

## REFERENCES

1. World Health Organization. *Visceral Leishmaniasis: Control Strategies and Epidemiological Situation Update in East Africa, Report of a WHO Bi-Regional Consultation Addis Ababa, Ethiopia*. (2015). Available from: <http://www.who.int/leishmaniasis/resources/978924150965/en/>
2. Alvar J, Vélez ID, Bern C, Herrero M, Desjeux P, Cano J, et al. WHO leishmaniasis control team leishmaniasis worldwide and global estimates of its incidence. *PLoS One* (2012) 7(5):e35671. doi:10.1371/journal.pone.0035671
3. Ready PD. Epidemiology of visceral leishmaniasis. *Clin Epidemiol* (2014) 6:147–54. doi:10.2147/CLEP.S44267
4. Kaye P, Scott P. Leishmaniasis: complexity at the host-pathogen interface. *Nat Rev Microbiol* (2011) 9:604–15. doi:10.1038/nrmicro2608
5. Rodrigues V, Cordeiro-da-Silva A, Laforge M, Silvestre R, Estaquier J. Regulation of immunity during visceral *Leishmania* infection. *Parasit Vectors* (2016) 9:118. doi:10.1186/s13071-016-1412-x
6. Stäger S, Rafati S. CD8<sup>+</sup> T cells in *Leishmania* infections: friends or foes? *Front Immunol* (2012) 3:5. doi:10.3389/fimmu.2012.00005
7. Kamhawi S, Oliveira F, Valenzuela JG. Using humans to make a human leishmaniasis vaccine. *Sci Transl Med* (2014) 6(234):234fs18. doi:10.1126/scitranslmed.3009118
8. Lundsgaard C, Lund O, Kesmir C, Brunak S, Nielsen M. Modeling the adaptive immune system: predictions and simulations. *Bioinformatics* (2007) 23(4):3265–75. doi:10.1093/bioinformatics/btm471
9. Patronov A, Doytchinova I. T-cell epitope vaccine design by immunoinformatics. *Open Biol* (2013) 3:120139. doi:10.1098/rsob.120139
10. Palatnik-de-Sousa CB. Vaccines for leishmaniasis in the fore coming 25 years. *Vaccine* (2008) 26:1709–24. doi:10.1016/j.vaccine.2008.01.023
11. Seyed N, Taheri T, Rafati S. Post-genomics and vaccine improvement for *Leishmania*. *Front Microbiol* (2016) 7:467. doi:10.3389/fmicb.2016.00467
12. Black M, Trent A, Tirrell M, Olive C. Advances in the design and delivery of peptide subunit vaccines with a focus on toll-like receptor agonists. *Expert Rev Vaccines* (2010) 9(2):157–73. doi:10.1586/erv.09.160
13. Panda AK. Induction of anti-tumor immunity and T-cell responses using nanodelivery systems engrafting TLR-5 ligand. *Expert Rev Vaccines* (2011) 10(2):155–7. doi:10.1586/erv.10.164
14. Joshi MD, Unger WJ, Storm G, van Kooyk Y, Mastrobattista E. Targeting tumor antigens to dendritic cells using particulate carriers. *J Control Release* (2012) 161(1):25–37. doi:10.1016/j.jconrel.2012.05.010
15. Varypataki EM, Silva AL, Barnier-Quer C, Collin N, Ossendorp F, Jiskoot W. Synthetic long peptide-based vaccine formulations for induction of cell mediated immunity: a comparative study of cationic liposomes and PLGA nanoparticles. *J Control Release* (2016) 226:98–106. doi:10.1016/j.jconrel.2016.02.018
16. Hirosue S, Kourtis IC, van der Vlies AJ, Hubbell JA, Swartz MA. Antigen delivery to dendritic cells by poly(propylene sulfide) nanoparticles with disulfide conjugated peptides: cross presentation and T cell activation. *Vaccine* (2010) 28:7897–906. doi:10.1016/j.vaccine.2010.09.077
17. Taki A, Smooker P. Small wonders – the use of nanoparticles for delivering antigen. *Vaccines (Basel)* (2015) 3(3):638–61. doi:10.3390/vaccines3030638
18. Danhier F, Ansorena E, Silva JM, Coco R, Le Breton A, Préat V. PLGA-based nanoparticles: an overview of biomedical applications. *J Control Release* (2011) 161(2):505–22. doi:10.1016/j.jconrel.2012.01.043
19. Silva AL, Soema PC, Slüter B, Ossendorp F, Jiskoot W. PLGA particulate delivery systems for subunit vaccines: linking particle properties to immunogenicity. *Hum Vaccin Immunother* (2016) 12(4):1056–69. doi:10.1080/21645515.2015.1117714
20. Tafaghodi M, Khamesipour A, Jaafari MR. Immunization against leishmaniasis by PLGA nanospheres encapsulated with autoclaved *Leishmania major* (ALM) and CpG-ODN. *Parasitol Res* (2011) 108(5):1265–73. doi:10.1007/s00436-010-2176-4
21. Santos DM, Carneiro MW, de Moura TR, Fukutani K, Clarencio J, Soto M, et al. Towards development of novel immunization strategies against leishmaniasis using PLGA nanoparticles loaded with kinetoplastid membrane protein-11. *Int J Nanomedicine* (2012) 7:2115–27. doi:10.2147/IJN.S30093
22. Lima SAC, Resende M, Silvestre R, Tavares J, Ouassis A, Lin PK, et al. Characterization and evaluation of BNIPDaotc-loaded PLGA nanoparticles for visceral leishmaniasis: *in vitro* and *in vivo* studies. *Nanomedicine* (2012) 7(12):1839–49. doi:10.2217/Nnm.12.74
23. Etna MP, Giacomini E, Severa M, Pardini M, Aguiló N, Martín C, et al. A human dendritic cell-based *in vitro* model to assess *Mycobacterium tuberculosis* SO<sub>2</sub> vaccine immunogenicity. *ALTEX* (2014) 31(4):397–406. doi:10.14573/altex.1311041
24. Stoel M, Pool J, de Vries-Idema J, Zaaraoui-Boutahar F, Bijl M, Andeweg AC, et al. Innate responses induced by whole inactivated virus or subunit influenza vaccines in cultured dendritic cells correlate with immune responses *in vivo*. *PLoS One* (2015) 10(5):e0125228. doi:10.1371/journal.pone.0125228
25. Banchereau R, Baldwin N, Cepika AM, Athale S, Xue Y, Yu CI, et al. Transcriptional specialization of human dendritic cell subsets in response to microbial vaccines. *Nat Commun* (2014) 5:5283. doi:10.1038/ncomms6283
26. Maertzdorf J, Kaufmann SH, Weiner J. Molecular signatures for vaccine development. *Vaccine* (2015) 33(40):5256–61. doi:10.1016/j.vaccine.2015.03.075
27. Yang AX, Chong N, Jiang Y, Catalano J, Puri RK, Khleif SN. Molecular characterization of antigen-peptide pulsed dendritic cells: immature dendritic cells develop a distinct molecular profile when pulsed with antigen peptide. *PLoS One* (2014) 9(1):e86306. doi:10.1371/journal.pone.0086306
28. Costa V, Righelli D, Russo F, De Berardinis P, Angelini C, D'Apice L. Distinct antigen delivery systems induce dendritic cells' divergent transcriptional response: new insights from a comparative and reproducible computational analysis. *Int J Mol Sci* (2017) 18(3):E494. doi:10.3390/ijms18030494
29. Agallou M, Athanasou E, Koutsogiannis O, Dotsika E, Karagouni E. Experimental validation of multi-epitope peptides including promising MHC class I- and II-restricted epitopes of four known *Leishmania infantum* proteins. *Front Immunol* (2014) 5:268. doi:10.3389/fimmu.2014.00268
30. Rammensee H, Bachmann J, Emmerich NP, Bachor OA, Stevanović S. SYFPEITHI: database for MHC ligands and peptide motifs. *Immunogenetics* (1999) 50:213–9. doi:10.1007/s002510050595
31. Doytchinova IA, Guan P, Flower DR. EpiJen: a server for multistep T cell epitope prediction. *BMC Bioinformatics* (2006) 7:131. doi:10.1186/1471-2105-7-131
32. Hamdy S, Elamanchili P, Alshamsan A, Molavi O, Satou T, Samuel J. Enhanced antigen-specific primary CD4<sup>+</sup> and CD8<sup>+</sup> responses by co-delivery of ovalbumin and toll-like receptor ligand monophosphoryl lipid

- A in poly(d,L-lactic-co-glycolic acid) nanoparticles. *J Biomed Mater Res A* (2007) 81:652–62. doi:10.1002/jbm.a.31019
33. Yan MGJ, Dong W, Liu Z, Ouyang P. Preparation and characterization of a temperature-sensitive sulfobetaine polymer-trypsin conjugate. *Biochem Eng J* (2006) 30(1):48–54. doi:10.1016/j.bej.2006.02.001
  34. Lee H, Park TG. Conjugation of trypsin by temperature-sensitive polymers containing a carbohydrate moiety: thermal modulation of enzyme activity. *Biotechnol Prog* (1998) 14(3):508–16. doi:10.1021/Bp9701224
  35. Weissenböck A, Wirth M, Gabor F. WGA-grafted PLGA-nanospheres: preparation and association with Caco-2 single cells. *J Control Release* (2004) 99(3):383–92. doi:10.1016/j.jconrel.2004.07.025
  36. Agallou M, Margaroni M, Karagouni E. Cellular vaccination with bone marrow derived dendritic cells pulsed with a peptide of *Leishmania infantum* KMP-11 and CpG oligonucleotides induces protection in a murine model of visceral leishmaniasis. *Vaccine* (2011) 29(31):5053–64. doi:10.1016/j.vaccine.2011.04.089
  37. Yu G, Wang LG, Han Y, He QY. clusterProfiler: an R package for comparing biological themes among gene clusters. *OMICS* (2012) 16(5):284–7. doi:10.1089/omi.2011.0118
  38. Gene Ontology Consortium. Gene ontology consortium: going forward. *Nucleic Acids Res* (2015) 43(Database issue):D1049–56. doi:10.1093/nar/gku1179
  39. Luo W, Brouwer C. Pathview: an R/bioconductor package for pathway-based data integration and visualization. *Bioinformatics* (2013) 29(14):1830–1. doi:10.1093/bioinformatics/btt285
  40. Carrión J, Folgueira C, Alonso C. Immunization strategies against visceral leishmaniasis with the nucleosomal histones of *Leishmania infantum* encoded in DNA vaccine or pulsed in dendritic cells. *Vaccine* (2008) 26(20):2537–44. doi:10.1016/j.vaccine.2008.03.003
  41. Gouzelou E, Haralambous C, Antoniou M, Christodoulou V, Martinković F, Živičnjak T, et al. Genetic diversity and structure in *Leishmania infantum* populations from southeastern Europe revealed by microsatellite analysis. *Parasit Vectors* (2013) 6:342. doi:10.1186/1756-3305-6-342
  42. Titus RG, Marchand M, Boon T, Louis JA. A limiting dilution assay for quantifying *Leishmania major* in tissues of infected mice. *Parasite Immunol* (1985) 7:545–55. doi:10.1111/j.1365-3024.1985.tb00098.x
  43. Chen KY, Liu J, Ren EC. Structural and functional distinctiveness of HLA-A2 allelic variants. *Immunol Res* (2012) 53(1–3):182–90. doi:10.1007/s12026-012-8295-5
  44. Longmate J, York J, La Rosa C, Krishnan R, Zhang M, Senitzer D, et al. Population coverage by HLA class-I restricted cytotoxic T-lymphocyte epitopes. *Immunogenetics* (2001) 52(3–4):165–73. doi:10.1007/s002510000271
  45. Kazzaz J, Singh M, Ugozzoli M, Chesko J, Soenawan E, O'Hagan DT. Encapsulation of the immune potentiators MPL and RC529 in PLG microparticles enhances their potency. *J Control Release* (2006) 110:566–73. doi:10.1016/j.jconrel.2005.10.010
  46. Li Y, Pei Y, Zhang X, Gu Z, Zhou Z, Yuan W, et al. PEGylated PLGA nanoparticles as protein carriers: synthesis, preparation and biodistribution in rats. *J Control Release* (2001) 71:203–11. doi:10.1016/S0168-3659(01)00218-8
  47. De Groot AS, Sbai H, Aubin CS, McMurry J, Martin W. Immuno-informatics: mining genomes for vaccine components. *Immunol Cell Biol* (2002) 80(3):255–69. doi:10.1046/j.1440-1711.2002.01092.x
  48. Resende DM, Caetano BC, Dutra MS, Penido ML, Abrantes CF, Verly RM, et al. Epitope mapping and protective immunity elicited by adenovirus expressing the *Leishmania* amastigote specific A2 antigen: correlation with IFN-gamma and cytolytic activity by CD8+ T cells. *Vaccine* (2008) 26(35):4585–93. doi:10.1016/j.vaccine.2008.05.091
  49. Elfaki ME, Khalil EA, De Groot AS, Musa AM, Gutierrez A, Younis BM, et al. Immunogenicity and immune modulatory effects of *in silico* predicted *L. donovani* candidate peptide vaccines. *Hum Vaccin Immunother* (2012) 8(12):1769–74. doi:10.4161/hv.21881
  50. Basu R, Roy S, Walden P. HLA class I-restricted T cell epitopes of the kinetoplastid membrane protein-11 presented by *Leishmania donovani*-infected human macrophages. *J Infect Dis* (2007) 195(9):1373–80. doi:10.1086/513439
  51. Seyed N, Zahedifard F, Safaiyan S, Gholami E, Doustdari F, Azadmanesh K, et al. *In silico* analysis of six known *Leishmania major* antigens and *in vitro* evaluation of specific epitopes eliciting HLA-A2 restricted CD8 T cell response. *PLoS Negl Trop Dis* (2011) 5(9):e1295. doi:10.1371/journal.pntd.0001295
  52. Rezvan H, Rees R, Ali S. Immunogenicity of MHC class I peptides derived from *Leishmania mexicana* Gp63 in HLA-A2.1 transgenic (HHDII) and BALB/C mouse models. *Iran J Parasitol* (2012) 7(4):27–40.
  53. Bijkher MS, van den Eeden SJ, Franken KL, Melief CJ, Offringa R, van der Burg SH. CD8+ CTL priming by exact peptide epitopes in incomplete Freund's adjuvant induces a vanishing CTL response, whereas long peptides induce sustained CTL reactivity. *J Immunol* (2007) 179(8):5033–40. doi:10.4049/jimmunol.179.8.5033
  54. Melief CJ, van der Burg SH. Immunotherapy of established (pre)malignant disease by synthetic long peptide vaccines. *Nat Rev Cancer* (2008) 8(5):351–60. doi:10.1038/nrc2373
  55. Neisig A, Roelse J, Sijts AJ, Ossendorp F, Feltkamp MC, Kast WM, et al. Major differences in transporter associated with antigen presentation (TAP)-dependent translocation of MHC class I-presented peptides and the effect of flanking sequences. *J Immunol* (1995) 154(3):1273–9.
  56. Wang QM, Sun SH, Hu ZL, Zhou FJ, Yin M, Xiao CJ, et al. Epitope DNA vaccines against tuberculosis: spacers and ubiquitin modulates cellular immune responses elicited by epitope DNA vaccine. *Scand J Immunol* (2004) 60(3):219–25. doi:10.1111/j.0300-9475.2004.01442.x
  57. Nezafat N, Ghasemi Y, Javadi G, Khoshnoud MJ, Omidinia E. A novel multi-epitope peptide vaccine against cancer: an *in silico* approach. *J Theor Biol* (2014) 349:121–34. doi:10.1016/j.jtbi.2014.01.018
  58. Schubert B, Kohlbacher O. Designing string-of-beads vaccines with optimal spacers. *Genome Med* (2016) 8(1):9. doi:10.1186/s13073-016-0263-6
  59. de Oliveira LM, Morale MG, Chaves AA, Cavalher AM, Lopes AS, Diniz Mde O, et al. Design, immune responses and anti-tumor potential of an HPV16 E6E7 multi-epitope vaccine. *PLoS One* (2015) 10(9):e0138686. doi:10.1371/journal.pone.0138686
  60. Velders MP, Weijzen S, Eiben GL, Elmishad AG, Kloetzel PM, Higgins T, et al. Defined flanking spacers and enhanced proteolysis is essential for eradication of established tumors by an epitope string DNA vaccine. *J Immunol* (2001) 166(9):5366–73. doi:10.4049/jimmunol.166.9.5366
  61. Bergmann CC, Yao Q, Ho CK, Buckwold SL. Flanking residues alter antigenicity and immunogenicity of multi-unit CTL epitopes. *J Immunol* (1996) 157(8):3242–9.
  62. Alexander J, Fikes J, Hoffman S, Franke E, Sacci J, Appella E, et al. The optimization of helper T lymphocyte (HTL) function in vaccine development. *Immunol Res* (1998) 18(2):79–92. doi:10.1007/Bf02788751
  63. El Bissati K, Chentouf AA, Krishack PA, Zhou Y, Woods S, Dubey JP, et al. Adjuvanted multi-epitope vaccines protect HLA-A\*11:01 transgenic mice against *Toxoplasma gondii*. *JCI Insight* (2016) 1(15):e85955. doi:10.1172/jci.insight.85955
  64. Ghaffari-Nazari H, Tavakkol-Afshari J, Jaafari MR, Tahaghoghi-Hajghorbani S, Masoumi E, Jalali SA. Improving multi-epitope long peptide vaccine potency by using a strategy that enhances CD4+ T help in BALB/c mice. *PLoS One* (2015) 10(11):e0142563. doi:10.1371/journal.pone.0142563
  65. Dolenc I, Seemüller E, Baumeister W. Decelerated degradation of short peptides by the 20S proteasome. *FEBS Lett* (1998) 434(3):357–61. doi:10.1016/S0014-5793(98)01010-2
  66. Farhadi T, Ranjbar MM. Designing and modeling of complex DNA vaccine based on MOMP of *Chlamydia trachomatis*: an *in silico* approach. *Netw Model Anal Health Inform Bioinform* (2017) 6:1. doi:10.1007/s13721-016-0142-5
  67. Akhoo BA, Slathia PS, Sharma P, Gupta SK, Verma V. *In silico* identification of novel protective VS.G antigens expressed by *Trypanosoma brucei* and an effort for designing a highly immunogenic DNA vaccine using IL-12 as adjuvant. *Microb Pathog* (2011) 51(1–2):77–87. doi:10.1016/j.micpath.2011.01.011
  68. Margaroni M, Agallou M, Kontonikola K, Karidi K, Kammona O, Kiparissides C, et al. PLGA nanoparticles modified with a TNF $\alpha$  mimicking peptide, soluble *Leishmania* antigens and MPLA induce T cell priming *in vitro* via dendritic cell functional differentiation. *Eur J Pharm Biopharm* (2016) 105:18–31. doi:10.1016/j.ejpb.2016.05.018
  69. Pajot A, Michel ML, Fazilleau N, Pancré V, Auriault C, Ojcius DM, et al. A mouse model of human adaptive immune functions: HLA-A2.1/HLA-DR1-transgenic H-2 class I-class II-knockout mice. *Eur J Immunol* (2004) 34(11):3060–9. doi:10.1002/eji.200425463
  70. Pascolo S. HLA class I transgenic mice: development, utilization and improvement. *Expert Opin Biol Ther* (2005) 5(7):919–38. doi:10.1517/14712598.5.7.919
  71. Firat H, Garcia-Pons F, Tourdot S, Pascolo S, Scardino A, Garcia Z, et al. H-2 class I knockout, HLA-A2.1-transgenic mice: a versatile animal model for pre-clinical evaluation of antitumor immunotherapeutic strategies. *Eur J Immunol*

- (1999) 29(10):3112–21. doi:10.1002/(SICI)1521-4141(199910)29:10<3112::Aid-Immu3112>3.0.Co;2-Q
72. Iranpour S, Nejati V, Delirezh N, Biparva P, Shirian S. Enhanced stimulation of anti-breast cancer T cells responses by dendritic cells loaded with poly lactic-co-glycolic acid (PLGA) nanoparticle encapsulated tumor antigens. *J Exp Clin Cancer Res* (2016) 35(1):168. doi:10.1186/s13046-016-0444-6
73. Hamdy S, Haddadi A, Hung RW, Lavasanifar A. Targeting dendritic cells with nano-particulate PLGA cancer vaccine formulations. *Adv Drug Deliv Rev* (2011) 63(10–11):943–55. doi:10.1016/j.addr.2011.05.021
74. Chong CSW, Cao M, Wong WW, Fischer KP, Addison WR, Kwon GS, et al. Enhancement of T helper type 1 immune responses against hepatitis B virus core antigen by PLGA nanoparticle vaccine delivery. *J Control Release* (2005) 102(1):85–99. doi:10.1016/j.jconrel.2004.09.014
75. Lutsiak ME, Kwon GS, Samuel J. Biodegradable nanoparticle delivery of a Th2-biased peptide for induction of Th1 immune responses. *J Pharm Pharmacol* (2006) 58(6):739–47. doi:10.1211/jpp.58.6.0004
76. Elamanchili P, Lutsiak CM, Hamdy S, Diwan M, Samuel J. “Pathogen-mimicking” nanoparticles for vaccine delivery to dendritic cells. *J Immunother* (2007) 30(4):378–95. doi:10.1097/Cji.0b013e31802cf3e3
77. Ferrington DA, Gregerson DS. Immunoproteasomes: structure, function, and antigen presentation. *Prog Mol Biol Transl Sci* (2012) 109:75–112. doi:10.1016/B978-0-12-397863-9.00003-1
78. Callahan MK, Garg M, Srivastava PK. Heat-shock protein 90 associates with N-terminal extended peptides and is required for direct and indirect antigen presentation. *Proc Natl Acad Sci U S A* (2008) 105:1662–7. doi:10.1073/pnas.0711365105
79. Ichiyanagi T, Imai T, Kajiwara C, Mizukami S, Nakai A, Nakayama T, et al. Essential role of endogenous heat shock protein 90 of dendritic cells in antigen cross-presentation. *J Immunol* (2010) 185(5):2693–700. doi:10.4049/jimmunol.1000821
80. Bougnères L, Helft J, Tiwari S, Vargas P, Chang BH, Chan L, et al. A role for lipid bodies in the cross-presentation of phagocytosed antigens by MHC class I in dendritic cells. *Immunity* (2009) 31(2):232–44. doi:10.1016/j.jimmuni.2009.06.022
81. Bousso P. T-cell activation by dendritic cells in the lymph node: lessons from the movies. *Nat Rev Immunol* (2008) 8(9):675–84. doi:10.1038/nri2379
82. Suthar MS, Ramos HJ, Brassil MM, Netland J, Chappell CP, Blahnik G, et al. The RIG-I-like receptor LGP2 controls CD8<sup>+</sup> T cell survival and fitness. *Immunity* (2012) 37(2):235–48. doi:10.1016/j.jimmuni.2012.07.004
83. Nishimura H, Yajima T, Muta H, Podack ER, Tani K, Yoshikai Y. A novel role of CD30/CD30 ligand signaling in the generation of long-lived memory CD8<sup>+</sup> T cells. *J Immunol* (2005) 175(7):4627–34. doi:10.4049/jimmunol.175.7.4627
84. Burkett PR, Koka R, Chien M, Chai S, Boone DL, Ma A. Coordinate expression and trans presentation of interleukin (IL)-15R $\alpha$  and IL-15 supports natural killer cell and memory CD8<sup>+</sup> T cell homeostasis. *J Exp Med* (2004) 200:825–34. doi:10.1084/jem.20041389
85. Sandau MM, Schluns KS, Lefrancois L, Jameson SC. Cutting edge: transpresentation of IL-15 by bone marrow-derived cells necessitates expression of IL-15 and IL-15R alpha by the same cells. *J Immunol* (2004) 173:6537–41. doi:10.4049/jimmunol.173.11.6537
86. Kapsenberg ML. Dendritic-cell control of pathogen-driven T-cell polarization. *Nat Rev Immunol* (2003) 3(12):984–93. doi:10.1038/nri1246
87. Diwan M, Elamanchili P, Cao M, Samuel J. Dose sparing of CpG oligodeoxy-nucleotide vaccine adjuvants by nanoparticle delivery. *Curr Drug Deliv* (2004) 1(4):405–12. doi:10.2174/156720104334597
88. Miah MA, Yoon CH, Kim J, Jang J, Seong YR, Bae YS. CISH is induced during DC development and regulates DC-mediated CTL activation. *Eur J Immunol* (2012) 42(1):58–68. doi:10.1002/eji.201141846
89. Meng L, Bai Z, He S, Mochizuki K, Liu Y, Purushe J, et al. The Notch ligand DLL4 defines a capability of human dendritic cells in regulating Th1 and Th17 differentiation. *J Immunol* (2016) 196(3):1070–80. doi:10.4049/jimmunol.1501310
90. Jung ID, Noh KT, Lee CM, Chun SH, Jeong SK, Park JW, et al. Oncostatin M induces dendritic cell maturation and Th1 polarization. *Biochem Biophys Res Commun* (2010) 394(2):272–8. doi:10.1016/j.bbrc.2010.02.153
91. Vigne S, Palmer G, Martin P, Lamacchia C, Strelbel D, Rodriguez E, et al. IL-36 signaling amplifies Th1 responses by enhancing proliferation and Th1 polarization of naïve CD4<sup>+</sup> T cells. *Blood* (2012) 120(17):3478–87. doi:10.1182/blood-2012-06-439026
92. Kotturi MF, Assarsson E, Peters B, Grey H, Oseroff C, Pasquetto V, et al. Of mice and humans: how good are HLA transgenic mice as a model of human immune responses? *Immunome Res* (2009) 5:3. doi:10.1186/1745-7580-5-3
93. Agallou M, Margaroni M, Athanasiou E, Toubanaki DK, Kontonikola K, Karidi K, et al. Identification of BALB/c immune markers correlated with a partial protection to *Leishmania infantum* after vaccination with a rationally designed multi-epitope cysteine protease a peptide-based nanovaccine. *PLoS Negl Trop Dis* (2017) 11(1):e0005311. doi:10.1371/journal.pntd.0005311
94. Alves-Silva MV, Nico D, Morrot A, Palatnik M, Palatnik-de-Sousa CB. A chimera containing CD4+ and CD8+ T-cell epitopes of the *Leishmania donovani* nucleoside hydrolase (NH36) optimizes cross-protection against *Leishmania amazonensis* infection. *Front Immunol* (2017) 8:100. doi:10.3389/fimmu.2017.00100
95. Martins VT, Lage DP, Duarte MC, Carvalho AM, Costa LE, Mendes TA, et al. A recombinant fusion protein displaying murine and human MHC class I- and II-specific epitopes protects against *Leishmania amazonensis* infection. *Cell Immunol* (2017) 313:32–42. doi:10.1016/j.cellimm.2016.12.008
96. Loeillet C, Bañuls AL, Hide M. Study of *Leishmania* pathogenesis in mice: experimental considerations. *Parasit Vectors* (2016) 9:144. doi:10.1186/s13071-016-1413-9

**Conflict of Interest Statement:** The authors declare that the research was conducted in the absence of any commercial or financial relationships that could be construed as a potential conflict of interest.

Copyright © 2017 Athanasiou, Agallou, Tatsoglou, Kammona, Hatzigeorgiou, Kiparissides and Karagouni. This is an open-access article distributed under the terms of the Creative Commons Attribution License (CC BY). The use, distribution or reproduction in other forums is permitted, provided the original author(s) or licensor are credited and that the original publication in this journal is cited, in accordance with accepted academic practice. No use, distribution or reproduction is permitted which does not comply with these terms.



OPEN ACCESS

**Edited by:**

Jeffrey K. Actor,  
UTHealth Science Center,  
United States

**Reviewed by:**

Sampa Santra,  
Harvard Medical School,  
United States

Darren Woodside,  
Texas Heart Institute,  
United States

**\*Correspondence:**

José Ronnie Carvalho de  
Vasconcelos  
jrvcasconcelos@gmail.com.br

<sup>†</sup>These authors have contributed  
equally to this work.

<sup>#</sup>In memoriam.

**Specialty section:**

This article was submitted to  
Vaccines and Molecular  
Therapeutics,  
a section of the journal  
*Frontiers in Immunology*

**Received:** 30 May 2017

**Accepted:** 26 September 2017

**Published:** 13 October 2017

**Citation:**

Ferreira CP, Cariste LM, Santos Virgilio FD, Moraschi BF, Monteiro CB, Vieira Machado AM, Gazzinelli RT, Bruna-Romero O, Menin Ruiz PL, Ribeiro DA, Lannes-Vieira J, Lopes MF, Rodrigues MM and Vasconcelos JRC (2017) LFA-1 Mediates Cytotoxicity and Tissue Migration of Specific CD8<sup>+</sup> T Cells after Heterologous Prime-Boost Vaccination against *Trypanosoma cruzi* Infection. *Front. Immunol.* 8:1291.  
doi: 10.3389/fimmu.2017.01291

# LFA-1 Mediates Cytotoxicity and Tissue Migration of Specific CD8<sup>+</sup> T Cells after Heterologous Prime-Boost Vaccination against *Trypanosoma cruzi* Infection

**Camila Pontes Ferreira**<sup>1,2†</sup>, **Leonardo Moro Cariste**<sup>1,3†</sup>, **Fernando Dos Santos Virgilio**<sup>1,2</sup>, **Barbara Ferri Moraschi**<sup>1,2</sup>, **Caroline Brandão Monteiro**<sup>3</sup>, **Alexandre M. Vieira Machado**<sup>4</sup>, **Ricardo Tostes Gazzinelli**<sup>4,5</sup>, **Oscar Bruna-Romero**<sup>6</sup>, **Pedro Luiz Menin Ruiz**<sup>3</sup>, **Daniel Araki Ribeiro**<sup>3</sup>, **Joseli Lannes-Vieira**<sup>7</sup>, **Marcela de Freitas Lopes**<sup>8</sup>, **Mauricio Martins Rodrigues**<sup>1,2‡</sup> and **José Ronnie Carvalho de Vasconcelos**<sup>1,2,3\*</sup>

<sup>1</sup> Molecular Immunology Laboratory, Center of Molecular and Cellular Therapy, São Paulo, Brazil, <sup>2</sup> Department of Microbiology, Immunology and Parasitology, Federal University of São Paulo (UNIFESP), São Paulo, Brazil, <sup>3</sup> Department of Biosciences, Federal University of São Paulo, São Paulo, Brazil, <sup>4</sup> René Rachou Research Center, Fiocruz, Minas Gerais, Brazil, <sup>5</sup> Division of Infectious Disease and Immunology, Department of Medicine, University of Massachusetts Medical School, Worcester, MA, United States, <sup>6</sup> Department of Microbiology, Immunology and Parasitology, Federal University of Santa Catarina, Florianópolis, Brazil, <sup>7</sup> Biology Interactions Laboratory, Oswaldo Cruz Institute, Fiocruz, Rio de Janeiro, Brazil, <sup>8</sup> Institute of Biophysics Carlos Chagas Filho, Federal University of Rio de Janeiro, Rio de Janeiro, Brazil

Integrins mediate the lymphocyte migration into an infected tissue, and these cells are essential for controlling the multiplication of many intracellular parasites such as *Trypanosoma cruzi*, the causative agent of Chagas disease. Here, we explore LFA-1 and VLA-4 roles in the migration of specific CD8<sup>+</sup> T cells generated by heterologous prime-boost immunization during experimental infection with *T. cruzi*. To this end, vaccinated mice were treated with monoclonal anti-LFA-1 and/or anti-VLA-4 to block these molecules. After anti-LFA-1, but not anti-VLA-4 treatment, all vaccinated mice displayed increased blood and tissue parasitemia, and quickly succumbed to infection. In addition, there was an accumulation of specific CD8<sup>+</sup> T cells in the spleen and lymph nodes and a decrease in the number of those cells, especially in the heart, suggesting that LFA-1 is important for the output of specific CD8<sup>+</sup> T cells from secondary lymphoid organs into infected organs such as the heart. The treatment did not alter CD8<sup>+</sup> T cell effector functions such as the production of pro-inflammatory cytokines and granzyme B, and maintained the proliferative capacity after treatment. However, the specific CD8<sup>+</sup> T cell direct cytotoxicity was impaired after LFA-1 blockade. Also, these cells expressed higher levels of Fas/CD95 on the surface, suggesting that they are susceptible to programmed cell death by the extrinsic pathway. We conclude that LFA-1 plays an important role in the migration of specific CD8<sup>+</sup> T cells and in the direct cytotoxicity of these cells.

**Keywords:** vaccination, *Trypanosoma cruzi*, migration, integrins, specific CD8<sup>+</sup> T cells

## INTRODUCTION

Chagas disease, caused by the intracellular parasite *Trypanosoma cruzi*, is a major public health problem, with about seven million people infected worldwide (1). CD8<sup>+</sup> T cells are crucial for controlling the multiplication of intracellular pathogens such as *T. cruzi*. These cells control the infection by secreting cytokines such as IFN- $\gamma$  and TNF- $\alpha$ , or by direct cytotoxicity against infected target cells (2). The heterologous prime-boost vaccination strategy has shown significant results in the induction of specific CD8<sup>+</sup> T cells and the generation of an optimal protective immune response. Among several possible combinations of vectors for this type of immunization, we used a plasmid vector for priming and an adenovirus-Ad5 vector (replication-defective human Ad type 5) for boosting, both containing an insertion of the ASP-2 gene (*T. cruzi*'s amastigote surface protein 2 gene). This type of immunization was capable of protecting A/Sn mice that are highly susceptible to experimental infection with *T. cruzi* (3, 4).

The results obtained in preclinical experimental models with heterologous prime-boost immunization have boosted recent clinical trials (5–10). In 2013, the first results of a Phase II clinical trial were published. In that study, a number of volunteers, who were vaccinated with plasmid DNA followed by immunization with Ad5, both encoding the genes of the apical membrane antigen 1 and the immunodominant surface protein of the *Plasmodium falciparum* circumsporozoite protein, developed immunity to malaria (11).

To the CD8<sup>+</sup> T cells exert their effector function, these cells must migrate to non-lymphoid peripheral tissues where the infection occurs. Our group recently demonstrated that the protection generated by heterologous prime-boost immunization regimen depends on the recirculation of specific CD8<sup>+</sup> T cells, since immunized and protected A/Sn mice became susceptible to the experimental challenge with *T. cruzi* after FTY720 drug treatment (12). This immunosuppressive drug reduces lymphocyte recirculation by altering T cell signaling via sphingosine-1-phosphate receptor-1 (S1Pr1). This leads in sustained inhibition of S1Pr1 signaling, trapping T cells within the secondary lymphoid with no impairment of T cell activation (12, 13). Based on this knowledge, we hypothesized that other molecules, such as integrins, could be involved in the CD8<sup>+</sup> T cell migration. The integrins are heterodimers that composed of an alpha and beta chain; LFA-1 is composed of  $\alpha$ L $\beta$ 2 (CD11a/CD18) chains, and VLA-4, of  $\alpha$ 4 $\beta$ 1 (CD49d/CD29) chains. These molecules play an important role in the formation of immunological synapses and signal transduction, which result, for example, in cell migration, activation, and/or proliferation (14, 15). During transendothelial migration, chemokine-triggered activation of both LFA-1 and VLA-4 leads them to change their conformations and strongly bind to intercellular adhesion molecules (ICAMs and VCAMs, respectively) on endothelial cells and, thus, migrate into the tissues (16). In  $\beta$ 2 integrin-deficient mice, LFA-1 shows a significant reduction in the *in vitro* lymphocyte migration, strengthening the role of this molecule in leukocyte migration (17). The LFA-1 role in lymphocyte migration has also been demonstrated in the experimental autoimmune encephalomyelitis,

in which regulatory CD4<sup>+</sup> T cells can migrate to the CNS *via* LFA-1 (18). Its role has also been demonstrated in allografts, and the antagonism of this molecule is a very effective inhibitor of acute rejection, thus prolonging allograft survival in rodents (19). VLA-4 has also been studied in liver allograft rejections, where it seems responsible for the migration of effector CD8<sup>+</sup> T cells and transplant rejection along with LFA-1 (20, 21). During infection by intracellular parasites such as *T. cruzi*, specifically by the Colombian strain, there is a predominance of effector CD8<sup>+</sup> T lymphocytes (CTLs) with high expression of LFA-1 and VLA-4 in the myocardium of infected mice (22). In addition, the high expression of LFA-1 on the surface of Pfn<sup>+</sup>CD8<sup>+</sup> T cells during the acute and chronic phases has been demonstrated (23). However, the dominance of these cells in cardiac tissue favors the progression of the inflammatory reaction, culminating in Chronic Chagas heart disease (24).

Herein, we tested whether LFA-1 and VLA-4 integrins were key mediators for T cell-mediated protective immunity against *T. cruzi* infection. For that purpose, mice were vaccinated with heterologous prime-boost vaccine (recombinant plasmid DNA/AdHu5), challenged and treated with blocking antibodies to LFA-1 and/or VLA-4. Our results demonstrate that LFA-1, but not VLA-4, is essential for protective immune response of highly susceptible mice against *T. cruzi* infection. Also, the study demonstrated that LFA-1 mediates CD8<sup>+</sup> T cells migration into infected tissues, such as the heart, and plays an important role in CD8<sup>+</sup> T cells cytotoxicity for parasite clearance.

## MATERIALS AND METHODS

### Ethics Statement

This study was carried out in strict accordance with the recommendations in the Guide for the Care and Use of Laboratory mice of the Brazilian National Council of Animal Experimentation (<http://www.mctic.gov.br/mctic/opencms/textogeral/concea.html>). The protocol was approved by the Ethical Committee for Animal Experimentation at the Federal University of São Paulo (Id # CEP 7559051115).

### Mice and Parasites

Female 5- to 8-week-old A/Sn or C57BL/6 mice were purchased from the Federal University of São Paulo. ICAM-1-deficient mice were kindly supplied by Dr. João Santana, Ribeirão Preto School of Medicine-FMPR. Parasites of the Y strain of *T. cruzi* were used in this study (2, 3). Blood trypomastigotes of the Y strain of *T. cruzi* were maintained by weekly passages in A/Sn mice at the Xenodiagnosis Laboratory of Dante Pazzenese Cardiology Institute. Bloodstream trypomastigotes were obtained from mice infected 7–28 days earlier with parasites of the Y strain. For *in vivo* experiments, each mouse was inoculated with 150 trypomastigotes (A/Sn) or 10<sup>4</sup> trypomastigotes (C57BL/6) diluted in 0.2 mL phosphate-buffered saline (PBS) and administrated subcutaneously (s.c.) in the base of the tail. Parasitemia was determined by collecting 5  $\mu$ L of blood, and parasites were counted on the light microscope (25).

## Immunization Protocol

In this study, we used the heterologous prime-boost immunization protocol with plasmid pIgSPCl.9 and the human replication-defective adenovirus type 5 containing the ASP-2 gene, as described previously (3, 26). Briefly, this immunization consists of a dose of plasmid DNA as a prime (pcDNA3 control or pIgSPClone9). The mice were intramuscularly inoculated (i.m.) with 50 µg of plasmid DNA into each *tibialis anterioris* muscle. Three weeks after the first immunization, mice were boosted with  $2 \times 10^8$  plaque-forming units of the adenoviral vectors Adβ-gal or AdASP-2. Both injections were performed *via* intramuscular route (*tibialis anterior muscle*).

## Peptide

TEWETGQI peptide was synthesized by GenScript and obtained at purity higher than 95%. The TEWETGQI epitope expressed on ASP-2 surface is target of CD8<sup>+</sup> T cells and was identified previously (27). It was used for specific CD8<sup>+</sup> T cell stimulation *in vitro* and *ex vivo*. The H2K<sup>K</sup>-TEWETGQI multimer, labeled with fluorophore APC, was purchased from Immudex (Copenhagen, Denmark) and used for specific CD8<sup>+</sup> T cell detection in tissues.

## Treatment with Monoclonal Antibodies

Anti-LFA-1 (anti-CD11a, clone M17-4) and anti-VLA-4 (anti-CD49d, clone PS/2) monoclonal antibodies were purchased from BioXcell; in addition, we used Rat IgG2a (clone 2A3) isotype control. The *in vivo* treatment was performed with 10 i.p. injections of 250 µg of mAb/mouse (every 48 h after infection, until day 20 after infection). The concentration of LFA-1 used for *in vivo* treatment was the same used by Reisman et al. (28). To evaluate the efficiency of LFA-1 integrin blockade, C57BL/6 mice were infected with  $10^4$  trypomastigote forms of Y strain, and 12 days post infection, the splenocytes were harvested and incubated *in vitro* for 24 h at 30°C with monoclonal 250 µg/mL of 2A3 isotype control or anti-LFA-1 in complete medium [1% NEAA, 1% L-glutamine, 1% vitamins and 1% pyruvate, 0.1% 2-ME, 10% fetal bovine serum (FBS) (HyClone)]. After incubation, splenocytes were washed and labeled with anti-CD8 PerCP (clone 53-6.7, BD) and anti-CD11a FITC (clone 2D7, BD), fixed with 1% paraformaldehyde and analyzed by flow cytometry. Concomitantly, we also evaluated the blockade of the LFA-1 molecule stimulating splenocytes *in vitro* with 1 µg/mL anti-CD3 (clone 145-2C11, eBioscience) in complete medium for 72 h at 37°C and 5% CO<sub>2</sub>. On the second day of incubation, 250 µg of 2A3 isotype control or anti-LFA-1 monoclonal antibodies were added to the culture. On the third day of culture, cells were harvested and labeled with anti-CD8 PerCP and anti-CD11a FITC for flow cytometric analysis. LFA-1 expression was performed on gated CD8<sup>+</sup> T cells, according to Figures S1A,B in Supplementary Material, treatment with monoclonal anti-LFA-1 blocked most LFA-1 molecule expressed on activated CD8<sup>+</sup> T cells and after anti-LFA-1 FITC staining there was a lower CD11a MFI on the surface of these cells, indicating that there is competition between anti-LFA-1 monoclonal antibodies used for *in vivo* blocking (clone M17-4) and anti-CD11a FITC (clone 2D7, BD) used for flow cytometry labeling.

## Real-time PCR

Hearts, livers, and spleens from the *T. cruzi*-infected, immunized, and/or treated mice with anti-LFA-1 A/Sn were used for extracting DNA. The extraction protocol, the specific primers for a satellite DNA region of the parasite, and the RT-PCR reaction using the TaqMan Universal Master Mix II with UNG were adapted from Piron and colleagues (29). For the race plates, we used StepOnePlus (Applied Biosystems<sup>®</sup>), and distilled water for negative control reaction.

## Enzyme-Linked Immunospot (ELISPOT) Assay

Sterile PBS containing 10 µg/mL of anti-mouse IFN-γ monoclonal antibody (clone R4-6A2, Pharmingen) was added onto nitrocellulose 96-well flat-bottom plates; after 24 h, the plates were washed with RPMI and blocked with RPMI containing 10% FBS for 2 h. Following,  $1 \times 10^6$  responder cells from spleen, liver, or lymph node were incubated with  $3 \times 10^5$  antigen-presenting cells in complete medium [1% NEAA, 1% L-glutamine, 1% vitamins and 1% pyruvate, 0.1% 2-ME, 10% FBS (HyClone), and 20 U/mL mouse recombinant IL-2 (SIGMA)]. The plate was incubated in the presence or absence of 10 µM of peptide TEWETGQI. After 24 h, the plates were washed three times with PBS, and five times with PBS-Tween 20 (0.05% Tween). Each well received biotinylated anti-mouse monoclonal antibody (clone XMG1.2, Pharmingen) diluted in PBS-0.05% Tween 20 at a final concentration of 2 µg/mL. The plates were incubated with streptavidin-peroxidase (BD) and developed by adding peroxidase substrate (50 mM Tris-HCl, pH 7.5, containing 1 mg/mL DAB and 1 µL/mL 30% hydrogen peroxide, both from SIGMA). The number of IFN-γ-producing cells was determined using a stereoscope.

## Intracellular Cytokine Staining

Two million cells from the spleen, lymph node, or liver were treated with ACK buffer (NH<sub>4</sub>Cl, 0.15 M; KHCO<sub>3</sub>, 10 mM; Na<sub>2</sub>-EDTA 0.1 mM; pH = 7.4). ICS was performed after *in vitro* culture of splenocytes in presence or absence of 10 µM of peptide TEWETGQI as described previously (25). Cells were washed three times in plain RPMI and resuspended in cell culture medium consisting of RPMI 1640 medium supplemented with 10 mM HEPES, 0.2% sodium bicarbonate, 59 mg/L of penicillin, 133 mg/L of streptomycin, 10% HyClone FBS, 2 mM L-glutamine, 1 mM sodium pyruvate, 55 µM 2-mercaptoethanol. The viability of the cells was evaluated using 0.2% trypan blue exclusion dye to discriminate between live and dead cells. Cell concentration was adjusted to  $2 \times 10^6$  cells/mL in cell culture medium containing CD107a FITC antibody (clone 1D4B, BD), anti-CD28 (clone 37.51, BD), BD Golgi-Plug (1 µL/mL), and monensin (5 µg/mL) and incubated no longer than 12 h in V-bottom 96-well plates (Corning) in a final volume of 200 µL in duplicate, at 37°C in a humid environment containing 5% CO<sub>2</sub>. After 12 h incubation, cells were stained for surface markers with anti-CD8 PERCP antibody (clone 53-6.7, BD) on ice for 30 min. To detect IFN-γ, TNF or granzyme B by intracellular staining, cells were then washed twice in buffer containing PBS, 0.5% bovine serum

albumin (BSA), and 2 mM EDTA, fixed and permeabilized with BD perm/wash buffer. After being washed twice with BD perm/wash buffer, cells were stained for intracellular markers using APC-labeled anti-IFN- $\gamma$  (clone XMG1.2, BD), PE-labeled anti-TNF- $\alpha$  (clone MP6-XT22, BD), and anti-granzyme B PE (clone GB11, INVITROGEN) for 20 min on ice. Finally, cells were washed twice with BD perm/wash buffer and fixed in 1% PBS–paraformaldehyde. At least 700,000 cells were acquired on a BD FACS Canto II flow cytometer and then analyzed with FlowJo. Figures S3A,B in Supplementary Material shows the representative ICS gate strategies.

## Purification of Liver and Heart

### Lymphocytes

The perfused liver was lysed with collagenase buffer composed of 0.2 mg/mL collagenase IV (SIGMA), 0.02 mg/mL DNase (SIGMA), and 5% FBS. The leukocytes were separated on a 35% Percoll gradient (GE Healthcare), followed by centrifugation at 600  $\times$  g for 20 min and at 4°C. The pellet was suspended in RPMI 1640 (SIGMA) with 10% FBS (30). For the purification of the lymphocytes of the heart, we followed the protocol of Gutierrez et al. (31). Briefly, hearts collected from five mice at day 20 d.p.i. were minced, pooled, and incubated for 1 h at 37°C with RPMI 1640, supplemented with NaHCO<sub>3</sub>, penicillin–streptomycin gentamicin, and 0.05 g/mL of liberase blendzyme CI (Roche, Basel, Switzerland). The organs were processed in a Medimachine (BD Biosciences) in PBS containing 0.01% BSA. After tissue digestion and washes, cell viability was assessed by trypan blue exclusion, counted in a hemocytometer.

## Flow Cytometry Analysis

Splenocytes were treated with ACK buffer for red cell lysis and washed with RPMI with 10% FBS. The spleen, heart, lymph node, and liver cells were stained with H2K<sup>k</sup>-TEWETGQI multimer for 10 min at RT. The cell surface was stained for 30 min at 4°C. The following antibodies were used for surface staining: anti-CD3 APC/Cy7 (clone 145-2C11, BD), anti-CD8 PERCP or anti-CD8 PACIFIC BLUE (clone 53-6.7, BD), anti-CD11a FITC (clone 2D7, BD), anti-CD11c APC/Cy7 (clone HL3, BD), anti-CD44 FITC (clone IM7, BD), anti-CD62L PE (clone MEL-14, BD), anti-CXCR3 PERCP/Cy5.5 (clone 173, BioLegend), anti-CD27 FITC (clone LG3A10, BD), anti-CD4 PE/Cy7 (clone RM4-5, BD), anti-KLRG1 FITC (clone 2F1, eBioscience), anti-CD49d PE/Cy7 (clone R1-2, BD), anti-CD69 PERCP (clone H1.2F3, BD), anti-CD43 PE/Cy7 (1B11, BioLegend), anti-CD95 PE/Cy7 (clone JO2, BD), anti-CD25 FITC (clone LG3A10, BD), anti-CD127 PE (clone SB/199, BD), anti-CD122 FITC (clone TM- $\beta$ 1, BD), anti-CD38 PE (clone 90, BD), anti- $\beta$ 7 PERCP (clone FIB27, BioLegend), anti-CD31 FITC (clone MEC 13.3, BD), anti-CD272 PE (clone 8F4, eBioscience), anti-PD-1 FITC (clone J43, eBioscience), anti-CTLA-4 PE (clone UC10-4B9, eBioscience), and anti-CCR7 PE (clone 4B12, BD). At least 500,000 cells were acquired on a BD FACS Canto II flow cytometer and analyzed with FlowJo 8.7.

## In Vivo Proliferation Assay

A/Sn were immunized with ASP-2 using the heterologous “prime-boost” vaccination regimen and infected with 150

trypomastigotes forms of *T. cruzi*. At the moment of infection, mice were treated with monoclonal antibodies (LFA-1 or 2A3 isotype control) and 2 mg of BrdU (5-bromo-2'-deoxyuridine, SIGMA) by route i.p., at every 48 h, until the 20th day after challenge. Then, 2  $\times$  10<sup>6</sup> splenocytes were treated with ACK buffer for red cell lysis, washed with RPMI plus 10% FBS, and stained with H2K<sup>k</sup>-TEWETGQI multimer and anti-CD8 antibody. The specific CD8<sup>+</sup> T cells were stained according BrdU-FITC Kit protocol (BD Pharmingen) for analysis of BrdU incorporation. A minimum of 700,000 cells were acquired on a BD FACS Canto II flow cytometer and analyzed with FlowJo 8.7.

## In Vivo Cytotoxicity Assay

For the *in vivo* cytotoxicity assays, splenocytes collected from naive A/Sn mice were treated with ACK buffer to lyse the red blood cells, as described by Silverio et al. (23). The cells were divided into two populations and were labeled with the fluorogenic dye carboxyfluorescein diacetate succinimidyl ester (CFSE; Molecular Probes, Eugene, OR, USA) at a final concentration of 10  $\mu$ M (CFSE<sup>high</sup>) or 1  $\mu$ M (CFSE<sup>low</sup>). CFSE<sup>high</sup> cells were coated with 2.5  $\mu$ M of the TEWETGQI ASP-2 peptide for 40 min at 37°C. CFSE<sup>low</sup> cells remained uncoated. Subsequently, CFSE<sup>high</sup> cells were washed and mixed with equal numbers of CFSE<sup>low</sup> cells before intravenous injection (2  $\times$  10<sup>7</sup> cells per mouse) into *T. cruzi*-infected, immunized and/or treated mice with anti-LFA-1 A/Sn recipients that were sedated with diazepam (20 mg/kg). Spleen cells from the recipient mice were collected at 20 h after adoptive cell transfer and fixed with 1.0% paraformaldehyde. At least 100,000 cells were acquired on a BD FACS Canto II flow cytometer and analyzed with FlowJo 8.7. The percentage of specific lysis was determined using the following formula:

$$\% \text{ lysis} = 1 - \frac{(\% \text{CFSE}^{\text{high}} \text{ infected}/\% \text{CFSE}^{\text{low}} \text{ infected})}{(\% \text{CFSE}^{\text{high}} \text{ naive}/\% \text{CFSE}^{\text{low}} \text{ naive})} \times 100$$

## Histology and Immunohistochemistry

The mice's heart, spleen, and liver were fixed in 10% formalin, and then dehydrated, embedded in paraffin blocks, and sectioned on a microtome. Staining was obtained with hematoxylin and eosin, and the number of amastigotes nests was quantified using a light microscope with 40 $\times$  objective lens. Overall, 50 fields/group were counted. For immunohistochemistry the hearts of the animals were removed and frozen in Tissue-Tek O.C.T. (Sakura Finetek), and the 7  $\mu$ m thickness cuts were made in the cryostat (Leica) and then fixed in ice-cold acetone for 15 min. The samples were stained with 20  $\mu$ g of the biotinylated anti-CD8 antibody (clone 53-6.7, RD systems) for 12 h in the wet chamber, and after incubation was labeled with streptavidin Alexa Fluor® 488 (Thermo Fischer) at the concentration of 0.5 mg/mL, diluted 1:100 for 1 h and room temperature. The DAPI (4',6-diamidino-2-phenylindole, SIGMA) dye was used for labeling the 5 mg/mL cell nucleus, diluted 1:1,000 for 15 min at room temperature. The images were acquired in the Confocal Leica TCS SP8 CARS microscope of the Institute of Pharmacology and Molecular Biology (INFAR)

of the Paulista School of Medicine of the Federal University of São Paulo. The images were obtained using the 63× objective and processed by the ImageJ program.

## Statistical Analysis

The number of parasites/mL corresponding to the peak of parasitemia, the number of IFN- $\gamma$ -producing cells (ELISPOT), and the absolute number of CD8<sup>+</sup> T cells were compared by analysis of unidirectional variance (ANOVA); subsequently, the Tukey's HSD test was used. To compare the survival of mice after challenge with *T. cruzi*, we used the Log-rank test. The receptor expression was compared using MFI (mean fluorescence intensity), and the naïve group MFI was taken as the baseline. MFI was determined by the FlowJo software. Differences were considered significant when *P* value was <0.05.

## RESULTS

### LFA-1 Is Essential for Survival of A/Sn Mice during the Experimental Challenge with *T. cruzi*

Previously, we demonstrated that treatment with FTY720, which retains CD8<sup>+</sup> T cells in the lymph nodes *via* blockade of receptor S1Pr1, culminates in death of immunized mice. As LFA-1 and VLA-4 integrins were expressed on those specific CD8<sup>+</sup> T cells we investigated the role of these molecules following immunization and *T. cruzi* infection. To this end, immunized and infected mice were treated with 250 µg of monoclonal antibodies anti-LFA-1 and/or anti-VLA-4 every 48 h to block those molecules. Initially, we analyzed blood parasitemia and, as shown in **Figure 1A**, mice treated with anti-LFA-1 (green) antibody had increased blood parasitemia when compared with the group only immunized and treated with the control isotype (red), whereas mice treated with anti-VLA-4 (yellow) had a parasite burden similar to the immunized (red). To examine whether these two integrins exhibit synergism, one group was treated with both antibodies simultaneously (**Figure 1A**, blue group). Simultaneous treatment resulted in increased blood parasitemia, but this increase was not significant when compared with the group treated with anti-LFA-1 only, indicating that LFA-1, but not VLA-4, is important to control blood parasites. With respect to survival (**Figure 1B**), all mice treated with anti-LFA-1 died after 26 days, whereas all anti-VLA-4-treated mice and isotype control treated mice survived. Therefore, no statistical differences were observed in the survival rate between the mice treated with anti-LFA-1 (green) and the mice treated with both antibodies (blue), but there were differences in survival rate between the mice treated with anti-LFA-1 and mice treated with isotype control. Therefore, during LFA-1 blockade, mice displayed increased blood parasitemia and succumbed after challenge with *T. cruzi*, while VLA-4 blockade does not interfere with parasitemia and survival of treated mice.

To confirm the role of LFA-1 during *T. cruzi* infection, C57BL/6 mice naturally resistant to *T. cruzi* infection were infected and treated. C57BL/6 mice treatment with anti-LFA-1 was able to control blood parasitemia until 12th day after infection, but after

that, the blood parasitemia increased and all mice treated with anti-LFA-1 rapidly succumbed to infection (**Figures 1C,D**) when compared the mice treated with the isotype control.

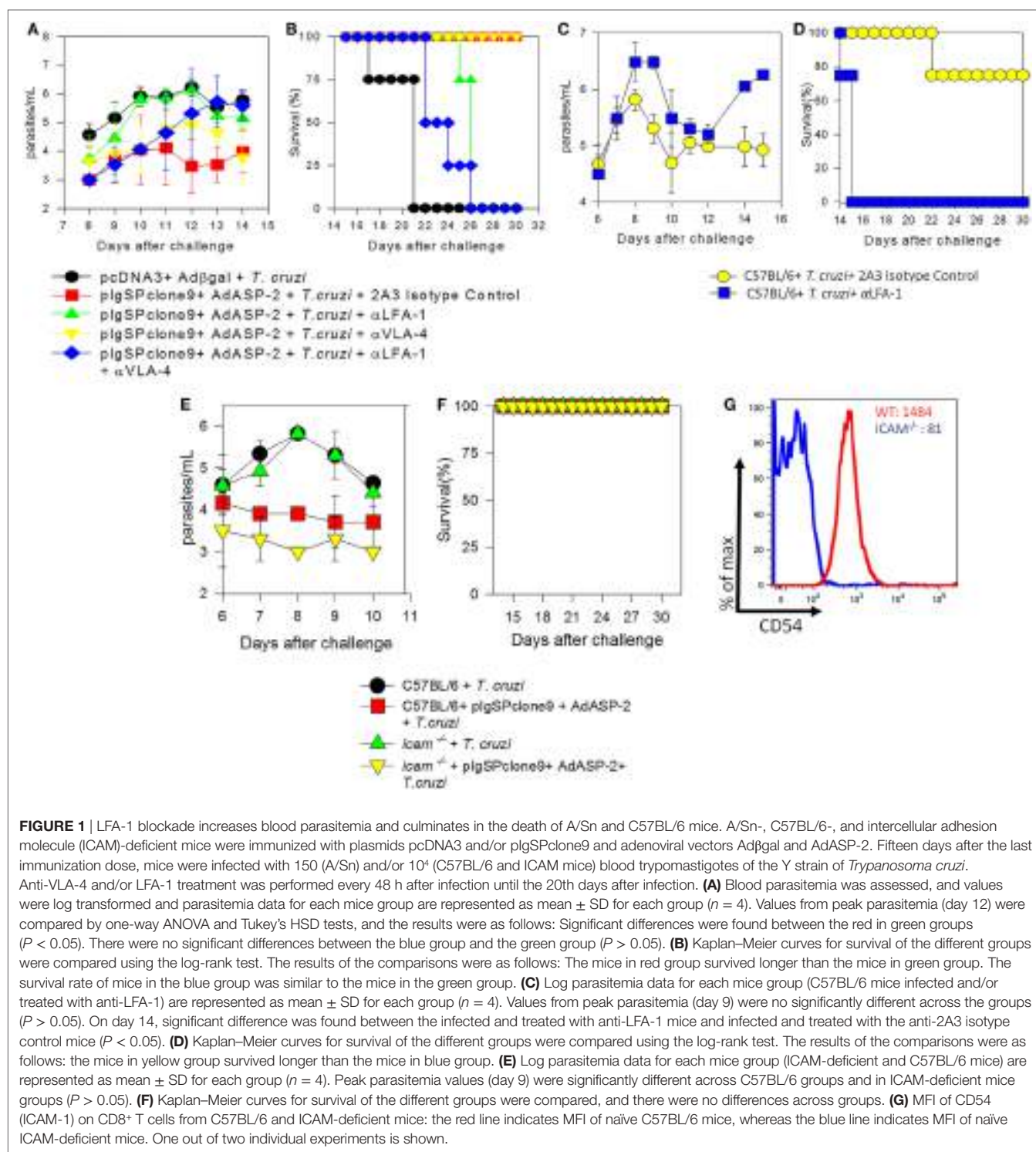
Since LFA-1 blockade increased mouse susceptibility to infection by *T. cruzi*, we investigated the importance of the ICAM-1 integrin, a major ligand of LFA-1. To this end, genetically ICAM-1-deficient mouse was used. These mice were immunized and infected for parasitemia and survival analysis. Both C57BL/6 and ICAM-1 knockout mice displayed similar parasitemia, and the two groups immunized with the ASP-2 gene showed a decreased parasitemia when compared with the vector control immunized groups (**Figure 1E**). In addition, all mice survived the experimental challenge with *T. cruzi* (**Figure 1F**). **Figure 1G** shows the expression of CD54 (ICAM-1) on spleen of CD8<sup>+</sup> T cells of WT and deficient mice, and, as expected, the latter ones have lower expression of CD54 compared with WT mice. Altogether, these results indicate that the absence of ICAM-1 does not increase susceptibility to *T. cruzi* infection and suggest that, even though ICAM-1 is a major ligand of LFA-1, there is another ligand (i.e., ICAM-2) that binds to LFA-1 allowing it to exert its functions.

### LFA-1 Blockade Increases Tissue Parasite of Immunized and Infected A/Sn Mice

Since anti-VLA-4 treatment did not interfere in the mice parasitemia and/or survival, all following experiments were performed by blocking LFA-1 integrin only. As the LFA-1 blockade leads to increased blood parasitemia and rapid death of the mice, we investigated whether the parasitic increase also occurs in the tissues of infected, immunized, and/or anti-LFA-1-treated A/Sn mice. The heart, liver, and spleen of these mice were extracted after the 20th day of infection for quantification of the parasite's DNA by real-time PCR; in addition, the number of amastigote nests in the heart was quantified using hematoxylin–eosin staining. There was a statistical increase in the number of amastigote nests in the hearts of the LFA-1-treated mice compared with the immunized and infected group, and the largest amount of nests was found in the hearts of mice solely infected (**Figures 2A,B**). In addition, LFA-1 blockade resulted in the increase of parasites in the tissues analyzed compared with immunized, infected mice. The spleen showed higher parasite increase, followed by hearts and livers respectively (**Figure 2C**). These results demonstrate that treatment with anti-LFA-1 increases blood parasitemia, which will reflect on increased tissue parasite burden.

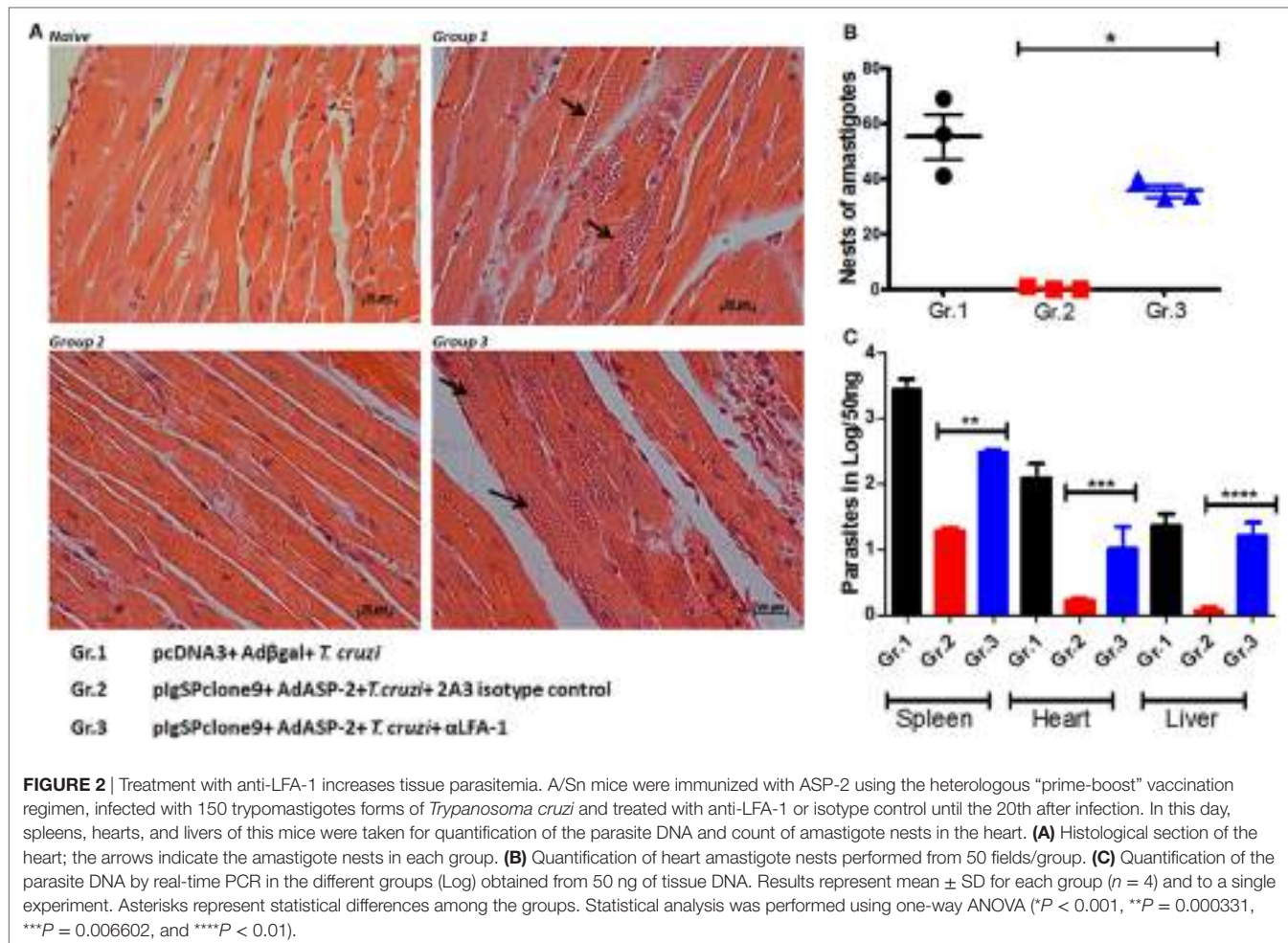
### LFA-1 Blockade Increases the Expression Level of the Fas/CD95 Molecule on the Surface of Effector CD8<sup>+</sup> T Cells

We analyzed whether LFA-1 blockade affects effector phenotype and activation of specific CD8<sup>+</sup> T cells. To this end, splenocytes were stained with anti-CD8 and H2K<sup>K</sup> TEWETQGI-multimer, and surface markers. In previous results obtained by our group, we demonstrated that immunization followed by infection induces specific CD8<sup>+</sup> T cells with the phenotype of effector cells (TE), which is characterized by the expression of CD11a<sup>high</sup>, CD44<sup>high</sup>, CD62L<sup>low</sup>, and CD127<sup>low</sup> (25, 26). Anti-LFA-1 treatment increased



the frequency and the absolute number of specific CD8<sup>+</sup> T cells in the spleen (Figures 3A,B). In addition, as there is competition between the antibodies used for *in vivo* blockade and flow cytometric labeling, we observed a decrease in CD11a MFI in the anti-LFA-1-treated groups (Figure 3C). In general, the markers whose expression levels increased in the anti-LFA-1-treated group (Gr.3) in comparison with the infected group (Gr.1) or

the immunized and infected group (Gr.2) were as follows: CD27, CD43, CD69, and CD95 (Figure 3C). Our group has also demonstrated that the cells generated by immunization followed by infection expressed lower levels of CD95 on the surface compared with infected only group, and these cells were also resistant to death induced by anti-CD95 (12). Moreover, markers CD183, CD38, and PD-1 also displayed increased expression levels on the



surface of specific CD8<sup>+</sup> T cells after treatment with anti-LFA-1 (Gr.3) compared with Gr.2 (Figure 3C). KLRL1, however, had similar MFI among the three groups, and these groups showed low expression of markers CD122, BTLA, CTLA-4, and CD25. These results suggest that anti-LFA-1 treatment does not impair specific CD8<sup>+</sup> T cells in the spleen. Instead, there is a greater frequency and absolute number of these cells. In addition, the treatment did not alter the phenotype of effector CD8<sup>+</sup> T cells (TE); however, we found in the spleen of treated mice that those CD8<sup>+</sup> T cells expressed high levels of CD95.

### Specific CD8<sup>+</sup> T Cells Accumulate in Secondary Lymphoid Organs and Decrease Migration into the Heart after LFA-1 Blockade

After demonstrating that anti-LFA-1 treatment increases blood and tissue parasitemia and leads to mice death, our hypothesis was that specific CD8<sup>+</sup> T cells cannot migrate into the infected tissues since LFA-1 is associated with leukocyte migration. To test our hypothesis, we measured in the spleen, lymph, blood, liver, and heart the frequency of specific CD8<sup>+</sup> T cells. For that propose, the cells were labeled with anti-CD8 and H2K<sup>K</sup>-TEWETGQI

multimer. We found higher frequency and increment in the absolute numbers of specific CD8<sup>+</sup> T cells in spleens and lymph nodes, but not in the blood and liver of the anti-LFA-1-treated group when compared with the infected and immunized group (Figures 4A–F). A dramatic influx reduction of specific CD8<sup>+</sup> T cells after anti-LFA-1 treatment (Figure 4A) was observed in group 3 hearts. In addition, we found that specific CD8<sup>+</sup> T cells in the spleen, blood, and heart of the infected group (Gr.1) and the immunized and infected group (Gr.2) expressed high levels of CD11a, whereas the cells in the immunized, infected, and anti-LFA-1-treated group (Gr.3) showed decreased CD11a MFI due to the competition described earlier (Figure 4G). We also evaluated the frequency of total CD8<sup>+</sup> T cells in the spleen, blood, and heart and, as shown in Figure S2 in Supplementary Material, there was a reduction in the frequency of CD8<sup>+</sup> T cells in the heart of the anti-LFA-1-treated group (Figures S2A–D in Supplementary Material). Furthermore, by immunohistochemistry, there is a decrease in the number of CD8<sup>+</sup> T cells in the heart of animals treated with anti-LFA-1 (Figures S2E,F in Supplementary Material). The number of CD8<sup>+</sup> T cells in the heart of the treated group was similar to the infected group, and in relation to the immunized group, treatment with anti-LFA-1 decreased the migration of CD8<sup>+</sup> T cells to the heart, observed

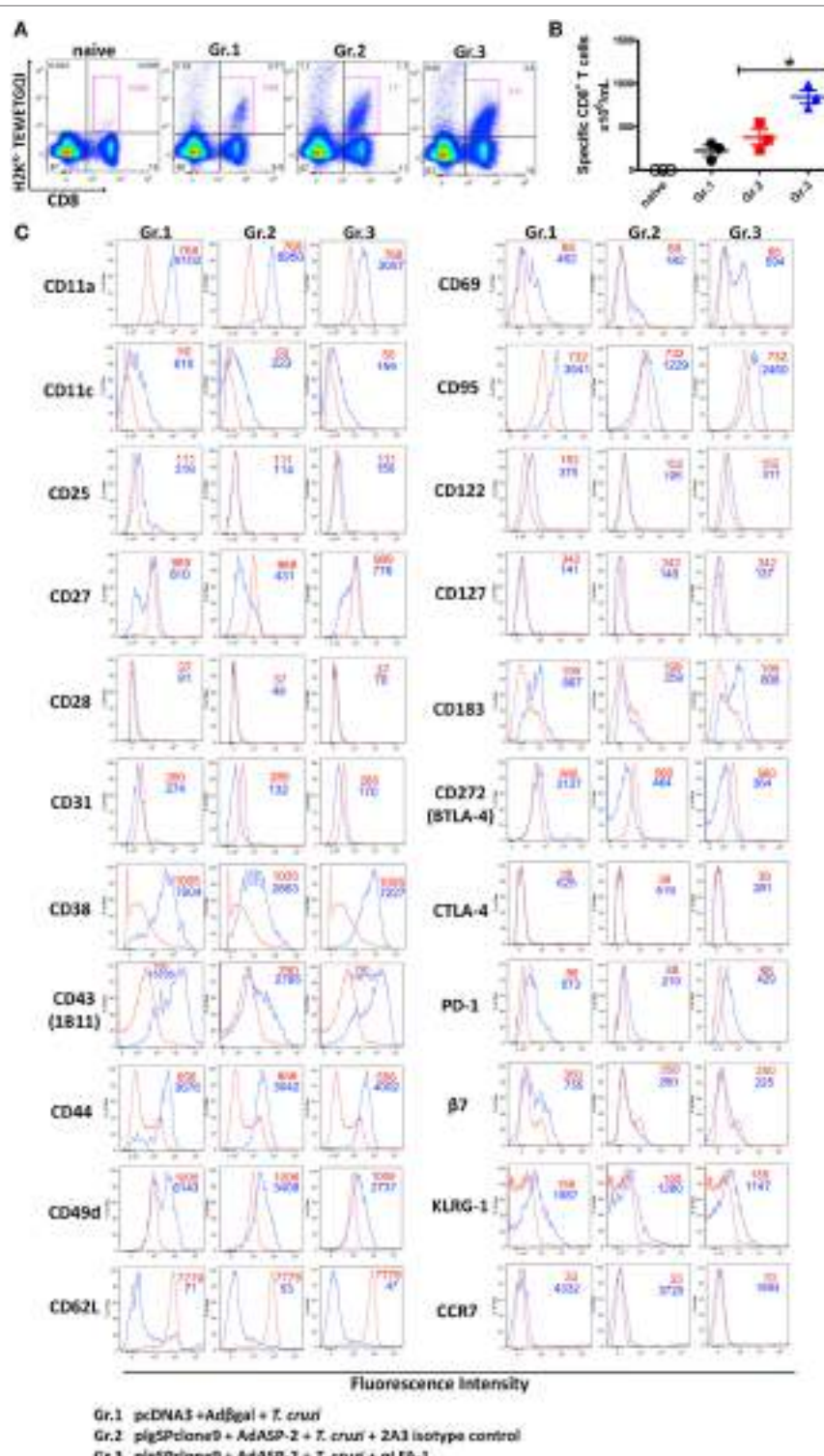


**FIGURE 3 |** Effector CD8<sup>+</sup> T lymphocytes express high levels of CD95 on the surface after anti-LFA-1 treatment. A/Sn mice were immunized with ASP-2 using the heterologous “prime-boost” vaccination regimen, infected with 150 trypanomastigotes forms of *Trypanosoma cruzi* and treated with anti-LFA-1 or isotype control until the 20th after infection. In this day, the splenic cells were labeled with H2K<sup>-</sup>TEWETGQI multimer, anti-CD8 and surface markers. **(A)** The frequency of specific CD8<sup>+</sup> T cells in the spleen. **(B)** Absolute number of specific CD8<sup>+</sup> T cells in the spleen. **(C)** Histograms with MFI of each marker analyzed in different groups. The red line represents the *naive* group, whereas the blue line represents groups 1, 2, and 3. Results in panels **(A,B)** are individual values with the mean  $\pm$  SD of groups ( $n = 4$ ), while in panel **(C)** representative analyses are shown for four mice per experiment. The experiment was performed two or more times with similar results. Statistical analysis was performed using the one-way ANOVA. Asterisks denote statistically significant differences between the groups 2 and 3 ( $P < 0.05$ ).

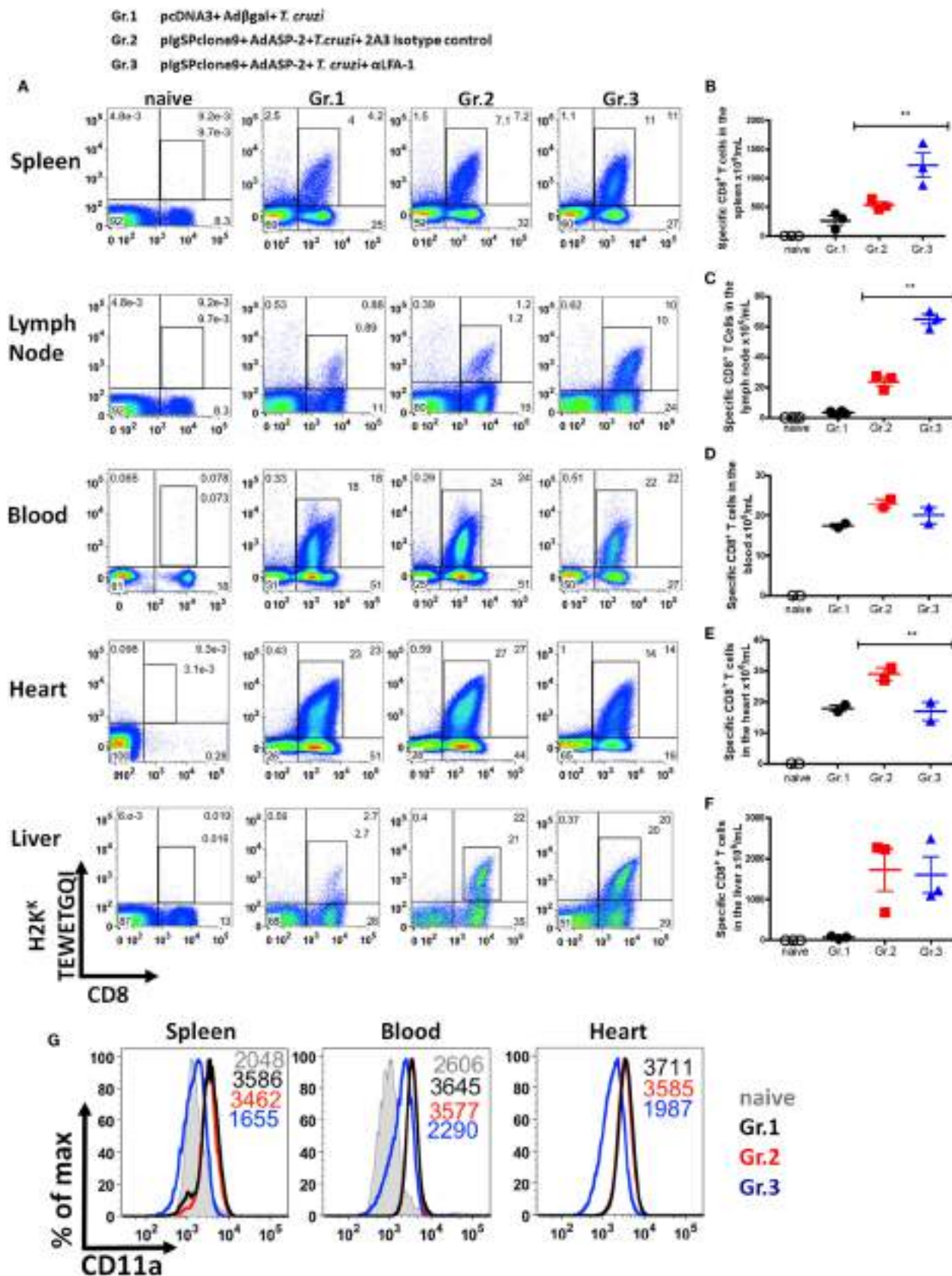


FIGURE 4 | Continued

**FIGURE 4 |** Continued

Specific CD8<sup>+</sup> T cells accumulate in the spleen and lymph node and do not migrate into the heart after anti-LFA-1 treatment. A/Sn mice were immunized with ASP-2 using the heterologous “prime-boost” vaccination regimen, infected with 150 trypanomastigotes forms of *Trypanosoma cruzi* and treated with anti-LFA-1 or isotype control until the 20th after infection. In this day, spleen, heart, liver, lymph nodes, and blood cells of the immunized, infected, and treated or not with anti-LFA-1 were labeled with anti-CD8 and H2K<sup>K</sup>-TEWETGQI multimer. **(A)** Frequency of specific CD8<sup>+</sup> T cells in the spleen, lymph node, blood, heart, and liver, respectively. **(B–F)** Absolute number of specific CD8<sup>+</sup> T cells in the spleen, lymph node, blood, heart, and liver, respectively. The results for the spleen, lymph node, and liver are representative values of an individual in each group ( $n = 4$ ) with mean  $\pm$  SD. While the results for the blood and heart were taken from a pool of five individuals per group, values of an individual of each repetition ( $n = 2$ ) with mean  $\pm$  SD. Statistical analysis was performed using the one-way ANOVA. **(G)** Histograms represent MFI of specific CD8<sup>+</sup> T cells that express CD11a onto the surface in the spleen, blood, and heart, respectively, and the group naïve the MFI of CD11a was analyzed onto the surface of CD8<sup>+</sup> T cells. Asterisks denote statistically significant differences between of groups 2 and 3 (\*\* $P < 0.001$ ).

by the low number of these cells in the cardiac tissue. These results corroborate the decrease in specific CD8<sup>+</sup> T cells in those organs. Therefore, during LFA-1 blockade, specific CD8<sup>+</sup> T cells accumulate in the secondary lymphoid organs, such as spleen and lymph node, and cannot migrate into the heart, as observed by the lower frequency of these cells in that organ.

### Specific CD8<sup>+</sup> T Cells Degranulate and Produce IFN- $\gamma$ and TNF- $\alpha$ after Anti-LFA-1 Treatment

Having in mind the important role of IFN- $\gamma$  during infection by *T. cruzi* (2), we analyzed whether the anti-LFA-1 treatment may alter production of IFN- $\gamma$  by specific CD8<sup>+</sup> T cells. We also analyzed the effector function of specific CD8<sup>+</sup> T cells in the spleen, liver, and lymph nodes regarding TNF- $\alpha$  production and indirect cytotoxicity involving cell surface mobilization of CD107a. The gate strategy used to evaluate the production of cytokines and the polyfunctionality of specific CD8<sup>+</sup> T cells is illustrated in Figures S3A,B in Supplementary Material. In the spleen of the anti-LFA-1-treated group, compared with the immunized and infected group, there was an increase in the percentage of polyfunctional specific CD8<sup>+</sup> T cells, that is, cells that are capable of degranulating and, at the same time, producing IFN- $\gamma$  and TNF- $\alpha$ . Such increase in polyfunctionality of specific CD8<sup>+</sup> T cells after anti-LFA-1 treatment was also observed in lymph nodes and liver (Figures 5A,B). In addition, anti-LFA-1 treatment also culminated in an increase in the amplitude of the immune response, i.e., the percentage of specific CD8<sup>+</sup> T cells producing IFN- $\gamma$  or TNF- $\alpha$  or degranulating, in the spleen, lymph node, and liver (Figure 5C). The number of specific CD8<sup>+</sup> T cells producing IFN- $\gamma$  was higher in the anti-LFA-1-treated group (Gr.3), when compared with Gr.2, and this increase occurred in the spleen, the lymph node, and liver (Figure 5D). Altogether, these results show that LFA-1 blockade does not affect the effector function of specific CD8<sup>+</sup> T cells regarding IFN- $\gamma$  and TNF- $\alpha$  secretion and degranulation. The increase in the effector function is probably due to the accumulation of specific cells in spleen and lymph node after treatment with anti-LFA-1.

### Specific CD8<sup>+</sup> T Cells Reduce Direct Cytotoxicity against Target Cells after Treatment with Anti-LFA-1

First, we tested whether treatment had impaired the frequency and absolute numbers of specific CD8<sup>+</sup> T cells. As we can see, there was an increase in the frequency and absolute numbers of specific

CD8<sup>+</sup> T cells in the anti-LFA-1-treated group (Figures 6A,B). We concluded that the treatment did not interfere with specific CD8<sup>+</sup> T cell expansion. Since specific CD8<sup>+</sup> T cells are capable of secreting IFN- $\gamma$  and TNF- $\alpha$  after LFA-1 blockade in the spleen, we assessed whether the treatment had impaired specific CD8<sup>+</sup> T cells proliferative capacity. The proliferation of specific CD8<sup>+</sup> T cells in the spleen was analyzed *in vivo* by thymidine BrdU analog incorporation. We found that a similar proportion of the H2K<sup>K</sup>-TEWETGQI CD8<sup>+</sup> cells incorporated BrdU *in vivo* in non-treated or treated mice indicating that the proliferative capacity of these cells was not significantly different (Gr. 2 and Gr. 3, Figure 6C). However, the infected mice have a greater proliferation in comparison with groups 2 and 3 (Figures 6C,D).

Another effector function triggered by specific CD8<sup>+</sup> T cells is the direct cytotoxicity against the target cells. Here, we analyzed whether this function had been affected by the treatment. For that purpose, we used *in vivo* cytotoxicity assay. Figure 7A shows representative histograms containing two populations P1 (CFSE<sup>low</sup>) and P2 (CFSE<sup>high</sup>) showing the specific lysis of H2K<sup>K</sup>-TEWETGQI peptide-labeled CFSE<sup>high</sup> cells from Gr.1, Gr.2, and Gr.3 groups (Figure 7A). Surprisingly, we observed that the immunized mice treated with anti-LFA-1 had significantly decreased cytotoxicity when compared with the immunized group (Figure 7B). The specific CD8<sup>+</sup> T cells from the immunized mice have 80% cytotoxicity whereas the anti-LFA-1-treated cells showed a 29% percentage drop. Figure 7C shows that the numbers of CFSE<sup>low</sup> cells were similar across groups 1, 2, and 3, while the number of cells CFSE<sup>high</sup> decreased in groups 2 (non-treated) and 3 (treated) compared with group 1 (Figure 7D).

The reduction of cytotoxicity did not affect the amount of granzyme B produced by specific CD8<sup>+</sup> T cells in the anti-LFA-1-treated group. We observed that MFI and the percentage of specific CD8<sup>+</sup> T cells that produce granzyme B were similar across the groups (Figures 7E,F). These results demonstrate that treatment with LFA-1 directly affects the cytotoxicity of specific CD8<sup>+</sup> T cells and the impairment of this function may be one of the factors responsible for the reversal protection generated by immunization observed after LFA-1 blockade.

## DISCUSSION

Our group previously demonstrated that the recirculation of specific CD8<sup>+</sup> T cells generated by heterologous prime-boost immunization and *T. cruzi* infection is of paramount importance to the protection of A/Sn mice, which are highly susceptible to infection by *T. cruzi* (12, 13). Given that integrins play an important role

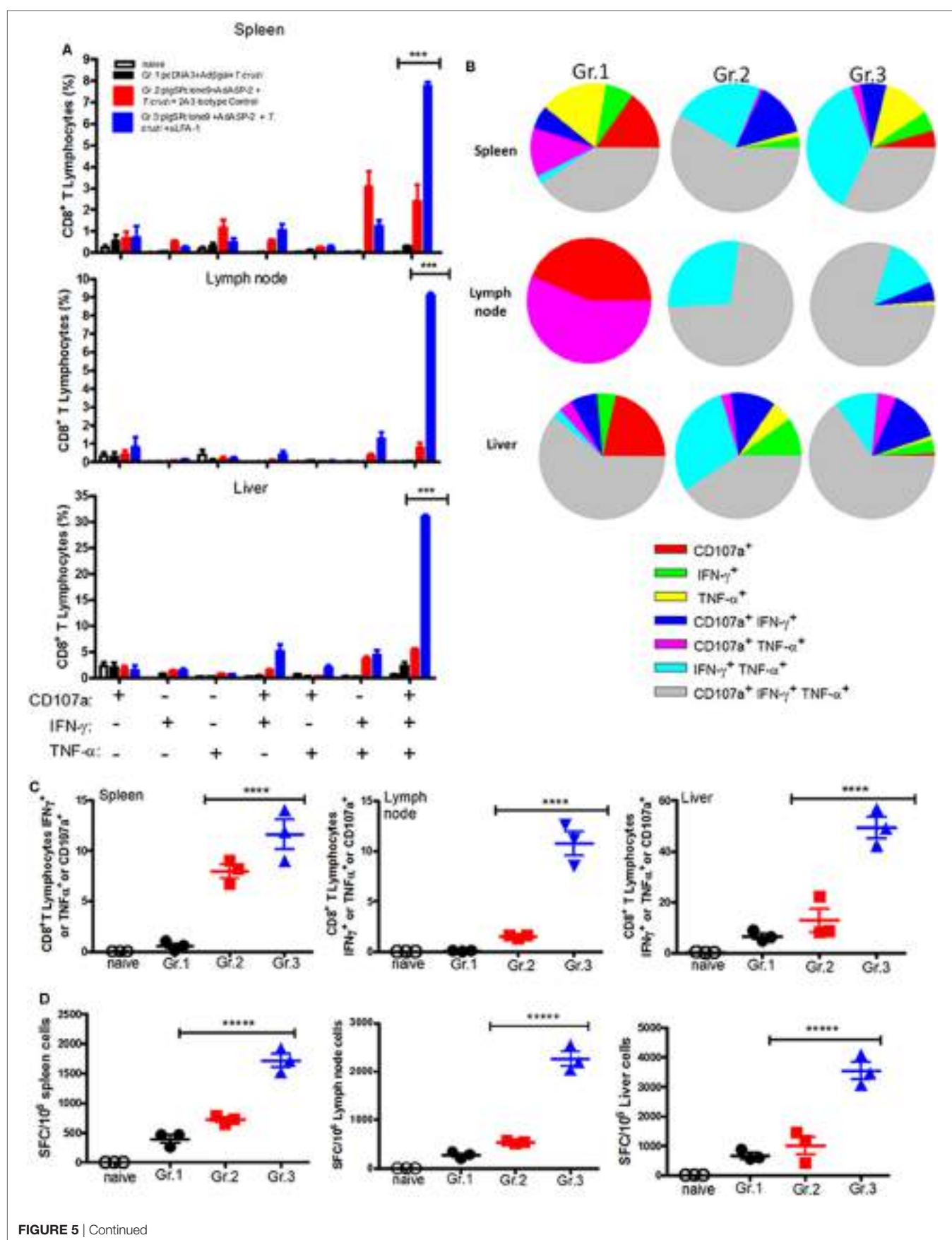
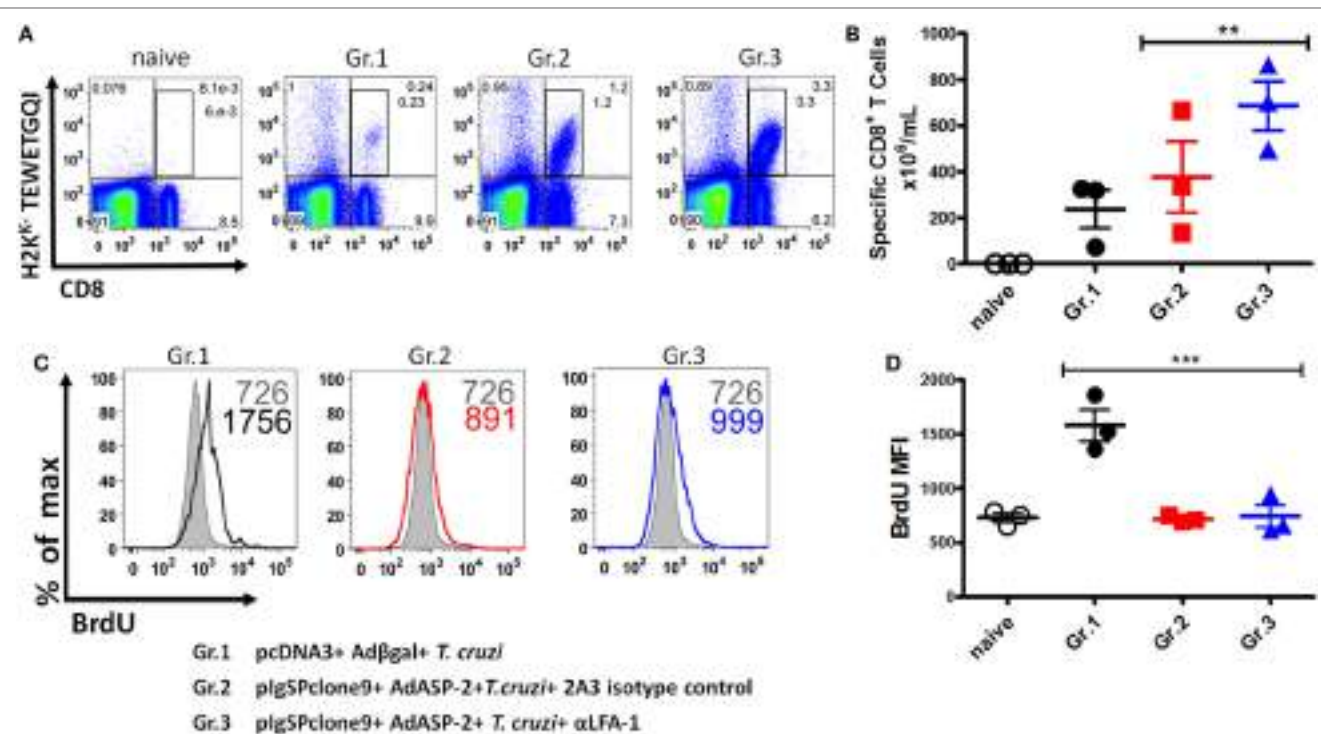


FIGURE 5 | Continued

**FIGURE 5 | Continued**

Anti-LFA-1 treatment increases the polyfunctionality of specific CD8<sup>+</sup> T cells in the spleen, liver, and lymph node, and the number of IFN- $\gamma$ -producing cells. A/Sn mice were immunized with ASP-2 using the heterologous “prime-boost” vaccination regimen, infected with 150 trypanomastigotes forms of *Trypanosoma cruzi*, and treated with anti-LFA-1 or isotype control until 20th days after infection. In this day, splenocytes and cells of inguinal lymph nodes were collected. Furthermore, leukocytes from the liver were isolated by Percoll. These cells were restimulated *in vitro* in the presence of the peptide TEWETGQL at a final concentration of 10 mM. After 12 h, cells were stained for CD8, IFN- $\gamma$ , and TNF- $\alpha$ . Frequencies were initially estimated for any CD8<sup>+</sup> that expressed surface CD107a, IFN- $\gamma$ , or TNF- $\alpha$  after stimulation *in vitro* with peptide TEWETGQL. **(A)** Percentage of specific CD8<sup>+</sup> T cells performing each of the functions shown in the graph combinations; (+) indicates presence, while (-) indicates absence of CD107a/IFN- $\gamma$ /TNF- $\alpha$ . **(B)** Pie chart represents the fraction of specific CD8<sup>+</sup> T cells that carry each of the combinations shown in the legend. **(C)** Amplitude of the immune response, i.e., the percentage of CD8<sup>+</sup> T cells that are performing at least one of the functions indicated. **(D)** ELISPOT graph of the IFN- $\gamma$ -producing cells. Results are representative of two independent experiments with the mean  $\pm$  SD of each individual shown in the graphs ( $n = 4$ ). Asterisks show statistical difference between the groups. Statistical analysis was performed using one-way ANOVA ( $P < 0.05$ ). Boolean analysis was performed using FlowJo software. SFC, spot-forming cell.



**FIGURE 6 |** Specific CD8<sup>+</sup> T cells can proliferate after the treatment with anti-LFA-1. A/Sn mice were immunized with ASP-2 using the heterologous “prime-boost” vaccination regimen, infected with 150 trypanomastigotes forms of *Trypanosoma cruzi*, and treated with anti-LFA-1 or isotype control until 20th days after infection. Mice received 2 mg of 5-bromo-2'-deoxyuridine (BrdU) every 48 h. In this day, spleen was harvested for the proliferation assay. 2  $\times$  10<sup>6</sup> splenocytes were labeled with H2K<sup>K</sup>-TEWETGQL multimer, anti-CD8 and anti-BrdU. **(A,B)** The frequency and absolute number of specific CD8<sup>+</sup> T cells in the spleen, respectively. **(C,D)** Histograms with MFI of BrdU in the groups and graph of the MFI mean of the specific CD8 T cells expressing BrdU. The graphs represent the mean  $\pm$  SD for each individual ( $n = 3$ ). Representative results of two independent experiments. Statistical analysis was performed using one-way ANOVA test (\*\* $P < 0.01$ ; \*\*\* $P < 0.005$ ).

in cell-cell and cell-extracellular matrix interactions, and that these interactions are responsible for the intracellular signal transduction that culminates in cell migration (14) and formation of the immunological synapse (15), the aim of this study was to analyze the role of LFA-1 and VLA-4 integrins in specific CD8<sup>+</sup> T cells migration. During activation of specific CD8<sup>+</sup> T cells, there was an increase in the expression level of CD11a (LFA-1) and CD49d (VLA-4) chains (12). In addition, an increase in effector CD8<sup>+</sup> T cells that express molecules LFA-1/ICAM-1 and VLA-4/VCAM-1 occurred in the hearts of mice infected with *T. cruzi*, suggesting the role of these molecules in the migration of specific CD8<sup>+</sup> T cells into infected tissues (22, 23, 32). Here, we investigated the hypothesis that these molecules participate in the

migration of specific CD8<sup>+</sup> T cells generated by immunization and infection. LFA-1 blockade, but not VLA-4, makes vaccinated A/Sn and infected C57BL/6 mice susceptible to infection with *T. cruzi*. The increased susceptibility of A/Sn mice was accompanied by increased parasitemia and tissue parasite burden, as well as rapid death of these mice. Even though VLA-4 does not play any role in our model, it participates in the migration of specific CTLs into the heart of C3H/He mice when infected with the Colombian strain of *T. cruzi* (22). Because we did not see any role of VLA-4 in the mice parasitemia and survival our study was conducted toward LFA-1 role.

To analyze the role of ICAM-1, a major ligand for LFA-1, we used ICAM-1 KO mice and challenged them with blood

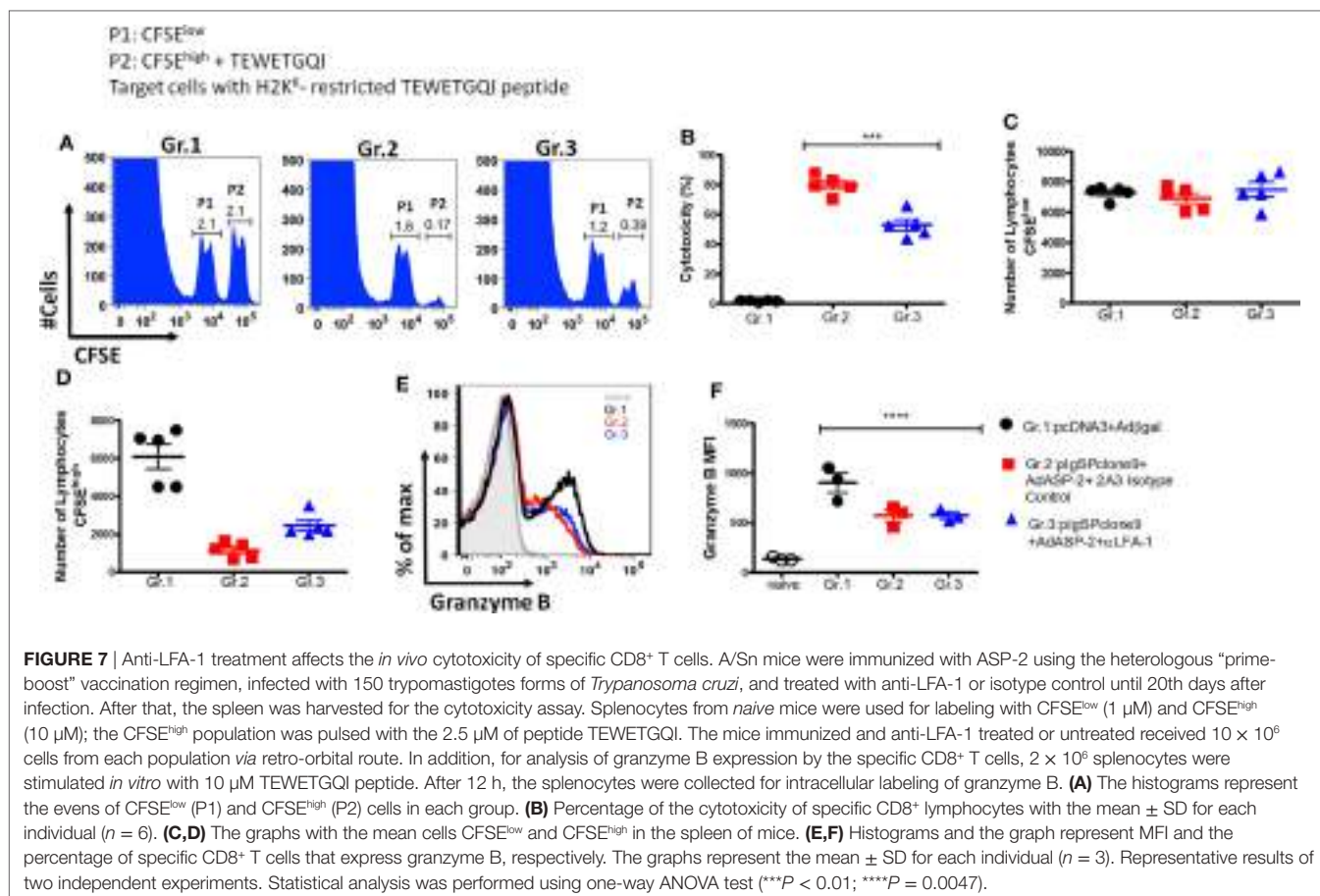


**FIGURE 7 |** Anti-LFA-1 treatment affects the *in vivo* cytotoxicity of specific CD8<sup>+</sup> T cells. A/Sn mice were immunized with ASP-2 using the heterologous “prime-boost” vaccination regimen, infected with 150 trypanomastigotes forms of *Trypanosoma cruzi*, and treated with anti-LFA-1 or isotype control until 20th days after infection. After that, the spleen was harvested for the cytotoxicity assay. Splenocytes from naive mice were used for labeling with CFSE<sup>low</sup> (1  $\mu$ M) and CFSE<sup>high</sup> (10  $\mu$ M); the CFSE<sup>high</sup> population was pulsed with the 2.5  $\mu$ M of peptide TEWETGQI. The mice immunized and anti-LFA-1 treated or untreated received  $10 \times 10^6$  cells from each population *via* retro-orbital route. In addition, for analysis of granzyme B expression by the specific CD8<sup>+</sup> T cells,  $2 \times 10^6$  splenocytes were stimulated *in vitro* with 10  $\mu$ M TEWETGQI peptide. After 12 h, the splenocytes were collected for intracellular labeling of granzyme B. **(A)** The histograms represent the events of CFSE<sup>low</sup> (P1) and CFSE<sup>high</sup> (P2) cells in each group. **(B)** Percentage of the cytotoxicity of specific CD8<sup>+</sup> lymphocytes with the mean  $\pm$  SD for each individual ( $n = 6$ ). **(C,D)** The graphs with the mean cells CFSE<sup>low</sup> and CFSE<sup>high</sup> in the spleen of mice. **(E,F)** Histograms and the graph represent MFI and the percentage of specific CD8<sup>+</sup> T cells that express granzyme B, respectively. The graphs represent the mean  $\pm$  SD for each individual ( $n = 3$ ). Representative results of two independent experiments. Statistical analysis was performed using one-way ANOVA test (\*\* $P < 0.01$ ; \*\*\* $P = 0.0047$ ).

tryponastigotes of the Y strain of *T. cruzi*, which did not affect the susceptibility of these mice to infection. This may be related to the redundancy of ligands by which a receptor can connect to alternate ligands without complete loss of functions performed by a receptor (33–35).

LFA-1 acts as a co-stimulatory molecule participating in the activation of T lymphocytes (36), and it has been shown that this molecule activates CD4<sup>+</sup> T cells and induces secretion of cytokines such as IFN- $\gamma$  and IL-17 (37). Therefore, we evaluated whether LFA-1 blockade impairs the activation of specific CD8<sup>+</sup> T cells or interferes with phenotype of effector CD8<sup>+</sup> T cells (TE). Our group has characterized the profile of CD8<sup>+</sup> T cells induced by immunization that displays a phenotype of effector CD8<sup>+</sup> T cells (TE). TE cells are characterized by expression of CD44<sup>high</sup>, CD62L<sup>low</sup>, and CD127<sup>low</sup> (26), and we evaluated this profile and other activation markers on the cells from anti-LFA-1-treated mice. The anti-LFA-1 blockade decreased the CD11a MFI on specific CD8<sup>+</sup> T cells surface by approximately 50%. In addition, treatment did not affect the phenotype of effector CD8<sup>+</sup> T cells as well as the expression of early and late activation markers, such as CD69 and CD44, respectively. Results obtained by Gérard and colleagues also showed that the absence of LFA-1 does not reduce the expression of CD69 on CD8<sup>+</sup> T cells (38).

The lower expression of CD95 in the cells induced upon vaccination was the main difference to CD8<sup>+</sup> T cells generated by the infection, which had higher levels of CD95 (25). There is an

increase in the expression of Fas/CD95 on some specific CD8<sup>+</sup> T cells after immunization and treatment with anti-LFA-1. This result suggests that specific CD8<sup>+</sup> T cells in mice treated with anti-LFA-1 may be more susceptible to programmed cell death by the extrinsic pathway. Similar results were shown by Borthwick and colleagues, who found that LFA-1 blockade reduces the survival of T lymphocytes, thus suggesting the important role of LFA-1 in survival signals during the process of T cells migration (39). Otherwise, reduction of migration to tissues upon LFA-1 blockade might increase effector CD8 T-cells expressing Fas in the secondary lymphoid organs.

Indeed, there is an impaired migration of specific CD8<sup>+</sup> T cells after LFA-1 blockade. The number of these cells was quantified in the spleen, heart, liver, lymph nodes, and blood after anti-LFA-1 treatment. The treatment led to an increase in the frequency and absolute number of specific CD8<sup>+</sup> T cells in the spleen and lymph node, and a decreased frequency mainly in the heart. However, despite the apparent decrease in the overall number of CD8 T cells in blood, this decrease was not statistically significant (Figure S2 in Supplementary Material). We have previously described that specific-peptide CD8<sup>+</sup> activation occurs in the lymph nodes after subcutaneous infection by *T. cruzi* and also in vaccinated model (12, 13). We approached this subject by administering the immunosuppressive drug FTY720 (12, 13). In both models, this drug reduced lymphocyte recirculation by interfering with T cell signaling *via* S1Pr1. This

interference resulted in inhibition of S1Pr1 signaling, effectively trapping T cells within the lymph node without inhibiting T cell activation. FTY720 administration significantly impaired protective immunity supporting the hypothesis that T cell recirculation is critical for the protective immunity they mediate (12, 13). Here, we have not addressed how these cells accumulate more in the lymph after treatment with anti-LFA-1. However, our data confirm that recirculation of these cells is necessary to exert their effector function in the peripheral tissues. Thus, blocking the integrin LFA-1, we observed the same accumulation not only in the lymph node but also in the spleen. However, in our immunization, infection, and treatment model, there was no change in the number of specific CD8<sup>+</sup> T cells in the peripheral blood (Figure S2 in Supplementary Material), probably because of the increased accumulation of CD8<sup>+</sup> T cells in the spleen and lymph node. This phenomenon may be specific to our immunization and infection model but has not yet been explored in details or found in another model. One explanation might be that the blockage of LFA-1 integrin expressed by CD8<sup>+</sup> T cells prevents the interactions with its ligand might be required to exit from lymph node. Another explanation might be due the decreased speed or movement of these cells (40). These issues need to be further addressed in our vaccination and infection model. These results confirm that LFA-1 is important to the migration of specific CD8<sup>+</sup> T cells into infected tissues such as the heart, and the decline of these cells should be one of the causes for increased parasitemia in that organ. Recent studies have shown that LFA-1 blockade, and not VLA-4, reduces migration speed of T lymphocytes, leading to decreased antigen scanning by T cells (41) and, hence, lower immune response and higher parasitemia.

We also evaluated whether anti-LFA-1 treatment would affect the effector function of specific CD8<sup>+</sup> T cells, since these cells accumulated in the spleen are incapable of controlling the number of parasites. We analyzed the production of pro-inflammatory cytokines, crucial for controlling *T. cruzi* multiplication, such as IFN- $\gamma$  and TNF- $\alpha$ , and observed that there was accumulation of polyfunctional specific CD8<sup>+</sup> T cells capable of degranulating and simultaneously producing TNF- $\alpha$  and IFN- $\gamma$  in the spleen, lymph node and liver. As the LFA-1 blockade retained CD8<sup>+</sup> T cells in the spleen and lymph node, we believe that this accumulation led to increased effector function of these cells. In the liver, in which there was no accumulation of such cells, the increase in intracellular cytokine production can be explained by the fact that LFA-1 blockade does not affect the production of those cytokines. In addition, it has been shown that high doses of anti-LFA-1 were required for impairing the production of those mediators (42). Finally, specific CD8<sup>+</sup> T cells proliferated after LFA-1 blockade, and this result was consistent with the data obtained by Gérard et al. (38).

Another important function triggered by specific CD8<sup>+</sup> T cells is the direct cytotoxicity against target cells. NK cytotoxic cells and CTLs of chagasic patients express perforin and granzyme B, suggesting the importance of these mediators to the host immune response (43). In addition, specific CD8<sup>+</sup> T cells induced by immunization are cytotoxic and can produce perforin (2). Anti-LFA-1 treatment decreased the 80% cytotoxicity of specific CD8<sup>+</sup> T cells in the immunized group to 60% after treatment. Similar results were obtained by Petit et al.,

whereas LFA-1 blockade was responsible for a 50% decrease of direct cytotoxicity triggered by CD8<sup>+</sup> T cells (42). In addition, the decrease in cytotoxicity is independent of cytotoxic granule production and degranulation because there was no decrease in the amount of granzyme B and CD107a in specific CD8<sup>+</sup> T cells treated with anti-LFA-1. We believe that cytotoxicity is impaired not because of the reduction of cytotoxic granules but because LFA-1 is important to maintain stability between target and cytotoxic cells. The role of LFA-1 in maintaining a stable contact between the cells was demonstrated by blocking  $\beta 2$  chain of LFA-1, since absence of such molecule impaired the formation time of cell protrusions, as well as the stability of the immunological synapse (44–47). Also, it has been shown that LFA-1 blockade impairs close contact between effector T cells and antigen-presenting cells (48).

The reduction of direct cytotoxicity may explain why specific CD8<sup>+</sup> T cells cannot control the number of parasites in the spleen even if accumulation of these cells occurs during LFA-1 blockade. In addition, our results suggest that LFA-1 plays an important role in the migration of specific CD8<sup>+</sup> T cells into the heart and the survival of these cells. Finally, we believe that impairment of direct cytotoxicity and lower migration of specific CD8<sup>+</sup> T cells into the heart are the major causes of lack of protection to *T. cruzi* infection upon immunization and treatment with anti-LFA-1.

## ETHICS STATEMENT

This study was carried out in strict accordance with the recommendations in the Guide for the Care and Use of Laboratory mice of the Brazilian National Council of Animal Experimentation (<http://www.cobea.org.br/>). The protocol was approved by the Committee on the Ethics of Animal Experiments of the Institutional Animal Care and Use Committee at the Federal University of São Paulo (Id # CEP 7559051115).

## AUTHOR CONTRIBUTIONS

CF, LC, and JV conceived and designed the experiments. CF, LC, FV, BM, CM, PR, and DA performed the experiments. CF and LC analyzed the data and prepared the figures. AM, RG, O-BR, and MR contributed with reagents and materials. CF and JV wrote the manuscript. ML, JL-V, CM, and BM performed the final review of the article. All the authors read and approved the final article.

## ACKNOWLEDGMENTS

This work is a tribute to the memory of Professor Mauricio Martins Rodrigues.

## FUNDING

This research was supported by the Fundação de Amparo à Pesquisa do Estado de São Paulo (FAPESP, programa Jovem Pesquisador Processo: 2012/22514-3), CF (processo FAPESP: 2015/08814-2); LC (Processo FAPESP: 2017/11499-7); BM (2014/19422-5). CF, LC, and BM were recipients of fellowship from FAPESP. JV, O-BR, ML, AM, RG, JL-V, DA, and

MR are recipients of fellowships from CNPq. CM and BCA are recipients of fellowships from Coordenação de Aperfeiçoamento de Pessoal de Nível Superior (CAPES). JL-V is recipient of fellowships from UFRJ. RG is supported by a grant from the US National Institutes of Health (NIAID R01AI116577).

## REFERENCES

- World Health Organization. *Chagas Disease (American trypanosomiasis)*. World Health Organization (2016). Available from: <http://www.who.int/chagas/epidemiology/en/>
- De Alencar BCG, Persechini PM, Haolla FA, Oliveira G, Silverio JC, Lannes-Vieira J, et al. Perforin and gamma interferon expression are required for CD4(+) and CD8(+) T-cell-dependent protective immunity against a human parasite, *Trypanosoma cruzi*, elicited by heterologous plasmid DNA prime-recombinant adenovirus 5 boost vaccination. *Infect Immun* (2009) 77(10):4383–95. doi:10.1128/IAI.01459-08
- Vasconcelos JRC, Hiyane MI, Marinho CRF, Claser C, Machado AV, Gazzinelli RT, et al. Protective immunity against *Trypanosoma cruzi* infection in a highly susceptible mouse strain after vaccination with genes encoding the amastigote surface protein-2 and trans-sialidase. *Hum Gene Ther* (2004) 15(9):878–86. doi:10.1089/hum.2004.15.878
- Machado AV, Cardoso JE, Claser C, Rodrigues MM, Gazzinelli RT, Bruna-Romero O. Long-term protective immunity induced against *Trypanosoma cruzi* infection after vaccination with recombinant adenoviruses encoding amastigote surface protein-2 and trans-sialidase. *Hum Gene Ther* (2006) 17(9):898–908. doi:10.1089/hum.2006.17.898
- Freel SA, Lamoreaux L, Chattopadhyay PK, Saunders K, Zarkowsky D, Overman RG, et al. Phenotypic and functional profile of HIV-inhibitory CD8 T cells elicited by natural infection and heterologous prime/boost vaccination. *J Virol* (2010) 84(10):4998–5006. doi:10.1128/JVI.00138-10
- Jaoko W, Karita E, Kayitenkore K, Omosa-Manyonyi G, Allen S, Than S, et al. Safety and immunogenicity study of multiclade HIV-1 adenoviral vector vaccine alone or as boost following a multiclade HIV-1 DNA vaccine in Africa. *Plos One* (2010) 5(9):e12873. doi:10.1371/journal.pone.0012873
- Koup RA, Roederer M, Lamoreaux L, Fischer J, Novik L, Nason MC, et al. Priming immunization with DNA augments immunogenicity of recombinant adenoviral vectors for both HIV-1 specific antibody and T-cell responses. *Plos One* (2010) 5(2):e9015. doi:10.1371/journal.pone.0009015
- Hill AV, Reyes-Sandoval A, O'Hara G, Ewer K, Lawrie A, Goodman A, et al. Prime-boost vectored malaria vaccines: progress and prospects. *Hum Vaccin* (2010) 6:78–83. doi:10.4161/hv.6.1.10116
- Schooley RT, Spritzler J, Wang H, Lederman MM, Havlir D, Kuritzkes DR, et al. AIDS clinical trials group 5197: a placebo-controlled trial of immunization of HIV-1-infected persons with a replication-deficient adenovirus type 5 vaccine expressing the HIV-1 core protein. *J Infect Dis* (2010) 202(5):705–16. doi:10.1086/655468
- De Rosa SC, Thomas EP, Bui J, Huang Y, deCamp A, Morgan C, et al. HIV-DNA priming alters T cell responses to HIV-adenovirus vaccine even when responses to DNA are undetectable. *J Immunol* (2011) 187(6):3391–401. doi:10.4049/jimmunol.1101421
- Chuang I, Sedegah M, Cicatelli S, Spring M, Polhemus M, Tamminga C, et al. DNA prime/adenovirus boost malaria vaccine encoding *P. falciparum* CSP and AMA1 induces sterile protection associated with cell-mediated immunity. *PLoS One* (2013) 8(2):e55571. doi:10.1371/journal.pone.0055571
- Vasconcelos JR, Dominguez MR, Neves RL, Ersching J, Araújo A, Santos LI, et al. Adenovirus vector-induced CD8<sup>+</sup> T effector memory cell differentiation and recirculation, but not proliferation, are important for protective immunity against experimental *Trypanosoma cruzi* infection. *Hum Gene Ther* (2014) 25(4):350–63. doi:10.1089/hum.2013.218
- Dominguez MR, Ersching J, Lemos R, Machado AV, Bruna-Romero O, Rodrigues MM, et al. Re-circulation of lymphocytes mediated by sphingosine-1-phosphate receptor-1 contributes to resistance against experimental infection with the protozoan parasite *Trypanosoma cruzi*. *Vaccine* (2012) 30(18):2882–91. doi:10.1016/j.vaccine.2012.02.037
- Hogg N, Laschinger M, Giles K, McDowell A. T-cell integrins: more than just sticking points. *J Cell Sci* (2003) 116(11):4695–705. doi:10.1242/jcs.00876
- Dustin ML. The cellular context of T cell signaling. *Immunity* (2009) 30(4):482–92. doi:10.1016/j.jimmuni.2009.03.010
- Shamri R, Grabovsky V, Gauguet JM, Feigelson S, Manevich E, Kolanus W, et al. Lymphocyte arrest requires instantaneous induction of an extended LFA-1 conformation mediated by endothelium-bound chemokines. *Nat Immunol* (2003) 6(5):497–506. doi:10.1038/ni1194
- Woolf E, Grigorova I, Sagiv A, Grabovsky V, Feigelson SW, Shulman Z, et al. Lymph node chemokines promote sustained T lymphocyte motility without triggering stable integrin adhesiveness in the absence of shear forces. *Nat Immunol* (2007) 8(10):1076–85. doi:10.1038/ni1499
- Glatigny S, Duhen R, Arbelaez C, Kumari S, Bettelli E. Integrin alpha L controls the homing of regulatory T cells during CNS autoimmunity in the absence of integrin alpha 4. *Sci Rep* (2015) 16(5):7834. doi:10.1038/srep07834
- Kwun J, Farris AB, Song H, Mahle WT, Burlingham WJ, Knechtle SJ. Impact of leukocyte function-associated antigen-1 blockade on endogenous allo-specific T cells to multiple minor histocompatibility antigen mismatched cardiac allograft. *Transplantation* (2015) 99(12):2485–93. doi:10.1097/TP.0000000000000805
- Harning R, Pelletier J, Lubke K, Takei F, Merluzzi VJ. Reduction in the severity of graft-versus-host disease and increased survival in allogenic mice by treatment with monoclonal antibodies to cell adhesion antigens LFA-1 alpha and MALA-2. *Transplantation* (1991) 52:842–5. doi:10.1097/00007890-199111000-00017
- Kariya T, Ueta H, Xu XD, Koga D, Ezaki T, Yu E, et al. Direct evidence for activated CD8<sup>+</sup> T cell transmigration across portal vein endothelial cells in liver graft rejection. *J Gastroenterol* (2016) 51(10):985–98. doi:10.1007/s00535-016-1169-1
- Dos Santos PV, Roffé E, Santiago HC, Torres RA, Marino AP, Paiva CN, et al. Prevalence of CD8(+) alpha beta T cells in *Trypanosoma cruzi*-elicited myocarditis is associated with acquisition of CD62Llow LFA-1 highVLA-4 high activation phenotype and expression of IFN-gamma-inducible adhesion and chemoattractant molecules 1. *Microbes Infect* (2001) 3:971–84. doi:10.1016/S1286-4579(01)01461-7
- Silvero JC, Pereira IR, Cipitelli Mda C, Vinagre NF, Rodrigues MM, Gazzinelli RT, et al. CD8<sup>+</sup> T-cells expressing interferon gamma or perforin play antagonistic roles in heart injury in experimental *Trypanosoma cruzi*-elicited cardiomyopathy. *PLoS Pathog* (2012) 8(4):e1002645. doi:10.1371/journal.ppat.1002645
- Michailowsky V, Celes MR, Marino AP, Silva AA, Vieira LQ, Rossi MA, et al. Intercellular adhesion molecule 1 deficiency leads to impaired recruitment of T lymphocytes and enhanced host susceptibility to infection with *Trypanosoma cruzi*. *J Immunol* (2004) 1:463–70. doi:10.4049/jimmunol.173.1.463
- Vasconcelos JR, Bruna-Romero O, Araújo AF, Domínguez MR, Ersching J, de Alencar BC, et al. Pathogen-induced proapoptotic phenotype and high CD95 (Fas) expression accompany a suboptimal CD8<sup>+</sup> T-cell response: reversal by adenoviral vaccine. *PLoS Pathog* (2012) 8(5):e1002699. doi:10.1371/journal.ppat.1002699
- Rigato PO, de Alencar BC, Vasconcelos JR, Domínguez MR, Araújo AF, Machado AV, et al. Heterologous plasmid DNA prime-recombinant human adenovirus 5 boost vaccination generates a stable pool of protective long-lived CD8<sup>+</sup> T effector memory cells specific for a human parasite, *Trypanosoma cruzi*. *Infect Immun* (2011) 79(5):2120–30. doi:10.1128/IAI.01190-10
- Tzelepis F, de Alencar BC, Penido ML, Gazzinelli RT, Persechini PM, Rodrigues MM. Distinct kinetics of effector CD8<sup>+</sup> cytotoxic T cells after infection with *Trypanosoma cruzi* in naïve or vaccinated mice. *Infect Immun* (2006) 74(4):2477–81. doi:10.1128/IAI.74.4.2477-2481.2006

## SUPPLEMENTARY MATERIAL

The Supplementary Material for this article can be found online at <http://www.frontiersin.org/article/10.3389/fimmu.2017.01291/full#supplementary-material>.

28. Reisman N, Floyd T, Wagener M, Kirk A, Larsen C, Ford M. LFA-1 blockade induces effector and regulatory T-cell enrichment in lymph nodes and synergizes with CTLA-4lg to inhibit effector function. *Blood* (2011) 118(22):5851–61. doi:10.1182/blood-2011-04-347252
29. Piron M, Fisa R, Casamitjana N, López-Chejade P, Puig L, Vergés M, et al. Development of a real-time PCR assay for *Trypanosoma cruzi* detection in blood samples. *Acta Trop* (2007) 103(3):195–200. doi:10.1016/j.actatropica.2007.05.019
30. Hintermann E, Ehser J, Christen U. The CYP2D6 animal model: how to induce autoimmune hepatitis in mice. *J Vis Exp* (2012) 3(60):3644. doi:10.3791/3644
31. Gutierrez F, Mariano F, Oliveira C, Pavanelli W, Guedes P, Silva G, et al. Regulation of *Trypanosoma cruzi*-induced myocarditis by programmed death cell receptor 1. *Infect Immun* (2011) 79:1873–81. doi:10.1128/IAI.01047-10
32. Zhang L, Tarleton RL. Persistent production of inflammatory and anti-inflammatory cytokines and associated MHC and adhesion molecule expression at the site of infection and disease in experimental *Trypanosoma cruzi* infections. *Exp Parasitol* (1996) 84(2):203–13. doi:10.1006/expp.1996.0106
33. Martin SD, Spinger TA. Intercellular adhesion de-1 (CAM-1) is a ligand for lymphocyte function-associated antigen 1 (LFA-1). *Cell* (1987) 51:813–9. doi:10.1016/0092-8674(87)90104-8
34. Rahman A, Fazal F, Hug tightly and say goodbye: role of endothelial ICAM-1 in leukocyte transmigration. *Antioxid Redox Signal* (2009) 11(4):823–39. doi:10.1089/ARS.2008.2204
35. Ley K. Pathways and bottlenecks in the web of inflammatory adhesion molecules and chemoattractants. *Immunol Res* (2001) 24(1):87–95. doi:10.1385/IR:24:1:87
36. Bachmann MF, McKall-Faienza K, Schmits R, Bouchard D, Beach J, Speiser DE, et al. Distinct roles for LFA-1 and CD28 during activation of naive T cells: adhesion versus costimulation. *Immunity* (1997) 7:549–57. doi:10.1016/S1074-7613(00)80376-3
37. Mori M, Hashimoto M, Matsuo T, Fujii T, Furu M, Ito H, et al. Cell-contact-dependent activation of CD4+ T cells by adhesion molecules on synovial fibroblasts. *Mod Rheumatol* (2017) 27(3):448–56. doi:10.1080/14397595.2016.1220353
38. Gérard A, Khan O, Beemiller P, Oswald E, Hu J, Matloubian M, et al. Secondary T cell–T cell synaptic interactions drive the differentiation of protective CD8+ T cells. *Nat Immunol* (2013) 14(4):356–63. doi:10.1038/ni.2547
39. Borthwick NJ, Akbar AA, Buckley C, Pilling D, Salmon M, Jewell AP, et al. Transendothelial migration confers a survival advantage to activated T lymphocytes: role of LFA-1/ICAM-1 interactions. *Clin Exp Immunol* (2003) 134:246–52. doi:10.1046/j.1365-2249.2003.02298.x
40. Reichardt P, Patzak I, Jones K, Etemire E, Gunzer M, Hogg N. A role for LFA-1 in delaying T-lymphocyte egress from lymph nodes. *EMBO J* (2013) 32(6):829–43. doi:10.1038/emboj.2013.33
41. Katakai T, Habiro K, Kinashi T. Dendritic cells regulate high-speed interstitial T cell migration in the lymph node via LFA-1/ICAM-1. *J Immunol* (2013) 191(3):1188–99. doi:10.4049/jimmunol.1300739
42. Petit AE, Demotte N, Scheid B, Wildmann C, Bigirimana R, Gordon-Alonso M, et al. A major secretory defect of tumour-infiltrating T lymphocytes due to galectin impairing LFA-1-mediated synapse completion. *Nat Commun* (2016) 7:12242. doi:10.1038/ncomms12242
43. Dotiwala F, Mulik S, Polidoro RB, Ansara JA, Burleigh BA, Walch M, et al. Killer lymphocytes use granzysin, perforin and granzymes to kill intracellular parasites. *Nat Med* (2016) 22(2):210–6. doi:10.1038/nm.4023
44. Hivrozand C, Saitaki M. Biophysical aspects of T lymphocyte activation at the immune synapse. *Front Immunol* (2016) 15(7):46. doi:10.3389/fimmu.2016.00046
45. Kinashi T. Intracellular signalling controlling integrin activation in lymphocytes. *Nat Rev Immunol* (2005) 5(7):546–59. doi:10.1038/nri1646
46. Sigal A, Bleijs DA, Grabovsky V, van Vliet SJ, Dwir O, Figdor CG, et al. The LFA-1 integrin supports rolling adhesions on ICAM-1 under physiological shear flow in a permissive cellular environment. *J Immunol* (2000) 165:442–52. doi:10.4049/jimmunol.165.1.442
47. Morgan MM, Labno CM, Van Seventer GA, Denny MF, Straus DB, Burkhardt JK. Superantigen-induced T cell: B cell conjugation is mediated by LFA-1 and requires signaling through Lck, but not ZAP-70. *J Immunol* (2001) 167:5708–18. doi:10.4049/jimmunol.167.10.5708
48. Friedman RS, Jacobelli J, Krummel MF. Surface-bound chemokines capture and prime T cells for synapse formation. *Nat Immunol* (2006) 7(10):1101–8. doi:10.1038/ni1384

**Conflict of Interest Statement:** The authors declare that the research was conducted in the absence of any commercial or financial relationships that could be construed as a potential conflict of interest.

Copyright © 2017 Ferreira, Cariste, Santos Virgílio, Moraschi, Monteiro, Vieira Machado, Gazzinelli, Bruna-Romero, Menin Ruiz, Ribeiro, Lannes-Vieira, Lopes, Rodrigues and Vasconcelos. This is an open-access article distributed under the terms of the Creative Commons Attribution License (CC BY). The use, distribution or reproduction in other forums is permitted, provided the original author(s) or licensor are credited and that the original publication in this journal is cited, in accordance with accepted academic practice. No use, distribution or reproduction is permitted which does not comply with these terms.



# Vaccine Containing the Three Allelic Variants of the *Plasmodium vivax* Circumsporozoite Antigen Induces Protection in Mice after Challenge with a Transgenic Rodent Malaria Parasite

## OPEN ACCESS

### Edited by:

Abdul Qader Abbady,  
Atomic Energy Commission of Syria,  
Syria

### Reviewed by:

Stasya Zarling,  
Walter Reed Army Institute of  
Research, United States  
Geert Leroux-Roels,  
Ghent University, Belgium

### \*Correspondence:

Irene S. Soares  
isoares@usp.br

*<sup>†</sup>In memoriam.*

### Specialty section:

This article was submitted to  
Vaccines and Molecular  
Therapeutics,  
a section of the journal  
Frontiers in Immunology

**Received:** 30 May 2017

**Accepted:** 25 September 2017

**Published:** 11 October 2017

### Citation:

Gimenez AM, Lima LC, Françoso KS,  
Denapoli PMA, Paratieri R,  
Bargieri DY, Thibierge J-M,  
Andolina C, Nosten F, Renia L,  
Nussenzweig RS, Nussenzweig V,  
Amino R, Rodrigues MM and  
Soares IS (2017) Vaccine Containing  
the Three Allelic Variants of the  
*Plasmodium vivax* Circumsporozoite  
Antigen Induces Protection in Mice  
after Challenge with a Transgenic  
Rodent Malaria Parasite.  
Front. Immunol. 8:1275.  
doi: 10.3389/fimmu.2017.01275

Alba Marina Gimenez<sup>1</sup>, Luciana Chagas Lima<sup>1,2</sup>, Katia Sanches Françoso<sup>2</sup>,  
Priscila M. A. Denapoli<sup>1</sup>, Raquel Panatieri<sup>3,4</sup>, Daniel Y. Bargieri<sup>4</sup>, Jean-Michel Thibierge<sup>3</sup>,  
Chiara Andolina<sup>5,6</sup>, Francois Nosten<sup>5,6</sup>, Laurent Renia<sup>7</sup>, Ruth S. Nussenzweig<sup>8</sup>,  
Victor Nussenzweig<sup>8</sup>, Rogerio Amino<sup>3</sup>, Mauricio M. Rodrigues<sup>1†</sup> and Irene S. Soares<sup>2\*</sup>

<sup>1</sup>Department of Microbiology, Immunology and Parasitology, Center of Cellular and Molecular Therapy (CTCMol), Federal University of São Paulo, São Paulo, Brazil, <sup>2</sup>Department of Clinical and Toxicological Analyses, School of Pharmaceutical Sciences, University of São Paulo, São Paulo, Brazil, <sup>3</sup>Unit of Malaria Infection and Immunity, Institut Pasteur, Paris, France,

<sup>4</sup>Department of Parasitology, University of São Paulo, São Paulo, Brazil, <sup>5</sup>Shoklo Malaria Research Unit, Mahidol-Oxford Tropical Medicine Research Unit, Faculty of Tropical Medicine, Mahidol University, Mae Sot, Thailand, <sup>6</sup>Centre for Tropical Medicine and Global Health, Nuffield Department of Medicine Research Building, University of Oxford, Oxford, United Kingdom, <sup>7</sup>Singapore Immunology Network, Biopolis, Agency for Science Technology and Research, Singapore, Singapore,

<sup>8</sup>New York University School of Medicine, New York, NY, United States

*Plasmodium vivax* is the most common species that cause malaria outside of the African continent. The development of an efficacious vaccine would contribute greatly to control malaria. Recently, using bacterial and adenoviral recombinant proteins based on the *P. vivax* circumsporozoite protein (CSP), we demonstrated the possibility of eliciting strong antibody-mediated immune responses to each of the three allelic forms of *P. vivax* CSP (PvCSP). In the present study, recombinant proteins representing the PvCSP alleles (VK210, VK247, and *P. vivax*-like), as well as a hybrid polypeptide, named PvCSP-All epitopes, were generated. This hybrid containing the conserved C-terminal of the PvCSP and the three variant repeat domains in tandem were successfully produced in the yeast *Pichia pastoris*. After purification and biochemical characterization, they were used for the experimental immunization of C57BL/6 mice in a vaccine formulation containing the adjuvant Poly(I:C). Immunization with a recombinant protein expressing all three different allelic forms in fusion elicited high IgG antibody titers reacting with all three different allelic variants of PvCSP. The antibodies targeted both the C-terminal and repeat domains of PvCSP and recognized the native protein on the surface of *P. vivax* sporozoites. More importantly, mice that received the vaccine formulation were protected after challenge with chimeric *Plasmodium berghei* sporozoites expressing CSP repeats of *P. vivax* sporozoites (Pb/PvVK210). Our results suggest that it is possible to elicit protective immunity against one of the most common PvCSP alleles using soluble recombinant proteins expressed by *P. pastoris*. These recombinant proteins are promising candidates for clinical trials aiming to develop a multiallele vaccine against *P. vivax* malaria.

**Keywords:** malaria, *Plasmodium vivax*, recombinant vaccine, circumsporozoite protein, prime-boost regimens

## INTRODUCTION

Morbidity due to malaria is prevalent worldwide and is reflected by millions of cases every year, which are almost entirely attributable to *Plasmodium falciparum* and *Plasmodium vivax* parasite species infection (1). *P. vivax* is the most geographically widespread species of human malaria, predominating in the regions of North and South America, South and Southeast Asia, Western Pacific, and Eastern Mediterranean; according to the WHO 2015 World Malaria Report, this malarial species was responsible for 13.8 million cases worldwide in 2015 (1). Complicated malaria and deaths due to *P. vivax* malaria have been reported in different endemic regions (2). Despite the studies on *P. vivax* malaria being neglected in the last few decades (3–5), currently, there is a consensus that studies aiming to control and eliminate this important tropical disease are of high priority (6). In this context, the development of a *P. vivax* vaccine would represent a great advancement in malaria control strategies. Unfortunately, only four clinical trials based on the *P. vivax* antigens (PvDBP, ScPvs25, N-R&C peptides and VMP001) have been completed according to the NIH website.<sup>1</sup>

The circumsporozoite protein (CSP) is the most abundant component of sporozoite surface and is involved in the initial stages of invasion of mammalian host hepatocytes [reviewed in Ref. (7, 8)]. As the first protein associated with an effective protection against malaria (9, 10), the majority of trials in experimental animals and humans are based on the CSP. This protein is an important target for antibodies and CD4<sup>+</sup> and CD8<sup>+</sup> T cells that can eliminate the preerythrocytic stages of the parasite (11). RTS,S, the most advanced vaccine so far, directed to the *P. falciparum* CSP, now named as Mosquirix™, is currently scheduled to begin a pilot phase in sub-Saharan Africa in 2018, according to WHO program (12). This formulation uses the hepatitis B surface antigen as a matrix for the conserved C-terminal portion and central repeat domain of CSP combined to powerful adjuvant systems (AS), which is a liposomal suspension (AS01) presentation of the immunostimulants monophosphoryl lipid A (MPL) and saponin purified from *Quillaja saponaria* (QS21). The Phase III efficacy of RTS,S against all malaria episodes between children and young infants residents of African endemic areas ranges from 28% (three-dose group) to 36% (four-dose group) (13). These promising RTS,S results justify investment in the CSP as a target for *P. vivax* vaccines.

As described for the CSPs of other species of *Plasmodium*, the primary structure of *P. vivax* CSP (PvCSP) has three major defined domains. The central repeat domain is flanked by highly conserved regions, the N- and C-terminal domains. All three domains can be targets of specific antibodies. However, only antibodies directed against the central repeat domain of PvCSP have been associated to protective efficacy against *P. vivax* in *Aotus nancymaae* monkeys (14). Sequencing of the genes encoding the CSPs of different strains of *P. vivax* uncovered the presence of three different alleles at the central repeat domain. These alleles have been described in different parts of the world (15–19).

This strain diversity adds complexity for the development of a multiallelic vaccine against *P. vivax* malaria. The CSPs designated VK210, VK247, and *P. vivax*-like are almost identical in their N- and C-terminal domains, but differ in the central repeat region.

*P. vivax* CSP-derived antigens have been combined into multivalent formulations or chimeric synthetic molecules in attempts to obtain protective immunity against *P. vivax*. Recombinant PvCSP-derived proteins expressed in *Escherichia coli* and yeast were tested as vaccines with very limited success (20) and thus were not pursued further. Peptides based on the N-terminal region, central repeats, and C-terminal region of PvCSP-VK210 formulated in Montanide ISA 720 or Montanide ISA 51 adjuvants were immunogenic in BALB/c mice, *Aotus* monkeys (21), and healthy human volunteers (22). Recently, a PvCSP-based vaccine named Rv21 was demonstrated to be highly protective against challenge in rodent models to malaria (23). However, these vaccines did not consider the three allelic variants of PvCSP.

The most advanced recombinant protein formulation for *P. vivax* is the vaccine VMP001 (vivax malaria protein 001) (24). VMP001, obtained in bacteria *E. coli*, merges the central variant epitopes of VK210 and VK247 flanked by the amino- and carboxy-terminal regions of PvCSP, and was immunogenic in C57BL/6 (25), *Rhesus* monkeys (26), and human naive volunteers (27). The clinical trial results from Phase I/IIa showed VMP001 to be immunogenic, inducing humoral and cellular immune responses to the vaccine antigen. A significant delay in time to parasitemia was seen in 59% of vaccinated subjects compared to the control group. However, vaccination did not induce sterile protection (27). Immunogenicity to PvCSP was also achieved by our group, with *E. coli* constructs fusing all of the three variants, in C57BL/6 mice (28, 29). In these studies, the induced antibodies against the PvCSP chimeric constructs were able to recognize epitopes from each of the variants (VK210, VK247, and *P. vivax*-like) inserted in the central region (28, 29). However, the recombinant PvCSP used in these studies were expressed using prokaryotic systems as insoluble proteins, complicating large scale production. Thus, antigen expression as soluble secreted proteins using eukaryotic systems such as *Pichia pastoris* may represent a long-term advantage in an effort to solve this problem.

Based on these findings, we generated three new recombinant proteins based on the central regions of these variants, that contain immunodominant epitopes for B cells, and the conserved C-terminal region of PvCSP. Additionally, we generated a fourth recombinant protein, which contains the C-terminal region and epitopes from the three *P. vivax* CSP alleles fused as a single polypeptide, called yPvCSP-All epitopes. All recombinant proteins were successfully produced as soluble secreted proteins in the yeast *P. pastoris*. The present study describes the immunogenicity of the different formulations and analysis for protection against the PvCSP-VK210 allele.

## MATERIALS AND METHODS

### Ethics Statement

This study was performed in strict accordance with the recommendations in the Guide for the Care and Use of Laboratory

<sup>1</sup><https://clinicaltrials.gov>.

Animals of the Brazilian National Council for the Control of Animal Experimentation (CONCEA).<sup>2</sup> The protocol was approved by the Committees on the Ethics of Animal Experiments of the Faculty of Pharmaceutical Sciences of University of São Paulo, Brazil (CEUA No. 362/2012), and the Institutional Animal Care and Use Committee at the Federal University of São Paulo (CEP No. 0172/12 and CEUA No. 1463171214). The study with human blood obtained from infected Thai patients was approved by Oxford Tropical Research Ethics Committee (reference OX28-09).

## Recombinant Proteins Expressed in *P. pastoris* Yeast

### Genetic Design and Construction of yPvCSP Recombinant Proteins

Synthetic genes encoding the recombinant proteins yPvCSP-VK210, yPvCSP-VK247, yPvCSP-*P. vivax*-like, and yPvCSP-All epitopes were synthetized by GenScript USA, Inc. (Piscataway, NJ, USA) using codon optimization to improve expression in *P. pastoris*. Figure 1 shows a schematic representation of these

recombinant proteins. The synthetic genes were cloned into the pUC57 vector and were subsequently subcloned into the *P. pastoris* expression vector pPIC9K (Invitrogen, Carlsbad, CA, USA). Amplified plasmids were linearized with *Sal*I and transformed into the GS115 strain (*his4*<sup>-</sup>) of *P. pastoris* by electroporation. Clones transformed with plasmid pPIC9K-PvCSP-VK210, pPIC9K-PvCSP-VK247, pPIC9K-PvCSP-*P. vivax*-like, or pPIC9K-PvCSP-All epitopes were screened for high copy-number integration by G418 selection, according to the manufacturer's instructions (Pichia Expression Kit, Invitrogen).

### Expression and Purification of Recombinant Proteins

Clones with a Mut<sup>+</sup> phenotype that were secreting high levels of each recombinant protein were selected. The induction of protein expression was performed as described, with some modifications (30). A Mut<sup>+</sup> transformant was initially grown overnight in 200 mL of BMGY medium (1% w/v yeast extract, 2% w/v peptone, 1.34% w/v yeast nitrogen base without amino acids, 4 × 10<sup>-5</sup>% w/v biotin, 1% w/v glycerol, and 0.1 M potassium phosphate, pH 6.0) at 28–30°C with vigorous shaking. The cells were harvested, resuspended in 1 L BMMY (BMGY with glycerol replaced with 0.5% v/v methanol), and incubated again for 72 h. Methanol was added every 24 h to a final concentration of 1% v/v. After induction for 72 h, the cells were removed by centrifugation and the culture supernatant was clarified by filtration with a 0.45-μm membrane (Merck Millipore, MA, USA). The supernatant was applied to a HisTrap FF column coupled to a FPLC ÄKTA prime plus (GE Healthcare, Chicago, IL, USA), which was previously equilibrated with 20 mM sodium phosphate/0.5 M NaCl, pH 8.0. Bound proteins were eluted with a 0–500 mM imidazole (Sigma-Aldrich, St. Louis, MO, USA) gradient in 20 mM sodium phosphate/0.5 M NaCl, pH 8.0. Fractions containing protein were detected by SDS-PAGE and Coomassie blue staining, pooled, and used in a second-purification step by anionic exchange chromatography using a Resource Q column coupled to a FPLC ÄKTA prime plus (GE Healthcare, Chicago, IL, USA). The protein was eluted using a 0–1 M NaCl linear gradient in 20 mM Tris-HCl, pH 8.0, and analyzed by SDS-PAGE. The peaks corresponding to each recombinant protein that had a high degree of purity were collected and dialyzed against phosphate-buffered saline (PBS). The protein concentration was determined by the Bradford method (BioRad, Hercules, CA, USA) using bovine serum albumin (BSA; Sigma-Aldrich, St. Louis, MO, USA) as a standard.

### Characterization of Recombinant yPvCSP Immunoblotting

For immunologic characterization, the recombinant proteins were fractionated by 12% SDS-PAGE under reducing conditions and were transferred from the gel to nitrocellulose membranes (Hybond N, GE Healthcare, Chicago, IL, USA). The membranes were blocked for up to 1 h using fat free milk in PBS (5% w/vol) and bovine serum albumin (2% w/vol) containing 0.1% Tween 20 (PBS-T). The blots were incubated for 1 h at room temperature (RT) with the appropriate primary antibody diluted in PBS-T, as described (31). The primary antibodies used were (i) mouse monoclonal antibodies (MAbs) to His<sub>6</sub> (GE Healthcare, Chicago, IL, USA) diluted 1:1,000; (ii) MAb 2F2 (MRA-184) to PvCSP from

<sup>2</sup><http://www.mctic.gov.br/mctic/opencms/textogeral/concea.html>.

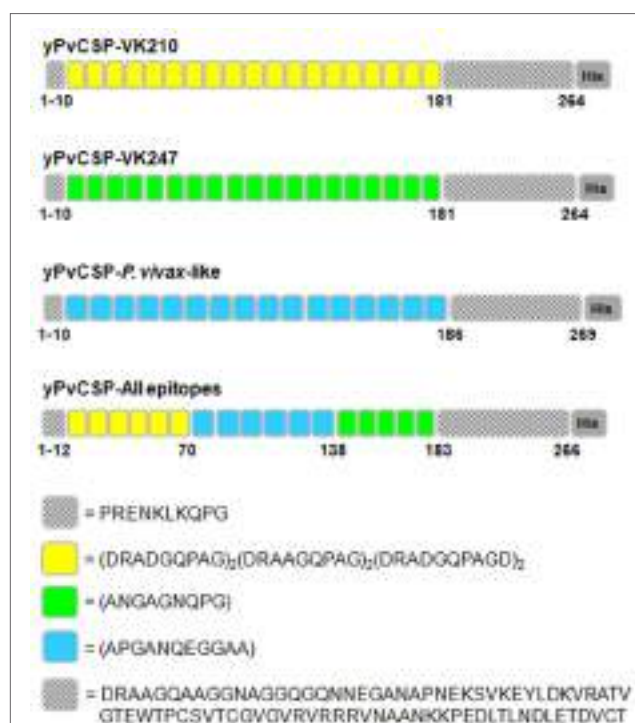


**FIGURE 1 |** Schematic representation of the *Plasmodium vivax* circumsporozoite protein (CSP) recombinant antigens. The individual recombinant proteins have the specific individual repeats [yPvCSP-VK210 ( $n = 19$ ), yPvCSP-VK247 ( $n = 19$ ), or yPvCSP-*P. vivax*-like ( $n = 16$ )] and the C-terminal (CT) region. For each repeat sequence, the amino acids positions and the histidine tag are indicated. The classic repeat sequence VK210 is represented in yellow, VK247 in green, and *P. vivax*-like in blue. The yPvCSP-All epitopes merges the repeats of all three allelic variants described above ( $n = 6/6/5$  repeat sequences of VK210/*P. vivax*-like/VK247, respectively) and the CT region.

the VK210 strain (1 µg/mL) (32); and (iii) MAb 2E10E9 (MRA-185) to PvCSP from the VK247 strain (1 µg/mL) developed by Dr. Alan Cochrane (Unpublished data). The hybridomas used for the production of MRA-184 and MRA-185 were obtained from the Malaria Research and Reference Reagent Resource Center (MR4), Manassas, VA, USA.

After washing twice with PBS-T, peroxidase-labeled goat anti-mouse IgG (Sigma-Aldrich, St. Louis, MO, USA) diluted 1:1,000 in PBS-T was added for 1 h. The reaction was developed using a chemiluminescence detection assay (ECL, GE Healthcare, Chicago, IL, USA).

### Reverse-Phase High-Performance Liquid Chromatography (RP-HPLC)

Purified proteins were analyzed by RP-HPLC using a C18 column (4.6 × 250 mm; 300 µm particle size) coupled to an HPLC LCMS-2020 LC/MS system (Shimadzu, Kyoto, Japan). The HPLC procedure was performed at RT ( $\approx$ 25°C) using a binary gradient of 0.1% trifluoroacetic acid (TFA, Solvent A) and 0.1% TFA in a 9:1 (v/v) solution of acetonitrile:water (Solvent B) with a two-step solvent gradient starting at 0–20%, followed by 20–100%, at a rate of 1 mL/min for 40 min. The elution was monitored with a UV-Visible absorbance detector (Shimadzu SPD M20A) at 220 and 280 nm.

### Recombinant Proteins Expressed in *E. coli*

In order to determine the specificity of IgG antibodies, flagellin-fusion proteins His<sub>6</sub>FliC-PvCS-VK210 (31), His<sub>6</sub>FliC-PvCS-VK247 and His<sub>6</sub>FliC-PvCS-*P. vivax*-like (28), were used individually on ELISA plates for analyzing the specificity of the antibodies against each of the repeats sequences, as these proteins do not have the C-terminal region. The His<sub>6</sub>FliC protein (31), used as a carrier for the individual repeat sequences, is a recombinant flagellin derived from *Salmonella Typhimurium* and produced in *E. coli*. In order to determine the specificity of the antibodies against C-terminal region, No repeats protein (29) was used. This recombinant protein contains only the PvCSP N-terminal region fused with the C-terminal region.

These recombinant proteins were produced in *E. coli* using the method previously described (33). Following this, purification was performed by affinity chromatography (HisTrap FF column, GE Healthcare, Chicago, IL, USA) and subsequent anion-exchange chromatography (Resource Q column, GE Healthcare, Chicago, IL, USA) as described above.

### Immunization Schedule

For immunological assays, 6–8 weeks old C57BL/6 female mice were subcutaneously (s.c.) immunized thrice, following the schedule described in the figures ( $n = 6$  mice per group). For each dose, the indicated amount of protein was administered with high-molecular-weight Poly(I:C) adjuvant (50 µg/dose/mouse) (InvivoGen, San Diego, CA, USA). A volume of 50 µL was injected s.c. into each footpad (first dose) and a final volume of 100 µL was injected s.c. at the base of the tail (second and third doses). After each immunization, blood was collected from the tail, and the sera were analyzed for the presence of antibodies

against each recombinant protein. For the protection experiment, mice were intraperitoneally immunized thrice, following the schedule described in Figure 8A.

## Immunological Assays

### Antibody Measurement

Antibodies against each recombinant protein in mouse sera were detected by enzyme-linked immunosorbent assay (ELISA), as described previously (29). The recombinant proteins were employed as solid phase-bound antigens (200 ng/well), and a volume of 50 µL of each solution was added to each well of a 96-well plate. After overnight incubation at RT, plates were washed with a solution of PBS and 0.05% PBS-T and blocked with a solution of PBS, 2.5% (w/v) skimmed milk, and 2.5% BSA for 2 h at 37°C. Serial dilutions (1/2) of murine polyclonal sera (100 µL) were added to wells in duplicate, followed by incubation for 1 h at 37°C. After washing with PBS-T, 50 µL aliquots of peroxidase-labeled goat anti-mouse IgG (Sigma, St. Louis, MO, USA), diluted 1:1,000, were added to each well and incubated for 1 h at 37°C. The enzymatic reaction was developed with o-phenylenediamine (1 mg/mL) (Sigma) diluted in phosphate-citrate buffer (pH 5.0) containing hydrogen peroxide [0.03% (vol/vol)]. The enzymatic reaction was stopped by the addition of 50 µL of a solution containing 4 N H<sub>2</sub>SO<sub>4</sub>. The optical density at 492 nm (OD<sub>492</sub>) was measured using a SpectraMax Plus 384 Microplate Reader. Anti-PvCSP titers were determined based on the highest dilution of sera that yielded an A<sub>492</sub> higher than 0.1. This cut-off value was set at 3 SDs above the mean A<sub>492</sub> obtained from naïve mice against the recombinant proteins.

For detection of IgG subclass responses, secondary antibodies specific to mouse IgG1, IgG2b, and IgG2c were used (Southern Technologies, Chattanooga, TN, USA). Results are expressed as the mean values of IgG titers  $\pm$  SD.

### Immunofluorescence Assay

*Anopheles cracens* mosquitoes were fed on human blood obtained from infected Thai patients using Hemotek® membrane-feeding system (34). After 2 weeks, aseptically dissected infected salivary glands were disrupted in a glass tissue grinder and the sporozoite preparation was deposited on glass slides. Slides were dried at RT and kept frozen at –20°C before use.

Slides containing wild-type VK210 *P. vivax* sporozoites were fixed with cold methanol for 10 min and blocked with PBS–3% BSA for 30 min at RT. Slides were then incubated in a humid chamber for 1 h at RT with sera from mice immunized with the mix of the three CSP alleles (VK210, VK247, and *P. vivax*-like) or with the yPvCSP-All epitopes recombinant protein (dilution 1:100 in PBS–3% BSA). MAb 2F2 (anti-PvCSP-VK210) and sera from mice immunized with adjuvant only (dilution 1:50 in PBS–3% BSA) were used as a positive and negative controls, respectively. Slides were washed three times with PBS-T before the addition of a dilution 1:500 in PBS–3% BSA of anti-mouse IgG conjugated to Alexa Flour 568 (Thermo Fisher Scientific, Waltham, MA, USA). The slides were incubated for 1 h at RT, washed three times with PBS-T and incubated for 15 min with 4',6-Diamidino-2-Phenylindole Dihydrochloride (DAPI, Invitrogen, Carlsbad, CA, USA). Binding was visualized using a fluorescence microscope

DMI6000B/AF6000 (Leica) coupled to a digital camera system (DFC 365 FX) and the images were treated and analyzed using the open-source software ImageJ.

### Cytokine Measurement

To measure the number of cells secreting interferon gamma (IFN- $\gamma$ ), splenocytes collected from immunized C57BL/6 mice were used for enzyme-linked immunospot (ELISPOT) assays. This procedure was performed by using mouse IFN- $\gamma$  capture antibody (BD Biosciences) to coat flat-bottom Multiscreen HTS plates (Millipore) overnight at 4°C. After three washes with PBS-T, the plates were blocked with R10 [(fetal calf serum (10%) (v/v), RPMI 1640), Gibco], for 2 h at 37°C and 5  $\times$  10<sup>5</sup> cells/well mice splenocytes were stimulated overnight at 37°C, 5% CO<sub>2</sub>, in the presence of recombinant proteins (yPvCSP-VK210, yPvCSP-VK247, yPvCSP-*P. vivax*-like, and yPvCSP-All epitopes, 10 mg/mL) or ConA (2.5 mg/mL) diluted in RPMI 1640-IL2 [IL-2 0.03% (v/v)]. Plates were then washed 3 times with PBS, and mouse IFN- $\gamma$  detection antibody biotinylated [XMG 1.2, (1:200), Pharmingen] was added to the plates overnight at 4°C. Streptavidin-labeled peroxidase [(1:500), BD, Biosciences] was added to the plates, after six PBS-T washes, for 2 h and spots were visualized with 4',6-diamidino-2-phenylindole, dihydrochloride (1 mg/mL).

To determine the intracellular expression of IFN- $\gamma$  and tumor necrosis factor alpha (TNF- $\alpha$ ), intracellular cytokine staining (ICS) was used. These assays were performed as in previous studies (29, 35). Basically, ICS was evaluated following the *in vitro* culture of splenocytes in the presence or absence of an antigenic stimulus. Cells were washed three times in RPMI 1640 medium (pH 7.4) and resuspended in cell culture medium consisting of RPMI 1640 medium (pH 7.4) supplemented with 10 mM HEPES, 0.2% sodium bicarbonate, 59 mg/L of penicillin, 133 mg/L of streptomycin, and 10% fetal bovine serum (Hyclone, Logan, UT, USA). Cell viability was evaluated using 0.2% trypan blue exclusion dye. Cell density was adjusted to 5  $\times$  10<sup>6</sup> cells/mL in cell culture media containing anti-CD28 (2  $\mu$ g/mL), BD GolgiPlug (10  $\mu$ g/mL), monensin (5  $\mu$ g/mL), and FITC-labeled anti-CD107a (2  $\mu$ g/mL). Final concentrations of 10  $\mu$ g/mL of the indicated recombinant proteins or 2  $\mu$ g/mL of Concanavalin A (ConA; Sigma-Aldrich, St. Louis, MO, USA) were added. The cells were cultivated in V-bottom 96-well plates (Corning, New York, NY, USA) in a final volume of 200  $\mu$ L in duplicate, at 37°C in a humid environment containing 5% CO<sub>2</sub>. After a 12 h incubation, cells were stained for surface markers with PerCP-Cy5.5-labeled anti-CD4 (clone RM4-5) or PE Cy7-labeled CD8 (clone 53-6.7) on ice for 20 min. To detect IFN- $\gamma$  and TNF- $\alpha$  by intracellular staining, cells were then washed twice in PBS/0.5% BSA/2 mM EDTA, fixed and permeabilized with BD Fixation/Permeabilization solution. Cells were stained for intracellular markers using APC-labeled anti-IFN- $\gamma$  (Clone XMG1.2) and PE-labeled anti-TNF- $\alpha$  (clone MP6-XT22). Finally, cells were washed twice with BD perm/wash buffer and fixed in 1% PBS-paraformaldehyde. At least 50,000 cells were acquired on a BD FACS Canto II flow cytometer and then analyzed with FlowJo 8.7 software. Gating strategy is depicted in Figure S1 in Supplementary Material.

### Mice Infection and Parasitemia Analysis

Sporozoites (spz) from *Plasmodium berghei* ANKA expressing *P. vivax* circumsporozoite VK210 repeats (Pb/PvVK210) were obtained as described elsewhere (36). Transgenic Pb/PvVK210 spz were maintained in female *Anopheles stephensi* mosquitoes. The total number of spz was determined using a Kova glass slide and 4,000 spz in 1  $\mu$ L of PBS were microinjected s.c. in the footpad of C57BL/6 mice previously immunized as described above. Thin-blood smears were prepared daily from day 3 to day 10 after challenge, on glass slides from a drop of blood obtained from tails. Blood smears were air-dried, fixed with methanol, and Giemsa stained. Percentages of parasitized erythrocytes were determined by microscopic examination of ~3,000 erythrocytes each in Giemsa-stained smears.

For analysis of the hepatic infection, livers of immunized mice were harvested 42 h after sporozoite challenge and frozen in liquid nitrogen. Ground tissue was resuspended in Trizol reagent (Invitrogen) and total RNA was extracted according to the manufacturer's instructions. After treatment with turboDNase (Ambion), 2  $\mu$ g of total RNA was used for cDNA synthesis, using the superscript II reverse transcriptase and random primers (d(N)9, New England Biolabs). For each sample, a reaction without reverse transcriptase was used for controlling DNA contamination. The real time PCR was performed with 1/20 of the cDNA reaction using the iTaq Universal SYBR Green Supermix (Biorad) and the primers for the mouse HPRT (Fwd, 5'-CCTGCTGGATTACATTAAAGCACTG-3'; Rev5'-GTCAAGGGCATATCCAACAAAC-3') or for the *P. berghei* 18S rRNA (Fwd, 5'-AAGCATTAAATAAAGCGAACATACATCCT TAC-3'; Rev, 5'-GGAGATTGGTTTGACGTTATGTG-3'). Reactions were run in triplicate in three independent experiments according to the following conditions: (1  $\times$  95°C for 5 min; 40  $\times$  95°C for 15 s, 60°C for 30 s; 1  $\times$  55°C to 95°C in 13 min).

### Statistical Analysis

For immunological responses analyses, values were log-transformed and compared using one-way ANOVA followed by Tukey's HSD tests.<sup>3</sup> For parasitemia analyses, the non-parametric Mann-Whitney test was performed. Differences were considered statistically significant when  $P < 0.05$ .

## RESULTS

### Four Recombinant Proteins Based on the Sequences of *P. vivax* CSPs Were Successfully Produced in the Yeast *P. pastoris* as Soluble Secreted Proteins

Recombinant proteins representing the PvCSP alleles (VK210, VK247, and *P. vivax*-like) as well as the hybrid polypeptide yPvCSP-All epitopes were generated. This hybrid contained the conserved C-terminal of the *P. vivax* CSP and the three variant repeat domains in tandem. The proteins were purified and their integrity and purity was evaluated by SDS-PAGE,

<sup>3</sup><http://faculty.vassar.edu/lowry/VassarStats.html>.

immunoblotting, and RP-HPLC (**Figure 2**). A reduced gel stained with Coomassie blue showed that the proteins migrated between 40 and 55 kDa (**Figure 2A**). **Figure 2B** shows that the purified proteins were recognized by specific MAbs generated

against radiation-attenuated *P. vivax* sporozoites (MAb VK210 2F2 and MAb VK247 2E10.E9), as well as monoclonal anti-His antibody. Recognition was also observed for the entire hybrid polypeptide. The purity of the proteins, after the combination of

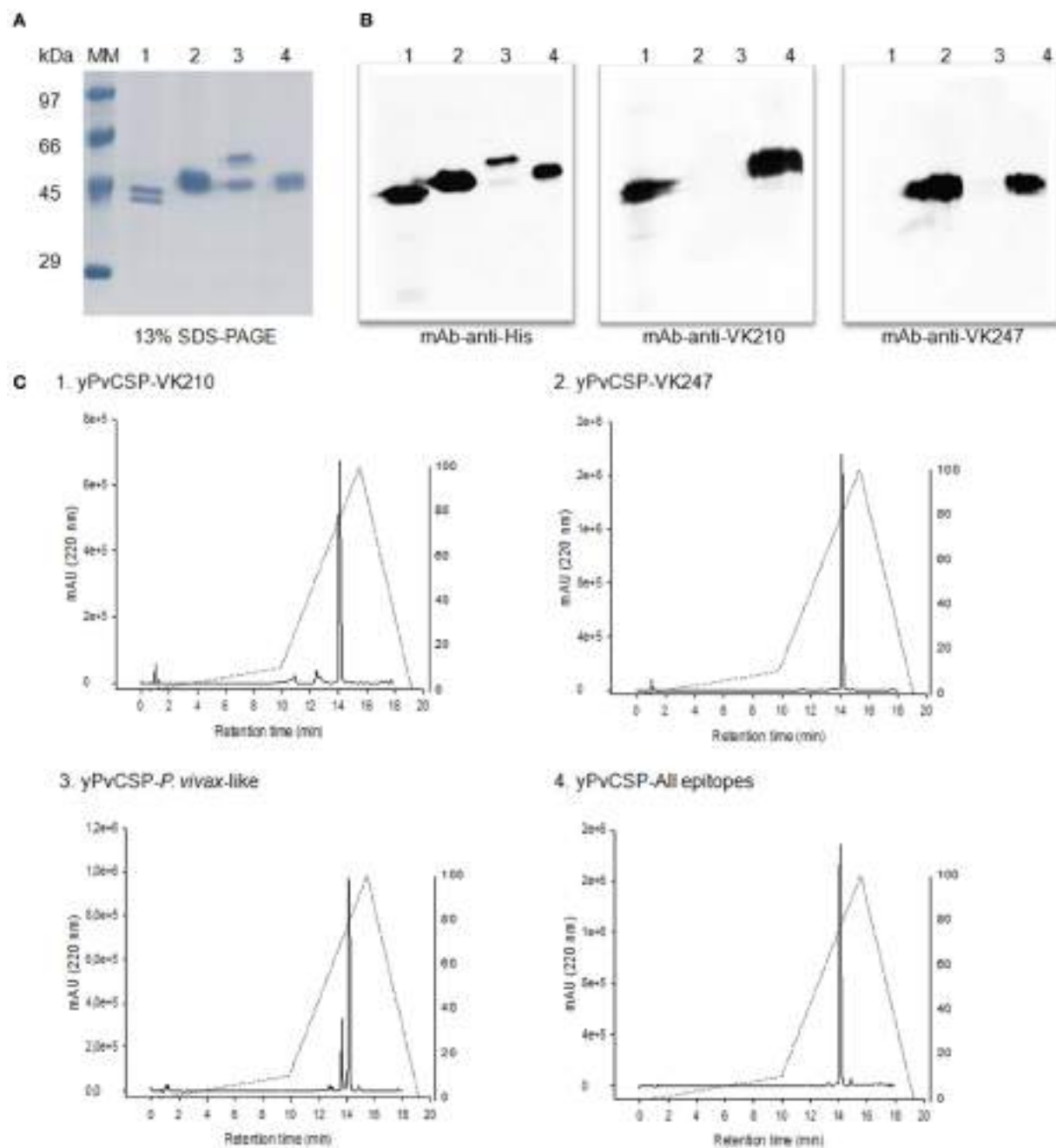


**FIGURE 2 |** Purification and biochemical characterization of the *Plasmodium vivax* circumsporozoite protein (CSP) recombinant proteins. **(A)** 13% SDS-PAGE under reduced conditions stained with Coomassie blue. Proteins migrate between 50 and 55 kDa. Fractions were 2 µg of: (1) yPvCSP-VK210, (2) yPvCSP-VK247, (3) yPvCSP-*P. vivax*-like, and (4) yPvCSP-All epitopes. **(B)** Western blot using 1 µg of the same fractions of proteins described above. Antibodies used were monoclonal antibody (MAB) anti-His, MAb VK210 (2F2), and MAb VK247 (2E10.E9). The secondary antibody used was anti-mouse IgG HRP-labeled, and detection was performed by ECL assay. **(C)** The purity of proteins, after the combination of chromatographic methods, was analyzed by reverse-phase high-performance liquid chromatography (RP-HPLC), in which the gradient elution was developed combining 0.1% trifluoroacetic acid (TFA) in water and 0.1% TFA in 90% acetonitrile, 24°C, 1 mL/min for 40 min, in a C18 column.

chromatographic methods, was analyzed by RP-HPLC. Analysis of RP-HPLC chromatograms revealed high purity of these recombinant proteins (Figure 2C).

## Vaccine Containing the Three Allelic Forms of the *P. vivax* CSP Was Immunogenic in Mice

The serum IgG responses to PvCSP antigens were determined in C57BL/6 mice immunized s.c. with the purified proteins in the presence of the adjuvant Poly(I:C). Six mice per group were immunized with three doses containing 1 µg of each protein or adjuvant alone administered as described in Section “Materials

and Methods,” at 28-day intervals. Formulations containing the mix of the three CSP alleles (VK210, VK247, and *P. vivax*-like, 1 µg of each protein/animal/dose) or the hybrid polypeptide (yPvCSP-All epitopes, 3 µg of protein/animal/dose) were also tested. The antibody titers were analyzed by ELISA according to the timeline described in Figure 3A. These homologous prime-boost vaccination regimens were highly immunogenic in the mouse model, eliciting a high and long-lasting specific antibody immune response (Figure 3B).

To better characterize the anti-PvCSP response, the IgG subtypes of the generated antibodies were analyzed and the IgG1/IgG2c ratio was calculated. All mouse sera presented detectable levels of all IgGs in the groups immunized with the proteins

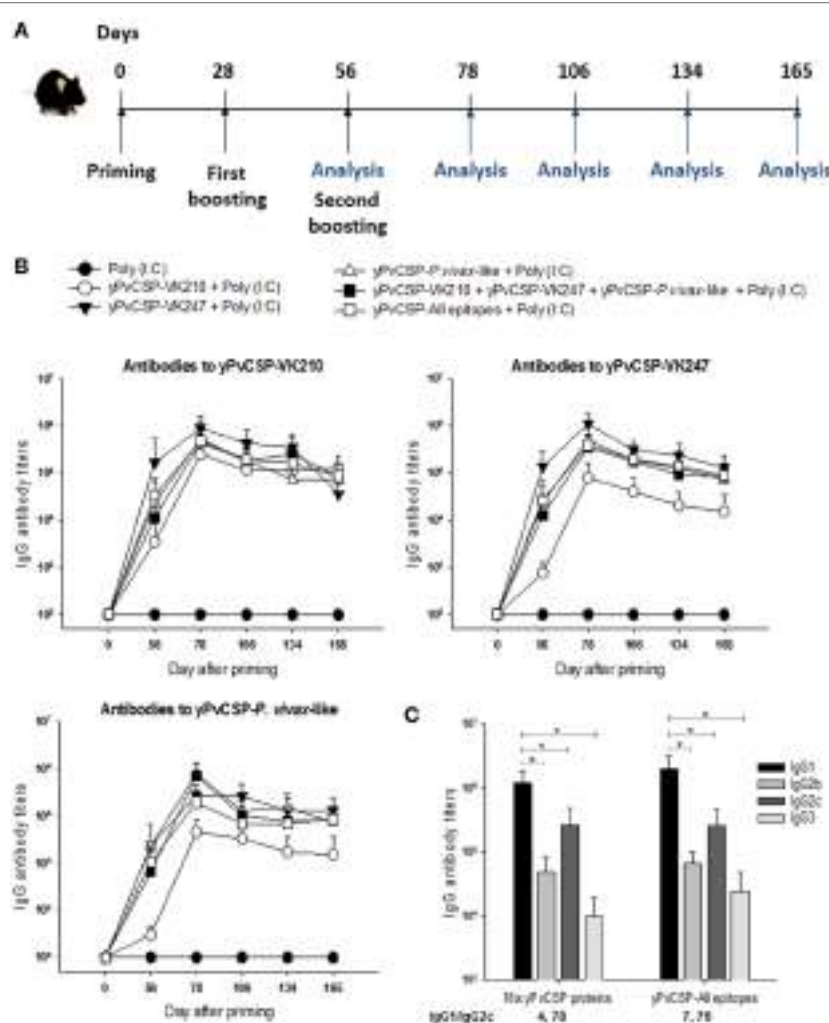


**FIGURE 3 |** Specific antibody response in mice immunized with *Plasmodium vivax* circumsporozoite protein (PvCSP) recombinants. **(A)** C57BL/6 mice were immunized s.c. with three doses 28 days apart with the purified proteins in the presence of the adjuvant Poly(I:C), whereby the antibody response was analyzed according to the timeline described. **(B)** The IgG antibody serum titers against recombinant proteins representing each allelic form of PvCSP were analyzed by ELISA. The results are expressed as the means  $\pm$  SD ( $n = 6$ ). Mouse groups were immunized with: (1) Poly(I:C); (2) Poly(I:C) plus yPvCSP-VK210 (1 µg/dose/mouse); (3) Poly(I:C) plus yPvCSP-VK247 (1 µg/dose/mouse); (4) Poly(I:C) plus yPvCSP-*P. vivax*-like (1 µg/dose/mouse); (5) Poly(I:C) plus a protein mix [yPvCSP-VK210 (1 µg/dose/mouse) + yPvCSP-VK247 (1 µg/dose/mouse) + yPvCSP-*P. vivax*-like (1 µg/dose/mouse)]; or (6) Poly(I:C) plus yPvCSP-All epitopes (3 µg/dose/mouse). **(C)** IgG isotypes were determined by ELISA in sera of mice from groups 5 and 6 described above. Asterisk denotes statistical differences ( $P < 0.01$ ) when comparing IgG1 isotype with IgG2b, IgG2c and IgG3.

individually, mixed, or fused. An analysis of the IgG1/IgG2c anti-PvCSP-VK210 ratio (**Figure 3C**), showed a polarized Th2-like response (IgG1/IgG2c > 1). Similar results were observed against PvCSP-VK247 (data not shown).

To delineate the specificity of anti-yPvCSP-All epitopes antibodies, when compared with immunizations performed with individual yPvCSP proteins or protein mix, the mouse serum was tested against three recombinant proteins containing only the repeats fused to flagellin (FliC) of *Salmonella enterica* serovar Typhimurium [FliC-PvCSP-repeats (28)], and one recombinant protein containing only PvCSP N- and C-terminal regions [No repeats (29)] (**Figure 4A**). Interestingly, all FliC-PvCSP-repeats variants and the No-repeats protein were recognized in sera from mice immunized with protein mix or with yPvCSP-All epitopes, whereas no significative cross-reaction among repeat sequences was observed in animals immunized with individual yPvCSP

proteins (**Figure 4B**). We concluded that the immunization with a recombinant protein expressing all the three different allelic variants in fusion elicited high IgG antibody titers reacting with all three different allelic variants of PvCSP. The antibodies were targeted to both the C-terminal and the repeat domains of PvCSP.

In addition, we determined whether sera from mice immunized with the prime-boost immunization regimen reacted with *P. vivax* sporozoites in immunofluorescence assays. We observed that sera from both groups of mice that were immunized with a formulation containing the yPvCSP-All epitopes and protein mixture reacted to sporozoites of the *P. vivax* VK210 strain (**Figures 5A,B**). Antibody recognition was specific, as control sera from mice immunized with the adjuvant Poly(I:C) did not react (**Figure 5C**), and the sera-stained sporozoites showed a pattern of staining on the surface of the sporozoites similar to that observed with the monoclonal antibody anti-VK210 (**Figure 5D**).

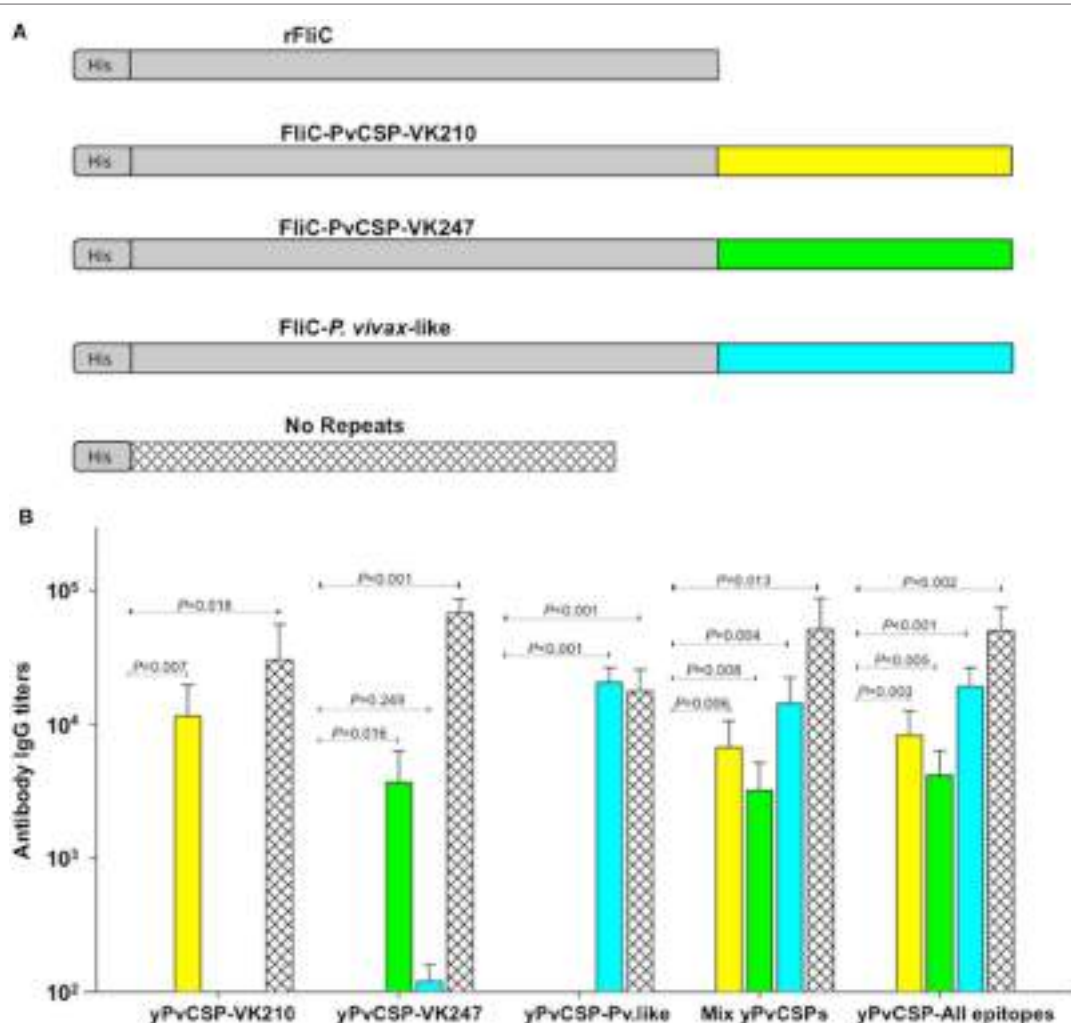


**FIGURE 4 |** Specificity of IgG antibody in mice immunized with *Plasmodium vivax* circumsporozoite protein (CSP) recombinants. **(A)** Schematic representation of recombinant proteins used as a substrate bound to the plates in the ELISA assay. **(B)** C57BL/6 mice were immunized s.c. with the purified proteins in the presence of the adjuvant Poly(I:C) according to the timeline described in **Figure 3A**. The specificity of IgG antibody serum titers toward rFliC, FliC-PvCSP-repeats and No repeats proteins were analyzed by ELISA in sera of mice from groups 2 to 6 described in **Figure 3B**. The results are expressed as mean  $\pm$  SD ( $n = 6$  animals/group).  $P$  values are indicated. Differences were considered statistically significant when  $P < 0.05$ .

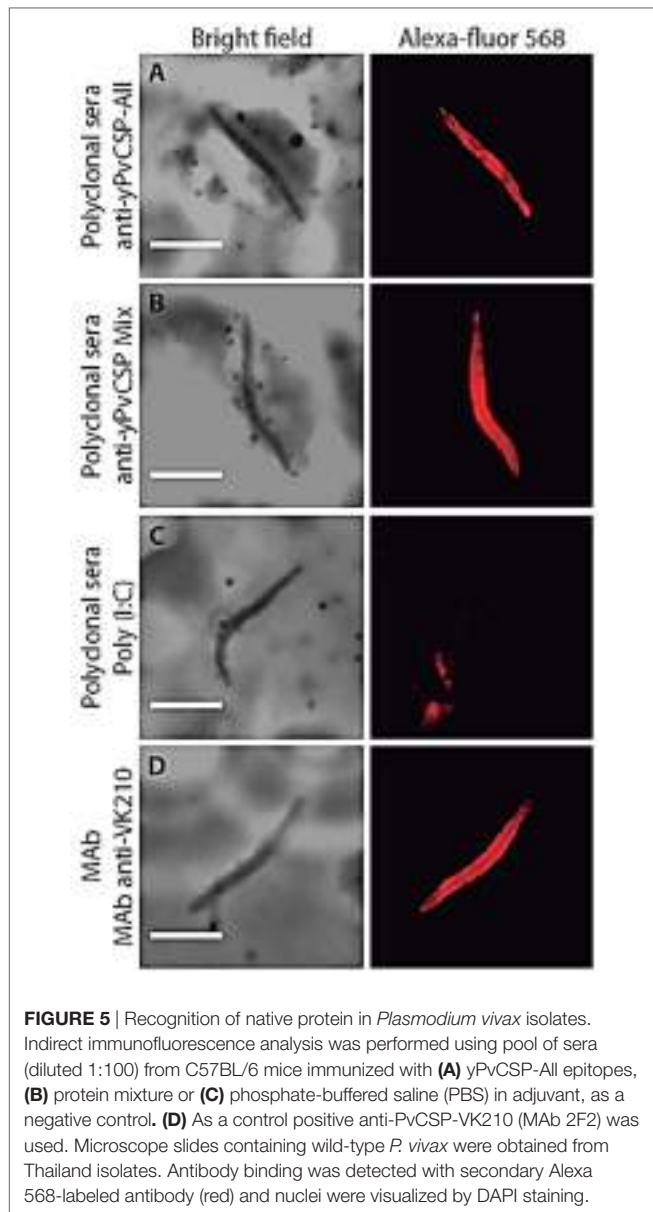


**FIGURE 5 |** Recognition of native protein in *Plasmodium vivax* isolates. Indirect immunofluorescence analysis was performed using pool of sera (diluted 1:100) from C57BL/6 mice immunized with **(A)** yPvCSP-All epitopes, **(B)** protein mixture or **(C)** phosphate-buffered saline (PBS) in adjuvant, as a negative control. **(D)** As a control positive anti-PvCSP-VK210 (MAb 2F2) was used. Microscope slides containing wild-type *P. vivax* were obtained from Thailand isolates. Antibody binding was detected with secondary Alexa 568-labeled antibody (red) and nuclei were visualized by DAPI staining.

## yPvCSP-All Epitopes and Protein Mix Induced Low Activation of CD4<sup>+</sup> and CD8<sup>+</sup> T Cells

We selected two vaccine formulations (yPvCSP-All epitopes and protein mix) to evaluate the ability of the induction of the T cell-mediated immune responses in immunized C57BL/6 mice. We measured IFN- $\gamma$  secretion by ELISPOT assay. We also evaluated the production of inflammatory cytokines (IFN- $\gamma$  and TNF- $\alpha$ ) by CD4<sup>+</sup> and CD8<sup>+</sup> T cells using ICS. **Figure 6A** shows a schematic representation of the immunization schedule. Spleen cells were stimulated *in vitro* with recombinant proteins representing the three allelic forms of PvCSP.

Overall, very low levels of CD4<sup>+</sup> and CD8<sup>+</sup> T cells producing any cytokine were detected. Positive controls performed in parallel with stimulation with ConA were consistently successful

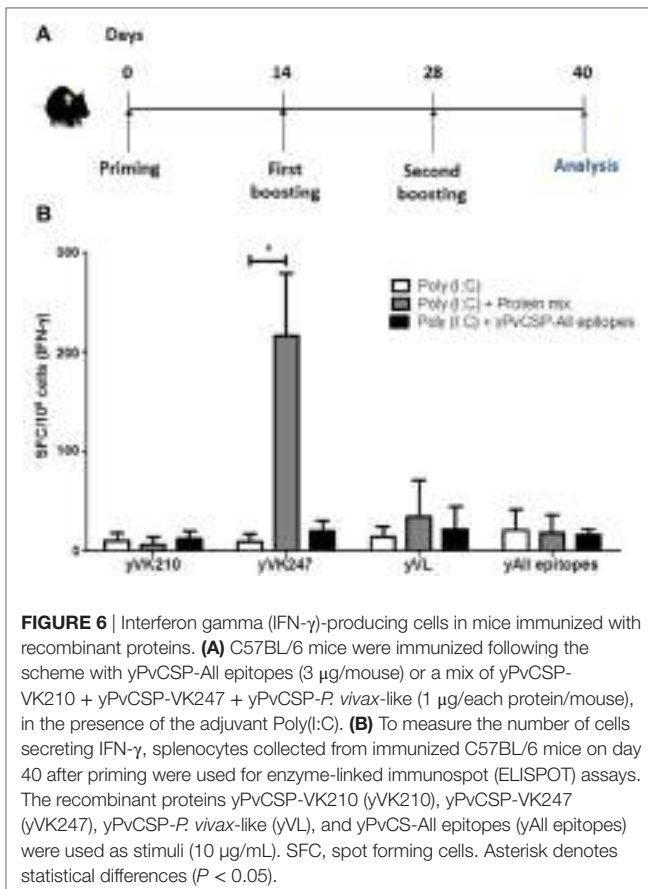


**FIGURE 6 |** Interferon gamma (IFN- $\gamma$ )-producing cells in mice immunized with recombinant proteins. **(A)** C57BL/6 mice were immunized following the scheme with yPvCSP-All epitopes (3  $\mu$ g/mouse) or a mix of yPvCSP-VK210 + yPvCSP-VK247 + yPvCSP-*P. vivax*-like (1  $\mu$ g/each protein/mouse), in the presence of the adjuvant Poly(I:C). **(B)** To measure the number of cells secreting IFN- $\gamma$ , splenocytes collected from immunized C57BL/6 mice on day 40 after priming were used for enzyme-linked immunospot (ELISPOT) assays. The recombinant proteins yPvCSP-VK210 (yVK210), yPvCSP-VK247 (yVK247), yPvCSP-*P. vivax*-like (yVL), and yPvCSP-All epitopes (yAll epitopes) were used as stimuli (10  $\mu$ g/mL). SFC, spot forming cells. Asterisk denotes statistical differences ( $P < 0.05$ ).

(data not shown). A higher number of IFN- $\gamma$ -producing cells were observed in the group immunized with the protein mix and stimulated with recombinant yPvCSP-VK247, but not in the animals immunized with the yPvCSP-All epitopes when the splenocytes were stimulated with the same protein (**Figure 6B**). This difference is in agreement with previous results (29) and could be due to a different processing or antigen presentation of the VK247 epitope.

We also attempted to detect IFN- $\gamma$  and TNF- $\alpha$  using ICS (**Figure 7**). Using Boolean gating analysis, we were able to detect low but significant simultaneous production of both cytokines by CD4<sup>+</sup> T cells derived from mice immunized with the protein mix in a splenocyte culture restimulated with yPvCSP-VK247 recombinant protein (**Figure 7A**). We also observed that CD8<sup>+</sup> T cells derived from mice immunized with the protein yPvCSP-All epitopes were able to produce low but significant levels of TNF- $\alpha$  in a splenocyte culture pulsed with the antigen yPvCSP-*P. vivax*-like (**Figure 7B**). On the other hand, we did not detect any specific responses (IFN- $\gamma$  or TNF- $\alpha$ ) in CD4<sup>+</sup> or CD8<sup>+</sup> T cells after restimulation with recombinant yPvCSP-VK210.

Similarly, we attempt to detect a cytotoxic response in vaccinated mice by measuring CD107a expression in CD4<sup>+</sup> or CD8<sup>+</sup> T cells after stimulation with the recombinant proteins. Under the experimental conditions, we did not detect significant differences in CD107a expression when compared to mice immunized with adjuvant only (Figure S2 in Supplementary Material).

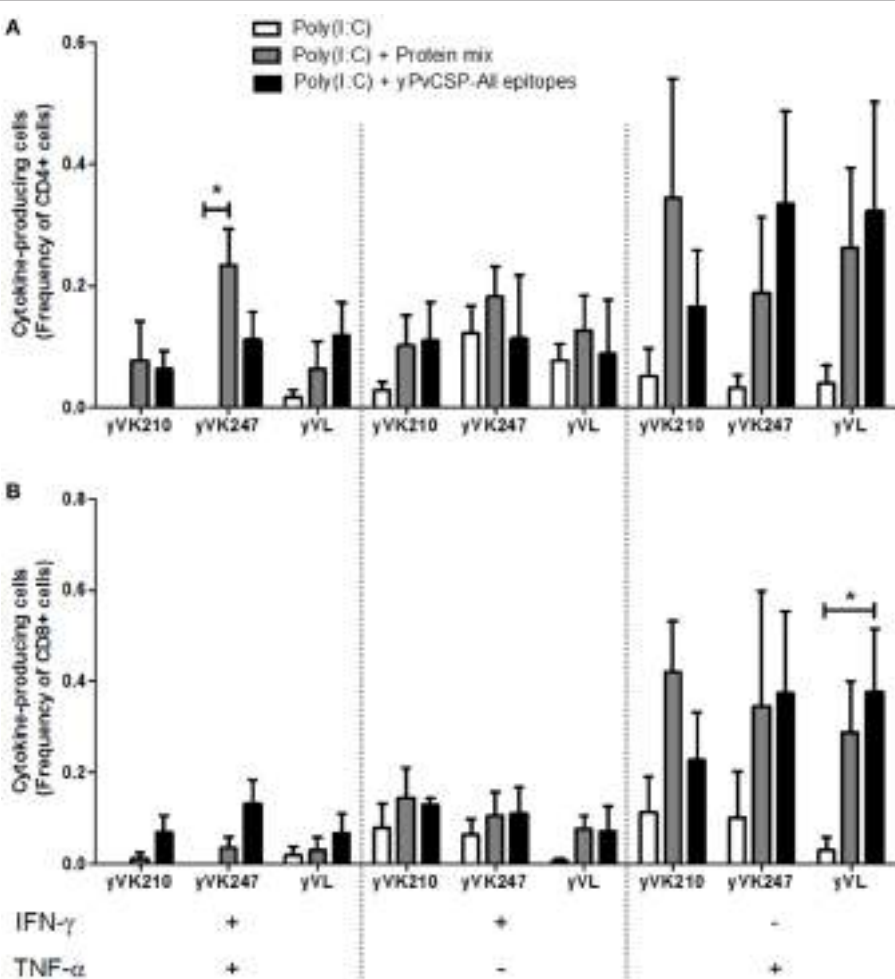


**FIGURE 7 |** CD4<sup>+</sup> and CD8<sup>+</sup> T cell-mediated immunity of mice immunized with recombinant proteins. C57BL/6 mice were immunized s.c. with the recombinant proteins following the scheme described in **Figure 6A**. To determine the intracellular expression of interferon gamma (IFN- $\gamma$ ) and tumor necrosis factor alpha (TNF- $\alpha$ ), intracellular cytokine staining (ICS) was performed following the *in vitro* culture of splenocytes in the presence or absence of the antigenic stimuli yPvCSP-VK210 (yVK210), yPvCSP-VK247 (yVK247), and yPvCSP-*P. vivax*-like (yVL). **(A)** Frequency of CD4<sup>+</sup> cytokine-producing cells. **(B)** Frequency of CD8<sup>+</sup> cytokine-producing cells. Asterisks denote statistically significant ( $P < 0.05$ ) higher frequencies of cells from mice immunized with the recombinant proteins when compared to cells from mice injected with adjuvant only. Media backgrounds of all samples were subtracted before plotting.

## A Vaccine Containing the Three Allelic Forms of the *P. vivax* CSP Induces Protection against Infection in Mice after Challenge with Chimeric Parasite Pb/PvVK210

We used the chimeric parasite Pb/PvVK210, in which the repeats of the PbCSP were replaced by those of the PvCSP (VK210), to evaluate the potential efficacy of the yPvCSP-All epitopes vaccine against a sporozoite infection *in vivo*. C57BL/6 mice were immunized with yPvCSP-All epitopes in the presence of Poly(I:C), in a three-dose prime-boost immunization regimen (**Figure 8A**). The immunization-challenge schedule is described in **Figure 8A**.

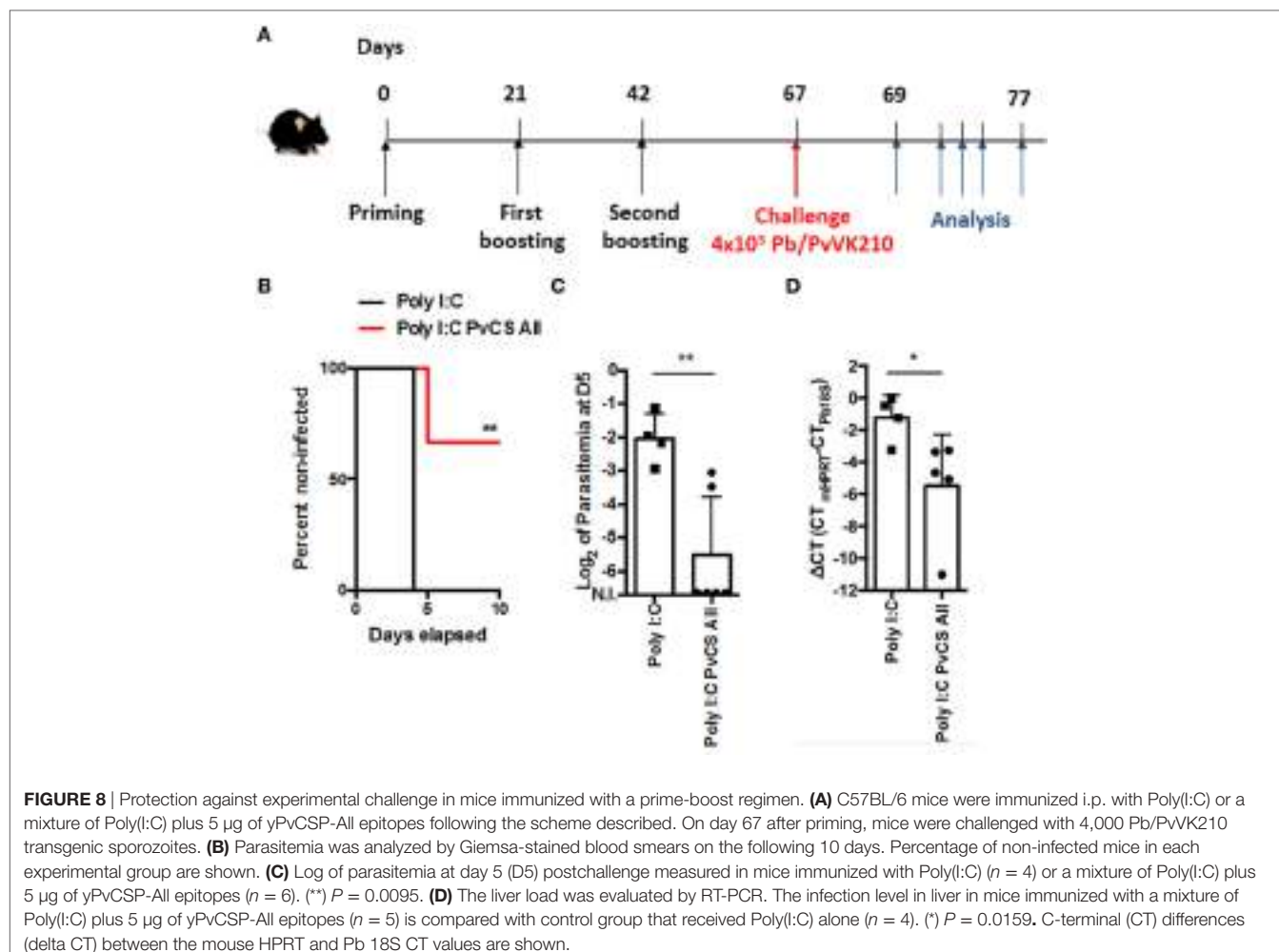
This experimental design involved challenge with 4,000 Pb/PvVK210 sporozoites on day 25 after boost. As shown in **Figure 8B**, the immunization with three doses of 5  $\mu$ g of protein/mouse/dose

was protective for 4/6 mice until day 10 postchallenge, whereas all control mice became infected by day 4 postchallenge. This protection corresponded to a ~10-fold decrease in parasitemia at day 5, when infected blood cells in mice that only received adjuvant still increase exponentially (**Figure 8C**,  $P = 0.0095$ ).

Finally, we evaluated the liver stage parasite burden in immunized mice challenged with Pb/PvVK210 sporozoites. The liver parasite burdens in mice group immunized with a mixture of Poly(I:C) plus 5  $\mu$ g of yPvCSP-All epitopes was 20 times lower compared with control group that received Poly(I:C) alone ( $P = 0.0159$ ) (**Figure 8D**).

## DISCUSSION

In the past decade, diverse efforts toward the development of an effective vaccine against malaria have increased the knowledge



about the level of protection necessary—although also often not enough—to achieve disease-preventative immunity. For preerythrocytic vaccines, there is a consensus on the requirement of high serum levels of IgG antibodies specific to the repeat sequences of the CSP antigen, both for *P. falciparum* and for *P. vivax*. In addition, protection has been related to the frequency of CD4<sup>+</sup> T cells expressing proinflammatory cytokines; thus, several approaches have been trialed in order to produce both a strong antibody response and cell-mediated immunity.

In several studies focusing on RTS,S formulations, the generation of antibodies against the central repeat region of *P. falciparum* CSP has been recognized as key factor to achieve some level of protective effect [reviewed in Ref. (11)]. Accordingly, ELISA titers to the CSP repeats are significantly higher in protected individuals, whereas opsonizing antibodies would not contribute to protection and the C-terminal-targeted antibody contribution remains undefined (37).

In *P. vivax*, the development of a vaccine targeting the CSP antigen has been limited for several decades to preclinical immunization models developed mostly in mice. In previous works, we were able to successfully elicit high titers of antibodies recognizing the three allelic forms of the PvCSP antigen, by using homologous or heterologous prime-boost immunization regimens (29).

These immunizations were carried out using the same adjuvant employed here, Poly(I:C), which is a synthetic analog of double-stranded RNA capable of activating toll-like receptor type 3 and therefore eliciting a virus-like immune response in humans (38). However, the recombinant protein expression from the bacterial system yielded high levels of unfolded protein, mostly recovered from inclusion bodies, which have to be denatured to obtain purified proteins. These production difficulties led us to develop novel CSP-based recombinant proteins to be expressed in a eukaryotic system such as *P. pastoris*. Our group has been employing this protein-production system successfully for the last few years, enabling the easy production of highly purified, stable, properly folded, and immunogenic proteins to be used for the development of vaccines against protozoa parasites (30, 39). These features, also shown in this work, would be a great advantage for the following scaling process in order to obtain a vaccine formulation, which could be distributed in several endemic areas.

Recently, results from the first in-human clinical trial aiming to develop a vaccine against *P. vivax* (VMP001) were published. This formulation contains a recombinant protein comprising N-terminal, C-terminal, VK210, and VK247 repeat domains. As mentioned, vaccination did not induce sterile protection;

however, a significant delay in the prepatent period was associated with the presence of anti-VK210 repeats-specific responses (27).

Interestingly, although specific antibodies were generated against all regions of the CSP in all vaccinated individuals, CD4<sup>+</sup> T cell responses specific to repeat and C-terminal regions were detected in only 17% of vaccinated subjects, whereas 90% of subjects showed strong cellular responses to the N-terminal region (27). As this response was not protective against natural challenge (i.e., infected-mosquito bites), we think that immunodominant epitopes of the *P. vivax* CSP-N-terminal region could be hampering the recognition or antigen presentation of repeat-specific domains. Therefore, the absence of the N-terminal region in our formulations, which were able to induce a repeat-specific antibody and cellular responses in mice, could present an advantage when compared to VMP001 formulations.

To our knowledge, this is the first report of a vaccine potentially protective against all the three allelic variants of *P. vivax* CSP. The results presented herein show that immunization with our recombinant proteins was able to induce a strong humoral immune response, eliciting Abs against all three repeat regions as well against C-terminal region. Although immunization with single variants generated antibodies with some level of cross-reaction between the different variants of PvCSP, we showed in previous studies that the cross-reactivity between IgG antibodies is very limited and would not be possible to use a single variant as a universal vaccine (28). Furthermore, cross-reactivity is expected to be due essentially to Abs recognizing the C-terminal region, present in all the proteins. As Abs against the repeat regions of PvCSP were demonstrated to be associated to protection in *A. nancymaae* monkeys (14), the vaccine formulation containing the hybrid polypeptide (yPvCS-All epitopes) was selected for protection assays, aiming at further development of an anti-*P. vivax* vaccine. The relevant proportion of the antibody titer specific for each of the repeat regions induced by immunization with yPvCSP-All epitopes indicates that one (instead of three) stable protein could be able to confer protection against all the three allelic variants of *P. vivax* sporozoites.

The precise reason why the All epitopes vaccine elicited a very low cytokine response measured in the ICS assay and an undetectable response in the ELISpot assay is not clear to date. A challenging objective of future works will be to find adjuvants, delivering systems or expression strategies able to improve CSP-specific cellular responses. Combined use of viral vectors and potent adjuvants was recently reported to improve CD8<sup>+</sup> T cell responses against preerythrocytic malaria (40). We are currently working on some of these strategies using new adjuvants, adenovirus-delivered antigens and Virus-like particles formulations in order to further develop cell-mediated responses.

In summary, the strong humoral response showed in this work, with a significant ( $>10^4$ ) proportion of antibodies targeting repeats sequences, and the low but detectable CD4<sup>+</sup> and CD8<sup>+</sup> T cell-mediated responses, indicate that this formulation should be highly immunogenic in humans, generating immunity to all three variants of PvCSP. Furthermore, the significant protection elicited after challenge with 4,000 Pb/PvVK210 sporozoites should indicate a more effective protection against natural infection, in which ~100 sporozoites are released per bite (41).

Although the protection found here was not sterilizing to all animals, it has been hypothesized that a candidate *P. vivax* vaccine with low efficacy against primary infection may potentially reduce transmission by preventing relapses (42). In addition, still it is possible to improve the protective immunity of the recombinant vaccine yPvCSP-All epitopes combining with other potent adjuvants (Adjuvant Systems) (43). Taken together, our results are encouraging for testing our vaccine formulations in clinical trials, aiming to the development of a multi-allelic vaccine against *P. vivax* malaria.

## ETHICS STATEMENT

This study was performed in strict accordance with the recommendations in the Guide for the Care and Use of Laboratory Animals of the Brazilian National Council for the Control of Animal Experimentation (CONCEA) (<http://www.mctic.gov.br/mctic/opencms/textogeral/concea.html>). The protocol was approved by the Committees on the Ethics of Animal Experiments of the Faculty of Pharmaceutical Sciences of University of São Paulo, Brazil (CEUA No. 362/2012), and the Institutional Animal Care and Use Committee at the Federal University of São Paulo (CEP No. 0172/12 and CEUA No. 1463171214). The study with human blood obtained from infected Thai patients was approved by Oxford Tropical Research Ethics Committee (reference OX28-09).

## AUTHOR CONTRIBUTIONS

Designed the study and associated protocols: MR, RA, and IS. Performed research work: AG, LL, KF, PD, RP, and J-MT. Analyzed data: AG, LL, KF, DB, MR, RA, and IS. Contributed reagents and materials: CA, FN, LR, RN, and VN. Wrote the manuscript: AG, RA, and IS. All authors read and approved the final version of the manuscript.

## ACKNOWLEDGMENTS

We would like to thank Dr. Marcelo Y. Icimoto for helping with biochemical characterization analyses and Renata Albuquerque for helping with flow cytometer handling and analyses. We also thank Vander Jampaulo for performing some experiments involved in the initial standardization of the project. We are in debt to Fidel Zavala for providing the chimeric *P. berghei* sporozoites. This work is dedicated in memory of Professor Mauricio Martins Rodrigues, a brilliant scientist who devoted his life to the study of parasite vaccines.

## FUNDING

This work was supported by grants from Fundação de Amparo à Pesquisa do Estado de São Paulo (FAPESP 2012/13032-5), Instituto Nacional de Ciência e Tecnologia de Vacinas (INCTV-CNPq). AMG is recipients of fellowship from FAPESP, PD from CAPES, LL, IS, and MR from CNPq. CA and FN are supported by the Wellcome Trust (Program Grant 089179) and were part of the Wellcome Trust Mahidol University Oxford Tropical

Medicine Research Program funded by the Wellcome Trust. LR is supported by funding from the Singapore Immunology Network (SiGN) and the Horizontal Program on Infectious Diseases under the Agency for Science, Technology and Research (A\*STAR, Singapore).

## REFERENCES

- WHO. *World Malaria Report 2015*. Geneva: WHO Library (2016).
- Rahimi BA, Thakkinstian A, White NJ, Sirivichayakul C, Dondorp AM, Chokejindachai W. Severe vivax malaria: a systematic review and meta-analysis of clinical studies since 1900. *Malar J* (2014) 13:481. doi:10.1186/1475-2875-13-481
- Price RN, Tijitra E, Guerra CA, Yeung S, White NJ, Anstey NM. Vivax malaria: neglected and not benign. *Am J Trop Med Hyg* (2007) 77:79–87.
- Mueller I, Galinski MR, Baird JK, Carlton JM, Kocher DK, Alonso PL, et al. Key gaps in the knowledge of *Plasmodium vivax*, a neglected human malaria parasite. *Lancet Infect Dis* (2009) 9:555–66. doi:10.1016/S1473-3099(09)70177-X
- Carlton JM, Sina BJ, Adams JH. Why is *Plasmodium vivax* a neglected tropical disease? *PLoS Negl Trop Dis* (2011) 5:e1160. doi:10.1371/journal.pntd.0001160
- Bassat Q, Velarde M, Mueller I, Lin J, Leslie T, Wongsrichanalai C, et al. Key knowledge gaps for *Plasmodium vivax* control and elimination. *Am J Trop Med Hyg* (2016) 95(6 Suppl):62–71. doi:10.4269/ajtmh.16-0180
- Mueller I, Shakri AR, Chitnis CE. Development of vaccines for *Plasmodium vivax* malaria. *Vaccine* (2015) 33:7489–95. doi:10.1016/j.vaccine.2015.09.060
- Birkett AJ. Status of vaccine research and development of vaccines for malaria. *Vaccine* (2016) 34:2915–20. doi:10.1016/j.vaccine.2015.12.074
- Nussenzweig RS, Vanderberg J, Most H, Orton C. Protective immunity produced by the injection of x-irradiated sporozoites of *Plasmodium berghei*. *Nature* (1967) 216:160–2. doi:10.1038/216160a0
- Clyde DF. Immunization of man against falciparum and vivax malaria by use of attenuated sporozoites. *Am J Trop Med Hyg* (1975) 24:397–401. doi:10.4269/ajtmh.1975.24.397
- Cohen J, Nussenzweig V, Nussenzweig R, Vekemans J, Leach A. From the circumsporozoite protein to the RTS, S/AS candidate vaccine. *Hum Vaccin* (2010) 6:90–6. doi:10.4161/hv.6.1.9677
- World Health Organization. Malaria vaccine: WHO position paper, January 2016 – recommendations. *Vaccine* (2017). doi:10.1016/j.vaccine.2016.10.047
- Clemens J, Moorthy V. Implementation of RTS,S/AS01 malaria vaccine – the need for further evidence. *N Engl J Med* (2016) 374:2596–7. doi:10.1056/NEJMMe1606007
- Yadava A, Hall CE, Sullivan JS, Nace D, Williams T, Collins WE, et al. Protective efficacy of a *Plasmodium vivax* circumsporozoite protein-based vaccine in *Aotus nancymaae* is associated with antibodies to the repeat region. *PLoS Negl Trop Dis* (2014) 8:e3268. doi:10.1371/journal.pntd.0003268
- Arnot DE, Barnwell JW, Tam JP, Nussenzweig V, Nussenzweig RS, Enea V. Circumsporozoite protein of *Plasmodium vivax*: gene cloning and characterization of the immunodominant epitope. *Science* (1985) 230:815–8. doi:10.1126/science.2414847
- Rosenberg R, Wirtz RA, Lanar DE, Sattabongkot J, Hall T, Waters AP, et al. Circumsporozoite protein heterogeneity in the human malaria parasite *Plasmodium vivax*. *Science* (1989) 245:973–6. doi:10.1126/science.2672336
- Qari SH, Goldman IF, Povoa MM, Oliveira S, Alpers MP, Lal AA. Wide distribution of the variant form of the human malaria parasite *Plasmodium vivax*. *J Biol Chem* (1991) 266:12627–300.
- Qari SH, Shi YP, Goldman IF, Udhayakumar V, Alpers MP, Collins WE, et al. Identification of *Plasmodium vivax*-like human malaria parasite. *Lancet* (1993) 341:780–3. doi:10.1016/0140-6736(93)90559-Y
- Qari SH, Shi YP, Povoa MM, Alpers MP, Deloron P, Murphy GS, et al. Global occurrence of *Plasmodium vivax*-like human malaria parasite. *J Infect Dis* (1993) 168:1485–9. doi:10.1093/infdis/168.6.1485
- Collins WE, Nussenzweig RS, Ballou WR, Ruebush TK II, Nardin EH, Chulay JD, et al. Immunization of *Saimiri sciureus* boliviensis with recombinant vaccines based on the circumsporozoite protein of *Plasmodium vivax*. *Am J Trop Med Hyg* (1989) 40:455–64. doi:10.4269/ajtmh.1989.40.455
- Arevalo-Herrera M, Vera O, Castellanos A, Cespedes N, Soto L, Corradin G, et al. Preclinical vaccine study of *Plasmodium vivax* circumsporozoite protein derived-synthetic polypeptides formulated in montanide ISA 720 and montanide ISA 51 adjuvants. *Am J Trop Med Hyg* (2011) 84:21–7. doi:10.4269/ajtmh.2011.10-0110
- Arevalo-Herrera M, Soto L, Perlaza BL, Cespedes N, Vera O, Lenis AM, et al. Antibody-mediated and cellular immune responses induced in naïve volunteers by vaccination with long synthetic peptides derived from the *Plasmodium vivax* circumsporozoite protein. *Am J Trop Med Hyg* (2011) 84:35–42. doi:10.4269/ajtmh.2011.09-0507
- Salman AM, Montoya-Diaz E, West H, Lall A, Atcheson E, Lopez-Camacho C, et al. Rational development of a protective *P. vivax* vaccine evaluated with transgenic rodent parasite challenge models. *Sci Rep* (2017) 7:46482. doi:10.1038/srep46482
- Bell BA, Wood JF, Bansal R, Ragab H, Cargo J III, Washington MA, et al. Process development for the production of an *E. coli* produced clinical grade recombinant malaria vaccine for *Plasmodium vivax*. *Vaccine* (2009) 27:1448–53. doi:10.1016/j.vaccine.2008.12.027
- Yadava A, Sattabongkot J, Washington MA, Ware LA, Majam V, Zheng H, et al. A novel chimeric *Plasmodium vivax* circumsporozoite protein induces biologically functional antibodies that recognize both VK210 and VK247 sporozoites. *Infect Immun* (2007) 75:1177–85. doi:10.1128/IAI.01667-06
- Vanloubbeeck Y, Pichyangkul S, Bayat B, Yongvanitchit K, Bennett JW, Sattabongkot J, et al. Comparison of the immune responses induced by soluble and particulate *Plasmodium vivax* circumsporozoite vaccine candidates formulated in AS01 in rhesus macaques. *Vaccine* (2013) 31:6216–24. doi:10.1016/j.vaccine.2013.10.041
- Bennett JW, Yadava A, Tosh D, Sattabongkot J, Komisar J, Ware LA, et al. Phase 1/2a trial of *Plasmodium vivax* malaria vaccine candidate VMP001/AS01B in malaria-naïve adults: safety, immunogenicity, and efficacy. *PLoS Negl Trop Dis* (2016) 10:e0004423. doi:10.1371/journal.pntd.0004423
- Leal MT, Camacho AG, Teixeira LH, Bargieri DY, Soares IS, Tararam CA, et al. Immunogenicity of recombinant proteins consisting of *Plasmodium vivax* circumsporozoite protein allelic variant-derived epitopes fused with *Salmonella enterica* serovar typhimurium flagellin. *Clin Vaccine Immunol* (2013) 20:1418–25. doi:10.1128/CVI.00312-13
- Teixeira LH, Tararam CA, Lasaro MO, Camacho AG, Ersching J, Leal MT, et al. Immunogenicity of a prime-boost vaccine containing the circumsporozoite proteins of *Plasmodium vivax* in rodents. *Infect Immun* (2014) 82:793–807. doi:10.1128/IAI.01410-13
- Vicentini EC, Francoso KS, Rocha MV, Iourtov D, Dos Santos FL, Kubrusly FS, et al. Invasion-inhibitory antibodies elicited by immunization with *Plasmodium vivax* apical membrane antigen-1 expressed in *Pichia pastoris* yeast. *Infect Immun* (2014) 82:1296–307. doi:10.1128/IAI.01169-13
- Camacho AG, Teixeira LH, Bargieri DY, Boscardin SB, Soares IS, Nussenzweig RS, et al. TLR5-dependent immunogenicity of a recombinant fusion protein containing an immunodominant epitope of malarial circumsporozoite protein and the FliC flagellin of *Salmonella typhimurium*. *Mem Inst Oswaldo Cruz* (2011) 106(Suppl 1):167–71. doi:10.1590/S0074-02762011000900021
- Nardin EH, Nussenzweig V, Nussenzweig RS, Collins WE, Harinasuta KT, Tapchaisri P, et al. Circumsporozoite proteins of human malaria parasites *Plasmodium falciparum* and *Plasmodium vivax*. *J Exp Med* (1982) 156:20–30. doi:10.1084/jem.156.1.20
- Bargieri DY, Rosa DS, Braga CJ, Carvalho BO, Costa FT, Espindola NM, et al. New malaria vaccine candidates based on the *Plasmodium vivax* merozoite surface protein-1 and the TLR-5 agonist *Salmonella typhimurium* FliC flagellin. *Vaccine* (2008) 26:6132–42. doi:10.1016/j.vaccine.2008.08.070

## SUPPLEMENTARY MATERIAL

The Supplementary Material for this article can be found online at <http://www.frontiersin.org/article/10.3389/fimmu.2017.01275/full#supplementary-material>.

34. Andolina C, Landier J, Carrara V, Chu CS, Franetich JF, Roth A, et al. The suitability of laboratory-bred *Anopheles cracens* for the production of *Plasmodium vivax* sporozoites. *Malar J* (2015) 14:312. doi:10.1186/s12936-015-0830-0
35. Vasconcelos JR, Bruna-Romero O, Araujo AF, Dominguez MR, Ersching J, de Alencar BC, et al. Pathogen-induced proapoptotic phenotype and high CD95 (Fas) expression accompany a suboptimal CD8+ T-cell response: reversal by adenoviral vaccine. *PLoS Pathog* (2012) 8:e1002699. doi:10.1371/journal.ppat.1002699
36. Espinosa DA, Yadava A, Angov E, Maurizio PL, Ockenhouse CF, Zavala F. Development of a chimeric *Plasmodium berghei* strain expressing the repeat region of the *P. vivax* circumsporozoite protein for in vivo evaluation of vaccine efficacy. *Infect Immun* (2013) 81:2882–7. doi:10.1128/IAI.00461-13
37. Chaudhury S, Ockenhouse CF, Regules JA, Dutta S, Wallqvist A, Jongert E, et al. The biological function of antibodies induced by the RTS,S/AS01 malaria vaccine candidate is determined by their fine specificity. *Malar J* (2016) 15:301. doi:10.1186/s12936-016-1348-9
38. Caskey M, Lefebvre F, Filali-Mouhim A, Cameron MJ, Goulet JP, Haddad EK, et al. Synthetic double-stranded RNA induces innate immune responses similar to a live viral vaccine in humans. *J Exp Med* (2011) 208:2357–66. doi:10.1084/jem.20111171
39. Gimenez AM, Francoso KS, Ersching J, Icimoto MY, Oliveira V, Rodriguez AE, et al. A recombinant multi-antigen vaccine formulation containing *Babesia bovis* merozoite surface antigens MSA-2a1, MSA-2b and MSA-2c elicits invasion-inhibitory antibodies and IFN-gamma producing cells. *Parasit Vectors* (2016) 9:577. doi:10.1186/s13071-016-1862-1
40. Milicic A, Rollier CS, Tang CK, Longley R, Hill AVS, Reyes-Sandoval A. Adjuvanting a viral vectored vaccine against pre-erythrocytic malaria. *Sci Rep* (2017) 7:7284. doi:10.1038/s41598-017-07246-0
41. Medica DL, Sinnis P. Quantitative dynamics of *Plasmodium yoelii* sporozoite transmission by infected anopheline mosquitoes. *Infect Immun* (2005) 73: 4363–9. doi:10.1128/IAI.73.7.4363-4369.2005
42. White M, Amino R, Mueller I. Theoretical implications of a pre-erythrocytic *Plasmodium vivax* vaccine for preventing relapses. *Trends Parasitol* (2017) 33:260–3. doi:10.1016/j.pt.2016.12.011
43. Garcon N, Di Pasquale A. From discovery to licensure, the adjuvant system story. *Hum Vaccin Immunother* (2017) 13:19–33. doi:10.1080/21645515.2016.1225635

**Conflict of Interest Statement:** The authors declare that the research was conducted in the absence of any commercial or financial relationships that could be construed as a potential conflict of interest.

Copyright © 2017 Gimenez, Lima, Françoso, Denapoli, Panatieri, Bargieri, Thiberge, Andolina, Nosten, Renia, Nussenzweig, Nussenzweig, Amino, Rodrigues and Soares. This is an open-access article distributed under the terms of the Creative Commons Attribution License (CC BY). The use, distribution or reproduction in other forums is permitted, provided the original author(s) or licensor are credited and that the original publication in this journal is cited, in accordance with accepted academic practice. No use, distribution or reproduction is permitted which does not comply with these terms.



# What Is Known about the Immune Response Induced by *Plasmodium vivax* Malaria Vaccine Candidates?

**Carolina López<sup>1,2</sup>, Yoelis Yépes-Pérez<sup>1,3</sup>, Natalia Hincapié-Escobar<sup>1</sup>, Diana Díaz-Arévalo<sup>1,4</sup> and Manuel A. Patarroyo<sup>1,5\*</sup>**

<sup>1</sup>Molecular Biology and Immunology Department, Fundación Instituto de Immunología de Colombia (FIDIC), Bogotá, Colombia, <sup>2</sup>PhD Programme in Biomedical and Biological Sciences, Universidad del Rosario, Bogotá, Colombia,

<sup>3</sup>MSc Programme in Microbiology, Universidad Nacional de Colombia, Bogotá, Colombia, <sup>4</sup>Universidad de Ciencias Aplicadas y Ambientales (UDCA), Bogotá, Colombia, <sup>5</sup>Basic Sciences Department, School of Medicine and Health Sciences, Universidad del Rosario, Bogotá, Colombia

## OPEN ACCESS

### Edited by:

Irene S. Soares,  
University of São Paulo, Brazil

### Reviewed by:

Georges Snounou,  
Centre National de la Recherche Scientifique (CNRS), France

Daniel Olive,

Institut national de la santé et de la recherche médicale, France  
Josué Da Costa Lima-Junior,  
Oswaldo Cruz Foundation, Brazil

### \*Correspondence:

Manuel A. Patarroyo  
mapatarr.fidic@gmail.com

### Specialty section:

This article was submitted to  
Vaccines and Molecular Therapeutics,  
a section of the journal  
*Frontiers in Immunology*

**Received:** 05 November 2016

**Accepted:** 25 January 2017

**Published:** 13 February 2017

### Citation:

López C, Yépes-Pérez Y, Hincapié-Escobar N, Díaz-Arévalo D and Patarroyo MA (2017) What Is Known about the Immune Response Induced by *Plasmodium vivax* Malaria Vaccine Candidates? *Front. Immunol.* 8:126.  
doi: 10.3389/fimmu.2017.00126

Malaria caused by *Plasmodium vivax* continues being one of the most important infectious diseases around the world; *P. vivax* is the second most prevalent species and has the greatest geographic distribution. Developing an effective antimalarial vaccine is considered a relevant control strategy in the search for means of preventing the disease. Studying parasite-expressed proteins, which are essential in host cell invasion, has led to identifying the regions recognized by individuals who are naturally exposed to infection. Furthermore, immunogenicity studies have revealed that such regions can trigger a robust immune response that can inhibit sporozoite (hepatocytic stage) or merozoite (erythrocyte stage) invasion of a host cell and induce protection. This review provides a synthesis of the most important studies to date concerning the antigenicity and immunogenicity of both synthetic peptide and recombinant protein candidates for a vaccine against malaria produced by *P. vivax*.

**Keywords:** malaria, *Plasmodium vivax*, immune response, antigenicity, immunogenicity

## INTRODUCTION

Malaria is one of the most important vector-transmitted diseases, affecting a large part of the world's population. Around 214 million new cases appeared in 2015, and 438,000 people died from the disease. This disease is caused by parasites from the phylum Apicomplexa, genus *Plasmodium*, and

**Abbreviations:** Spz, sporozoites; RBC, red blood cells; NT, N-terminal; pexel/VTS, *Plasmodium* export element/vacuolar translocation signal; Mrz, merozoites; NFκB, nuclear factor kappa B; PRRs, pattern recognition receptors; PAMPs, pathogen-associated molecular patterns; MHC, major histocompatibility complex; NK, natural killer; IFN-γ, interferon gamma; TNF, tumor necrosis factor; LDH, lactate dehydrogenase; TAT, thrombin-antithrombin III; HNE, human neutrophil elastase; IL, interleukin; Th1, T helper 1; Th2, T helper 2; CXCL9, chemokine (C-X-C motif) ligand 9; CCL2, chemokine (C-C motif) ligand 2; CCL5, chemokine (C-C motif) ligand 5; Ig, immunoglobulin; i.v., intravenously; HLA, human leukocyte antigen; CSP, circumsporozoite protein; TRAP, thrombospondin-related adhesive protein; GPI, glycosphingolipidylinositol; PNG, Papua New Guinea; LSP, long synthetic peptides; TLR, toll-like receptor; CpG, cytosine and guanine separated by one phosphate; GLA, glucopyranosyl lipid A; TSR, thrombospondin type 1 repeat; MSP, merozoite surface protein; ELISA, enzyme-linked immunosorbent assay; EGF, epidermal growth factor; HABPs, high activity binding peptides; AMA-1, apical membrane antigen-1; rPvAMA-1, recombinant *Plasmodium vivax* apical membrane antigen-1; FcγR-Fc, Fc-gamma receptors; PP, poly-proline; TCR, T-lymphocyte receptor; ADCI, antibody-dependent cell-mediated inhibition; DBP, Duffy binding protein; DARC, Duffy antigen receptor for chemokines; rDBP, recombinant Duffy binding protein; PBMC, peripheral blood mononuclear cell; RBP, reticulocyte-binding proteins; HARBPs, high affinity reticulocyte-binding peptides.

is transmitted by the bite of a female mosquito from the genus *Anopheles* infected by the parasite (1).

Five species cause malaria in humans: *P. falciparum*, *P. vivax*, *P. malarie*, *P. ovale*, and *P. knowlesi*. Acute febrile disease symptoms appear 10–15 days after the bite of an infected mosquito. Initial symptoms include fever, headache, shivering, and vomiting; if not treated early on, and depending on the species responsible for the disease, severe anemia, metabolic acidosis, or cerebral malaria may be produced, and even lead to death (1).

Studying the proteins involved in *P. vivax* invasion has not been easy, mainly due to technical restrictions such as a lack of continuous culture *in vitro*, meaning that studying the parasite's biology has been limited, as well as the identification of new antigens and their evaluation *in vitro* (2, 3).

Infection by more than one *Plasmodium* species is usually omitted in routine diagnosis by microscopy (4, 5), leading to an overestimation of the amount of cases caused by coinfection in endemic areas and thus to treatment failure (6). Drug resistance since the first report in 1989 (7) has been increasing worldwide throughout Southeast Asia [Indonesia, China, Thailand, Papua New Guinea (PNG)], South America (the Brazilian and Peruvian Amazon region, Colombia), Africa (Madagascar, Ethiopia), Pakistan, and Turkey (8, 9).

Such resistance appears to be related to mutations regarding multidrug resistance 1 (*mdr1*) gene and variation in the gene's number of copies, presumably due to selective pressure by first-line chloroquine treatment (10, 11).

Even though malaria caused by *P. vivax* has been considered benign (unlike that caused by *P. falciparum*), severe *P. vivax* malaria has emerged during the last few years with some cases leading to death (12–17). In spite of *P. vivax* malaria having a greater global distribution, it is still considered a neglected infection, thereby leading to socioeconomic impact factors being understated in endemic regions, causing more than US\$2 billion per year costs worldwide (18). The forgoing means that investment and efforts must be focused on developing a vaccine against *P. vivax* malaria.

Antigenicity studies arise from evaluating the immune response induced in individuals naturally exposed to the infection. On the other hand, immunogenicity assays evaluate *in vitro* or *in vivo* the immune response induced when vaccine candidates are used for immunization (Figures 1 and 2).

The present review summarizes classical studies that have been carried out to date concerning the antigenicity and immunogenicity of the most important proteins considered candidates for a vaccine against *P. vivax* malaria. Although the use of a single-stage protein is not enough to provide a successful sterile vaccine, it has represented an important advance in identifying hundreds of malarial antigens that can be combined to develop a multistage, multi-epitope sterile vaccine.

## MALARIA: INFECTION BY *P. vivax*

Around 90% of the clinical cases presented are the result of infection by two of the most relevant species: *P. falciparum* or *P. vivax*. *P. vivax* malaria is the second most important around the world and is the most prevalent on the Asian and American continents. Such infection is characterized by relapses several years after the

first infection, since a latent form called hypnozoite occurs during hepatic phase. This stage is difficult to diagnose, allowing the parasite to survive in the host for longer (1, 19, 20).

Infection begins with the vector inoculating sporozoites (Spz) into the host's skin; these Spz are motile and travel through the blood stream, later being carried to the liver. Sinnis et al. have named a "skin stage" of infection because they have proposed that this interaction between Spz and cells at the injection site means that Spz may remain in the injection site for 2–3 h, maybe in hair follicles, giving rise to infective merozoites (Mrz) (21, 22). Regarding *P. berghei* expressing GFP (a rodent parasite), it has been observed that Spz have a random gliding-movement. Moreover, Spz glide into the skin, interacting with blood vessel walls. Lymphatic vessels also become invaded to drain lymph nodes near the injection site where some Spz can partially develop into exoerythrocytic stages (23–25).

Sporozoites migrate from the skin to liver cells (these becoming infected first) and then cross/traverse endothelial cells and use cell traversal machinery to pass through the endothelium, thereby beginning the hepatic stage that might go unnoticed clinically (26, 27). Some parasites remain as hypnozoites during this stage, and others go into the blood stream giving rise to the erythrocyte stage where the disease's clinical manifestations are presented.

The severity of the disease during the erythrocyte stage depends on various factors, such as the location of parasitized red blood cells (RBC) in the target organs, the local and systemic action of the parasite's bioactive products, pro-inflammatory cytokine production, as well as innate and adaptive immune system cytokine and chemokine regulators, and the activation, recruiting, and infiltration of inflammatory cells (28).

After invading the hepatocytes, each Spz replicates within the parasitophorous vacuole by a family of parasite proteins having an NT export motif called pexel/VTS (*Plasmodium* export element/vacuolar translocation signal) (29–31). The circumsporozoite protein (CSP) enters the hepatocyte's cytoplasm using the pexel/VTS motif and a nuclear localization signal to go into the nucleus. CSP in the nucleus induces the expression of the host's genes, where the NFκB transcription factor controls the expression of genes involved in inflammation (32), controlling biological functions such as metabolic transport, the cell cycle, the immune response, and apoptosis, thereby creating a favorable setting for parasite growth (31).

The *Plasmodium* erythrocyte stage begins when an infected hepatocyte ruptures and releases close to 30,000 Mrz into the blood stream, undertaking an initial journey as merosomes to the lungs and then becoming disseminated in the circulation. Each Mrz infects an immature RBC (reticulocyte), which generates 16 new Mrz 48 h later (33).

## IMMUNE RESPONSE REGARDING MALARIA

Innate and adaptive immune system molecules are involved in disease pathogenesis and control. Clinical immunity to malaria can be acquired during three phases: immunity to the disease, immunity to symptomatic infection, and partial immunity to

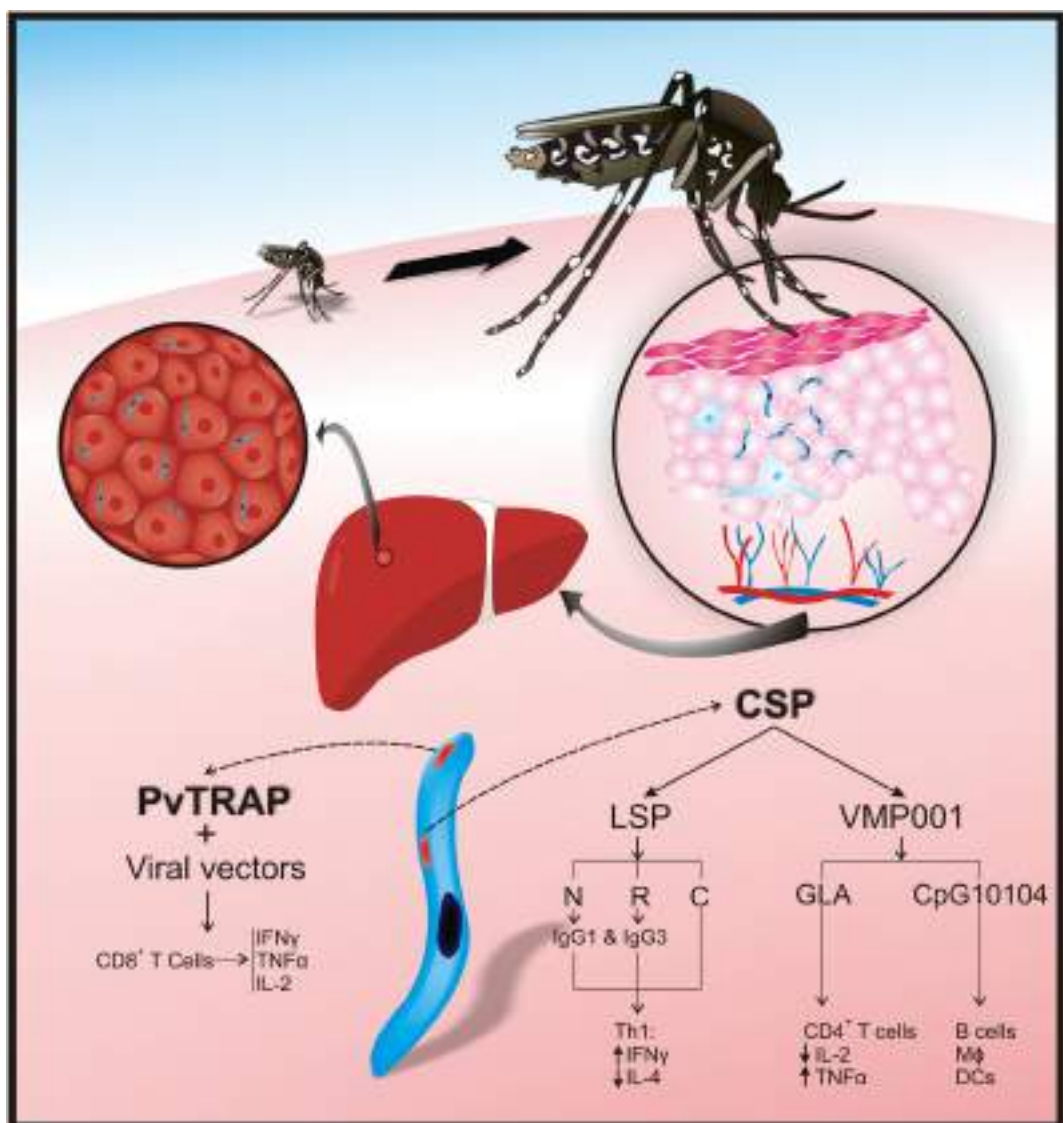


**FIGURE 1 |** *Plasmodium vivax* preerythrocyte stage protein immunogenicity. After sporozoites have been inoculated into the skin by *Anopheles* mosquitoes, they travel to the liver via the bloodstream and enter hepatocytes thereby initiating the preerythrocyte stage. *P. vivax* circumsporozoite protein (CSP) and thrombospondin-related adhesive protein (PvTRAP) are involved in hepatocyte recognition and binding in a mammalian host. In CSP, the N-terminal (NT) and repeat region facilitate parasite binding to hepatocytes. Adaptive immune responses against PvCSP and PvTRAP control invasion of hepatocytes by cytokines [CD4<sup>+</sup> T-helper 1 (Th1) and CD4<sup>+</sup> T-helper 2 (Th2) cells], cytophilic antibodies, and CD8<sup>+</sup> T-cells. Interferon gamma (IFN- $\gamma$ ) increases and interleukin (IL)-4 decreases after vaccination with CSP-long synthetic peptides [CSP-LSP-N terminal; CSP-LSP-R (repeat region), and CSP-LSP-N terminal]. Cytophilic antibodies (IgG1 and IgG3) are produced after vaccination with CSP-LSP-N; CSP-LSP-R. Immunization with PvCSP recombinant vaccine (VMP 001) combined with CpG10104 has induced protection and activation of B-cells, macrophages (MΦ), and dendritic cells (DCs). When this recombinant vaccine is formulated with glucopyranosyl lipid A (GLA), there is activation of CD4<sup>+</sup> T-cells, production of tumor necrosis factor-alpha (TNF- $\alpha$ ), and reduction of IL-2. Immunization with PvTRAP, expressed in viral vectors, induces activation of CD8 T-cells and production of IFN- $\gamma$ , TNF- $\alpha$ , and IL-2.

parasitemia (28). The premunition (absence of fever with infection and lower densities of parasitemia) is present in places where malaria is endemic and in people that had suffered of several infections through the years (8–15 years), thus acquiring natural immune responses that lower the risk of clinical disease (34). The term was coined early in the 1900s during epidemiological studies with patients from endemic areas that can control the parasitemia and develop a subclinical infection (35). It is characterized by a

slow acquisition rate, present just in holo- or hyper-endemic areas, rapidly lost, strain dependent, IgG dependent, and directed toward blood-stage parasites; although the immune response induced is strong, it is not a sterilizing immunity. The protection mechanism has not been completely described, but there is evidence that cytophilic antibodies and memory cells produced after repeated infections with *Plasmodium* variants are responsible for this kind of protection (34, 36–39).

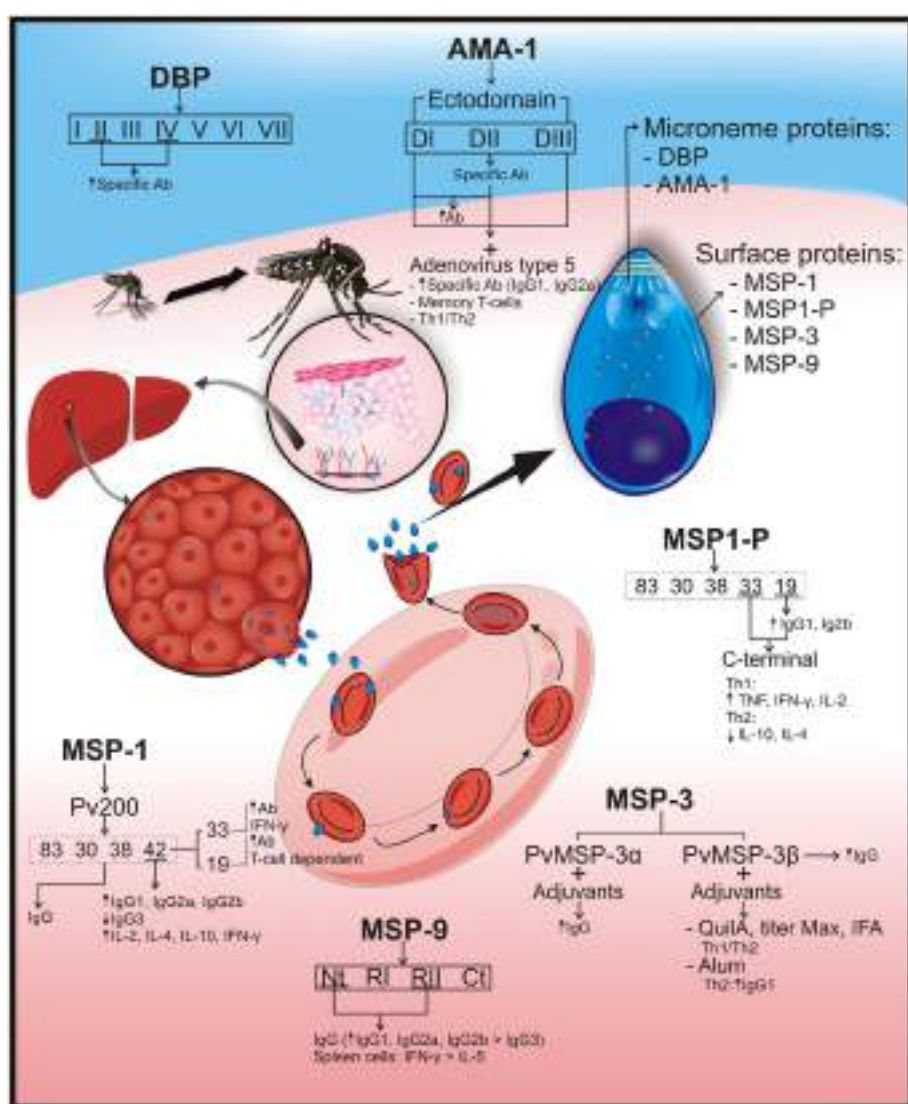


**FIGURE 2 |** *Plasmodium vivax* erythrocyte stage protein immunogenicity. *P. vivax* parasites are differentiated into tissue schizonts in hepatic cells, which, after thousands of replications, are released into the bloodstream as merozoites (Mrz). These Mrz predominantly invade reticulocytes, and their infection cycle is repeated every 48 h. Several surface and microneme merozoite proteins have been identified as vaccine candidates. Surface proteins would include merozoite surface protein-1 (MSP-1/Pv200), which is an abundant ligand on merozoite surface and is essential for reticulocyte invasion. MSP-1 was cleaved into 83, 30, 38, 42 (33 and 19) kDa fragments; immunization with the complete protein induced IgG production. MSP-1–42 fragment increased IgG1, IgG2a, and IgG2b production but not that of IgG3, as well as interleukin (IL)-2, IL-4, IL-10, and interferon gamma (IFN- $\gamma$ ) production in vaccinated mice. Immunization with 19-kDa fragments produced high antibody titers that were T-cell dependent. Higher antibody and IFN- $\gamma$  production was observed after vaccination with the 33-kDa fragment. Another surface protein is merozoite surface protein-1 paralog (MSP1-P), which was also cleaved into 83, 30, 38, 42, 33, and 19 kDa; the last two fragments (C-terminal region) induced a Th1 cytokine response profile, having high tumor necrosis factor (TNF), IFN- $\gamma$ , and IL-2, but low IL-10 and IL-4 cytokines (Th2 profile). High IgG1 and IgG2b titers were observed in vaccinated animals with 19-kDa fragment. Merozoite surface protein-3 (MSP-3): PvMSP3- $\alpha$  block II is highly immunogenic and induces IgG production. The PvMSP-3 $\beta$  region with Quil A, Titer Max, or IFA adjuvants has produced a balanced Th1/Th2 response and IgG but became directed toward a Th2 response when formulated with Alum. Merozoite surface protein-9 (MSP-9) immune response against NT and repeat region II was mainly IgG, having greater IgG1, IgG2a, and IgG2b titers than IgG3 isotype production. These two regions also induced higher IFN- $\gamma$  than IL-5 production in spleen cells. The following are microneme proteins: the Duffy binding protein (DBP) is a surface receptor for invading human reticulocytes and is divided into seven regions where regions II (main ligand domain) and IV induce specific antibody production. Apical membrane antigen-1 (AMA-1) is essential during cell host invasion, and its ectodomain defines three subdomains (DI, DII, and DIII). Immunization with AMA-1 induced high IgG antibody titers. Vaccinating mice with human adenovirus type 5 and rAMA-1 have produced long-lived specific antibodies (IgG1 and IgG2a), memory T-cell, and Th1/Th2 balance immune responses. An arrow pointing upwards ( $\uparrow$ ) indicates an increase in antibody titers or cytokine production; an arrow pointing downwards ( $\downarrow$ ) shows reduced cytokine or antibody production.

An innate immune response is triggered during *Plasmodium* infection as first line of defense, followed by an adaptive immune response, which includes T-cells, B-cells, and antibodies. A mosquito inoculates Spz into a host's skin when biting; these can remain in the skin for up to 6 h after inoculation (40). Such retention affects the place for antigen presentation and the location and type of response so induced.

Dendritic cells (DCs) present antigens, depending on the anatomic environment and the resulting immune response. These cells, through pattern recognition receptors, recognize the pathogen-associated molecular patterns (PAMPs) exhibited by the parasite. The mechanism of action regarding such recognition triggers intracellular signals enabling DC maturation (41). Three PAMPs have been described in *P. falciparum*: hemozoin, immunostimulatory nucleic acid motifs, and glycosylphosphatidylinositol anchors [glycophosphatidylinositol (GPI) anchors] (42).

The parasite's main source of protein is RBC hemoglobin. Hemoglobin hydrolysis releases lipophilic prosthetic group—heme—which is extremely toxic for the parasite. Heme detoxification is thus necessary and is achieved by converting heme into an insoluble crystalline material called hemozoin (Hz) (43). Regarding *P. falciparum* infection, Hz binds DNA inside host cell phagolysosomes and cytosol, and toll-like receptor (TLR)9 is activated by nucleic acids, NLRP3, AIM2, and other cytosolic sensors (42, 44–46).

In terms of AT content in the genome, *P. falciparum* has the highest AT content (82%) and *P. vivax* the lowest AT content (56%). On the other hand, *in silico* analysis has shown that *P. falciparum* contains ~300 CpG and ~6,000 AT-rich motifs and *P. vivax* ~2,000 CpG and ~5,500 AT-rich motifs. The release of CpG *Plasmodium* DNA into phagolysosomes produces an innate immune response activating TLR9 (42, 44, 47).

Glycophosphatidylinositol anchors connect surface proteins with the protozoan plasma membrane; they are essential toxins for parasite viability (48). They turn on the innate response because they induce cytokine synthesis and are recognized by TLRs such as TLR1-TLR2 or TLR2-TLR6 (depending on GPI anchor activation containing three or two fatty acid chains, respectively) and TLR4 (49–51).

Some functions described for DCs have been T- and B-lymphocyte activation, immune tolerance, natural killer (NK) cell activation, and macrophage activation (52). For example, a third of Spz are drained to regional lymph nodes where they become internalized by skin-derived DCs (CD103+) and presented to CD8+ T-cells (26).

Some studies have shown that infected RBC bind to DCs, inhibit their maturation, and cannot stimulate a T-lymphocyte response in acute *P. falciparum* infection. Other studies have shown that inhibition depends on contacting a larger amount of infected RBC per DC (53, 54).

Antigens begin to be presented on hepatocyte surface during the hepatic stage in context of the major histocompatibility complex (MHC) class I molecules expressed on all nucleated cells to become recognized by CD8+ T-cells (55).

Immune response during the erythrocyte stage is mainly mediated by antibodies while a cellular response predominates

during the hepatic stage (56). CD4+ T-, B-, and NK cells also play an important role in the immune response induced by the parasite during the erythrocyte stage since immunity depends on memory B-cell production and lifespan, following infection (57).

During *P. vivax* infection, some individuals can acquire immunity naturally; such immunity consists of a cytokine production-mediated cellular immune response, cytokine receptors, and proteolytic enzymes forming part of the host response to infection, as well as IgG antibodies. Patients having moderate parasitemia in endemic regions of Colombia have high IFN- $\gamma$  and TNF- $\alpha$  levels, a pro-inflammatory cytokine profile correlated with the response found in an unstable transmission region. The balance in interleukin (IL)-10/TNF- $\alpha$  rate could prevent increased parasitemia and host pathology (58).

A study by Hemmer et al. evaluated the production of lactate dehydrogenase (as hemolysis parameter), TNF- $\alpha$  (which produces a response to parasite products and has antiparasitic activity), thrombin–antithrombin III (pro-coagulant activity parameter), and human neutrophil elastase (its secretion becoming increased by parasite products, having antiparasitic activity) in a population infected by *P. falciparum* and *P. vivax* or *P. ovale* (59).

The parasitemia/response rate of each parameter was greater in patients suffering *P. vivax* or *P. ovale* malaria than *P. falciparum*; regarding parasitemia, TNF- $\alpha$  response was stronger in *P. vivax* or *P. ovale* infection than *P. falciparum*. The increase of these factors in *P. vivax* infection helped to control parasitemia, while they led to complications in *P. falciparum* infection such as host response-mediated severe malaria (59). Studies have shown that *P. falciparum* parasitemia levels decrease when coinfected with either *P. vivax* or other *Plasmodium* species, compared to single infection (60), thereby attributing a possible attenuating role to other *P. falciparum* species (60–62).

Another study that compared the immune response of patients suffering complicated and uncomplicated malaria caused by *P. vivax* reported a higher IFN- $\gamma$ /IL-10 rate in patients having complicated disease, as well as higher TNF- $\alpha$  level. They concluded that the severity of disease caused by *P. vivax* was correlated with pro-inflammatory immune response activation and cytokine imbalance (63).

Interleukin-10 acts as immunoregulator by controlling the effects of other cytokines produced by CD4+ Th1 and CD8+ T-cells in *Plasmodium* infection. The overproduction of cytokines such as IFN- $\gamma$  by these cells not only helps to increase phagocytosis for eliminating the parasite but also produces immunopathological effects associated with the disease. However, studies involving another group of patients suffering *P. vivax* malaria found high levels of IFN- $\gamma$  and IL-10 in patients with previous episodes of malaria. Polymorphism studies regarding the IL-10 gene promoter in populations from endemic regions have shown that polymorphisms neither influence the production of this cytokine nor its regulatory function regarding the immune response (64, 65).

Goncalves et al. evaluated the cytokine pattern in uncomplicated symptomatic *P. vivax* and *P. falciparum* infection in a low malaria transmission region in Brazil to test the hypothesis that *P. vivax* infection causes a greater pro-inflammatory cytokine response than infection by other *Plasmodium* species. They

found a greater anti-inflammatory cytokine response than in *P. falciparum* infection, but similar pro-inflammatory cytokine response. The response of anti-inflammatory cytokines such as IL-10 and IL-10/TNF- $\alpha$ , IL-10/IFN- $\gamma$  and IL-10/IL-6 ratios in clinical malaria caused by *P. vivax* was short-lived and positively correlated with parasitemia rather than with the symptoms. This means that there must be a balance between inflammatory cytokine and regulator responses (66).

Network analysis was one of the approaches adopted by Mendoca et al. for understanding the interaction between different blood biomarkers for inflammation, tissue damage, and oxidative stress and the immunopathogenesis of malaria. They concluded that when studying uninfected individuals from endemic regions, the network of interactions showed high density between these biomarkers, limiting the symptoms but not the infection. IL-10 and IL-4 have connections with chemokine (C-X-C motif) ligand 9 (CXCL9) in uninfected people and with chemokine (C-C motif) ligand 2 and IFN- $\gamma$  in people having asymptomatic *P. vivax* infection (67, 68).

Such interactions revealed a protective role for IL-4 and IL-10 cytokines due to their modulating effect on these pro-inflammatory cytokine and chemokine. The network of biomarkers in patients suffering mild malaria consisted of IFN- $\gamma$ , tumor necrosis factor (TNF), and chemokine (C-C motif) ligand 5, while the interaction occurred between CXCL9 and IL-12 in symptomatic patients. CXCL9 was associated with regulatory cytokines thereby suggesting their role in resistance to infection, as well as being associated at the beginning with symptoms when linked to IL-12. Patients who had a fatal outcome regarding the disease had an interaction between TNF, IFN- $\gamma$ , and IL-10, the latter modulating the Th1 response, negatively regulating TNF and IFN- $\gamma$ , due to an IL-12p70 suppression that could lead to death (67, 68).

Cytokine profile variations have been observed in malaria-dengue coinfection. TNF levels have increased in patients with coinfection regarding single infection thereby highlighting the role of IL-6, INF- $\gamma$ , and IL-7 (68). Regarding the humoral response, antibodies play an import role in protection against malaria, and this has been demonstrated in different studies. Cohen et al. showed that passive transfer of antibodies from malaria-immune individuals to naïve young children suffering severe clinical malaria reduced the parasite density and clinical symptoms related to this disease (69). This experiment was confirmed by further studies where adult patients controlled the clinical symptoms and parasitemia after receiving intravenously injections of sera from people living in malaria-endemic areas (70, 71).

Immunoglobulins can protect or arrest disease progression in different ways; neutralizing anti-Spz antibodies can block Spz from invading hepatocytes (72–74). Mrz can be opsonized in the erythrocyte stage by specific antibodies that activate cell-mediated death or prevent the invasion of RBC and block the proteins responsible for binding to molecules on cell surface.

Studies in malaria-endemic areas have suggested that high IgG3 and IgG1 cytophilic antibody titers are associated with protection (75). *In vitro* studies have shown that monocytes can kill asynchronous malaria parasites in the presence of cytophilic IgG3

and IgG1 antibodies (76). These antibodies facilitate phagocytosis and kill *Plasmodium* parasites since cross-linked Fc $\gamma$ R-Fc induce a respiratory burst. Antibody responses against *P. vivax* CSP-1 (77), PvMSP-1 (78–81), PvRBP1 (82, 83), PvAMA-1 (84), and PvMSP-3 $\alpha$  (85, 86) have been characterized by IgG1 and IgG3 predominance, which are associated with malaria exposure and malaria protection; Tables 1 and 2 summaries the results obtained in each study.

## MHC Molecules and the Immune Response

Major histocompatibility complex proteins have high polymorphism in human beings; antigen-binding capability varies from one allele to another, increasing or reducing their affinity (55). The forgoing is essential for developing an effective vaccine inducing a protective immune response.

Major histocompatibility complex antigen-presenting molecules are divided into two large groups. Class I present intracellular antigens and can couple eight to nine amino acid-long peptides due to the smaller size of their grooves. Class II recognizes extracellular antigens and can display 13–18 amino acid-long peptides (109).

The genes encoding class II MHC proteins in humans are called human leukocyte antigen (HLA) and are in chromosome 6. They have alpha and beta subunits, an immunoglobulin domain, and a short transmembrane portion. They have genes from three classes of protein: HLA-DP, HLA-DQ, and HLA-DR; the most polymorphic locus is HLA-DR at expense of a highly polymorphic beta subunit, unlike the alpha subunit, which is monomorphic in humans (110).

The peptide's binding site is formed by two almost parallel alpha helix regions above a beta sheet. The peptides are bound in the groove formed by the helices, with their terminal residues extended. The peptides adopt an extended poly-proline type II conformation exposing the peptide backbone to MHC conserved hydrogen-bonding residues covering the groove. Such conformation allows a peptide's side-chains to bind to the groove of the MHC binding site, as well as allowing the side-chains to bind to MHC pockets in positions 1, 4, 6, and 9. The others bind to the T-lymphocyte receptor (TCR)-binding site (55, 111).

Major histocompatibility complex class II molecules, expressed constitutively on antigen-presenting cell surface (DCs, macrophages, and B-lymphocytes) recognize extracellular peptides processed by the endosome/lysosome pathway, which are edited by the HLA-DM molecule. MHC class II presents the antigen to the TCR of CD4+ T-lymphocyte (T-helper) (55).

The CSP is one of the most important proteins described to date in Spz. Previous studies involving individuals residing in *P. vivax* malaria-endemic regions in Brazil have shown low responses for antibodies directed against the repeat region. An association has been reported between the HLA-DR16\* allele and antibody response to *P. vivax* VK247 variant CSP repeats, as well as an association between the HLA-DR7\* allele and a lack of antibody response to VK210 variant CSP repeats (112).

A study involving an infected population in Brazil evaluated the relationship between HLA-DRB1\* alleles and the antibody

**TABLE 1 |** *PvCSP peptide antigenicity*.

Antigen	Sequence	Country	N	Prevalence of individuals having anti-antigen reactivity (IgG)	Reference
N	SSILLVLDFFTHCGHNVDSLKAINLNQVNFFNVDASSLGAAAHVGQSASRSGRLGENPDDEEGDAKKKDGGKAEEFKNPRENKLKPGQ	Colombia	80	35%	(87)
R	GDRADGQPA	Colombia	80	61%	(87)
C	YLDKV RATV GTEWTPCSVTCGV GVR VRRV NAANKKPKEDLT LNDLET DVC TMDCAGIFN VSN S LGLVILL	Colombia	80	39%	(87)
PvCS-NRC	KAEPKNPREN KI KQPGDRAD	Colombia	42	58%	(88)
PvNR1R2	GQPAGDRADGQPA-PEG-KAEPKNPREN KI KQPGENGAGDQPGANGAGNQPG-PEG-NNEGANA PNEKS VKEY LDKV/RATV/GTEWTPC SVTCGV GVR VRRV NAANKKPKEDLT LNDLET DVC TMDCAG	Papua New Guinea (PNG)	32	69%	(89)
VMP 001	LGAAHVVGQSASRSGRLGENPDDEEGDAKKKDGGKAEPKNPREN KI KQPGANGAGNQPGANGAGNQPGDADGQ	Colombia	36	81%	(90)
rPvCSP-c	Recombinant PvCSP with two copies of VK210 repetitive region (GDP(A/D)GQPA) and one of VK247 (ANGAGNGPG) PAGDRADGQPA GQPA	PNG	42	24%	(91)
	Recombinant PvCSP with four copies of the VK210 repetitive region (Belem strain) and three of VK247 (PNG strain)	Thailand	50	82%	(92)
		Brazil	40	65%	
		Thailand/Korea	114	73%	

response to CSP, MSP-1, AMA-1, and Duffy binding protein (DBP) peptides. A significant association was found between high MSP-1 antibody levels (especially to the *Pv*200L fragment) and the HLA-DR3\* allele; while no association was found between CSP, AMA-1, and DBP antibody production and HLA-DRB1\* alleles (113).

During the erythrocyte phase, the merozoite surface protein (MSP) family is the responsible of the interaction between Mrz and reticulocytes. *Pv*MSP-1, *Pv*MSP-3, and *Pv*MSP-9 are potential vaccine candidates since they are exposed to the immune system and are recognized by antibodies from naturally infected individuals. A study by Lima-Junior et al. evaluated IgG antibody response to *P. vivax* MSP-1, MSP-3 $\alpha$ , and MSP-9; a relationship between HLA-DRB1\*04 individuals and high antibody response to *Pv*MSP3<sub>CT</sub> and *Pv*MSP3<sub>NT</sub> and HLA-DQB1\*03 individuals, and response to *Pv*MSP3<sub>CT</sub> was observed (86).

IgG response was positively associated with HLA-DRB1\*04 and HLA-DQB1\*03 individuals regarding *Pv*MSP-9 repeat regions and the NT region. Such response involving high antibody levels was associated with a possible selective pressure by *P. vivax* in the Amerindian population. Antibody responses for *Pv*MSP-9 were more correlated with the time spent living in a malaria-endemic area and not with a particular HLA-DRB1\* allele (86).

Ferreira et al. constructed and expressed a synthetic gene encoding promiscuous T-helper epitopes bound to the *Pv*RBP1<sub>435-777</sub> sequence. Although it has been observed in clinical assays that candidates for a vaccine against *P. vivax* are poorly immunogenic, they predicted that this chimerical protein (called *Pv*RMC-RBP1) would be recognized by multiple HLA alleles. Epidemiological and serological studies proved the preservation of B-cell conformational epitopes in the chimeric protein. However, no association was found between HLA-DRB1\* and HLA-DQB1\* alleles and IgG antibody responses to the chimeric or native proteins. This seemed to be because *Pv*RBP1 had multiple promiscuous T-cell epitopes, which did not induce specific genetic restriction (83).

## Non-HLA Host Polymorphism

Miller et al. proved (for the first time) the hypothesis that the Duffy negative erythrocytes are resistant to *P. vivax* infection in Africans (114). The Duffy antigen or Duffy antigen receptor for chemokines (DARC) is expressed on RBC surface (115). Its encoding genetic locus having three alleles [FY\*A (Fy<sup>a</sup>) and FY\*B (Fy<sup>b</sup>) with SNP of differences and FY\*O] has a negative serological phenotype Fy(a–b–) (116, 117). The absence of DARC expression in RBC is due to a point mutation (T46C) in the GATA box of this gene's promoter (118, 119).

Duffy negative patients infected with *P. vivax* have been found during the last few years (56, 120). Mendes et al. reported that Duffy negative individuals from Africa's West Coast were infected with different strains of *P. vivax*, and they concluded that the parasite evolved quickly and used other receptors different to Duffy to invade RBC (121).

The balance between innate and adaptive immune response is important in the development of immunopathology and clinical severity in several infectious diseases. Sohail et al. have investigated polymorphisms in the TNF- $\alpha$  gene promoter region and

**TABLE 2 | Erythrocyte phase protein antigenicity.**

Protein	Protein region	Country	N	Prevalence of individuals having anti-antigen reactivity (IgG)	Reference
Merozoite surface protein-1 (MSP-1)	N-terminal (NT) C-terminal	Brazil (Pará)	37	51.4% 64.1%	(78)
MSP-1	C-terminal ( <i>Pv</i> 200 <sub>18</sub> —18 kDa fragment)	Republic of Korea (Northern Province of Kyunggi)	421	88.1% (IgG) 94.5% (IgM)	(93)
MSP-1	<i>Pv</i> 200L	Colombia (Buenaventura)	69	52.2%	(94)
MSP-1	C-terminal ( <i>Pv</i> 200 <sub>19</sub> —19 kDa fragment)	Turkey (Province of Sanliurfa)	82	69.5% (IgM) 53.6% (IgG) 7.3% (IgA)	(95)
Merozoite surface protein-1 paralog	C-terminal ( <i>Pv</i> MSP1P-19) C-terminal ( <i>Pv</i> MSP1P-33)	Republic of Korea (Province of Gyeonggi Gangwon)	30	73% (IgG3) 43% (IgG1) 57% (IgG1)	(81)
<i>Pv</i> MSP3- $\alpha$	Full length C-terminal NT	Brazil	276	77% 54% 39%	(86)
<i>Pv</i> MSP3- $\alpha$	Full length Repeat block I Repeat block II C-terminal NT	Brazil (Rondonia State)	282	78% 64% 53% 54% 39%	(85)
<i>Pv</i> MSP3- $\alpha$	Repeat block I Repeat block II C-terminal NT	Papua New Guinea (PNG)	264	36% 38% 65% 38%	(96)
<i>Pv</i> MSP3- $\alpha$	FP-1 (aa 359–798)	Brazil (Amazon region)	220	68%	(97)
<i>Pv</i> MSP3- $\beta$	FP-1 (aa 35–375) FP-2 (aa 385–654) FP-3 (aa 35–654)	Brazil (Amazon region)	220	26% 64.5% 66%	(97)
<i>Pv</i> MSP-9	<i>Pv</i> MSP9-Nt <i>Pv</i> MSP9-RI-RII <i>Pv</i> MSP9-Ct	Brazil (Ribeirinha, Colina)	306	74%	(98)
<i>Pv</i> MSP-9	<i>Pv</i> MSP9-NT V <sub>147</sub> -K <sub>159</sub> ; V <sub>438</sub> -D <sub>449</sub> ; K <sub>325</sub> -I <sub>339</sub> ; P <sub>434</sub> -I <sub>448</sub> ; A <sub>443</sub> -K <sub>456</sub>	Brazil (Rondonia state)	142	61.2% (IFN- $\gamma$ ) 49% (IL-4)	(99)
<i>Pv</i> MSP-9	<i>Pv</i> MSP9-Nt <i>Pv</i> MSP9-RI-RII	PNG	183	45.9% 8.7%	(96)
Duffy binding protein (DBP)	DBPII-IV	PNG (Mandang)	100	60%	(100)
DBP	DBPII-IV	Colombia (Buenaventura)	92	40%	(101)
Apical membrane antigen-1 (AMA-1)	PV66/AMA-1	Brazil (North)	221	85% (IgG) 48.5% (IgM)	(102)
AMA-1	DI DII DIII DI-DII DII-DIII Ectodomain	Brazil (Amazonas region)	100	13% 65% 12% 60% 58% 70%	(103)
AMA-1	<i>Pv</i> AMA-1	Iran	84	81%	(104)
AMA-1	<i>Pv</i> AMA-1	Brazil	1,330	52.5%	(105)
AMA-1	<i>Pv</i> AMA-1	Brazil	83	73%	(106)

(Continued)

**TABLE 2 | Continued**

Protein	Protein region	Country	N	Prevalence of individuals having anti-antigen reactivity (IgG)	Reference
PvRBP1	Full length <i>PvRBP1</i> <sub>431–748</sub> <i>PvRBP1</i> <sub>733–1407</sub>	Brazil (Rondonia state)	294	66% 41% 47%	(82)
PvRBP1	<i>PvRMC-RBP1</i> <i>PvRBP1</i> <sub>23–751</sub>	Brazil (Rondonia state)	253	47% 60%	(83)
PvRBP1	Coiled-coil and C-terminal peptides	Republic of Korea	16	68%	(107)
PvRBP2	Repeat sequence peptides NT and repeat sequence peptides Coiled-coil and C-terminal peptides			62% 68–87% 62–68%	
PvRBP1	<i>PvRBP1a-34</i> <i>PvRBP1b-32</i>	Republic of Korea	104	34% 39%	(108)

its association with vivax infection in an Indian population. They found that TNF-308A and TNF-1031C were associated with vivax infection (very low frequency) in the study population (122). Other research has shown that IL1B, IL4R, IL12RB1, and TNF genes were associated with susceptibility to *P. vivax* malaria in a population from Brazil's Pará state, reporting  $-5,839\text{C}>\text{T}$  SNP promoter association with *P. vivax* malaria susceptibility (123).

Da Silva et al. have shown an Amazonian population's many host polymorphisms association with susceptibility or resistance to malaria infection. SNPs in the IL-10, CTL4 and TLR4 genes have been significantly associated with lower risk of clinical malaria, while a SNP in the IRF1 gene has displayed an enhanced risk. An intronic SNP in LTA was associated with protection, and one SNP on the TNF promoter was associated with susceptibility to clinical malaria (124).

Another study found no differences regarding IL6-176G>C polymorphism distribution in participants making up the different clinical groups of vivax malaria in a Brazilian population. No association was found between TNF-308G and clinical manifestations of malaria and no haplotype having DDX39B (22 C>G and 348 C>T) and TNF-308G> was identified or polymorphisms increasing the risk of clinical vivax malaria. Moreover, study participants having the genotype combination described here associated with resistance against manifestations of *P. vivax* infection (CG/CC/GG/GG) also had lower levels of pro-inflammatory TNF and IL-6, suggesting that DDX39B confers protection against malaria pathogenesis by reducing inflammatory response (125).

## ***P. vivax* PREERYTHROCYTE PHASE PROTEIN ANTIGENICITY AND IMMUNOGENICITY**

### ***P. vivax* CSP**

One of the predominant surface proteins in Spz is the CSP; it is expressed during the preerythrocyte phase and plays a fundamental role during hepatocyte invasion (126). This protein is a candidate for a vaccine against malaria in the preerythrocyte

phase since various studies have shown that anti-CSP antibodies block hepatocyte invasion (88, 127, 128).

Circumsporozoite protein in the different *Plasmodium* species has a highly conserved structure; it consists of an NT extreme (N), a species-specific central repeat region (R) located between two conserved regions (region I and region II), and a GPI anchor in the C-terminal extreme (129). The repeat region contains an immunodominant B-cell epitope, which is associated with its immunogenic potential (130).

Furthermore RTS,S/AS01, the most advanced recombinant vaccine to date for preventing malaria caused by *P. falciparum*, is designed from *P. falciparum* circumsporozoite protein (*PfCSP*) repeat region peptides and C-terminal region T- and B-epitopes, coexpressed with hepatitis B surface antigen. Phase III clinical studies have shown 33–50% efficacy 1-year post-immunization in 5- to 17-month-old infants (89, 92, 131). However, after a 7-year follow-up, the vaccine efficacy declined to 4.4%, with a 16.6% efficacy against all episodes of clinical malaria in the low-exposure cohort and to  $\sim 2.4\%$  in the high-exposure cohort (132). Furthermore, no vaccine efficacy was observed against severe malaria in children and young infants immunized with RTS,S/AS0 (133). Given that CSP has been widely studied in *P. falciparum*, and among different *Plasmodium* species, this protein is considered as a potential target for designing a vaccine against *P. vivax* (134–137).

Three allele variants of the *P. vivax* circumsporozoite protein (*PvCSP*) have been described: VK210, VK247, and vivax-like CSP-P, which differ at repeat region sequence level (138, 139). VK210 has greater global distribution, being found in countries like Brazil (140), India (141), Thailand (142), and Peru (143), while VK247 is found in some regions of Colombia and Brazil (144), and vivax-like CSP-P in Brazil (140), Indonesia, Madagascar, and PNG (139).

Antigenicity studies in people exposed to the disease in different endemic regions have found variable prevalence in individuals responding to different *PvCSP* fragments (87) (Table 1). Preclinical studies and phase I clinical assays (Table 3) have been carried out regarding *P. vivax* with long synthetic peptides (LSP)

having more than 70 *Pv* amino acids from *PvCSP* amino terminal (N), carboxyl terminal (C), and repeat (R) regions linked to tetanus toxoid peptide (87). Immunized non-human primates from the genus *Aotus* spp. produced specific antibody response recognizing both LSP and CSP since the first immunization (87). LSP has also induced a Th1-type immune response characterized by increased IFN- $\gamma$  and reduced IL-4 production in T-lymphocytes stimulated *in vitro* (87, 137).

High IFN- $\gamma$  production *in vitro* and cytophilic antibodies (IgG1 and IgG3) capable of recognizing fragments from the *PvCSP* N- and R-regions have been produced by LSP (as in experimental models) in phase I clinical assays. By contrast, the C-terminal region has not been immunogenic in humans (77).

Specific B- and T-cell epitopes must be included to stimulate an immune response thereby enabling recognition by class I and class II MHC molecules. Two modified LSP, *PvCS-NRC* (137 aa) and *PvNR<sub>1</sub>R<sub>2</sub>* (131 aa) have induced a strong antigen-specific antibody response in immunized mice. They have inhibited Spz invasion of hepatoma cells (HepG2A-16) *in vitro* by 65 and 90% for both *PvCS-NRC* and *PvNR<sub>1</sub>R<sub>2</sub>*, respectively (88, 128). *PvCS-NRC* has included conserved regions I and II and the repeat region sequence from VK210 and VK247 variants (88, 129). *PvNR<sub>1</sub>R<sub>2</sub>* has been improved by including B-epitopes, T-epitopes, and cytotoxic lymphocytes epitopes (128).

Immunogenic fragments of CSP have been evaluated in a recombinant vaccine (VMP 001) expressed in *Escherichia coli* encoding a *PvCSP* chimera (149). VMP 001 has triggered a potent immune response in BALB/c mice following a third immunization. The antibodies so produced were capable of agglutinating live Spz, indicating a loss of Spz-infective capability (150). r*PvCSP*-c, a recombinant protein similar to VMP 001 (91), has shown antibody-specific reactivity against variants VK210 and VK247 (151).

Formulations have been made with adjuvants or TLR agonists to maximize vaccine candidate fragments' immune response. Regarding adjuvants, assays involving BALB/c mice and *Aotus* spp. monkeys have proved that formulation with Freund's, Montanide ISA270, and Montanide ISA51 adjuvants, which have not led to significant differences concerning specific antibody production. However, clinical assays have revealed greater immunogenicity (having greater antibody titers and IFN- $\gamma$  production) when

Montanide ISA 51 adjuvant was used (145). Other adjuvant that has been tested is the inert nanoparticles, which is coated with the *P. berghei* CSP and induced CD8 T cell immunity without pro-inflammatory signals and also induced IFN- $\gamma$  production levels determined to be required for sterile protection in the *P. berghei* challenge model (152).

*PvCSP* has been formulated with TLR agonists helping to improve the immune response. *Aotus nancymaae* immunized with VMP 001 plus a TLR9 agonist (CpG 10104) have produced high antibody titers since the first dose, antibodies directed against the C-terminal region, and the VK210 variant repeat region predominating. It was seen that 66.7% of immunized primates became protected following experimental challenge (153), associated with the activation of B-cells, macrophages, and DCs by the CpG 10104 agonist (154).

Other formulations have been evaluated by using new agonists. When using VMP 001 for immunization with the TLR4 agonist (glucopyranosyl lipid A) it was found that this created a CD4+ cell response with high IL-2 production but low TNF levels (90). Fusing a polypeptide covering the *PvCSP* immuno-dominant region coformulated with the FliC agonist (*Salmonella typhimurium* flagellin) produced a PAMPs-dependent immune response via TLR5 (155).

The results of *PvCSP* vaccine phase I/II of *Pv*(VMP001/AS01B) have been published recently; it induced an antibody, cell-mediated immune response and delayed the latent period, but it did not induce sterile protection (146). Experience with *P. falciparum* vaccines has demonstrated that single-stage and single-target antigens cannot induce long-lived, sterile protection (133). The next generation *P. vivax* vaccine should include multiple targets, especially those needed for binding to host cells and those blocking transmission.

## Thrombospondin-Related Adhesive Protein (*PvTRAP*)

The thrombospondin-related adhesive protein (TRAP) has also been evaluated as a potential preerythrocyte phase vaccine candidate. TRAP is a type I transmembrane protein, expressed in the micronemes and translocate to Spz surface during hepatocyte invasion. The ectodomain consists of an A domain, a thrombospondin type 1 repeat (TSR), and a repeat region, which is variable among species. The A and TSR regions are cell adhesion domains that interact with hepatocyte membrane receptors thereby enabling invasion (156–158).

This protein has been studied in *P. berghei* and *P. falciparum* as vaccine candidate; these studies showed a significant reduction in parasites during hepatic phase, mediated by CD8+ cytotoxic T-lymphocytes but involving low antibody production (159, 160) *P. falciparum* (161).

A *P. vivax* study with *PvTRAP* LSP involved immunizing mice and *Aotus* spp., which were then experimentally challenged. A good antibody response against the peptide was produced in mice, but only 50% recognized Spz. Four immunizations were needed in *Aotus* for obtaining a significant antibody titer, but IFN- $\gamma$  levels did not increase; four of the six monkeys became protected following experimental challenge (162).

**TABLE 3 |** *Plasmodium vivax* vaccine clinical trials.

Stage	Protein	Name	Type	Clinical trial	Reference
Preerythrocytic	PvCSP	CSP-N, -R, -C	LSP	Phase Ib	(77, 145)
	PvCSP	VMP001	Rec	Phase I, IIa	(146)
Transmission blocking	Pvs25	ScPvs25/ISA51	Rec	Phase I	(147)
	Pvs25	Pvs25H/Alhydrogel	Rec	Phase I	(148)
Erythrocytic	PvDBP	ChAd63 PvDBP	Viral vector	Phase Ia	www.clinicaltrials.gov NCT01816113

LSP, long synthetic peptide; Rec, recombinant; CSP, circumsporozoite protein.

Mice immunized with *Pv*TRAP expressed in viral vectors have induced a better immune response associated with high IFN- $\gamma$  production and TNF- $\alpha$  by CD8+ T-lymphocytes and the production of high antibody titers specific against *Pv*TRAP. A marked increase in IL-2 production from CD8+ lymphocytes has been seen after inoculating Spz, indicating an active response in the liver (163).

One of the main problems in developing an antimalarial vaccine using *Pv*TRAP has been its high genetic polymorphism observed in different isolates from different regions around the world (164). An approach to preventing these problems would involve studying proteins' conserved regions instead of using immune-dominant antigens, which are highly polymorphic.

## ***P. vivax* ERYTHROCYTE PHASE PROTEIN ANTIGENICITY AND IMMUNOGENICITY**

### **Merozoite Surface Protein-1 (MSP-1)**

The MSP family has been the most studied candidate from the erythrocyte asexual phase when developing an effective vaccine against malaria. The MSP-1 belongs to this family, being one of the most studied and currently important for both *P. falciparum* and *P. vivax* (165).

The MSP-1 analog in *P. vivax* is encoded by the *Pv*200 gene (166), having a 200-kDa molecular weight (167). The proteolytic processing profile is thought to be similar than for *P. falciparum* MSP-1, leading to 4 fragments: 83, 30, 38, and 42 kDa; further cleavage of the last one (C-terminal region) produces 33 and 19 kDa polypeptides, which are released to the blood stream. A 19-kDa portion remained bound to the recently formed ring phase following reticulocyte invasion (79, 168).

A study in *Pv* exposed individuals found IgG responses to r*Pv*200L (like the *Pf*190L fragment) indicating that the protein has high antigenicity. Sera from immunized animals showed IgG-specific antibodies capable of recognizing this protein *Pv*. The authors highlighted the fact that the observed response had a protective tendency since *Aotus* spp. developed low parasitemia peaks following *P. vivax* challenge (94).

The 19-kDa C-terminal fragment has been one of the most studied from MSP-1 (*Pv*200). Kaslow and Kumar studied *Pv*200<sub>19</sub> protein immunogenic capability in mice vaccinated with three doses. An increase in antibodies was observed in sera, which became increased with the second vaccination, this being attributed to a booster for helping epitopes in *Pv*200<sub>19</sub>. The response was T-cell dependent, suggesting that an immune response to a vaccine based on this protein could be boosted by natural infection (169).

Studies in an endemic area of Brazil by Soares et al. detected IgG antibodies against MSP-1 C-terminal and NT region. Response to the C-terminal region increased according to patients' number of previous episodes of malaria, an increase of up to 80% being observed in patients who had suffered more than four episodes. Moreover, *in vitro* proliferation was observed in 47% of the individuals and IFN- $\gamma$  production 54% of them. This study suggests that the C-terminal region contains two immunogenic epidermal growth factor (EGF)-like domains

which induce T-cell and antibody responses against *P. vivax* during natural infection in humans (78). Later studies with the C-terminal region, specifically *Pv*MSP-1<sub>19</sub>, have shown that these two EGF-like domains function as a binding portion in *Pv*MSP-1 interaction with erythrocytes (170).

Later studies by Soares et al. found that antibody titers against *Pv*MSP-1<sub>19</sub> became rapidly reduced (by up to 13-fold) in infected individuals and those who had received treatment against the disease. Antibody response against the NT region became reduced, even though such reduction was not significant. The decrease of antibodies directed against the C-terminal region could have contributed toward cases of reinfection in high-risk areas (171). Fernandez-Becerra et al. evaluated IgG subclasses in children, finding a predominant IgG1-type response against the C-terminal region and low IgG3 and IgG4 percentages. The predominant antibodies in adults were IgG3, a correlation between antibodies against the C-terminal region and age being observed (172).

High antibody titers against *Pv*200<sub>19</sub> have been observed in infected soldiers in the republic of Korea *Pv*, mostly IgG and IgM to a lesser extent; these were maintained for a long period of time (from 4 to 6 months) following recovery from malaria (173). Another study showed that IgG antibody permanence was maintained for more than 5 months, while IgM-type remained negative 2–4 months after the onset of symptoms (93).

The major responses in Turkey (where *P. vivax* is the only *Plasmodium* species present in the area) were IgG, IgM, and IgA to a lesser extent. It is worth highlighting the fact that *Pv*MSP-1<sub>19</sub> was highly antigenic in individuals who are naturally exposed to the infection and, since no other Plasmodia are infecting in that area, the response observed cannot be attributable to a crossed reactivity (95).

Rosa et al. characterized the *MSP-1*<sub>19</sub> recombinant protein's antigenic and immunogenic properties together with two T-helper epitopes (the universal pan allelic DR epitope and a new internal MSP-1 epitope from the 33-kDa C-terminal region). It was seen that T-helper epitopes did not modify protein recognition by human IgG. The complete recombinant protein was immunogenic in marmosets (*Callithrix jacchus jacchus*), but only when Freund's adjuvant was used (174).

A study of immune response and protection was conducted in our institute, two groups of *Aotus* spp. (one splenectomized and the other not) were immunized with two recombinant polypeptides (r*Pv*MSP-1<sub>14</sub> and r*Pv*MSP-1<sub>20</sub>) from the MSP-1 33-kDa C-terminal region containing high activity binding peptides (HABPs) to reticulocytes. Most immunized monkeys recognized the r*Pv*MSP-1<sub>14</sub>, r*Pv*MSP-1<sub>20</sub>, or the mix of HABPs by enzyme-linked immunosorbent assay (ELISA) and denatured *Pv*MSP-1 42 and 33-kDa fragments by Western blot. Although half the animals immunized with the r*Pv*MSP-1<sub>14</sub> and r*Pv*MSP-1<sub>20</sub> mixture were protected, some monkeys did not produce antibodies against the vaccine candidate. This suggested that protection was not only mediated by a humoral immune response (175). The next study involved vaccinating *Aotus* spp. monkeys with the two above mentioned recombinant polypeptides but in three doses. *Aotus* spp. produced antibodies capable of recognizing the native protein and managed to control parasitemia in four out of the five immunized

monkeys. Interestingly, some animals produced high IFN- $\gamma$  levels and controlled parasitemia but displayed low antibody titers; conversely, some other animals were protected having high antibody titers but low IFN- $\gamma$  levels (176).

Other studies have found that anti-*PvMSP-1* antibodies (predominantly IgG), recognizing the NT region, are associated with a reduced risk of infection and clinical protection against the *PvMSP-1*. Although these antibodies do not recognize the C-terminal region (79), there have been reports that the C-terminal region is immunogenic and capable of naturally stimulating antibody production in new infections (78, 93, 173).

The MSP-1 protein's 42-kDa fragment has also been studied due to its potential as vaccine candidate; its immunogenicity was evaluated in mice. High IgG1, IgG2a, and IgG2b antibody levels were observed while IgG3-type response was low. A high proliferative response also found high IL-2, IL-4, IL-10, and IFN- $\gamma$  levels being detected in culture supernatants (177). Greater prevalence of recognition of *PvMSP1<sub>19</sub>* than *PvMSP1<sub>42</sub>* was found when a naturally acquired humoral immune response was reported (178).

An MSP-1 paralog has been identified recently (*PvMSP1-P*); its immune response was characterized using different protein fragments (83, 30, 38, 42, 33, and 19 kDa). The NT (83 kDa) fragment and two from the C-terminal region (33 and 19 kDa) were recognized by sera from infected patients living in endemic areas (179).

IgG1 and IgG3 (IgG2b in mice) were the predominant responses in patients from endemic regions, as in immunized mice. The C-terminal region induced a predominantly Th1 profile of cytokine response having high TNF, IFN- $\gamma$ , and IL-2, but low levels of IL-10 and IL-4 cytokines (Th2 profile), showed greater lymphoproliferative response than the MSP1-19 fragment. The correlation between parasitemia and anti-MSP1P antibody level suggest that it does not contribute strongly to inhibiting parasite growth (81).

Due to its colocation with MSP1, it has been thought that it played a similar role in erythrocyte invasion; however, analyzing the sequences has suggested different roles for each protein. Cytoadherence assays demonstrated that MSP1-P could be an essential adhesion molecule regarding *P. vivax* invasion to erythrocytes, is immunogenic in humans, and is a potential vaccine candidate against *P. vivax* (179).

### Merozoite Surface Protein-3 (MSP-3)

The *P. vivax* merozoite surface protein-3 (*PvMSP3*) is a member of the MSP family characterized by having a highly polymorphic alanine-rich central domain (180). It has a relatively conserved N- and C-terminal domain and two central blocks of seven repeats forming tertiary supercoiled helices in their structure (180–182). It is expressed in schizonts and is associated with Mrz surface during the erythrocyte phase (180).

Its homolog in *P. falciparum* has been studied as a vaccine candidate in preclinical (183) and phase I assays, protection was associated with reduced parasitemia by cytophilic antibodies inducing antibody-dependent cell-mediated inhibition of parasite growth mechanism (184). It has been shown to be highly

immunogenic in *P. vivax*, having a high prevalence of antibodies directed against *PvMSP-3 $\alpha$*  block II (96).

A correlation has been described between time spent living in an endemic region and the number of previous episodes of malaria, involving an increase in IgG1 and IgG3 anti-*PvMSP-3 $\alpha$*  (85, 86, 96). A naturally acquired response has been found toward 15 antigenic determinants, mainly located in repeat regions (85). Other studies have reported the C-terminal region as being the most antigenic, having a significant increase in IgG in a population from Brazil (97) and PNG (96). However, it has been found the antibodies directed against block II are associated with protection against clinical episodes of *P. vivax* malaria, having greater than 500 parasites/ $\mu$ L parasitemia (96).

Interestingly, no response against *PvMSP-3 $\alpha$*  was produced in immunogenicity studies with C57BL/6 mice, while high antibody titers were produced with *PvMSP-3 $\beta$*  following the second and third immunization (97). Incorporating adjuvants (Quil A, TiterMax, or IFA) has maximized the response against *PvMSP-3 $\alpha$* , indicating that another parasite's molecules must act as adjuvant for *PvMSP-3 $\alpha$*  antigenic presentation during natural infection (96, 97). Regarding cellular response, *PvMSP-3 $\beta$*  with Quil A, Titer Max, or IFA adjuvants have produced a balanced Th1/Th2 response, while the Alum adjuvant directed response toward Th2 with a significant murine IgG1 increase. Alum co-formulated with the TLR9 agonist (CpG ODN 1826) balanced the Th1/Th2 relationship, increasing Th1 response due to pro-inflammatory cytokine production (97).

### Merozoite Surface Protein-9 (MSP-9)

The *P. vivax* merozoite surface protein-9 (*PvMSP-9*) is also a potential vaccine candidate. Some studies have shown that this protein is conserved among *Plasmodium* species infecting humans, rodents, and primates. Furthermore, antibodies produced against *PvMSP9* homologs in *P. cynomolgi* and *P. knowlesi* can inhibit Mrz invasion of erythrocytes (180).

The *P. vivax*, *P. knowlesi*, and *P. cynomolgi* *msp-9* genes encode a hydrophobic signal peptide and repeat motifs upstream of the stop codon and a C-terminal region having two species-specific blocks of repeat amino acids (*PvMSP9-R1* and *PvMSP9-R2*). Together with *P. falciparum* has four cysteine residues close to the NT giving the MSP-9 family's structural and functional characteristics. This protein is expressed during schizogony and is organized on Mrz surface during schizont development and segmentation (180, 185).

The cellular and humoral immune response of BALB/c mice immunized with *PvMSP9-Nt*, *PvMSP9-RI* recombinants, and the mixture of both recombinants was evaluated for testing *PvMSP-9* immunogenicity. Antibody response in mice was determined by ELISA and was mainly IgG; there were greater titers for IgG1, IgG2a, and IgG2b isotypes than IgG3. Regarding cellular response, the amount of spleen cells secreting IFN- $\gamma$  was higher than those secreting IL-5. Moreover, sera from patients living in an endemic region of Brazil recognized the two recombinant regions, demonstrating that both were immunogenic (186).

A study was carried out on a population, which was naturally exposed to *P. vivax* infection in Brazil, and the immune response against *PvMSP9-R1R2* and *PvMSP-N* terminal domains was

evaluated. Of the 306 individuals in this study, 74% had IgG antibodies that recognized at least one of the recombinant proteins, thereby indicating that these proteins are antigenic during natural infection, especially *PvMSP9*-RIRII. When the IgG subclasses were evaluated, IgG1 was predominant for *PvMSP9*-RIRII and *PvMSP9*-N terminus, and IgG2 was prevalent for *PvMSP9*-RII. Furthermore, five synthetic peptides predicted to bind to HLA-DR alleles were chosen, and the overall cellular response frequency for at least one of the peptides was 58% for IFN- $\gamma$  and 41% for IL-4. No association was found between IFN- $\gamma$  production and IgG levels regarding recombinant proteins. Lima-Junior et al. thus concluded that *PvMSP9* C-terminal and NT domains are immune response targets for individuals living in *P. vivax* endemic regions. The reactivity index for IgG has been positively correlated with time spent living in an endemic area; conversely, IgG3 reactivity did not predominate regarding response to the recombinant proteins. It has been shown that *PvMSP9* NT region peptides induce memory T-cell response where IFN- $\gamma$  and IL-4 cytokines produced in significant proportion by individuals from endemic regions has indicated the presence of T-cell epitopes (98).

Another study involving volunteers from an endemic region of the Amazon region showed that the response of cells producing IFN- $\gamma$  was significantly greater than those regarding IL-4. The results obtained for 5 of the 11 peptides selected contained *PvMSP9* promiscuous T-cell epitopes. The core sequence (ASIDSMI) shared by three of the peptides was highly immunogenic; another peptide could have had two immunodominant epitopes, one in the overlapping core region and another in the C-terminal region, which produced a cellular response in 23 volunteers (99).

The specific response of IgG to *PvMSP9*-N terminal has been associated with protection against symptomatic *P. vivax* infection in children aged less than 3 years old in a PNG endemic region. Such antibodies specific for *PvMSP9* were prevalent in children suffering frequent infections and have been associated with protection in children who have not had these infections. The authors concluded that two classes of antibodies are produced against the *PvMSP9* NT region, one produced by short-lived memory B-cells and the other by long-lived cells (96).

## Duffy Binding Protein (DBP)

*Plasmodium vivax* Mrz requires antigens from the Duffy blood group as surface receptor for invading human reticulocytes (114). *P. vivax* DBP adhesion to its receptor on erythrocytes [Duffy antigen receptor for chemokines (DARC)] is essential for the parasite to continue developing during the asexual phase in human blood (114, 187). *PvDBP* is a 140-kDa protein, which is located in the micronemes; it has been divided into four important regions: a peptide signal sequence (region I), two cysteine-rich regions separated by a non-homologous hydrophilic region (region II, identified as the erythrocyte-binding domain, and region VI), and transmembrane domain (region VII) (188–191). *PvDBP* is a main target to use as vaccine candidate since its importance during parasite invasion and its ability to induce antibodies against the parasite's asexual phases (114, 192).

Serological evaluation in a PNG endemic area has shown that a humoral immune response was common and increased

with age, suggesting a possible booster effect regarding antibody response in some cases by repeated exposure to the infection (100). A similar pattern has been observed in an endemic region of Colombia where a positive correlation was found between increased antibody response and patients' age. Also, an immunologic boost for DBP was found, even in endemic areas having a low transmission level (101). The forgoing shows that DBP<sub>II</sub> was naturally antigenic in people residing in endemic regions.

Children having high antibody levels against DBP<sub>II</sub> has been associated with delayed reinfection time with the same *P. vivax* variant; however, such association was not observed when evaluating MSP1-19 (193). In other studies have been observed that naturally acquired neutralizing antibodies against DBP are short-lived, increasing with acute infection, and are strain specific (194, 195).

Antibodies from plasma from naturally exposed people and from animals immunized with recombinant Duffy binding protein (rDBP) have blocked the specific interaction between the *PvDBP* ligand domain *in vitro* and its receptor on erythrocyte surface; such inhibitory activity has been correlated with antibody titers (196, 197). The forgoing shows DBP's potential as vaccine candidate due to its essential role as adhesion molecule (196).

The cytokine production of individuals exposed to *P. vivax* was analyzed; IFN- $\gamma$ , IL-10, and IL-2 induction was observed. The response was seen to depend on individuals' age and the specific DBP<sub>II</sub> variant, producing partially acquired immunity to *P. vivax* in these populations (198). Similarly, epitopes mapped from the DBP<sub>II</sub> critical binding region have produced a humoral response, accompanied by increased antibody levels associated with patients' increased age, suggesting recognition through repeated infection. Some individuals recognized rDBP<sub>II</sub> but not linear epitopes, indicating the presence of conformational epitopes; such cases occur regularly in young people or subjects suffering first acute *P. vivax* infection, suggesting that multiple infections are needed for the recognition of linear epitopes (199).

The DBP binding domain (DBP<sub>II</sub>) is polymorphic, tending to compromise the efficacy of any vaccine associated with strain-specific immunity (192). Due to the high rate of polymorphism observed in DBP region II, an in-depth investigation was made of the relative importance of conserved and polymorphic residues in this region by directed mutagenesis. The mutations causing the loss of ligand function were mainly produced in discontinuous groups of conserved residues, while almost all mutations in polymorphic residues did not alter RBC binding (200). Such polymorphism has been seen to have a synergic effect on the antigenic nature of DBP (201). Sera from patients reacted to denatured, non-reduced, and native rDBP, indicating immunogenic conserved linear B-epitopes (100). The immune efficacy of a DBP<sub>II</sub> vaccine depends on inducing antibodies, and this response should be optimized toward conserved epitopes to protect against *P. vivax* (197).

Since DBP region II epitopes have been shown to be immunogenic, studies have established universal epitopes, which can be presented by different HLA-DR alleles inducing an effective cellular and humoral immune response, making them a candidate for a subunit-based vaccine (202). Antigenicity studies using *PvDBP*<sub>II</sub> universal epitopes have shown that lymphoproliferation,

IL-6, and IFN- $\gamma$  production is induced in peripheral blood mononuclear cells (PBMCs) from individuals exposed to infection. Such results have suggested that these epitopes having affinity for HLA-DR molecules can be good components of a vaccine against *P. vivax* (203).

Polymorphisms observed in DARC have also been associated with *P. vivax* infection severity and susceptibility in humans. Individuals with low DARC expression (a single negative allele) have a greater probability of having anti-MSP1 and anti-DBP antibodies than individuals having high DARC expression (double positive alleles). Individuals having high expression of DARC have been found to be associated with greater susceptibility to infection, exhibiting low frequency and magnitude of specific antibody response against *P. vivax* during the blood stage. This could indicate that one of *P. vivax*'s primary mechanisms for evading host immunity works through indirect negative regulation of DARC, influencing the humoral response against erythrocyte invasion and parasite development (204).

### Apical Membrane Antigen-1 (AMA-1)

The AMA-1 in *Plasmodium* is a transmembrane protein, which is localized in the micronemes. It seems to be essential during cell host invasion and is present in all *Plasmodium* species (205, 206). Eight disulfide bonds have been identified in the AMA-1 ectodomain of 66 kDa, defining three different subdomains (DI, DII, and DIII) (207). Immune responses induced by AMA-1 from different *Plasmodium* species have shown potent parasite-inhibitory effects both in animals and *in vitro* thus suggesting AMA-1 as a potential vaccine candidate (208).

*Plasmodium vivax* AMA-1 ectodomain (PV66/AMA-1) has been shown to be highly immunogenic in rhesus monkeys, inducing high IgG antibody titers; however, these suffer a rapid decline. A slight reduction in parasitemia has been observed in *P. cynomolgi*-challenged animals previously immunized with PV66 (209).

Mice immunized with human adenovirus type 5 and rAMA-1 have produced long-lived specific antibodies (including IgG1 and IgG2a) and memory T-cell proliferative responses. Memory T-cell responses were effector- and central-type, central memory predominating (210). In mice it was observed that response was both Th1 and Th2 following three immunizations and persisted for 1 year following the first immunization. On the other hand, the antibodies produced were capable of recognizing the native protein located on *P. vivax* parasites (211).

When evaluating the immune response against two *PvAMA-1* variants (A and B), there were no significant differences regarding the prevalence of IgG response. A marked switching in isotypes, which became increased with age, was also seen. The predominant cytophilic antibodies recognized *PvAMA1A* (IgG1) and *PvAMA1B* (IgG1–IgG3). The immune-epidemiological data in this research were similar regarding the two variants, this implied that one of these forms could be used in a universal erythrocyte stage *PvAMA-1* antigen-based vaccine (212).

An IgG response was observed in people residing in endemic regions exposed to *P. vivax* in Brazil, IgG1 being the dominant subclass. This antibody response was slightly lower than that observed with MSP1<sub>19</sub> and increased by 100% in individuals

having had more than three episodes. Sequences of *PvAMA-1* variable domain from different isolates have been seen to have limited polymorphism in this country (102).

This protein has been seen to be involved in Mrz invasion and contains an extracellular portion containing three different domains (207). When evaluating DI, DII, and DIII, separately or in combination in *P. vivax*-infected individuals, a greater immune response toward proteins containing the domain II was observed. Inhibition assays using the *PvAMA-1* ectodomain led to common epitopes being identified within the DI–DII domains, which were recognized by antibodies from people residing in endemic regions. Immunization in mice having the *PvAMA-1* ectodomain induced high levels of antibodies, predominantly against DI–II (103).

A linear B-epitope was also identified between amino acids 290–307 (SASDQPTQYEEEMTDYQK) in domain II, this peptide was recognized by sera from individuals naturally infected by *P. vivax* (213).

Recombinant *P. vivax* apical membrane antigen-1 DII was formulated with six adjuvants and was highly immunogenic regardless of the adjuvant used. DII-specific antibodies recognized native AMA-1 protein, demonstrating that it is immunogenic and indicating that this protein region could be evaluated as part of a subunit-based vaccine against malaria caused by *P. vivax* (214).

### Reticulocyte-Binding Proteins (RBP)

Reticulocyte-binding proteins include *PvRBP1* and *PvRBP2* and their variants *PvRBP1a* and b and *PvRBP2a*, b, and c, and other family members (215). RBP1 is a homodimer bound by disulfide bonds, binds non-covalently to RBP2, and forms a protein complex (216). They are colocalized in the apical zone in Mrz micronemes and contain a transmembrane domain toward the C-terminal extreme, possessing repeat regions in *PvRBP2* and reticulocyte-binding domains (108, 215, 217–219).

It is thought that RBPs could participate in reticulocyte invasion since no infection by *P. vivax* has been observed in mature erythrocytes (220). Their reticulocyte-binding ability has also been reported, but the specific receptors have yet to be identified (219). It has recently been found that only *PvRBP2b* binds specifically to reticulocytes (221). Due to their participation in infection, they have been studied as erythrocyte phase vaccine candidates, aimed at blocking Mrz invasion of reticulocytes (218).

High affinity reticulocyte-binding peptides (HARBPs) have been identified, 5 in a fragment from the region I of *PvRBP1* NT extreme (222) and 24 throughout the whole protein (223). The highly-conserved region III (between amino acids 1,941–2,229) had the greatest amount of HARBPs (223) and, when used as immunogen, it induced high antibody titers in *Aotus nancymaae* monkeys, able to recognize the full *PvRBP1* in parasite lysate. T-lymphocytes became activated following the second and third doses, but no protection was obtained after experimental challenge (224). Due to studies involving other *P. falciparum* proteins showing that highly conserved sequences are not immunogenic, in spite of having high binding capability, it has been suggested that changes must be made in some amino acids to increase the immune response and induce protection based on studies of critical binding residues for HARBPs from region III (224).

Antigenicity studies have found a direct relationship between higher anti-*PvRBP1* antibody titers and the number of previous episodes, the time spent residing in an endemic region and age (82, 83, 219, 224). The immune response to *PvRBP1* has also been associated with greater IgG1 and IgG3 cytophilic antibody presence against fragments from polymorphic regions (82, 83).

Studies regarding different populations where an acquired response to B-epitopes (107) and various fragments from *PvRBP1* and *PvRBP2* variants (108, 219) have shown high prevalence of IgG antibodies against fragments from repeat region, the super-coiled helix, and *PvRBP1* C-terminal region (107) (**Table 2**). Regarding the NT region (including the most polymorphic region of the *PvRBP1a* and b variants) (108), IgG prevalence was intermediate in a population from Thailand, while no antibody response against *PvRBP1b* was found in a population from the Republic of Korea (219).

On the other hand, *PvRBP2* has been seen to have greater antibody prevalence against NT region, repeat region (107), and *PvRBP2c* variant fragments (219). *PvRBP2c* is one of the most polymorphic variants, probably having the greatest global distribution, associated with the prevalence of this variant's recognition (219). *PvRBP2b* and *PvRBP1a* have been correlated with lower risk of parasitemia in a cohort study of PNG children (221). Regarding other proteins such as *PvDBP*, *PvRBP* antigenicity is much lower (82, 108).

### Antigenicity and/or Immunogenicity of Non-Classical Vaccine Candidates

In spite of the technical limitations involved in studying *P. vivax* proteins, other proteins characterized as being promising vaccine candidates have been studied during the last few years. One such is merozoite surface protein-10 (*PvMSP10*) having NT and C-terminal regions with two EGF-like domains and a GPI anchor (225). Colombian individuals exposed to *P. vivax* infection have shown reactivity to recombinant *PvMSP10*; r*PvMSP10* has also elicited high antibody titers against the protein in immunized *Aotus* monkeys but no protection after challenge (226). Infected Korean individuals had 42% IgG prevalence, IgG1 and IgG3 antibodies predominating. Immunized mice have shown a Th1 response-biased immune response (227).

The *Pv34* protein was characterized based on homology of the *P. falciparum* *Pf34* protein, and antigenicity was evaluated in PBMCs from individuals previously exposed to infection. Stimulation with r*Pv34* induced proliferation in 71% of individuals and high IL-2, IFN- $\gamma$ , and IL-4 production (Th1/Th2 profile), such response being attributed to recognition of T- and B-epitopes responsible for a combined immune response (228).

Another protein characterized was *PvRON-1*, based on its homologous *PfASP* protein in *P. falciparum*. This protein's antigenicity was evaluated using sera from people having had previous *P. vivax* infection. The results showed that *PvRON-1* was expressed during natural infection and could generate an antibody response in the host (229).

An antigenicity and immunogenicity study of *P. vivax* rhoptry-associated leucine (Leu) zipper-like protein-1 (*PvRALP-1*) was carried out on patient serum samples and immunized mice.

*PvRALP-1* was recognized in samples from patient sera, IgG1 and IgG3 being the predominant subclasses, although without significant differences with the other subclasses; Th1/Th2 response was balanced in immunized mice (230).

The CelTOS microneme protein characterized and tested for *P. falciparum*, having 98% homology with *P. vivax*, should be considered for further studies since cross-species protection has been demonstrated in preclinical studies (231). It has been described as vaccine target by blocking transmission infection or preerythrocytic stage due to its cell traversal function in Spz and ookinetes (232). A recent study proved ~20% prevalence of antibodies against *PvCelTOS* in a Thai population (233). More studies related to immunogenicity, and antigenicity potential are needed and should involve new proteins characterized during the last few years, related to host cell invasion during different life cycle stages, such as rhoptry neck proteins.

### TRANSMISSION BLOCKING *P. vivax* VACCINE CANDIDATES

One of the methodologies used for controlling malaria infection has been the search for transmission blocking vaccines, through strategies for preventing ookinete development in the vector (234). The assays conducted for transmission blocking have been focused on two main proteins, *Pvs25* and *Pvs28*, expressed on gametocyte surface. Anti-sera have recognized *Pv25* in zygotes and mature ookinetes, and *Pv28* more in mature ookinetes (235).

Immunogenicity tested with recombinant proteins *Pvs25* and *Pvs28* in mice has shown a splenic T-cell proliferative response. Anti-sera from mice immunized with a *Pvs25–28* chimera had a high antibody titer compared to mice immunized with *Pvs25* or *Pvs28* alone. Anti-*Pvs25–28* and anti-*Pvs25* had higher transmission blocking than anti-*Pvs28* (235, 236).

Studies had demonstrated that *P. vivax* *Sall* strain recombinant *Pvs25* and *Pvs28* had transmission blocking capability, even with natural isolates, thus overcoming genetic polymorphism between isolates (237). Higher transmission blocking has been described as a direct function of antibody titers in sera (238–240).

Different vaccination schemes have been tested, varying adjuvant, dose, expression system (148, 237, 238, 240, 241). Phase I clinical trials determining security and immunogenicity in humans have shown high transmission blocking capability in humans, demonstrating these antigens' potential as vaccine candidates (147, 148).

### CONCLUSION

This review has summarized immune responses induced by *P. vivax* vaccine candidates, which are essential in host cell invasion. Classical vaccine development has been focused on immunodominant antigens such as sporozoite and MSPs, which are recognized by sera from partially protected individuals who are naturally exposed to infection. However, surface proteins, for example *PvMSP1* and *PvCSP*, have high allelic polymorphism (164, 242, 243) and are under positive selection by the immune response. After several natural infections, many of these epitopes

have shown an ability to generate a strong immune response in individuals without clinical symptoms, showing an association with IFN- $\gamma$  effector T-cell activation and generation of cytophilic antibody subclasses. Similar immune responses have been observed in animal models immunized with these polymorphic immunodominant antigens. Nevertheless, the success for this kind of vaccines has been limited, since the cross protectivity obtained for the remaining strains is very low and induces a short-lived immune response (244, 245). Moreover, parasites change their cell targets and molecules during preerythrocytic, erythrocytic, and sexual stages, and single-antigen/single-stage vaccines do not induce sterile protection. It has been observed that *P. falciparum* parasites hide their amino acid conserved domains of the proteins involved in the invasion of host cells, showing immune dominant and polymorphic epitopes to the immune system (246).

Other methodologies are needed to solve these kinds of issue. An alternative is to develop an antimalarial vaccine (246), focused on synthetic peptides designed on conserved regions of Spz and Mrz proteins having high hepatic cell or RBC-binding ability. Although these peptides are not immunogenic, *P. falciparum* and *P. vivax* studies have shown that such peptides can be modified by changing their critical RBC-binding residues for others having similar mass but opposite polarity, making them highly immunogenic and protective (247, 248).

Another problem in the development of an antimalarial vaccine concerns the many haplotypes present in the exposed population. The HABPs can also be modified that fit properly inside the peptide-binding region of MHCII. In studies with *P. falciparum* with a MSP-2 HABP that has been modified to bind to HLA-DR $\beta$ 1\*0403 molecules with high affinity, it was shown that *Aotus* monkeys bearing HLA-DR $\beta$ 1\*0403-like molecules,

produced high antibody titers with sterile immunity after challenge with *P. falciparum* FVO. This was a proof-of-concept immune protection-inducing protein structures demonstrating that specifically modified HABPs are able to induce sterile protection against malaria by engaging the proper TCR/pMHCII interactions (249).

Evaluation of conserved epitopes and non-immunodominant antigens important in parasite adhesion and invasion of erythrocytes should be prioritized for multistage, multi-epitope, minimal subunit-based, chemically synthesized antimalarial development, covering a large part of the HLA-DR $\beta$ 1\* population in endemic areas to protect them against malarial parasites.

## AUTHOR CONTRIBUTIONS

CL conceived the work and drafted the manuscript; YY-P drafted the manuscript and designed the figures; NH-E and DD-A drafted the manuscript; MP critically revised the manuscript for important intellectual content. All authors have revised the manuscript and given their approval for the version to be submitted.

## ACKNOWLEDGMENTS

We would like to thank Jason Garry for translating and thoroughly revising the manuscript and Professor Manuel Elkin Patarroyo for his suggestions.

## FUNDING

This work was financed by the Colombian Science, Technology and Innovation Department (COLCIENCIAS) through grant RC # 0309-2013.

## REFERENCES

- WHO. In: Press W, editor. *World Malaria Report*. (2015). p. 280.
- Udomsangpetch R, Kaneko O, Chotivanich K, Sattabongkot J. Cultivation of *Plasmodium vivax*. *Trends Parasitol* (2008) 24(2):85–8. doi:10.1016/j.pt.2007.09.010
- Mueller I, Galinski MR, Baird JK, Carlton JM, Kocher DK, Alonso PL, et al. Key gaps in the knowledge of *Plasmodium vivax*, a neglected human malaria parasite. *Lancet Infect Dis* (2009) 9(9):555–66. doi:10.1016/S1473-3099(09)70177-X
- Jiang N, Chang Q, Sun X, Lu H, Yin J, Zhang Z, et al. Co-infections with *Plasmodium knowlesi* and other malaria parasites, Myanmar. *Emerg Infect Dis* (2010) 16(9):1476–8. doi:10.3201/eid1609.100339
- Nino CH, Cubides JR, Camargo-Ayala PA, Rodriguez-Celis CA, Quinones T, Cortes-Castillo MT, et al. *Plasmodium malariae* in the Colombian Amazon region: you don't diagnose what you don't suspect. *Malar J* (2016) 15(1):576. doi:10.1186/s12936-016-1629-3
- Mayxay M, Pukrittayakamee S, Newton PN, White NJ. Mixed-species malaria infections in humans. *Trends Parasitol* (2004) 20(5):233–40. doi:10.1016/j.pt.2004.03.006
- Rieckmann K, Davis D, Hutton D. *Plasmodium vivax* resistance to chloroquine? *Lancet* (1989) 334(8673):1183–4. doi:10.1016/S0140-6736(89)91792-3
- Khatoon L, Baliraine FN, Bonizzoni M, Malik SA, Yan G. Prevalence of antimalarial drug resistance mutations in *Plasmodium vivax* and *P. falciparum* from a malaria-endemic area of Pakistan. *Am J Trop Med Hyg* (2009) 81(3):525–8.
- Price RN, von Seidlein L, Valecha N, Nosten F, Baird JK, White NJ. Global extent of chloroquine-resistant *Plasmodium vivax*: a systematic review and meta-analysis. *Lancet Infect Dis* (2014) 14(10):982–91. doi:10.1016/S1473-3099(14)70855-2
- Suwannarusk R, Chavchich M, Russell B, Jaidee A, Chalfein F, Barends M, et al. Amplification of pvmdr1 associated with multidrug-resistant *Plasmodium vivax*. *J Infect Dis* (2008) 198(10):1558–64. doi:10.1086/592451
- Khim N, Andrianaranjaka V, Popovici J, Kim S, Ratsimbason A, Benedet C, et al. Effects of mefloquine use on *Plasmodium vivax* multidrug resistance. *Emerg Infect Dis* (2014) 20(10):1637–44. doi:10.3201/eid2010.140411
- Prakash J, Singh A, Kumar N, Saxena R. Acute renal failure in *Plasmodium vivax* malaria. *J Assoc Physicians India* (2003) 51:265–7.
- Nautiyal A, Singh S, Parameswaran G, DiSalle M. Hepatic dysfunction in a patient with *Plasmodium vivax* infection. *Medsc Gen Med* (2005) 7(1):8.
- Tjitra E, Anstey NM, Sugiarto P, Warikar N, Kenangalem E, Karyana M, et al. Multidrug-resistant *Plasmodium vivax* associated with severe and fatal malaria: a prospective study in Papua, Indonesia. *PLoS Med* (2008) 5(6):e128. doi:10.1371/journal.pmed.0050128
- Naha K, Dasari S, Prabhu M. Spectrum of complications associated with *Plasmodium vivax* infection in a tertiary hospital in South-Western India. *Asian Pac J Trop Med* (2012) 5(1):79–82. doi:10.1016/S1995-7645(11)60251-4
- Rizvi I, Tripathi DK, Chughtai AM, Beg M, Zaman S, Zaidi N. Complications associated with *Plasmodium vivax* malaria: a retrospective study from a tertiary care hospital based in Western Uttar Pradesh, India. *Ann Afr Med* (2013) 12(3):155. doi:10.4103/1596-3519.117624
- Kumar R, Agarwal D, Kumar P. Severe *Plasmodium vivax* malaria in children: an emerging threat. *J Pediatr Sci* (2014) 6:e210. doi:10.17334/jps.99493

18. Price RN, Tjitra E, Guerra CA, Yeung S, White NJ, Anstey NM. Vivax malaria: neglected and not benign. *Am J Trop Med Hyg* (2007) 77(6 Suppl): 79–87.
19. Guerra CA, Howes RE, Patil AP, Gething PW, Van Boeckel TP, Temperley WH, et al. The international limits and population at risk of *Plasmodium vivax* transmission in 2009. *PLoS Negl Trop Dis* (2010) 4(8):e774. doi:10.1371/journal.pntd.0000774
20. White NJ. Determinants of relapse periodicity in *Plasmodium vivax* malaria. *Malar J* (2011) 10(1):1. doi:10.1186/1475-2875-10-297
21. Sinnis P, Coppi A. A long and winding road: the *Plasmodium* sporozoite's journey in the mammalian host. *Parasitol Int* (2007) 56(3):171–8. doi:10.1016/j.parint.2007.04.002
22. Gueirard P, Tavares J, Thibierge S, Bernex F, Ishino T, Milon G, et al. Development of the malaria parasite in the skin of the mammalian host. *Proc Natl Acad Sci U S A* (2010) 107(43):18640–5. doi:10.1073/pnas.1009346107
23. Amino R, Thibierge S, Martin B, Celli S, Shorte S, Frischknecht F, et al. Quantitative imaging of *Plasmodium* transmission from mosquito to mammal. *Nat Med* (2006) 12(2):220–4. doi:10.1038/nm1350
24. Vaughan AM, Aly AS, Kappe SH. Malaria parasite pre-erythrocytic stage infection: gliding and hiding. *Cell Host Microbe* (2008) 4(3):209–18. doi:10.1016/j.chom.2008.08.010
25. Menard R, Tavares J, Cockburn I, Markus M, Zavala F, Amino R. Looking under the skin: the first steps in malarial infection and immunity. *Nat Rev Microbiol* (2013) 11(10):701–12. doi:10.1038/nrmicro3111
26. Good MF, Doolan DL. Malaria vaccine design: immunological considerations. *Immunity* (2010) 33(4):555–66. doi:10.1016/j.immuni.2010.10.005
27. Duffy PE, Sahu T, Akue A, Milman N, Anderson C. Pre-erythrocytic malaria vaccines: identifying the targets. *Expert Rev Vaccines* (2012) 11(10):1261–80. doi:10.1586/erv.12.92
28. Schofield L, Grau GE. Immunological processes in malaria pathogenesis. *Nat Rev Immunol* (2005) 5(9):722–35. doi:10.1038/nri1686
29. Hiller NL, Bhattacharjee S, van Ooij C, Liolios K, Harrison T, Lopez-Estrano C, et al. A host-targeting signal in virulence proteins reveals a secretome in malarial infection. *Science* (2004) 306(5703):1934–7. doi:10.1126/science.1102737
30. Marti M, Good RT, Rug M, Knuepfer E, Cowman AF. Targeting malaria virulence and remodeling proteins to the host erythrocyte. *Science* (2004) 306(5703):1930–3. doi:10.1126/science.1102452
31. Singh AP, Buscaglia CA, Wang Q, Levay A, Nussenzweig DR, Walker JR, et al. *Plasmodium* circumsporozoite protein promotes the development of the liver stages of the parasite. *Cell* (2007) 131(3):492–504. doi:10.1016/j.cell.2007.09.013
32. Aggarwal BB. Nuclear factor-kappaB: the enemy within. *Cancer Cell* (2004) 6(3):203–8. doi:10.1016/j.ccr.2004.09.003
33. Baer K, Klotz C, Kappe SH, Schnieder T, Frevert U. Release of hepatic *Plasmodium yoelii* merozoites into the pulmonary microvasculature. *PLoS Pathog* (2007) 3(11):e171. doi:10.1371/journal.ppat.0030171
34. Baird JK, Jones TR, Danudirgo EW, Annis BA, Bangs MJ, Basri H, et al. Age-dependent acquired protection against *Plasmodium falciparum* in people having two years exposure to hyperendemic malaria. *Am J Trop Med Hyg* (1991) 45(1):65–76.
35. Christophers SR. The mechanism of immunity against malaria in communities living under hyper-endemic conditions. *Indian J Med Res* (1924) 12(2):273–94.
36. Brown KN, Brown IN. Immunity to malaria: antigenic variation in chronic infections of *Plasmodium knowlesi*. *Nature* (1965) 208(5017):1286–8. doi:10.1038/2081286a0
37. Pérignon JL, Druihle P. Immune mechanisms underlying the premunition against *Plasmodium falciparum* malaria. *Mem Inst Oswaldo Cruz* (1994) 89:51–3. doi:10.1590/S0074-02761994000600013
38. Doolan DL, Dobaño C, Baird JK. Acquired immunity to malaria. *Clin Microbiol Rev* (2009) 22(1):13–36. doi:10.1128/CMR.00025-08
39. Snounou G, Pérignon J-L. Malariaotherapy-insanity at the service of malariology. *Adv Parasitol* (2013) 81(6):223–55. doi:10.1016/B978-0-12-407826-0.00006-0
40. Yamauchi LM, Coppi A, Snounou G, Sinnis P. *Plasmodium* sporozoites trickle out of the injection site. *Cell Microbiol* (2007) 9(5):1215–22. doi:10.1111/j.1462-5822.2006.00861.x
41. Amorim KN, Chagas DC, Sulczewski FB, Boscardin SB. Dendritic cells and their multiple roles during malaria infection. *J Immunol Res* (2016) 2016:2926436. doi:10.1155/2016/2926436
42. Gazzinelli RT, Kalantari P, Fitzgerald KA, Golenbock DT. Innate sensing of malaria parasites. *Nat Rev Immunol* (2014) 14(11):744–57. doi:10.1038/nri3742
43. Jani D, Nagarkatti R, Beatty W, Angel R, Slebodynick C, Andersen J, et al. HDP-a novel heme detoxification protein from the malaria parasite. *PLoS Pathog* (2008) 4(4):e1000053. doi:10.1371/journal.ppat.1000053
44. Parroche P, Lauw FN, Goutagny N, Latz E, Monks BG, Visintin A, et al. Malaria hemozoin is immunologically inert but radically enhances innate responses by presenting malaria DNA to toll-like receptor 9. *Proc Natl Acad Sci U S A* (2007) 104(6):1919–24. doi:10.1073/pnas.0608745104
45. Coban C, Igari Y, Yagi M, Reimer T, Koyama S, Aoshi T, et al. Immunogenicity of whole-parasite vaccines against *Plasmodium falciparum* involves malarial hemozoin and host TLR9. *Cell Host Microbe* (2010) 7(1):50–61. doi:10.1016/j.chom.2009.12.003
46. Ghosh D, Stumhofer JS. Do you see what I see: recognition of protozoan parasites by toll-like receptors. *Curr Immunol Rev* (2013) 9(3):129–40. doi:10.2174/1573395509666131203225929
47. Sharma S, DeOliveira RB, Kalantari P, Parroche P, Goutagny N, Jiang Z, et al. Innate immune recognition of an AT-rich stem-loop DNA motif in the *Plasmodium falciparum* genome. *Immunity* (2011) 35(2):194–207. doi:10.1016/j.immuni.2011.05.016
48. Schofield L, Hackett F. Signal transduction in host cells by a glycosylphosphatidylinositol toxin of malaria parasites. *J Exp Med* (1993) 177(1):145–53. doi:10.1084/jem.177.1.145
49. Krishnegowda G, Hajjar AM, Zhu J, Douglass EJ, Uematsu S, Akira S, et al. Induction of proinflammatory responses in macrophages by the glycosylphosphatidylinositol of *Plasmodium falciparum*: cell signaling receptors, glycosylphosphatidylinositol (GPI) structural requirement, and regulation of GPI activity. *J Biol Chem* (2005) 280(9):8606–16. doi:10.1074/jbc.M413541200
50. Gazzinelli RT, Denkers EY. Protozoan encounters with toll-like receptor signalling pathways: implications for host parasitism. *Nat Rev Immunol* (2006) 6(12):895–906. doi:10.1038/nri1978
51. Durai P, Govindaraj RG, Choi S. Structure and dynamic behavior of Toll-like receptor 2 subfamily triggered by malarial glycosylphosphatidylinositol of *Plasmodium falciparum*. *FEBS J* (2013) 280(23):6196–212. doi:10.1111/febs.12541
52. Wykes MN, Good MF. What really happens to dendritic cells during malaria? *Nat Rev Microbiol* (2008) 6(11):864–70. doi:10.1038/nrmicro1988
53. Skorokhod OA, Alessio M, Mordmuller B, Arese P, Schwarzer E. Hemozoin (malarial pigment) inhibits differentiation and maturation of human monocyte-derived dendritic cells: a peroxisome proliferator-activated receptor-gamma-mediated effect. *J Immunol* (2004) 173(6):4066–74. doi:10.4049/jimmunol.173.6.4066
54. Elliott SR, Spurck TP, Dodin JM, Maier AG, Voss TS, Yosaatmadja F, et al. Inhibition of dendritic cell maturation by malaria is dose dependent and does not require *Plasmodium falciparum* erythrocyte membrane protein 1. *Infect Immun* (2007) 75(7):3621–32. doi:10.1128/IAI.00095-07
55. Stern LJ, Calvo-Calle JM. HLA-DR: molecular insights and vaccine design. *Curr Pharm Des* (2009) 15(28):3249–61. doi:10.2174/138161209789105171
56. Lima-Junior Jda C, Pratt-Riccio LR. Major histocompatibility complex and malaria: focus on *Plasmodium vivax* infection. *Front Immunol* (2016) 7:13. doi:10.3389/fimmu.2016.00013
57. Riley EM, Stewart VA. Immune mechanisms in malaria: new insights in vaccine development. *Nat Med* (2013) 19(2):168–78. doi:10.1038/nm.3083
58. Praba-Egge AD, Montenegro S, Arevalo-Herrera M, Hopper T, Herrera S, James MA. Human cytokine responses to meso-endemic malaria on the Pacific Coast of Colombia. *Ann Trop Med Parasitol* (2003) 97(4):327–37. doi:10.1179/000349803235002399
59. Hemmer CJ, Holst FG, Kern P, Chiwakata CB, Dietrich M, Reisinger EC. Stronger host response per parasitized erythrocyte in *Plasmodium vivax* or ovale than in *Plasmodium falciparum* malaria. *Trop Med Int Health* (2006) 11(6):817–23. doi:10.1111/j.1365-3156.2006.01635.x
60. Alfrangis M, Lemnge MM, Moon R, Theisen M, Bygbjerg I, Ridley RG, et al. IgG reactivities against recombinant rhoptry-associated protein-1

- (rRAP-1) are associated with mixed *Plasmodium* infections and protection against disease in Tanzanian children. *Parasitology* (1999) 119(Pt 4):337–42. doi:10.1017/S0031182099004825
61. Maitland K, Williams TN, Newbold CI. *Plasmodium vivax* and *P. falciparum*: biological interactions and the possibility of cross-species immunity. *Parasitol Today* (1997) 13(6):227–31. doi:10.1016/S0169-4758(97)01061-2
  62. Smith T, Genton B, Baea K, Gibson N, Narara A, Alpers MP. Prospective risk of morbidity in relation to malaria infection in an area of high endemicity of multiple species of *Plasmodium*. *Am J Trop Med Hyg* (2001) 64(5–6):262–7.
  63. Andrade BB, Reis-Filho A, Souza-Neto SM, Clarencio J, Camargo LM, Barral A, et al. Severe *Plasmodium vivax* malaria exhibits marked inflammatory imbalance. *Malar J* (2010) 9:13. doi:10.1186/1475-2875-9-13
  64. Langhorne J, Ndungu FM, Sponaas AM, Marsh K. Immunity to malaria: more questions than answers. *Nat Immunol* (2008) 9(7):725–32. doi:10.1038/nifi.205
  65. Medina TS, Costa SP, Oliveira MD, Ventura AM, Souza JM, Gomes TF, et al. Increased interleukin-10 and interferon-gamma levels in *Plasmodium vivax* malaria suggest a reciprocal regulation which is not altered by IL-10 gene promoter polymorphism. *Malar J* (2011) 10:264. doi:10.1186/1475-2875-10-264
  66. Goncalves RM, Scopel KK, Bastos MS, Ferreira MU. Cytokine balance in human malaria: does *Plasmodium vivax* elicit more inflammatory responses than *Plasmodium falciparum*? *PLoS One* (2012) 7(9):e44394. doi:10.1371/journal.pone.0044394
  67. Mendonça VR, Queiroz AT, Lopes FM, Andrade BB, Barral-Netto M. Networking the host immune response in *Plasmodium vivax* malaria. *Malar J* (2013) 12(1):1. doi:10.1186/1475-2875-12-69
  68. Mendonça VR, Andrade BB, Souza LC, Magalhaes BM, Mourao MP, Lacerda MV, et al. Unravelling the patterns of host immune responses in *Plasmodium vivax* malaria and dengue co-infection. *Malar J* (2015) 14:315. doi:10.1186/s12936-015-0835-8
  69. Cohen S, Mc GI, Carrington S. Gamma-globulin and acquired immunity to human malaria. *Nature* (1961) 192:733–7. doi:10.1038/192733a0
  70. Sabchareon A, Burnouf T, Ouattara D, Attanath P, Bouharoun-Tayoun H, Chantavanich P, et al. Parasitologic and clinical human response to immunoglobulin administration in falciparum malaria. *Am J Trop Med Hyg* (1991) 45(3):297–308.
  71. Gysin J, Moisson P, Pereira da Silva L, Druihle P. Antibodies from immune African donors with a protective effect in *Plasmodium falciparum* human infection are also able to control asexual blood forms of the parasite in *Saimiri* monkeys. *Res Immunol* (1996) 147(6):397–401. doi:10.1016/0923-2494(96)82048-7
  72. Hollingdale MR, Nardin EH, Tharavanij S, Schwartz AL, Nussenzweig RS. Inhibition of entry of *Plasmodium falciparum* and *P. vivax* sporozoites into cultured cells; an in vitro assay of protective antibodies. *J Immunol* (1984) 132(2):909–13.
  73. Nardin E, Zavala F, Nussenzweig V, Nussenzweig RS. Pre-erythrocytic malaria vaccine: mechanisms of protective immunity and human vaccine trials. *Parasitologia* (1999) 41(1–3):397–402.
  74. Rathore D, Nagarkatti R, Jani D, Chattopadhyay R, de la Vega P, Kumar S, et al. An immunologically cryptic epitope of *Plasmodium falciparum* circumsporozoite protein facilitates liver cell recognition and induces protective antibodies that block liver cell invasion. *J Biol Chem* (2005) 280(21):20524–9. doi:10.1074/jbc.M414254200
  75. Bouharoun-Tayoun H, Attanath P, Sabchareon A, Chongsuphajaisiddhi T, Druihle P. Antibodies that protect humans against *Plasmodium falciparum* blood stages do not on their own inhibit parasite growth and invasion in vitro, but act in cooperation with monocytes. *J Exp Med* (1990) 172(6):1633–41. doi:10.1084/jem.172.6.1633
  76. Bouharoun-Tayoun H, Oeuvray C, Lunel F, Druihle P. Mechanisms underlying the monocyte-mediated antibody-dependent killing of *Plasmodium falciparum* asexual blood stages. *J Exp Med* (1995) 182(2):409–18. doi:10.1084/jem.182.2.409
  77. Arévalo-Herrera M, Soto L, Perlaza BL, Céspedes N, Vera O, Lenis AM, et al. Antibody-mediated and cellular immune responses induced in naïve volunteers by vaccination with long synthetic peptides derived from the *Plasmodium vivax* circumsporozoite protein. *Am J Trop Med Hyg* (2011) 84(2 Suppl):35–42. doi:10.4269/ajtmh.2011.09-0507
  78. Soares IS, Levitus G, Souza JM, Del Portillo HA, Rodrigues MM. Acquired immune responses to the N-and C-terminal regions of *Plasmodium vivax* merozoite surface protein 1 in individuals exposed to malaria. *Infect Immun* (1997) 65(5):1606–14.
  79. Nogueira PA, Alves FP, Fernandez-Becerra C, Pein O, Santos NR, da Silva LHP, et al. A reduced risk of infection with *Plasmodium vivax* and clinical protection against malaria are associated with antibodies against the N terminus but not the C terminus of merozoite surface protein 1. *Infect Immun* (2006) 74(5):2726–33. doi:10.1128/IAI.74.5.2726-2733.2006
  80. Versiani FG, Almeida ME, Melo GC, Versiani FO, Orlandi PP, Mariuba LA, et al. High levels of IgG3 anti ICB2-5 in *Plasmodium vivax*-infected individuals who did not develop symptoms. *Malar J* (2013) 12:294. doi:10.1186/1475-2875-12-294
  81. Cheng Y, Shin E-H, Lu F, Wang B, Choe J, Tsuoboi T, et al. Antigenicity studies in humans and immunogenicity studies in mice: an MSP1P subdomain as a candidate for malaria vaccine development. *Microb Infect* (2014) 16(5):419–28. doi:10.1016/j.micinf.2014.02.002
  82. Tran TM, Oliveira-Ferreira J, Moreno A, Santos F, Yazdani SS, Chitnis CE, et al. Comparison of IgG reactivities to *Plasmodium vivax* merozoite invasion antigens in a Brazilian Amazon population. *Am J Trop Med Hyg* (2005) 73(2):244–55.
  83. Ferreira AR, Singh B, Cabrera-Mora M, De Souza ACM, Marques MTQ, Porto LCS, et al. Evaluation of naturally acquired IgG antibodies to a chimeric and non-chimeric recombinant species of *Plasmodium vivax* reticulocyte binding protein-1: lack of association with HLA-DRB1\* /DQB1\* in malaria exposed individuals from the Brazilian Amazon. *PLoS One* (2014) 9(8):e105828. doi:10.1371/journal.pone.0105828
  84. Yildiz Zeyrek F, Palacpac N, Yuksel F, Yagi M, Honjo K, Fujita Y, et al. Serologic markers in relation to parasite exposure history help to estimate transmission dynamics of *Plasmodium vivax*. *PLoS One* (2011) 6(11):e28126. doi:10.1371/journal.pone.0028126
  85. Lima-Junior JC, Jiang J, Rodrigues-da-Silva R, Banic D, Tran T, Ribeiro R, et al. B cell epitope mapping and characterization of naturally acquired antibodies to the *Plasmodium vivax* merozoite surface protein-3 $\alpha$  (PvMSP-3 $\alpha$ ) in malaria exposed individuals from Brazilian Amazon. *Vaccine* (2011) 29(9):1801–11. doi:10.1016/j.vaccine.2010.12.099
  86. Lima-Junior JC, Rodrigues-da-Silva RN, Banic DM, Jiang J, Singh B, Fabricio-Silva GM, et al. Influence of HLA-DRB1 and HLA-DQB1 alleles on IgG antibody response to the *P. vivax* MSP-1, MSP-3 $\alpha$  and MSP-9 in individuals from Brazilian endemic area. *PLoS One* (2012) 7(5):e36419. doi:10.1371/journal.pone.0036419
  87. Herrera S, Bonelo A, Perlaza BL, Valencia AZ, Cifuentes C, Hurtado S, et al. Use of long synthetic peptides to study the antigenicity and immunogenicity of the *Plasmodium vivax* circumsporozoite protein. *Int J Parasitol* (2004) 34(13):1535–46. doi:10.1016/j.ijpara.2004.10.009
  88. Céspedes N, Arévalo-Herrera M, Felger I, Reed S, Kajava AV, Corradin G, et al. Antigenicity and immunogenicity of a novel chimeric peptide antigen based on the *P. vivax* circumsporozoite protein. *Vaccine* (2013) 31(42):4923–30. doi:10.1016/j.vaccine.2013.05.082
  89. Agnandji ST, Lell B, Fernandes JF, Abossolo BP, Methogo B, Kabwende AL, et al. A phase 3 trial of RTS, S/AS01 malaria vaccine in African infants. *N Engl J Med* (2012) 367(24):2284–95. doi:10.1056/NEJMoa1208394
  90. Lumsden JM, Pichyangkul S, Srichairatanakul U, Yongvanitchit K, Limsalakpatch A, Nurmukhambetova S, et al. Evaluation of the safety and immunogenicity in rhesus monkeys of a recombinant malaria vaccine for *Plasmodium vivax* with a synthetic toll-like receptor 4 agonist formulated in an emulsion. *Infect Immun* (2011) 79(9):3492–500. doi:10.1128/IAI.05257-11
  91. Rui E, Fernandez-Becerra C, Takeo S, Sanz S, Lacerda MV, Tsuoboi T, et al. *Plasmodium vivax*: comparison of immunogenicity among proteins expressed in the cell-free systems of *Escherichia coli* and wheat germ by suspension array assays. *Malar J* (2011) 10(1):1. doi:10.1186/1475-2875-10-192
  92. Neafsey DE, Juraska M, Bedford T, Benkeser D, Valim C, Griggs A, et al. Genetic diversity and protective efficacy of the RTS, S/AS01 malaria vaccine. *N Engl J Med* (2015) 373(21):2025–37. doi:10.1056/NEJMoa1505819
  93. Park J-W, Moon S-H, Yeom J-S, Lim K-J, Sohn M-J, Jung W-C, et al. Naturally acquired antibody responses to the C-terminal region of merozoite surface protein 1 of *Plasmodium vivax* in Korea. *Clin Diagn Lab Immunol* (2001) 8(1):14–20. doi:10.1128/CDLI.8.1.14-20.2001

94. Valderrama-Aguirre A, Quintero G, Gomez A, Castellanos A, Perez Y, Mendez F, et al. Antigenicity, immunogenicity, and protective efficacy of *Plasmodium vivax* MSP1 PV200l: a potential malaria vaccine subunit. *Am J Trop Med Hyg* (2005) 73(5 Suppl):16–24.
95. Zeyrek FY, Babaoglu A, Demirel S, Erdogan DD, Ak M, Korkmaz M, et al. Analysis of naturally acquired antibody responses to the 19-kd C-terminal region of merozoite surface protein-1 of *Plasmodium vivax* from individuals in Sanliurfa, Turkey. *Am J Trop Med Hyg* (2008) 78(5):729–32.
96. Stanisic DI, Javati S, Kiniboro B, Lin E, Jiang J, Singh B, et al. Naturally acquired immune responses to *P. vivax* merozoite surface protein 3 $\alpha$  and merozoite surface protein 9 are associated with reduced risk of *P. vivax* malaria in young Papua New Guinean children. *PLoS Negl Trop Dis* (2013) 7(11):e2498. doi:10.1371/journal.pntd.0002498
97. Bitencourt AR, Vicentini EC, Jimenez MC, Ricci R, Leite JA, Costa FT, et al. Antigenicity and immunogenicity of *Plasmodium vivax* merozoite surface protein-3. *PLoS One* (2013) 8(2):e56061. doi:10.1371/journal.pone.0056061
98. Lima-Junior JC, Tran TM, Meyer EV, Singh B, De-Simone SG, Santos F, et al. Naturally acquired humoral and cellular immune responses to *Plasmodium vivax* merozoite surface protein 9 in Northwestern Amazon individuals. *Vaccine* (2008) 26(51):6645–54. doi:10.1016/j.vaccine.2008.09.029
99. Lima-Junior JC, Banic DM, Tran TM, Meyer VS, De-Simone SG, Santos F, et al. Promiscuous T-cell epitopes of *Plasmodium* merozoite surface protein 9 (PvMSP9) induces IFN-gamma and IL-4 responses in individuals naturally exposed to malaria in the Brazilian Amazon. *Vaccine* (2010) 28(18):3185–91. doi:10.1016/j.vaccine.2010.02.046
100. Fraser T, Michon P, Barnwell JW, Noe AR, Al-Yaman F, Kaslow DC, et al. Expression and serologic activity of a soluble recombinant *Plasmodium vivax* Duffy binding protein. *Infect Immun* (1997) 65(7):2772–7.
101. Michon PA, Arevalo-Herrera M, Fraser T, Herrera S, Adams JH. Serologic responses to recombinant *Plasmodium vivax* Duffy binding protein in a Colombian village. *Am J Trop Med Hyg* (1998) 59(4):597–9.
102. Rodrigues MHC, Rodrigues KM, Oliveira TR, Cômodo AN, Rodrigues MM, Kocken CH, et al. Antibody response of naturally infected individuals to recombinant *Plasmodium vivax* apical membrane antigen-1. *Int J Parasitol* (2005) 35(2):185–92. doi:10.1016/j.ijpara.2004.11.003
103. Múfalo BC, Gentil F, Bargieri DY, Costa FT, Rodrigues MM, Soares IS. *Plasmodium vivax* apical membrane antigen-1: comparative recognition of different domains by antibodies induced during natural human infection. *Microbes Infect* (2008) 10(12):1266–73. doi:10.1016/j.micinf.2008.07.023
104. Haghj AM, Khoramizade MR, Nateghpour M, Mohebali M, Edrissian GH, Eshraghian MR, et al. A recombinant *Plasmodium vivax* apical membrane antigen-1 to detect human infection in Iran. *Korean J Parasitol* (2012) 50(1):15–21. doi:10.3347/kjp.2012.50.1.15
105. Cunha MG, Silva ES, Sepúlveda N, Costa SP, Saboia TC, Guerreiro JF, et al. Serologically defined variations in malaria endemicity in Pará state, Brazil. *PLoS One* (2014) 9(11):e113357. doi:10.1371/journal.pone.0113357
106. Tomaz FMMB, da Cruz Furini AA, Capobianco MP, Póvoa MM, Trindade PCA, Fraga VD, et al. Humoral immune responses against the malaria vaccine candidate antigen *Plasmodium vivax* AMA-1 and IL-4 gene polymorphisms in individuals living in an endemic area of the Brazilian Amazon. *Cytokine* (2015) 74(2):273–8. doi:10.1016/j.cyto.2015.03.020
107. Han J-H, Li J, Wang B, Lee S-K, Nyunt MH, Na S, et al. Identification of immunodominant B-cell epitope regions of reticulocyte binding proteins in *Plasmodium vivax* by protein microarray based immunoscreening. *Korean J Parasitol* (2015) 53(4):403. doi:10.3347/kjp.2015.53.4.403
108. Han J-H, Lee S-K, Wang B, Muñoz F, Nyunt MH, Na S, et al. Identification of a reticulocyte-specific binding domain of *Plasmodium vivax* reticulocyte-binding protein 1 that is homologous to the PfRh4 erythrocyte-binding domain. *Sci Rep* (2016) 6:26993. doi:10.1038/srep26993
109. Neefjes J, Jongsma ML, Paul P, Bakke O. Towards a systems understanding of MHC class I and MHC class II antigen presentation. *Nat Rev Immunol* (2011) 11(12):823–36. doi:10.1038/nri3084
110. Ujvari B, Belov K. Major histocompatibility complex (MHC) markers in conservation biology. *Int J Mol Sci* (2011) 12(8):5168–86. doi:10.3390/ijms12085168
111. Mazza C, Malissen B. What guides MHC-restricted TCR recognition? *Semin Immunol* (2007) 19(4):225–35. doi:10.1016/j.smim.2007.03.003
112. Oliveira-Ferreira J, Pratt-Riccio LR, Arruda M, Santos F, Ribeiro CT, Goldberg AC, et al. HLA class II and antibody responses to circumsporozoite protein repeats of *P. vivax* (VK210, VK247 and *P. vivax*-like) in individuals naturally exposed to malaria. *Acta Trop* (2004) 92(1):63–9. doi:10.1016/j.actatropica.2004.02.011
113. Storti-Melo LM, da Costa DR, Souza-Neiras WC, Cassiano GC, Couto VS, Povoa MM, et al. Influence of HLA-DRB-1 alleles on the production of antibody against CSP, MSP-1, AMA-1, and DBP in Brazilian individuals naturally infected with *Plasmodium vivax*. *Acta Trop* (2012) 121(2):152–5. doi:10.1016/j.actatropica.2011.10.009
114. Miller LH, Mason SJ, Clyde DF, McGinniss MH. The resistance factor to *Plasmodium vivax* in blacks. The Duffy-blood-group genotype, FyFy. *N Engl J Med* (1976) 295(6):302–4. doi:10.1056/NEJM197608052950602
115. Michon P, Woolley I, Wood EM, Kastens W, Zimmerman PA, Adams JH. Duffy-null promoter heterozygosity reduces DARC expression and abrogates adhesion of the *P. vivax* ligand required for blood-stage infection. *FEBS Lett* (2001) 495(1–2):111–4. doi:10.1016/S0014-5793(01)02370-5
116. Iwamoto S, Li J, Sugimoto N, Okuda H, Kajii E. Characterization of the Duffy gene promoter: evidence for tissue-specific abolishment of expression in Fy(a-b-) of black individuals. *Biochem Biophys Res Commun* (1996) 222(3):852–9. doi:10.1006/bbrc.1996.0833
117. Hamblin MT, Di Renzo A. Detection of the signature of natural selection in humans: evidence from the Duffy blood group locus. *Am J Hum Genet* (2000) 66(5):1669–79. doi:10.1086/302879
118. Tournamille C, Colin Y, Cartron JP, Le Van Kim C. Disruption of a GATA motif in the Duffy gene promoter abolishes erythroid gene expression in Duffy-negative individuals. *Nat Genet* (1995) 10(2):224–8. doi:10.1038/ng0695-224
119. Lopez C, Saravia C, Gomez A, Hoebeke J, Patarroyo MA. Mechanisms of genetically-based resistance to malaria. *Gene* (2010) 467(1–2):1–12. doi:10.1016/j.gene.2010.07.008
120. Woldearegai TG, Kremsner PG, Kun JF, Mordmuller B. *Plasmodium vivax* malaria in Duffy-negative individuals from Ethiopia. *Trans R Soc Trop Med Hyg* (2013) 107(5):328–31. doi:10.1093/trstmh/trt016
121. Mendes C, Dias F, Figueiredo J, Mora VG, Cano J, de Sousa B, et al. Duffy negative antigen is no longer a barrier to *Plasmodium vivax* – molecular evidences from the African West Coast (Angola and Equatorial Guinea). *PLoS Negl Trop Dis* (2011) 5(6):e1192. doi:10.1371/journal.pntd.0001192
122. Sohail M, Kaul A, Bali P, Raziuddin M, Singh MP, Singh OP, et al. Alleles -308A and -1031C in the TNF-alpha gene promoter do not increase the risk but associated with circulating levels of TNF-alpha and clinical features of vivax malaria in Indian patients. *Mol Immunol* (2008) 45(6):1682–92. doi:10.1016/j.molimm.2007.10.002
123. Sortica VA, Cunha MG, Ohnishi MD, Souza JM, Ribeiro-Dos-Santos AK, Santos NP, et al. IL1B, IL4R, IL12RB1 and TNF gene polymorphisms are associated with *Plasmodium vivax* malaria in Brazil. *Malar J* (2012) 11:409. doi:10.1186/1475-2875-11-409
124. da Silva Santos S, Clark TG, Campino S, Suarez-Mutis MC, Rockett KA, Kwiatkowski DP, et al. Investigation of host candidate malaria-associated risk/protective SNPs in a Brazilian Amazonian population. *PLoS One* (2012) 7(5):e36692. doi:10.1371/journal.pone.0036692
125. Mendonça VR, Souza LC, Garcia GC, Magalhães BM, Lacerda MV, Andrade BB, et al. DDX39B (BAT1), TNF and IL6 gene polymorphisms and association with clinical outcomes of patients with *Plasmodium vivax* malaria. *Malar J* (2014) 13(1):1. doi:10.1186/1475-2875-13-278
126. Aldrich C, Magini A, Emiliani C, Dottorini T, Bistoni F, Crisanti A, et al. Roles of the amino terminal region and repeat region of the *Plasmodium berghhei* circumsporozoite protein in parasite infectivity. *PLoS One* (2012) 7(2):e32524. doi:10.1371/journal.pone.0032524
127. Persson C, Oliveira GA, Sultan AA, Bhanot P, Nussenzweig V, Nardin E. Cutting edge: a new tool to evaluate human pre-erythrocytic malaria vaccines: rodent parasites bearing a hybrid *Plasmodium falciparum* circumsporozoite protein. *J Immunol* (2002) 169(12):6681–5. doi:10.4049/jimmunol.169.12.6681
128. Céspedes N, Jiménez E, Lopez-Perez M, Rubiano K, Felger I, Alonso P, et al. Antigenicity and immunogenicity of a novel *Plasmodium vivax* circumsporozoite derived synthetic vaccine construct. *Vaccine* (2014) 32(26):3179–86. doi:10.1016/j.vaccine.2014.04.007
129. Rathore D, Sacci JB, de la Vega P, McCutchan TF. Binding and invasion of liver cells by *Plasmodium falciparum* sporozoites Essential involvement

- of the amino terminus of circumsporozoite protein. *J Biol Chem* (2002) 277(9):7092–8. doi:10.1074/jbc.M106862200
130. Nussenzweig V, Nussenzweig RS. Rationale for the development of an engineered sporozoite malaria vaccine. *Adv Immunol* (1989) 45:283–334. doi:10.1016/S0065-2776(08)60695-1
131. White MT, Verity R, Griffin JT, Asante KP, Owusu-Agyei S, Greenwood B, et al. Immunogenicity of the RTS, S/AS01 malaria vaccine and implications for duration of vaccine efficacy: secondary analysis of data from a phase 3 randomised controlled trial. *Lancet Infect Dis* (2015) 15(12):1450–8. doi:10.1016/S1473-3099(15)00239-X
132. Olotu A, Fegan G, Wambua J, Nyangweso G, Leach A, Lievens M, et al. Seven-year efficacy of RTS,S/AS01 malaria vaccine among young African children. *N Engl J Med* (2016) 374(26):2519–29. doi:10.1056/NEJMoa1515257
133. Rts SCTP. Efficacy and safety of RTS,S/AS01 malaria vaccine with or without a booster dose in infants and children in Africa: final results of a phase 3, individually randomised, controlled trial. *Lancet* (2015) 386(9988):31–45. doi:10.1016/S0140-6736(15)60721-8
134. Zavala F, Tam JP, Barr PJ, Romero P, Ley V, Nussenzweig RS, et al. Synthetic peptide vaccine confers protection against murine malaria. *J Exp Med* (1987) 166(5):1591–6. doi:10.1084/jem.166.5.1591
135. Weiss WR, Berzofsky J, Houghten RA, Sedegah M, Hollindale M, Hoffman SL. AT cell clone directed at the circumsporozoite protein which protects mice against both *Plasmodium yoelii* and *Plasmodium berghei*. *J Immunol* (1992) 149(6):2103–9.
136. Marussig M, Rénia L, Motard A, Miltgen F, Pétour P, Chauhan V, et al. Linear and multiple antigen peptides containing defined T and B epitopes of the *Plasmodium yoelii* circumsporozoite protein: antibody-mediated protection and boosting by sporozoite infection. *Int Immunol* (1997) 9(12):1817–24. doi:10.1093/intimm/9.12.1817
137. Doolan DL, Hoffman SL. IL-12 and NK cells are required for antigen-specific adaptive immunity against malaria initiated by CD8+ T cells in the *Plasmodium yoelii* model. *J Immunol* (1999) 163(2):884–92.
138. Rosenberg R, Wirtz RA, Lanar DE, Sattabongkot J, Hall T, Waters AP, et al. Circumsporozoite protein heterogeneity in the human malaria parasite *Plasmodium vivax*. *Science* (1989) 245(4921):973–6. doi:10.1126/science.2672336
139. Qari SH, Shi V-P, Povoa MM, Alpers MP, Deloron P, Murphy GS, et al. Global occurrence of *Plasmodium vivax*-like human malaria parasite. *J Infect Dis* (1993) 168(6):1485–9. doi:10.1093/infdis/168.6.1485
140. Machado RL, Póvoa MM. Distribution of *Plasmodium vivax* variants (VK210, VK247 and *P. vivax*-like) in three endemic areas of the Amazon region of Brazil and their correlation with chloroquine treatment. *Trans R Soc Trop Med Hyg* (2000) 94(4):377–81. doi:10.1016/S0035-9203(00)90110-X
141. Cochrane AH, Nardin EH, De Arruda M, Maracic M, Clavijo P, Collins WE, et al. Widespread reactivity of human sera with a variant repeat of the circumsporozoite protein of *Plasmodium vivax*. *Am J Trop Med Hyg* (1990) 43(5):446–51.
142. Wirtz R, Rosenberg R, Sattabongkot J, Webster H. Prevalence of antibody to heterologous circumsporozoite protein of *Plasmodium vivax* in Thailand. *Lancet* (1990) 336(8715):593–5. doi:10.1016/0140-6736(90)93393-4
143. Franke ED, Lucas CM, San Roman E, Wirtz RA. Prevalence of antibody to the variant repeat of the circumsporozoite protein of *Plasmodium vivax* in Peru. *Am J Trop Med Hyg* (1992) 46(6):708–10.
144. Gonzalez J, Hurtado S, Arevalo-Herrera M, Herrera S. Variants of the *Plasmodium vivax* circumsporozoite protein (VK210 and VK247) in Colombian isolates. *Mem Inst Oswaldo Cruz* (2001) 96(5):709–12. doi:10.1590/S0074-02762001000500023
145. Herrera S, Fernández OL, Vera O, Cárdenas W, Ramírez O, Palacios R, et al. Phase I safety and immunogenicity trial of *Plasmodium vivax* CS derived long synthetic peptides adjuvanted with montanide ISA 720 or montanide ISA 51. *Am J Trop Med Hyg* (2011) 84(2 Suppl):12–20. doi:10.4296/ajtmh.2011.09-0516
146. Bennett JW, Yadava A, Tosh D, Sattabongkot J, Komisar J, Ware LA, et al. Phase 1/2a Trial of *Plasmodium vivax* malaria vaccine candidate VMP001/AS01 B in malaria-naïve adults: safety, immunogenicity, and efficacy. *PLoS Negl Trop Dis* (2016) 10(2):e0004423. doi:10.1371/journal.pntd.0004423
147. Wu Y, Ellis RD, Shaffer D, Fontes E, Malkin EM, Mahanty S, et al. Phase 1 trial of malaria transmission blocking vaccine candidates Pfs25 and Pvs25 formulated with montanide ISA 51. *PLoS One* (2008) 3(7):e2636. doi:10.1371/journal.pone.0002636
148. Malkin EM, Durbin AP, Diemert DJ, Sattabongkot J, Wu Y, Miura K, et al. Phase 1 vaccine trial of Pvs25H: a transmission blocking vaccine for *Plasmodium vivax* malaria. *Vaccine* (2005) 23(24):3131–8. doi:10.1016/j.vaccine.2004.12.019
149. Bell BA, Wood JF, Bansal R, Ragab H, Cargo J, Washington MA, et al. Process development for the production of an *E. coli* produced clinical grade recombinant malaria vaccine for *Plasmodium vivax*. *Vaccine* (2009) 27(9):1448–53. doi:10.1016/j.vaccine.2008.12.027
150. Yadava A, Sattabongkot J, Washington MA, Ware LA, Majam V, Zheng H, et al. A novel chimeric *Plasmodium vivax* circumsporozoite protein induces biologically functional antibodies that recognize both VK210 and VK247 sporozoites. *Infect Immun* (2007) 75(3):1177–85. doi:10.1128/IAI.01667-06
151. Cheng Y, Ito D, Sattabongkot J, Lim CS, Kong D-H, Ha K-S, et al. Serological responses to a soluble recombinant chimeric *Plasmodium vivax* circumsporozoite protein in VK210 and VK247 population. *Malar J* (2013) 12(1):1. doi:10.1186/1475-2875-12-323
152. Wilson KL, Xiang SD, Plebanski M. Montanide, Poly I:C and nanoparticle based vaccines promote differential suppressor and effector cell expansion: a study of induction of CD8 T cells to minimal *Plasmodium berghei* epitope. *Front Microbiol* (2015) 6:29. doi:10.3389/fmicb.2015.00029
153. Yadava A, Hall CE, Sullivan JS, Nace D, Williams T, Collins WE, et al. Protective efficacy of a *Plasmodium vivax* circumsporozoite protein-based vaccine in *Aotus nancymaae* is associated with antibodies to the repeat region. *PLoS Negl Trop Dis* (2014) 8(10):e3268. doi:10.1371/journal.pntd.0003268
154. Krieg AM, Yi A-K, Matson S, Waldschmidt TJ, Bishop GA, Teasdale R, et al. CpG motifs in bacterial DNA trigger direct B-cell activation. *Nature* (1995) 374(6522):546–9. doi:10.1038/374546a0
155. Camacho AGA, Teixeira LH, Bargieri DY, Boscardin SB, Soares IDS, Nussenzweig RS, et al. TLR5-dependent immunogenicity of a recombinant fusion protein containing an immunodominant epitope of malarial circumsporozoite protein and the FliC flagellin of *Salmonella typhimurium*. *Mem Inst Oswaldo Cruz* (2011) 106:167–71. doi:10.1590/S0074-02762011000900021
156. Rogers WO, Malik A, Mellouk S, Nakamura K, Rogers MD, Szarfman A, et al. Characterization of *Plasmodium falciparum* sporozoite surface protein 2. *Proc Natl Acad Sci U S A* (1992) 89(19):9176–80. doi:10.1073/pnas.89.19.9176
157. Ogunbanwo JA, Pendyala PR, Malhotra P, Chauhan VS. Expression, purification and characterization of a recombinant *Plasmodium vivax* thrombospondin related adhesive protein (PvTRAP). *Int J Biomed Sci* (2006) 2(3):251.
158. Swearingen KE, Lindner SE, Shi L, Shears MJ, Harupa A, Hopp CS, et al. Interrogating the *Plasmodium* sporozoite surface: identification of surface-exposed proteins and demonstration of glycosylation on CSP and TRAP by mass spectrometry-based proteomics. *PLoS Pathog* (2016) 12(4):e1005606. doi:10.1371/journal.ppat.1005606
159. Hafalla JCR, Bauza K, Friesen J, Gonzalez-Aseguinolaza G, Hill AV, Matuschewski K. Identification of targets of CD8+ T cell responses to malaria liver stages by genome-wide epitope profiling. *PLoS Pathog* (2013) 9(5):e1003303. doi:10.1371/journal.ppat.1003303
160. Longley RJ, Bauza K, Ewer KJ, Hill AV, Spencer AJ. Development of an in vitro assay and demonstration of *Plasmodium berghei* liver-stage inhibition by TRAP-specific CD8+ T cells. *PLoS One* (2015) 10(3):e0119880. doi:10.1371/journal.pone.0119880
161. Ewer KJ, O'Hara GA, Duncan CJ, Collins KA, Sheehy SH, Reyes-Sandoval A, et al. Protective CD8+ T-cell immunity to human malaria induced by chimpanzee adenovirus-MVA immunisation. *Nat Commun* (2013) 4:2836. doi:10.1038/ncomms3836
162. Castellanos A, Arévalo-Herrera M, Restrepo N, Gulloso L, Corradin G, Herrera S. *Plasmodium vivax* thrombospondin related adhesion protein: immunogenicity and protective efficacy in rodents and *Aotus* monkeys. *Mem Inst Oswaldo Cruz* (2007) 102(3):411–6. doi:10.1590/S0074-02762007005000047
163. Bauza K, Malinauskas T, Pfander C, Anar B, Jones EY, Billker O, et al. Efficacy of a *Plasmodium vivax* malaria vaccine using ChAd63 and modified vaccinia Ankara expressing thrombospondin-related anonymous protein

- as assessed with transgenic *Plasmodium berghei* parasites. *Infect Immun* (2014) 82(3):1277–86. doi:10.1128/IAI.01187-13
164. Chenet SM, Tapia LL, Escalante AA, Durand S, Lucas C, Bacon DJ. Genetic diversity and population structure of genes encoding vaccine candidate antigens of *Plasmodium vivax*. *Malar J* (2012) 11(1):1. doi:10.1186/1475-2875-11-68
165. Wang Q, Zhao Z, Zhang X, Li X, Zhu M, Li P, et al. Naturally Acquired Antibody Responses to *Plasmodium vivax* and *Plasmodium falciparum* Merozoite Surface Protein 1 (MSP1) C-Terminal 19 kDa Domains in an Area of Unstable Malaria Transmission in Southeast Asia. *PLoS ONE* (2016) 11(3):e0151900. doi:10.1371/journal.pone.0151900
166. Del Portillo HA, Longacre S, Khouri E, David PH. Primary structure of the merozoite surface antigen 1 of *Plasmodium vivax* reveals sequences conserved between different *Plasmodium* species. *Proc Natl Acad Sci U S A* (1991) 88(9):4030–4. doi:10.1073/pnas.88.9.4030
167. del Portillo HA, Gysin J, Mattei DM, Khouri E, Udagama PV, Mendis KN, et al. *Plasmodium vivax*: cloning and expression of a major blood-stage surface antigen. *Exp Parasitol* (1988) 67(2):346–53. doi:10.1016/0014-4894(88)90081-1
168. Freeman RR, Holder AA. Surface antigens of malaria merozoites. A high molecular weight precursor is processed to an 83,000 mol wt form expressed on the surface of *Plasmodium falciparum* merozoites. *J Exp Med* (1983) 158(5):1647–53. doi:10.1084/jem.158.5.1647
169. Kaslow DC, Kumar S. Expression and immunogenicity of the C-terminus of a major blood-stage surface protein of *Plasmodium vivax*, Pv200 19, secreted from *Saccharomyces cerevisiae*. *Immunol Lett* (1996) 51(3):187–9. doi:10.1016/0165-2478(96)02570-9
170. Han H-J, Park S-G, Kim S-H, Hwang S-Y, Han J, Traicoff J, et al. Epidermal growth factor-like motifs 1 and 2 of *Plasmodium vivax* merozoite surface protein 1 are critical domains in erythrocyte invasion. *Biochem Biophys Res Commun* (2004) 320(2):563–70. doi:10.1016/j.bbrc.2004.06.008
171. Soares IS, da Cunha MG, Silva MN, Souza JM, Del Portillo HA, Rodrigues MM. Longevity of naturally acquired antibody responses to the N-and C-terminal regions of *Plasmodium vivax* merozoite surface protein 1. *Am J Trop Med Hyg* (1999) 60(3):357–63.
172. Fernandez-Becerra C, Sanz S, Brucet M, Stanisic DI, Alves FP, Camargo EP, et al. Naturally-acquired humoral immune responses against the N-and C-termini of the *Plasmodium vivax* MSP1 protein in endemic regions of Brazil and Papua New Guinea using a multiplex assay. *Malar J* (2010) 9(1):1. doi:10.1186/1475-2875-9-29
173. Park CG, Chwae Y-J, Kim J-I, Lee J-H, Hur GM, Jeon BH, et al. Serologic responses of Korean soldiers serving in malaria-endemic areas during a recent outbreak of *Plasmodium vivax*. *Am J Trop Med Hyg* (2000) 62(6):720–5.
174. Rosa DS, Iwai LK, Tzelepis F, Bargieri DY, Medeiros MA, Soares IS, et al. Immunogenicity of a recombinant protein containing the *Plasmodium vivax* vaccine candidate MSP1 19 and two human CD4+ T-cell epitopes administered to non-human primates (*Callithrix jacchus jacchus*). *Microb Infect* (2006) 8(8):2130–7. doi:10.1016/j.micinf.2006.03.012
175. Sierra AY, Barrero CA, Rodriguez R, Silva Y, Moncada C, Vanegas M, et al. Splenectomised and spleen intact *Aotus* monkeys' immune response to *Plasmodium vivax* MSP-1 protein fragments and their high activity binding peptides. *Vaccine* (2003) 21(27):4133–44. doi:10.1016/S0264-410X(03)00455-9
176. Barrero CA, Delgado G, Sierra AY, Silva Y, Parra-Lopez C, Patarroyo MA. Gamma interferon levels and antibody production induced by two PvMSP-1 recombinant polypeptides are associated with protective immunity against *P. vivax* in *Aotus* monkeys. *Vaccine* (2005) 23(31):4048–53. doi:10.1016/j.vaccine.2005.02.012
177. Dutta S, Ware LA, Barbosa A, Ockenhouse CF, Lanar DE. Purification, characterization, and immunogenicity of a disulfide cross-linked *Plasmodium vivax* vaccine candidate antigen, merozoite surface protein 1, expressed in *Escherichia coli*. *Infect Immun* (2001) 69(9):5464–70. doi:10.1128/IAI.69.9.5464-5470.2001
178. Chen J-H, Wang Y, Ha K-S, Lu F, Suh I-B, Lim CS, et al. Measurement of naturally acquired humoral immune responses against the C-terminal region of the *Plasmodium vivax* MSP1 protein using protein arrays. *Parasitol Res* (2011) 109(5):1259–66. doi:10.1007/s00436-011-2370-z
179. Cheng Y, Wang Y, Ito D, Kong D-H, Ha K-S, Chen J-H, et al. The *Plasmodium vivax* merozoite surface protein 1 paralog is a novel erythrocyte-binding ligand of *P. vivax*. *Infect Immun* (2013) 81(5):1585–95. doi:10.1128/IAI.01117-12
180. Galinski MR, Corredor-Medina C, Povoa M, Crosby J, Ingravallo P, Barnwell JW. *Plasmodium vivax* merozoite surface protein-3 contains coiled-coil motifs in an alanine-rich central domain. *Mol Biochem Parasitol* (1999) 101(1):131–47. doi:10.1016/S0166-6851(99)00063-8
181. Rayner J, Corredor V, Feldman D, Ingravallo P, Iderabdullah F, Galinski M, et al. Extensive polymorphism in the *Plasmodium vivax* merozoite surface coat protein MSP-3 $\alpha$  is limited to specific domains. *Parasitology* (2002) 125(5):393–405. doi:10.1017/S0031182002002317
182. Rayner JC, Huber CS, Feldman D, Ingravallo P, Galinski MR, Barnwell JW. *Plasmodium vivax* merozoite surface protein PvMSP-3 $\beta$  is radically polymorphic through mutation and large insertions and deletions. *Infect Genet Evol* (2004) 4(4):309–19. doi:10.1016/j.meegid.2004.03.003
183. Hisaeda H, Saul A, Reece JJ, Kennedy MC, Long CA, Miller LH, et al. Merozoite surface protein 3 and protection against malaria in *Aotus nancymai* monkeys. *J Infect Dis* (2002) 185(5):657–64. doi:10.1086/339187
184. Audran R, Cachat M, Lurati F, Soe S, Leroy O, Corradin G, et al. Phase I malaria vaccine trial with a long synthetic peptide derived from the merozoite surface protein 3 antigen. *Infect Immun* (2005) 73(12):8017–26. doi:10.1128/IAI.73.12.8017-8026.2005
185. Vargas-Serrato E, Barnwell JW, Ingravallo P, Perler FB, Galinski MR. Merozoite surface protein-9 of *Plasmodium vivax* and related simian malaria parasites is orthologous to p101/ABRA of *P. falciparum*. *Mol Biochem Parasitol* (2002) 120(1):41–52. doi:10.1016/S0166-6851(01)00433-9
186. Oliveira-Ferreira J, Vargas-Serrato E, Barnwell JW, Moreno A, Galinski MR. Immunogenicity of *Plasmodium vivax* merozoite surface protein-9 recombinant proteins expressed in *E. coli*. *Vaccine* (2004) 22(15–16):2023–30. doi:10.1016/j.vaccine.2003.07.021
187. Horuk R, Chitnis CE, Darbonne WC, Colby TJ, Rybicki A, Hadley TJ, et al. A receptor for the malarial parasite *Plasmodium vivax*: the erythrocyte chemokine receptor. *Science* (1993) 261(5125):1182–4. doi:10.1126/science.7689250
188. Wertheimer SP, Barnwell JW. *Plasmodium vivax* interaction with the human Duffy blood group glycoprotein: identification of a parasite receptor-like protein. *Exp Parasitol* (1989) 69(3):340–50. doi:10.1016/0014-4894(89)90083-0
189. Fang X, Kaslow DC, Adams JH, Miller LH. Cloning of the *Plasmodium vivax* Duffy receptor. *Mol Biochem Parasitol* (1991) 44(1):125–32. doi:10.1016/0166-6851(91)90228-X
190. Adams JH, Sim BK, Dolan SA, Fang X, Kaslow DC, Miller LH. A family of erythrocyte binding proteins of malaria parasites. *Proc Natl Acad Sci U S A* (1992) 89(15):7085–9. doi:10.1073/pnas.89.15.7085
191. Chitnis CE, Miller LH. Identification of the erythrocyte binding domains of *Plasmodium vivax* and *Plasmodium knowlesi* proteins involved in erythrocyte invasion. *J Exp Med* (1994) 180(2):497–506. doi:10.1084/jem.180.2.497
192. Ntumngia FB, Adams JH. Design and immunogenicity of a novel synthetic antigen based on the ligand domain of the *Plasmodium vivax* Duffy binding protein. *Clin Vaccine Immunol* (2012) 19(1):30–6. doi:10.1128/CVI.05466-11
193. Cole-Tobian JL, Michon P, Biasor M, Richards JS, Beeson JG, Mueller I, et al. Strain-specific Duffy binding protein antibodies correlate with protection against infection with homologous compared to heterologous *Plasmodium vivax* strains in Papua New Guinean children. *Infect Immun* (2009) 77(9):4009–17. doi:10.1128/IAI.00158-09
194. Ceravolo I, Sanchez B, Sousa T, Guerra B, Soares I, Braga E, et al. Naturally acquired inhibitory antibodies to *Plasmodium vivax* Duffy binding protein are short-lived and allele-specific following a single malaria infection. *Clin Exp Immunol* (2009) 156(3):502–10. doi:10.1111/j.1365-2249.2009.03931.x
195. Choontong P, Panichakul T, Permmongkol C, Barnes SJ, Udomsangpetch R, Adams JH. Characterization of inhibitory anti-Duffy binding protein II immunity: approach to *Plasmodium vivax* vaccine development in Thailand. *PLoS One* (2012) 7(4):e35769. doi:10.1371/journal.pone.0035769
196. Michon P, Fraser T, Adams JH. Naturally Acquired and vaccine-elicited antibodies block erythrocyte cytoadherence of the *Plasmodium vivax* Duffy binding protein. *Infect Immun* (2000) 68(6):3164–71. doi:10.1128/IAI.68.6.3164-3171.2000

197. Chootong P, McHenry AM, Ntumngia FB, Sattabongkot J, Adams JH. The association of Duffy binding protein region II polymorphisms and its antigenicity in *Plasmodium vivax* isolates from Thailand. *Parasitol Int* (2014) 63(6):858–64. doi:10.1016/j.parint.2014.07.014
198. Xainli J, Baisor M, Kastens W, Bockarie M, Adams JH, King CL. Age-dependent cellular immune responses to *Plasmodium vivax* Duffy binding protein in humans. *J Immunol* (2002) 169(6):3200–7. doi:10.4049/jimmunol.169.6.3200
199. Xainli J, Cole-Tobian JL, Baisor M, Kastens W, Bockarie M, Yazdani SS, et al. Epitope-specific humoral immunity to *Plasmodium vivax* Duffy binding protein. *Infect Immun* (2003) 71(5):2508–15. doi:10.1128/IAI.71.5.2508-2515.2003
200. VanBuskirk KM, Sevova E, Adams JH. Conserved residues in the *Plasmodium vivax* Duffy-binding protein ligand domain are critical for erythrocyte receptor recognition. *Proc Natl Acad Sci U S A* (2004) 101(44):15754–9. doi:10.1073/pnas.0405421101
201. VanBuskirk KM, Tobian JLC, Baisor M, Sevova ES, Bockarie M, King CL, et al. Antigenic drift in the ligand domain of *Plasmodium vivax* Duffy binding protein confers resistance to inhibitory antibodies. *J Infect Dis* (2004) 190(9):1556–62. doi:10.1086/424852
202. Saravia C, Martinez P, Granados DS, Lopez C, Reyes C, Patarroyo MA. Identification and evaluation of universal epitopes in *Plasmodium vivax* Duffy binding protein. *Biochem Biophys Res Commun* (2008) 377(4):1279–83. doi:10.1016/j.bbrc.2008.10.153
203. Martinez P, Lopez C, Saravia C, Vanegas M, Patarroyo MA. Evaluation of the antigenicity of universal epitopes from PvDBP11 in individuals exposed to *Plasmodium vivax* malaria. *Microbes Infect* (2010) 12(14):1188–97. doi:10.1016/j.micinf.2010.08.007
204. Maestre A, Muskus C, Duque V, Agudelo O, Liu P, Takagi A, et al. Acquired antibody responses against *Plasmodium vivax* infection vary with host genotype for Duffy antigen receptor for chemokines (DARC). *PLoS One* (2010) 5(7):e11437. doi:10.1371/journal.pone.0011437
205. Waters AP, Thomas A, Deans J, Mitchell G, Hudson DE, Miller LH, et al. A merozoite receptor protein from *Plasmodium knowlesi* is highly conserved and distributed throughout *Plasmodium*. *J Biol Chem* (1990) 265(29):17974–9.
206. Cheng Q, Saul A. Sequence analysis of the apical membrane antigen I (AMA-1) of *Plasmodium vivax*. *Mol Biochem Parasitol* (1994) 65(1):183–7. doi:10.1016/0166-6851(94)90127-9
207. Hodder AN, Crewther PE, Matthew ML, Reid GE, Moritz RL, Simpson RJ, et al. The disulfide bond structure of *Plasmodium* apical membrane antigen-1. *J Biol Chem* (1996) 271(46):29446–52. doi:10.1074/jbc.271.46.29446
208. Remarque EJ, Faber BW, Kocken CH, Thomas AW. Apical membrane antigen 1: a malaria vaccine candidate in review. *Trends Parasitol* (2008) 24(2):74–84. doi:10.1016/j.pt.2007.12.002
209. Kocken CH, Dubbeld MA, Van Der Wel A, Pronk JT, Waters AP, Langermans JA, et al. High-level expression of *Plasmodium vivax* apical membrane antigen 1 (AMA-1) in *Pichia pastoris*: strong immunogenicity in *Macaca mulatta* immunized with *P. vivax* AMA-1 and adjuvant SBAS2. *Infect Immun* (1999) 67(1):43–9.
210. Bouillet LÉM, Dias MO, Dorigo NA, Moura AD, Russell B, Nosten F, et al. Long-term humoral and cellular immune responses elicited by a heterologous *Plasmodium vivax* apical membrane antigen 1 protein prime/adenovirus boost immunization protocol. *Infect Immun* (2011) 79(9):3642–52. doi:10.1128/IAI.05048-11
211. Salavatifar M, Zakeri S, Roodbari NH, Djadid ND. High-level expression, purification and characterization of a recombinant *Plasmodium vivax* apical membrane antigen 1: implication for vivax malaria vaccine development. *Cell J* (2015) 17(3):520.
212. Salavatifar M, Zakeri S, Abouie Mehrizi A, Mirkhazemi S, Dinparast Djadid N. Evaluation of naturally acquired antibody responses to two variant forms of *Plasmodium vivax* apical membrane antigen-1 in individuals living in areas of low and unstable malaria transmission of Iran. *Arch Iran Med* (2015) 18(12):834–43.
213. Bueno LL, Lobo FP, Morais CG, Mourão LC, de Ávila RAM, Soares IS, et al. Identification of a highly antigenic linear B cell epitope within *Plasmodium vivax* apical membrane antigen 1 (AMA-1). *PLoS One* (2011) 6(6):e21289. doi:10.1371/journal.pone.0021289
214. Gentil F, Bargieri DY, Leite JA, Francoso KS, Patricio MB, Espindola NM, et al. A recombinant vaccine based on domain II of *Plasmodium vivax* apical membrane antigen 1 induces high antibody titres in mice. *Vaccine* (2010) 28(38):6183–90. doi:10.1016/j.vaccine.2010.07.017
215. Li J, Han E-T. Dissection of the *Plasmodium vivax* reticulocyte binding-like proteins (PvRBPs). *Biochem Biophys Res Commun* (2012) 426(1):1–6. doi:10.1016/j.bbrc.2012.08.055
216. Galinski M, Barnwell J. *Plasmodium vivax*: merozoites, invasion of reticulocytes and considerations for malaria vaccine development. *Parasitol Today* (1996) 12(1):20–9. doi:10.1016/0169-4758(96)80641-7
217. Galinski MR, Medina CC, Ingravallo P, Barnwell JW. A reticulocyte-binding protein complex of *Plasmodium vivax* merozoites. *Cell* (1992) 69(7):1213–26. doi:10.1016/0092-8674(92)90642-P
218. Galinski MR, Xu M, Barnwell JW. *Plasmodium vivax* reticulocyte binding protein-2 (PvRBP-2) shares structural features with PvRBP-1 and the *Plasmodium yoelii* 235 kDa rhoptry protein family. *Mol Biochem Parasitol* (2000) 108(2):257–62. doi:10.1016/S0166-6851(00)00219-X
219. Hietanen J, Chim-ong A, Chiramanewong T, Gruszczik J, Roobsoong W, Tham W-H, et al. Gene models, expression repertoire, and immune response of *Plasmodium vivax* reticulocyte binding proteins. *Infect Immun* (2016) 84(3):677–85. doi:10.1128/IAI.01117-15
220. Prajapati SK, Singh OP. Insights into the invasion biology of *Plasmodium vivax*. *Front Cell Infect Microbiol* (2013) 3:8. doi:10.3389/fcimb.2013.00008
221. Franca CT, He WQ, Gruszczik J, Lim NT, Lin E, Kiniboro B, et al. *Plasmodium vivax* reticulocyte binding proteins are key targets of naturally acquired immunity in young Papua New Guinean children. *PLoS Negl Trop Dis* (2016) 10(9):e0005014. doi:10.1371/journal.pntd.0005014
222. Cantor EM, Lombo TB, Cepeda A, Espinosa AM, Barrero CA, Guzmán F, et al. *Plasmodium vivax*: functional analysis of a highly conserved PvRBP-1 protein region. *Mol Biochem Parasitol* (2001) 117(2):229–34. doi:10.1016/S0166-6851(01)00355-3
223. Urquiza M, Patarroyo MA, Marí V, Ocampo M, Suárez J, López R, et al. Identification and polymorphism of *Plasmodium vivax* RBP-1 peptides which bind specifically to reticulocytes. *Peptides* (2002) 23(12):2265–77. doi:10.1016/S0196-9781(02)00267-X
224. Rojas-Caraballo J, Delgado G, Rodriguez R, Patarroyo MA. The antigenicity of a *Plasmodium vivax* reticulocyte binding protein-1 (PvRBP1) recombinant fragment in humans and its immunogenicity and protection studies in *Aotus* monkeys. *Vaccine* (2007) 25(18):3713–21. doi:10.1016/j.vaccine.2006.12.041
225. Perez-Leal O, Sierra AY, Barrero CA, Moncada C, Martinez P, Cortes J, et al. Identifying and characterising the *Plasmodium falciparum* merozoite surface protein 10 *Plasmodium vivax* homologue. *Biochem Biophys Res Commun* (2005) 331(4):1178–84. doi:10.1016/j.bbrc.2005.04.031
226. Giraldo MA, Arevalo-Pinzon G, Rojas-Caraballo J, Mongui A, Rodriguez R, Patarroyo MA. Vaccination with recombinant *Plasmodium vivax* MSP-10 formulated in different adjuvants induces strong immunogenicity but no protection. *Vaccine* (2009) 28(1):7–13. doi:10.1016/j.vaccine.2009.09.046
227. Cheng Y, Wang B, Sattabongkot J, Lim CS, Tsuboi T, Han E-T. Immunogenicity and antigenicity of *Plasmodium vivax* merozoite surface protein 10. *Parasitol Res* (2014) 113(7):2559–68. doi:10.1007/s00436-014-3907-8
228. Mongui A, Angel DI, Gallego G, Reyes C, Martinez P, Guhl F, et al. Characterization and antigenicity of the promising vaccine candidate *Plasmodium vivax* 34kDa rhoptry antigen (Pv34). *Vaccine* (2009) 28(2):415–21. doi:10.1016/j.vaccine.2009.10.034
229. Moreno-Perez DA, Montenegro M, Patarroyo ME, Patarroyo MA. Identification, characterization and antigenicity of the *Plasmodium vivax* rhoptry neck protein 1 (PvRON1). *Malar J* (2011) 10:314. doi:10.1186/1475-2875-10-314
230. Cheng Y, Li J, Ito D, Kong DH, Ha KS, Lu F, et al. Antigenicity and immunogenicity of PvRALP1, a novel *Plasmodium vivax* rhoptry neck protein. *Malar J* (2015) 14:186. doi:10.1186/s12936-015-0698-z
231. Bergmann-Leitner ES, Mease RM, de la Vega P, Savranskaya T, Polhemus M, Ockenhouse C, et al. Immunization with pre-erythrocytic antigen CelTOS from *Plasmodium falciparum* elicits cross-species protection against heterologous challenge with *Plasmodium berghei*. *PLoS One* (2010) 5(8):e12294. doi:10.1371/journal.pone.0012294

232. Kariu T, Ishino T, Yano K, Chinzei Y, Yuda M. CelTOS, a novel malarial protein that mediates transmission to mosquito and vertebrate hosts. *Mol Microbiol* (2006) 59(5):1369–79. doi:10.1111/j.1365-2958.2005.05024.x
233. Longley RJ, Reyes-Sandoval A, Montoya-Díaz E, Dunachie S, Kumpitak C, Nguitragool W, et al. Acquisition and longevity of antibodies to *Plasmodium vivax* preerythrocytic antigens in Western Thailand. *Clin Vaccine Immunol* (2016) 23(2):117–24. doi:10.1128/CVI.00501-15
234. Peiris JS, Premawansa S, Ranawaka MB, Udagama PV, Munasinghe YD, Nanayakkara MV, et al. Monoclonal and polyclonal antibodies both block and enhance transmission of human *Plasmodium vivax* malaria. *Am J Trop Med Hyg* (1988) 39(1):26–32.
235. Hisaeda H, Stowers AW, Tsuboi T, Collins WE, Sattabongkot JS, Suwanabun N, et al. Antibodies to malaria vaccine candidates Pvs25 and Pvs28 completely block the ability of *Plasmodium vivax* to infect mosquitoes. *Infect Immun* (2000) 68(12):6618–23. doi:10.1128/IAI.68.12.6618-6623.2000
236. Hisaeda H, Collins WE, Saul A, Stowers AW. Antibodies to *Plasmodium vivax* transmission-blocking vaccine candidate antigens Pvs25 and Pvs28 do not show synergism. *Vaccine* (2001) 20(5–6):763–70. doi:10.1016/S0264-410X(01)00402-9
237. Sattabongkot J, Tsuboi T, Hisaeda H, Tachibana M, Suwanabun N, Rungruang T, et al. Blocking of transmission to mosquitoes by antibody to *Plasmodium vivax* malaria vaccine candidates Pvs25 and Pvs28 despite antigenic polymorphism in field isolates. *Am J Trop Med Hyg* (2003) 69(5):536–41.
238. Arevalo-Herrera M, Solarie Y, Yasnot MF, Castellanos A, Rincon A, Saul A, et al. Induction of transmission-blocking immunity in *Aotus* monkeys by vaccination with a *Plasmodium vivax* clinical grade PVS25 recombinant protein. *Am J Trop Med Hyg* (2005) 73(5 Suppl):32–7.
239. Miura K, Keister DB, Muratova OV, Sattabongkot J, Long CA, Saul A. Transmission-blocking activity induced by malaria vaccine candidates Pfs25/Pvs25 is a direct and predictable function of antibody titer. *Malar J* (2007) 6:107. doi:10.1186/1475-2875-6-107
240. Saul A, Hensmann M, Sattabongkot J, Collins WE, Barnwell JW, Langermanns JA, et al. Immunogenicity in rhesus of the *Plasmodium vivax* mosquito stage antigen Pvs25H with alhydrogel and montanide ISA 720. *Parasite Immunol* (2007) 29(10):525–33. doi:10.1111/j.1365-3024.2007.00971.x
241. Blagborough AM, Musiychuk K, Bi H, Jones RM, Chichester JA, Streatfield S, et al. Transmission blocking potency and immunogenicity of a plant-produced Pvs25-based subunit vaccine against *Plasmodium vivax*. *Vaccine* (2016) 34(28):3252–9. doi:10.1016/j.vaccine.2016.05.007
242. Espinosa AM, Sierra AY, Barrero CA, Cepeda LA, Cantor EMA, Lombo TB, et al. Expression, polymorphism analysis, reticulocyte binding and serological reactivity of two *Plasmodium vivax* MSP-1 protein recombinant fragments. *Vaccine* (2003) 21(11):1033–43. doi:10.1016/S0264-410X(02)00660-6
243. Tanabe K, Escalante A, Sakihama N, Honda M, Arisue N, Horii T, et al. Recent independent evolution of MSP1 polymorphism in *Plasmodium vivax* and related simian malaria parasites. *Mol Biochem Parasitol* (2007) 156(1):74–9. doi:10.1016/j.molbiopara.2007.07.002
244. Achtman A, Bull P, Stephens R, Langhorne J. Longevity of the immune response and memory to blood-stage malaria infection. In: Langhorne J, editor. *Immunology and Immunopathogenesis of Malaria*. Berlin, Heidelberg: Springer (2005). p. 71–102.
245. Villegas-Mendez A, Inkson CA, Shaw TN, Strangward P, Couper KN. Long-lived CD4+ IFN- $\gamma$ + T cells rather than short-lived CD4+ IFN- $\gamma$ + IL-10+ T cells initiate rapid IL-10 production to suppress anamnestic T cell responses during secondary malaria infection. *J Immunol* (2016) 197(8):3152–64. doi:10.4049/jimmunol.1600968
246. Patarroyo ME, Alba MP, Reyes C, Rojas-Luna R, Patarroyo MA. The Malaria Parasite's Achilles' Heel: functionally-relevant invasion structures. *Curr Issues Mol Biol* (2015) 18:11–20. doi:10.21775/cimb.018.011
247. Cifuentes G, Bermudez A, Rodriguez R, Patarroyo M, Patarroyo M. Shifting the polarity of some critical residues in malarial peptides' binding to host cells is a key factor in breaking conserved antigens' code of silence. *Med Chem* (2008) 4(3):278–92. doi:10.2174/157340608784325160
248. Patarroyo ME, Bermudez A, Patarroyo MA. Structural and immunological principles leading to chemically synthesized, multiantigenic, multistage, minimal subunit-based vaccine development. *Chem Rev* (2011) 111(5):3459–507. doi:10.1021/cr100223m
249. Patarroyo MA, Bermudez A, Lopez C, Yépez G, Patarroyo ME. 3D analysis of the TCR/pMHCII complex formation in monkeys vaccinated with the first peptide inducing sterilizing immunity against human malaria. *PLoS One* (2010) 5(3):e9771. doi:10.1371/journal.pone.0009771

**Conflict of Interest Statement:** The authors declare that the research was conducted in the absence of any commercial or financial relationships that could be construed as a potential conflict of interest.

Copyright © 2017 López, Yépez-Pérez, Hincapié-Escobar, Díaz-Arévalo and Patarroyo. This is an open-access article distributed under the terms of the Creative Commons Attribution License (CC BY). The use, distribution or reproduction in other forums is permitted, provided the original author(s) or licensor are credited and that the original publication in this journal is cited, in accordance with accepted academic practice. No use, distribution or reproduction is permitted which does not comply with these terms.



# Plasmodium vivax Cell-Traversal Protein for Ookinete and Sporozoite: Naturally Acquired Humoral Immune Response and B-Cell Epitope Mapping in Brazilian Amazon Inhabitants

## OPEN ACCESS

### Edited by:

Clarisa B. Palatnik-de-Sousa,  
Federal University of Rio de Janeiro,  
Brazil

### Reviewed by:

Manuel Alfonso Patarroyo,  
Fundación Instituto de Inmunología  
de Colombia (FIDIC), Colombia  
Daniel Youssef Bargieri,  
University of São Paulo, Brazil

### \*Correspondence:

Josué da Costa Lima-Junior  
josue@ioc.fiocruz.br

### Specialty section:

This article was submitted to  
Vaccines and Molecular  
Therapeutics,  
a section of the journal  
*Frontiers in Immunology*

**Received:** 10 November 2016

**Accepted:** 17 January 2017

**Published:** 07 February 2017

### Citation:

Rodrigues-da-Silva RN, Soares IF,  
Lopez-Camacho C,  
Martins da Silva JH,  
Perce-da-Silva DS, Téva A,  
Ramos Franco AM, Pinheiro FG,  
Chaves LB, Pratt-Riccio LR,  
Reyes-Sandoval A, Banic DM and  
Lima-Junior JC (2017) Plasmodium  
vivax Cell-Traversal Protein for  
Ookinete and Sporozoite: Naturally  
Acquired Humoral Immune Response  
and B-Cell Epitope Mapping in  
Brazilian Amazon Inhabitants.  
*Front. Immunol.* 8:77.  
doi: 10.3389/fimmu.2017.00077

Rodrigo Nunes Rodrigues-da-Silva<sup>1</sup>, Isabela Ferreira Soares<sup>1</sup>, Cesar Lopez-Camacho<sup>2</sup>,  
João Hermínio Martins da Silva<sup>3</sup>, Daiana de Souza Perce-da-Silva<sup>4</sup>, Antônio Têva<sup>5</sup>,  
Antônia Maria Ramos Franco<sup>6</sup>, Francimeire Gomes Pinheiro<sup>6</sup>, Lana Bitencourt Chaves<sup>1</sup>,  
Lilian Rose Pratt-Riccio<sup>7</sup>, Arturo Reyes-Sandoval<sup>2</sup>, Dalma Maria Banic<sup>4</sup> and  
Josué da Costa Lima-Junior<sup>1\*</sup>

<sup>1</sup>Laboratory of Immunoparasitology, Oswaldo Cruz Institute, Fiocruz, Rio de Janeiro, Brazil, <sup>2</sup>Nuffield Department of Medicine, The Jenner Institute, The Henry Wellcome Building for Molecular Physiology, University of Oxford, Oxford, UK,

<sup>3</sup>Computational Modeling Group, Fiocruz, Fortaleza, Brazil, <sup>4</sup>Laboratory of Clinical Immunology, Oswaldo Cruz Institute, Fiocruz, Rio de Janeiro, Brazil, <sup>5</sup>Laboratory of Immunodiagnostics, Department of Biological Sciences, National School of Public Health, Fiocruz, Rio de Janeiro, Brazil, <sup>6</sup>Laboratory of Leishmaniasis and Chagas Disease, National Institute of Amazonian Research, Manaus, Brazil, <sup>7</sup>Laboratory of Malaria Research, Oswaldo Cruz Institute, Fiocruz, Rio de Janeiro, Brazil

The cell-traversal protein for ookinete and sporozoite (CeTOS), a highly conserved antigen involved in sporozoite motility, plays an important role in the traversal of host cells during the preerythrocytic stage of *Plasmodium* species. Recently, it has been considered an alternative target when designing novel antimalarial vaccines against *Plasmodium falciparum*. However, the potential of *Plasmodium vivax* CeTOS as a vaccine target is yet to be explored. This study evaluated the naturally acquired immune response against a recombinant *P. vivax* CeTOS (PvCeTOS) (IgG and IgG subclass) in 528 individuals from Brazilian Amazon, as well as the screening of B-cell epitopes *in silico* and peptide assays to associate the breadth of antibody responses of those individuals with exposition and/or protection correlates. We show that PvCeTOS is naturally immunogenic in Amazon inhabitants with 94 individuals (17.8%) showing specific IgG antibodies against the recombinant protein. Among responders, the IgG reactivity indexes (RIs) presented a direct correlation with the number of previous malaria episodes ( $p = 0.003$ ;  $r = 0.315$ ) and inverse correlation with the time elapsed from the last malaria episode ( $p = 0.031$ ;  $r = -0.258$ ). Interestingly, high responders to PvCeTOS (RI > 2) presented higher number of previous malaria episodes, frequency of recent malaria episodes, and ratio of cytophilic/non-cytophilic antibodies than low responders (RI < 2) and non-responders (RI < 1). Moreover, a high prevalence of the cytophilic antibody IgG1 over all other IgG subclasses ( $p < 0.0001$ ) was observed. B-cell epitope mapping revealed five immunogenic regions in PvCeTOS, but no associations between the specific IgG response to peptides and

exposure/protection parameters were found. However, the epitope (*PvCeltos<sub>I136-E143</sub>*) was validated as a main linear B-cell epitope, as 92% of IgG responders to *PvCeltos* were also responders to this peptide sequence. This study describes for the first time the natural immunogenicity of *PvCeltos* in Amazon individuals and identifies immunogenic regions in a full-length protein. The IgG magnitude was mainly composed of cytophilic antibodies (IgG1) and associated with recent malaria episodes. The data presented in this paper add further evidence to consider *PvCeltos* as a vaccine candidate.

**Keywords:** *PvCeltos*, *P. vivax*, vaccines, epitope mapping, epitope prediction, malaria vaccines, malaria

## INTRODUCTION

Malaria remains a major public health problem worldwide. It is caused by protozoan parasites of the genus *Plasmodium*, being responsible for nearly 438,000 deaths and 150–300 million new infections in 2015 (1) and the reason of enormous socioeconomic impact in endemic settings (2). Among the *Plasmodium* species able to infect humans, *Plasmodium falciparum* and *Plasmodium vivax* are the most prevalent malaria parasites. *P. falciparum* is extremely prevalent in Africa and is responsible for the majority of cases and deaths worldwide, while *P. vivax* is the most prevalent species outside Africa (3). Despite the reduction in the number of malaria cases and deaths over the past decade (1), the emergence of drug resistance and the significant ongoing burden of morbidity and mortality emphasize the need for an effective malaria vaccine. Unfortunately, potential *P. vivax* vaccine candidates lag far behind those for *P. falciparum* (4). Currently, besides the RTS, S vaccine, there are 30 candidate vaccine formulations in clinical trials against *P. falciparum*, while there is only one against *P. vivax* (5). These data allied to the impact caused by the high *P. vivax* prevalence (2), the severity of the disease (6–11), and the emergence of strains resistant to chloroquine (12–14) and primaquine (15–17), reiterate the importance of identifying and exploring the potential of vaccine candidates against *P. vivax* as an essential step in the development of a safe and affordable vaccine.

Malaria liver-stage vaccines are one of the leading strategies and the only approach that has demonstrated complete, sterile protection in clinical trials. Therefore, vaccines targeting sporozoite and liver-stage parasites, when parasite numbers are low, can lead to the elimination of the parasite before it advances to the symptomatic stage of the disease (18). Corroborating this idea, the sterile protection against *P. falciparum* by immunization with radiation-attenuated sporozoites was demonstrated in several studies (19–21) and the protection lasted for at least 10 months and extended to heterologous strain parasites (22). Based on these findings, sporozoite surface antigens are one of the most promising vaccine targets against malaria, to protect and prevent the symptoms and block its transmission. To date, RTS,S, the subunit vaccine consisting of a portion of *P. falciparum* circumsporozoite protein (CSP), conferred partial protection in Phase III trials and fell short of community-established vaccine efficacy goals (23–26). Conversely, Gruner and collaborators have demonstrated that the sterile protection against sporozoites can be obtained in the absence of specific immune responses to

CSP (27). In addition, a recent study found 77 parasite proteins associated with sterile protection against irradiated sporozoites (28). Collectively, these data reinforce the concept that a multivalent anti-sporozoite vaccine targeting several surface-exposed antigens would induce a higher protection efficacy.

In this scenario, cell-traversing protein of *Plasmodium* ookinetes and sporozoites, a highly conserved protein among *Plasmodium* species, emerged as a novel target in the development of a vaccine against *Plasmodium* parasites (29). This secretory microneme protein is translocated to the sporozoites and ookinetes surface, being necessary for sporozoites and ookinetes to break through cellular barriers and establish infection in the new host, having a crucial role on cell-transversal ability in both stages (29, 30). The disruption of the genes encoding *Celtos* in *Plasmodium berghei* reduces the infectivity in the mosquito host and also the infectivity of the sporozoite in the liver, almost eliminating their ability to cell pass (29). Interestingly, *P. falciparum* *Celtos* (*PfCeltos*) was naturally recognized by acquired antibodies in exposed populations (31), able to induce cross-reactive immunity against *P. berghei* and inhibit sporozoite motility and invasion of hepatocytes *in vitro* (32). However, the knowledge about *P. vivax* *Celtos* (*PvCeltos*) has remained limited. Only recently, a study reported *PvCeltos* as naturally immunogenic in infected individuals from Western Thailand. Our group, investigating the genetic diversity of genes encoding *PvCeltos* in field isolates from five different regions of the Amazon forest, reveals a highly-conserved profile. Together, both findings support the potential of *PvCeltos* as an interesting target on *P. vivax* sporozoite surface, but further studies are still necessary to consolidate this protein as an alternative in future multitarget vaccines. Therefore, the present study aimed at evaluating the naturally acquired humoral immune response against *PvCeltos* in exposed populations from Brazilian Amazon, determining the antibody subclass profile, identifying its B-cell epitopes and verifying the existence of associations between the specific IgG and subclass response against *PvCeltos* and epidemiological data that can reflect the exposition and/or protection degree.

## PARTICIPANTS AND METHODS

### Study Area and Volunteers

A cross-sectional cohort study was conducted involving 528 individuals from Rio Preto da Eva (2°50'50"S/59°56'28"W), located north of the Amazon River and 80 km distant from Manaus, the capital of Amazon state. This city has an area of 6,000 km<sup>2</sup>

and a population of about 22,000 people, who live in rural areas inside the forests. Transmission of malaria in the Amazon occurs throughout the whole year, with seasonal fluctuations with maximum transmission occurring during the dry season from May to October and prevalence of infections by *P. vivax*, responsible for more than 85% of reported malaria cases.

Samples and survey data were collected from November 2013 to March 2015. In addition, we also included, as control subjects, 10 naive individuals living in Manaus, and with no reported previous malaria episodes. Written informed consent was obtained from all adult donors or from parents of donors in the case of children. The study was reviewed and approved by the Fundação Oswaldo Cruz Ethical Committee and the National Ethical Committee of Brazil.

## Epidemiological Survey

In order to evaluate the possible influence of epidemiological factors on humoral immunity against PvCeITOS, all donors were interviewed upon informed consent prior to blood collection. The survey included questions related to personal exposure to malaria, such as years of residence in the endemic area, recorded individual and family previous malaria episodes, use of malaria prophylaxis, presence/absence of symptoms, and personal knowledge of malaria transmission. All epidemiological data were stored in Epi-Info for subsequent analysis (Centers for Disease Control and Prevention, Atlanta, GA, USA).

## Malaria Diagnosis and Blood Sampling

Venous peripheral blood was drawn into heparinized tubes and plasma collected after centrifugation ( $350 \times g$ , 10 min). Plasma samples were stored at  $-20^{\circ}\text{C}$  and transported to our laboratory. Thin and thick blood smears of all donors were examined for malaria parasites. Parasitological evaluations were done by examination of 200 fields at  $1,000\times$  magnification under oil-immersion and a research expert in malaria diagnosis examined all slides. Donors positive for *P. vivax* and/or *P. falciparum* at the time of blood collection were subsequently treated using the chemotherapeutic regimen recommended by the Brazilian Ministry of Health.

## Recombinant PvCeITOS Expression in HEK-293T Cells

As previously described (33), the *P. vivax* sequence for CeITOS (Salvador I; Uniprot accession number Q53UB7) was cloned in the expression vector pHLSec, which is flanked by the chicken  $\beta$ -actin/rabbit  $\beta$ -globin hybrid promoter with a signal secretion sequence and a Lys-His6 tag. The protein was expressed upon transient transfection in HEK-293T cells with endotoxin-free plasmids in roller bottles ( $2,125 \text{ cm}^2$ ). The secreted protein was purified from the supernatant by immobilized Ni Sepharose affinity chromatography. The presence of proteins in the elution samples was confirmed using 6xHis epitope tag antibody [horseradish peroxidase (HRP) conjugate] in a Western blot. The sample was concentrated using an Amicon Ultra centrifugal filter system (Life Technologies) until reaching 10 ml of final volume. Contaminant proteins and salts were removed from the concentrate by size exclusion purification (SEC) using Superdex

medium in the column. Protein concentration after recovery was tested using a Bradford protein assay, and purity was assessed by silver staining and by Western blotting.

## Antibody Assays

Anti-PvCeITOS specific antibodies were evaluated on plasma samples from 528 exposed individuals from Brazilian Amazon and 10 healthy individuals, who had no reported malaria episodes, using enzyme-linked immunosorbent assay (ELISA), essentially as previously described (33, 34). Briefly, MaxiSorp 96-well plates (Nunc, Rochester, NY, USA) were coated with PBS containing  $1.5 \mu\text{g/ml}$  of recombinant protein. After overnight incubation at  $4^{\circ}\text{C}$ , the plates were washed and blocked for 1 h at  $37^{\circ}\text{C}$ . Individual plasma samples diluted 1:100 in PBS-Tween containing 5% non-fat dry milk (PBS-Tween-M) were added in duplicate wells. After 1 h at  $37^{\circ}\text{C}$  and three washings with PBS-Tween, bound antibodies were detected with peroxidase-conjugated goat antihuman IgG (Sigma, St. Louis) and followed by addition of *o*-phenylenediamine and hydrogen peroxide. Optical density was identified at 492 nm using a SpectraMax 250 ELISA reader (Molecular Devices, Sunnyvale, CA, USA). The results for total IgG were expressed as reactivity indexes (RIs), which were calculated by the mean optical density of an individual's tested sample divided by the mean optical density of 10 non-exposed control individuals' samples plus 3 standard deviations. Subjects were scored as responders to PvCeITOS if the RI of IgG against the recombinant protein was higher than 1. Additionally, the RIs of IgG subclasses were evaluated on responders individuals by a similar method, using peroxidase-conjugated goat antihuman IgG1, IgG2, IgG3, and IgG4 (Sigma, St. Louis).

## B Cell Epitope Prediction on PvCeITOS

The prediction of linear B-cell epitopes was carried out using the program BepiPred (35), which is based on hidden Markov model profiles of known antigens, and also incorporates hydrophilicity and secondary structure prediction. For each input FASTA sequence, the server outputs a prediction score for each amino acid. The recommended cutoff of 0.35 was used to determine potential B-cell linear epitopes, ensuring sensibility of 49% and specificity of 75% to this approach. Linear B-cell epitopes are predicted to be located at the residues with the highest scores. In this study, BepiPred was used to predict B-cell linear epitopes and to evaluate the prediction value of peptides containing short amino acid sequences of PvCeITOS.

The Emini surface accessibility (ESA) was used to evaluate the probability of predicted linear B-cell epitopes to be exposed on the surface of the protein. This approach calculates the surface accessibility of hexapeptides and values greater than 1.0 indicate an increased probability of being found on the surface (36). Sequences with BepiPred score above 0.35 and ESA score above 1.0 were considered potential linear B-cell epitopes in regions that could be accessed by naturally acquired antibodies.

## B-Cell Epitope Mapping of PvCeITOS

A peptide library of 32 PvCeITOS synthetic 15-mer peptides overlapping by nine amino acids (GenOne Biotechnologies; purity 95% based on HPLC) was synthesized. To evaluate the specific

response to each peptide, the peptide array was performed using MaxiSorp 96-well plates (Nunc, Rochester, NY, USA) coated with PBS containing 5 µg/ml of each peptide in duplicates. After overnight incubation at 4°C, the plates were washed with PBS and blocked with PBS-Tween containing 5% non-fat dry milk (PBS-Tween-M) for 1 h at 37°C. Individual plasma samples were diluted 1:100 with PBS-Tween-M and added in duplicate wells for each sequence and the plates incubated at room temperature for 1 h. After three washings with PBS-Tween, bound antibodies were detected with peroxidase-conjugated goat antihuman IgG (Sigma, St. Louis) followed by addition of *o*-phenylenediamine and hydrogen peroxide. The absorbance was read at 492 nm using an ELISA reader (Spectramax 250, Molecular Devices, Sunnyvale, CA, USA). The results for total IgG were expressed as RIs, which were calculated by the mean optical density of the tested samples plus 3 standard deviations of pools of control individuals. Subjects were scored as positive if the RI was higher than 1.

## Root Mean Square Fluctuation (RMSF) and Electrostatic Potential Surface Calculation

Molecular dynamics simulations were carried out using GROMACS 5.1.2 (37) software package. Gromos53a6 (38) force field was used. Simple point charge water model (39) was used to solvate the system. Charges were neutralized using Na<sup>+</sup> and Cl<sup>-</sup> ions. Steepest descent method was used for energy minimization. Further, 100 ps temperature equilibration was carried out at a temperature of 300 K in the presence of position restraints of 1,000 KJ/mol and the pressure coupling of 1,000 ps at 1 bar of atmospheric pressure. After equilibration, the simulation of 200,000 ps (200 ns) without position restraints was carried out. All simulations were run three times, and consistent results were recorded. RMSF was analyzed from simulation trajectory using GROMACS utilities. The Electrostatic potential surface for the PvCetTOS was calculated using APBS (40) and visualized in PyMOL (Pymol LLC) and the electrostatic potential surfaces for the contours from -3kT/e (red) to +3kT/e (blue) were visualized. The figures were rendered using PyMol.

## Statistical Analysis

All statistical analyzes were carried out using Prism 5.0 for Windows (GraphPad Software, Inc.). The one-sample Kolmogorov-Smirnov test was used to determine whether a variable was normally distributed. The Mann-Whitney test was used to compare RIs of IgG against recombinant PvCetTOS between studied groups. Differences in proportions of the RI of IgG subclasses and epidemiological parameters were evaluated by Fisher's exact test and associations between antibody responses and epidemiological data were determined by Spearman rank test. A two-sided *p* value <0.05 was considered significant.

## RESULTS

### Epidemiological Profile of Studied Individuals

Most studied individuals were adults and naturally exposed to malaria infection throughout the years (Table 1). Age ranged

**TABLE 1 | Summary of the epidemiological data of the studied population.**

	Overall	PvCetTOS IgG responders	PvCetTOS IgG non-responders (NRs)
<b>Gender—N (%)</b>			
Male	284 (53.8%)	55 (58.5%)	229 (52.8%)
Female	244 (46.2%)	39 (41.5%)	205 (47.2%)
Total	528	94	434
<b>Malaria exposure—median (IR)</b>			
Age (years)	36 (25–50)	38 (21–55.5)	36 (21–50)
Time of residence in endemic area (years)	33 (19–49)	35 (21–55)	33 (19–48)
Number of previous malaria episodes (n)	4 (2–10)	4.5 (2–10)	4 (2–10)
Time since the last malaria episode (months)	51 (24–91)	60 (13.7–89.2)	51 (24–90.5)
Frequency of recent malaria episodes (%)	12.7%	16.0%	13.1%
<b>Previous malaria species contracted—N (%)</b>			
Never infected	7 (1.3%)	0 (0%)	7 (1.6%)
<i>Plasmodium falciparum</i>	32 (6.1%)	5 (5.3%)	27 (6.2%)
<i>Plasmodium vivax</i>	125 (23.7%)	25 (26.6%)	100 (23%)
Both species	158 (29.9%)	31 (33%)	127 (29.3%)
Not reported/remember	206 (39%)	33 (35.1%)	173 (39.9%)

Values of age, time of residence in endemic areas, number of previous malaria episodes, and time elapsed from the last malaria episode represent the median (interquartile range), while the parameter "frequency of recent malaria episodes" represents the percentage of individuals who reported malaria episode in the last year. The frequency of individuals who present recent malaria episodes was compared by Fisher's test, and other epidemiological parameters were compared by Mann-Whitney test. No statistical difference was observed between epidemiological parameters of responders and NR individuals.

from 10 to 89 years with an average of 36.9. The proportion of men was significantly higher (53.8%) than for women (46.2%;  $\chi^2 = 5.761$ , *p* < 0.0164). Regarding the previous personal history of malaria, only seven individuals reported no malaria episode (1.3%). Among those who remembered the *Plasmodium* species, the majority (29.9%) reported infections by *P. falciparum* and *P. vivax*. The number of past malaria episodes also varied greatly among donors, ranging from 0 to 50 (mean = 7.74 ± 16.5). Finally, the time elapsed since the last malaria episode ranged from 0 to 480 months (mean = 71.7 ± 77.9). Interestingly, a correlation trend was observed between the time of residence in the endemic area and the number of previous malaria infections (*p* = 0.0003; *r* = 0.153). Collectively, the epidemiological inquiry indicated that the studied population had different degrees of exposure and/or immunity.

### PvCetTOS Is Naturally Immunogenic with the Prevalence of Cytophilic Antibodies in Brazilian Amazon Individuals

To test if the PvCetTOS is a target for naturally acquired antibodies in Amazon individuals, we first assessed the IgG reactivity profile against the recombinant protein. The plasma samples collected from the 528 individuals living in the endemic area reveal a low frequency of responders to PvCetTOS, since only 17.8% of the studied population (94 individuals) presented

specific IgG antibodies against the protein. Interestingly, the epidemiological data were similar between responders and NRs against this protein (**Table 1**). On both groups, responders and NRs, the age, time of residence in endemic area, the number of previous malaria episodes, the number of recent malaria episodes, the frequency of individuals with recent malaria episodes, and months elapsed from the last malaria episode were similar ( $p > 0.05$ ).

Among the group of responders to PvCelTOS, the RI ranged from 1.01 to 19.93 (median = 1.205; interquartile range = 1.082; 1.552), reflecting a wide spectrum in magnitude of naturally acquired IgG response. The IgG subclass profile was marked by IgG1, the most prevalent subclass, present in 65.96% of responders, and with major RI (median = 1.15; interquartile range = 0.86–1.68) compared to IgG2 (median = 0.9; interquartile range = 0.66–1.2), IgG3 (median = 0.88; interquartile range = 0.72–1.06), and IgG4 (median = 0.62; interquartile range = 0.51–0.76) (**Figure 1**). Moreover, IgG3 RIs were directly correlated to the number of recent malaria episodes ( $p = 0.003$ ;  $r = 0.315$ ; Figure S1A in Supplementary Material) and inversely associated with the time elapsed from the last malaria episode ( $p = 0.031$ ;  $r = -0.258$ ; Figure S1B in Supplementary Material).

## High IgG RIs against PvCelTOS Are Driven by Cytophilic Antibodies and Associated with Recent Infections

In order to identify possible factors that could be associated with this large spectrum of reactivity against PvCelTOS in IgG-positive

individuals, we explored epidemiological data among responders. Initially, we observed that the RI against PvCelTOS was directly correlated with the number of previous malaria episodes ( $p = 0.047$ ;  $r = 0.227$ ; Figure S1C in Supplementary Material) and inversely correlated with the time elapsed from the last malaria episode ( $p = 0.045$ ;  $r = -0.24$ ; Figure S1D in Supplementary Material). Based on these findings, responder individuals were divided into two subgroups: high responders (HRs; individuals who had RI of IgG against PvCelTOS higher than 2) and low responders (LRs; individuals who had RI of IgG against PvCelTOS between 1 and 2). **Figure 2A** illustrates the means of epidemiological parameters of HRs, LRs, and NRs to PvCelTOS. Interestingly, while NRs and LRs presented a very similar profile of epidemiological parameters, HRs presented a statistically higher number of previous malaria episodes in comparison to NR and LR ( $p = 0.0058$ ;  $p = 0.0051$ , respectively). Moreover, despite no statistical differences could be observed on the time elapsed from the last malaria episode ( $p = 0.15$  in ANOVA test), the frequency of individuals who reported recent episodes of malaria was higher in HR (41.6%) than LR (12%,  $p = 0.02$ ) and NR (13.1%,  $p = 0.016$ ). Moreover, the proportion of RIs of cytophilic over non-cytophilic antibodies (IgG1 + IgG3/IgG2 + IgG4) presented direct correlation with RI of IgG of responder individuals ( $p = 0.0016$ ;  $r = 0.32$ ), suggesting that higher RI could be associated with a cytophilic profile of humoral response against PvCelTOS. Interestingly, although the proportion of individuals with cytophilic profile was similar in both groups, HR and LR (83% and 78%, respectively), the ratio of (cytophilic/non-cytophilic) antibodies was significantly higher in HR than LR ( $p = 0.0076$ ) (**Figure 2B**).

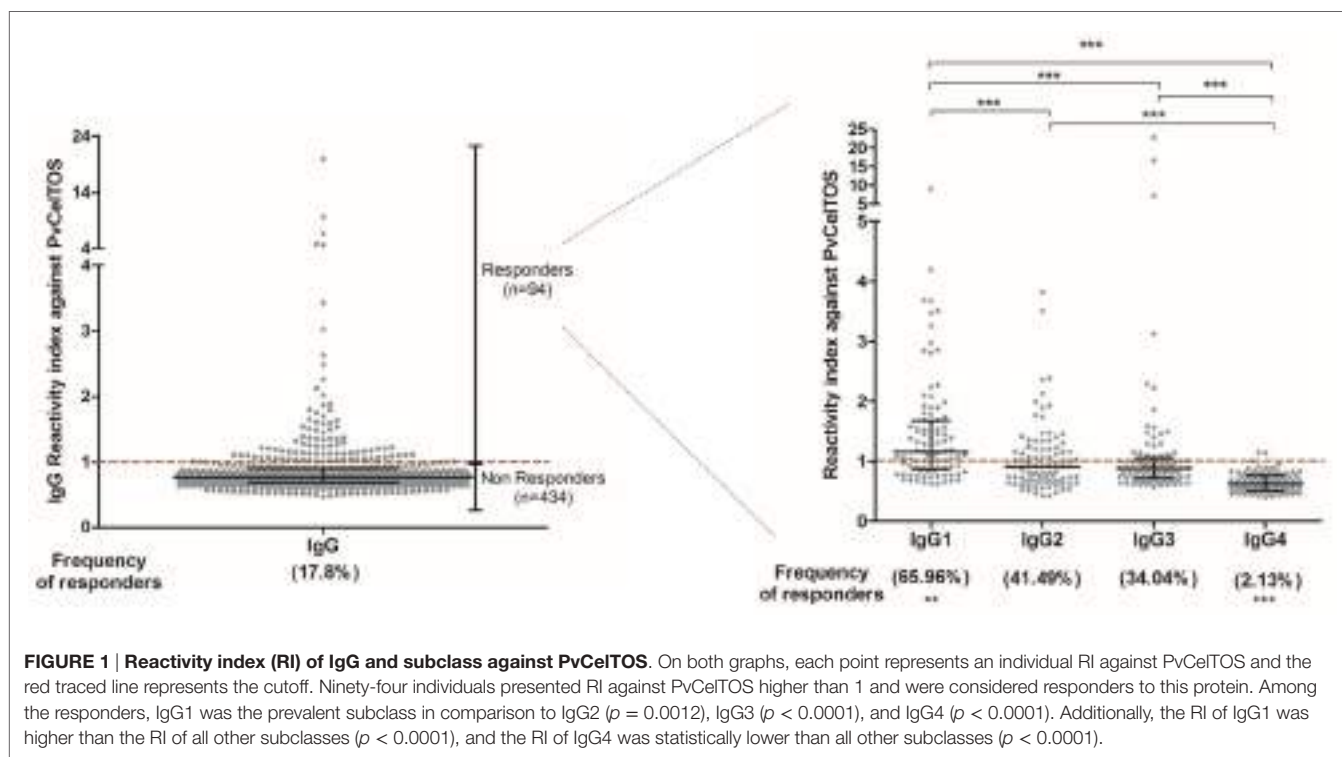
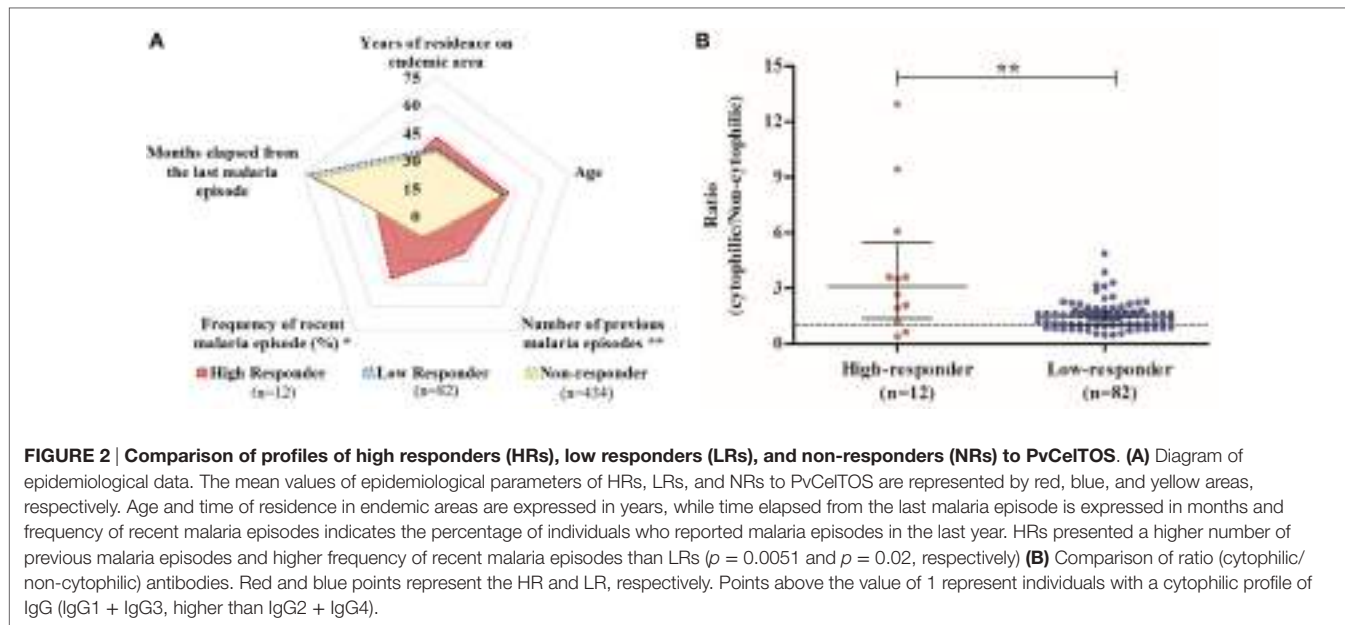


**FIGURE 1 | Reactivity index (RI) of IgG and subclass against PvCelTOS.** On both graphs, each point represents an individual RI against PvCelTOS and the red traced line represents the cutoff. Ninety-four individuals presented RI against PvCelTOS higher than 1 and were considered responders to this protein. Among the responders, IgG1 was the prevalent subclass in comparison to IgG2 ( $p = 0.0012$ ), IgG3 ( $p < 0.0001$ ), and IgG4 ( $p < 0.0001$ ). Additionally, the RI of IgG1 was higher than the RI of all other subclasses ( $p < 0.0001$ ), and the RI of IgG4 was statistically lower than all other subclasses ( $p < 0.0001$ ).



## Five Immunogenic Regions Identified in PvCelTOS and Two Linear B-Cell Epitopes Broadly Recognized by Naturally Acquired IgG Antibodies

Four B-cell linear epitopes were predicted *in silico* in the entire sequence of PvCelTOS (PvCelTOS<sub>K6-N13</sub>; PvCelTOS<sub>G38-R57</sub>; PvCelTOS<sub>I136-E143</sub>; PvCelTOS<sub>K166-S191</sub>).

In order to validate the prediction data and identify possible non-predicted immunogenic regions of PvCelTOS, plasma from IgG responders to PvCelTOS was tested against 32 overlapping peptides corresponding to the complete amino acid sequence. First, 10 peptides (N13-L27; S19-V33; E73-I87; L79-K93; S97-A111; P127-V141; I133-G147; P139-V153; L181-L195; E182-D196) were broadly recognized by responders to PvCelTOS (Figure 3). Two of the predicted epitopes (PvCelTOS<sub>I136-E143</sub> and PvCelTOS<sub>K166-S191</sub>) were present (partially or entirely) in peptides confirmed as naturally immunogenic. Interestingly, peptides I133-G147 and E182-D196 were recognized by IgG specific antibodies of responders to PvCelTOS in frequencies higher than 50% (92% and 54%, respectively) and presented median of RI higher than 1 (1.79 and 1.14, respectively). In addition, peptides P127-V141, P139-V153, and L181-L195 were located besides the most immunogenic peptides and presented overlapped sequences, which were also recognized by IgG antibodies in moderate frequencies. Peptide I133-G147 (ASTIKPPRVSEDAYF) presented the highest IgG RI ( $p < 0.0001$  by ANOVA test) and the highest frequency of recognition (92%) compared to all other peptides. While it contains the entire sequence of predicted epitope PvCelTOS<sub>I136-I43</sub>, peptides P127-V141 and P139-V153, which contain only the partial sequence of the predicted epitope, presented minor frequencies of recognition (38% and 39%, respectively;  $p < 0.0001$  on Fisher's exact test). The peptides L181-L195 and 186-196 were both

partially inserted in the predicted linear epitope PvCelTOS<sub>I66-I91</sub> and could be the immune dominant sequence of this longer predicted epitope. These data supported the prediction of linear B-cell epitopes PvCelTOS<sub>I136-E146</sub> and PvCelTOS<sub>K166-S191</sub>. Conversely, peptides N13-L27, S19-V33, and S97-A111 also presented frequency of recognition about 40% (38, 40, and 36%, respectively). After the confirmation of five immunogenic regions and two immunodominant epitopes in PvCelTOS, we also compared the RI and frequencies between HR and LR for PvCelTOS. However, no differences were found.

## Main B Cell Epitopes Are Present on PvCelTOS Surface

Peptides that presented overlapped amino acids and were recognized by more than 20% of responders to PvCelTOS (Figure 3) were grouped as immunogenic regions. All peptides inserted in identified immunogenic regions are listed in Table 2 with their respective frequencies of recognition, BepiPred and ESA scores. In this context, we identified five immunogenic regions PvCelTOS<sub>N13-V33</sub>, PvCelTOS<sub>E73-K93</sub>, PvCelTOS<sub>S97-A111</sub>, PvCelTOS<sub>P127-V153</sub>, and PvCelTOS<sub>L181-D196</sub>, in which B-cell epitopes could be inserted. Interestingly, the peptides with higher frequency of specific responders (I133-G147, L181-L195, and 182-186) presented a good combination of BepiPred and ESA score. The molecular dynamics and electrostatic potential surface of PvCelTOS indicate regions P127-V153, N13-V33, and L181-D186 as more flexible than E73-K93 and S97-A111 (Figure 4A). Regarding solvent exposure, all immunogenic regions were exposed and accessible in solution. Interestingly, the immunogenic regions L181-D196 and E73-K93 are part of a very negatively charged region, while N13-V33 and P127-V153 are in a mostly neutral-positive region (Figure 4B).

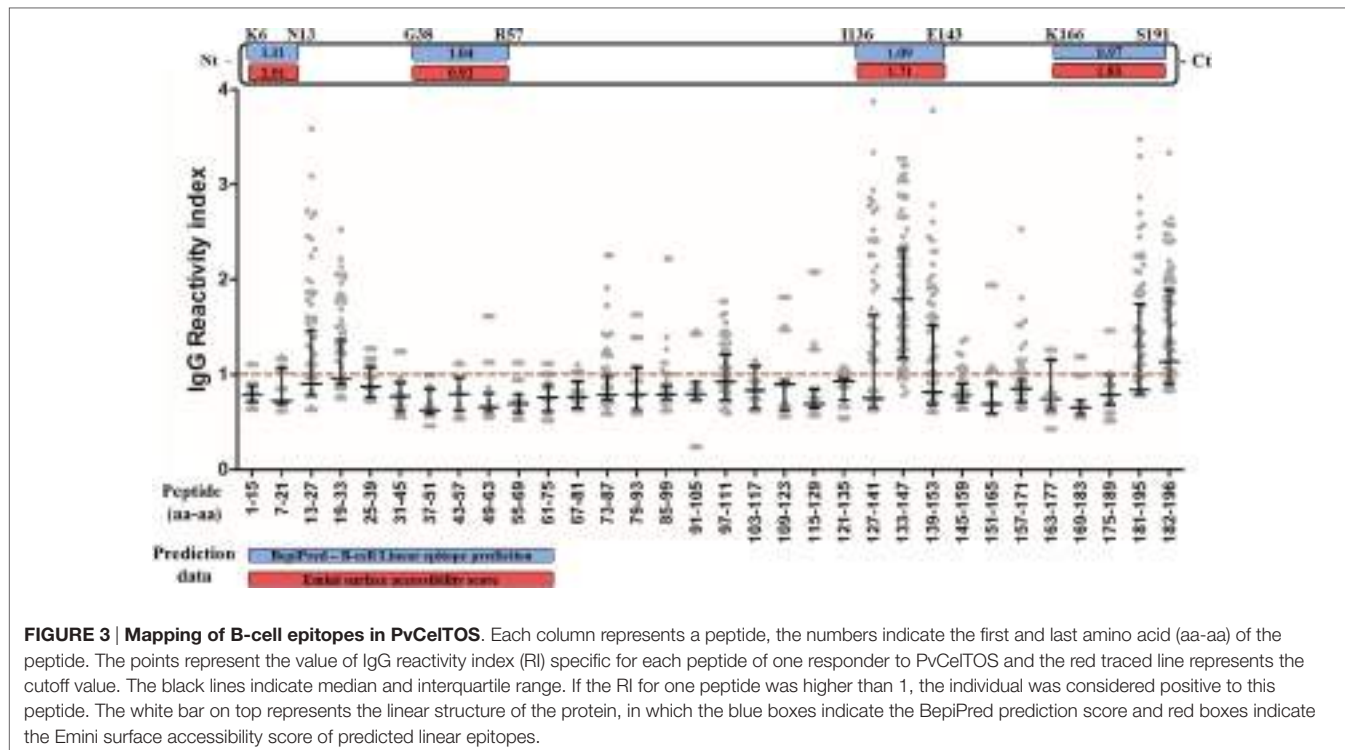


**FIGURE 3 | Mapping of B-cell epitopes in PvCelTOS.** Each column represents a peptide, the numbers indicate the first and last amino acid (aa-aa) of the peptide. The points represent the value of IgG reactivity index (RI) specific for each peptide of one responder to PvCelTOS and the red traced line represents the cutoff value. The black lines indicate median and interquartile range. If the RI for one peptide was higher than 1, the individual was considered positive to this peptide. The white bar on top represents the linear structure of the protein, in which the blue boxes indicate the BepiPred prediction score and red boxes indicate the Emini surface accessibility score of predicted linear epitopes.

## DISCUSSION

Despite significant advances in the understanding of the biology of *Plasmodium* parasites and the immune response elicited by these pathogens, there is not yet a subunit vaccine capable of providing long-lasting protection. The cell-traversing protein for ookinete and sporozoite (CelTOS) has been considered a potential novel alternative for a vaccine against malaria (29, 32, 41), but the knowledge on *P. vivax* CelTOS potential remains scarce. Unfortunately, many conventional vaccinology strategies applied to *P. falciparum* are especially difficult when dealing with non-cultivable microorganisms such as *P. vivax*. Consequently, seroepidemiological studies have played a significant role in the identification and validation of *P. vivax* vaccine candidates (42–48). Therefore, we confirmed the naturally acquired humoral response against PvCelTOS (IgG and IgG subclass) and identified five B-cell epitopes along the entire PvCelTOS amino acid sequence, which were recognized by IgG antibodies from malaria-exposed populations from Brazilian Amazon.

Plasma samples were collected in three cross-sectional studies with Brazilian Amazon communities between 2013 and 2015. The profile of the studied individuals shows that our population included rainforest region natives and migrants from non-endemic areas of Brazil who had lived in the area for more than 10 years. The majority of individuals reported a prior experience with *P. vivax* and/or *P. falciparum* malaria. Concerning malaria history, the highly variable range of number of previous infections, time of residence in endemic areas, and time since the last infection suggests differences in exposure and immunity, since it is well known that the acquisition of clinical immunity mediated by antibodies depends on continued exposure to the parasite

(49–51). The correlation between time of residence in endemic areas and months since the last infection observed in our study also indicates that this phenomenon could be occurring in low/medium endemic areas like the Brazilian Amazon. Therefore, the selection of these individuals was ideal to detect the presence of antibodies against the new recombinant antigen and distinguish whether the alterations found were related to malaria exposure and/or indicatives of protection.

First, we found 94 individuals presenting specific antibodies to PvCelTOS and confirmed the natural immunogenicity of PvCelTOS among exposed individuals from Brazilian Amazon. Recently, Longley and collaborators also reported the first evidence of naturally induced IgG responses to PvCelTOS in human volunteers from Western Thailand (33). Interestingly, the frequency of responders to PvCelTOS observed in our studied population (17.8%) was similar to the frequency observed by Longley on uninfected and clinical malaria individuals (33). Moreover, the low humoral reactivity against PvCelTOS is commonly found in other *Plasmodium* preerythrocytic antigens (48, 52, 53). The short life of specific antibodies, host genetic factors, and/or epidemiological parameters could be possible reasons for the low frequency of responders against PvCelTOS in endemic areas. The short life of specific PvCelTOS humoral response hypothesis does not seem to occur since Longley et al. verified that IgG positivity and magnitude of response were present over the 1-year period in the absence of *P. vivax* infections (33). Our study also describes anti-PvCelTOS antibodies in individuals who reported no malaria in the last 10 years or more. However, in both cases, the contact between human host and sporozoite antigens in transmission areas was not evaluated. In relation to host genetic factors, there is a significant body of

**TABLE 2 | Identification of immunogenic regions in PvCelTOS.**

Immunogenic region	Sequence	Reactivity index (RI) Mean (CI 95%)	Responders (%)	Position	Peptide sequence	Specific responders (%)	BepiPred score	ESA score
PvCelTOS <sub>113-V33</sub>	NKVNPRV <b>SIICAFELAL</b> FCFVN	1.17 (1.07–1.27)	45%	13–27	NKVNPRV <b>SIICAFELAL</b>	38%	-1.52	0.35
PvCelTOS <sub>573-K33</sub>	EVIGNELADNIA <b>NEIVSSLQK</b>	0.93 (0.88–0.99)	30%	19–33	<b>SIICAFELAL</b> FCFVN	40%	-2.37	0.07
PvCelTOS <sub>397-A111</sub>	SFLQS <b>GFDYKTQLKA</b>	0.95 (0.89–1.01)	36%	73–87	EVIGNELADNIA <b>NEIVSSLQK</b>	22%	0.01	0.70
PvCelTOS <sub>5127-W153</sub>	PTEKIVASTIKPPRV <b>SEDAYFLLGPVV</b>	1.39 (1.27–1.50)	69%	97–111	LADNIA <b>NEIVSSLQK</b> TQLKA	20%	0.14	0.56
PvCelTOS <sub>1191-D196</sub>	<u>LEEEEADEFSD<b>ELLDD</b></u>	1.32 (1.21–1.44)	53%	127–141	SFLQS <b>GFDYKTQLKA</b>	36%	0.12	0.91
				139–153	PTEKIVASTIKPPRV	38%	0.69	0.89
				181–195	IKPPRV <b>SEDAYFLLGPVV</b>	92%	0.52	1.14
				182–196	PRV <b>SEDAYFLLGPVV</b>	39%	-0.08	0.75
					LEEEEADEFSD <b>ELLDD</b>	43%	0.95	2.15
					EEEEADEFSD <b>ELLDD</b>	54%	0.84	2.08

Peptides with overlapping and recognized by more than 20% of responders to PvCelTOS were grouped in immunogenic regions. The RI of an immunogenic region represents the mean of RI of all peptides inserted in that immunogenic region with a confident interval of 95%. The frequency of recognition of immunogenic regions was defined based on the number of individuals with RI to immunogenic region higher than 1. The peptides combined in an immunogenic region were listed with their respective frequencies of recognition, BepiPred score, and Emni surface accessibility (ESA) score. Overlapped mers were signified by underlined bold typeface on immunogenic region sequence.

evidences of its influence in malaria outcomes and the capacity to mount a humoral immune response (54–57). To date, associations of HLA class II on humoral immune response to malaria antigens were reported in individuals living in malaria-endemic areas from Brazilian Amazon (58, 59) and in human vaccine trials (60–62). In *P. vivax* preerythrocytic targets, the presence of HLA-DRB1\*03 and DR5 was associated with the absence of antibody response to the CSP amino-terminal region (48) and HLA-DRB1\*07 was related to the absence of specific antibodies for CSP repeats of VK210 (52). Moreover, Chaves and collaborators reported that PvCelTOS gene sequence is highly conserved among isolates from different Brazilian geographic regions (unpublished data), suggesting a low selective pressure by immune response against PvCelTOS. In our view, the influence of immunogenetic factors in PvCelTOS-specific humoral response are feasible, but more studies are still necessary to confirm this hypothesis.

Regarding the influence of epidemiological factors, we initially tried to investigate the associations between exposition to malaria and the frequency of IgG responders to PvCelTOS. Surprisingly, although the association of epidemiological data with specific response against *Plasmodium* antigens was well characterized on several studies (63–65), we observed a similar epidemiological profile between responders and NRs to PvCelTOS. Therefore, we focused on the search of distinct epidemiological and IgG subclass profiles among PvCelTOS responder individuals. The knowledge about the antibody subclass profile is critical to suggest functional antimalarial immunity and to evaluate potential vaccine candidates. Cytophilic antibodies (IgG1 and IgG3) are frequently prevalent on immune serum from high-transmission areas (66–69) and often correlate with protection from disease (70–72). In our study, IgG1 presented higher frequencies of responders and median RI than all other subclasses. Moreover, IgG3 RIs were directly associated with the number of malaria episodes over the last 12 months and inversely correlated with the time elapsed from the last malaria episode, suggesting that recent *P. vivax* infections can raise the levels of anti-PvCelTOS specific IgG3. The sterile protective immunity to malaria was recently associated with a panel of antigens (28), and the relationship of cytophilic antibodies and reduced risk of symptoms are a common finding in high endemic areas (70–74). However, in our study, concerning the higher levels of IgG1 for PvCelTOS and the association of IgG3 levels with recent infections, we cannot confirm or discard its role as part of protective humoral response until more conclusive studies, such as sporozoite inhibition by anti-PvCelTOS specific antibodies, are conducted. In the same way, among responders, IgG RIs were directly correlated with the number of previous malaria episodes and inversely correlated with the time elapsed from the last malaria episodes, suggesting that antibody levels for PvCelTOS could be associated with recent infections.

The influence of epidemiological parameters on immunity to malaria was previously observed in studies from Brazilian Amazon population. Based on previous studies that associated high levels of antibodies with multiple preerythrocytic antigens with reduced risk of clinical malaria in children (75) and decreased risk of infection in adults (68), we also aimed to investigate if

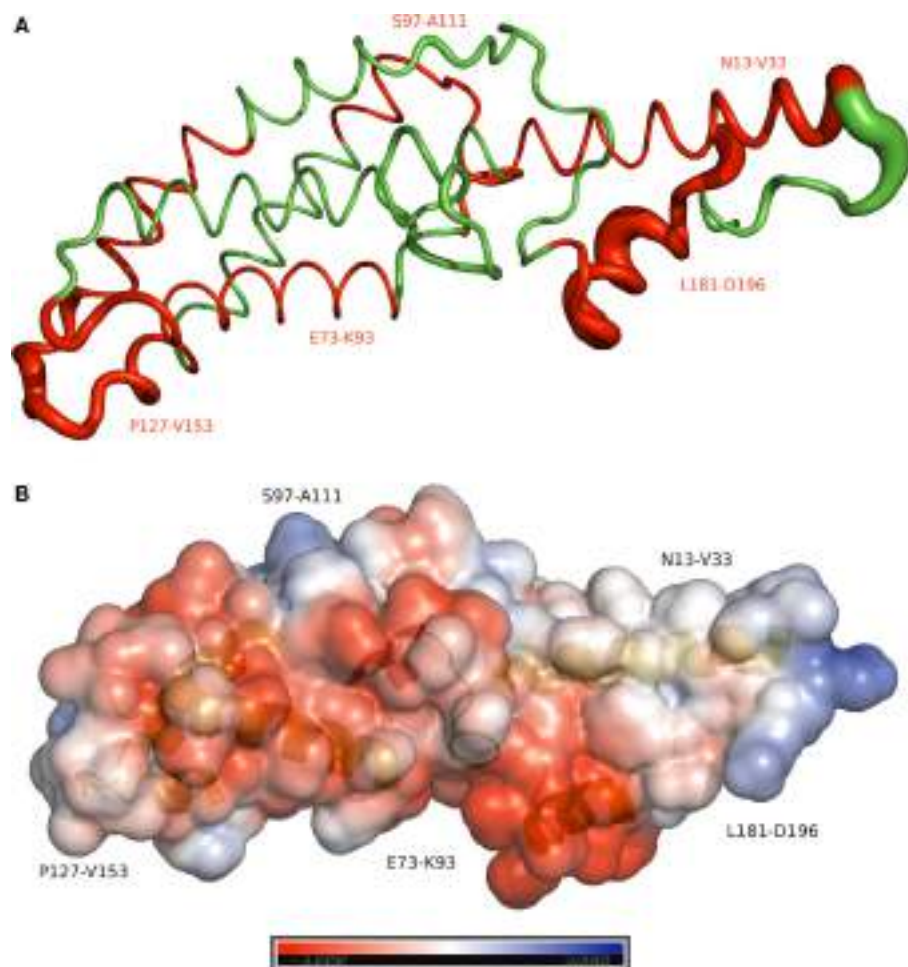


**FIGURE 4 | Molecular dynamics and electrostatic potential surface for the PvCelTOS.** **(A)** Sausage plot of the PvCelTOS. The red color identifies the immunogenic regions of PvCelTOS. Thickness depicts relative fluctuation as calculated during molecular dynamics. The thinnest segments represent the most stable regions of the protein. **(B)** The surface model shows the electrostatic potential surface of the PvCelTOS, representing the positive (blue) and negative (red) charges. The secondary structure in the background represents the immunogenic region.

the epidemiological parameters could reveal new findings about the role of exposition on PvCelTOS immunogenicity. Therefore, we subdivided the large spectrum IgG RIs among PvCelTOS responders into HRs ( $RI > 2$ ) and LRIs ( $RI < 2$ ). Although LRIs and NRs to PvCelTOS presented similar exposition factors to malaria, interestingly, HR individuals presented a remarkable higher number of previous malaria episodes, frequency of recent malaria episodes, and a higher ratio of cytophilic/non-cytophilic antibodies than LRIs. This observation suggested that higher level of exposition to malaria induced a more intense and improved humoral response against PvCelTOS. Unfortunately, the cross-sectional design of our study limited the investigation to retrospective malaria histories, and the best approximation of an individual's protection was the estimated amount of time that had passed since their last malaria episode, which presented no significant association with IgG response against PvCelTOS. Prospective studies on humoral immune responses and studies addressing the ability of these antibodies to interfere the motility/

invasion of sporozoites (76, 77) will provide more evidences of the protective role of anti-PvCelTOS antibodies.

Information at the amino acid level about the epitopes of proteins recognized by antibodies is important for their use as biological tools and for understanding general molecular recognition events (78). In this context, epitope prediction programs have been widely used in malaria research (4, 79–81). Nevertheless, the use of chemically prepared arrays of short peptides is a more powerful tool to identify and characterize epitopes recognized by antibodies (46, 82, 83). It is also important to mention that in order to raise antibodies for a peptide, a minimum length of six amino acids is required, and peptides of  $>10$  amino acids are generally required for the induction of antibodies that may bind to the native protein (84). In this context, the synthesis of 15 amino acid peptides, with 9 overlapping, has allowed the identification of PvCelTOS B-cell epitopes encompassed in sequences ranging from 15 to 27 amino acids in length. Therefore, after the confirmation of PvCelTOS as naturally immunogenic in exposed populations, the present

paper describes for the first time the fine B cell epitope mapping of a full-length protein. Initially, 10 peptides were specifically recognized by naturally acquired antibodies from PvCelTOS responders. After a combination of *in silico* approaches and recognition of overlapped peptides, five immunogenic regions were confirmed (PvCelTOS<sub>13-33</sub>, PvCelTOS<sub>73-93</sub>, PvCelTOS<sub>97-111</sub>, PvCelTOS<sub>127-153</sub>, and PvCelTOS<sub>181-196</sub>) in different frequencies and RIs. Moreover, the main linear epitope (ASTIKPPRVSEDAYF) presented highest IgG RI and frequency compared to all other naturally recognized peptides, suggesting that the majority of naturally acquired antibodies against PvCelTOS are directed to the C-terminal region. Moreover, T cell responses to PvCelTOS may also help to determine the immunodominant repertoire in individuals living in malaria-endemic regions, which could also supply information for the development of a vaccine for PvCelTOS. In humans, PfCelTOS derivative peptides elicited proliferative and IFN- $\gamma$  responses in *ex vivo* ELISPOT assays using peripheral blood mononuclear cells from naturally exposed individuals living in Ghana (30).

Recently, CelTOS was demonstrated as highly conserved protein across several large groups of apicomplexan parasites including *Plasmodium* spp., *Cytauxzoon*, *Theileria*, and *Babesia* and considered essential to cell infection, traversal, and membrane disruption (85). Despite the genetical differences between PfCelTOS and PvCelTOS, it is important to mention that Bergmann-Leitner and colleagues immunized mice and rabbits with recombinant PfCelTOS and also observed specific antibodies for linear B-cell epitopes at C-terminal (82). These observations suggested that CelTOS could present a similar conformation among species, with similar regions targeted by antibodies. We considered that the exposition of linear epitopes is a critical step to their recognition by circulating antibodies; therefore, the combination of ESA, molecular dynamics, and electrostatic potential surface was used as a complementary approach to predict the exposition of epitope sequences on protein surface. All immunogenic regions identified were exposed and accessible to antibodies. This finding could be important in a future subunit vaccine composition based on these identified regions. However, the potential of these specific antibodies directed main PvCelTOS epitopes in the inhibition of sporozoite motility, invasion, and/or traversal remains to be investigated.

## REFERENCES

- W.H.O. *World Malaria Report*. Geneva: WHO (2015).
- Richie TL, Saul A. Progress and challenges for malaria vaccines. *Nature* (2002) 415(6872):694–701. doi:10.1038/415694a
- W.H.O. *World Malaria Report 2014*. Geneva: WHO (2014).
- Rodrigues-da-Silva RN, Martins da Silva JH, Singh B, Jiang J, Meyer EV, Santos F, et al. In silico identification and validation of a linear and naturally immunogenic B-cell epitope of the *Plasmodium vivax* malaria vaccine candidate merozoite surface protein-9. *PLoS One* (2016) 11(1):e0146951. doi:10.1371/journal.pone.0146951
- WHO. *Tables of Malaria Vaccine Projects Globally ("Rainbow Tables")*. (2015). Available from: [http://www.who.int/immunization/research/development/Rainbow\\_tables/en/](http://www.who.int/immunization/research/development/Rainbow_tables/en/)

## AUTHOR CONTRIBUTIONS

JL-J did study designing, performed experiments, data analysis, manuscript preparation, and manuscript review. RR-d-S did study designing, performed experiments, data analysis, and manuscript preparation. IS performed experiments. CL-C did recombinant protein expression and manuscript review. JM did molecular dynamics and bioinformatics and manuscript review. DP-d-S performed collection of blood and epidemiological data. AF did fieldwork support. AT performed collection of blood and epidemiological data and diagnosis. FP did fieldwork support. LC performed experiments. LP-R did data analysis and manuscript review. AR-S did recombinant protein expression, data analysis, and manuscript review. DB did study designing, fieldwork support, manuscript review, and data analysis.

## ACKNOWLEDGMENTS

We are grateful to all volunteers who made this study possible.

## FUNDING

This study was supported by the Brazilian National Research Council – CNPq/PAPES. JL-J is recipient of FAPERJ APQ1 (E-26/210.653/2015), Jovem Cientista do Nosso Estado (E26/203.255/2016), and CNPq-Universal research grants (445150/2014-9). AR-S is supported by a Wellcome Trust Career Development Fellowship 097395/Z/11/Z.

## SUPPLEMENTARY MATERIAL

The Supplementary Material for this article can be found online at <http://journal.frontiersin.org/article/10.3389/fimmu.2017.00077/full#supplementary-material>.

**FIGURE S1 | Associations of humoral response and exposition parameters in responders to PvCelTOS.** (A) Spearman correlation between IgG3 reactivity index (RI) and number of recent malaria episodes; (B) Spearman correlation between IgG3 and months elapsed since the last malaria episode; (C) Spearman correlation between anti-PvCelTOS IgG reactivity index and number of previous malaria episodes; and (D) Spearman correlation between anti-PvCelTOS IgG RI and months elapsed since the last malaria episode.

- Tan LK, Yacoub S, Scott S, Bhagani S, Jacobs M. Acute lung injury and other serious complications of *Plasmodium vivax* malaria. *Lancet Infect Dis* (2008) 8(7):449–54. doi:10.1016/S1473-3099(08)70153-1
- Price RN, Tjitra E, Guerra CA, Yeung S, White NJ, Anstey NM. Vivax malaria: neglected and not benign. *Am J Trop Med Hyg* (2007) 77(6 Suppl):79–87.
- Rahimi BA, Thakkinstian A, White NJ, Sirivichayakul C, Dondorp AM, Chokejindachai W. Severe vivax malaria: a systematic review and meta-analysis of clinical studies since 1900. *Malar J* (2014) 13:481. doi:10.1186/1475-2875-13-481
- O'Brien AT, Ramirez JF, Martinez SP. A descriptive study of 16 severe *Plasmodium vivax* cases from three municipalities of Colombia between 2009 and 2013. *Malar J* (2014) 13:404. doi:10.1186/1475-2875-13-404
- Gouglas A, Karageorgopoulos DE, Dimitriadou A, Melas N, Kranidiotis G, Voutsinas D, et al. Severe *Plasmodium vivax* malaria complicated with acute

- respiratory distress syndrome: a case associated with focal autochthonous transmission in Greece. *Vector Borne Zoonotic Dis* (2014) 14(5):378–81. doi:10.1089/vbz.2012.1192
11. Zubairi AB, Nizami S, Raza A, Mehraj V, Rasheed AF, Ghanchi NK, et al. Severe *Plasmodium vivax* malaria in Pakistan. *Emerg Infect Dis* (2013) 19(11):1851–4. doi:10.3201/eid1911.130495
  12. Price RN, von Seidlein L, Valecha N, Nosten F, Baird JK, White NJ. Global extent of chloroquine-resistant *Plasmodium vivax*: a systematic review and meta-analysis. *Lancet Infect Dis* (2014) 14(10):982–91. doi:10.1016/S1473-3099(14)70855-2
  13. de Santana Filho FS, Arcanjo AR, Chehuan YM, Costa MR, Martinez-Espinosa FE, Vieira JL, et al. Chloroquine-resistant *Plasmodium vivax*, Brazilian Amazon. *Emerg Infect Dis* (2007) 13(7):1125–6. doi:10.3201/eid1307.061386
  14. Ruebush TK II, Zegarra J, Cairo J, Andersen EM, Green M, Pillai DR, et al. Chloroquine-resistant *Plasmodium vivax* malaria in Peru. *Am J Trop Med Hyg* (2003) 69(5):548–52.
  15. Nayar JK, Baker RH, Knight JW, Sullivan JS, Morris CL, Richardson BB, et al. Studies on a primaquine-tolerant strain of *Plasmodium vivax* from Brazil in Aotus and Saimiri monkeys. *J Parasitol* (1997) 83(4):739–45. doi:10.2307/3284254
  16. Kristensen KL, Dragsted UB. Recurrent *Plasmodium vivax* malaria due to dose-dependent primaquine resistance: a case report. *Scand J Infect Dis* (2014) 46(1):63–5. doi:10.3109/00365548.2013.822093
  17. Arias AE, Corredor A. Low response of Colombian strains of *Plasmodium vivax* to classical antimalarial therapy. *Trop Med Parasitol* (1989) 40(1):21–3.
  18. Swearingen KE, Lindner SE, Shi L, Shears MJ, Harupa A, Hopp CS, et al. Interrogating the Plasmodium Sporozoite Surface: Identification of Surface-Exposed Proteins and Demonstration of Glycosylation on CSP and TRAP by Mass Spectrometry-Based Proteomics. *PLoS Pathog* (2016) 12(4):e1005606. doi:10.1371/journal.ppat.1005606
  19. Clyde DF, McCarthy VC, Miller RM, Hornick RB. Specificity of protection of man immunized against sporozoite-induced falciparum malaria. *Am J Med Sci* (1973) 266(6):398–403. doi:10.1097/00000441-197309000-00002
  20. Rieckmann KH, Carson PE, Beaudoin RL, Cassells JS, Sell KW. Letter: sporozoite induced immunity in man against an Ethiopian strain of *Plasmodium falciparum*. *Trans R Soc Trop Med Hyg* (1974) 68(3):258–9. doi:10.1016/0035-9203(74)90129-1
  21. Egan JE, Hoffman SL, Haynes JD, Sadoff JC, Schneider I, Grau GE, et al. Humoral immune responses in volunteers immunized with irradiated *Plasmodium falciparum* sporozoites. *Am J Trop Med Hyg* (1993) 49(2):166–73.
  22. Hoffman SL, Goh LM, Luke TC, Schneider I, Le TP, Doolan DL, et al. Protection of humans against malaria by immunization with radiation-attenuated *Plasmodium falciparum* sporozoites. *J Infect Dis* (2002) 185(8):1155–64. doi:10.1086/339409
  23. Olotu A, Fegan G, Wambua J, Nyangweso G, Awuondo KO, Leach A, et al. Four-year efficacy of RTS,S/AS01E and its interaction with malaria exposure. *N Engl J Med* (2013) 368(12):1111–20. doi:10.1056/NEJMoa1207564
  24. Rts SCTP, Agnandji ST, Lell B, Fernandes JF, Abossolo BP, Methogo BG, et al. A phase 3 trial of RTS,S/AS01 malaria vaccine in African infants. *N Engl J Med* (2012) 367(24):2284–95. doi:10.1056/NEJMoa1208394
  25. Bejon P, Cook J, Bergmann-Leitner E, Olotu A, Lusingu J, Mwacharo J, et al. Effect of the pre-erythrocytic candidate malaria vaccine RTS,S/AS01E on blood stage immunity in young children. *J Infect Dis* (2011) 204(1):9–18. doi:10.1093/infdis/jir222
  26. Olotu A, Lusingu J, Leach A, Lievens M, Vekemans J, Msham S, et al. Efficacy of RTS,S/AS01E malaria vaccine and exploratory analysis on anti-circumsporozoite antibody titres and protection in children aged 5–17 months in Kenya and Tanzania: a randomised controlled trial. *Lancet Infect Dis* (2011) 11(2):102–9. doi:10.1016/S1473-3099(10)70262-0
  27. Gruner AC, Mauduit M, Tewari R, Romero JF, Depinay N, Kayibanda M, et al. Sterile protection against malaria is independent of immune responses to the circumsporozoite protein. *PLoS One* (2007) 2(12):e1371. doi:10.1371/journal.pone.0001371
  28. Trieu A, Kayala MA, Burk C, Molina DM, Freilich DA, Richie TL, et al. Sterile protective immunity to malaria is associated with a panel of novel *P. falciparum* antigens. *Mol Cell Proteomics* (2011) 10(9):M111007948. doi:10.1074/mcp.M111.007948
  29. Kario T, Ishino T, Yano K, Chinzei Y, Yuda M. CelTOS, a novel malarial protein that mediates transmission to mosquito and vertebrate hosts. *Mol Microbiol* (2006) 59(5):1369–79. doi:10.1111/j.1365-2958.2005.05024.x
  30. Anum D, Kusi KA, Ganeshan H, Hollingdale MR, Ofori MF, Koram KA, et al. Measuring naturally acquired ex vivo IFN-gamma responses to *Plasmodium falciparum* cell-traversing protein for ookinetes and sporozoites (CelTOS) in Ghanaian adults. *Malar J* (2015) 14:20. doi:10.1186/s12936-014-0539-5
  31. Kusi KA, Bosomprah S, Dodo D, Kyei-Baafour E, Dickson EK, Mensah D, et al. Anti-sporozoite antibodies as alternative markers for malaria transmission intensity estimation. *Malar J* (2014) 13:103. doi:10.1186/1475-2875-13-103
  32. Bergmann-Leitner ES, Mease RM, De La Vega P, Savranskaya T, Polhemus M, Ockenhouse C, et al. Immunization with pre-erythrocytic antigen CelTOS from *Plasmodium falciparum* elicits cross-species protection against heterologous challenge with *Plasmodium berghei*. *PLoS One* (2010) 5(8):e12294. doi:10.1371/journal.pone.0012294
  33. Longley RJ, Reyes-Sandoval A, Montoya-Diaz E, Dunachie S, Kumpitak C, Nguitragool W, et al. Acquisition and longevity of antibodies to *Plasmodium vivax* preerythrocytic antigens in Western Thailand. *Clin Vaccine Immunol* (2016) 23(2):117–24. doi:10.1128/CVI.00501-15
  34. Stanisic DI, Fowkes FJ, Koinari M, Javati S, Lin E, Kiniboro B, et al. Acquisition of antibodies against *Plasmodium falciparum* merozoites and malaria immunity in young children and the influence of age, force of infection, and magnitude of response. *Infect Immun* (2015) 83(2):646–60. doi:10.1128/IAI.02398-14
  35. Larsen JE, Lund O, Nielsen M. Improved method for predicting linear B-cell epitopes. *Immunome Res* (2006) 2:2. doi:10.1186/1745-7580-2-2
  36. Emini EA, Hughes JV, Perlow DS, Boger J. Induction of hepatitis A virus-neutralizing antibody by a virus-specific synthetic peptide. *J Virol* (1985) 55(3):836–9.
  37. Berendsen HJC, van der Spoel D, van Drunen R. GROMACS: a message-passing parallel molecular dynamics implementation. *Comput Phys Commun* (1995) 91(1–3):13. doi:10.1016/0010-4655(95)00042-E
  38. Oostenbrink C, Villa A, Mark AE, van Gunsteren WF. A biomolecular force field based on the free enthalpy of hydration and solvation: the GROMOS force-field parameter sets 53A5 and 53A6. *J Comput Chem* (2004) 25(13):1656–76. doi:10.1002/jcc.20090
  39. William LJ, Chandrasekhar J, Madura JD, Impey RW, Klein ML. Comparison of simple potential functions for simulating liquid water. *J Chem Phys* (1983) 79:926–35. doi:10.1063/1.445869
  40. Baker NA, Sept D, Joseph S, Holst MJ, McCammon JA. Electrostatics of nanosystems: application to microtubules and the ribosome. *Proc Natl Acad Sci U S A* (2001) 98(18):10037–41. doi:10.1073/pnas.181342398
  41. Bergmann-Leitner ES, Legler PM, Savranskaya T, Ockenhouse CF, Angov E. Cellular and humoral immune effector mechanisms required for sterile protection against sporozoite challenge induced with the novel malaria vaccine candidate CelTOS. *Vaccine* (2011) 29(35):5940–9. doi:10.1016/j.vaccine.2011.06.053
  42. Bueno LL, Morais CG, Soares IS, Bouillet LE, Bruna-Romero O, Fontes CJ, et al. *Plasmodium vivax* recombinant vaccine candidate AMA-1 plays an important role in adaptive immune response eliciting differentiation of dendritic cells. *Vaccine* (2009) 27(41):5581–8. doi:10.1016/j.vaccine.2009.07.031
  43. Amarasinghe S, Kathriarachchi H, Udagama P. Conserved regions of *Plasmodium vivax* potential vaccine candidate antigens in Sri Lanka: conscious in silico analysis of prospective conformational epitope regions. *Asian Pac J Trop Med* (2014) 7(10):832–40. doi:10.1016/S1995-7645(14)60146-2
  44. Xia H, Fang Q, Jangpatrapongska K, Zhiyong T, Cui L, Li B, et al. A comparative study of natural immune responses against *Plasmodium vivax* C-terminal merozoite surface protein-1 (PvMSP-1) and apical membrane antigen-1 (PvAMA-1) in two endemic settings. *EXCLI J* (2015) 14:926–34. doi:10.17179/excli2015-388
  45. Lima-Junior JC, Tran TM, Meyer EV, Singh B, De-Simone SG, Santos F, et al. Naturally acquired humoral and cellular immune responses to *Plasmodium vivax* merozoite surface protein 9 in Northwestern Amazon individuals. *Vaccine* (2008) 26(51):6645–54. doi:10.1016/j.vaccine.2008.09.029
  46. Lima-Junior JC, Jiang J, Rodrigues-da-Silva RN, Banic DM, Tran TM, Ribeiro RY, et al. B cell epitope mapping and characterization of naturally acquired antibodies to the *Plasmodium vivax* merozoite surface protein-3alpha

- (PvMSP-3alpha) in malaria exposed individuals from Brazilian Amazon. *Vaccine* (2011) 29(9):1801–11. doi:10.1016/j.vaccine.2010.12.099
47. Ladeia-Andrade S, Ferreira MU, Scopel KK, Braga EM, Bastos Mda S, Wunderlich G, et al. Naturally acquired antibodies to merozoite surface protein (MSP)-1(19) and cumulative exposure to *Plasmodium falciparum* and *Plasmodium vivax* in remote populations of the Amazon Basin of Brazil. *Mem Inst Oswaldo Cruz* (2007) 102(8):943–51. doi:10.1590/S0074-02762007000800009
  48. Storti-Melo LM, da Costa DR, Souza-Neiras WC, Cassiano GC, Couto VS, Povoa MM, et al. Influence of HLA-DRB-1 alleles on the production of antibody against CSP, MSP-1, AMA-1, and DBP in Brazilian individuals naturally infected with *Plasmodium vivax*. *Acta Trop* (2012) 121(2):152–5. doi:10.1016/j.actatropica.2011.10.009
  49. Braga EM, Barros RM, Reis TA, Fontes CJ, Morais CG, Martins MS, et al. Association of the IgG response to *Plasmodium falciparum* merozoite protein (C-terminal 19 kD) with clinical immunity to malaria in the Brazilian Amazon region. *Am J Trop Med Hyg* (2002) 66(5):461–6.
  50. Baird JK. Age-dependent characteristics of protection v. susceptibility to *Plasmodium falciparum*. *Ann Trop Med Parasitol* (1998) 92(4):367–90. doi:10.1080/00034989859366
  51. Soe S, Theisen M, Roussilhon C, Aye KS, Druilhe P. Association between protection against clinical malaria and antibodies to merozoite surface antigens in an area of hyperendemicity in Myanmar: complementarity between responses to merozoite surface protein 3 and the 220-kilodalton glutamate-rich protein. *Infect Immun* (2004) 72(1):247–52. doi:10.1128/IAI.72.1.247-252.2004
  52. Oliveira-Ferreira J, Pratt-Riccio LR, Arruda M, Santos F, Daniel Ribeiro CT, Goldberg AC, et al. HLA class II and antibody responses to circumsporozoite protein repeats of *P. vivax* (VK210, VK247 and *P. vivax*-like) in individuals naturally exposed to malaria. *Acta Trop* (2004) 92(1):63–9. doi:10.1016/j.actatropica.2004.02.011
  53. Yildiz Zeyrek F, Palacpac N, Yuksel F, Yagi M, Honjo K, Fujita Y, et al. Serologic markers in relation to parasite exposure history help to estimate transmission dynamics of *Plasmodium vivax*. *PLoS One* (2011) 6(11):e28126. doi:10.1371/journal.pone.0028126
  54. Modiano D, Petrarca V, Sirima BS, Luoni G, Nebie I, Diallo DA, et al. Different response to *Plasmodium falciparum* in west African sympatric ethnic groups: possible implications for malaria control strategies. *Parassitologia* (1999) 41(1–3):193–7.
  55. Modiano D, Chiucchiini A, Petrarca V, Sirima BS, Luoni G, Roggero MA, et al. Interethnic differences in the humoral response to non-repetitive regions of the *Plasmodium falciparum* circumsporozoite protein. *Am J Trop Med Hyg* (1999) 61(4):663–7.
  56. Brisebarre A, Kumlungui B, Sawadogo S, Afridi S, Fumoux F, Rihet P. Genome-wide significant linkage to IgG subclass responses against *Plasmodium falciparum* antigens on chromosomes 8p22-p21, 9q34 and 20q13. *Genes Immun* (2015) 16(3):187–92. doi:10.1038/gene.2014.66
  57. Afridi S, Atkinson A, Garnier S, Fumoux F, Rihet P. Malaria resistance genes are associated with the levels of IgG subclasses directed against *Plasmodium falciparum* blood-stage antigens in Burkina Faso. *Malar J* (2012) 11:308. doi:10.1186/1475-2875-11-308
  58. Beck HP, Felger I, Barker M, Bugawan T, Genton B, Alexander N, et al. Evidence of HLA class II association with antibody response against the malaria vaccine SPF66 in a naturally exposed population. *Am J Trop Med Hyg* (1995) 53(3):284–8.
  59. Banic DM, Goldberg AC, Pratt-Riccio LR, De Oliveira-Ferreira J, Santos F, Gras-Masse H, et al. Human leukocyte antigen class II control of the immune response to p126-derived amino terminal peptide from *Plasmodium falciparum*. *Am J Trop Med Hyg* (2002) 66(5):509–15.
  60. Nardin EH, Oliveira GA, Calvo-Calle JM, Castro ZR, Nussenzweig RS, Schmeckpeper B, et al. Synthetic malaria peptide vaccine elicits high levels of antibodies in vaccinees of defined HLA genotypes. *J Infect Dis* (2000) 182(5):1486–96. doi:10.1086/315871
  61. Murillo LA, Rocha CL, Mora AL, Kalil J, Goldenberg AK, Patarroyo ME. Molecular analysis of HLA DR4-beta 1 gene in malaria vaccinees. Typing and subtyping by PCR technique and oligonucleotides. *Parasite Immunol* (1991) 13(2):201–10. doi:10.1111/j.1365-3024.1991.tb00275.x
  62. Stephens HA, Brown AE, Chandanayangyong D, Webster HK, Sirikong M, Longta P, et al. The presence of the HLA class II allele DPB1\*0501 in ethnic Thais correlates with an enhanced vaccine-induced antibody response to a malaria sporozoite antigen. *Eur J Immunol* (1995) 25(11):3142–7. doi:10.1002/eji.1830251123
  63. Maitland K, Williams TN, Bennett S, Newbold CI, Peto TE, Viji J, et al. The interaction between *Plasmodium falciparum* and *P. vivax* in children on Espiritu Santo island, Vanuatu. *Trans R Soc Trop Med Hyg* (1996) 90(6):614–20. doi:10.1016/S0035-9203(96)90406-X
  64. Luxemburger C, Thwai KL, White NJ, Webster HK, Kyle DE, Maelankirri L, et al. The epidemiology of malaria in a Karen population on the western border of Thailand. *Trans R Soc Trop Med Hyg* (1996) 90(2):105–11. doi:10.1016/S0035-9203(96)90102-9
  65. Kaneko A, Chaves LF, Taleo G, Kalko M, Isozumi R, Wickremasinghe R, et al. Characteristic age distribution of *Plasmodium vivax* infections after malaria elimination on Aneityum Island, Vanuatu. *Infect Immun* (2014) 82(1):243–52. doi:10.1128/IAI.00931-13
  66. Bouharoun-Tayoun H, Druilhe P. *Plasmodium falciparum* malaria: evidence for an isotype imbalance which may be responsible for delayed acquisition of protective immunity. *Infect Immun* (1992) 60(4):1473–81.
  67. Chelimo K, Ofulla AV, Narum DL, Kazura JW, Lanar DE, John CC. Antibodies to *Plasmodium falciparum* antigens vary by age and antigen in children in a malaria-holoendemic area of Kenya. *Pediatr Infect Dis J* (2005) 24(8):680–4. doi:10.1097/01.inf.0000172151.28851.fd
  68. John CC, Moormann AM, Pregibon DC, Sumba PO, McHugh MM, Narum DL, et al. Correlation of high levels of antibodies to multiple pre-erythrocytic *Plasmodium falciparum* antigens and protection from infection. *Am J Trop Med Hyg* (2005) 73(1):222–8.
  69. Stanisic DI, Richards JS, McCallum FJ, Michon P, King CL, Schoepflin S, et al. Immunoglobulin G subclass-specific responses against *Plasmodium falciparum* merozoite antigens are associated with control of parasitemia and protection from symptomatic illness. *Infect Immun* (2009) 77(3):1165–74. doi:10.1128/IAI.01129-08
  70. Aribot G, Rogier C, Sarthou JL, Trape JF, Balde AT, Druilhe P, et al. Pattern of immunoglobulin isotype response to *Plasmodium falciparum* blood-stage antigens in individuals living in a holoendemic area of Senegal (Dielmo, west Africa). *Am J Trop Med Hyg* (1996) 54(5):449–57.
  71. Metzger WG, Okenu DM, Cavanagh DR, Robinson JV, Bojang KA, Weiss HA, et al. Serum IgG3 to the *Plasmodium falciparum* merozoite surface protein 2 is strongly associated with a reduced prospective risk of malaria. *Parasite Immunol* (2003) 25(6):307–12. doi:10.1046/j.1365-3024.2003.00636.x
  72. Nebie I, Diarra A, Ouedraogo A, Soulama I, Bougouma EC, Tiono AB, et al. Humoral responses to *Plasmodium falciparum* blood-stage antigens and association with incidence of clinical malaria in children living in an area of seasonal malaria transmission in Burkina Faso, West Africa. *Infect Immun* (2008) 76(2):759–66. doi:10.1128/IAI.01147-07
  73. Shi YP, Sayed U, Qari SH, Roberts JM, Udhayakumar V, Oloo AJ, et al. Natural immune response to the C-terminal 19-kilodalton domain of *Plasmodium falciparum* merozoite surface protein 1. *Infect Immun* (1996) 64(7):2716–23.
  74. Roussilhon C, Oeuvelray C, Muller-Graf C, Tall A, Rogier C, Trape JF, et al. Long-term clinical protection from falciparum malaria is strongly associated with IgG3 antibodies to merozoite surface protein 3. *PLoS Med* (2007) 4(11):e320. doi:10.1371/journal.pmed.0040320
  75. John CC, Tande AJ, Moormann AM, Sumba PO, Lanar DE, Min XM, et al. Antibodies to pre-erythrocytic *Plasmodium falciparum* antigens and risk of clinical malaria in Kenyan children. *J Infect Dis* (2008) 197(4):519–26. doi:10.1086/526787
  76. Mishra S, Nussenzweig RS, Nussenzweig V. Antibodies to *Plasmodium circumsporozoite protein* (CSP) inhibit sporozoite's cell traversal activity. *J Immunol Methods* (2012) 377(1–2):47–52. doi:10.1016/j.jim.2012.01.009
  77. Stewart MJ, Nawrot RJ, Schulman S, Vanderberg JP. *Plasmodium berghei* sporozoite invasion is blocked in vitro by sporozoite-immobilizing antibodies. *Infect Immun* (1986) 51(3):859–64.
  78. Reineke U, Sabat R. Antibody epitope mapping using SPOT peptide arrays. *Methods Mol Biol* (2009) 524:145–67. doi:10.1007/978-1-59745-450-6\_11
  79. Lima-Junior JC, Banic DM, Tran TM, Meyer VS, De-Simone SG, Santos F, et al. Promiscuous T-cell epitopes of *Plasmodium* merozoite surface protein 9 (PvMSP9) induces IFN-gamma and IL-4 responses in individuals naturally exposed to malaria in the Brazilian Amazon. *Vaccine* (2010) 28(18):3185–91. doi:10.1016/j.vaccine.2010.02.046

80. Lin HH, Zhang GL, Tongchusak S, Reinherz EL, Brusic V. Evaluation of MHC-II peptide binding prediction servers: applications for vaccine research. *BMC Bioinformatics* (2008) 9(Suppl 12):S22. doi:10.1186/1471-2105-9-S12-S22
81. Bueno LL, Lobo FP, Morais CG, Mourao LC, de Avila RA, Soares IS, et al. Identification of a highly antigenic linear B cell epitope within *Plasmodium vivax* apical membrane antigen 1 (AMA-1). *PLoS One* (2011) 6(6):e21289. doi:10.1371/journal.pone.0021289
82. Bergmann-Leitner ES, Chaudhury S, Steers NJ, Sabato M, Delvecchio V, Wallqvist AS, et al. Computational and experimental validation of B and T-cell epitopes of the in vivo immune response to a novel malarial antigen. *PLoS One* (2013) 8(8):e71610. doi:10.1371/journal.pone.0071610
83. Lin M, McRae H, Dan H, Tangorra E, Laverdiere A, Pasick J. High-resolution epitope mapping for monoclonal antibodies to the structural protein Erns of classical swine fever virus using peptide array and random peptide phage display approaches. *J Gen Virol* (2010) 91(Pt 12):2928–40. doi:10.1099/vir.0.023259-0
84. Dyrberg T, Oldstone MB. Peptides as antigens. Importance of orientation. *J Exp Med* (1986) 164(4):1344–9. doi:10.1084/jem.164.4.1344
85. Jimah JR, Salinas ND, Sala-Rabanal M, Jones NG, Sibley LD, Nichols CG, et al. Malaria parasite CelTOS targets the inner leaflet of cell membranes for pore-dependent disruption. *Elife* (2016) 5:e20621. doi:10.7554/eLife.20621

**Conflict of Interest Statement:** The authors declare that the research was conducted in the absence of any commercial or financial relationships that could be construed as a potential conflict of interest.

Copyright © 2017 Rodrigues-da-Silva, Soares, Lopez-Camacho, Martins da Silva, Perce-da-Silva, Téva, Ramos Franco, Pinheiro, Chaves, Pratt-Riccio, Reyes-Sandoval, Banic and Lima-Junior. This is an open-access article distributed under the terms of the Creative Commons Attribution License (CC BY). The use, distribution or reproduction in other forums is permitted, provided the original author(s) or licensor are credited and that the original publication in this journal is cited, in accordance with accepted academic practice. No use, distribution or reproduction is permitted which does not comply with these terms.



# Linear Epitopes of *Paracoccidioides brasiliensis* and Other Fungal Agents of Human Systemic Mycoses As Vaccine Candidates

Luiz R. Travassos<sup>1\*</sup> and Carlos P. Taborda<sup>2,3</sup>

<sup>1</sup>Department of Microbiology, Immunology and Parasitology, Federal University of São Paulo, São Paulo, Brazil, <sup>2</sup>Department of Microbiology, Institute of Biomedical Sciences, University of São Paulo, São Paulo, Brazil, <sup>3</sup>Laboratory of Medical Mycology IMTSP/LIM53/HCFMUSP, University of São Paulo, São Paulo, Brazil

## OPEN ACCESS

### Edited by:

Clarisa B. Palatnik-de-Sousa,  
Federal University of Rio de Janeiro,  
Brazil

### Reviewed by:

Ji Wang,  
Harvard Medical School, USA  
Ramaswamy Kalyanasundaram,  
University of Illinois at Chicago, USA

### \*Correspondence:

Luiz R. Travassos  
luiztravassos@gmail.com

### Specialty section:

This article was submitted to  
Vaccines and Molecular  
Therapeutics,  
a section of the journal  
Frontiers in Immunology

Received: 15 December 2016

Accepted: 16 February 2017

Published: 10 March 2017

### Citation:

Travassos LR and Taborda CP (2017)  
Linear Epitopes of *Paracoccidioides brasiliensis* and Other Fungal Agents of Human Systemic Mycoses As Vaccine Candidates.  
*Front. Immunol.* 8:224.  
doi: 10.3389/fimmu.2017.00224

Dimorphic fungi are agents of systemic mycoses associated with significant morbidity and frequent lethality in the Americas. Among the pathogenic species are *Paracoccidioides brasiliensis* and *Paracoccidioides lutzii*, which predominate in South America; *Histoplasma capsulatum*, *Coccidioides posadasii*, and *Coccidioides immitis*, and the *Sporothrix* spp. complex are other important pathogens. Associated with dimorphic fungi other important infections are caused by yeast such as *Candida* spp. and *Cryptococcus* spp. or mold such as *Aspergillus* spp., which are also fungal agents of deadly infections. Nowadays, the actual tendency of therapy is the development of a pan-fungal vaccine. This is, however, not easy because of the complexity of eukaryotic cells and the particularities of different species and isolates. Albeit there are several experimental vaccines being studied, we will focus mainly on peptide vaccines or epitopes of T-cell receptors inducing protective fungal responses. These peptides can be carried by antibody inducing  $\beta$ -(1,3)-glucan oligo or polysaccharides, or be mixed with them for administration. The present review discusses the efficacy of linear peptide epitopes in the context of antifungal immunization and vaccine proposition.

**Keywords:** peptide, vaccine, antibody, fungi, *Paracoccidioides*

## SYSTEMIC FUNGAL INFECTIONS AND CURRENT TREATMENT: A SHORT INTRODUCTION

Distinct groups of fungi can cause systemic mycoses: geographically delimited thermal-dimorphic fungi, classical yeast such as *Cryptococcus* spp. and *Candida* spp., or molds like *Aspergillus* spp., *Fusarium* spp., and *Penicillium* spp.

Thermal-dimorphic fungi are a group of ascomycetes endemic in certain regions, agents of the most common diseases, such as paracoccidioidomycosis, occurring in the vast area from south Mexico to the north of Argentina; coccidioidomycosis in the Americas with particular incidence in the USA (California, Texas, Utah, New Mexico, Arizona, and Nevada), Mexico, Colombia, Venezuela, northeast of Brazil, and north of Argentina; North American blastomycosis, with high incidence in Canada, eastern USA, sporadic cases in Argentina, and endemic areas in middle and eastern Africa; histoplasmosis, found in the Americas, Southeast Asia, and Africa; and the *Sporothrix schenckii* complex with worldwide distribution (1). These fungi usually present propagules in the

soil, vegetal, or animal excrement. The infection usually starts *via* the respiratory route except for sporotrichosis that rarely occurs by inhalation of fungal propagules, rather arising from surface injuries by fungus-contaminated objects or cat scratches (1).

Most of patients developing *Candida* spp. and *Cryptococcus* spp. infections are immunodeficient suffering from AIDS, diabetes, or have been administered immunosuppressive drugs as in organ transplantation procedures, indwelling catheter for a short or long time, although primary infections can also occur without association with other conditions (2, 3). *Aspergillus fumigatus*, *Fusarium* spp., and *Penicillium* spp. can cause different types of infection. Patients undergoing hematopoietic stem cell transplantation for treatment of hematological malignancy have considerable risk of developing fatal fungal infection (4, 5). Whereas infection by *Candida* spp. occurs mainly by endogenous yeast, this is not an exclusive pathway. Infections by *Cryptococcus* spp., *A. fumigatus*, *Fusarium* spp., and *Penicillium* spp. occur by inhalation of fungal propagules (2–5).

There is no trustworthy quantitation of people infected by systemic mycosis in the World; however, Brown et al. (6) estimated that more than 2,050,000 people yearly infected with the 10 most significant invasive fungal agents/mycoses including *Aspergillus*, *Candida*, *Cryptococcus*, mucormycosis, *Pneumocystis*, *Blastomyces*, *Coccidioides*, *Histoplasma*, *Penicillium*, and *Paracoccidioides* (6).

There are few groups of antifungal drugs effective in the treatment of systemic fungal disease. Most of them belong to four classes: polyenes, azoles, echinocandins, and pyrimidine (7). Other antimicrobial drugs also have antifungal action such as trimethoprim-sulfamethoxazole that is used with relative success in the treatment of patients with paracoccidioidomycosis (8). Treatment and the option for antifungal drugs depend on the severity of the disease and time of use (9).

There are many reports on drug resistance in systemic fungal infections involving almost all classes of antimicrobial drugs. In paracoccidioidomycosis, resistance to ketoconazole and trimethoprim-sulfamethoxazole may be related to the agent species (*Paracoccidioides brasiliensis* or *Paracoccidioides lutzii*) [reviewed in Ref. (9)] or the melanization process, which enhances the resistance of yeast cells to amphotericin B (10). The biofilm formation in *Candida* spp. can enhance resistance of yeast cells to antifungal drugs (11, 12), and the *Candida albicans* biofilm is intrinsically resistant to the host immune system [reviewed in Ref. (12)]. Such resistance appears to be multifactorial involving conventional resistance mechanisms as the increased efflux pump, and mechanisms specific to the biofilm as the production of an extracellular matrix containing β-glucan and extracellular DNA [reviewed in Ref. (11)]. The resistance to azoles by efflux pump proteins in *Candida albicans* may involve overexpression of Cdr1p (ATP-binding cassette) and CaMdr1p (major facilitator superfamily) as reviewed in Ref. (13).

Due to the increasing resistance, several groups of researchers focus on safer and effective new antifungal compounds. Authors have isolated *Paracoccidioides* spp. (14) and *Candida* (15) susceptible to curcumin. The use of ajoene derived from garlic with antifungal activity against *Paracoccidioides brasiliensis* (16), *Scedosporium prolificans* (17), and dermatophytes (18) has

also been reported. Antiretroviral protease inhibitors such as Saquinavir and Ritonavir have shown inhibitory activity against *Histoplasma capsulatum* (19) and *Candida albicans* (20). In addition, several other reports showing the antifungal activities of different compounds with potential use in patients have appeared, still without clearance from regulatory institutions.

Generally, the immune system is important to achieve good therapeutic results in association with antifungal drugs. The status of innate and adaptive immune system plays a central role in the protection against foreign pathogens. In contrast to immunocompetent individuals, immunosuppressed patients are much more susceptible to fungal infections some of them fatal (21, 22).

The cellular immune system is essential to protect and eliminate fungal pathogens; in general, dendritic cells (DCs), macrophages, and neutrophils are central in the mechanisms of fungal elimination. Antigenic peptides are presented to lymphocytes with subsequent eliciting of T-cell and B-cell effective responses (21–24). Differentiation of CD4<sup>+</sup> T cells along a T-helper (Th) cell type 1 (Th1) or type 2 (Th2) pathway and development of specific Th responses determine host's susceptibility or resistance to invasive fungal infections. A Th1 response is induced by cytokines, such as IFN-γ, interleukin (IL)-6, tumor necrosis factor (TNF)-α, and IL-12. The main Th2 cytokines are IL-4 and IL-10. IFN-γ activates macrophages and increases fungistatic and fungicidal activities. Th17 cells and IL-22 are involved in the activation and repair of epithelial barriers, and while activated by IL-17 are crucial for antifungal defense and control of the NK cells (21–25).

The function of antibody-mediated immunity against fungal infections was believed to have little or no role in protection against fungal diseases in the past (26). However, since Dromer et al. showed that a monoclonal antibody to *Cryptococcus neoformans* was effective against the fungal infection (27), a series of protective monoclonal antibodies against medically important fungi have been described (26). The protective mechanism of antibody-mediated immunity depends on opsonization, Fc receptor-dependent ADCC, immunoglobulin subclasses, genetic background, status of the cellular immune system, fungal burden, amount of patient administered monoclonal antibodies, among other characteristics (26).

Antifungal drugs are the basis of systemic mycoses treatment in both immunocompetent and immunosuppressed patients. However, immunosuppression or anergy may interfere with chemotherapy efficiency. Vaccination (therapeutic or prophylactic) may boost the immune system and add to the protective effect of antifungal drugs allowing for reduction of the time of treatment and prevention of relapse. In this review, we focus mainly on vaccines and epitope description.

## **Paracoccidioides brasiliensis**

The major diagnostic antigen of *Paracoccidioides brasiliensis* is the 43 kDa glycoprotein (gp43) discovered in 1986 by Puccia et al. (28). A detailed description of gp43 was reviewed in Travassos et al. (29). Epitopes in the gp43 are peptide in nature so that patients' sera reacted with the deglycosylated antigen (30). Several mAbs were raised to the gp43 and tested either *in vivo* against lung infections by *Paracoccidioides brasiliensis* or in

phagocytosis assays with peritoneal and alveolar macrophages. Most mAbs stimulated the phagocytosis of yeast forms (31). MAbs 3E, which was effective both in the reduction of fungal burdens in infected animals and in the promotion of phagocytosis, was tested for binding to a panel of gp43 internal peptides. The mAb 3E epitope lied within the sequence NHVRIPIGYWAV shared with *A. fumigatus*, *Aspergillus oryzae*, and *Blumeria graminis* sequences from  $\beta$ -1,3-glucanases (29).

Other protein antigens eliciting protective antibodies have been described but the B-cell epitopes were not characterized. In relation to the recently recognized *P. lutzii* species, the gp43 and 27 kDa antigens were less expressed in *P. lutzii* and PS2 genotype of *Paracoccidioides brasiliensis* (32). The gp43 ortholog in *P. lutzii* contains few epitopes in common with the *Paracoccidioides brasiliensis* gp43, contributing to serological diagnostic difficulties in patients infected with *P. lutzii* (33).

The gp43 elicits an IFN- $\gamma$ -mediated T-CD4 $^{+}$  response, which is protective against the lung infection by *Paracoccidioides brasiliensis*. The gp43 was cloned, sequenced, and expressed in bacteria as a recombinant fusion protein (34). The amino acid sequence was deduced from a 987-bp fragment obtained by PCR amplification. Similarities of 56–58% were found with exo-1,3- $\beta$ -D-glucanases of *Saccharomyces cerevisiae* and *Candida albicans*. The open-reading frame was found in a 1,329 bp fragment, encompassing two exons and one intron. The gp43 gene encodes 416 amino acids with a leader peptide of 35 aa. Epitopes able to elicit hypersensitivity in both guinea pigs (35) and humans (36) were described. A peptide of 15 amino acids (QTLIAIHTLAIRYAN) obtained from a collection of gp43 internal peptides, which was also located using DNAStar, Protean analysis Sette algorithm for Ia $^d$  binding peptides (37), contained the T-CD4 $^{+}$  epitope, and was called P10 (38). The functional activities of P10 analogs and truncated peptides were studied. Peptides of 12 aa or longer, which is the size required for MHC II antigen presentation, were active. The sequence HTLAI is an essential domain of the epitope. Gene polymorphism studies showed that the P10 sequence is highly conserved in *Paracoccidioides brasiliensis* isolates (39). In contrast, the corresponding sequences of *Candida albicans* and *S cerevisiae* exo-glucanases differed from P10 (40).

As with the gp43, P10 induces a Th1 lymphocyte response, which is protective against the intratracheal (i.t.) infection by virulent *Paracoccidioides brasiliensis*. IFN- $\gamma$  is a key cytokine in this response as it has been shown to activate macrophages for increased fungicidal activity against *Paracoccidioides brasiliensis* and *Blastomyces dermatitidis* (41). It also plays a role in the organization of granulomas. Mice deficient in the IFN- $\gamma$  are highly susceptible to *Paracoccidioides brasiliensis* infection. IFN- $\gamma$ -receptor (but not IFN- $\alpha$ -R and IFN- $\beta$ -R), IFN- $\gamma$ , and IRF-1 KO mice were 100% killed 3–4 weeks following i.t. infection with virulent *Paracoccidioides brasiliensis*. P10 failed to protect those KO mice (40).

## P10 AS A VACCINE CANDIDATE

P10 contains the T-CD4 $^{+}$  epitope that is presented by MHC II molecules from murine H-2 haplotypes a, b, and d (38). The promiscuous nature of P10, if also shown with HLA-DR

molecules, could represent an important attribute of this peptide to be used in a human vaccine to paracoccidioidomycosis. Iwai et al. (42) tested P10 and the analogous peptide gp43 (180–194), which included an N-terminal lysine and omitted the C-terminal asparagine, a glycosylated residue in the gp43. Both peptides bound to the nine prevalent HLA-DR molecules confirming their ability to be presented by different MHC II antigens. Gp43 (180–194) and four other peptides identified by TEPITOPE algorithm were recognized by 53 and 32–47%, respectively, of patients with treated paracoccidioidomycosis. Seventy-four percent of patients recognized a combination of five promiscuous gp43 peptides. TEPITOPE scanned 25 Caucasian HLA-DR antigens with P10 and analogous peptides, all containing the HTLAI core sequence, being predicted to bind to 90% of them. The four peptides that were predicted to bind to a large number of HLA-DR molecules, in addition to Gp43 (180–194), were Gp43 (45–59): IGGWLLEPWISPSV; Gp43 (94–108): TEDDFKNIAAGLNHV; Gp43 (106–120): LNHVRIPIGYWAVNP; and Gp43 (283–298): IDQHVKLACS LPHGRL (42). These peptides could be added to P10 or Gp43 (180–194) in case the single epitope-based vaccine may not be powerful enough to induce full protective immunity. Indeed, multiple B-cell and T-cell epitopes in a pool or as a multi-epitope polypeptide were reported to increase immunogenicity (43, 44).

In the mouse experimental infection, P10 alone exerted an efficient antifungal immunity against i.t. infections by virulent *Paracoccidioides brasiliensis* strains (Figure 1). A classical demonstration by histopathology shows murine lung sections from i.t.-infected BALB/c mice with large granulomas and numerous fungal cells as compared to preserved lung parenchyma, few or no detectable granulomas, very few or absence of fungal elements, in P10 immunized mice (45). Early experiments used complete Freund adjuvant as an adjuvant to both gp43 and P10. Mayorga et al. (46) showed that mice treated with the cationic lipid dioctadecyl-dimethylammonium bromide (DODAB) followed in efficiency by bacterial flagellin, both adjuvants to P10, were best protected against fungal infection as demonstrated by the lowest numbers of viable yeast cells and reduced granuloma formation and fibrosis. IFN- $\gamma$  and TNF- $\alpha$ , in contrast to IL-4 and IL-10, were secreted in the lungs of mice immunized with P10 in combination with these adjuvants. When combined with antifungal drugs, P10 was protective even in animals submitted to severe immune suppression (47). P10 immunization together with itraconazole or sulfamethoxazole and trimethoprim chemotherapy resulted in 100% survival of infected immunocompromised mice, up to 200 days postinfection, whereas untreated anergic mice died within 80 days.

P10 is primarily an antigenic peptide that is presented by MHC II molecules to induce a Th1 T-CD4 $^{+}$  cell proliferation, which exerts an IFN- $\gamma$ -dependent antifungal protection. Generally, T-CD4 $^{+}$  cells confer resistance through secretion of cytokines such as IFN- $\gamma$ , TNF- $\alpha$ , GM-CSF, and IL-17A, which can activate neutrophils, macrophages, DCs, and inflammatory monocytes for fungal killing and clearance. Activation of B cells leads to the secretion of protective antibodies (22, 48).

There is, however, some evidence of an immunomodulatory effect of P10 *in vivo*, which parallels the biological effects of

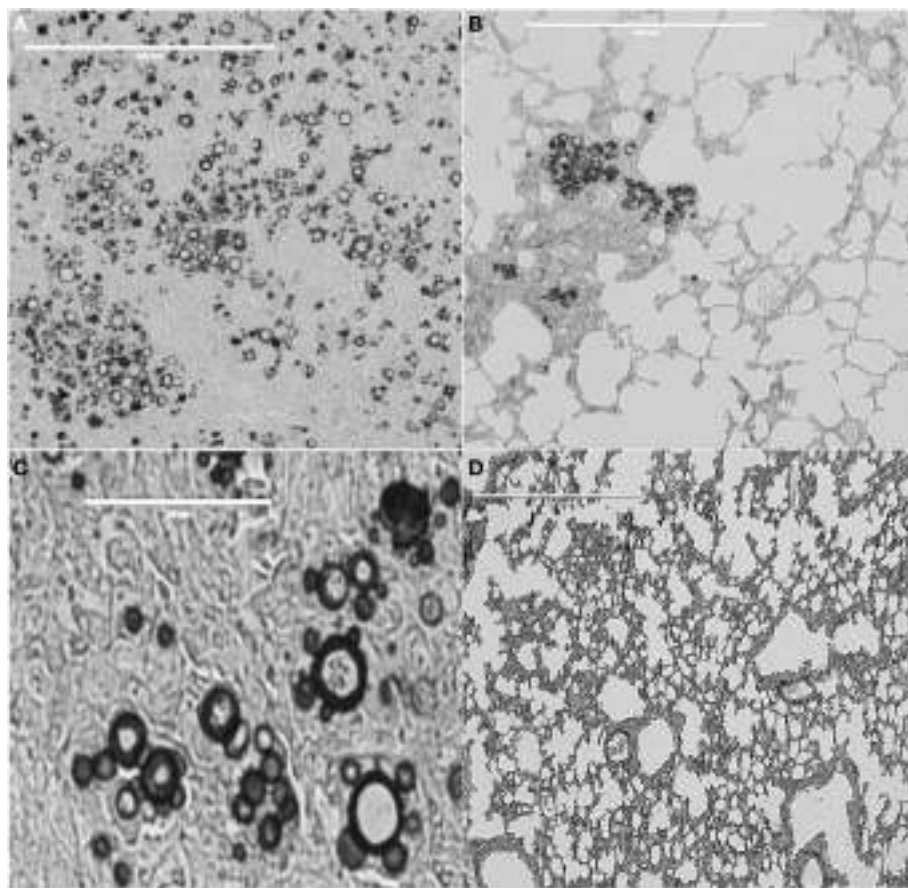


**FIGURE 1 | Lung tissue from BALB/c mice infected with *Paracoccidioides brasiliensis* vaccinated or not with peptide P10.** **(A)** Lung tissue of control only infected mice. Bar, 400  $\mu$ m. **(B)** Lung tissue of mice infected with *Paracoccidioides brasiliensis* and vaccinated with P10 in presence of cationic lipid. Bar, 400  $\mu$ m. **(C)** Highly magnified lung tissue of control, only infected mice. Bar, 50  $\mu$ m. **(D)** Lung tissue of mice infected with *Paracoccidioides brasiliensis* and vaccinated with P10 in presence of cationic lipid. Bar, 400  $\mu$ m. Slides were stained with Grocott-Gomori methenamine silver. Pictures were taken using EVOS fluorescence microscopy (AMG). The Animal Care and Use Committee of the University of São Paulo approved all *in vivo* testing.

isolated immunoglobulin CDRs and fragments of transcription factors (49, 50). These short peptides were able to activate bone-marrow DCs, which in turn started an immune response protective against antigenically unrelated metastatic murine melanoma.

A similar effect was observed with the combination of P10 and the TLR-5-binding *Salmonella typhimurium* FliCi flagellin (51), using the same metastatic melanoma system. Compounds were administered intranasally into C57Bl/6 mice, challenged intravenous (i.v.) with syngeneic B16F10-Nex2 murine melanoma cells. A marked reduction in the number of pulmonary tumor cell nodules was observed with a significant increase in the survival of challenged animals. Noticeable immunological responses were the M1 lung macrophages and secretion by lymph node cells and splenocytes of IL-12p40 and IFN- $\gamma$  when they were restimulated with tumor antigens.

Therefore, P10 acts not only as a specific Th1 *Paracoccidioides brasiliensis* antigen but also as a non-specific immunomodulatory peptide, much like a series of other anti-cancer peptides (49).

*Ex vivo* P10-primed bone-marrow DCs were administered to *Paracoccidioides brasiliensis* i.t.-infected mice (52). There followed a significantly reduced fungal burden and decreased pulmonary damage. Increased production of IFN- $\gamma$  and IL-12 and reduction in IL-10 and IL-4 compared to the untreated or unprimed, DCs-treated mice were obtained. A vaccine, therefore, with P10-primed DCs has the potential of rapid protection against the development of serious paracoccidioidomycosis in infected patients.

## P10 MINI-GENE THERAPY

An early plasmid vaccine with a mammalian expression vector carrying the gp43 gene induced specific antifungal antibodies and a T cell-mediated immune response under the control of the CMV promoter (53). The IFN- $\gamma$ -mediated immune response, which was effective against the i.t. infection by *Paracoccidioides brasiliensis*, lasted for at least 6 months after DNA-vaccine administration. Plasmids with P10 mini-gene insert (pP10) and also with IL-12 insert (pIL-12) were later used in an immunoprophylactic

protocol and their association completely eliminated the fungal elements [colony forming units (CFUs)] in the lungs from i.t.-infected animals (54). In a therapeutic protocol, empty plasmids were inactive and only the combination of both pP10 and pIL-12 achieved maximal protection using both BALB/c and B10.A (susceptible) mouse strains.

In a long-term protocol in which plasmids were administered in B10.A susceptible mice, 30 days after infection and the animals were sacrificed 6 months after infection, the pP10 vaccine alone reduced lung CFUs more than 100-fold and the combination of pP10 and pIL-12, virtually eliminated all fungal cells with recovery of the lung architecture. These are very encouraging results toward the use of gene therapy with P10 DNA insert, along with pIL-12 for a long lasting immune protection against paracoccidioidomycosis.

The above-described results are a remarkable example of effective immune responses elicited by a single epitope against a systemic fungal infection. Their complexity, however, is far from being completely understood. Owing to persistent antigen stimulation and active immune response, the infection by *Paracoccidioides brasiliensis* is characterized by granuloma formation and fibrosis. Remarkably, the association of the cationic lipid (DODAB) and P10 resulted in significant reduction of pulmonary fibrosis in animals developing paracoccidioidomycosis.

## OTHER AGENTS OF SYSTEMIC MYCOSES

### *Coccidioides immitis* and *Coccidioides posadasii*

As with *Paracoccidioides brasiliensis*, T cell-mediated immunity seems to be most important in the protection against *Coccidioides* infection (55–57). High titers of antibodies correlate with poor clinical prognosis, although there is evidence showing that a specific humoral response can modulate the immune response and contribute to host resistance (55–57).

A cell wall associated proline-rich antigen known as antigen 2 (Ag2) and Ag2/Pra showed to be protective against *Coccidioides* infection using an experimental model (58, 59). A recombinant rAg2/Pra protein and a genetic vaccine with AG@/PRA elicited protective CD4<sup>+</sup> T-cell-mediated response, although the route of immunization with both antigens showed some inconsistency (59).

Herr et al. (59) showed that *Coccidioides posadasii* produces a homologous proline-rich antigen denominated Prp2, which shows 69% protein identity and 86% similarity to Ag2/Pra. Protection against intra nasal challenge of C57BL/6 mice was verified by subcutaneous vaccination with single bacterially expressed homolog, rAg2/Pra or rPrp2 in association with rAg2/Pra in the presence of the CpG oligodeoxynucleotides adjuvant (59). A significant improvement of protective immunity induced by vaccination with combined rAg2/Pra and rPrp2 proteins was observed when compared to immunization with the single recombinant proteins (59).

Peptide libraries from proline-rich Ag2/Pra and Prp2 were used for mapping CD4<sup>+</sup> T-cell epitope by analysis of the T-cell

response in an IFN- $\gamma$ -ELISPOT assay. Six sequences of Ag2/Pra overlapping peptides (TRLTDFKCHCSKPELPGQIT, HCSKPELPGQITPCVVEACP, PIDIPPVDTTAPEPSETAE, TTAAPEPSETAEPTAEPTEE, PTEEPTAEPTEAEPTHE, and PTAEPTAEPTHEPTEEPTAV) and three sequences of Prp2 (EKLTD FKCHCAKPELPGKIT, DTRTPTQPPSTSPSAPQPTA, and PSTS PSAPQPTACI-PKRRRA) induced IFN- $\gamma$  by CD4<sup>+</sup> T cells isolated from mice immunized with either rAg2/Pra or rPrp2 (59). Albeit some peptides exhibited high similarity in their sequences, cross-reactions with T cells from either rAg2/Pra or rPrp2-immunized mice were not observed. Peptide sequences with high T-cell stimulatory response from homologous immunized mice contained one or more TXXP sequences. The XX residues, however, of TXXP motifs of Ag2/Pra and Prp2 differed (59).

Hurtgen et al. (60) described a strategy for the construction and immunological evaluation of a recombinant epitope-based vaccine. The use of a computational algorithm (ProPred), which identified putative T-cell epitopes predicted to bind promiscuously to human MHC class II molecules, revealed three antigens: aspartyl protease (Pep1), alpha-mannosidase (Amn1), and phospholipidase B as potential vaccine candidates (60). T-cell reactivity of synthetic peptides carrying all predicted epitopes was tested by IFN- $\gamma$  ELISPOT assay.

A single, bacteria-expressed, and recombinant epitope-based vaccine was constructed with five promiscuous, immunodominant T-cell epitopes derived from Pep1 (MRNSILLAATVLLGCTSAKVHL and HVRALGQKYFGSLP SSQQQTV), Amn1 (PAKVDVLLAQSLKLADVLKF and NGLA TTGTLVLEWTRLSDIT), and P1b (TPLVVYIPNYPYTTWS NIST). The upstream 20-mer peptide had the N-terminal of each epitope flanked by Ii-Key fragment (LRMKLPKS), and the C termini in four of the five peptides were flanked by CPGPG spacer to avoid processing of junctional epitopes (60).

C57BL/6 mice immunized with the epitope-based vaccine admixed with synthetic CpG ODN adjuvant or loaded on yeast glucan particles, and then challenged intranasally with *Coccidioides posadasii*, induced an infiltration of active T helper-1 (Th1), Th2 and Th17 cells, enhanced IFN- $\gamma$  and IL-17, and reduced lung fungal burden with prolonged animal survival (60).

In some infections by dimorphic fungi, even in the absence of CD4<sup>+</sup> T cells, mice had long-term survival mediated by vaccine-induced IL-17-producing CD8<sup>+</sup> T cells (61). Recombinant CD4<sup>+</sup> and CD8<sup>+</sup> T-cell epitopes joined by non-immunogenic linkers were loaded on glucan particles (composed primarily of  $\beta$ -1,3-glucan) which delivered the vaccine to APCs. Beta-glucan activates the alternative pathway of complement with deposition of C3 fragments, thus leading to phagocytosis by DCs and macrophages mediated by complement receptors and dectin-1. A decapeptide (EP67) agonist of active C-terminal region of human complement C5a acted as an adjuvant enhancing antigen presentation by macrophages and DCs but not neutrophils due to its high affinity for C5a receptors (C5aR/CD88) (61). This adjuvant was effective when conjugated with lysine residues on the surface of live arthroconidia from the vaccine strain. EP67 directs the vaccine to C5aR-bearing macrophages and DCs, inducing phagocytosis and antigen presentation. BALB/c mice immunized with EP67 conjugated, live vaccine, increased survival and decreased

inflammatory pathology, fungal burden, and neutrophils in the lungs (62). EP67 conjugated with epitope-based protein vaccines may provide an effective mechanism to further augment Th17 immunity (61). The use of glucan particles as a delivery and adjuvant compound as used here to treat coccidiomycosis could become in the future an important carrier of peptide antigens eliciting protective immune cellular responses, thus following the pioneering work in *Candida albicans*. Coincidentally with *Candida albicans*, the cellular response elicited against *Coccidioides* was also characterized by increased Th17 immunity.

### ***Histoplasma capsulatum***

Scheckelhoff and Deepe described an immunogenic heat shock protein-60 region (F3, fragment 3), which conferred protection against experimental *Histoplasma* infection (63, 64). A T-cell clone from C57BL/6 mice expressing V $\beta$  8.1/8.2 $^{+}$  T cells was generated after subcutaneous rHsp60 immunization and was efficacious for rHsp60-induced protective effect. TCR analysis showed that a subset of V $\beta$  8.1/8.2 $^{+}$  that produced IFN- $\gamma$  and reacted with F3, shared a common CDR3 sequence, DGGQG (64). It seems that a distinct subset of V $\beta$  8.1/8.2 $^{+}$  T cells is crucial for generating a protective response following rHsp60 immunization.

CD4 $^{+}$  T-cell depletion during primary infection by *H. capsulatum* led to animal's death, whereas lack of CD8 $^{+}$  T cells decreased fungal clearance (65). Remarkably, however, CD4 $^{+}$  T cells are dispensable in vaccine immunity to *H. capsulatum* [reviewed in Ref. (66)]. In the absence of CD4 $^{+}$  T cells, CD8 $^{+}$  T cells must be present exclusively during vaccine induction. Alternatively, immune CD8 $^{+}$  T cells generated in wild type mice, in the absence of CD4 $^{+}$  T cells, were adoptively transferred to mice infected with *Blastomyces* giving rise to effector cells lowering by 15-fold the lung CFU compared to no T cells. In both *H. capsulatum* and *B. dermatitidis* infections, when CD4 $^{+}$  T cells are absent, CD8 $^{+}$  T cells participate as effectors of vaccine immunity against these fungi (67). Likely, MHC-I molecules cross-present exogenous fungal antigens to vaccine-induced CD8 $^{+}$  T cells. These results point to the feasibility of developing vaccines against fungal infections in patients with immune deficiencies such as AIDS. They also illustrate the plasticity of the immune system adding unsuspected functional roles to cells and soluble mediators.

### ***Aspergillus fumigatus***

Invasive aspergillosis has significant incidence in immunocompromised hosts, with high mortality rate. Ito et al. demonstrated that sonication of *A. fumigatus* hyphae liberated an antigen able to protect corticosteroid immunosuppressed mice from invasive aspergillosis (68). Subcutaneous vaccination with recombinant allergen Asp f3, a 19 kDa protein recognized by antibodies from mice exposed intranasally to *A. fumigatus* conidia, with or without TiterMax adjuvant was protective (68). Two T-cell epitopes have been identified, and orthologs of Asp f3 have also been found in other *Aspergillus* species, *Coccidioides posadasii*, *Penicillium citrinum*, *Candida albicans*, *Candida boidinii*, *S. cerevisiae*. Since Asp f3 could mediate allergic bronchopulmonary aspergillosis, authors focused on eliminating its allergenic property after mapping the reactive epitopes. Several truncated forms of Asp f3 were synthesized and by using mass spectrometric analysis, two

peptides were identified, 11-mer (PGAFTPVC SAR) and 13-mer (HVPEYIEKLPEIR), able to stimulate Asp f3-specific T cells (68).

The protection mediated by Asp f3 was investigated in experimentally infected mice. After vaccination, specific Asp f3 pre-infection IgG titers did not differ in resistant and susceptible mice and passive transfer of Asp f3 antibodies did not protect immunosuppressed mice from aspergillosis. In fact, the antigen is not accessible unless both cell walls and membrane have been permeabilized (69). Depletion of CD4 $^{+}$  T cells, however, reduced the survival of rAsp f3-vaccinated mice. Transference of purified CD4 $^{+}$  T cells from rAsp f3-vaccinated mice into non-vaccinated mice conferred protection (69).

Consecutive 5-aa overlapping peptides from Asp f3 (15–168) sequence were synthesized. Mice were vaccinated subcutaneously with non-allergenic recombinant Asp f3 (15–168)-based vaccine, suspended in TiterMax adjuvant. Five weeks after the second immunization, mice were immunosuppressed with subcutaneous injection of cortisone acetate (2.5 mg) in suspension with methylcellulose (0.5%) and Tween 80 (0.1%) for 10 days. Mice were then anesthetized and intranasally inoculated with three million conidia. Significant protection was observed with such rAsp f3 vaccination (69).

Diaz-Arevalo et al. refined the previous search for immunogenic Asp f3 epitopes (70). T-cell proliferation with a set of overlapping synthetic 20-mer peptides was carried out. T cells from Asp f3 (15–168)-vaccinated non-infected mice as well as vaccinated infected survivors showed proliferative responses to the synthetic peptides: VCSARHVPEYIEKLPEIRAK (residues 60–79) and EIRAKGVDVAVLAYNDAYV (residues 75–94). Sera from vaccinated survivors of experimental *A. fumigatus* challenge and from non-surviving mice were analyzed. Elevated titers of IgG to VCSARHVPEYIEKLPEIRAK were found only in the surviving group suggesting that the deduced sequence contains both a B-cell epitope and a T-cell epitope (70).

Vaccination of a susceptible population to an opportunistic disease like invasive aspergillosis was approached by Stevens et al. (56). The least immunocompromised patients might be considered as an initial step. Candidates to immunization could include chronic granulomatous disease patients, transplant, leukemics, solid tumor at diagnosis, rheumatic or inflammatory bowel, and intensive care unit patients. Donors of hematopoietic stem cell transplants are also immunization candidates. As mentioned above, CD8 $^{+}$  T cells can be used in CD4-deficient hosts, and vaccines can be used aiming at stimulating the immune response, reducing immunosuppression, or acting synergistically with antifungal therapy.

### ***Candida albicans***

Invasive candidiasis is often associated with immunosuppression, prolonged antibiotic treatment, and anatomical lesions like surgery or venous catheter. A mortality of >30% is observed. Other clinical forms of candidiasis such as skin infections, oropharyngeal mucosa, and vaginal are most frequent but less severe. Knowledge of protective immune responses in candidiasis is thus a major aspect to be pursued in the field of systemic mycoses. Bär et al. used immunoproteomics to investigate natural T-cell epitopes of *Candida albicans*. The authors identified an MHC II-bound

peptide that is recognized by 1/4 of all *Candida albicans*-specific Th cells, a remarkably high frequency of interaction (71).

Four peptides were identified, with overlapping sequences, derived from a homologous region of the related adhesins Als1 and Als3. The longest of the three identified Als1/Als3-derived peptides (amino acid residues 236–253) was chosen for further analysis, referred to as pALS [sequences, indicating in bold the predicted MHC II-binding epitope: KGLNDWNYPV<sup>SSESFS(Y/T)</sup>]. The novel antigenic peptide of Bär et al. has an important role in fungal pathogenicity. It is functionally conserved in non-albicans *Candida* species, and most importantly, the epitope-specific T cells are not only murine but also human. Human memory Th cells responded to peptide stimulation, and vaccination of mice with the peptide elicited a T cell-dependent anti-candidiasis immune response (71). The pALS peptide of *Candida albicans*, carrying a promiscuous epitope, and eliciting a protective antifungal immune response, is functionally similar to *Paracoccidioides brasiliensis* P10, a peptide candidate of a vaccine against systemic paracoccidioidomycosis (see above section). pALS-specific T cells from the cervical lymph nodes of orally infected mice secreted IL-17A, but not IFN- $\gamma$  or IL-4 (71).

Another methodology was used by Wang et al. (72), who evaluated a hybrid phage as a potential vaccine candidate without adjuvant against *Candida albicans*. The ability of hybrid phage displaying epitope SLAQVKYTSASSI to induce an immune protective response was studied in a mouse model. Strong cellular and humoral immune responses were induced similar to recombinant rSap2 protein immunization. Protection against intravenous lethal challenge with *Candida albicans* was observed in BALB/c mice immunized with hybrid phage confirming its great potential as a vaccine inducing strong Th1 and Th17 response without adjuvant (72).

A vaccine that could be effective against *Candida albicans* and a variety of other human pathogenic fungi was proposed by Cassone and coworkers (73, 74), based on *Laminaria digitata*'s  $\beta$ -glucan (laminarin). To increase the immunogenicity of the glucan, it was conjugated with the diphtheria toxoid CRM197. The conjugate was protective against systemic and vaginal *Candida albicans* infections, by eliciting anti- $\beta$ -glucan antibodies, mainly IgG2b. These antibodies bound to and inhibited growth of both *Candida albicans* and *A. fumigatus* hyphae.

To understand the nature of the epitopes recognized by protective antibodies to these conjugates, studies were carried out with the following compounds, in addition to the laminarin-diphtheria toxoid (CRM197) conjugate, which was protective against fungal infections in mice (75): natural curdlan (Curd)-CRM197; linear 15-mer-CRM197 or 1,6-branched-17-mer-CRM197  $\beta$ -(1,3)-glucan-derived oligosaccharides. Anti- $\beta$ -(1,3)-glucan IgG antibodies were specifically raised by Curd-CRM197 and 15-mer-CRM197 oligosaccharide immunization. These antibodies protected mice against lethal infection by *Candida albicans*. Contrariwise, immunization with the 1,6-branched-17-mer CRM197 oligosaccharide elicited both anti- $\beta$ -(1,6) and anti- $\beta$ -(1,3) glucan IgG, which was not protective (75).

Conjugation of  $\beta$ -glucan to a carrier protein induces the production of antibodies that are protective against major fungal pathogens such as *Aspergillus* spp. and *Cryptococcus* spp., in

addition to *Candida* spp. Growth-inhibitory  $\beta$ -glucan-specific antibodies combined with a protein, such as Als3 or Hyr1, could enhance the magnitude of protective antibodies as well as reduce the chances of *Candida albicans* immune evasion (76). The importance of a multivalent vaccine in comparison with the univalent anti- $\beta$ -glucan-specific antibodies (42) was further evaluated by using mixed pALS with curdlan for protective immunization. Mice were challenged 3 weeks later i.v., with a high dose of *Candida albicans*. Immunization with curdlan alone was not sufficient for protection but the combination with pALS greatly increased the number of mice protected from fatal systemic candidiasis. The enhanced survival upon immunization with pALS plus curdlan correlated with the induction of pALS-specific IL-17A-producing CD4 $^{+}$  T cells. Data show therefore that pALS-specific Th17 lymphocytes do protect mice from candidiasis (71).

On Table 1, we summarize the linear peptides carrying epitopes potentially effective in antifungal vaccine development.

## PAN-FUNGAL VACCINES

Recent studies showed that attenuated *Blastomyces dermatitidis* conferred protective effects by T-cell recognition of an unknown but conserved antigen [reviewed in Ref. (42)]. Wüthrich et al. using transgenic CD4 $^{+}$  T cells identified an amino acid determinant within chaperone calnexin that is conserved across ascomycetes (77). Calnexin, an ER protein, localizes to the surface of yeast, hyphae, and spores (77). Infection with dimorphic or opportunistic fungi induces calnexin-specific CD4 $^{+}$  T cells (77). Vaccine of calnexin in glucan particles elicited calnexin-specific CD4 $^{+}$  T cells and resistance to infection by *B. dermatitidis*, *H. capsulatum*, *Pseudogymnoascus* (*Geomyces*) *destructans*, *Fonsecaea pedrosoi*, and *A. fumigatus* (77). Authors investigated regions of conserved sequences, which represent shared epitopes recognized by the 1807-T cell receptor. Using an algorithm that predicts six regions of overlapping peptide and a second algorithm developed by Marc Jenkins refined the analysis (77). Peptides of 13-mer were synthesized, representing 10 predicted epitopes, and they were tested for binding to the 1807-T cell receptor. The peptide #1 (LVVKNPAAHHAIS) activated naive 1807-T cells as measured by their reduced expression of CD62L, increased expression of CD44, and stimulated production of IFN- $\gamma$ . None of the other calnexin peptides induced IFN- $\gamma$  production by 1807-T cells (77). To investigate the biological relevance of peptide #1 in medically important fungi with conserved calnexin sequences, naïve 1807-T cells were transferred into mice before infection or vaccination with these fungi (77). One week later, activation of 1807 and endogenous Ag-specific CD4 $^{+}$  T cells using calnexin peptide-MHC class II tetramer were analyzed. *B. dermatitidis*, *A. fumigatus*, *H. capsulatum*, *Coccidioides posadasii*, *F. pedrosoi*, and *Pseudogymnoascus* (*Geomyces*) *destructans* expanded and activated 1807 and tetramer-positive CD4 $^{+}$  T cells *in vivo*. Fungi that did not trigger expansion of tetramer-positive CD4 $^{+}$  T cells included *Candida albicans*, *Cryptococcus neoformans*, and *Pneumocystis jiroveci*, and any tetramer-positive CD8 $^{+}$  T cells detected in vaccinated mice (77). Vaccination with calnexin formulated in glucan particles or Adjuplex induces protective immunity against lethal, pulmonary fungal infection with *B.*

**TABLE 1 | Linear peptide sequences with potential use as vaccine components.**

Fungi (reference)	Name of antigen and linear peptide sequence	Immune cell	Animal model delivery	Results adjuvancy
<i>Paracoccidioides brasiliensis</i> (38, 46, 52, 54)	P10 QTLLIAHTLAIKYAN	CD4+ Th1 cell	BALB/c mice/ CFA, alum, CL, flagellin, DC, DNA plasmid	Protection against i.t. challenge, reduction of fungal burden, efficacy of DNA vaccine
<i>Coccidioides</i> spp. (59)	Antigen 2 (Ag2)/Pra 1P6: TRLTDFKCHCSKPELPGQIT; 1P7: HCSKPELPGQITPCVVEACP; 1P12: PIDIPPVDTTAAPE-PSETAE; 1P13: TTAAPEPSETAEPTEAEPTEE; 1P15: PTEEPTAEPTEAEPTEAEPTHE; 1P16: PTAEPTAEPTHEPTEEPAV	CD4+ Th1 cell	C57BL/6 mice/ CpG ODN	Elicit T-cell response in mice immunized with rAg2/Pra; IFN- $\gamma$ ELISPOT
<i>Coccidioides</i> spp. (59)	PrP2 2P6: EKLTDfkCHCAkPELPGKIT; 2P13: DTRTPTQPPSTSPSAPQPTA; 2P14: PSTSPSAPQPTACI-PKRRRA	CD4+ Th1 cell	C57BL/6 mice/ CpG ODN	Elicit T-cell response in mice immunized with rPrP2; IFN- $\gamma$ ELISPOT
<i>Coccidioides</i> spp. (60)	Predicted T-cell epitopes Pep1 P1: MRNSILLAATVLLGCTSAKVHL; P2: HVRALGQKYFGSLPSSQQQT	CD4+ T cells	HLA-DR4 C57BL/6 mice/ CpG ODN	Elicit T-cell response in mice immunized with rEBV; IFN- $\gamma$ ELISPOT
<i>Coccidioides</i> spp. (60)	Predicted T-cell epitopes Amn1 P10: PAKVDVLLAQSLKLADVLKF; P11: NGLATTGTLVLEWTRLSDIT	CD4+ T cells	HLA-DR4 C57BL/6 mice/ CpG ODN	Elicit T-cell response in mice immunized with rEBV; IFN- $\gamma$ ELISPOT
<i>Coccidioides</i> spp. (60)	Predicted T-cell epitopes phospholipidase B (Plb) P6: TPLVYYIPNYPYTTWSNIST	None	HLA-DR4 C57BL/6 mice/ CpG ODN	Failed to elicit T-cell response from mice immunized with rEBV; IFN- $\gamma$ ELISPOT
<i>Coccidioides</i> spp. (60)	Recombinant epitope-based vaccine rEBV Include the five selected epitope peptides (Pep1, Amn1 and Plb), N-terminal leader peptides and glycine/proline spacer sequences (CPGPG)	CD4+ Th1, Th2 and Th17 cells	HLA-DR4 C57BL/6 mice/ CpG ODN or GPs plus OVA complex	(a) <i>In vitro</i> T-cell response in mice immunized with rEBV; IFN- $\gamma$ ELISPOT. (b) rEBV + CpG ODN and i.n. challenge: reduction of lung CFU but not significant survival. (c) rEBV + GPs: 10-fold-higher T-cell response with Pep1-P1 and significant enhanced survival.
<i>Histoplasma capsulatum</i> (64)	CDR3 fragment DGGQQG	V $\beta$ 8.1/8.2+ T cells	C57BL/6 and athymic nude mice/ TCR $\alpha/\beta^{-/-}$ and IFN- $\gamma^{-/-}$ mice	(a) rHsp60 or fragment 3 (F3) confers protection after i.n. challenge. (b) Depletion of V $\beta$ 8.1/8.2+ T cells from immunized rHsp60 mice abolish the protection to lethal and sublethal challenges.
<i>Aspergillus</i> spp. (68, 78)	Asp f3 B12: PGAFTPVCAR, C3: HVPEYIEKLPEIR	T cell	CF-1 mice/ TiterMax	(a) rASP f3 confer protection to corticosteroid immunosuppressed CF-1 mice against i.n. infection with conidia. (b) T-cell proliferation to rAsp f3 variants and trypsin-derived peptides (B12 and C3) in immunized CF-1 mice.
<i>Aspergillus</i> spp. (68, 70)	Asp f3 P4: VCSARHVPEYIEKLPEIRAK; P5: EIRAKGVDVAVLAYNDAYVCSAR	B and T cells	CF-1 mice/ TiterMax	(a) CD4+ T cells are required for rAsp f3 vaccine protection. (b) Proliferation of T cells from rAsp f3-vaccinated mice and tested by luminometric ATP cell titer quantification in positively selected T cells after stimulation. (c) P4: VCSARHVPEYIEKLPEIRAK IgG titers were elevated only in the surviving vaccinated and <i>Aspergillus fumigatus</i> challenged mice.
<i>Candida albicans</i> (71)	pALS (ALS1, ALS3) KGLND <b>WNYPVSSESFS(Y)T</b>	CD4+ Th17 cell	C57BL/6 and JHT mice/IFA mixed with curdlan or CpG	(a) Peptide-loaded MHCI complex from DC1940 cells isolated and sequenced by liquid chromatography coupled to MS/MS. (b) Mice immunized with pALS mixed with IFA plus curdlan and i.v. infected with <i>Candida albicans</i> protected from fatal systemic disease. (c) pALS is recognized by human memory T cells.

(Continued)

**TABLE 1 | Continued**

Fungi (reference)	Name of antigen and linear peptide sequence	Immune cell	Animal model delivery adjuvancy	Results
<i>Candida albicans</i> (72)	Hybrid phage displaying epitope SLAQVKYTSASSI Recombinant Sap2 (rSap2)	B and T cells	BALB/c mice/ TE buffer or CFA	(a) Decreased colonization of <i>Candida albicans</i> in kidneys and spleens from mice immunized with hybrid phage (TE) or rSap2 (CFA). (b) Mice immunized with hybrid phage (TE) or rSap2 (CFA) prolong survival against <i>Candida albicans</i> infection.
Pan fungal (77)	Calnexin peptide #1 LVVKNPAAHHAIS Recombinant calnexin (rCalnexin)	CD4 <sup>+</sup> Th1 and Th17 cells	C57BL/6/ GP-MSA and yeast RNA; LPS	(a) Calnexin (ER protein) has <i>Blastomyces dermatitidis</i> , <i>H. capsulatum</i> , <i>Coccidioides posadasii</i> , and <i>Paracoccidioides brasiliensis</i> conserved regions. (b) Immunized mice with rCalnexin formulated in GP reduced lung and spleen CFU in mice infected with <i>B. dermatitidis</i> or <i>Coccidioides posadasii</i> and prolonged survival. (c) Soluble calnexin peptide #1 plus LPS delivery by i.v. route improved expansion of calnexin-specific T cells.

CFA, complete Freund adjuvant; IFA, incomplete Freund adjuvant; CL, cationic lipid; DC, dendritic cells; CpG ODN, synthetic oligodeoxynucleotide containing unmethylated CpG dinucleotides; i.t., intratracheal; i.n., intranasal; i.v., intravenous; rEBV, bacterium-expressed recombinant epitope-based vaccine; GPs, yeast cell wall-derived glucan particles; GMP, glucan mannan particles; CFU, colony forming unit; OVA, chicken ovalbumin; MSA, mouse serum albumin.

*dermatitidis* and *Coccidioides posadasii*. Fungal burdens were reduced 10-fold in lung and spleen samples (77).

## FINAL REMARKS

Albeit most single- or pan-antifungal vaccine in development focus on protein/peptide, live-attenuated fungi, immune stimulatory adjuvants, antigens presented by DCs, combination of polysaccharide with protein where polysaccharide acts as a carrier or as a mixing adjuvant, and on passive immunotherapy, the synthesis of linear oligosaccharides of β-glucan becomes also an alternative to a pan-fungal vaccine.

Liao et al. (78) developed a series of synthetic β-glucan oligosaccharides coupled to keyhole limpet hemocyanin (KLH) to generate glycoconjugates that contained structurally well-defined carbohydrate antigens. The authors have demonstrated, using a mouse model, that the conjugate of KLH and octa-β-glucan can elicit protective immune responses against *Candida albicans* (78).

Although short peptides carrying epitopes mediating immune responses may display remarkable activities, even acting as

antigens and immunomodulatory molecules, it seems that multivalent vaccines may be superior to univalent ones, thus supporting Cassone's views on *Candida albicans* vaccines (76). Development of an immune response against "multiple unrelated virulence traits" will probably be "a better approach."

## AUTHOR CONTRIBUTIONS

LT and CT wrote and revised the paper.

## ACKNOWLEDGMENTS

The authors acknowledge Leandro B. Roque da Silva, University of São Paulo, for picture support.

## FUNDING

This work was supported by FAPESP (2016/08730-6, 2010/51423-0) and CAPES. LT and CT are research fellows of the CNPq.

## REFERENCES

- Souza ACO, Taborda CP. Epidemiology of dimorphic fungi. In: *Reference Module in Life Sciences*. Elsevier (2017). doi:10.1016/B978-0-12-809633-8.12056-4
- Coelho C, Casadevall A. Cryptococcal therapies and drug targets: the old, the new and the promising. *Cell Microbiol* (2016) 18:792–9. doi:10.1111/cmi.12590
- Cassone A, Cauda R. *Candida* and candidiasis in HIV-infected patients: where commensalism, opportunistic behavior and frank pathogenicity lose their borders. *AIDS* (2012) 26:1457–72. doi:10.1097/QAD.0b013e3283536ba8
- Al-Bader N, Sheppard DC. Aspergillosis and stem cell transplantation: an overview of experimental pathogenesis studies. *Virulence* (2016) 7:950–66. doi:10.1080/21505594.2016.1231278
- Datta K, Hamad M. Immunotherapy of fungal infections. *Immunol Invest* (2015) 44:738–76. doi:10.3109/08820139.2015.1093913
- Brown GD, Denning DW, Gow NAR, Levitz SM, Netea MG, White TC. Hidden killers: human fungal infections. *Sci Transl Med* (2012) 4:1–9. doi:10.1126/scitranslmed.3004404
- Agarwal AK, Tripathi SK, Xu T, Jacob MR, Li XC, Clark AM. Exploring the molecular basis of antifungal synergies using genome-wide approaches. *Front Microbiol* (2012) 3:115. doi:10.3389/fmicb.2012.00115
- Bocca AL, Amaral AC, Teixeira MM, Sato PK, Sato P, Shikanai-Yasuda MA, et al. Paracoccidioidomycosis: eco-epidemiology, taxonomy and clinical and therapeutic issues. *Future Microbiol* (2013) 8:1177–91. doi:10.2217/fmb.13.68
- de Oliveira HC, da Silva JF, Scorzoni L, Marcos CM, Rossi SA, de Paula e Silva ACA, et al. Importance of adhesins in virulence of *Paracoccidioides* spp. *Front Microbiol* (2015) 6:303. doi:10.3389/fmicb.2015.00303
- Da Silva MB, Marques AF, Nosanchuk JD, Casadevall A, Travassos LR, Taborda CP. Melanin in the dimorphic fungal pathogen *Paracoccidioides brasiliensis*: effects on phagocytosis, intracellular resistance and drug susceptibility. *Microbes Infect* (2006) 8:197–205. doi:10.1016/j.micinf.2005.06.018
- Taff HT, Mitchell KF, Edward JA, Andes DR. Mechanisms of *Candida* biofilm drug resistance. *Future Microbiol* (2013) 8:1325–37. doi:10.2217/fmb.13.101
- Liu X, Wang D, Yu C, Li T, Liu J, Sun S. Potential antifungal targets against a *Candida* biofilm based on an enzyme in the arachidonic acid cascade – a review. *Front Microbiol* (2016) 7:1925. doi:10.3389/fmicb.2016.01925

13. Prasad R, Rawal MK. Efflux pump proteins in antifungal resistance. *Front Pharmacol* (2014) 5:202. doi:10.3389/fphar.2014.00202
14. Martins CVB, Da Silva DL, Neres ATM, Magalhães TFF, Watanabe GA, Modolo LV, et al. Curcumin as a promising antifungal of clinical interest. *J Antimicrob Chemother* (2009) 63:337–9. doi:10.1093/jac/dkn488
15. Neelofar K, Shreaz S, Rimple B, Muralidhar S, Nikhat M, Khan LA. Curcumin as a promising anticandidal of clinical interest. *Can J Microbiol* (2011) 57:204–10. doi:10.1093/jac/dkn488
16. Thomaz L, Apitz-Castro R, Marques AF, Travassos LR, Taborda CP. Experimental paracoccidioidomycosis: alternative therapy with ajoene, compound from *Allium sativum*, associated with sulfamethoxazole/trimethoprim. *Med Mycol* (2008) 46:113–8. doi:10.1080/13693780701651681
17. Davis SR, Perrie R, Apitz-Castro R. The in vitro susceptibility of *Scedosporium prolificans* to ajoene, allitridium and a raw extract of garlic (*Allium sativum*). *J Antimicrob Chemother* (2003) 51:593–7. doi:10.1093/jac/dkg144
18. Ledezma E, López JC, Marin P, Romero H, Ferrara G, De Sousa L, et al. Ajoene in the topical short-term treatment of tinea cruris and tinea corporis in humans. Randomized comparative study with terbinafine. *Arzneimittelforschung* (1999) 49:544–7. doi:10.1055/s-0031-1300459
19. Goughenour KD, Rapple CA. Antifungal therapeutics for dimorphic fungal pathogens. *Virulence* (2016) 19:1–11. doi:10.1080/21505594.2016.1235653
20. Dos Santos ALS. HIV aspartyl protease inhibitors as promising compounds against *Candida albicans* André Luis Souza dos Santos. *World J Biol Chem* (2010) 1:21–30. doi:10.4331/wjbc.v1.i2.21
21. Marcos CM, de Oliveira HC, de Melo WC, da Silva JE, Assato PA, Scorzoni L, et al. Anti-immune strategies of pathogenic fungi. *Front Cell Infect Microbiol* (2016) 6:142. doi:10.3389/fcimb.2016.00142
22. Romani L. Immunity to fungal infections. *Nat Rev Immunol* (2011) 11:275–88. doi:10.1038/nri2939
23. Travassos LR, Rodrigues EG, Iwai LK, Taborda CP. Attempts at a peptide vaccine against paracoccidioidomycosis, adjuvant to chemotherapy. *Mycopathologia* (2008) 165:341–52. doi:10.1007/s11046-007-9056-1
24. Loures FV, Araújo EF, Feriotti C, Bazar SB, Calich VLG. TLR-4 cooperates with dectin-1 and mannose receptor to expand Th17 and Tc17 cells induced by *Paracoccidioides brasiliensis* stimulated dendritic cells. *Front Microbiol* (2015) 6:261. doi:10.3389/fmicb.2015.00261
25. Rathore JS, Wang Y. Protective role of Th17 cells in pulmonary infection. *Vaccine* (2016) 34:1504–14. doi:10.1016/j.vaccine.2016.02.021
26. Casadevall A, Pirofski LA. Immunoglobulins in defense, pathogenesis, and therapy of fungal diseases. *Cell Host Microbe* (2012) 11:447–56. doi:10.1016/j.chom.2012.04.004
27. Dromer F, Salamero J, Contrepois A, Carbon C, Yeni P. Production, characterization, and antibody specificity of a mouse monoclonal antibody reactive with *Cryptococcus neoformans* capsular polysaccharide. *Infect Immun* (1987) 55:742–8.
28. Puccia R, Schenkman S, Gorin PAJ, Travassos LR. Exacellular components of *Paracoccidioides brasiliensis*: identification of a specific antigen. *Infect Immun* (1986) 53:199–206.
29. Travassos LR, Goldman G, Taborda CP, Puccia R. Insights in *Paracoccidioides brasiliensis* pathogenicity. In: Kavanagh K, editor. *New Insights in Medical Mycology*. Netherlands: Springer (2007). p. 241–65.
30. Puccia R, Travassos LR. The 43-kDa glycoprotein from the human pathogen *Paracoccidioides brasiliensis* and its deglycosylated form: excretion and susceptibility to proteolysis. *Arch Biochem Biophys* (1991) 289:298–302. doi:10.1016/0003-9861(91)90475-X
31. Buijsse-Filho R, Puccia R, Marques AF, Pinto FA, Muñoz JE, Nosanchuk JD, et al. The monoclonal antibody against the major diagnostic antigen of *Paracoccidioides brasiliensis* mediates immune protection in infected BALB/c mice challenged intratracheally with the fungus. *Infect Immun* (2008) 76:3321–8. doi:10.1128/IAI.00349-08
32. Arantes TD, Bagagli E, Nino-Vega G, San-Blas G, Theodoro RC. *Paracoccidioides brasiliensis* and *Paracoccidioides lutzii*, a secret love affair. *Rev Inst Med Trop Sao Paulo* (2015) 57:25–30. doi:10.1590/S0036-46652015000700006
33. Batista J, De Camargo ZP, Fernandes GF, Vicentini AP, Fontes CJF, Hahn RC. Is the geographical origin of a *Paracoccidioides brasiliensis* isolate important for antigen production for regional diagnosis of paracoccidioidomycosis? *Mycoses* (2010) 53:176–80. doi:10.1111/j.1439-0507.2008.01687.x
34. Cisalpino PS, Puccia R, Yamauchi LM, Cano MIN, Da Silveira JF, Travassos LR. Cloning, characterization, and epitope expression of the major diagnostic antigen of *Paracoccidioides brasiliensis*. *J Biol Chem* (1996) 271:4553–60. doi:10.1074/jbc.271.8.4553
35. Rodrigues EG, Travassos LR. Nature of the reactive epitopes in *Paracoccidioides brasiliensis* polysaccharide antigen. *J Med Vet Mycol* (1994) 32:77–81. doi:10.1080/02681219480000111
36. Sarava ECO, Altermani A, Franco MF, Unterkircher CS, Camargo ZP. *Paracoccidioides brasiliensis*-gp43 used as paracoccidioidin. *J Med Vet Mycol* (1996) 34:155–61. doi:10.1080/02681219680000261
37. Sette A, Buus S, Appella E, Smith JA, Chesnut R, Miles C, et al. Prediction of major histocompatibility complex binding regions of protein antigens by sequence pattern analysis. *Proc Natl Acad Sci U S A* (1989) 86:3296–300. doi:10.1073/pnas.86.9.3296
38. Taborda CP, Juliano MA, Puccia R, Franco M, Travassos LR. Mapping of the T-cell epitope in the major 43-kilodalton glycoprotein of *Paracoccidioides brasiliensis* which induces a Th-1 response protective against fungal infection in BALB/c mice. *Infect Immun* (1998) 66:786–93.
39. Morais FV, Barros TF, Fukada MK, Cisalpino PS, Puccia R. Polymorphism in the gene coding for the immunodominant antigen gp43 from the pathogenic fungus *Paracoccidioides brasiliensis*. *J Clin Microbiol* (2000) 38:3960–6.
40. Travassos LR, Taborda CP, Iwai LK, Cunha-Neto E, Puccia R. The gp43 from *Paracoccidioides brasiliensis*: a major diagnostic antigen and vaccine candidate. In: Domer GS, Kobayashi JE, editors. *The Mycota XII, Human Fungal Pathogens*. Berlin, Heidelberg: Springer-Verlag (2004). p. 279–96.
41. Brummer E, Hanson LH, Restrepo A, Stevens DA. In vivo and *in vitro* activation of pulmonary macrophages by IFN-gamma for enhanced killing of *Paracoccidioides brasiliensis* or *Blastomyces dermatitidis*. *J Immunol* (1988) 140:2786–9.
42. Iwai LK, Yoshida M, Sidney J, Shikanai-Yasuda MA, Goldberg AC, Juliano MA, et al. In silico prediction of peptides binding to multiple HLA-DR molecules accurately identifies immunodominant epitopes from gp43 of *Paracoccidioides brasiliensis* frequently recognized in primary peripheral blood mononuclear cell responses from sensitized individuals. *Mol Med* (2003) 9:209–19.
43. Meleno RH, Langeveld JP, Schaaper WM, Slootstra JW. Synthetic peptide vaccines: unexpected fulfillment of discarded hope? *Biologics* (2001) 29:233–6. doi:10.1006/biol.2001.0298
44. Alexander J, Oseroff C, Dahlberg C, Qin M, Ishioka G, Beebe M, et al. A decaepitope polypeptide primes for multiple CD8+ IFN-gamma and Th lymphocyte responses: evaluation of multiepitope polypeptides as a mode for vaccine delivery. *J Immunol* (2002) 168:6189–98. doi:10.4049/jimmunol.168.12.6189
45. Travassos LR, Rittner GMG, Taborda C. Paracoccidioidomycosis: advance towards a molecular vaccine. In: Giese M, editor. *Molecular Vaccines*. Wien: Springer-Verlag (2013). p. 257–68. doi:10.1007/978-3-7091-1419-3\_14
46. Mayorga O, Muñoz JE, Lincopan N, Teixeira AF, Ferreira LCS, Travassos LR, et al. The role of adjuvants in therapeutic protection against paracoccidioidomycosis after immunization with the P10 peptide. *Front Microbiol* (2012) 3:154. doi:10.3389/fmicb.2012.00154
47. Muñoz JE, Luft VD, Amorim J, Magalhães A, Thomaz L, Nosanchuk JD, et al. Immunization with P10 peptide increases specific immunity and protects immunosuppressed BALB/c mice infected with virulent yeasts of *Paracoccidioides brasiliensis*. *Mycopathologia* (2014) 178:177–88. doi:10.1007/s11046-014-9801-1
48. Nanjappa SG, Klein BS. Vaccine immunity against fungal infections. *Curr Opin Immunol* (2014) 28:27–33. doi:10.1016/j.coi.2014.01.014
49. Massaoka MH, Matsuo AL, Figueiredo CR, Girola N, Farias CF, Pasqualoto K, et al. A subtraction tolerization method of immunization allowed for Wilms' tumor protein-1 (WT1) identification in melanoma and discovery of an anti-tumor peptide sequence. *J Immunol Methods* (2014) 414:11–9. doi:10.1016/j.jim.2014.08.003
50. Figueiredo CR, Matsuo AL, Azevedo RA, Massaoka MH, Girola N, Polonelli L, et al. A novel microtubule de-stabilizing complementarity-determining region C36L1 peptide displays antitumor activity against melanoma *in vitro* and *in vivo*. *Sci Rep* (2015) 5:14310. doi:10.1038/srep14310
51. de Melo FM, Braga CJ, Pereira FV, Maricato JT, Origassa CS, Souza MF, et al. Anti-metastatic immunotherapy based on mucosal administration of flagellin and immunomodulatory P10. *Immunol Cell Biol* (2015) 93:86–98. doi:10.1038/icb.2014.74
52. Magalhães A, Ferreira KS, Almeida SR, Nosanchuk JD, Travassos LR, Taborda CP. Prophylactic and therapeutic vaccination using dendritic cells primed with

- peptide 10 derived from the 43-kilodalton glycoprotein of *Paracoccidioides brasiliensis*. *Clin Vaccine Immunol* (2012) 19:23–9. doi:10.1128/CVI.05414-11
53. Pinto AR, Puccia R, Diniz SN, Franco MF, Travassos LR. DNA-based vaccination against murine paracoccidioidomycosis using the gp43 gene from *Paracoccidioides brasiliensis*. *Vaccine* (2000) 18:3050–8. doi:10.1016/S0264-410X(00)00074-8
54. Rittner GMG, Muñoz JE, Marques AF, Nosanchuk JD, Taborda CP, Travassos LR. Therapeutic DNA vaccine encoding peptide P10 against experimental paracoccidioidomycosis. *PLoS Negl Trop Dis* (2012) 6:e1519. doi:10.1371/journal.pntd.0001519
55. Yoon HJ, Clemons KV. Vaccines against *Coccidioides*. *Korean J Intern Med* (2013) 28:403–7. doi:10.3904/kjim.2013.28.4.403
56. Stevens DA, Clemons KV, Liu M. Developing a vaccine against aspergillosis. *Med Mycol* (2011) 49(Suppl 1):S170–6. doi:10.3109/13693786.2010.497775
57. Benard G. An overview of the immunopathology of human paracoccidioidomycosis. *Mycopathologia* (2008) 165:209–21. doi:10.1007/s11046-007-9065-0
58. Cox RA, Magee DM. Coccidioidomycosis: host response and vaccine development. *Clin Microbiol Rev* (2004) 17:804–39. doi:10.1128/CMR.17.4.804-839.2004
59. Herr RA, Hung CY, Cole GT. Evaluation of two homologous proline-rich proteins of *Coccidioides posadasii* as candidate vaccines against coccidioidomycosis. *Infect Immun* (2007) 75:5777–87. doi:10.1128/IAI.00807-07
60. Hurtgen BJ, Hung CY, Ostroff GR, Levitz SM, Cole GT. Construction and evaluation of a novel recombinant T cell epitope-based vaccine against coccidioidomycosis. *Infect Immun* (2012) 80:3960–74. doi:10.1128/IAI.00566-12
61. Cole GT, Hung CY, Sanderson SD, Hurtgen BJ, Wüthrich M, Klein BS, et al. Novel strategies to enhance vaccine immunity against coccidioidomycosis. *PLoS Pathog* (2013) 9:e1003768. doi:10.1371/journal.ppat.1003768
62. Hung CY, Hurtgen BJ, Bellecourt M, Sanderson SD, Morgan EL, Cole GT. An agonist of human complement fragment C5a enhances vaccine immunity against *Coccidioides* infection. *Vaccine* (2012) 30:4681–90. doi:10.1016/j.vaccine.2012.04.084
63. Deepe GS Jr, Gibbons R, Brunner GD, Gomez FJ. A protective domain of heat-shock protein 60 from *Histoplasma capsulatum*. *J Infect Dis* (1996) 174:828–34. doi:10.1093/infdis/174.4.828
64. Scheckelhoff M, Deepe GS. The protective immune response to heat shock protein 60 of *Histoplasma capsulatum* is mediated by a subset of V $\beta$ 8.1/8.2+ T cells. *J Immunol* (2002) 169:5818–26. doi:10.4049/jimmunol.169.10.5818
65. Allendörfer R, Brunner GD, Deepe GS Jr. Complex requirements for nascent and memory immunity in pulmonary histoplasmosis. *J Immunol* (1999) 162:7389–96.
66. Horwath MC, Fecher RA, Deepe GS Jr. *Histoplasma capsulatum*, lung infection and immunity. *Future Microbiol* (2015) 10:967–75. doi:10.2217/fmb.15.25
67. Wüthrich M, Filutowicz HI, Warner T, Deepe GS, Klein BS. Vaccine immunity to pathogenic fungi overcomes the requirement for CD4 help in exogenous antigen presentation to CD8+ T cells: implications for vaccine development in immune-deficient hosts. *J Exp Med* (2003) 197:1405–16. doi:10.1084/jem.20030109
68. Ito JI, Lyons JM, Diaz-arevalo D, Hong TB, Kalkum M. Vaccine progress. *Med Mycol* (2009) 47:394–400. doi:10.1080/13693780802552614
69. Diaz-Arevalo D, Ito JI, Kalkum M. Protective effector cells of the recombinant Asp f3 anti-aspergillosis vaccine. *Front Microbiol* (2012) 3:299. doi:10.3389/fmich.2012.00299
70. Diaz-Arevalo D, Bagramyan K, Hong TB, Ito JI, Kalkum M. CD4+ T cells mediate the protective effect of the recombinant asp f3-based anti-aspergillosis vaccine. *Infect Immun* (2011) 79:2257–66. doi:10.1128/IAI.01311-10
71. Bär E, Gladiatov A, Bastidas S, Roschitzki B, Acha-Orbea H, Oxenius A, et al. A novel Th cell epitope of *Candida albicans* mediates protection from fungal infection. *J Immunol* (2012) 188:5636–43. doi:10.4049/jimmunol.1200594
72. Wang Y, Su Q, Dong S, Shi H, Gao X, Wang L. Hybrid phage displaying SLAQVKYTSASSI induces protection against *Candida albicans* challenge in BALB/c mice. *Hum Vaccin Immunother* (2014) 10:1057–63. doi:10.4161/hv.27714
73. Torosantucci A, Bromuro C, Chiani P, De Bernardis F, Berti F, Galli C, et al. A novel glyco-conjugate vaccine against fungal pathogens. *J Exp Med* (2005) 202:597–606. doi:10.1084/jem.20050749
74. Cassone A, Torosantucci A. Opportunistic fungi and fungal infections: the challenge of a single, general antifungal vaccine. *Expert Rev Vaccines* (2006) 5:859–67. doi:10.1586/14760584.5.6.859
75. Bromuro C, Romano M, Chiani P, Berti F, Tortini M, Proietti D, et al. Beta-glucan-CRM197 conjugates as candidates antifungal vaccines. *Vaccine* (2010) 28:2615–23. doi:10.1016/j.vaccine.2010.01.012
76. Cassone A. Development of vaccines for *Candida albicans*: fighting a skilled transformer. *Nat Rev Microbiol* (2013) 11:884–91. doi:10.1038/nrmicro3156
77. Wüthrich M, Brandhorst TT, Sullivan TD, Filutowicz H, Sterkel A, Stewart D, et al. Calnexin induces expansion of antigen-specific CD4+ T cells that confer immunity to fungal ascomycetes via conserved epitopes. *Cell Host Microbe* (2015) 17:452–65. doi:10.1016/j.chom.2015.02.009
78. Liao G, Zhou Z, Burgula S, Liao J, Yuan C, Wu Q, et al. Synthesis and immunological studies of linear oligosaccharides of  $\beta$ -glucan as antigens for anti-fungal vaccine development. *Bioconjug Chem* (2015) 26:466–76. doi:10.1021/bc500575a

**Conflict of Interest Statement:** The authors declare that the research was conducted in the absence of any commercial or financial relationships that could be construed as a potential conflict of interest.

Copyright © 2017 Travassos and Taborda. This is an open-access article distributed under the terms of the Creative Commons Attribution License (CC BY). The use, distribution or reproduction in other forums is permitted, provided the original author(s) or licensor are credited and that the original publication in this journal is cited, in accordance with accepted academic practice. No use, distribution or reproduction is permitted which does not comply with these terms.



# The Immune Epitope Database and Analysis Resource in Epitope Discovery and Synthetic Vaccine Design

**Ward Fleri\***, **Sinu Paul**, **Sandeep Kumar Dhanda**, **Swapnil Mahajan**, **Xiaojun Xu**,  
**Bjoern Peters** and **Alessandro Sette**

Division of Vaccine Discovery, La Jolla Institute for Allergy and Immunology, La Jolla, CA, USA

## OPEN ACCESS

### Edited by:

Clarisa B. Palatnik-de-Sousa,  
Federal University of Rio de Janeiro,  
Brazil

### Reviewed by:

Daniel Olive,  
Institut national de la santé et de la  
recherche médicale (INSERM),  
France  
Arun Kumar,  
Health Sciences North, Canada

### \*Correspondence:

Ward Fleri  
wflier@lji.org

### Specialty section:

This article was submitted to  
Vaccines and Molecular  
Therapeutics,  
a section of the journal  
Frontiers in Immunology

**Received:** 22 December 2016

**Accepted:** 27 February 2017

**Published:** 14 March 2017

### Citation:

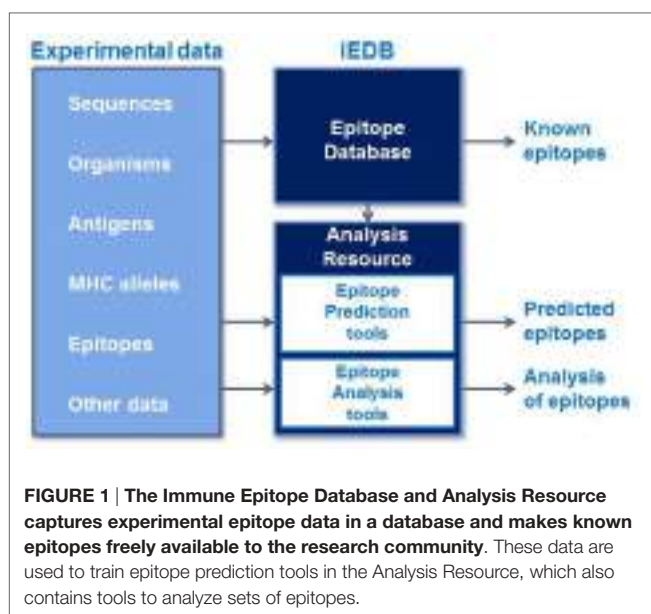
Fleri W, Paul S, Dhanda SK, Mahajan S, Xu X, Peters B and Sette A (2017) The Immune Epitope Database and Analysis Resource in Epitope Discovery and Synthetic Vaccine Design. *Front. Immunol.* 8:278.  
doi: 10.3389/fimmu.2017.00278

The task of epitope discovery and vaccine design is increasingly reliant on bioinformatics analytic tools and access to depositories of curated data relevant to immune reactions and specific pathogens. The Immune Epitope Database and Analysis Resource (IEDB) was indeed created to assist biomedical researchers in the development of new vaccines, diagnostics, and therapeutics. The Analysis Resource is freely available to all researchers and provides access to a variety of epitope analysis and prediction tools. The tools include validated and benchmarked methods to predict MHC class I and class II binding. The predictions from these tools can be combined with tools predicting antigen processing, TCR recognition, and B cell epitope prediction. In addition, the resource contains a variety of secondary analysis tools that allow the researcher to calculate epitope conservation, population coverage, and other relevant analytic variables. The researcher involved in vaccine design and epitope discovery will also be interested in accessing experimental published data, relevant to the specific indication of interest. The database component of the IEDB contains a vast amount of experimentally derived epitope data that can be queried through a flexible user interface. The IEDB is linked to other pathogen-specific and immunological database resources.

**Keywords:** epitope, prediction, T cell, antibody, vaccines, MHC class I, MHC class II, immunogenicity

## INTRODUCTION

The Immune Epitope Database and Analysis Resource (IEDB) is a freely available resource that contains an extensive collection of experimentally measured immune epitopes and a suite of tools for predicting and analyzing epitopes (Figure 1). The IEDB includes antibody and T cell epitopes for infectious diseases, allergens, autoimmune diseases, and transplant/alloantigens studied in humans, non-human primates, mice, and other animal species. Life science researchers can use the IEDB to develop new vaccines, diagnostics, and therapeutics. The database is populated using information captured or curated from peer-reviewed scientific literature and from data submitted by researchers. As of December 2016, over 18,000 references have been curated, and the database contains over 260,000 epitopes and over 1,200,000 B cell, T cell, MHC binding, and MHC ligand elution assays (positive and negative). Because the database is continually being updated with new literature and data submissions, the IEDB provides researchers designing vaccines with a comprehensive collection



of experimental data in a single data repository that can be used to query for known epitopes and their immunogenic responses.

The tools in the Analysis Resource<sup>1</sup> (1, 2) fall into two general categories: prediction and analysis tools. Prediction tools predict the outcome of experiments, such as MHC class I or class II binding, MHC class I processing and immunogenicity, and for predicting linear and discontinuous (conformational) B cell epitopes. The epitope prediction tools are valuable resources for vaccine developers when experimentally measured epitopes are not available in the IEDB. In this review, we briefly describe the basic principles of machine learning algorithms, on which the prediction tools are based, and some basic principles of tool evaluation. Next, we describe the MHC class I and class II binding prediction tools hosted in the analysis resource.

The tools for class I cover a broad range of alleles, including 83 human, 8 chimpanzee, 18 macaque, and other non-primates. The accuracy of these predictions is very high, with AUC values greater than 0.9. For MHC class II binding, the breadth of allele data is less extensive, involving 24 human alleles and 3 mouse alleles. There are also pan predictions that extrapolate from these alleles to predict binding for other alleles. The class II binding predictions are being retrained with new data as of the end of 2016. The accuracy of class II binding predictions has improved significantly over the past 10 years, from AUC of 0.76 to 0.87, but it is lower than class I. Subsequently, we describe T cell processing predictions which combine MHC binding with other parts of the MHC class I cellular pathway, namely proteasomal cleavage and TAP transport, generated from independent experimental datasets. There are also predictors trained on eluted MHC ligands that provide an overlay of the signals from MHC binding and MHC processing presentation pathway. The processing prediction tools offer a relatively small but statistically significant

increase in accuracy compared to using the MHC binding prediction alone.

The Analysis Resource includes several B cell epitope prediction tools, based on a number of classical approaches such as hydrophilicity scales or amino acid properties, independently developed by different authors and reimplemented in the Analysis Resource. There are also predictors based on machine learning and structure-based approaches. The accuracy of B cell epitope prediction tools is generally rather poor, having AUC values ranging from 0.6 to 0.7. Finally, we will describe analysis tools. The analysis tools enable users to analyze known epitope sequences, assembled either from IEDB queries or other sources. These tools include epitope conservancy analysis, population coverage, and epitope clustering.

In the general categories of analysis tools, there are tools with which users can estimate the fraction of individuals expected to respond to a given set of peptides with the Population Coverage tool, calculate conservancy of a peptide within a protein, and cluster peptides based on sequence identity. The Population Coverage tool gives vaccine designers insight to the efficacy of their vaccine to regional and global populations, while the conservancy analysis tool identifies regions of a protein or antigen that are conserved and are potential targets for vaccines.

## MACHINE LEARNING AND EVALUATING PREDICTION QUALITY

MHC binding experiments measure the affinity between an MHC and isolated peptides, usually expressed as IC<sub>50</sub> concentration with low IC<sub>50</sub> value implying a high affinity binder (3). Because even a small virus can result in tens of thousands of peptide fragments as a result of processing by a cell's MHC class I pathway, experimentalist can rarely afford to measure each of them. Machine learning approaches can develop a function that predicts affinity binding for a given peptide sequence (4, 5). Artificial neural networks (ANNs), support vector machines, linear programming, and hidden Markov models (HMMs) find this function and differ primarily in how they define "find," their respective function spaces, and how they measure affinity binding. The calculation of a scoring matrix offers a relatively simple example. With a scoring matrix, the binding affinity for the sequence is computed based on the amino acid and its position in the binding groove. The values for each residue in the sequence are summed to yield the overall binding for the entire sequence. The position-specific scoring matrix is derived by varying the values of the matrix until the sums for known, measured peptides approximate the measured affinities. To evaluate how well this function works for predicting MHC class I peptide binding, objective methods to evaluate prediction quality are necessary.

Peptide binding datasets, far larger than any previously assembled, were originally compiled in 2006 (6). The dataset covered 48 MHC class I alleles from 88 different datasets with a variety of peptide lengths with a total of 50,000 IC<sub>50</sub> values. This collection allowed the IEDB team to perform a thorough comparison of different prediction algorithms, including a number of publicly available prediction websites, such as SYFPEITHI (7) and BIMAS

<sup>1</sup><http://tools.iedb.org>.

(8), and computed the correlation between the measured IC<sub>50</sub> values and each algorithm's predicted score, be it a heuristic score as for SYFPEITHI or a half-life of binding score as for BIMAS. To evaluate performance, given the different predicted scoring systems of the algorithms, we reformulated the problem in terms of predicting which peptides bind with an IC<sub>50</sub> value less than 500 nM, an established threshold associated with immunogenicity for 80–90% of all epitopes.

This allowed computing the number of true negatives, true positives, false negatives, and false positives. By systematically varying the predicted score threshold from low to high, one can calculate the rate of true positives and false positives as a function of the threshold to derive an ROC curve. The area under this ROC curve is the AUC value and that has a number of important statistical properties (9). It is independent of the predicted scale because it compares the rank of your matrices and it is independent of the composition of the dataset, such as having different proportions of binders and non-binders. The AUC value is essentially capturing the probability that given two peptides, one a binder and the other a non-binder, the predicted score will be higher for the binder compared to the non-binder. An AUC value of 0.5 is equivalent to a random prediction and a value of 1.0 is equivalent to a perfect prediction.

In evaluating the different web server predictors, we discovered that it was difficult to separate the performance of the algorithms from the datasets used to train them. To correct for this effect, we used a cross-validation approach, where the dataset is split into five subsets. The algorithm is then trained on the data in four of the subsets and predicts the values in the fifth. This process is then repeated four more times, with each subset being omitted from training and used to compare predictions (10).

## MHC CLASS I BINDING PREDICTIONS

Antigen-specific T cells do not directly recognize native antigens, but rather the T Cell receptor binds a molecular complex formed by an MHC molecule and a peptide epitope. In order for a peptide to be bound and presented by the MHC molecule, the antigen needs to be processed by the cell (11). Antigens are cleaved by the proteasome and transported into the endoplasmic reticulum (ER), through the Golgi, and finally presented in a closed groove on the MHC class I molecule. The MHC class I molecule is expressed by almost all nucleated cells and presents cleaved segments of the antigen to the CD8+ T cells. Its binding groove is closed at both ends and can accommodate peptides of 8–15 amino acids in length. MHC molecules are highly polymorphic and thousands of different variants exist. The peptide binding specificity is also very broad, and a given MHC can bind and present a number of different peptides (12).

Given the large number of variants possible and this broad specificity, experimental characterization of all peptide–MHC interactions is experimentally challenging. Binding prediction methods facilitate the selection of potential epitopes. The methods are developed using experimental peptide binding data for different MHC alleles to train machine learning algorithms that in turn can be used to predict the binding for any arbitrary peptide.

The IEDB database resource houses binding data for 173 MHC class I molecules, which includes 119 human alleles for HLA-A, B, and C. It also has data for macaque, chimpanzee, mouse, cattle, pig, and rat (13). The machine learning methods are periodically retrained when sufficient amount of new data become available in the IEDB. The prediction routines were last retrained in 2013, and the training sets are publicly available at <http://tools.iedb.org/main/datasets/>. The available methods and their performance have been published starting from 2005 and have seen an improvement in performance over that time (14, 15).

## The Web Interface for MHC Class I Binding Predictive Tools

The primary interface for epitope prediction tools is through a web interface, which is described below. Users can access the MHC class I binding prediction tool from the IEDB home page or directly at <http://tools.iedb.org/mhci/>. The class I home page has numerous tabs to assist users, including a Help tab for detailed explanations on inputs and outputs, an Example tab with specific examples and a Reference tab with publications related to the methods. From the Download tab, the user can download the scoring matrices for the various methods and a link to the dataset used for retraining the class I binding prediction tools in 2013 (16). Tool developers are encouraged to make use of these data. In addition, users can download a standalone version of the binding prediction tool that can be hosted on the user's own server. Finally, the Contact tab has a link to the IEDB help desk at [help@iedb.org](mailto:help@iedb.org) that has the goal of responding within one business day of receiving a help request.

To perform class I binding predictions, the user inputs one or more sequences as plain text, separating the sequences with blanks, or in FASTA format, or specifies a file containing the proteins. Next, a user can select a preferred method from a list including IEDB recommended, consensus (17), netMHCpan (10, 18), ANN (4, 19–22), scoring matrix method (SMM) (5), SMMPPMBEC (23), Combinatorial Library (24), PickPocket (25), and netMHCcons (26). The IEDB recommended method is the default setting and usually is consensus, a combination of three different methods (ANN, SMM, and Combinatorial Library). If these methods are not available for the selected allele, netMHCpan will be used instead. The user next specifies MHC species (human, mouse, non-human primates, and others) and specific alleles. Multiple alleles and epitope lengths (9–14) can be specified. For humans, the most frequent alleles are available for selection by default, and a reference set of the 27 most frequent alleles (97% of the global population) and peptide lengths of 9 and 10 can also be selected.

## Output of MHC Class I Binding Predictive Tools

When the user clicks the submit button, the protein sequence is parsed into all possible peptides for the specified length and the predicted binding affinity for each is calculated. The tool compares the predicted affinity to that of a large set of randomly selected peptides and assigns a percentile rank (lower percentile rank corresponds to higher binding affinity), which is method

independent since not all methods predict IC<sub>50</sub> values. In the Consensus method (17), the median value of the three values is used. Results are presented by default sorted by predicted percentile rank, but results can also be sorted by sequence position. Users can filter results by a designated percentile rank cutoff.

The results page lists the input protein sequence, the table of results, a link to download the results as a CSV file, and a list of citations associated with the methods used. The output table includes columns for the allele, peptide start and end positions, the peptide length, the peptide sequence, the method(s) used, and the percentile rank. Checking a box at the top of the results table can expand the results. The output table can be sorted by clicking on each column header.

There are three main strategies for selecting potential binders. The first involves selecting all peptides with IC<sub>50</sub> value less than 500 nM, a threshold previously associated with immunogenicity (3). A second recommended strategy is to pick the top 1% of peptides for each allele/length combination. The third strategy is to pick peptides with percentile ranks below 1% (27). A further study regarding the strength of affinity for different alleles and their repertoire size indicated that repertoire size differs for each allele (28). We derived from this study allele-specific binding thresholds for the 38 most common HLA-A and HLA-B alleles. A link at the top of the Help tab accesses a table of alleles and their associated affinity cutoff IC<sub>50</sub> values.

## Standalone Version and Application Program Interface (API)

The MHC class I binding tools are also available in a standalone version that runs on a Linux operating system and can be downloaded from the Download tab. Because the standalone version is hosted locally on hardware of the user's choosing, an internet connection is not needed and users do not need to worry about their web browser timing out. Instructions for installing the software are provided in the accompanying README file.

All users can also access the MHC binding prediction tools using the API. The API uses a Representational State Transfer, an application that uses HTTP requests to GET, PUT, POST, or DELETE data from web servers. In this manner, users can send parameters over the internet directly to the IEDB web servers. No special software needs to be installed locally to use the API, and users will always access the latest version of the tools, unlike the standalone versions that need to be updated on local servers with each new release of the prediction tools. The API can also be incorporated into scripts and pipelines. In addition to the MHC class I binding prediction tool, APIs exist for several other prediction tools, including class II binding, linear antibody epitope, class I processing, class I immunogenicity, and MHC-NP. Documentation for using these APIs can be found on the Tool-API tab.<sup>2</sup> The features and attributes of the web, standalone, and API versions of the tools are summarized in Figure 2.

<sup>2</sup><http://tools.iedb.org/main/tools-api/>.

## MHC CLASS I PROCESSING PREDICTION TOOLS

When a virus infects a host, it gets inside the cell, replicates, and spreads throughout the host. The virus and other components are degraded by a process known as antigen processing, which results in some of the peptide fragments being presented on the surface in the context of MHC class I epitopes that are recognized by CD8 T cells that can kill the cell, produce cytokines, proliferate, and form memory populations. Antigen processing is a complex enzymatic process with key players such as the proteasome complex that generates short peptides. Some of these fragments are transported from the cytosol into the ER by binding to TAP, where they undergo further trimming of N-terminal residues and then bind to MHC complexes. These are then transported to the cell surface where they can be presented to T cells (11).

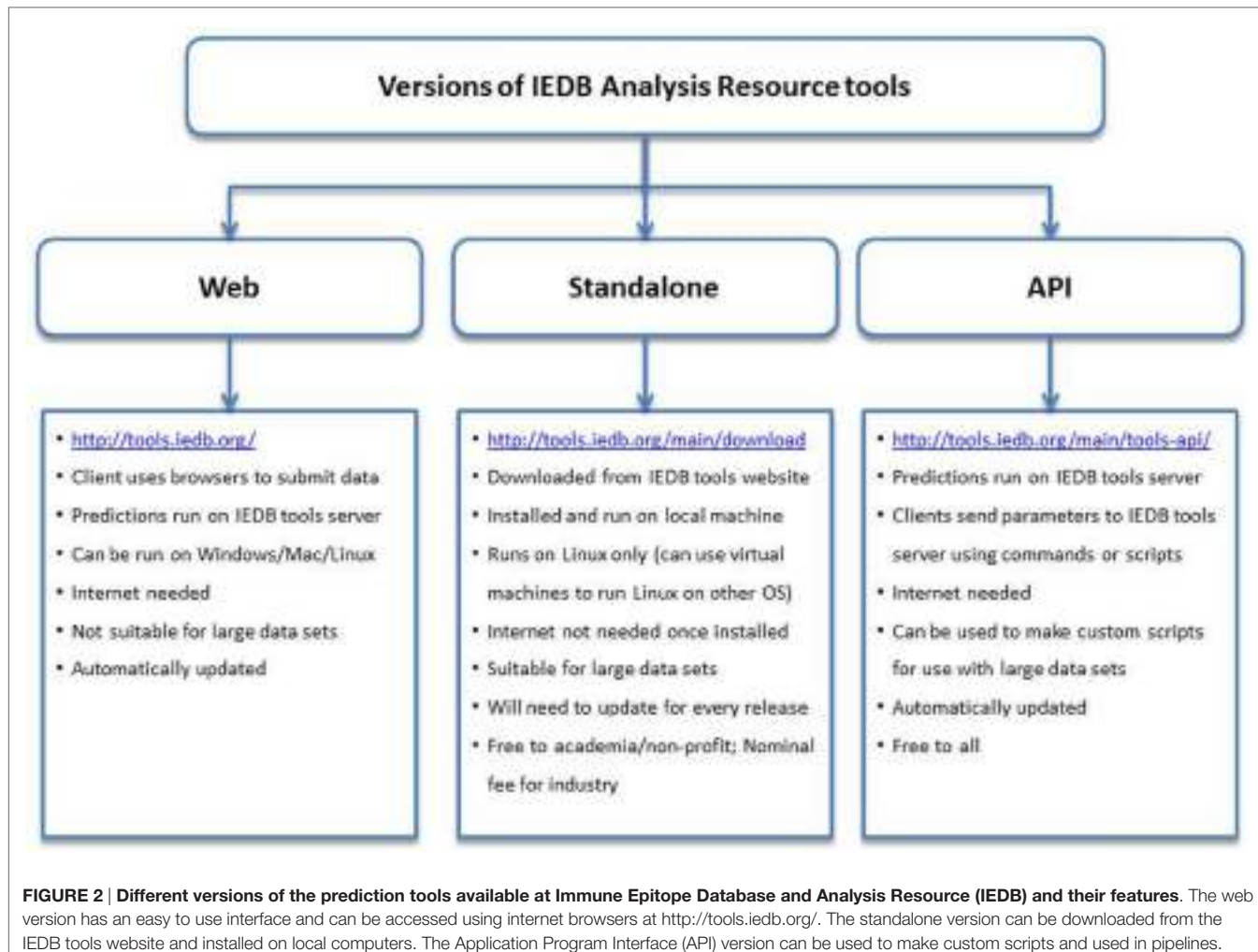
To predict the outcome of antigen processing and presentation, proteasomal cleavage, TAP transport, MHC class I binding, and T cell receptor peptide–MHC interaction can be considered. Each step of this pathway has a corresponding specificity or efficacy. As a first approximation, about 15% of all peptides that can be made from a protein are actually transported into the ER and about 2.5% of peptides that are made will bind to an MHC molecule. About 50% of peptides presented on the cell surface will be recognized by a T cell receptor (29).

There are two different types of processing tools in the Analysis Resource. One combines proteasomal cleavage, the transfer of peptide fragments by TAP, and MHC binding. The other type is neural network trained directly on naturally processed and presented peptides. The NetChop method (30, 31) models the cleavage and generation of the C-terminus of peptides based on data from naturally processed peptides and it is combined with other neural network based approaches [NetCTL (32) and NetCTLpan (33)]. Processing prediction tools include the MHC-NP tool developed by a research group outside the IEDB team, based on MHC elution experiments to assess the probability that a given peptide is naturally processed and binds to a given MHC molecule (34). Figure 3 provides a summary of the various tools involved in antigen processing and the different steps of processing with which they are associated.

## Combined Predictors

This tool can be found on the T Cell Tools section of the web interface, similar to that of the MHC class I binding, with added sections for proteasome cleavage and TAP transport. Users can select between two proteasome types—immunoproteasome and constitutive proteasome. Since their specificities are very similar (35), the immunoproteasome is recommended for use and is set by default.

TAP transports peptides into the ER that are potentially N-terminally extended from the ligand that end up in MHC (36). This means that the peptide that binds to MHC does not necessarily need to be a good substrate for TAP, but needs to be an N-terminally extended precursor of a TAP substrate. Accordingly, the TAP transport input section has two input fields, maximum precursor extension and alpha factor. The TAP transport method



takes a precursor of up to an extension of 1 into account. The alpha factor is a weighting factor that takes into account the uncertainty of not knowing which peptides are involved. A detailed discussion on the selection of these values has been published elsewhere (37). For most users, we recommend the use of the default values of 1 for the maximum precursor extension and 0.2 for the alpha factor as these worked best in predicting TAP transport overall.

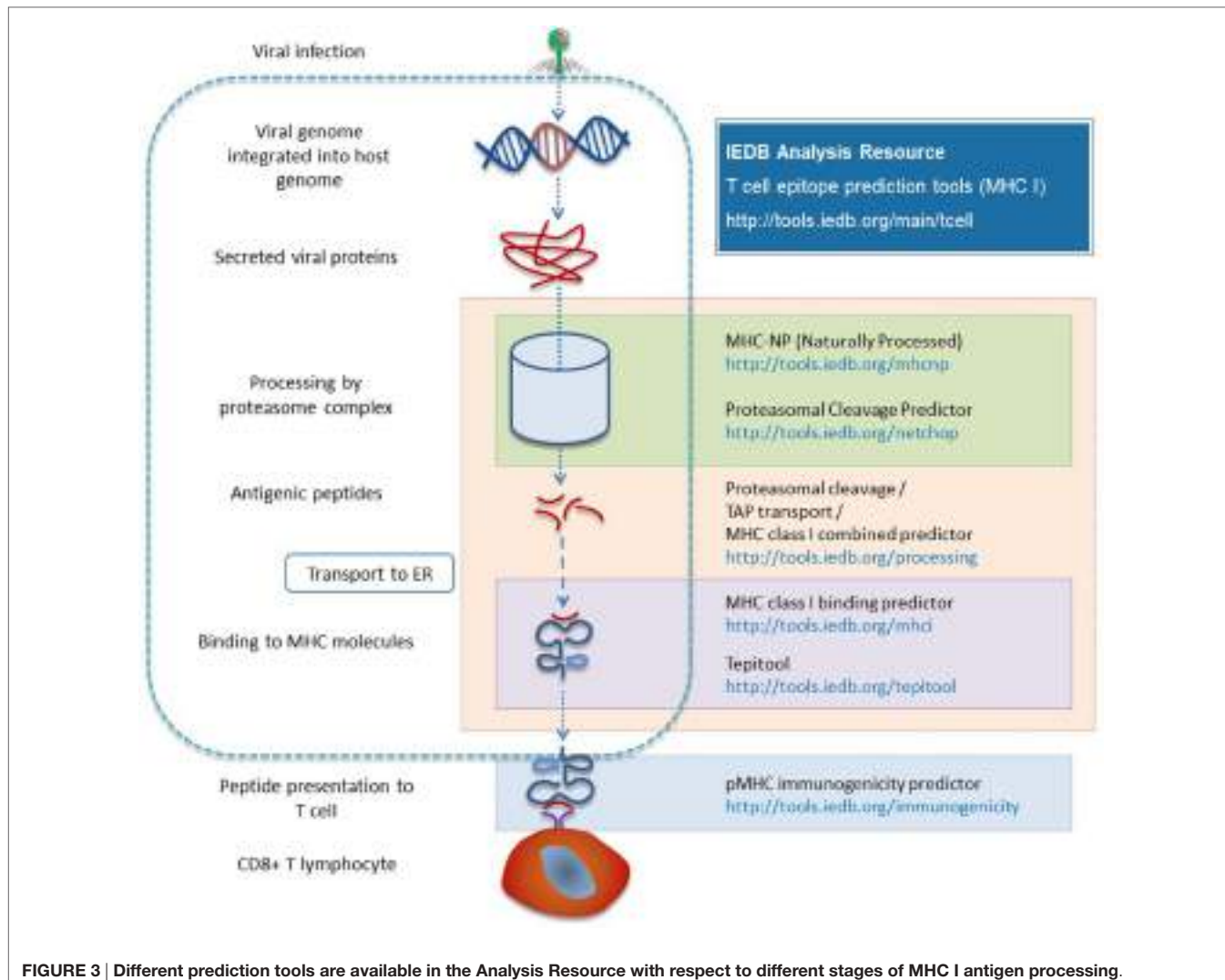
The output includes columns for the allele, start and end positions, peptide length, and sequence, plus columns for proteasome, TAP, MHC, and Total scores. The proteasome score indicates how well the peptide with its C-terminus could have been generated. The TAP transport score evaluated the ability of the peptide or its N-terminally prolonged precursor to be generated. The MHC score is the  $-\log_{10}$  of the IC50 value, so in this case a higher MHC score indicates a better binder. The total score is the sum of these three scores.

There are several caveats associated with the combined predictor and the other processing prediction tools. Based on our evaluation of the performance of prediction methods, we found that the processing predictions were better than the MHC binding predictions alone when predicting eluted peptides (38). However,

eluted peptides are typically identified by mass spectrometry, which requires the peptide to be reasonably abundant to allow for detection. In actuality, an immune response could occur with few peptides on a cell. So there is a potential bias that eluted data over-represents the “best possible” ligands and the difference between the processing predictions and the binding-only predictions may not be relevant in practice. When we benchmarked the ability to predict T cell epitopes, the improvement was not statistically significant. In conclusion, while processing predictions make sense in terms of the biology, the IEDB team recommends using the MHC class I binding predictions, which are trained on much larger datasets. For situations where the binding predictions provide too many candidate epitopes, using the processing scores instead can offer another filter to reduce the number of peptides to investigate.

## Other Processing Tools

Additional processing predictors are the neural network based tools, NetChop (30, 31), NetCTL (32), and NetCTLpan (33). NetChop is the proteasomal cleavage predictor based on an analysis of C-terminus residues in eluted ligands. NetCTL uses



the NetMHC method and combines it with NetChop and TAP transport method. NetCTLpan uses the NetChop, TAP transport method, and NetMHCpan.

The input interface is again similar to the other binding and processing tools, allowing the user to specify one of the three prediction methods and the protein sequence(s) of interest. NetChop predicts C-terminal cleavage based on two approaches, either the C-term 3.0 method, which uses specificities for the C-terminals based on eluted MHC ligands, or the 20S 3.0 method, which uses the analysis of proteasomal cleavage digests similar to the combined predictor. C-term 3.0 is not actually a proteasome prediction because it derives the specificity of the C-terminals statistically from eluted ligands that reflect the TAP transport specificity, but it performs better than 20S 3.0 and is, therefore, presented as the default value for all three methods. There are six publications that provide further details on the methods.

An additional processing method is MHC-NP, which was contributed to the IEDB by the Giguère group. While it covers

a limited number of mouse and human MHC class I alleles, MHC-NP won a benchmark performance contest at the Second Machine learning Competition in Immunology.<sup>3</sup> The IEDB is open to hosting tools from external groups on the Analysis Resource and welcomes the opportunity to do so.

## THE T CELL IMMUNOGENICITY PREDICTOR

The Analysis Resource has a T cell immunogenicity predictor tool that predicts the relative ability of a given set of peptides bound in an MHC complex to be recognized by a T cell. To develop the tool, we assembled datasets of peptides that have similar MHC binding affinity and then separated the ones that are recognized by T cells from the ones that are not recognized by T cells. We then observed that certain amino acids, such as tryptophan, phenylalanine, and

<sup>3</sup><http://bio.dfci.harvard.edu/DFRMLI/HTML/natural.php>.

isoleucine, are enriched in immunogenic peptides while other residues, such as serine, methylamine, and lysine, are depleted. Studies suggest that tryptophan and phenylalanine have long side chains that have a greater ability to make contact with the T cell receptor, possibly making them more immunogenic than other residues (39). We used the enrichment and depletions score to generate propensity scales than can be used to evaluate a peptide directly (39).

The tool has only been validated for 9-mers. By default, the tool masks the first, second, and C-terminus residues, the ones most likely to be directly responsible for MHC binding. The remaining residues in positions 3–8 are then the ones most likely to be in contact with the T cell and they are evaluated using the propensity scale and a score is calculated. A positive score indicates a likelihood of T cell recognition and a negative score indicates that recognition is less likely. We have conducted extensive studies to validate this approach. The tool has AUC values of 0.65–0.69, which is rather poor but still statistically significant. It offers an advantage over the processing tools in that it is independent of MHC binding.

It is worth noting that proteasomal cleavage, TAP transport, and MHC binding have undergone coevolution to a large extent, so that MHC molecules have evolved to bind peptides that are in the ER (38). So processing prediction tools are predicting dependent variables. As a result, their combination does not provide vastly improved predictions. In contrast, the immunogenicity tool focuses on residues that are not involved in these other predictions, and thus, its results are independent of the other processing prediction tools. Therefore, the IEDB team recommends using the MHC class I binding predictions to select candidate peptides for measurement and supplement that with the immunogenicity predictor to further reduce candidates to test.

## MHC CLASS II BINDING PREDICTIONS

The MHC class II antigen-processing pathway applies to exogenous proteins from extracellular sources, such as bacteria or fungus, which are engulfed by the cell and cleaved by proteases in the lysosome (11). The MHC class II molecules are synthesized by the ER and have two chains, alpha and beta, which assemble together to make a complete MHC class II chain. After a series of complex cellular processing events, MHC class II carrying specific peptides derived from degradation of these proteins are presented on the cell surface to T cell scrutiny (11).

The basic structure and principles for class II and class I binding prediction have many things in common but there are also some important differences (Table 1). With regard to structure, MHC class I molecules have a single alpha chain that impacts binding and the binding cleft lies between the alpha 1 and alpha 2 domains. Because the binding groove is closed, it can only accommodate shorter peptides (8–14 amino acids). MHC class II molecules though have two chains, alpha and beta that impact binding (12). The binding groove is open and can accommodate longer peptides (13–25 amino acids). MHC class I molecules are present in all nucleated cells. Class II molecules are found only in antigen presenting cells, such as macrophage cells, B cells, or dendritic cells (12).

**TABLE 1 | Comparison of MHC class I and class II epitope prediction tools available in the IEDB.**

Features	MHC class I	MHC class II
Structure	3 Alpha chains, 1 beta-2 microglobulin	2 Alpha chains, 2 beta chains
Peptide binding chain	Alpha	Alpha and beta
Binding cleft	Closed	Open
Loci	A, B, and C	DP, DQ, and DR
Antigen presenting cells	All nucleated cells	Dendritic, macrophage and B cells
Responding lymphocytes	Cytotoxic T cells (CD8+)	T helper cells (CD4+)
URL for IEDB predictions	<a href="http://tools.iedb.org/mhci">http://tools.iedb.org/mhci</a>	<a href="http://tools.iedb.org/mhcii">http://tools.iedb.org/mhcii</a>
Binding core	9 residues	9 residues
Residues flanking the binding core	NA	0–5 on each side
Recommended cutoff (IEDB Consensus percentile rank)	1.0	10.0
Peptide length accepted	8–14-mer	15-mer
Algorithms available	8 (Consensus, NetMHCpan, artificial neural network, SMMPPMBEC, SMM, Comblib, PickPocket and NetMHCcons)	6 (Consensus, NetMHCIpan, NN-align, SMM-align, Combinatorial library, Sturniolo)
Host species for which prediction is available	8 (human, mouse, gorilla, chimpanzee, cow, macaque, pig, and rat)	2 (human and mouse)
Total number of alleles available	3,600	DPA = 17, DPB = 128, DQA = 28, DQB = 104, DR = 256

IEDB, Immune Epitope Database and Analysis Resource; SMM, scoring matrix method.

With regard to nomenclature (40), only the alpha chain is variable in class I molecules so the nomenclature is “HLA” followed by the locus, typically A, B, or C, an asterisk, and certain digits that define the kind of allele it represents. An example for class I is HLA-B\*07:02. For class II molecules, both the alpha and beta chains affect binding and both chains are variable for the DP and DQ loci. As such, both chains need to be specified, such as HLA-DPA1\*01:03/DPB1\*02:01. For the DR locus, only the beta chain is variable so it is the only one that needs to be specified, for example HLA-DRB1\*01:01.

Another important difference pertains to the binding core. Because the open binding groove accommodates longer peptides, only part of the peptide binds or interacts with the class II molecule. The binding core is typically nine amino acids in length with neighboring or flanking residues. As a result, it is difficult to identify which residues are actually involved in the binding process. For proper binding, the binding core needs to be aligned with the binding groove. Flanking residues also interact with the class II molecule outside the binding groove, but because peptide lengths typically vary from 15 to 23 residues, the flanking residues

are also challenging to identify. As a result, MHC class II binding prediction is more challenging than that for class I molecules (41–45).

## MHC Class II Binding Prediction Tool Web Version

The web interface for the MHC class II binding prediction tool has many similarities to the class I interface. The tool can be accessed by links on the IEDB home page or directly at <http://tools.iedb.org/mhcii> and has tabs for Help, Example, Reference, Download, and Contact. Users can find a sequence of interest by clicking on the NCBI sequence browser and cut/paste it into the sequence field. The format for the sequences can be plain text or FASTA. Users can also upload a file with their sequences as plain text.

Several different prediction methods are available including IEDB recommended, Consensus (41, 46), netMHCIIpan (47, 48), SMM-align (49), Sturniolo (50), and NN-align (51). The default method is IEDB recommended. Users can specify the species and locus for humans (DR, DP, and DQ) and mouse (H-2-I), and the associated alleles. Finally, users can specify the output results to be sorted by percentile rank or sequence position. The IEDB team continuously evaluates and enhances algorithms and develops new algorithms, so the IEDB recommended methods can change over time. Each method generates a percentile rank and a binding affinity score.

The user selects the species, locus, and alleles. As in the class I binding tool, only the most frequent alleles are listed for HLA-DR. There are five or six alleles available for the DP and DQ loci. Thus, there are fewer alleles available, because less data are available for training the algorithms (44). By default, the alpha and beta chains are combined. If the user wants to specify the chains separately for DP and DQ, they can check a box to enable this option. For the DR locus, only the beta chain is displayed since the alpha chain is invariant.

A reference set of 27 most common alleles (52) that can provide global coverage can be selected by checking the appropriate box. Users also have the option to upload allele selections in a text file using the allele names. The tool parses the input protein sequences into 15-mers and predicts the binding affinity for each peptide. It then compares the predicted affinity for each peptide with that of a large set of randomly selected peptides to determine its percentile rank. The Consensus method uses the median rank of the three constitutive methods. As before, the lower the percentile rank, the better the binder.

Users can download the results in a CSV file and the web output lists the allele in the first column, followed by the start and end sequence positions, the peptide sequence, method used, and the percentile rank. The results can be expanded by checking the box at the top of the table, which reveals the different scores for the methods used. The expanded view also lists the nine amino acid binding core computed by each method.

As for class I, there are several recommended approaches to selecting binders, including selecting peptides that have percentile rank less than or equal to 10.0, or IC<sub>50</sub> values less than or equal to 1,000 nM, the experimentally determined threshold for

class II immunogenicity (53). Another approach is to select a desired percentage of the peptides within the peptide set sorted by percentile rank for users who want to study a fixed number of best possible peptides.

Because the tool breaks down input sequences into all possible 15-mers, many of these sequences will have the same predicted 9-mer binding core. One way to reduce this redundancy is to preprocess the input protein sequence by splitting it into a series of 15-mers that overlap by 10 residues and submit this series as input instead of the entire protein sequence. An overlap of 10 is recommended because it can capture the minimal number of 15-mers with all possible 9-mer binding cores with at least one flanking residue on both sides. Alternatively, the user can post-process results when the entire protein sequence is used as input by selecting the best binding (lowest percentile score) peptide among those with the same binding core. Because this process is more involved than the pre-processing approach, the pre-processing approach is recommended.

## Prediction of Promiscuous Binders and Immunodominant Epitopes

A peptide that binds to multiple MHC molecules is referred to as a promiscuous binder. Promiscuous binders may be associated with strong antigenicity (54, 55) and can provide extensive population coverage (52, 55). To predict promiscuous class II binders, the binding prediction tool can be used as described but raising the binding percentile rank threshold to 20 from 10, opting to use the 27 reference alleles that covers 94% of the global population. Once the run is submitted and completed, users can download the results into a CSV formatted file and use a spreadsheet program to find the sequences that have percentile rank below 20, and then count the number of alleles that bind each 15-mer peptide. We recommend selecting sequences that bind at least 50% of the alleles with a percentile rank cutoff of 20%.

In an independent study, we analyzed peptide datasets with measured immune responses from house dust mite, Timothy grass, *Mycobacterium tuberculosis*, cockroach allergens, and Pertussis (44). The aim of the study was to devise prediction strategies not at the level of single alleles, but rather at the level of the general population. After extensive experimentation, we discovered that a combined prediction for a set of seven alleles, representative of prototypic binding supertypes, could capture 50% immune response with 20% of the peptides. Users can generate 15-mers overlapping by 10 residues from their protein of interest, predict binding for these seven alleles, compute the median consensus percentile rank of the seven values for each peptide, and select all peptides with a median consensus percentile rank less than or equal to 20.0. This group of peptides will capture ~50% of the immune response in a general human population (44).

## TepiTool

The IEDB team has recently developed TepiTool, a T cell Epitope Tool that provides a user-friendly interface for MHC class I and

II binding predictions, by using IEDB team's recommendations as defaults, to automatically select the top peptides (56). The TepiTool interface is a step-by-step wizard that guides the user through input parameters and desired outputs. It is currently available at <http://tools.iedb.org/tepi tool> on the Analysis Resource Labs web page.

TepiTool guides the user through six separate steps, specifying inputs about their sequences (step 1), host species and MHC class (step 2), and alleles (step 3). For class I alleles, there are several options that the user can pick via radio buttons. The user can select from the list of frequently occurring alleles (frequency greater than 1% in the global population), a list of all available alleles, a list of representative alleles from different HLA supertypes, the panel of 27 allele reference set, or they can choose to upload an allele file. In step 4, the user is presented with several options regarding the selection of peptides, including low, moderate, or high number of peptides and different lengths of peptides. The user also has the option to select their own settings regarding removing or keeping duplicate peptides (to facilitate setting up of pools for screening). The user also has the option of including only peptides that are conserved in a specified percentage of sequences. By default, the percentage is set to 50%, but it can be changed in 10% increments up or down. All during this process, the selected parameters are summarized in a panel on the right of the web page.

In step 5, the user selects the prediction method (IEDB recommended, Consensus, SMM, or ANN) and the output (predicted percentile rank, predicted IC<sub>50</sub> or MHC-specific binding thresholds, the top X% or the top X number of peptides based on percentile rank). The recommended threshold of 500 nM is provided as a default if the IC<sub>50</sub> option is chosen. In all cases, the number of peptides in the predicted results is shown in the summary panel on the right. In the sixth and final step, the user reviews input parameters and selected options before submission. The user can also specify a job name and an email address to be notified when the run is completed.

On the output page, a table of concise results and the best binders based on the chosen criteria are listed at the top. This table contains the peptide start and end positions, peptide sequence, percentile rank, allele name, and the level of conservancy (if this option was chosen). The output also contains links to download the complete results citation information for the tools used, the input sequence, and a summary of the other input parameters.

MHC class II binding predictions are performed similarly, and in step 3, the user can select custom allele sets, the seven-allele, or the reference set of 27 most frequent alleles. In step 4, the default setting is for a moderate number of predicted peptides with duplicate peptides removed and the input protein will be automatically split into 15-mers overlapping by 10 amino acids. An overlap of 8 will be used if the “low number of peptides” option is used, and the overlap of 10 if the “high number of peptides” option is chosen. Alternatively, the tool performs the post-processing step of removing largely overlapping peptides from the prediction set by picking the top peptide from the overlapping set of peptides based on percentile rank.

## SEQUENCE-BASED B CELL EPITOPE PREDICTIONS

B cell epitope prediction tools can be accessed from the Analysis Resource pull-down menu or the link on the IEDB home page.<sup>4</sup> On the web page for this tool, users must input either a protein Swiss-Prot ID or a sequence in plain text format and select the method for the prediction. A description of the different methods can be found on the Help tab, including the references and amino acid scales used in these methods. As with the T cell prediction tools, there is also an Example tab that contains several sample cases that can help familiarize users to the input and output formats and a Reference tab that lists the publications that describe the methods.

Historically, physicochemical properties such as hydrophilicity (57), surface accessibility (58), beta-turns (59, 60), and flexibility (61) were correlated with the occurrence of B cell epitopes in proteins. We implemented these four amino acid physicochemical properties-based methods in this tool. In addition, we implemented a semi-empirical method which makes use of physicochemical properties of amino acids and their frequencies of occurrence to predict linear B cell epitopes (62) and a machine-learning based B cell linear epitope prediction method called BepiPred (63). BepiPred is a prediction method that is based on a combination of HMM and Parker's hydrophilicity and Levitt's secondary structure scales. For this reason, BepiPred is the default method. With an AUC value of 0.66, its prediction performance is relatively poor, but better than the other methods available on the web page.

BepiPred results page contains a plot of the predicted score versus the sequence position (Figure 4). The user can adjust the window size and score threshold. The score for a single residue position incorporates the neighboring residues defined by the specified window size, which has a default value of 7. The threshold value is based on the sensitivity and specificity. For BepiPred, a threshold value of 0.35 corresponds to a sensitivity of 0.49 and specificity of 0.75 (63). Increasing the threshold will reduce the sensitivity and increase the specificity, which will reduce false positives but reduce the number of possible epitopes (true positives). A threshold of 0.90 corresponds to a sensitivity of 0.25 and a specificity of 0.91, and a threshold of 1.30 corresponds to a sensitivity of 0.13 and a specificity of 0.96. Below the chart is a table that displays the predicted peptides, start and end positions, sequence, and its length. A second table lists the predicted residue score for each position and an Assignment column that indicates a predicted epitope position with an “E.” For the other methods, the threshold value is automatically set as the average score value, and both the window size and threshold values can be modified by the user.

## STRUCTURE-BASED EPITOPE PREDICTIONS

The IEDB Analysis Resource has two structure-based methods for predicting discontinuous epitopes—DiscoTope (64, 65)

<sup>4</sup><http://www.iedb.org>.

[Home](#) [Help](#) [Example](#) [Reference](#) [Download](#) [Contact](#)

## Bepipred Linear Epitope Prediction Results

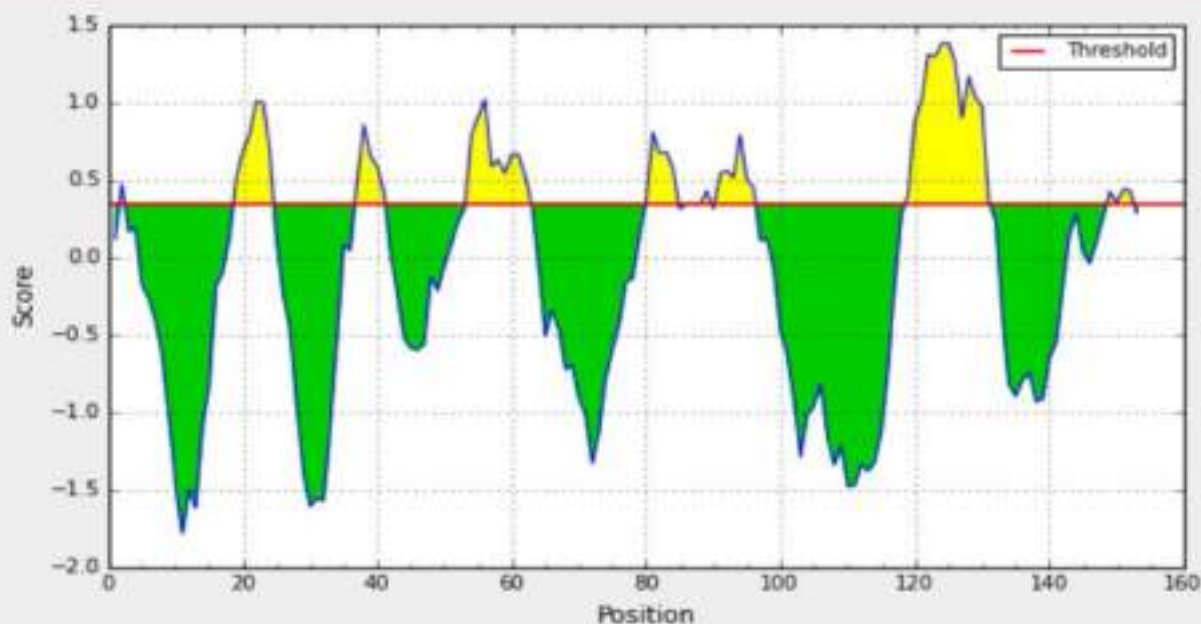
### Input Sequences

1 VLSEGEWQLV LHWAKVEAD VAGHGQDILI RLFKSHPETL EKFDRFKHLK TEAEMKASED  
 61 LKKHGVTVLT ALGAILKKKG HHEAELKPLA QSHATKHKIP IKYLEFISEA IIHVLHSRHP  
 121 GNFGADAGGA MNKAIELFRK DIAAKYKELG YOG

Center position: 4 Window size: 7

Threshold: 0.35

Recalculate



Average: -0.105 Minimum: -1.784 Maximum: 1.390

### Predicted peptides:

No.	Start	End	Peptide	Length
1	2	2	L	1
2	19	24	ADVAGH	6
3	37	41	PETLE	5
4	54	62	EMKASEDLK	9
5	80	84	GHHEA	5
6	87	87	K	1
7	89	89	L	1

**FIGURE 4 | BepiPred results.** BepiPred results for predicting linear epitopes in sperm whale myoglobin protein (Swissprot ID: P02185). Users can change the window size and score threshold (highlighted in a red box) and recalculate the results. A red line is drawn in the Score versus residue position plot at the chosen score threshold value to predict epitopes. Predicted epitope residue positions are colored in yellow. Predicted peptide table below the plot lists all the predicted linear epitopes and their positions in the protein.

and ElliPro (66). Both make use of the proteins' geometrical properties. There are also protein–protein docking algorithms that can be used for antigen–antibody interaction prediction. To use structure based prediction tools, the user must provide a three-dimensional (3D) structure of the antigen–antibody complex such as the ones provided by the Protein Data Bank.<sup>5</sup> The search feature on the home page of the PDB allows the user to search 3D structures of a protein by key word, PDB ID, or a sequence, while an advanced sequence search feature allows one to run BLAST on an input sequence to find relevant structures in the PDB database. Clicking on the desired structure will open a structure specific web page from which the structure coordinates can be downloaded in PDB format for use in the prediction tools. FASTA files are also available for download. PDB ID or a PDB format file is a required input for the DiscoTope epitope prediction method. If a 3D structure is not available in the PDB, there are homology modeling or comparative modeling methods, servers, and databases that can accessed, as described below.

The performance of ElliPro was evaluated in two separate studies in 2007 (67) and 2012 (65). The 2007 benchmark used 42 X-ray structures of antibody–antigen complexes and ElliPro obtained an AUC value of 0.73, a score better than several other predictors, including Epitopia (68), PEPITO (69), and DiscoTope 1 (64). Two antibody–protein docking tools were benchmarked and had AUC values less than 0.60. The 2012 benchmark used 52 X-ray structures of antibody–antigen complexes. In this study, ElliPro had an AUC value of 0.69 and was outperformed by DiscoTope 1.1 (AUC = 0.71) and DiscoTope 2.0 (AUC = 0.73). Overall, the performance of all the structure-based methods has average AUC value less than 0.75. This relatively poor performance might be due to the limited number of structures that can be used to train the algorithms. As more antibody–antigen complexes are deposited in the PDB, the quality of the structure-based predictions may improve.

## The DiscoTope Method for B Cell Epitope Prediction

DiscoTope 2.0 (65) was trained on 75 X-ray structures of antibody–protein complexes and it takes into account multiple epitopes of an antigen. It assigns each residue a score calculated as a linear combination of normalized values from Parker's hydrophilicity scale, amino acid propensity, the number of contacts within 10 Å for each atom, and the area of relative solvent accessibility. The DiscoTope web page requires three inputs: the PDB ID, a PDB chain ID, and the version of DiscoTope to use. If a user has generated a PDB file from homology modeling, that file can be specified and uploaded as well. The IEDB team recommends the use of DiscoTope 2.0, but it involves a more complex calculation than version 1.1 and subsequently takes longer to run. Users making a large number of runs might, therefore, want to use version 1.1. Different default score thresholds are used by the two different versions.

<sup>5</sup><http://www.rcsb.org>.

The initial DiscoTope results page displays a plot of the DiscoTope score versus the amino acid position of the protein, with the score threshold displayed as a red horizontal line and epitope candidate positions colored in green. Users can also select a Table View and a 3D View.

The 3D View initiates a JSmol applet that graphically displays the 3D protein structure along with the same table that is displayed in the Table View (Figure 5). The orientation of the 3D protein structure can be changed in JSmol using a computer mouse and visualization settings can be changed by right-clicking the mouse button to reveal a list of display options. Each row in the table has a button labeled CPK, which when clicked will highlight the residue in the structure model.

## ElliPro

Like DiscoTope, ElliPro can be accessed from the IEDB home page from the Analysis Resource pull-down menu or via the link in the right-hand panel. ElliPro (67) predicts epitopes in three steps. It first approximates the protein shape with an ellipsoid. It next calculates a protrusion index (PI) (70) for each and every residue. The PI is determined by constructing an ellipsoid that encompasses as many residues as possible but excludes that particular residue. Once the ellipsoid is constructed, it computes the ratio of the number of residues contained in the ellipsoid to the total number of residues to produce the PI. In the third step, the program clusters neighboring residues based on PI values to predict epitopes. There are two prediction parameters as inputs. The minimum score has a default value of 0.5 and indicates that any residue with a PI greater than 0.5 is considered an epitope candidate. The maximum distance parameter has a default value of 6, which means that only residues within a 6 Å distance will be clustered together within one epitope.

The ElliPro results page contains two tables, the first one for predicted linear epitopes and the second for predicted discontinuous epitopes. The former includes columns for the chain ID, start and end positions of the epitope, the peptide sequence, the number of residues, the ElliPro score, and buttons to view the 3D structure with a JSmol applet. The JSmol rendering of the protein will show the epitope as spheres and the rest of the protein as lines. The ElliPro score is the average value of the PI for all residues involved. The predicted epitopes are presented in descending order based on their scores. The second table has essentially the same information except each residue is listed with its chain ID, amino acid notation, and sequence position. At the bottom of the page is a link so users can view the individual residue scores in a table and a plot of score versus sequence position.

## Homology Modeling for B Cell Epitope Predictions

If the user has an amino acid sequence for their protein of interest but a PDB structure is not available, the user needs to perform homology modeling to generate a PDB file. In this case, we recommend using Protein Model Portal (PMP).<sup>6</sup> Users can enter

<sup>6</sup><http://www.proteinmodelportal.org>.

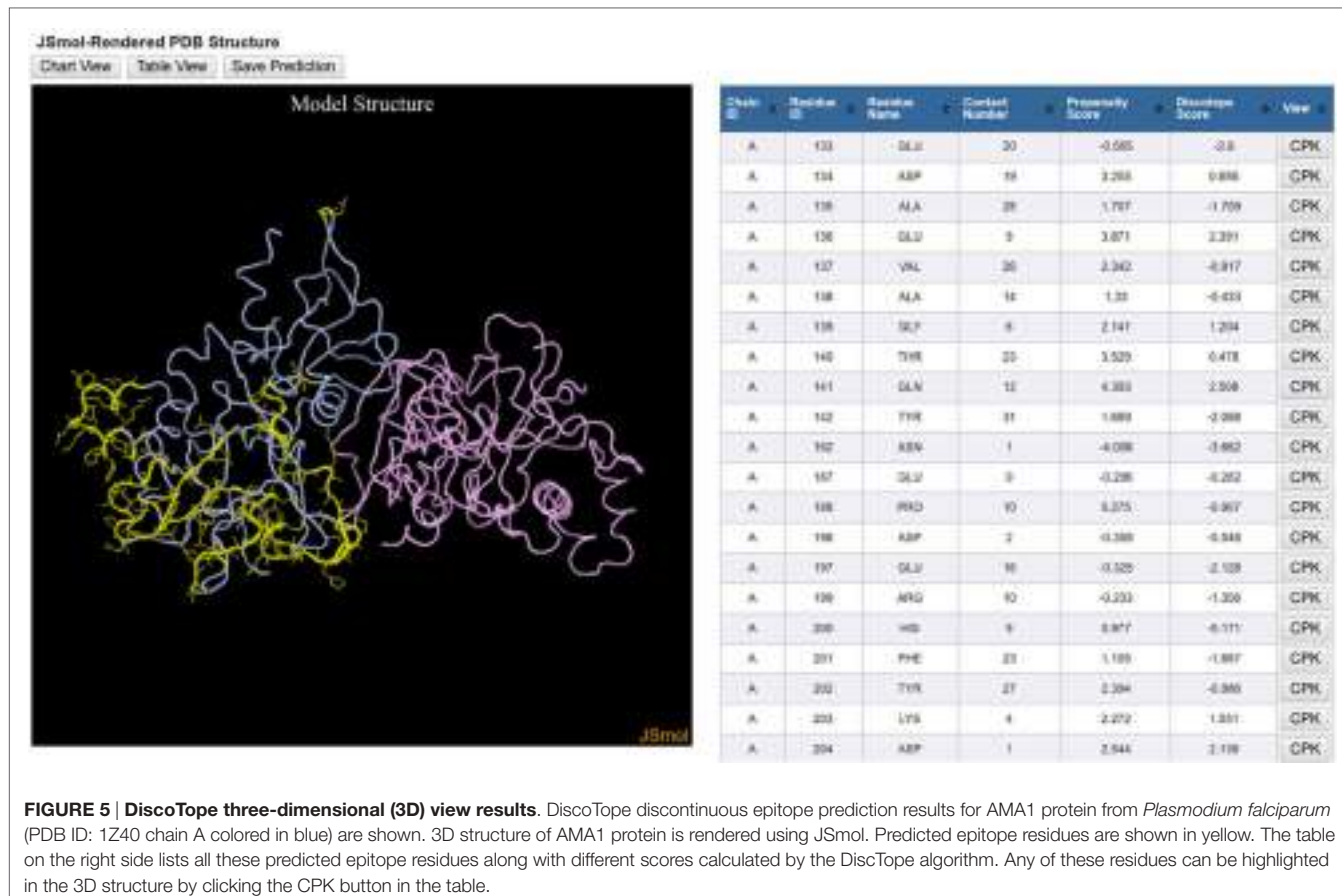


**FIGURE 5 | DiscoTope three-dimensional (3D) view results.** DiscoTope discontinuous epitope prediction results for AMA1 protein from *Plasmodium falciparum* (PDB ID: 1Z40 chain A colored in blue) are shown. 3D structure of AMA1 protein is rendered using JSmol. Predicted epitope residues are shown in yellow. The table on the right side lists all these predicted epitope residues along with different scores calculated by the DiscTope algorithm. Any of these residues can be highlighted in the 3D structure by clicking the CPK button in the table.

their protein sequence in the search field and hit the Search button. PMP will search major protein databases, such as UniProt, Swiss-Prot, and NCBI, and display results of the query. Users can then select a record and obtain a PDB-formatted file. If no models are found, the user can click the Submit button at the bottom of the query result page to submit their target protein sequence to one of PMP's registered homology modeling services. The subsequent page displays a list of the protein modeling servers along with a brief description of their server policy. Among them MODELLER is one of the prominent homology modeling suites that has gained vast popularity over the years (71). Once users select a server, registers for it, and submit their sequence, they will receive an email informing them that their results are ready to be retrieved.

The I-TASSER server was the number one server for protein structure prediction in community-wide contests for CASP7, CASP8, CASP9, CASP10, and CASP11 (72, 73). It also has a relatively simple user interface and easily understood parameters. However, I-TASSER is very popular and busy, and a protein of 1,000 amino acids could take several days before the job is finished. I-TASSER will provide five predicted homology models by default. Each model has a C-score that indicates the level of confidence of the model. I-TASSER also generates a TM score that indicates how close the top ranked structure is to a natural structure. We recommend only considering the models that have

C-scores greater than  $-1.50$  and using the model with the highest C-score if possible, even though a C-score meeting this empirical criterion does not necessarily guarantee the reliability of the model chosen. Once the user has obtained the PDB file of their homology model, they can specify the file for upload for their ElliPro run.

## Methods for Modeling and Docking of Antibody and Protein 3D Structures

The B cell page of the Analysis Resource has a link to a web page that provides information on available methods for modeling and docking antibody and protein 3D structures. The first step in the process is taking the antibody and antigen sequences and developing structure models. If a structure exists in the PDB, this step can be skipped. For modeling the antigen, one can use the protein structure modeling process previously described. For antibody modeling, however, there are specific programs available that take advantage of the inherent structure of an antibody. RosettaAntibody (74) and PIGS (75) are two applications that model antibodies. PIGS, or Prediction of ImmunoGlobulin Structure, is easier to use and has been implemented in the Analysis Resource. Once models for the antigen and antibody have been generated, the docking can be modeled with many different protein–protein docking programs including PatchDock (76) and ClusPro (77).

PIGS can be accessed from the Analysis Resource's B Cell Tools tab. As with the other tools in the Analysis Resource, PIGS has Help, Example, and Reference tabs. Users also have the option of uploading a sequence file with the light and heavy chain information instead. The PIGS results page displays a JSmol rendering of the modeled antibody structure. Each chain has its own color as do the light and heavy chain loops (L1, L2, L3, H1, H2, H3). There is a button at the bottom of the results page to download the structure file. This file can be opened in a text editor where the user can examine the alignment of the target sequence to the canonical antibody template. If the user wants to edit the alignment, they will have to go to the PIGS home website<sup>7</sup> since this feature has not been implemented in the IEDB.

With structure files for the antibody and the antigen, the user can now use one of the antibody–antigen docking programs. PatchDock<sup>8</sup> is relatively fast and has good accuracy and a straightforward and easy to understand user interface. The Complex Type input parameter should be set to “Antibody–antigen.” The antibody should be specified as the receptor molecule and the antigen specified as the ligand molecule since the antibody–antigen docking is optimized for this configuration. The Clustering RMSD field is used for clustering the results. Because there can be many results, the program clusters them to be able to present representative ones. PatchDock recommends using 4.0 Å in protein–protein docking. Once a job is submitted, PatchDock typically returns results within a few minutes. The results are ranked by the geometric shape complementarity score (Score), where the higher score indicates a better result. Values are also presented for the approximate interface area of the complex (Area) and the atomic contact energy. The page has a link to visualize the candidate with a Jmol applet and a link to download the results. Users can improve the solutions using the FireDock (78, 79) link at the bottom of the page. PatchDock performs a rigid-body computation so the backbone does not move. FireDock is an efficient method for refining the rigid-body docking solutions of PatchDock.

ClusPro<sup>9</sup> is another well-known docking server and was the first web-based antibody–antigen docking program publicly available. ClusPro also incorporates electrostatic interaction energy and desolvation energy. ClusPro accepts both PDB IDs and uploaded PDB files as input. Under Advanced Options, there is an Antibody Mode, where the user can check the boxes to use the Antibody Mode and to automatically mask non-CDR regions. The resulting models can be downloaded and visualized on this page.

## Analysis Tools

The IEDB's analysis tools most frequently used are the population coverage tool, the epitope conservancy tool, and the epitope clustering tool. The population coverage tool (80) calculates the fraction of individuals that are predicted to respond to a given set of epitopes with known MHC restriction, based on HLA

genotypic frequencies from <http://allelefrequencies.net> (81) assuming no linkage disequilibrium between HLA loci. Example data sets from the tab of the same name can be selected. The user can enter either epitope names or sequences, and then selects the population geographical location of interest. Results show what fraction of the population are expected to respond to at least one peptide, how many peptides on average each subject is expected to respond, and to how many peptides 90% of donors can potentially respond. Results are presented in graphical and tabular form.

The epitope conservancy analysis (82) tool calculates the degree of conservancy of an epitope within a given protein sequence set at different degrees of sequence identity. The degree of conservation is defined as the fraction of protein sequences that contain the epitope at a given identity level. In practice, the user inputs a set of epitopes and a set of protein sequences, and specifies the sequence identity threshold. The results page shows the number of protein sequences where each epitope is conserved at the given identity threshold. Users can click on a link to view details for a given epitope, which shows the subsequences in each protein that match the epitope sequence. With an identity threshold of 100%, the matches are identical, but lower thresholds allow varying degrees of amino acid substitutions.

The epitope cluster analysis tool (2) groups epitopes together based on sequence similarity. It is common to have variants of the same epitope tested by different labs that synthesize peptides of different lengths or use different isoforms of proteins. This can result in largely redundant sequences in a group. This tool takes epitope sequences as input and groups them by a user-specified level of identity.

## CONCLUSION

The IEDB and the Analysis Resource provide researchers interested in vaccine design and evaluation with useful bioinformatics resources in the context of data and tools. In this paper, we have described the features of the epitope prediction and analysis tools and how to use them (Figure 6). The MHC class I binding and processing prediction tools calculate putative epitopes and their affinity to a wide assortment of MHC alleles, which correlates to CD8+ recognition and immune response. Evaluations have shown these predictions to have very good accuracy. The MHC class II binding tools, while not as accurate as the class I tools, have improved significantly over the years as more binding data have become available to train the machine learning algorithms that drive the predictions. For both class I and class II binding prediction tools, reference sets of HLA alleles have been derived that provide over 95% global population coverage, an important feature for developing drugs. These tools are helpful in developing a set of likely high affinity binding peptides that can be synthesized for experimental analysis. A user-friendly interface named TepiTool has been developed to guide users through the process of making class I and class II binding predictions. It facilitates the selection of different input parameters, including the IEDB recommended default values and the reference allele sets, and it allows the user to select output criteria, such as the top binders based on percentile rank or promiscuity in the case of class II alleles. The class I immunogenicity tool predicts the

<sup>7</sup><http://circe.med.uniroma1.it/pigs/>.

<sup>8</sup><http://bioinfo3d.cs.tau.ac.il/PatchDock/>.

<sup>9</sup><https://cluspro.bu.edu/>.

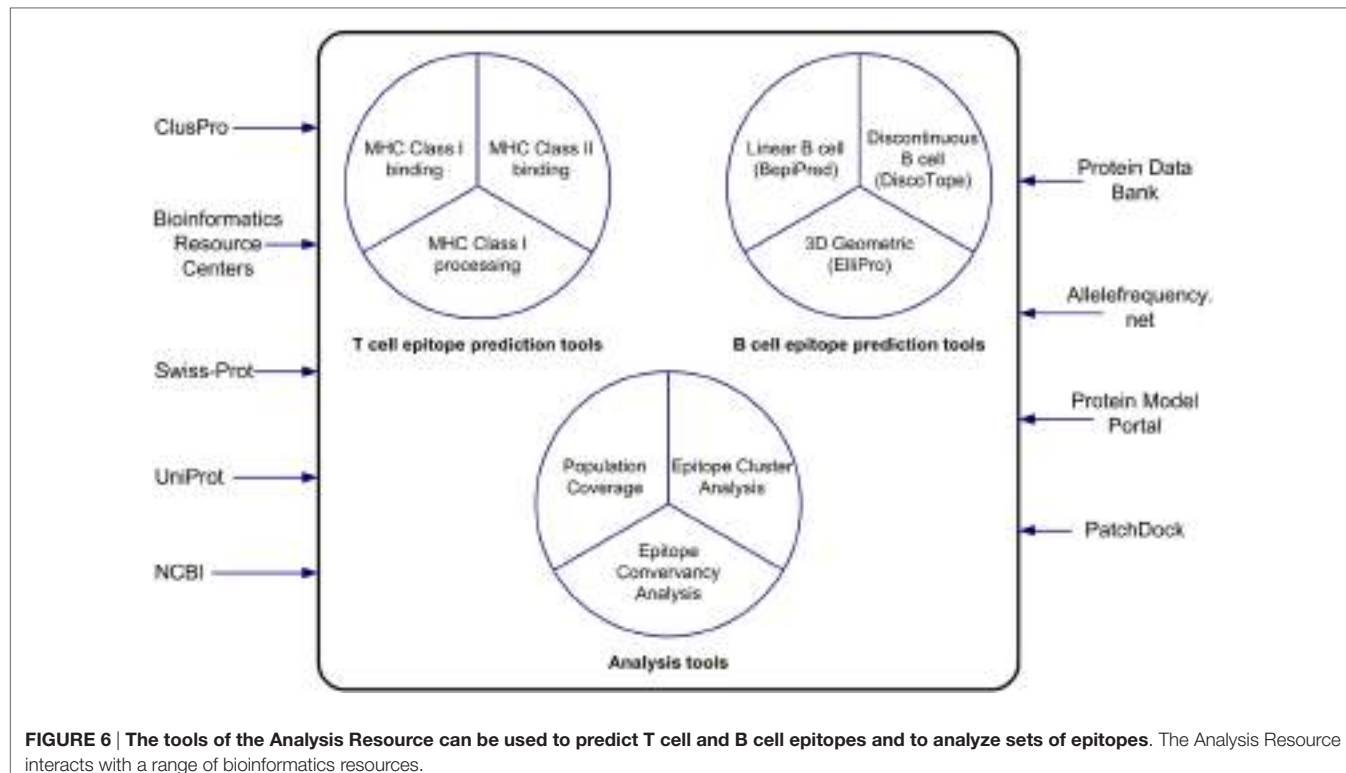


**FIGURE 6 |** The tools of the Analysis Resource can be used to predict T cell and B cell epitopes and to analyze sets of epitopes. The Analysis Resource interacts with a range of bioinformatics resources.

immunogenicity of peptide–MHC complex in a manner that is independent of MHC restriction.

The development of B cell epitope predictors is an ongoing area of research. The Analysis Resource offers tools for predicting linear and conformational antibody epitopes using several approaches, including amino acid scales, machine learning techniques, and molecular geometrical properties. Although not providing a performance similar to that of MHC class I and class II predictors, the B cell epitope tools can identify candidate antigen regions likely to bind antibodies. The Analysis Resource also provides a tool for predicting the population coverage of T cell epitope-based vaccines so that vaccines can be designed to maximize coverage. The epitope conservancy analysis tool was designed to analyze the variability and conservation of epitopes within a given set of protein sequences, useful information in developing peptide-based vaccines since conserved epitopes would be expected to be immunogenic

across multiple strains or possibly species. In all, the IEDB offers a valuable and free bioinformatics resource to the vaccine design community.

## AUTHOR CONTRIBUTIONS

WF generated the first draft of the manuscript; SP and SD provided content and figures for the T cell sections; SM provided content and figures for the B cell section, XX provided content for the B cell section; AS and BP edited successive rounds of the manuscript.

## FUNDING

This work was supported by the National Institute of Allergy and Infectious Diseases (contract number HHSN272201200010C).

## REFERENCES

- Zhang Q, Wang P, Kim Y, Haste-Andersen P, Beaver J, Bourne PE, et al. Immune epitope database analysis resource (IEDB-AR). *Nucleic Acids Res* (2008) 36:W513–8. doi:10.1093/nar/gkn254
- Kim Y, Ponamarenko J, Zhu Z, Tamang D, Wang P, Greenbaum J, et al. Immune epitope database analysis resource. *Nucleic Acids Res* (2012) 40:W525–30. doi:10.1093/nar/gks438
- Sette A, Vitiello A, Reherman B, Fowler P, Nayersina R, Kast WM, et al. The relationship between class I binding affinity and immunogenicity of potential cytotoxic T cell epitopes. *J Immunol* (1994) 153:5586–92.
- Nielsen M, Lundegaard C, Worning P, Lauemøller SL, Lamberth K, Buus S, et al. Reliable prediction of T cell epitopes using neural networks with novel sequence representations. *Protein Sci* (2003) 12:1007–17. doi:10.1110/ps.0239403
- Peters B, Sette A. Generating quantitative models describing the sequence specificity of biological processes with the stabilized matrix method. *BMC Bioinformatics* (2005) 6:132. doi:10.1186/1471-2105-6-132
- Peters B, Bui H, Frankild S, Nielsen M, Lundegaard C, Kostem E, et al. A community resource benchmarking predictions of peptide binding to MHC-I molecules. *PLoS Comput Biol* (2006) 2:e65. doi:10.1371/journal.pcbi.0020065

7. Rammensee HG, Bachmann J, Emmerich NPN, Bachor OA, Stevanović S. SYFPEITHI: database for MHC ligands and peptide motifs. *Immunogenetics* (1999) 50:213–9. doi:10.1007/s002510050595
8. Parker KC, Bednarek MA, Coligan JE. Scheme for ranking potential HLA-A2 binding peptides based on independent binding of individual peptide side-chains. *J Immunol* (1994) 152:163–75.
9. Lasko TA, Bhagwat JG, Zou KH, Ohno-Machado L. The use of receiver operating characteristic curves in biomedical informatics. *J Biomed Inform* (2005) 38:404–15. doi:10.1016/j.jbi.2005.02.008
10. Nielsen M, Lundsgaard C, Blicher T, Lamberth K, Harndahl M, Justesen S, et al. NetMHCpan, a method for quantitative predictions of peptide binding to any HLA-A and -B locus protein of known sequence. *PLoS One* (2007) 2:e796. doi:10.1371/journal.pone.0000796
11. Murphy K, editor. *Janeway's Immunobiology*. New York: Garland Science (2011).
12. Paul S, Kolla RV, Sidney J, Weiskopf D, Fleri W, Kim Y, et al. Evaluating the immunogenicity of protein drugs by applying in vitro MHC binding data and the immune epitope database and analysis resource. *Clin Dev Immunol* (2013) 2013. doi:10.1155/2013/467852
13. Vita R, Overton JA, Greenbaum JA, Ponomarenko J, Clark JD, Cantrell JR, et al. The immune epitope database (IEDB) 3.0. *Nucleic Acids Res* (2015) 43(D1):D405–12. doi:10.1093/nar/gku938
14. Zhang L, Udaka K, Mamitsuka H, Zhu S. Toward more accurate pan-specific MHC-peptide binding prediction: a review of current methods and tools. *Brief Bioinform* (2012) 13:350–64. doi:10.1093/bib/bbr060
15. Nielsen M, Andreatta M. NetMHCpan-3.0: improved prediction of binding to MHC class I molecules integrating information from multiple receptor and peptide length datasets. *Genome Med* (2016) 8:1. doi:10.1186/s13073-016-0288-x
16. Kim Y, Sidney J, Buus S, Sette A, Nielsen M, Peters B. Dataset size and composition impact the reliability of performance benchmarks for peptide-MHC binding predictions. *BMC Bioinformatics* (2014) 15:1. doi:10.1186/1471-2105-15-241
17. Mouttaftsi M, Peters B, Pasquetto V, Tscharke DC, Sidney J, Bui H, et al. A consensus epitope prediction approach identifies the breadth of murine TCD8-cell responses to vaccinia virus. *Nat Biotechnol* (2006) 24:817–9. doi:10.1038/nbt1215
18. Hoof I, Peters B, Sidney J, Pedersen LE, Sette A, Lund O, et al. NetMHCpan, a method for MHC class I binding prediction beyond humans. *Immunogenetics* (2009) 61:1–13. doi:10.1007/s00251-008-0341-z
19. Lundsgaard C, Lamberth K, Harndahl M, Buus S, Lund O, Nielsen M. NetMHC-3.0: accurate web accessible predictions of human, mouse and monkey MHC class I affinities for peptides of length 8–11. *Nucleic Acids Res* (2008) 36:W509–12. doi:10.1093/nar/gkn202
20. Buus S, Lauemöller S, Worning P, Kesmir C, Frimurer T, Corbet S, et al. Sensitive quantitative predictions of peptide MHC binding by a ‘query by committee’ artificial neural network approach. *Tissue Antigens* (2003) 62:378–84. doi:10.1034/j.1399-0039.2003.00112.x
21. Lundsgaard C, Lund O, Nielsen M. Accurate approximation method for prediction of class I MHC affinities for peptides of length 8, 10 and 11 using prediction tools trained on 9mers. *Bioinformatics* (2008) 24:1397–8. doi:10.1093/bioinformatics/btn128
22. Lundsgaard C, Nielsen M, Lund O. The validity of predicted T-cell epitopes. *Trends Biotechnol* (2006) 24:537–8. doi:10.1016/j.tibtech.2006.10.001
23. Kim Y, Sidney J, Pinilla C, Sette A, Peters B. Derivation of an amino acid similarity matrix for peptide: MHC binding and its application as a Bayesian prior. *BMC Bioinformatics* (2009) 10:394. doi:10.1186/1471-2105-10-394
24. Sidney J, Assarsson E, Moore C, Ngo S, Pinilla C, Sette A, et al. Quantitative peptide binding motifs for 19 human and mouse MHC class I molecules derived using positional scanning combinatorial peptide libraries. *Immunome Res* (2008) 4:2. doi:10.1186/1745-7580-4-2
25. Zhang H, Lund O, Nielsen M. The PickPocket method for predicting binding specificities for receptors based on receptor pocket similarities: application to MHC-peptide binding. *Bioinformatics* (2009) 25:1293–9. doi:10.1093/bioinformatics/btp137
26. Karosiene E, Lundsgaard C, Lund O, Nielsen M. NetMHCcons: a consensus method for the major histocompatibility complex class I predictions. *Immunogenetics* (2012) 64:177–86. doi:10.1007/s00251-011-0579-8
27. Weiskopf D, Angelo MA, de Azeredo EL, Sidney J, Greenbaum JA, Fernando AN, et al. Comprehensive analysis of dengue virus-specific responses supports an HLA-linked protective role for CD8+ T cells. *Proc Natl Acad Sci U S A* (2013) 110:E2046–53. doi:10.1073/pnas.1305227110
28. Paul S, Weiskopf D, Angelo MA, Sidney J, Peters B, Sette A. HLA class I alleles are associated with peptide-binding repertoires of different size, affinity, and immunogenicity. *J Immunol* (2013) 191:5831–9. doi:10.4049/jimmunol.1302101
29. Assarsson E, Sidney J, Oseroff C, Pasquetto V, Bui H, Frahm N, et al. A quantitative analysis of the variables affecting the repertoire of T cell specificities recognized after vaccinia virus infection. *J Immunol* (2007) 178:7890–901. doi:10.4049/jimmunol.178.12.7890
30. Kesmir C, Nussbaum AK, Schild H, Detours V, Brunak S. Prediction of proteasome cleavage motifs by neural networks. *Protein Eng* (2002) 15:287–96. doi:10.1093/protein/15.4.287
31. Nielsen M, Lundsgaard C, Lund O, Kesmir C. The role of the proteasome in generating cytotoxic T-cell epitopes: insights obtained from improved predictions of proteasomal cleavage. *Immunogenetics* (2005) 57:33–41. doi:10.1007/s00251-005-0781-7
32. Larsen MV, Lundsgaard C, Lamberth K, Buus S, Brunak S, Lund O, et al. An integrative approach to CTL epitope prediction: a combined algorithm integrating MHC class I binding, TAP transport efficiency, and proteasomal cleavage predictions. *Eur J Immunol* (2005) 35:2295–303. doi:10.1002/eji.200425811
33. Stranzl T, Larsen MV, Lundsgaard C, Nielsen M. NetCTLpan: pan-specific MHC class I pathway epitope predictions. *Immunogenetics* (2010) 62:357–68. doi:10.1007/s00251-010-0441-4
34. Giguère S, Drouin A, Lacoste A, Marchand M, Corbeil J, Laviolette F. MHC-NP: predicting peptides naturally processed by the MHC. *J Immunol Methods* (2013) 400:30–6. doi:10.1016/j.jim.2013.10.003
35. Peters B, Janek K, Kuckelkorn U, Holzhütter H. Assessment of proteasomal cleavage probabilities from kinetic analysis of time-dependent product formation. *J Mol Biol* (2002) 318:847–62. doi:10.1016/S0022-2836(02)00167-5
36. Lauvås G, Kakimi K, Niedermann G, Ostankovitch M, Yotnda P, Firat H, et al. Human transporters associated with antigen processing (TAPs) select epitope precursor peptides for processing in the endoplasmic reticulum and presentation to T cells. *J Exp Med* (1999) 190:1227–40. doi:10.1084/jem.190.9.1227
37. Peters B, Bulik S, Tampe R, Van Endert PM, Holzhütter HG. Identifying MHC class I epitopes by predicting the TAP transport efficiency of epitope precursors. *J Immunol* (2003) 171:1741–9. doi:10.4049/jimmunol.171.4.1741
38. Tenzer S, Peters B, Bulik S, Schoor O, Lemmel C, Schatz M, et al. Modeling the MHC class I pathway by combining predictions of proteasomal cleavage, TAP transport and MHC class I binding. *Cell Mol Life Sci* (2005) 62:1025–37. doi:10.1007/s00018-005-4528-2
39. Calis JJ, Maybeno M, Greenbaum JA, Weiskopf D, De Silva AD, Sette A, et al. Properties of MHC class I presented peptides that enhance immunogenicity. *PLoS Comput Biol* (2013) 9:e1003266. doi:10.1371/journal.pcbi.1003266
40. Marsh S, Albert E, Bodmer W, Bontrop R, Dupont B, Erlich H, et al. Nomenclature for factors of the HLA system, 2010. *Tissue Antigens* (2010) 75:291–455. doi:10.1111/j.1399-0039.2010.01466.x
41. Wang P, Sidney J, Kim Y, Sette A, Lund O, Nielsen M, et al. Peptide binding predictions for HLA DR, DP and DQ molecules. *BMC Bioinformatics* (2010) 11:568. doi:10.1186/1471-2105-11-568
42. Chaves FA, Lee AH, Nayak JL, Richards KA, Sant AJ. The utility and limitations of current web-available algorithms to predict peptides recognized by CD4 T cells in response to pathogen infection. *J Immunol* (2012) 188:4235–48. doi:10.4049/jimmunol.1103640
43. Andreatta M, Karosiene E, Rasmussen M, Stryhn A, Buus S, Nielsen M. Accurate pan-specific prediction of peptide-MHC class II binding affinity with improved binding core identification. *Immunogenetics* (2015) 67:641–50. doi:10.1007/s00251-015-0873-y
44. Paul S, Arlehamn CSL, Scriba TJ, Dillon MBC, Oseroff C, Hinz D, et al. Development and validation of a broad scheme for prediction of HLA class II restricted T cell epitopes. *J Immunol Methods* (2015) 422:28–34. doi:10.1016/j.jim.2015.03.022
45. Andreatta M, Nielsen M. Gapped sequence alignment using artificial neural networks: application to the MHC class I system. *Bioinformatics* (2016) 32:511–517. doi:10.1093/bioinformatics/btv639

46. Wang P, Sidney J, Dow C, Mothé B, Sette A, Peters B. A systematic assessment of MHC class II peptide binding predictions and evaluation of a consensus approach. *PLoS Comput Biol* (2008) 4:e1000048. doi:10.1371/journal.pcbi.1000048
47. Nielsen M, Lundsgaard C, Blicher T, Peters B, Sette A, Justesen S, et al. Quantitative predictions of peptide binding to any HLA-DR molecule of known sequence: NetMHCIIpan. *PLoS Comput Biol* (2008) 4:e1000107. doi:10.1371/journal.pcbi.1000107
48. Karosiene E, Rasmussen M, Blicher T, Lund O, Buus S, Nielsen M. NetMHCIIpan-3.0, a common pan-specific MHC class II prediction method including all three human MHC class II isotypes, HLA-DR, HLA-DP and HLA-DQ. *Immunogenetics* (2013) 65:711–24. doi:10.1007/s00251-013-0720-y
49. Nielsen M, Lundsgaard C, Lund O. Prediction of MHC class II binding affinity using SMM-align, a novel stabilization matrix alignment method. *BMC Bioinformatics* (2007) 8:238. doi:10.1186/1471-2105-8-238
50. Sturniolo T, Bono E, Ding J, Raddrizzani L, Tuereci O, Sahin U, et al. Generation of tissue-specific and promiscuous HLA ligand databases using DNA microarrays and virtual HLA class II matrices. *Nat Biotechnol* (1999) 17:555–61. doi:10.1038/9858
51. Nielsen M, Lund O. NN-align. An artificial neural network-based alignment algorithm for MHC class II peptide binding prediction. *BMC Bioinformatics* (2009) 10:296. doi:10.1186/1471-2105-10-296
52. Greenbaum J, Sidney J, Chung J, Brander C, Peters B, Sette A. Functional classification of class II human leukocyte antigen (HLA) molecules reveals seven different supertypes and a surprising degree of repertoire sharing across supertypes. *Immunogenetics* (2011) 63:325–35. doi:10.1007/s00251-011-0513-0
53. Southwood S, Sidney J, Kondo A, del Guercio M, Appella E, Hoffman S, et al. Several common HLA-DR types share largely overlapping peptide binding repertoires. *J Immunol* (1998) 160:3363–73.
54. Tangri S, Mothé BR, Eisenbraun J, Sidney J, Southwood S, Briggs K, et al. Rationally engineered therapeutic proteins with reduced immunogenicity. *J Immunol* (2005) 174:3187–96. doi:10.4049/jimmunol.174.6.3187
55. Oseroff C, Sidney J, Kotturi MF, Kolla R, Alam R, Broide DH, et al. Molecular determinants of T cell epitope recognition to the common Timothy grass allergen. *J Immunol* (2010) 185:943–55. doi:10.4049/jimmunol.1000405
56. Paul S, Sidney J, Sette A, Peters B. TepiTool: a pipeline for computational prediction of T cell epitope candidates. *Curr Protoc Immunol* (2016) 114:1–18. doi:10.1002/cipm.12
57. Parker J, Guo D, Hodges R. New hydrophilicity scale derived from high-performance liquid chromatography peptide retention data: correlation of predicted surface residues with antigenicity and X-ray-derived accessible sites. *Biochemistry* (1986) 25:5425–32. doi:10.1021/bi00367a013
58. Emini EA, Hughes JV, Perlow DS, Boger J. Induction of hepatitis A virus-neutralizing antibody by a virus-specific synthetic peptide. *J Virol* (1985) 55:836–9.
59. Pellequer J, Westhof E, Van Regenmortel MH. Correlation between the location of antigenic sites and the prediction of turns in proteins. *Immunol Lett* (1993) 36:83–99. doi:10.1016/0165-2478(93)90072-A
60. Chou P, Fasman G. Prediction of the secondary structure of proteins from their amino acid sequence. *Adv Enzymol Relat Areas Mol Biol* (1978) 47:45–148.
61. Karplus P, Schulz G. Prediction of chain flexibility in proteins. *Naturwissenschaften* (1985) 72:212–3. doi:10.1007/BF01195768
62. Kolaskar A, Tongaonkar PC. A semi-empirical method for prediction of antigenic determinants on protein antigens. *FEBS Lett* (1990) 276:172–4. doi:10.1016/0014-5793(90)80535-Q
63. Larsen JEP, Lund O, Nielsen M. Improved method for predicting linear B-cell epitopes. *Immunome Res* (2006) 2:1. doi:10.1186/1745-7580-2-1
64. Haste Andersen P, Nielsen M, Lund O. Prediction of residues in discontinuous B-cell epitopes using protein 3D structures. *Protein Sci* (2006) 15:2558–67. doi:10.1110/ps.062405906
65. Krugelum JV, Lundsgaard C, Lund O, Nielsen M. Reliable B cell epitope predictions: impacts of method development and improved benchmarking. *PLoS Comput Biol* (2012) 8:e1002829. doi:10.1371/journal.pcbi.1002829
66. Ponomarenko J, Bui H, Li W, Fuseder N, Bourne PE, Sette A, et al. ElliPro: a new structure-based tool for the prediction of antibody epitopes. *BMC Bioinformatics* (2008) 9:1. doi:10.1186/1471-2105-9-514
67. Ponomarenko JV, Bourne PE. Antibody-protein interactions: benchmark datasets and prediction tools evaluation. *BMC Struct Biol* (2007) 7:1. doi:10.1186/1472-6807-7-64
68. Rubinstein ND, Mayrose I, Martz E, Pupko T. Epitopia: a web-server for predicting B-cell epitopes. *BMC Bioinformatics* (2009) 10:287. doi:10.1186/1471-2105-10-287
69. Sweredoski MJ, Baldi P. PEPITO: improved discontinuous B-cell epitope prediction using multiple distance thresholds and half sphere exposure. *Bioinformatics* (2008) 24:1459–60. doi:10.1093/bioinformatics/btn199
70. Thornton JM, Edwards MS, Taylor WR, Barlow DJ. Location of ‘continuous’ antigenic determinants in the protruding regions of proteins. *EMBO J* (1986) 5:409–13.
71. Webb B, Sali A. Comparative protein structure modeling using Modeller. *Curr Protoc Bioinformatics* (2016) 54:5.6.1–5.6.37. doi:10.1186/1471-2105-11-568
72. Zhang Y. I-TASSER server for protein 3D structure prediction. *BMC Bioinformatics* (2008) 9:1. doi:10.1186/1471-2105-9-40
73. Yang J, Yan R, Roy A, Xu D, Poisson J, Zhang Y. The I-TASSER suite: protein structure and function prediction. *Nat Methods* (2015) 12:7–8. doi:10.1038/nmeth.3213
74. Sircar A, Kim ET, Gray JJ. RosettaAntibody: antibody variable region homology modeling server. *Nucleic Acids Res* (2009) 37:W474–9. doi:10.1093/nar/gkp387
75. Marcatili P, Olimpieri PP, Chailyan A, Tramontano A. Antibody modeling using the prediction of immunoglobulin structure (PIGS) web server. *Nat Protoc* (2014) 9:2771–83. doi:10.1038/nprot.2014.189
76. Schneidman-Duhovny D, Inbar Y, Nussinov R, Wolfson HJ. PatchDock and SymmDock: servers for rigid and symmetric docking. *Nucleic Acids Res* (2005) 33:W363–7. doi:10.1093/nar/gki481
77. Comeau SR, Gatchell DW, Vajda S, Camacho CJ. ClusPro: a fully automated algorithm for protein-protein docking. *Nucleic Acids Res* (2004) 32:W96–9. doi:10.1093/nar/gkh354
78. Andrusier N, Nussinov R, Wolfson HJ. FireDock: fast interaction refinement in molecular docking. *Proteins* (2007) 69:139–59. doi:10.1002/prot.21495
79. Mashiah E, Schneidman-Duhovny D, Andrusier N, Nussinov R, Wolfson HJ. FireDock: a web server for fast interaction refinement in molecular docking. *Nucleic Acids Res* (2008) 36:W229–32. doi:10.1093/nar/gkn186
80. Bui HH, Sidney J, Dinh K, Southwood S, Newman MJ, Sette A. Predicting population coverage of T-cell epitope-based diagnostics and vaccines. *BMC Bioinformatics* (2006) 7:153. doi:10.1186/1471-2105-7-153
81. Gonzalez-Galarza FF, Takeshita LY, Santos EJ, Kempson F, Maia MH, da Silva AL, et al. Allele frequency net 2015 update: new features for HLA epitopes, KIR and disease and HLA adverse drug reaction associations. *Nucleic Acids Res* (2015) 43:D784–8. doi:10.1093/nar/gku1166
82. Bui HH, Peters B, Assarsson E, Mbawuike I, Sette A. Ab and T cell epitopes of influenza A virus, knowledge and opportunities. *Proc Natl Acad Sci U S A* (2007) 104:246. doi:10.1073/pnas.0609330104

**Conflict of Interest Statement:** The authors declare that the research was conducted in the absence of any commercial or financial relationships that could be construed as a potential conflict of interest.

Copyright © 2017 Fleri, Paul, Dhanda, Mahajan, Xu, Peters and Sette. This is an open-access article distributed under the terms of the Creative Commons Attribution License (CC BY). The use, distribution or reproduction in other forums is permitted, provided the original author(s) or licensor are credited and that the original publication in this journal is cited, in accordance with accepted academic practice. No use, distribution or reproduction is permitted which does not comply with these terms.



OPEN ACCESS

**Edited by:**

Daniela Santoro Rosa,  
Federal University of  
São Paulo, Brazil

**Reviewed by:**

Vijay Panchanathan,  
Perdana University, Malaysia  
Armelle Phalipon,  
Institut Pasteur, France

**\*Correspondence:**

Ekaterina A. Kurbatova  
kurbatova6162@yandex.ru;  
Nelli K. Akhmatova  
anelly@mail.ru;  
Nikolay E. Nifantiev  
nen@ioc.ac.ru

**Specialty section:**

This article was submitted  
to Vaccines and  
Molecular Therapeutics,  
a section of the journal  
*Frontiers in Immunology*

**Received:** 18 October 2016

**Accepted:** 18 May 2017

**Published:** 02 June 2017

**Citation:**

Kurbatova EA, Akhmatova NK,  
Akhmatova EA, Egorova NB,  
Yastrebova NE, Sukhova EV,  
Yashunsky DV, Tsvetkov YE,  
Gening ML and Nifantiev NE (2017)

Neoglycoconjugate of  
Tetrasaccharide Representing One  
Repeating Unit of the *Streptococcus*  
*pneumoniae* Type 14 Capsular  
Polysaccharide Induces the  
Production of Opsonizing IgG1  
Antibodies and Possesses the  
Highest Protective Activity As  
Compared to Hexa- and  
Octasaccharide Conjugates.

*Front. Immunol.* 8:659.

doi: 10.3389/fimmu.2017.00659

# Neoglycoconjugate of Tetrasaccharide Representing One Repeating Unit of the *Streptococcus pneumoniae* Type 14 Capsular Polysaccharide Induces the Production of Opsonizing IgG1 Antibodies and Possesses the Highest Protective Activity As Compared to Hexa- and Octasaccharide Conjugates

Ekaterina A. Kurbatova<sup>1\*</sup>, Nelli K. Akhmatova<sup>1\*</sup>, Elina A. Akhmatova<sup>2</sup>, Nadezhda B. Egorova<sup>1</sup>, Natalya E. Yastrebova<sup>1</sup>, Elena V. Sukhova<sup>2</sup>, Dmitriy V. Yashunsky<sup>2</sup>, Yury E. Tsvetkov<sup>2</sup>, Marina L. Gening<sup>2</sup> and Nikolay E. Nifantiev<sup>2\*</sup>

<sup>1</sup>Laboratory of Therapeutic Vaccines, Mechnikov Research Institute for Vaccines and Sera, Moscow, Russia,

<sup>2</sup>Laboratory of Glycoconjugate Chemistry, N. D. Zelinsky Institute of Organic Chemistry, Russian Academy of Sciences, Moscow, Russia

Identifying protective synthetic oligosaccharide (OS) epitopes of *Streptococcus pneumoniae* capsular polysaccharides (CPs) is an indispensable step in the development of third-generation carbohydrate pneumococcal vaccines. Synthetic tetra-, hexa-, and octasaccharide structurally related to CP of *S. pneumoniae* type 14 were coupled to bovine serum albumin (BSA), adjuvanted with aluminum hydroxide, and tested for their immunogenicity in mice upon intraperitoneal prime-boost immunizations. Injections of the conjugates induced production of opsonizing anti-OS IgG1 antibodies (Abs). Immunization with the tetra- and octasaccharide conjugates stimulated the highest titers of the specific Abs. Further, the tetrasaccharide ligand demonstrated the highest ability to bind OS and CP Abs. Murine immune sera developed against tetra- and octasaccharide conjugates promoted pathogen opsonization to a higher degree than antisera against conjugated hexasaccharide. For the first time, the protective activities of these glycoconjugates were demonstrated in mouse model of generalized pneumococcal infections. The tetrasaccharide conjugate possessed the highest protective activities. Conversely, the octasaccharide conjugate had lower protective activities

**Abbreviations:** CP, capsular polysaccharide; BSA, bovine serum albumin; OS, oligosaccharide; Ab, antibody; MALDI-TOF, matrix laser desorption ionization time-of-flight; ELISA, enzyme-linked immunosorbent assay.

and the lowest one showed the hexasaccharide conjugate. Seras against all of the glycoconjugates passively protected naive mice from pneumococcal infections. Given that the BSA-tetrasaccharide induced the most abundant yield of specific Abs and the best protective activity, this OS may be regarded as the most promising candidate for the development of conjugated vaccines against *S. pneumoniae* type 14 infections.

**Keywords:** *Streptococcus pneumoniae* type 14, synthetic oligosaccharide, glycoconjugate vaccine protective activity, antibody specificity, opsonophagocytosis, biotinylated oligosaccharide

## INTRODUCTION

*Streptococcus pneumoniae* are Gram-positive bacteria that cause invasive and non-invasive, often lethal, infections in multiple anatomic locations in adults and children (1, 2). Pneumococci capsules are one of the major virulence factors for this class of bacteria (3). Based on the chemical structure of capsular polysaccharides (CPs), more than 90 different serotypes of *S. pneumoniae* have been identified, approximately 20 of which are responsible for 80–90% of all pneumococcal infections (4, 5).

Epidemiologic data have shown that vaccination is an effective way to prevent pneumococcal infection. Studies of unconjugated polysaccharide-based pneumococcal vaccine of the first-generation confirmed its efficacy and safety in adults (6). At the same time, disadvantages of such vaccines have been observed, including inefficiency in children less than 2 years of age and in certain risk groups (7), absence of boosting effects upon revaccination, suggesting insufficient development of immune memory (8).

These disadvantages of polysaccharide vaccines have been overcome in carbohydrate vaccines of the second-generation consisting of CP conjugated to a protein carrier. This results in switching the syntheses of antibodies (Abs) to the carbohydrate component of the conjugate from IgM to IgG, their affinity maturation, formation of immunological memory, and protection of the host from infection by inducing complement-mediated opsonophagocytosis (8–11). The use of pneumococcal conjugate vaccines of the second-generation based on CP of clinically relevant serotypes of *S. pneumoniae* led to a significant reduction in the incidence of pneumococcal infections (5).

However, the use of native CP for production of conjugated vaccines has a number of disadvantages connected with difficulties in bacteria cultivation, isolation, and purification of CP and, in some cases, unsuccessful conjugation of CP to protein carriers (12). A promising direction is the development of carbohydrate pneumococcal vaccines of the third-generation based on synthetic oligosaccharides (OSs) related to the structurally defined regions of CP coupled to protein carriers (13).

To date, the structures of pneumococcal CP of different serotypes have been well described (14). Numerous synthetic OSs that bear structural similarities to CP of serotypes 1–4, 6A/B, 7F, 8, 9A/V, 14, 17F, 18C, 19A/F, 22F, 23F, 27, and 29 have been characterized (15). Several of these OSs have been conjugated to carrier proteins and tested as potential vaccines (13, 16). Advantages of OS-protein conjugate-based vaccines include the absence of bacterial impurities, high serotype specificity of immune responses, and ability of some of them to induce stronger Ab responses compared with traditional conjugated vaccines (16), known and

specific engineering of the chemical structures of the synthetic OS allowing for controlled conjugations to carrier proteins, and standardized methods that comply with modern vaccine production requirements. Well-established chemical structures of OS favor to determine the role of specific CP features on the formation of immune responses.

*Streptococcus pneumoniae* CP type 14 consists of branched tetrasaccharide repeating units (17) (**Figure 1**). This CP has relatively low immunogenicity when compared with other pneumococcal CP serotypes (18). The CP type 14 serotype is very common in the human population (1–3, 19, 20) and frequently infects younger children (14). Previously, the tetrasaccharide ligand ( $\beta$ -D-Gal-(1 $\rightarrow$ 4)- $\beta$ -D-Glc-(1 $\rightarrow$ 6)-[ $\beta$ -D-Gal-(1 $\rightarrow$ 4)]- $\beta$ -D-GlcNAc) was described as a good candidate to serve as the *S. pneumoniae* type 14 conjugated vaccine ligand (21). However, these data have not been substantiated with experiments demonstrating protective activity in murine models.

Here, we present for the first time the comparative study of the ability of tetra-bovine serum albumin (BSA), hexa-BSA, and octa-BSA conjugates related to CP of *S. pneumoniae* type 14 to induce anti-CP and anti-OS opsonizing Abs and the evaluation of the efficacy of each neoglycoconjugate in the models of active and passive protection of mice.

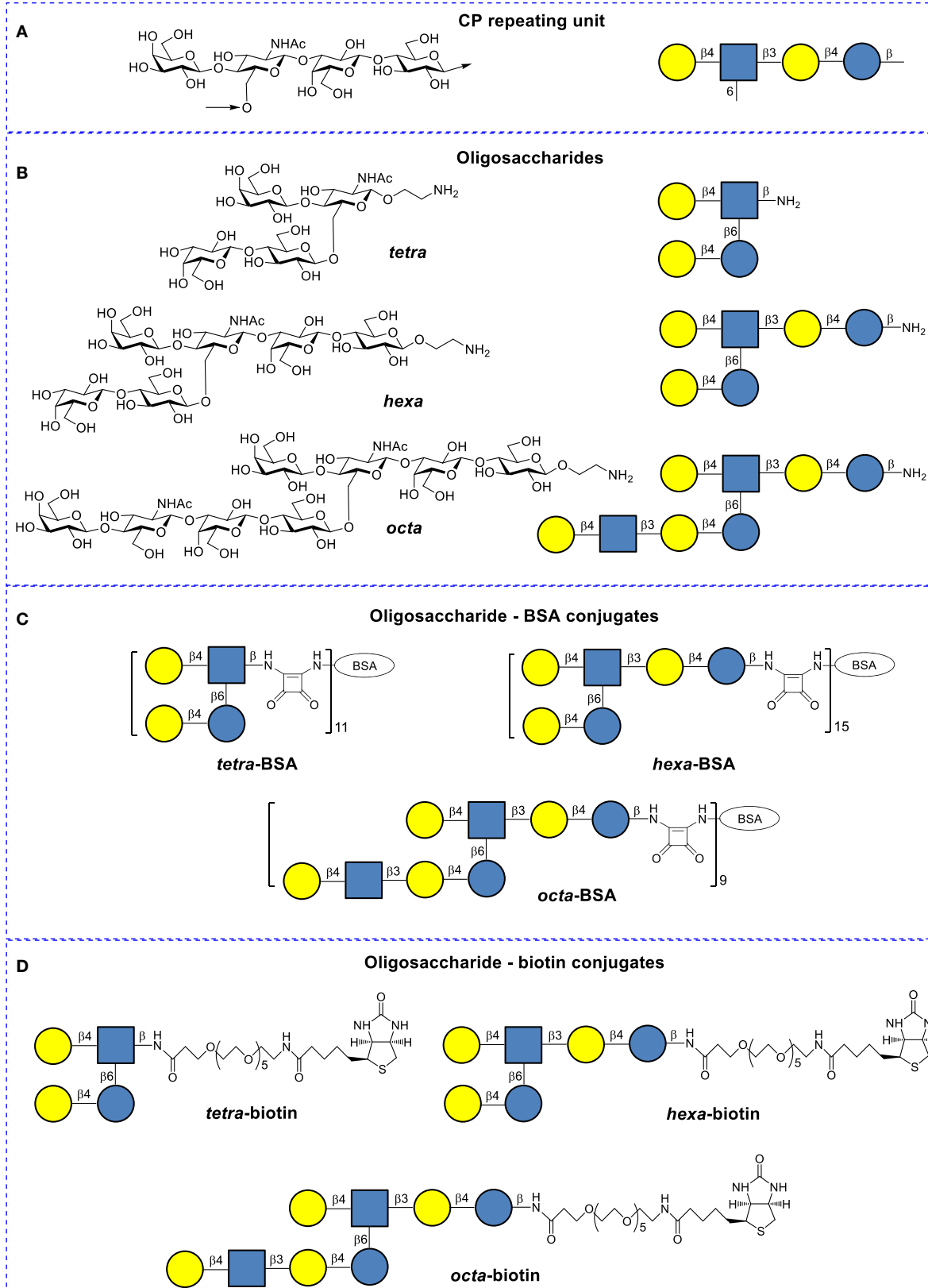
## MATERIALS AND METHODS

### Synthetic OSs and Their Conjugates

Oligosaccharides were conjugated to BSA (Sigma-Aldrich, USA) and biotin (structures and designations are given in **Figure 1**), as previously described (22, 23). BSA has been frequently used as a protein carrier in engineered immunogenic glycoconjugates and other types of biomolecular systems (24). Matrix laser desorption ionization time-of-flight data demonstrate that the tetra-BSA, hexa-BSA, and octa-BSA conjugates contained on average 11, 15, and 9 OS ligands per protein molecule, corresponding to carbohydrate contents (by weight) of 10, 19, and 16%, respectively (22).

### Synthetic and Bacterial CPs

*Streptococcus pneumoniae* serotype 14 synthetic CP containing an average of 10 tetrasaccharide repeats per polymer was generated using polycondensation reactions (25). Bacterial CPs were obtained from the laboratory strain of *S. pneumoniae* type 14 #883 isolated on April 22, 2012, from a child with acute otitis media at the Microbiology department of the “Scientific Center of Children’s Health” of the Ministry of Health of the Russian Federation (Moscow). The strain was expanded in semi-synthetic

**FIGURE 1 | Continued**

**FIGURE 1 | Continued**

Structures of *Streptococcus pneumoniae* type 14 capsular polysaccharides and their conjugates. **(A)** Repeating unit of the *S. pneumoniae* type 14 CP (structural and symbolic representations). **(B)** Synthetic spacer-armed oligosaccharides (OSs) used to prepare bovine serum albumin (BSA) and biotin conjugates (structural and symbolic representations). **(C)** BSA conjugates of synthetic OSs. **(D)** Biotin conjugates of synthetic OSs.

nutrient media. Isolation of CP was previously described (26). The presence of CP in the preparation was confirmed by NMR spectrometry.

## Animals

BALB/c male mice aged 6–8 weeks and 2 “Chinchilla” rabbits weighing 2.5 kg were purchased from the Scientific and Production Center for Biomedical Technologies (Moscow, Russia) and kept in the vivarium of the Mechnikov Research Institute for Vaccines and Sera. The housing, husbandry, blood sampling, and sacrificing conditions conformed to the European Union guidelines for the care and use of laboratory animals. Experimental designs were approved by the Mechnikov Research Institute for Vaccines and Sera Ethics Committee.

## Immunization

Mice were immunized intraperitoneally with tetra-BSA, hexa-BSA, and octa-BSA conjugates adjuvanted with aluminum hydroxide (Sigma-Aldrich Co., USA). Animals were dosed twice, on days 0 and 14 of the experiments. A single dose of glycoconjugates ranged from 10 to 1.25 µg (carbohydrate content) in twofold dilutions in saline. Aluminum hydroxide was added in an amount of 25 µL (250 µg) per immunizing dose and stored overnight at 4°C. Similar immunization schedules were used for immunization of mice with doses of the Prevenar-13 (Pfizer, USA) pneumococcal conjugate vaccine containing aluminum phosphate as an adjuvant, and doses of the Pneumo-23 (Aventis Pasteur, France) polysaccharide vaccine. Prevenar-13 murine vaccinations were single doses of either 2.2 or 1.1 µg per immunization (equivalent to 1 or 1/2 the recommended dose for humans). The Prevnar-13 vaccine contained *S. pneumoniae* type 14 CP conjugated with the inactive diphtheria toxin, CRM<sub>197</sub>, as the protein carrier. Pneumo-23 murine vaccinations were a single dose of 5 µg CP (corresponding to 1/5 of the dose recommended for humans). Antibacterial sera were recovered by repeated immunization of rabbits with inactivated *S. pneumoniae* type 14 bacteria.

## Measurement of Ab Response to CP and OS

Murine sera were collected 14 days after the second immunization with the OS conjugates, or with CRM<sub>197</sub>-CP included in the Prevenar-13 vaccine, as described earlier. Ab titers were measured by enzyme-linked immunosorbent assay (ELISA) from individual blood samples of 6–12 mice/dose (the results of two experiments), or from pooled sera of 6 mice/conjugate, as previously described (27). To prepare for the titer assays, flat-bottom plates (Biomedicals, Russia) were coated with *S. pneumoniae* type 14 bacterial CP (1 µg/well) or synthetic CP (0.5 µg/well). Wells were also coated with CP, tetra-BSA, hexa-BSA, and octa-BSA conjugates (0.4 µg/well) to determine murine post-immunization

Ab titers. Rabbit anti-mouse peroxidase-conjugated IgG1 Abs (gamma 1 chain; Rockland Immunochemicals, Inc., USA) were used as secondary Abs.

Antibody titers to OSs of glycoconjugate-immunized mice were detected on streptavidin-coated 96-well plates (Pierce®, Thermo Scientific Inc., USA) with binding capacities of 5 pmol biotin/well. OS-biotin conjugates were adsorbed on streptavidin-coated 96-well plates at 15 pmol/well. Washes were performed with phosphate-buffered saline (PBS) (Sigma, USA) supplemented with 0.05% Tween 20 (Panreac Syntesis, Spain). ELISA was performed according to the manufacturer's instructions. Briefly, 150 nM solutions diluted in PBS of each biotinylated OS (100 µL/well) were transferred into streptavidin-coated wells. OSs were incubated for 2 h with shaking (300 RPM) at room temperature. Each well was washed three times with 200 µL of wash buffer. Serial dilutions of antisera were prepared and added to each well. Plates were incubated for 30 min at room temperature. Each well was washed three times with 200 µL of wash buffer. Secondary rabbit anti-mouse peroxidase-conjugated IgG1 Abs or goat anti-rabbit peroxidase-conjugated IgG Abs (Thermo Scientific, USA) were added to each well. After 30 min of incubation with shaking (300 RPM) at room temperature, wells were washed three times with 200 µL of wash buffer. Enzyme substrate aliquots were added, followed by incubation for 15 min at room temperature. Optical densities (ODs) were determined with a microplate reader (iMark, Japan) at 450 nm. Antibody titers are expressed as dilution of serum or as log<sub>10</sub> values.

## Antigen-Binding Capacity of Glycoconjugates-Induced Ab

To study the Ab-binding capacity in the sera of mice immunized with OS-conjugates, CP, or bacteria, biotinylated OSs were adsorbed on the bottom of streptavidin-coated 96-well plates (Thermo Scientific, USA) with a binding capacity of 5 pmol biotin/well. After adding immune antisera (90 µL/well), a concentration gradient of the OS ligands and synthetic CP or bacterial CP in PBS (1–10 µg/well) was inoculated into the wells. PBS (10 µL) was added in the control wells. The ELISA reaction procedures were the same as described earlier. Incubations with ligands and CP were carried out for 1 h at 37°C. Plates were washed three times with 200 µL/well of PBS-Tween 20. Next, working dilutions of peroxidase-conjugated rabbit anti-mouse IgG1 Abs (Rockland Immunochemicals, USA) or goat anti-rabbit peroxidase-conjugated IgG Abs (Thermo Scientific, USA) were added, as appropriate. Plates were incubated for 45 min at 37°C and then washed three times with 200 µL/well of PBS-Tween 20. Next, 100 µL of TMB was added per well to stain the bound reaction products. After 15 min, the reactions were quenched with 1 M H<sub>2</sub>SO<sub>4</sub>. ODs were determined at 450 nm with a microplate reader. The results were presented here as 50% inhibitory concentration

( $IC_{50}$ ) values.  $IC_{50}$  values were the concentrations of inhibitors that led to a twofold decrease of the OD and were calculated using calibration curves.

Flat-bottom plates (Biomedicals, Russia) coated with synthetic CP (0.5  $\mu$ g/well) were also used. The procedure was the same as described earlier.

### Opsonophagocytosis Assay

The opsonizing activities of Abs elicited against the glycoconjugates were quantified by measuring uptake of heat-killed *S. pneumoniae* type 14 bacterial cells by neutrophils and monocytes in the peripheral blood of untreated mice. Heat-killed bacteria were labeled by fluorescein isothiocyanate (FITC). FITC-labeled bacteria ( $10^9$  cells/mL) were treated with sera (10  $\mu$ L) from non-immunized mice ( $n = 6$ ) or the antisera (10  $\mu$ L) from mice ( $n = 6$  for each conjugate) vaccinated twice with each of the synthetic conjugates (10  $\mu$ g of carbohydrate) and then harvested 2 weeks after the second immunization. Either (1) heat-killed FITC-labeled bacteria, (2) heat-killed FITC-labeled bacteria treated by non-immune sera, or (3) heat-killed FITC-labeled bacteria treated with antiserum to each BSA conjugate were added to peripheral blood from non-immunized mice ( $n = 10$ ). Sera and antisera were added to the bacteria at a 1:1 ratio and then incubated for 20 min at 37°C and washed by centrifugation (2,500 g, 10 min) in RPMI-1640 (Sigma, USA). The number of neutrophils and monocytes that internalized FITC-labeled bacteria was determined by flow cytometry (Cytomix FC-500, Beckman Coulter, USA, with CXP software). Cell population gates were determined by front and side light scattering and cell size; there were 10,000 cells/gate. The results were presented as the percentage of neutrophils or monocytes that phagocytized heat-killed FITC-labeled *S. pneumoniae* type 14 cells.

### Glycoconjugates-Induced Passive Protection in Naive Mice

BALB/c mice were intraperitoneally immunized once with 25  $\mu$ L of pooled immune sera obtained from the glycoconjugate-exposed mice ( $n = 6$ ) as described earlier; each single dose of each glycoconjugate was 10  $\mu$ g (carbohydrate content) per mouse. Each serum was tested in eight unexposed mice. Control injections (25  $\mu$ L) included sera from non-immunized mice given to unexposed mice ( $n = 8$ ), and eight unexposed mice received only saline. Two hours after the serum inoculations, mice were challenged with intraperitoneal exposure to *S. pneumoniae* type 14. Mortality rates were calculated 7 days post-infection.

### Glycoconjugate-Induced Active Protection in Immunized Mice

BALB/c mice were immunized twice intraperitoneally with each glycoconjugate in twofold dilutions from 10 to 1.25  $\mu$ g (carbohydrate content) per mouse on days 0 and 14. The same animals were challenged after 2 weeks interval with  $5 \times 10^8$  colony forming units of *S. pneumoniae* type 14/0.5 mL. Non-immunized control mice (8–10 animals/group) were also challenged with the type 14 bacteria. As reference agents, Pneumo-23 and Prevenar-13 were given at single doses of 5 and 1.1  $\mu$ g of CP *S. pneumoniae* type 14, respectively, and injected according to the same schedule as

described earlier. The results of three experiments were measured. Mortality rates were calculated at 7 days post-infection.

### Statistical Analysis

Groups were compared using Mann–Whitney rank sum tests for independent samples. Yates-corrected Chi-square tests were used to evaluate survival of mice after the challenges.  $P$  values of  $\leq 0.05$  were considered statistically significant (STATISTICA 10 software).

## RESULTS

### Anti-CP Response Induced by the Glycoconjugates

Only IgG1 Ab titer levels were assessed in the sera of glycoconjugate-immunized mice, as the level of IgG2a, IgG2b, and IgG3 was previously shown to be low in exposed animals (26). Post-immunization anti-CP Ab titer levels were determined in individual murine blood sera in ELISA using *S. pneumoniae* type 14 CP as the coating antigen (Figure 2). The highest IgG1 Ab titers were induced against glycoconjugate injections at the dose of 10  $\mu$ g (carbohydrate content). Ab titers to tetrasaccharide conjugates (Figure 2A) had no difference with hexasaccharide conjugates (Figure 2B) and were lower than to the octasaccharide conjugates (Figure 2C) ( $P < 0.05$ ).

IgG1 Ab titers in sera of mice immunized with conjugated pneumococcal vaccine Prevenar-13 (contains *S. pneumoniae* type 14 CP-CRM<sub>197</sub>) were evaluated using each neoglycoconjugates, synCP, and bacCP as coating antigens (Figure 3). The highest titers of IgG1 Abs in the same sera to Prevenar-13 were detected against the tetra-BSA conjugate, lower titers were detected against the hexa-BSA and octa-BSA conjugates, and the lowest titer of IgG1 Abs was detected against synCP and bacCP.

In contrast to *S. pneumoniae* type 14 CP, the tetra-BSA conjugate possessed the highest ability to recognize CP-induced IgG1 Abs.

### Anti-OS Response Induced by the Glycoconjugates

The titers of anti-OS IgG1 Abs were measured against biotinylated OSs in the pooled sera of glycoconjugate-immunized mice (Figure 4A). The highest levels of IgG1 anti-OS Abs were observed in the sera of mice immunized with the tetra-BSA and octa-BSA conjugates. The lowest level of Abs was detected in the serum generated by exposure to the hexa-BSA conjugate ( $P < 0.05$ ).

Titer levels of IgG1 Abs to tetra-, hexa-, and octasaccharide in pooled sera from these two groups of mice immunized with the pneumococcal conjugate vaccine Prevenar-13 at doses of either 1.1 or 2.2  $\mu$ g (CP content) were also measured using biotinylated OS (Figure 4B). Ab titers were higher with administration of the 2.2- $\mu$ g/mouse dose, when compared with the lower dose (1.1- $\mu$ g/mouse;  $P < 0.05$ ). The titers of IgG1 Abs to the tetra- and octasaccharide in both pooled sera exceeded the level of Abs generated against the hexasaccharide ( $P < 0.05$ ).

Investigations of two antibacterial sera obtained by repeated immunization of rabbits with inactivated bacterial cells revealed differences between the levels of anti-OS Abs detected using

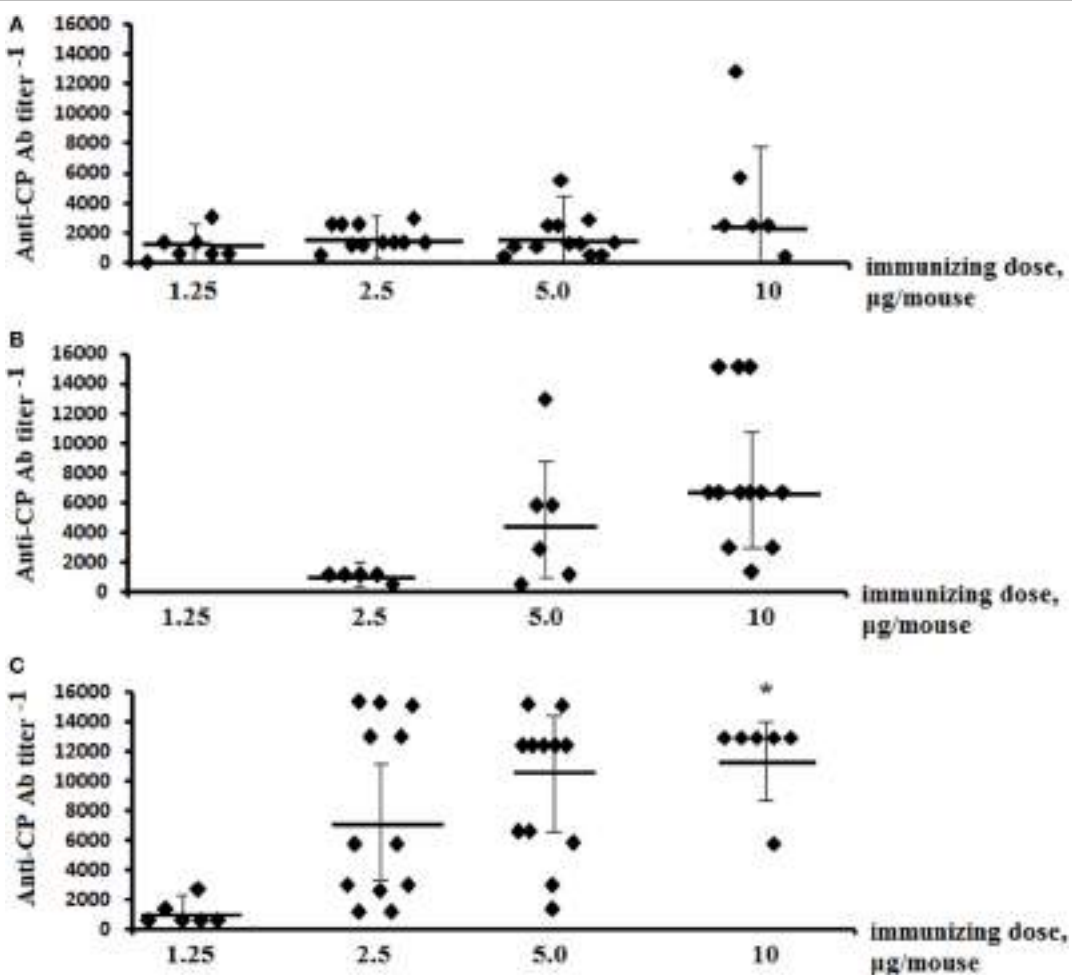


**FIGURE 2 |** Anti-CP IgG1 antibody (Ab) titers in mice immunized with the glycoconjugates. BALB/c mice were immunized intraperitoneally with tetra-bovine serum albumin (BSA) **(A)**, hexa-BSA **(B)**, and octa-BSA **(C)** conjugates adsorbed on aluminum hydroxide twice over 14 days at 1.25–10 µg/dose (the hexa-BSA conjugate was injected at 2.5–10 µg/dose). Anti-CP IgG1 Ab titers in murine blood sera were determined by enzyme-linked immunosorbent assay 2 weeks after the second immunization. *Streptococcus pneumoniae* type 14 bacterial CP was used as the coating antigens. The data from two experiments were summarized. For each glycoconjugate, blood was taken from 6 to 12 mice. The data represent individual anti-CP IgG1 Ab titers, bars indicates median  $\pm$  SD. Mann–Whitney Rank Sum tests were used to evaluate significance. Differences in the anti-CP IgG1 Ab titers between tetra-BSA and octa-BSA conjugates at the immunizing dose of 10 µg/mouse, \* $P < 0.05$ .

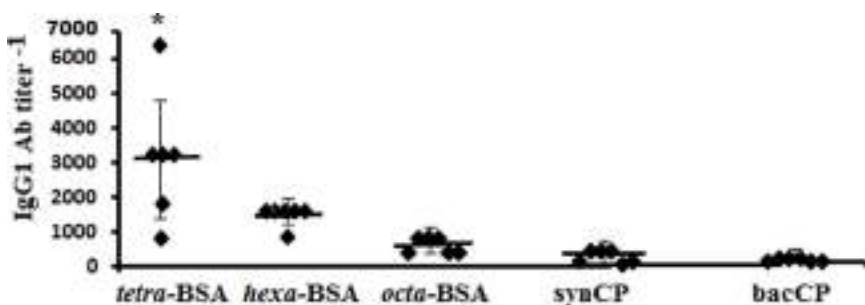


**FIGURE 3 |** IgG1 antibody (Ab) titer in mice immunized with *Streptococcus pneumoniae* type 14 CP. BALB/c mice received two intraperitoneal immunizations with the conjugated pneumococcal vaccine Prevenar-13 with aluminum phosphate as adjuvant at 1.1 µg (content of *S. pneumoniae* type 14 CP) per dose. The tetra-bovine serum albumin (BSA), hexa-BSA, and octa-BSA conjugates, and synthetic (synCP) and bacterial CP (bacCP) were capture antigens, coating the enzyme-linked immunosorbent assay plates. The data are represented by individual titers of IgG1 Abs, bars indicate median  $\pm$  SD. Mann–Whitney Rank Sum tests were used to determine significance. For differences in the level of Abs detected against tetra-BSA and octa-BSA conjugates, \* $P < 0.05$ .

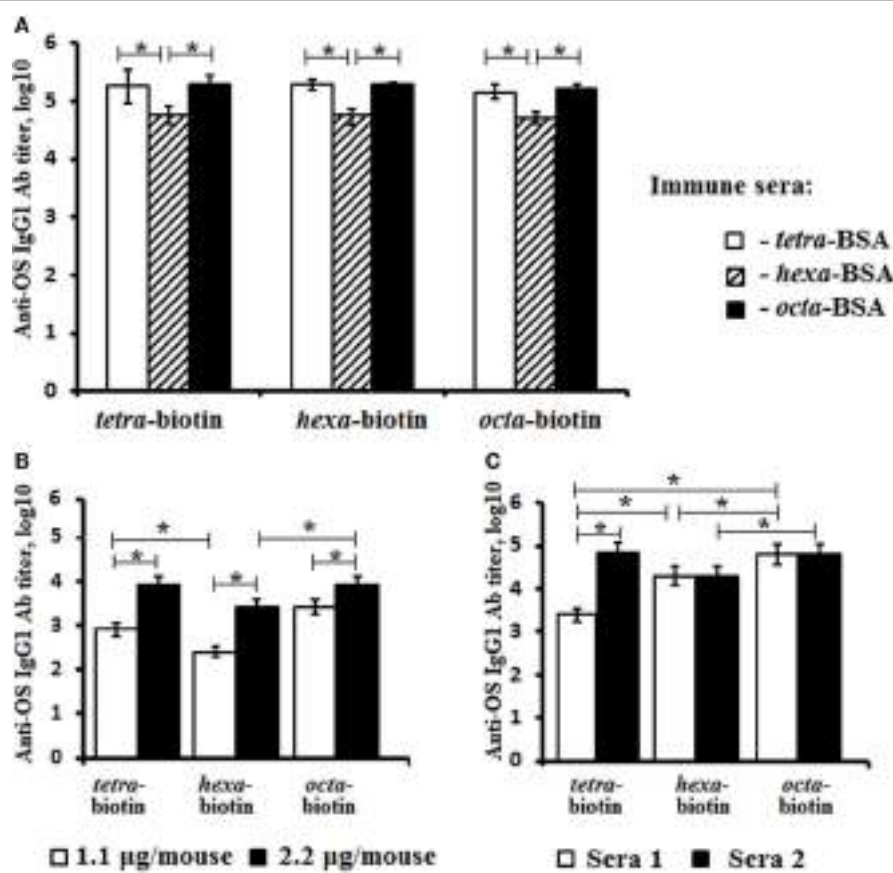


**FIGURE 4 |** Anti-OS IgG1 antibody (Ab) titer in mice immunized with the OS-conjugates, CP, or bacteria. The biotinylated oligosaccharides tetra-biotin, hexa-biotin, and octa-biotin were applied as coating antigens. **(A)** Fourteen days after the second immunization, IgG1 Ab titers were determined in the pooled sera of BALB/c mice ( $n = 6$ ) intraperitoneally vaccinated with a single dose (10  $\mu$ g) of each conjugate adsorbed on aluminum hydroxide. **(B)** Fourteen days after the second immunization, the IgG1 Ab titers were measured in the pooled sera of two groups of BALB/c mice ( $n = 6$ ) who were intraperitoneally vaccinated with single doses of either 1.1 or 2.2  $\mu$ g (CP content) of *Streptococcus pneumoniae* type 14 CP-CPM<sub>197</sub> adsorbed on aluminum phosphate. **(C)** The level of IgG Abs in rabbits ( $n = 2$ ) immunized with inactive *S. pneumoniae* type 14 bacterial cells. Ab titers were transformed to log<sub>10</sub>.  $n = 6$  assays per antiserum. The data are displayed as a mean value  $\pm$  SD. Mann-Whitney Rank Sum tests were used to determine significance,  $^*P < 0.05$ .

biotinylated OS (Figure 4C). In antibacterial serum 1, IgG Ab titers to the tetrasaccharide were lower than hexa- and octasaccharide Ab titers (Log<sub>10</sub>, 3.4 vs. 4.3 and 4.8, respectively;  $P < 0.05$ ). Conversely, serum 2 had higher levels of IgG Abs against the tetra- and octasaccharides with the lowest level of Abs generated against the hexasaccharide ( $P < 0.05$ ).

Antibodies in glycoconjugate-induced sera, as well as anti-CP and anti-pneumococcal whole cell sera of animals recognized synthetic OSs of different length.

### Antigen-Binding Capacity of the Glycoconjugate-Induced Abs

Antigen-binding capacities of the Abs in the immune sera to OS-conjugates, CP, or bacteria were tested in ELISA using streptavidin plates coated with biotinylated tetra-, hexa-, and octasaccharides (Figure 5). Inhibition of binding was carried out by blocking binding reactions with biotinylated OS after incubation with the tetra-, hexa-, and octasaccharide ligands, as well as synCP and bacCP into immune sera.

In the system tetra-BSA antisera/tetra-biotin, the tetrasaccharide ligand had the highest inhibitory capacity, followed by synCP and bacCP (Figure 5A). For the hexa-BSA antisera/hexa-biotin, the best inhibitory activities were demonstrated by the tetra- and hexasaccharide ligands, synCP, and bacCP (Figure 5B). For the octa-BSA antisera/octa-biotin, the highest inhibitory activity possessed the tetrasaccharide ligand and synCP (Figure 5C). Taken together, the tetrasaccharide ligand had the maximal abilities to inhibit binding between anti-OS IgG1Abs and bound biotinylated OS.

In CRM<sub>197</sub>-CP-exposed sera/tetra-biotin, the tetrasaccharide ligand, as well as synCP and bacCP, had high inhibitory activity (Figure 5D). The tetrasaccharide ligand, as well as synCP and bacCP, inhibited interactions of anti-CP Abs with hexa-biotin in a higher degree than the hexa- and octasaccharide. The same results were obtained in the system CRM<sub>197</sub>-CP-antisera/octa-biotin. Thus, the tetrasaccharide ligand exhibited maximal binding inhibitions between anti-CP IgG1 Abs and biotinylated OS.

For the first rabbit antibacterial sera (Sera 1), the tetrasaccharide ligand and synCP possessed the highest inhibitory activity

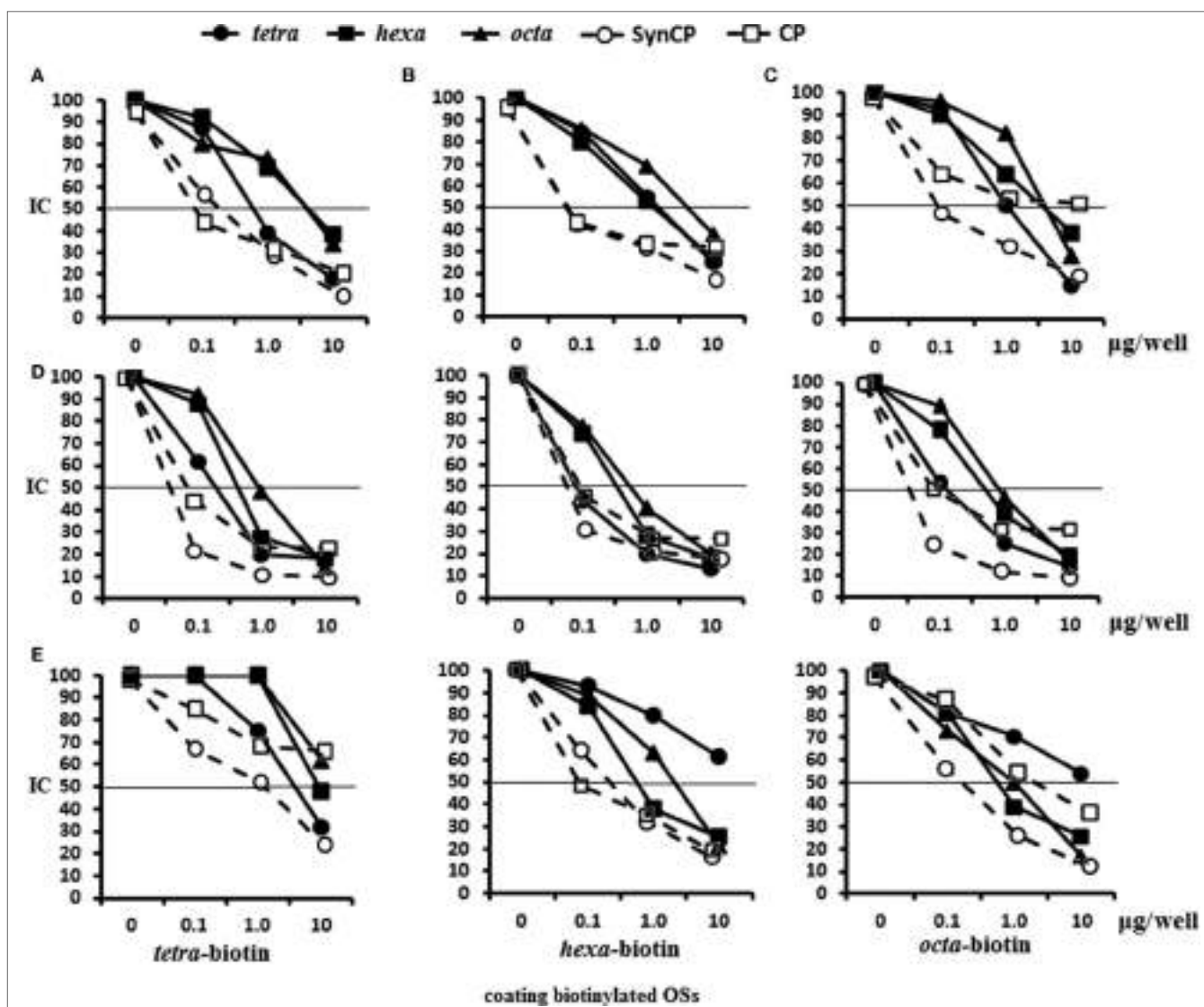


**FIGURE 5 |** Inhibition of IgG1 antibodies (Abs) in mice immune sera with OS ligands and CP. Enzyme-linked immunosorbent assay inhibition assays were performed using streptavidin-coated plates with tetra-biotin, hexa-biotin, and octa-biotin adsorbed on their surfaces. **(A–C)** Inhibition of IgG1 Abs in the pooled sera of BALB/c mice ( $n = 6$ ) that were immunized twice intraperitoneally with glycoconjugates at 10 µg/dose. Sera were obtained 14 days after the second immunization. Serum samples for all glycoconjugates were diluted 1:4,000. The tetra-, hexa-, and octasaccharide ligands, synCP, and bacCP were used as inhibitors and applied in amounts ranging from 0 to 10 µg/well. The horizontal line indicates the IC<sub>50</sub> at the point of intersection of the inhibition curves. **(A)** Tetra-bovine serum albumin (BSA) conjugate antiserum was tested against tetra-biotin capture material. **(B)** Hexa-BSA conjugate antiserum was tested against hexa-biotin capture material. **(C)** Octa-BSA conjugate antiserum was tested against octa-biotin capture material. **(D)** Inhibition of IgG1 Abs was measured in the pooled sera of BALB/c mice immunized twice intraperitoneally over 2 weeks with the conjugated pneumococcal vaccine, Prevenar-13, at 1.1 µg of *Streptococcus pneumoniae* type 14 CP per single dose. The dilutions of sera tested against the tetra-biotin and octa-biotin coating antigens were 1:500; hexa-biotin was diluted 1:300. **(E)** Inhibition of IgG Abs was measured in serum harvested from rabbits that were immunized multiple times with inactivated *S. pneumoniae* type 14 bacteria. The dilution of rabbit sera tested against tetra-biotin coating antigens was 1:300, against hexa-biotin and octa-biotin coating antigens was 1:3,000;  $n = 3$  per data point.

against tetra-biotin (Figure 5E). Interestingly, when hexa-biotin was the coating antigen, high inhibitory activities were revealed for the hexa- and octasaccharide ligands, as well as for synCP and bacCP. Hexa- and octasaccharide, as well as synCP and bacCP, possessed high inhibitory activities against octa-biotin. In case of the rabbit antibacterial serum, the tetrasaccharide inhibited IgG Abs only in the tetra-biotin system, because when being tested against the hexa-biotin and octa-biotin, the working dilution of

the serum was 1:3,000, and Abs to the tetrasaccharide fragment of CP (titer 1:3,200) could not be identified.

The abilities of the OS ligands, as well as synCP and bacCP, to inhibit the binding of either glycoconjugate or CP antisera to synCP coating antigens were studied (Figure 6). In this case, IgG Abs were determined, as the level of IgG1 was universally low. For the sera of mice immunized with the tetra-BSA (Figure 6A), hexa-BSA (Figure 6B), and octa-BSA conjugates (Figure 6C), the

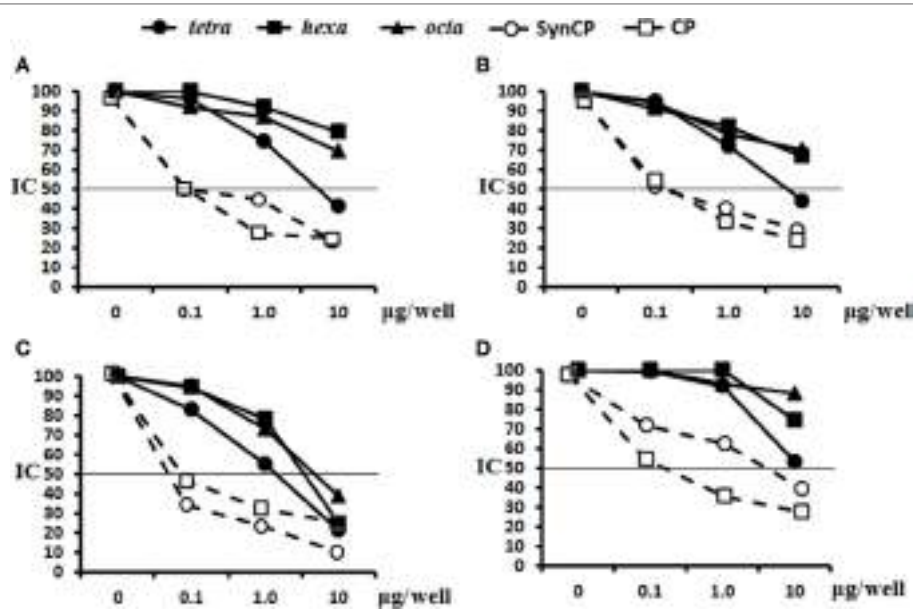


**FIGURE 6 |** Inhibition of IgG antibodies (Abs) recognizing SynCP as the coating antigen with OS ligands and CP. Pooled immune sera were obtained after double intraperitoneal immunization of BALB/c mice ( $n = 6$  for each glycoconjugate) with the OS-bovine serum albumin (BSA) conjugates adsorbed on aluminum hydroxide (10 µg of carbohydrate/single dose). The tetra-, hexa-, and octasaccharide ligands, as well as synCP and bacCP, were used as inhibitory materials at concentrations of 0–10 µg/well. The horizontal line indicates the IC<sub>50</sub> level at the point of intersection of the inhibition curves. **(A)** Inhibition of IgG Abs was measured in tetra-BSA conjugate sera at a dilution of 1:400. **(B)** Inhibition of IgG Abs was measured in hexa-BSA conjugate sera at a dilution of 1:400. **(C)** Inhibition of IgG Abs was measured in octa-BSA conjugate sera at a dilution of 1:1,600. **(D)** Inhibition of IgG Abs was measured in *Streptococcus pneumoniae* type 14 CP-CRM<sub>197</sub> at a dilution of 1:200. Immune sera were obtained after immunization of mice ( $n = 6$ ) with Prevenar-13 adsorbed on aluminum phosphate at 2.2 µg (content of *S. pneumoniae* type 14 CP) per single dose.

tetrasaccharide ligand, as well as synCP and bacCP, possessed the highest inhibitory activities. The hexa- and octasaccharides only demonstrated inhibitory activities in the octa-BSA conjugate/synCP reactions. In the serum of mice immunized with *S. pneumoniae* type 14 CP-CRM<sub>197</sub> (Prevenar-13), the highest inhibitory activities were detected for the tetrasaccharide ligand, synCP, and bacCP (Figure 6D). The tetrasaccharide ligand was the only one to reach IC<sub>50</sub> for inhibiting interactions in the sera to Prevenar-13.

In general, these data provided clear evidence that the tetrasaccharide ligand possessed the best capacity to bind to anti-OS, anti-CP, and antibacterial Abs.

## Opsonophagocytic Capacity of Glycoconjugate-Induced Sera

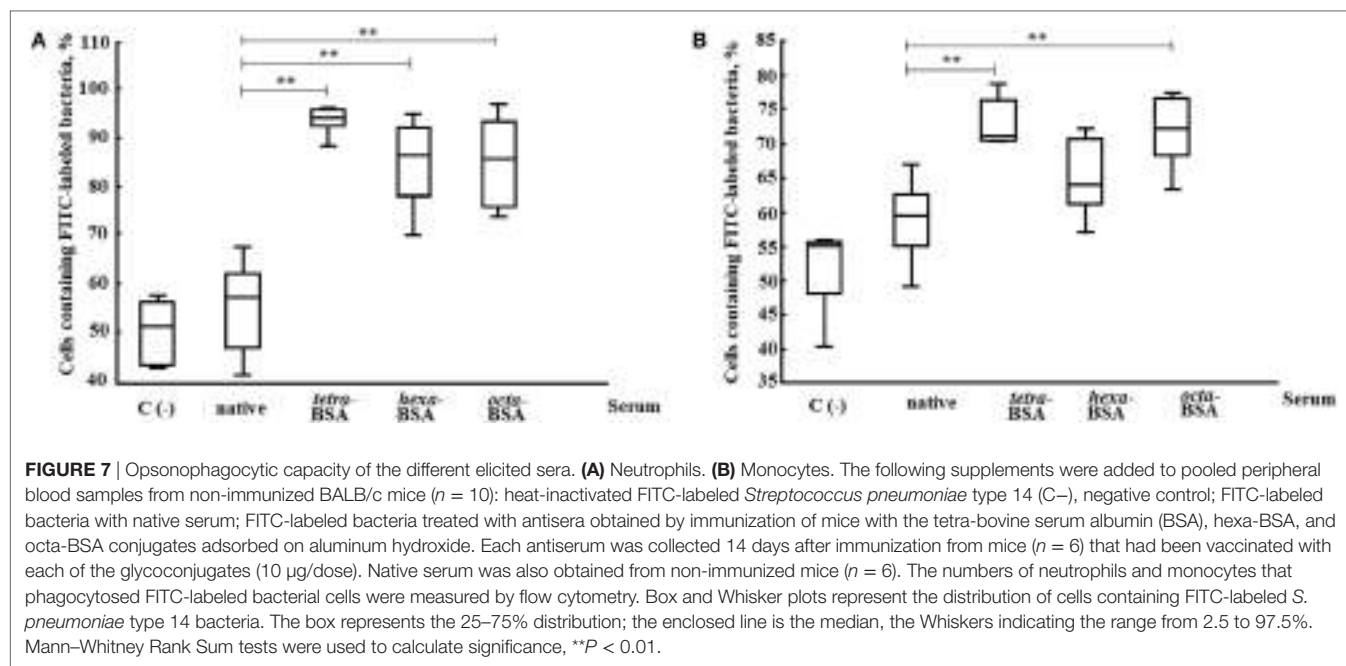
Opsonophagocytosis rates of heat-killed *S. pneumoniae* type 14 bacteria by neutrophils and monocytes collected from murine peripheral blood samples were examined by flow cytometry (Figure 7). The percentages of neutrophils (Figure 7A) and monocytes (Figure 7B) that phagocytosed heat-inactivated FITC-labeled bacterial cells of *S. pneumoniae* type 14 were quantified from blood samples of naive mice. The total number of active neutrophils that phagocytosed *S. pneumoniae* type 14 bacteria significantly increased in samples exposed to glycoconjugate antisera as compared with control samples without sera (C−), or samples supplemented with native sera ( $P < 0.01$ ). No differences in the opsonizing rates between the antisera were revealed in this

experiment. Similarly, monocytes captured *S. pneumoniae* type 14 bacterial cells in the presence of sera to the tetra-BSA and octa-BSA conjugates as compared with the native serum or the control (C−;  $P < 0.01$ ). The lowest phagocytic activities of monocytes were observed after incubating bacteria with hexa-BSA conjugate anti-sera; no significant difference was found in monocyte phagocytosis rates of hexa-BSA-treated and native serum-treated bacteria.

To summarize, the Abs induced by the tetra- and octasaccharide conjugates possessed the highest opsonophagocytic capacity.

## Passive Protection Elicited by the Glycoconjugate-Induced Abs

Naive mice received a single intraperitoneal administration of glycoconjugate-induced serum followed by challenge with a lethal dose of *S. pneumoniae* type 14 (Table 1). The reference group of mice received native sera. Two hours after treatment, all groups of mice were challenged with a lethal dose of *S. pneumoniae* type 14. The number of mice surviving on day 7 (D7) after the challenge was given (Table 1). No serum was injected into control mice. The sera to the tetra-BSA and hexa-BSA conjugates protected six out of eight mice, while all the mice in the control group died ( $P < 0.01$ ). The sera to the octa-BSA conjugate protected five out of eight mice ( $P < 0.05$ ). The native serum protected three out of eight mice. Yates-corrected Chi-square tests, between the control and other groups, \* $P < 0.05$ , \* $P < 0.01$ . The titers of Abs to CP in the glycoconjugate-induced sera were significantly higher in comparison with the mice given native sera (Mann-Whitney Rank Sum test, \* $P < 0.05$ ).

**TABLE 1 |** Passive protection of mice with immune sera to the glycoconjugates.

Immune sera to glycoconjugates	Anti-CP antibodies titer, log <sub>10</sub>	Survivors	
		D0	D7
Tetra-bovine serum albumin (BSA)	3.65 ± 0.61*	8	6**
Hexa-BSA	3.82 ± 0.58*	8	6**
Octa-BSA	4.07 ± 0.60*	8	5*
Native sera	2.17 ± 0.36	8	3
Control	<2.0	8	0

\* $P < 0.05$ , \*\* $P < 0.01$ .

Thus, all glycoconjugate-induced sera possessed the preventive capacities.

## Active Protection upon Challenge of Glycoconjugate-Immunized Mice

The results of three experiments of protective activities of glycoconjugates challenged with a lethal dose of *S. pneumoniae* type 14 are given (Table 2). In the first experiment (Exp. 1, Table 2), the tetra-BSA conjugate protected mice from infections (more than 4 LD<sub>50</sub>) at doses of 2.5, 5.0, and 10 µg compared with controls (naive mice;  $P < 0.01$ ,  $P < 0.001$ , and  $P < 0.001$ , respectively). For the hexa-BSA conjugate, the optimal immunizing dose was 10 µg ( $P < 0.01$ ). The octa-BSA conjugate protected mice at immunizing doses of 5 and 10 µg ( $P < 0.001$  and  $P < 0.01$ , respectively). Yates-corrected Chi-square test, \*\* $P < 0.01$ , \*\*\* $P < 0.001$ .

In the second experiment (Exp. 2, Table 2), mice were immunized with lower doses (1.25 µg) of the conjugates and challenged with 4 LD<sub>50</sub> of *S. pneumoniae* type 14. Here, the hexa-BSA conjugate was not tested, because in the previous experiment it did not protect the animals from infection at the lowest doses. The highest protection was induced by the tetra-BSA conjugate ( $P < 0.001$ ), whereas the octa-BSA conjugate applied at the same

**TABLE 2 |** Protective activity of the glycoconjugates.

Experimental series	Immunogen	Single dose (carbohydrate content) per mouse, µg	Survivors	
			D0	D7
1	Tetra-bovine serum albumin (BSA)	2.5	8	8***
		5.0	8	8***
		10	8	7**
		2.5	8	1
		5.0	8	2
	Octa-BSA	10	8	7**
		2.5	8	3
		5.0	8	8***
		10	8	6**
		Control	Saline	0
2	Tetra-BSA	1.25	10	10***
	Octa-BSA	1.25	10	7**
	CP-CRM <sub>197</sub>	1.1	4	4***
	Control	Saline	10	0
3	Hexa-BSA	10	10	10***
	CP	5.0	10	2
	Control	Saline	10	1

\* $P < 0.01$ , \*\* $P < 0.001$ .

dose was less effective ( $P < 0.01$ ). Additionally, the *S. pneumoniae* type 14 CP-CRM<sub>197</sub> conjugate at a dose equivalent to the doses of the BSA conjugates protected all mice from infections.

In the third experiment (Exp. 3, Table 2), the protective activity of the hexa-BSA conjugate was analyzed at the most effective single immunizing dose (10 µg of carbohydrate per mouse) and compared with the *S. pneumoniae* type 14 CP (5 µg of carbohydrate per mouse) from a commercial polysaccharide vaccine. In this case, 1.9 LD<sub>50</sub> was used as the infectious dose of *S. pneumoniae* type 14, lower than in the two previous experiments. The CP

administered without an adjuvant did not protect the mice against the infection, whereas the hexa-BSA conjugate adsorbed on aluminum hydroxide at the most effective single immunizing dose (10 µg/mouse) protected all immunized mice.

Thus, it was revealed that all neoglycoconjugates adsorbed on aluminum hydroxide possessed protective activity. The protective activity of the tetra-BSA conjugate was significantly higher than that of the hexa-BSA and octa-BSA conjugates (Exp. 1, **Table 2**). Given the strong protective capabilities of the tetra-BSA conjugate, the tetrasaccharide ligand seems the best of these candidates for development of an *S. pneumoniae* type 14 vaccine.

## DISCUSSION

Selection of an optimal OS ligand possessing sufficient protective activity is the major barrier faced by developers of neoglycoconjugate vaccines. Modern chemical methods allow efficient syntheses of OSs representing potential protective epitopes of bacterial polysaccharides suitable for vaccine development (28–32). This study presented comparative immunological data of three potential protective epitopes of the *S. pneumoniae* type 14 CP. The tetra-, hexa-, and octasaccharide OS units differed from one another structurally and consisted of 1, 1.5, and 2 repeating units related to the CP of *S. pneumoniae* type 14.

The chemical structure of the OSs is an important factor in determining the immunogenicity of epitopes (15). Among the structurally unique tetra-, penta-, and hexasaccharides related to the *S. pneumoniae* type 14 CP, there exists a range of capabilities to stimulate induction of anti-CP IgG Abs (21, 33). It has been demonstrated that octasaccharides possessing different chemical structures and, generally, OSs with higher chain lengths are immunologically active with capacity to bind anti-CP Abs. Conjugates of long-chain OSs induce specific Abs, which subsequently promote phagocytosis of *S. pneumoniae* type 14 bacterial cells (21, 33, 34). Investigation of a large group of OSs (from tri- to dodecasaccharides) possessing varying chemical structures and conjugated to CRM<sub>197</sub> revealed that the tetrasaccharide conjugate elicited Ab production and promoted the phagocytosis of *S. pneumoniae* type 14 bacteria. However, these data were not confirmed by *in vivo* protective activity assays of the conjugated tetrasaccharide in animal models (21).

All glycoconjugates synthesized and reported here displayed immunogenic properties and elicited anti-CP and anti-OS IgG1 Ab production. Notably, the tetra-BSA conjugate possessed the highest protective properties in murine *S. pneumoniae* type 14 infection challenge models as compared with hexa-BSA and octa-BSA conjugates, but induced lower titers of anti-CP IgG1 Abs. Abs to the short-length OSs may have less opportunity to recognize chemically treated CP, as treatment may hide antigenic determinants; antigenic determinants may be more accessible to Abs generated against OSs with longer carbohydrate chains. However, we showed in a previous study that tetra-BSA conjugate-induced Abs more actively agglutinated live *S. pneumoniae* type 14 cells than did hexa-BSA - and octa-BSA -induced Abs; their activity equaled that of commercial serotype-specific rabbit pneumococcal antisera (35).

Conjugated tetrasaccharide as coating antigen in ELISA possessed higher diagnostic capabilities than CP detecting the higher

level of CP-induced IgG1 Abs than either the conjugated long-chain octasaccharide or high-molecular weight CP. Probably, anti-CP IgG1 Abs did not fit precisely to the conformational epitope of CP of *S. pneumoniae* type 14, or because inappropriate epitopes were exposed on the surface of immobilized CP. Thus, the anti-CP IgG1 Ab titers reported in sera to commercial polysaccharide-based pneumococcal vaccines may occur lower than real levels detected in the same sera against tetrasaccharide conjugate. Therefore, it is reasonable to use the tetrasaccharide conjugate as the coating antigen in ELISA to determine anti-CP IgG1 Ab titers.

Post-vaccination, anti-OS IgG1 Ab titers measured in murine blood sera with ELISA using biotinylated OSs were higher than those detected using bacterial or synthetic CPs. The presence of shared carbohydrate fragments in the different OS ligands may explain the observation that each OS could cross-inhibit binding of other glycoconjugate Abs as well as the antibacterial sera. As a result, these experiments did not identify the types and abundance of anti-OS Abs present in the sera of animals exposed to CP. However, the tetrasaccharide ligand possessed the highest binding capacity to Abs generated in OS-immunized murine sera, as well as anti-CP and anti-pneumococcal whole cell sera.

All glycoconjugate-induced antisera promoted phagocytosis of *S. pneumoniae* type 14 bacterial cells by neutrophils and monocytes in peripheral blood of non-immunized mice. All antisera also induced passive protection of naive mice from pneumococcal infections. Similar preventive efficacies of each anti-OS serum may have occurred because the highest effective doses of each glycoconjugate were used to generate the immune sera. Perhaps, differences in opsonophagocytic and preventive activity of sera could be detected if lower immunizing doses for obtaining glycoconjugate-induced sera would be used.

Here, it was revealed for the first time that tetra-BSA, hexa-BSA, and octa-BSA conjugates adsorbed on aluminum hydroxide protected mice against *S. pneumoniae* type 14 infections. The feasibility of using aluminum hydroxide as an adjuvant to stimulate high levels of Ab production against conjugated synthetic OS was demonstrated previously (26). The tetra-BSA conjugate had the highest protective activity that was comparable to those demonstrated by the commercially available conjugated pneumococcal vaccine, Prevenar-13.

Based on the results of these immunological studies, including *in vivo* protective activity assays in murine models, we conclude that the tetrasaccharide corresponding to one repeating unit of CP is an excellent candidate for the development of a neoglycoconjugate *S. pneumoniae* type 14 vaccine. Additionally, tetrasaccharide-based coating antigens can be applied to ELISA for reliable determination of anti-CP Ab titers.

## CONCLUSION

The neoglycoconjugate of the tetrasaccharide, which is composed of one repeating unit of *S. pneumoniae* type 14 CP, induced the formation of opsonizing Abs and possessed stronger protective activity in mice challenged with the lethal doses of pneumococcal bacteria as compared to the hexa- and octasaccharide conjugates. These data support application of the tetrasaccharide

as a component for development of synthetic or semi-synthetic pneumococcal vaccines.

## ETHICS STATEMENT

BALB/c male mice aged 6–8 weeks and two “Chinchilla” rabbits weighing 2.5 kg were purchased from the Scientific and Production Centre for Biomedical Technologies, Branch “Andreevka” (Moscow, Russia) and kept in the vivarium of the Mechnikov Research Institute for Vaccines and Sera. The housing, husbandry, blood sampling, and sacrificing conditions conformed to the European Union guidelines for the care and use of laboratory animals. The design of experiments was approved by the Ethics Committee of Mechnikov Research Institute for Vaccines and Sera.

## AUTHOR CONTRIBUTIONS

EK planned the studies on Ab responses in mice and rabbits and summarized the results. NA studied the protective and

preventive activities of sera in mice, opsonophagocytosis assays, and statistical analyses of data. EA performed the ELISA inhibition tests using different coating antigens and immune sera. NE summarized the results, compared the data with contemporary literature, and statistically analyzed the results. NY obtained the capsular polysaccharides and rabbit immune sera. ES performed the chemical syntheses of the oligosaccharides and analyzed the results. DY performed the chemical syntheses, conjugated the OS with protein carriers and analyzed the results. YT performed the chemical synthesis, conjugated the OS with protein carriers and summarized the results. MG summarized the results, and compared the data with contemporary literature. NN planned the study, analyzed the results, and compared the data with contemporary literature.

## FUNDING

This work was supported by the Russian Science Foundation (grant no. 14-50-00126).

## REFERENCES

- Hausdorff WP, Bryant J, Paradiso PR, Siber GR. Which pneumococcal serogroups cause the most invasive disease: implications for conjugate vaccine formulation and use, part I. *Clin Infect Dis* (2000) 30:100–21. doi:10.1086/313609
- Inostroza J, Vinet AM, Retamal G, Locra P, Ossa G, Facklam R, et al. Influence of patient age on *Streptococcus pneumoniae* serotypes causing invasive disease. *Clin Diagn Lab Immunol* (2001) 8(3):556–9. doi:10.1128/CDLI.8.3.556-559.2001
- AlonsoDeVelasco E, Verheul AF, Verhoef J, Snippe H. *Streptococcus pneumoniae*: virulence factors, pathogenesis, and vaccines. *Microbiol Rev* (1995) 59:591–603.
- van Dam JE, Fleer A, Snippe H. Immunogenicity and immunochemistry of *Streptococcus pneumoniae* capsular polysaccharides. *Antonie Van Leeuwenhoek* (1990) 58:1–47. doi:10.1007/BF02388078
- WHO position paper. Pneumococcal conjugate vaccine for childhood immunization—WHO position paper. *Wkly Epidemiol Rec* (2007) 82:93–104.
- Musher DM, Manoff SB, McFetridge RD, Liss CL, Marchese RD, Raab J, et al. Antibody persistence ten years after first and second doses of 23-valent pneumococcal polysaccharide vaccine, and immunogenicity and safety of second and third doses in older adults. *Hum Vaccin* (2011) 7(9):919–28. doi:10.4161/hv.7.9.15996
- Leventer-Roberts M, Feldman BS, Brufman I, Cohen-Stavi CJ, Hoshen M, Balicer RD. Effectiveness of 23-valent pneumococcal polysaccharide vaccine against invasive disease and hospital-treated pneumonia among people aged ≥65 years: a retrospective case-control study. *Clin Infect Dis* (2015) 60(10):1472–80. doi:10.1093/cid/civ096
- Siegrist CA. Vaccine immunology. In: Plotkin SA, Orenstein AW, Offit PA, editors. *Vaccines. 5th ed.* Philadelphia, Pa: Saunders Elsevier (2008). p. 17–36.
- Stein KE. Thymus-independent and thymus-dependent responses to polysaccharide antigens. *J Infect Dis* (1992) 165(Suppl 1):49–52. doi:10.1093/infdis/165-Supplement\_1-S49
- Avci FY, Li X, Tsuji M, Kasper DL. Carbohydrates and T cells: a sweet two-some. *Semin Immunol* (2013) 25(2):146–51. doi:10.1016/j.smim.2013.05.005
- Mitchison NA. The carrier effect in the secondary response to haptene-protein conjugates. II. Cellular cooperation. *Eur J Immunol* (1971) 1:18–25. doi:10.1002/eji.1830010104
- Soubal JP, Peña L, Santana D, Valdés Y, García D, Pedroso J, et al. Procedimiento de conjugación del polisacárido capsular de *Streptococcus pneumoniae* serotipo 6B a toxido tetánico. *Biotechol Apl* (2013) 30(3):199–215.
- Gening ML, Kurbatova EA, Tsvetkov YE, Nifantiev NE. Development of approaches to a conjugated carbohydrate vaccine of the third generation against *Streptococcus pneumoniae*: the search for optimal oligosaccharide ligands. *Russ Chem Rev* (2015) 84(11):1100–13. doi:10.1070/RCR4574
- Ovodov YS. Bacterial capsular antigens. Structural patterns of capsular antigens. *Biochemistry (Mosc)* (2006) 71:937–54. doi:10.1134/S000629790609001X
- Kamerling JP. Pneumococcal polysaccharides: a chemical view. In: Tomasz A, editor. *Streptococcus pneumoniae Molecular Biology and Mechanism of Disease*. New York: Mary Ann Libert, Inc (2000). p. 81–114.
- Jansen WT, Snippe H. Short-chain oligosaccharide protein conjugates as experimental pneumococcal vaccines. *Indian J Med Res* (2004) 119(Suppl):7–12.
- Lindberg B, Lönngran J, Powell DA. Structural studies on the specific type 14 pneumococcal polysaccharide. *Carbohydr Res* (1977) 58:177–86. doi:10.1016/S0008-6215(00)83413-8
- Landesman SH, Schiffman G. Assessment of the antibody response to pneumococcal vaccine in high-risk populations. *Rev Infect Dis* (1981) 3:184–96. doi:10.1093/clinids/3.Supplement\_1.S184
- Jauneikaitė E, Jefferies JM, Hibberd ML, Clarke SC. Prevalence of *Streptococcus pneumoniae* serotypes causing invasive and non-invasive disease in South East Asia: a review. *Vaccine* (2012) 30:3503–14. doi:10.1016/j.vaccine.2012.03.066
- Satcher D, Hughes JM, Cohen ML, Thacker SB, Goodman RA, Hewitt SM, et al. Prevention of pneumococcal disease: recommendations of the Advisory Committee on Immunization Practices (ACIP). *MMWR Recomm Rep* (1997) 46(8):1–24.
- Safari D, Dekker HAT, Joosten AF. Identification of the smallest structure capable of evoking opsonophagocytic antibodies against *S. pneumoniae* type 14. *Infect Immun* (2008) 76:4615–23. doi:10.1128/IAI.00472-08
- Sukhova EV, Yashunsky DV, Tsvetkov YE, Kurbatova EA, Nifantiev NE. Synthesis of oligosaccharide fragments of the *Streptococcus pneumoniae* type 14 capsular polysaccharide and their neoglycoconjugates with bovine serum albumin. *Russ Chem Bull Int Ed* (2014) 63(2):511–21. doi:10.1007/s11172-014-0462-5
- Chizhov AO, Sukhova EV, Khatuntseva EA, Tsvetkov YE, Nifantiev NE. High-resolution mass spectra of biotinylated, HEG-spacer molecular probes with oligosaccharide fragments of the capsular polysaccharides from *Streptococcus pneumoniae*. *Mendelev Commun* (2015) 25:457–9. doi:10.1016/j.mencom.2015.11.020
- Ananikov VP, Khokhlova EA, Egorov MP, Sakharov AM, Zlotin SG, Kucherov AV, et al. Organic and hybrid molecular systems. *Mendelev Commun* (2015) 25:75–82. doi:10.1016/j.mencom.2015.03.001
- Kochetkov NK, Nifant'ev NE, Backinowsky LV. Synthesis of the capsular polysaccharide of *Streptococcus pneumoniae* type 14. *Tetrahedron* (1987) 43(13):3109–21. doi:10.1016/S0040-4020(01)86852-6
- Akhmatova NK, Kurbatova EA, Akhmatov EA, Egorova NB, Logunov DY, Gening ML, et al. The effect of a BSA conjugate of a synthetic hexasaccharide related to the fragment of capsular polysaccharide of *Streptococcus pneumoniae*

- type 14 on the activation of innate and adaptive immune responses. *Front Immunol* (2016) 7:248. doi:10.3389/fimmu.2016.00248
27. Kurbatova EA, Vorobiov DS, Semenova IB, Sukhova EV, Yashunsky DV, Tsvetkov YE, et al. Development of approaches to creation of experimental test system for evaluation of antigenic activity of synthetic oligosaccharide ligands related to fragments of the *Streptococcus pneumoniae* type 14 capsular polysaccharide. *Biochemistry (Mosc)* (2013) 78:819–24. doi:10.1134/S0006297913070122
28. Wessels MR, Kasper DL. Antibody recognition of the type 14 pneumococcal capsule. *J Exp Med* (1989) 169:2121–31. doi:10.1084/jem.169.6.2121
29. Verez-Bencomo V, Fernandez-Santana V, Hardy E, Toledo ME, Rodriguez A, Baly A, et al. A synthetic conjugate polysaccharide vaccine against *Haemophilus influenzae* type b. *Science* (2004) 305:522–5. doi:10.1126/science.1095209
30. Granoff DM, McHugh YE, Raff HV, Mokatrin AS, van Nest GA. MF59 adjuvant enhances antibody responses of infant baboons immunized with *Haemophilus influenzae* type b and Neisseria meningitidis group C oligosaccharide-CRM197 conjugate vaccine. *Infect Immun* (1997) 65:1710–5.
31. Gening ML, Maira-Litran T, Kropec A, Skurnik D, Grout M, Tsvetkov YE, et al. Synthetic  $\beta(1 \rightarrow 6)$ -linked N-acetylated and non-acetylated oligoglucosamines used to produce conjugate vaccines for bacterial pathogens. *Infect Immun* (2010) 78:764–72. doi:10.1128/IAI.01093-09
32. Gening ML, Tsvetkov YE, Pier GB, Nifantiev NE. Synthesis of oligo- $\beta(1 \rightarrow 6)$ -glucosamines corresponding to the fragments of the surface polysaccharide of *Staphylococcus aureus*. *Carbohydr Res* (2007) 342:567–75. doi:10.1016/j.carres.2006.08.010
33. Mawas F, Niggemann J, Jones C, Corbel MJ, Kamerling JP, Vliegenthart JFG. Immunogenicity in a mouse model of a conjugate vaccine made with a synthetic single repeating unit of type 14 pneumococcal polysaccharide coupled to CRM197. *Infect Immun* (2002) 70(10):5107–14. doi:10.1128/IAI.70.9.5107-5114.2002
34. Safari D, Rijkers G, Snijpe H. The complex world of polysaccharides. In: Karunaratne DN, editor. *The Future of Synthetic Carbohydrate Vaccines: Immunological Studies on Streptococcus pneumoniae Type 14*. (Chap. 24), Rijeka, Croatia: InTech (2012). p. 617–34.
35. Kurbatova EA, Akhmatova EA, Akhmatova NK, Egorova NB, Yastrebova NE, Romanenko EE, et al. The use of biotinylated oligosaccharides related to fragments of capsular polysaccharides from *Streptococcus pneumoniae* serotypes 3 and 14 as a tool for assessment of the level of vaccine-induced antibody response to neoglycoconjugates. *Russ Chem Bull Int Ed* (2016) 65:1608–16. doi:10.1007/s11172-016-1488-7

**Conflict of Interest Statement:** The authors declare that the research was conducted in the absence of any commercial or financial relationships that could be construed as potential conflicts of interest.

Copyright © 2017 Kurbatova, Akhmatova, Akhmatova, Egorova, Yastrebova, Sukhova, Yashunsky, Tsvetkov, Gening and Nifantiev. This is an open-access article distributed under the terms of the Creative Commons Attribution License (CC BY). The use, distribution or reproduction in other forums is permitted, provided the original author(s) or licensor are credited and that the original publication in this journal is cited, in accordance with accepted academic practice. No use, distribution or reproduction is permitted which does not comply with these terms.



# The Length of N-Glycans of Recombinant H5N1 Hemagglutinin Influences the Oligomerization and Immunogenicity of Vaccine Antigen

Agnieszka Katarzyna Maciola<sup>1</sup>, Maria Anna Pietrzak<sup>1</sup>, Piotr Kosson<sup>2</sup>, Mariusz Czarnocki-Cieciura<sup>3,4</sup>, Krzysztof Śmiertanka<sup>5</sup>, Zenon Minta<sup>6</sup> and Edyta Kopera<sup>1\*</sup>

<sup>1</sup> Institute of Biochemistry and Biophysics, Polish Academy of Sciences, Warsaw, Poland, <sup>2</sup> Mossakowski Medical Research Centre, Polish Academy of Sciences, Warsaw, Poland, <sup>3</sup> Laboratory of Protein Structure, International Institute of Molecular and Cell Biology, Warsaw, Poland, <sup>4</sup> Laboratory of RNA Biology and Functional Genomics, Institute of Biochemistry and Biophysics, Polish Academy of Science, Warsaw, Poland, <sup>5</sup> Department of Poultry Diseases, National Veterinary Research Institute, Pulawy, Poland

## OPEN ACCESS

### Edited by:

Marc H. V. Van Regenmortel,  
Centre national de la recherche  
scientifique (CNRS), France

### Reviewed by:

Mark Agostino,  
Curtin University, Australia  
Hans Dieter Klenk,  
Philipps University of  
Marburg, Germany

### \*Correspondence:

Edyta Kopera  
ekopera@ibb.waw.pl

To the memory of Professor Krystyna  
Grzelak and Professor Włodzimierz  
Zagórski-Ostoja.

### Specialty section:

This article was submitted to  
Vaccines and Molecular  
Therapeutics,  
a section of the journal  
*Frontiers in Immunology*

Received: 09 November 2016

Accepted: 30 March 2017

Published: 20 April 2017

### Citation:

Maciola AK, Pietrzak MA, Kosson P, Czarnocki-Cieciura M, Śmiertanka K, Minta Z and Kopera E (2017) The Length of N-Glycans of Recombinant H5N1 Hemagglutinin Influences the Oligomerization and Immunogenicity of Vaccine Antigen. *Front. Immunol.* 8:444. doi: 10.3389/fimmu.2017.00444

Hemagglutinin glycoprotein (HA) is a principle influenza vaccine antigen. Recombinant HA-based vaccines become a potential alternative for traditional approach. Complexity and variation of HA N-glycosylation are considered as the important factors for the vaccine design. The number and location of glycan moieties in the HA molecule are also crucial. Therefore, we decided to study the effect of N-glycosylation pattern on the H5 antigen structure and its ability to induce immunological response. We also decided to change neither the number nor the position of the HA glycosylation sites but only the glycan length. Two variants of the H5 antigen with high mannose glycosylation (H5<sub>hm</sub>) and with low-mannose glycosylation (H5<sub>Man5</sub>) were prepared utilizing different *Pichia* strains. Our structural studies demonstrated that only the highly glycosylated H5 antigen formed high molecular weight oligomers similar to viral particles. Further, the H5<sub>hm</sub> was much more immunogenic for mice than H5<sub>Man5</sub>. In summary, our results suggest that high mannose glycosylation of vaccine antigen is superior to the low glycosylation pattern. Our findings have strong implications for the recombinant HA-based influenza vaccine design.

**Keywords:** avian influenza, H5N1, N-glycosylation, high-mannose glycosylation, low-mannose glycosylation, recombinant hemagglutinin, *Pichia pastoris*

## INTRODUCTION

Traditional manufacturing of influenza vaccines involves using living viruses and presents unique technical and biosafety challenges. Serious limitations of the egg-based method forced researchers for a new solution in the area of influenza vaccine development. Alternative methods are now being explored. A relevant characteristic of the influenza virus is its capacity to change constantly, which is caused by mutations in the genes encoding two proteins: hemagglutinin (HA) and neuraminidase (1). Those changes are usually activated by two mechanisms: antigenic shift and antigenic drift. Both

**Abbreviations:** HA, hemagglutinin; Man, mannose; GlcNA, N-acetylglucosamine; HexNAc, N-acetylhexosamine; AOX, alcohol oxidase; Endo H, endoglycosidase H; PAGE, polyacrylamide gel electrophoresis; IEC, ion exchange chromatography; SEC, size exclusion chromatography; MALS, multi-angle light scattering; MALDI-MS, matrix-assisted laser desorption/ionization mass spectrometry; TEM, transmission electron microscopy; HI, hemagglutination inhibition.

of them may cause the formation of a highly pathogenic virus. The capacity of influenza virus to change constantly is a great challenge for the vaccine production and the main reason why the composition of an influenza vaccine must be reviewed and updated each year.

Recombinant technology enables to obtain the protein product within several weeks, thus the time scale for the influenza vaccine production is much more attractive. As the infection-blocking antibodies are directed mainly against the hemagglutinin protein, a dynamic development in a HA-based subunit vaccine research is currently being observed. This type of vaccines contain recombinant HA protein obtained by means of genetic engineering in different expression systems (2–5). Hemagglutinin is a homotrimeric protein anchored on the surface of the virus. Each monomer consists of two subunits: HA1 and HA2, linked by a disulfide bond. The protein undergoes N-linked glycosylation and its final molecular weight (MW) is approximately 80 kDa.

Glycosylation is the most common post-translation modification by which oligosaccharides are covalently attached to either the side chain of asparagine (N-linked) or serine/threonine (O-linked). In the recent years, glycosylation, especially the N-linked one, has become an area of intensive study due to its ability to impact virus biology (6, 7). It was shown that the N-glycosylation of the influenza hemagglutinin plays an important role in the life cycle of influenza virus and influences its antigenic fitness. Indeed, oligosaccharides attached to the globular head of HA were shown to modulate virus antigenic properties (8–10) and its receptor binding (11, 12). The oligosaccharides attached to the stem region were suggested to play a critical role in HA cleavage, replication, and pH stability (13–15). The other research groups also showed that the N-glycosylation is required for the efficient folding and oligomerization of HA protein (7, 16–20).

Because the complexity and variation of hemagglutinin glycosylation are considered as the important factors for the influenza vaccine design, it was of interest to study whether the low-mannose glycosylation pattern improves immunogenicity of the H5 influenza antigen. In this study, we used a glycoengineered *Pichia pastoris* strain, which is capable to modify glycoproteins with Man<sub>5</sub>GlcNAc<sub>2</sub> N-glycans. It was reported that all human cells use this glycan moiety as a foundation to form complex glycans (21). Previously, we showed that immunization with the subunit vaccine based on the extracellular region of H5 hemagglutinin with deletion of the multibasic cleavage site fully protected chickens from lethal infections by the highly pathogenic H5N1 virus (22). We also demonstrated that such an antigen spontaneously oligomerized into spherical structures. For the antigen production, we utilized very simple, low-cost, and efficient yeast expression system. In order to obtain antigen variants with a different N-glycosylation pattern, recombinant proteins were produced in KM 71 or GlycoSwitch® *P. pastoris* strain. Thus, we obtained high-mannose (H5<sub>hm</sub>) and low-mannose glycosylated (H5<sub>Man5</sub>) H5 antigens having identical protein backbone and only differing in their N-linked glycans. Since differences in the glycosylation pattern of the recombinant proteins might have an impact on their structures, we first specifically investigated this aspect. Then, we compared the immunological properties of the H5<sub>hm</sub> and H5<sub>Man5</sub> antigens *in vivo* applying mice model.

Our results are highly relevant to the subject of recombinant influenza vaccine antigens.

## MATERIALS AND METHODS

### Cloning of H5 Hemagglutinins

The DNA encoding the extracellular domain of HA with deletion of the cleavage site (EpiFluDatabase Accession No. EPI15789) from H5N1 avian influenza virus (A/swan/Poland/305-135V08/2006 clade 2.2.2) was cloned into pJAZs1 vector using *Bsa*I (Thermo Scientific, USA) and pPICZαC using *Cla*I and *Not*I restriction sites. pJAZs1/H5<sub>Man5</sub> and pPICZαC/H5<sub>hm</sub> plasmids were linearized with *Pme*I (Thermo Scientific, USA) and used for the electroporation of the SuperMan5 (GlycoSwitch, Biogrammatics, USA) and KM 71 (his4, aox1:ARG4, arg4) (Invitrogen, USA) *P. pastoris* strains. Positive clones were transformed to a fresh YPD agar plate with Zeocine (Invitrogen, USA). The yeast transformants were screened for insertion by PCR with 5' AOX I and 3' AOX I primers. Yeast clones with verified inserts were grown as previously described (23). The presence of recombinant proteins both in medium and cells (control) was detected by SDS-PAGE and Western blotting.

### Purification of Recombinant HA Protein

Yeast medium was concentrated using tangential flow filtration (TFF) with 10 kDa cutoff Biomax cassette (Millipore, USA) and diafiltrated with 10 mM Tris pH 7.6 (Buffer A). Samples were centrifuged (14,000 rpm, 5 min, 4°C) followed by injection into HiTrap Q HP column. Proteins were eluted with 10 mM Tris pH 7.6 and 1 M NaCl (Buffer B) using a linear gradient from 10 to 45% of Buffer B at a flow rate of 0.25 ml/min. Fractions containing H5 proteins were collected, pooled, lyophilized, and stored at –20°C. H5 antigens were next loaded on a Superdex 200 10/300 GL column (GE Healthcare, UK), pre-equilibrated with 10 mM Tris pH 7.6 with 200 mM NaCl and the protein elution was monitored at 280 nm. MW standards (Bio-Rad, USA) were used to calibrate the column and to identify the MWs of proteins present in the samples.

### Mass Spectrometry Analysis

H5 antigens were denatured with denaturing buffer at 95°C for 10 min. The reaction mix containing denatured HA protein and 0.125 U of endoglycosidase H (Endo H, New England Biolabs, USA) was incubated at 37°C for 1 h. The non-treated protein sample was used as a control. The protein was analyzed using SDS-PAGE. The gel bands containing deglycosylated polypeptides were excised and analyzed by LC-MS-MS/MS (liquid chromatography coupled to tandem mass spectrometry) as previously described (23). Fragmentation spectra of peptides indicated by Mascot as N-glycosylated were manually investigated.

### Size Exclusion Chromatography (SEC)-Multi-Angle Light Scattering (MALS) Analysis

The averaged MW of H5<sub>hm</sub> and H5<sub>Man5</sub> oligomers present in the SEC profile after final purification step was determined by

SEC-MALS. To this end, protein samples from selected SEC fractions (100  $\mu$ l) were reinjected into a Superose 6 Increase column (GE Healthcare) equilibrated with a SEC-MALS buffer (10 mM Tris pH 7.6, 200 mM NaCl) at a 0.5 ml/min flow rate. Elution of the proteins was monitored by three online detectors: UV detector (1,220 Infinity LC System, Agilent Technologies, USA), light scattering detectors (DAWN HELEOS II, Wyatt Technology, USA), and refractive index detector (Optilab T-rEX, Wyatt Technology). Data analysis and MW calculations were performed using the ASTRA 6 software (Wyatt Technology).

### Transmission Electron Microscopy (TEM)

The H5<sub>hm</sub> protein sample was applied to the clean side of carbon on mica and negatively stained with 2% (w/v) sodium silico tungstate. A grid was then placed on top of the carbon film which was subsequently air dried. Images were taken under low-dose conditions (less than 20 e-/A<sup>2</sup>) with a T12 FEI electron microscope at 120 kV using an ORIUS SC1000 camera (Gatan, Inc., Pleasanton, CA, USA).

### Hemagglutination Assay

Hemagglutination test was performed according to the standard protocol. Briefly, twofold dilution of the H5 antigens was incubated with 1% chicken erythrocytes for 30 min at room temperature.

### Immunization Experiments

The experimental and control groups consisted of 10 7-week-old Balb/c mice. The animals were kept at a constant temperature of 22–24°C. In the first experiment, mice were immunized with 25  $\mu$ g of H5<sub>hm</sub> oligomers, H5<sub>hm</sub> oligomers and monomers, and H5<sub>Man5</sub> monomers dissolved in saline solution and supplemented with Alhydrogel (aluminum hydroxide, Gentaur, Germany). 100  $\mu$ l of vaccine was administered by subcutaneous injection into the neck skin fold. There were three injections (first application of antigen and/or adjuvant + two booster shots) at an interval of 3 weeks between each dose in order to monitor immunological response. In the second experiment, mice were immunized twice with 5  $\mu$ g of H5<sub>hm</sub> monomers or oligomers and 25  $\mu$ g of H5<sub>hm</sub> monomers. An adequate portion of the protein was dissolved in saline plus adjuvant. Control mice received only a specific adjuvant. Blood samples were taken 14 days after each injection in order to determine the level of antibodies. Sera were stored at –20°C.

### Enzyme-Linked Immunoabsorbant Assay (ELISA)

Collected sera were assayed for antibodies against H5 HA by an ELISA method, using MediSorp plates (Nunc, Denmark) coated with mammalian cell-expressed HA (19-529, ΔRRRKRR, 6xHis-tag at C-terminus, Immune Technology, USA) of H5N1 virus (A/Bar-headed Goose/Qinghai/12/05 H5N1, clade 2.2, 99.61% of aminoacid sequence similarity to A/swan/Poland/305-135V08/2006) diluted in PBS to 3  $\mu$ g/ml. Sera samples, taken from individual groups at each time point of experiment were pooled, serially diluted in 2% BSA/PBS and applied onto the coated plates (o/n, 4°C). Sera samples from mice immunized with H5 protein were tested in parallel with sera from sham-immunized

mice (negative controls). Bound antibodies were subsequently detected with horseradish peroxidase (HRP)-labeled goat antibodies against mouse IgG ( $\gamma$ -chain specific, Sigma-Aldrich, USA) at 1:1,000 dilution in 2% BSA/PBS (1 h, 37°C). TMB was used as a HRP substrate. After incubation for 30 min at room temperature, the reaction was stopped by addition of 0.5 M sulfuric acid. The absorbance was measured at 450 nm (A<sub>450</sub>) with a microplate reader (Synergy HTI; BioTek Instruments, USA). Endpoint titer was defined as the highest dilution producing an A<sub>450</sub> value fourfold higher than the mean A<sub>450</sub> value of the control group.

### Hemagglutination Inhibition (HI) Test

Sera samples were heat inactivated at 56°C for 30 min and then were pretreated by kaolin and chicken erythrocytes to avoid a false positive reaction in HI test (24). The pretreated sera (10  $\mu$ l of sera in serial twofold dilutions) were incubated for 25 min in titration plate with four HA units of the inactivated antigen A/turkey/Poland/35/2007 H5N1, clade 2.2.3 (99.22% of aminoacid sequence similarity to A/swan/Poland/305-135V08/2006). Next, a 1% suspension of chicken erythrocytes was added and incubated for 30 min. The HI titer was assessed as the reciprocal of the highest dilution in which hemagglutination was inhibited.

## RESULTS

### Purification of the H5<sub>hm</sub> and H5<sub>Man5</sub> Antigens

The extracellular domain of H5N1 hemagglutinin (residues 17-531, ΔRRRKRR) was selected because it adopted the correct three-dimensional structure required for higher oligomerization. The vaccine based on this HA domain fully protected chickens from lethal infections by the highly pathogenic H5N1 virus (22). This time, in order to obtain the antigens with a native protein sequence, we excluded any affinity tags. Antigen variants with different N-glycosylation patterns were produced in the KM 71 or GlycoSwitch® *P. pastoris* strain. The last is engineered to produce proteins with Man<sub>5</sub>GlcNAc<sub>2</sub> Asn-linked glycans. Finally, we obtained the high-mannose (H5<sub>hm</sub>) and low-mannose glycosylated (H5<sub>Man5</sub>) H5 antigens having identical protein backbone and only differing in their N-linked glycans. In order to increase a sample-to-volume ratio and to simplify the utilization of the ion exchange chromatography (IEC), the yeast medium was concentrated. Various methods were tested, e.g., trichloroacetic acid, ammonium sulfate, dry dialysis using Aquacide and TFF. The last one proved to be the most efficient method (data not shown). Not only it allowed us to concentrate the medium up to 10-fold but also to diafiltrate the protein samples with the IEC buffer. SDS-PAGE analysis after the IEC (Figures 1A,B) showed a high level of purity only for the H5<sub>hm</sub> protein (Figure 1C). Both recombinant antigens were clearly the major components of the IEC preparations but the purity of H5<sub>Man5</sub> antigen (Figure 1D) had to be improved during the next purification step applying size exclusion chromatography (see N-Glycan-Dependent Structure of the H5<sub>hm</sub> and H5<sub>Man5</sub> Antigens). Yield as high as 200 mg of the purified H5<sub>hm</sub> protein

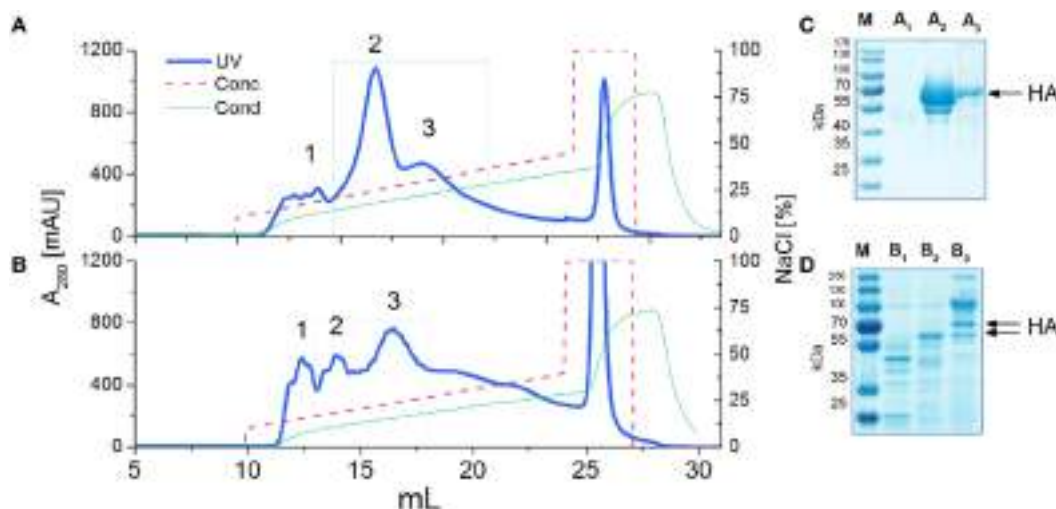


**FIGURE 1 | Ion exchange chromatography (IEC) (A,B) and SDS-PAGE analysis (C,D) of H5 antigens.** IEC chromatograms (A,B) present typical purification profiles of H5<sub>hm</sub> and H5<sub>Man5</sub> proteins, respectively. Absorbance at 280 nm is shown. HiTrapQ column was pre-equilibrated with 10 mM Tris/HCl pH 7.6 (Buffer A). Proteins were eluted with 10 mM Tris/HCl pH 7.6; 1 M NaCl (Buffer B) applying a linear gradient from 10% B to 45% B at flow rate 0.25 ml/min. Collected fractions (1, 2, 3) were analyzed on 4–12% SDS-PAGE (C,D) following Coomassie staining. HA protein was detected in peak no 2 and 3 [(C): line A<sub>2</sub> and A<sub>3</sub>; (D): line B<sub>2</sub> and B<sub>3</sub>]. Fractions with H5<sub>hm</sub> or H5<sub>Man5</sub> protein were pooled, lyophilized, and stored in –20/–80°C.

**TABLE 1 | N-glycosylated peptides from the H5<sub>hm</sub> and H5<sub>Man5</sub> proteins confirmed by LC/MS/MS analysis.**

Residue	Region	Amino acid sequence	Mass	Antigen
22-35	HA1	<b>N</b> VTVTHAQDILEK + HexNAc	1,669.85	H5 <sub>hm</sub> H5 <sub>Man5</sub>
163-189	HA1	<b>S</b> YNNTNQEDLLVLWGIHHPNDAAEQTR + HexNAc	3,337.56	H5 <sub>hm</sub>
278-304	HA1	CQTPIGAI <b>N</b> SSMPFHNIHPLTIGECPK + HexNAc	3,221.53	H5 <sub>hm</sub> H5 <sub>Man5</sub>
478-491	HA2	<b>N</b> GTYDYPQYSEAR + HexNAc	1,894.78	H5 <sub>hm</sub> H5 <sub>Man5</sub>

*N-linked glycosylation sites are bold and underlined. Molecular mass of modified peptides (one HexNAc attached to the asparagine residue) was determined by spectrometer. HexNAc (N-acetylhexosamine).*

per 1 l was achieved after the IEC procedure. The efficiency of the H5<sub>Man5</sub> antigen production was rather modest (1.5 mg/l), making the utilization of GlycoSwitch® *P. pastoris* strain as a vaccine platform unattractive.

In order to examine *N*-glycosylation sites of recombinant HA antigens, we used a standard proteomic procedure for Endo H treated proteins. Mass spectrometry analysis confirmed that four sites in H5<sub>hm</sub> and three sites in H5<sub>Man5</sub> are glycosylated (Table 1; Supplementary Material). Three *N*-glycosylated sites (N22, N286, N478) confirmed by LC/MS/MS analysis were common for the H5<sub>hm</sub> and H5<sub>Man5</sub> proteins. Additionally N165 was confirmed for the H5<sub>hm</sub> protein. The structures of glycosylated H5<sub>hm</sub> and H5<sub>Man5</sub> monomer and trimer are presented in Figure 2.

## N-Glycan-Dependent Structure of the H5<sub>hm</sub> and H5<sub>Man5</sub> Antigens

Size exclusion chromatography disclosed significant differences in oligomeric status of the H5<sub>hm</sub> and H5<sub>Man5</sub> protein variants (Figure 3). The H5<sub>hm</sub> antigen was eluted in several separate peaks (Figure 3A), suggesting the presence of various oligomeric forms. Although three peaks were seen in the chromatogram of the H5<sub>Man5</sub> protein (Figure 3B), SDS-PAGE analysis confirmed

that the HA protein was eluted only in a single peak corresponding to the molecular mass of a monomer (Figure 3D, line B<sub>2</sub>). The eluted fractions were subjected to gel electrophoresis under native conditions. Native PAGE analysis revealed high MW forms in the sample of H5<sub>hm</sub> (Figure 3C). Further, both H5<sub>hm</sub> and H5<sub>Man5</sub> monomer fractions from SEC referred to the reference band mass between 240 and 480 kDa which was much closer to the molecular mass of trimeric or tetrameric form. To better understand oligomerization status of the H5<sub>hm</sub> and H5<sub>Man5</sub> antigens and to gain a more precise measurements of their various oligomeric forms, we performed size exclusion chromatography coupled to multi-angle light scattering (SEC-MALS) experiments and by matrix-assisted laser desorption/ionization mass spectrometry (MALDI-MS). SEC-MALS analysis revealed that the major peak in the H5<sub>hm</sub> SEC profile (LMW fraction; peak #4 in Figure 3A) contained mostly monomeric form of the H5<sub>hm</sub> antigen (weight-averaged MW of 81 kDa, Figure 4D, Table 2). By contrast, HMW fractions (peaks 1–3, Figure 3A) contained higher oligomeric forms of H5<sub>hm</sub>. These forms ranging from dimers to trimers (peak b, Figure 4B and peak b, Figure 4C, weight-averaged MW of 167 and 215 kDa, respectively, Table 2) to pentamers/hexamers and even higher oligomers (peak a, Figure 4A, calculated MWs ranging from ~400 to ~700 kDa). This suggests

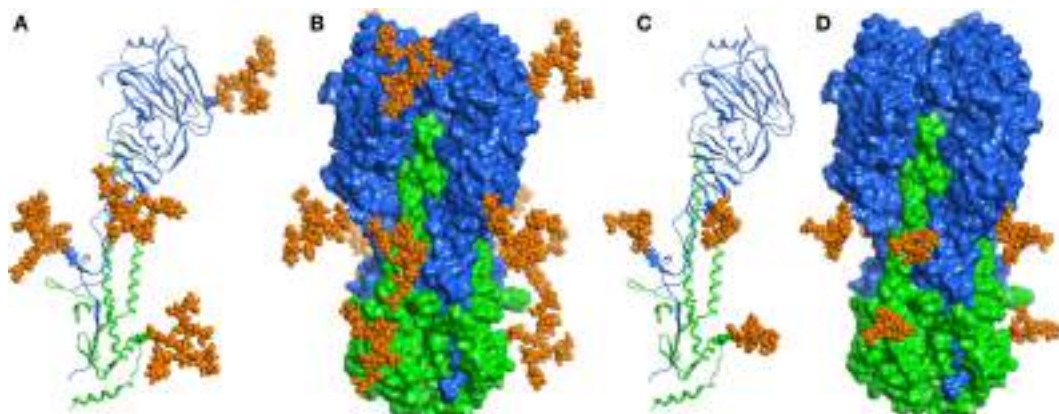


**FIGURE 2 | Structural representations of the molecular models of *N*-glycosylated H5<sub>hm</sub> (A,B) and H5<sub>Mans</sub> (C,D) monomers and trimers.** HA1 domain was depicted in blue ribbon representation, HA2 domain—in green one, and oligosaccharides—in orange atomistic ball one. The sugar-bonded asparagines were also depicted in atomistic representations according to their respective domain colors. The models were constructed based on the crystallographic structure of the H5 hemagglutinin (PDB ID code 5E2Y).

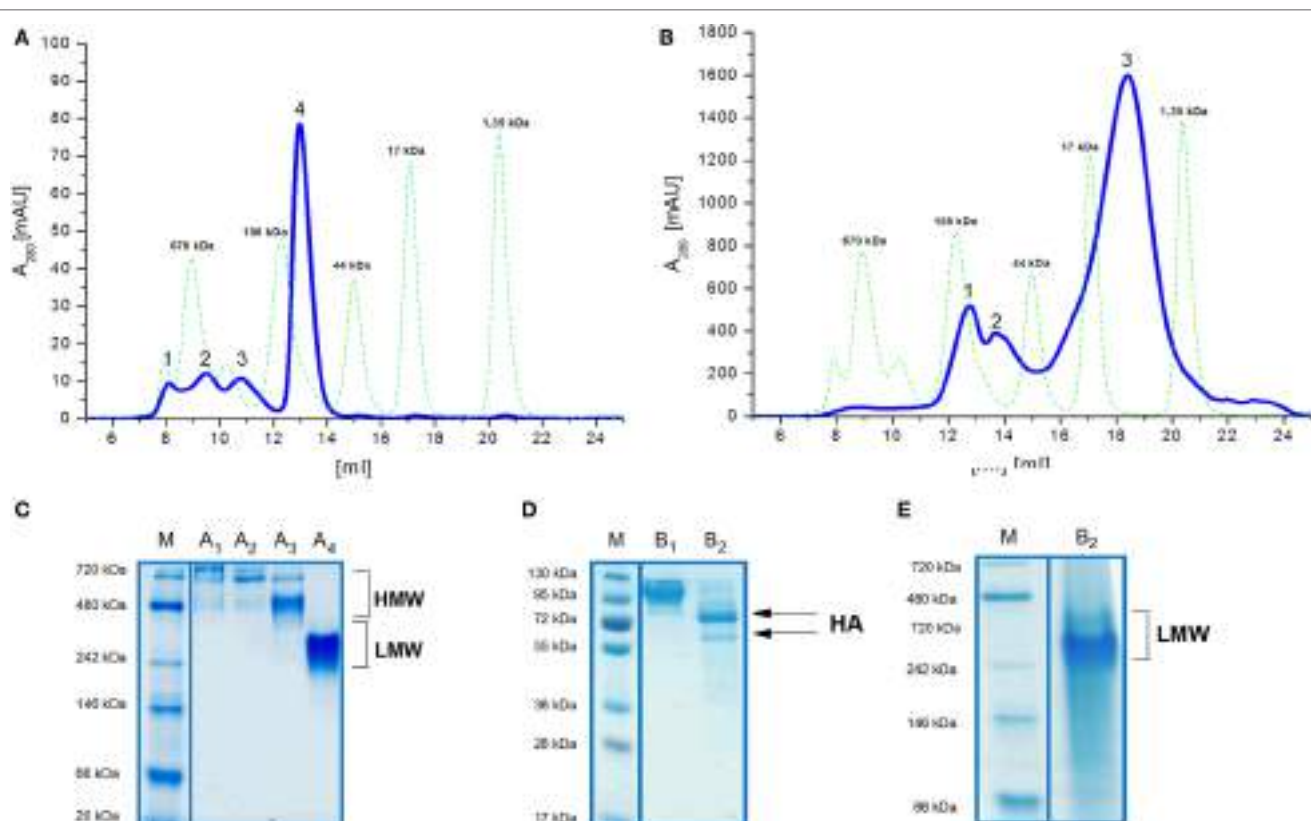


**FIGURE 3 | Size exclusion chromatography (SEC) (A,B) of H5 antigens on Superdex 200 10/300 GL column and Native PAGE analysis (C,E) of SEC fractions.** Chromatograms of the ion exchange chromatography–elution fractions (A,B). Molecular weight (MW) standard is indicated by the green dotted line. Fractions of the H5<sub>hm</sub> or H5<sub>Mans</sub> proteins were lyophilized separately and dissolved in water followed by 4–7% Native PAGE (C,E). SEC fractions of the H5<sub>Mans</sub> protein were additionally analyzed on 4–12% SDS-PAGE (D) following Coomassie staining.

that the HMW fraction on H5<sub>hm</sub> antigen comprises a mixture of different oligomeric forms of the H5<sub>hm</sub> protein. In contrast, the H5<sub>Mans</sub> antigen contained exclusively monomeric form of the H5

protein (weight-averaged MW of 67 and 66 kDa for peaks a and b respectively, (Figure 4E) which suggests different structural conformation of the population present in peak 2, Figure 3B,

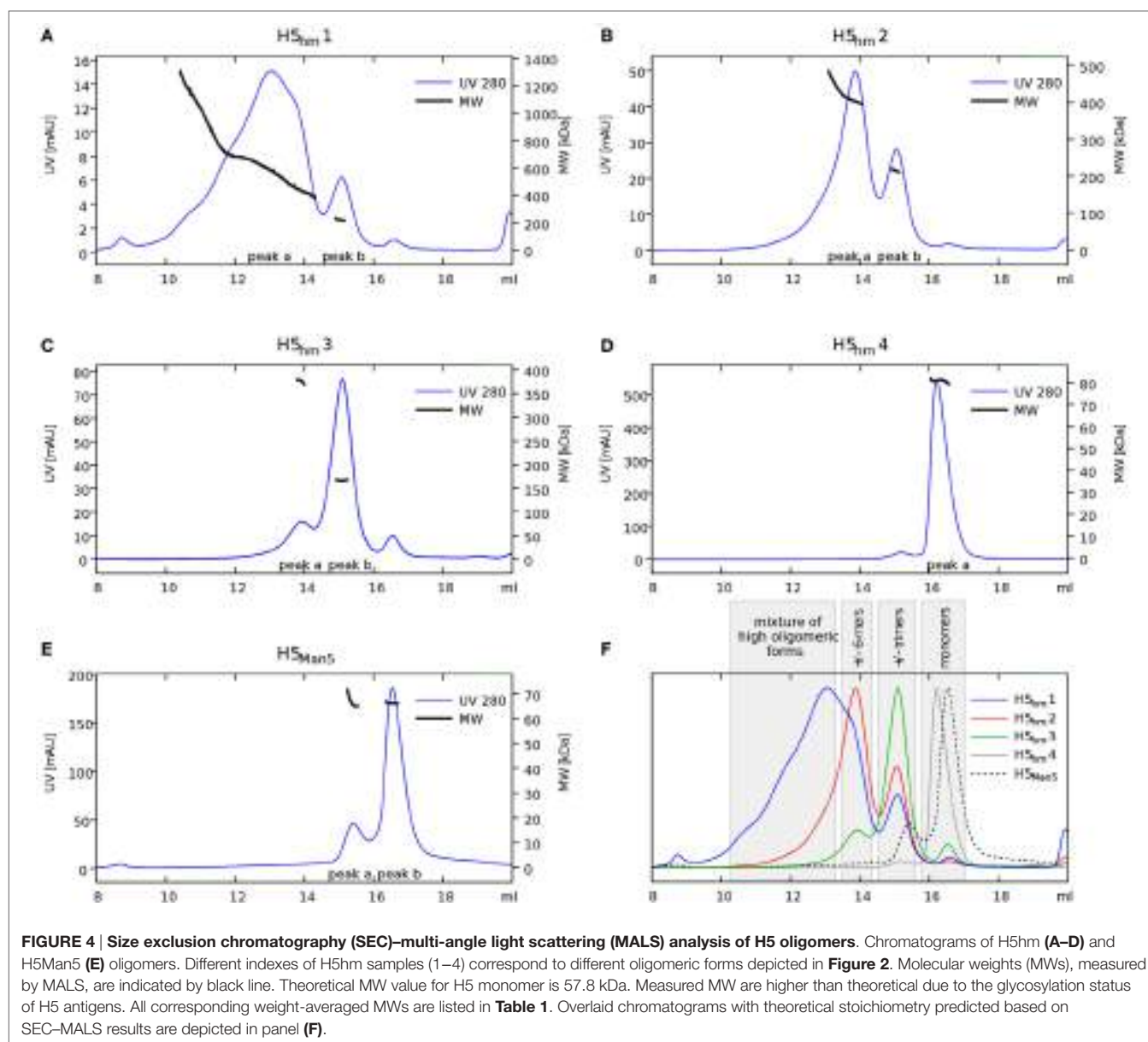


**TABLE 2 | Weight-averaged molecular weights (MWs) of H5 oligomers calculated by size exclusion chromatography–multi-angle light scattering analysis.**

Sample	Peak	MW (kDa)	Oligomeric state
H5hm1	a	645	Mixture of high oligomeric forms (9-mer on average)
	b	222	Trimer
H5hm2	a	418	Mixture of high oligomeric forms (hexamer on average)
	b	215	Trimer
H5hm3	a	376	Mixture of high oligomeric forms (pentamer on average)
	b	167	Dimer
H5hm4	a	81	Monomer
H5Man5	a	67	Monomer
	b	66	Monomer

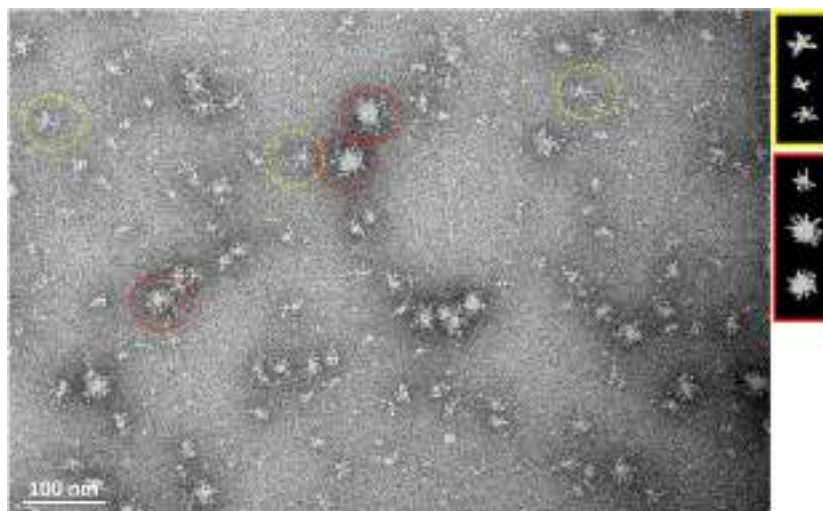
Corresponding chromatograms are present in Figure 4.

Table 2). All the chromatograms with theoretical stoichiometry predicted based on SEC-MALS results were overlaid and are presented in (Figure 4F).

Matrix-assisted laser desorption/ionization mass spectrometry analysis confirmed that the LMW fraction of the H5<sub>hm</sub> antigen from SEC column contains aside from monomer also dimer and trimer. In the sample of the H5<sub>Man5</sub> antigen, MALDI spectrometer detected only monomers (Supplementary Material).

Transmission electron microscopy showed that HMW oligomers formed regular, spherical nanostructures with an average size of 30 nm in diameter (Figure 5). However, the morphology of the H5<sub>hm</sub> nanostructures visualized by TEM is variable, e.g., rosette-like structures were also seen.

The activity of the purified H5<sub>hm</sub> and H5<sub>Man5</sub> antigens was assessed by hemagglutination assay using chicken red blood cells. This method is a surrogate assay to measure the functionality



**FIGURE 5 | Transmission electron microscopy of the purified H5<sub>hm</sub> antigen.** Images were obtained at nominal 30,000 magnification. The white scale bar represents 100 nm. Spherical (red circle) and rosette-like structures (yellow circle) were visualized.

of the influenza antigen. As a positive control, we used the inactivated A/chicken/Belgium/150/1999 H5N2 virus. Efficient HA-mediated hemagglutination was observed for the H5<sub>hm</sub> HMW oligomers or a mixture of the H5<sub>hm</sub> HMW and LMW oligomers. Hemagglutination test was negative for the H5<sub>Man5</sub> antigen (Figure 6). This is consistent with previous data suggesting that only the high MW HA oligomers are able to bind to multiple red blood cells to create the lettices structures measured in the hemagglutination assay. The immunogenicity of the H5<sub>hm</sub> and H5<sub>Man5</sub> antigens were tested *in vivo*.

### N-Glycan-Dependent Induction of Humoral Response in Mice

To test the effect of the *N*-glycan length on the antigen immunogenicity, mice were immunized with both H5<sub>hm</sub> and H5<sub>Man5</sub> antigen variants at the same dose. Furthermore, for the H5<sub>hm</sub> antigen, we tested the HMW oligomers and a mixture of HMW and LMW oligomers. Both H5<sub>hm</sub> and H5<sub>Man5</sub> variants elicited specific anti-HA-IgG antibodies after first administration of the vaccine; however, significant differences between these two antigens at each of measurement point were observed (Figures 7A–C). Also, the significant differences in the immunological properties between these two antigens were disclosed in HI test (Figure 7D). Although all groups were HI positive, both assays indicated that high-mannose glycosylated H5 antigen is superior to the H5<sub>Man5</sub>. Furthermore, what was surprising for us, both ELISA and HI assays showed that the H5<sub>hm</sub> HMW oligomers mixed with LMW oligomers induced much stronger humoral response than the H5<sub>hm</sub> HMW oligomers solely. The HI titers as high as 2,048 were observed in the group immunized with the mixed H5<sub>hm</sub> HMW and LMW oligomers (Figure 7D). These results prompted us to follow up the immunization experiment. During the next mice immunization, we tested

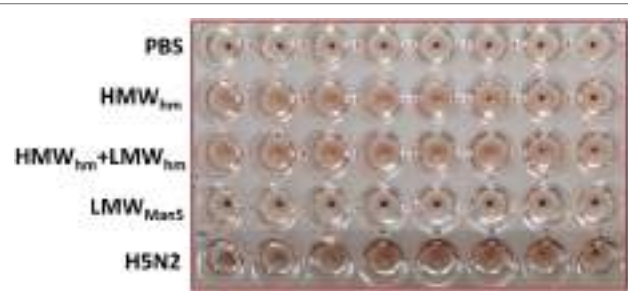


**FIGURE 6 | Hemagglutination of chicken red blood cells by the H5<sub>hm</sub> and H5<sub>Man5</sub> proteins.** Twofold dilution of the H5 antigens were incubated with 1% chicken erythrocytes (30 min, RT). Two forms (HMW and LMW oligomers) of H5<sub>hm</sub> antigen were tested. As a positive control, an inactivated H5N2 virus (A/chicken/Belgium/150/1999) was used.

the H5<sub>hm</sub> HMW and LMW oligomers separately and the lower dose of vaccine was applied. Mice were immunized twice with different H5<sub>hm</sub> forms. Figures 7E,F present the results obtained from the ELISA test. The second immunization trial showed that one dose of LMW oligomers of the H5<sub>hm</sub> antigen induced much stronger immunological response than the HMW oligomers. Further, booster injection confirmed that the LMW oligomers were more immunogenic for mice than the H5<sub>hm</sub> HMW oligomers.

### DISCUSSION

Various studies have shown that additional glycosylation sites introduced to HA molecules by site-directed mutagenesis abolish virus virulence and impact its immunogenicity (25, 26). Therefore, we decided to study the effect of *N*-glycosylation pattern without changing the number or the position of glycosylation

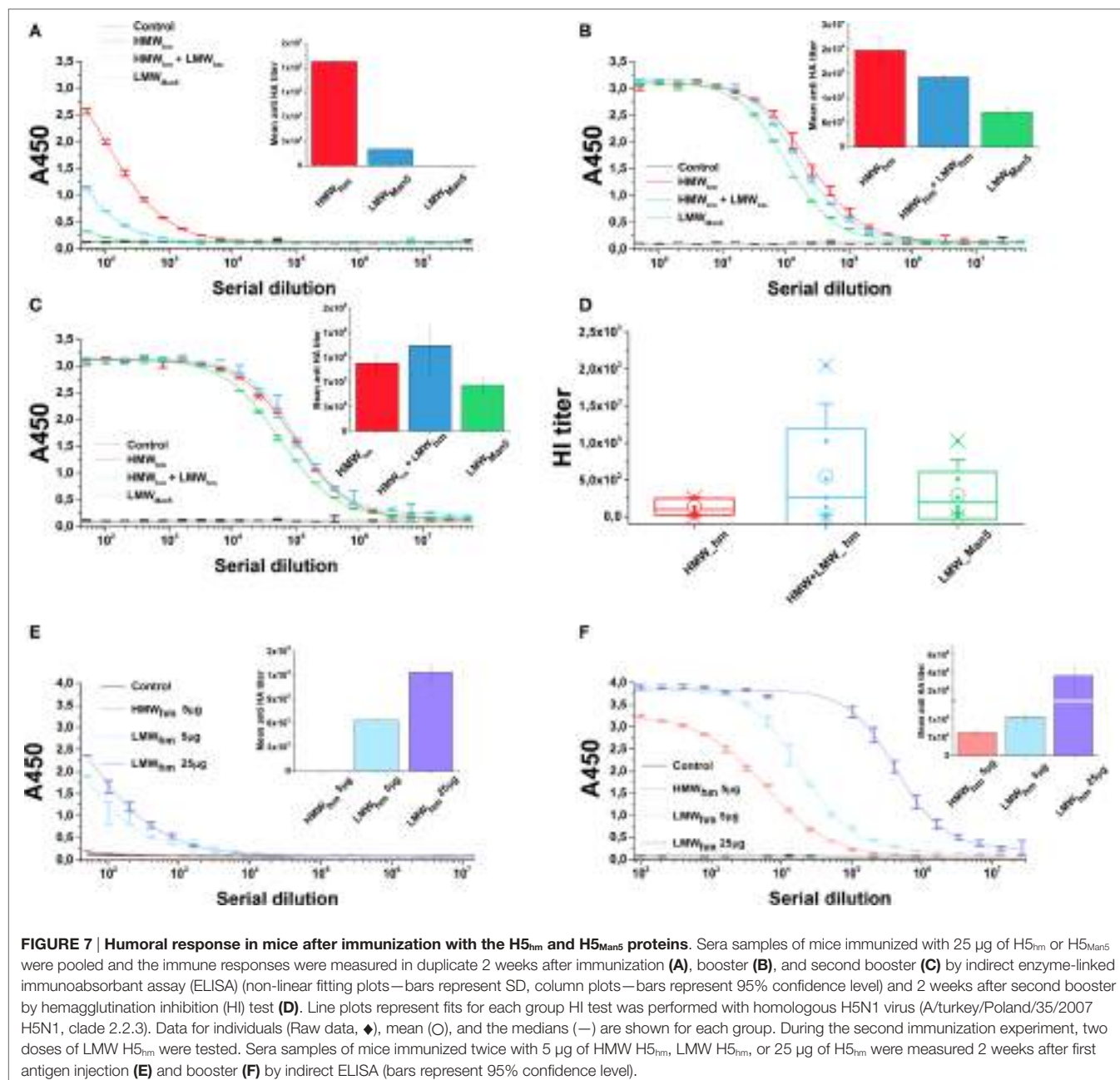


**FIGURE 7 |** Humoral response in mice after immunization with the H5<sub>hm</sub> and H5<sub>Man5</sub> proteins. Sera samples of mice immunized with 25 µg of H5<sub>hm</sub> or H5<sub>Man5</sub> were pooled and the immune responses were measured in duplicate 2 weeks after immunization (**A**), booster (**B**), and second booster (**C**) by indirect enzyme-linked immunoabsorbant assay (ELISA) (non-linear fitting plots—bars represent SD, column plots—bars represent 95% confidence level) and 2 weeks after second booster by hemagglutination inhibition (HI) test (**D**). Line plots represent fits for each group HI test was performed with homologous H5N1 virus (A/turkey/Poland/35/2007 H5N1, clade 2.2.3). Data for individuals (Raw data, ♦), mean (○), and the medians (—) are shown for each group. During the second immunization experiment, two doses of LMW H5<sub>hm</sub> were tested. Sera samples of mice immunized twice with 5 µg of HMW H5<sub>hm</sub>, LMW H5<sub>hm</sub>, or 25 µg of H5<sub>hm</sub> were measured 2 weeks after first antigen injection (**E**) and booster (**F**) by indirect ELISA (bars represent 95% confidence level).

sites. We also abandoned the idea of the addition of any foreign sequence either to enhance the oligomerization or facilitate the purification process. Although these fusion carriers are usually short peptide sequences, the changes that adding them may introduce to a protein are unpredictable. We obtained KM 71 and GlycoSwitch *Pichia* strains with stable expression of two variants of H5 antigen, with high-mannose glycosylation (H5<sub>hm</sub>) and low-mannose glycosylation (H5<sub>Man5</sub>). To test the immunological response in mice, we used three H5N1 isolates from clade 2.2. The amino acid homology between these isolates varies between 99.22 and 99.61%. The rationale for usage of three HA antigens is to mimic more natural conditions, where the circulation of genetically identical viruses is short lived, considering the

fast evolution of influenza viruses. Therefore, we created a “near-homologous” setting because the H5N1 isolates used for the preparation of HA antigen, for ELISA and HI test, all belong to clade 2.2 H5N1, the predominant genotype during 2005/2006 epidemic of HPAI. Our immunization experiments showed that the H5<sub>hm</sub> antigen induced significantly stronger HA-antibody response than the H5<sub>Man5</sub> antigen. The mean anti-HA antibodies titer as high as  $1.5 \times 10^6$  after the third dose of the H5<sub>hm</sub> vaccine was detected. However, it is well known that protective immunity correlates with HI titers rather than antigen-binding antibodies. Indeed, HI tests showed that the antigen with high-mannose glycosylation gave higher neutralizing antibodies titer than the low-glycosylated H5 antigen. It was reported by Lin and

colleagues that recombinant H5 antigen with high-mannose glycans was highly immunogenic and elicited strong immunological response (27). Recently, Liu and colleagues showed a very positive effect of high-mannose type glycosylation on the immunogenicity of recombinant H1, H5, and H7 antigens (28). On the other hand, Chen and colleagues reported that monoglycosylated H1 induced higher HI-antibodies titer and exhibited higher neutralizing capacity than fully glycosylated HA (29). The same effect was observed for the H5 protein (12). However, in above studies, antigen variants were forced to form trimers since the transmembrane domain was replaced with the residues that are trimerization segment.

In our study, the differences in the immunological properties may be explained by the differences in the oligomeric status of the H5<sub>hm</sub> and H5<sub>Man5</sub> antigens. Structural analysis showed that the high-mannose glycosylated antigen but not Man<sub>5</sub> oligomerized into spherical like structures. The H5<sub>hm</sub> antigen also formed low molecular oligomers like dimers/trimers and these oligomers combined with monomers were more immunogenic for mice than high MW oligomers. For the H5<sub>Man5</sub> antigen, only monomeric forms were detected. Gallagher and colleagues demonstrated that glycosylation state had an impact on hemagglutinin oligomerization. They showed that although no individual oligosaccharide side chain was necessary or sufficient for the folding, the mutant HAs having less than five oligosaccharides formed intracellular aggregates (18). The differences in oligomeric status of the antigens may be also caused by the number of glycosylated sites in the antigens. Mass spectrometry analysis confirmed that four sites in H5<sub>hm</sub> and three sites in H5<sub>Man5</sub> are glycosylated. Without any mutation, N165 is not glycosylated in the H5<sub>Man5</sub> antigen. Further studies are necessary to explore the effect of the N-glycosylation on the recombinant hemagglutinin oligomerization.

A low-cost production of vaccine with the specific match to the genetics of current outbreak's virus is strongly required. In this study, we used the *P. pastoris* cells to produce a soluble H5 antigens. The *P. pastoris* expression system has been commonly utilized as a platform to produce various proteins significant for medical industry, including vaccine antigens (Shanvac™, Elovac™, Gavac™). The another crucial issue for an influenza vaccine to be licensed for use is a development of efficient process for the purification of the protein product. We optimized both of vaccine production steps (expression and purification); however, the efficient production process was achieved only for high-mannose H5 protein. The efficiency of the H5<sub>Man5</sub> antigen production was rather low, thus the utilization of GlycoSwitch® *P. pastoris* strain as a vaccine platform is unattractive. For the high-mannose H5 antigen, which was proved to be much more immunogenic, the excellent efficiency up to 150 mg of highly purified protein from 1 l of culture medium (6,000 doses) was obtained. This efficiency presumably could be easily scaled up using bioreactors.

In summary, the N-glycosylation influences the biological properties of the influenza H5 antigens. The presence and the number of carbohydrate moieties (mannose) had an impact on the oligomerization and the immunogenicity of the H5<sub>hm</sub> and H5<sub>Man5</sub>

antigens. Structural analysis showed that the high-mannose glycosylated antigen not only formed low molecular oligomers like dimers and trimers but also oligomerized into spherical structures similar to influenza virions. The high-mannose H5 antigen induced significantly stronger HA-antibody response than the H5<sub>Man5</sub> antigen. These results might be highly relevant for the influenza vaccine design.

## ETHICS STATEMENT

Immunization studies were conducted at the Institute of Experimental Medicine PAS (Warsaw, Poland) under the control of Bioethics Committee (Permission No 21/2014).

## AUTHOR CONTRIBUTIONS

AM and MP performed the experiments, MC-C conducted SEC-MALS analysis, PK conducted mice experiment. ZM and KŚ contributed H5N1 virus and performed HI analysis. AM, MP, and EK participated in study design and data analysis. All authors participated in manuscript and figures preparation and have read and approved the final manuscript.

## ACKNOWLEDGMENTS

The authors thank Dr. Marcin Mielecki for constructing the molecular models of the highly glycosylated and low-glycosylated monomeric and trimeric hemagglutinin H5. They also thank Agata Malinowska from the Mass Spectrometry Laboratory IBB PAS for the assistance with the MS results analysis. This work used the platforms of the Grenoble Instruct centre (ISBG; UMS 3518 CNRS-CEA-UJF-EMBL) with support from FRISBI (ANR-10-INSB-05-02) and GRAL (ANR-10-LABX-49-01) within the Grenoble Partnership for Structural Biology (PSB). The authors thank Dr. Christine Moriscot and Dr. Guy Schoehn from the Electron Microscopy platform of the Integrated Structural Biology of Grenoble. The equipment used was sponsored in part by the Centre for Preclinical Research and Technology (CePT), a project co-sponsored by European Regional Development Fund and Innovative Economy, The National Cohesion Strategy of Poland (Innovative economy 2007–2013, Agreement POIG.02.02.00-14-024/08-00). The authors thank Piotr Baran from the Institute of Biotechnology and Antibiotics for MALDI-MS analysis.

## FUNDING

This work was supported by Grant No. PBS2/A7/14/2014 from the National Centre for Research and Development.

## SUPPLEMENTARY MATERIAL

The Supplementary Material for this article can be found online at <http://journal.frontiersin.org/article/10.3389/fimmu.2017.00444/full#supplementary-material>.

## REFERENCES

- Wiley DC, Skehel JJ. The structure and function of the hemagglutinin membrane glycoprotein of influenza virus. *Annu Rev Biochem* (1987) 56:365–94. doi:10.1146/annurev.biochem.56.1.365
- Moresco KA, Stallknecht DE, Swayne DE. Evaluation and attempted optimization of avian embryos and cell culture methods for efficient isolation and propagation of low pathogenicity avian influenza viruses. *Avian Dis* (2010) 5:622–6. doi:10.1637/8837-040309-Reg.1
- Verma S, Dimitrova M, Munjal A, Fontana J, Crevar CJ, Carter DM, et al. Oligomeric recombinant H5 HA1 vaccine produced in bacteria protects ferrets from homologous and heterologous wild-type H5N1 influenza challenge and controls viral loads better than subunit H5N1 vaccine by eliciting high-affinity antibodies. *J Virol* (2012) 86:12283–93. doi:10.1128/JVI.01596-12
- Buckland B, Boulanger R, Fino M, Srivastava I, Holtz K, Khratkov N, et al. Technology transfer and scale-up of the Flublok recombinant hemagglutinin (HA) influenza vaccine manufacturing process. *Vaccine* (2014) 32:5496–502. doi:10.1016/j.vaccine.2014.07.074
- Le Mauff F, Mercier G, Chan P, Burel C, Vaudry D, Bardot M, et al. Biochemical composition of haemagglutinin-based influenza virus-like particle vaccine produced by transient expression in tobacco plants. *Plant Biotechnol J* (2015) 13:717–25. doi:10.1111/pbi.12301
- Vigerust DJ, Shepherd VL. Virus glycosylation: role in virulence and immune interactions. *Trends Microbiol* (2007) 5:211–8. doi:10.1016/j.tim.2007.03.003
- Sun X, Jayaraman A, Maniprasad P, Raman R, Houser KV, Pappas C, et al. N-linked glycosylation of the hemagglutinin protein influences virulence and antigenicity of the 1918 pandemic and seasonal H1N1 influenza A viruses. *J Virol* (2013) 87:8756–66. doi:10.1128/JVI.00593-13
- Skehel JJ, Stevens DJ, Daniels RS, Douglas AR, Knossow M, Wilson IA, et al. A carbohydrate side chain on hemagglutinins of Hong Kong influenza viruses inhibits recognition by a monoclonal antibody. *Proc Natl Acad Sci U S A* (1984) 6:1779–83. doi:10.1073/pnas.81.6.1779
- Abe Y, Takashita E, Sugawara K, Matsuzaki Y, Muraki Y, Hongo S. Effect of the addition of oligosaccharides on the biological activities and antigenicity of influenza A/H3N2 virus hemagglutinin. *J Virol* (2004) 18:9605–11. doi:10.1128/JVI.78.18.9605-9611.2004
- Zhang X, Chen S, Jiang Y, Huang K, Huang J, Yang D, et al. Hemagglutinin glycosylation modulates the pathogenicity and antigenicity of the H5N1 avian influenza virus. *Vet Microbiol* (2015) 175:244–56. doi:10.1016/j.vetmic.2014.12.011
- Tsuchiya E, Sugawara K, Hongo S, Matsuzaki Y, Muraki Y, Li ZN, et al. Effect of addition of new oligosaccharide chains to the globular head of influenza A/H2N2 virus haemagglutinin on the intracellular transport and biological activities of the molecule. *J Gen Virol* (2002) 83:1137–46. doi:10.1099/0022-1317-83-12-3067
- Wang CC, Chen JR, Tseng YC, Hsu CH, Hung YF, Chen SW, et al. Glycans on influenza hemagglutinin affect receptor binding and immune response. *Proc Natl Acad Sci U S A* (2009) 106:18137–42. doi:10.1073/pnas.0909696106
- Desphande KL, Fried VA, Ando M, Webster RG. Glycosylation affects cleavage of an H5N2 influenza virus hemagglutinin and regulates virulence. *Proc Natl Acad Sci U S A* (1987) 1:36–40.
- Kawaoka Y, Webster RG. Interplay between carbohydrate in the stalk and the length of the connecting peptide determines the cleavability of influenza virus hemagglutinin. *J Virol* (1989) 63:3296–300.
- Zhang X, Chen S, Yang D, Wang X, Zhu J, Peng D, et al. Role of stem glycans attached to haemagglutinin in the biological characteristics of H5N1 avian influenza virus. *J Gen Virol* (2015) 96:1248–57. doi:10.1099/vir.0.000082
- Copeland CS, Doms RW, Bolzau EM, Webster RG, Helenius A. Assembly of Influenza hemagglutinin trimers and its role in intracellular transport. *J Cell Biol* (1986) 103:1179–91. doi:10.1083/jcb.103.4.1179
- Hurtley SM, Bole DG, Hoover-Litty H, Helenius A, Copeland CS. Interactions of misfolded influenza virus hemagglutinin with binding protein (BiP). *J Cell Biol* (1989) 108:2117–26. doi:10.1083/jcb.108.6.2117
- Gallagher PJ, Henneberry JM, Sambrook JE, Gething MJ. Glycosylation requirements for intracellular transport and function of the hemagglutinin of influenza virus. *J Virol* (1992) 66:7136–45.
- Roberts PC, Garten W, Klenk HD. Role of conserved glycosylation sites in maturation and transport of influenza A virus hemagglutinin. *J Virol* (1993) 67:3048–60.
- Daniels R, Kurowski B, Johnson AE, Hebert DN. N-linked glycans direct the cotranslational folding pathway of influenza hemagglutinin. *Mol Cell* (2003) 11:79–90. doi:10.1016/S1097-2765(02)00821-3
- Kornfeld R, Kornfeld S. Assembly of asparagine-linked oligosaccharides. *Ann Rev Biochem* (1985) 54:631–6. doi:10.1146/annurev.bi.54.070185.003215
- Pietrzak M, Maciola A, Zdanowski K, Protas-Kulkowska AM, Olszewska M, Śmiertanka K, et al. An avian influenza H5N1 virus vaccine candidate based on the extracellular domain produced in yeast system as subviral particles protects chickens from lethal challenge. *Antiviral Res* (2016) 133:242–9. doi:10.1016/j.antiviral.2016.08.001
- Kopera E, Dvornyk A, Kosson P, Florys K, Saczyńska V, Dębski J, et al. Expression, purification and characterization of glycosylated influenza H5N1 hemagglutinin produced in *Pichia pastoris*. *Acta Biochim Pol* (2014) 61:597–602.
- Bizanov G, Tamosunas V. Immune response induced in mice after intragastric administration with Sendai virus in combination with extract of *Uncaria tomentosa*. *Scand J Lab Anim Sci* (2005) 32:201–7.
- Vigerust DJ, Ulett KB, Boyd KL, Madsen J, Hawgood S, McCullers JA. N-linked glycosylation attenuates H3N2 influenza viruses. *J Virol* (2007) 81:8593–600. doi:10.1128/JVI.00769-07
- Wanzeck K, Boyd KL, McCullers JA. Glycan shielding of the influenza virus hemagglutinin contributes to immunopathology in mice. *Am J Respir Crit Care Med* (2011) 183:767–73. doi:10.1164/rccm.201007-1184OC
- Lin SC, Jan JT, Dionne B, Butler M, Huang MH, Wu CY, et al. Different immunity elicited by recombinant H5N1 hemagglutinin proteins containing pauci-mannose, high-mannose, or complex type N-glycans. *PLoS One* (2013) 8:e66719. doi:10.1371/journal.pone.0066719
- Liu WC, Lin YL, Spearman M, Cheng PY, Butler M, Wu SC. Influenza virus hemagglutinin glycoproteins with different N-glycan patterns activate dendritic cells in vitro. *J Virol* (2016) 90:608560–96. doi:10.1128/JVI.00452-16
- Chen JR, Yu YH, Tseng YC, Chiang WL, Chiang MF, Ko YA, et al. Vaccination of monoglycosylated hemagglutinin induces cross-strain protection against influenza virus infections. *Proc Natl Acad Sci U S A* (2014) 111:2476–81. doi:10.1073/pnas.1323954111

**Conflict of Interest Statement:** The authors declare that the research was conducted in the absence of any commercial or financial relationships that could be construed as a potential conflict of interest.

Copyright © 2017 Maciola, Pietrzak, Kosson, Czarnocki-Cieciura, Śmiertanka, Minta and Kopera. This is an open-access article distributed under the terms of the Creative Commons Attribution License (CC BY). The use, distribution or reproduction in other forums is permitted, provided the original author(s) or licensor are credited and that the original publication in this journal is cited, in accordance with accepted academic practice. No use, distribution or reproduction is permitted which does not comply with these terms.

# Advantages of publishing in Frontiers



## OPEN ACCESS

Articles are free to read for greatest visibility and readership



## FAST PUBLICATION

Around 90 days from submission to decision



## HIGH QUALITY PEER-REVIEW

Rigorous, collaborative, and constructive peer-review



## TRANSPARENT PEER-REVIEW

Editors and reviewers acknowledged by name on published articles



## REPRODUCIBILITY OF RESEARCH

Support open data and methods to enhance research reproducibility



## DIGITAL PUBLISHING

Articles designed for optimal readership across devices



FOLLOW US  
@frontiersin



IMPACT METRICS  
Advanced article metrics track visibility across digital media



EXTENSIVE PROMOTION  
Marketing and promotion of impactful research



LOOP RESEARCH NETWORK  
Our network increases your article's readership

### Frontiers

Avenue du Tribunal-Fédéral 34  
1005 Lausanne | Switzerland

Visit us: [www.frontiersin.org](http://www.frontiersin.org)

Contact us: [info@frontiersin.org](mailto:info@frontiersin.org) | +41 21 510 17 00